THESIS

# ALTERATION OF ORGANIC MATTER AND COPPER MINERALIZATION IN THE MIDCONTINENT RIFT, USA

Submitted by

Max Schultz

Department of Geosciences

In partial fulfillment of the requirements

For the Degree of Master of Science

Colorado State University

Fort Collins, Colorado

Summer 2017

Master's Committee:

Advisor: John Ridley

Sally Sutton
Alan Kennan

# ABSTRACT

# ALTERATION OF ORGANIC MATTER AND COPPER MINERALIZATION IN THE MIDCONTINENT RIFT, USA

This study applies petrographic, organic and isotopic geochemical analyses in an effort to discern the vertical and lateral dimensions or conduits of detectable main stage mineralization partial oxidation, heating, and fluid flow in and near the sediment-hosted stratiform Cu deposits in the Midcontinent Rift. Field and core samples from a 100 km traverse along strike of the Nonesuch Formation are analyzed at atomic, molecular, micro- and macroscopic levels for comparison to address the problem. Analytical tools - optical petrography (68 samples), Rock-Eval II (RE; 74 samples) pyrolysis, gas chromatography and gas chromatography-mass spectroscopy (GC and GC-MS; 9 samples), as well as stable isotopic analyses of C and O ($\delta^{13}$C and $\delta^{18}$O; 27 samples) - and their results here compared indicate that partial oxidation of organic matter (OM) does not exclusively co-occur with Cu mineralization.

Two morphologies of OM with distinct geochemical and petrographic characteristics have been identified. Filamentous organic matter (FOM) is generally darker colored opaque inertinite while amorphous organic matter (AOM) is lighter in color and commonly translucent. Reflected and transmitted light microscopy identified disseminated chalcocite and chalcopyrite mineralization; this mineralization coincides with darker average AOM color (higher thermal alteration index or TAI). Most of the seven identified vertically breached dark gray shaley laminations are Cu mineralized and situated in the lower to middle portion of their respective sections.

Outcrop samples show significantly lower quotients of RE hydrogen index to oxygen index (HI/OI) and values of total organic carbon (TOC) than do drill core specimens. Core profiles show gradients of increasing HI and decreasing OI stratigraphically up-section, when outlier values are excluded, and the HI gradient is steeper with respect to stratigraphic position than is typical for sedimentary basins. Oxygen index values increase with proximity to Cu minerals and the lowest HI samples are from in and adjacent to mineralized rock at or near White Pine, MI. Most Cu mineralized samples show OI above 30 mg $CO_2$/g TOC with HI under 72 mg HC/g TOC and the opposite is true for the HI of most unmineralized samples.

The FOM shows a lower H/C ratio than does the AOM. Darker colored AOM and lower HI/OI quotients than in unmineralized Nonesuch Formation material are apparent in Cu mineralized samples. The lowest $T_{max}$ and highest HI values are in unmineralized orange (low TAI) AOM, and nearly 70% of the darker brown AOM samples are Cu mineralized. No overall correlation between other RE parameters, Cu mineralization and TAI is apparent, however. All of the samples containing breached shaley laminae show low TOC but show no other relation to RE parameters.

Four measures of organic maturity - the production, thermal alteration, and methylphenanthrene-1 indices, and the $C_{29}$ Ts/($C_{29}$ hopane + $C_{29}$ Ts) parameter - show bidirectionally increasing thermal maturity of OM outward from the four central sampling sites. This aligns with multiple previous studies which have reported a paleothermal low in the vicinity of the Iron River syncline. A strong linear correlation on cross plot of $C_{29}$ sterane $\beta\beta/(\beta\beta+\alpha\alpha)$ versus $C_{29}$ sterane $S/(S+R\ \alpha\alpha\alpha)$ suggests that the gas chromatography-mass spectroscopy samples experienced similar heating rates in the subsurface.

A single organofacies source is suggested by the pristane/$n$-$C_{17}$ and phytane/$n$-$C_{18}$ quotients and their crossplot. The distribution of tricyclic terpanes and the presence of 1,2,5-TMN in all samples, with the occurrence of $C_{32}$ αα methylhopanes a majority of gas chromatography-mass spectroscopy samples concur with recent paleobiological reports of a significant cyanobacterial contribution to Nonesuch Formation OM.

Three generic patterns of OM alteration are distinguished by GC and GC-MS: least altered, partially altered, and altered; no relation to Cu mineralization is apparent for any of the three categories. Least altered samples have whole rock extract chromatograms typical of source rocks in the upper half of the oil window - a broad, smooth GC trace, dominated by *n*-alkanes $n$-$C_{11}$ to $n$-$C_{14}$ with associated peak clusters of monomethyl alkanes commonly associated with Proterozoic carbonaceous rocks. Altered samples show sharp narrow whole rock extract GC traces distinguished by 2-4 dominant *n*-alkanes, lack peaks of clusters of homologous sets of monomethyl alkanes, and have lesser abundance of alkanes, and a conspicuous higher abundance and broader array of polycyclic aromatic hydrocarbons (PAHs). The partially altered sample shows a bimodal GC trace distinct from those of the other two categories. Rock-Eval II HI values overlap for the altered and least altered samples, whereas the OI values are higher for altered samples, with the latter also showing the highest $T_{max}$ value.

The presence of sterane and terpane biomarkers at White Pine, MI discounts previous studies' assertion that their absence indicates a strictly localized oxidative destruction of such compounds during Cu mineralization. All analyzed samples have significant non-biomarker PAHs and derivatives thereof, including: 3-methylbiphenyl, phenanthrenes, trimethylnaphthalenes, dibenzothiophene (DBT), dibenzofuran (DBF), fluorene, benzofluoranthene, benzopyrene, perylene; this suggests widespread, regional aromatization associated with localized Cu mineralization.  In contrast, diminished values of DBT and DBF relative to either methylated or dimethylated homologues in Cu mineralized samples are interpreted to reflect a localized effect of epigenetic OM oxidation associated with mineralization and alteration.  The pristane/*n*-$C_{17}$ is elevated in the Cu mineralized samples, consistent with localized oxidative destruction of *n*-alkanes during mineralization.  It is suggested that dehydrocyclization of phenylphenanthrenes during Cu mineralization formed the observed benzofluoranthenes and benzopyrenes.  The phenanthrene/Σmethylphenanthrene parameter shows regular relation to HI/OI quotient, although it is less well correlated to Cu mineralization, HI or OI than in other studies.

Decreased concentrations of saturated compounds associated with Cu mineralization, as well as moretane/hopane, $C_{29}$ Ts/($C_{29}$ hopane + $C_{29}$ Ts), and trimethylnaphthalene index measures, and an interpreted thermal cracking of long chain hydrocarbons to form diamantanes during Cu mineralization, indicate localized increases in maturity of OM occurs in Cu mineralized samples in the central portion of the sampling traverse (within the overall thermal maturity low in the central sites of the sampling traverse).  However, aside from diminished abundance of saturated hydrocarbons, some counterexamples to these Cu mineralization-associated organic maturation parameters exist, and no regular relation of any of these measures to depth is apparent.

A ternary plot comparing relative abundances of DBT, DBF and fluorene shows the gas chromatography-mass spectroscopy samples clustered nearest to the thiohydrocarbon DBT vertex of the plot, with the implication of relatively little oxidative alteration but considerable S introduction for the subset of GC-MS samples.  In contrast, the position of the GC-MS samples on the DBT/phytane axis of the plot comparing DBT/phytane versus pristane/phytane suggests relatively little introduction of S with significant aromatization.

An overall trend of low $\delta^{18}O$ at lower $\delta^{13}C$ exists for carbonates of the Nonesuch Formation. No relation between carbonate vein, concretion or laminite isotopic ratios of C or O and depth or proximity to mineralization or between isotope ratios and elemental composition is apparent. Still, the most negative stable isotopic ratios co-occur with sections of Nonesuch Formation in which OM is mostly strongly oxidized, based on OI values. The upper end of isotopic ratios of carbonate C and O approximates that of Copper Harbor Formation stromatolites, which is taken to be the primary carbonate composition in the sequence. The relatively broad spread to more negative $\delta^{13}C$ values can be interpreted as a result of variable degrees of mixing with C derived by oxidation of indigenous OM. The lack of relation of carbonate isotopic ratios to distance to Cu mineralization suggests that OM oxidation likely took place throughout the Nonesuch Formation and was neither restricted to, nor strongly heightened in, Cu mineralized rocks.

# ACKNOWLEDGEMENTS

This work would not have been possible without financial and intellectual support at CSU, particularly from John Ridley.  Sally Sutton, Sven Egenhoff, and Judy Hannah each drove me forward, shared knowledge and enthusiasm for this project.  The SEG Graduate Student Fellowship and the Malcolm McCallum Scholarship smoothed my path forward and brighten the way ahead.  I am fortunate to have had such strong graduate program compatriots – Marissa Boraas, Jake McCane, and others – to assist in the many steps to this final product.  My journey would not have been possible without the three human fundaments of any task that I tackle: Bob and Donna, and my dear Desirée.  I cannot thank Philip Wells, Daniel Gourley, Z.L. Lucius, Teddy Schafer, Tom Kasper and Lucile Fiske enough for their support.

# DEDICATION

A #2 dot-filling standardized test might not seem like a ticket to the Promised Land, but that is how my Uncle Orton Lynn Gray sprung my mother from the dead-end of servile Middle American womanhood. Rural North Dakota, late 1960s, Orton said, “Hey Donna, so there is this test called the ACT and I think that you should take it.” She did so, and the joys of university and biochemistry and worldliness became her. Orton Gray’s thirst for knowledge, his genuine egalitarian equanimity, his very offbeat self, and his humanitarian nature made Woodworth, North Dakota just the right spot for my mother to be in that time. We miss him, and work to carry on in his noble steps.

# TABLE OF CONTENTS

## *1. Introduction*

### *1.1 Problem and Context*

Industry estimates suggest that many kilotons of recoverable Cu as fine-grained disseminated sulfides are in place in and near the White Pine Mine, northern Michigan (Johnson, 2014). Current commercial interest, historic production greater than 3.5 billion pounds Cu, and incomplete understanding of the mode of metallization in the SSC deposits of northern Michigan justify the present analysis: A combined geochemical investigation with the goal of identifying pathways of Cu-associated hydrothermal fluid flow (Sirois, 2015).

Economic Cu ores, with variable minor Ag, sit near the base of the 200 m thick shaley siltstones of the 1.08 Ga Nonesuch Formation; the ores are stratiform bodies up to a few kilometers strike extent and up to a few meters thick in the lowest few meters of the Nonesuch Formation or extending up to 5 meters into the underlying redbed clastic sedimentary rocks of the Copper Harbor Conglomerate (Ensign *et al.*, 1968; Brown, 1971). At the White Pine Mine and the Copperwood prospect, Cu emplacement is thought to have occurred by reduction of oxidized, Cu-bearing fluids upon flow into and through the dark gray shales and interaction with reduced C therein. Cu deposition by this mechanism would likely overlap spatially with oxidation of OM in the Nonesuch Formation; such hydrothermally affected OM would plausibly show distinct organic geochemical alteration signatures. This mode of emplacement may also have imprinted distinct isotopic signatures in carbonates in the Nonesuch Formation.

Genetic models for this style of deposit will benefit from a clearer understanding of the relationship of fluid flow to structural features (e.g.: the Keweenaw Fault, basement topography). Future Cu extraction could be streamlined by better constraints on zones of greatest Cu concentration. Future exploration for analogous deposits elsewhere in the region will benefit from this study's determination if haloes of organic alteration of barren hostrocks adjacent to Cu mineralization can serve as indicators of proximity to economic Cu deposits or of hydrothermal fluid conduits.

### *1.2 Objectives*

Comparative analysis of RE pyrolitic and GC-MS parameters with organic petrography to ascertain the degree of syn-mineralization oxidation of organic matter (OM) in the Nonesuch Formation is the main objective of this study. Ideally this provides a means of delineating paleohydrothermal fluid conduits. Stable isotope data on C and O from carbonate laminites, concretions, and veins provide supporting data to identify the extent of hydrothermal mobilization of $C_{org}$ to neomineralized, $C_{carb}$.

### *1.3 Study Area and Geologic History*

#### *1.3.1 Physiography and Genesis of the Midcontinent Rift System*

The samples in this survey come from a short segment on the southeast margin of the more than 2,000 km long, 40-90 km wide, Superior arm of the Mesoproterozoic Midcontinent rift system of North America (Figure 1). The rift cuts across Precambrian basement terranes of ages ranging from 1.85 Ga to older than 2.5 Ga (Bickford, 1988). Rift opening and abundant rift-filling volcanism likely occurred between 1109 and 1087 Ma (Davis and Sutcliff, 1985). Major magmatic activity in the rift was focused in two pulses -1109-1105 Ma and 1100-1094 Ma (Paces and Miller, 1993). Volcanic rocks dominated during active rifting and sedimentation dominated the post-rift subsidence phase, depositing what became the more than 30 km thick rift fill beneath today's Lake Superior (Behrendt *et al.*, 1988). Twenty kilometers of mostly subaerial volcanic rocks underlie a 5 km-thick mixed series of sedimentary and volcanic rocks; a further 7 km sedimentary rock sequence sits above the mixed unit (Ojakangas *et al.*, 2001).

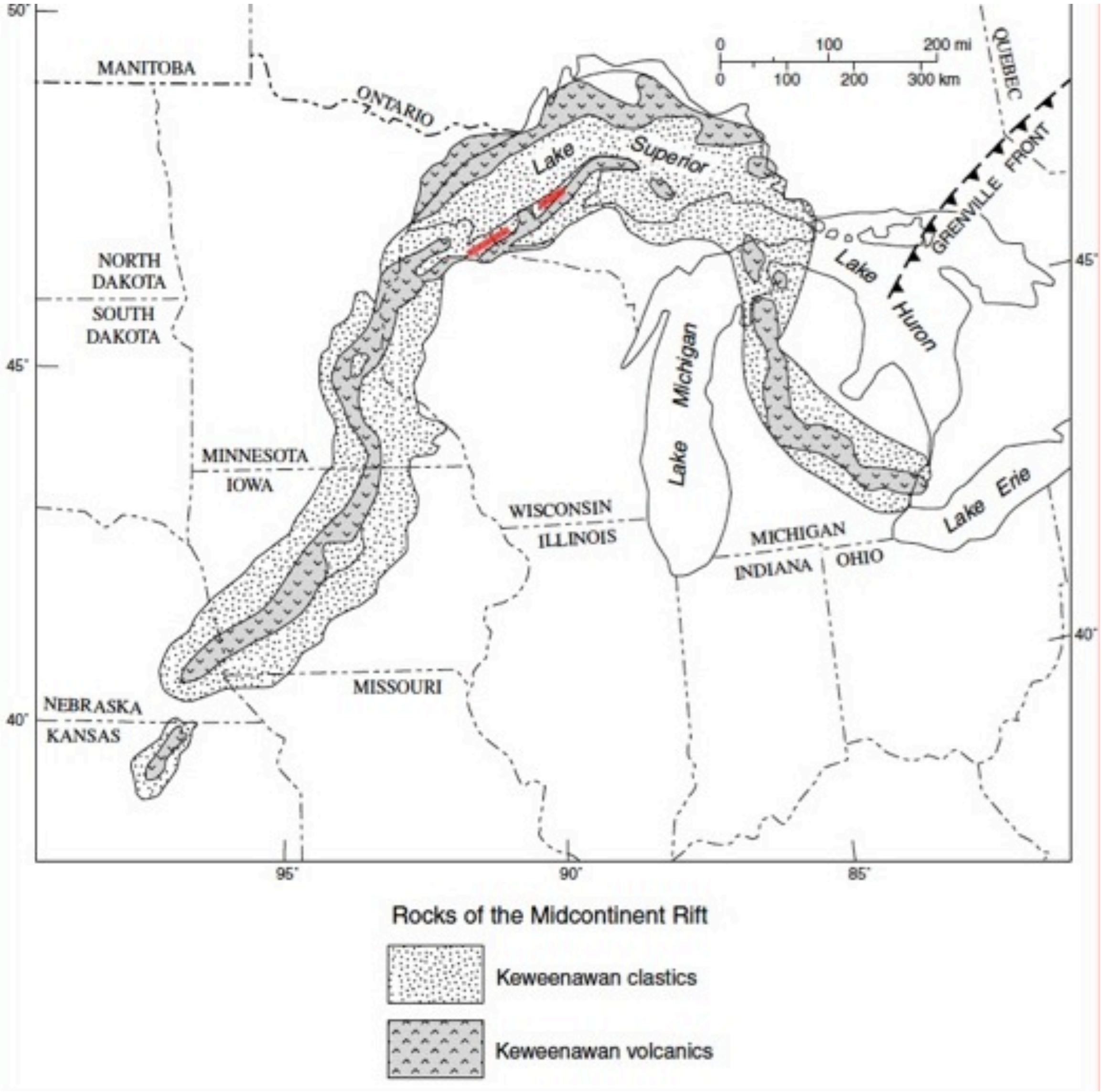

Figure 1: Location of the North American Midcontinent rift system, from Ojakangas *et al.* (2001). Samples in this study come from the red-highlighted lineament in the Superior arm of the rift.

Near to the end of rift extension, the Grenville Province to the southeast experienced tectonic compression (Cannon and Hinze, 1992). Grenville compression partially inverted the original graben-bounding normal faults into major reverse faults. This, and broad folding at 30-50 m.y. after extension ceased, suggest that tectonic stresses of the Grenville orogen overwhelmed and partially closed the Midcontinent rift system (Cannon and Hinze, 1992).

The nature and form of the Midcontinent rift are attributable to at least two different driving forces. Basinal void space formed first by rift extension and later, flexural crustal subsidence/sagging caused by rift-fill loading above low-viscosity mantle material (Nyquist and Wang, 1988). During rift extension a system of axial half-grabens developed, separated along the length of the rift by structural accommodation zones (Ojakangas *et al.*, 2001). It is generally accepted that tectonic extension energized by a mantle plume caused initial rift opening and voluminous volcanism (Van Schmus, 1992; Cannon and Nicholson (1992). Basin filling occurred both along the rift axis and in basins flanking a central, post-volcanic horst. See Figure 2. Paleomagnetic measurements and interpretation by Elmore and van der Voo (1982) and others suggest that rift filling occurred at low latitudes in a tropical to subtropical climate.

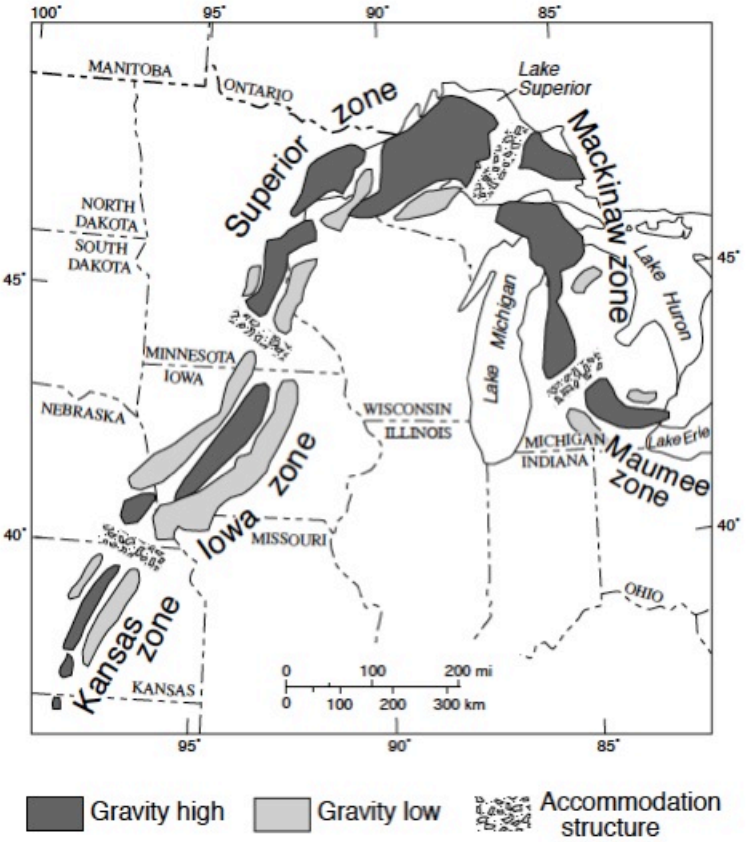

Figure 2: Schematic map of the gravitational trend of the Midcontinent rift system showing major tectonic zones. The geophysical trends seen here result from differences in the lithology of rift-fill rock sequences. From Ojakangas *et al.* (2001).

The conditions that formed the Midcontinent rift provided some important elements for SSC deposit genesis, namely a thick pile of mafic rocks, a sufficiently steep geothermal gradient, and a low-latitude rift basin setting. Isotopic, petrochemical, and geophysical evidence support the presence of a hotspot in the genesis of the rift (Miller and Nicholson, 2013). The massive volume (1.3-2.0 x $10^6$ $km^3$) of primitive, mafic rock extruded over a geologically short period and the comparatively moderate crustal extension of the rift would require the anomalous hot asthenosphere of a mantle plume (Cannon, 1992; Hutchinson *et al.*, 1990).

### *1.3.2 Stratigraphy of the Midcontinent Rift System*

Rift fill rocks, the Keweenawan Supergroup, are exposed only in the Lake Superior area, commonly in thick monoclinal columns that dip toward the rift axis beneath the lake. Reverse faults associated with Grenville compression repeat the section in some areas. Three major lithologic components are present: 1) a thick edifice of subaerial lava flows, 2) local accumulations of plutonic to hypabyssal intrusive rocks, and 3) the upper sequence of post-extension, sag-period sedimentary rocks (Miller and Nicholson, 2013). The bulk of the Keweenawan Supergroup rocks are extrusives of the Bergland and Powder Mill Groups and consist of huge volumes of subaerial tholeiitic basalts with minor rhyolite. Early post-rift red-bed sedimentary rocks are mostly intrabasinally-derived material that was dominantly deposited in fluvial settings: this is the Oronto Group. Above the Oronto Group is the progressively more mature red-bed fluvial sediment of the Bayfield Group, of extra-basinal provenance (Ojakangas *et al.*, 2001; Figure 3 and Figure 4).

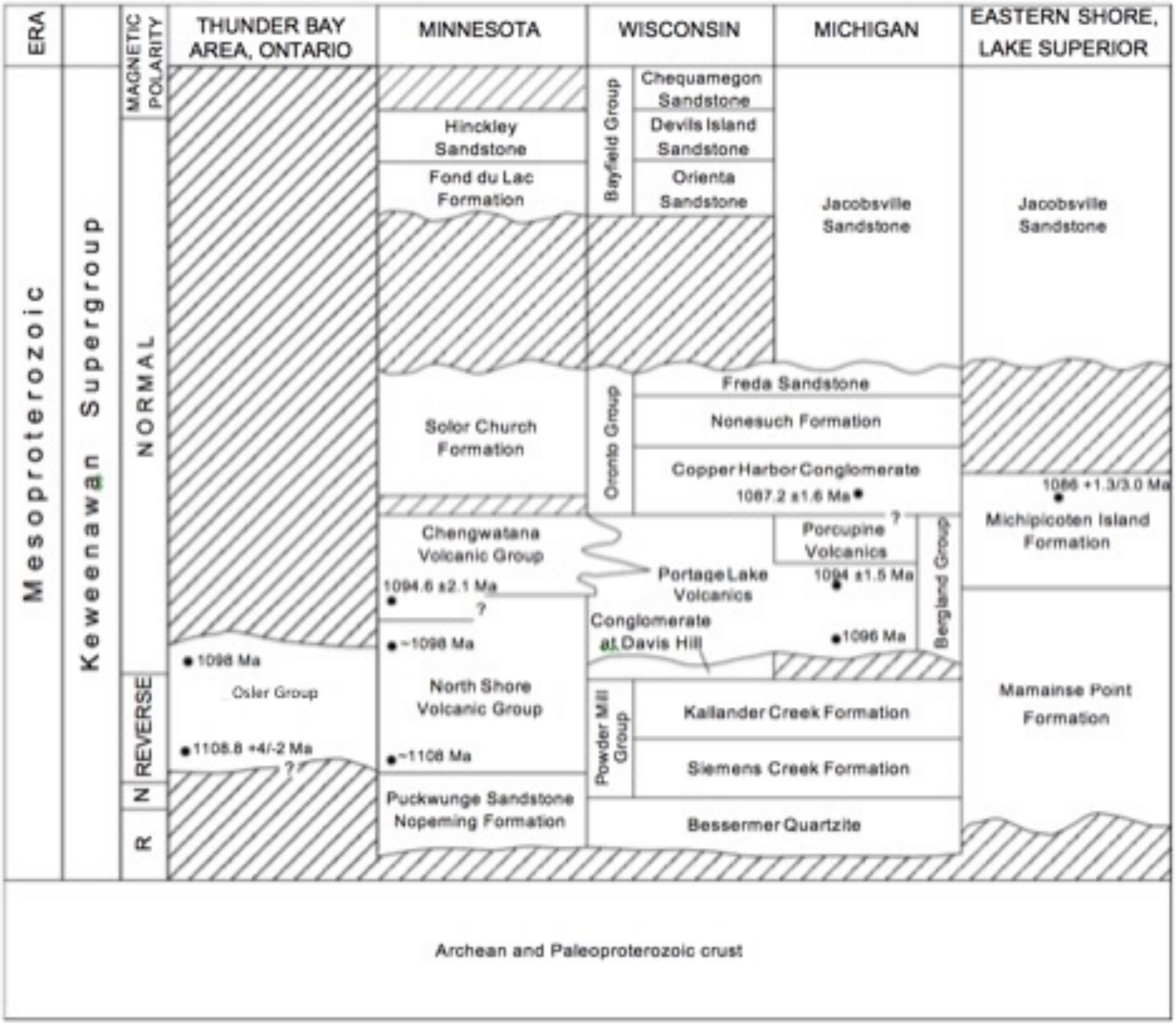

Figure 3: The comparative stratigraphy of the full Keweenawan Supergroup in the Lake Superior region. From Ojakangas *et al.*, 2001.

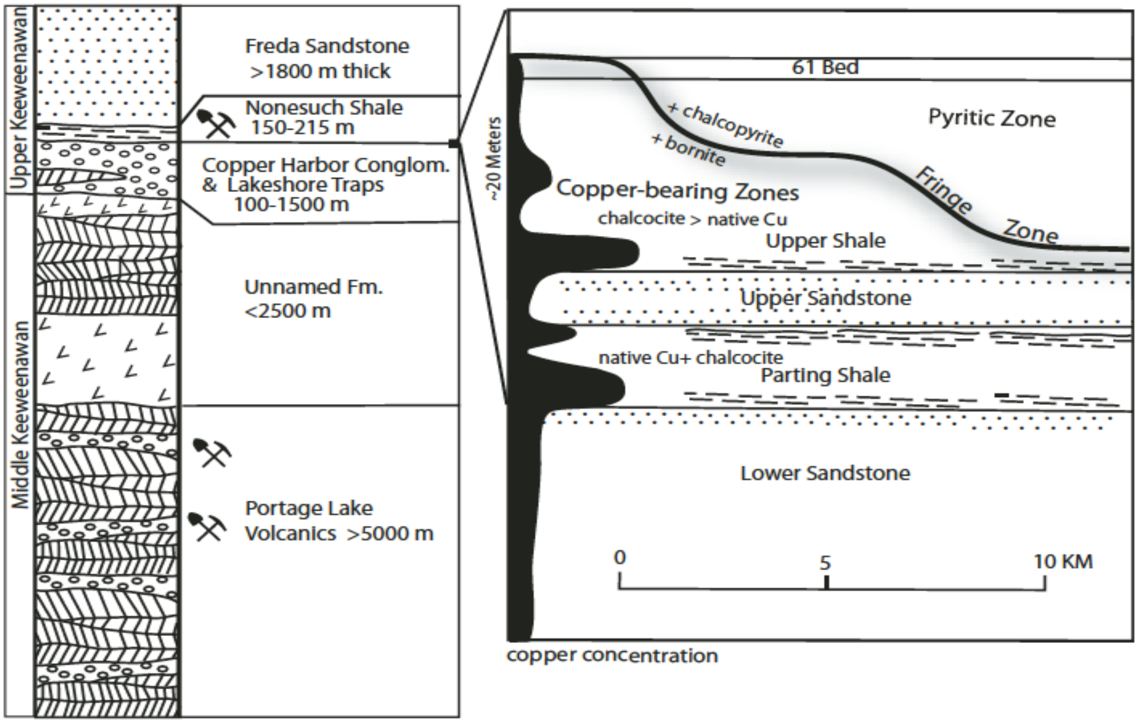

Figure 4: Stratigraphic column of the Midcontinent Rift, Upper Peninsula Michigan, showing SSC deposits of the Nonesuch and the native Cu deposits more intimately associated with mafic rocks. The detail shows Cu concentration in layers of Nonesuch Formation at White Pine. Notice the "fringe zone" slightly cutting across stratigraphic horizons. From Schmidt and Rogers, 2007.

### *1.3.2.1 Bergland Group*

The Portage Lake Volcanics are the base of the Bergland Group in northern Wisconsin and Upper Michigan. These are dominantly olivine-rich flood basalts, 3-5 km thick in the Keweenaw Peninsula, with minor interlayered felsic volcanic and sedimentary units (Davis and Paces, 1990). The Bergland Group bears about 1% rhyolite in the deep central grabens of the Midcontinent rift. Rift flanking zones, like those preserved as the Porcupine Volcanics and the North Shore Volcanic Group, show as much as 10-25% rhyolite (Cannon and Nicholson, 1992). Indeed, the Porcupine Volcanics, intersected by the sampling traverse of this study, are a rhyolite-andesite volcanic sequence.

#### *1.3.2.2 Oronto Group*

The transgressive-regressive sequence of the Oronto Group was deposited in three units atop the Bergland Group Volcanics as extrusive volcanism diminished (Elmore *et al.,* 1989). The Copper Harbor Formation, up to 2 km thick, shows intermittent, upward-decreasing, basalt flows of the Lakeshore Traps in its lower 1,000 m. Clast-supported conglomerate composes the lower part of the Copper Harbor Formation; clasts are dominantly volcanic, mainly sourced from Bergland Group rocks. The upper part of the Copper Harbor Formation is largely volcanic-derived sandstone with minor siltstone. This fining-upward and fining-basinward sequence records a prograding alluvial fan complex (Ojakangas *et al.,* 2001). Pauses in Copper Harbor Formation sedimentation are evidenced by the presence of rare stromatolitic beds, sometimes associated with calcite pseudomorphs after gypsum, as well as carbonate-filled syneresis or mud-desiccation shrinkage cracks (Elmore, 1984). Evaporite mineral pseudomorphs, the red color of the unit and shrinkage cracks may be interpreted as recording deposition in an arid or semi-arid environment. Formation water encountered in the Copper Harbor conglomeratic sandstones at White Pine Mine is an alkaline brine with a chloride and TDS content approximately twice that of seawater, a condition which partly satisfies the requisite Cu solubility for economic SSC deposition (Johnson, 2014, Ridley, 2013).

Red conglomeratic sandstone and dark-gray siltstone to shale are interbedded and interlaminated in the lowest 6 m of the Nonesuch Formation and the basal contact (atop the Copper Harbor Formation) is arbitrarily placed at the base of the lowest 1 m thick unit containing dark-gray siltstone and shale (cf. White, 1971). The Nonesuch Formation is a mostly fine-grained sequence of gray to black shale and siltstone with minor light gray sandstone. Cu-ore and petroleum seeps are found in the lowest 10 m of the Nonesuch Formation at the White Pine Mine (Ojakangas *et al.*, 2001). The lower portion of the Nonesuch Formation shows textures suggesting sedimentation of mud and silt from suspension in a low-energy, standing-water, depositional setting.  A transition from quiet-water to an increasingly fluvial-influenced depositional system is inferred from coarsening-upward sequences observed in the upper portion of the Nonesuch Formation (Imbus, 1988).

The fine-grained, often carbonaceous, sediment of the Nonesuch Formation and its association with continental red-bed alluvial fan and fluvial deposits, suggest a lacustrine environment of deposition.  Sedimentary structures observed by the author (Figure 5, cf. Suszek, 1997) recent Os isotope data (Cumming, 2012), rare but partially preserved anhydrite/gypsum nodules, and paleogeographic reconstructions suggesting that the nearest coastline was 800 km distant, further support lacustrine, non-marine, deposition (Ojakangas *et al.,* 2001; Elmore *et al.,* 1989).  However, marine embayment/estuarine environment of Nonesuch Formation deposition have also been suggested.  Evidence for marine deposition includes: 1) the presence of organic molecular fossils similar to those found in Phanerozoic oils of marine origin (Pratt *et al.,* 1991), 2) high total S content, S/C ratio and S isotope dispersion that is characteristic of syngenetic sulfides formed by reduction of seawater sulfate (Burnie *et al.,* 1972; Hieshima and Pratt, 1991), and 3) an intimate association of framboidal pyrite to OM in the Nonesuch Formation.

Figure 5: Straight to semi-arcuate infilled cracks 15 m stratigraphically above Nonesuch Formation base, Presque Isle River. Rock hammer head at right for scale.

The Freda Formation, up to 3600 m thick, shows stacked cyclic sequence packages of red-brown sandstone, siltstone, mudstone, and shale. Freda Formation depositional sequences are both fining-upward and coarsening-upward. The environment of deposition was a braided stream network; this system interfingers with, and ultimately overlaps the top of the Nonesuch Formation (Daniels, 1982).

### *1.3.3 Climate*

The samples in this study come from a present-day continental to semi-maritime climate. Lake Superior's proximity moderates air temperatures in the sample area and prevailing northerly winds provide for cold winters, cool summers, and regularly high humidity throughout the year (U.S. E.P.A., 1992). The mean annual temperature for the area is 40° F, with summertime highs in the low 80's and wintertime lows near 0° F, according to the National Oceanic and Atmospheric Administration. Annual precipitation by rainfall is 80 cm, and yearly snowfall regularly totals 450 cm (Michigan State University, 1998).

## *1.4 The Nonesuch Formation Sediment Hosted Stratiform Copper Deposits*

At White Pine Mine the Cu-bearing beds are mainly in the lower 7 m of the Nonesuch Formation. There, local usage describes four stratigraphic units, which are, in ascending order, the lower sandstone (the upper most Copper Harbor Formation conglomeratic sandstone bed), the parting shale, the upper sandstone, and the upper shale (White and Wright, 1955). The extent of individual Cu-bearing beds at White Pine is measurable in square miles (White and Wright, 1955). At White Pine Cu is present mainly in the upper and parting shales where mining nomenclature provides 12 distinct lithostratigraphic units through which five laterally extensive foci of greatest Cu enrichment (up to 3% Cu by weight) are recognized. An informal naming scheme has been developed for the lowermost Nonesuch Formation’s beds, to aid miners in distinguishing the ore zones (Figure 6, from White and Wright, 1955). Overall stratigraphy at White Pine Mine and the Copperwood deposit are depicted in Figures 7 and 8.

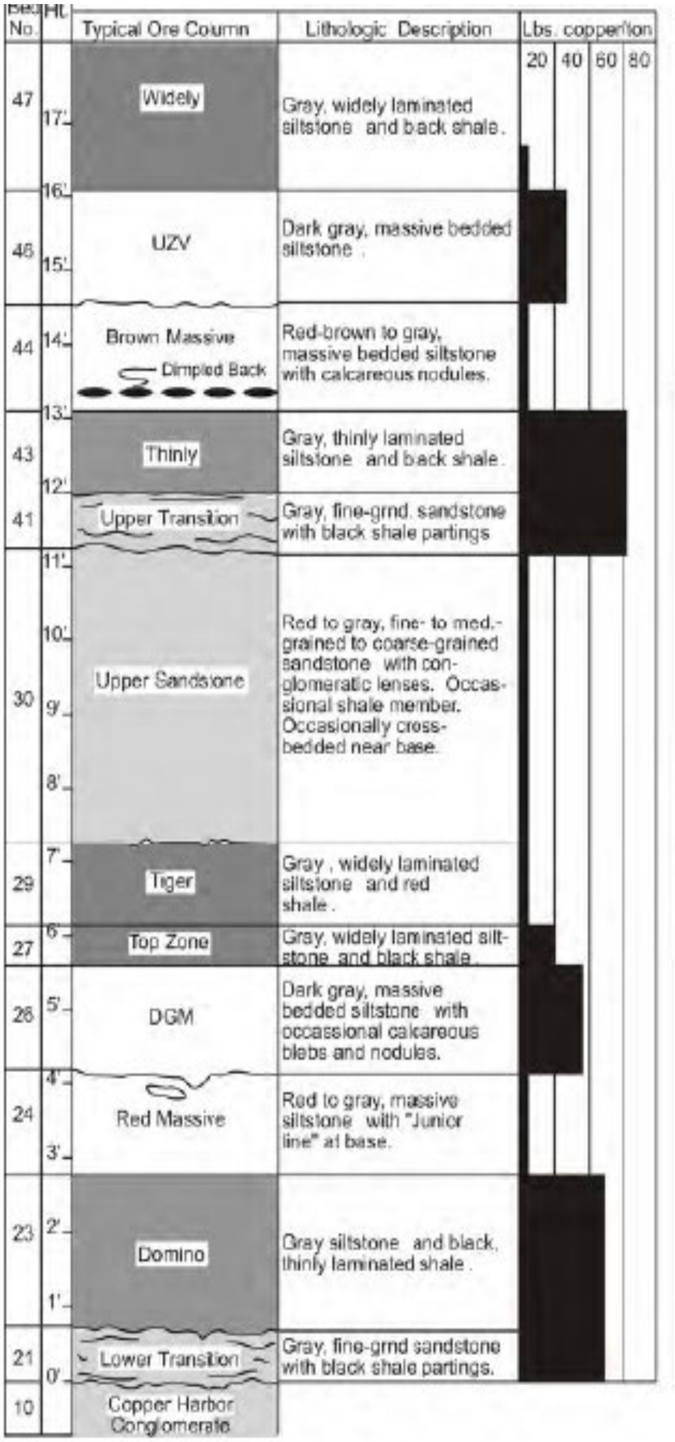

Figure 6: Mining nomenclature and typical thicknesses, ore grades of beds in the area of the White Pine Mine. From White and Wright, 1955.

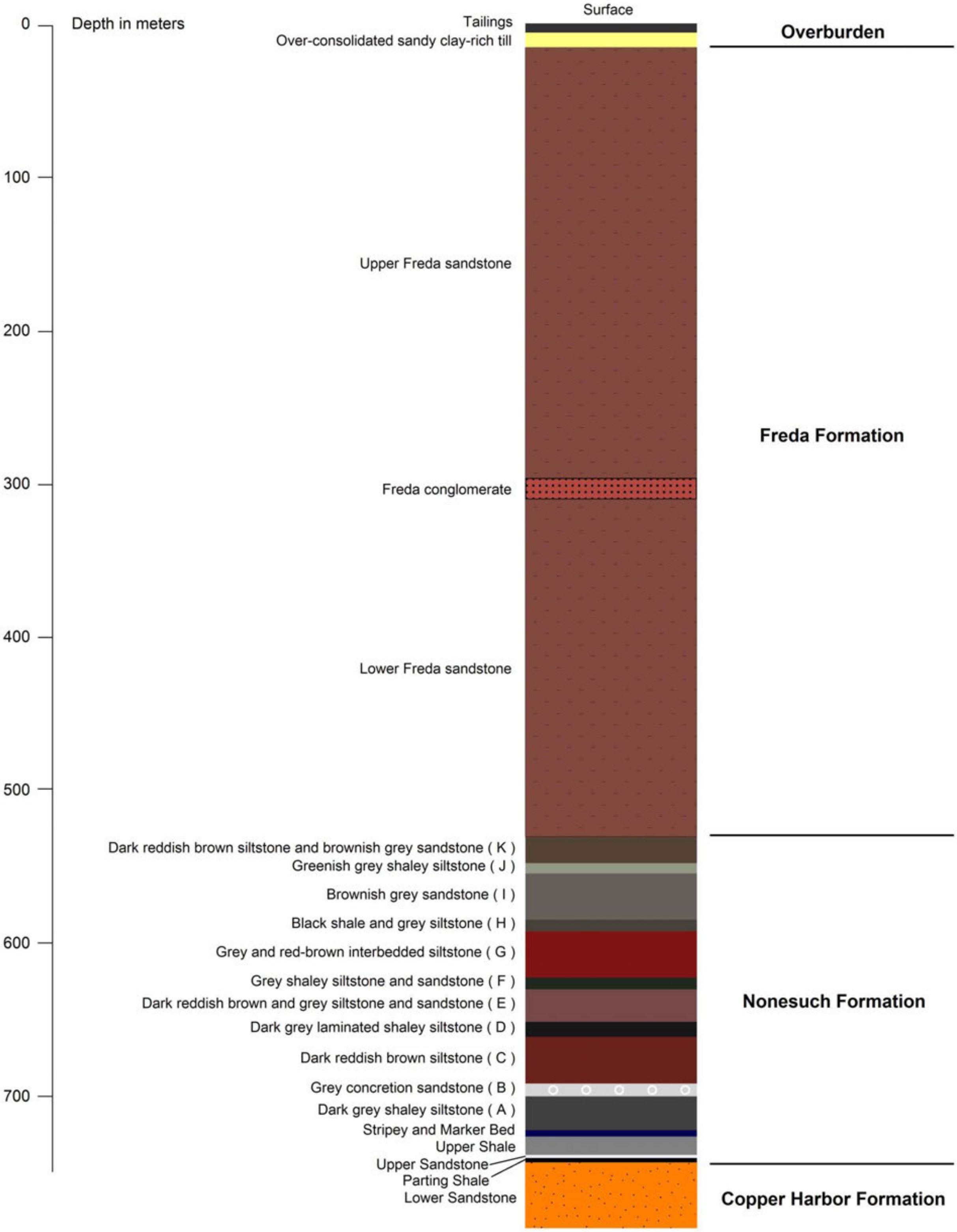

Figure 7: A general stratigraphic column at the White Pine Mine, from Sirois, 2015.

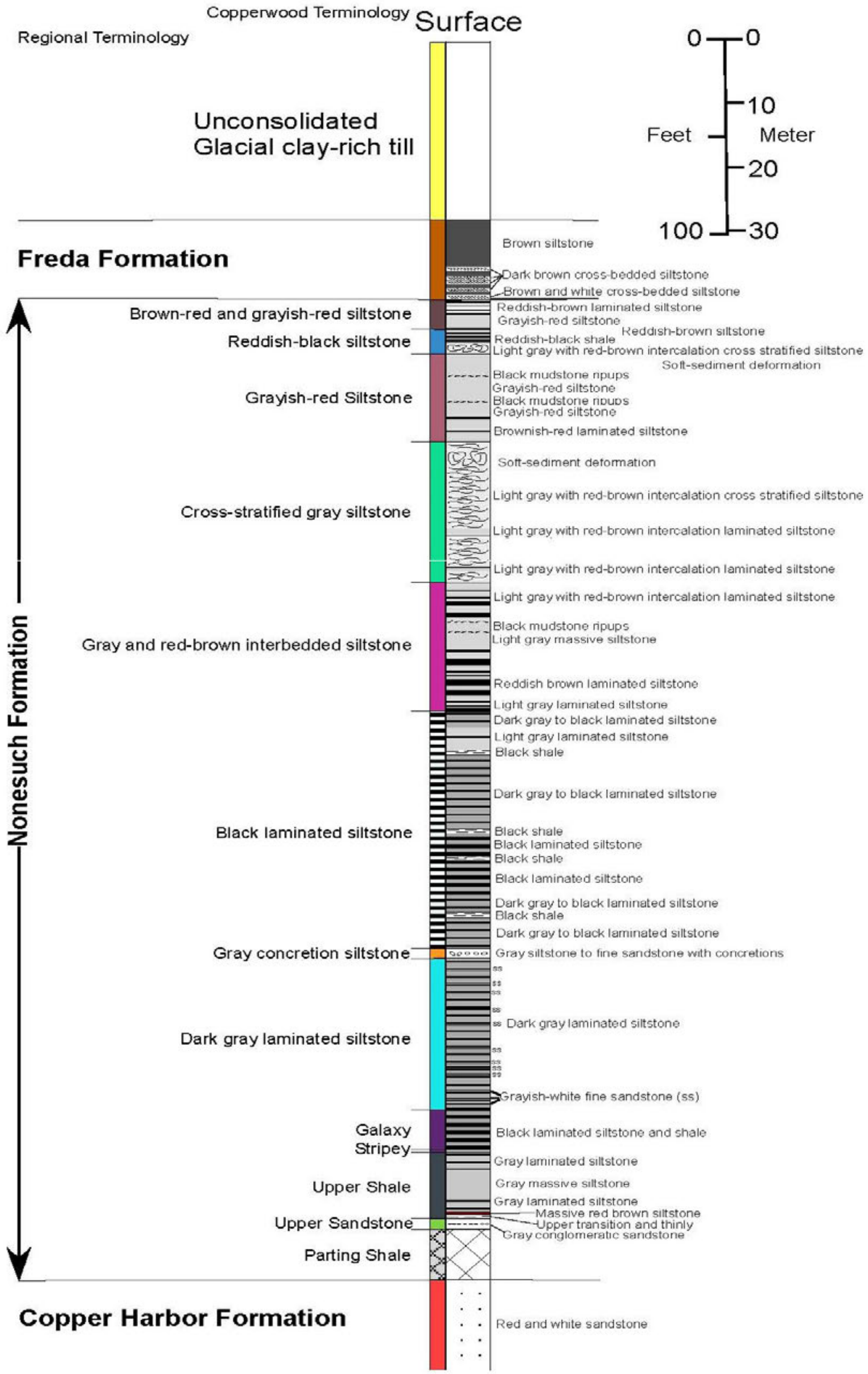

Figure 8: A generalized stratigraphic column at the Copperwood deposit, from Sirois, 2015.

Sediment hosted stratiform Cu deposits worldwide rank second only to porphyry Cu deposits in terms of Cu production (Robb, 2003). The Cu deposits of the Nonesuch Formation show many of the characteristic features of this deposit type. Recent economic Cu-focused studies of the Nonesuch Formation include those by Bornhorst and Williams (2013) Johnson (2014) and Sirois (2015). The thin but laterally extensive White Pine main stage cupriferous zone, localized in reduced carbonaceous horizons near to the boundary between reduced and oxidized sedimentary facies shows many hallmarks of the deposit type, especially the association with continental redbeds and evaporites (Brown and Chartrand, 1983). Total organic content (TOC) is generally less than 0.3% for the Nonesuch Formation in northern Michigan and Wisconsin, but select finely laminated calcareous and non-calcareous silty shales show TOC ranging from 0.25 to 2.8%, with an average of 0.6% (Imbus *et al.*, 1988; Hieshima *et al.*, 1989).

The lowest 15 m of the White Pine Nonesuch Formation can be divided into packages that display chemical and petrographic evidence of penetration by ascending fluids (Sutton *et al.*, 2013). Copper mineralization as sulfides is mainly restricted to the lowest 5 m, sometimes with modest enrichment of Ag, V, and Zn (Sutton *et al.*, 2013). This basal zone has the greatest abundance of vertical fracture fillings and vertically breached shale laminae (Sutton *et al.*, 2013). The next 5 m package is low in S, trace metals and Cu, although native Cu does occur. Greater S concentration, with modest increases in Cu, As, Cd, Mo, Pb, Sb, characterizes the third 5 m package (Sutton *et al.*, 2013). Content of $C_{org}$ varies according to the 5 m packages above; TOC is below 0.5% in the lowest 5 m package, below 0.2% in the second package and rises gradually above (Sutton *et al.*, 2013).

Three structural domains recording three deformation episodes and two stages of Cu mineralization are recognized at the White Pine Mine. Mauk *et al.* (1989) describe: 1) synsedimentary extensional growth faults; 2) a set of NE-SW trending high angle normal faults crosscutting (post-dating) main-stage mineralization, and; 3) S-dipping thrust faults accompanying second stage Cu mineralization. The first Cu mineralization stage is the early diagenetic SSC event, the "main stage" of White Pine ore emplacement (e.g. White and Wright, 1955). The distinct second stage Cu mineralization accompanied thrusting and introduced mainly native Cu focused in calcite-rich veins, especially in the southwestern portion of the mine (Ruiz *et al.*, 1984). Ho and Mauk (1996) instead reported second-stage mineralization as dominantly chalcocitic, concluding that it resulted from reduction of sulfate introduced as a component of the mineralizing fluids.

Similar to other SSCs, ore is found mainly as very fine-grained disseminated Cu sulfides (White and Wright, 1966). Native Cu, silver and silver sulfides (e.g. acanthite) are also important ore minerals (Johnson, 2014). As at other deposits of this type, White Pine and Copperwood sulfide minerals (and metals) show lateral and vertical zonation, although the Nonesuch Formation deposit ores are dominantly chalcocitic (Brown, 1978). The general main stage sulfide zonation is: barren (no sulfide, often with hematite) => native Cu => chalcocite => bornite => chalcopyrite => galena => sphalerite => greenockite => pyrite (Brown, 1978). This zonation progresses upward through the Nonesuch Formation as well as inward from the paleo-margin of the basin (Brown, 1978).

The geometry and textural relations of sulfide minerals of the transition between the cupriferous and pyritic zones (the fringe surface) are important to genetic explanation (Seasor and Brown, 1989). The top of the cupriferous zone is independent of lateral facies changes and transgresses bedding (Brown, 1971). Significantly, the fringe surface is stratigraphically lower where greater amounts of introduced Cu were precipitated in the basal Nonesuch Formation beds

(Misra, 2000). Sulfide minerals at the fringe show textures interpreted to reflect a systematic step-by-step replacement of fine-grained diagenetic pyrite by chalcopyrite, bornite, digenite, and, finally, chalcocite (White, 1960). Most workers now accept a post-sedimentary, syndiagenetic ore emplacement model (Robb, 2003). Ore fluids are thought to have evolved by interaction with Cu-substituted minerals (e.g., hematite, magnetite, biotite, hornblende and pyroxene) in the clastic, oxidized sedimentary sequence of the Copper Harbor Formation (Brown, 2009). These fluids are likely to have been characterized by low temperatures (under 130°C), a near-neutral pH (6-7.5), moderate salinity (up to 20 wt% NaCl equivalent), and oxidized conditions (Robb, 2003). Such conditions, would favor Cu transport as cuprous chloride complexes with aqueous S species as dominantly sulfate ions (Rose, 1976). See Figures 9 and 10. Ore fluids encountering the reducing environment of the Nonesuch Formation then precipitated metals by three mechanisms: 1) deposition of native Cu; 2) conversion of precursor pyrite to chalcocite, and; 3) deposition of chalcocite with Cu and S derived entirely from the fluid phase (likely by thermochemical sulfate reduction; Ho and Mauk, 1996). These mechanisms explain ore mineral replacement textures, geometry and relation of the fringe surface to ore concentrations, and vertical mineral zoning with the most soluble sulfide minerals (galena, sphalerite, greenockite) farthest along the path of the upward circulating fluids (Brown, 1978; Seasor and Brown, 1989). All three mechanisms require a reducing agent external to the ascending ore fluid.

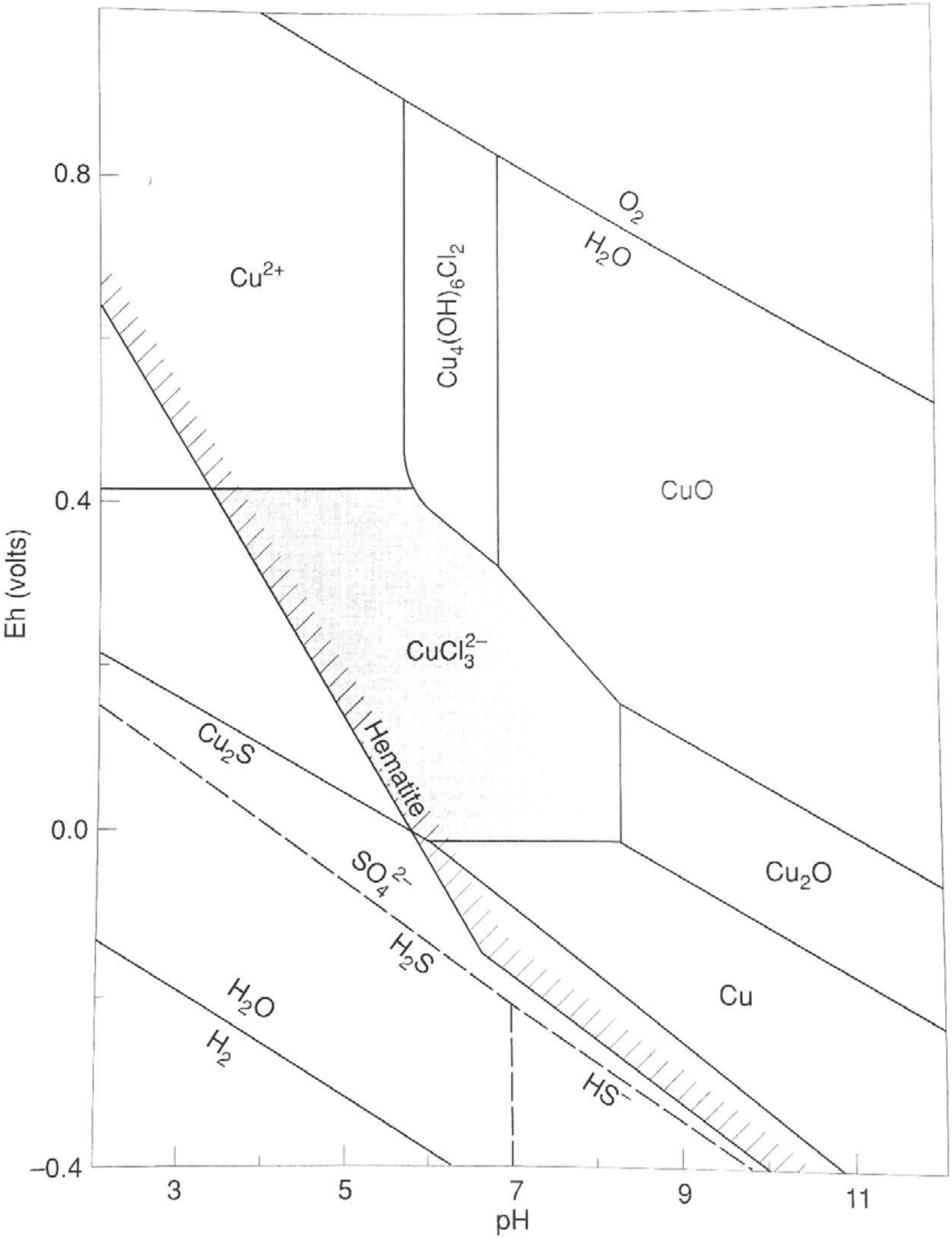

Figure 9: Pourbaix (Eh-pH) plot for the system Cu-O-H-S-Cl at 25°C (with $\Sigma S = 10^{-4}$ m and $Cl^- = 0.5$ m). Illustrated fields show the range of stability for hematite, various S species and the cuprous-chloride complex for conditions most likely compatible with the formation of SSC deposits (Robb, 2003). The brine ascending through the Copper Harbor Formation is thought to have had Eh-pH conditions in the zone of stability for cuprous chloride complexes (at center, $CuCl_3^{2-}$). Copper became unstable in solution after mixing of brine with reductive fluids in the lower Nonesuch Formation, precipitating chalcocite and other ore minerals.

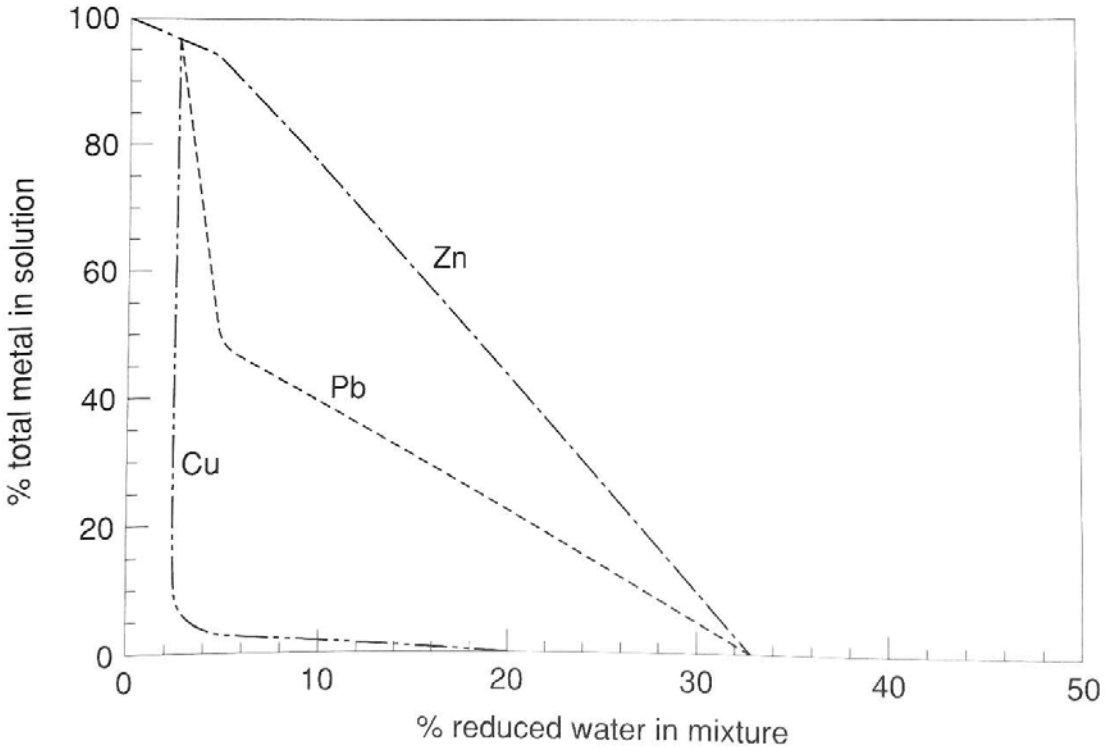

Figure 10: Model showing the effects of mixing a typical SSC-type ore fluid with a reduced fluid on metal precipitation. The sequence of deposition is the same as the zonation of metals observed in at White Pine and in the Kupferschiefer (Robb, 2003).

Ho and Mauk (1996) used differences in S isotope signatures to conclude that S enrichment in the Nonesuch Formation might have occurred by hydrothermal activity. If chalcocite formation occurred by reduction of sulfate in the ore fluids, this would result in net S addition to the sediments as well as increased S to C ratios in mineralized versus unmineralized samples (Ho and Mauk, 1996). Indeed, molar S/C ratios show trends associated with Cu deposition in the lower Nonesuch Formation at White Pine, especially in areas affected by second-stage mineralization (Mauk and Hieshima, 1992).

### *1.5 Organic Geochemical Background*

Organic matter (OM) refers to material formed by living organisms and containing C-C bonds. Given suitable conditions, OM accumulates and is preserved in the rock record; diagenetic, catagenetic, and metagenetic evolution of OM occurs with increasing degrees and durations of burial and heating. Bitumen (organic matter soluble in organic solvents), kerogen (the organic-insoluble portion of OM in sedimentary rocks), pyrobitumen (infusible and insoluble bitumen), and petroleum form by burial, diagenesis and catagenesis of primary OM. See Figures 11 through 15. Tissot and Welte (1976), Hunt (1995), among others, cover these processes in detail.

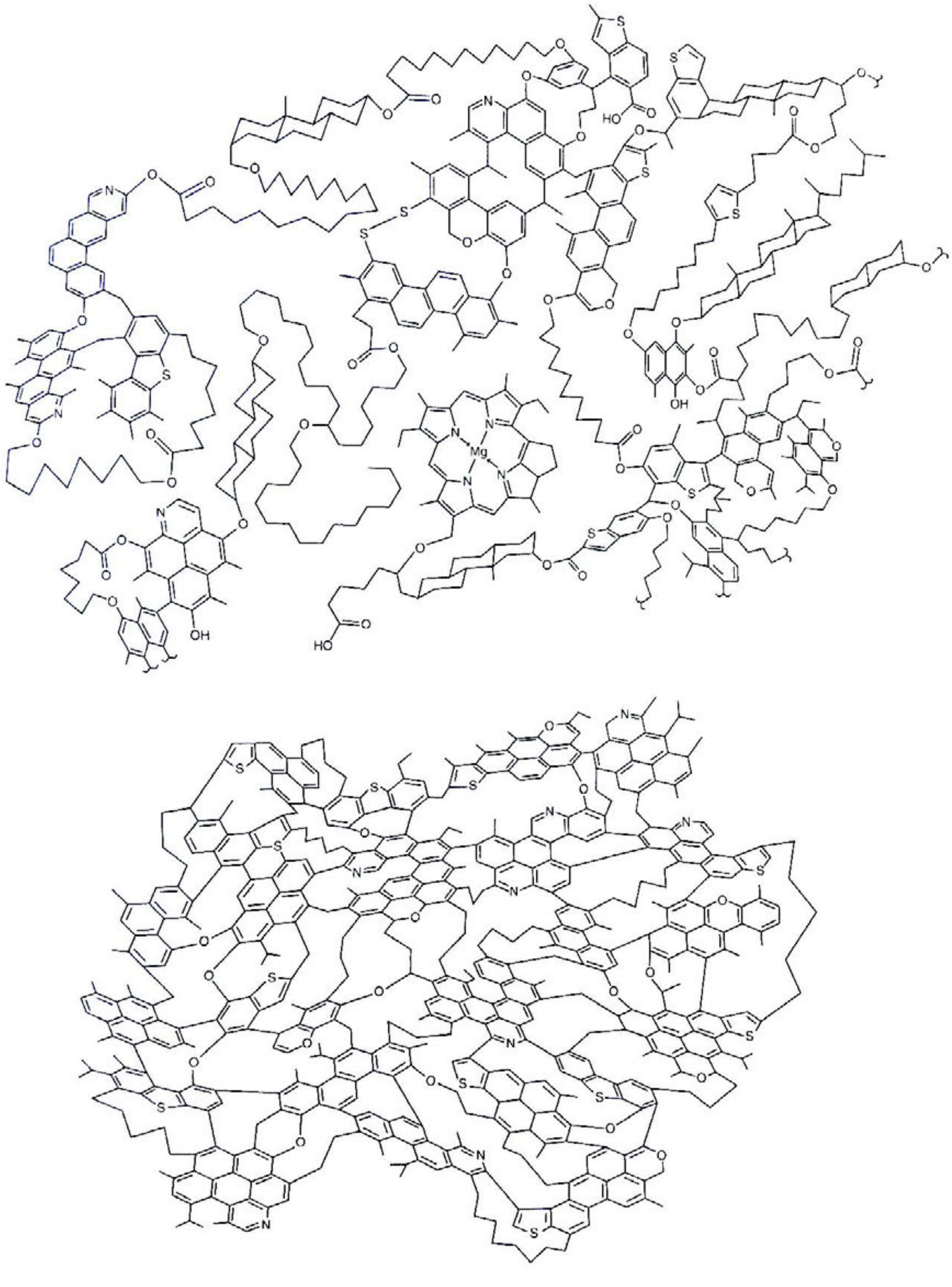

Figure 11: Schematic structural characteristics of Type II kerogen: a) at the end of diagenesis (atomic H/C = 1.25, O/C = 0.09); and b) at the end of catagenesis (H/C = 0.73, O/C = 0.03). Kerogen and bitumen each increase in aromaticity with increasing thermal maturity, especially above artificial levels $R_o$ greater than 0.9% (Craddock et al., 2015). This similarity likely results from loss of aliphatic chains from both organic fractions during petroleum generation. Killops and Killops, 2005.

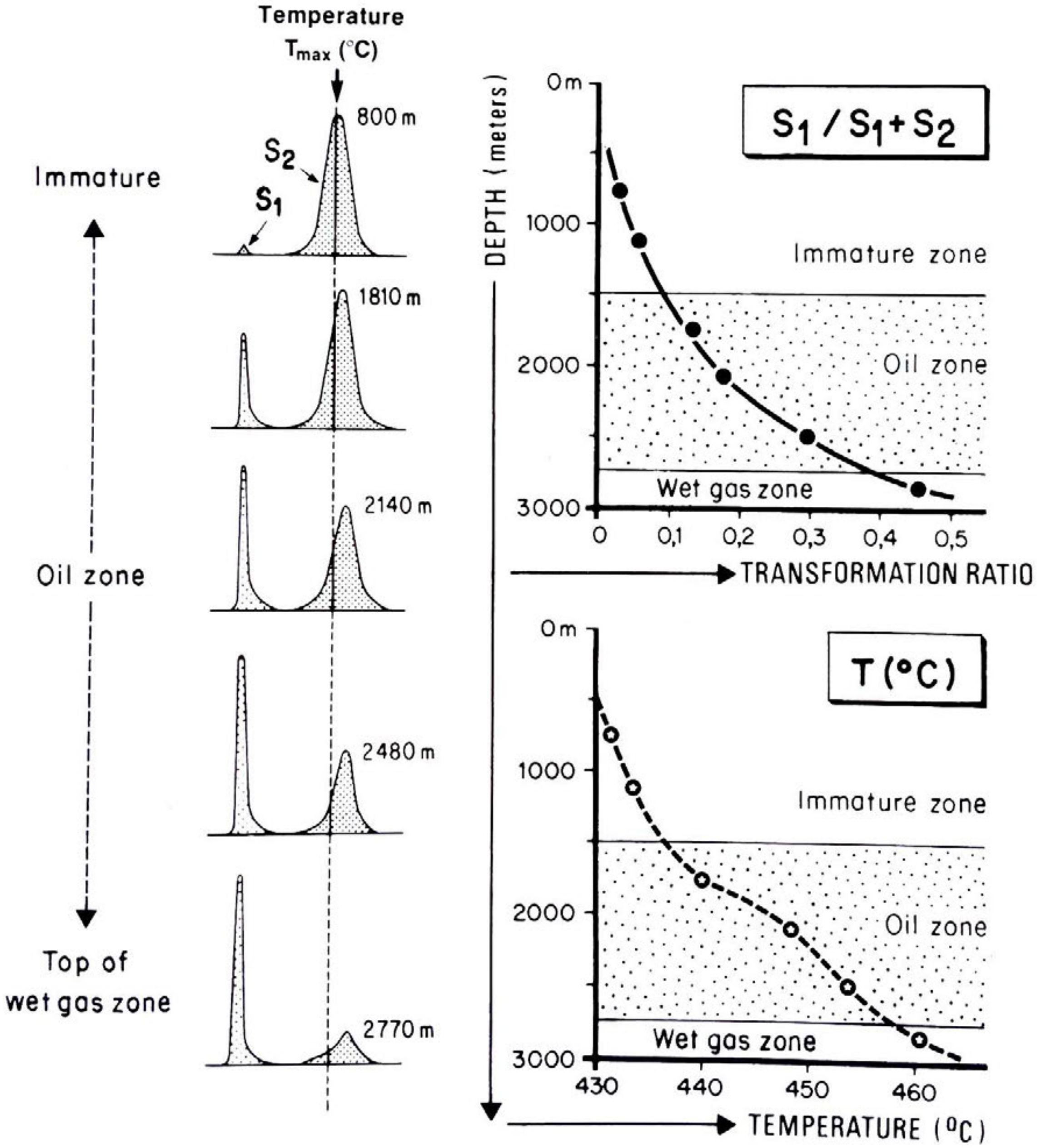

Figure 12: Maturation trends by Rock-Eval pyrolysis are generally predictable: increasing maturity coincides with increasing $S_1$ and $T_{max}$ but decreasing $S_2$ values. From Tissot and Welte, 1984.

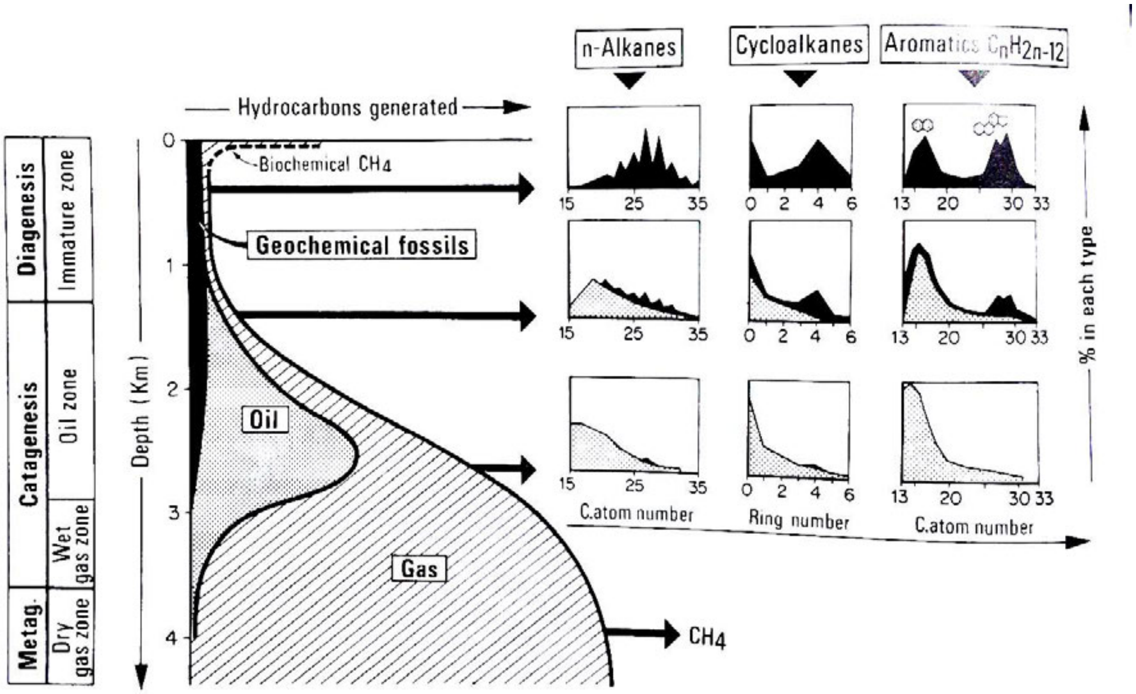

Figure 13: Schematic HC formation as function of source rock burial. The evolution of the HC composition is shown in insets for three structural types. Depths are illustrative only and correspond to an average for Mesozoic and Paleozoic rocks. Other actors exerting significant influence include: kerogen type, burial history, and geothermal gradient. From Taylor *et al*., 1998.

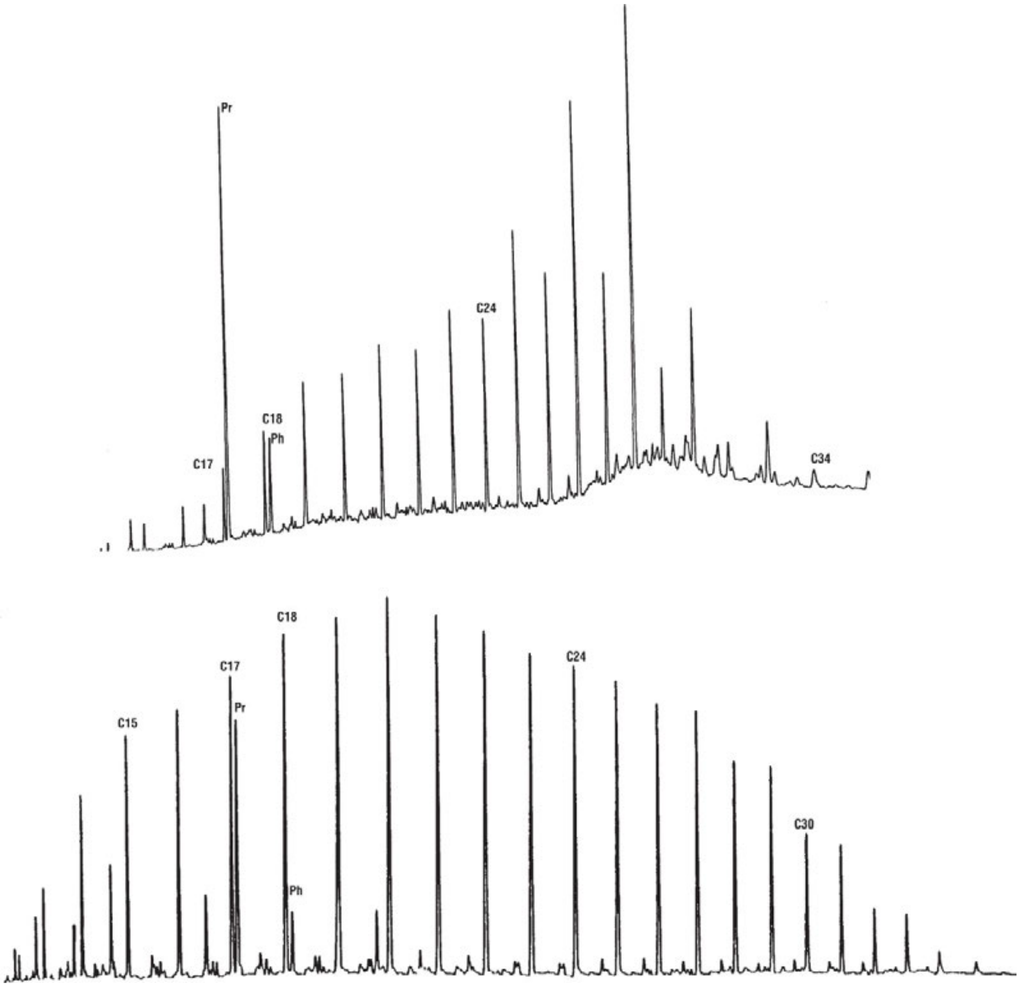

Figure 14: Gas chromatograms of saturated HCs from an immature extract of coaly organic matter (top) and from an oil believed to have been sourced from a similar facies (bottom). Both show many of the same characteristics - high wax content, odd $C_n$ preference in the wax range, high pristane/phytane ratio - but maturity effects have altered many of the details. (Waples and Curiale, 1999).

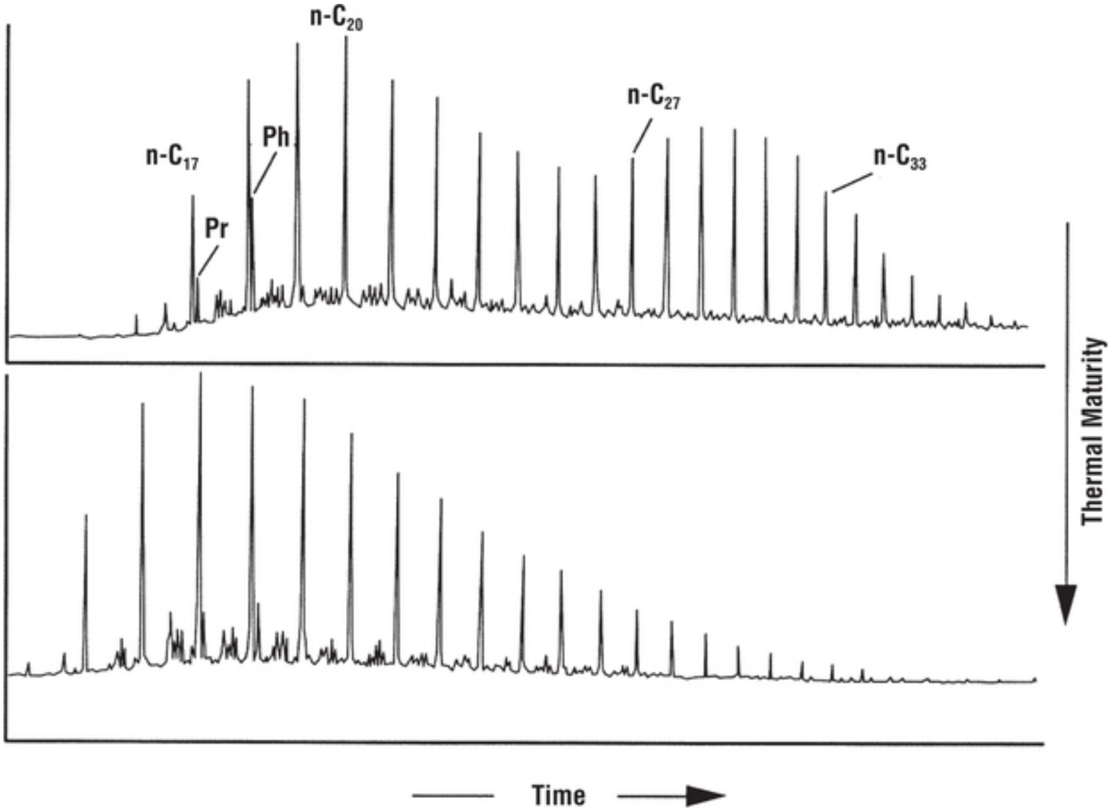

Figure 15: Gas chromatograms of two oils from Wyoming. Both were sourced from the Permian Phosphoria Formation but are hosted in different strata. The bimodal distribution of *n*-alkanes in the top oil is consistent with a lower thermal maturity than that of the unimodal *n*-alkane distribution of the oil at the bottom. (Waples and Curiale, 1999).

### *1.5.1 Kerogen Classification*

The nature of precursor OM determines the kerogen type produced in early diagenesis. See Figure 16. Kerogen is typified by ratios of contained $C_{org}$, H, and O, commonly on van Krevelen diagrams, as in Figure 17. Organic petrologists refer to distinctive kerogen types, which they subdivide based on their chemical composition, inferred origins and appearance (Tissot and Welte, 1984). See Table 1.

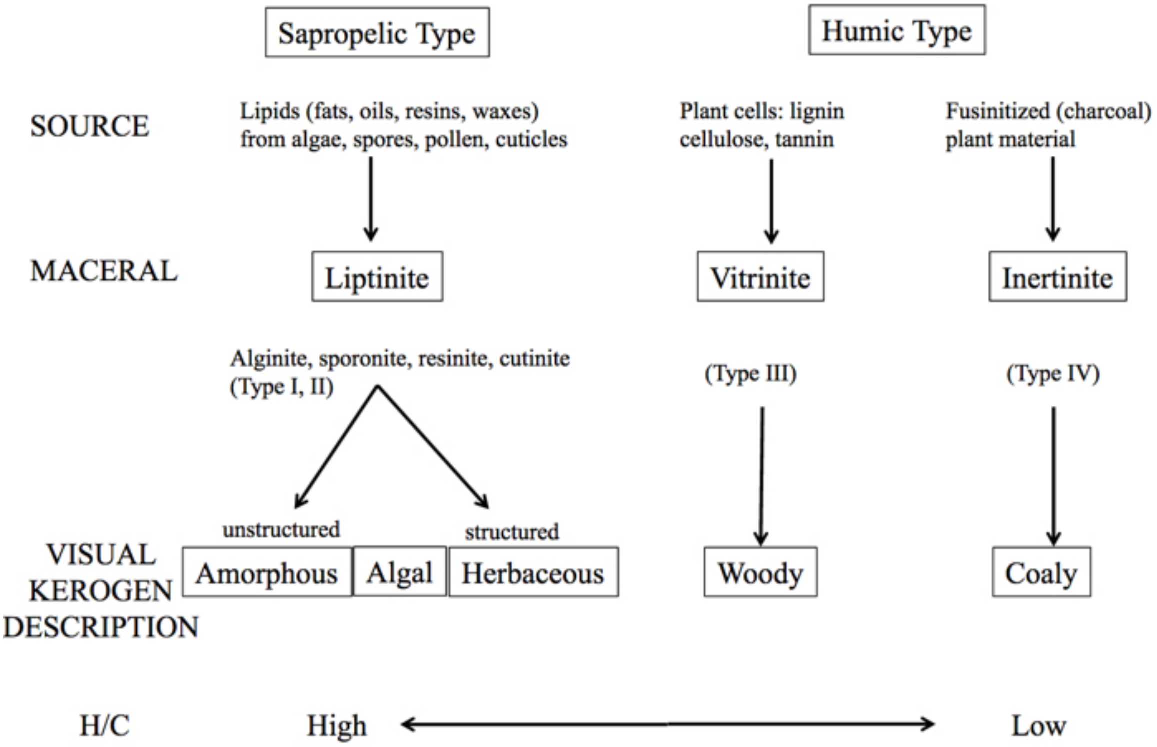

Figure 16: The nature of the primary organic matter determines the kerogen type formed during diagenesis. From McCarthy *et al*., 2011.

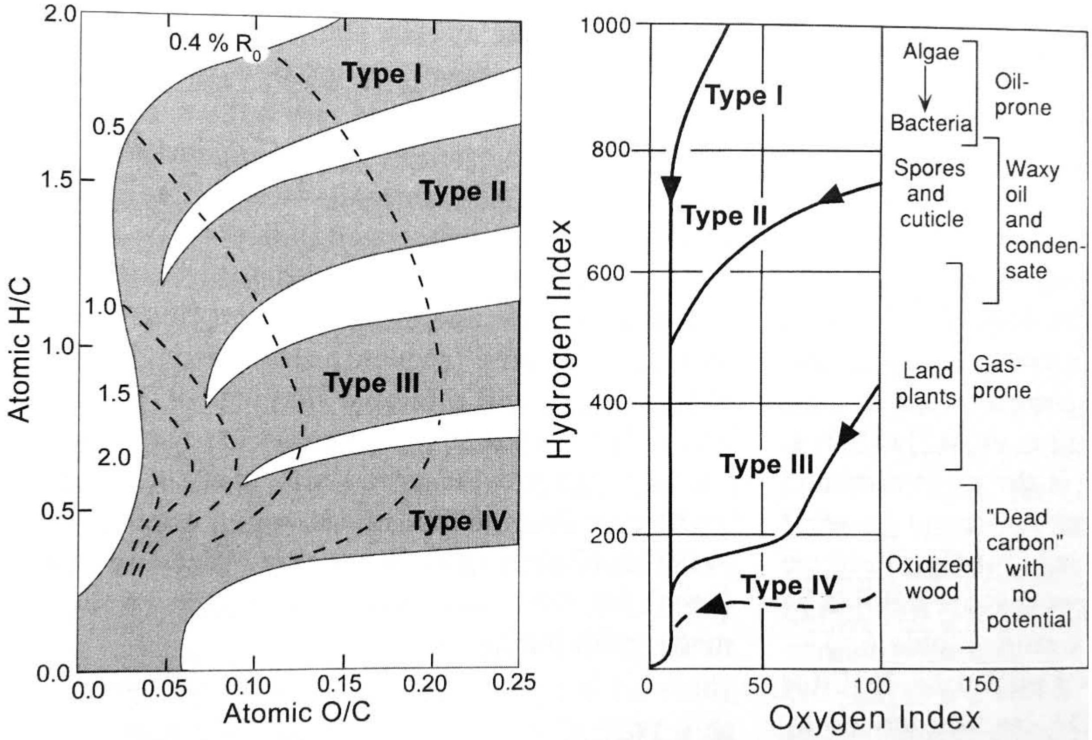

Figure 17: Kerogen types and maturation paths, defined by atomic H/C and O/C ratios (van Krevelen diagram) and also by hydrogen and oxygen indices (Modified van Krevelen diagram). Potter *et al*., 2005.

Table 1: Types of kerogen, as classified by van Krevelen diagram, with respective matter source/nature. Potter *et al.*, 2005.

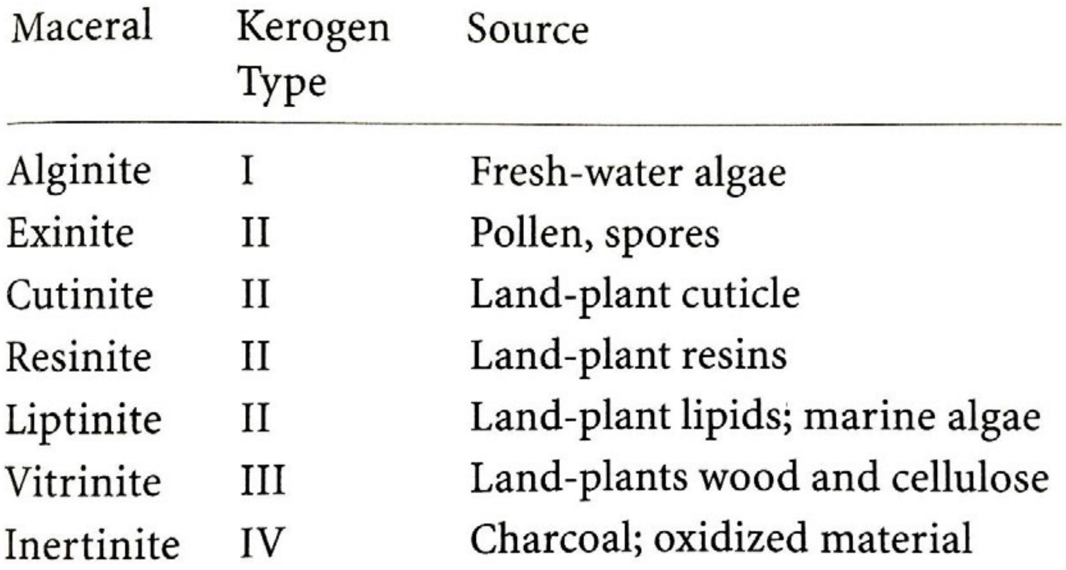

| Maceral | Kerogen Type | Source |
|---|---|---|
| Alginite | I | Fresh-water algae |
| Exinite | II | Pollen, spores |
| Cutinite | II | Land-plant cuticle |
| Resinite | II | Land-plant resins |
| Liptinite | II | Land-plant lipids; marine algae |
| Vitrinite | III | Land-plants wood and cellulose |
| Inertinite | IV | Charcoal; oxidized material |

The distribution of components in parent kerogens influences the HCs generated at the peak of oil formation; see Figure 18**.** Type I kerogens consist mainly of algal and amorphous kerogen, and are prone to oil generation. Type II kerogens are derived from mixed terrestrial and marine material; waxy oil is the dominant economic product of Type II kerogen maturation. Woody, terrestrial material most prone to gas generation upon maturation comprises Type III kerogen. Type IV kerogen is derived from residual organic matter found in sediments that have been reworked after erosion. Type IV kerogen may have experienced alteration by subaerial weathering, combustion or biologic oxidation prior to ultimate burial and is considered dead or inert C due to its relatively H-poor chemistry; there is no potential to generate HCs in these inertinites (Hunt, 1995). Kerogens of the first three types are indistinguishable from Type IV inertinites at very high maturities using only Rock-Eval pyrolysis (Tissot and Welte, 1984).

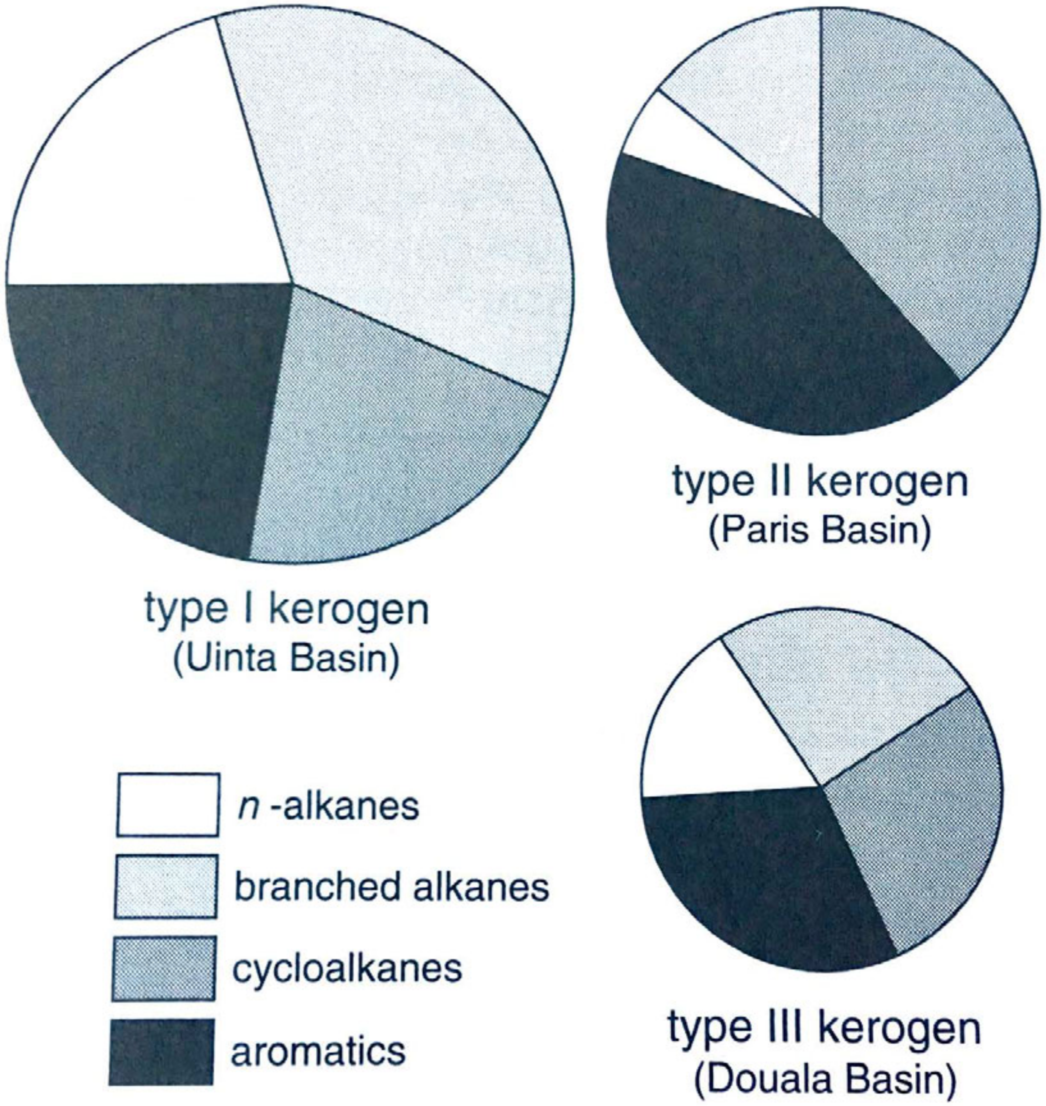

Figure 18: Distribution of HCs generated from samples representing different kerogen types at the peak of oil formation. Areas are proportional to amount of HCs per unit mass of $C_{org}$. From Killops and Killops, 2005.

The biota from which kerogen is derived are constructed from a relatively few simple molecular components that are mostly unchanged over geologic time (Hunt, 1995). Carbohydrates, proteins, lipids, resins, pigments, and other classes of organic building blocks are the structures of life and metabolic systems. Flora and fauna contain differing proportions of the major constituents that produce unique chemical signatures - biochemical fossils or biomarkers. Together, these factors lead to production of different, distinct kerogen types and a broad array of biochemical fossils.  These biomarkers can be isolated from whole rocks (as bituminous extracts and kerogen pyrolyzates) and also from crude oils.  Bituminous extracts (rock extracts) are obtained by organic solvent extraction of 5 grams of sample pulp (finely ground rock) placed in a cellulose thimble and extracted with dichloromethane using Soxhlet apparatus (Bjorlykke, 2013).  The ratios and distributions of such biomarkers (and, to some extent, those of HCs generally) are utilized to interpret the provenance, the depositional and thermal history of preserved OM (cf. Peters *et al.,* 2005; Engel and Macko, 1987; Killops and Killops, 2005).  This is depicted in Figure 19.

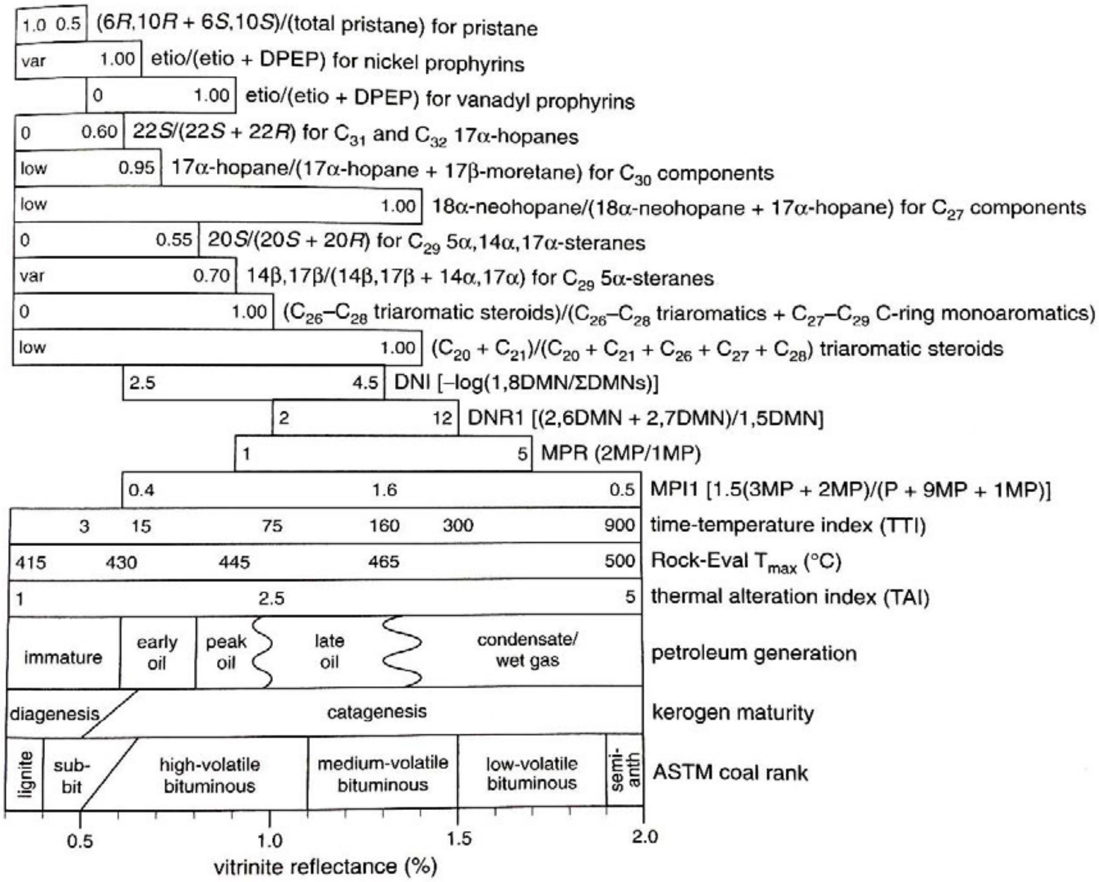

Figure 19: Approximate correlation of various maturity parameters with stages of petroleum generation.  Killops and Killops, 2005.

### *1.6 Organic Geochemistry with Specific Reference to Precambrian Organic Matter*

Organic matter preserved in Precambrian rocks is unique in that it has persisted despite its vast period of existence in crustal rocks vulnerable to tectonic recycling and significant stresses related to high pressures and temperatures. Such ancient OM is also unique in that it was generated in differing biotic and ecosystemic regimes, leading to distinct chemical differences from more recently generated OM.

The mean TOCs of Precambrian sedimentary rocks are lower than those of comparable Phanerozoic lithofacies, probably reflecting lower primary productivity/biomass generation, as well as metagenetic C loss and erosion of many representative Precambrian environments (Engel and Macko, 1993). The UCLA Precambrian Paleobiology Group showed 67% of their 315 samples as below 0.5% TOC, 17% of their samples as between 0.5 and 1.0% TOC, 14% of their samples with TOC between 1 and 5% TOC, and 2% of samples with TOC greater than 5% (Hayes *et al.,* 1983). Reimer *et al.* (1979) reported Early Archean sediments of the South African Swaziland Sequence with an average of 0.43% TOC. This is similar to the mean TOC finding of 0.38% by Imbus *et al.* (1988) for the Nonesuch Formation. Precambrian kerogens display as much chemical variability as kerogens in the Phanerozoic record (McKirdy and Hahn, 1982).

Precambrian Type I kerogen, H-rich, presents petrologically as thin films of lamellar alginite and also as discrete ellipsoid or disc-shaped algal bodies (McKirdy and Kanstler, 1980). Type I organic morphologies are derived from bloom or mat-forming cyanobacteria, partially reworked by anaerobic bacteria, thus incorporating lipid-rich bacterial cells (McKirdy *et al.,* 1980). The inferred depositional environments for this material are: 1) evaporitic, alkaline playa-lacustrine facies similar to those of the Observatory Hill Beds, Officer Basin, S. Australia (atomic H/C = 1.19-1.37 with atomic O/C = 0.05-0.1), and 2) marine phosphorites of the

Ordovician Beetle Creek Formation, Georgina Basin, Queensland, Australia (atomic H/C = 1.13 with O/C = 0.05-0.1), and the similar Lesser Karatau deposit, Former USSR (atomic H/C = 0.53), and the Areyonga Formation, Amadeus Basin, N. Territory, Australia (atomic H/C = 0.53 and O/C = 0.05-0.2; Powell *et al.,* 1975). The latter two lower H/C values reflect their higher degree of thermal alteration due to deeper burial (McKirdy and Hahn, 1982). Precambrian Type I kerogen generally presents a pyrolysis-hydrogenation-gas chromatography (PH-GC) pyrogram in which *n*-alkanes up to $C_{25}$ or higher are dominant; simple aromatics (benzene, toluene, etc.) occur in very low concentrations relative to aliphatic moieties of equivalent $C_n$, though this is dependent upon kerogen rank (McKirdy and Hahn, 1982). Likely precursors of this highly aliphatic OM include lipid-rich planktonic chlorophytes, or bacterial/microbial mats (McKirdy *et al.,* 1980).

Precambrian Type II kerogen, such as that of the 1.45 Ga McMinn Formation, McArthur Basin, N. Territory, Australia occupy an intermediate position on a van Krevelen plot (H/C = 0.5-0.9 and O/C = 0.07-0.2, at low levels of maturity/oxidation; Peat *et al.,* 1978). This material can be a mixture of Type I and III kerogens, but has also been described as a derivative of acritarchs, bacterial lipids, or amorphous sapropelized algal/protozoan remains (McKirdy and Hahn, 1982). It may be in some part a derivative of sporopollenin, a chemically resistant biopolymer in the cell walls of certain algae (Brooks and Shaw, 1972). It presents petrologically mainly as lamalginite although some reports indicate the presence of amorphous algal or protozoan remains and some acritarchs (Engel and Macko, 1993). This material differs little in PH-GC pyrograms from Precambrian Type I OM but it is significantly more naphthenic. The maturation of such Precambrian Type II OM occurs by progressive shortening of aliphatic chains and a loss of alkyl groups, as well as generally increasing aromatization of alicyclic rings

(McKirdy and Hahn, 1982). Such Precambrian Type II OM has been isolated from bituminous shales and carbonates of the 0.8 Ga Bitter Springs Formation, Amadeus Basin, Australia (atomic H/C = 0.80-0.85) and from several units within the 1.6-1.7 Ga McArthur Group, McArthur Basin, Australia (atomic H/C = 0.75-0.92; Saxby, 1976). Among the Precambrian sequences known to contain kerogens that have not matured well past the peak oil window (Rock-Eval $T_{max}$ below 450°C) are a number of units generally of a similar composition (H/C = 0.70-1.66 and HI = 150-740; Engel and Macko, 1993). This group contains kerogen of Type I and Type II.

Oxygen-rich, H-poor kerogen (Type III or Type IV) is preserved in very low concentrations in certain Proterozoic and also Paleozoic stromatolitic carbonates and cherts (atomic H/C 0.5-0.8 with O/C = 0.05-0.4, and atomic H/C = 0.4-0.6 with O/C = 0.1-0.4, respectively) presuming minimal maturation/oxidation (McKirdy, 1976). Such kerogen of this age is likely derived from cyanobacterial mucillage and from algal and bacterial pectic tissue (McKirdy *et al.,* 1980). Type IV kerogen presumably underwent partial oxidation during early diagenesis (McKirdy and Hahn, 1982). The saturated portion of these and other humic Precambrian kerogens often shows an odd $C_n$ preference in the $C_{10}$+ range, possibly reflecting derivation from bacterial cell-wall lipids (McKirdy *et al.*, 1980). A distinct group of Precambrian Type II/III (H/C = 0.90-1.17 and HI = 100-484) kerogens have been reported (Engel and Macko, 1993). Significantly, at least one member of this latter group is thought to have undergone bacterial degradation (sapropelization) of the primary algal biota, and possibly partial oxidation *prior* to compaction and lithification, which may explain the trend towards Type III kerogen (Crick *et al.,* 1988). See Table 3.

Table 3: Origins, chemical characteristics, typical associated depositional environments, and Cambrian and Precambrian examples of kerogen. Engel and Macko, 1993.

| Kerogen type | Source | Chemical characterization | Depositional environment | Precambrian and Cambrian examples |
|---|---|---|---|---|
| I | Lipid-rich chlorophytes and cyanophytes (eg: *Tasmanites, Gloecapsomorpha)* Bloom and mat-forming cyanophytes; acritarchs; archaebacteria | Hydrogen-rich (alginite coalification track), *n*-alkanes up to $C_{25}$ dominate pyrolyzate; simple aromatic hydrocarbons (benzene, toluene, ethylbenzene, and the xylenes) occur in very low concentrations relative to aliphatic moieties of similar carbon numbers | Reported from Ordovician and older rocks for which anoxic lacustrine or marine environments may be inferred | Beetle Crk Fm., Geogina Basin, Queensland (phosphorite restricted marine shelf); Observatory Hill Fm., Officer Basin, S. Australia (Cambrian dolomitic argillaceous mudstone; alkaline playa lake, evaporitic) |
| II | Partially degraded (sapropelized) algae and zooplankton; bacterial lipids; acritarchs | Intermediate coalification track, complex chemical composition; pyrolysates differ little in aromaticity from Type I kerogen but are considerably more naphthenic; *n*-alkyl chains prominent but shorter and present in lower concentration relative to branched and cyclic alkyl moieties | Various anoxic to suboxic environments, including lacustrine and marine sabkha to outer shelf | Ouldburra Fm., Officer Basin, S. Australia (micritic carbonate; shallow marine to evaporitic); McMinn Fm., McArthur Basin, N. Terr., Australia (shale and siltstone; outer marine shelf); Velkerri Fm., McArthur Basin (pyritic mudstone and siltstone) |
| III | Geochemically gellified algal humic acids incorporating some bacterial lipids. | Oxygen-rich, hydrogen-poor; pyrolysate commonly displays an odd-carbon-number predominance in the $C_{10+}$ range which may be a biomarker for bacterial cell wall lipids; simple aromatic hydrocarbons prominent relative to short-chain *n*-alkyl moieties | Suboxic, shallow to deep marine | Pertatatak Fm., Amadeus Basin, N. Terr., Australia (shale and siltstone; outer marine shelf); Bitter Springs Fm., Amadeus Basin, N. Terr., Australia (dolomite, partly anhydritic; shallow marine to evaporitic) |
| IV | Partially oxidized algal cellulose and sheath mucillage; bacterial pectic tissue | As above, but with lower pyrolyzate yield | Oxic, shallow marine. Typically found in very low concentrations in certain late Proterozoic stromatolitic carbonates and cherts for which an inter- to supra-tidal environment may be inferred | Wilkawillina Limestone, Arrowie Basin, S. Australia (stromatolitic limestone); Wonoka Fm., Adelaide Geosyncline, S. Australia (stromatolitic limestone) |

The saturate fraction of typical Precambrian extracted OM generally presents a classic "marine signature;" that is, a prevalence of $C_{12}$ to $C_{20}$ *n*-alkanes, often with predominantly odd over even $C_n$ homologs in the vicinity of *n*-$C_{15}$ and *n*-$C_{17}$ (Tissot and Welte, 1984). This *n*-alkane signature is thought to result from the decarboxylation of the corresponding normal fatty acids (especially *n*-$C_{16}$ and *n*-$C_{18}$ homologs) which are important lipid constituents of planktonic and benthic organisms (Engel and Macko, 1993).

Branched alkane species increase in abundance in oils with increasing geologic age (Hoering, 1981). Both *iso*- and *anteiso*-alkanes (2- and 3-methyl-substituted, respectively) are common components of most Precambrian oils and extracts (Engel and Macko, 1993). Monomethyl alkanes such as the 4-, 5-, and 6-methyl-substituted alkanes and the midchain methyl-substituted isomers - so-called "X compounds," first reported in Omani oils by Klomp (1980) - are found in unusual abundances in Precambrian oils and extracts. These singly branched alkanes, among the most distinctive compounds found in Precambrian-sourced hydrocarbons, and are widely believed to form by rearrangements and cracking of C skeletons during long periods of kerogen maturation (Engel and Macko, 1993). Summons *et al.* (1988) posited a bacterial origin to the midchain methyl-substituted alkanes found exclusively in Precambrian and Early Paleozoic oils and extracts, whereas later workers ascribe them to cyanobacterial input (George *et al.,* 2008).

A broad selection of isoprenoid HCs have been reported from Precambrian oils and extracts. The $C_{12}$ to $C_{20}$ regular (head-to-tail linked) isoprenoid alkanes are the most commonly reported isoprenoid compounds (Engel and Macko, 1993).

Steranes (tetracyclic compounds derived from steroids and sterols via diagenetic and catagenetic degradation and saturation) in Precambrian oils and sediments provide definitive evidence of eukaryotic inputs to their precursor OM, and to their thermal maturity. The presence of steranes in the 1.7 Ga Barney Creek Formation of the McArthur Basin provides evidence for the presence of eukaryotes which is significantly earlier than the age of well-established fossil evidence for these organisms (1.4 Ga; Summons and Walter, 1990). Sterane distributions and ratios may be used to infer maturity levels of Precambrian rocks, despite their lesser abundance in Neoproterozoic as compared to Mesozoic rocks. Hopanes associated with bacterial inputs are generally abundant in Precambrian rocks as compared to their occurrence in younger strata (Ourisson and Rohmer, 1992).

### *2. Studies of Relations Between Organic Matter and Metal Ore*

The general view that OM plays a role in some forms of ore mineralization is evidenced by occurrence of OM in sedimentary rocks in association with metallic ores at, for example, the Pb, Zn and Ag deposits of the McArthur Basin of Australia (Logan *et al.,* 2001; Summons *et al.,* 1988), Cu deposits of the European Kupferschiefer (Püttman *et al.,* 1989) and SSC deposits of northern Michigan, USA (Ho *et al.,* 1990; Ho and Mauk, 1996). Additional accounts of organics-ore association include those of U (e.g., Gize, 2000), Au (e.g., Fairmaid *et al.,* 2011; Ilchik *et al.,* 1986), Hg (e.g., Lavric *et al.,* 2003; Gize, 2000), and in particular the large deposits of Mississippi Valley Type Pb-Zn deposits (e.g., Disnar and Sureau, 1990).

Organic geochemistry has been applied to OM-associated mineral deposits to identify HC biomarkers of major organic precursors and molecular alterations indicative of important Earth processes such as thermal maturity and biodegradation (e.g., Logan *et al.,* 2001; Rieger *et al.,* 2008). Some workers have reported correlation of trends between biomarker/abiotic HC parameters and metal enrichments (Hulen and Collister, 1999; Spangenberg and Macko, 1998).

With analytical advances it is now possible to use organic geochemical parameters to search for thermal anomalies associated with hydrothermal ore deposits and to map conduits of ore-emplacing paleofluids (Ilchik *et al.,* 1986). Significantly, the organic parameters inferred to represent hydrothermalism may occupy larger areas than the orebodies themselves, potentially offering a means of exploration. Still, few would confidently claim to totally understand the relevance of organics to the mineralization process, although the review by Greenwood *et al.* (2013) highlights promising insightful outcomes from several well-studied OM-ore associations. See also the 2000 edition of Reviews in Economic Geology on *Ore Genesis and Exploration, v. 3: The roles of organic matter* (eds. T.H. Giordano et al).

### *2.1 Kupferschiefer Stratiform Copper*

The Upper Permian cupriferous shale, or Kupferschiefer, of northern Europe shares many geologic and interpreted genetic features with the Nonesuch Formation SSCs (Ridley, 2013). The stratigraphic term Kupferschiefer describes a thin (less than 4 m) bed of marine bituminous marl occupying an estimated 600,000 $km^2$ extent, from Poland in the east across Germany and the North Sea to northeast England, where it is called the Marl Slate and lacks reported economic Cu concentrations (Vaughan *et al.*, 1989). It has been exploited for Ag, Cu, and other base metals since the Middle Ages and is regarded as the type example of a shale-hosted, strata-bound, disseminated sulfide deposit (Speczik *et al*., 1986). The term Rote Fäule was first used by miners to describe barren, red-colored rocks found in the vicinity of the ore. It is applied to rocks of the Weisseliegende (white sandstone), Kupferschiefer, and Zechsteinkalk layers which exhibit various types of red coloration caused by disseminated hematite and goethite (Vaughan *et al.*, 1989). Some workers early on interpreted the Rote Fäule to represent a shallow-water equivalent of the black, Cu-bearing shales but a diagenetic origin is suggested and widely accepted based on the presence of hematite pseudomorphs after syngenetic pyrite (Jowett *et al.,* 1987).

Organic C content generally decreases from bottom to top in the Kupferschiefer, which reflects decreasing preservation with increasing oxygenation of the Zechstein Sea (Püttman *et al.*, 1989). However, the lowest TOC values are found in the bottom-most samples of the basal, most-altered Rote Faule (Bechtel *et al.*, 2000). The change from black shale to red shale (Rote Fäule) across Cu ores in the Kupferschiefer is interpreted to be a result of near complete epigenetic oxidation and dissolution of indigenous OM during flow of Cu-bearing fluids on the up-flow margins of the ores (Speczik and Püttman, 1987).

### 2.1.1 Organic Geochemical Studies of the Kupferschiefer

The Kupferschiefer has been a topic of OM-ore study since the middle 1980s. Kotarba *et al.* (2006) applied RE, GC/GC-MS, and compound class-specific SI methods to examine thermal maturity and source rock prospectivity of the Permian Kupferschiefer, building upon a significant body of organic geochemical studies of Cu ore-organic relations in the region.

Overall Kupferschiefer mineralized and highly oxidized ore-adjacent areas) show: 1) kerogens depleted in H equivalents (low HI; Sun and Püttman, 2001); 2) a dominance of aromatic compounds in EOM, especially PAHs; 3) lower MPI1 (demethylation) and lower MDR; 4) saturated HCs depleted in n-alkanes of intermediate to high molecular weight; and, 5) a higher degree of OM degradation indicated by increasing phenanthrene/methylphenanthrene ratio (demethylation), than do barren, least-altered samples (Bechtel *et al.,* 2000). Barren samples do however show increasing maturity with depth as reflected by generally decreasing HI and increasing $T_{max}$ values, diminished EOM yields and correlation of MPI1 and depth in agreement with the relation of MPI1 to organic maturity (Bechtel *et al.,* 2000).

The Bechtel *et al.* (2000) study is most closely analogous to this study, in terms of deposit type, analytical tools and end goals, although Sun and Püttman (2001) replicated some of their findings. Sun (1998) showed that mineralized and barren Kupferschiefer samples are Type II and Type III kerogens on modified van Krevelen plots (cf. Bechtel *et al.,* 2000). All barren Kupferschiefer samples fall within the area where Type II OM dominates, whereas the Rote Fäule and some of the mineralized samples do not (Bechtel, *et al.,* 2000). Departures from the expected thermal evolution pathways for a given kerogen are seen in Figure 20 from Bechtel *et al.* (2000). Sun (1998) suggested that secondary oxidation of OM during mineralization altered Type II kerogen to the Type II-III mixture observed. Alternatively, this could reflect multiple OM source types, $C_{carb}$ interferences during pyrolysis of organic-lean, carbonate-rich samples.

Discrimination thereof necessitated kerogen typing by crossplots of HI versus $T_{max}$, as in Figure 21. The mineralized Kupferschiefer samples show a slight negative correlation between HI and burial depth (Figure 22), with HI values significantly reduced at a given depth compared with the barren samples.

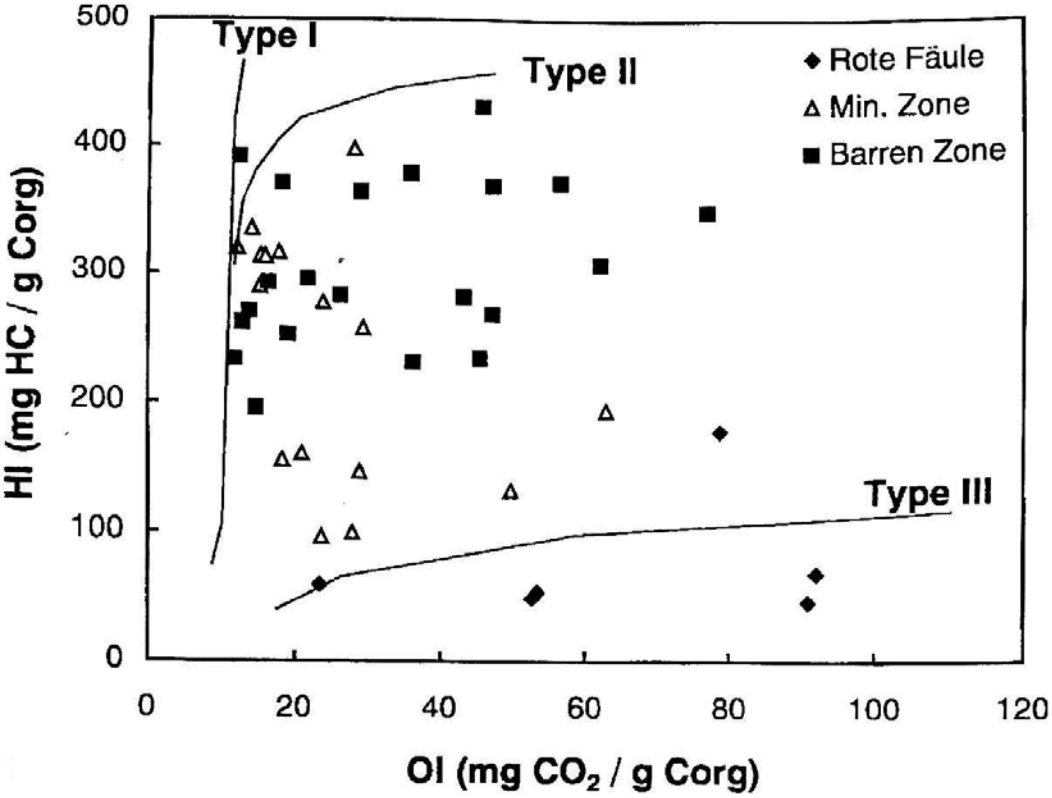

Figure 20: Modified van Krevelen diagram of Rock-Eval pyrolysis on Kupferschiefer SSC samples. Maturation pathways typical for the different kerogen types are indicated. Bechtel *et al.*, 2000.

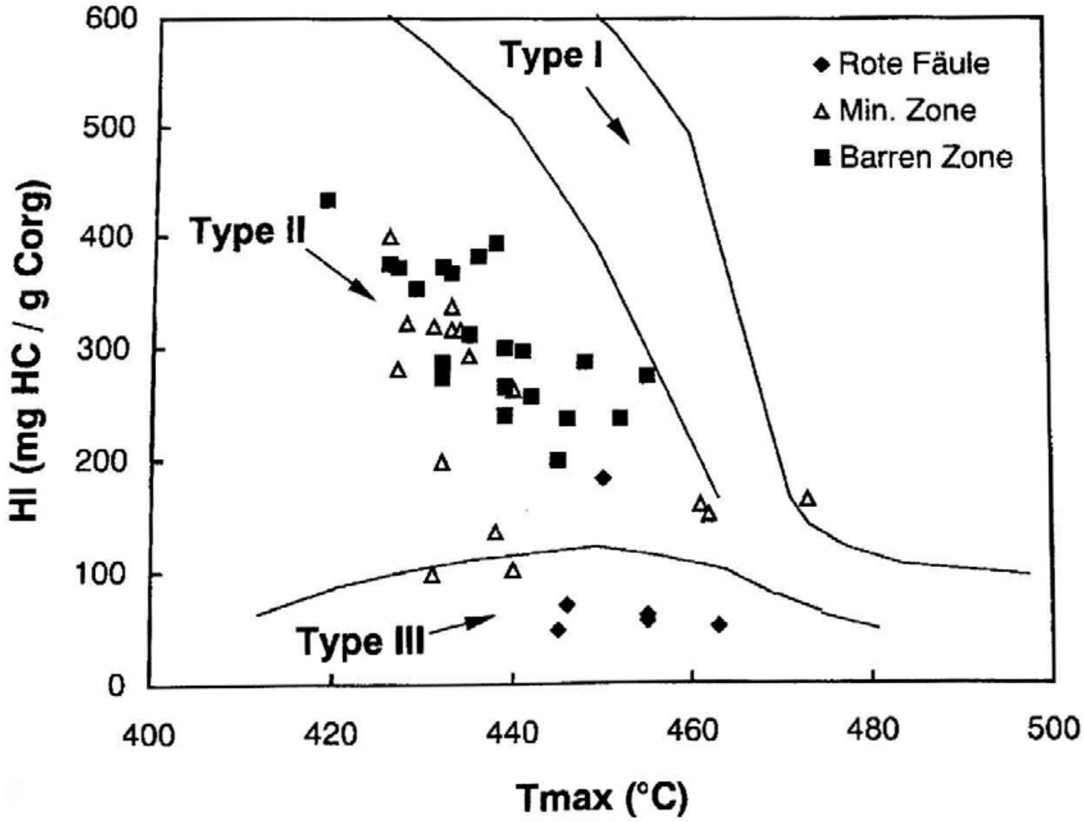

Figure 21: Relationship between HI and temperature of maximum pyrolysis yield ($T_{max}$) for Kupferschiefer SSC samples. Fields in the diagram are labeled according to the predominance of the respective kerogen type. Bechtel *et al.*, 2000.

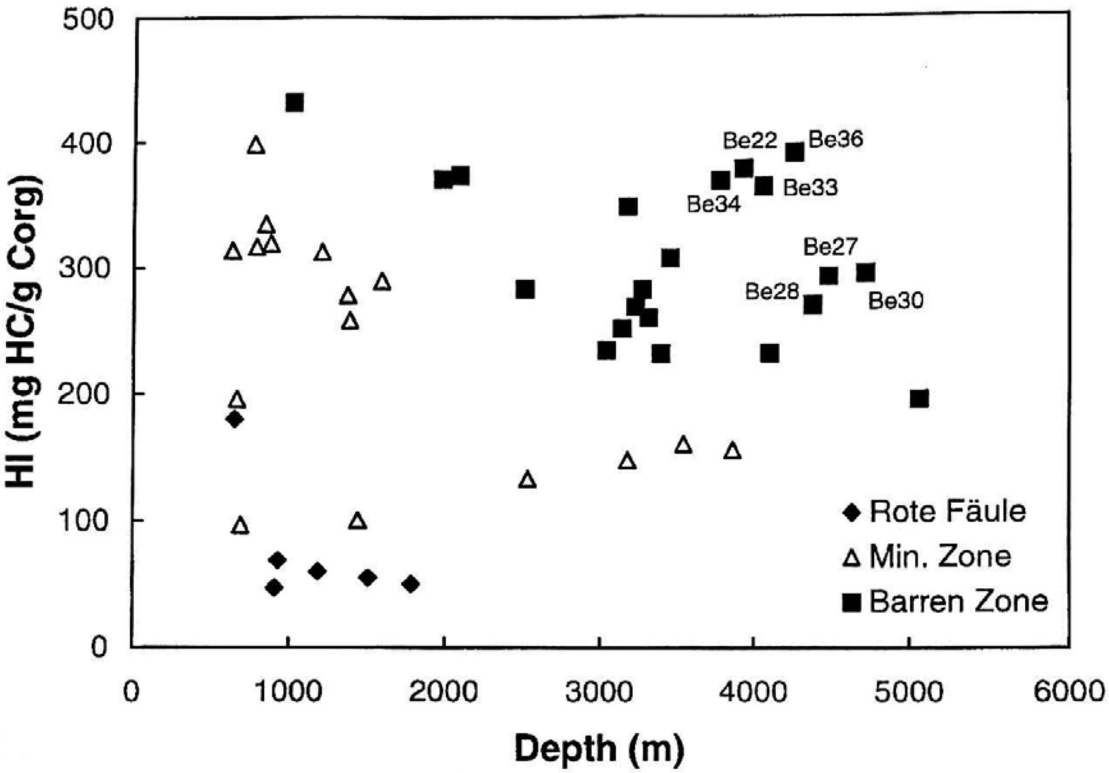

Figure 22: Correlation plot of HI versus downhole depths of the Kupferschiefer. Bechtel *et al.*, 2000.

Organic matter from highly mineralized samples adjacent to Rote Fäule and especially from Rote Fäule samples show low HI and higher OI values than does the whole sample set of Bechtel *et al.* (2000; cf. Sun and Püttman, 2001). Bechtel *et al.* (2000) interpreted their similarly broad scatter of HI versus OI data points (Figure 20) to reflect OM degradation due to both burial-induced thermal maturation and oxidation associated with base metal mineralization.

The vast majority of barren Kupferschiefer samples show relatively low $T_{max}$ values (Figure 23). In comparison, mineralized and ore-proximal Kupferschiefer samples plot in different fields on the $T_{max}$ versus depth diagram. The Rote Fäule samples show highest $T_{max}$ values (despite the present shallow burial depth of Kupferschiefer in the localities from which these samples were collected). In fact, the increasing $T_{max}$ values towards the Rote Faule are characteristic of OM degradation by partial oxidation by ascending oxidizing brines in and just above the Rote Faule.

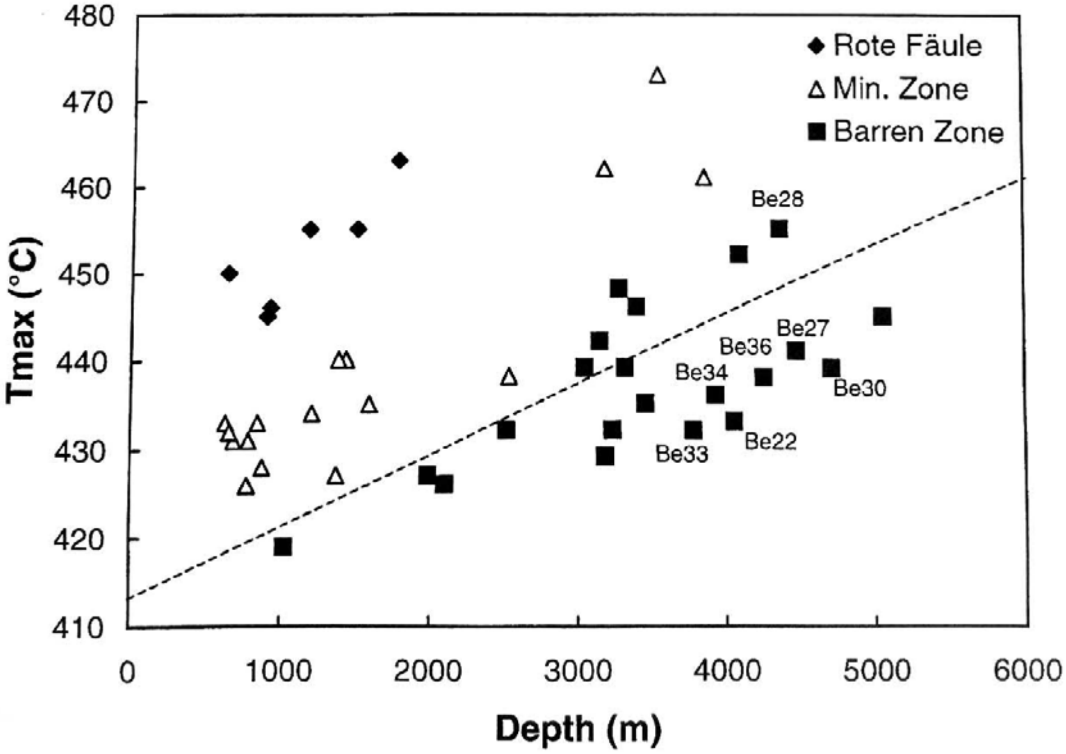

Figure 23: Correlation plot of $T_{max}$ versus downhole depths of the Kupferschiefer. Bechtel *et al*., 2000.

With decreasing distance to the Rote Fäule, the EOM yield decreased from 50-70 mg/g $C_{org}$ to values between 25-35 mg/g $C_{org}$ (Bechtel *et al.,* 2000). See Figure 24. This trend parallels a general increase in the aromatic portion of EOM from 20-38% in Pb-Zn mineralized samples (lacking Cu) up to 40-54% aromatics in the most-altered Rote Faule samples. Increasing aromatic EOM yield accompanies a decrease in the proportion of saturated HC in EOM from Pb-Zn mineralized samples to Rote Fäule samples. Barren zone samples give greater yield of EOM and a wider range of values (33-61 mg/g $C_{org}$); the wider spread of values is in part due to this subset's broader span of sample collection depths due to km-scale vertical structural offsets (Bechtel *et al.,* 2000).

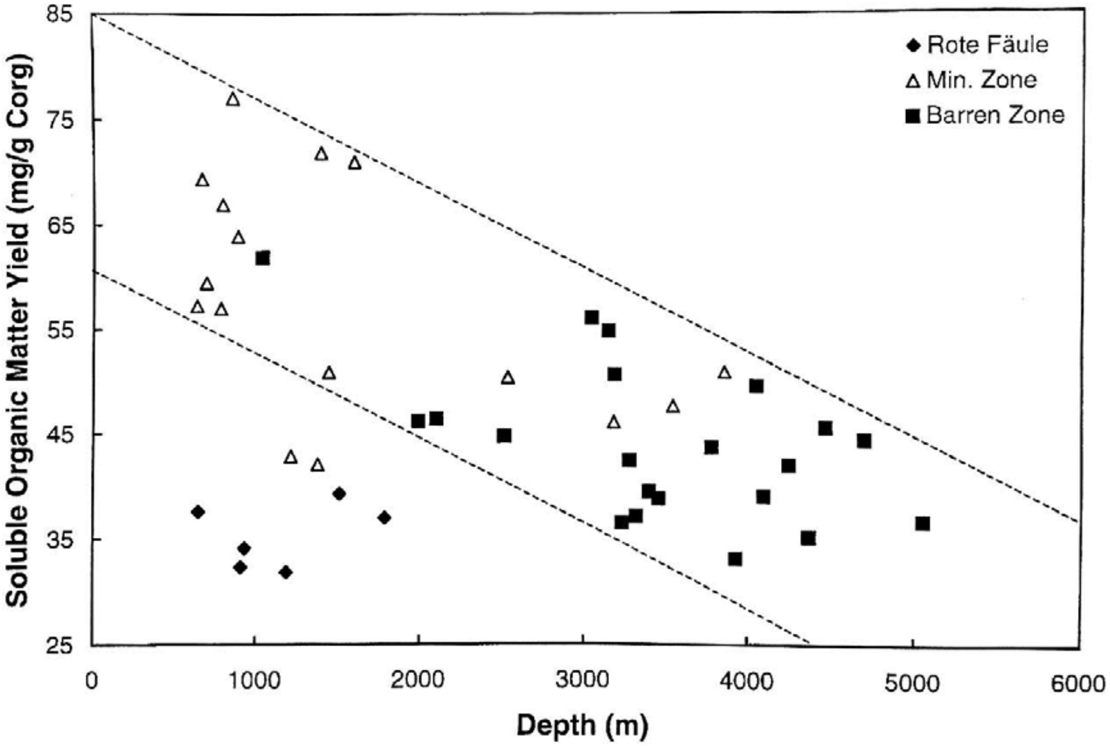

Figure 24: Plot of the $C_{org}$-normalized, $C_{15}$+ soluble organic matter yield vs. downhole depths of the Kupferschiefer (Bechtel *et al*., 2000).

Multiple studies of the Permian Kupferschiefer describe distinct differences in the saturate and aromatic fractions of extracted OM and of the vitrinite reflectance for ore-proximal versus ore-distal samples (Sun, 1998; Bechtel *et al.,* 2000). This evidence for oxidative alteration of OM in highly mineralized Kupferschiefer samples near the most-altered Rote Fäule zones coincides with correlations of RE and EOM yields versus the present sample depths. Aromatic compositions changed with decreasing distance to the most-altered and mineralized zones by increasing abundance of PAH (Bechtel, *et al.,* 2000). This trend was posited by Sun and Püttman (2001) to result from dealkylation of oxy-alkylated aromatics to produce DBF, among other aromatics. Sun (1998) found that vitrinite reflectance increased with proximity to ore and Rote Fäule, coincident with increasing aromaticity. Proximity to mineralized and most-altered zones correlate with increases in the ratio of phenanthrene to methylphenanthrenes (and thus, also to decreases in the MPI1 with proximity to ore, possibly by demethylation of methylphenanthrenes; Bechtel *et al.,* 2000).

The aromatic portion's GC traces from Pb-Zn mineralized samples at greater distance to the Rote Fäule zone are successively dominated by phenanthrene, methyl-, dimethyl-, and trimethyl-phenanthrenes (Figure 25, Bechtel *et al.,* 2000). Further aromatic constituents include biphenyl, DBF, and DBTs. The Cu-mineralized zone shows the same compounds, but with reduced intensities of the methylphenanthrene and increasing number of aromatic rings. Increased aromaticity is defined by the appearance of PAHs including fluoranthrene, pyrene, and benzo(k)fluoranthrene (Figure 26). Rote Fäule samples show these PAHs and also benzo(a)anthracene, triphenylene, and chrysene as the dominant aromatic compounds (Figure 27). Barren zone samples show PAHs at only minor intensities in comparison (Bechtel *et al.,* 2000).

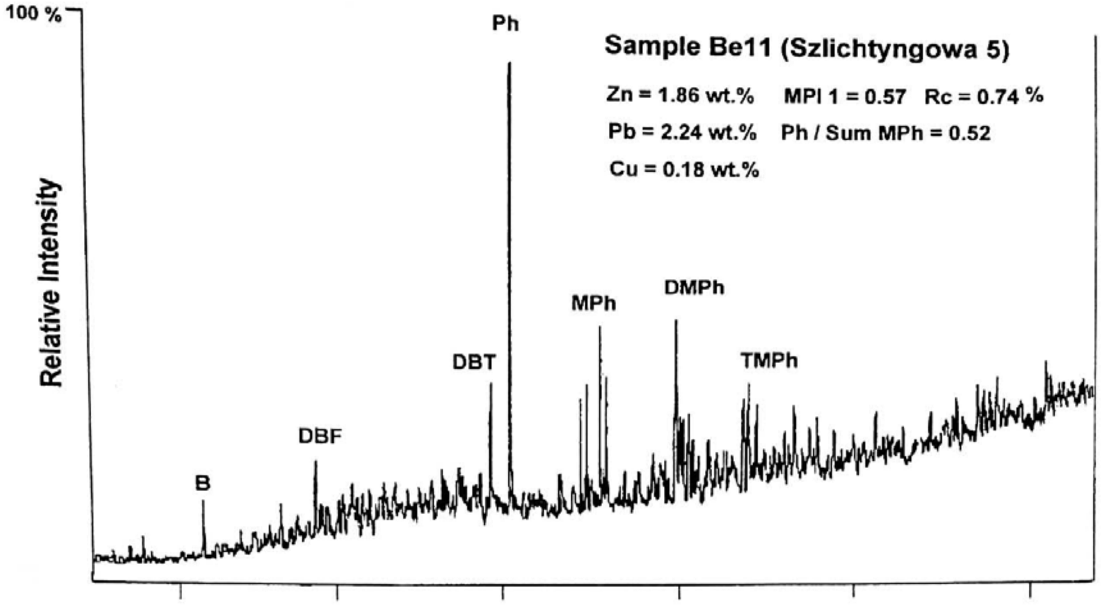

Figure 25: Gas chromatogram of the aromatic HC fraction from a Kupferschiefer sample representative of the Pb-Zn mineralized zone. B = biphenyl; DBF = dibenzofuran; DBT = dibenzothiophene; Ph = phenanthrene; MPh = methylphenanthrenes; DMPh = dimethylphenanthrenes; TMPh = trimethylphenanthrenes. Bechtel *et al*., 2000.

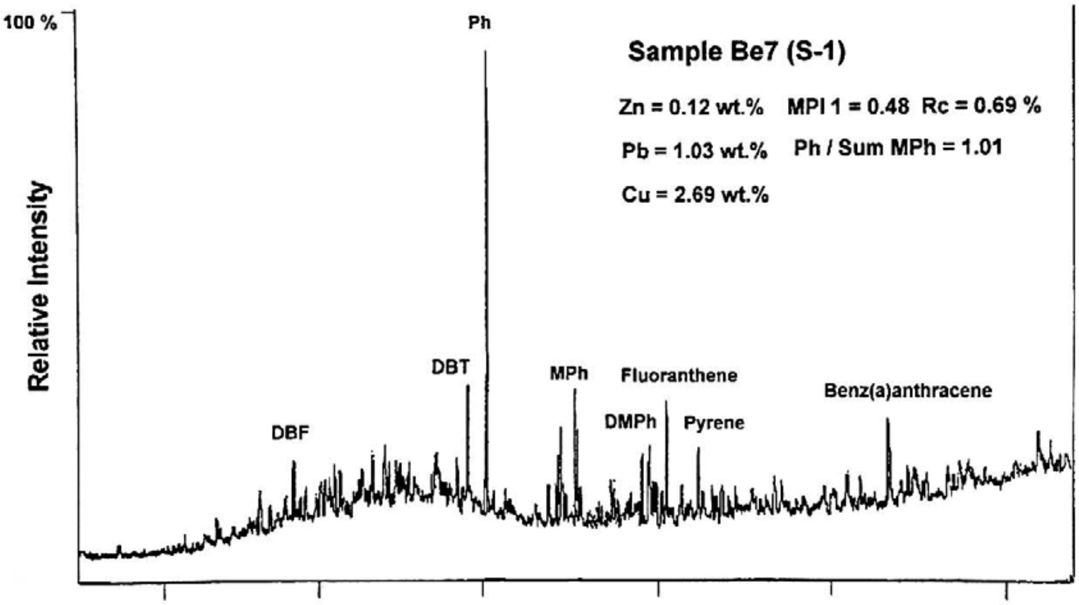

Figure 26: Gas chromatogram of the aromatic HC fraction from a Kupferschiefer sample representative of the Cu mineralized zone.  DBF = dibenzofuran; DBT = dibenzothiophene; Ph = phenanthrene; MPh = methylphenanthrenes; DMPh = dimethylphenanthrenes.  Bechtel *et al*., 2000.

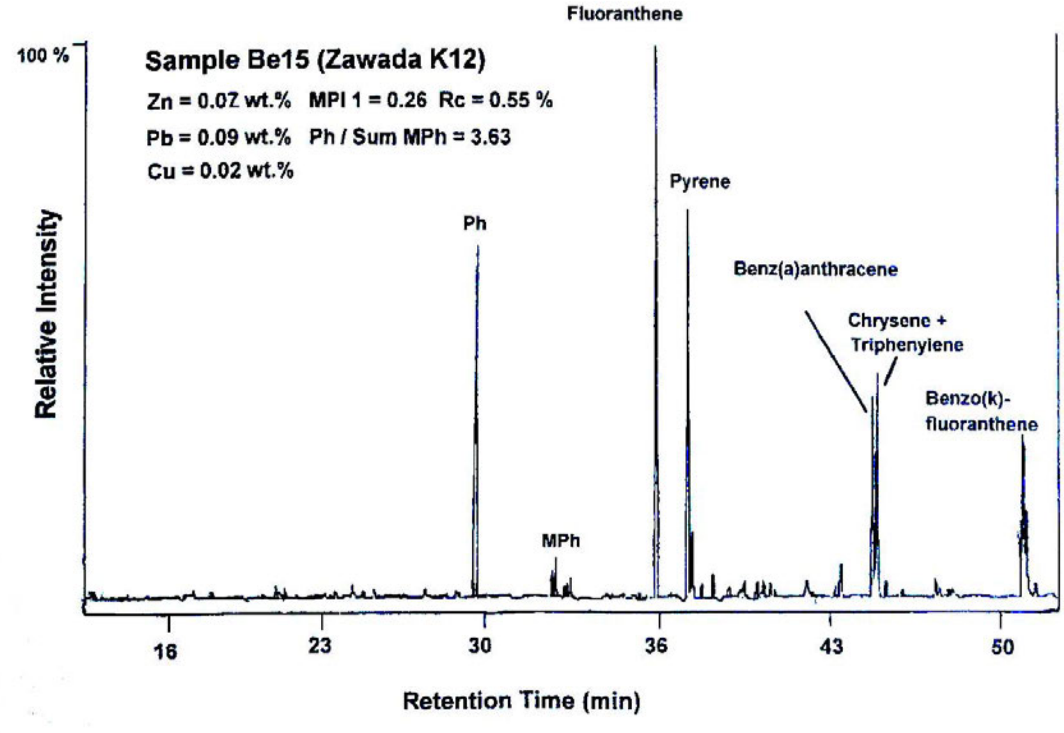

Figure 27: Gas chromatogram of the aromatic HC fraction from a Kupferschiefer sample representative of the Rote Faule zone.  Ph = phenanthrene; MPh = methylphenanthrenes.  Bechtel *et al*., 2000.

The methylphenanthrene index (MPI1) averaged 0.8 for Rote Fäule and mineralized samples, and ~0.96 for the barren, ore-distal samples; MPI1 values decrease towards the Rote Fäule, as shown in Figure 28 (Bechtel *et al.,* 2000; cf. Sun, 1998). The observed MPI1 depression in highly mineralized samples is thought to result from H donation during thermochemical sulfate reduction by alkylated phenanthrenes.

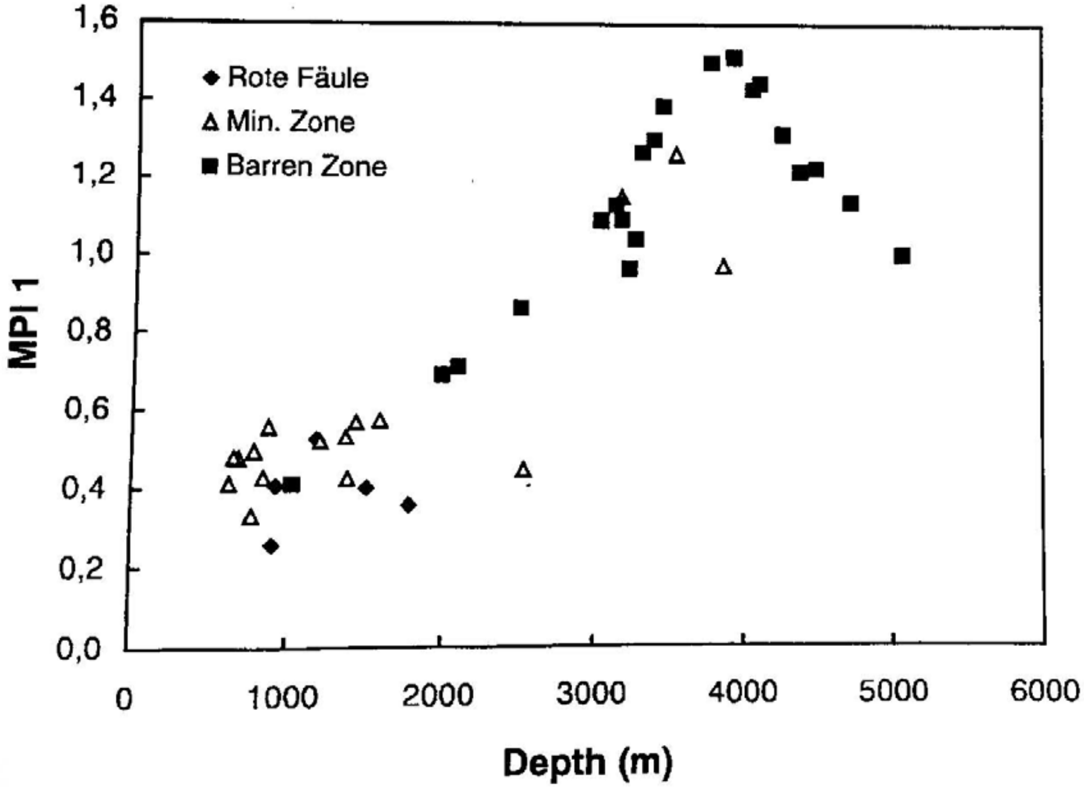

Figure 28: Correlation plot of the methylphenanthrene index, sensu Radke, *et al*., 1982. From Bechtel *et al*., 2000.

The values of the methyldibenzothiopene ratio (MDR) increase continuously from 2.2 to 7.2 with increasing depth (Figure 29). For samples presently at less than 2000 m depth, there is a broad scatter of MDR values; this is thought to reflect varied degrees of OM degradation by oxic brines associated with Cu ore emplacement in the Kupferschiefer.

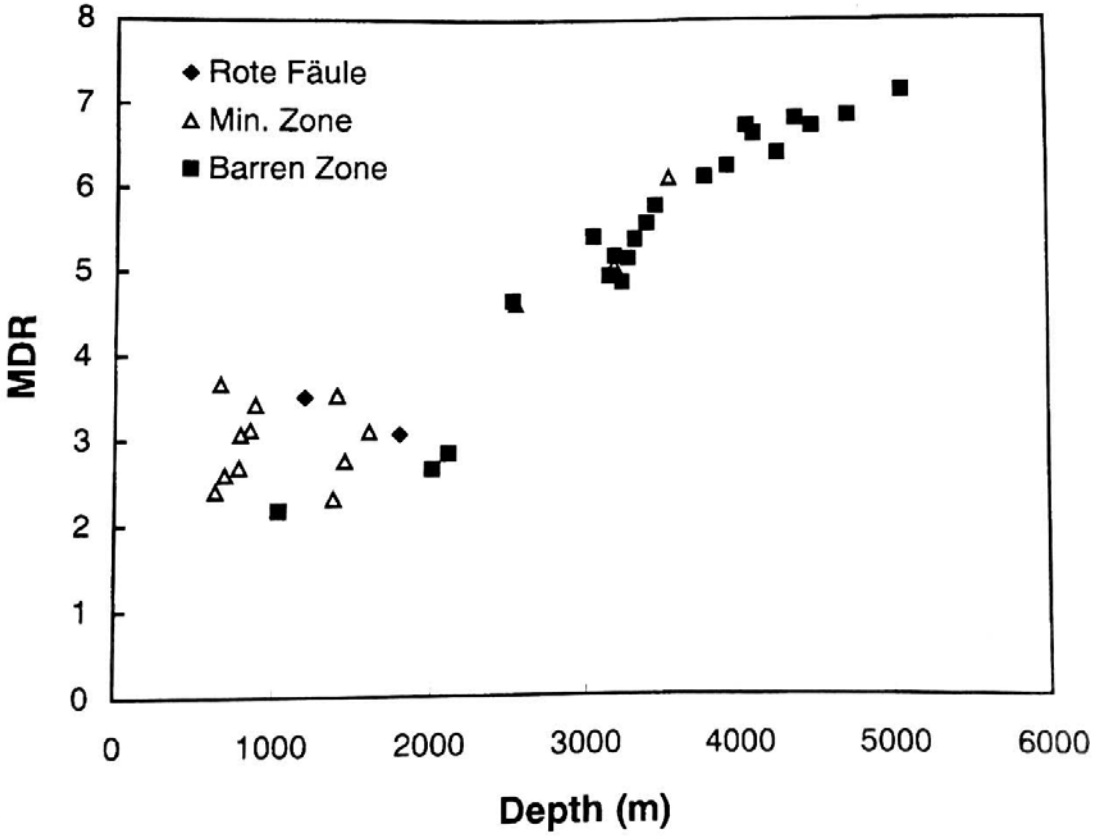

Figure 29: Correlation plot of the methyldibenzothiophene ratio (MDR of Radke *et al*., 1982) of the Kupferschiefer. From Bechtel *et al*., 2000.

The depletion of MPs relative to phenanthrene in EOM can be used to quantify the extent of OM alteration by the oxidizing hydrothermal brines (Püttman *et al.,* 1989). Speczik (1994) tied increasing Cu grade to vitrinite reflectance as well as Ph/ΣMPh to plot a classic bell-curve by these three parameters from GC/GC-MS and VR data. Speczik (1994) showed that values for the Ph/ΣMPh provide a measure for the intensity of alteration. Unoxidized and weakly oxidized samples showed Ph/ΣMPh = 0.6-1.2, while oxidized samples give values between 1.5 and 3.0 (Speczik, 1994). Bechtel *et al.* (2000) showed averaged Ph/ΣMPh for Rote Fäule and mineralized samples of 0.82 and 0.457 for barren ore-distal rocks. Clear boundaries between

Rote Fäule, mineralized, and barren Kupferschiefer samples are apparent in the plot of HI versus Ph/ΣMPh, shown in Figure 30 from Bechtel *et al.* (2000).

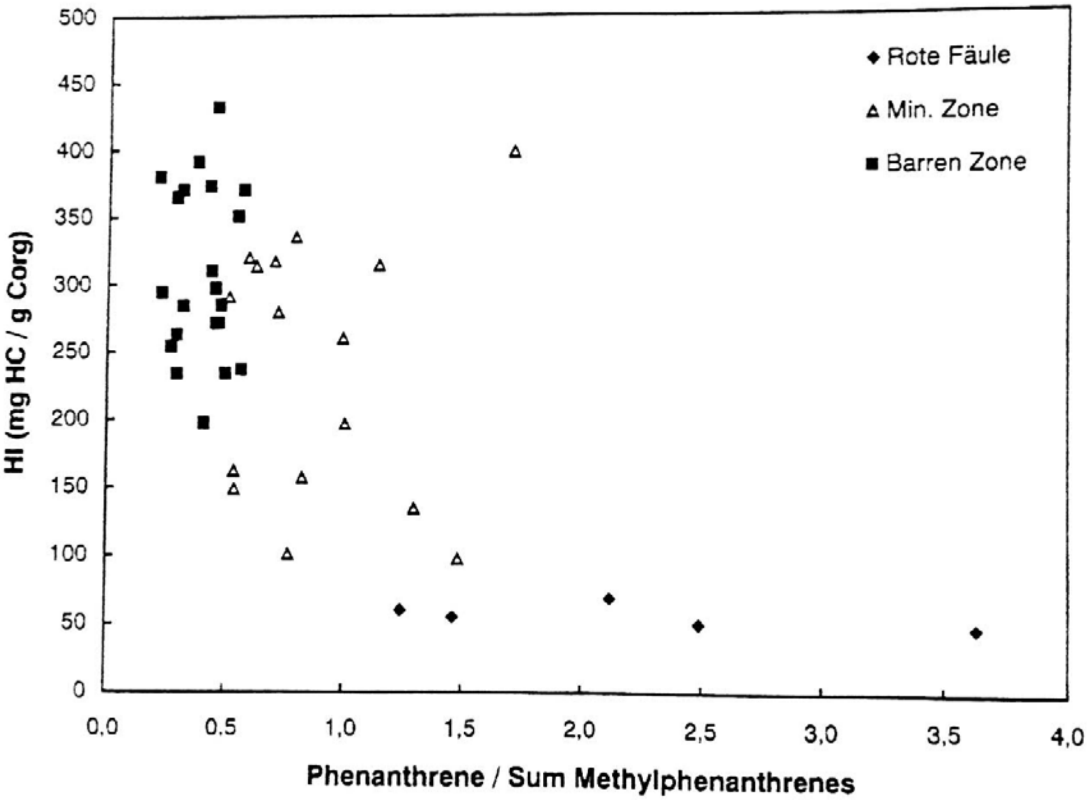

Figure 30: Hydrogen index vs. the Ph/ΣMPh ratio of Kupferschiefer samples, from barren, mineralized, and Rote Faule zones. Bechtel *et al.*, 2000.

Bechtel *et al.* (2000) showed that mineralized and ore-proximal rocks have higher abundances of pristane and phytane relative to heptadecane ($n$-$C_{17}$) and octadecane ($n$-$C_{18}$) than do unmineralized ore-distal barren samples in the Kupferschiefer. Their values for ore-proximal and mineralized samples averaged 0.76 and 0.79, respectively, and ore-distal samples averaged 1.22 for pristane/$n$-$C_{17}$ and 1.54 for phytane/$n$-$C_{18}$ (Bechtel *et al.,* 2000).

The isotopic composition of $C_{org}$ and $C_{carb}$ showed changes corresponding to the alteration patterns of OM elucidated by GC-MS and RE data (Bechtel *et al.,* 2000). Kupferschiefer kerogens as well as bitumens in and proximal to the most altered zone showed enrichment of $^{13}C$ relative to ore-distal, unaltered samples as in Figure 31 (Bechtel *et al.*, 2000;

Sun and Püttman, 2001). This can be explained by preferential release of isotopically light $C_{org}$ through progressive degradation of OM (Sun and Püttman, 2001). Conversely, Kupferschiefer calcites of Rote Fäule samples are depleted in $^{13}C$ and $^{18}O$ to the highest extent relative to barren samples, followed by calcite of the mineralized zone as shown by Figure 32 (Bechtel *et al.,* 2000). This negative correlation suggests the generation of carbonate from isotopically light $CO_2$ liberated by degradation of OM. Oxidative conversion of $C_{org}$ into carbonates after deposition of the sediment is the best explanation given the trends in C isotopic composition of OM and calcite (Bechtel *et al.,* 2000).

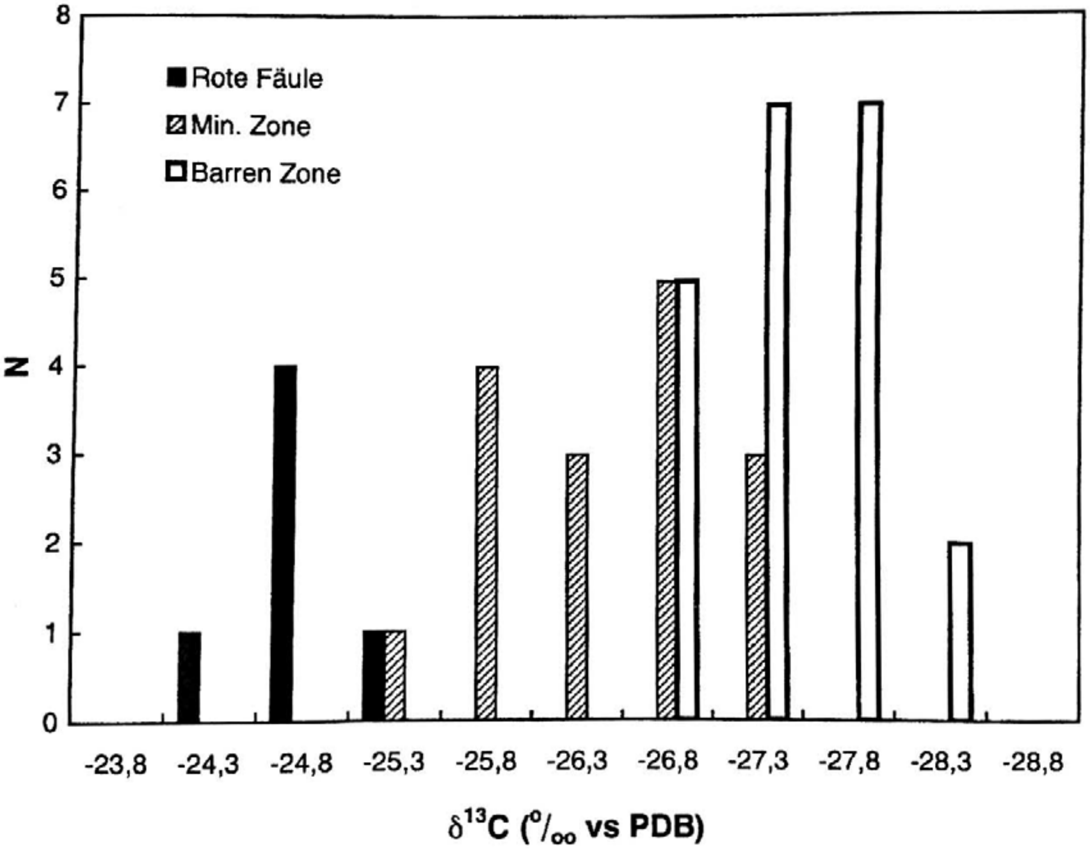

Figure 31: Histogram of the $\delta^{13}C$ values of the total $C_{org}$ from the Kupferschiefer of the Polish Zechstein Basin. Bechtel *et al.*, 2000.

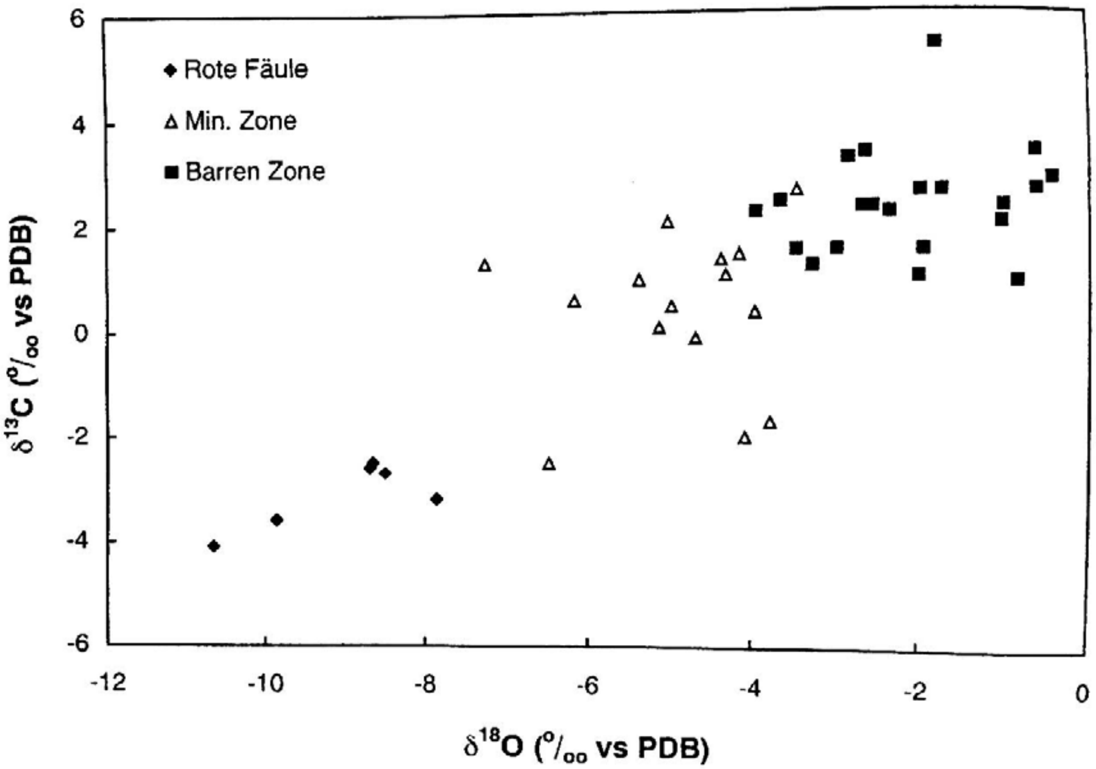

Figure 32: $\delta^{13}C$ vs. $\delta^{18}O$ diagram of calcites from the Kupferschiefer of Poland. Bechtel *et al.*, 2000.

The multiple independent lines of evidence corroborate and convince this observer of the veracity of the conclusion of Bechtel, *et al.* (2000): Within the Polish Cu deposits, the OM of the Kupferschiefer acted as a geochemical trap by its reducing potential, precipitating metal sulfides from ascending, oxidizing brines caused by decreasing Eh conditions.

### *2.2 Alligator Ridge Gold and Organic Alteration*

Ilchik *et al.* (1986) quantified OM maturation by RE to map Au hydrothermal enrichment conduits. They showed that OI and HI values more accurately reflect Au, As and Sb enrichments than did mineral alteration patterns observable in the field. Mineralized samples showed HI values ranging from 1 to 55, while the HI range for unmineralized samples was 10 to 76; deposit-distal background samples showed a similar HI range to those of unmineralized mine samples. Select pyrograms (Figure 33) representing each of the three classes of all samples show a significant decrease of the $S_2$ peak (and resultant HI depression) for samples proximal to, or bearing, ore-grade Au concentrations.  This significant increase in organic maturity above background in both mineralized and unmineralized samples indicates that thermal effects of hydrothermal fluid flow are more extensive than ore grade or other field-observable mineralogic alteration patterns (Ilchik *et al.*, 1986).

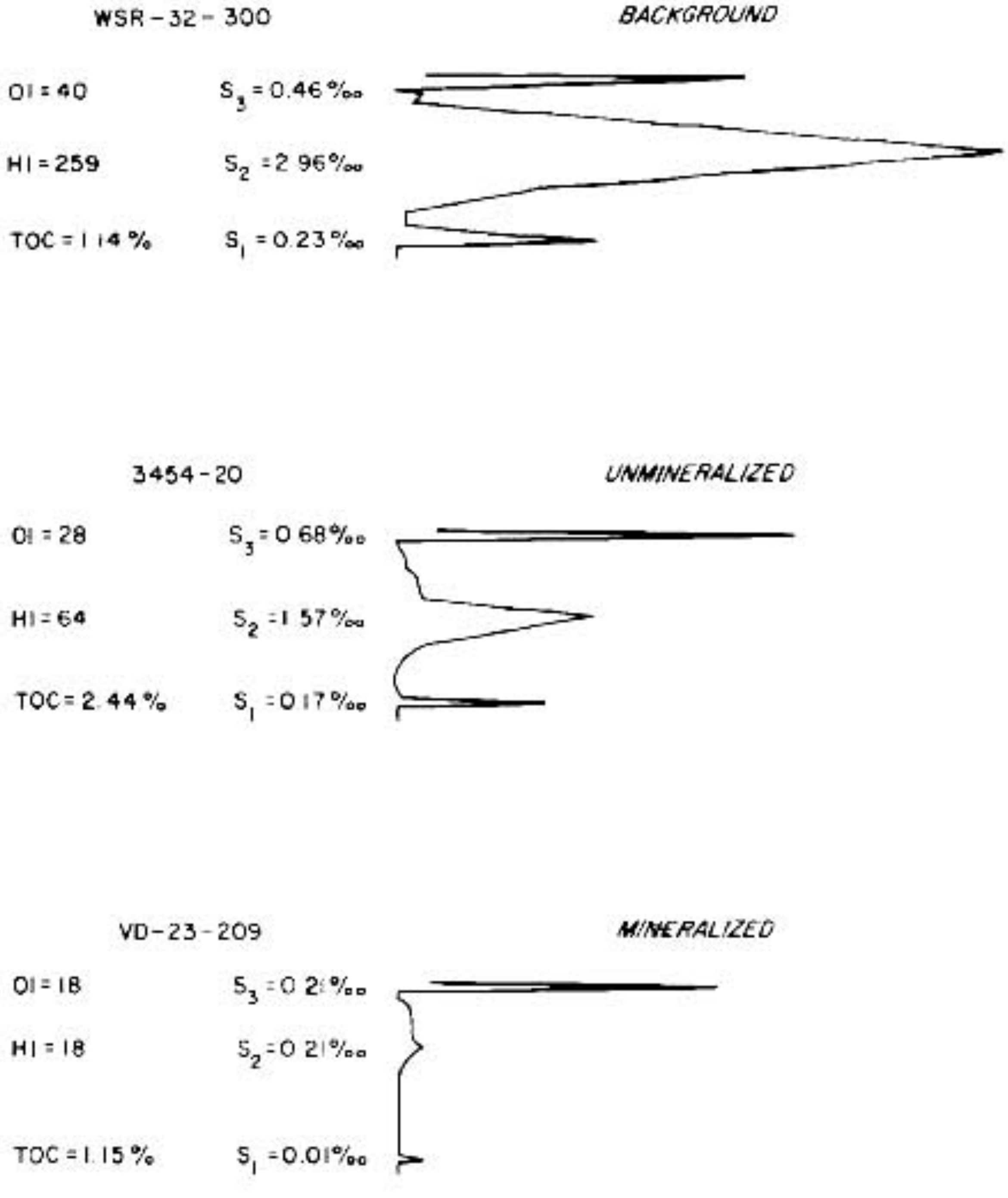

Figure 33: Effects of hydrothermalism on kerogens of the Pilot Shale at Alligator Ridge, NV, as determined by pyrolysis. Pyrograms representative of mineralized, unmineralized, and background samples are on the right. Note the decreases in the $S_1$ and $S_2$ peaks caused by hydrothermal activity (Ilchik *et al*., 1986).

Ilchik *et al.* (1986) showed HI isopleths at Vantage II, which they interpreted as isotherms for the hydrothermal event. Heat flow is controlled by fluid advection rather than conduction through the rock matrix, so the isotherms extend in the direction of maximum fluid flow (as in Figure 34, from Ilchik *et al.,* 1986). Rock-Eval maturity parameters can thus serve as useful proxies for mapping hydrothermal flow patterns associated with sediment-hosted precious metal deposits.

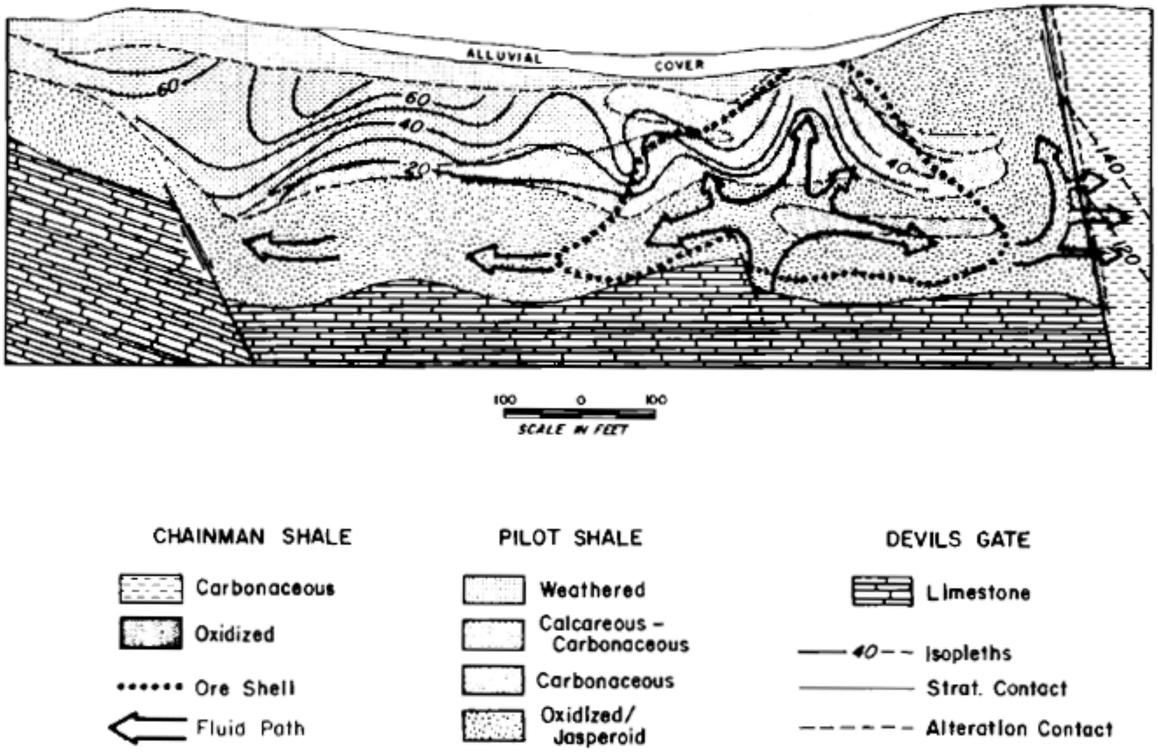

Figure 34: Hydrogen index isopleths and proposed mineralizing fluid pathways at Alligator Ridge Vantage II and III orebodies. Most samples come from 50-100 feet below present topographic surface. Arrows indicate proposed fluid flow path (Ilchik *et al.,* 1986).

The OI range for mineralized and unmineralized samples is significantly greater than for the background samples. Background samples showed OI between 10 and 45, whereas both mineralized and unmineralized samples gave OI between 0 and 150 - an oxidation anomaly associated with ore deposition. One mineralized sample registered an OI value of 303 (Ilchik *et al.,* 1986). Visually prominent oxidation features in the deposit proper - destruction of sulfide minerals and OM - coincide with elevated OI values; these samples are mostly found adjacent to significant hematite concentrations.

### *2.3 Idrija Mercury Deposit*

Rock-Eval pyrolysis parameters and GC-MS study of the molecular composition of regional barren rocks, host rocks, and mine ores revealed oxidative degradation of indigenous and migrated OM at the world-class Hg deposit at Idrija, Slovenia (Lavric *et al.,* 2003). The study also applied stable isotopic analyses of kerogens, bitumens, pyrobitumens, and some *n*-alkanes to provide mine-scale constraints on ore fluid pathways and insights as to the nature of hydrothermal alteration of the Idrija OM (cf. Palinkas *et al.,* 2001).

Idrija bitumens from mineralized samples were depleted in aliphatic HC and enriched in PAH, S-PAH and hydrogenated PAH relative to unmineralized and regional samples. Idrija deposit's PAH may have formed by: 1) pyrolytic fragmentation of organic compounds followed by reformation (cyclization, aromatization, annelation), and 2) transformation of biological precursors (eg: saturated cyclic compounds) by dehydrogenation and dealkylation. Efficiency of both processes increase with elevated temperature: higher temperatures will show higher PAH contents and mixtures of degraded biomarkers and residual immature biomarkers (Engel and Macko, 1993). Thermochemical sulfate reduction involved with cinnabar precipitation may have further enhanced aromatization of Idrija HC by S catalysis. Lavric *et al.* (2003) concluded that the occurrence of hydrogenated PAH in the Idrija ore samples indicated a higher degree of alteration and the pathway of hydrothermal fluids. It seems probable that the high concentrations of S-PAH in Idrija mineralized samples were formed during mineralization and related to hydrothermally mediated reduction of sulfate by OM (Lavric *et al.,* 2003).

### *3. Previous Organic Geochemical Studies of the Nonesuch Formation*

The OM in the Nonesuch Formation was produced and accumulated around 1.087 Ga (Cumming *et al.,* 2013). Organic matter thought to be indigenous to the Nonesuch Formation is found as kerogen, bitumen, pyrobitumen in pore spaces, and as seep oil, fluid inclusion oil and vein inclusion pyrobitumen. This occurrence is spectacular for several reasons: life was still very primitive, limiting production potential; also, the preservation of the Nonesuch Formation without tectonic destruction or sufficient heating to completely destroy its OM is outstanding for rocks of this age (Erwin, 2015; Hunt, 1995).

Nishio (1919) early suggested the importance of OM-Cu relations in the ore deposits of the Nonesuch Formation. Barghoorn *et al.* (1965) put out the first detailed microscopic study of the Nonesuch Formation's OM by petrographic and biologic examination of kerogen isolates. Further detailed organic petrography of the Nonesuch Formation includes works by Imbus (1988), Thompson and Rizer (1993), King (2009), Colbert (2011), and Fourgani (2012). Significant contributions to the known paleoecology and paleoenvironment of Nonesuch Formation deposition include those by Elmore *et al.* (1989), Pratt *et al.* (1991) and Cumming *et al.* (2013). Petroleum prospectivity of the Nonesuch Formation OM was central to the publications of Imbus *et al.* (1988), Uchytil *et al.* (1997) and Hegarty *et al.* (2007). Advances in high-sensitivity organic analytical mechanics drove a boom of OM-focused geochemical research on the Nonesuch Formation in the late 1980s and 1990s. Degradation of OM similar to that recorded in the Kupferschiefer ores has been inferred for the Nonesuch Formation ores through low *n*-alkane contents of whole rock extracts, (Ho *et al.,* 1990; Ho and Mauk, 1996), higher apparent thermal maturity of OM in ore (Hieshima and Pratt, 1991) and lower solvent extraction yields of HC in ore (Mauk and Hieshima, 1992). Imbus *et al.* (1992) reported a relatively broad range $\delta^{13}C$ for Nonesuch Formation kerogens from Michigan and Wisconsin, and a strong enrichment in $^{13}C$ in samples below 0.15% TOC.

### *3.1 Origin and Character of Nonesuch Formation Organic Matter*

Early optical study of kerogen concentrates under incident white light by Barghoorn *et al.* (1965) identified an anastomose filamentous organic material (FOM) that was interpreted by Moore *et al.* (1969) to represent fungal or actinomycete mats. Strother and Wellman (2016) encountered small (10 micron maximum dimension), ellipsoidal organic-walled microfossils in the Nonesuch Formation, as well as in the coeval lacustrine mudstones of the Torridon Group of the north-west Scottish Highlands. Individual cells of the newly identified microfossil, *Eohalothece lacustrina*, are associated with benthic microbial biofilms. The majority of such samples have been recovered in palynological preparations in the form of large, apparently planktonic colonies.

Rock-Eval pyrolysis HI and OI values from 41 Nonesuch Formation samples plot over a fairly broad area on a modified van Krevelen diagram (Imbus *et al.*, 1992). A simplistic interpretation might invoke a large range in thermal maturity to explain apparent disproportionation of H (decreasing HI down the Type I or II coalification tracks), however thermal maturity is generally equivalent throughout the basin, and HI shows no clear relation to TOC level or lithology differences (Imbus *et al.*, 1992). Per that study, Type I kerogens (HI above 300, OI below 10), indicating probable algal origin, are found only in the eastern (Michigan) Nonesuch Formation, whereas two Michigan and one Wisconsin Type II kerogens (HI below 300, OI under 25) are reported by Imbus *et al.* (1992). Contribution of terrestrial higher-plant material to produce Type II-III kerogen (OI above 25) could not have occurred at this time in the Precambrian but such kerogen is nonetheless present in eastern lower and upper divisions. This is attributed to hydrothermal alteration of OM during mineralization for the two lower eastern Nonesuch Formation samples (cf. Ho *et al.,* 1990), whereas the upper eastern division Type II-III kerogens are thought to have been oxidized in shallow ponded environments prior to deep burial (cf. Milavec, 1986). Kerogens whose HI and OI values preclude typing may be attributed to extensive degradation via oxidation, prolonged heating, microbial activity or low initial TOC.

Colbert (2011) showed the presence of mid-chain substituted monomethyl alkanes as well as 1,2,5-TMN from inclusion oil in calcite from White Pine, interpreted to derive from a cyanobacterial source (cf. George *et al.,* 2008). Imbus *et al.* (1992) put forth the *b/e* parameter (comparing the abundance of branched-cyclic alkanes relative to that of *n*-alkanes), which suggests a greater bacterial biomass contribution to the aromatic, generally western (Wisconsin) kerogens.

### *3.2 Organic Maturity of the Nonesuch Formation*

#### *3.2.1 Petrographic Appearance and Maturity*

The filamentous organic matertial (FOM) of the Nonesuch Formation fluoresces under blue light (Organic Petrography 1 - OP 1) in all eastern (Michigan) samples, but does not fluoresce where identified in the great majority of western (Wisconsin) samples (Imbus *et al.,* 1988). The Michigan FOM is orange whereas the Wisconsin FOM is a dark-orange red color under incident light (Imbus *et al.,* 1988). The two distinct organic petrographies also show a continuum between end-member kerogen pyrolysate compositions by pyrolysis-gas chromatography-mass spectrometry. Organic Petrography 1 kerogens are mainly aliphatic whereas the mostly western kerogens of OP 2 are distinct in their significantly higher content of aromatic compounds (Imbus *et al.,* 1988). This greater aromaticity may represent a higher degree of kerogen maturity, as is suggested by the co-occurrence of bitumen-like granular black material in OP2 (eg: Teichmüller, 1982). It has, however, been shown that relatively high aromaticity of kerogen pyrolysates does not always represent increased thermal maturation (Eglinton *et al.,* 1988). The distinct optical petrographic and organic geochemical evidences were interpreted by Imbus *et al.* (1988) to represent variable primary production or preservation differences superimposed over maturity differences between the Nonesuch Formation in Michigan (eastern samples) and Wisconsin (western samples). Regional differences in kerogen appearance led Imbus *et al.* (1988) to tentatively suggest a thermal maturity trend increasing westward.

Colbert (2011) reported yellow fluorescence color present in at least some of the inclusions in all of that study's samples. This indicates early- to peak-oil window maturity (cf. Killops and Killops, 2005).

### *3.2.2 Geochemical Maturity*

Biomarker maturity ratios from high sensitivity GC-MS on inclusion oil from near White Pine Mine by Colbert (2011) suggest an early- to peak-oil window maturity for the HCs. However, the wide range of fluid inclusion homogenization temperatures along with an inconsistency between these and the biomarker data indicate that the thermal history of the Colbert (2011) inclusion oil is more complex than that of typical oils. Outside of the White Pine area, the Nonesuch Formation is moderately mature with respect to petroleum generation (Pratt *et al.,* 1991). Rock-Eval $T_{max}$ values from Presque Isle and Iron River syncline suggest maturity equivalent to the initial phase of oil generation (Pratt *et al.,* 1991). In contrast to kerogen color observations interpreted to indicate a westward-increasing maturity trend, maturity-related molecular parameters seen in bitumens show no consistent trends across the Michigan and

Wisconsin portions of the Nonesuch Formation (octene/*m*- + *p*-xylenes, % $n$-$C_8$/$n$-$C_{8-22}$, $R_c$; Imbus *et al.,* 1992).

Likewise, the range of $T_{max}$ values reported by Imbus *et al.* (1992) show no regional east-west segregation, and generally correspond to the early oil generation thermal regime. Uchytil *et al.* (1997) report $T_{max}$ values in the early to early-middle oil generation window. Other workers have reported $T_{max}$ values for the Nonesuch Formation in the marginally mature (incipient oil generation) range of organic maturity (Palacas, 1997). Ho *et al.* (1989) interpreted $T_{max}$ values for White Pine samples to mean that the rocks had not experienced heating much higher than 100°C. Others (Barghoorn *et al.,* 1965) cited abundant porphyrins in the lower Nonesuch Formation Formation and inferred temperatures limited to under about 120-175°C, depending upon duration of heating.

At White Pine, Fourgani (2012) found that the highest TOC values occur in the unmineralized pyrite zone and that Type III and IV kerogens dominate. Given that Type III and IV kerogens generally form from Phanerozoic plants, this suggests either erroneous data or alteration of the OM at White Pine; a general lack of fluorescence of this OM could be interpreted as further evidence of thermochemical alteration (Fourgani, 2012). Fourgani (2012) reported variable maturity indicated by a wide range of $T_{max}$ and $R_o$ values for White Pine samples: some White Pine samples showed as post-mature while others gave values indicating immaturity with respect to HC generation.

General thermal maturity of OM from the White Pine Mine is interpreted to be higher than that of bitumen from unmineralized Nonesuch Formation strata (Pratt *et al.,* 1991). Unmineralized core extracts are enriched in hopanes versus steranes by factors of 2 to 8 compared to a factor of 0.4 for seep petroleum, probably due to preferential thermal destruction or alteration of hopanes compared with steranes (Pratt *et al.,* 1991). Indeed, overall thermal maturity at White Pine Mine is consistent with peak petroleum generation, while outside the mine thermal maturity is consistent with the onset of petroleum generation (Price *et al.,* 1996).

### *3.3 White Pine Oil Studies*

Active seeps in the White Pine Mine extrude crude oil and salty water (up to 30% TDS, mostly Ca-Na-Cl; Brown, 2006). Petroleum seeps from the roof of the mine via joints and boltholes. At White Pine some oil inclusions in calcite as well as native Cu bear pyrobitumen or petroleum; some of these are thought to be contemporaneous to second-stage mineralization (Nishioka *et al.,* 1985). Petroleum also occurs locally in pores of the "lower sandstone," in association with pyrobitumen cements (Mauk, 1993). Biomarker and stable C isotope analysis strongly support an oil-source rock correlation between the Nonesuch Formation OM and petroleum seeps in the mine (e.g., Pratt *et al.,* 1991). Gas chromatograms of petroleum and pyrobitumen reflect *n*-alkane rich liquid HCs with a homologous series of monomethyl and *n*-alkanes (Mauk and Burruss, 2002).

The same study (Mauk and Burruss, 2002) ruled out significant biodegradation based on low pristane/phytane, pristane/$n$-$C_{17}$ and phytane/$n$-$C_{18}$ ratios found in inclusion oils. This is supported by the reasonable supposition that fluid migration and entrapment occurred at temperatures too hot for biodegradation to occur (Mauk and Burruss, 2002).

Pyrobitumen inclusions in vein calcite are associated with second-stage mineralization at White Pine; the texture of these inclusions indicates that these are primary inclusions trapped during calcite growth (Kelly and Nishioka, 1985). Pyrobitumen commonly forms by thermal degradation of oils, and may be the case in this situation (cf. Price *et al.,* 1996). Mauk and Burrus (2002), favoring a water-washing genesis of calcite inclusion pyrobitumen at White Pine, ruled out a strictly thermal origin, stating that "all geothermometry" indicates low temperatures at the mine site. Exsolution and migration of a gas-rich HC phase - phase separation - can alternatively leave a pyrobitumen residue. Mauk and Burruss (2002) excluded phase separation as the primary means of petroleum alteration at White Pine based on the observed similarity of chromatograms of bitumen extracted from both mineralized and unmineralized Nonesuch Formation to those of inclusion oils from White Pine.

Seep petroleum samples from the unfaulted northeastern part of the White Pine Mine have a lower thermal maturity (early oil window) than do those from seeps in the thrusted, twice-mineralized, southwestern domain (late oil window), as inferred from *n*-alkane distributions (Mauk and Hieshima, 1992). Mauk and Hieshima (1992) suggested that exogenous petroleum mixing with locally generated HCs might explain this disparity. Another possibility is that seep petroleum is mostly endogenous to the local White Pine Mine Nonesuch Formation, and experienced different degrees of hydrothermally mediated chemical alteration. The latter interpretation is supported by similarities in the isotopic compositions of individual *n*-alkanes from seep petroleum and from petroleum in the "lower sandstone" (Mauk *et al.,* 1993). The spatial overlap between inferred higher maturity and brittle structural deformation suggests that hydrothermal activity associated with second-stage mineralization locally enhanced thermal maturity of seep petroleums near to compressional faults (Mauk and Hieshima, 1992). Indigeneity of petroleum is further supported by similar distributions of acyclic isoprenoids, monomethyl alkanes, cyclohexanes, triterpanes and $C_{27}$ to $C_{29}$ steranes between the petroleum from the White Pine Mine seeps and extracts of nonmineralized cores (Pratt *et al.,* 1991). It is significant that the pyrobitumen cements and veins of the "lower sandstone" may have formed as a result of oxidation of precursor petroleum during second-stage mineralization (Mauk and Hieshima, 1992).

### *3.4 Other Thermal Constraints for the Nonesuch Formation*

Price *et al.* (1996) built time-temperature histories for a variety of potential Nonesuch Formation burial histories; these were then evaluated by comparison to organic and inorganic thermal maturity indicators. This modeling indicates that maximum temperatures for the Nonesuch Formation, 110-125°C, were reached at about 1075 Ma and coincided with maximum burial depth of less than 6, and more likely, 4 km (Price *et al.*, 1996). Hegarty *et al.* (2007) proposed much later maturation (ca. 200-300 Ma) in Midcontinent rift fill rocks, but that study focused on a sub-basin in what is now western Iowa. Heat flow estimates and thermal conductivity measurements were used by Mauk and Hieshima (1992) to estimate a maximum paleotemperature between 140-150°C for 4 km burial depth and 280-300°C for a 6 km burial.

Colbert's (2011) FI study of White Pine area indicates that aqueous and oil inclusions were trapped in calcite of the Nonesuch Formation during diagenesis at temperatures between 100-130°C. That study suggested that the inclusions were then heated to levels of at least 150°C for a short period of time, either shortly after diagenesis or around 200-300 Ma, with some indication that maximum post-entrapment temperatures exceeded 250°C (cf. Mauk and Hieshima, 1992; Hegarty *et al.*, 2007). It is possible that heating these samples beyond 150°C during microthermometry caused additional re-equilibration of some of the calcite-hosted inclusions, which could have caused an artificial skew toward higher temperatures in the data histograms (Colbert, 2011).

Apatite fission track and vitrinite reflectance led Hegarty *et al.* (2007) to conclude that Nonesuch Formation equivalents in western Iowa experienced maximum burial to a depth of 4 km, at about 200-300 Ma. Others have bracketed the maximum burial of the Nonesuch in the White Pine region between 1.5 and 3.6 km (e.g., Brown, 1971; White, 1971, Nishioka, 1983). For this author, the up to 4 km of overlying Freda Formation beneath an angular unconformity to the Paleozoic rocks above it suggest that at least 3 km may be taken as a minimum burial depth for the Nonesuch Formation.

Illite/smectite geothermometry (Price and McDowell, 1993; Li *et al.*, 1995) suggests a northeastern increasing thermal maturity trend. They suggested maximum paleotemperatures of 115°C, 160°C, and 190°C for Presque Isle syncline, White Pine, and Houghton area Nonesuch Formation, respectively. This gradient (opposite to that reported by Imbus *et al.,* 1992) parallels northeasterly increases in the amount of uplift on the Keweenaw Fault as well as progressively more pervasive alteration and native Cu mineralization in the Portage Lake Volcanics (Price and McDowell, 1993). However, Essene and Peacor (1995) point out inherent inaccuracies for technique. Price and McDowell (1993) also report a significant thermal maturity low in the Iron River syncline, west of White Pine Mine (shown in Figure 35).

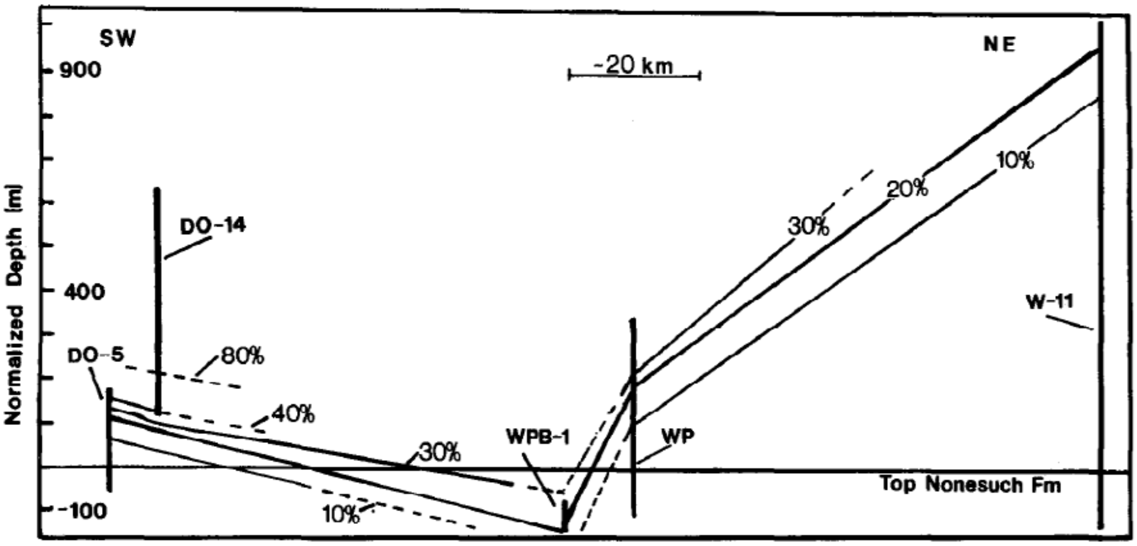

Figure 35: Price and McDowell (1993) cross-section schematic of horizontal and vertical illite/smectite expandability. The Iron River syncline area - the location of the WPB-1 - is depicted here as a thermal low. Their data show a modest increase in thermal maturity to the southwest in the Nonesuch Formation, but the overall trend increases in thermal maturity to the northeast.

Other lines of evidence have been applied to constrain paleotemperatures at White Pine. Brown (1971) inferred, by his observation of pink bornite at White Pine that paleotemperatures were below 75°C (pink bornite exsolves chalcopyrite at higher temperatures). The same paper noted the presence of djurlite ($Cu_{1.96}S$) and, based on that mineral's breakdown to chalcocite and digenite above that 93°C, asserted that value as a thermal maximum for the Nonesuch Formation. Fluid inclusion homogenization temperatures from vein calcite (which may be early or be late fault-associated) and the observation of monoclinic calcite constrained vein-filling temperatures to the range 70-100°C (Nishioka, 1983).

## *3.5 Isotopic Ratios of the Nonesuch Formation*

### *3.5.1 Nonesuch Formation Carbonate Carbon and Oxygen Isotopes*

Cupriferous waters entered the site of the Nonesuch Formation SSC deposits as oxidized fluids and became reduced on interaction with OM, which was presumably oxidized to form $CO_2$ (Ridley, 2013). At other SSC deposits, it has been shown that enrichment of OM in $^{13}C$ towards oxidized ore-associated zones and that this enrichment correlates with more negative $\delta^{13}C$ values of $C_{carb}$ (Bechtel *et al.*, 2000). This negative correlation is thought to reflect the generation of carbonate from isotopically light $CO_2$ released through the degradation of OM (Bechtel *et al.*, 2000). The bulk of the carbonate in the "regular" Nonesuch Formation samples of Imbus (1990) plot in the zone of "common diagenetic cements" on the $\delta^{18}O$ versus $\delta^{13}C$ crossplot; this set of samples partly coincides in isotopic composition with those determined for Copper Harbor Formation sediments and hydrothermal-derived calcites associated with the underlying Keweenawan Portage Lake Volcanics. Imbus (1990) interpreted this coincidence to mean that the carbonate chemistry of the lake waters was possibly influenced by hydrothermally derived fluids. These "remarkable" isotopic similarities among Nonesuch Formation, Copper Harbor

Formation and Portage Lake Lava Series hydrothermal carbonates were interpreted by Imbus *et al.* (1992) to suggest a shared hydrothermal synmineralization genesis of calcite. Cross correlation of C cycle parameters (TOC, %$CaCO_3$, $\delta^{13}C$, and $\delta^{18}O$) suggest a relationship between primary productivity and carbonate precipitation in the Michigan Nonesuch Formation and evidence organic cycling in the Wisconsin Nonesuch Formation (Imbus, 1990).

### *3.5.2 Nonesuch Formation Kerogen Pyrolyzate Carbon Isotope Ratios*

Ho *et al.*'s (1989) analysis of kerogen pyrolyzate C from the lower Nonesuch Formation at White Pine identified $\delta^{13}C$ values between -34 and -31‰; this is similar to the mean $\delta^{13}C$ value of -32.68‰ (±1.5, overall range -27 to -34‰) for the 218 kerogen pyrolyzates in the 1992 Imbus *et al.*, study. Overall these values are $^{13}C$ depleted relative to those commonly observed in Phanerozoic-Precambrian kerogens (Schidlowski, 1987). The observed strong $^{13}C$ enrichment in samples below 0.15% TOC throughout the Nonesuch Formation may result from any or a combination of: destruction of isotopically light OM constituents by oxidation, microbial activity or alteration by mineralizing fluids (Imbus *et al.*, 1992). That study thus excluded the low TOC-higher $\delta^{13}C$ from consideration when it described the geographic segregation of kerogen $\delta^{13}C$: eastern samples from middle to low stratigraphic position are enriched in $^{13}C$ relative to those of the western Nonesuch Formation, in Wisconsin. In contrast, when the low TOC-higher $\delta^{13}C$ values are considered, the western samples specifically - and the formation overall - show enrichment in $^{13}C$ up section (Imbus *et al.*, 1992). A strong trend of kerogen $^{13}C$ depletion is apparent with increasing % $CaCO_3$ in the eastern samples of Imbus *et al*. (1992), as well as across the region. Both of the two previous trends may be interpreted as suggesting the possibility of oxidative destruction of OM by ascending ore fluids liberating isotopically light C and proximal remineralization of such as carbonate. Overall it has been concluded that negligible isotope fractionation of kerogen from the mineralization processes and associated oxidation of $C_{org}$ occurred in the Nonesuch Formation (Greenwood *et al.*, 2013).

### *3.6 White Pine Chlorite Homogenization Halo*

Li *et al.* (1995) found a zonation in the chemical composition of detrital-shaped chlorites in the Nonesuch Formation. They posited that the narrower range of Fe/Fe+Mg ratios in the White Pine area than for unmineralized samples collected away from the mine is an alteration halo. Li *et al.* (1995) presumed that high water-rock ratios drove chlorite homogenization in the vicinity of the White Pine orebody based on the finding of Price and McDowell (1993) of only minor changes in the inferred regional paleotemperatures in this part of the Midcontinent rift. Still, given the 85 km length of their sampling traverse, from White Pine east-northeast to Houghton, Michigan, Li *et al.* (1995) acknowledged that the chemical differences in chlorites might result from variations inherited from different sedimentary provinces.

### *3.7 Organic Matter-Copper Relations at White Pine*

Previous White Pine deposit petrographic and organic analyses have suggested that regular relations between organic geochemical maturity/oxidation parameters and Cu ores exist on the deposit-scale. A similar degree of oxidation to that of ore-proximal Kupferschiefer is noted for White Pine Mine OM by comparison to the data of Bechtel *et al.* (2000) from the Kupferschiefer. At White Pine, the OM in and near to the 5 m-thick ore zone is strongly oxidized according to RE data; this material has not followed the normal maturation trend expected for lacustrine or shallow marine restricted basin OM (Sutton *et al.*, 2013). Still, no conclusive regional-scale thermochemical alteration pattern has been firmly established for the Nonesuch Formation like the correlations between RE/GC-MS parameters and Cu enrichment shown by Bechtel *et al.* (2000). Ore fluid conduits and pathways for the Nonesuch Formation are not well constrained, neither broadly nor at individual deposits (cf. Ilchik *et al.,* 1986).

Bulk parameters and petrographic indicators of organic matter content in the Nonesuch Formation appear to indicate that organic matter and petroleum served as direct, or very nearly direct, reductants. Copper-rich beds at White Pine (up to 1-4% Cu) are mainly of well-laminated, dark gray to black, organic-rich shale; oxidized strata contain up to 1% Cu, often less than 0.05%, while the richest ores are in the darker gray units (Mauk *et al.*, 1991; Misra, 2000). At Copperwood too, there is an overall negative correlation with the level of host rock oxidation in the lower Cu bearing sequence and the abundance of chalcocite (Sirois, 2015). These relationships hint that OM throughout the Nonesuch Formation served as a reducing agent during Cu mineralization (Ho and Mauk, 1996). However, redox reactions in ore deposition may have locally conserved $C_{org}$ because the TOC values of mineralized and unmineralized samples are similar (Ho and Mauk, 1996).

Some evidence suggests that mixing of the oxic cupriferous brine with reduced pore fluids from the lower carbonaceous siltstones of the Nonesuch Formation occurred in the several meters just beneath the lithostratigraphic boundary with the Copper Harbor Formation. At White Pine, most of the "lower sandstone"/uppermost Copper Harbor Formation material is not visibly altered in hand sample, a coarse- to fine-grained red sandstone, but in places has been "bleached" to a gray or greenish gray; many White Pine Mine drill core logs record this "gray sandstone" just below the main ore horizon. Most of the gray sandstone is unmineralized, but in places, the "bleached" sandstone hosts rich disseminations of native Cu as well as chlorite and pyrobitumen cements (Butler and Burbank, 1929 and Mauk *et al.*, 1991). Very little calcite cement remains in these samples, but in its place as a cement is a black pitchy HC which is up to 2% of the rock's constituents (Butler and Burbank, 1929). The "bleached" rock's greenish coloration occurs due to chlorite fringes about sand grains and the former reddish ferric oxides are absent, having apparently been reduced to ferrous oxide, which may in part have gone into chlorite (Butler and Burbank, 1929).

Rock-Eval pyrolyses of mineralized Nonesuch Formation samples have not generally been informative for provenance studies because of their low OM content and their significant progress down maturation curves. For example, Ho *et al.* (1989) identified two Cu mineralized samples each with low HI and OI (70 mg HC/g TOC and 40-50 mg $CO_2$/g TOC) that they interpreted as typical of thermally degraded OM in which source distinctions have been destroyed.

Bitumens from both mineralized and unmineralized lower Nonesuch Formation at White Pine show gas chromatograms in which the *n*-alkanes are depleted relative to other Proterozoic bitumens (Ho and Mauk, 1996). This suggests that thermal maturation of the Nonesuch Formation at White Pine coincided with hydrothermal ore emplacement. In this respect, it is significant that pristane/*n*-C17 and phytane/*n*-C18 ratios are lower in mineralized than unmineralized samples (Ho and Mauk, 1996). As compared to mineralized strata, extractable OM from unmineralized White Pine Mine strata showed higher ratios of pristane/phytane, more pronounced odd C preference and *n*-alkanes of higher $C_n$ (Hieshima and Pratt, 1991). Lower EOM yields are reported for the mineralized White Pine Mine samples (Hieshima and Pratt, 1991).

### *3.8 Water-Washing and the Nonesuch Formation's Organic Geochemistry at White Pine*

Significant degradation of bitumen in both mineralized and unmineralized samples of the lower Nonesuch Formation is reported, which may be attributed to either regional-scale water washing or biodegradation (Ho and Mauk, 1996.) The solubility of a given $C_n$ compound decreases in the following order: aromatics > cycloalkanes > normal alkanes (Engel and Macko, 1993). The $C_1$-$C_{17}$ fraction of the White Pine inclusion oils shows extensive but variable depletion of normal, branched, cyclic, and aromatic HCs; these patterns are consistent with water-washing as the dominant form of alteration of White Pine inclusion oils (Mauk and Burruss, 2002). This observation led Mauk and Burruss, (2002) to estimate levels of depletion (relative to a least-depleted sample) of both isoprenoids $C_{13}$-$C_{20}$ and *n*-alkanes $C_6$-$C_{17}$ for oils from vein inclusions at White Pine. That study concluded that the strata at White Pine experienced water:oil ratios ranging from 200:1 to "very much greater" than 9000:1. This range of values is significantly elevated relative to water:oil ratios (110±40) typically estimated for petroleum-producing sedimentary basins (Ballentine *et al.*, 1996). The extremely high water:petroleum ratios align with reports of water-washing of petroleum at other hydrothermal ore deposits and at oceanic spreading centers (Disnar and Heroux, 1995; Simoneit and Fetzer, 1995). The hydrothermal genesis of ore at White Pine Mine means that high water:oil ratios are not unexpected. Certainly it is reasonable to expect that unaltered rocks in sedimentary basins have experienced a lesser degree of aqueous through-flow than rocks in hydrothermal ore deposits (Criss and Taylor, 1986).

## *4. Methods*

### *4.1 Thin Section Microscopy*

Singly polished ultra-thin (20 micron) sections of field and core samples prepared by Leek Petrographics of Denver were integral for determining the nature and content of organic, Cu, and carbonate materials. Samples were examined by transmitted and reflected light microscopy on a Leica DM2500P microscope and hand sample examination on a Leica MZ16 microscope at CSU.

Other workers have reported kerogen color of a given sample as the "lightest" (tending toward yellow) repeatedly observable color for each specimen (cf. Hayes *et al.*, 1983). In this work, kerogen color is reported as the median of the observed color extrema for each observed organic morphology. Thermal Alteration Index (TAI) colors and values are after those by Jones and Edison (1978). This index is aligned with the Rock-Eval II parameters in Mastalerz *et al.* (2016). See Figure 36.

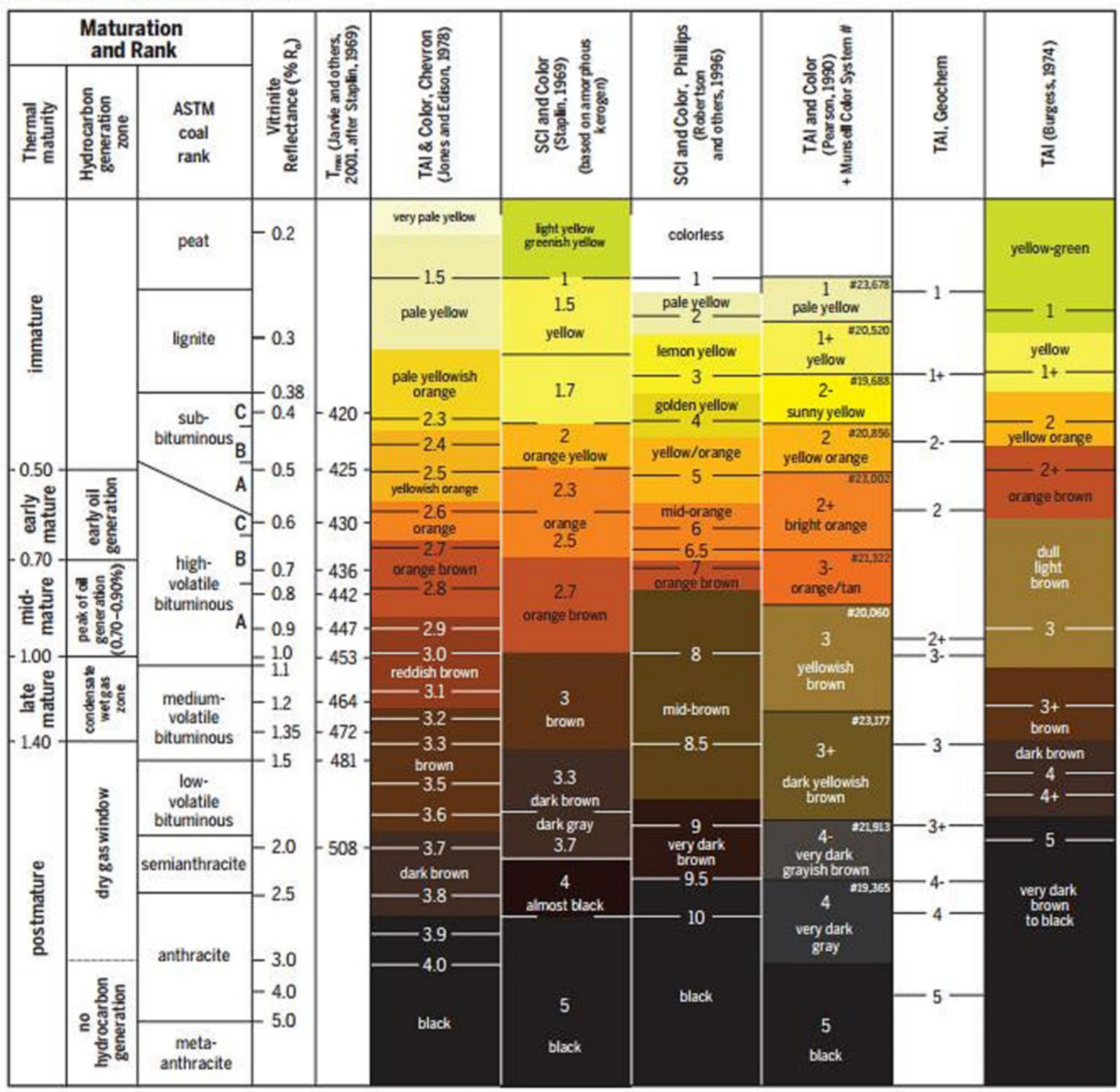

Figure 36: Selected TAI and spore color index scales and their approximate correspondence to the vitrinite reflectance and $T_{max}$ values. From Mastalerz *et al*., 2016.

### *4.2 Rock-Eval II Pyrolysis*

Rock-Eval II pyrolysis selectively quantifies and characterizes bitumen and kerogen in a given HC source rock sample. The technique utilizes flame-ionization detection (FID) to measure the concentration of organic species in the gas stream generated during each period of oven step heating. This gives a quantitative measure of each group of components. Pyrograms, cross-plots of time and FID response are used to depict the results of RE analyses, as in Figure

12 (Tissot and Welte, 1984). Weatherford Geochemical Service Group in Shenandoah, Texas performed the RE and LECO TOC analyses for this study.

Samples for RE II analyses are ground and sieved through a -60 mesh (250 micron) screen. After grinding, 2 grams of sample material is loaded into a metal crucible. The sample is then placed in an electric oven that has been previously cleaned of potential contaminants. The sample is then step-heated in an inert (He) atmosphere. The sample is held isothermally at 300° C for three minutes. Volatiles are removed from the oven and conveyed to the FID in a $N_2$ gas stream, which prevents the sample from combusting. Free HCs (oil and gas already in the rock) volatilized during the first step comprise the $S_1$ peak, reported in milligrams HC per gram of rock. This is represented graphically as the area beneath the peak $S_1$ in Figure 12. Note that non-indigenous HCs introduced by migration or contaminations by drilling fluids are included in the $S_1$ peak, if they are present.

Temperature is then increased to 550° C at a rate of 25° C/min and the $S_2$ and $S_3$ peaks are measured from the pyrolitic degradation of kerogen in the sample. Nonvolatile HCs thermally cracked and volatilized in this second step, as well as heavy HCs (greater than $C_{40}$) released here comprise the $S_2$ peak (Hunt, 1995). The $S_2$ peak is used to determine the HI and the $T_{max}$ value, the temperature at which $S_2$ yield is at a maximum. $T_{max}$ depends on the maturity and original nature of the kerogen. The HI is the ratio of the amount of petroleum generated ($S_2$) to the total content of organic material (TOC) of the sample ($100xS_2/TOC = HI$; Hunt, 1995). The production index (PI) is the ratio $S_1/(S_1+S_2)$.

The $CO_2$ released from kerogen cracking in the 300°-390° C range is separated from the HCs and stored until heating is completed. The O content of the kerogen controls the quantity of $CO_2$ that is formed. This $CO_2$ is then released and a thermal conductivity detector measures its abundance in the known volume of gas. This gives the $S_3$ peak, in milligrams of $CO_2$ per gram of rock. The ratio between the quantity of $CO_2$ formed by pyrolysis ($S_3$) and TOC is the oxygen index (OI = 100x$S_3$/TOC).

At the start of each analytical session a known, well-categorized source rock standard sample (of Mancos shale) is pyrolyzed; standards are analyzed every six samples to ensure proper instrument calibration and function. Variability in analytical results on the standard are acceptable if within a narrow range (+/- 3° C for $T_{max}$ values for example; Weatherford Geochemical Services Pamphlet).

### *4.2.1 Total Organic Carbon Analysis*

The LECO method of analysis determined the TOC of samples in this study. This process measures the TOC value by combusting the $C_{org}$ present and measuring the $CO_2$ produced on a LECO 600 C analyzer. Ground rock samples 0.1 grams in mass were treated in concentrated HCl for a minimum of two hours to remove carbonates. Samples were separated from acid by filtration and then dried at 110° C in a LECO crucible for at least an hour. The LECO 600 operates with detection limits to 0.01 weight percent $CO_2$ (Weatherford Geochemical Services Pamphlet).

The amount of $CO_2$ generated on heating is proportional to the amount of $C_{org}$ (TOC) of the sample. The LECO method for TOC determination does not include measurement of low molecular weight bitumen present in the sample. Such pre-existing short-chain HCs would be volatilized during drying, and thus the LECO TOC value may underestimate the true TOC, relative to other techniques (Peters, 1986).

### *4.2.2 Rock-Eval and LECO TOC Inaccuracies and Thresholds for Reliability*

Rock-Eval and LECO TOC parameters are at best imperfect: Snowdon (1995) showed that localized depression of $T_{max}$ values is commonly coincident with high gamma-ray log signature and elevated HI and TOC. The presence of S-rich (and thus thermally labile) kerogen might be responsible for some instances of $T_{max}$ depression. Other inaccuracies may be attributed to mineral matrix composition: rock components may either retain HC compounds, generally lowering $S_1$ or $S_2$ peaks while increasing $T_{max}$, or liberating inorganic $CO_2$ and increasing $S_3$ and OI (Fowler *et al.*, 2014). The presence of inorganic $CO_2$ generated during pyrolysis (by incomplete HCl carbonate leaching or by $CO_2$ released from clay minerals) may generate erroneous, inflated TOC values (Hunt, 1995).

Jiang *et al.* (2016) demonstrate a total loss of free HCs below $C_{10}$ in less than 24 hours when powdered, low TOC samples were exposed to open air. This resulted in a 38% decrease in the $S_1$ peak. Similarly, they demonstrate a 29% decrease in the $S_1$ peak when powdered samples were stored in sealed containers for 7 days prior to RE. In their study, volatile losses occurred at much slower rates for higher (above 11%) TOC samples. This supports at least partial control on $S_1$ depression by adsorption/desorption of light (sub-$C_{10}$) HCs on *in-situ* OM and mineral matrix.

Rock-Eval and TOC parameters are thus reliable only above threshold TOC, $S_1$ and $S_2$ values. Mineral matrix effects are important if TOC, $S_1$ and $S_2$ are low, but are not significant where samples have TOC greater than 5%. Other workers report different threshold values: a decrease in the HI due to mineral matrix effects must be taken into account for samples with TOC less than 1.5% (Peters, 1996). Oxygen index has questionable significance if TOC is less than or equal to 0.5% (Sykes and Snowdon, 2002).

$T_{max}$ values for samples with $S_2$ peaks less than 0.5 mg HC/g rock are often inaccurate - such $T_{max}$ values are unreliable unless a distinct, definitive kerogen peak is noted on the pyrogram (Weatherford Geochemical Services Pamphlet). Sykes and Snowdon (2002) suggest 0.2 mg HC/g rock as the $S_2$ value below which $T_{max}$ values are unreliable.

### *4.3 Light Stable Isotope Principles, Fractionation and the Delta Notation*

Most elements consist of more than one stable isotope. These various isotopes of an element have slightly different chemical and physical properties because of their mass differences - the lighter isotopes move faster and form weaker bonds (Rollinson, 1994). Chemical reactions may thus measurably change these isotopic ratios by fractionation. Thus the isotopic ratios of diagenetic minerals may give evidence of prevailing conditions during their genesis (Longstaffe and Ayalon, 1988). Various isotope standards (defined as 0‰) are used for reporting isotopic compositions. Carbon and oxygen stable isotope ratios in this study are reported relative to the VPDB, or Vienna Pee Dee Formation Belemnite standard. The origin and nature of $C_{carb}$ in the Nonesuch Formation is explored by the stable isotopic ratios of C and O ($\delta^{13}C$ and $\delta^{18}O$, respectively). The stable isotopic notation and principles are described by Sharpe (2007), Kreulen (1988), Andres and Fallick (1986) and others.

### *4.3.1 Carbonate Stable Isotope Ratio Determination*

Carbonate laminite and vein samples were extracted from hand specimens using a 0.9 mm diamond-bit microdrill at CSU. Sample weights of 20-100 mg were soaked for three hours in 10% hydrogen peroxide to oxidize and release $C_{org}$. They were then rinsed with deionized water and dried under heat lamp.

The University of New Mexico CSI lab analyzed the carbonate samples by the method described by Spotl and Vennemann (2003). The samples were loaded in 12 mL borosilicate exetainers, at which time the exetainers were flushed with He and the samples were reacted for 12 hours with $H_3PO_4$ at 50° C. The evolved $CO_2$ was measured by continuous flow Isotope Ratio Mass Spectrometer using a Gasbench device coupled to a Thermo Fisher Scientific Delta V Plus Isotope Ratio Mass Spectrometer. Reproducibility was better than 0.1‰ for both $\delta^{13}C$ and $\delta^{18}O$

(both VPDB) based on repeats of a laboratory standard (Carrara Marble). The laboratory standard was calibrated versus NBS 19, for which the $\delta^{13}C$ is 1.95‰ and $\delta^{18}O$ is 2.2‰.

### *4.4 Soxhlet, Gas Chromatography and Mass Spectroscopy*

Organic extraction and molecular analyses ("biomarker analysis") for this study were performed by Weatherford Geochemical Service Group in Shenandoah, Texas, and the overview of analytical conditions and procedures comes from their Geochemical Services Pamphlet. Organic extractions utilized 5 grams of sample pulp (ground to -60 mesh) that was placed in a cellulose Soxhlet thimble and then extracted with dichloromethane using Soxhlet apparatus; this method obtained total HC extracts of 9 samples. Both Soxhlet thimble and apparatus are run through the extraction process prior to sample addition to minimize likelihood of extract contamination. Freshly activated Cu metal is added at the start of the extraction process to ensure removal of any elemental S that might be extracted with the bitumen. Extraction continues until no additional color is observed leaching from the sample (usually 12-20 hours). At this point the extract is collected, filtered through a Whatman #40 filter paper. Solvent is then carefully evaporated from the filtrate and the EOM yield obtained by transferring it to a pre-massed sample vial. Each total extract was split into two aliquots; the first was stored for total extract analysis and gravimetric yield determination.

Nine samples from four profiles over 20 km of strike extent (BIR, cores WPB-1, 517 and 523) from the Iron River syncline and WP mine areas were analyzed by GC and GC-MS. All profiles are marked by Cu mineralization at the base of the Nonesuch Formation. The samples are from about 3 to 25 m above the base of the Nonesuch Formation and collectively straddle the mineralized/barren fringe so that they are variably in or above ore zones, or in and above sub-ore concentrations of Cu at the base of the Nonesuch Formation.

Biomarker analysis samples were selected on the basis of requirements for reliable data of TOC greater than 0.2% and higher $S_1$ and $S_2$ production during RE pyrolysis. The requirements dictated that OI ranged from 10-60 and samples with OI greater than 75 were not analyzed. The limited size and organic leanness of the samples meant that GC and GC-MS data was obtainable only for the saturated and aromatic fractions of the whole rock extracts, and not for the resins, polar and NSO components.

### *4.4.1 Extract Gas Chromatography*

This study's column chromatography was done by injection of a 0.1 - 1.0 µL sample from the second aliquots into a split/split-less port of an Agilent 6890N GC held at a temperature of 275° C. From there the sample passes through a 60 m x 0.25 mm Agilent DB-1 column using a constant pressure of He as the carrier gas. The column oven is programmed to hold at 30° C for 5 minutes but then to increase to 320° C at 3° C/minute at which point it is held at this final temperature for 20 minutes. Components eluting the column are detected using an FID held at 350° C. The addition of an internal standard prior to injection allows these components to be identified. Under these conditions, compounds from $n$-$C_4$ to $n$-$C_{42}$ are observed, with *n*-alkanes, key isoprenoids and key aromatic compounds reported. Extract standards are run periodically to check retention times and other chromatographic performance criteria (Weatherford Geochemical Services, 2000).

### *4.4.2 Gas Chromatography-Mass Spectrometry Principles and Analysis*

Two analytical tools - gas chromatography (GC) and mass spectrometry (MS) - can be combined into a single instrument (GC-MS) to analyze mixtures of compounds. The GC separates the mixture and the MS records the masses of components eluted at different times. The GC-MS records mass fraction gas chromatograms for the mixture, which plot the amount of each component versus its retention time (time required to travel through the column, or elute).

Each component of the mixture is characterized by its retention time in the gas chromatogram and the mass of its molecular ion and fragments thereof.

Prior to GC-MS analysis, the saturate and aromatic components are separated by medium pressure liquid chromatography, to avoid possible interferences. Both saturate and aromatic fractions are examined using an HP 6890 GC equipped with an HP 7683 auto-sampler, on-column injector and the HP 5973 mass selective detector.

The saturates are separated using a 60 m DB-5 column using a column oven program that starts at 100° C and ends at 320° C with a total run time of 118.5 minutes. The aromatics are separated using a 60 m DB-1 column using a column oven program that starts at 70° C and ends at 315° C with a total run time of 131.33 minutes. Helium is used as the carrier gas. Both saturate and aromatic GC runs use the on-column injection technique with the injector temperature programmed at 3° C above that of the column oven. The MSD is operated in the selected ion mode (SIM).

For saturate biomarker analysis, ions are collected in two time windows; window 1 covers from 5-30.00 minutes; window 2 extends from 30.00-118.5 minutes. The dwell time is set to 20 milliseconds for each mass in both windows. For aromatic biomarker analysis, ions are collected in two time windows; window 1 extends from 5-77.8 minutes; window 2 extends from 77.8-131.33 minutes. Again, both windows are set to 20 milliseconds dwell time for each mass. The components are quantified relative to an internal standard that is added to the fraction after the liquid chromatographic separation (Weatherford Geochemical Services Pamphlet).

Weatherford identified the majority of peaks for both aromatic and saturated fraction GC-MS chromatograms. However, a significant proportion of the dominant peaks on the aromatic TIC and on the "biomarker" high *m/z* fragmentograms were left unidentified in the Weatherford analysis.  In the absence of authentic chemical reference standards analyzed under the same GC-MS conditions, certainty of identification is not total.  The majority of the peaks unidentified by Weatherford were thus tentatively identified by the author at CSU by manual comparison of a given chromatogram or mass spectrum with chromatograms and mass spectra available in the U.S. National Library of Medicine’s Pubchem.gov Open Chemistry Database.  Additionally, tentative compound identification was based on comparison of the mass spectra and relative retention times of the unknown peaks to chromatograms in the broad array of GC-MS literature. The mass spectra were used specifically to differentiate between suspected components by their distinct fragmentation patterns.

### 5. Sampling

Outcrop and core sampling of the Nonesuch Formation yielded 76 samples for pyrolytic analysis, 74 of which were thin-sectioned and polished for petrographic microscopy; 32 of these samples were also analyzed for stable isotopic ratios, and 9 for biomarkers by GC-MS. See Appendix A: Samples Collected.

The samples give a roughly 100 km near-linear WSW-ENE span of 11 stratigraphic transects. The transects cover an average of 96 m, ranging from 60 to 200 m, covering 30-100% of the Nonesuch Formation thickness at a given site. An overview map is shown in Figure 37. Imbus' (1990) samples cover a significantly larger spatial spread than do the samples in this study. Imbus included four samples in the 100 km to the west of this study's westernmost site (Copper Falls, Mellen, Wisconsin), and one sample from the easternmost Nonesuch Formation outcrop, near Houghton, Michigan some 80 km northeast of this study's easternmost sample site. Hegarty *et al.* (2007) examined the organic maturity of Nonesuch Formation equivalents as far west as Iowa; the Uchytil, *et al.* (1997) traverse covers 240 km west-southwest from Houghton, Michigan into northwest Wisconsin. Pratt, *et al.* (1991) analyzed samples from White Pine, Michigan into northern Wisconsin, with about 60 samples from Bear Creek Company Cu exploration cores. Li *et al.* (1995) sampled between White Pine and Houghton, Michigan in their SEM investigation of clay-Cu relationships; likewise, Ho and Mauk (1996) sampled from Presque Isle syncline to Houghton. Other previous studies cover a lesser geographic extent than do those of this study, being limited mainly to White Pine Mine proper (Kelly and Nishioka, 1985; Ho *et al.*, 1989; Mauk and Hieshima, 1992; Mauk and Burruss, 2002; Fourgani, 2012; Sutton *et al.*, 2013).

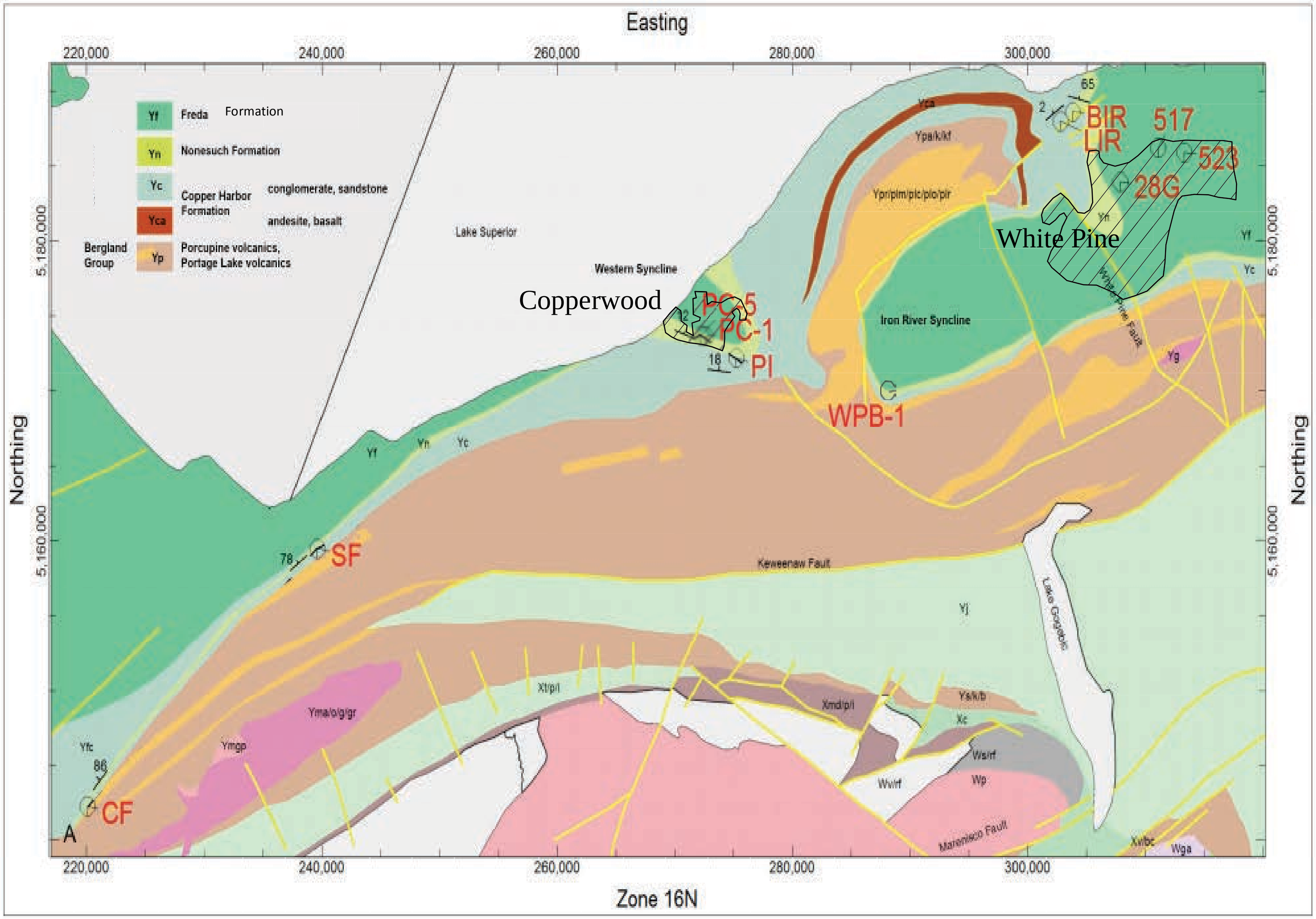

Figure 37: The sampling traverse, a roughly 100 km near-linear WSW-ENE span of 11 stratigraphic transects, each covering much or all of the Nonesuch Formation section. Sampling sites are labeled in red lettering.

### *5.1 Core Samples*

Extensive diamond drill core exploration for SSC deposits in the Michigan Upper Peninsula produced hundreds of meters of Nonesuch Formation core material during the late 1950s and early 1960s. Further drilling in the mid-1990s and early 2000s produced still more core. Much of this material has been transferred from industry to public curation by organizations including the Michigan Department of Environmental Quality (MDEQ) and Michigan Technical University (MTU). Core samples in this study come from drillholes WPB-1, PC-1, PC-5, 517, 523 and 28G, as shown in overview map.

#### *5.1.1 Michigan Department of Environmental Quality Core Samples*

The author visited the MDEQ geologic core repository at Marquette, MI in April 2015. The MDEQ core facility is not climate-controlled and appears to sometimes permit outside precipitation/moisture into the core storage bays.

All of the cores in this study had previously been sampled extensively, and not much material remained in the potential ore zone at the lowest 5 m of the cores. The Nonesuch Formation is generally fairly well-indurated but in many dark gray, fine-grained silty to shaley sections, the core had fallen apart and consisted of jumbled chunks of indeterminate original position in the core. These disintegrated zones were not sampled in this study. This, coupled with previous sampling, and the MDEQ mandate to retain at least 1/2 of the core material for a given segment, commonly precluded sampling the darkest gray organic-rich zones in the lower Nonesuch Formation.

Core sample candidates were identified first with preference for visually apparent organic richness. The intact (not disaggregated) darkest gray, most organic-rich samples were then selected for a spacing giving greatest focus on the lowest 10 m of the Nonesuch Formation. Samples of about 20 g each were selected. Some of these came as pre-cut 1/4 vertical splits, some as 1/2, and others as whole core for splitting at CSU.

Two days of sampling from five diamond drill cores netted 37 segments. The PC boreholes were drilled in 1959 and the WPB-1 borehole in 1961. The 517 and 523 boreholes were both drilled in 1995 and are 27 mm diameter core. The PC boreholes and the WPB-1 borehole are 47.6 mm diameter core.

#### *5.1.2 MTU Core Samples*

Colbert (2011) sampled 47.6 mm diameter core material from borehole 28G, housed at the MTU repository in Houghton, MI. Borehole 28G was drilled in 1983 in the White Pine Mine vicinity. Colbert's sample spacing gives greatest resolution in the lowest 10 m of the Nonesuch Formation in borehole 28G. The author selected a subset of Colbert's 28G borehole samples on the basis of visually apparent organic richness.

### *5.2 Outcrop Samples*

Outcrops of the Nonesuch Formation occur in riverbeds and banks in the western Upper Peninsula of Michigan. Samples from five of the most complete sections were analyzed for this survey. These sites are river-incised canyons and gorges with extensive vegetative cover, commonly showing relatively discontinuous and often diminutive bedrock outcroppings. (Figures 38, 39, 40).


Figure 38: The Saxon Falls, MI, sample site.  Note line of bedding strike expressed as river-spanning riffle. Nonesuch Formation crops out at right.

Figure 39: Saxon Falls, Montreal River, MI sample site:Top of Copper Harbor Conglomerate behind hammer, Nonesuch Formation base closer to point of view. Notice the strong positive outcropping habit of the Copper Harbor Conglomerate relative to the weak topographic expression of the finer-grained Nonesuch Formation.

Figure 40: Fractured fissile shaley siltstone at Copper Falls, Bad River, WI. The majority of samples from this site were too broken to collect as singular specimens.

The riverside position and common, sometimes pervasive, fracturing in these locations present some possibility of geologically recent, shallow oxidation of OM, especially given the relatively high dissolved O contents of such perennially cool (temperature) river waters (USGS National Water Information System). As such, samples ideally originated more than 5 cm distant from fractures, but this criterion - to minimize the likelihood and potential extent of recent OM oxidation - was not met for the majority of the rocks collected by the author. Samples were collected as high above apparent peak river level as possible, and were generally collected between 1 and 2.5 m above river. Most outcrop pyrolysis samples in this study (27 of 41) were collected by the author during fieldwork in September 2015; the balance come from material collected by Sarah Colbert in 2010 and stored at CSU. Weathered surfaces were avoided in sample collection in the interest of minimizing shallow, recent oxidation. Visibly weathered surfaces were cut or ground off prior to RE, LECO, and GC/GC-MS analyses in the interest of minimizing inclusion of OM that may have undergone recent or shallow oxidation by weathering processes.

### *5.2.1 Copper Falls, Potato Creek, Saxon Falls, and Presque Isle River Outcrop Samples*

Three out of four field sites visited by the author were sampled with particular attention to visually apparent organic richness, presence/absence of secondary Cu minerals, calcite veining, sedimentary texture and near-surface oxidation. Samples were taken from intervals of the darkest color, finest grain size and as far from fractures and flowing water as possible. Samples for which these conditions are not met may give unreliable pyrolysis and GC-MS data and are noted as such in the analysis and discussion.

Irregular outcroppings, interbedded discontinuous lenses of redbed conglomeratic sandstone material with shaley siltstone and inaccuracies in previous maps complicated the identification of the Nonesuch Formation-Copper Harbor Formation contact. Nonetheless, each sample has been assigned a quantitative height above the base of the Nonesuch Formation, as defined by White (1971). Surface estimation of the distance up-section from the base of the Nonesuch Formation to each sample site was corrected for structural dip and for deviation from perpendicular surface transit. One site, Potato Creek, showed very extensive (60 m high) outcrops of a near homogeneous, coarse-grained crossbedded redbed sandstone that occupied the location previously mapped as Nonesuch Formation (cf. Cannon *et al.*, 1996). The section at Potato Creek was not sampled.

At the three sections sampled by the author, interbedded red sandstone and gray shale are prominent in the lowest 10 m of the Nonesuch Formation. Well-cemented medium-grained conglomeratic red sandstone episodically recurs in 1-3 m thick beds, diminishing in abundance up-section. The sandstone interbeds were typically separated by 1-4 m of finer-grained shaley dark gray to gray siltstone.

At Copper Falls State Park, the Nonesuch Formation is intermittently exposed on both sides of the Bad River. Strata strike averages 240°, 80° N at Copper Falls. See Figure 41. There the Proterozoic sediments are incised to form cliffs and the outcrops range from river level to many tens of meters above river level. The Nonesuch Formation is very pervasively fractured and commonly fissile at river level at Copper Falls. Root penetration and water-wet sample surfaces were common for most samples at Copper Falls. Sampling was restricted to less than 7 m above river level. Some samples are pervasively fractured (as in Figure 42) but still included for more complete coverage. Samples from the north side of the river are suffixed A while south side samples are suffixed B (as in Figure 41).

Figure 41: Sample locations at Copper Falls, Bad River, WI.

**IMAGE**

Figure 42: Pervasive fracture and root penetration of outcrops at Copper Falls was more prevalent than at Saxon Falls or Presque Isle River sample sites.

The Saxon Falls, MI section - on the east side of the Montreal River - exposes almost the entire extent of the Nonesuch Formation at river level and in places along the rim of the river gorge, 33 m above river level. Two sampling transects of the exposed Nonesuch Formation were taken there, one near river level and one at the rim (Figure 43). Strata strike dip roughly 240°, 80° N at Saxon Falls. Samples from the rim are suffixed A while those from the lower exposure are suffixed B. These two separate collections are combined in the data analysis. River-level samples commonly showed pervasive fracturing perpendicular to bedding. About one third of the river-level Saxon Falls samples showed thin faintly iridescent blue veneers on weathered surfaces, interpreted to be secondary Cu minerals, eg: azurite or covellite; it is possible that this veneer is actually an Mn oxide such as pyrolusite. As shown in Figures 44 and 45, rounded, discrete biscuit-like weathering geometries at the base of conglomeratic sandstone incursions were present. No infilling material was present between the positive relief structures, which are taken by the author to represent casts of dessication cracks; this is interpreted to support a lacustrine, rather than marine, environment of deposition.

Figure 43: Sample locations at Saxon Falls, Montreal River, MI.

Figure 44: Biscuit-shaped positive relief structures at 104 m above Nonesuch Formation base, Saxon Falls, MI. Right side is down-section in this image.

Figure 45: At left, notice the semi-polygonal, rounded biscuit-like positive relief structures on underside of a coarser-grained (lithologically very similar to Copper Harbor Conglomerate material) incursion at Saxon Falls. Down-section is to the right side of the image. Site is 77 m above Nonesuch Formation base. Therse are provisionally interpreted as the underside of desiccated mud as interpreted by the author on the basis of their continuous network. It is also possible that they result from a post-lithification structural disturbance.

The Nonesuch Formation is almost entirely exposed at Presque Isle River site, mostly less than 5 m above river level, and on both sides of the river. Strata strike ~280°, 20° N at the Presque Isle River site (Figure 46). Most samples come from the east side of the river, and not more than 5 m distal to the river. Minor, very small HC seeps were intermittently apparent in eddies near the riverbanks at this site. Secondary Cu minerals - especially malachite - were apparent as mottled crustiform coatings at the majority of sampling locations at Presque Isle River within 30 m of Nonesuch Formation base. See Figure 47. At about 15 m vertically up-section from the base of the Nonesuch Formation, and again at 26 m up-section, *ex-situ*/loose small boulders showed continuous and straight to semi-arcuate void-filling networks of material distinct from the host rock.  These blocks were too large to remove from the field.  See Figures 5, 48.  These are interpreted to be relict mud-crack infillings rather than syneresis cracks: the former suggest a lacustrine environment of deposition.  The blocks are probably close to their original stratigraphic position, as suggested by similarities in lithology to their surrounding outcrops.

Figure 46: Sample locations downstream of Lepisto Falls, Presque Isle River, MI.

Figure 47: Sample PI-7, at 15 m above Nonesuch Formation base, was collected adjacent to obvious secondary copper mineral crust.

Figure 48: Site is 15 m above Nonesuch Formation base, Presque Isle River, MI. Infilling of cracks interpreted by the author to result from desiccation of wet sediments prior to burial. Note speckled veneer of probable malachite, bottom R.

### *5.2.2 Big Iron and Little Iron River Outcrop Samples*

Colbert (2011) collected samples from stream outcrops of the Nonesuch Formation at both the Big Iron River (BIR) and the Little Iron River (LIR). Incomplete Nonesuch Formation sections are exposed at both sites. At BIR, the best outcrop expression is of the upper and middle Nonesuch Formation, at the upstream southern end of the section. Colbert gathered material at roughly regular intervals with particular attention to visible veins, secondary Cu minerals or other unusual features. Stratigraphic position of these samples was recorded in terms of surface meters downsection from the top of the Nonesuch Formation at BIR, from north to south. At LIR, samples were taken from south to north, from the Copper Harbor up section into the Nonesuch Formation. Trigonometric correction for stratal dip has been applied but the depths of these samples are best viewed in terms of their relative position rather than as absolute numerical height above the Nonesuch Formation base.

Fourteen outcrop samples in this study come from Colbert's material. The author selected for outcrop samples from the Colbert study on the basis of visually apparent organic richness and to minimize the presence of fractures in the hand samples. Some samples are pervasively fractured but still included in the interest of maximum spatial resolution of sampling.

## *6. Results*

### *6.1 Petrography of Organic Matter, Copper, and Calcite*

Organic matter is present in 87% of thin sections in one or both of two distinct morphologies. Amorphous translucent isotropic material (AOM) in laminar masses of yellow and orange to dark brown coloration is commonly found in association with a more discrete filamentous organic matter (FOM; 67% of AOM co-occurs with FOM, and vice versa). The FOM is typically black, opaque material that presents as both singular wisps and continuous wavy agglomerations thereof; the FOM resembles inertinized alginite of Teichmüller (1982). Less than 10% of the FOM is translucent and lighter colored (ranging to orange in one instance, in sample BIR 13), whereas the AOM is 85% translucent and generally brown to orange in color. The rare slides that show FOM without AOM show a range of FOM color, from TAI = 2.6 to 3.8 (orange to dark brown). Similarly, the small proportion (7% of total FOM) of translucent reddish brown to brown FOM (TAI = 2.9 to 3.6) is apparent in slides that also host AOM of reddish brown to brown color (TAI = 2.9 to 3.6). Thermal Alteration Index values for AOM average to 3.12 and to 3.86 for FOM. Collectively, the AOM coloration corresponds to the early mature to late mature range as in Mastalerz *et al.* (2016), and the FOM to post-mature TAI values.

Fluffy amorphinite can be compacted and pressed into wavy sheets which decrease in size with increased degradation (Teichmüller, 1982). While this might suggest the derivation of FOM by compaction and alteration of the AOM, the co-occurrence of both morphologies (and rarely, translucent FOM with AOM) in single samples, both in association and as discrete entities, argues against a genetic relation.

The AOM sometimes appears as granules with patchy extent – this is often as a partial AOM coating of quartz grains. The color of the AOM on quartz grains is excluded from consideration here as it is difficult to distinguish from other mineral veneers (especially hematite) on quartz and other translucent silicate grains.

A small minority of samples show bituminous inclusions, which are often associated with calcite veins and brecciated Nonesuch Formation hostrock. One of the bituminous inclusions is apparent as a bedding-concordant fracture filling solid with shrinkage cracks. The margins of this mass show higher reflectance than does the center and it is adjacent to several disseminated fine grained chalcocite masses.

Pyrobitumen in concentric anisotropic orange to black (PPL transmitted) mottled reflecting material is present in two heavily fractured, thickly calcite veined samples, intimately associated with chalcocite as interstitial material between detrital mineral grains. It is possible that this anisotropic orange to black material, which easily ground away during a second hand polishing with Ag tarnish compound, represents neobiogenic growths of HC oxidizing bacteria or fungi. The slide was cut in 2016, so it is most likely (to this observer) that this material is pyrobitumen (cf. Barghoorn *et al.*, 1965).

Copper minerals are present in 25% of thin sectioned samples, mostly as very fine grained subhedral angular masses of chalcocite, often showing incipient or complete replacement of pyrite grains, and to a lesser extent, of framboids. Lesser chalcopyrite (10% of thin section samples), covellite, and bornite are also present as very fine grained subhedral grains from rounded to angular, and commonly replacing pyrite.

Petrographic observation reveals three main calcite morphologies: as vein-filling material, calcite matrix cement in silt laminations, and concretionary masses contorting and sometimes cutting beds (both concordant and discordant to bedding). Calcite is also present as pervasive cement independent of clast lithology/grain size; one sample shows a localized halo of matrix calcite focused around clay-rich rip-up clasts in sandstone matrix.  While calcite occurrence is relatively common in the Nonesuch Formation, it occurs in a minority of samples and only rarely occupies an entire sample.  Appendix A gives detailed sample descriptions, hand sample images and thin section photomicrographs.

Thin (sub-mm wide) discordant or layer parallel calcite veins and rounded concretions are interpreted to be syn-diagenetic.  Concretions were present prior to matrix cementation as the grains in the shale are arranged around them but do not show clear deformation or replacement (Figure A20, A29).  Also, Cu minerals on the edges of the calcite nodules indicate that this calcite precipitated prior to Cu mineralization (Figure A30).  Mauk *et al.* (1993) made the same interpretation based on their observation of a four-fold lesser compactional deformation of individual bedding laminae within such nodules as compared to laminae immediately outside of the concretions. Vein calcite occupies brittle deformed fractures, suggesting formation later in diagenesis than the concretionary nodules.  Primary origin is possible for the layer parallel segregations (laminites) that cement detrital silt-size grains and do not disturb bedding as do the clearly diagenetic concretions.  However, Mauk *et al*. (1993) placed these laminite cements later in the diagenetic sequence based on textural observations indicating that the laminite calcite growth post-dates quartz overgrowths in the siltstones of the lower Nonesuch Formation.

The color of a given hand sample can serve as a crude proxy for the redox history of the rock: greenish hues can be caused by elevated chlorite (ferrous iron) content while red color in rocks commonly results from higher content of hematite with its ferric iron.  Sample selection favoring the darkest gray, most OM-rich samples and the general absence (or unreliable identification) of the "bleached [reduced] gray sandstone" meant that no systematic effort to qualitatively or quantitatively distinguish the hematite or chlorite contents of the rocks in this study was undertaken.

### *6.2 Rock-Eval and LECO TOC – Overall Patterns*

Overall this study shows lower TOC (ranging from 0.01 to 0.86%) than prior organic geochemical surveys of the Nonesuch Formation in this region. Hieshima *et al.* (1989) reported upper range TOC values of 0.8 to 1.2% for the Nonesuch Formation, and Imbus *et al.* (1988) reported a range of Nonesuch Formation TOC values from zero to 2.5%. Figure 49 shows TOC values of representative samples of Imbus *et al.* (1988) and representative upper-range TOC core samples and high C outcrop samples of this study. Although select high TOC values in this study are broadly similar to those previously reported for the Nonesuch Formation, many samples - mostly those collected from outcrops - are significantly lower in TOC. There are three possible explanations for this discrepancy. One explanation is that the samples in this study experienced significant oxidation of OM during extended weathering in outcrop or decades of storage without curation for OM preservation. Another possible explanation is that preferential disaggregation of organic-rich intervals led to sampling of better-indurated, less organic-rich samples. It is also possible that extensive previous sampling of high C intervals of finite core material exhausted available material for destructive analyses.

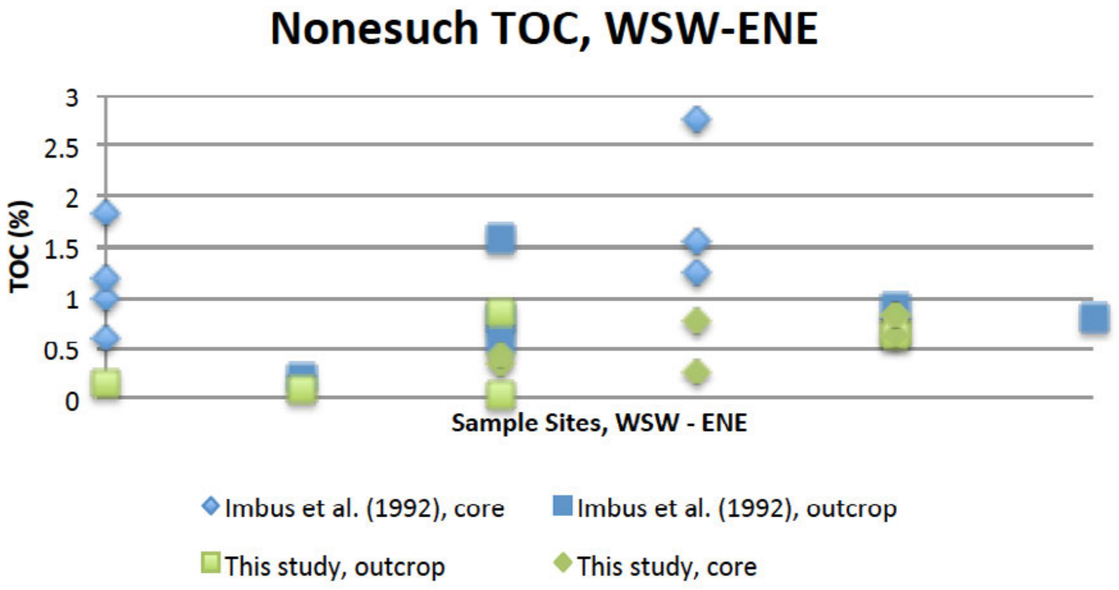

Figure 49: Representative TOC samples of Imbus *et al.* (1991) versus upper range (cores) and TOC maxima (outcrop) of this study. Samples are grouped regionally from WSW to ENE, but are not horizontally scaled.

Higher TOC values on average are found in core samples, rather than those collected from outcrop. This difference may reflect the greater ease of identifying organic-rich intervals in cores versus in outcrop, and also the non-outcropping habit of the more readily weathered organic rich portions of the Nonesuch Formation.

Average TOC for the unmineralized RE and thin section sampled subset is 0.22%, but this is higher (0.34%) when outcrop samples are excluded; unmineralized outcrop samples of this subset show average TOC of 0.11%. Mineralized core samples showed TOC similar to that of mineralized outcrop samples (0.18 and 0.19%, respectively). The HI/OI ratio of outcrop samples was smaller than that for core material in both mineralized (0.51 and 1.54, respectively) and unmineralized (0.20 and 1.91, respectively) samples. Taken together this strongly suggests that recent near-surface outcrop oxidation strongly influences organic composition.

All samples in this study had a measurable $S_1$ peak, but many lacked a clearly defined $S_2$ peak. The $S_2$ peak is absent or poorly defined in the majority of outcrop samples, and is only recorded in those samples showing TOC greater than 0.25%. All samples from the lowermost 5 m of the Nonesuch Formation have low $S_2$.

A Modified van Krevelen plot of this study's samples, Figure 50, depicts two distinct populations: a group at low OI (under 50 mg $CO_2$/g TOC) and with low to moderate HI (less than 10 to 360 mg HC/g TOC) and a scatter of samples to high OI at relatively low HI. The two populations can be discerned on the basis of TOC - all but one sample with OI greater than 75 mg/g show TOC less than 0.12%. The first group overlaps, but extends to lower HI at higher OI, the field identified by Imbus *et al*. (1991) in their regional oil and gas prospectivity study of the Nonesuch Formation (dashed line).

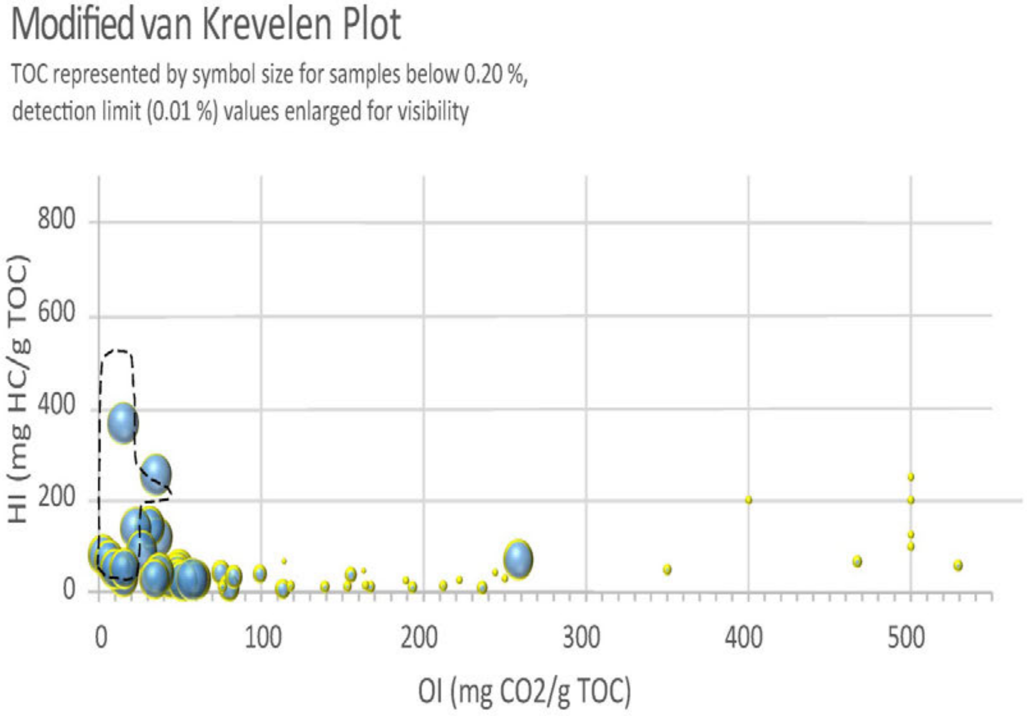

Figure 50: Modified van Krevelen plot of the organic matter in the Nonesuch Formation. The outlined field shows the range of values from a wider survey of the Nonesuch Formation by Imbus *et al.* (1991). Symbol size is scaled by TOC in order to emphasize more reliable data.

The distribution of HI with $T_{max}$ is shown in Figure 51. $T_{max}$ values below 400° C cannot be representative of kerogen transformations, and all of these data points were flagged as unreliable because of low pyrolysis yields and no clear $S_2$ peak. The low $T_{max}$ values are nearly all from samples with low TOC and low pyrolyzable yields. Samples which produced clearly quantifiable $S_2$ peaks on heating all have TOC greater than 0.35% and have $T_{max}$ dominantly in the range 430 to 440° C. In the subset of samples producing clear $S_2$ peaks there is a minor increase in $T_{max}$ with decreasing HI, which would be consistent with a range of maturity. High

$T_{max}$ outliers are both outcrop samples (BIR 13 and BIR 16) and both have unusual pyrograms with extended duration or double $S_2$ peaks suggesting the presence of unusual volatile high molecular weight HCs.

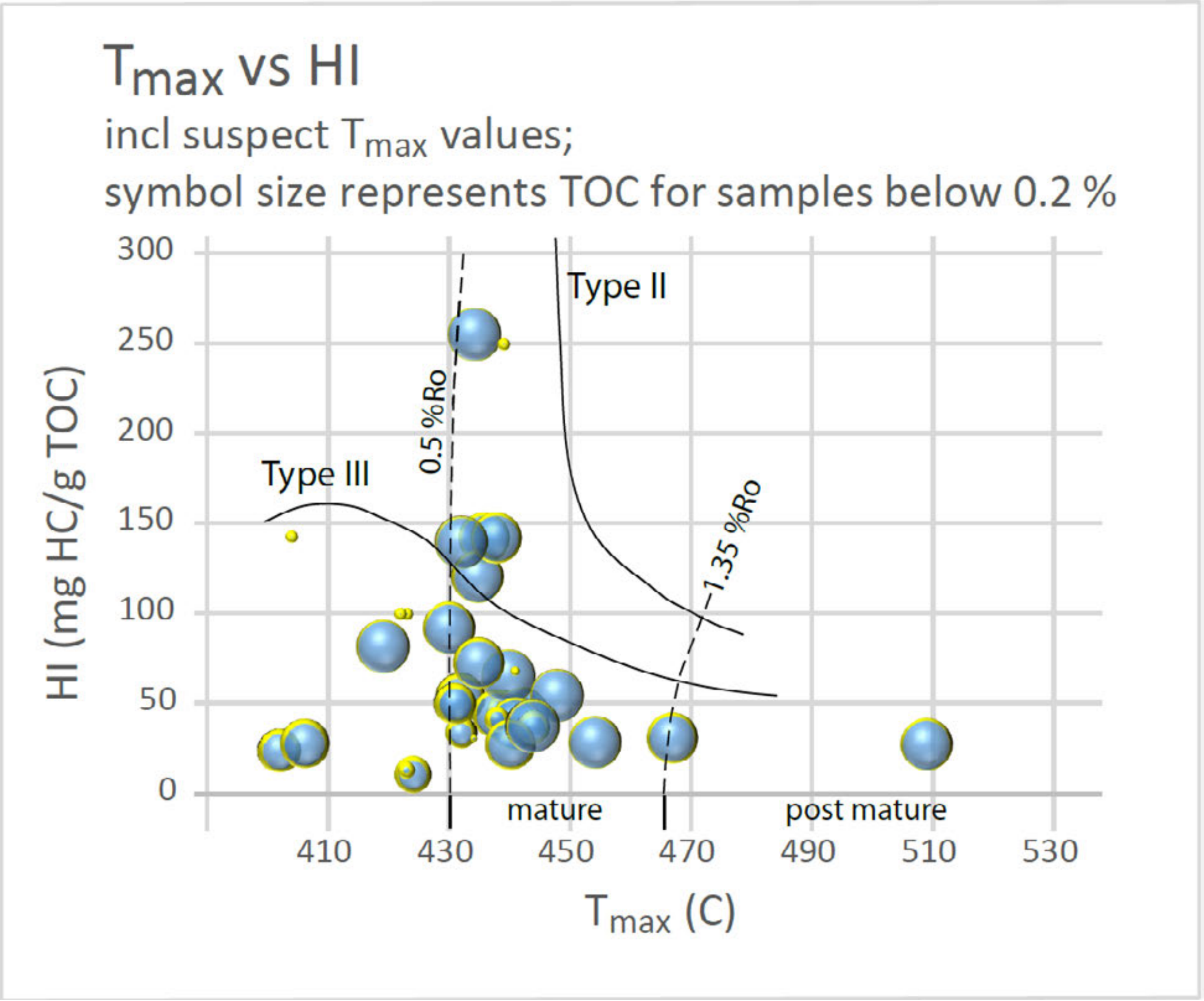

Figure 51: Temperature of maximum $S_2$ yield ($T_{max}$) versus HI for the Nonesuch Formation. The solid lines show typical evolution paths of Type I and II kerogen on maturation; the dashed lines are approximate contours of vitrinite reflectance along paths of kerogen (after Hunt, 1995). Symbol size is scaled by TOC in order to emphasize more reliable data.

The combined overall implication of the Modified van Krevelen plot and the $T_{max}$-HI plot is a Type III organic matter origin. Given the age and the high HI of a minority of samples, it is interpreted to have been Type I or II. Apparent maturities by PI and HI indices and on $T_{max}$ are mainly mature (greater than 0.15, less than 100, and greater than 435° C, respectively; cf. Peters and Cassa, 1994). These maturity indicators do show some variability from marginally immature to late-mature to slightly post-mature indications. The majority of well-characterized samples are late-mature by these measures (especially by HI). The least mature samples are those from highest in the stratigraphic section in the Western syncline (PIR samples) and Iron River syncline (WPB samples).

The observed correlation between low TOC and high OI indicates a probable preferential oxidation of OM in C-lean samples. Two possible explanations for this relationship exist: 1) Oxidation of organic matter may have been pervasive throughout the Nonesuch Formation, but its extent was buffered in organic-rich samples, or 2) At least some samples of low TOC were originally richer but now are lean because they are strongly oxidized. The timing and extent of oxidation is not clear. The low TOC and high OI of the broadly fractured sample groups from the stream outcrop profiles at CF, SF and most from PI sections are interpreted to result at least in part from recent weathering in the wet climate.

There is generally a negative correlation between $T_{max}$ and HI, and for HI versus OI, but the scatter is relatively wide in both Figure 50 and 51. It is notable that the overall negative sloping HI versus OI trend is steeper for mineralized than for unmineralized samples. Organic C content is uniformly very low in the FOM-only samples, which average to less than 0.1% TOC (these fall into the zone of inertinite on the modified van Krevelen plot). In contrast, the AOM-only samples are C-rich by comparison (average 0.46%). The AOM-only samples show up as a mixture of Type II-III and Type IV OM on modified van Krevelen plots, with slightly greater prevalence of more H-rich Type II-III material present. The AOM-only $T_{max}$ values are generally in the 435-450° C range, while the FOM-only samples' $T_{max}$ values are unreliable because of low $S_2$ response.

Excluding the lowest TOC (less than 0.15%) and highest OI (greater than 100 mg/g) samples reveals regional and vertical patterns in the HI, and to a lesser degree, OI, value distributions. All of the highest HI samples are from the middle and upper levels of the Nonesuch Formation in the Western syncline (samples PIR) and the Iron River syncline (WPB samples). If one further excludes the lone sample collected from greater than 104 m above the Formation base, core profiles show a gradient of increasing HI, and a trend of diminishing OI with stratigraphic height (Figures 52 and 53). Similarly, these core profiles show an overall positive correlation between HI/OI ratio and stratigraphic height (Figure 54).

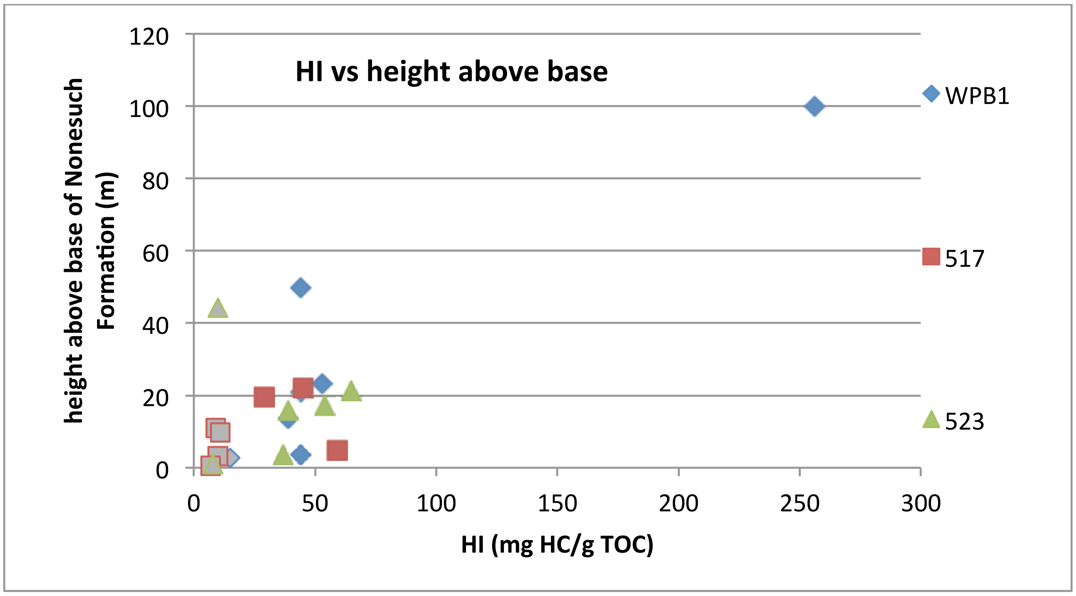

Figure 52: Hydrogen index in samples relative to height above the base of the Nonesuch Formation in three core profiles. The greyed symbols are regarded as unreliable due to low yields. Note that values of HI of less than about 15 are imprecise because they are calculated assuming an $S_2$ RE pyrolysis peak of 0.01 mg HC/g TOC even in cases where this peak cannot be readily identified on the pyrogram.

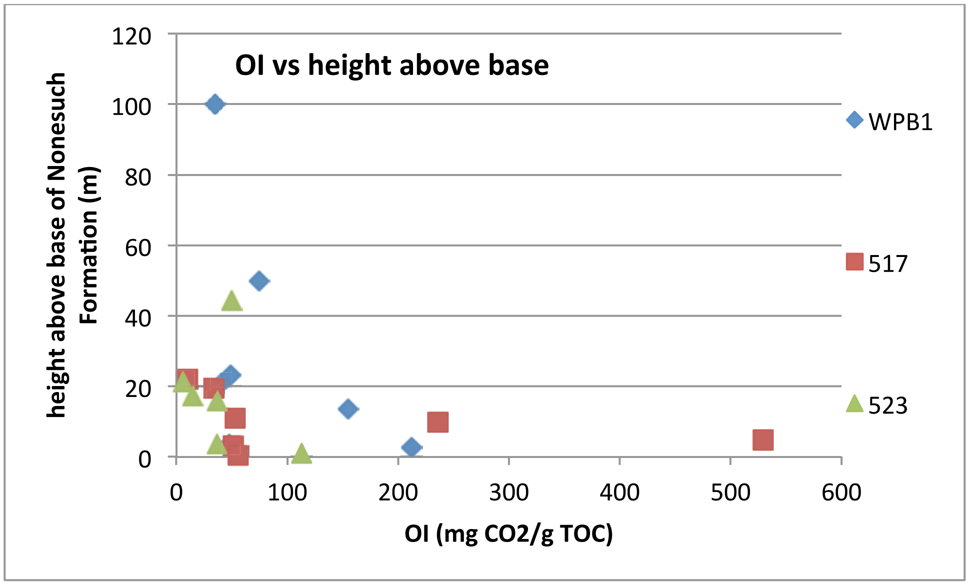

Figure 53: Oxygen index in samples relative to height above the base of the Nonesuch Formation in three core profiles.  Negative correlation is apparent in all three core profiles as well as for the group overall.

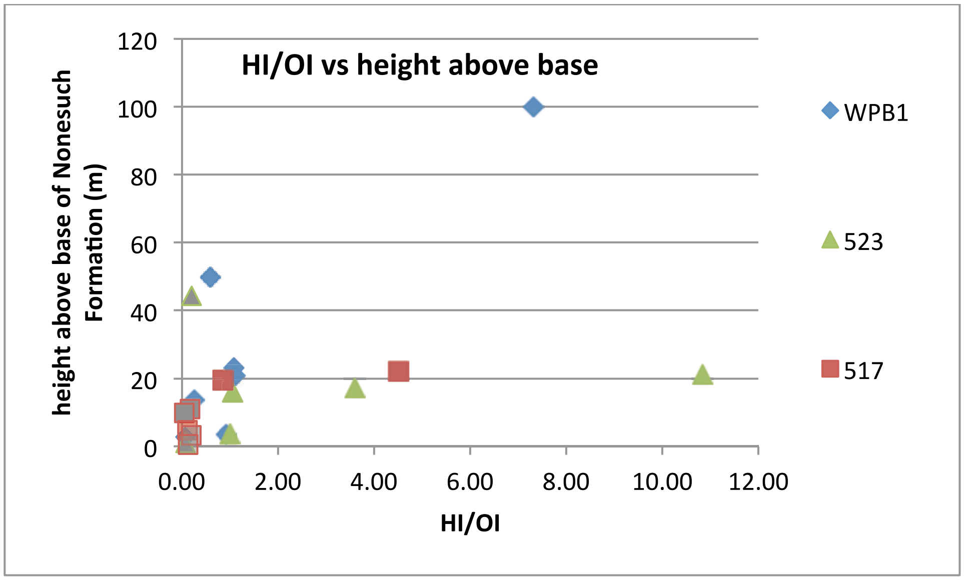

Figure 54: Overall positive correlation between HI/OI ratio and stratigraphic height for three selected core profiles. The greyed symbols are regarded as unreliable due to low yields (they are calculated assuming an $S_2$ RE pyrolysis peak of 0.01 mg HC/g TOC even in cases where this peak cannot be readily identified on the pyrogram).

Exluding the lowest TOC, high OI (under 0.15% and above 100 mg/g), stratigraphically outlying (above 104 m) samples, as well as the three profiles for which only one or two data points are available (PI, LIR, 28G), reveals mixed positive and negative correlations between HI and stratigraphic position for the other profiles (PC1, PC5, BIR, SF and CF).  The same is true with respect to the relationship between OI and stratigraphic height for this subset of samples. However, the remaining profiles show dominantly (4 of 5) positive correlation of HI/OI ratio versus stratigraphic position (Figure 55).

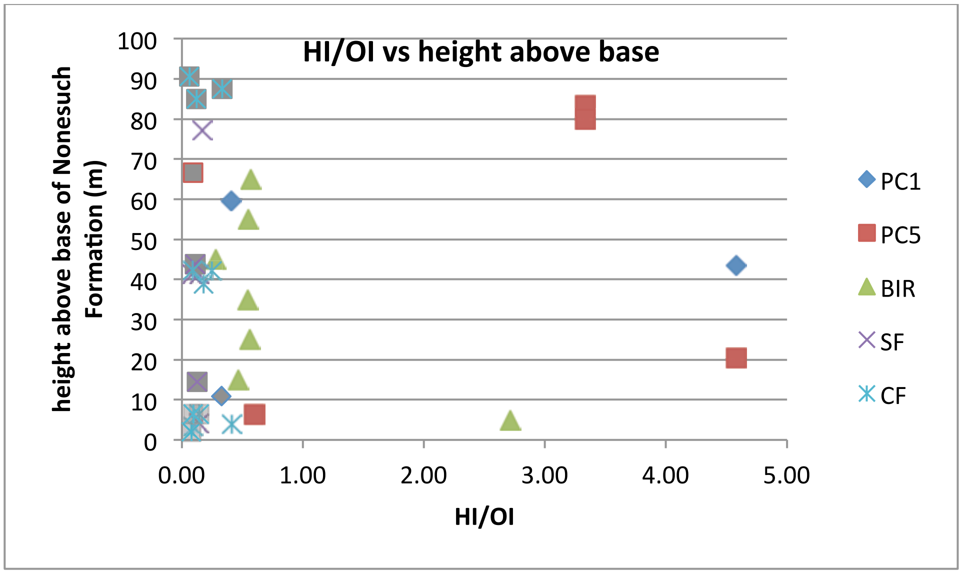

Figure 55: Dominantly positive correlation of HI/OI ratio and stratigraphic height for the remaining profiles containing at least three points. The greyed symbols are regarded as unreliable due to low yields (they are calculated assuming an $S_2$ RE pyrolysis peak of 0.01 mg HC/g TOC even in cases where this peak cannot be readily identified on the pyrogram).

No statistically significant correlation between HI or HI/OI and stratigraphic height is apparent, even with the exclusion of fewer data points for a third, even broader subset of samples. The line of best fit is positive for both stratigraphic height versus HI as well as versus HI/OI (Figures 56 and 57). The excluded outliers are: 1) four data points within 60 m above the base of the formation, all with HI above 200, and; 2) two points with very high OI (above 2200), and; 3) the LIR and PIR samples, for which only one or two points remain in this subset.

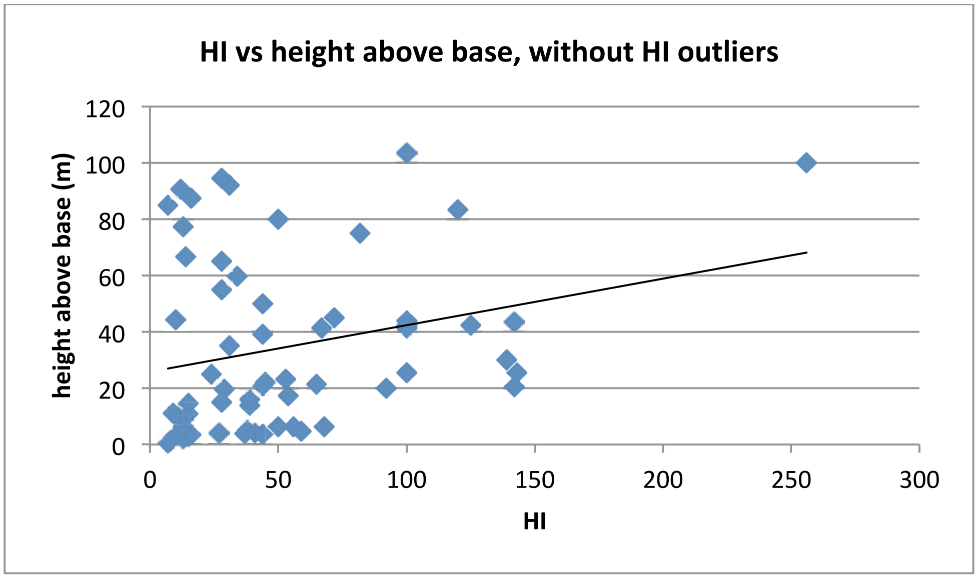

Figure 56: Statistically insignificant correlation line for HI versus stratigraphic height for the larger dataset. The slope of the line of best fit is nonetheless positive.

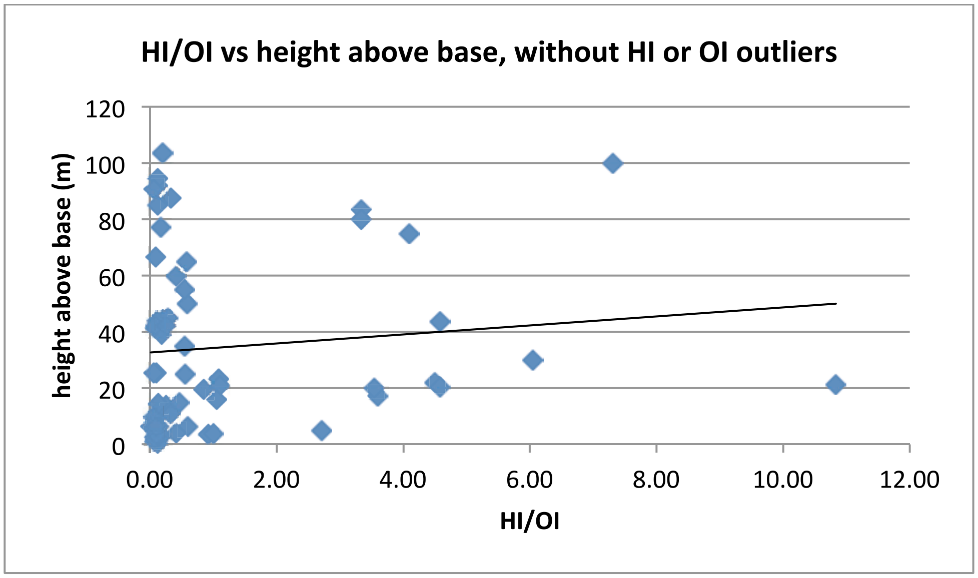

Figure 57: Statistically insignificant but nonetheless positive line of best fit for the plot of HI/OI versus stratigraphic height.

### *6.2.1 Rock-Eval and LECO TOC Relation to Copper Mineralization*

The lowest HI samples are from in or adjacent to mineralized rock at and near White Pine. No such relation with high OI samples exists. Most (28/42) unmineralized samples for which RE and thin section data exists show HI greater than 72 mg HC/g TOC; in contrast, nearly all RE/thin section analyzed Cu-mineralized samples (20/23) show OI greater than 30 and HI below 72 mg HC/g TOC. A majority (8/14) of the unmineralized high HI samples show OI values above 258 (these 8 samples average 682 OI, while the 14 samples as a whole average OI of 376). Average TOC for the high OI, low HI mineralized samples is 0.14%, whereas the few mineralized samples with higher HI show higher average TOC of 0.73%. A majority (14/23) of mineralized samples show low HI/OI (less than 0.33); greater than 90% of mineralized samples with HI/OI less than 0.33 show TOC below 0.15%.

No statistically significant correlation exists between TOC and TAI values of AOM, for either mineralized or unmineralized samples (excluding from consideration the samples lacking AOM altogether, as in Figure 58). Similarly, no statistically significant correlation of HI to TAI values of AOM for either mineralized and unmineralized samples (Figure 59). Mineralized samples show a slightly steeper negative slope than do unmineralized samples on this diagram. No correlation of OI to TAI of AOM values is apparent for either mineralized and unmineralized samples, as in Figure 60.

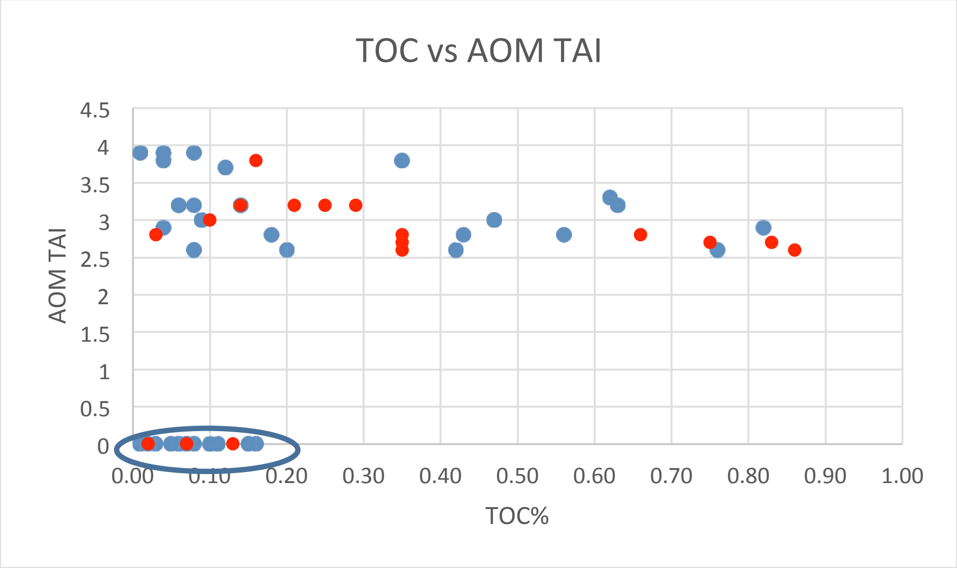

Figure 58: No statistically significant correlation of TOC and TAI values of AOM exists, for either mineralized or unmineralized samples. Samples lacking AOM altogether which are here depicted as TAI = 0, and are enclosed in the blue oval. Mineralized samples are red, unmineralized are blue.

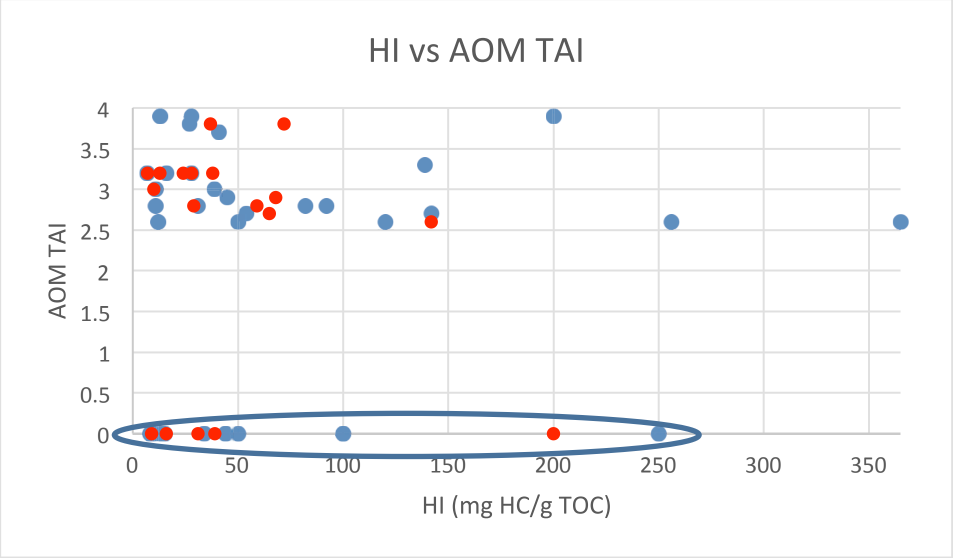

Figure 59: No correlation of HI to TAI values of AOM for either mineralized or unmineralized samples exists. Note that mineralized AOM-bearing samples show a slightly steeper negative slope than do unmineralized AOM-bearing samples. Mineralized samples are red, unmineralized are blue. Samples in which AOM was absent are depicted as TAI = 0, within the blue oval.

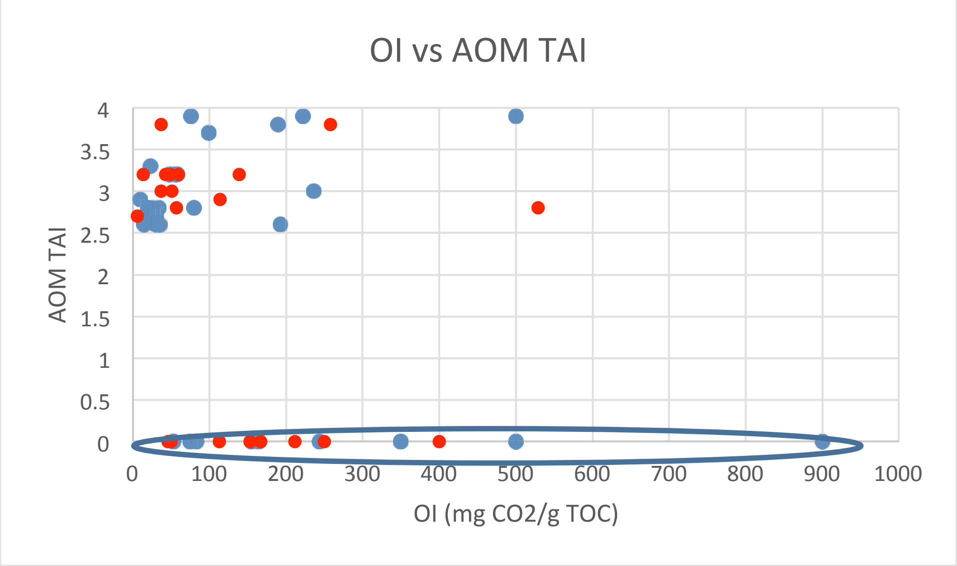

Figure 60: No strong correlation of lower OI at lower TAI of AOM is apparent. Mineralized samples are red, unmineralized are blue. The oval envelops the samples in which AOM was not observed.

No strong correlation between $T_{max}$ and AOM TAI values is apparent for mineralized samples if the low-$S_2$ samples are included. This is also the case if only the samples with reliable $T_{max}$ are considered (Figures 61, 62).

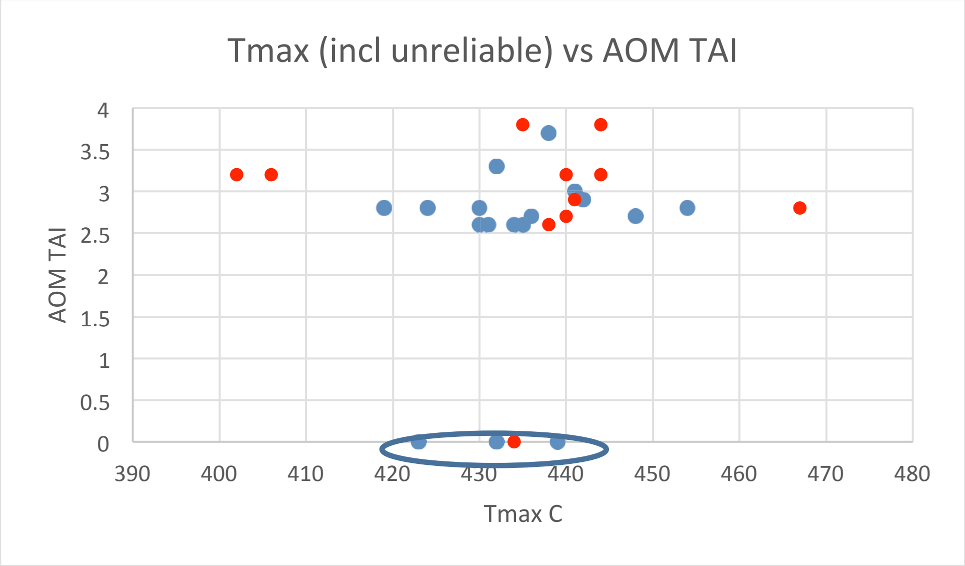

Figure 61: No strong correlation between AOM color (and TAI value) and $T_{max}$ is apparent for the broader set of barren and mineralized samples. Mineralized samples are red, unmineralized are blue. The oval envelops the samples in which AOM was not observed.

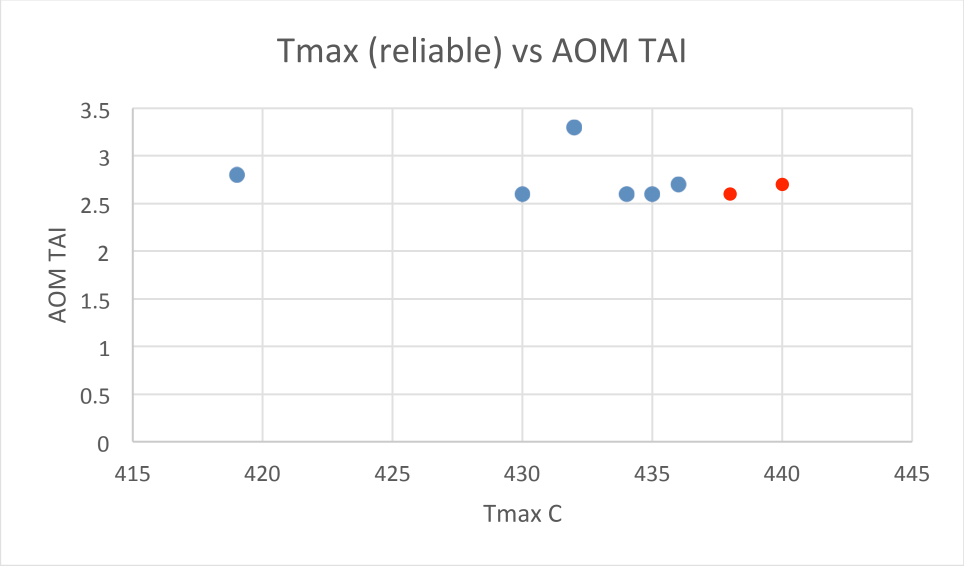

Figure 62: No strong correlation between AOM color (and TAI value) and $T_{max}$ is apparent for the reliable subset of $T_{max}$ values. Mineralized samples are red, unmineralized are blue.

No strong, reliable trends of HI, OI, or Tmax are apparent with respect to the color of organic matter, nor does OM color show a strong correlation to Cu mineralization (Figure 63). The lowest $T_{max}$ values and the highest HI values are for unmineralized samples with low TAI AOM (orange or orange brown). Most (67%) of the darkest (dark brown) AOM samples are mineralized (Figure 64).

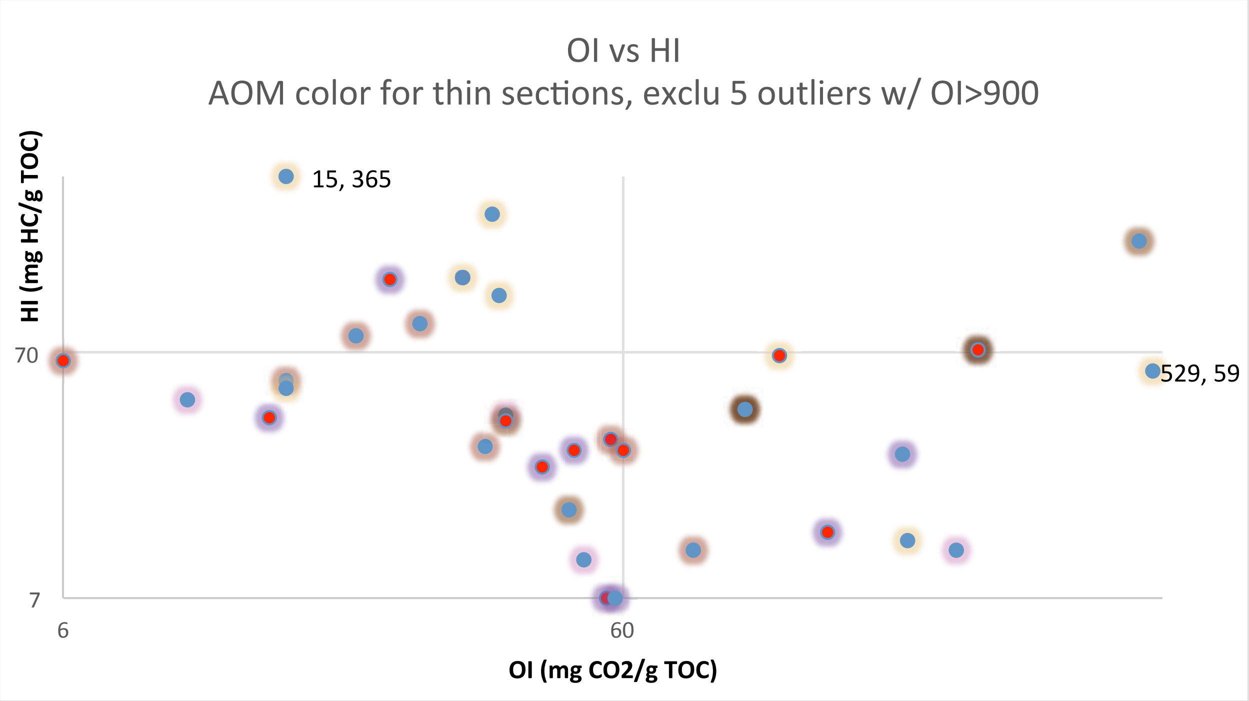

Figure 63: Color of AOM and mineralization with HI versus OI plot (excluding 5 outliers with OI greater than 900). Red data points are mineralized; blue points are barren of Cu minerals. The TAI color range and representative data point halo color scheme is: orange (2.6) - light orange halo; orange brown (2.7 to 2.8) - dark orange halo; reddish brown (2.9 to 3.1) - pink halo; brown (3.2 to 3.6) - purple halo; dark brown (3.7 to 3.8) - brown halo.

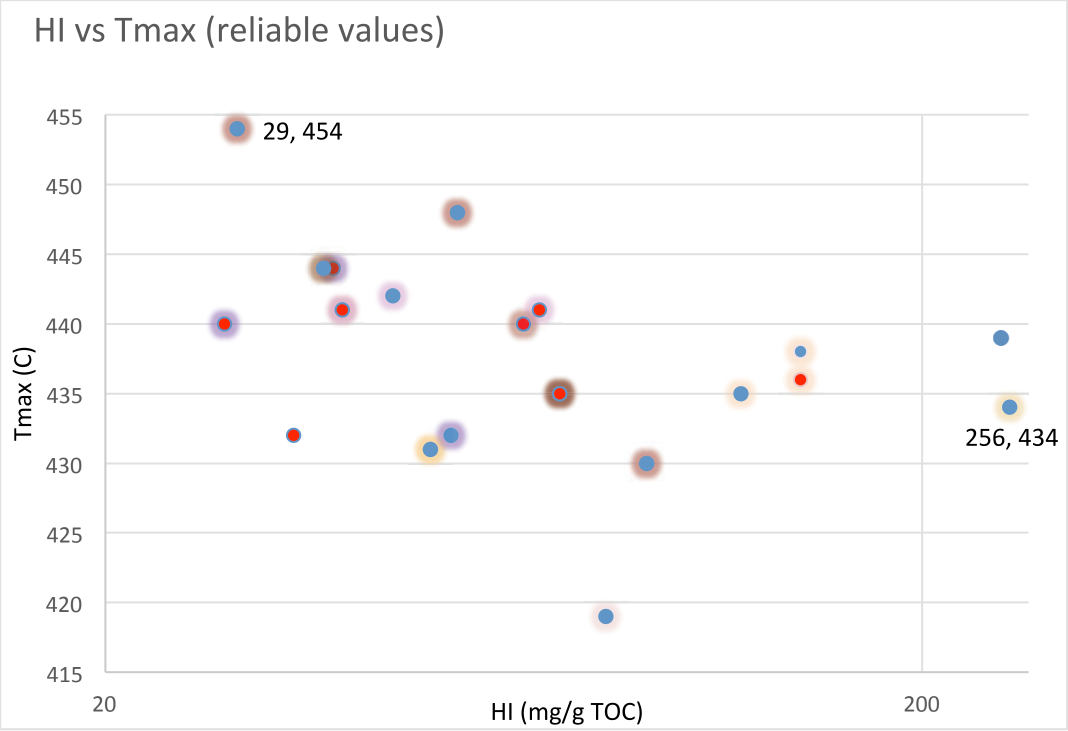

Figure 64: The TAI/ color of AOM and mineralization with HI versus $T_{max}$ values (excludes points with $S_2$ under 0.2, excepting those with discernible $S_2$ peaks). Red data points are mineralized; blue points are barren of Cu minerals. The TAI color range and representative data point halo color scheme is: orange (2.6) - light orange halo; orange brown (2.7 to 2.8) - dark orange halo; reddish brown (2.9 to 3.1) - pink halo; brown (3.2 to 3.6) - purple halo; dark brown (3.7 to 3.8) - brown halo. Samples lacking AOM in thin section show no halo.

Mineralized samples for which RE and thin section data exists (n = 23) show an average HI/OI ratio of 1.02 with average AOM and FOM TAI values (excluding samples for which OM of a given type is absent in thin section) of 3.13 and 3.83, respectively. In contrast, unmineralized samples for which RE and thin section data exists (n = 33) show average HI/OI ratio of 2.08 with average AOM and FOM TAI average values of 2.95 and 3.86, respectively.

Many samples show dark gray to black thin (sub 10 mm thickness) continuous even parallel laminations of fine shaley organic-rich material alternate in varve-like patterns with thin to medium thickness (10 to 100 mm) light gray siltstone laminations. Abrupt vertical disruptions to, and sub cm scale offsets of, the continuous nature of the thin dark gray shaley laminations are apparent in a minority (7 total) of samples, most of which are in the lower or middle Nonesuch

Formation (see Appendix A, Figures A36, A50, A55, A59). The majority of these features show ductile rather than brittle deformation, although the broken shaley lamination in CF-3A (Figure A55) shows sharp angular margins to the fractures. Some of these “breached shaley laminations,” as described by Sutton *et al*. (2013), show silty light gray material penetrating and migrated stratigraphically upward through the overlying shaley laminae. A majority (6 of 7) of these samples are Cu-mineralized or adjacent (sub 20 m distant) to Cu mineralization, and only one is barren, distal to mineralization and in the upper one-third of the Nonesuch Formation. No reliable $T_{max}$ values exist for these samples. All of the breached shaley laminae samples with TOC data (6 of 7) show TOC below 0.36%, and most are under 0.10% (4 of 6). No correlation of AOM or FOM color to mineralization is apparent in these breached shaley laminated samples, nor do clear patterns of OM Type, HI or OI to mineralization exist (Table 4). It is possible that these sedimentary structures represent clastic dikes extruded upward during pre-lithification compaction of the Nonesuch Formation: By such a mechanism, the quartz-rich (overall less compactible) silty material distorted and was extruded upward through the somewhat cohesive but more readily distorted shaley dark gray laminae. It is yet not possible to ascribe a genetic syn-mineralization upward fluid flow mechanism to these features; however, their occurrence as generally near to or in Cu mineralized rocks seems to support this conclusion of Sutton *et al*. (2013).

.

Table 4: The RE and other parameters for samples showing vertically disrupted shaley laminations. Samples in which vertically offset and broken shaley laminae were observed have previously been suggested to result from penetration and disturbance by ascending fluids associated with ore. Comparison of RE, LECO, Cu enrichment (or proximity to enrichment)) and stratigraphic position reveals no clear patterns or correlation of these measures for this study’s Nonesuch Formation samples.

| LIR 3 | 28G 571 | CF 3A | SF 1A | BIR 14 | BIR 11 | BIR 10 | Sample |
|---|---|---|---|---|---|---|---|
| 0.01 | 0.09 | 0.06 | 0.01 | 0.21 | - | 0.35 | TOC % |
| - | - | 16 | 200 | 24 | - | 72 | HI |
| - | - | 48 | 500 | 43 | - | 258 | OI |
| min'd | min'd | distal | adjacent | min'd | min'd | min'd | Cu |
| lower 1/3 | lower 1/3 | upper 1/3 | lower 1/3 | lower 1/3 | middle 1/3 | middle 1/3 | Strat. Position |
| AOM absent | AOM absent | 3.2 | 3.9 | 3.2 | 3.2 | 3.8 | AOM TAI |
| FOM absent | 3.9 | 3.9 | 3.9 | 3.9 | 3.2 | 3.9 | FOM TAI |

### *6.3 Stable Isotopes*

Samples come from eight profiles at stratigraphic heights from the base to the middle Nonesuch Formation. The data here replicate many of the aspects of the larger dataset of Imbus *et al.* (1991). Delta$^{18}$O values range from -14 to -5 ‰ (VPDB); $\delta^{13}$C from -13 to -1.5 ‰ (VPDB) with two outliers of significantly lower $\delta^{13}$C (-31 and -26 ‰). A narrower cluster of isotope compositions is apparent in most samples from the lower Nonesuch Formation (lowest 20 m) with $\delta^{18}$O = -9.5 to -7 ‰ and $\delta^{13}$C = -4 to -1.5 ‰.

No strong overall relation between carbonate vein, concretion or laminite isotope values and depth or proximity to mineralization, or between isotope values and elemental composition of the OM in the matrix of the samples is apparent (Figures 65, 66, 67). However, it is noted that the most strongly negative $\delta^{13}$C values do co-occur throughout the Nonesuch Formation sections with the most oxidized samples (by OI, as in Figure 68). No regular pattern of HI/OI or HI values versus isotopic composition of carbonates is apparent (Figures 69, 70). Similarly, no relationship between calcite stable isotope values and OM color and TAI values exists.

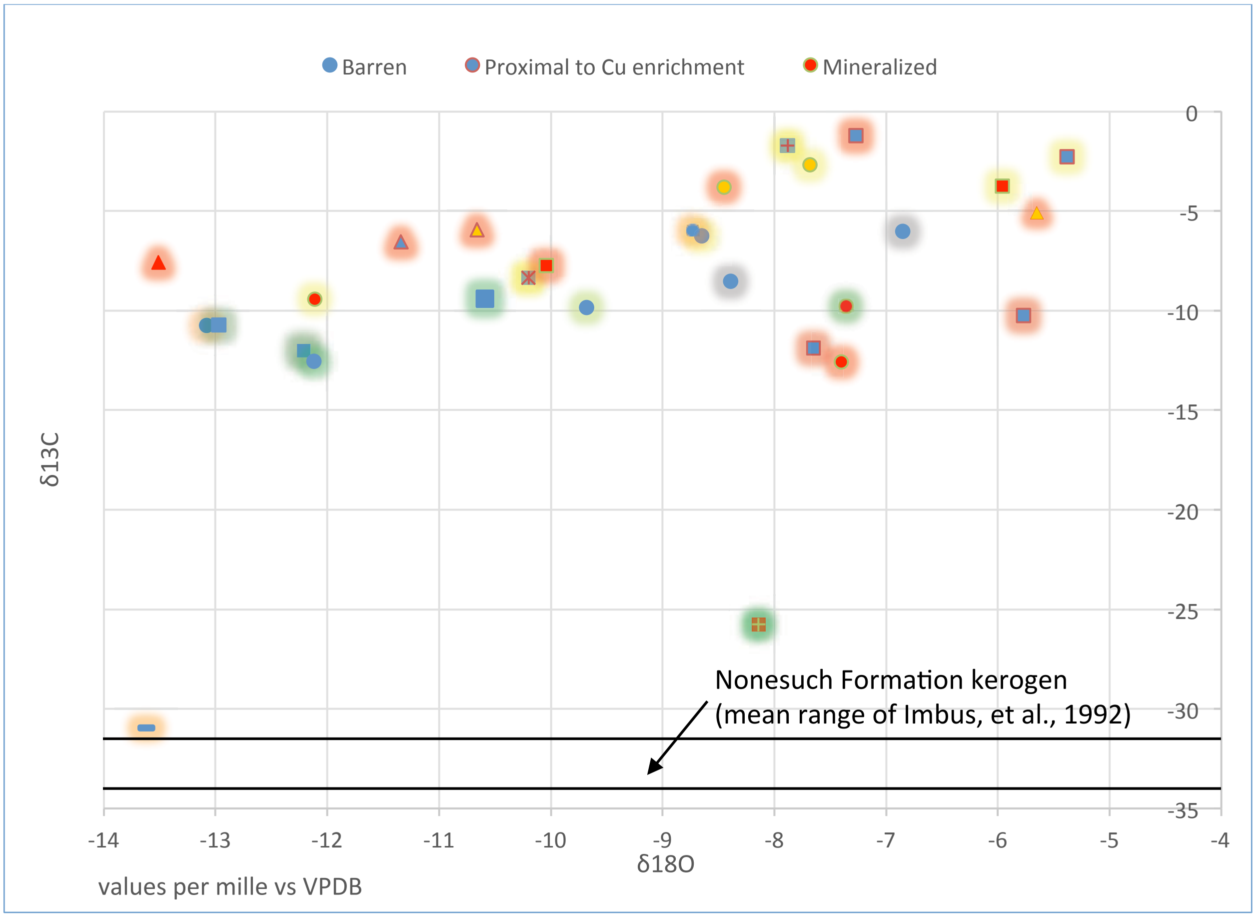

Figure 65**:** The halo indicates a percentile range for each sample, based on the depth of the sample within a given site's Nonesuch Formation thickness. Red - lowest (0-5%); yellow - low (5-22%); green - middle (23-60%); gray - highest (60-100%). Point shape indicates morphology of calcite sample: triangle - conjugate veins at 45˚ to lamination; horizontal dash - vertical vein (90˚ to lamination); asterisk in square - calcite halo about internally laminated, darker-colored rip-up clasts; circle - matrix calcite segregated on light gray thin silty discontinuous laminae; square - matrix calcite segregated on light gray thin silty continuous laminae; cross shape in square - calcite segregation as blebby, ovoid concretions which disturb lamination.

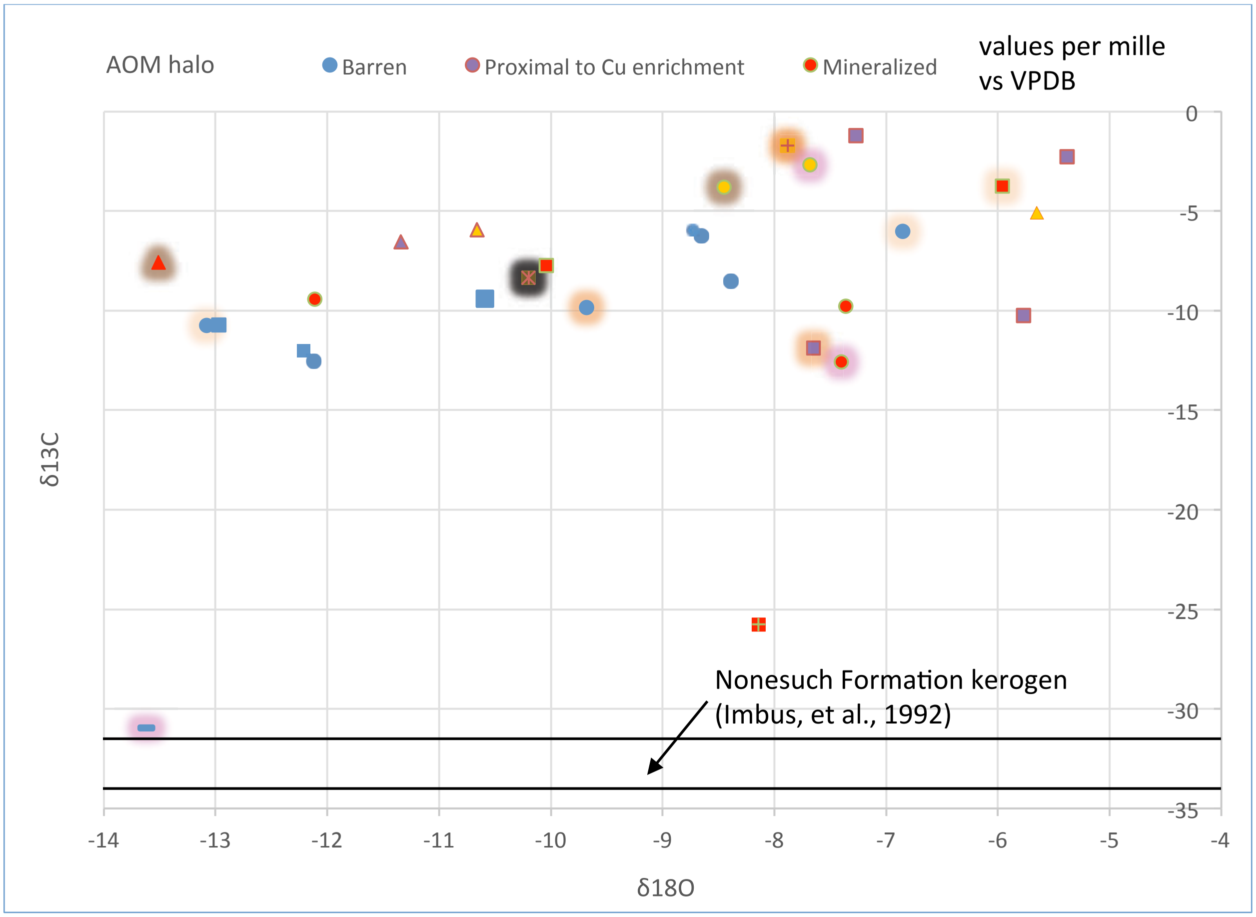

Figure 66: The halo color indicates the TAI value range in which the AOM of each sample fits: orange (2.6) - light orange; orange brown (2.7 to 2.8) – dark orange; reddish brown (2.9 to 3.1) – pink; brown (3.2 to 3.6) – purple; dark brown (3.7 to 3.8) – brown; black (3.9) – black.  Point shape indicates morphology of calcite sample: triangle - conjugate veins at 45˚ to lamination; horizontal dash - vertical vein (90˚ to lamination); asterisk in square - calcite halo about internally laminated, darker-colored rip-up clasts; circle - matrix calcite segregated on light gray thin silty discontinuous laminae; square - matrix calcite segregated on light gray thin silty continuous laminae; cross shape in square - calcite segregation as blebby, ovoid concretions which disturb lamination.

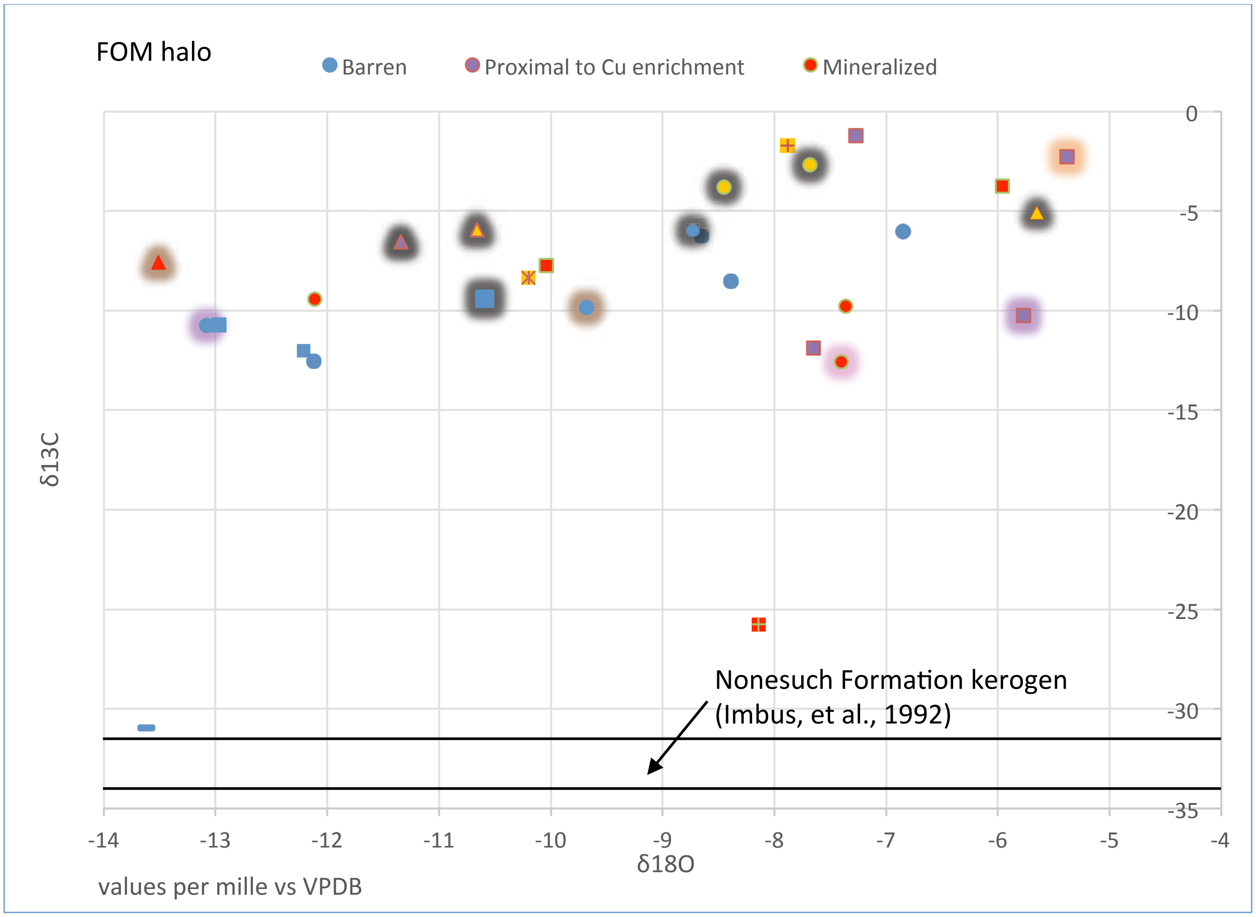

Figure 67: The halo color indicates the TAI value range in which the FOM of each sample fits: orange (2.6) - light orange; orange brown (2.7 to 2.8) – dark orange; reddish brown (2.9 to 3.1) – pink; brown (3.2 to 3.6) – purple; dark brown (3.7 to 3.8) – brown; black (3.9) – black. Point shape indicates morphology of calcite sample: triangle - conjugate veins at 45˚ to lamination; horizontal dash - vertical vein (90˚ to lamination); asterisk in square - calcite halo about internally laminated, darker-colored rip-up clasts; circle - matrix calcite segregated on light gray thin silty discontinuous laminae; square - matrix calcite segregated on light gray thin silty continuous laminae; cross shape in square - calcite segregation as blebby, ovoid concretions which disturb lamination.

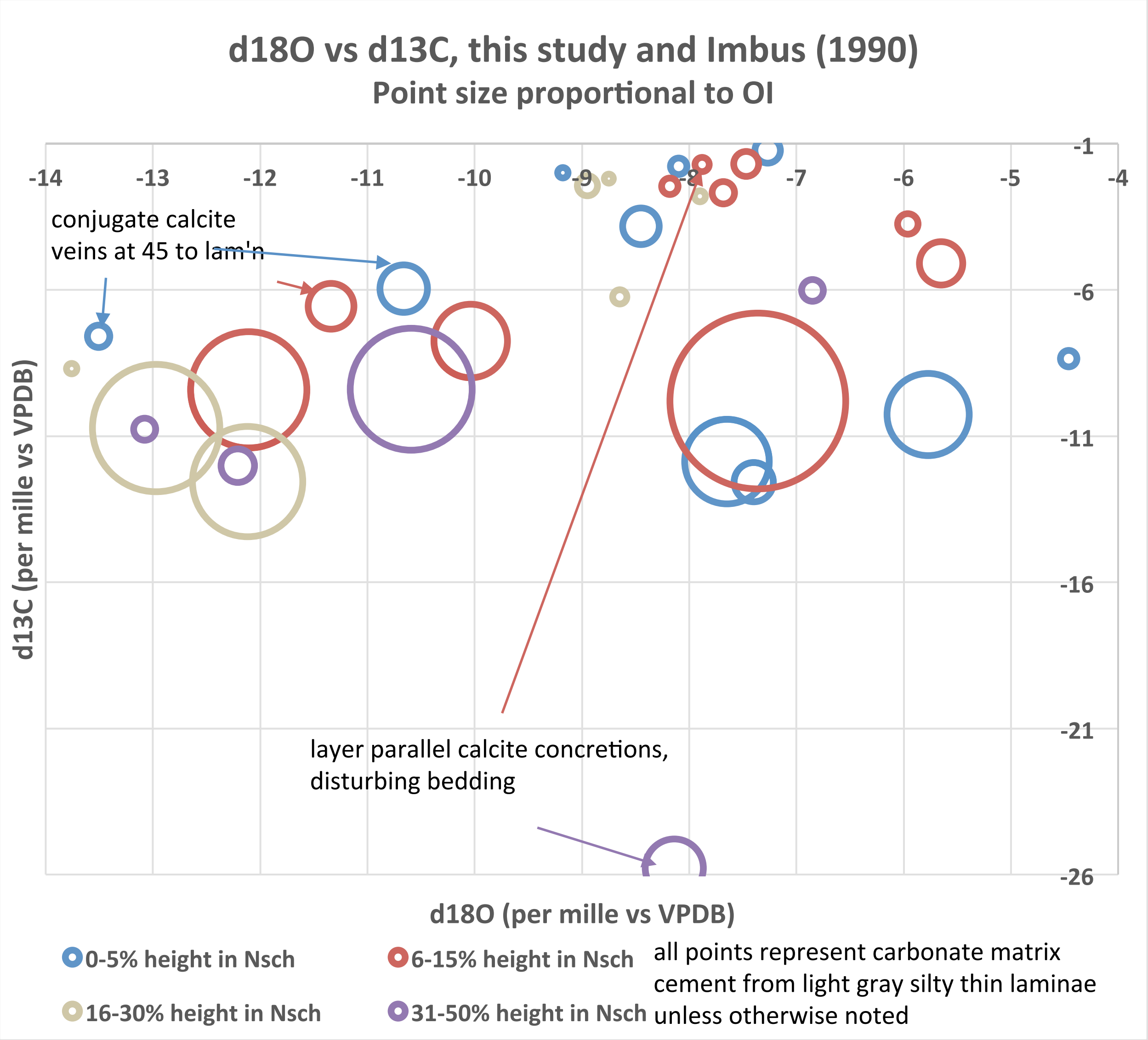

Figure 68: Stable isotope versus OI values for samples with thin section petrographic observations by stratigraphic position.

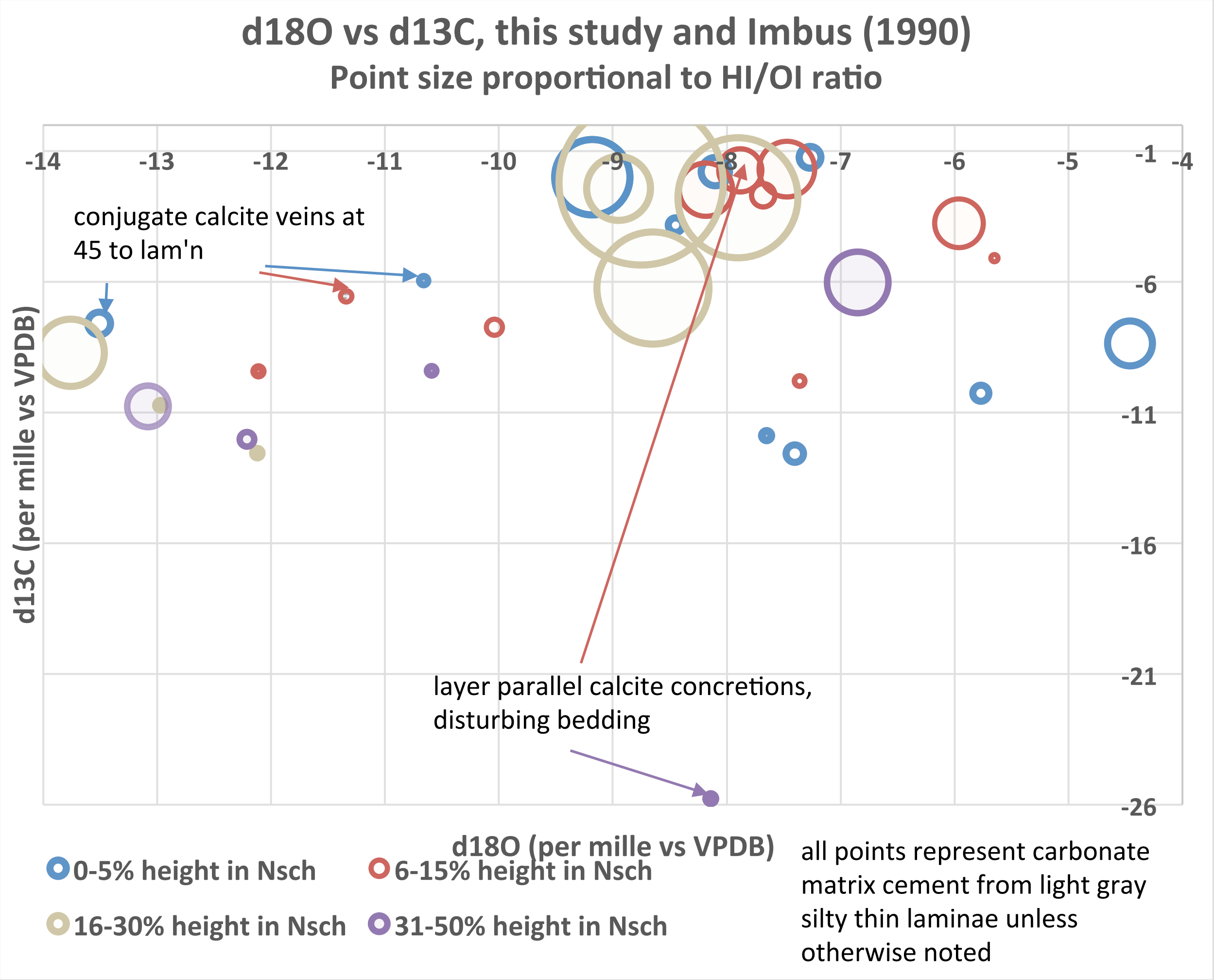

Figure 69: Stable isotope versus HI/OI values for samples with thin section petrographic observations by stratigraphic position.

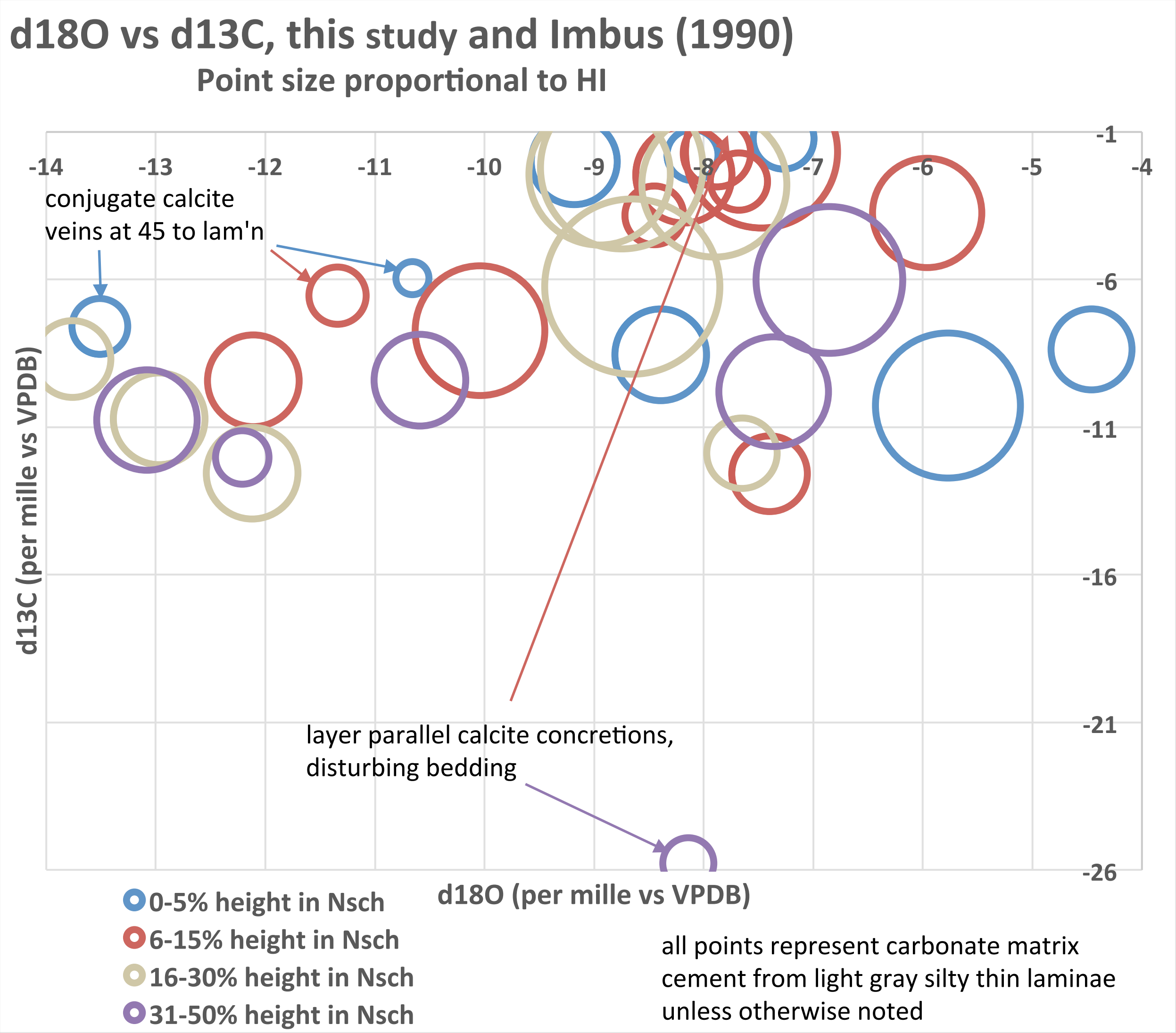

Figure 70: Stable isotope versus HI values for samples with thin section petrographic observations by stratigraphic position.

An overall trend from all the data of lower δ$^{13}$C at lower δ$^{18}$O is apparent. The higher end of the range closely resembles the isotopic compositions of carbonates in stromatolites in the underlying Copper Harbor Formation (Imbus *et al*., 1992), and is taken as the composition of primary carbonate in the sequence. More negative δ$^{13}$C can be interpreted as results of variable degrees of mixing with C derived by the oxidation of indigenous OM: the two low δ$^{13}$C outliers have isotope values indicative of partial or complete oxidation of OM. More negative δ$^{18}$O may result from interaction with an external fluid of any source, or from equilibration of carbonates with clay or other silicate minerals in the host sequence.

Two outliers with significantly lower $\delta^{13}C$ could well result from oxidation of organic matter in ore deposition. The liberated light $C_{org}$ was either reincorporated as $C_{carb}$ immediately adjacent to ore in the mineralized sample, or the isotopically light $C_{org}$ in $CO_2$ migrated up-section and was re-deposited as $C_{carb}$ in the vein sample (523-7). The position of the vein sample (523-7) 60 m above the base of the Nonesuch Formation alternatively suggests widespread organic oxidative effects throughout the Nonesuch Formation, rather than strictly localized OM oxidation and $C_{org}$ re-deposition as carbonate associated with Cu mineralization.

The three low-angle vein samples are more interesting: these three stratigraphically lowest vein conjugates at 45º to lamination show less negative $\delta^{13}C$ values than the upper Nonesuch Formation veins of Imbus et al. (1992) possibly indicating a greater degree of oxidatively-mobilized $C_{org}$ being reincorporated as $C_{carb}$ higher in the Nonesuch Formation through fracture-filling diagenetic calcite growth.

The lack of relations between distance to mineralization and carbonate C and O isotope values indicate that OM oxidation likely took place throughout the Nonesuch Formation and was neither restricted to mineralized sequences nor was heightened significantly in mineralized rock sequences.

## *6.4 Molecular Makeup of Organic Matter*

### *6.4.1 Whole-Rock Extract Gas Chromatography*

Nine samples from four profiles over 20 km strike length (BIR, cores WPB-1, 517 and 523) from the Iron River syncline and WP mine areas were analyzed by GC and GC-MS. Each of the four profiles show Cu mineralization in the lowermost Nonesuch Formation. The samples are from about 3 to 25 m above the base of the Nonesuch Formation and collectively straddle the mineralization fringe such that they are variably in, above ore zones, or in and above sub-ore concentrations of Cu at the base of the Nonesuch Formation.

Samples for these analyses were chosen based on requirements for reliable data of TOC greater 0.2% and higher $S_1$ and $S_2$ production during RE pyrolysis. The requirements meant that OI ranged from 10 to 60 and samples with high OI (above 75) were not analyzed. The limited size and organic leanness of the samples meant that it was possible only to obtain whole extract GC data and GC-MS data for saturate and aromatic fractions (for biomarker contents and associated maturity indices), but not for resins, polar and NSO components. Table 5 lists selected compound contents and ratios of the nine extracts.

The BIR samples (from the Top Zone, the Dark Gray Massive and Domino members of the WP mining scheme) all show disseminated chalcocite, often replacing pyrite. The BIR 16 thin section shows blue fluorescing oil inclusions which were observed by Colbert (2011) to give an average fluid inclusion homogenization temperature of 159° C (range 94 to 200° C). The BIR GC-MS samples were collected stratigraphically below two thin section samples showing probable pyrobitumen similar to that described by Barghoorn *et al*. (1965).

The WPB samples are both adjacent (under 10 m distal) to Cu mineralization, while the 523 samples are mixed, one is adjacent and the other distal. The 517 samples are both distal to Cu mineralization.

Three generic patterns are identified from the nine chromatograms and are classified as "least altered," "partially altered," and "altered" (Figure 71). Least altered samples (Table 5, Figure 72a) have chromatograms typical of source rocks in the upper half of the oil window.

The five least altered samples have RE pyrolysis HI from 29 to 54 and OI from 10 to 37.

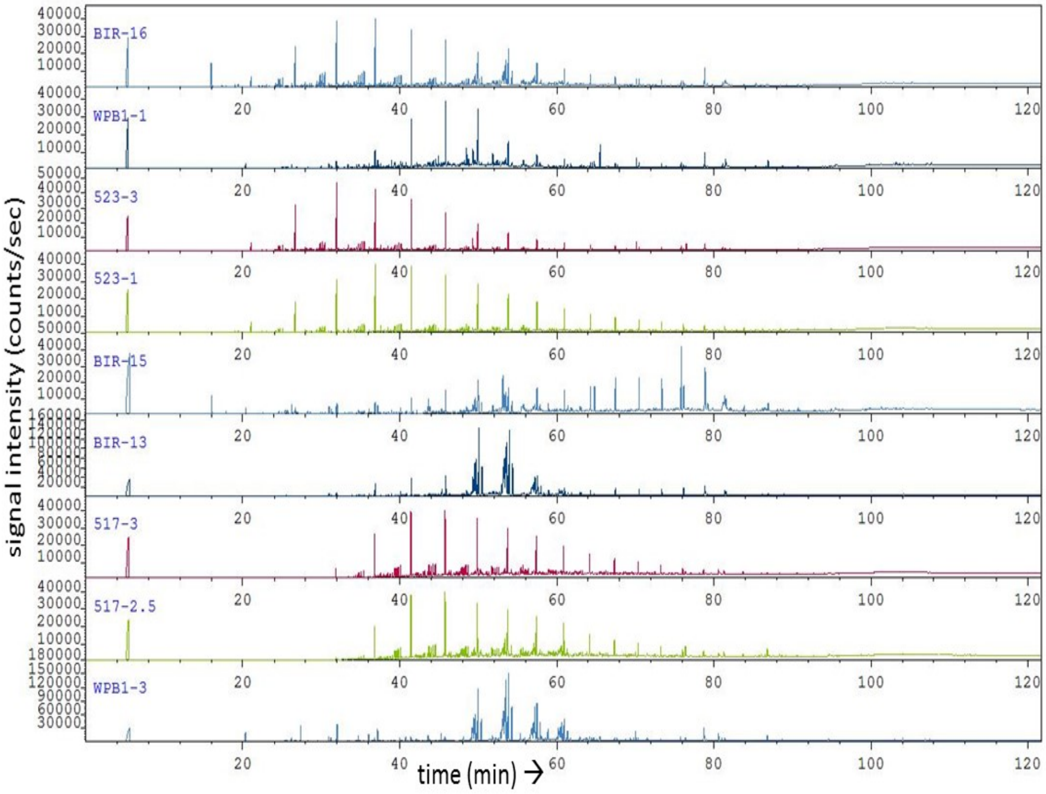

Figure 71: Least altered samples show broad, smooth whole extract GC traces, whereas the altered (BIR 13, WPB-1 and WPB-3) samples show distinctly different, sharper peak distributions over narrower ranges of elution times. The bimodal distribution of the less altered BIR 15 sample stands out from the other unimodal peak distributions.

Table 5: Selected chemical parameters, compound ratios, and indices from the Nonesuch Formation. For definitions, refer to list of acronyms. D = index normally indicative of depositional environment; M = index normally indicative of maturity.

| | | less altered | | | | | slightly altered | altered | | |
|---|---|---|---|---|---|---|---|---|---|---|
| Sample# | | 523.1 | 523.3 | 517-2.5 | 517-3 | BIR-16 | BIR-15 | BIR-13 | WPB-1 | WPB1-3 |
| TOC | | 0.75 | 0.47 | 0.56 | 0.8 | 0.63 | 0.25 | 0.35 | 0.27 | 0.23 |
| HI | | 54 | 39 | 29 | 45 | 38 | 24 | 31 | 44 | 44 |
| OI | | 19 | 37 | 34 | 10 | 14 | 60 | 57 | 48 | 40 |
| S1 | | 0.14 | 0.09 | 0.07 | 0.19 | 0.25 | 0.04 | 0.05 | 0.04 | 0.02 |
| S2 | | 0.09 | 0.18 | 0.16 | 0.37 | 0.24 | 0.07 | 0.11 | 0.12 | 0.1 |
| EOM (ppm) | | 581 | 175 | 138 | 405 | 285 | 86 | 122 | 172 | 118 |
| color/TAI of AOM | | orange brown (2.7) | red brown (2.9) | orange brown (2.8) | red brown (2.9) | orange brown (3.2) | orange brown (2.8) | orange brown (3.2) | no TS | no TS |
| color/TAI of FOM | | n/a | black, 3.9 | n/a | n/a | n/a | n/a | black, 3.9 | no TS | no TS |
| Cu | | no, adjacent (4 m) | no, distal (12 m) | no, distal (15 m) | no, distal (17 m) | chalcocite, widespread | chalcocite, rare | chalcocite, widespread | no, adjacent (1 m) | no, adjacent (10 m) |
| m above base of Nonesuch Formation | | 15.9 | 17.3 | 19.5 | 22.1 | lowermost | low | middle | 3.6 | 20.9 |
| **GC parameters** | | | | | | | | | | |
| Pristane/Phytane | | 1.73 | 1.71 | 0.67 | 1.05 | 1.03 | 1.2 | 1.4 | 1.81 | 0.24 |
| Pristane/*n* $C_{17}$ | | 0.12 | 0.13 | 0.1 | 0.09 | 0.12 | 0.37 | 0.14 | 0.45 | 0.05 |
| Phytane/*n* $C_{18}$ | | 0.1 | 0.12 | 0.19 | 0.11 | 0.2 | 0.4 | 0.25 | 0.45 | 0.42 |
| CPI (Carbon Preference) Hunt | | 0.88 | 0.48 | 1.16 | 1.19 | 0.57 | 1.56 | 0.78 | 0.78 | 1.71 |
| Normal Paraffins (%) | | 36.8 | 34.4 | 26.5 | 27 | 25.7 | 19.3 | 23.7 | 20.4 | 16.3 |
| Isoprenoids (%) | | 3.1 | 2.4 | 2.5 | 2.6 | 2.4 | 2.7 | 1.8 | 4.6 | 1.3 |
| Phenanthrene/*n* $C_{18}$ | | 0.02 | 0.07 | 0.03 | 0.03 | 0.09 | 0.35 | 0.62 | 0.28 | 0.54 |
| Resolved Unknowns (%) | | 58.3 | 63.1 | 71 | 70.3 | 71.8 | 77.5 | 74 | 74.8 | 81.6 |
| **Steranes (m/z 217; 218)** | | | | | | | | | | |
| dia (S+R)/ ααα steranes (S+R) $C_{27}$ | M | 0 | 1.51 | 0.91 | 0 | 3.28 | 1.44 | 1.7 | 1.32 | 1.11 |
| S/S+R ($C_{29}$ ααα) (217) | M | | 0.28 | 0.37 | | | 0.31 | 0.25 | 0.37 | 0.29 |
| ββ/(ββS+ααR) $C_{29}$ (217) | M | 0 | 0.34 | 0.48 | | 0.23 | 0.35 | 0.26 | 0.41 | 0.36 |
| **Terpanes (m/z 191)** | | | | | | | | | | |
| C23 triterpanes/C21 triterpanes | D | 1.55 | 1.74 | 2.14 | 1.97 | 1.37 | 2.58 | 1.77 | 0.95 | 1.22 |
| Norhopane/Hopane | D | 0.82 | 0.77 | 0.68 | 0.71 | 0.83 | 0.84 | 0.98 | 1.44 | 1.12 |
| Moretane/Hopane | M | | 0.19 | 0.15 | | | 0.14 | 0.17 | 0.41 | 0.35 |
| Ts/(Ts+Tm) trisnorhopanes | M/D | | 0.47 | 0.36 | | 0.47 | 0.54 | 0.47 | 0.09 | 0.18 |
| $C_{29}$Ts/$C_{29}$ Hopane | M | | 0.27 | | | 0.32 | 0.34 | 0.23 | 0.03 | 0.09 |
| $H_{32}$ S/(R+S) Homohopanes | M | | 0.54 | 0.59 | | 0.61 | 0.58 | 0.59 | 0.59 | 0.59 |
| Steranes/Hopanes | D | 0.66 | 0.9 | 0.4 | 0.19 | 0.89 | 0.65 | 1.05 | 0.13 | 0.29 |
| **Triaromatic and Monoaromatic Steroids** | | | | | | | | | | |
| ($C_{20}$+$C_{21}$)/S TAS | M | | | 0.27 | 0.55 | 0.46 | 0.38 | 0.44 | 0.23 | 0.31 |
| TAS #1 20/(20+27) | M | | | 0.4 | 0.7 | 0.68 | 0.55 | 0.68 | 0.54 | 0.61 |
| TAS #2 21/(21+28) | M | | | 0.61 | 0.82 | 0.77 | 0.74 | 0.74 | 0.54 | 0.57 |
| **Phenanthrenes, Naphthalenes, and Dibenzothiophenes** | | | | | | | | | | |
| MPI-1 (methylphenanthrene) | M | 0.67 | 0.73 | 0.83 | 0.87 | 1.05 | 0.83 | 0.88 | 0.33 | 0.09 |
| MPI-2 | M | 0.78 | 0.87 | 0.96 | 1.03 | 1.29 | 1 | 1.05 | 0.4 | 0.11 |
| DNR-1 (dimethylnaphthalene) | M | 5.27 | 6.65 | 3.34 | 5.79 | 2.58 | 7.82 | 10.53 | 8.38 | 2.99 |
| DNR-2 | M | 1.9 | 2.31 | 1.63 | 2.32 | 1.08 | 1.47 | 2.3 | 2.41 | 1.45 |
| MDR (methyldibenzothiophene) | M | 5.4 | 8.29 | 2.27 | 3.61 | 4.05 | 11.35 | 11.29 | 4.84 | 1.93 |
| MDR23 | M | 0.46 | 0.43 | 0.73 | 0.94 | 0.36 | 0.36 | 0.37 | 0.25 | 0.04 |
| MDR1 | M | 0.15 | 0.1 | 0.51 | 0.35 | 0.17 | 0.06 | 0.06 | 0.11 | 0.05 |
| phenanthrene/sum methylphenanthrenes | M | 0.67 | 0.59 | 4.58 | 0.43 | 0.59 | 1.14 | 1.11 | 2.15 | 4.16 |
| phenanthrene/sum dimethylphenanthrenes | M | 0.37 | 0.39 | 0.34 | 0.28 | 0.5 | 1.85 | 2.04 | 2.63 | 14.54 |
| fluorene/sum methylfluorenes | | 1.5 | 1.87 | 1.06 | 1.08 | 1.08 | 1.04 | 2 | 2.34 | 2.21 |
| dibenzofuran/sum dimethyl-DBF | | 2.29 | 0.07 | 0.47 | 0.47 | 1.11 | 1.87 | 4.1 | 5.17 | 97.01 |
| DBT/MDBT | | 0.69 | 0.06 | 0.39 | 0.42 | 0.81 | 0.91 | 0.88 | 1.15 | 3.22 |
| dimethylnaphthalene index | | 2.51 | 2.7 | 2.45 | 2.96 | 1.92 | 2.14 | 2.67 | 3.04 | 1.91 |
| trimethylnaphthalene index | | 2.28 | 2.16 | 1.83 | 1.88 | 2.05 | 2.6 | 2.81 | 2.55 | 2.33 |
| DBT/Phenanthrene | M | 0.08 | 0.08 | 0.01 | 0.13 | 0.03 | 0.04 | 0.02 | 0.06 | 0.15 |

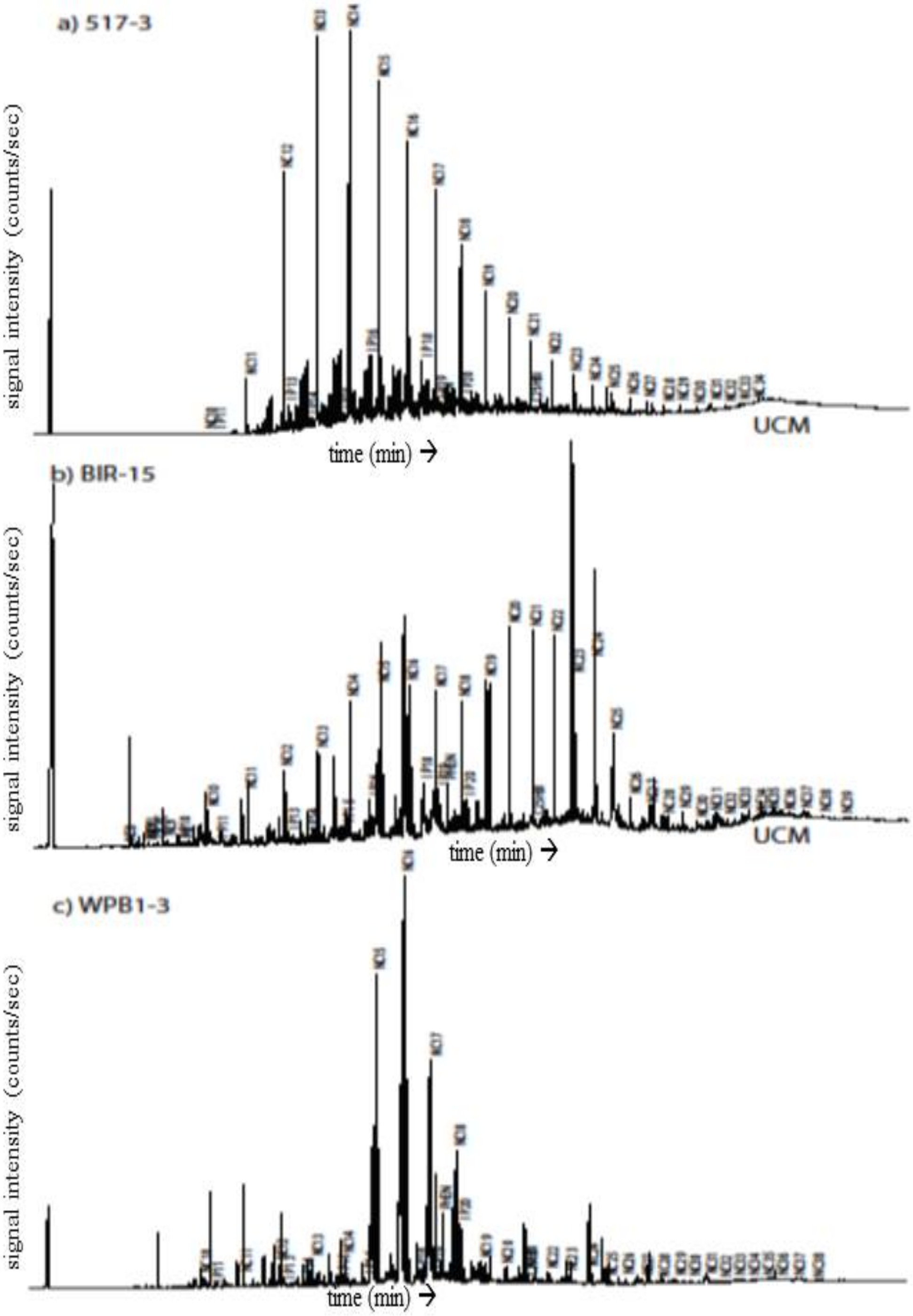

Figure 72: Representative Soxhlet whole extract chromatograms for the Nonesuch Formation. Peak identification was for these chromatograms were largely provided by proprietary software of Weatherford Laboratories. UCM = unresolved complex mixture; NC = *n*-alkane with C number; IP = isoprenoid with C number; PHEN = phenanthrene.

The least altered extracts are dominated by *n*-alkanes, with highest concentrations at *n*-$C_{11}$ to *n*-$C_{14}$ and a smooth decrease to higher lengths (Figure 72a). Their UCM is small and peaks at high C number. None of the least altered extracts show any marked odd/even *n*-alkane preference (CPI is about 1). Pristane/phytane is generally uniform and slightly above one, although the 523 samples both show a slight odd over even preference and the 517-2.5 sample favors even C numbers (values around 1.7 and a value of 0.67, respectively). Pristane/heptadecane and phytane/octadecane ratios are uniform and low (0.1 to 0.2). Each of the least altered samples' traces have significant clusters of peaks interpreted as multiple isomers of monomethylalkanes, as are typical of Precambrian source rocks and oils. The one mineralized sample characterized as least altered shows twice the phenanthrene response of the other least altered samples.

The samples typified as altered (Table 5, example in Figure 72c) are distinguished by a sharp maximum of *n*-alkanes over a narrow range (*n*-$C_{13}$ to *n*-$C_{16}$, *n*-$C_{15}$ to *n*-$C_{18}$ and *n*-$C_{15}$ to *n*-$C_{16}$, respectively). Hydrogen indices are in the same range as for unaltered samples (37 to 44) but OIs are slightly higher (40, 48, 52). The highest $T_{max}$ of the GC-MS samples is 467° C and is for the altered sample BIR 13. Normal alkanes as a percentage of total resolved compounds are less abundant than in least altered samples (16-20% compared to greater than 25%). Clusters of peaks from homologous sets of monomethylalkanes are not apparent and have been replaced by multiple resolved peaks of other compounds that elute at similar times as midrange *n*-alkanes. Some of these are isoprenoids, but the most prominent are PAHs like the trimethylnaphthalenes (between *n*$C_{15}$ and *n*$C_{16}$ and prominent on BIR 15, WPB-3 and BIR 13) and dimethylnaphthalenes (between *n*$C_{14}$ and *n*$C_{15}$ and prominent on the WPB and BIR 13, 15 chromatograms). Fluoranthene is dramatically present as such a PAH peak on the WPB1 chromatogram, and to a lesser extent on the WPB-3 and BIR 13 whole rock extract GC chromatograms (cf. Liang *et al.,* 2005). Pristane/phytane ratios differ between the three samples, spanning the range of this measure for all GC-MS samples (0.24 to 1.81), but may be unreliable due to peak overlap.  Phytane/octadecane ratios are higher in the three altered samples than in all of the less altered samples, and are mostly higher than the slightly altered sample.  Phenanthrene forms a distinct and moderately prominent peak.  The percentage range of resolved unknowns is higher for the altered samples than for any of the least altered samples.  There is no significant increase in the size of the UCM for the altered samples relative to the less- and unaltered samples.

The partially altered sample, BIR 15, is identifiable based on its chromatogram with characteristics intermediate between least altered and altered (Figure 72b).  Hydrogen index is slightly lower than for altered and least altered samples (28) but OI is higher than for any other GC-MS sample (60).  The range of *n*-alkanes is similar to that of least altered samples, but the concentration of high molecular mass alkanes are lower and there are double maxima at *n*-$C_{16}$ and *n*-$C_{23}$ rather than smooth decreases with increasing C number.  Normal alkanes form 19% of resolved compounds.  As with the altered samples, there is no significant increase in the UCM, the peak clusters from homologous sets of monomethylalkanes are replaced by resolved peaks near mid-range *n*-alkanes.

The least altered extracts are largely similar to most extracts previously analyzed from Nonesuch Formation shales and siltstones (Ho *et al.*, 1990; Hieshima and Pratt, 1991; Pratt *et al.*, 1991; Mauk and Hieshima, 1992; Ho and Mauk, 1996; Uchityl *et al.*, 1997).

### *6.4.2 Saturate Gas Chromatography-Mass Spectroscopy*

This study’s GC analyses of saturated HC fractions show a significant difference in the HC composition of mineralized and unmineralized samples (Figure 73).  Püttman *et al.* (1990) noted disparity in the saturate portion TIC chromatograms across Cu mineralization in the

Kupferschiefer, with saturate content lesser and overall range of chain length diminished for samples in mineralized zones. Here, however, the mineralized BIR samples show broader ranges of saturate compound elution times (and chain lengths), with abundances similar to those for barren samples. Overall, abundances of saturated compounds generally increase with depth, whereas increasing depth correlates to a narrowing of the range of detected compounds (except for the 517 profile). It is notable that the samples categorized as “altered” by the overall total extract GC chromatogram show both narrowed (WPB-1 and WPB-3) and relatively broad (BIR 13) distributions of saturated compounds. In particular, the great similarity of the WPB sample saturate TIC traces to those of the “less altered” samples is remarkable. In this respect, the aromatic portion’s GC-MS results can offer a more reasonable means of distinguishing differences potentially associated with mineralization and hydrothermal alteration of organic matter.

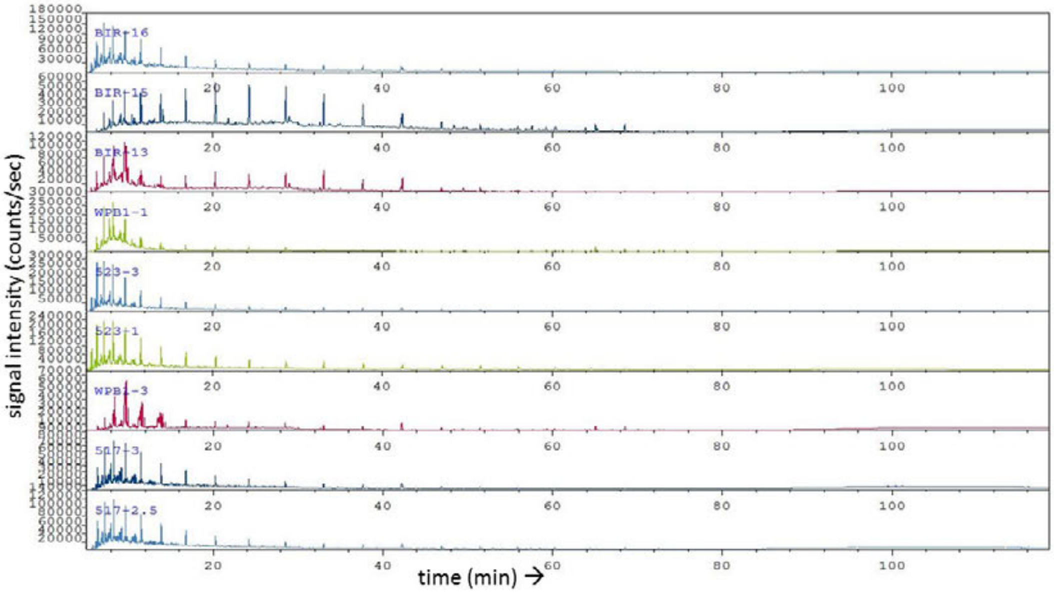

Figure 73: The saturate portion TIC for the Nonesuch Formation samples. Notice the broader range and similar abundance of detected compounds for the mineralized BIR samples. This finding is counter to the well-documented trend of diminished saturate compounds in mineralized Kupferschiefer samples.

The majority of the GC-MS samples in this study contain the $C_{32}$ 2-alpha methylhopanes, which are only known from cyanobacteria (cf. Dutkiewicz *et al.*, 2006 and Summons *et al.,* 1988). Only the 523-3, 517-3, and the BIR 16 samples did not contain these compounds, while the rest showed concentrations between 1 and 4 ppm total for the compounds.

The majority of the samples in this study show *m/z* 191 mass chromatograms in which tricyclic terpanes (*m/z* 191) maximize at $C_{23}$ and also include a series of extended tricyclic terpanes to at least $C_{30}$. This is true for 523-3 (10 ppm), 517-2.5 (14.5 ppm), BIR 13 (69.1 ppm), and BIR 15 (63.2 ppm) based on peak areas. Samples BIR 16, 517-3, and 523-1 maximize at $C_{23}$ as well, but show limited spread and lesser $C_{23}$ concentrations (10.3, 3.5, and 3.3 ppm, respectively and spreads to $C_{26}$, $C_{25}$, and $C_{24}$, respectively). The *m/z* 191 mass chromatograms for samples WPB-3 and WPB-1 respectively maximize at $C_{19}$ and $C_{20,}$ but significant concentrations of $C_{23}$ tricyclic terpanes are still apparent (32 and 37.6 ppm, correspondingly).

The distribution of tricyclic terpanes of these samples is typical of generation from algal and/or bacterial organic matter (cf. Dutkiewicz *et al*., 2006). The majority of the GC-MS samples in this study contain the $C_{32}$ 2-alpha methylhopanes, which are only known from cyanobacteria (cf. Dutkiewicz *et al*., 2006 and Summons *et al.,* 1988). Further, the presence of significant concentrations of 1,2,5-TMN in the aromatic fraction of all 9 samples indicates probable cyanobacterial input (cf. Colbert, 2011). This is in alignment with chroococcalian cyanobacterial cells and masses observed by Strother and Wellman (2016) in Nonesuch Formation kerogen concentrates.

Most samples in this study (excluding 517-3 and 523-1) show the $C_{21}$ molecule pregnane as the dominant sterane (*m/z* 217).

### *6.4.3 Aromatic Gas Chromatography-Mass Spectroscopy*

#### *6.4.3.1 Aromatic Gas Chromatography-Mass Spectroscopy Total Ion Current Chromatogram*

The GC-MS analysis on the aromatic fraction of extracts detected and quantified multiple mid- and higher-mass PAHs and monoaromatic and triaromatic steroid biomarkers (MAS and TAS). Signal to noise ratio was good for most mass fragmentograms, except for triaromatic methyl steroids (*m/z* 245) in three least altered samples that are dominated by *n*-alkanes (core samples from NE WP mine area 517-3, 523-1, 523-3).

The aromatic compound 1,2,5-TMN, elsewhere linked to unicellular photosynthetic inputs (cf. Peters *et al*., 2005), is present in all samples in significant concentrations (excepting the 0.5 ppm in 517-3).

Overall there are similarities and differences between the traces of the different samples. All samples have a large number of unidentified peaks at early elution times on the *m/z* 231 (TAS) fragmentogram. These are derivatives of pregnane and similar molecules with C numbers from 19 to 21 (Figure 74). Samples from WPB have much higher concentrations of multiple early-eluting aromatic steroids than all other samples.

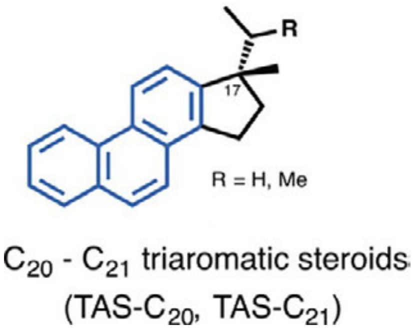

Figure 74: Structure of sterane TAS molecules derived from aromatization of homopregnane ($C_{20}$) and pregnane ($C_{21}$). Aeppli *et al.*, 2014.

All samples have high to extremely high concentrations of non-biomarker PAHs and derivative compounds, notably 3-methylbiphenyl, phenanthrene, trimethylnaphthalenes, methylphenanthrenes and dimethylphenanthrenes. In addition, biphenyl, dibenzofuran, dibenzothiophene, fluorene and derivatives were quantified in all samples.

Phenanthrene dominates the BIR 13 aromatic TIC; methylphenanthrene peaks are the second most prominent compounds, with DBF the fourth most abundant compound, based on the similarities of the Nonesuch Formation sample in the *m/z* 178, 192, 206, and 220 mass fragmentograms to those found in the literature (Ré-Poppi and Santiago Silva, 2002). An unidentified mixed-mass spectra peak is third highest. Also apparent are the dimethylphenanthrene and lesser trimethyldibenzothiophene peaks (Figure 75).

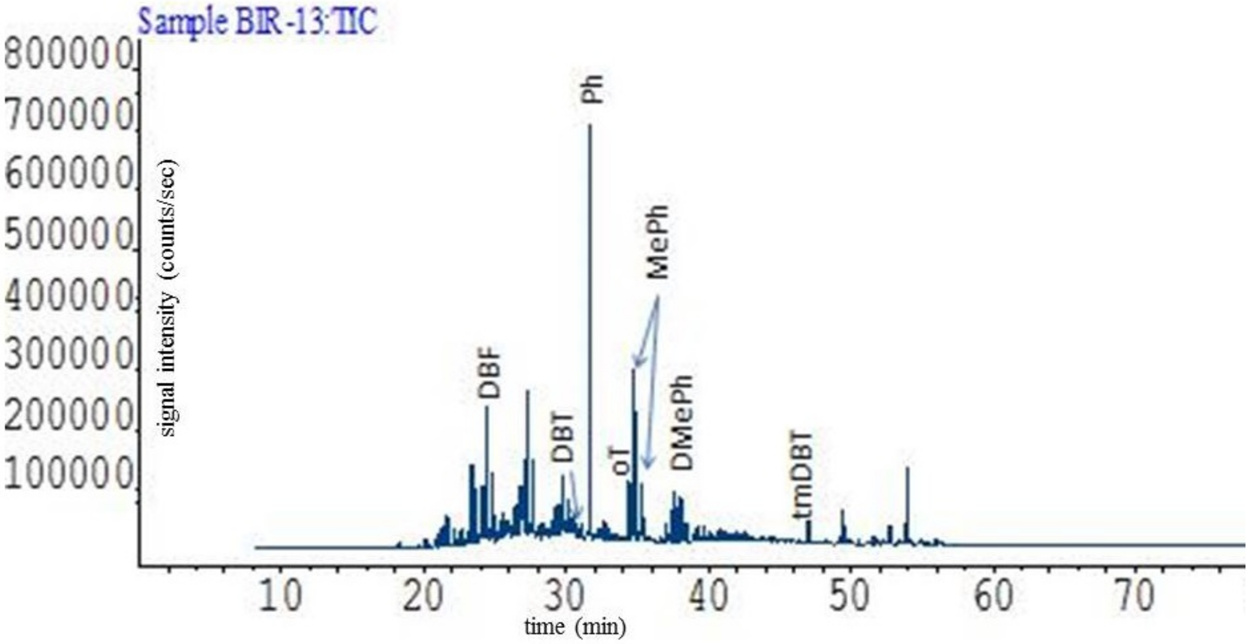

Figure 75: The TIC for the aromatic portion of the BIR 13 sample is dominated by phenanthrene (Ph), and successively by its methylated homologues (methyl-, dimethyl-, ethyl-). The four methylphenanthrene peaks are together depicted as MePh. Eluting just prior to the dimethylphenanthrenes (DmePh) and the methylphenanthrenes is the o-terphenyl (oT) peak, the internal reference standard. The next two smaller peaks represent various co-eluted, unidentified ions of *m/z* below 178.The late eluting peaks are of mixed mass. The minor trimethyldibenzothiophene peak is labeled tmDBT.

The WPB-3 sample's aromatic portion is strongly dominated by the phenanthrene and o-terphenyl (internal reference standard) peaks respectively (Figure 76). The unidentified large peak between DBF and DBT on the WPB chromatogram shows five different *m/z* fragment contributors on its mass spectrum. The unidentified large peak between DBF and DBT shows no identifiable *m/z* dominance. Benzo(b)naphthothiophene (cf. Rospondek *et al.*, 2007) is apparent as a late-eluting *m/z* 234 constituent of minor abundance. Trimethyldibenzothiophene is the latest-eluting peak identified.

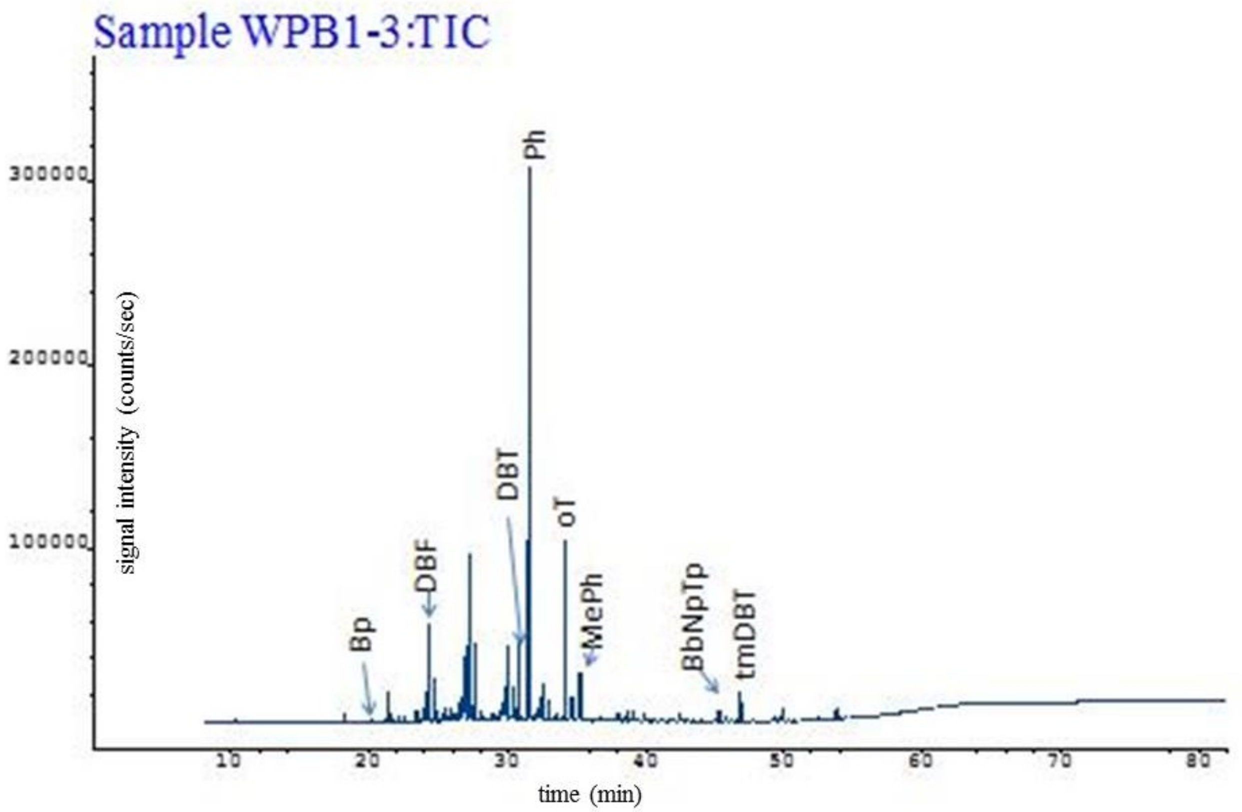

Figure 76: Phenanthrene (Ph) and o-terphenyl (oT, internal reference standard) dominate the aromatic TIC of WPB-3. The unidentified large peak between DBF and DBT shows no identifiable *m/z* dominance. Benzo(b)naphthothiophene (BbNpTp) (cf. Rospondek *et al.* (2007)) is apparent as a late-eluting *m/z* 234 constituent of minor abundance. Trimethyldibenzothiophene (tmDBT) is the latest-eluting peak identified. The methylphenanthrene peaks are together depicted as MePh. Biphenyl (Bp) is the earliest eluting compound on this chromatogram.

The WPB-1 sample's aromatic TIC (Figure 77) dominant peak is the phenanthrene (o-terphenyl being the reference standaard), with lesser methylbiphenyl as the second most abundant compound and a C3-naphthalene couplet third with TMN compounds making up the fourth most abundant peak.

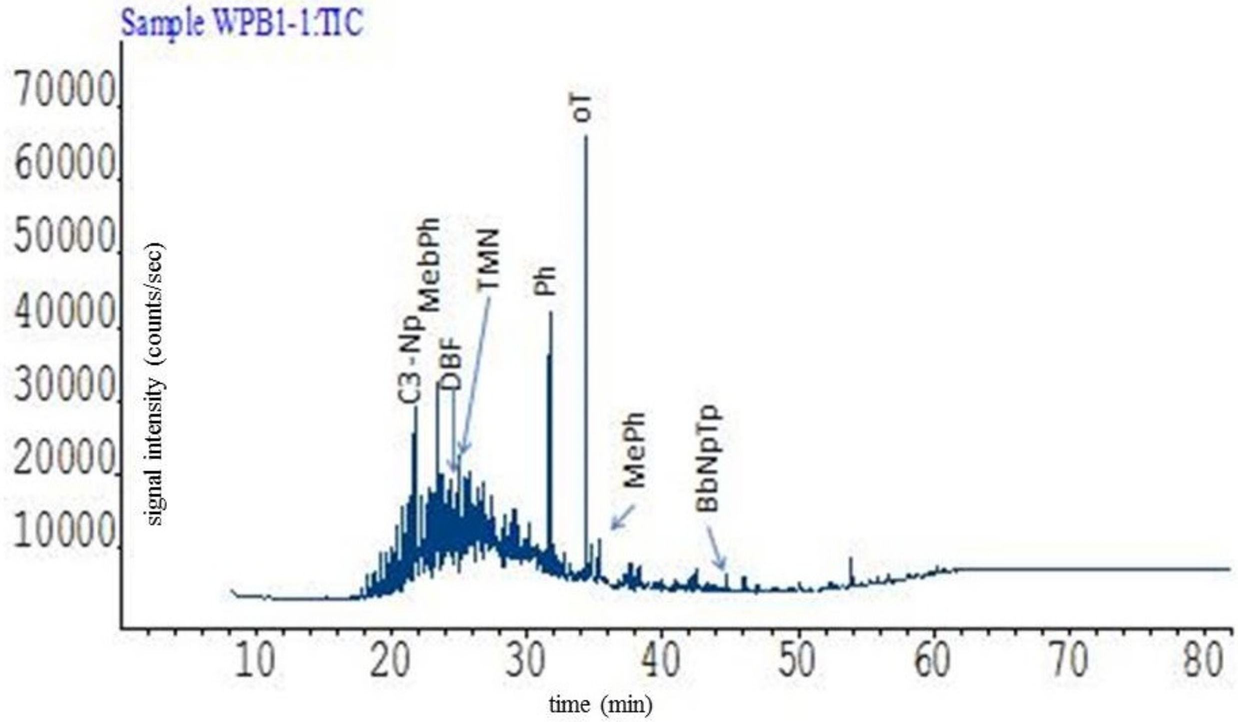

Figure 77: Internal reference standard o-terphenyl (oT) is most noticeable on the WPB1 aromatic TIC; the phenanthrene (Ph) peak is the most prominent indigenous derived peak on the aromatic TIC of WPB-1. Methylbiphenyl (MebPh) is the second most abundant compound and a C3-naphthalene (C3-Np) couplet is third with TMN compounds making up the fourth most abundant peak. DBF is apparent as well. The four methylphenanthrene (MePh) peaks are together depicted as MePh. Benzo(b)naphthothiophene is apparent as the latest eluting identified compound. The peak similar to that which was tentatively identified as the trimethyldibenzothiophenes does not show a singular mass dominance and remains unidentified for WPB1.

The least altered BIR 16 aromatic TIC shows the same strongly dominant phenanthrene maximum as do the other mineralized as well as the altered samples. The mineralized BIR samples also all show the second most abundant aromatic constituents as the methylphenanthrenes (around 34.8 minutes, *m/z* 192). See Figures 78 to 83.

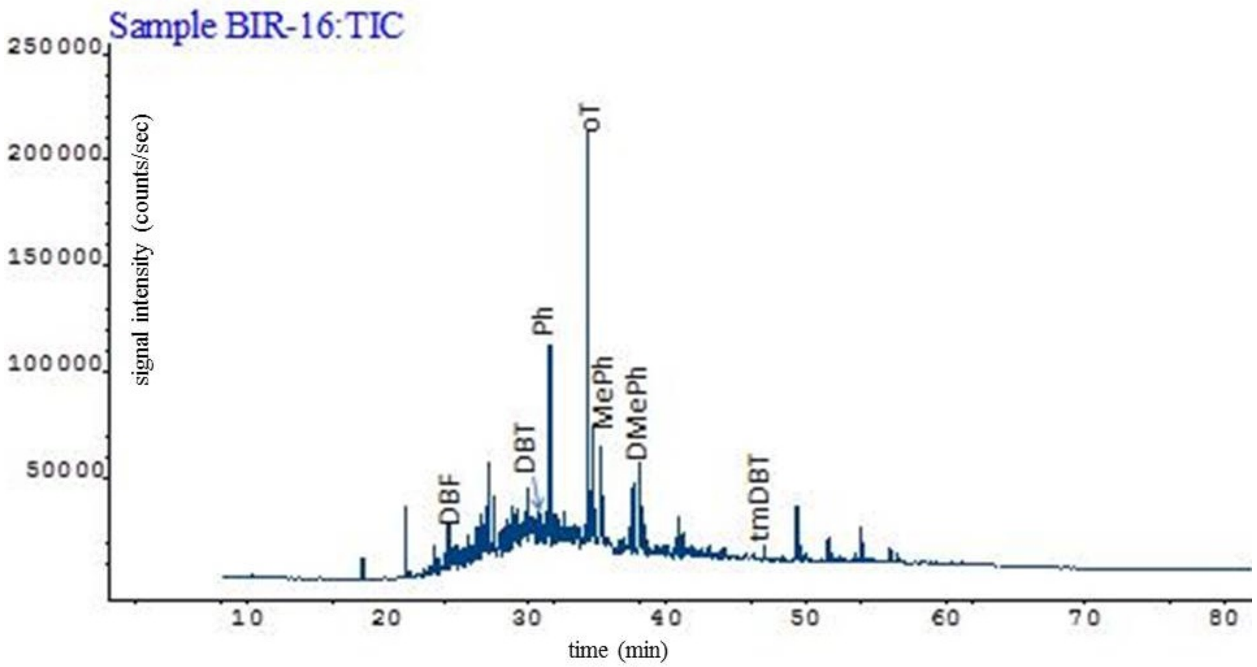

Figure 78: The total ion chromatogram for the aromatic portion of the mineralized but least organically altered BIR 16 sample.

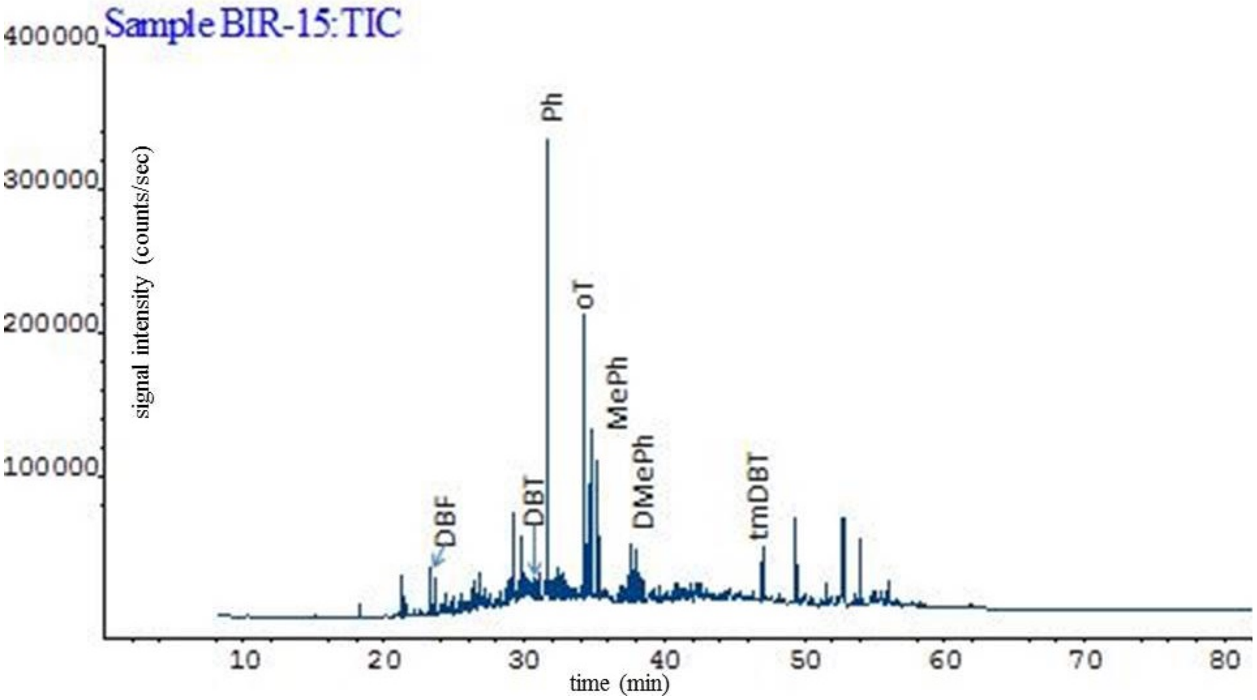

Figure 79: The aromatic fraction total ion chromatogram for the BIR 15 sample, mineralized and slightly altered.

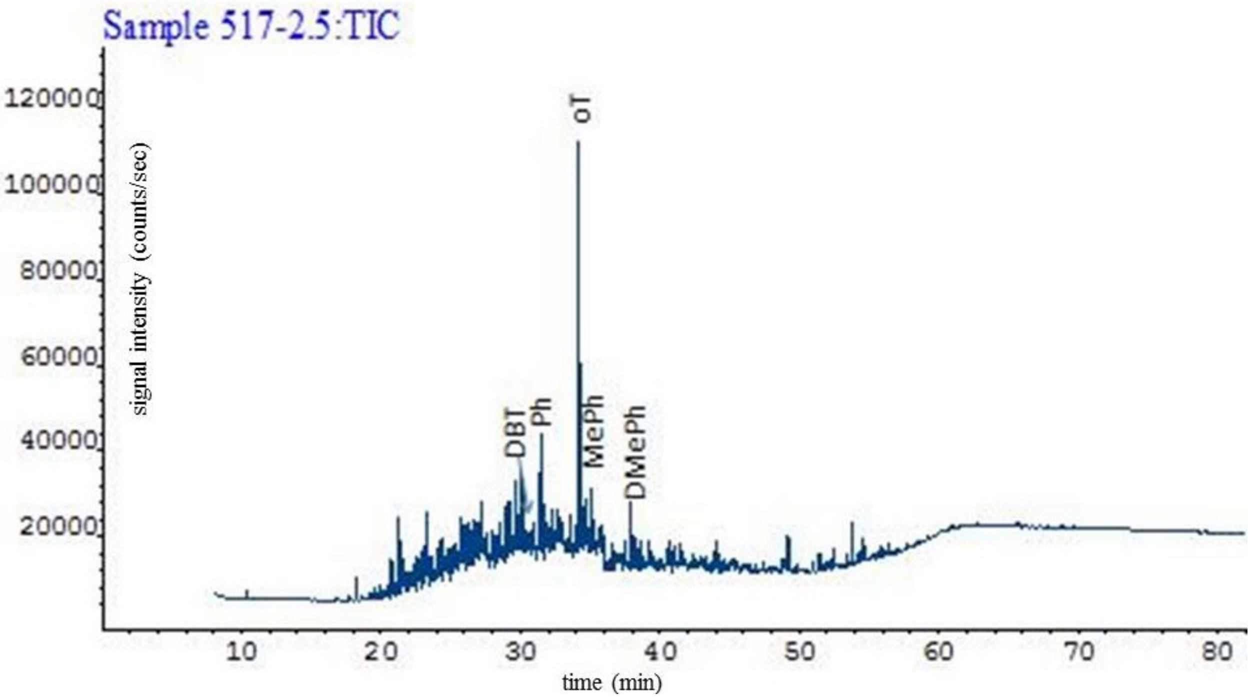

Figure 80: The aromatic TIC for the unmineralized distal to Cu mineralization and least organically altered sample 517-2.5.

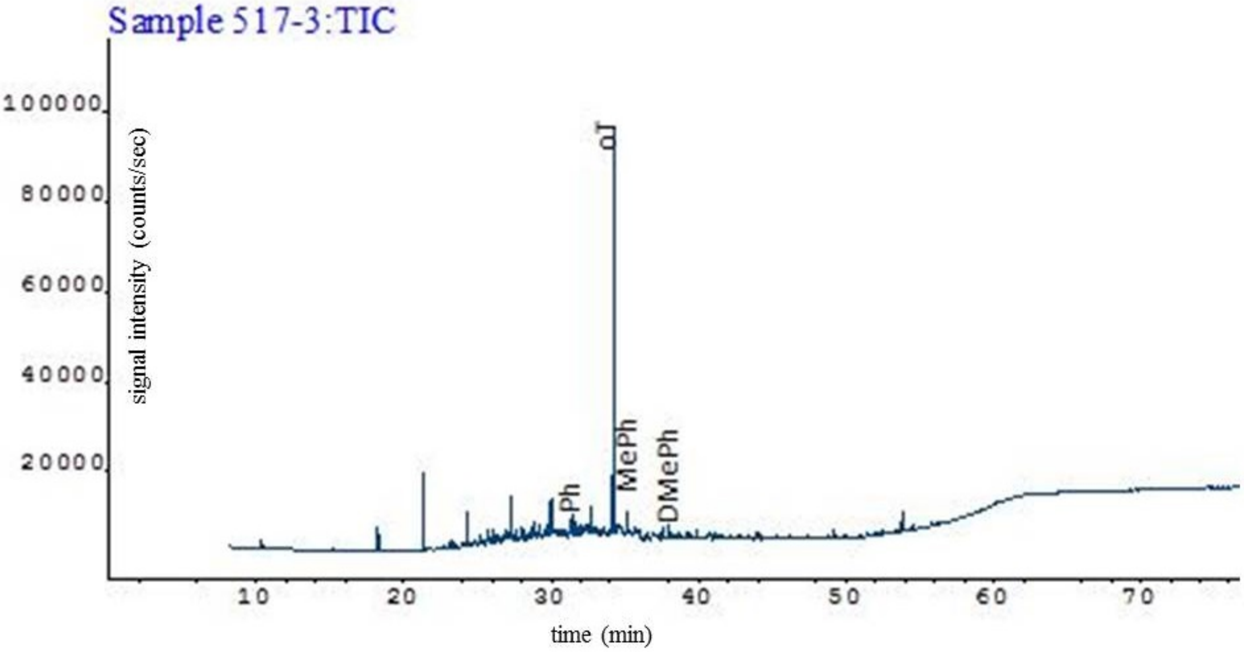

Figure 81: The total ion chromatogram for aromatic portion of sample 517-3, which is unmineralized and least organically altered as well as distal to Cu mineralization.

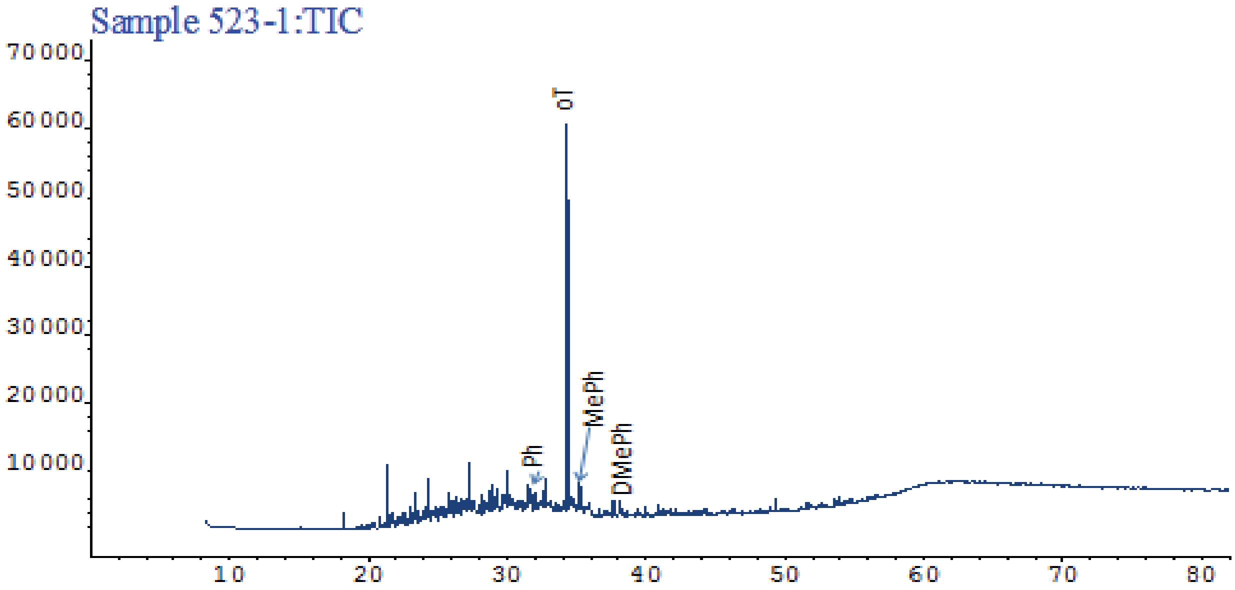

Figure 82: The TIC for the aromatic portion of 523-1. Unmineralized sample is within 5 m of overlying Cu mineralization.

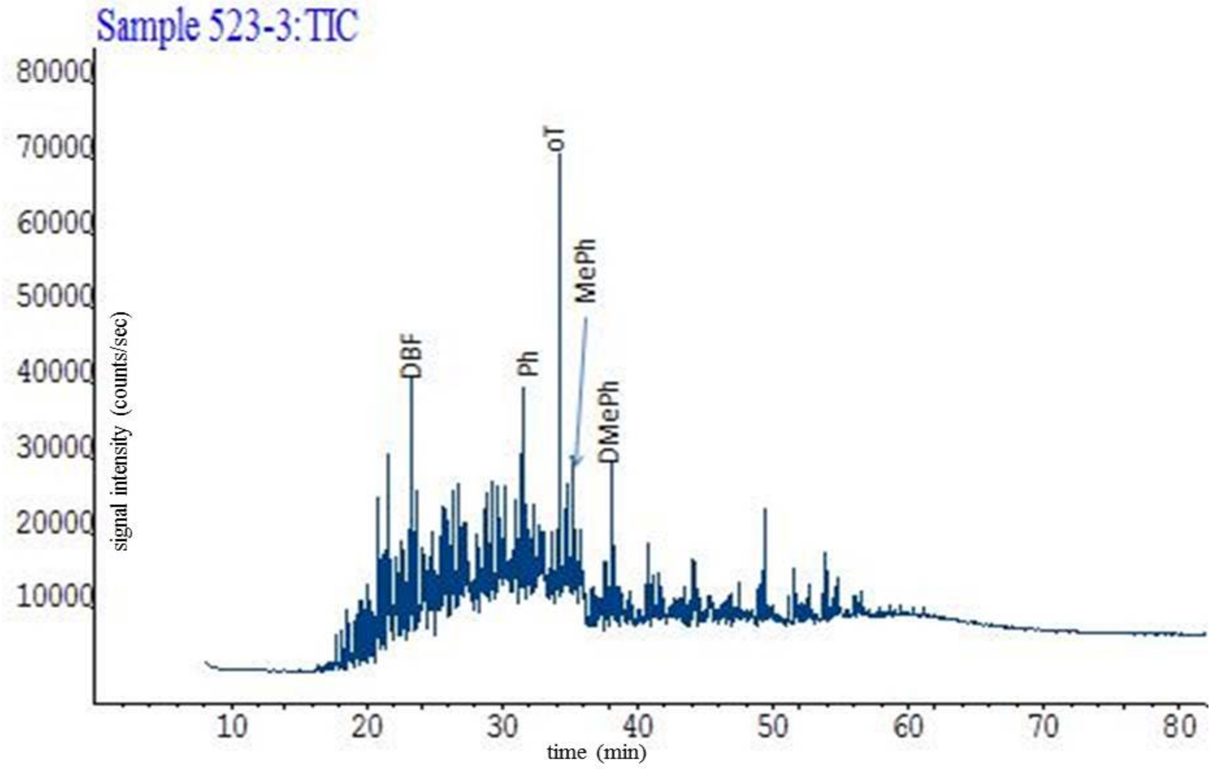

Figure 83: Total ion current chromatogram for the 523-3 sample's aromatic fraction. Unmineralized but semi-proximal to Cu mineralization (5.4 m below it, and 12.2 m above it).

Comparative aromatic TIC chromatograms are found in Figures 84 to 87.

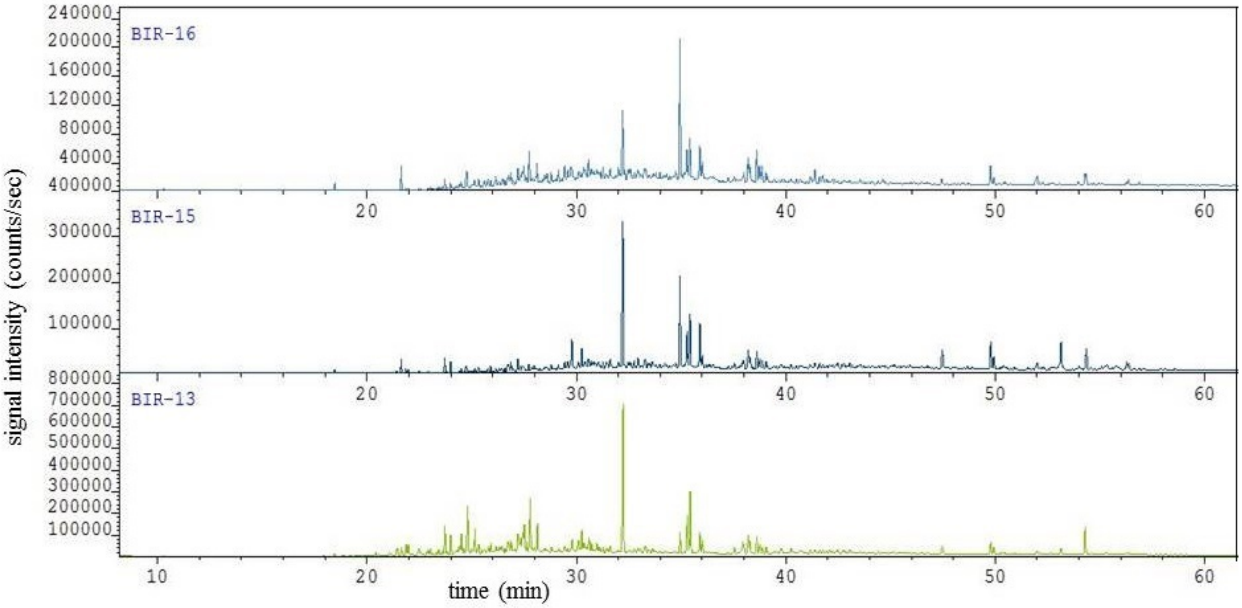

Figure 84: The aromatic portion TIC for the three mineralized BIR samples (sample BIR 16 is least altered, BIR 15 is slightly altered and BIR 13 is most altered). BIR 13 and BIR 15 (dark blue and green) show phenanthrene as the most abundant aromatic, and their second most abundant aromatic constituents as the methylphenanthrenes (around 34.8 minutes, *m/z* 192). The prominent maximum on BIR 16's aromatic TIC is the o-terphenyl (*m/z* 230, internal reference standard), which is also apparent as the second highest peak on the other BIR samples.

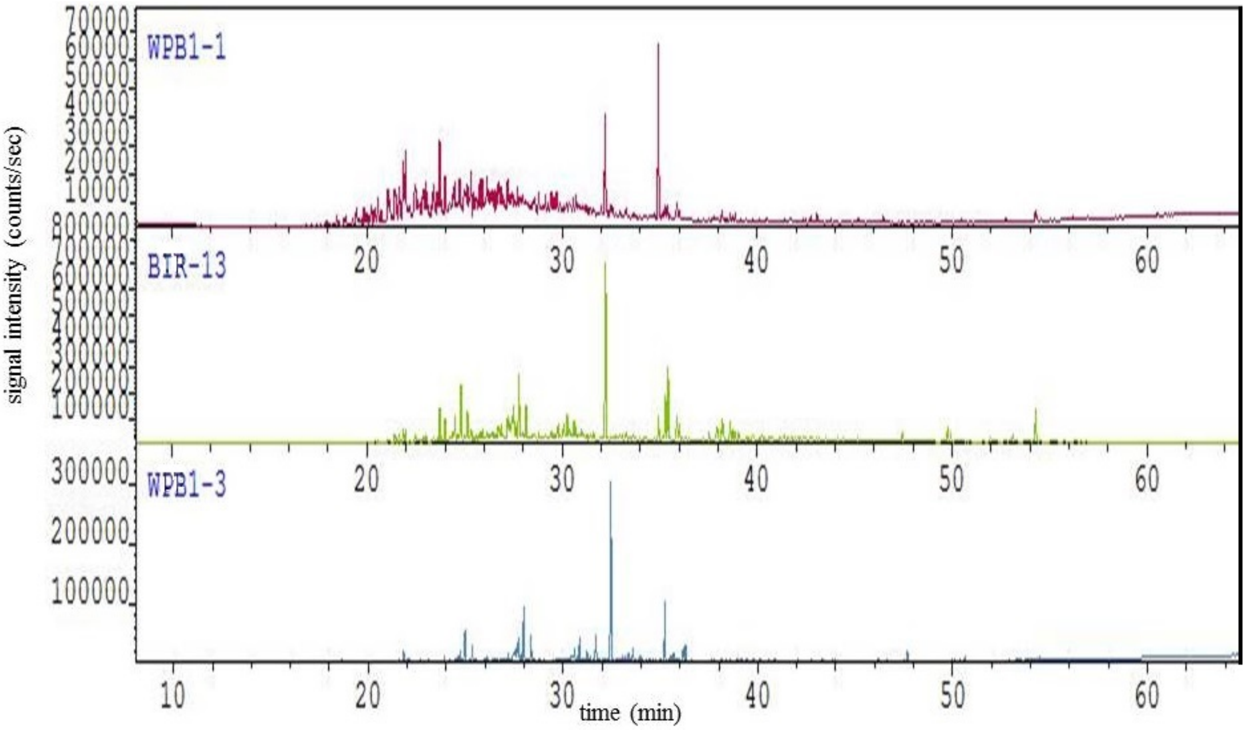

Figure 85: Aromatic TIC for most altered samples. The WPB-1 is the lowest in section of the three, and shows the broadest UCM.

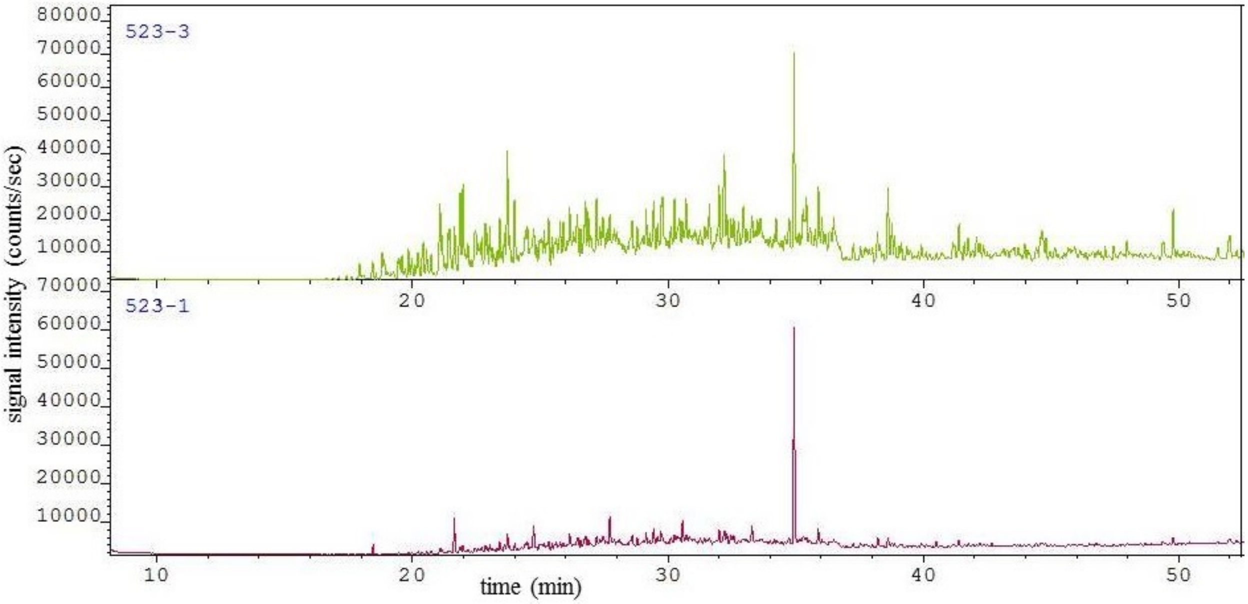

Figure 86: The TIC for the aromatic portion of the 523 samples showing their shared maximum as the *m/z* 230 internal reference standard o-terphenyl.

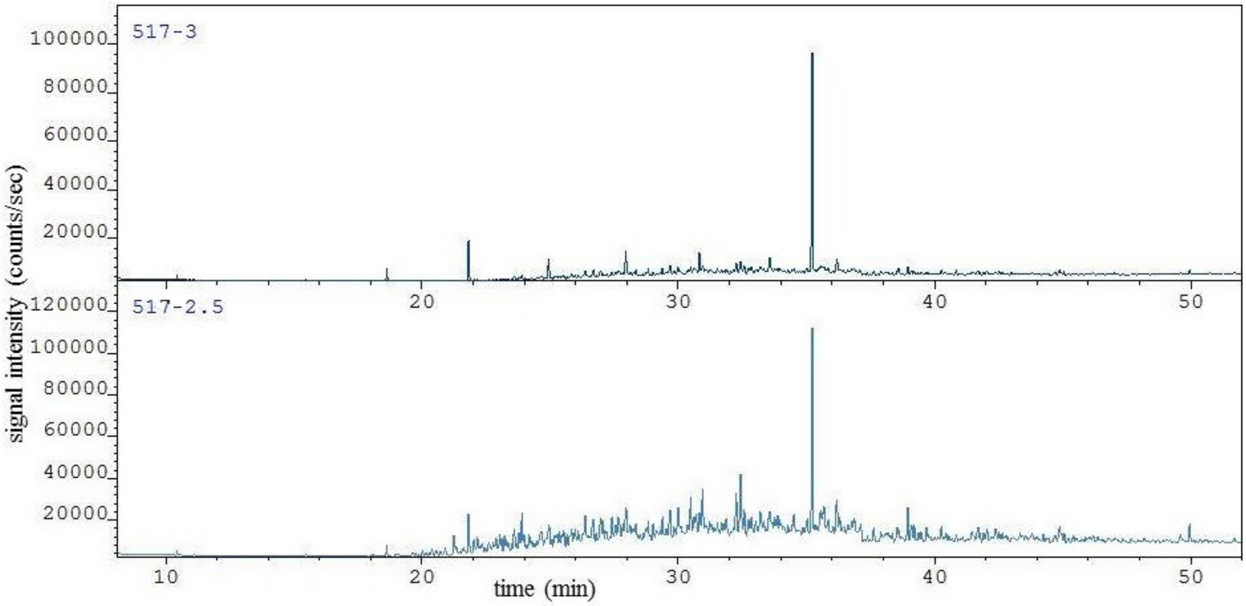

Figure 87: The TIC for the aromatic portion of the 517 samples showing their shared maximum at *m/z* 230, the o-terphenyl reference standard.

### *6.4.3.2 Aromatic Gas Chromatography-Mass Spectroscopy Ion Chromatograms*

The MAS (*m/z* 253) chromatogram for BIR 13 (Figure 88) shows the benzo(e)pyrene as the dominant compound, followed closely in abundance by benzo(a)pyrene. Lesser benzofurans and perylene are also present.

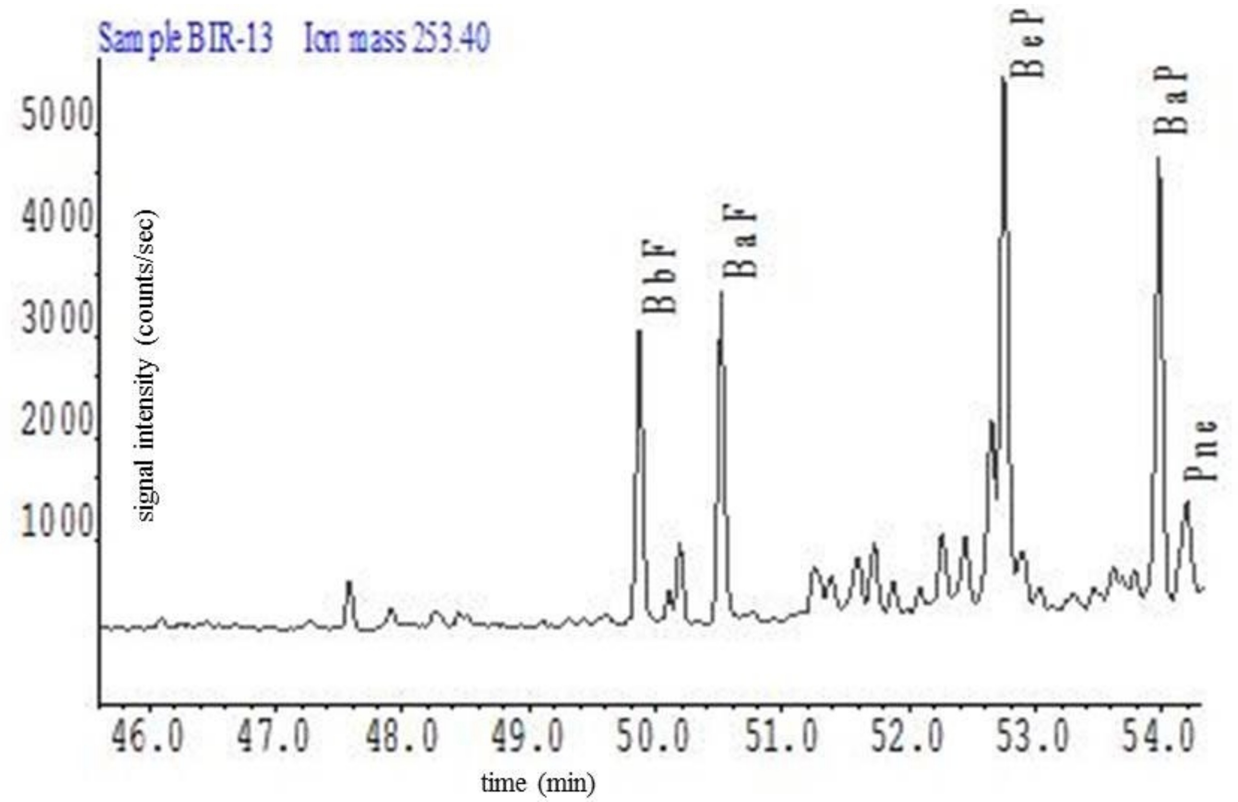

Figure 88: The BIR 13 *m/z* 253 chromatogram shows identical peaks to the more abundant PAH compounds of BIR 15, BIR 16 and WPB-1. The benzo(e)pyrene (BeP) peak most prominent, secondary abundance of benzo(a)pyrene (BaP). The benzo(a)fluoranthene (BaF) and benzo(b)fluoranthene (BbF) peaks are also apparent as third and fourth most abundant, followd by perylene (Pne).

The TAS chromatogram (*m/z* 231) of BIR 13 shows the most abundant TAS compound being the $C_{21}$ homopregnane-derivative diasterane - pictured in Figure 74 - at just 25% the abundance of the three maximum peak heights, which are unidentified because they consist of multiple co-eluting mass fragments.

The BIR 13 *m/z* 245 aromatic chromatogram's most abundant triaromatic methylsteroids identified by Weatherford are below 20% the height of the most abundant peak, which is dominated by *m/z* 226 contribution, likely benz(a)anthracene.

Comparison with the *m/z* 252 chromatogram (in order to identify fragmentation ratios to aid in peak identification) and the literature reveals that the WPB-3 *m/z* 253 chromatogram shows the benzo(a)pyrene peak most prominent, secondary abundance of benzo(e)pyrene and perylene as the third most abundant component. The next four highest peaks show contribution from multiple co-eluting compounds and do not conform to expected breakdown ratios *m/z* 252/253; these remain unidentified. The benzo(a)fluoranthene and benzo(b)fluoranthene peaks are also apparent. It is probable that the earliest eluting peaks represent the phenylphenanthrenes, and also the 2,2-binaphthalene. See Figure 89. Grafka *et al.* (2015) proposed dehydrocylization of phenylphenanthrene parent molecules as the dominant genetic mechanism in the formation of benzo(b)fluoranthene and benzo(e)pyrene.

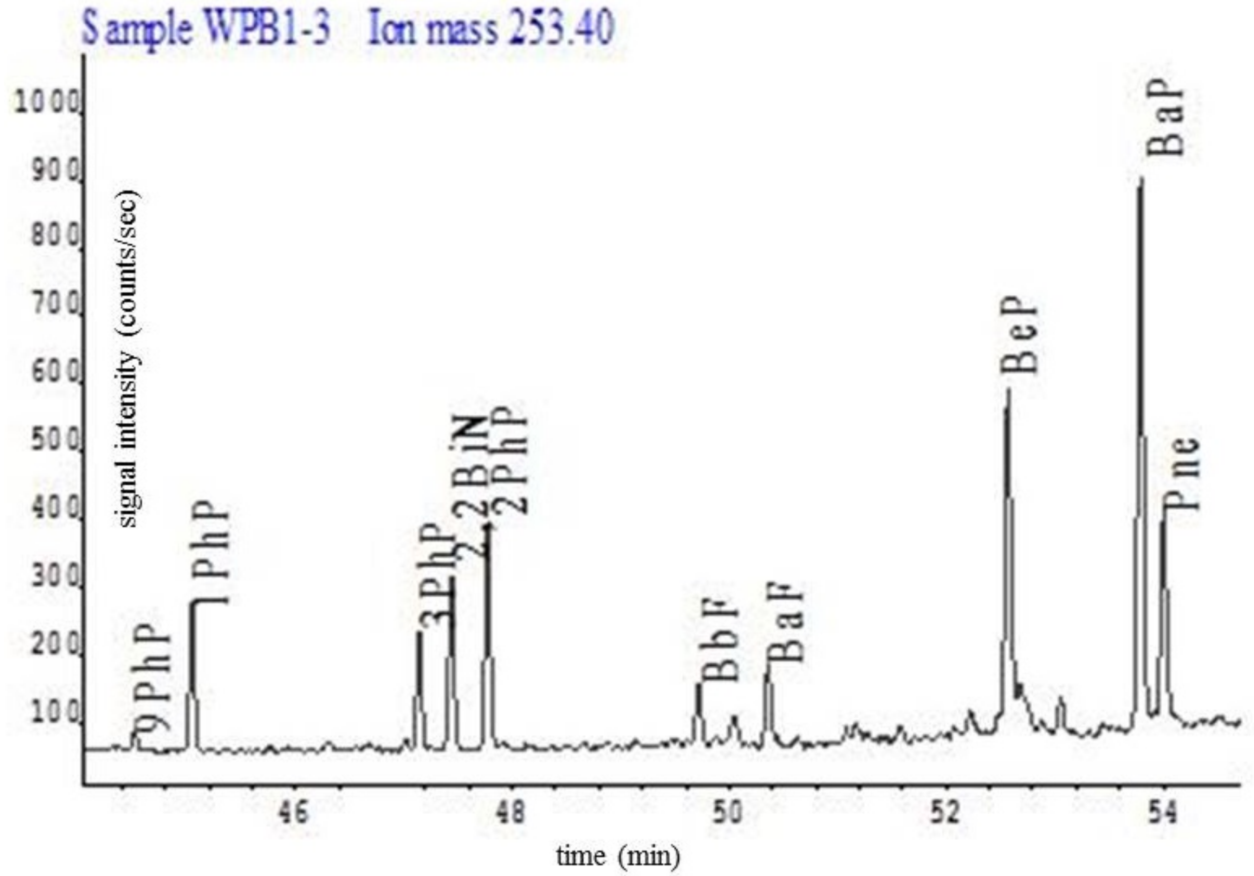

Figure 89: The *m/z* 253 MAS chromatogram for the WPB-3 sample. The benzo(a)pyrene (BaP) peak most prominent, secondary abundance of benzo(e)pyrene (BeP), and perylene (Pne) as the third most abundant component. The benzo(a)fluoranthene (BaF) and benzo(b)fluoranthene (BbF) peaks are also apparent. Grafka *et al.* (2015) proposed dehydrocylization of the PhP parent molecules for the formation of BbF and BeP.

The WPB-3 *m/z* 231 chromatogram shows dramatically lower abundance and greater noise than for the other altered *m/z* 231 plots. Again, though, early eluting peaks showed too mixed a composition for positive identification, but approach a factor of three greater peak height than the TAS compounds identified by Weatherford. No positive identification of the mixed compound co-eluting peaks early on the *m/z* 231 is possible for WPB-3 at this time. The *m/z* 245 is similar to that of WPB-1, with early-eluting mixed *m/z* contributed unidentified peaks dominant. It is clear that most of the unidentified early-eluting peaks bear some contribution from substituted *m/z* 230 compounds, likely methylphenylnaphthalene.

The MAS (*m/z* 253) chromatogram for WPB-1 shows benzo(a)pyrene as the dominant component, with lesser benzo(e)perylene and perylene (Figure 90). Early-eluting compounds on the *m/z* 253 are mixed mass signals, with the fourth highest showing a significant component of methylated homologues of phenanthrene; their resemblance to the phenylphenanthrenes and binaphthalene in WPB-3 suggests at least some contribution from these compounds.

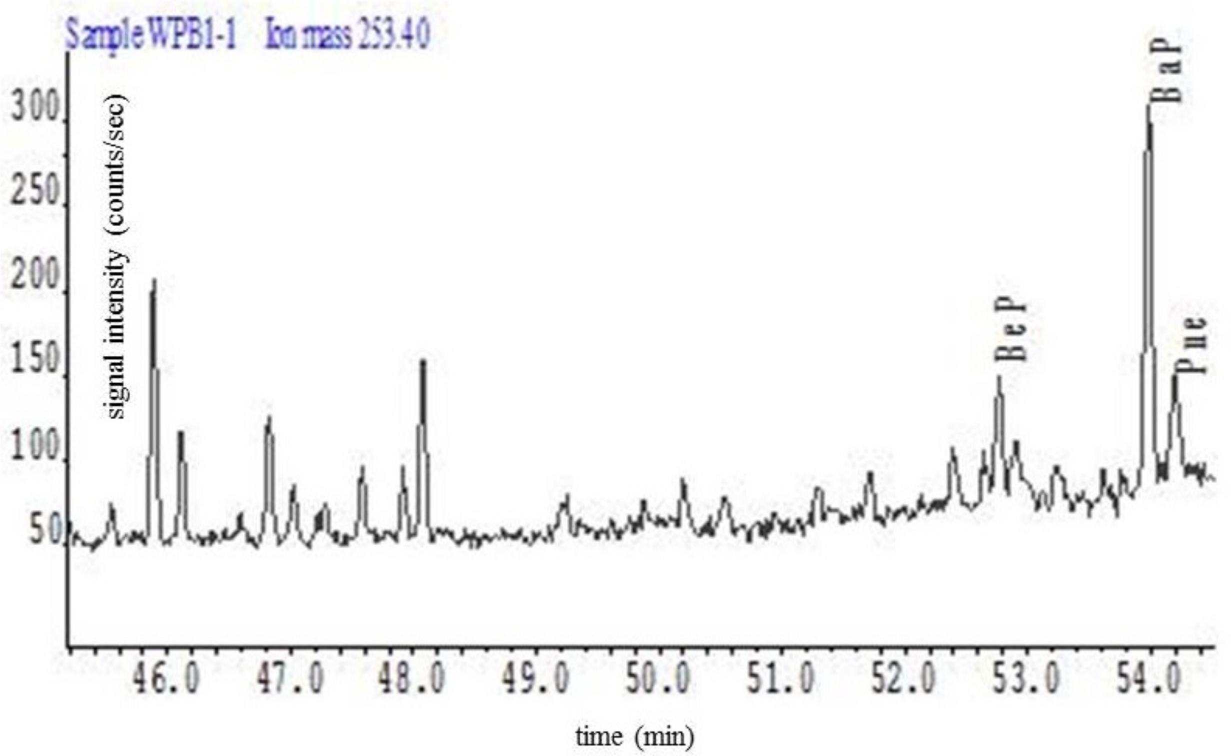

Figure 90: The benzo(a)pyrene (BaP) peak most prominent, secondary abundance of benzo(e)pyrene (BeP), and perylene (Pne) as the third most abundant component.

Far lesser abundance of the TAS compounds exist in WPB-1 than in the previous altered *m/z* 231 chromatograms. The WPB-1 *m/z* 231 (TAS) chromatogram shows the most abundant TAS compound being the $C_{21}$ at 75% the height of the highest peak. The maximum peak on the *m/z* 231, as well as the third and fourth highest peaks, show a mixture of contributing fragments and remain unidentified. The perylene identified in the *m/z* 253 chromatogram contributes about half the peak height of the highest peak on the *m/z* 231. The *m/z* 245 for the WPB-1 sample shows triaromatic methylsteroids as present, but they are well below the maximum height, early eluting *m/z* 220-rich probable methylated phenanthrene peak, which is 30% higher than the most abundant triaromatic methylsteroid. Figures 91 to 96 show the *m/z* 253 chromatograms for the remainder of the sample suite, while comparative *m/z* 253 chromatograms are found in Figures 97 and 98.

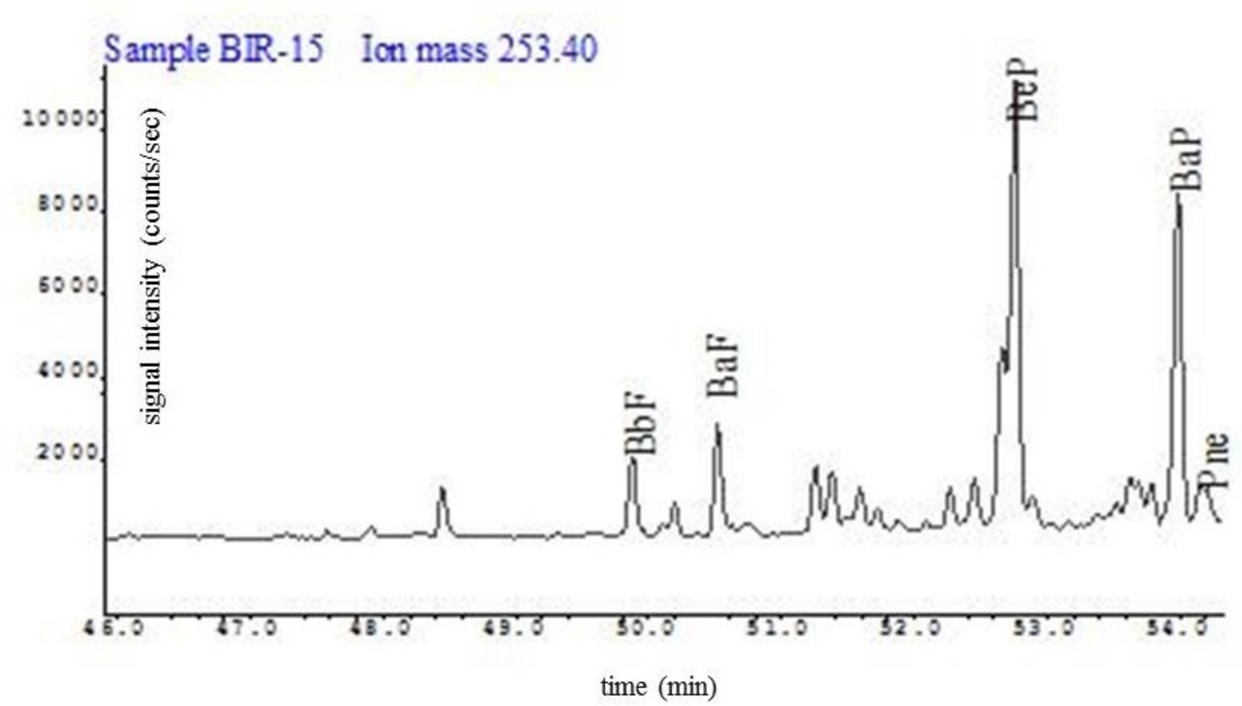

Figure 91: The *m/z* 253 chromatogram for the slightly altered, mineralized BIR 15 sample.

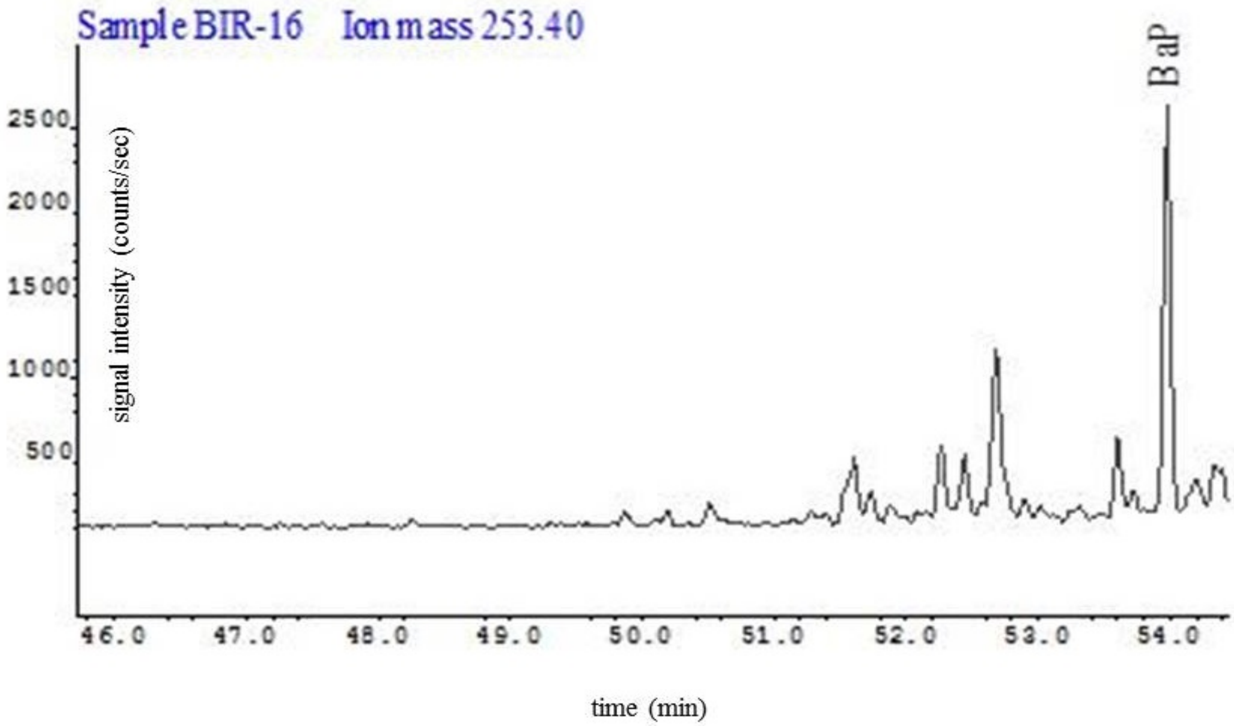

Figure 92: The *m/z* 253 chromatogram for the mineralized but least organically altered BIR 16.

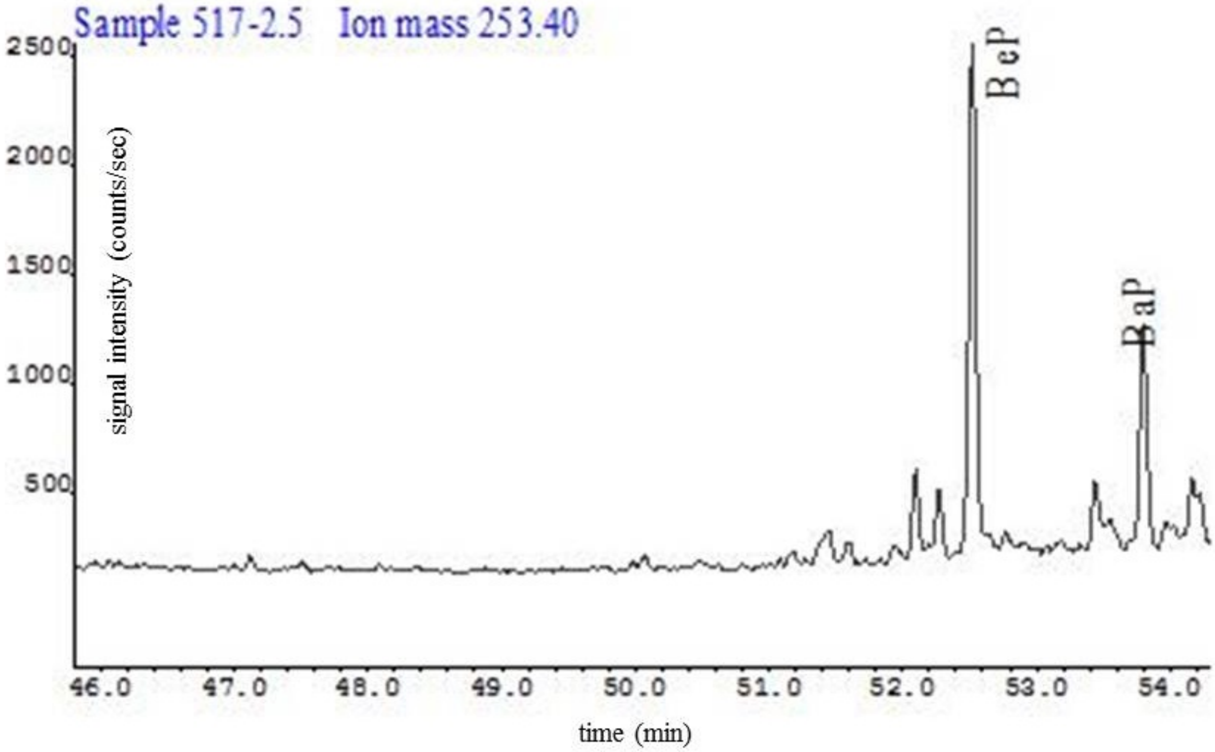

Figure 93: The *m/z* 253 chromatogram for the unmineralized, least altered and distal to Cu mineralization sample 517-2.5.

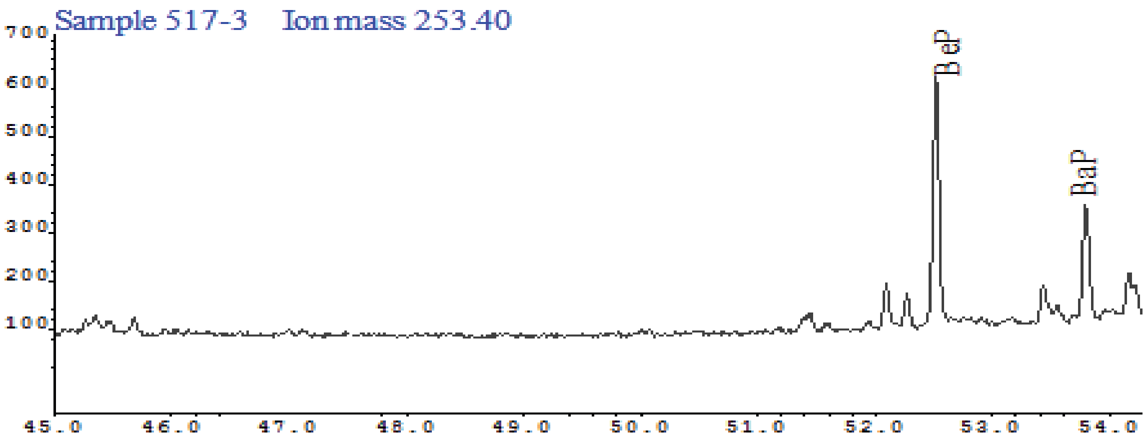

Figure 94: The *m/z* 253 chromatogram for the least organically altered, unmineralized and distal to Cu sulfide mineralization sample 517-3.

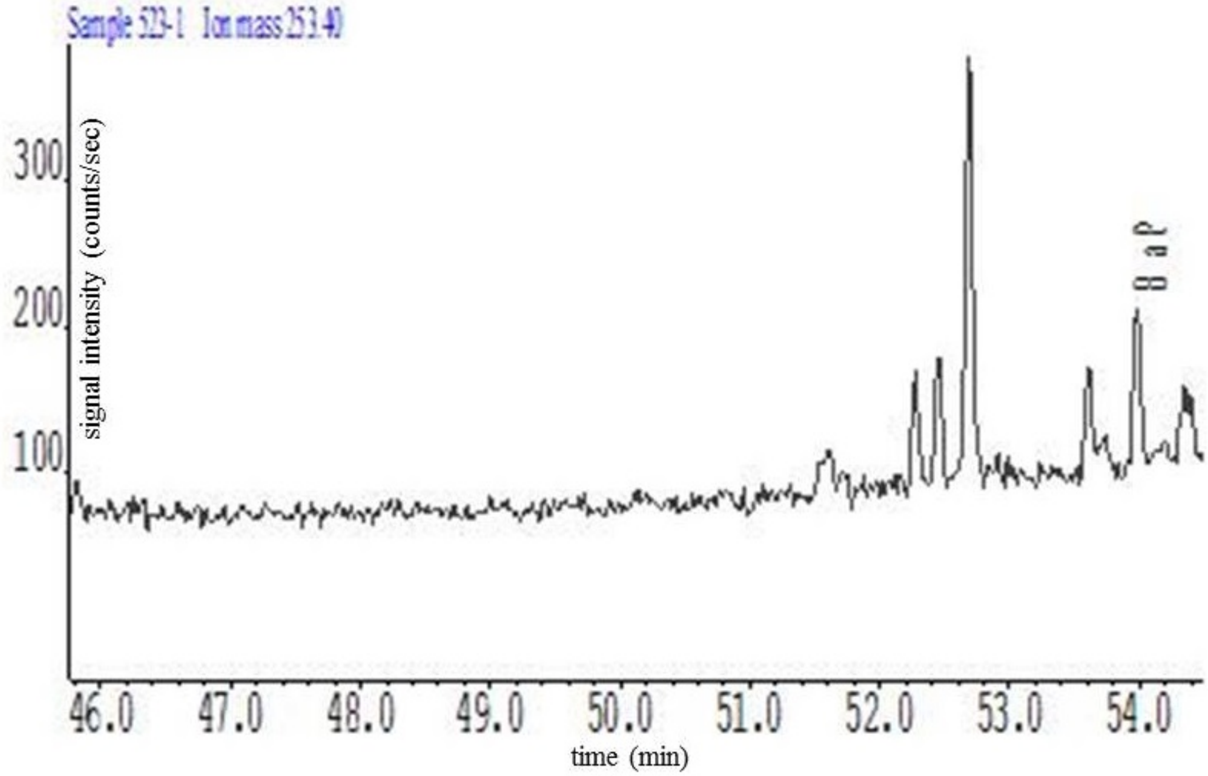

Figure 95: The *m/z* 253 chromatogram for the 523-1 sample. This sample is barren but within 5 m of the overlying Cu mineralization.

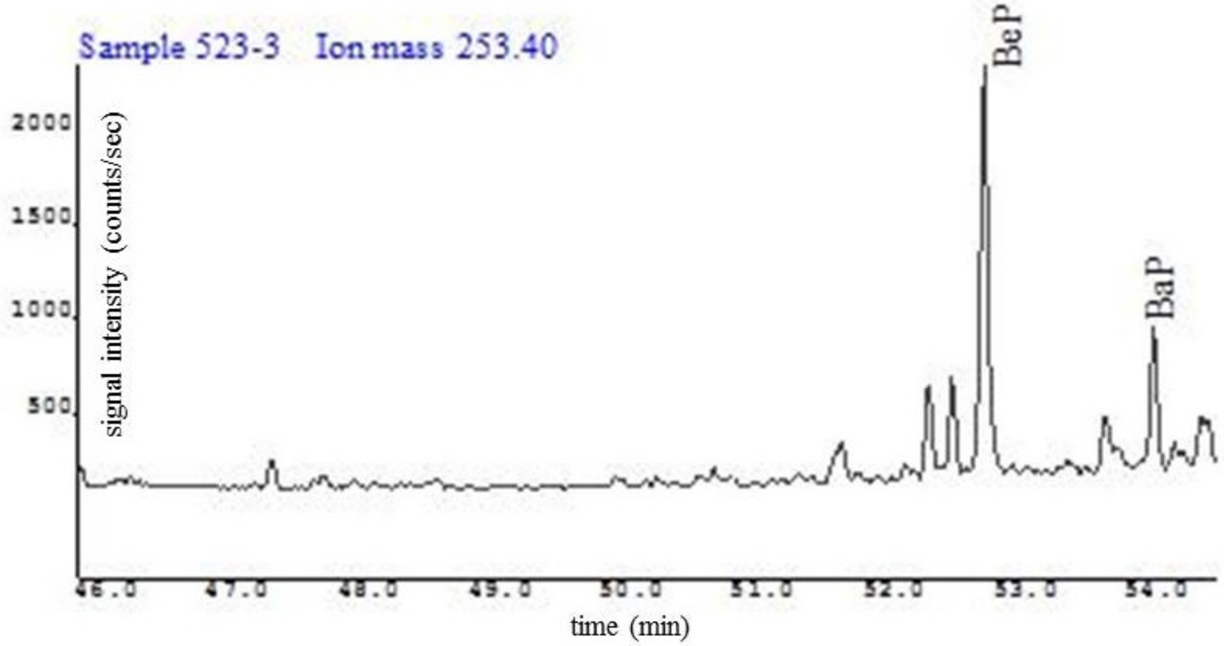

Figure 96: Ion *m/z* 253 chromatogram for sample 523-3. This sample is unmineralized, and 5.4 m below mineralization, as well as 12.2 m above Cu mineralization.

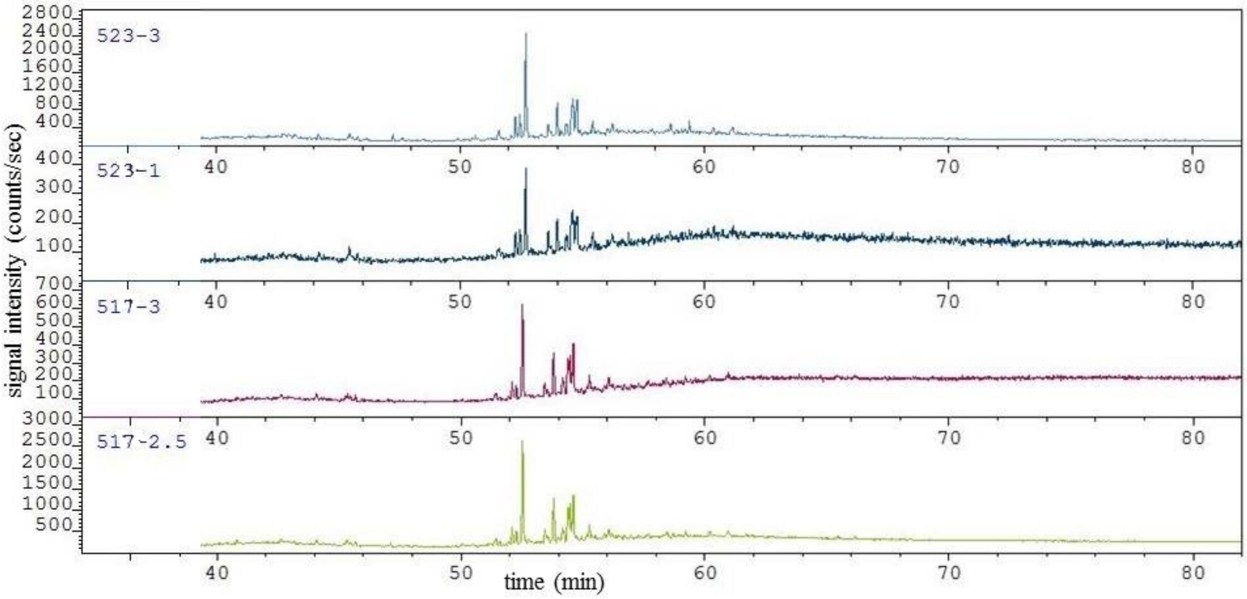

Figure 97: *M/z* 253 MAS chromatogram comparison for four of the least altered samples - 517(red and green) and 523 (light and dark blue) samples. Note the greater abundance of these compounds in the two samples from closest-to-base of Nonesuch Formation.

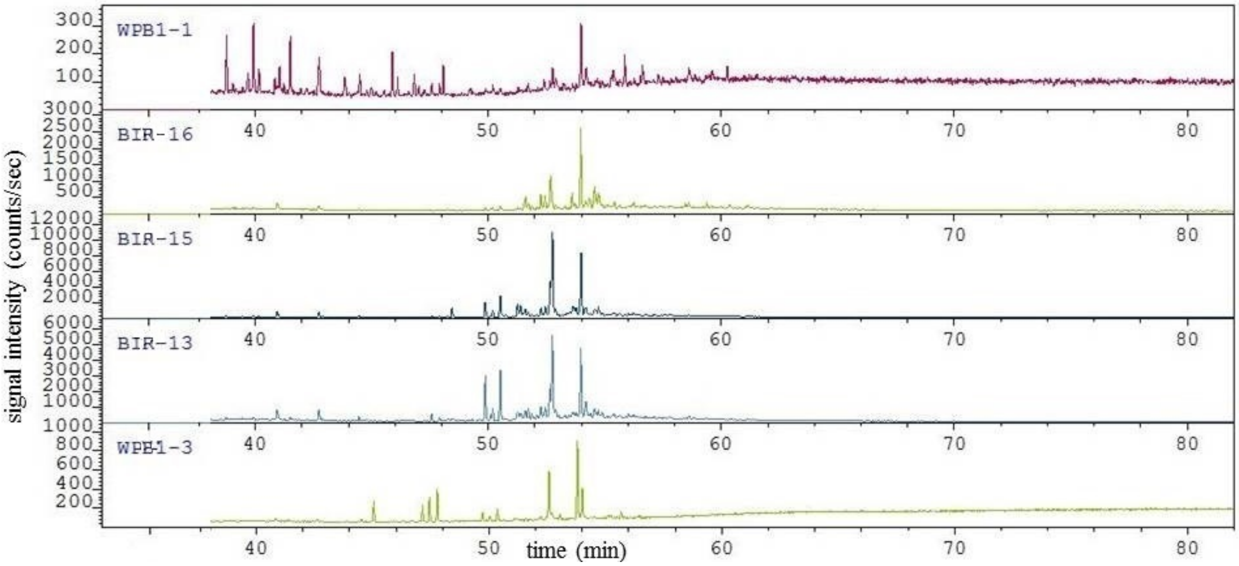

Figure 98: *M/z* 253 MAS chromatogram comparison for the WPB and BIR samples.

### *6.4.3.3 Polycyclic Aromatic Compound Ternary Plot*

Li *et al*. (2013) compared 150+ samples of known, varied depositional origin on ternary plots of the total contents of fluorene, dibenzothiophene and dibenzofuran, as well as their alkylated homologs Figure 99. Each of the un-alkylated parent molecules is depicted in Figure 100. Each corner represents the sum of GC-MS signal intensity (sums of areas under peaks identified on the chromatogram) for each of the homologous series, as identified by comparison with retention indices reported in literature and correlation with co-injection of internal standards. The authors put forth a preliminary diagram establishing diagnostic regions of the ternary plot most commonly occupied by each of several depositional/lithological classes of petroleum source rocks. Samples representing typical fluvial/deltaic/freshwater lacustrine shale, brackish/saline lacustrine shale, marine shale, marine carbonate and swamp environments were used in the ternary plots, as depicted in the diagnostic regions of Li and others (2013).

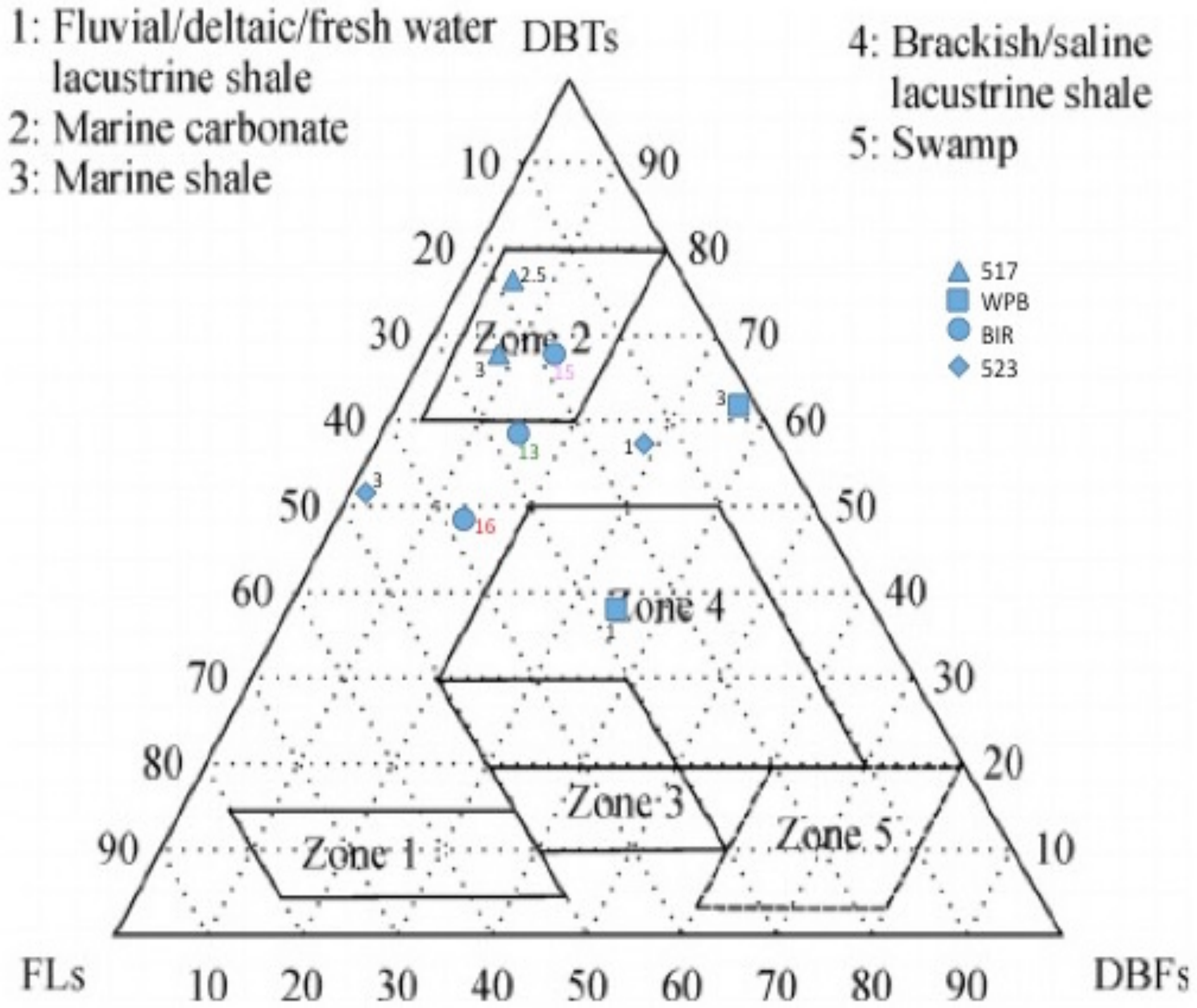

Figure 99: Ternary diagram of fluorenes, dibenzothiophenes (DBTs) and dibenzofurans (DBFs) of the aromatic GC-MS for Nonesuch Formation data. The diagnostic zones here were identified by comparison of 150+ samples of known source rock lithologies and depo-conditions. The ΣDBT-ΣDBF-Σfluorenes poles are defined slightly differently from the plot's originators, Li *et al.*, 2013.

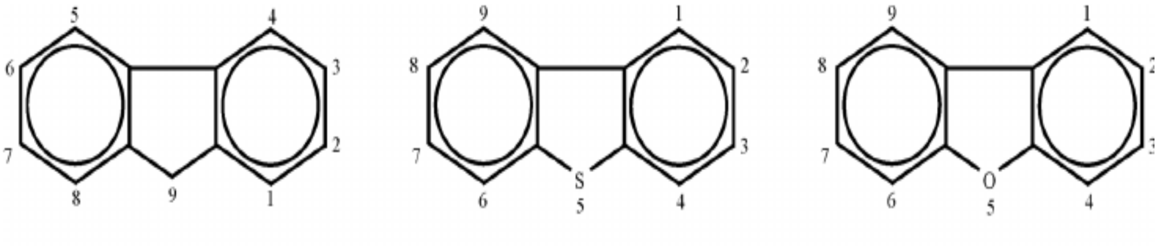

Fluorene (FL) Dibenzothiophene (DBT) Dibenzofuran (DBF)

Figure 100: Correlation of chemical structures of fluorene, DBT, and DBF. Dibenzothiophene is sometimes referred to as the "sulfur fluorene" and DBF the "oxygen fluorene." From Li *et al.,* 2013.

Of the nine Nonesuch Formation GC-MS samples, one plotted within the zone of typical brackish/saline lacustrine shales (Figure 99). Three of the GC-MS samples plotted within the zone of marine carbonate petroleum source rocks. The balance of samples fall near to the marine carbonate sector, in the 50% of the plot nearest to the DBT apex. These samples show relatively more S-PAHs than the "typical" marine carbonates, lacustrine and marine shales of zones 1, 2, and 3. The majority of samples showed less than 20% DBFs.

This study's ternary plot of ΣDBTs-ΣDBFs-Σfluorenes differs from those of the Li *et al.* (2008) study in several areas. First, no *m/z* 194 GC-MS analysis on the aromatic extracts was done and so we exclude the dimethylfluorenes (of which as many as 12 isomers have been previously identified in similar extracts, eg: Li *et al.*, 2008) from our calculations. This study does not include the DMDBTs because they were apparent on the *m/z* 212 chromatogram. Third, the MDBFs were not apparent as peaks in the *m/z* 196 chromatogram in the expected time range and were excluded. This study's GC-MS did not use an internal standard for identification of DMDBFs, and they were not included in the relative abundance calculations. Finally, our study did not apply the deuterated DBT ($C_{12}D_8S$) standard for more positive identification of trimethylated members of that series on the *m/z* = 192 chromatogram (as in the Li *et al.*, 2008, study).

## *7. Discussion and Interpretation*

Organic matter is the most temperature-sensitive solid constituent in sedimentary rocks (Peters *et al*., 2005). Petrographic and geochemical organic maturity parameters commonly utilized in petroleum prospectivity studies are applied here to assess the degree of organic maturation, as well as its relation to hydrothermal emplacement of disseminated Cu in the sedimentary Nonesuch Formation of the Midcontinent rift system. Over a dozen such parameters were assessed and compared - thermal alteration index (TAI) values, Rock-Eval parameters (the PI or production index quotient, $T_{max}$ values), Soxhlet extract yield and GC-MS molecular maturity indices (see Peters *et al.*, 2005 and Engel and Macko, 1993). These measures show varied indications of organic maturity for this study's samples, and differing relationships to geographic distribution as well as Cu mineralization and stratigraphic position.

The chemical and molecular makeup of OM in the Nonesuch Formation has been potentially influenced by varying degrees of alteration during sedimentation and early burial, and varying depths and temperatures of burial, both within a single profile and across the region of the study area. Other processes that may likely have altered the organic and Cu mineral chemistry of the Nonesuch Formation include syndiagenetic hydrothermal activity or groundwater flow unrelated to Cu ores, the hydrothermal fluids of Cu ores, oil migration into or out of the rocks, and weathering, either in outcrop or in core since sampling. It is not possible at present to specify whether - or the degree to which - each of these processes affected a given sample or set of samples.

## *7.1 Regional Variations in Apparent Maturity*

### *7.1.1 Production and Thermal Alteration Indices*

The PC-5, PC-1, PIR and WPB samples, in the central portion of the sampling traverse, show the lowest average PI values (0.35 to 0.5) while the WP vicinity samples and the samples from CF and SF show significantly higher average PI values (0.6 to 1.0). This mirrors the thermal maturity trends described by Price and McDowell (1993, Figure 35) as well as the westward increasing thermal maturity trend of Imbus *et al.* (1988). It is possible that the extremely low $S_2$ values of many of the SF and CF samples are responsible for artificially inflating the PI values used in this asserted bidirectional increase in thermal maturity. Significantly, AOM coloration is lightest and its TAI values are at minima for the sample set in the PC-5, PC-1, PIR and WPB samples. It must be noted that only one of the five PIR samples showed AOM for consideration by the TAI. No such relation to geographic distribution is apparent with respect to color or TAI of FOM.

### *7.1.2 Methylphenanthrene and Methyldibenzothiophene Indices*

The maturity indices that give most reliable results in this type of deposit (MPI1 and MDR, the methylphenanthrene and methyldibenzothiophene ratios, respectively) are correlated to calculated VR values ($R_c$ and $R_m$). The calculated VR values for MPI1 and MDR indices indicate early to peak oil window for this study's samples, excluding three very high MDR outliers (Table 5). The MPI1 is better correlated to PI values than is any other maturity parameter examined in this study (See Figure 101).

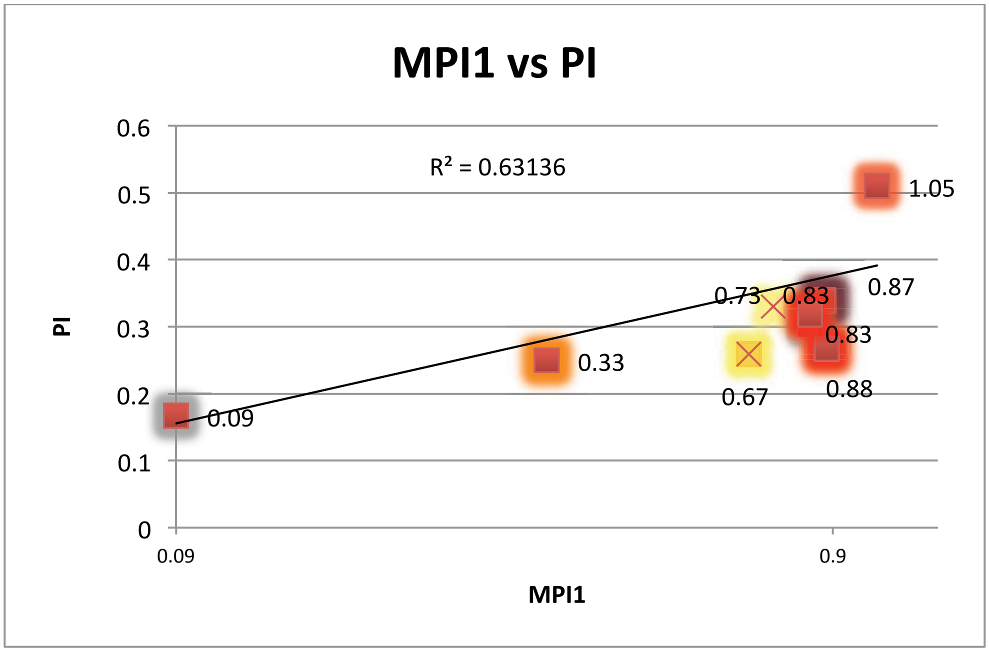

Figure 101: The strongest correlation of any GC-MS maturity parameter to RE maturity indicators is seen here in the plot of MPI1 versus PI. Red data points are mineralized, orange data points are within 1 m of mineralization, yellow are within 5 m (X'd data points are below the nearest Cu mineralization), gray points are sub 20 m to mineralization, and brown is within 25 m of mineralization.

Stojanovic *et al.* (2007) applied ratios based on the degradation of dimethylphenanthrene (DMPh) and trimethylphenanthrene (TMPh) into corresponding methylphenanthrenes and phenanthrene as aromatic maturity indicators for crude oil. The Phen/ΣDMPh (phenanthrene to sum dimethylphenanthrene) ratio is highest (2.6 to 14.5) for most altered samples, minimal in least altered samples (below 2, and dominantly below 0.5). Trimethylphenanthrenes were not identified fully enough to justify calculation of the phenanthrene to TMPh ratio.

### *7.1.3 Methylnaphthalene Indices*

Methylnapthalene isomerization ratios were shown by Radke (1987) and Stojanovic *et al.* (2007) to vary regularly in relation to established bulk maturity parameters. The dimethylnaphthalene index (1,3-)+(1,6-)+(1,7-)DMN/[(2,3-)+(1,4-)+(1,5-DMN) of Radke (1987) indicates a range of maturity broader than expected for so small of a dataset that is relatively uniform in maturity by other measures. The altered samples range from high maturity at the base of the Iron River syncline Nonesuch Formation, to submature some 16 m above at WPB-3, with the altered BIR 13 registering as medium high maturity. The other samples are variously sub- to medium maturity by this DMN index. The trimethylnaphthalene (TMN) index of Stojanovic *et al.* (2007) shows similarly tangled, though slightly less wide-ranging maturities, and no clear pattern with respect to geography. The TMN index is defined as: (1,3,6-TMN + 1,3,7-TMN)/(1,3,5-TMN + 1,4,6-TMN).

### *7.1.4 Pristane and Phytane Versus Associated Normal Alkanes*

The pristane/$nC_{17}$ versus phytane/$nC_{18}$ plot (Figure 102) indicates moderate to high maturity of OM. Figure 102 is also interpreted to suggest a single organofacies as the OM source (Seifert and Moldowan, 1986).

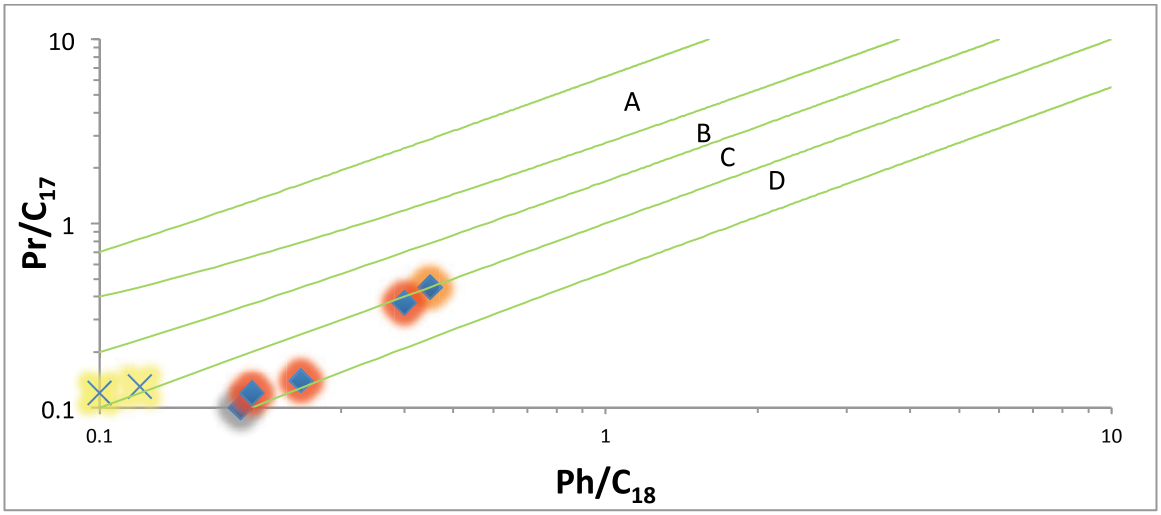

Figure 102: Relationship of normalized isoprenoid biomarker contents of Nonesuch Formation EOM. Maturity increases toward the origin. Lettered zones are associated with: terrestrial Type III OM deposited in suboxic conditions (A); Type III coaly OM (B); Type II-III mixed OM (C), and; Type I-II algal, marine OM deposited in reducing conditions (D; zones after Ashok, *et al.*, 2013). Red data points are mineralized, orange data points are within 1 m of mineralization, yellow are within 5 m (X'd data points are below the nearest Cu mineralization), gray points are sub 20 m to mineralization, and brown is within 25 m of mineralization.

### *7.1.5 Moretane and Hopane Comparison*

The moretane/hopane ratio decreases with thermal maturity, reaching thermal equilibrium at a value of 0.05 (equivalent to VR of 0.7%). Values range from 0.68 to 1.44 for this measure, suggesting thermally submature OM for the samples in this study. It is significant that the two most strongly altered samples (by TOC, MPI1, methylation ratios of PAHs), from WPB, are the least thermally mature by this measure.

### *7.1.6 Ts/Ts+Tm Trisnorhopane and $C_{29}$Ts/($C_{29}$ hopane + $C_{29}$Ts) Parameters*

The Ts/(Ts+Tm) terpane thermal maturity parameter compares the $C_{27}$ 17α-trisnorhopane (Tm) and 18α-trisnorhopane II (Ts) GC-MS signals, and reaches thermal equilibrium at unity, which is equivalent to 1.4% $R_0$ (postmature). The majority of nonzero values for samples in this study are in the range 0.37 to 0.54 (low to moderate maturity). Two of the 9 GC-MS samples show very low maturity by this measure (0.09 and 0.18): these are the WPB samples, for which the Ts/Ts+Tm value is half or less that of other areas. All samples outside of the WPB area are in the mature range by this measure, implying a thermal maturity low for the Iron River syncline area, as did Price and McDowell’s (1993) study.

The Ts/Ts+Tm trisnorhopane maturity measure is strongly source dependent and varies with changes in source rock lithology, Eh and pH (Peters *et al*., 2005). Co-elution with tricyclic or tetracyclic terpanes on *m/z* 191 mass chromatograms is possible, and may not be ruled out in the present absence of *m/z* 370 mass chromatograms.

The $C_{29}$Ts/($C_{29}$ hopane + $C_{29}$Ts) parameter's trend with maturity should be comparable with, though slightly less than, the maturity trend of the Ts/Ts+Tm trisnorhopane maturity/depositional measure (Peters *et al.,* 2005). The $C_{29}$Ts/($C_{29}$ hopane + $C_{29}$Ts) results of this study concur with the convention in the literature, suggesting that most samples are mature with respect to HC generation, and further supporting the interpreted paleothermal low in the vicinity of the WPB sample core drill hole.

### *7.1.7 Geographic Distribution of Sterane Maturity Parameter Values*

Living organisms possess sterols exclusively with the 20R configuration (Peters *et al.*, 2005). During diagenesis and catagenesis, steranes are gradually transformed to a mixture of 20R and 20S isomers, until they reach a thermal equilibrium value of about 0.55 for the 20S/(20R+20S) ratio (Figure 19). Thermal equilibrium is reached for this parameter at about 0.9% $R_O$, at the end of the peak oil generation window (also known as the S/S+R $C_{29}$ ααα ratio; Seifert and Moldowan, 1986). The S/S+R $C_{29}$ ααα sterane ratio for Nonesuch Formation GC-MS samples in this study (0.25 to 0.37 for the 6 of 9 samples with nonzero values) indicates low maturity and no pattern exists with respect to geographic distribution.

The ββ/(ββ+αα) $C_{29}$ sterane ratio increases with maturation from near-zero values to about 0.70 at thermal equilibrium (Peters and others, 2005). The range of values for the samples in this study (0.23 to 0.48) indicates thermal maturity in the early to peak oil generation window, without any ordered geographic distribution of values.

A cross plot of $C_{29}$ sterane ββ/(ββ+αα) versus $C_{29}$ sterane S/S+R ααα (Figure 103) shows that the studied EOM samples are low to moderately mature. The relatively strong linear correlation of the two parameters suggests that the samples experienced similar heating rates in the subsurface, and that analytical error was minimal (cf. Peters *et al.*, 2005).

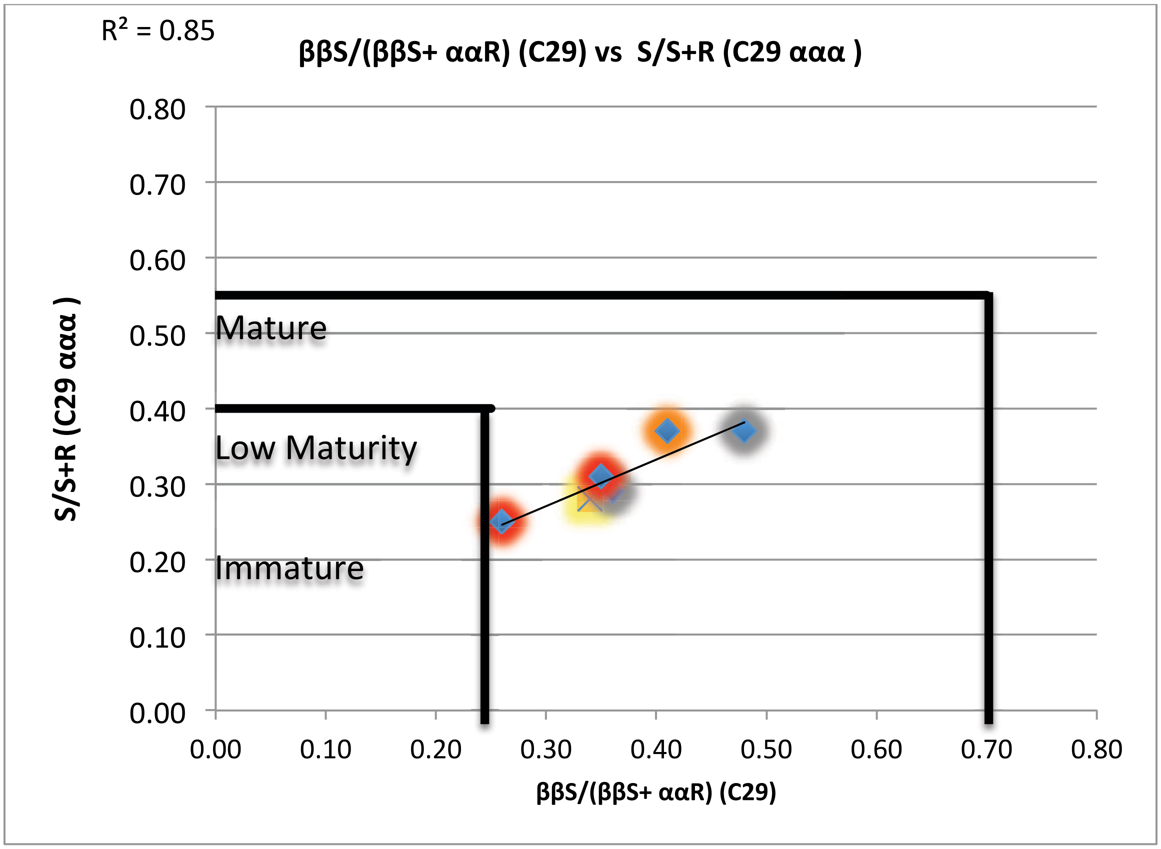

Figure 103: Cross plot of $C_{29}$ sterane ββ/(ββ+αα) versus $C_{29}$ sterane S/S+R ααα which shows that the studied EOM samples are low to moderately mature (maturity increases away from the origin; Peters *et al*., 2005). Red data points are mineralized, orange data points are within 1 m of mineralization, yellow are within 5 m (X'd data points are below the nearest Cu mineralziation), gray points are sub 20 m to mineralization, and brown is within 25 m of mineralization.

The ratio of diagenetic (S+R) to ααα (S+R) for the $C_{27}$ steranes indicates late oil window maturity and shows regular variation with position on the sampling traverse (Table 5, Figure 37). Thermal equilibrium is reached at 1.00 (equivalent to VR of 1.4%) for this parameter, and when the outliers (0, 3.28) are excluded, the values range from 0.91 to 1.7. The highest values for this parameter are mainly for the mineralized BIR samples.

### *7.1.8 Pregnane*

The steranes are nearly dominated by the $C_{21}$ molecule pregnane and to a lesser extent $C_{22}$ molecule homopregnane, which is consistent with high maturity, a large contribution of algal/bacterial matter, or both (cf. Dutkiewicz *et al*., 2006). Other studies have ascribed high abundance of pregnane to higher salinity in the depositional environment (cf. Mueller *et al.*, 1995).

### *7.1.9 Soxhlet Extractable Organic Matter Yield*

Soxhlet EOM yields show no regular pattern with respect to geographic locality, nor to AOM TAI (Table 5, Figure 37). Rock-Eval OI values are uniformly below 15 for higher EOM yielding samples (greater than 384 ppm), and lower yielding samples all show OI greater than 34. That the bitumen-rich samples show less oxidation of OM supports the TOC-OI negative correlation as representative of oxidative destruction of OM.

### *7.1.10 Long Versus Short Chain Triaromatic Steroids*

Higher concentrations of low molecular weight TAS compounds ($C_{20}$, $C_{21}$ derivatives of pregnane and homopregnane, respectively) relative to the longer chain $C_{26}$, $C_{27}$, and $C_{28}$ TASs have been interpreted to indicate higher levels of thermal maturity (Figure 19; Lillis *et al.*, 1998). The abundances and quotients of such low molecular weight TAS compounds relative to their longer-chain TAS homologues are generally higher for the BIR samples. However, the failure to detect these compounds in the 523 samples, and a high-quotient sample (517-3) coupled with a high abundance (peak heights in the thousands for 517-2.5) obscure what may be a regular pattern with respect to geographic position for this parameter.

### *7.1.11 Diamantanes*

Diamantanes are cage HCs that occur in all kinds of fossil fuels (Peters, *et al*., 2005). Due to their peculiar cage molecular structures - similar to a subunit of the diamond lattice – they have been widely used in the maturity assessment of highly mature to over-mature oils as well as source rocks since the 1990s (Ma, 2016). No diamantanes were detected in the aromatic portion, and while the saturate portion samples all show diamantane and methyldiamantanes, no other diamantane compound peaks were identified. No pattern of diamantane abundance is apparent with respect to geographic distribution. The saturate fraction GC-MS sample diamantanes showed similar degree of alkylation (15-20% unalkylated diamantane), and the methyldiamantane index, a maturity parameter created by Fang *et al.* (2016) showed no relation to geographic locality.

### *7.2 Variations in Apparent Maturity Related to Depth and Mineralization*

#### *7.2.1 Production and Thermal Alteration Indices*

The PI values do not correlate with Cu mineralization/distance to mineralization, AOM TAI, EOM yield or $T_{max}$ values. The degree of HC generation would ideally correspond to each of these parameters. Similarly, neither Soxhlet EOM yields nor TAI values show regular variation with respect to distance from Cu mineralization (Figures 66, 67, 104). The lack of correlation might suggest sample contamination, loss of free HCs or of kerogenous OM in outcrop/core storage, or that Cu mineralization, $S_1$ HC generation, and thermal alteration changing AOM color occurred as somewhat independent processes.

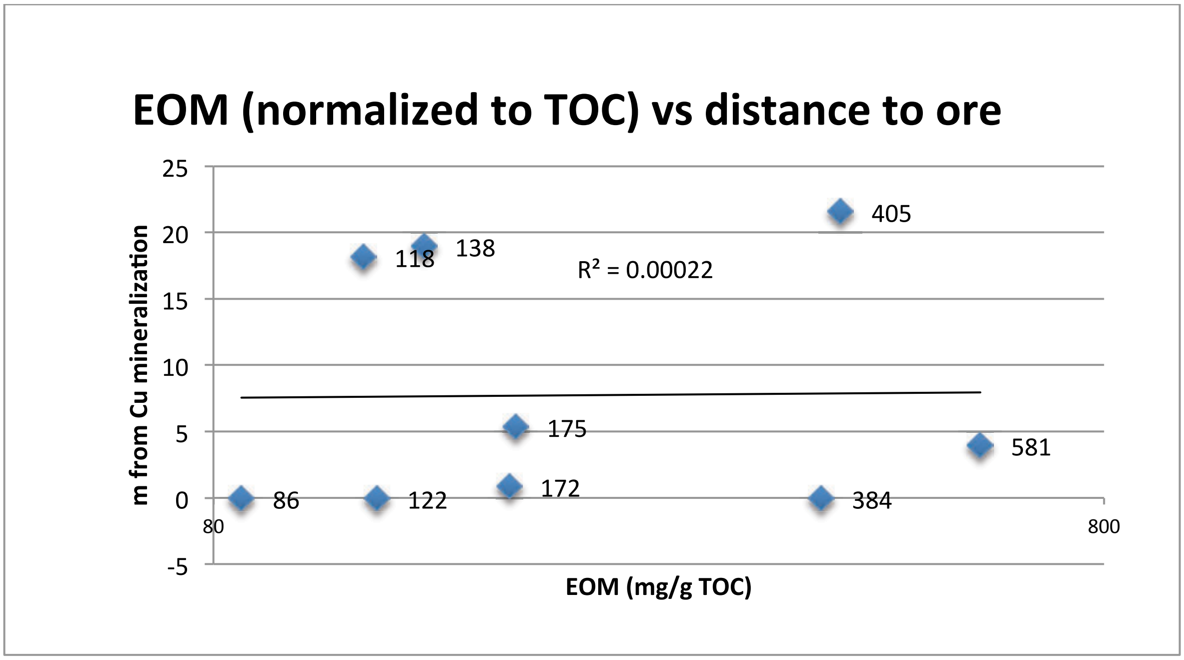

Figure 104: Normalized EOM yields versus distance to Cu mineralization, Nonesuch Formation.

### *7.2.2 Methylphenanthrene and Methyldibenzothiophene Indices*

Neither the MPI1 nor the MDR values (Figure 19) show regular variation with respect to Cu mineralization or depth. The Ph/ΣDMPh maturity parameter of Stojanovic *et al*. (2007) gives conflicting signals with respect to mineralization: mineralized samples range from submature to highly mature by the DMPh maturity measure. The same is true for the Ph/ΣDMPh value versus $T_{max}$, and HI parameters. However, Ph/ΣDMPh does align with OI values for the GC-MS samples of this study. The submature values by the Ph/ΣDMPh (as calibrated by Stojanovic *et al*., 2007) are all below OI = 41, and all GC-MS samples with OI greater than 40 show as high maturity by Ph/ΣDMPh. However, PI values decrease as Ph/ΣDMPh values increase to the mature range; one would expect the opposite trend of higher PI with higher Ph/ΣDMPh.

### *7.2.3 Pristane and Phytane Versus Associated Normal Alkanes*

The two samples that fall below the 0.1 pristane/*n*-$C_{17}$ cutoff for Figure 102 are both distal to Cu mineralization; one of these shows higher phytane/*n*-$C_{18}$ (0.42) and is 25 m away from Cu sulfide mineralization. The relation of low pristane/*n*-$C_{17}$ to greater distance from Cu mineralization contradicts the findings of Ho and Mauk (1996), while the apparent association of higher phytane/*n*-$C_{18}$ with Cu mineralization and proximity thereof agrees with their results.

### *7.2.4 Moretane and Hopane Comparison*

Two of the three low values (indicating greatest thermal maturity) for the moretane/hopane ratio are for Cu mineralized rocks. However, the other low value for this measure occurred in a less altered sample and the mineralized samples are not significantly outside the range of other samples with respect to moretane/hopane.

### *7.2.5 Ts/Ts+Tm Trisnorhopane and $C_{29}$Ts/($C_{29}$ hopane + $C_{29}$Ts) Parameters*

While incomplete data on the $C_{29}$Ts/($C_{29}$ hopane + $C_{29}$Ts) parameter complicates interpretation of its relation to mineralization, it should be noted that of the 6 samples for which data exists, mineralized samples make up two of three most mature values by this measure. No regular pattern with relation to depth is apparent for the $C_{29}Ts/(C_{29}$ hopane + $C_{29}Ts)$ maturity measure. The Ts/Ts+Tm trisnorhopane parameter is less clearly related than the previous maturity indicator to the spread of Cu mineralization, stratigraphic position or to the clear GC OM alteration pattern.

### *7.2.6 Diamantanes*

Diamantanes, colorless solid HCs, exhibit high density and resistance to oxidation, and can be produced by thermal cracking of long chain *n*-alkanes (Gordadze and Giruts, 2008). The two unmineralized samples classified as altered (WPB-1 and WPB-3) showed significantly lower total diamantane peak areas than did most other samples (the exception being 517-3). That the two lowest total diamantane peak areas of unmineralized samples (and presumably a lesser degree of thermal cracking of long chain *n*-alkanes; Gordadze and Giruts, 2008*)* occur in the two furthest-from-base unmineralized samples (WPB-3, 20.9 m above base; 517-3, 22.1 m above base) and that the absolute furthest-from-base sample is mineralized but shows a total diamantane value an order of magnitude greater than that of the WPB-3 could be interpreted to suggest enhancement of thermal cracking of long chain HCs during Cu mineralization. In this respect it seems significant that of the two unmineralized altered samples, the more distal to base and further from mineralization has less than half the diamantanes of its counterpart and maximizes at *n*-$C_{16}$ on the whole extract TIC whereas the mineralization-proximal of the two (WPB-1, sub 1 m distant to Cu mineralization) is lowest in section and maximizes at *n*-$C_{14}$. Enhanced thermal cracking of long chain HCs to diamondoids during mineralization would, however, have to have been limited to the site of Cu precipitation for the WPB-1 to be so close to Cu mineralization but show so little total diamantanes relative to the much higher diamantane content of the other GC-MS samples. The methyldiamantane index showed no relation to Cu mineral proximity, depth, RE parameters or EOM yield.

### *7.2.7 Methylnaphthalene Indices*

The mineralized and altered samples are medium to medium-high maturity by the TMN measure, while the less altered unmineralized samples are submature to medium mature. The DMN index shows no clear pattern with respect to depth or mineralization.

### *7.2.8 Sterane Maturity Parameters, Copper Mineralization and Depth*

As with geographic distribution, no meaningful pattern of sterane maturity parameters of Peters *et al*. (2005) is apparent. No relationship between the maturity parameters derived from the *m/z* 217 chromatogram and Cu mineralization or stratigraphic position exist.

### *7.2.9 Long Versus Short Chain Triaromatic Steroids*

Higher concentrations of low molecular weight TAS compounds ($C_{20}$, $C_{21}$ derivatives of pregnane and homopregnane, respectively) relative to the longer chain $C_{26}$, $C_{27}$, and $C_{28}$ TASs have been interpreted to indicate higher levels of thermal maturity (Figure 19; Lillis *et al.*, 1998). Neither abundances nor quotients of such low molecular weight TAS compounds relative to their longer-chain TAS homologues show regular variation with proximity to Cu mineralization or to organic alteration identified on the TIC chromatograms.

## *7.3 Evidence for OM Oxidation*

The presence of Nonesuch Formation sterane and terpane biomarkers away from White Pine (Pratt *et al.*, 1991) and the absence of sterane or terpane biomarkers at White Pine (Hoering, 1978; Imbus *et al.*, 1988) have previously been interpreted as resulting from oxidative destruction of such compounds during ore deposition (Peters *et al.*, 2005). This study's sterane and terpane biomarkers, recognized at White Pine and elsewhere indicate that this interpretation is not completely correct and that advances in analytical hardware necessitate re-examination of previous studies' analytical methods, data, and interpretations.

This study's directed sampling allows interpretation of OM oxidation regionally in the Nonesuch Formation and specifically in and above Cu mineralized zones. Still, it is not possible to quantify the extent of oxidation in any specific horizon in the Nonesuch Formation, nor to show consistently increasing degree of oxidation with increasing proximity to Cu mineralized zones.

### *7.3.1 Rock-Eval Evidence for OM Oxidation*

All analyzed profiles show a consistent pattern of decreasing HI towards the base of the Nonesuch Formation. This pattern spans approximately 100 m - the lower half of the Nonesuch Formation. The lowest HI values are substantially lower than in the ore and in the Rote Faule in the Kupferschiefer (Bechtel *et al*., 2001) and include some below ten. Such low values are probably unreliable because they are calculated from poorly defined peaks of production during RE pyrolysis. The pattern of decreasing HI towards the base of the Nonesuch Formation may be a result of higher temperature at the base of the formation, but the gradient of HI (up to 200 mg/g TOC per 100 m of section) is steeper than typically observed in sedimentary basins (e.g., Jin and Sonnenberg, 2012). Oxygen index has more scatter in each profile, likely related to the increased susceptibility of organic lean samples to changes in OI. Still, an increase in OI towards the base of the Nonesuch Formation can be inferred. Increases in OI from about 20 to 50 with proximity to Cu mineralization is apparent in organic rich samples, very similar to those recorded in the Kupferschiefer (Bechtel *et al*., 2000).

Organic matter of most of the lean samples is O rich and reasonably inferred to have been oxidized although the timing and context of this oxidation is not defined. We cannot rule out oxidation in outcrop and since coring, although the low UCM in all extracts shows that weathering was not a significant process beyond the differing degrees of alteration implied from molecular composition of the whole-rock extracts analyzed from organically richer samples. In contrast the isotopic compositions of carbonates indicate widespread syndiagenetic oxidation of OM, as suggested by Ho and Mauk (1996).

### *7.3.2 Relation of Hydrogen/Oxygen Index Ratio to Mineralization*

Copper bearing samples show a lower average HI/OI ratio than do unmineralized samples (1.1 and 2.0, respectively, and with exclusion of BIR with its oil inclusions). This suggests Cu deposition with direct reduction by locally-available OM, as does the low TOC-high OI correlation's greater prevalence in Cu mineralized samples. Greater than 90% of mineralized samples with HI/OI less than 0.33 show TOC below 0.15.

In contrast, the fact that unmineralized ore-distal samples show a lower average HI/OI ratio than do ore-adjacent unmineralized samples suggests that OM oxidation associated with ore hydrothermal fluid flow may have been a more broadly distributed effect rather than a local impact (HI/OI ratio values of 1.81 versus 2.62, respectively).

### *7.3.3 Petrographic and Geochemical Distinction of Filamentous Versus Amorphous Organic Matter*

Darkening or blackening of OM can be interpreted as representing oxidation of the organic constituents, and indeed, the black FOM-only samples are inertinite based on the RE data (Robert, 1980). The black, mostly opaque FOM is highly oxidized relative to the AOM - the 7 FOM-only samples for which RE data exists show an average HI/OI ratio of 0.18, whereas the same group of 16 AOM-only samples average 4.73. The four AOM-only samples showing reddish-brown or darker color (TAI = 3.0 or greater, coincident with late mature per Mastalerz *et al.*, 2016) average to 0.875 on the HI/OI ratio. Co-occurrence of AOM and FOM in mineralized and unmineralized samples suggests that this differing color and chemistry is not related to Cu mineralization.

### *7.3.4 Aromatization and Oxidation of Organic Matter*

The higher abundance of the benzopyrenes and benzofluoranthenes in the mineralized samples could plausibly be the result of oxidation of OM during mineralization. That the only observed occurrence of phenylphenanthrenes is in the two most strongly altered - but barren of Cu - samples (by TOC, MPI-1, ratios of unmethylated versus methylated PAHs, cf. Yawaranah *et al*., 1994), which show lesser abundance of the benzopyrenes and benzofluoranthenes than the mineralized GC-MS samples is significant. It has been documented that dehydrocyclization of phenylphenanthrenes during diagenetic oxidative hydrothermal alteration can generate the benzopyrenes and benzofluoranthenes (cf. Grafka *et al.*, 2015, Marynowski *et al.,* 2009, Marynowski and Wyszomirski, 2007). Given the observed differences in molecular makeup of these samples, it seems reasonable to conclude that such dehydrocyclization of the phenylphenanthrenes occurred during syndiagenetic oxidative hydrothermal alteration specifically associated with Cu mineralization, resulting in generation of the benzopyrenes and benzofluoranthenes.

All of the whole-rock organic extracts are from samples within to about 30 m above Cu mineralization zones at the base of the Nonesuch Formation and are within the zone of inferred HI reduction and slight OI increase. The GC and GC-MS data show variable degree of alteration within this sample subset. The most significant effects on molecular makeup of the OM that can be inferred to have occurred with alteration are aromatization (from the richness of the aromatic fraction of all extracts) and dehydrogenation (from the decrease in MPI-1 for example). None of these changes can be correlated with increased OI, and no O-containing compounds like ketones or carboxylic acids were detectable within the analysis, but could be present. Aromatization and dehydrogenation are, though, consistent with a decrease in HI and dehydrogenation and aromatization reactions inferred are consistent with oxidation (as in Shock *et al*., 2013). It is not clear that TSR was a significant process during Cu precipitation at White Pine. However, aromatization and dehydrogenation could have contributed to TSR and thus to the availability of sulfide for Cu precipitation by reactions similar to the schematic exchange:

$$C_6H_{14} + H_2SO_4 \text{-->} C_6H_6 + H_2S.$$

The least altered extracts are dominated by *n*-alkanes, with highest concentrations at *n*-$C_{11}$ to *n*-$C_{14}$ and a smooth decrease to higher lengths. The three altered samples show slightly higher OI and are distinguished by a sharp maximum of *n*-alkanes over a narrow range. The slightly altered sample (with the highest OI) shows a gas chromatogram with a range of *n*-alkanes that is similar to that of least altered samples, but the concentrations of high molecular mass alkanes are lower and there are double maxima at *n*-$C_{15}$ and *n*-$C_{24}$ rather than smooth decreases with increasing C number. This is consistent with the oxidative alteration of OM observed in the Kupferschiefer, where highly altered Rote Fäule material is characterized by a predominance of short chain *n*-alkanes (less than *n*-$C_{17}$) at the expense of mid- and long chain homologues (e.g., Kotarba *et al.*, 2006; Püttman *et al.*, 1989).

Concentrations of the thio- and oxo-aromatics dibenzothiophene and dibenzofuran, as well as the PAHs phenanthrene, benzofluoranthene, and benzopyrene are higher for mineralized and more altered samples.

### *7.3.5 Phenanthrene and its Methylated Homologues*

Speczik (1994) showed that low-rank vitrinite reflectance anomalies correlate well with the location of ore-grade occurrences of Cu sulfides in the Kupferschiefer. By comparison with these parameters, Speczik showed that values for the ratio phenanthrene/sum methylphenanthrenes (Ph/ΣMPh) provide a measure for the intensity of oxidative OM-alteration associated with ore deposition. Bechtel *et al.* (2000) successfully applied this ratio as a measure of Rote Fäule OM oxidation during hydrothermal alteration associated with proximal (single m-scale) Cu and minor precious metal mineralization, variably above, below, and concurrent with increased Ph/ΣMP ratios.  Unoxidized and weakly oxidized samples showed Ph/ΣMPh = 0.6-1.2, while oxidized samples give values between 1.5 and 3.0.

It was found that the ratio of phenanthrene to sum of methylphenanthrenes provides an imperfect but still apparent measure of the intensity of alteration.  The aromatic portion of the most altered extracts in this study are characterized by an increase in the ratio of phenanthrene to methylated phenanthrenes.

Excepting the least-altered sample that shows the maximum Ph/ΣMP value for the group, the slightly altered, most altered and mineralized samples show the highest range (1.1 to 4.2) and the least altered samples range from 0.43 to 0.67 and are barren of Cu.  No regular increase in biphenyl at the expense of phenanthrene in the most altered samples was apparent.

This study's samples do not show regular relation between HI, OI, and Ph/ΣMPh, as is clear in Figures 105 and 106.  The Ph/ΣMPh shows a closer (although statistically insignificant) correlation to the HI/OI ratio than to either the HI or the OI alone, which suggests that the measure is at least in some part aligned with the degree of oxidation of OM in a given sample. See Figure 107.

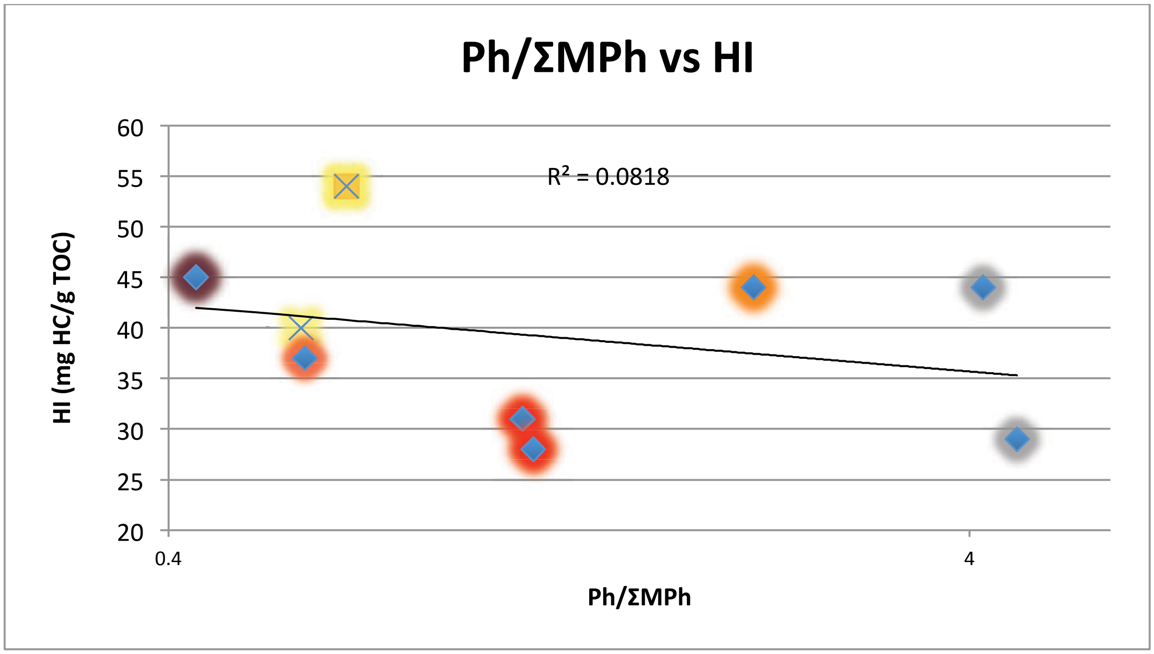

Figure 105: Note that the mineralized samples (BIR13, 15, 16, red) are under the 1.5 to 3 Ph/ΣMPh range of oxidized, Cu-bearing Kupferschiefer samples while the ore-adjacent WPB-1 (orange) sample shows Ph/ΣMPh of 2.15. That the barren ore-distal samples (gray are within 20 m of Cu mineralization; brown is up to 25 m away from Cu mineralization) occupy both ends of the spectrum similarly confounds this organic oxidation parameter's usefulness. Red data points are mineralized, orange data points are within 1 m of mineralization, yellow are within 5 m (X'd data points are below the nearest Cu sulfide mineralization), gray points are sub 20 m to mineralization, and brown is within 25 m of mineralization.

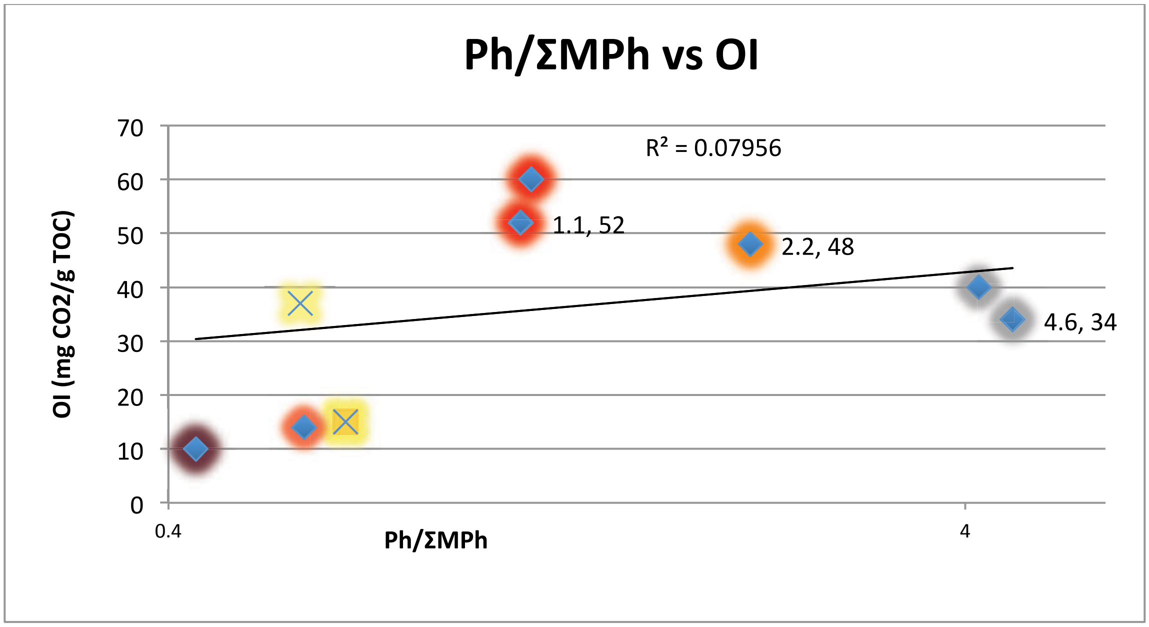

Figure 106: The Cu mineralized samples (BIR13, 15, 16, red) are below the 1.5 to 3 Ph/ΣMPh range of oxidized, Cu-bearing Kupferschiefer samples while the ore-adjacent WPB-1 (orange) sample shows Ph/ΣMPh of 2.15. Barren ore-distal data points are gray (within 20 m of Cu mineralization) and brown (up to 25 m away from Cu mineralization). Yellow data points indicate barren samples within 5 m of Cu mineralization (X indicates sample position beneath the nearby Cu concentration). Red points are mineralized.

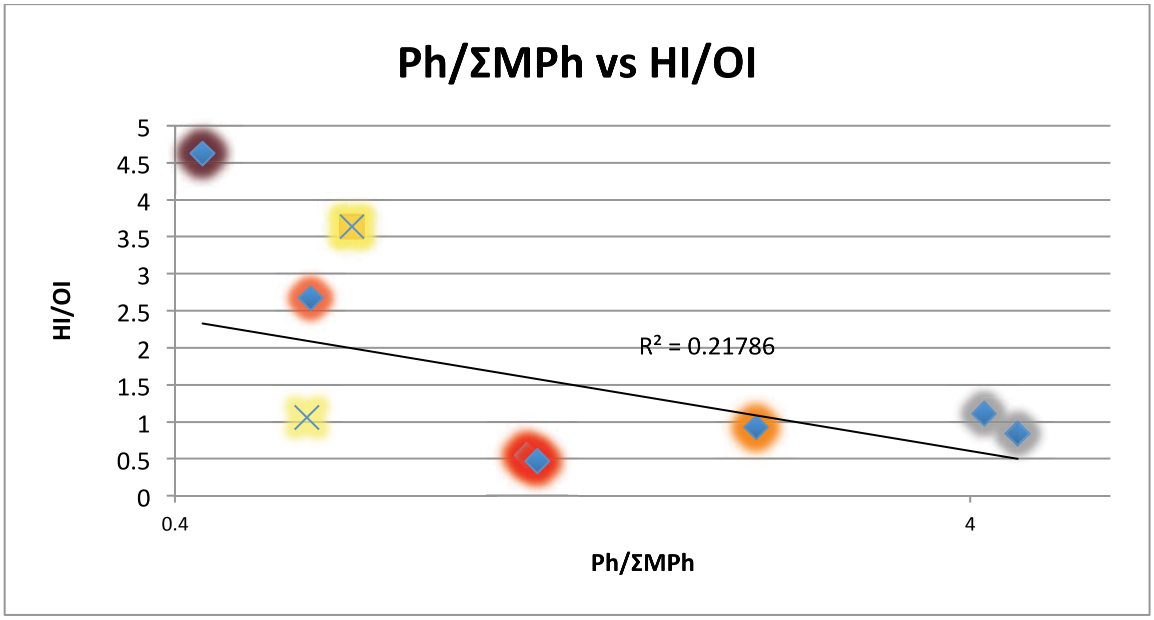

Figure 107: The Ph/ΣMPh shows a statistically insignificant but closer correlation to the HI/OI ratio than do any of the other GC-MS-RE parameter crossplots, which suggests that the measure is aligned with the degree of oxidation of OM in a given sample. Red data points are mineralized, orange data points are within 1 m of mineralization, yellow are within 5 m (X'd data points are below the nearest Cu mineralization), gray points are sub 20 m to mineralization, and brown is within 25 m of mineralization.

It is significant that the mineralized BIR samples show values between 0.6 and 1.1, in the unoxidized range. In contrast, the unmineralized, less than 20 m from ore, distal samples are above 4 on the Ph/ΣMPh ratio, and the ore-adjacent (within 1 m) sample, 523-1, is in the range Speczik *et al.* (2007) presented for mineralized, highly oxidized samples. However, 523-1 shows the highest HI and the second lowest OI of the group; the BIR samples show the highest *and* the lowest OI values. Two of the three samples showing the highest Ph/ΣMPh were not thin sectioned, and the TAI of the other is on the low end at 2.8, orange color (on AOM, no FOM present). The two darkest colored, highest TAI (both 3.2 AOM) GC-MS samples were the mineralized BIR 15 and 16 material, which showed broadly different Ph/ΣMPh values of 1.1 and 0.59, respectively. Based on OI, the more oxidized sample (BIR 15, with OI = 60) does show a higher, more oxidized Ph/ΣMPh value than BIR 16 (OI = 14). The study's overall average TAI value of 3.12 is not far below that of BIR 15 and 16, which is compatible with their overall less-oxidized Ph/ΣMPh values despite the disparity in the GC-MS parameter.

The two most strongly altered samples (with respect to TOC, MPI-1, Ph/ΣMPh, Ph/Σdimethylphenanthrenes, fluorene/Σmethylfluorenes and DBT/ΣDMDBTs), from the Iron River syncline, meet and exceed the range for "oxidized" Kupferschiefer samples as defined by Speczik (1994), 1.5 to 3. That the most strongly oxidized samples by this measure, WPB-3 and 517-2.5 (Phen/ΣMP ratios 4.2 and 4.6), are both nearly 20 m away from Cu mineralization testifies to a broad alteration of OM in the Nonesuch Formation.

Notably, the barren sample 523-1, taken just 4.5 m below chalcopyrite mineralization, shows in the "unoxidized" range (0.6 to 1.2, per Speczik, 1994); this could be construed as suggesting very localized, rather than pervasive, redox reactions of OM during Cu mineralization. However, the probable fracture-association and presumable focusing of fluids with such anomalous (as described by Brown, 1971) mineralization implies alteration could be highly localized.

### *7.3.6 Fluorene and its Methylated Homologues*

The altered extracts' aromatic portions are characterized by an increase in the ratio of fluorene to its methylated analogues. The BIR 13 and WPB samples are from 2 to 2.2 on the ratio fluorene/Σmethylfluorenes whereas the less altered and least altered samples are between 1 and 1.9. Neither HI/OI ratio, nor mineralization show regular relation to this ratio, nor does the TAI of AOM.

### *7.3.7 Dibenzofuran and its Dimethylated Homologues*

The methyldibenzofurans were not identified on the fragmentograms, but increases in the proportion of DBF to its dimethylated homologues imply de-methylation of DMDBF in the altered and mineralized samples. The ratio DBF/ΣDMDBF is between 4 and 100 for the most altered samples, between 1 and 4.1 for the mineralized samples. The DBF/ΣDMDBF ratio averages 0.88 for least altered samples, although an outlier of 2.3 is present in this group. Unmineralized least altered samples average below 0.83, outlier included. Overall, this is interpreted to suggest oxidative alteration of OM was most active in the altered and mineralized samples. No relationship to the color of contained OM is apparent, nor to HI/OI ratio.

### *7.3.8 Dibenzothiophene and its Methylated Homologues*

The aromatic portions of the most altered extracts in this study are characterized by a loss of methylated analogues and preservation of dibenzothiophene, as represented by the DBT/ΣMDBT ratio. Altered samples range from 0.9 to 3.2 on this measure, mineralized samples between 0.81 and 0.91, and least altered unmineralized samples are between 0.1 and 0.7. This suggests a localized effect of epigenetic oxidation associated with mineralization and alteration. No relation between this ratio and AOM TAI or HI/OI ratio is apparent, however.

### *7.3.9 Pristane to Phytane Ratio and Depositional Environment by Comparison to Dibenzothiophene Versus Phenanthrene*

In the Kupferschiefer, increases of the pristane to phytane ratio with proximity to Cu mineralization have been interpreted to result from increasing oxidation during deposition and diagenesis in the Kupferschiefer (Püttman *et al.*, 1989). This study's pristane/phytane ratio ranges from 1.03 to 1.81 for the group of samples that were either mineralized or within 10 m of Cu mineralization, whereas the samples more distal to Cu mineralization showed lower values for the measure (from 0.24 to 1.05). If one excludes the oil-inclusion bearing BIR 16 sample (HI/OI = 2.64, with its probably not closely indigenous OM content), this measure shows some association to the HI/OI ratio, with the majority of the former group ranging from 0.47 to 1.08 and the latter between 0.85 and 4.5. The outlier to this trend, 523-1, shows HI/OI and pristane/phytane of 3.6 and 1.73, respectively. This study's GC-MS sample set thus partially supports the findings of previous studies that either: 1) mineralizing hydrothermal alteration events result in oxidation of OM and increased pristane/phytane (e.g., Püttman *et al.*, 1989), or 2) increased thermal maturity interpreted have been driven by mineralizing fluids (cf. Gize, 2000).

A plot of pristane/phytane versus DBT/Phenanthrene (Figure 108, after Hughes *et al.*, 1995) positions the Nonesuch Formation samples in two plausibly correct depositional environment sectors (lacustrine hypersaline and marine shale/other lacustrine) and no relationship to mineralization or OM alteration is clear.  This may be interpreted as indicating a lesser degree of oxidative alteration of the samples.  It is worth noting that the S-aromatic (DBT) is sufficiently minimal in content relative to the abundant phenanthrene that all samples plot in the lowest 1/5 of their respective zones.  This can be interpreted as suggesting a relatively high degree of aromatization concurrent with minimal introduction of S for the whole group of GC-MS samples.  No relationship between alteration and mineralization, RE parameters, or AOM TAI is apparent on the plot of pristane/phytane versus DBT/Phenanthrene.

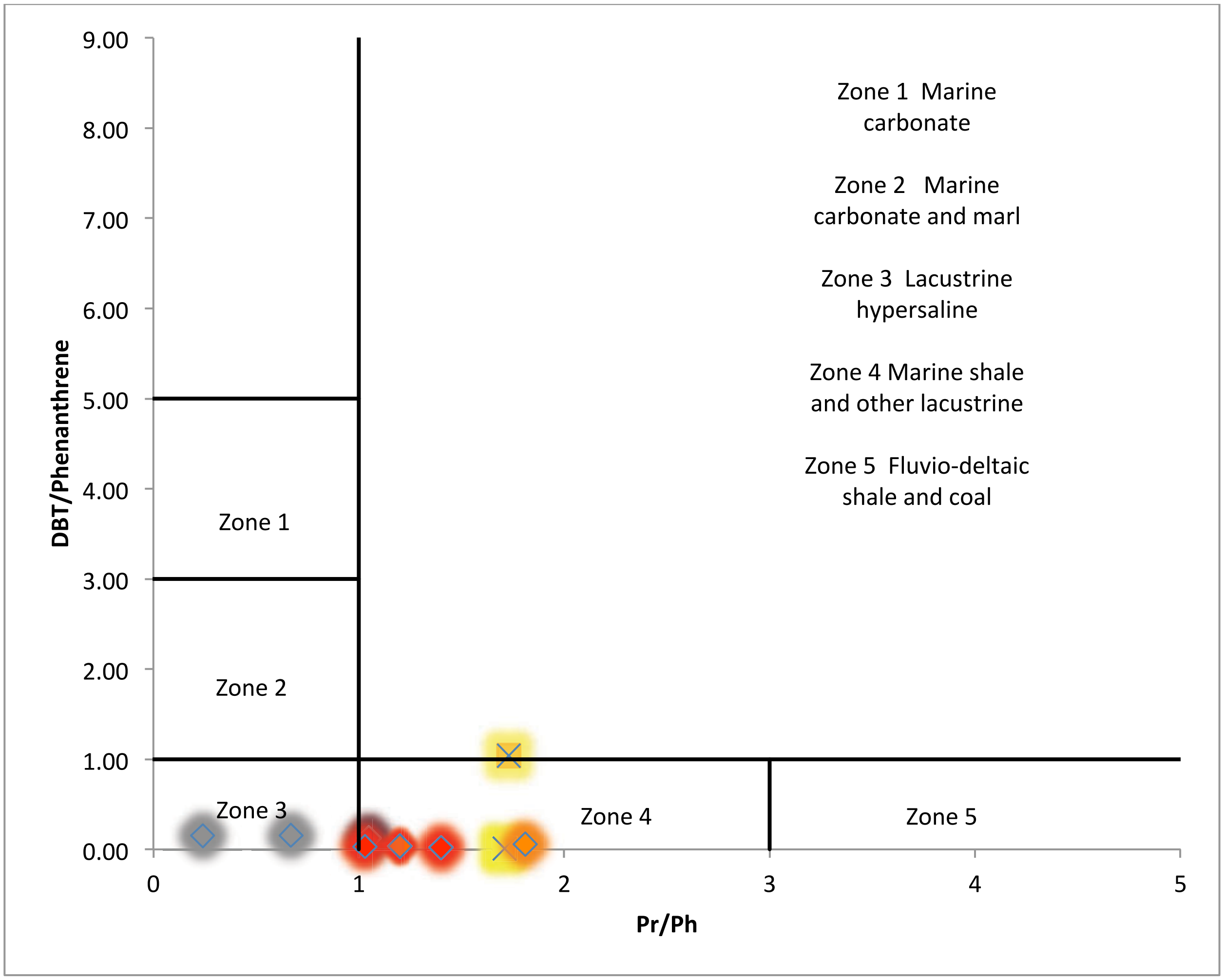

Figure 108: The Pr/Ph versus DBT/Phenanthrene plot, after Hughes *et al.* (1995). Red points are mineralized, orange is within 1 m of Cu mineralization, yellow is within 20 m, and gray is under 25 m distant. Data points stratigraphically below the proximal mineralization are X-marked.

### *7.3.10 Pristane to Normal Heptadecane Ratio*

In SSC deposits outside of the Midcontinent Rift, the ratio of isoprenoids to *n*-alkanes increases in association with Cu mineralization (Püttman *et al.*, 1989). Higher values for the pristane/*n*-$C_{17}$ and phytane/*n*-$C_{18}$ parameters have been interpreted to indicate increased oxidation of OM, but other influences such as variations in depositional environment, migration effects or biodegradation also may affect these measures.

Pristane/*n*-heptadecane ratios are higher in the three altered samples, consistent with preferential oxidation of the *n*-alkanes during alteration. However, these ratios are vulnerable to other factors, including migration, expulsion efficiency, water solubility, and biodegradation, and indeed, Ho and Mauk (1996) reported decreased rather than increased pristane/*n*-heptadecane and phytane/*n*-octadecane associated with mineralization.

It is significant that the two unmineralized samples closest to mineralization of Cu both show lower than average prevalence of isoprenoids for the unmineralized group of GC-MS samples. The prevalence of isoprenoids in mineralized GC-MS samples averages 2.8%, whereas unmineralized samples average 2.3% isoprenoids: this aligns with previous studies indicating increases in the ratio of isoprenoids to their respective associated *n*-alkanes with mineralization (Bechtel *et al.,* 2000), and interpreted increased thermal maturity in association with mineralization (Gize, 2000).

### *7.3.11 Sterane Maturity Parameters and Oxidation of Organic Matter*

The ratio of diagenetic (S+R) to ααα (S+R) for the $C_{27}$ steranes shows correlation to the OI values of this study's GC-MS samples, when the oil-included and poor GC-MS signal samples (three of these) are excluded (Figure 109). The $C_{27}$ diasterane (S+R) to ααα (S+R) $C_{27}$ sterane parameter increases with OI.

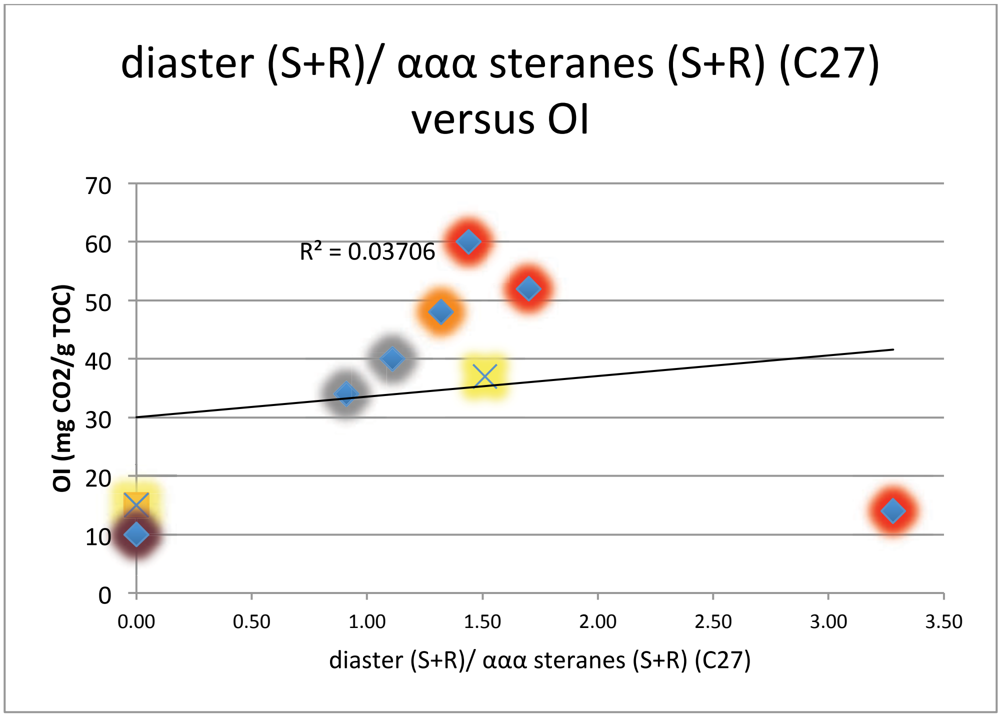

Figure 109: With the exclusion of the three samples below the line of best fit (due to oil inclusions in the mineralized BIR 16 and poor GC-MS resolution for the two leftmost, zero-value samples), the correlation between the $C_{27}$ diasteranes to ααα steranes is stronger. Red points are mineralized, orange is within 1 m of Cu mineralization, yellow is within 20 m, and gray is under 25 m distant. Data points stratigraphically below the proximal mineralization are X-marked.

The overall negative correlation of OI to the S/S+R $C_{29}$ ααα parameter is an expected maturity trend but the above trendline position of the mineralized and sub 1 m samples may be interpreted to suggest localized OM oxidation during Cu mineralization. See Figure 110.

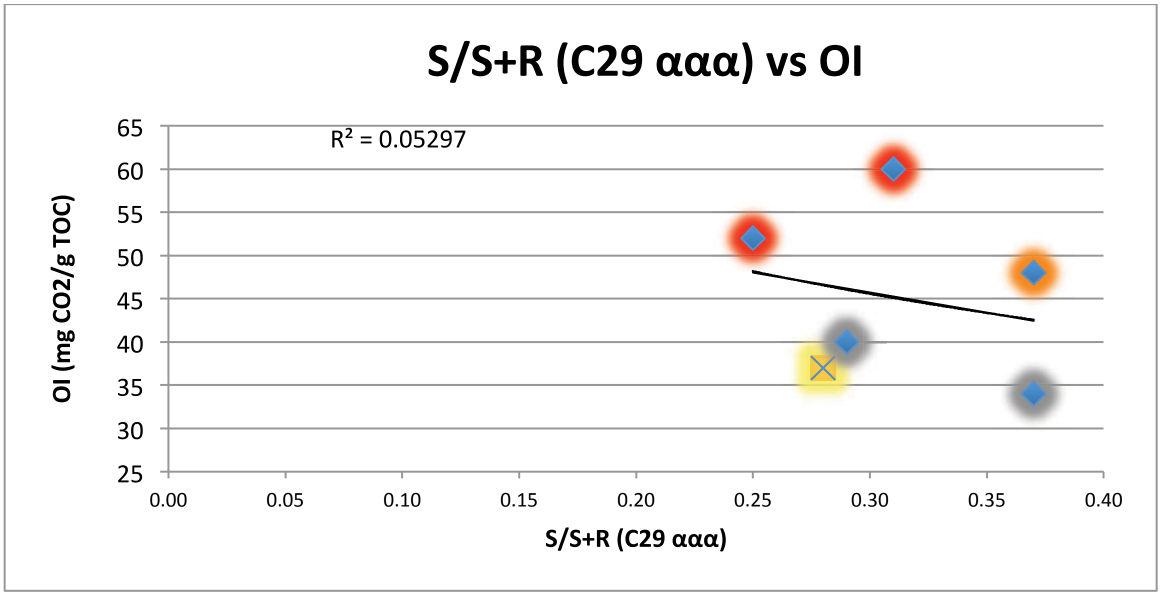

Figure 110: Red points are mineralized, orange is within 1 m of Cu mineralization, yellow is within 20 m, and gray is under 25 m distant. Data points stratigraphically below the proximal mineralization are X-marked. Increased biomarker ratio at decreased OI trend is expected for increased maturity, while the mineralized and nearest-mineralization above-trendline OI values can be seen to suggest local OM oxidation during mineralization. Red data points are mineralized, orange data points are within 1 m of mineralization, yellow are within 5 m, gray points are sub 20 m to mineralization, and brown is within 25 m of mineralization.

Oil inclusions in BIR 16 (the lowest OI, mineralized sample) observed by Colbert (2011) explain the unexpected positive trendline on the plot of OI-ββ/(ββ+αα) $C_{29}$. See Figure 111. The other BIR samples, both mineralized, show a greater degree of oxidation by OI than would be predicted by a trendline excluding all mineralized samples.

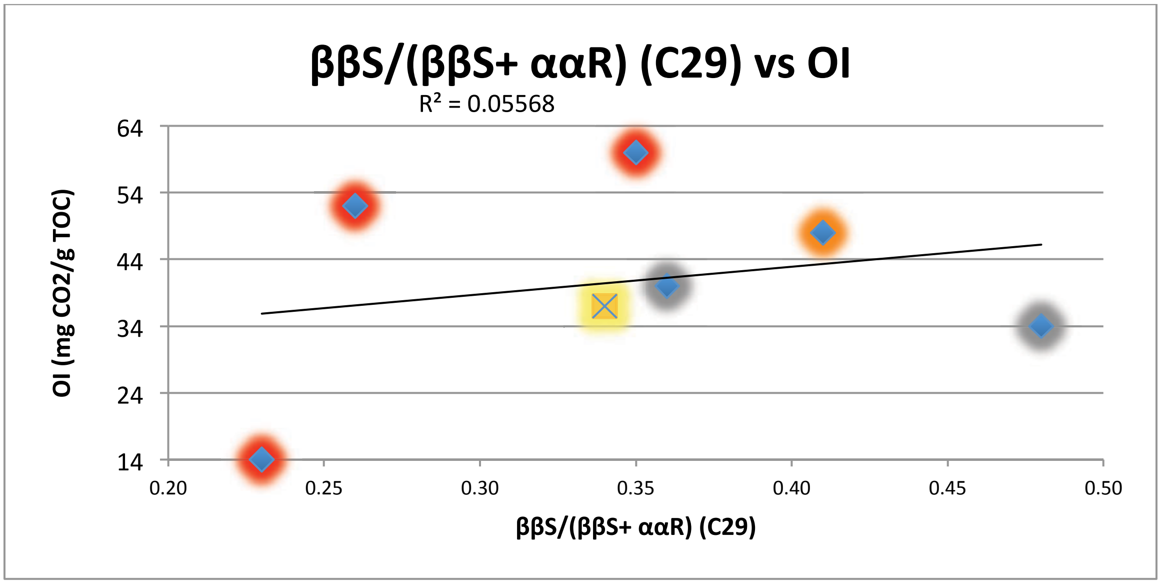

Figure 111: Oil inclusions in BIR 16 (the lowest OI, mineralized sample) observed by Colbert (2011) could explain the unexpected positive correlation. Red data points are mineralized, orange data points are within 1 m of mineralization, yellow are within 5 m (X'd data points are below the nearest Cu mineralization), gray points are sub 20 m to mineralization, and brown is within 25 m of mineralization.

### *7.3.12 Fluorene and Heteroatomic Fluorene Homologues*

The relative paucity of DBFs in the GC-MS samples (compared to those of Li *et al.*, 2015) can be interpreted to indicate relatively little oxidation of EOM in these samples. If the HCs in this study's Nonesuch Formation samples were generated during hydrothermalism by oxic brines, which to a degree oxidizes in-place organic kerogens, it seems reasonable to expect a relict signature of that oxidation in the form of enhanced DBF concentrations.

Fluorene is thought to derive from biphenyls; the DBT series lack clear biological precursors, while "natural" DBFs in crude oil and sedimentary organic matter have been described as metabolites of lichens or higher fungi. The prospect of significant contribution of lichen to lacustrine or marginal marine OM seems so unlikely that it is concluded that the relative lack of DBFs in this study's samples more likely represents marginal occurrence of OM oxidation during hydrothermalism associated with ore emplacement rather than significant inputs from lichen. Other studies suggested that DBFs may originate from dehydrated and condensed polysaccharides, which could conceivably be derived from algae or photosynthetic bacteria in the Nonesuch Formation (Sephton *et al*., 1999).

### *7.3.13 Polycyclic Aromatic Hydrocarbon Ternary Plot*

Li *et al*. (2013) noted that the relative abundance of DBT displays no regular relationship with the MDR maturity parameter, at least for marine shales. However, for the Type II and III organic-bearing Eocene suboxic lacustrine shales in their study, the DBT and DBF abundances did vary with depth. Specifically, the authors stated that the relative abundance of DBT gradually increases with increasing maturation, while the relative abundance of DBF does the opposite. Both compounds keep an approximately constant value in the window of oil generation. Those authors also note that biodegradation may lead to great variations of abundance in each of the DBT, fluorene, and DBF homologous series, in particular increasing DBT concentrations.

It is significant that total DBT content has been shown to decrease with increasing distance of migration of oil, similar to the carbazole (amine fluorene) content. The total DBT and alkyl-DBT content and relative content of isomers are controlled by both maturity and migration fractionation (Li *et al*., 2008). With increasing maturity, the MDR, the 2,4-/1,4-DMDBT and 4,6-/1,4-DMDBT ratios should be elevated due to the increasing amount of thermostable isomers (Chakhmakhchev *et al*., 1997).

The S enrichment of the Nonesuch Formation samples in this study, as indicated by their proximity to the relatively S enriched DBT point of the ternary plots, could be interpreted as evidence of widespread hydrothermalism (Figure 99). Specifically, high concentrations of DBTs are associated with thermochemical sulfate reduction (Wei *et al*., 2012). No geographic segregation with respect to ternary plot position is apparent. Absolute concentrations of DBT in petroleum have been shown to decrease with increasing migration (Li *et al*., 2008). The relatively high concentrations of DBT and the general lack of physical evidence of HC migrations might be interpreted to support indigeneity of the EOM in this study's GC-MS samples, although short distance (meter scale) migration cannot be ruled out. However, the one GC-MS sample - BIR 16 - showing definitive migrated solid bitumen (as well as Cu mineralization) presented 0.5% of the maximum observed DBT concentration of the sample suite, whereas unmineralized and non-bituminous samples like 523-3 presented lesser concentrations of DBT (0.04% of the maximum observed).

### *7.3.14 Stable Isotopes of Carbonate*

Strongly negative isotopic ratios of stable C and O in carbonates on two samples of the Nonesuch Formation may be interpreted as reflecting re-mineralization of isotopically light OM with a strongly negative isotopic signature, as suggested by Imbus *et al.* (1988). It is significant that one of the strongly negative $\delta^{13}C$ samples is from coarse grained, clearly secondary, calcite in bedding-perpendicular veins (523-7); very thin (sub-mm width) vertical and horizontal calcite-bearing fractures were present in 523-7, but only the vertical fracture was drilled. The other strongly negative $\delta^{13}C$ sample is from the layer-parallel calcite concretions that contort (but are not associated with changes in thickness of) the bedding of a chalcopyrite-rich sample (PIR-12). The organic matter of 523-7 is exclusively reddish brown AOM, while PIR-12 shows no OM in thin section. The redness of the 523-7 hand sample precluded RE analysis, whereas PIR-12's low TOC (0.03%) and $S_2$ disqualify the other RE parameters from reliable interpretation. Nonetheless, the relatively oxidized, Type IV position of the PIR-12 material (HI: 31, OI: 250) is potentially representative of localized oxidation and carbonate remineralization of OM in concert with Cu mineralization.

### *7.4 Distribution of OM Oxidation*

The aromatic maturity indices MPI1 and MDR indicate early to peak oil window at WP mine and similar or lower grade in the Iron River syncline. These are slightly lower grades than inferred from other indices ($T_{max}$, HI) and from temperatures inferred from clay mineralogy, which collectively indicate post-peak oil window for the WP area. The MPI1 gives calculated VR equivalent ($R_c$) maturities equivalent to the range between 0.77 and 1.0 for all samples from the WP mine area and significantly lower from Iron River syncline (0.42, 0.57). This measure shows varied patterns with depth and mineralization - the Cu mineralization proximal WPB sample that is closer to the base of the Nonesuch Formation is of higher $R_c$ maturity than is the sample 20 m above the base. The BIR samples show higher $R_c$ maturity with increasing degree of Cu mineralization and less regular pattern of MPI1 $R_c$ maturity to depth than at the Iron River syncline. The shallower 517 sample is less mature by this measure than the deeper sample, whereas the deeper, more distal to Cu mineralization 523 sample is more mature than the shallower sample that is closer to Cu mineralization.

The lower MPI1 from the Iron River syncline may be interpreted as a result of oxidative hydrothermal alteration, as in the Kupferschiefer (Bechtel *et al*., 2000), or of lower temperatures, as indicated by clay mineralogy (Price and McDowell, 1993).

The MDR gives calculated VR maturity of 0.71 to 1.01 for six of the nine samples, but significantly higher values (2.69, 7.63, 7.77) for three samples from the WP mine area which have partially altered or least altered GC traces. The outlier MDR VR equivalent maturity samples are significantly beyond the range of calibration (Radke *et al*., 1984). These outliers are thus unrealistic but still imply distinct OM characteristics in these samples.

The MPI1 and MDR maturity indices neither confirm nor rule out the proposal that the WP ore body is associated with a paleothermal anomaly (suggested by Mauk and Hieshima, 1992).

The ratio of diagenetic (S+R) to ααα (S+R) $C_{27}$ steranes shows a slight trend to lesser maturity for the Iron River syncline samples and maximal maturity concurrent with mineralization of the BIR samples. The moretane/hopane ratio has maximal values in the most altered WPB samples, suggesting lower thermal maturity in the Iron River syncline. Two of the three most mature samples by this measure are mineralized: BIR 13 and BIR 15. The high norhopane/hopane ratios of the two altered WPB samples suggests a marine carbonate facies for the Nonesuch Formation shales and siltstone (cf. Peters *et al.*, 2005). The BIR samples, all mineralized, show higher norhopane/hopane ratios than the least altered samples. The Ts/(Ts+Tm) and $C_{29}$Ts/($C_{29}$ hopane + $C_{29}$Ts) maturity parameters both show lesser maturity of OM in the Iron River syncline (submature) whereas they show higher maturity in the mineralized BIR samples. The Ts/(Ts+Tm) ratio in particular reaches maxima in the BIR samples. Each of the five above trends potentially reflect maturity influence affected by the OM oxidizing Cu mineralizing process.

There is a slight overall trend of increased HI to increasing S/S+R $C_{29}$ ααα ratio; this weak but positive correlation is counter to the expected maturity trend, and is clearly impacted by the low HI-low S/S+R $C_{29}$ ααα values of the hydrothermally mineralized BIR Nonesuch Formation samples. This may reflect increased thermal maturation of these samples during mineralization. See Figure 112.

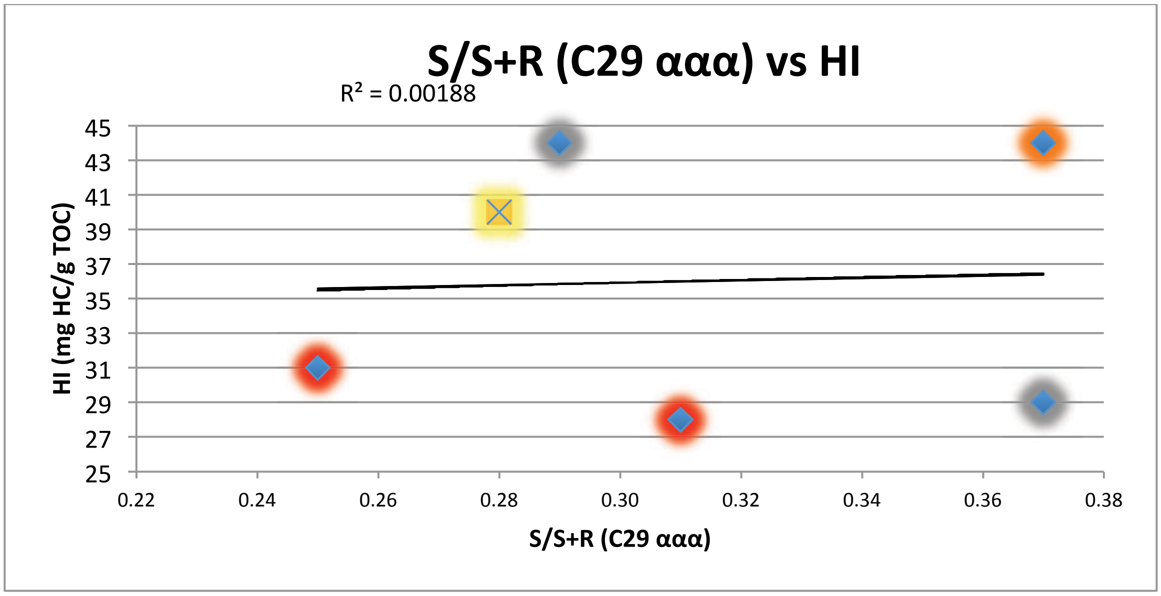

Figure 112: No statistically significant correlation exists between S/S+R $C_{29}$ ααα values and HI. The positive slope of the line of best fit is counter to expected maturity trends, largely due to low-rank position of the mineralized samples. Red points are mineralized, orange is within 1 m of Cu mineralization, yellow is within 20 m, and gray is under 25 m distant. Data points stratigraphically below the proximal mineralization are X-marked.

The ββ/(ββ+αα) $C_{29}$ maturity measure shows no correlation to HI, and the mineralized samples show low HI and lower maturity than most other GC-MS samples (Figure 113). In the absence of the aberrant mineralized data points, a strong negative correlation between these parameters would exist, as might be expected.

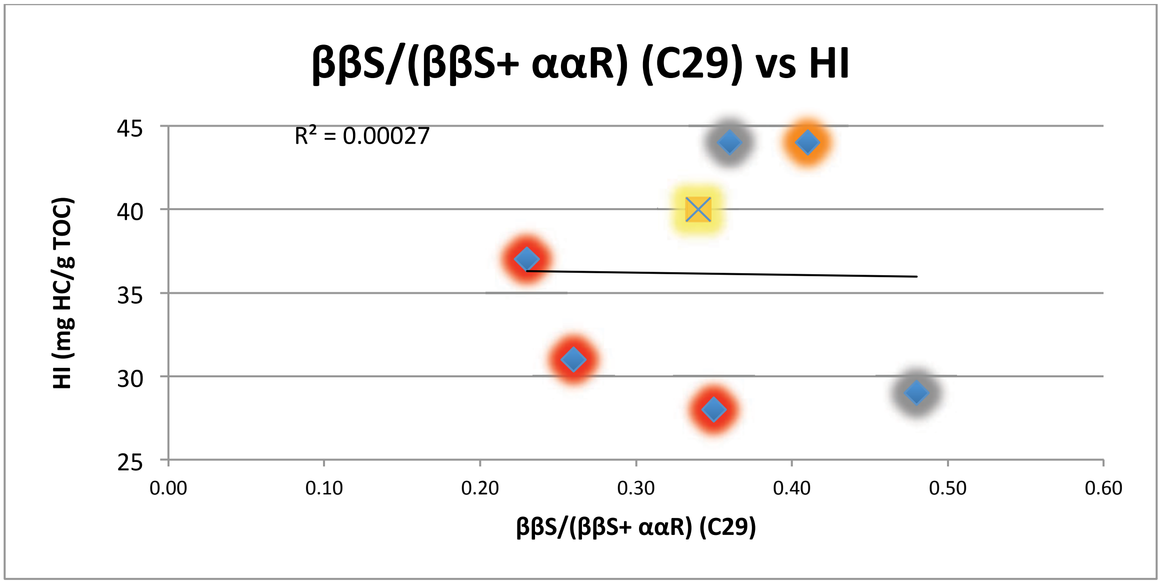

Figure 113: $C_{29}$ sterane ratio increases with maturation from near-zero values to about 0.70 at thermal equilibrium (Peters and others, 2005). This study's samples are in the early to peak oil generation window by this measure. Red points are mineralized, orange is within 1 m of Cu mineralization, yellow is within 20 m, and gray is under 25 m distant. Data points stratigraphically below the proximal mineralization are X-marked.

Of the two very low Ts/(Ts+Tm) samples, one is situated within 1 m of mineralization and the other is nearly 20 m away from mineralization. That the four highest Ts/(Ts+Tm) values (0.47 to 0.54) are found in the 3 mineralized and one of the sub 10 m distal to (and below) mineralization GC-MS samples may mean that mineralizing fluids played a role in increasing thermal maturity by this measure.

Other saturate fraction biomarker maturity parameters show less clear patterns with respect to depth, Cu mineralization and RE maturity parameters. The saturate parameters calculated from peak areas identified in ChromEdge Lite or provided by Weatherford but showing lesser correlation to Cu mineralization or RE parameters include: diahopane/hopane; $H_{32}$ S/R+S homohopane, triterpanes/hopanes; triterpanes/steranes; $C_{23}$ triterpanes/$C_{21}$ triterpanes; $C_{24}$ tetraterpanes/$C_{23}$ triterpanes; $C_{20}$-$C_{30}$ triterpanes/($C_{27}$-$C_{35}$ hopanes + $C_{20}$-$C_{30}$ triterpanes); steranes/hopanes; and, pregnane index.

## *8. Conclusion*

This study's data shows that geochemical and petrographic alteration of OM co-occurs with Cu mineralization on a widespread, regional scale, rather than strictly in the vicinity of zones of greatest Cu mineral concentrations:

- Two geochemically distinct populations of primary Proterozoic OM are petrographically different but often co-occur. Darker color, lesser H/C ratio and greater opacity of FOM than AOM are interpreted to result from processes operating prior to, and largely independent of, Cu mineralization. The color and hence TAI of AOM within a given sample is related, probably genetically, to Cu mineralization. However, no clear geographic or stratigraphic trends of AOM color exist, and AOM color does not darken with increasing proximity to Cu mineralization. No relationships between TAI values and GC, GC-MS, RE or stable isotopic geochemical patterns are apparent;
- Thermal maturity - as indicated by the PI, TAI, MPI1, Ts/Ts+Tm and the $C_{29}$ Ts/($C_{29}$ hopane + $C_{29}$ Ts) measures - shows bidirectionally increasing degrees of thermal alteration of OM distributed regionally outward from the four central sampling sites. On the local, sub 20-km scale, Cu mineralized samples show higher thermal maturity on the basis of moretane/hopane, $C_{29}$ Ts/($C_{29}$ hopane + $C_{29}$ Ts), TNy measures, as well as saturate and diamantane content. The analyzed GC-MS samples likely experienced similar heating rates in the subsurface.
- With the exclusion of outlier data points, Rock-Eval II core profiles show overall gradients of increasing HI with increasing stratigraphic height above the Copper Harbor Formation, whereas a negative OI relation to stratigraphic height exists. Taken together, that HI gradients span 30-100% of the Nonesuch Formation, are steeper than typically expected for such sedimentary basins, and that OI increases with proximity to Cu

mineralization but HI reaches minima in and adjacent to zones of Cu mineralization implies both broad scale and localized oxidation of OM in association with ore emplacement;

- Isoprenoid to corresponding *n*-alkane ratios, the distribution of tricyclic terpanes, the presence of 1,2,5-TMN in all samples and the widespread occurrence of $C_{32}$ α methylhopanes in a majority of GC-MS samples are interpreted to result from a single, dominant cyanobacterial OM source. These measures also imply a single paleoenvironment of production and deposition.
- Gas chromatography and GC-MS show three distinct populations of varied degree of OM alteration, which align to some degree with RE HI and OI values. The degree of OM alteration identified by GC and GC-MS does not clearly align with thermal maturity trends or with Cu mineralization - two of the altered samples are situated at the thermal maturity low in the center of the sample traverse (and are barren), whereas the other altered sample contains Cu minerals and is near to the thermal maximum in the vicinity of White Mine, MI. Lack of alignment of GC-MS alteration patterns to thermal maturity or to the presence or absence of Cu mineralization, as well as the overall similar style of OM alteration or degradation of those recorded in the altered and partially altered GC-MS samples to those earlier reported for both mineralized and unmineralized White Pine mine samples (Ho *et al.*, 1990; Mauk and Hieshima, 1992; Ho and Mauk, 1996) means that reactions specifically related to Cu deposition were not directly responsible for the three distinct GC-MS alteration patterns;
- Identification of a broad array of aromatic and PAHs throughout the GC-MS samples indicates widespread aromatization of OM, and with significant increases in the degree of

aromaticity relative to saturate compound content in Cu mineralized and organically altered samples;

- No simple relation between carbonate stable isotope ratios and depth or mineralization proximity is clear, although broad depletion of $^{13}C$ in carbonates concurrent with OM oxidation is implied by the overlap of strongly negative $\delta^{13}C$ values with sections of highest OI as well as the broad spread of $\delta^{13}C$ to more negative values relative to the interpreted primary carbonate composition. This concurs with data from the analogous Kupferschiefer indicating variable degrees of mixing of primary carbonate feedstock C with that derived by oxidation of indigenous OM;

Future studies could build upon this work by close examination of the potential relationship between the liberation of Fe from hematite during Cu mineralization and remineralization of Fe in association with ore mineral deposition. This would be best addressed by petrographic examination of the "bleached sandstone" and comparison with underlying, unbleached Copper Harbor Formation material. The organic geochemical composition of the pyrobitumen cements in the bleached sandstone is another worthwhile object of study, which may be well-addressed in a combined effort with consideration of the chlorite-hematite-organic alteration relations.

Future investigations of this type should ideally analyze only the absolutely freshest, unweathered outcrop samples possible. Outcrop samples must be from unfractured rock when possible, because OM is surficially oxidized, probably both microbiologically and abiogenically. Given the sensitivity of such analyses, core analysis would best be executed in the future on only the most recently collected and best curated drill core material available.

<u>*References*</u>

Aeppli, C. Nelson, R.K., Radovic, J.R., Carmichael, C.A., Valentine, D.L., and Reddy, C.M., 2014, Recalcitrance and degradation of petroleum biomarkers upon abiotic and biotic natural weathering of *Deepwater Horizon* oil. *Environmental Science and Technology*. **48**: 12: 6726-6734.

Andres, J.E., and, Fallick, R.D., 1986, Stable isotopes in sedimentary geology. *Journal of the Geological Society*. **100**:1375-1391.

Ashok, R., Saxena, R.K., Pande, H.C., Vartika, R., Mittal, A.K., and Pande, A., 2013, Oil-oil and oil-source correlation by application of compound specific isotope analysis: A frontier tool applied to Kali-Kuthalam area in Cauvery Basin. Society for Petroleum Geology India, 10th Biennial Conference.

Ballentine, C.J., O'Nions, R.K., and Coleman, M.L., 1996, A magnus opus: helium, neon, and argon isotopes in a North Sea oilfield. *Geochimica et Cosmochimica Acta*, **60**: 831-849.

Barghoorn, E.S., Meinschein, W.G., Schopf, J.W., 1965, Paleobiology of a Precambrian Shale. *Geology*, **148**: 461-472.

Behrendt, J.C., Green, A.G., Cannon, W.F., Hutchinson, D.R., Lee, M., Milkereit, B., Agena, W., Spencer, C., 1988, Crustal structure of the Midcontinent Rift System: results from the GLIMPCE deep seismic reflection profiles. *Geology*, **16**:81-85.

Bickford, M.E., 1988, The formation of continental crust, II: An application to the Proterozoic evolution of southern North America. *GSA Bulletin*, **100**:1375-1391.

Bechtel, A., Gratzer, R., Puttmann, W., and Oszezepalski, S., 2000, Geochemical characteristics across the oxic-anoxic interface within the Kupferschiefer of the Lubin-Sieroszowice mining district. *Chemical Geology*, **185**:9-31.

Brooks, J., and Shaw, G., 1972, Geochemistry of sporopollenin. *Chemical Geology*, **10**:69-87.

Brown, A.C., 2006, Genesis of native copper lodes in the Keweenaw district, northern Michigan: A hybrid evolved meteoric and metamorphogenic model. *Economic Geology*, **101**: 1437-1444.

Brown, A.C., and Chartrand, F.M., 1983, Stratiform copper deposits and interactions with co-existing atmospheres, hydrospheres, biospheres and lithospheres. *Precambrian Research*, **20**:533-542.

Brown, A.C., 1978, Stratiform copper deposits - evidence from their post-sedimentary origin. *Minerals Science Engineering*, **10**:172-181.

Brown, A.C., 1971, Zoning in the White Pine copper district, Ontonagon County, Michigan. *Economic Geology*, **66**:543-573.

Burnie, S., Schwarcz, H., and Crocket, J., 1972, A sulfur isotopic study of the White Pine Mine, Michigan. *Economic Geology*, **67**: 895-914.

Butler, B.S., and Burbank, W.S., 1929, Copper Deposits of Michigan: USGS Professional Paper 144.

Cannon, W., and Hinze, W., 1992, Speculations on the origin of the North American midcontinent rift. *Tectonophysics*, **213**:49-55.

Cannon, W., 1992, The midcontinent rift in the Lake Superior region with emphasis on its geodynamic evolution. *Tectonophysics*, **213**:41-48.

Cannon, W., and Nicholson, W., 1992, Middle Proterozoic midcontinent rift system, *in* U.S.G.S. Professional Paper 1556: Archean and Proterozoic Geology of the Lake Superior Region, U.S.A., 1993, *eds*. Sims, P., and Carter, L., 99 p.

Cannon, W., Woodruff, L.G., Nicholson, S.W., and Hedgman, C.A., 1996, Bedrock geologic map of the Ashland and the northern part of the Ironwood 30' X 60' quadrangles, Wisconsin and Michigan. U.S.G.S. Miscellaneous Geologic Investigations Map I-2566, scale 1:100,000.

Chakhmakhchev, A., Suzuki, M., Takayama, K., et al., 1997, Distribution of alkylated dibenzothiophenes in petroleum as a tool for maturity assessments. *Organic Geochemistry*, 26(7-8): 483-490.

Colbert, S.J., 2011, Fluid inclusion study of the Mesoproterozoic Nonesuch Formation - biogenic sources and thermal history of oil.

Craddock, P.R., et al., 2015, Evolution of kerogen and bitumen during thermal maturation via semi-open pyrolysis investigated by infrared spectroscopy. *Energy Fuels*, **29**:4:2197-2210.

Crick, I., Boreham, C., Cook, A., and Powell, T., 1988, Petroleum geology and geochemistry of Middle Proterozoic McArthur Basin, Northern Australia II: Assessment of source rock potential, *American Association of Petroleum Geologists Bulletin*, **72**:1495-1514.

Criss, R.E., and Taylor, Jr., H.P., 1986, Meteoric-hydrothermal systems, *in:* J.W. Valley, H.P. Taylor, Jr., and J.R. O'Neil, eds., Stable isotopes in high-temperature geological processes. *Mineralogical Society of America Reviews in Mineralogy*, **16**:373-424.

Cumming, V.M., Poulton, S.W., Rooney, A.D., and Selby, D., 2013, Anoxia in the terrestrial environment during the late Mesoproterozoic. *Geology*, **41**:583-586.

Cumming, V.M., 2012, Rhenium-osmium geochronology and geochemistry of ancient lacustrine sedimentary and petroleum systems, Durham theses, Durham University. 192 p.

Daniels, P., 1982, Upper Precambrian sedimentary rocks: Oronto Group, Michigan-Wisconsin. Geological Society of America, Memoir, **156**:107-133.

Davis, D., and Paces, J., 1990, Time resolution of geologic events on the Keweenaw Peninsula and implications for development of the midcontinent rift system. *Earth and Planetary Science Letters*, **97**:54-64.

Davis, D., and Sutcliffe, R.H., 1985, U-Pb ages from the Nipigon plate and northern Lake Superior. *Geologic Society of America Bulletin*, **96**:1572-1579.

Disnar, J.R., and Heroux, Y., 1995, *Degradation et lessivage des hydrocarbures de la formation ordovicienne de Thumb Mountain encaissant la gite Zn-Pb de Polaris (Territoires du Nord-Ouest, Canada)*. *Canadian Journal of Earth Sciences*, **32**:1017-1034.

Disnar, J.R., Surau, J.F., 1990, Organic matter in ore genesis - progress and perspectives. *Organic Geochemistry*, **16**: 577-599.

Dutkiewicz, A., Volk, H., George, S.C., Ridley, J., and Buick, R., 2006, Biomarkers from Huronian oil-bearing fluid inclusions: an uncontaminated record of life before the Great Oxidation Event. *Geology*, **34**: 673-678.

Eglinton, T.I., Philp, R.P., and Rowland, S.J., 1988, Flash pyrolysis of artifically matured kerogens from the Kimmeridge clay, U.K. *Organic Geochemistry*, **12**:33-41.

Elmore, R.D., Milavec, G., Imbus, S., and Engel, M., 1989, The Precambrian Nonesuch Formation of the North American midcontinent rift, sedimentology, and organic geochemical aspects of lacustrine deposition. *Precambrian Research*, **43**:191-213.

Elmore, R.D., 1984, The Copper Harbor Conglomerate: a late Precambrian fining-upward alluvial fan sequence in northern Michigan. GSA Bulletin, **95**:610-617.

Elmore, R.D., and van der Voo, R., 1982, Origin of hematite and its associated remanence in the Copper Harbor Conglomerate (Keweenawan), Upper Michigan. *Journal of Geophysical Research*, **87**:10918-10928.

Engel, M.H., and Macko, S.A., 1993, Organic Geochemistry, Springer, 832 p.

Ensign, C.O., Jr., and 8 others, 1968, Copper deposits in the Nonesuch Shale, White Pine, Michigan, *in* Ridge, J.D., ed., Ore Deposits of the United States 1933-1967, **1**: New York, American Institute of Mining, Metallurgical, and Petroleum Engineers, p. 459-488.

Erwin, D.H., 2015, Early metazoan life: divergence, environment and ecology. *Philosophical Transactions of the Royal Society*, **370**:1684.

Essene, E.J., and Peacor, D.R., 1995, Clay mineral thermometry - A critical perspective. *Clays and Clay Minerals*, **43**: 5:540-553.

Fairmaid, A.M., Kendrick, M.A., Phillips, D., Fu, B., 2011, The origin and evolution of mineralizing fluids in a sediment-hosted orogenic gold deposit, Ballarat East, Southeastern Australia. *Economic Geology,* **106**: 653-666.

Fang, C., Wei, W., Liu, D., and Liu, J., 2016, Evolution characteristics and applications of diamondoids in coal measures. *Journal of Natural Gas Geoscience,* **1**:1: 93-99.

Fourgani, Aiyda, 2012, Organic geochemistry of Mesoproterozoic Nonesuch Formation at White Pine, Michigan, USA. Colorado State University MS thesis, 160 p.

Fowler, M., Obermajer, M., and K.R. Stewart, 2014, Rock-Eval/TOC data for selected samples from twelve wells in the Jeanne d'Arc Basin, offshore Eastern Canada: Geological Survey of Canada Open File 7648.

George, S.C., and others, 2008, Preservation of hydrocarbons and biomarkers in oil trapped inside fluid inclusions for >2 billion years. *Geochimica et Cosmochimica Acta*, **72**: 844-870.

Giordano, T.H., et al. (eds.), 2000, Ore Genesis and Exploration, Reviews in Economic Geology. Kluwer, 895 p.

Gize, A.P., 2000, The organic geochemistry of gold, platinum, uranium and mercury deposits, *in* Giordano, T.H., et al. (eds.), Reviews in Economic Geology: Ore Genesis and Exploration: The Roles of Organic Matter, 217-250.

Gordadze, G.N., and Giruts, M.V., 2008, Synthesis of adamantane and diamantane hydrocarbons by high-temperature cracking of higher *n*-alkanes. *Petroleum Chemistry*, **48**:6: 414.

Grafka, O., Marynowski, L., and Simoneit, B., 2015, Phenyl derivatives of polycyclic aromatic compounds as indicators of hydrothermal activity in the Silurian black siliceous shales of the Bardzkie Mountains, Poland. *International Journal of Coal Geology*: **139**:1: 142-151.

Greenwood, P.F., Brocks, J.J., Grice, K., Schwark, L., Jaraula, C.M.B., Dick, J.M., and Evans, K.A., 2013, Organic geochemistry and mineralogy I: Characterization of organic matter associated with metal deposits. *Ore Geology Reviews*, **50**:1-27.

Hayes, J., Kaplan, I., and Wedeking, K., 1983, Precambrian organic geochemistry, preservation of the record, in: Earth's Earliest Biosphere (J. Schopf, ed.), Princeton University Press, Princeton, New Jersey, p. 93-134.

Hegarty, K.A., Foland, S.S., Cook, A.C., Green, P.F., and Doody, I.R., 2007, Direct measurement of timing: Underpinning a reliable petroleum system model for the Midcontinent rift system, *AAPG Bulletin*, **91**:7:959-979.

Hieshima, G., and Pratt, L., 1991, Sulfur/carbon ratios and extractable organic matter of the Middle Proterozoic Nonesuch Formation, North American midcontinent rift. *Precambrian Research*, **54**: 65-79.

Ho, E. and Mauk, J., 1996, Relationship between organic matter and copper mineralization in the Proterozoic Nonesuch Formation, northern Michigan. *Ore Geology Reviews*, **11**:71-88.

Hoering, T.C., 1978, Molecular fossils from the Precambrian Nonesuch Shale, *in* Ponnamperuma, C. (ed.) Comparative Planetology. Academic Press, New York, p. 243-255.

Hoering, T.C., 1981, Monomethyl acyclic hydrocarbons in petroleum and rock extracts. *Carnegie Institute of Washington, Yearbook*, **80**:389-393.

Hulen, J.B., Collister, J.W., 1999, The oil-bearing, carlin-type gold deposits of Yankee basin, Alligator Ridge district, Nevada. *Economic Geology Bulletin*, **94**: 1029-1049.

Hunt, J.M., 1995, Petroleum Geochemistry and Geology, 2nd ed., 743 p.

Hutchinson, D., White, R., Cannon, W., and Schulz, J., 1990, Keweenaw hot spot: Geophysical evidence for a 1.1 Ga mantle plume beneath the midcontinent rift system. Journal of Geophysical Research, **95***:*10869–10884.

Ilchik, R.P., Brimhall, G.H. Jr., and Schull, H.W., 1986, Hydrothermal maturation of indigenous organic matter at the Alligator Ridge Gold Deposits, Nevada. *Economic Geology*, **81**:113-130.

Imbus, S.W., Engel, M., Elmore, R., and Zumberge, J., 1988, The origin, distribution and hydrocarbon generation potential of the organic-rich facies in the Nonesuch Formation, Central North American Rift system: A regional study. *Organic Geochemistry*, **13**:207-219.

Imbus, S.W., 1990, Organic petrologic and geochemical studies on the Oronto group Nonesuch Formation (Middle Proterozoic) of the Midcontinent Rift System, northern Wisconsin and Upper Peninsula Michigan. University of Oklahoma PhD. Thesis, Norman, OK.

Imbus, S.W., Macko, S.A., Elmore, R.D., and Engel, M.H., 1992, Stable isotope (C, S, N) and molecular studies on the Precambrian Nonesuch Shale (Wisconsin-Michigan, USA): Evidence for differential preservation rates, depositional environment and hydrothermal influence. *Chemical Geology*, **101**:255-281.

Jiang, C., et al., 2016, Hydrocarbon evaporative loss from shale core samples as revealed by Rock-Eval and thermal desorption-gas chromatography analysis: Geochemical and geological implications. *Marine and Petroleum Geology*, **70**:9:294-303.

Jin, H., and Sonnenberg, S.A., 2012, Source rock potential of the Bakken Shales in the Williston Basin, North Dakota and Montana. Search and Discovery Article #20156.

Johnson, R.D., 2014, Technical Report on the White Pine copper property, White Pine, Michigan, USA: NI-43-101, Prepared for Highland Copper Company Inc., 76 p.

Jowett, E.C., and Rydzewski, A., and Jowett, R.J., 1987, THe Kupferschiefer Cu-Ag ore deposits in Poland: a re-appraisal of the evidence of their origin and presentation of a new genetic model. *Canadian Journal of Earth Science*, **24**:2016-2037.

Kelley, W.C., and Nishioka, G.K., 1985, Precambrian oil inclusions in late veins and the role of hydrocarbons in copper mineralization at White Pine, Michigan. *Geology*, **13**:334-337.

Killops, S., and Killops, V., 2005, Introduction to Organic Chemistry, Blackwell, 376 p.

King, N., 2009, Using copper mineralization to evaluate small-scale controls on mudstone permeability in the Nonesuch Formation. Colorado State University M.S. thesis, Fort Collins, CO.

Kotarba, M.J., Peryt, T.M., Kosakowski, P., and Wieclaw, D., 2006, Organic geochemistry, depositional history and hydrocarbon generation modelling of the Upper Permian Kupferschiefer and Zechstein Limestone strata in southwest Poland. *Marine and Petroleum Geology*, **23**:371-386.

Kreulen, R., 1988, Stable isotopes in sedimentary geology. *Sedimentary Geology*, **54**:4:350-351.

Lavric, J.V., Spangenberg, J.E., and Rezun, B., 2003, Organic geochemical records of hydrothermal alteration at Idrija mercury deposit, Slovenia. *Geologija*, **46**:1:129-134.

Li, G., Mauk, J.L., and Peacor, D.R., 1995, Preservation of clay minerals in the Precambrian (1.1 Ga) Nonesuch Formation in the vicinity of the White Pine copper mine, Michigan. *Clays and Clay Minerals*, **43**: 2: 361-376.

Li, M., Wang, T., Liu, J., Gao, L., 2008, Total alkyldibenzothiophenes content tracing the filling pathway of condensate reservoir in the Fushan Depression, South China Sea. *Science in China* D:Earth Scienes, 51:138-145.

Li, M., Wang, T., Bong, Z., Zhang, W., Sadik, A., and Hongbo, L., 2013, Ternary diagrams of fluorenes, dibenzothiophenes and dibenzofurans: Indicating depositional environment of crude oil source rocks. *Energy Exploration and Exploitation*, 31:4:569-588.

Li, S., Amrani, A., Pang, X., Haijun, Y., Said-Ahmad, W., Zhang, B., and Pang, Q., 2015, Quantitative source assessment of deep oils in the Tazhong Basin. *Organic Geochemistry*, 78:1-22.

Liang, F., Lu, M., Keener, T., Liu, Z., and Khang, S., 2005, The organic composition of diesel particulate matter, diesel fuel and engine oil of a non-road diesel generator. *Journal of Environmental Monitoring*, **7**: 983-988.

Lillis, P.G., Dolan, M.P., Warden, A., and King, D.J., 1998, Organic geochemistry of oils from Oil Spring and Florence Oil Field near Cañon City, Colorado. *USGS Open File Report 98-617*.

Logan, G.A., Hinman, M.C., Walter, M.R., Summon, R.E., 2001, Biogeochemistry of the 1640 Ma McArthur River (HYC) lead-zinc ore and host sediments, N. Territory, Australia. *Geochimica et Cosmochimica Acta*, **65**: 2317-2336.

Longstaffe, F.J., and Ayalon, A., 1988, Oxygen isotope studies of diagenesis and pore-water evolution in the western Canada sedimentary basin: Evidence from the Upper Cretaceous basal Belly River Sandstone, Alberta. *SEPM Journal of Sedimentary Research*, **58**:3:489-505.

Marynowski, L., and Simoneit, B.R.T., 2009, Widespread Upper Triassic to Lower Jurassic wildfire records from Poland: Evidence from charcoal and pyrolytic polycyclic aromatic hydrocarbons. *PALAIOS*, **24**:11: 785-798.

Marynowski, L., and Wyszomirski, P., 2007, Organic geochemical evidences of early diagenetic oxidation of terrestrial organic matter during the Triassic arid and semi arid climatic conditions. *Applied Geochemistry*, **23**:9:2612-2618.

Mastalerz, M., Hampton, L., and Drobniak, A., 2016, Evaluating thermal maturity using transmitted light techniques: color changes in structureless organic matter and palynomorphs, Indiana Geological Survey Ocassional Paper 73, 41 p.

Mauk, J.L., and Burruss, R.C., 2002, Water washing of Proterozoic oil in the Midcontinent Rift System. *AAPG Bulletin*, **86**:6:1113-1127.

Mauk, J.L., and Hieshima, G.B., 1992, Organic matter and copper mineralization at White Pine, Michigan, U.S.A. *Chemical Geology*, **99**:189-211.

Mauk, J.L., Kelly, W.C., van der Pluijm, B.A., and Seasor, R.W., 1993, Relations between deformation and sediment-hosted copper mineralization: Evidence from the White Pine portion of the midcontinent rift system. *Geology*, **20**:427-430.

Mauk, J.L., Seasor, R.W., Kelly, W.C., and van der Pluijm, B.A., 1989, The relationship between structure and second-stage copper mineralization in the White Pine district of the Midcontinent Rift, northern Michigan. *GSA Abstracts with Programs*, **21**: A130.

McCarthy, K., et al., 2011, Basic petroleum geochemistry for source rock evaluation. *Oilfield Review*, **23**:2:32-43.

McKirdy, D.M., 1976, Biochemical markers in stromatolites, *in*: Stromatolites, ed. M.R. Walter, p. 163-191. Amsterdam: Elsevier.

McKirdy D.M., and Hahn, J.H., 1982, The composition of kerogen and hydrocarbons in Precambrian rocks, *in*: Mineral Deposits and Evolution of the Biosphere, H.D. Holland and M. Schidlowski, eds. Berlin: Springer-Verlag. 420 p.

McKirdy, D.M., and Kanstler, A.J., 1980, Oil geochemistry and potential source rocks of the Officer Basin, South Australia. *Journal of the Australian Petroleum Exploration Association*, **20**:1:68-86.

McKirdy, D.M., McHugh, D.J., and Tardif, J.W., 1980, Comparative analysis of stromatolitic and other microbial kerogens by pyrolysis-hydrogenation-gas chromatography, *in:* Biogeochemistry of Ancient and Modern Environments, eds. P.A. Trudinger, M.R. Walter, and B.J. Ralph, p 187-200. Berlin: Springer-Verlag.

Milavec, G.J., 1986, The Nonesuch Formation: Precambrian sedimentation in an intracratonic rift. University of Oklahoma MS thesis, 142 p.

Miller, J., and Nicholson, S., 2013, Geology and mineral deposits of the 1.1 Ga midcontinent rift in the Lake Superior region - an overview: http://www.d.umn.edu/~mille066/Teaching/5100/Articles/Miller%20and%20Nicholson%202013.pdf.

Moore, L.R., Moore, J.R.M., and Spinner E., 1969, A geomicrobiological study of the Precambrian Nonesuch Shale. *Yorkshire Geologic Society Proceedings*, **37**: 351-394.

Nishio, K., 1919, Native copper and silver in the Nonesuch Formation, Michigan. *Economic Geology*, **14**: 324-334.

Nishioka, G.K., 1983, Origin of late veins in the White Pine copper deposits, northern Michigan: M.S. Thesis. University of Michigan, Ann Arbor, Michigan, 35 p.

Ojakangas, R., Morey, G., and Green, J., 2001, The Mesoproterozoic midcontinent rift system, Lake Superior Region, USA. *Sedimentary Geology*, **142**:421-442.

Ourisson, G., and Rohmer, M., 1992, Hopanoids 2, Biohopanoids: A novel class of bacterial lipids. *Accounts of Chemical Research*, **25**: 403-408.

Paces, J., and Miller, Jr., J., 1993, Precise U-Pb ages of Duluth Complex and related mafic intrusions, northeastern Minnesota: geochronological insights to physical, petrogenetic, paleomagnetic, and tectonomagnetic processes associated with the 1.1 Ga Midcontinent Rift System. *Journal of Geophysical Research*, **98**:13997-14013.

Palacas, J.G., 1997, Source-Rock Potential of Precambrian Rocks in Selected Basins of the United States. USGS Bulletin 2146-J.

Palinkas, L.A., Strmic, S., and Herlec, U., 2001: The ore-forming fluids in the Idria mercury mine, Slovenia. In: A. Piestrzynski et al. (eds.), Mineral deposits at the beginning of the 21st century - Swets and Zeitlinger, p. 321-324.

Peat, C.J., Muir, M.D., Plumb, K.A., McKirdy, D.M., and Norvick, M.S., 1978, Proterozoic microfossils from the Roper Group, Northern Territory, Australia. *Journal of Australian Geology and Geophysics*, **3**:1-17.

Peters, K.E., and Cassa, M.R., 1994, Applied source rock geochemistry, *in* Magoon, L.B., and Dow, W.G. (eds.) The Petroleum System - From Source to Trap. *AAPG Memoir* **60**:432-436.

Potter, E.P., Maynard, J.B., and Depetris, P.J., 2005, Mud and Mudstones. New York: Springer.

Powell, T.G., Cook, P.J., and McKirdy, D.M., 1975, Organic geochemistry of phosphorites: relevance to petroleum genesis. *AAPG Bulletin*, **59**:618-632.

Pratt, L., Summons, R., and Hieshima, G., 1991, Sterane and triterpane biomarkers in the Precambrian Nonesuch Formation, North American midcontinent rift. *Geochimica et Cosmochimica Acta*, **55**:911-916.

Price, K.L., Huntoon, J.E., and McDowell, S.D., 1996, Thermal history of the 1.1-Ga Nonesuch Formation, North American mid-continent rift, White Pine, Michigan: AAPG Bulletin, **80**:1:1-15.

Price, K.L., and McDowell, S.D., 1993, Illite/smectite geothermometry of the Proterozoic Oronto Group, midcontinent rift system: Clays and Clay Minerals, **41**:2:134-147.

Püttmann, W., Merz, C., and Speczik, S., 1989, The secondary oxidation of organic material and its influence on Kupferschiefer mineralization of Southwest Poland. *Applied Geochemistry*, **4**:151-161.

Radke, M., Willsch, H., Leythaeuser, D., and Teichmüller, M., 1982, Aromatic components of coal: relation of distribution pattern to rank. *Geochimica Cosmochimica Acta*, **46**: 1831-1848.

Radke, M., Leythaeuser, and Teichmüller, M., 1984, Relationships between rank and composition from coals of different origins. *Organic Geochemistry,* **10**:51-63.

Radke, M., Welte, D.H., and Wilsch, H., 1986, Maturity parameters based on aromatic hydrocarbons: influence of the organic matter type. *Organic Geochemistry*, **10**:51-63.

Radke, M., 1987, Organic geochemistry of aromatic hydrocarbons. *Advances in Petroleum Geochemistry*, **2**: 141-207.

Ré-Poppi, N., and Santiago-Silva, M.R., 2002, Identification of polycyclic aromatic hydrocarbons and methoxylated phenols in wood smoke emitted during production of charcoal. *Chromatographia*, **55**: 475-481.

Reimer, T., Barghoorn, E., and Margulis, L., 1979, Primary production in an Early Archean microbial ecosystem. *Precambrian Research,* **9**:93-104.

Rieger, A., Schwark, L., Cisternas, M.E., Miller, H., 2008, Genesis and evolution of bitumen in Lower Cretaceous lavas and implications is for strata-bound copper deposits, north Chile. *Econcomic Geology,* **103**:387-404.

Robert, P., 1980, The optical evolution of kerogen and geothermal histories applied to oil and gas exploration: *in* Durand, B., et al., Kerogen: Insoluble organic matter from sedimentary rocks: Paris, Edition Technip, p. 385-414.

Rollinson, H. R., 1994, Using Geochemical Data. Essex, England: Longman Scientific & Technical, 323 p.

Rospondek, M.F., Marynowski, L., and Gora, M., 2007, Novel arylated polyaromatic thiophenes: Phenylnaphtho[*b*]thiophenes and naphthylbenzo[*b*]thiophenes as markers of organic matter diagenesis buffered solutions. *Organic Geochemistry*, **38**: 1729-1756.

Rose, A.W., 1976, The effect of cuprous chloride complexes on the origin of redbed copper and related deposits. *Economic Geology*: **71**: 1036-1048.

Ruiz, J., Jones, L.M., and Kelly, W.C., 1984, Rubidium-strontium dating of ore deposits hosted by Rb-rich rocks, using calcite and other common Sr-bearing minerals. *Geology*, **12**:159-262.

Saxby, J.D., 1976, The significance of organic matter in ore genesis, *in:* Handbook of Stratabound and Stratiform Ore Deposits, ed. K.H. Wolf, p. 111-133. Amsterdam: Elsevier.

Schidlowski, M., 1987, Application of stable carbon isotopes to early biochemical evolution of Earth. *Annual Review of Earth Sciences*, **15**:47-72.

Schmidt, J.M., and Rogers, R.K., 2007, Metallogeny of the Nikolai large igneous province in southern Alaska and its influence on the mineral potential of the Talkeetna Mountains. *Geological Society of America Special Paper 431*:623-657.

Seasor, R.W., and Brown, A.C., 1989, Syngenetic and diagenetic concepts at the White Pine copper deposit, Michigan. *Geologic Association of Canada Special Paper*, **36**:257-268.

Sephton, M.A., Looy, C., Veefkind, R., Visscher, H., Brinkuis, H., and de Leeuw, J., 1999, Cyclic diaryl ethers in a Late Permian sediment, *Organic Geochemistry,* 30:4:267-273.

Seifert, W.K., and Moldowan, J.M., 1986, Use of biological markers in petroleum exploration. In: Methods in Geochemistry and Geophysics, **24**:261-290.

Sharpe, Z., 2007, Principles Of Stable Isotope Geochemistry. Upper Saddle River, N.J.: Pearson/Prentice Hall, 323 p.

Shock, E.L., Canovas, P., Yang, Z., Boyer, G., Johnson, K., Robinson, K., Fecteau, K., Windman, T., Cox, A., 2013, Thermodynamics of organic transformations in hydrothermal fluids. Reviews in Mineralogy and Geochemistry, **76**: 311-350.

Simoneit, B.R.T., and Fetzer, J.C., 1995, High molecular weight polycyclic aromatic hydrocarbons in hydrothermal petroleums - indicators of high temperatures and water washing (abs.). *AAPG Bulletin*, **79**:925.

Sirois, R., 2015, NI-43-101 Technical report on the Copperwood copper project, Michigan, USA, Prepared for Highland Copper Company, Inc., 154 p.

Snowdon, L., 1995, Rock-Eval $T_{max}$ suppression: Documentation and amelioration. *AAPG Bulletin*, **79**:1337-1348.

Spangenberg, J.E., Macko, S.A., 1998, Organic geochemistry of the San Vicente zinc-lead district, eastern Pucara Basin, Peru. *Chemical Geology*, **146:**1-43.

Stojanovic, K., Jovancicevic, B., Vitorovic, D., Pevneva, G., Golovko, J., and Golovko, A., 2007, New maturation parameters based on naphthalene and phenanthrene isomerization and dealkylation processes aimed at improved classification of crude oils (Southeastern Pannonian Basin, Serbia). *Geochemistry International*, **45**:8:781-797.

Strother, P.K., and Wellman, C.H., 2016, Paleoecology of a billion-year-old non-marine cyanobacterium from the Torridon Group and Nonesuch Formation. *Paleontology*, **59**:1:89-108.

Speczik, S., and Puttman, W., 1987, Origin of Kupferschiefer mineralization as suggested by coal petrology and organic geochemical studies. *Acta Geologica Polonica*, **37**:167-187.

Spotl, C., and Vennemann, T.W., 2003, Continuous-flow IRMS analysis of carbonate minerals. *Rapid Communications in Mass Spectrometry*, **17**:1004-1006.

Summons, R.E., Powell, T.G., Boreham, C.J., 1988, Petroleum geology and geochemistry of the middle Proterozoic Mcarthur Basin, N. Australia: composition of extractable hydrocarbons. *Geochimica et Cosmochimica Acta,* **52**:1747-1763.

Summons, R.E., and Walter, M.R., 1990, Molecular fossils and microfossils of prokaryotes and protists from Proterozoic sediments. *American Journal of Science*, **290-A**:212-244.

Sun, Y., 1998, Influences of secondary oxidation and sulfide formation on several maturity parameters in the Kupferschiefer. *Organic Geochemistry,* **29**:5-7:1419-1429.

Sun, Y., and Püttman, W., 2001, Oxidation of organic matter in the transition zone of the Zechstein Kupferschiefer from the Sangerhausen Basin, Germany. *Energy and Fuels,* **15**:817-829.

Suszek, T., 1997, Petrography and sedimentation of the Middle Proterozoic (Keweenawan) Nonesuch Formation, western Lake Superior region, midcontinent rift system: Geological Society of America, Special Paper, 312:195-210.

Sutton, S., Ridley, J., Fourgani, A., and King, N., 2013, Relationship of organic matter oxidation, Cu-mineralization and trace element geochemistry, Nonesuch Shale, Michigan, U.S.A. *Mineralogia Special Paper* **41**.

Sykes, R., and Snowdon, L., 2002, Guidelines for assessing the petroleum potential of coaly source rocks using Rock-Eval pyrolysis. *Organic Geochemistry*, **33**:12:1441-1455.

Taylor, G.H. et al., eds, 1998, Organic Petrology, Berlin, 704 p.

Teichmüller, M., 1982, Origin of the petrographic constituents of coal, *in* Stach's Textbook of Coal Petrology. (Stach et al., eds.), Gebruder-Bortraeger, Berlin, p.219-294.

Tissot, B.P., and Welte, D.H., 1984, Petroleum Formation and Occurrence. Springer: New York, 699 p.

U.S. Environmental Protection Agency, 1992, Mine Site Visit: Copper Range Company White Pine Mine, from: http://www3.epa.gov/epawaste/nonhaz/industrial/special/mining/techdocs/copper/copper4.pdf.

Uchytil, S.J., Jarvie, D.M., and Steffenson, C.K., 1997, Hydrocarbon prospectiveness of the Middle Proterozoic Nonesuch Formation in northern Wisconsin and Michigan, Wisconsin Geologic and Natural History Survey, 13 p.

Van Schmus, W., 1992, Tectonic setting of the midcontinent rift system. *Tectonophysics*, **213**:1-15.

Vaughn, D.J., Sweeney, M., Diedel, G.F., and Haranczyk, C., 1989, The Kupferschiefer: An overview with an appraisal of different types of mineralization. *Economic Geology*, **84**: 1003-1027.

Waples, D.W., and Curiale, J.A., 1999, Oil-oil and oil-source rock correlations, *in* Beaumount, E.A., and N.H. Foster, eds., *Exploring for oil and gas traps,* American Association of Petroleum Geologists, Tulsa, OK, p. 8-1 to 8-71.

White, W.S., and Wright, J.C., 1966, Sulfide mineral zoning in the basal Nonesuch Shale, northern Michigan. *Economic Geology*, **61**:1171-1190.

White, W.S., and Wright, J.C., 1955, The White Pine copper deposit, Ontonagon County, Michigan. *Economic Geology,* **49**:675-716.

White, W.S., 1971, A paleohydrologic model for the mineralization of the White Pine copper deposit: northern Michigan. *Economic Geology*, **66**:1-13.

White, W.S., 1960, The White Pine copper deposit. *Economic Geology*, **55**:402-410.

Yawanarajah, S., and Kruge, M., 1994, Lacustrine shales and oil shales from Stellarton Basin, Nova Scotia, Canada: Organofacies variations and use of polyaromatic hydrocarbons as maturity indicators. *Organic Geochemistry,* **21**: 153-170.

## *Appendix A: Sample Descriptions, Photomicrographs and Hand Sample Images*

### *White Pine Basin Core WPB1*

**WPB1-5,** 100.1 m above base

Finely interlaminated OM-rich layers, shale, wavy and crudely interlaminated with m.g. siltstone. Individual laminae are very thin and largely continuous across core, though discontinuous laminae are present (40%), lenticular. Lamina-sets of dominantly (over 75%) darker material vs dominantly lighter material are 5-10 mm thick - varve-like geometry. Darker, gray-black, thin (under.5 mm thick) wavier (concave up and down in small amplitude, 5 mm alternations) laminations of clay-size fraction OM particles present. Calcareous cement in light grayish white siltstone laminae - calcareous cemented light gray silty laminae encase dark gray finer silty lenticular lams in places, with sharp, irregular contact. Wispy to wavy discontinuous OM-rich laminae may be ripples; 35% shale, 65% silt. No ore present. Organic matter is amorphous and presents as orange (TAI = 2.6) groundmass associated with lowest-energy sectors of normal graded bedding, commonly associated with pyrite concentrations. Pyrite is sub- to euhedral and commonly about 5 microns but agglomerations approaching maximum dimension of 50 microns are also present. Two anastomosing whitish gray calcareous cemented fine silty laminae near the top of the sample sampled for stable isotopes. This is the cross-stratified gray siltstone of Figure 8. Darker laminae are composed of clay, mica, pyrite and OM. The opaque appearance of the darker layers is due in part to the presence of small spherical framboids of pyrite that are 10-20 microns diameter and concentrated in OM rich laminations. Light colored laminae are composed primarily of quartz silt.

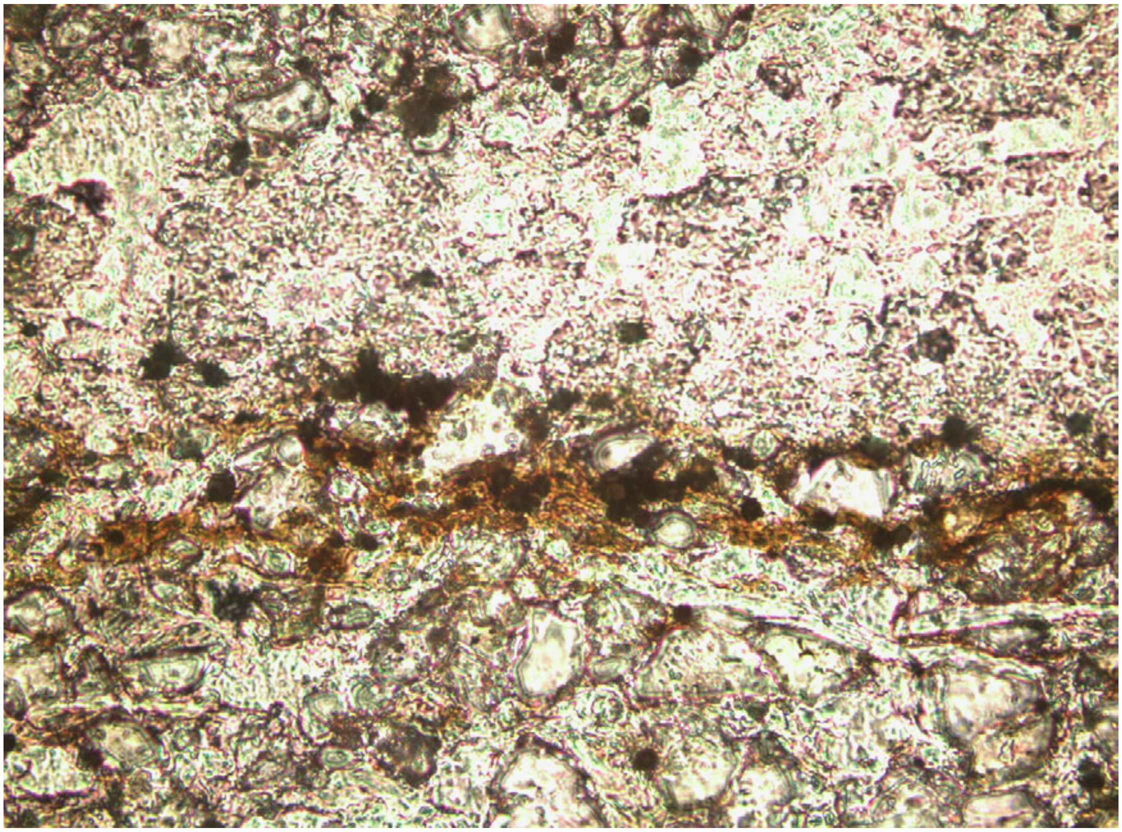

Figure A1: Transmitted light view of orange AOM with pyrite subhedra in association. Field of view is 350 microns wide. Sample WPB1-5.

Figure A2: Halved core sample of laminated shaly siltstone with mm scale at bottom. Light colored laminae are composed primarily of quartz silt. Darker laminae are composed of clay, mica, pyrite and OM. The opaque appearance of the darker layers is due in part to the presence of small spherical framboids of pyrite that are 10-20 microns diameter and concentrated in OM rich laminations. Sample WPB1-5.

**WPB1-7,** 49.9 m above base

Massive to crudely thinly laminated dark greenish-gray micaceous siltstone, coarse-grained with rare dark gray to gray-brown shale laminae. Sample is 85% silt/sand, 15% shale. Rare distinct bedding is apparent as 2 mm-wide darker, finer-grained wispy parallel to discordant, sub-parallel laminae, potentially representing penecontemporaneous deformation or intraformational rip-ups. Blotchy calcareous cemented, and with significant vein calcite in fracture at 45 degrees to bedding in hand sample. No Cu minerals or OM present in thin section. Hematite-coated quartz grains, subangular, present (about 1%). Brown blotchy exterior on cut surfaces of core, possibly surficial oxidation? This is the interbedded siltstone, gray to red-brown, of Figure 7.

Figure A3: Wet sediment deformed greenish gray micaceous siltstone, mm scale at R. Sample WPB1-7.

**WPB1-6,** 13.7 m above base

Homogenous pyritic silty mudstone, massive to very thinly laminated with most laminae lenticular and under 2mm wide. Multiple 1 cm thick concentrations of very thinly laminated grayish-black shale alternate with coarse gray siltstone. Black laminae are more continuous and parallel - despite the discontinuous presentation as in photo. Also present are thicker, fine-grained brownish gray laminae (to 2 cm); these are more laterally continuous and showing both irregular anastomosing and near-parallel forms. Pinkish white to transparent calcite/hematite filled fractures crosscut and offset bedding at 60°, sampled for stable isotopes. Isolated silt-rich pinkish-white calcite blebs (under 1 mm diameter) and some rare thin (sub 1 mm thick), laterally discontinuous subhorizontal calcite filled fractures. Discordant interlaminae present on bed-parallel end of sample, darker gray shale fragments to 3 mm, potentially rip-up clasts. Content: 85% silt, 15% shale overall. Thin section is massive, without OM-rich laminae; FOM present to 130 x 10 microns, black (TAI = 3.9), opaque, isotropic and showing higher reflectivity than AOM of WPB1-5. No Cu minerals in thin section (pyritic only), but assayed 0.01 wt. % Cu. This is the Thinly Bed of WP nomenclature (Figure 6).

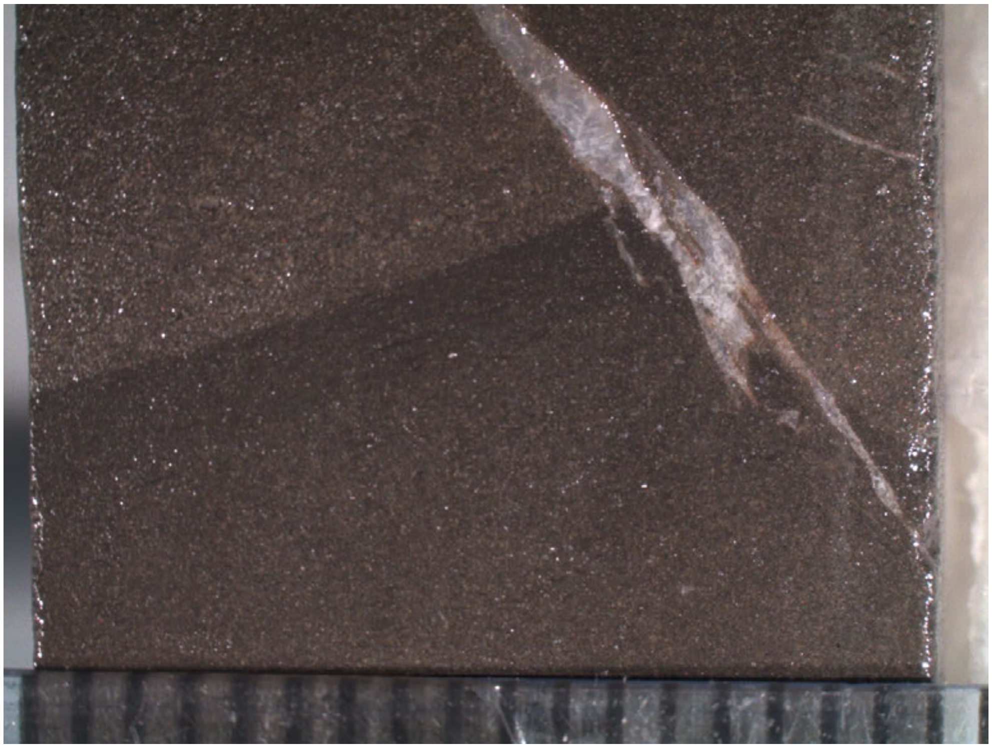

Figure A4: Hematitic calcite vein truncating/offsetting thick lamination, mm scale at bottom. Sample WPB1-6.

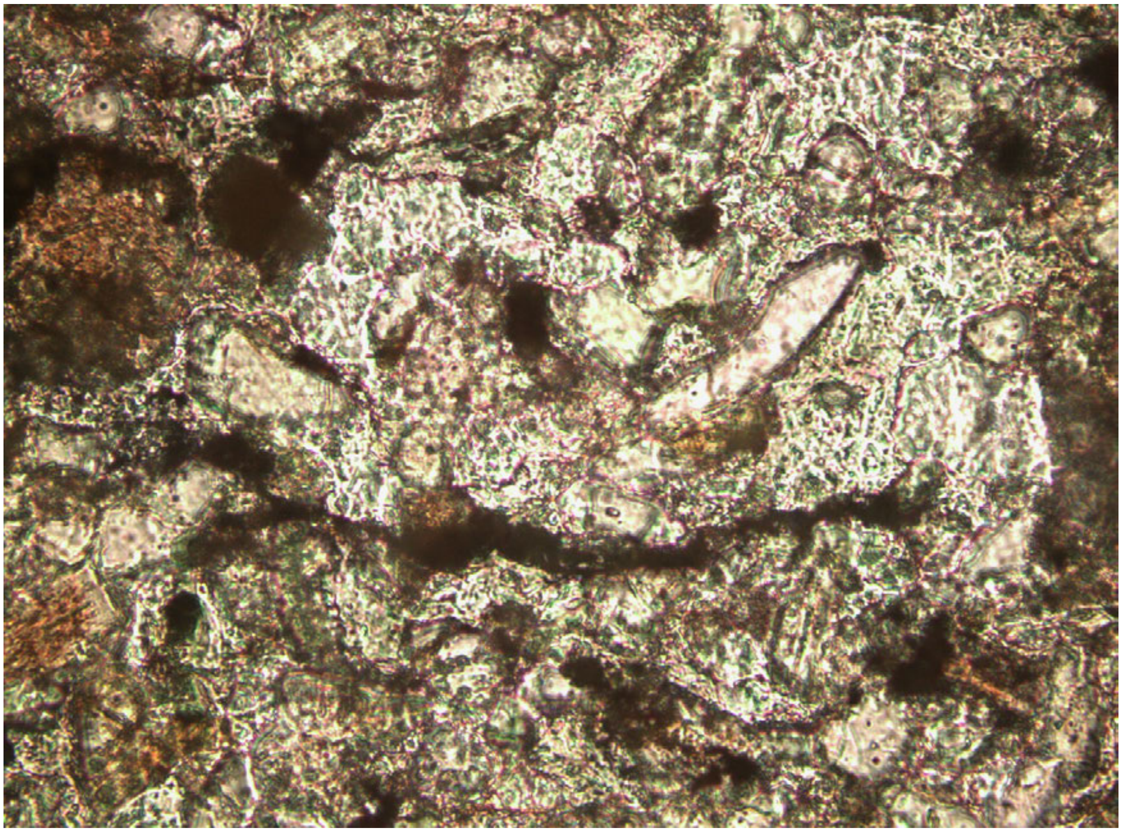

Figure A5: Filamentous OM in transmitted PPL, showing as opaque black wavy laminar material. Sample WPB1-6.

**WPB1-4**, 2.7 m above base

Light reddish-gray, blotchy coloration, coarse grained, massive siltstone, well-sorted and with very rare, faintly visible thin laminae of darker and finer-grained silt particles. Lamination is not ubiquitous and not observed in lighter areas, which appear massive. Calcite cement throughout. Pyritic with significant hematite (1% overall) and no Cu minerals aside from a lone very fine subhedral chalcopyrite grain; hematite is present both as quartz coatings (translucent) and as nearly opaque black to red, marginally translucent agglomerations. Sample is 100% siltstone. No OM apparent in thin section. Dark Gray Massive of Figure 6.

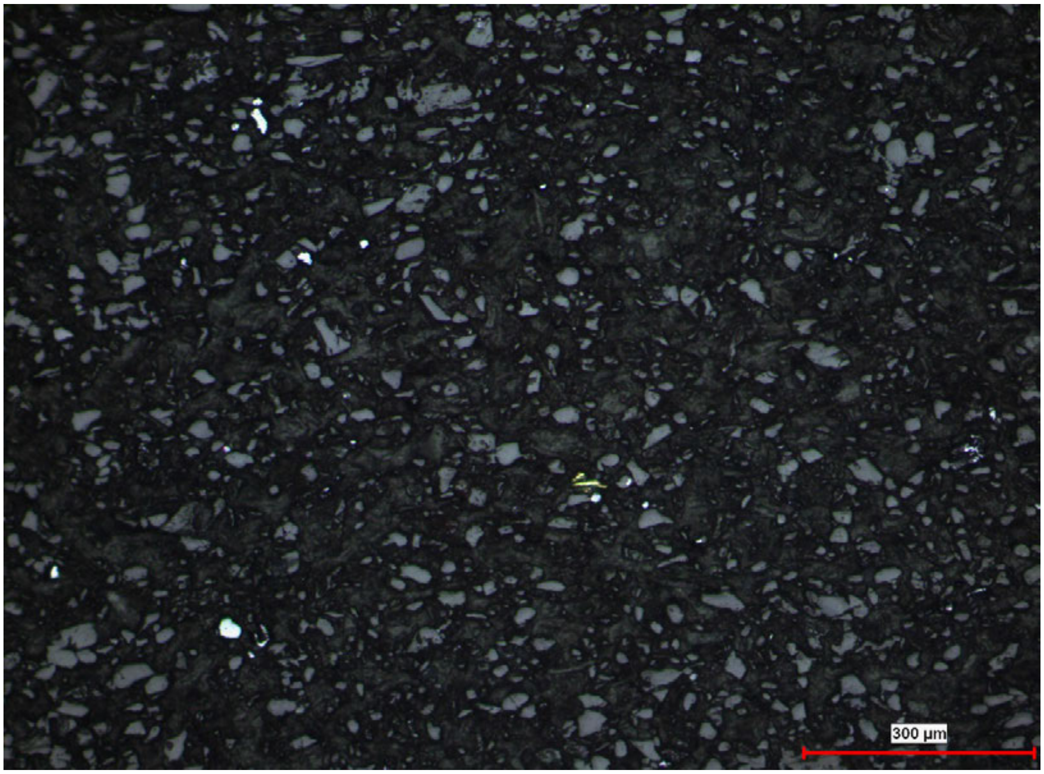

Figure A6: Lone chalcopyrite grain in sample WPB1-4, PPL REFL.

### *Core 517*

**517-1**, 206.7 m above base

Thin to very thin laminae in laminasets of OM-rich black, clay-size fraction layers alternating with grayish-white coarse siltstone layers. Grayish-black shale, variably continuous to sub-2 mm wide, in laminasets to 5 mm thick, wavy and parallel to wavy discontinuous laminated, between light grayish white coarse grained siltstone. Variable calcite content, with some lighter-color laminae very calcite-rich but others less so; calcite cement is not disseminated throughout. Convex down patterning in bases of light laminae, and some anastomosing/possibly folded dark, OM-rich black lams. No Cu minerals, and 49% silt, 51% shale. Amorphous OM presents as orange brown (TAI = 2.7) wavy lamellar masses of discontinuous OM-rich laminae, which are similar in appearance to lamalginite (some of this material is significantly darker, with TAI = 3.7 dark brown in places). The wavy discontinuous nature of the OM-rich laminations and their contortion about the larger-grained siltstone laminations at least in places evidence compactional deformation, as load structures. Hand sample shows thickly striped appearance (approximately 5 mm thick alternate light whitish gray banding = very thin lamina composite bedsets). Stable isotope sampled from 15% $CaCO_3$ cement in lighter gray laminae. Gray laminated siltstone of Figure 8, with pseudo-boudins of gray silt nearly encased in gray-black OM-rich laminae. Thin section shows FOM (opaque and black, TAI = 3.9) in close association with AOM (TAI = 2.6, orange) and v.f.g. phyllosilicate agglomerations, all of which in places show contorted bedding, but are elsewhere concordant with lamination.

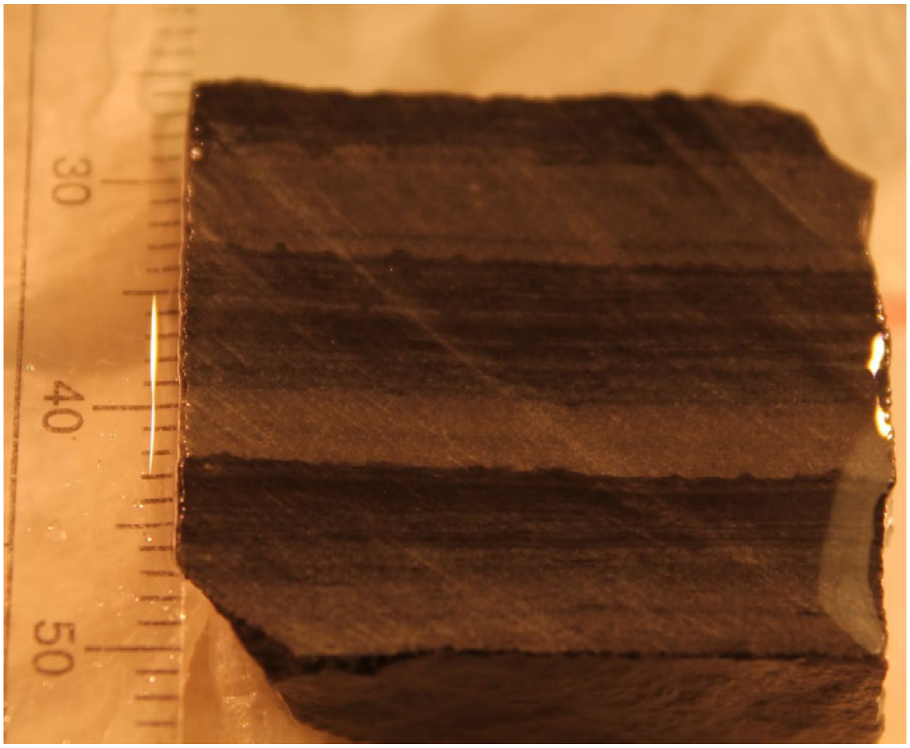

Figure A7: Hand sample showing laminasets with lode structures; mm scale at L. Sample 517-1.

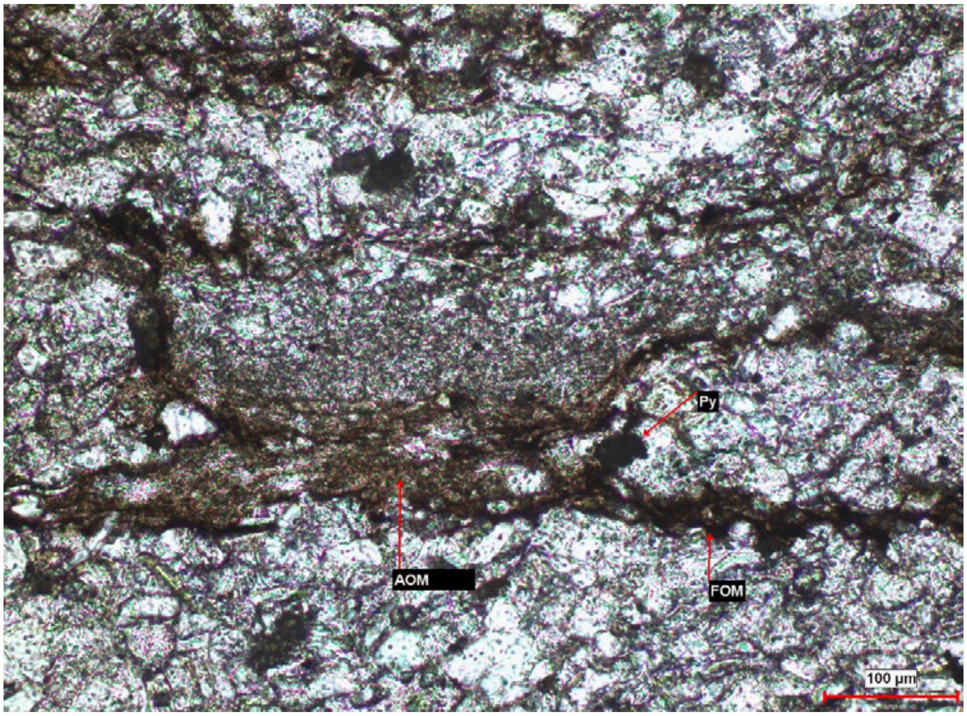

Figure A8: PPL lode structure - clay-rich lamination distorted by greater competence of silty quartz-rich laminae during compaction. The AOM is intimately associated with sub 2 micron clay mineral accumulations and pyrite. Sample 517-1.

**517-3**, 22.1 m above base

Black laminated siltstone and shale of WP nomenclature. Very very thin, alternate, gradationally-bounded, laminae of dark gray (f.g. silt/shale) to gray c.g. siltstone, with lighter layers commonly calcite-cemented. Laminae are wavy to gently undulating, often lenticular and less than 1 mm wide; 90% f.g. silt/shale, 10% m.g. silt. No Cu minerals in thin section. Bronze-gray sub 1 mm wide bedding aligned lenticular agglomerations of phyllosilicates apparent in hand sample. Translucent isotropic lamellar reddish brown AOM (TAI = 2.9) present as dispersed matrix in irregular mica-rich laminations with associated v.f.g. pyrite subhedra. No lamellar black opaque OM present.

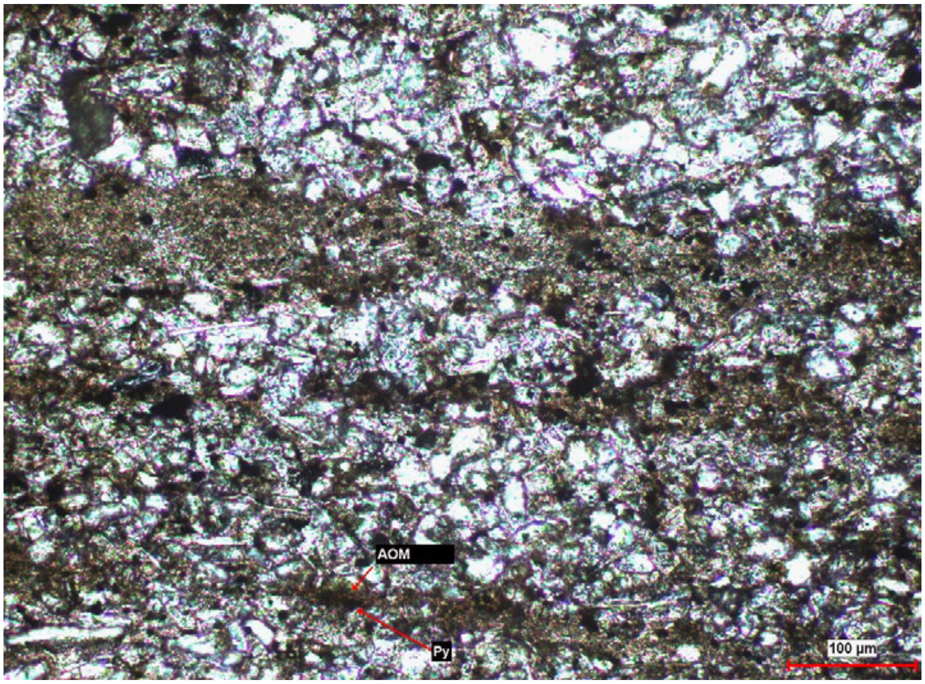

Figure A9: Thin section showing AOM and phyllosilicate-rich discontinuous laminations, with associated v.f.g. pyrite subhedra. Sample 517-3.

**517-2.5**, 19.5 m above base

Dark gray laminated siltstone of Figure 7. Very thin, continuous and parallel laminae in alternate dark gray fine grained siltstone/shale and lighter gray coarse-grained siltstone, both micaceous. Some laminae undulate, with darker gray staying similar thickness and lighter gray changing thickness - ripple laminations. Calcite cements lighter colored layers. Subhorizontal fracture-fill calcite present at base of core sample. Shows 50% f.g. silt/shale, 50% m.g and c.g. silt with 0% Cu assay. No Cu minerals; widespread pyrite, some framboidal. Widespread allogenic chlorite coating quartz grains. Significant amounts (but under 1% total area) of translucent isotropic amorphous orange brown OM (TAI = 2.8) present in lenticular, discontinuous slightly wavy clay-rich shale laminae.

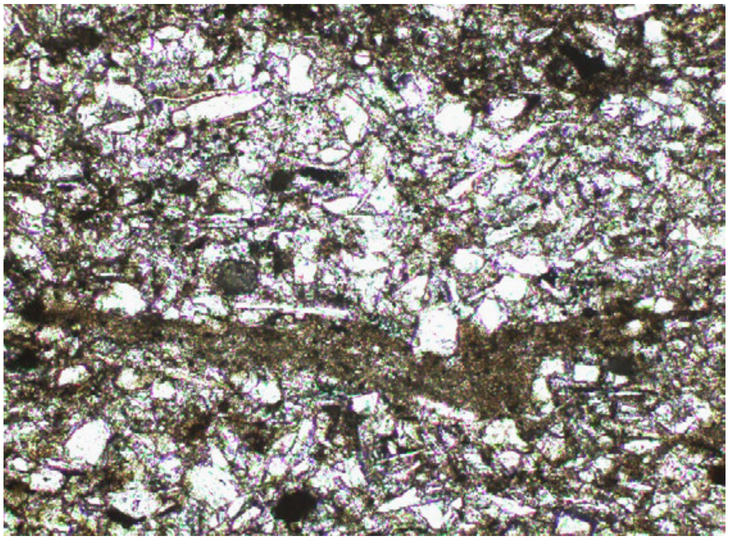

Figure A10: Orange brown AOM in PPL, concentrated in shale-size clay-rich discontinuous wavy laminations. Field of view is 0.6 mm wide, sample 517-2.5.

**517-4**, 11.1 m above base

Widely Bed of Figure 6. Massive gray-green siltstone and lighter gray siltstone, with rare thin discontinuous laminae, trough-shaped. Micaceous and bearing uneven subhorizontal (concave up/down on a 4 cm wavelength, 5 mm amplitude) calcite-filled fractures. Some (under 25% total) calcite cemented zones. One lone very thin, planar and parallel black opaque OM-rich shale layer, with irregularities, likely either rip-up clasts or folded laminae. Contains 90% m.g. silt, 10% shale and 0% Cu by assay. No Cu minerals. Significant hematite coating grains present, anisotropic. Filament of 100 x 10 micron opaque black (3.9 TAI) OM present, slightly undulating and proximal to pyrite agglomeration of similar dimension (130 x 30 microns).

Figure A11: Massive gray-green siltstone with rare continuous gradational-bounded OM-rich shale laminations, dark gray; 517-4.

**517-1.5**, 9.8 m above base

Brown Massive of Figure 6. Dark grayish-green massively bedded coarse-grained micaceous siltstone. No calcite matrix cement. Bedding sub-parallel fracture with calcite cement and brecciated siltstone suspended in neomineral cement. 90% silt/Ss, 10% shale. Assayed 0% Cu, no Cu mins in thin section; pyrite is common as single subhedral grains. Massive texture, with common allogenic hematite and chlorite coated quartz grains, subangular. In thin section, one single opaque black (TAI = 3.9) wisp of FOM, with associated concentration of clay-size fraction phyllosilicates and possibly reddish-brown AOM (TAI = 3.0), is distinct from adjacent pyrite. The hand sample contains a 2 mm wide wisp of black probable opaque FOM agglomerated concordant to massive bedding. Significant hematite present (0.5% total grains).

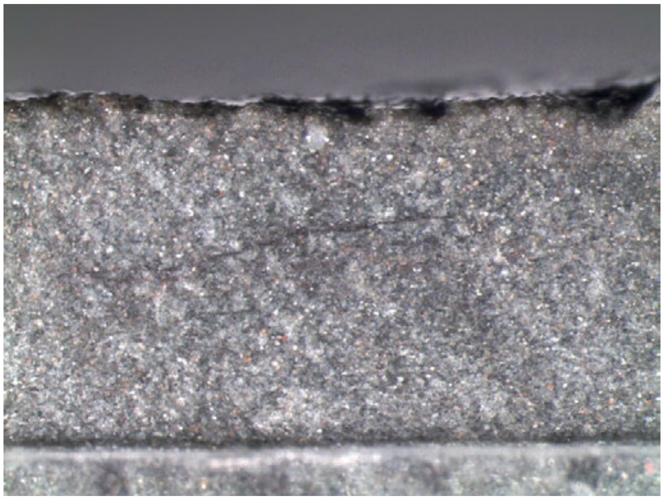

Figure A12: Carbonaceous wisp at 32x, FOM rip-up suggestive of possible algal mat origin (mm scale at bottom); 517-1.5.

**517-2,** 4.8 m above base

Upper Sandstone of Figure 6. Massive light gray siltstone (85%) with 1 mm thick continuous and discontinuous (lenticular) whitish laminae (even, parallel; no grain size change visible). Lighter layers are strongly calcite-cemented and show pinkish tint (hematite or kspar?). Significant oxidized iron stain on exterior of core - oxidized pyrite? 80% f.g. silt, 30% c.g. silt. Whitest lams have calcite cement (up to 40% locally) and few to no phyllosilicates. Collected 23 mg stable isotope sample from horizontal whitish gray to pinkish gray laminations, discontinuous. Sample comes from the middle of a fining-upward sequence and assayed 0.09% Cu. No Cu minerals in thin section. Strongly pyritiferous throughout, subhedral. Organic matter is randomly distributed throughout as isolated bed parallel masses of orange brown (TAI = 2.8). Hematite present as red incomplete coatings on anisotropic quartz grains.

**517-5**, 3.2 m above base

Red Massive unit of Figure 6. Brownish-gray massive coarse-grained siltstone with very thin dark gray shale laminae, (undulating lenticular, f.g. silt or shale) in laminasets (under 3 mm) between and with hematite-coated quartz-rich bronzy-reddish brown massive fine-grained thicker laminae. Coarser layers appear are more gray in color and finer laminae show reddish gray color. Non-calcareous. 65% silt, 35% shale. 0.06% Cu assay, no Cu minerals in thin section. Organic matter, if indeed present, is as reddish brown (TAI = 3.0) AOM matrix of rare clay-fraction dominant phyllosilicate-rich thin laminations. Black opaque FOM present in association with pyrite and AOM.

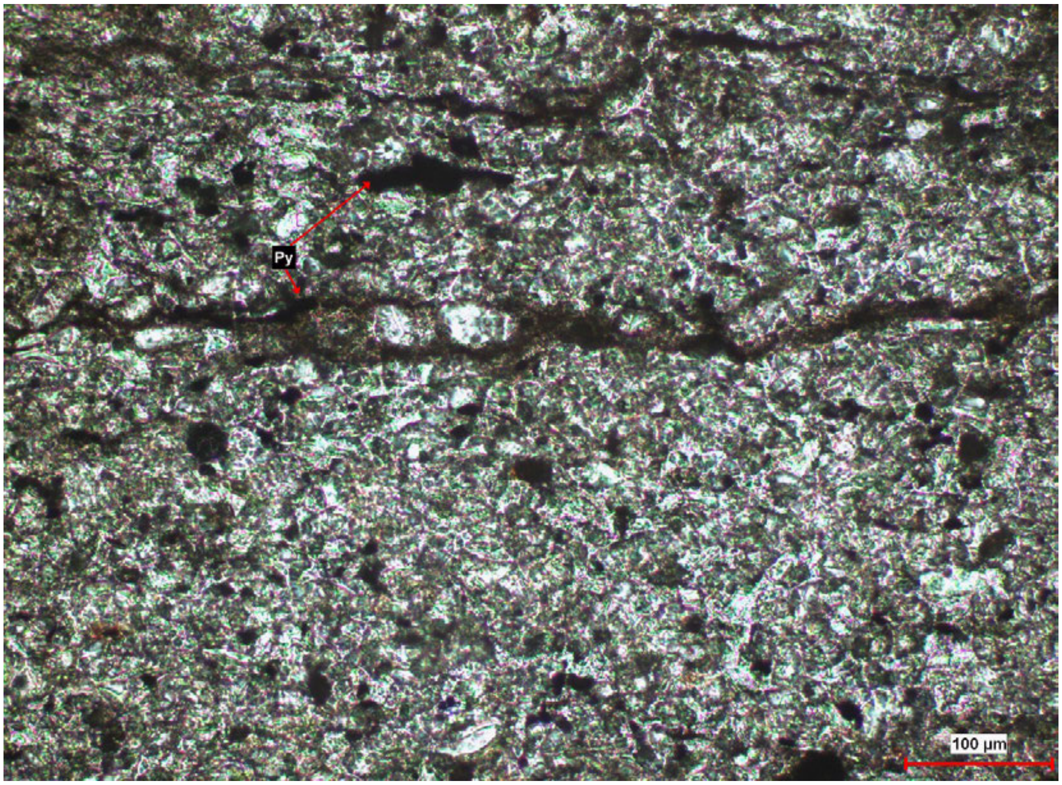

Figure A13: PPL of very thin, discontinuous shale laminations in massive siltstone, pyritic with FOM and reddish brown AOM in association. Sample 517-5.

**517-6**, 0.5 m above base

Sandy siltstone; gray-green crudely laminated micaceous sandy siltstone, non-calcareous with v.f.g. pyrite present in finer-grained green-gray laminae. Oxidation on grain surface as brown staining. Laminae are gently undulating in form and sometimes anastomose (contorted bedding juxtaposing coarse subangular micaceous quartz siltstone against finer-grained darker gray laminae, some overturned finer laminae observed). 60% silt, 40% shale. 1.88% Cu assay, but only very rare isolated v.f.g. subhedral chalcocite present in thin section, associated with mottled yellow-reflecting tarnish, possibly pyrobitumen. Organic matter is black opaque (TAI = 3.9) FOM, with faint hints of slightly translucent brown (TAI = 3.2) AOM, and concentrated in distorted very thin siltstone laminae; some AOM /FOM in association present near base of overground void. Domino Bed of WP nomenclature, as in Figure 6.

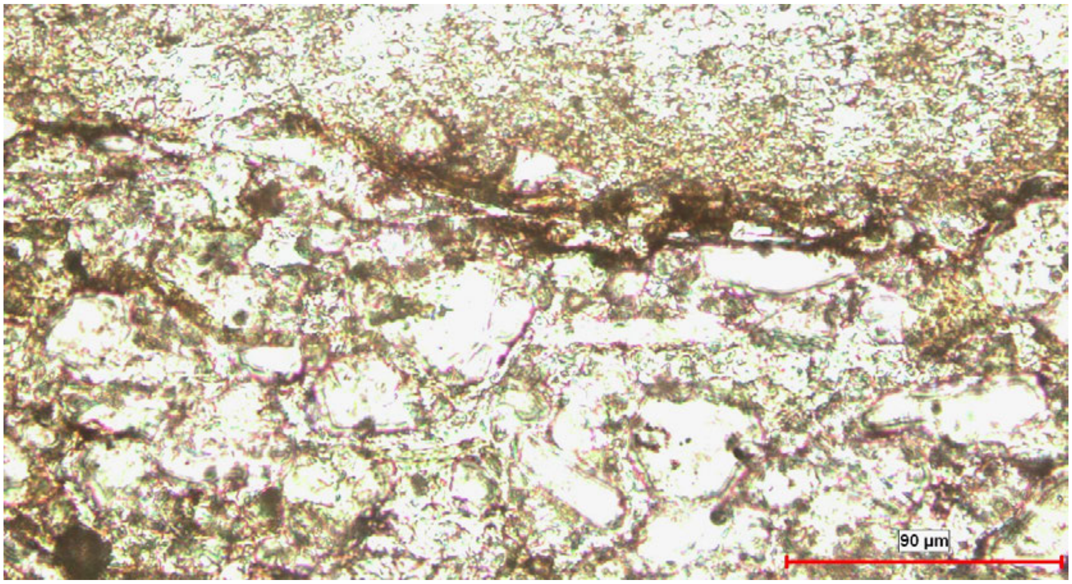

Figure A14: Brown AOM, slightly translucent (TAI = 3.2), concentrated at base of thin even parallel lamination of missing (overground) probable shale; AOM shows clay association and bounds FOM (black, opaque, TAI = 3.9). Sample 517-6.

Figure A15: Hand sample showing brown clay-rich layers. Field of view is 5 cm wide. Sample 517-6.

*Core 523*

**523-8**, 157.1 m above base

Dominantly massive, coarse-grained siltstone, green-gray, well-sorted. Massive siltstone shows sharp to gradational contacts with darker, continuous interlaminae. Such reddish-brown clay to fine silt laminae (sub-1 mm thick) are generally horizontal and sub-parallel, but undulating, convex-up, convex-down geometries exist; ripple marks and rip-up clasts of reddish, hematite-coated quart rich material are present. Isolated, minute (under 4 $mm^2$) pink domains of calcite cement are present in the massive green-gray siltstone; these are more concentrated proximal to the finer, darker laminae. Oxidized pyrite shows rusty red on weathered surfaces. Sample is 15% shale, 85% f.g. and m.g. silt. Assayed 0% Cu, and no Cu minerals in thin section. Organic matter not apparent in thin section. Brownish-red laminated siltstone of Figure 8.

Figure A16: Dominantly massive siltstone with visible crossbedding and pinkish calcite cement in isolated sub mm concentrations. Scale is mm ruled, top. Sample 523-8.

**523-7**, 59.5 m above base

Parallel, mostly even but with some minor irregularities, crisp to gradational bounded, thin to thick laminae of v.c.g. green-gray siltstone and maroon/red v.f.g. siltstone. Very narrow (sub 0.5 mm) vertical calcite-filled fracture, with subhorizontal fractures joining at high angles. Calcite vein and detrital (primary) pyrite present in sample. Hematitic growths common near pyrite accumulations and calcite blebs to 1 mm diameter are present. Sample is 60% shale, 40% silt, 0% Cu by assay, with dispersed reddish brown AOM (3.0 TAI) aligned with bedding. Significant (1%) hematite present, subhedral and dispersed. Sample is from the gray and red-brown siltstone of Figure 7.

**523-6**, 44.3 m above base

Sample is gray massive siltstone with oxidized subhedral f.g. pyrite. Sample shows sharp transition from massive reddish-gray v.f.g. silt/shale to massive dark gray v.f.g sandstone. Rare very thin blackish-gray discontinuous and wispy laminae also present. Massive dark gray sandstone grades back to v.f.g. reddish-gray siltstone/shale at base. Sample shows some interlamination in thin gradational wavy parallel to even parallel laminations. Transition shows undulating contact - in places the lower sandstone protrudes up into siltstone and "overhangs" siltstone (more gradational transition here). No OM apparent in thin section. Chalcopyrite present as rare, isolated v.f.g. subhedra, and pyrite dominates sulfides.

**523-4**, 21.3 m above base

Dark gray massive to thinly laminated (laterally discontinuous) laminae of finer-grained black sediment intercalated with gray v.f.g. sandstone. Sample contains multiple 4mm wide, very thin lenticular but mostly parallel and slightly undulating whiter-gray silt laminae. Some of the black laminae anastomose and inosculate. Two subhorizontal calcite veins/fractures (under 1 mm thick). Chalcopyrite is nearly ubiquitous as f.g. replacements of rounded subhedra pyrite and pyrite framboids. One laterally continuous fracture showing void space. Oxidized pyrites (sub-0.5 mm maximum dimension) present on exterior of core. Calcite cement present in lighter colored laminae. Sample is 65% shale, 35% silt/v.f.g. Ss. Isotropic, lamellar translucent orange-brown (TAI = 2.7) AOM accumulations interspersed with very fine phyllosilicates in lowest-energy, finest-grained laminae, and associated with pyrite. Filamentous OM, wavy and discontinuous with sulfide association, present (TAI = 3.9). Assayed 0% Cu, although chalcopyrite is apparent as very fine-grained subhedral masses in association with opaque FOM. Galaxy Bed of WP terminology, as in Figure 8.

Figure A17: Hand sample with mm scale, of chalcopyritic dark gray thinly wavy discontinuous laminated shaly siltstone. Sample 523-4.

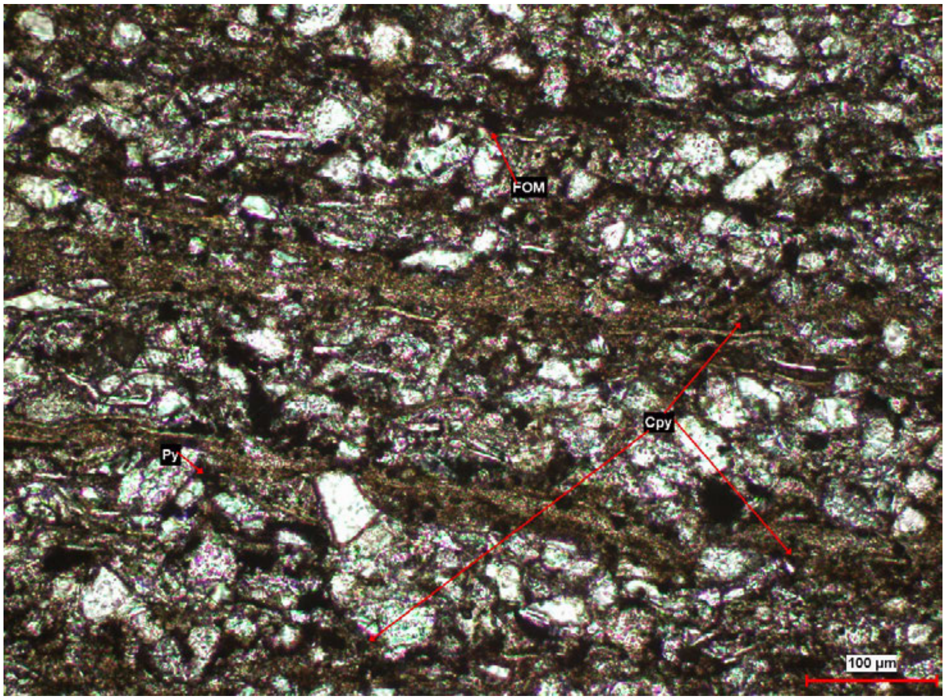

Figure A18: PPL of black FOM, with orange brown AOM, wavy and discontinuous with sulfide association (both pyrite and chalcopyrite). Sample 523-4.

**523-1**, 17.3 m above base

Sample is dark gray to very light gray very thinly laminated siltstone and darker gray-black shale laminae. Laminations are very thin, subhorizontal, even parallel to wavy, and commonly distorted by concretionary calcite. Numerous calcite concretions, some subhedral (up to 0.1 by

0.8 cm but mostly 0.5 mm max dim.), some having a greenish cast with few to no suspended detrital inclusions. Concretions locally disturb bedding, contorting dark layers concentrically or in lenticular bulges about concretions, large and small. This sample has the most intense calcite cement of the suite. Sampled 7 mg of the calcareous concretionary blebs sub-parallel to bedding (not from the too-thin to sample calcareous fracture at 60° to bedding). Some concretions are semispherical or at least circular, while most are elongate parallel to bedding. Sample assayed 0% Cu but shows chalcopyrite in association with calcite concretions and AOM in thin section. Organic matter is lightly translucent, laminar agglomerations, amorphous, orange brown (TAI = 2.7), associated with concentrations of pyrite; ovoid sub-10 mm darker orange constituents apparent in some discrete AOM grains. A strong association of lamellar OM to margins of clay-rich shale interlaminations is apparent. This is the Marker Bed of WP terminology, as in Figure 6. Sample contains 65% shale, 35% silt. Figure A19: Hand sample with mm scale at L of calcareous concretions distorting but concordant with silt and shale laminae. Figure A20, A21: Framboid and subhedra (f.g.) of pyrite, AOM, and calcite concretion disruption of thin laminae, PPL and REFL 100X.

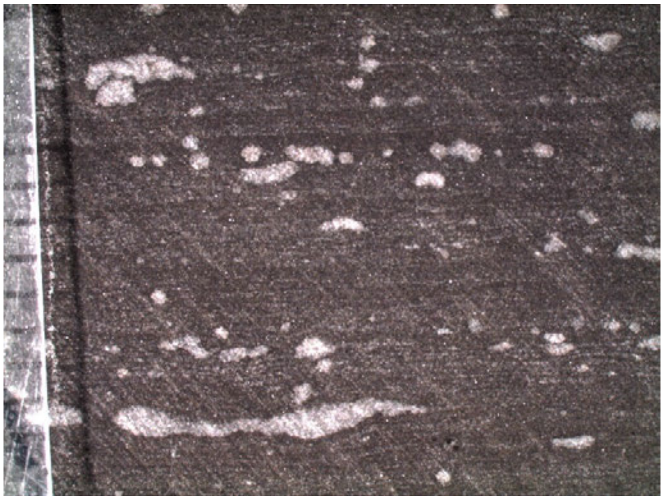

Figure A19: Hand sample with mm scale at L of calcareous concretions distorting but concordant with silt and shale laminae. Sample 523-1.

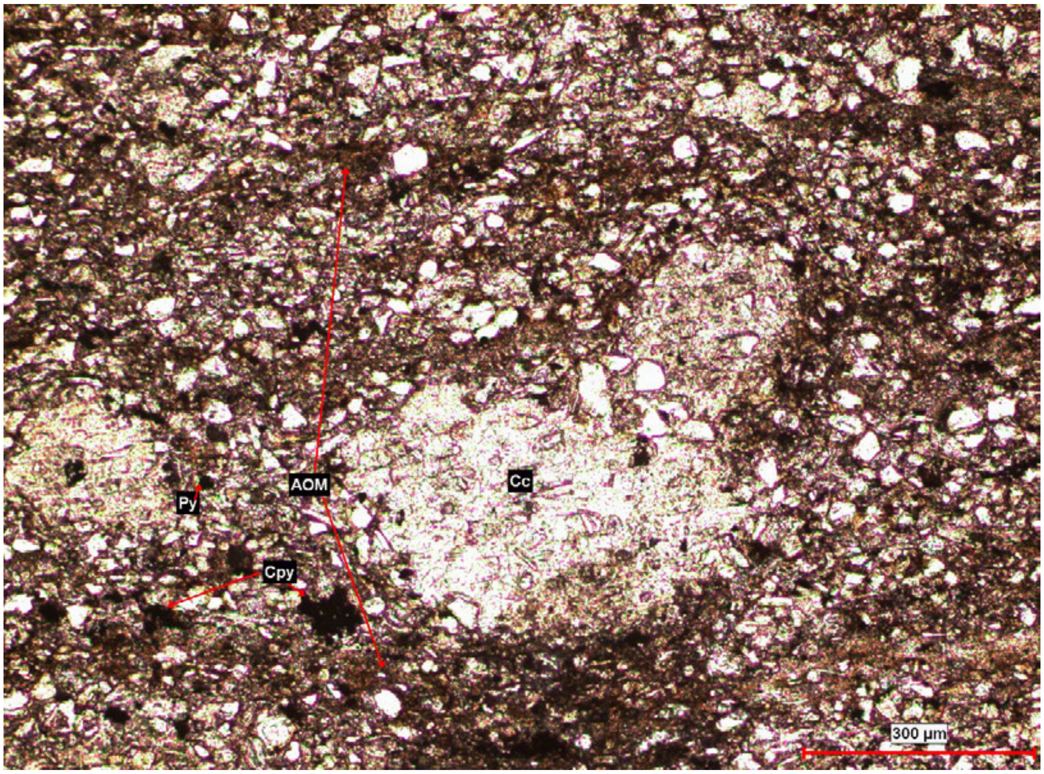

Figure A20: Pyrite, AOM, and calcite concretion disruption of thin laminae, PPL. Note chalcopyrite replacement of framboidal pyrite. Sample 523-1.

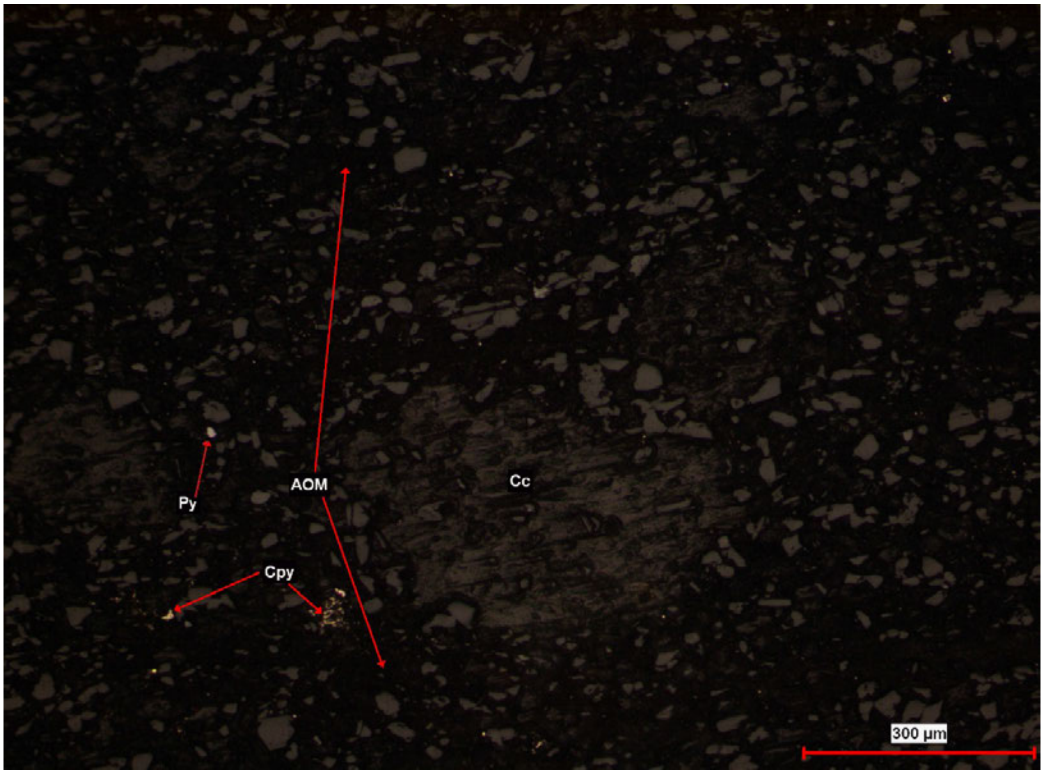

Figure A21: Pyrite, AOM, and calcite concretion disruption of thin laminae, REFL PPL. Note chalcopyrite replacement of framboidal pyrite. Sample 523-1.

**523-3**, 15.9 m above base

Sample is a dark gray shaley siltstone with very thin bronzy-gray shale laminae between dark-gray f.g. silt laminae and v.c.g. siltstone/v.f.g. qtzose sandstone laminae (high calcite, white to gray-white). Bronzy-gray shale and dark gray silt lams are sometimes irregular, wavy and anastomose, while white/gray-white c.g. silt/f.g. Silty layers are often lenticular/pseudo-boudinaged; even parallel lamination dominates overall. Bronzy-gray shale makes up 20%, dark gray silt is 45%, v.c.g. silt/v.f.g. sand is 35%. Sample assayed 0% but no Cu minerals in thin section. Amorphous reddish-brown (TAI = 3.0) faintly translucent OM concentrated in finest-grained layers and commonly intimately associated with pyrite, as bedding parallel aggregations. Black opaque FOM-rich continuous lamination present isotropic (TAI = 3.9) opaque laminae are closely associated with pyrite. The darker OM-rich laminae are often contorted and even when they show near parallel symmetry, silicate grains commonly distort the OM. This is the Stripey of WP terminology, as in Figure 6. Stable isotope sampled from 20% calcite content of thin silty gray laminations.

**523-2**, 3.7 m above base

Wispy black subparallel very thin laminations in dark gray siltstone at top 1 cm of core sample. Sample is mostly massive, dark gray siltstone with irregular, darker gray-black rip-up clast-rich, wispy black laminated finer silt and shale. Deformed laminae/rip-ups are largely concordant to bedding and are supported by massive quartzose siltstone. A small minority of rip-up clasts are calcite-cemented, light gray siltstone. Interformational rip-up conglomeratic siltstone are apparent, as well as a single sub 1 mm thick pink and white fracture-filling calcite zone at base (hematite). Pink and white calcite also form a 0.5 mm thick subvertical fracture-fill which offsets a sub 1 mm wide fracture of the same color and mineralogy.  Lamellar accumulations of amorphous isotropic brown (TAI = 3.2) organic matter wavy and slightly oblique to bedding are common.  Organic-rich zones are closely associated with dark brown to black (TAI = 3.8 to 3.9) opaque FOM, AOM and pyrite concentrations.  Sample assayed 0.98% Cu and incipient chalcocite replacement present on pyrite subhedra (anisotropic yellow mottled-reflecting tarnish present).  Sample is 85% silt, 15% shale.  Stable isotope sampled from conjugate calcite veins at 45° to bedding (not in thin section).  This sample is from the Upper Transition of WP terminology, as seen in Figure 6.

Figure A22: Hand sample with mm scale, showing one of the stable isotope sampled hematitic calcite veins oblique to bedding.  Sample 523-2.

**523-5**, 1.0 m above base

Light gray-green massive siltstone hosting bronzy-gray shale (irregular lenticular lamina 2 mm thick at bottom) with numerous discontinuous, somewhat discordant wispy black laminae (often near 45° to bedding) defines this sample.  Contorted bedding hints at pre-compaction slumping and faulting or rip-up clast inclusion.  Wispy black interlaminae offset by 0.1 mm wide calcite-filled fracture (some brecciation of light gray massive siltstone).  At least 7 subhorizontal, sub 1 mm wide calcite-filled fractures, some offset by the subvertical one. Some of the subhorizontal fractures anastomose. Anhedral, unoxidized chalcocite on fresh surface, but only weak incipient chalcocite replacement of pyrite is apparent in thin section. Some cohesive faulted fragments show different, more cohesive and subparallel (but still very wavy/irregular) thin laminations of all three lithologies above. Thin section is very thin, and OM is not apparent; it consists of 15% shale, 85% silt. The sample is 0.69 wt. % Cu by assay, and is from the Domino Bed of WP terminology (Figure 6).

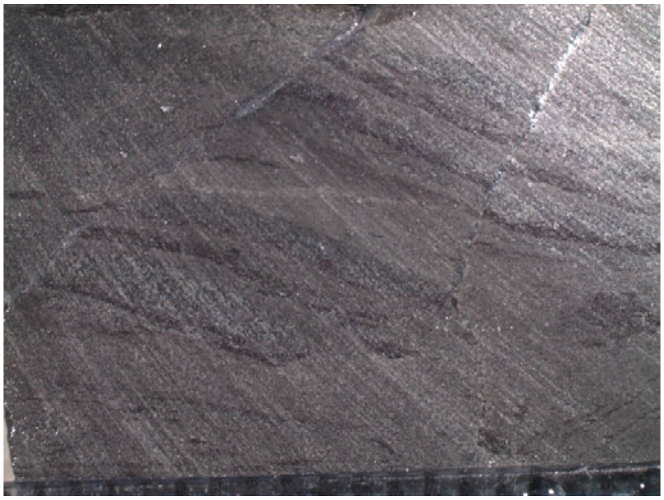

Figure A23: Fractured and faulted shaly siltstone shows folding and significant cm scale offsets. Millimeter scale at bottom. Sample 523-5.

*Core PC1*

**PC1-1**, 59.7 m above base

Sample composed of light gray very thinly to thickly laminated, c.g. siltstone laminae (with variable calcareous cement) with dark gray to grayish black shale laminae. Graded clay-silt couplet laminations, with silty material repeatedly fining upward to clay/shale in varve-like geometries dominate the sample. Laminations are wavy and parallel, continuous. Oxidized pyrite euhedra up to 0.5 mm are present. Sub 0.5 mm thick wavy/irregular black calcareous fracture w/o visible constituent grains, continuous across 2 cm width of core; (black color is discontinuous). Calcite for stable isotope analysis collected from gray silty laminae. Composition of sample is 70% silt, 30% shale and 0% Cu assay with no ore minerals present in thin section. Thin section ground away the darker, OM-rich shale laminations; no OM apparent in thin section. Minor hematite present.

**PC1-2**, 43.5 m above base

Light gray siltstone and dark gray shale laminae, both very thin, continuous across core, define this sample. Dark gray, v.f.g. silt laminae anastomose/inosculate in places, leaving lenticular light gray siltstone lams (6 mm x 0. 5mm). Darker laminae show small-amplitude wavy texture. Thin (0.5 mm thick), vuggy-centered horizontal fracture in c.g. gray siltstone bounded by brownish black f.g. siltstone lams (0.1 mm thick); f.g. brown bounding lams anastomose after 1 cm. Sample composition is 65% shale, 35% silt with 0% Cu by assay, and no Cu minerals. Lamellar bedding parallel AOM is translucent orange, associated with mica rich clay size fraction concentrations (TAI =2.7), contorting about quartz grains in laminae, and association with pyrite subhedra is common.

**PC1-3**, 10.9 m above base

Very thin, brown, lenticular to continuous and parallel shale laminae in massive gray f.g. siltstone, micaceous and massive, define this sample. Rare, faint light gray zones apparent, 1 mm thick and semi-continuous across core, in f.g. siltstone. Transition at end of sample is black wavy-crinkly, sub 1 mm thick semi-continuous fracture-fill or wispy lamination grading through gray f.g. siltstone to brown, f.g. siltstone/shale. Quartz grains with hematite coating common, as are pyritic accumulations with intimate-associated hematite coats on quartz. Sample is non-calcareous throughout, and 75% m.g. silt, 25% shale. 0.03% Cu assay, no Cu minerals in thin section. Thin section is massive and no OM is apparent. This is the Upper Shale of WP terminology, as in Figure 6.

**PC1-6**, 10.7 m above base

Sample is a brownish-red v.f.g. silt to shale sharply changing to greenish-gray c.g. silt, largely massive texture but with blotchy variegation. This specimen is mostly massive bedded c.g. silt to v.f.g. sand, subangular quartzose and micaceous. Some thin alternate laminae of both are present. Overall composition is 60% silt/sand, 40% shale/fine silt. Sample assayed 0.03% Cu, and two 0.75 mm diameter circular chalcocite agglomerations are notable, as well as near-total replacement of v.f.g. subhedral pyrite by chalcocite. Opaque black FOM (TAI = 3.9) and reddish-brown (3.1 = TAI) faintly translucent isotropic amorphous OM (up to 20 micron agglomerations) present, especially along margins of two 800-900 micron diameter circular chalcocite nodules. Circular chalcocite agglomerations are situated in line with two different semi-continuous organic-rich laminations with minor v.f.g. subhedral chalcocite along margins, as well as lesser v.f.g. covellite. Significant (0.5% total) hematite presence is apparent, mostly as grain coatings seen in thin section. This is the Brown Massive of Figure 6. Very soft Mohs scale (below 3) showing on scratch testing of the larger of two circular chalcocite OM-embedded masses, and a reddish-brown reflecting v.f.g. nonpleochroic isotropic-appearing material (hematite) dragged into scratch axis from adjacent margin of nodule. This material is also present on both parallel margins of scratch, and some has been dragged off the nodule to the distal edge - here it is opaque and appears isotropic, with bright red internal reflection.

Figure A24: Hand sample with mm scale at bottom showing 9 mm diameter chalcocite nodule and crudely laminated siltstone substrate.  Sample PC1-6.

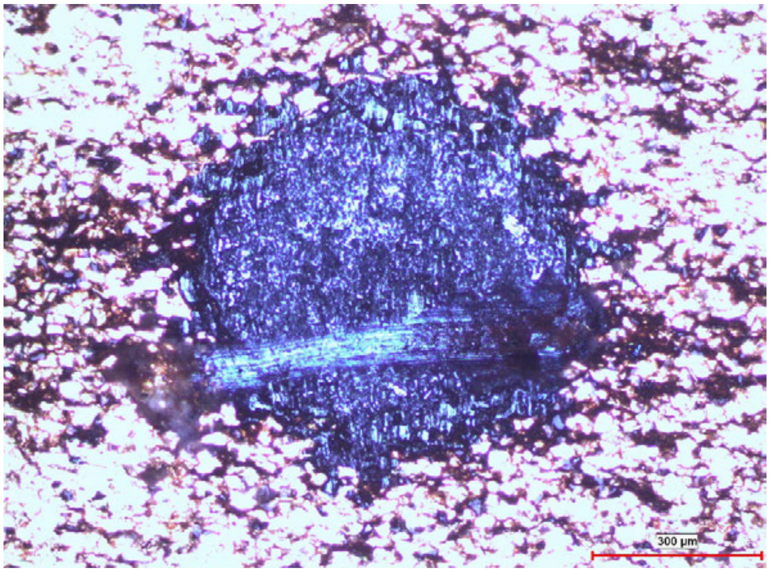

Figure A25: PPL and REFL chalcocite nodule to 0.9 mm diameter with minor v.f.g. subhedral chalcocite along margins, and v.f.g. hematite streaking into and along margins of nodule and intimately concentrated FOM and AOM.  Note bright blue covellite grain at R of nodule, just below center.  Sample PC1-6.

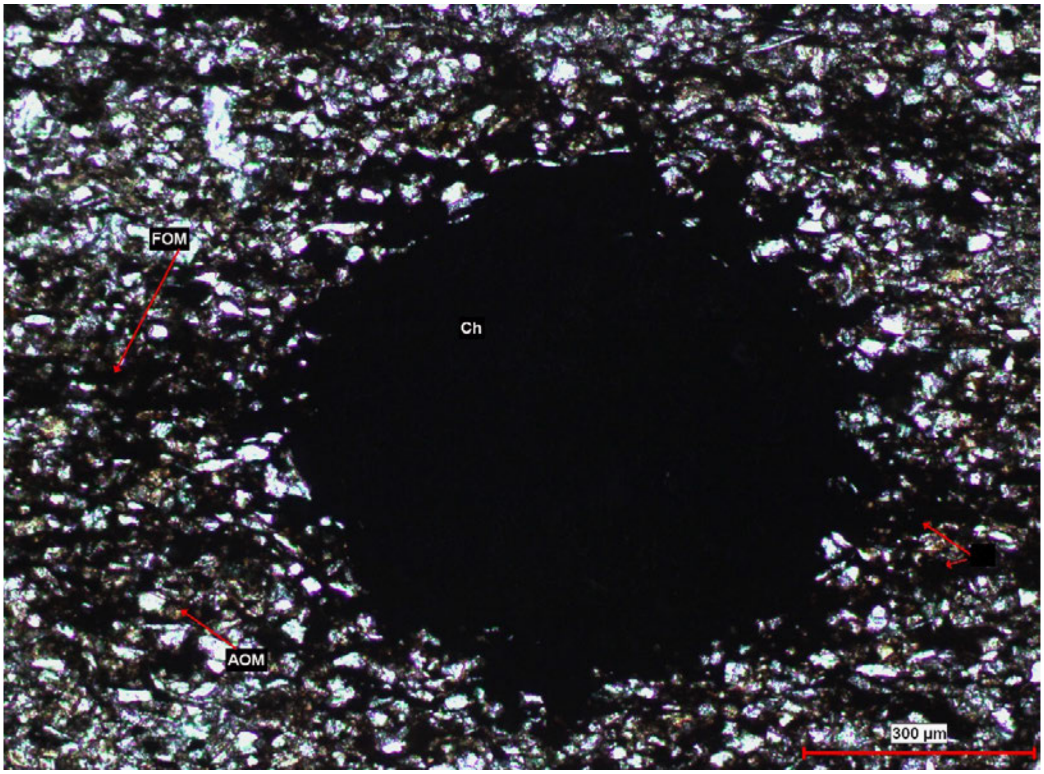

Figure A26: PPL chalcocite nodule to 0.9 mm diameter with minor v.f.g. subhedral chalcocite along margins, and v.f.g. hematite streaking into and along margins of nodule and intimately concentrated FOM and AOM. Arrows at bottom R indicate position of minor covellite. Sample PC1-6.

**PC1-4**, 10.1 m above base

This is the Brown Massive bed of Figure 6's WP terminology, and shows 0.025% Cu assay. The sample is mostly a massive gray f.g. siltstone alternating (~0.5 cm) with brownish-gray c.g. siltstone and v.f.g. sandstone, calcareous. Some rare black wispy discontinuous laminae apparent in hand sample (no grains visible, 1 mm wide x 0.1 mm thick.). Black wisps more prevalent in brownish coarser silt layers. Mostly (95%) silty nature defines the sample. Pyrite is the dominant sulfide, with very rare chalcopyrite in NE quadrant as v.f.g. sub- to euhedral grains. Several opaque black (3.9 = TAI) lamellar agglomerations of wavy discontinuous filamentous organic-rich material are present.

**PC1-5**, 2.4 m above base

As seen in Figure 6, this is the Red Massive of WP terminology, and it shows 0.17% Cu by assay. Sample is massive, reddish-brown siltstone and shale, micaceous. Rare black irregular lamination, 1 mm wide, 0.1 mm thick, exists, no grains visible; rare, darker brown round to irregular, black laminations under 1 mm wide (rip-ups?). Sample is dominantly (95+%) silt. Thin section shows AOM, translucent brown (TAI = 3.3) amorphous, with the darkest OM nearly opaque and rare, fracture-adjacent f.g. chalcocite and, minor v.f.g. covellite. Dominantly siltstone, with strong phyllosilicate concentrations associated with/mixed into AOM.

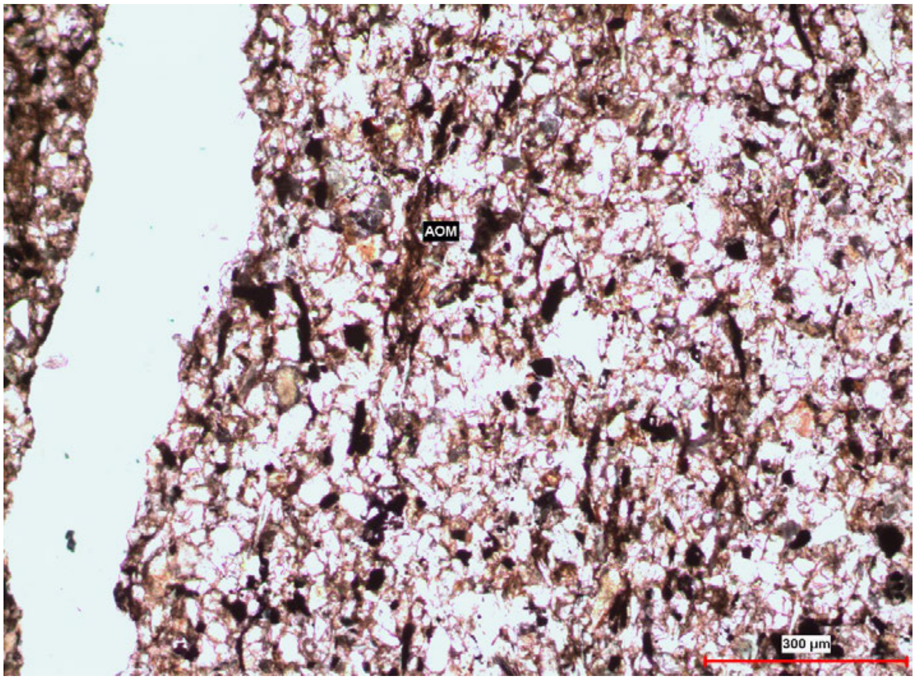

Figure A27: Amorpohous organic matter in PPL, showing opacity of chalcocite and covellite grains, as well as brown translucent AOM. Sample PC1-5.

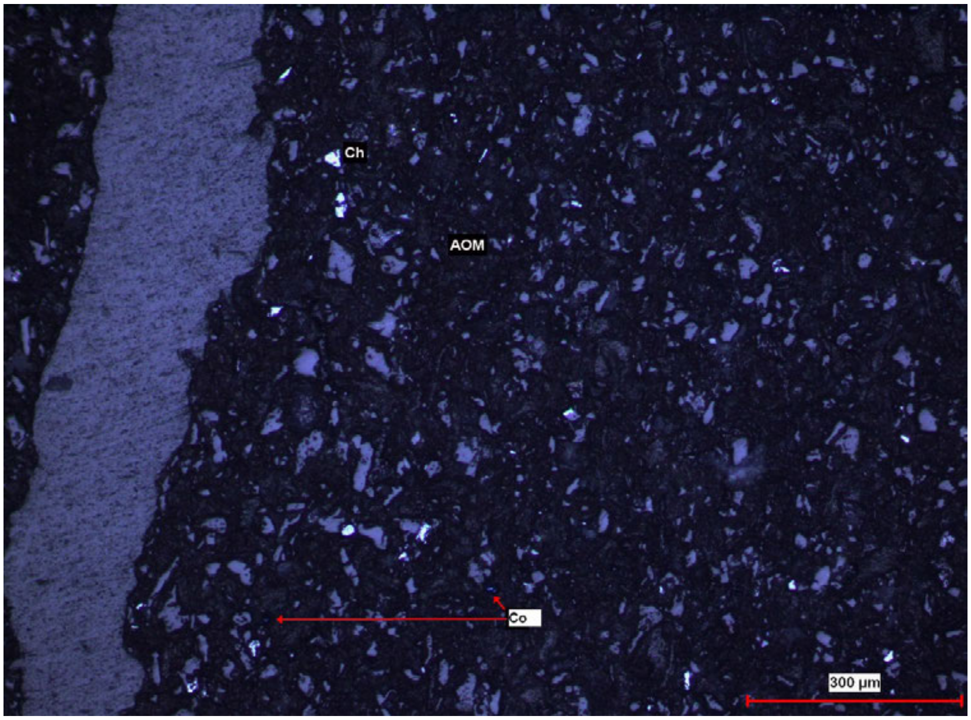

Figure A28: Covellite and chalcocite adjacent to fracture REFL PPL with AOM top center. Sample PC1-5.

*Core PC5*

**PC5-1**, 83.5 m above base

This sample is mostly gray siltstone, very thinly laminated, with very thin black, organic-rich shale laminae. Black laminations are wavy and parallel. Dark gray lams shift gradually up to light gray shale then up into gray siltstone. Non-calcareous (although vuggy fracture may represent calcite dissolution void) nature with respect to cement defines this sample, as does its composition: 80 to 95% silt, 5 to 20% shale/clay. Very f.g. oxidized sulfide is present. Majority of laminations are continuous and very thin, but the very finest - sub 0.5 mm thick - show rare, 3-4 stacked black laminations in a convex geometry, nearly or completely encasing gray lenticular silt laminations up to 3 mm wide. Very thin gray-green clay lams and very thin black laminae show some tears/discontinuities possibly indicating disruption during compaction or possibly due to vertical fluid movement. Wavy black laminations appear to have behaved more cohesively than silty layers, which form boudin-like geometries commonly 5 mm long. Pyrite framboids (to 80 microns diameter) common at silt/clay interfaces. Stable isotope sampled from gray slightly calcareous silty laminations. No Cu minerals are apparent in thin section. Organic matter is amorphous, aligned and associated with clay-rich laminations, commonly molded about quartz grains and associated with pyrite with TAI = 2.6 (orange); also present in a clay-rich lamination is a pyrite-associated brown translucent OM filament (TAI = 3.2).

**PC5-2**, 80.0 m above base

This is calcareous gray siltstone, m.g to c.g., very thinly laminated, with thin dark gray/black, laterally continuous OM-rich wavy laminae, often encasing lenticles of silt, which are less than 1mm thick; several anastomose carbonaceous laminations. Sample composition is 60%-40% silt/shale and it is pyritic, without any Cu minerals. Organic matter is amorphous, lamellar and distorted about quartz silt and smaller pyrite grains, giving a wavy black appearance associated with clay-rich zones (AOM is TAI = 2.6, FOM is TAI = 3.9). This is the black laminated siltstone of WP terminology (Figure 8).

**PC5-3**, 66.6 m above base

This sample is mainly massive, a brownish-gray siltstone made up of 95% silt/sand. Occasional calcite is present in irregular beds and blebs 1 mm to 20 mm thick, often as calcite cemented, silt bands. Organic matter is absent in thin section. No ore minerals, strictly disseminated pyrite, commonly showing hematite "smears" or haloes adjacent, coating neighboring quartz grains. This is the gray member of black laminated siltstone of Copperwood terminology (Figure 8).

**PC5-6**, 21.3 m above base

This is dark gray shale, very thinly laminated, parallel and continuous, (60%) with massive to crudely thin laminated (parallel and slightly wavy) light-gray, often lenticular c.g. siltstone and v.f.g. sandstone, calcareous. Uneven, gradational contacts are common between lithologies. Greenish gray phyllosilicate-rich layers are most continuous and sharpest-bounded, usually under 1 mm thick and very continuous, even parallel with slight waviness. Calcite-rich gray silt (15% calcite) laminae disrupt bedding in places and shows undulating gradational contact with darker gray shale layers. Silty grayish white laminae sampled for stable isotopes. Sample is pyritic with no Cu minerals. Rare organic matter present as orange (TAI = 2.6) lamellar both discordant and bedding aligned lamalginite-like filaments. As in Figure 6, this is the Marker bed of WP nomenclature.

**PC5-8**, 20.4 m above base

The sample shows irregular to wavy parallel, very thin black shale laminae with crudely-laminated, calcareous, silty gray laminae, and f.g. shaley gray very thin laminations of phyllosilicates. Gray-white calcareous concretions throughout distort laminations, and are sub 2 mm maximum dimension. Thin laminations dominate, and are continuous except for the silty gray laminae, some of which are discontinuous; overall composition is 60% shale, 40% silt. Chalcopyrite is present, replacing v.f.g. pyrite grains and framboids, dispersed throughout (in calcite concretions, phyllosilicate-rich laminae, and silty laminae). Amorphous orange (TAI = 2.6) translucent isotropic interstitial agglomerations crudely aligned with faint laminations. Stable isotope sampled from moderately calcareous silty gray thin laminae. This is the Marker bed of WP terminology seen also in Figure 6.

Figure A29: Irregular to wavy parallel, very thin black shale laminae with crudely-laminated, calcareous, silty gray laminae, and f.g. shaley gray very thin lams of phyllosilicates. Gray-white calcareous concretions throughout distort laminations, and are sub 2 mm maximum dimension. Thin laminations, continuous except for the silty gray laminae, some of which are discontinuous. Millimeter ruled scale at R. Sample PC5-8.

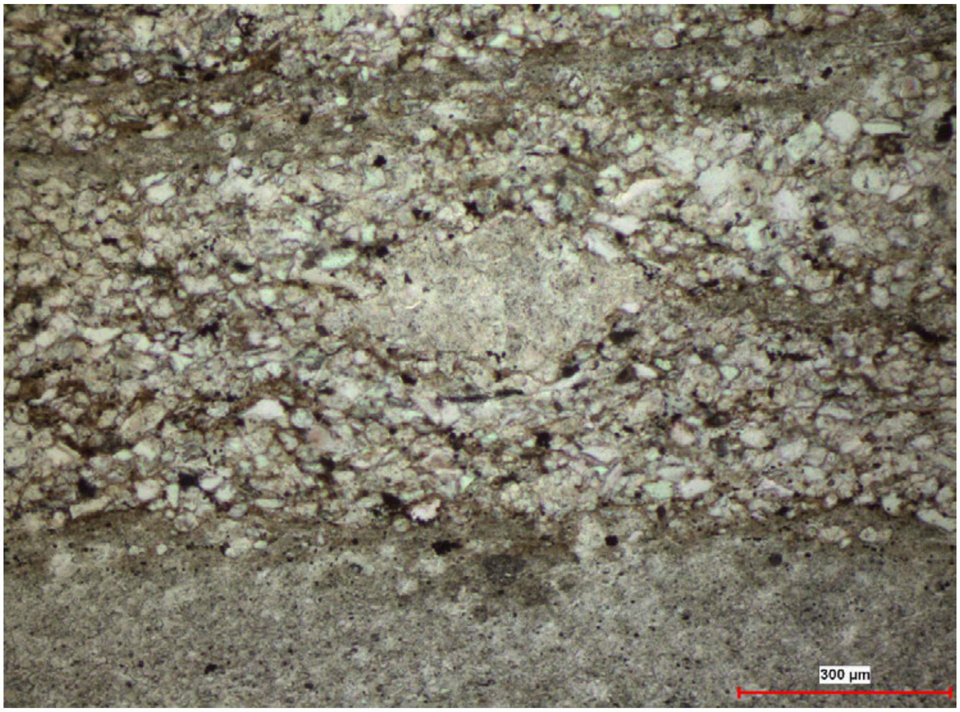

Figure A30: PPL shows calcite nodule at center, with opaques including chalcopyrite present, replacing v.f.g. round pyrite grains and framboids, dispersed outside of the calcite nodule (in both phyllosilicate-rich laminae and silty laminae). Amorphous orange OM present as translucent isotropic interstitial agglomerations crudely aligned with lamination. Sample PC5-8.

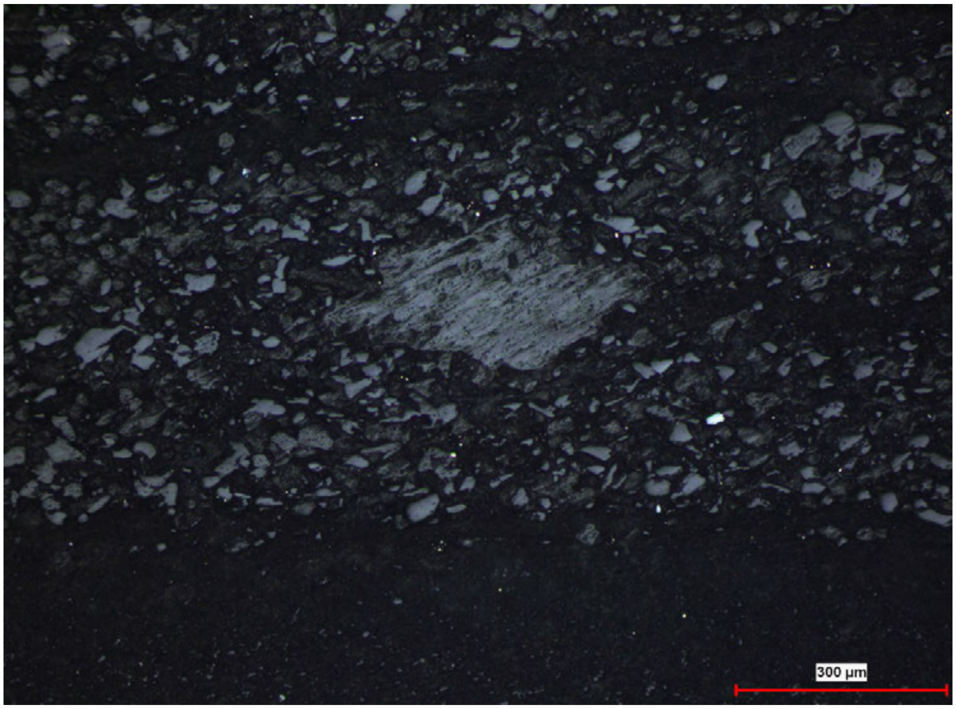

Figure A31: PPL shows calcite concretion at center, with brightly reflecting yellowish opaque chalcopyrite present, replacing v.f.g. round pyrite grains. Chalcopyrite is most apparent as miniscule bright yellow flecks (under 5 micron diameter) at margin of calcite mass at center. Sample PC5-8.

**PC5-4**, 8.1 m above base

This sample is massive, brownish-gray micaceous siltstone with rare, coarser-grained whitish-gray calcareous m.g. siltstone laminae (under 2 mm thick) and is 90% silt. Stable isotope analyzed carbonate materal was drilled from calcareous light gray silty laminae. This is the massive red-brown siltstone of the WP nomenclature (Figure 6) Upper Shale. Prominent hematite-coated quartz grains are common, and the sample is pyritic with no Cu minerals. Rare organic matter in a single wisp/filament of dark reddish brown (TAI = 3.15) lamellar, aligned and similar to lamalginite in appearance.

**PC5-7**, 6.4 m above base

This sample is dark grayish-red shale laminae with coarser-grained lighter gray siltstone, which is whiter in the calcareous-cemented lams (perhaps 1/10 of gray silty layers are calcite-cemented); the sample is 60% silt, 40% shale. It is pyritic with minor, rare chalcocite replacements of pyrite. Organic matter is reddish brown (TAI = 2.85), and pseudolamellar as short, discontinuous sheets and some filaments, both translucent and which are deformed about quartz grains. This sample is possibly same as Upper Sandstone of WP nomenclature (Figure 6).

**PC5-5**, 3.2 m above base

Massive, reddish-gray siltstone defines this sample, which is 80% silt, 20% shale. Massive siltstone with numerous lithic fragments on the microscopic scale. This is the Red Massive of Figure 6. Pyrite dominates the opaque minerals although rare v.f.g. chalcocite is present. Organic matter is amorphous reddish brown (TAI = 2.9), horizontally aligned, and with distortion about quartz grains. Significant hematite present as oxidative zone about sulfides. Chalcocite is as rare v.f.g. subhedra, present (NE quadrant extreme). Mottled yellow to green-reflecting opaque grain, possibly bituminous, present in SE quadrant, isotropic.

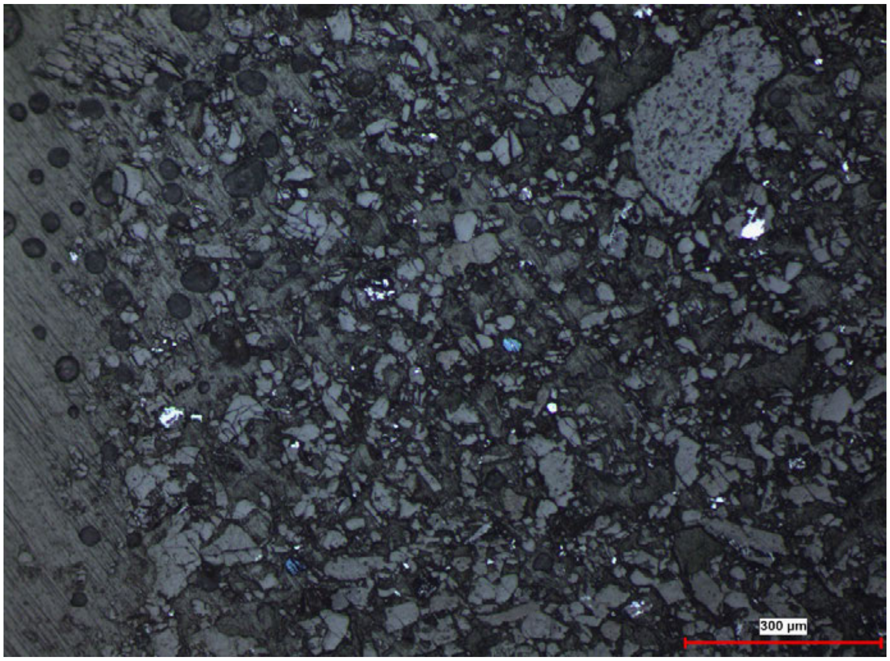

Figure A32: Pyritic with minor, rare chalcocite (center) replacements of pyrite, PPL REFL. Sample PC5-5.

## *Core 28G*

**28G-514’**, 17 m above mineralization

This is the Marker Bed of Figure 6. It is dark gray shaley siltstone with calcite nodules to 3 x 1 mm, displacing organic-rich thin wavy/undulating discontinuous laminations. Vertical calcite vein is present, as 1 mm thick, irregular, anastomosing and inosculating material, in places disturbing bedding. The sample is 60% silt, 40% shale. Also significant is pyrite as subhedral calcite vein-filling (along margins) neo-formed masses. Thin even parallel to wavy parallel laminae of darker gray finer-grained shale with thicker, silt-sized lighter gray laminations. Filamentous organic matter is lamellar, opaque and black, envelops silicate grains as a matrix-like mass (TAI = 3.9); this material is less prevalent than is widespread transparent lamellar AOM with TAI = 3.3, brown color.

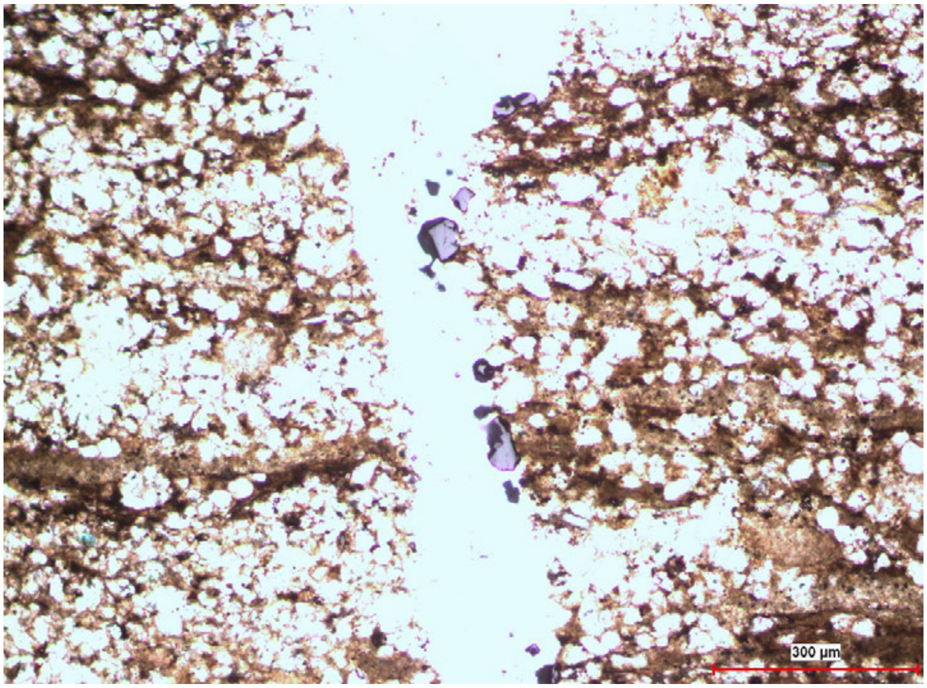

Figure A33: PPL REFL showing calcite vein with neomineral pyrite, brown AOM and black FOM. Sample 28G-514’.

**28G-520'**, 15 m above mineralization

As shown in Figure 6, this is the Marker Bed of WP terminology. The sample is a dark gray shaley siltstone with thin even parallel to wavy parallel alternate light gray (m.g. silt-dominated) laminae. Calcite vein disrupts/brecciates shaley siltstone, and shows masses of pyrite at its margins, in close association with most OM-rich laminations. Structureless AOM concentrated in dark gray, finest-grained laminations and is broadly distributed about quartz and other silicate grains. No Cu minerals. Organic matter is dominantly orange brown, unstructured AOM, isotropic and translucent, and encases subangular silicate grains (TAI = 2.8). Sample composition is 50% shale, 50% silt. Colbert (2011) reported fluid inclusion oil in the next sample down section, 28G-522'.

**28G-526'**, 12 m above mineralization

This is the Marker Bed shown in Figure 6. Dark gray continuous thinly laminated clay-size fraction dominates, with minor siltstone, light gray interpersed as thin interlaminae. A massive, calcite accumulation is present in a thick vein (1 cm width). Organic matter is dark brown, translucent isotropic and dominantly FOM, elsewhere as amorphous accumulations (TAI = 3.7). No Cu minerals in thin section, although pyrite is widespread.

**28G-539'**, 7 m above mineralization

This sample is a massive gray shale with visible pyrite, and calcite veins, with calcareous fractures showing primary OM-rich discontinuous laminations at the margins of fractures. Organic matter is present as filamentous lamellar concentrations of black opaque material (TAI = 3.9). Colbert (2011) reported oil inclusions in this sample and an oil homogenization temperature on them as 117 °C.  60% shale, 40% silt.  There is chalcopyrite present as very rare (sub-1% of sulfides apparent) v.f.g. anisotropic subhedra.

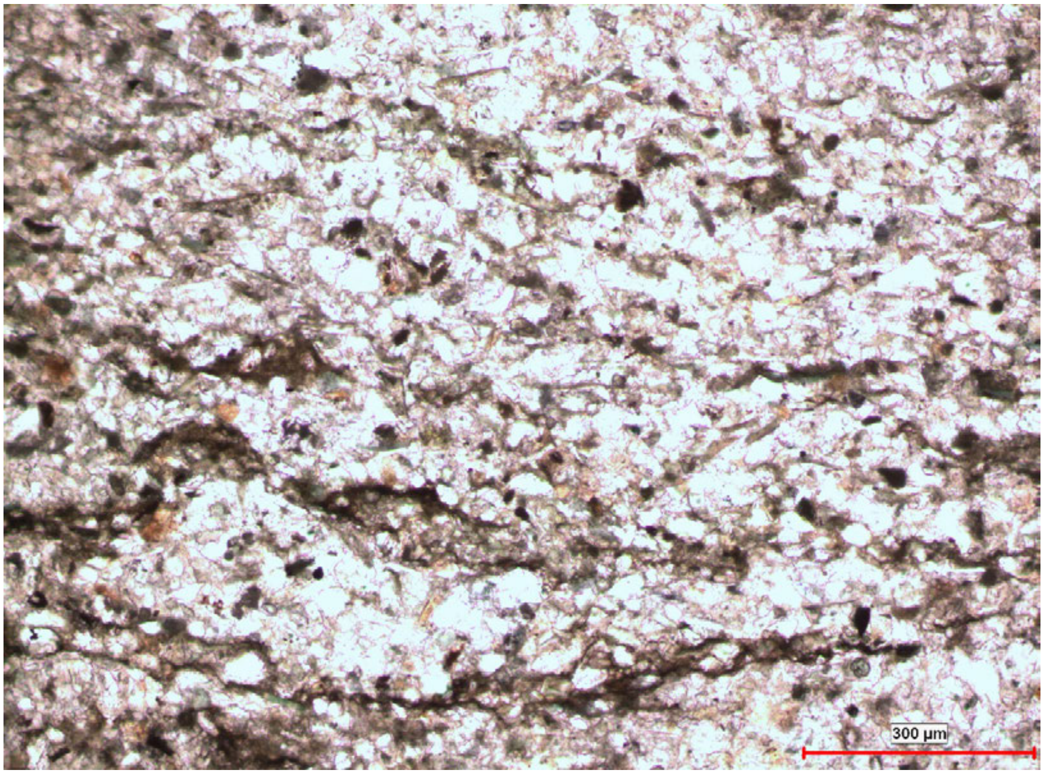

Figure A34: Filamentous opaque black OM with pyrite.  Sample 28G-539’.

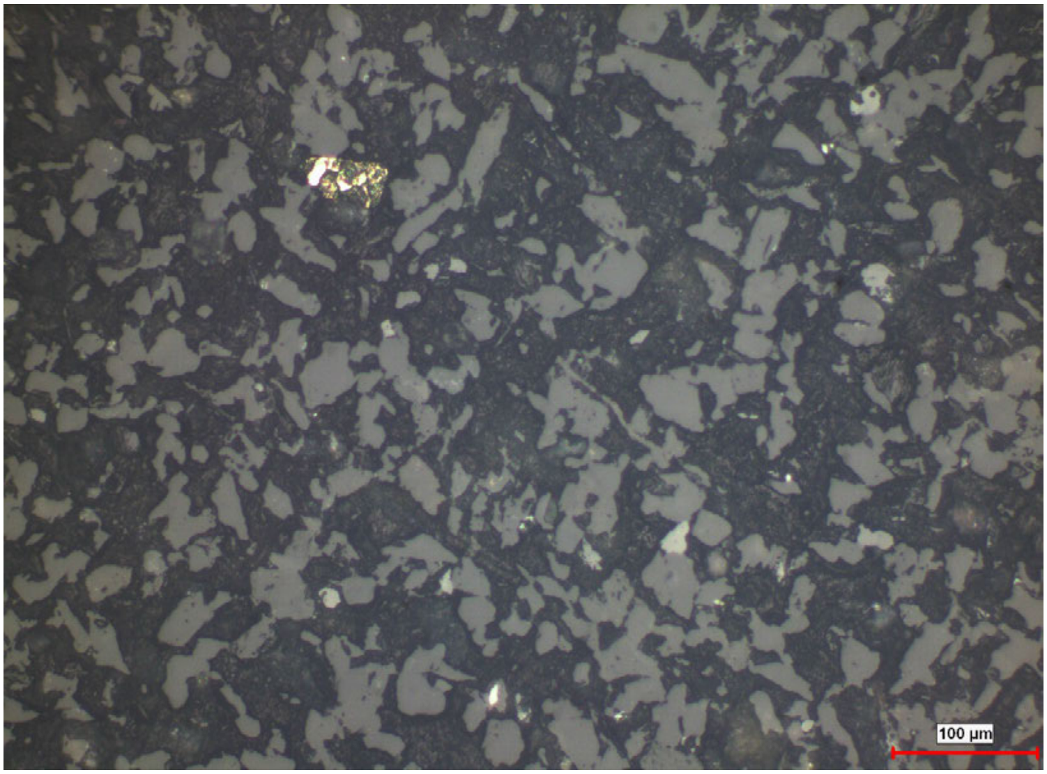

Figure A35: REFL PPL shows chalcopyrite, anhedral.  Sample 28G-539'.

**28G-571'**, mineralized

This is a red massive shale with pyrite and black opaque FOM.  No other organic matter is present in thin section.  Sample contains significant neoformed hematite growth about chalcocite as subangular masses.  Breached shaley lamination (FOM is amorphous, lamellar, and black - TAI 3.9) is apparent, with silty material disrupting OM-rich lamination.  Immediately above the breached lamination is a concentration of pyrite, with associated hematite.  Detrital chlorite present, but no neomineral chlorite growths.  Sample is noncalcareous and 60% shale, 40% silt. Chalcocite is present as very rare (sub 0.5% of sulfides apparent), incipient replacements of pyrite.

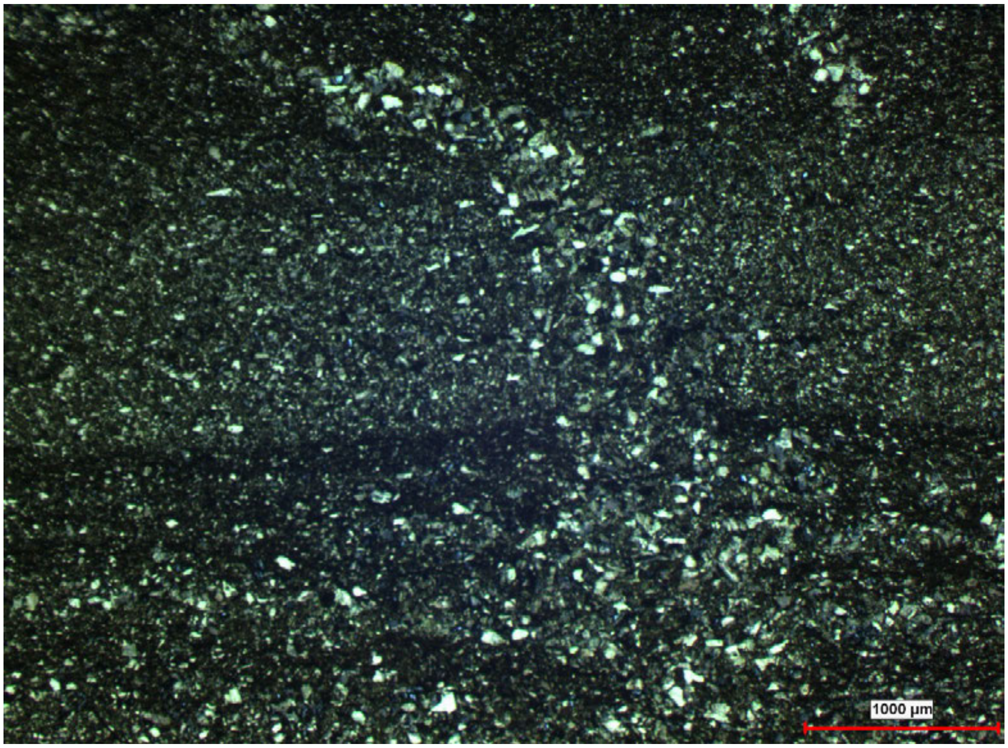

Figure A36: Silty dike breaching shaley lamination with very minor chalcocite at L center. PPL REFL. Sample 28G-571'.

**28G-572'**, Cu mineralized

This sample is of the Domino of WP terminology (Figure 6). Light gray sandy siltstone, crudely laminated micaceous sandy siltstone, non-calcareous. Interlaminae of darker gray carbonaceous content are gently undulating in form and sometimes anastomose. Lamellar, wavy FOM is opaque and black (TAI 3.9). Significant detrital chlorite is present, and reddish hematitic degradation of sulfides is widespread, in both v.f.g. (30 micron) and c.g. sulfides. Chalcocite replacements of pyrite are apparent as rare v.f.g. clasts.

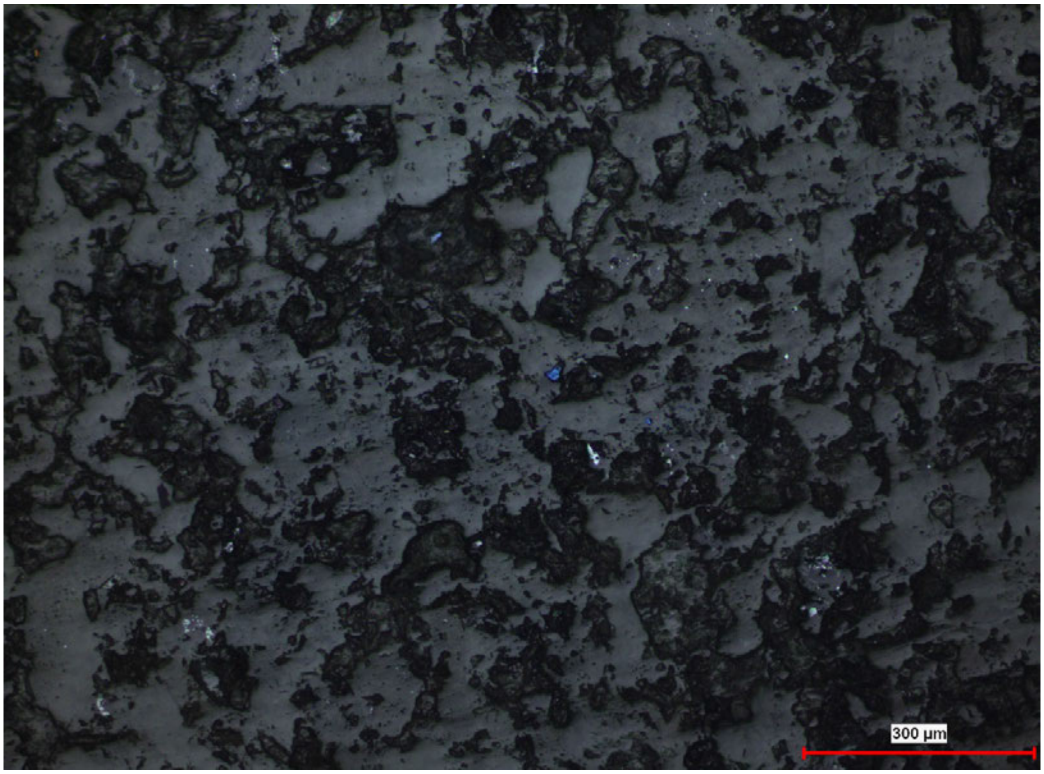

Figure A38: Chalcocite and pyrite PPL REFL.  Sample 28G-572’

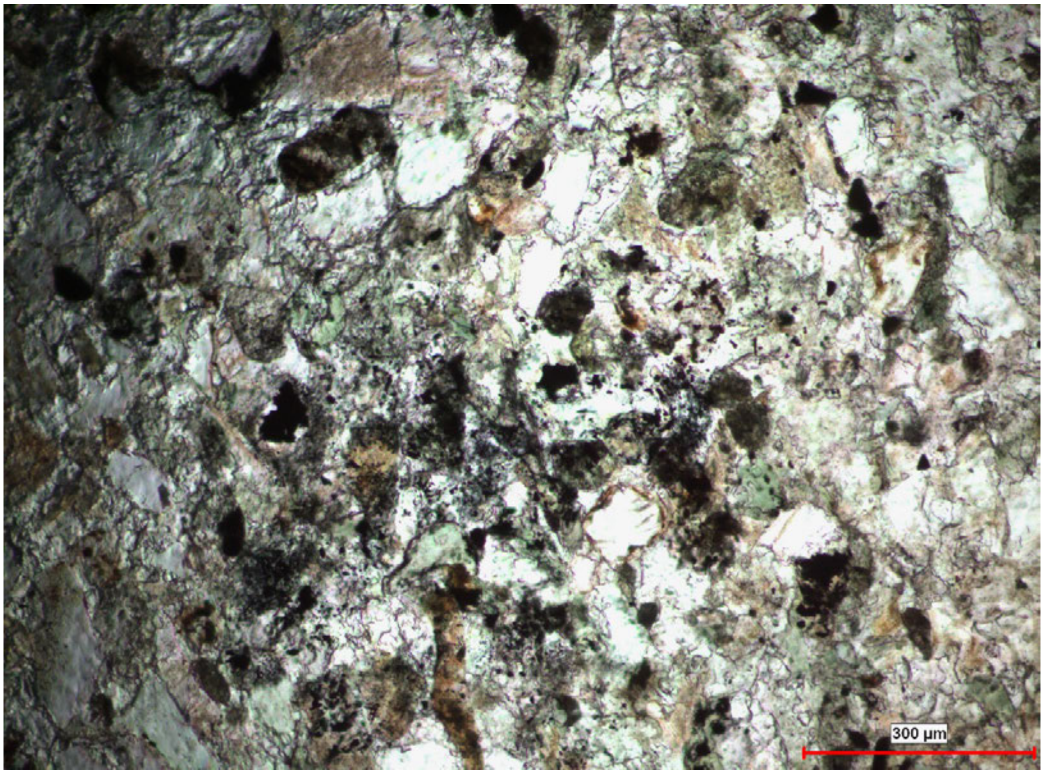

Figure A39: Chalcocite and pyrite PPL.  Sample 28G-572’.

*Presque Isle River Outcrop*

**PIR-12**, 92 m above base

The sample is an indistinctly bedded dark gray siltstone, m.g., with blotchy pink calcite-cemented irregular oblong forms (to 1 mm maximum) coloring 45% of sample light gray. Pyrite, disseminated and subhedral, focused in thin laminations. Composition is 60% silt, 40% shale. Calcareous blebs sampled for stable isotopes. Organic matter not present in slide, but hematite coated quartz common. At least 15 anisotropic chalcopyrite grains present with adjacent pyrite showing incipient chalcocite replacement. Significant chalcopyrite in PIR-11, sampled 89 m above base.

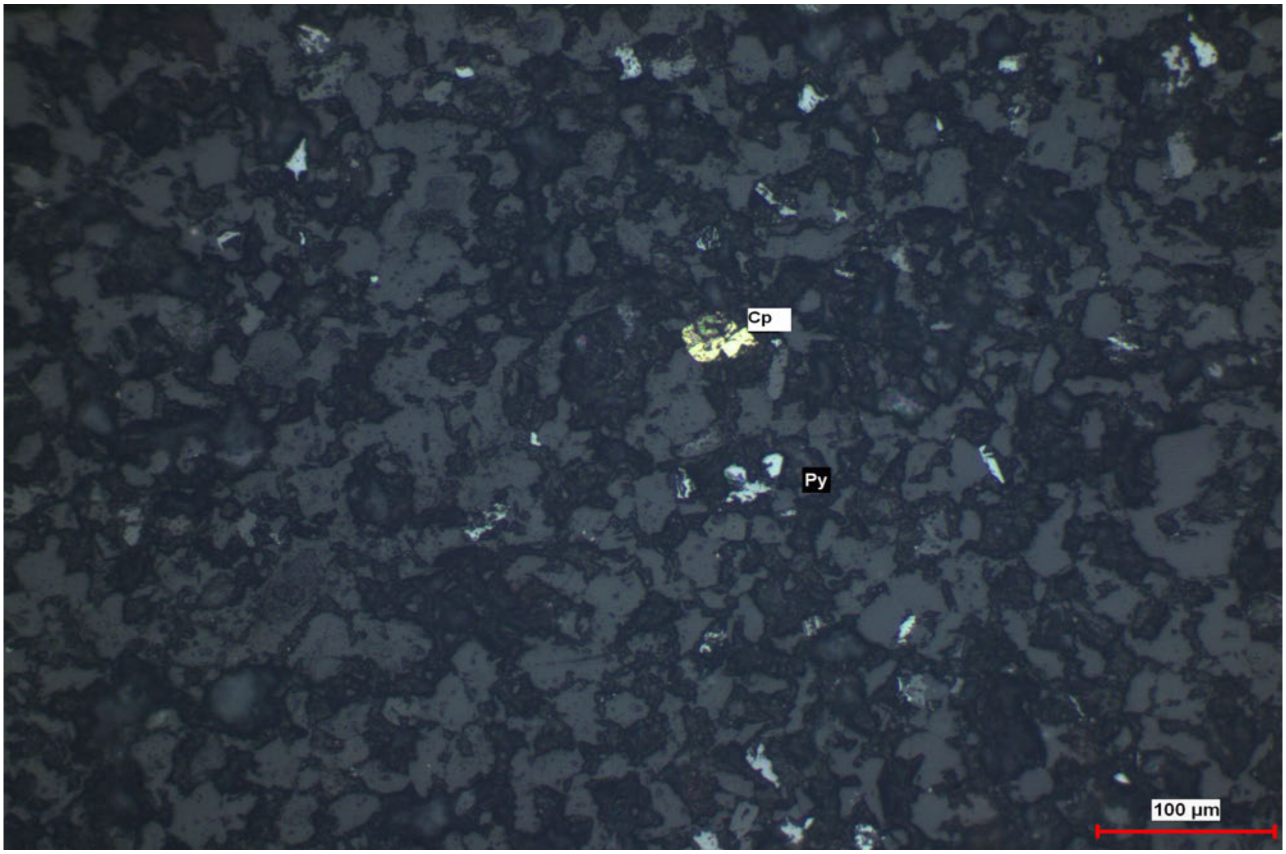

Figure A41: REFL PPL of chalcopyrite in matrix material, with incipient chalcocitization of adjacent pyrite grain. Sample PIR-12.

**PIR-10**, 59.9 m above base

This sample is green-gray thinly laminated (gently parallel even undulose to wavy) gray siltstone with dark gray shaly laminae. Fine anhedral pyrite disseminated throughout sample. Thin laminae of light gray m.g. silt are variably faintly calcareous, sampled for stable isotopes. No Cu minerals apparent. Isotropic orange (TAI = 2.6) lamellar translucent AOM with pyrite associated as small subhedra present in thin discontinuous slightly wavy laminations. Organic matter commonly encases more durable quartz grains, giving anastomose/inosculate appearance. Several subround translucent amorphous isotropic orange blebs of OM (to 30 microns maximum dimension) present.

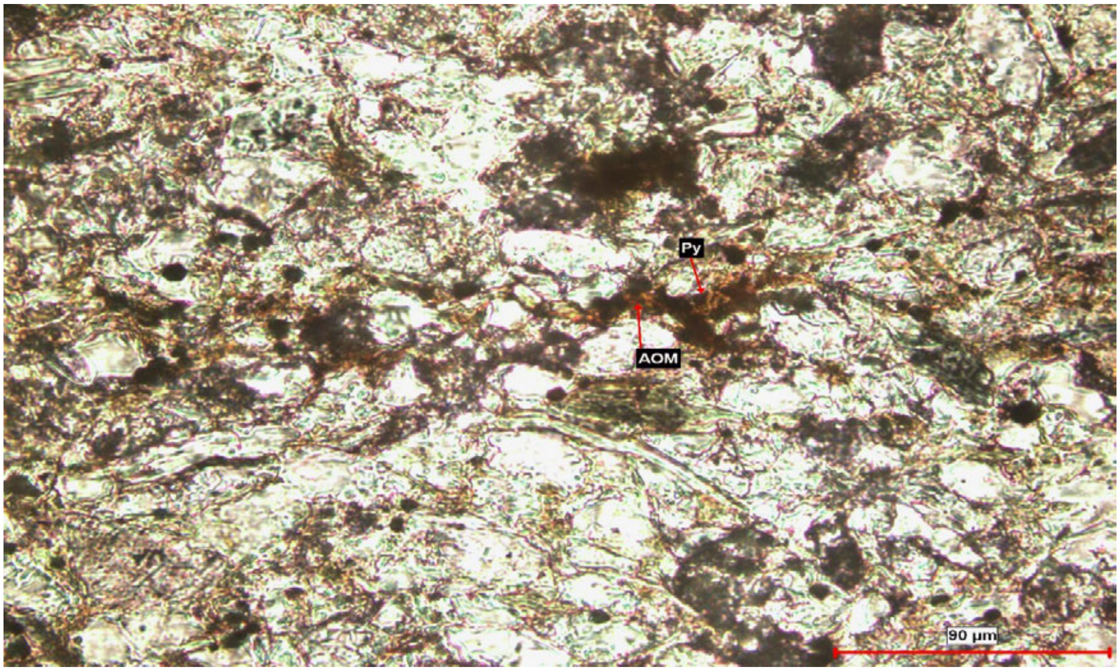

Figure A42: Isotropic orange (TAI = 2.6) lamellar translucent AOM with pyrite associated as small subhedra present in thin discontinuous slightly wavy laminations. PPL of sample PIR-10

**PIR-9**, 25.5 m above base

This sample is a gray to dark gray siltstone with some very thin grayish-black laminated f.g. silt to shale interlaminae (mostly straight, even parallel, with some gently undulose and some crossbedded fine laminae). Thin section is massive, with subhedral disseminated pyrite, and pyritic masses about silicates in agglomerations approaching 300 microns. Sample is well-cemented throughout with calcite cement, and sampled for stable isotopes. No Cu minerals or OM apparent, excepting one rare, isolated incipient chalcocite replacement of v.f.g. pyrite. Apparent oxidation (browning of shale layers) on surface of core sample, penetrates less than 2 mm.

**PIR-8**, 25.4 m above base

This sample is a massive gray siltstone, v.f.g. and dominantly quartzose. Pyrite dominates opaques, with very isolated (sub 1%) incipient chalcocite/bornite replacement of 100 x 90 micron pyrite grains, as well as a single bornite grain. Significant hematite-coated detrital quartz (about 20%) is present. No OM is apparent in thin section. Calcite-cemented laminations sampled for stable isotopes.

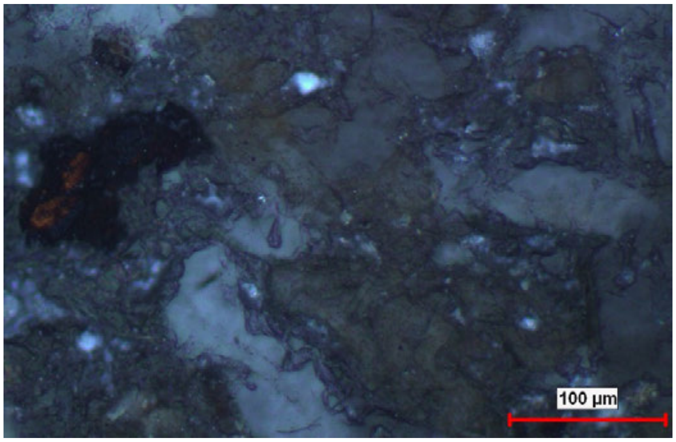

Figure A43: Anisotropy of lone bornite grain in left upper quadrant, XPL REFL. Sample PIR-8.

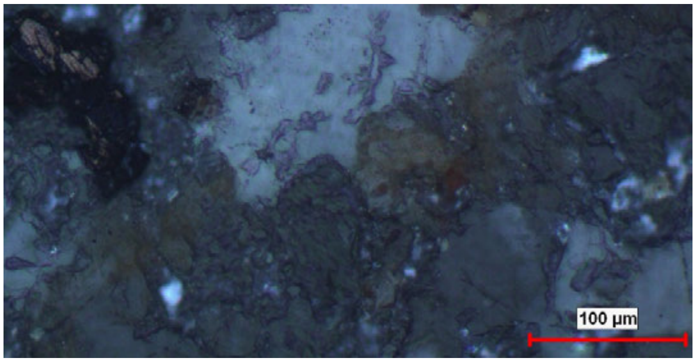

Figure A44: Anisotropy of lone bornite grain in left upper quadrant, XPL REFL. Sample PIR-8.

**PIR-7**, 14.9 m above base

This sample shows Cu-staining of malachite on exterior of brownish gray fissile m.g. siltstone, with lenticular siliceous concretions (5x20 cm). Composition is 90% siltstone, 10% shale, with rare interlaminae of micaceous darker gray siltstone. Mud or syneresis cracks apparent near sample site. Ripple mark showing normal graded bedding from m.g. subangular silicates in to v.f.g. phyllosilicates in thin section. No OM is apparent. Stable isotope sampled from siltstone calcite-cemented laminae. Significant hematite-coated quartz grains, subangular, are present (about 28%), as is neomineral chlorite (about 25%). The sample is pyritic with some incipient chalcocite replacements of framboids of 80 x 30 micron dimensions. Pyrite dominates the sample and chalcocite comprises around 2% of the sulfide minerals apparent. Many of the pyrites are bounded by hematite - oxidation in situ?

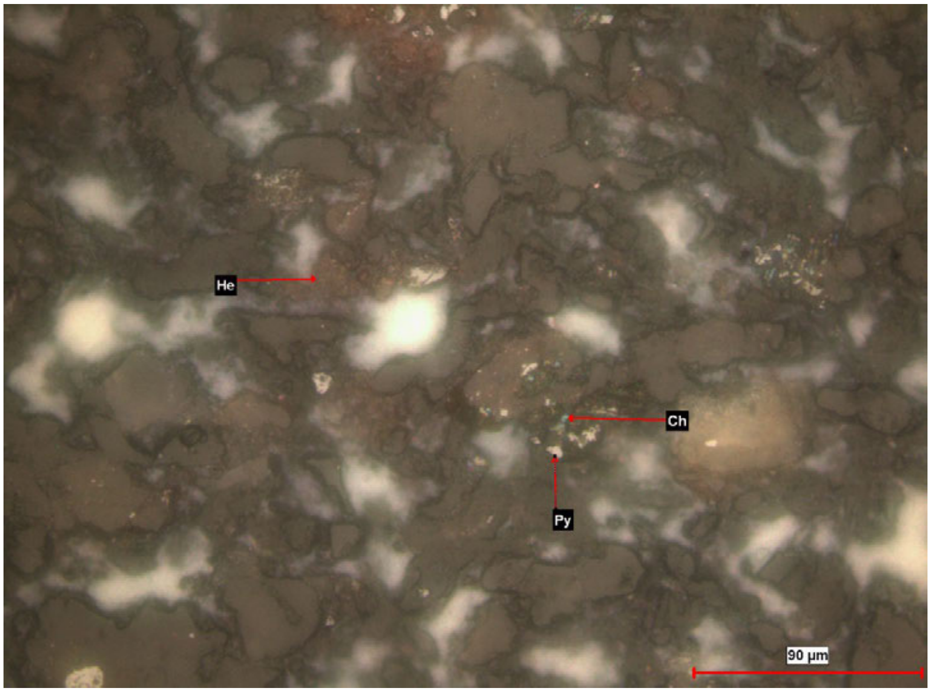

Figure A45: Incipient chalcocite on framboidal pyrite; pyrite dominates the sample and chalcocite comprises around 2% of the sulfide minerals apparent. PPL REFL. Note hematite about pyrite. Sample PIR-7.

**PIR-6**, 3.5 m above base

Red to white v.f.g. sandstone interlaminated with wavy/undulose c.g. silty lenticular to continuous thicker even parallel to wavy parallel laminated siltstone describe this sample. Ripple marks of finer material bound top and bottom of this noncalcareous specimen. This is the Lower Transition of WP terminology (Figure 6).

<u>*Saxon Falls Outcrop*</u>

**SF-4A**, 103.7 m above base

This sample shows thin ripple lamination in otherwise massive m.g. siltstone. 100% silt size clasts. Hematite coated quartz present; no OM apparent in thin section. Calcite-rich lamination sampled for stable isotopes. No Cu minerals apparent in thin section.

**SF-2B**, 94.6 m above base

This sample is thin even parallel to very thin discontinuous laminated dark gray OM-rich clay-size material in gray siltstone. Wispy black opaque FOM (TAI = 3.9) is apparent in association with dispersed AOM, black and opaque as intermixed matrix with v.f.g. shale-size phyllosilicate rich domains. Chlorite coating on detrital quartz grains common (15%) as well as very common quartz grains with hematite coating (20%). Composition is 80% siltstone, 20% clay-size and noobserved Cu minerals. Figure A46: Wispy black opaque FOM (TAI = 3.9) apparent in association with dispersed AOM, black and opaque as intermixed matrix with v.f.g. shale-size phyllosilicate rich domains.

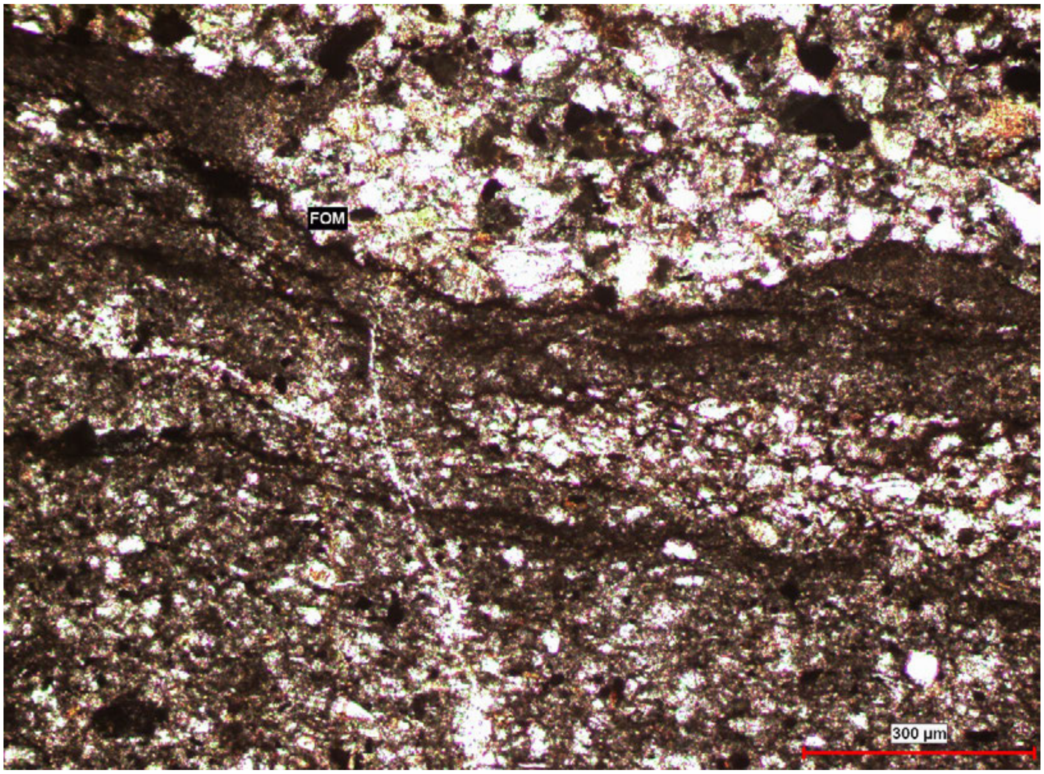

Figure A46: Wispy black opaque FOM (TAI = 3.9) apparent in association with dispersed AOM, black and opaque as intermixed matrix with v.f.g. shale-size phyllosilicate rich domains. Sample SF-2B

**SF-3B**, 77.2 m above base

Thickly laminated siltstone (gray) and shaley siltstone (dark gray), with thin calcareous laminations present describe this sample. It has opaque black (TAI = 3.9), very rare, FOM contorted about quartz clasts in overall wavy discontinuous laminar presentation. No Cu minerals, solely pyritic sulfides.

**SF-3A**, 43.8 m above base

This is a gray massive f.g. sandstone, red hematite coating quartz grains ubiquitous (to 25%). No OM apparent, and 100% sandstone. No Cu minerals. Stable isotope sampled from matrix calcite cement.

**SF-4B**, 41.3 m above base

This is a massive pyritic siltstone with significant hematite stained quartz (10%). No OM apparent, 100% siltstone in this sample. No Cu minerals. Stable isotope sampled from matrix calcite cement.

**SF-5B2**, 14.5 m above base

This specimen is a gray massive to thickly laminated, lenticular siltstone, showing en echelon 1 cm long, 1 mm wide pinkish white calcite filled fractures at 30 degrees to bedding. Massive in thin section, pyrite dominates sulfides. Calcite vein with isolated, rare very fine-grained chalcocite and covellite matrix grains in suspended in carbonate, replacing pyrite. Sample shows black wisps of opaque FOM (3.9 TAI), at 30 degrees to massive bedding, and is 100% siltstone.

This is likely the Galaxy bed of WP terminology (Figure 6). Sample has insufficient calcite for stable isotopes on calcite veins.

Figure A47: Hand sample showing massive bedded en echelon hematitic calcite veined siltstone. Sample SF-5B2:

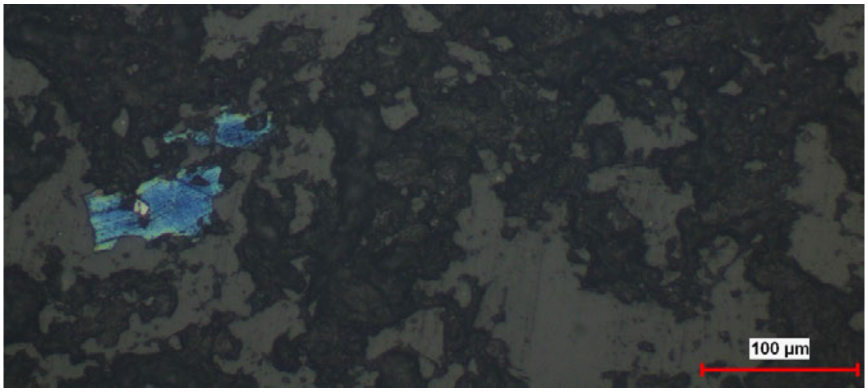

Figure A48: Covellite matrix grain suspended in calcite vein PPL and REFL. Sample SF-5B2.

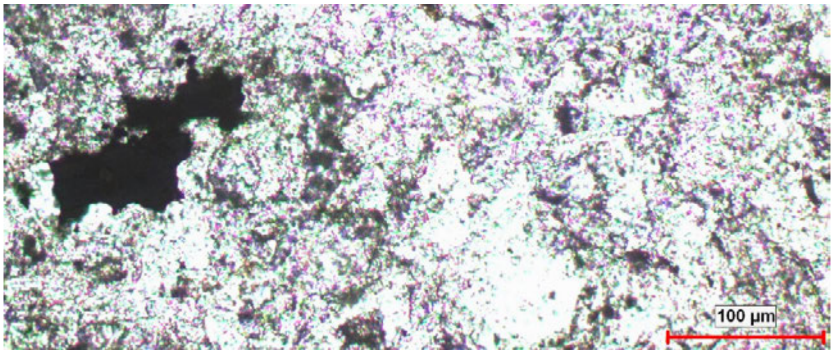

Figure A49: Covellite matrix grain suspended in calcite vein PPL.  Sample SF-5B2.

**SF-5B**, 14.5 m above base

This is a pervasively fractured massive dark gray siltstone.  No thin section.  This is similar in appearance to the Galaxy bed of WP terminology (Figure 6).

**SF-2A**, 13.0 m above base

This sample is a red m.g. quartzose lithic sandstone with 1 x 10 mm shale burgundy colored rip-up, rounded, set in massive matrix.  Rip-up clast shows dark red, horizontally and vertically fractured clay size fraction material, quartzose, and with black opaque (TAI = 3.9) AOM and significant bright red hematite grains, isotropic and translucent.  Compactional deformation of rip-up clast is evidenced by contorted margins where silt size grains impact and penetrate the rip-up.  Coarse calcite matrix cement localized around rip-up clast, sampled for stable isotopes.  Pyritiferous, but no Cu minerals apparent.

**SF-1A**, 7.8 m above base

This is a very thin even parallel continuous laminated siltstone (light gray) and mudrock (dark gray), pyritic.  Clay-poor, quartz dominant composition describe this sample’s component clasts.  Very thin calcite veinlet (vertical, and hematite-bounded in places) breaches shaley laminations, and slightly offsets lamination.  Very thin opaque black (TAI = 3.9) FOM-bearing lamination, discontinuous and wavy, present, associated with f.g. pyrite.  Composition is 60% siltstone, 40% clay-sized shale.  Opaque black (TAI = 3.9) dispersed AOM-bearing clay size-fraction lamination shows concentration of phyllosilicates and vertical displacement associated with vertical calcite veinlets.  No ore minerals are apparent and there is insufficient calcite in veinlet for reliable stable isotope sampling.

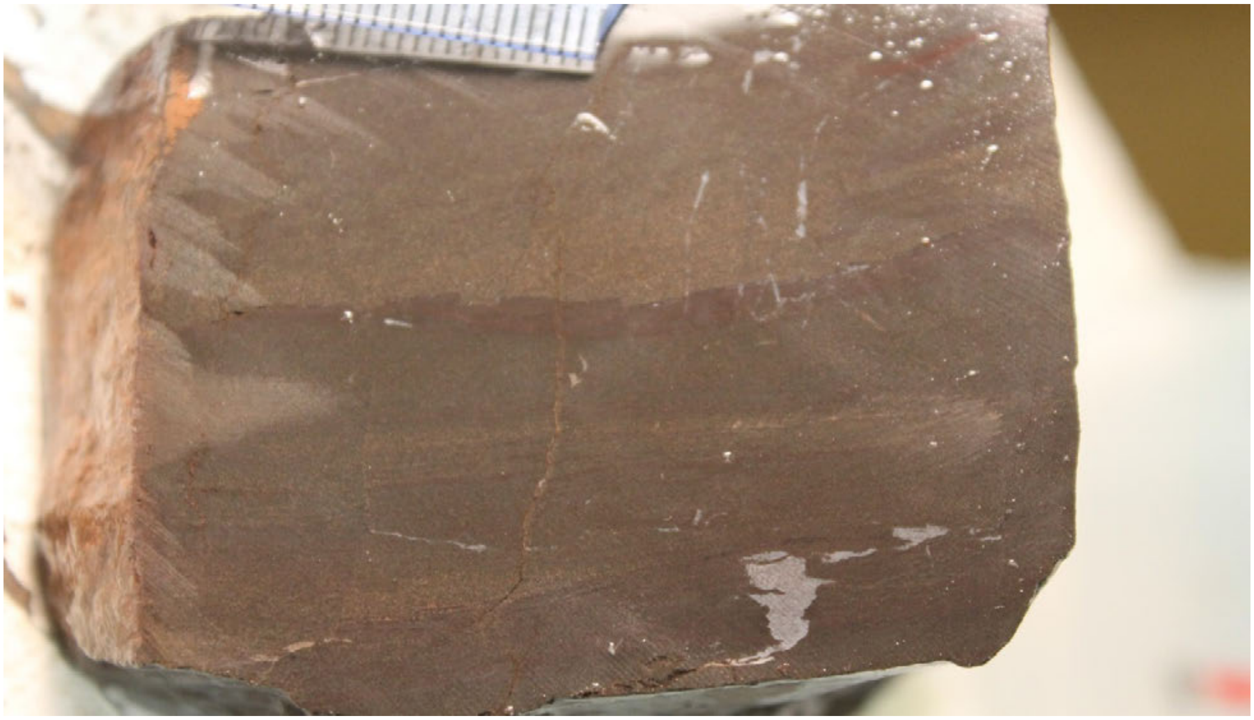

Figure A50: Hand sample showing calcareous concretion, vertical hematitic calcite veinlets, and vertically fractured, offset shaley laminae.  Note molar-tooth calcite concretion at bottom right.  Sample SF-1A.

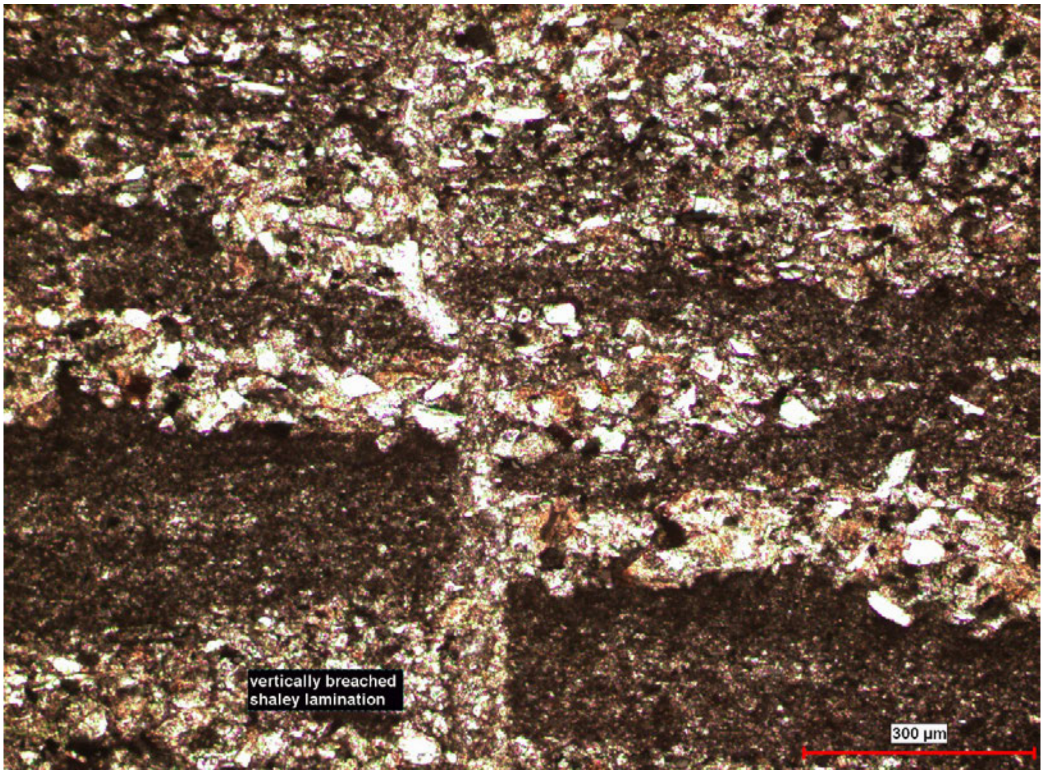

Figure A51: PPL opaque black (TAI = 3.9) dispersed AOM-bearing clay size-fraction lamination shows concentration of phyllosilicates and vertical displacement associated with vertical calcite veinlets. Sample SF-1A.

**SF-6B**, 4.1 m above base

This is a massive gray f.g. siltstone with less than 10% v.f.g. silt/shale as irregular, randomly oriented angular clasts (10 x 4 mm maximum) present - contorted bedding. Pyritic (disseminated subhedra to 30 microns, mostly sub 10 microns). This is possibly analogous to the Domino Scent of a Mule of WP nomenclature (Figure 6) and is 65% silt, 35% mudstone. Vertical calcite veinlet bisects sample. Faintly translucent, concentrations of AOM (TAI = 3.9) and clay-size fraction phyllosilicate-rich material apparent in distorted wavy interlaminations with quartzose siltstone laminations, both together as apparent rip-up clasts in massive siltstone. No Cu minerals.

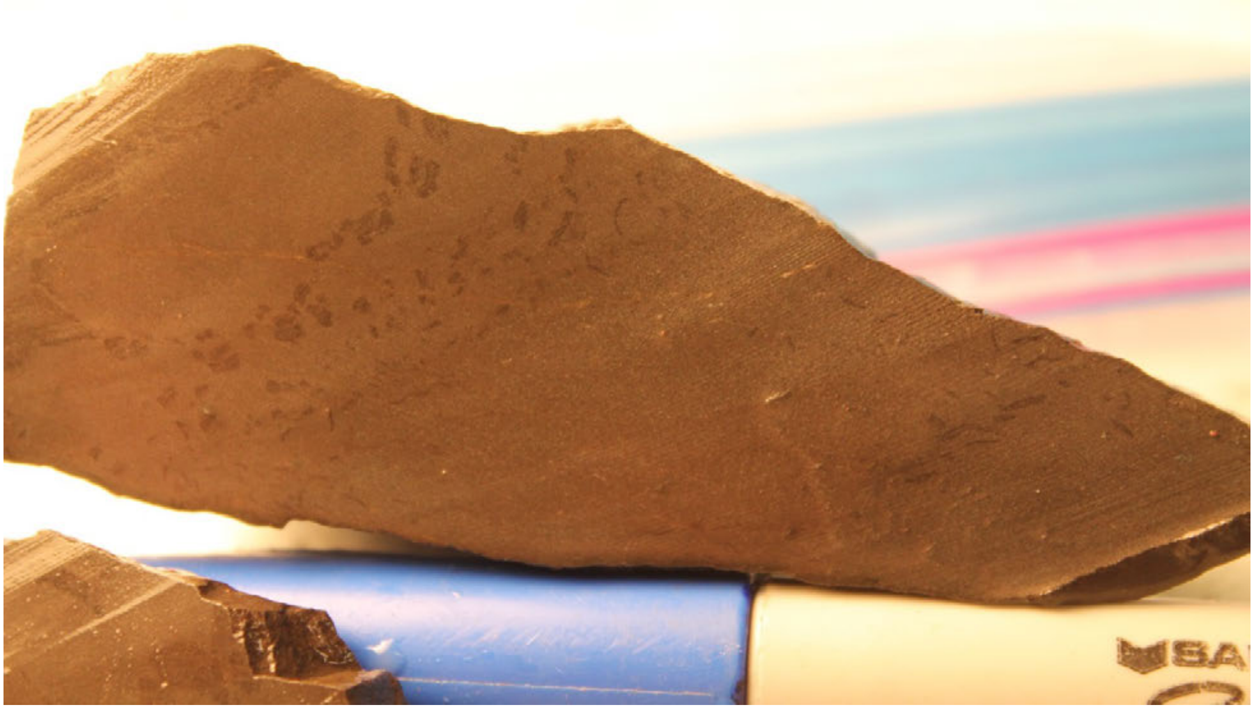

Figure A52: Hand sample showing contorted bedding/rip-up clasts of finer-grained shaley material, with minor hematitic veinlets.  Sample SF-6B.

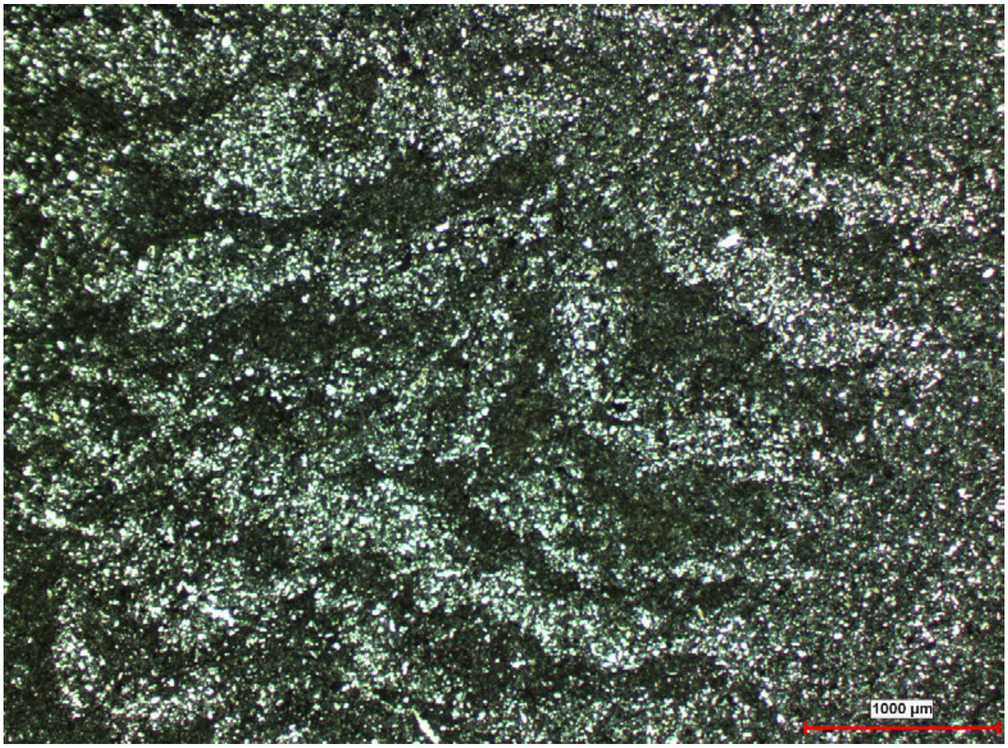

Figure A53: PPL overview of contorted bedding AOM-rich interlaminae with silt laminations in massive siltstone. Sample SF-6B.

*Copper Falls State Park Outcrop*

**CF-5B**, 90.6 m above base

This is dominantly black siltstone with minor (~7%) lenticular silty red-light-gray laminations, thin and thick. Hematite is present as isolated (20%) quartz grain coatings, subangular detrital quartz. Amorphous OM present in concordant but irregular and discontinuous lenticular accumulations, reddish brown in color (TAI = 2.9); some minor black opaque anastomosing OM also present (TAI = 3.9). No Cu minerals are present.

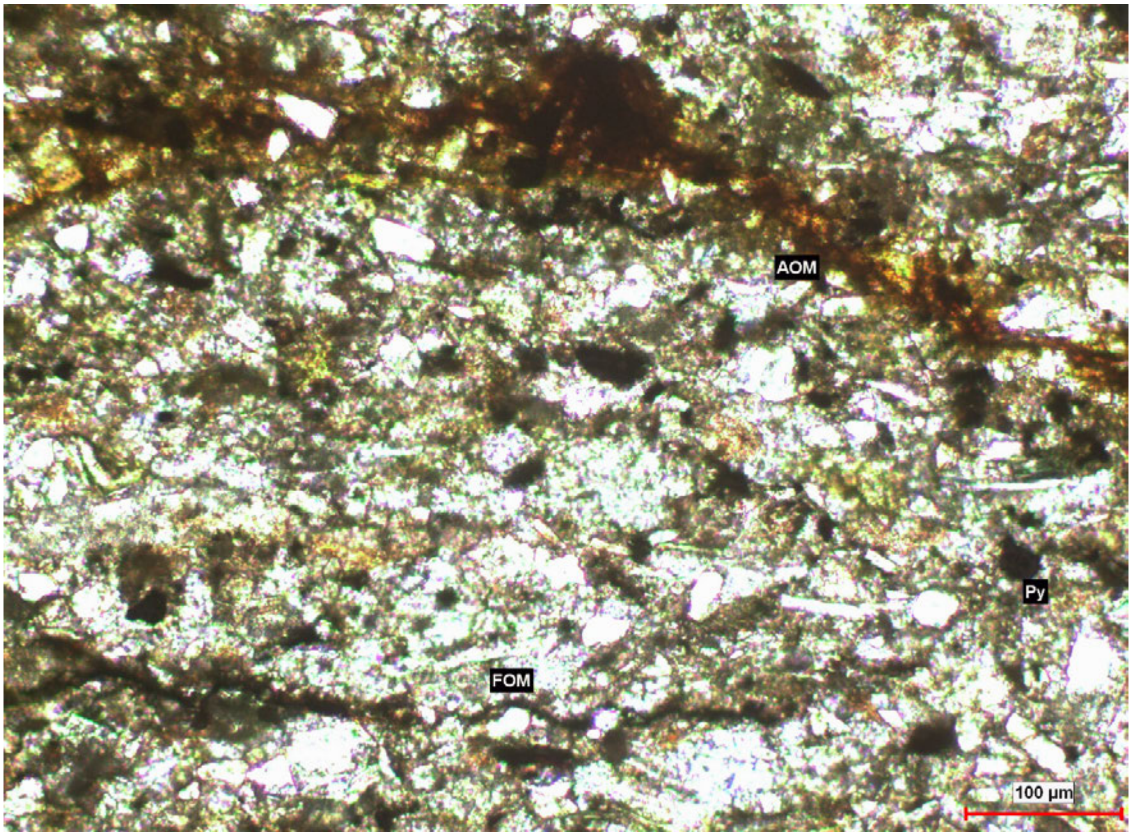

Figure A54: FOM and AOM present together. Sample CF-5B.

**CF-3A**, 87.5 m above base

This is a gray m.g. siltstone interlaminated (thickly, often even, wavy and continuous) with darker gray wavy continuous to broken lenticular shale laminations (breached). Pyrite, disseminated and euhedral to subhedral is present as very fine grains, no Cu minerals. Silty clastic dike intrudes clay-fraction rich thin lamination, and commonly disrupts/truncates clay-size fraction dominated laminations = breached shaley laminae. Filamentous anastomose and inosculate nearly opaque dark brown (TAI = 3.9) OM, discontinuous, suspends some quartz grains. Hematite coating on many of the silt fraction quartz grains.

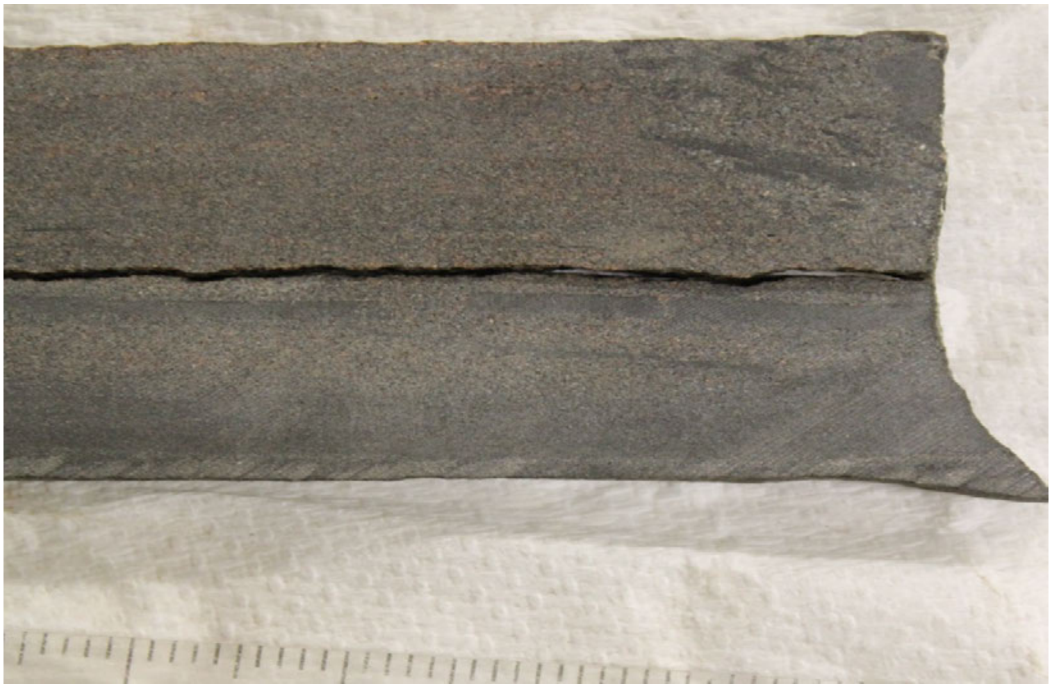

Figure A55: Fractured, offset shaley laminations, clay rich, in hand sample. Millimeter scale at bottom. Sample CF-3A.

**CF-4B**, 85.0 m above base

This sample shows black densely anastomosing (7%) even to wavy thin shale laminations with reddish gray and gray m.g. siltstone laminations (thick), coupled with dark gray uneven irregular m.g. silt laminations encasing lenticular silty red lams. No Cu minerals are apparent. Calcareous light gray siltstone laminae sampled for stable isotopes. During sample prep, oily residue (potentially originating in this sample) collected on sawing fluid surface. Composition is 80% siltstone, 20% shale. Filamentous organic matter dominates the organic fraction, as black opaque (TAI = 3.9), wavy material, inosculating/anastomosing about intervening silicate and pyrite grains. Hematite coated quartz silt-size grains are common (20%).

**CF-3B**, 42.3 m above base

Massive reddish-gray sandy siltstone with dark gray irregular discordant OM-rich domains to 10 by 5 mm, and discordant, discontinuous red to gray-red very thin internally wavy laminated material - rip-ups. No Cu minerals present in thin section. Rare isolated wavy black opaque FOM is present, (TAI = 3.9), intimately associated with pyrite. Hematite coating quartz and calcite is common in sand (55%) part of thin section, and significant hematite haloes about pyrite grains are present. No ore minerals are present.

**CF-4A**, 39.0 m above base

This sample is a pervasively fractured gray siltstone with rare (10%) darker gray silt laminae (even and parallel). Calcareous veins present, often concordant with FOM concentrations (zone of weakness?) not stable isotope sampled. No Cu minerals, pyrite common as v.f.g. subhedra. Thin discontinuous undulating anastomose/inosculate laminations contain OM as filaments of black opaque (TAI = 3.9) material. There is a significant halo of black opaque (TAI = 3.9) AOM about calcite concretion. This sample also shows FOM also present in concordant black opaque laminations.

**CF-2B''**, 6.4 m above base

Sample is a wavy, sometimes lenticular, irregular undulose thin dark gray shale interlaminae in gray siltstone, m.g. Copper secondary mineral stain was apparent in field. Strongly calcareous gray silt matrix sampled for stable isotopes. Red calcareous (calcite and hematite) vein present in hand sample. Chalcopyrite is widespread as very fine grained round granule and replacements of framboids to 50 microns. This sample is shaley overall (70%) with minor (30%) silt size fraction. Organic matter is filamentous, opaque black (TAI = 3.9), wavy and anastomose discontinuous, and commonly coexists spatially with chalcopyrite.

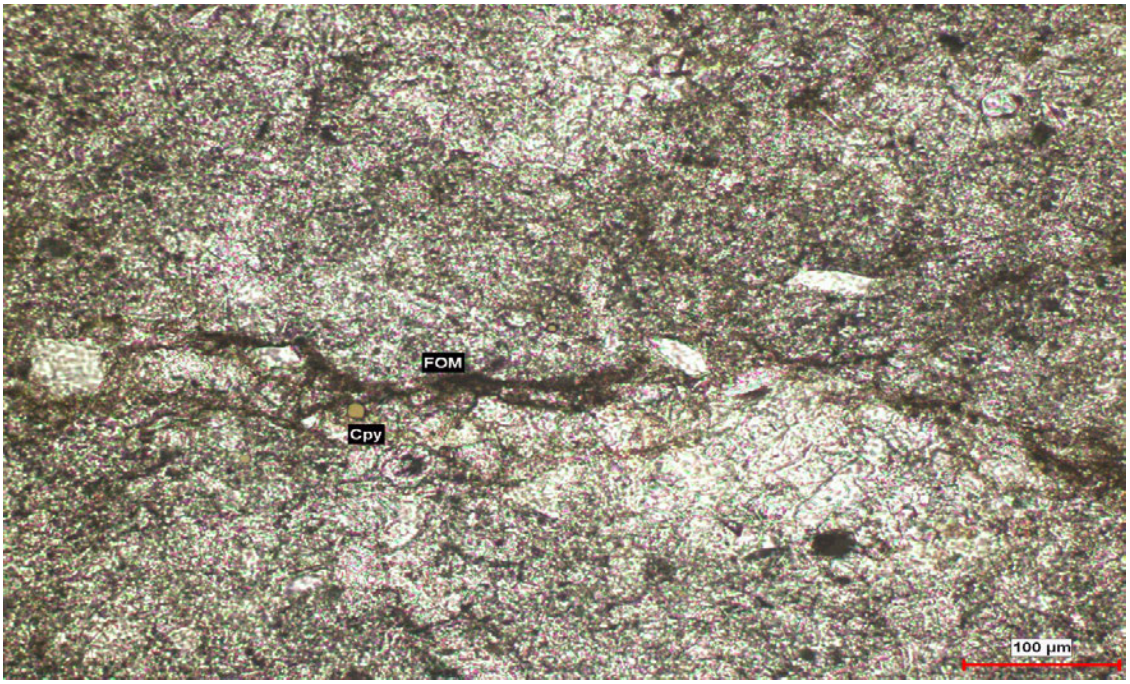

Figure A56: Chalcopyrite in black opaque FOM (TAI = 3.9). Sample CF-2B''.

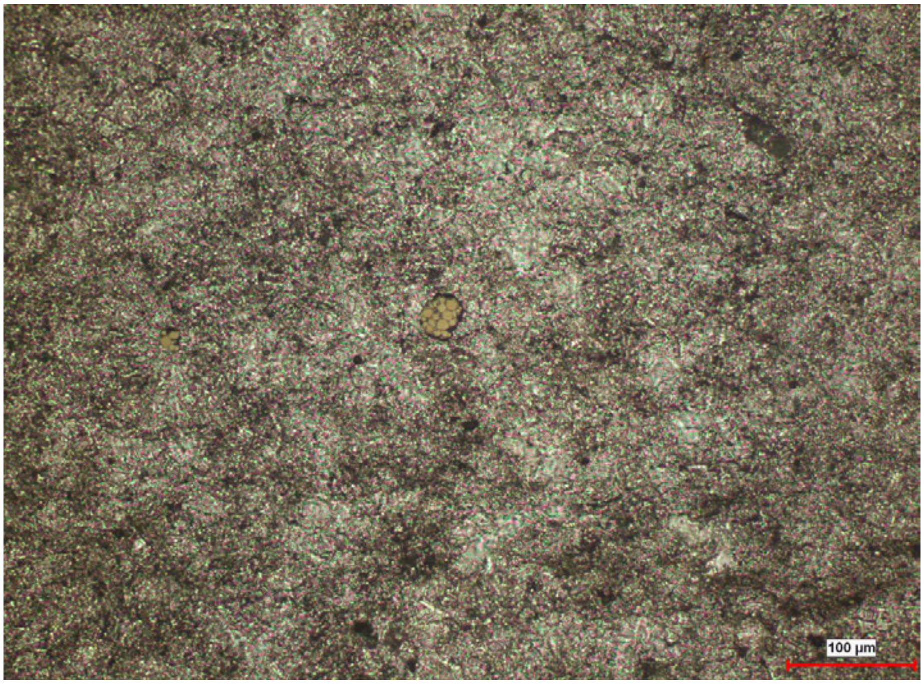

Figure A57: Chalcopyrite replacement of pyrite framboid. Sample CF-2B''.

**CF-2B'**, 6.4 m above base

This sample is a red to red-gray m.g. angular sandstone, massive to thick bedding, immediately (0.05 m) upsection from dark gray siltstone with malachite stain. 100% sand size clasts. Silty red matrix is slightly calcareous, dominantly hematite-coated quartz, sampled for stable isotopes. No OM apparent, nor are ore minerals.

**CF-2B**, 6.4 m above base

This sample is a gray and dark gray irregular/anastomosing interlaminated shale (dark gray) and m.g. siltstone (gray), which is pervasively fractured. Calcareous vein, pink, is likely hematitic.

**CF-2A**, 4.0 m above base

Sample is a gray siltstone, extremely fissile and fractured, thinly laminated with minor darker gray shale (even and parallel to wavy and discontinuous lenticular laminations). Organic matter is present as black opaque (TAI = 3.9) filaments, wavy and discontinuous, and as amorphous agglomerations of dark brown faintly translucent material about polishing/grinding voids (likely OM-rich or shale-rich previously; TAI = 3.7). Overall composition is 55% siltstone, 45% clay-size.

**CF-1B**, 3.4 m above base

This sample is a dark gray massive pyritic siltstone with rare, thin to thick gray-black shale interlaminations (discontinuous and undulating). Pervasively fractured, and with malachite stain on surface. Faintly calcareous gray silt laminations sampled for stable isotopes. Very thin sample (under 1.5 cm thick). Discontinuous hematitic calcite veinlet is present. Filamentous organic matter, opaque and black (TAI = 3.9) present, in association with concentrations of fine-grained chalcocite after pyrite, along transitions between clay-size fragment phyllosilicate rich zones and silty quartzose domains. Minimal f.g. pyrite is present. A hematite-lined calcite veinlet shows a suspended grain of secondary, very fine chalcocite. Overall composition is 70% silt, 30% clay-size grains.

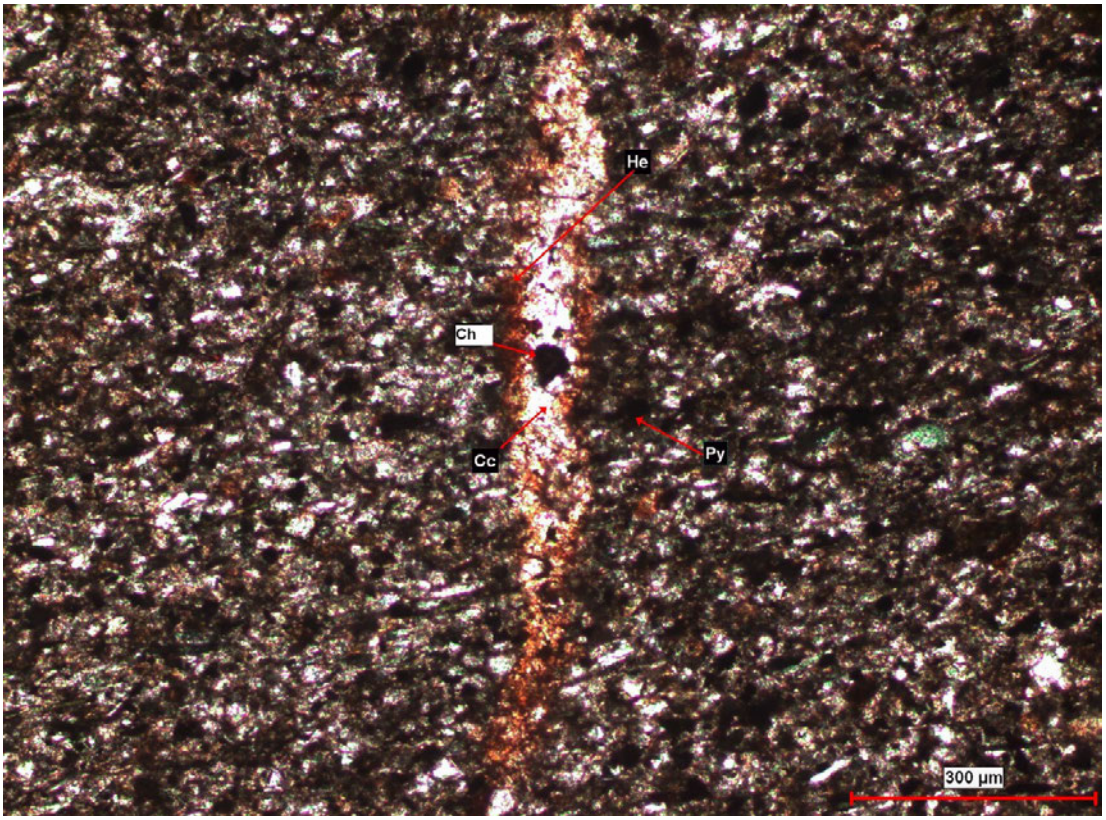

Figure A58: Sample CF-1B. PPL of chalcocite and hematite filling calcite vein, with adjacent pyrite.

**CF-1A-2**, 2.0 m above base

Thin black shale interlaminations between thick laminae of gray-red siltstone (hematite coated quartz very common - 80%), fissile. Significant but not pervasive fracture, as well as malachite/azurite staining present. Post-depositional fractures filled with pinkish white calcite (with minor associated hematite). Hematite coated quartz grains abundant in silt size fraction. Thin section shows calcite (subhedral) veins crosscutting and offsetting thin continuous subparallel shaley laminations. Rare wispy discontinuous opaque black OM (TAI = 3.9) present in two main laminae, both truncated by calcite vein. Overall composition is 95% m.g. silt, 5% clay-size. This sample is analogous in appearance to WP terminology’s Domino/Lower Sandstone (Figure 6). Pyrite is sole sulfide present, abundant and fine-grained.

**CF-1A**, 2.0 m above base

This sample shows igneous and cherty clasts in c.g. siltstone as gray red laminae, thick, alternate with gradationally bounded dark red f.g./m.g. silt laminae, crossbedded. Significant, nearly pervasive fracture dominates this sample, which is analogous to WP terminology's Domino/Lower Sandstone (Figure 6), and is 100% sandstone.

*Little Iron River Outcrop*

The LIR samples were collected at regular intervals between the top of the Copper Harbor Formation and the top of the Parting Sandstone of WP nomenclature, ascending from LIR-2.

**LIR-10**, Uppermost lower Nonesuch Formation

This is black, massive shale. Largely massive siltstone in thin section shows 3 discontinuous crudely laminar FOM in concordant concentrations of opaque black (TAI = 3.9) material. No Cu minerals are apparent.

**LIR-9**

As in Figure 6, this is the Stripey bed of WP nomenclature, a calcareous black to dark gray thickly interlaminated siltstone with lesser shale. Faint ripple lamination are present in thin section, as cuspate clay-rich laminae thin above projecting quartzose convex-up f.g. siltstone laminations, in lower right 1/10 of thin section. Orange brown (TAI = 2.8) amorphous organic matter is distinctly present as lamellar, translucent and largely bedding-concordant material, in association with silt-size laminations. Filamentous organic matter is rare but present as brown faintly translucent material with TAI = 3.2. No Cu minerals are apparent in thin section.

### LIR-8

This is a gray siltstone, massive to very thinly laminated. Continuous even parallel clay rich thin laminations show rare FOM (black, opaque, TAI = 3.9, with v.f.g. pyrite intimately associated) as well as lamellar translucent brown AOM also with strong pyrite association (TAI = 3.2). No Cu minerals are apparent in thin section.

### LIR-6

This is a calcareous, thinly laminated gray siltstone with thin dark gray shale interlaminations. Organic matter is filamentous and lamellar, concentrated in concordant forms, faintly translucent and isotropic with dark brown color (TAI = 3.8), strong association to v.f.g. pyrite; AOM also present in association with FOM, as transparent brown (TAI = 3.2) lamination-concordant masses. Lenticular, calcite-rich laminations show prominent m.g. subhedral calcite crystals, which in places offset FOM and AOM. In places calcite-rich zones bound organic material, with some disruption and displacement of segments of the organic rich laminae. No Cu minerals in thin section.

### LIR-5

This is massive siltstone with one faint, very crudely laminated bedding plane which shows clay and OM concentrations about subrounded quartz grains - probable rip-ups. Faintly opaque to translucent FOM present as wavy wisps of dark brown silicate-enveloping wisps of wavy/anastomose/inosculate agglomerations (TAI = 3.8). No Cu minerals apparent, with pyrite common as f.g. subhedral grains.

### LIR-4

This sample shows wavy contorted laminations in clay-fraction dominant zones that conform to siltstone laminations that are sometimes sausage-shaped - likely compactional lode structures. Organic matter is mostly present as amorphous discontinuous translucent isotropic lamellar concentrations, brown (TAI = 3.2), and concurrent with v.f.g. concentrations of phyllosilicates. Black FOM (TAI = 3.9) is also present as rare thin wavy isotropic opaque wisps. Hematite coated m.g. silt size quartz grains present as rare subangular red translucent anisotropic bodies. Cu minerals not present in thin section.

### LIR-3

This is a rock with gently undulating gray clay-rich thin laminations in light gray siltstone (thicker laminae). It shows breached phyllosilicate-rich v.f.g. shaley laminations in thin section, as photographed. Significant detrital chlorite is present, and 1% of grains are hematite coated quartz. Organic matter is not apparent in thin section. Chalcocite is present as rare v.f.g. subhedral grains, shown adjacent to yellow reflecting anisotropic mass of opaque chalcopyrite.

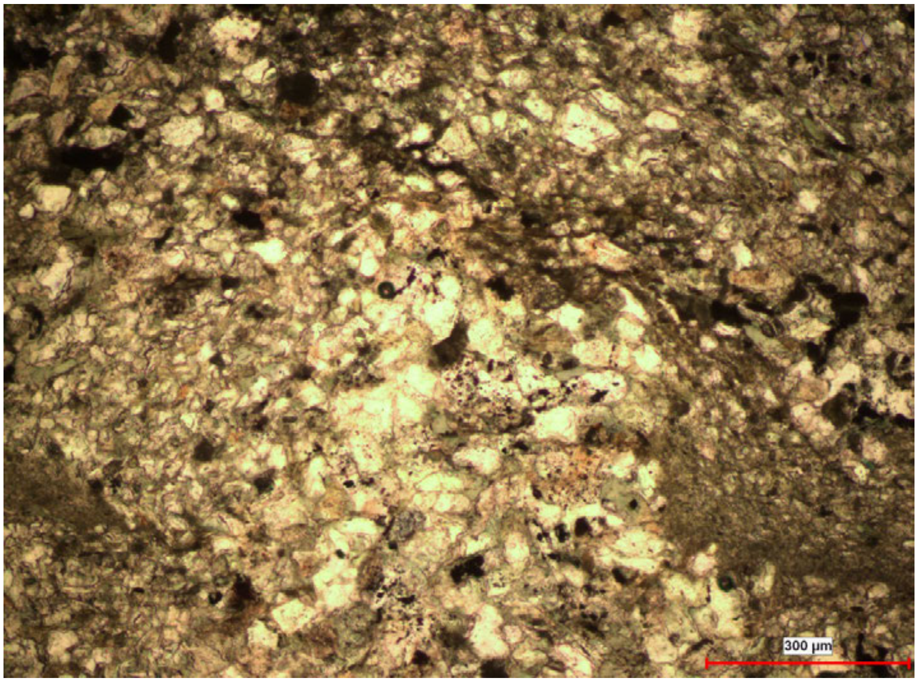

Figure A59: V.f.g. phyllosilicate-rich shale lamination showing siliciclastic silt-size clastic dike breaching the horizontal shale lamination, PPL.  Sample LIR3.

**LIR-2**, lowest sample (nearest Nonesuch Formation base)

This is Figure 6's parting shale, with native Cu at sample site.  It is a gray silty shale with thin alternate parallel light gray silty and dark gray f.g. silt to shale interlaminae; non-calcareous. Significant detrital hematite-coated quartz grains subangular.  Very rare Cu ore in thin section are chalcocite grains, v.f., subhedral, and intimately associated with yellow reflective probable pyrobitumen (as in photo).  Amorphous organic matter is apparent as brown translucent (TAI = 3.2) isotropic lamellar masses and also, more commonly, as margins of black opaque FOM-rich laminations (TAI = 3.9).  Bituminous, solid, anisotropic faintly translucent brown to dark brown bed-parallel mass with rounded ends fills bed-parallel void space (left by overground fracture fill or v.f.g. interval?).  The zones of greatest opacity and darkest color of this lamellar mass of bitumen coincide with highest reflectance (a faint bluish-gray mottled color).  Bituminous solid material shows higher reflectance along its exterior, with high-reflectance margins verging inward toward center of mass in locations where the vertical dimension thins the most - a "higher reflectance outer layer and a lower reflectance inner core suggesting overprinting by a post-emplacement rapid heating event" (cf. Glikson *et al.*, 2000 in Mastalerz *et al.*, 2000). Shrinkage cracks are apparent at one end of the bitumen mass, suggesting that this is pyrobitumen, which concurs with the anisotropic optical properties of the lamellar mass. Immediately above another set of shrinkage cracks in the bituminous material are multiple discrete agglomerations of chalcocite (initially tarnished to reflect mottled yellow, blue and green).

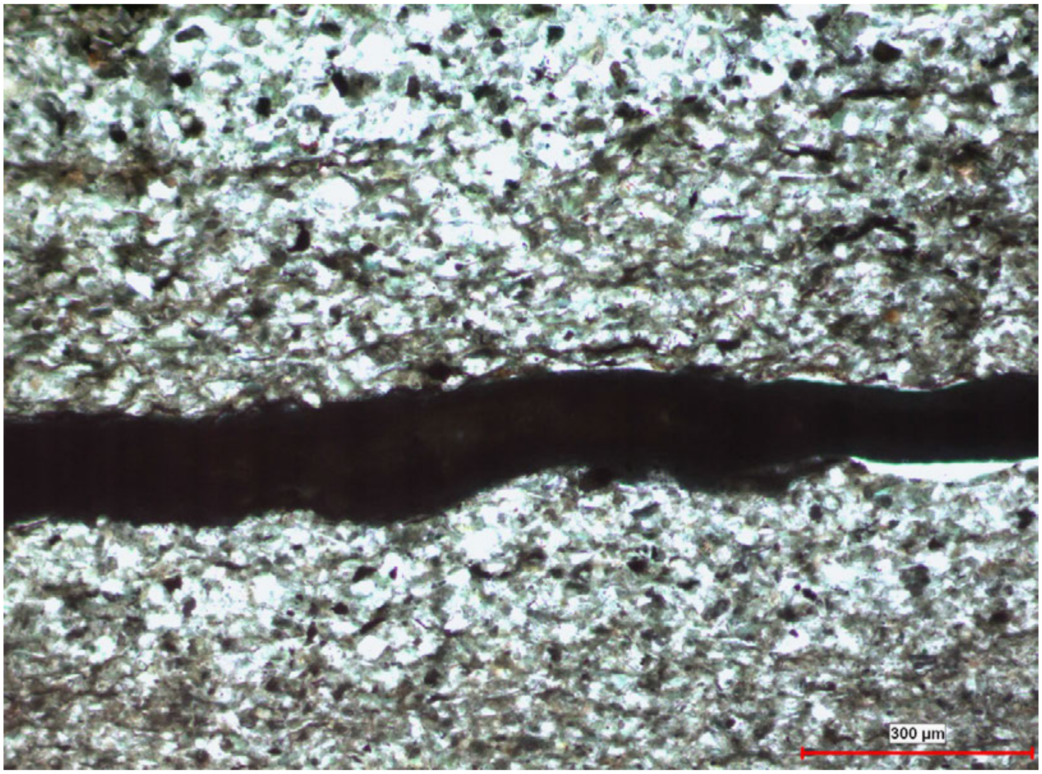

Figure A60: PPL solid bitumen in lamination concordant mass, showing zones of highest bitumen opacity (which are most reflective in next image). Sample LIR2.

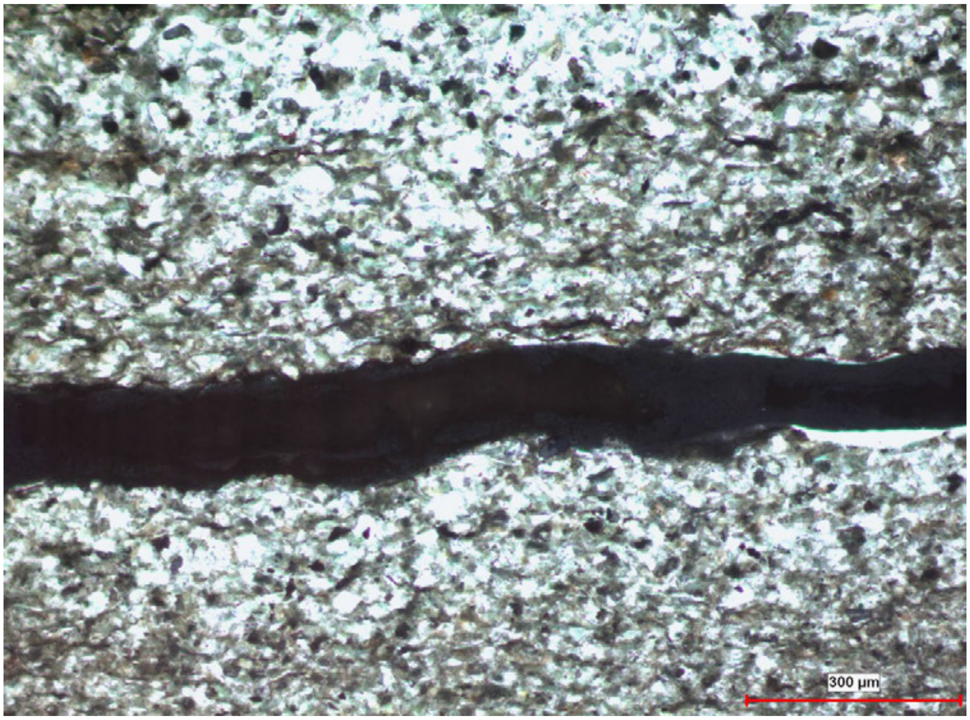

Figure A61: REFL PPL solid bitumen in lamination concordant mass, showing highest reflectivity coincident with highest opacity. Sample LIR 2.

Figure A62: PPL shrinkage cracks are apparent at one end of the solid bitumen mass - which may suggest that this is pyrobitumen, cf. Rasmussen and Buick (2000). Note also the dark gray translucent stain, potentially representing bitumen expelled in association with shrinkage crack contraction. Sample LIR 2.

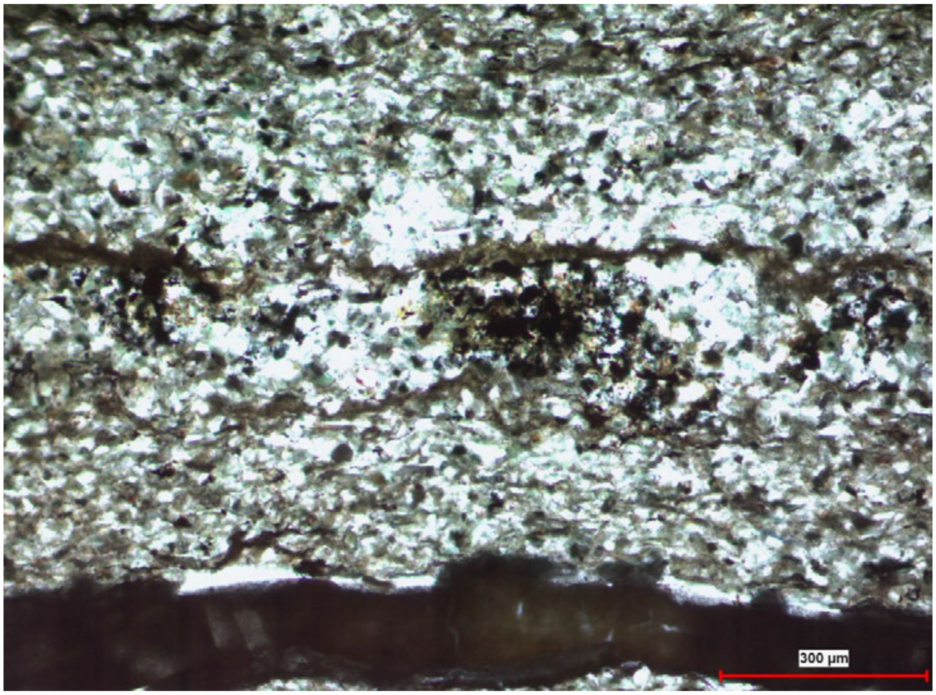

Figure A63: PPL. Immediately above another set of shrinkage cracks in the solid lamellar bituminous material are multiple discrete agglomerations of chalcocite (tarnished). Sample LIR2.

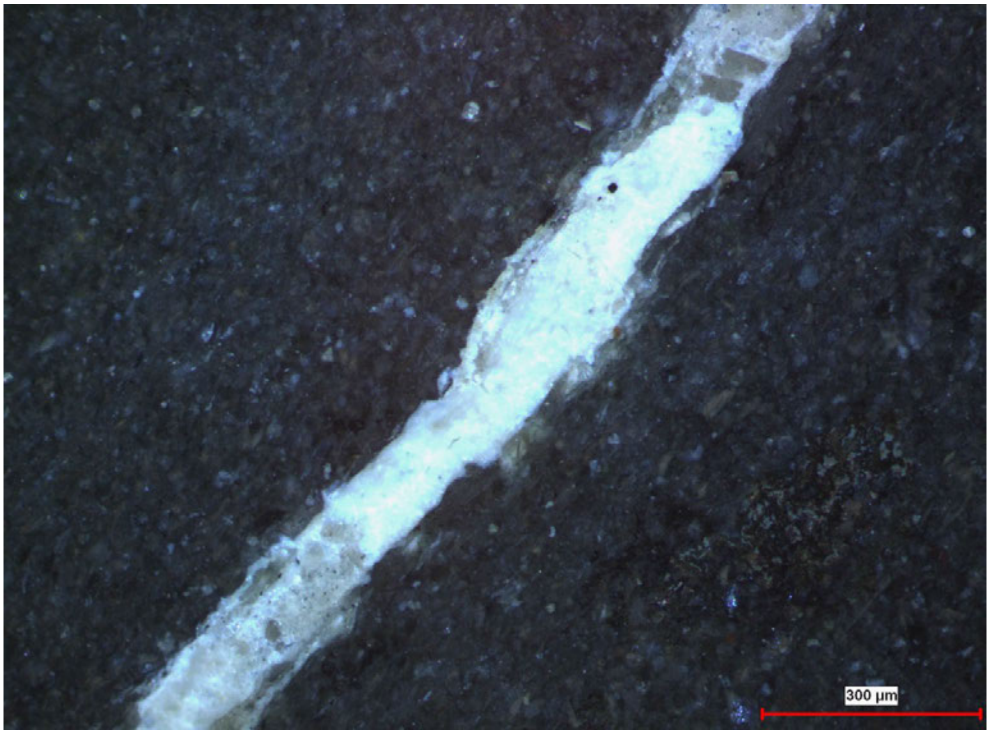

Figure A64: XPL REFL, showing subhedral chalcocite, tarnished (lower right). Sample LIR2. Note also anisotropy of the bituminous lamellar mass, as compared to Figure A65.

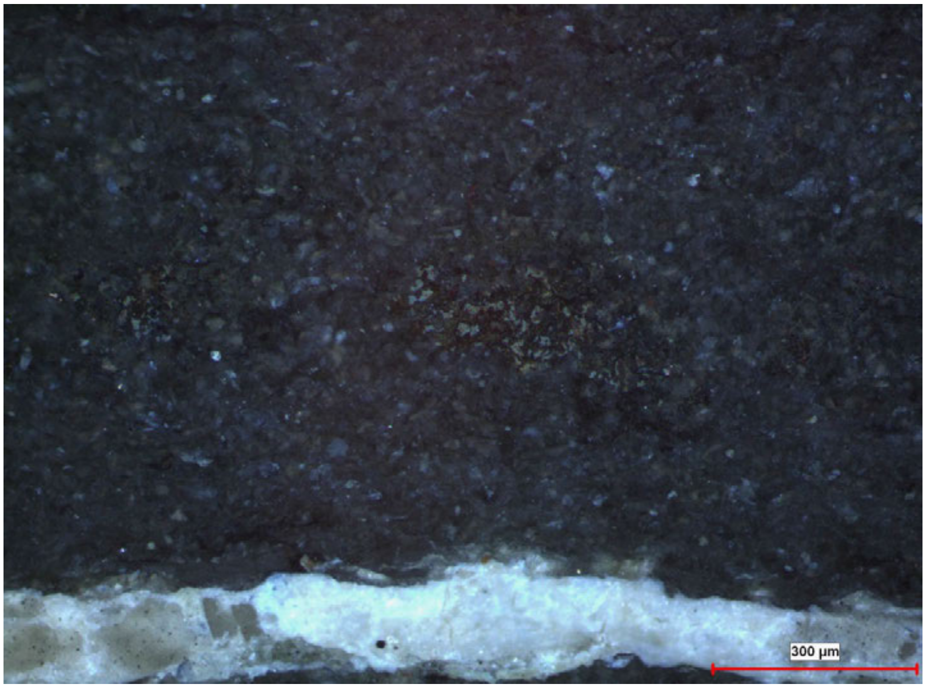

Figure A65: XPL REFL, showing anisotropy of solid bitumen in sample LIR2.

*Big Iron River Outcrop*

**BIR 7**, 700 m downstream from Nonesuch Formation top

This sample is a cross-stratified gray siltstone with wavy to discontinuous laminations that in places show concavity in darker laminae (possibly reflecting wet sediment contortion about more competent silt-size laminae). It is heavily fractured by calcite veins, with chalcocite anhedra as space-filling material (secondary to) between detrital mineral grains. The BIR slides were cut and polished in 2009 and 2010, and some of them contained an orange translucent concentric banded material about chalcocite anhedra - this orange material polished away easily by hand with mild abrasive anti-tarnish compound. The orange material surrounded c.g. anhedral chalcocite and also occupied chalcocite-bearing veins which offset bedding. The mottled reflectivity of such masses extended beyond the radial growths themselves, and occurred on adjacent grains, probably as a thin surface coating. This material is similar in appearance to the "residual petroleum" material described by Barghoorn *et al.* (1965) in transmitted light microscopy as "alternate sharply delineated layers and spheroids of reddish and light amber..HCs exhibiting varying degrees of devolatilization...and frequently arranged in an undulating concentric manner about a mineral center, often chalcocite." After a second polishing, the orange translucent material disappeared; it is debatable whether it was HC residue or a recent biogenic mass. Kerogenous AOM present as amorphous lamellar brown (TAI = 3.2) domains associated with finest-grained black opaque wavy to anastomose laminations. Fracture-filling chlorite about chalcocite grain, and many chalcocite grains distributed in black opaque FOM concentrations (TAI = 3.9), with chalcocite also commonly occurring in association with thin, bedding offsetting, fracture-filling pyrobitumen accumulations oblique to lamination. Medium grained chalcocite also present in silt-size discontinuous quartzose laminations.

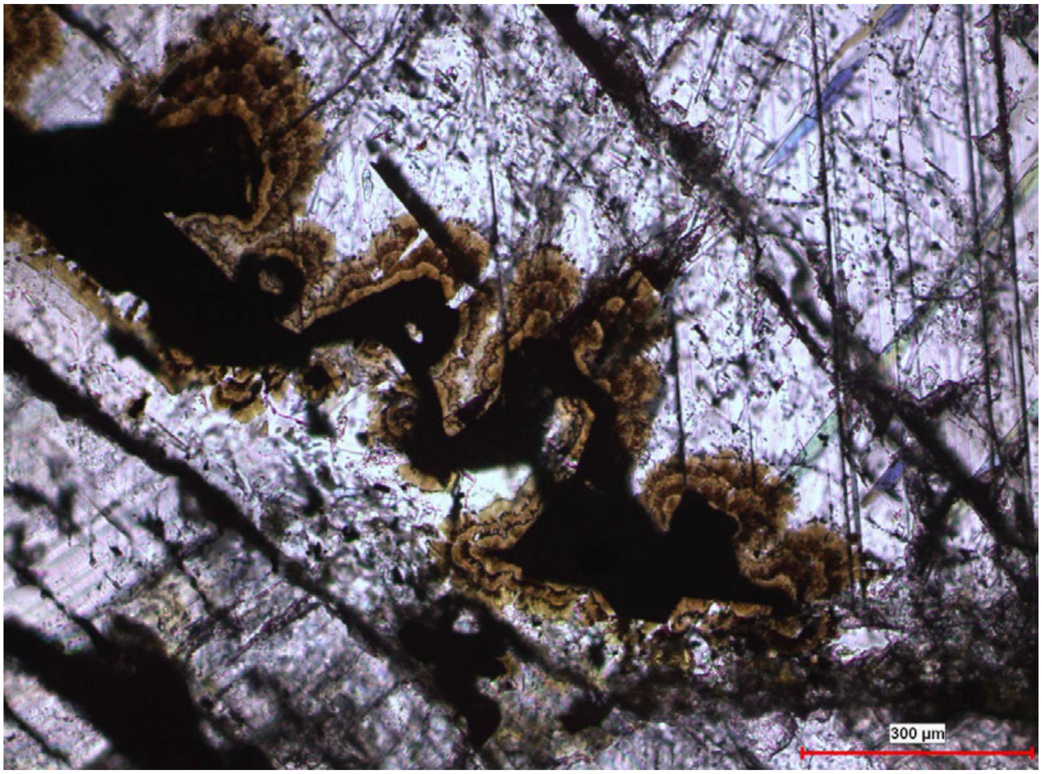

Figure A66: PPL orange banded concentric growths about chalcocite core. Sample BIR 7.

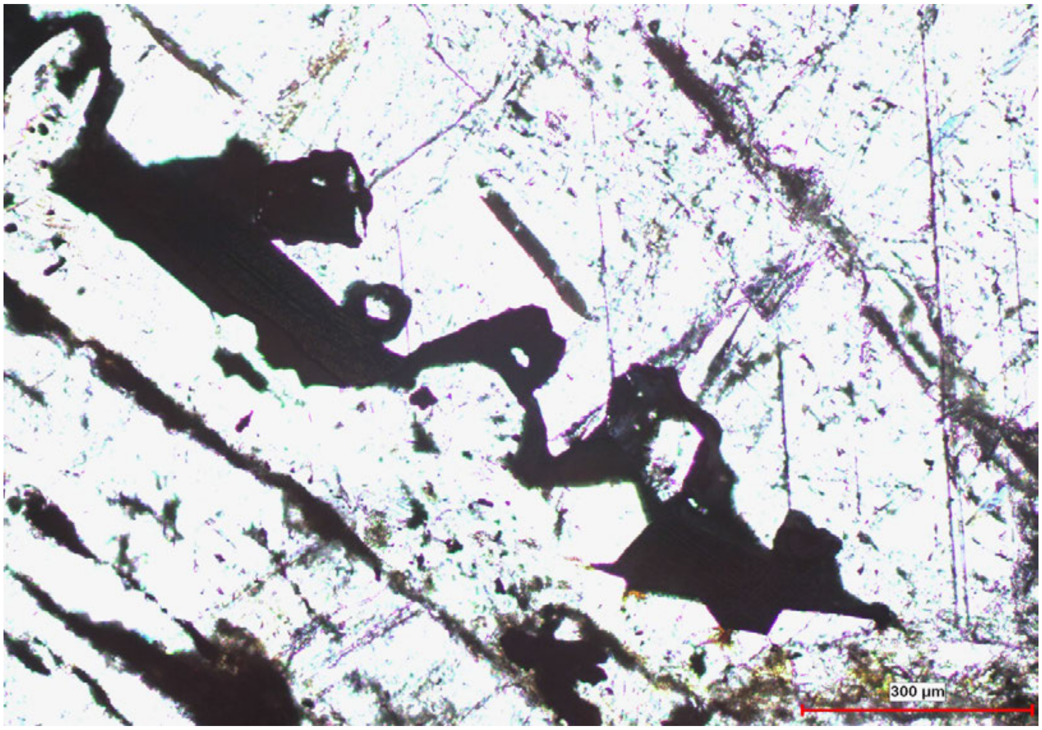

Figure A67: PPL of previous feature, but after removal of orange material by anti-tarnish hand polishing.  Sample BIR 7.

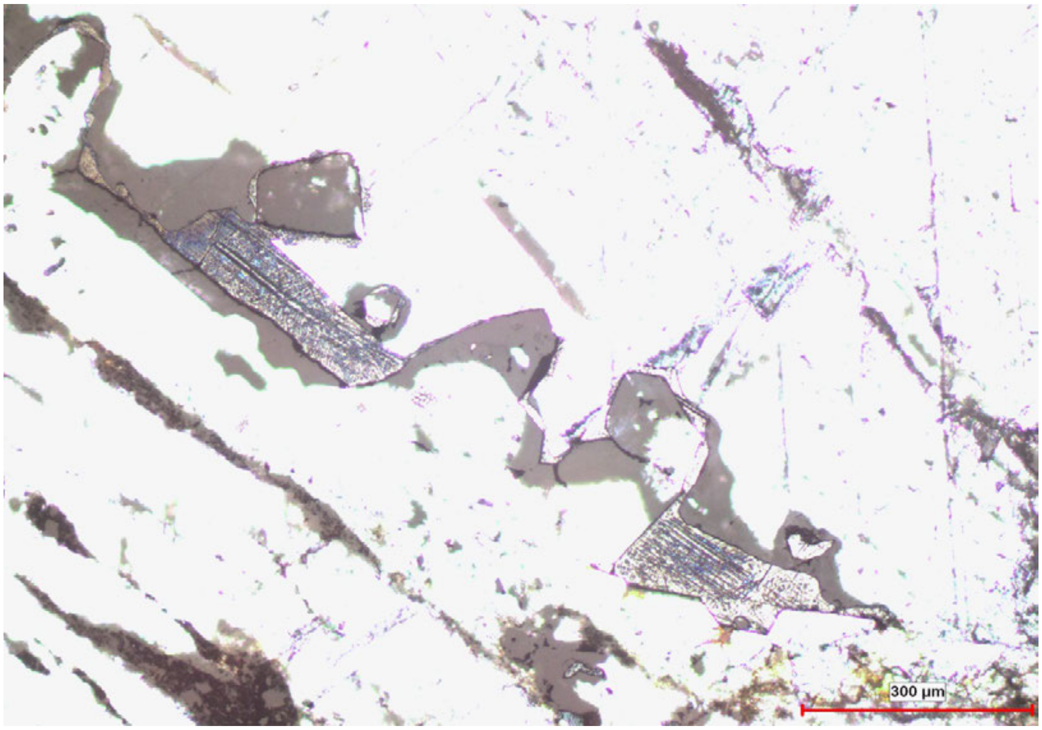

Figure A68: PPL and REFL showing the pyrobitumen/biogenic growth's chalcocite core and reflective nature. Sample BIR 7.

**BIR 8**, 720 m downstream from Nonesuch Formation top

This is a light gray thinly laminated siltstone with thin dark gray even parallel continuous interlaminated shale.  No thin section.

**BIR 10**, 760 m downstream from Nonesuch Formation top

This sample is a brecciated black shale with significant malachite stain, foliated appearance in hand sample, calcareous and pervasively fractured.  Calcite veins disrupt bedding in thin section, showing breached shaley laminae.  Translucent isotropic amorphous bedding concordant lamellar organic matter is brown (TAI = 3.2) but significant FOM is also apparent as wavy opaque accumulations of black (TAI = 3.9) material.  Very large anhedral chalcocite grains present, occupy secondary spaces in the same manner as in BIR 7.  Covellite is present and rare, as v.f.g. anisotropic masses in association with concentrations of chalcocite.  Incipient authigenic chlorite growths are commonly associated with chalcocite and covellite concentrations, in places envelop the Cu sulfides, and chloritic veins and vein margins also apparent.  Filamentous organic matter is apparent in shale clasts as black opaque (TAI = 3.9) lamellar material associated with dark brown AOM, faintly translucent (TAI = 3.8).  Orange to brown in transmitted light (PPL) to mottled bright yellow reflecting, chalcocite-associated concentric banded surficial material (polished away easily by hand, after initial preparation polish), possibly neo-biotic coating, or, possibly, devolatilized bituminous material similar to that of Barghoorn *et al*. (1965).

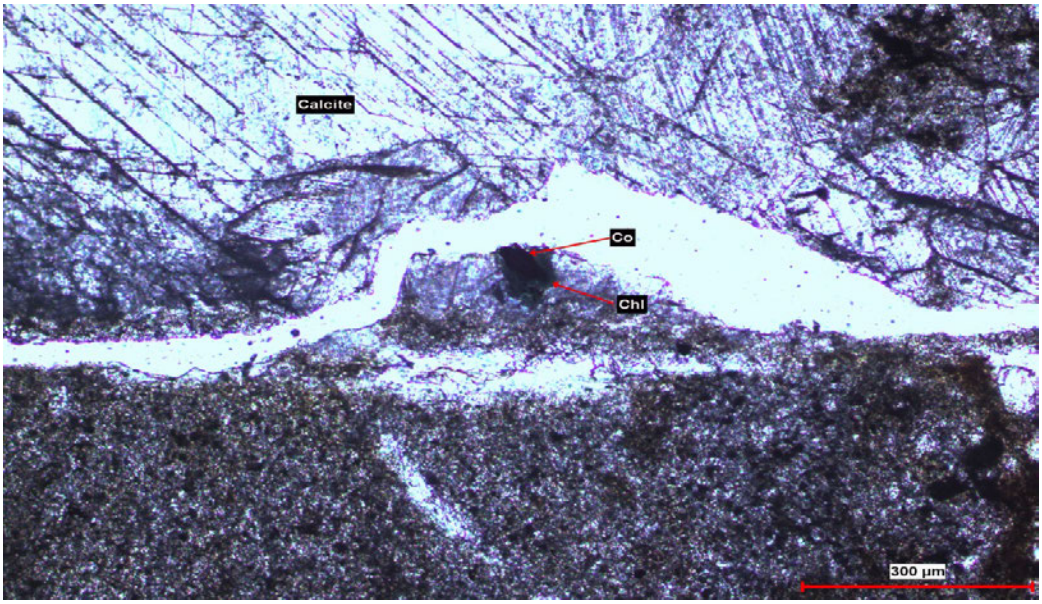

Figure A69: PPL - chlorite partially encasing f.g. covellite (anisotropy) on margin of c.g. calcite vein. Sample BIR 10.

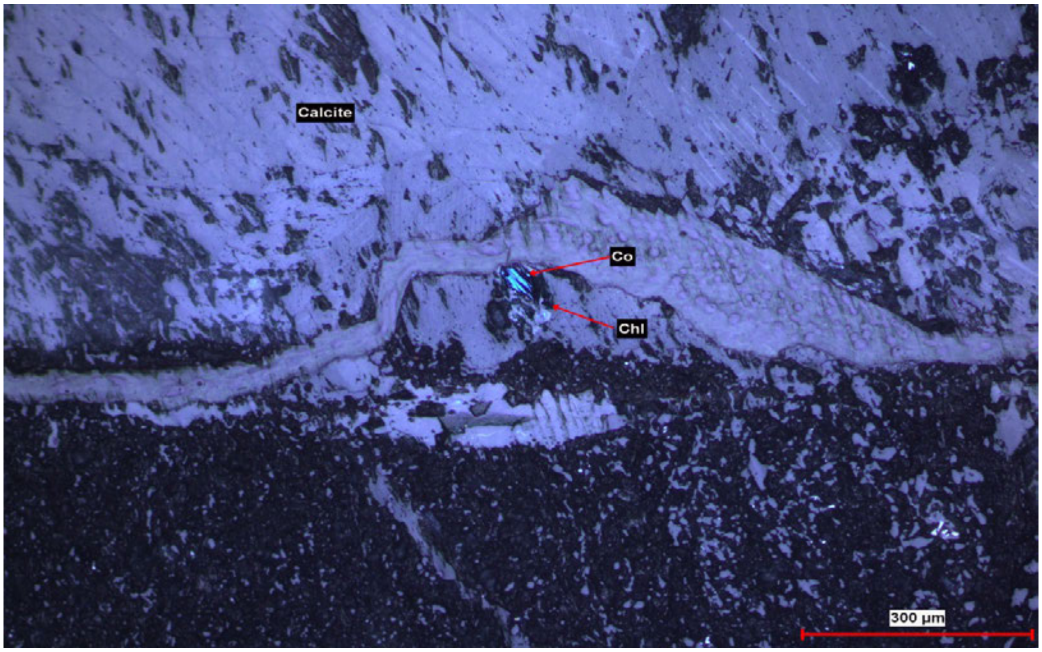

Figure A70: XPL and REFL – chlorite partially encasing an anhedral covellite grain, in association with vein calcite. Sample BIR 10.

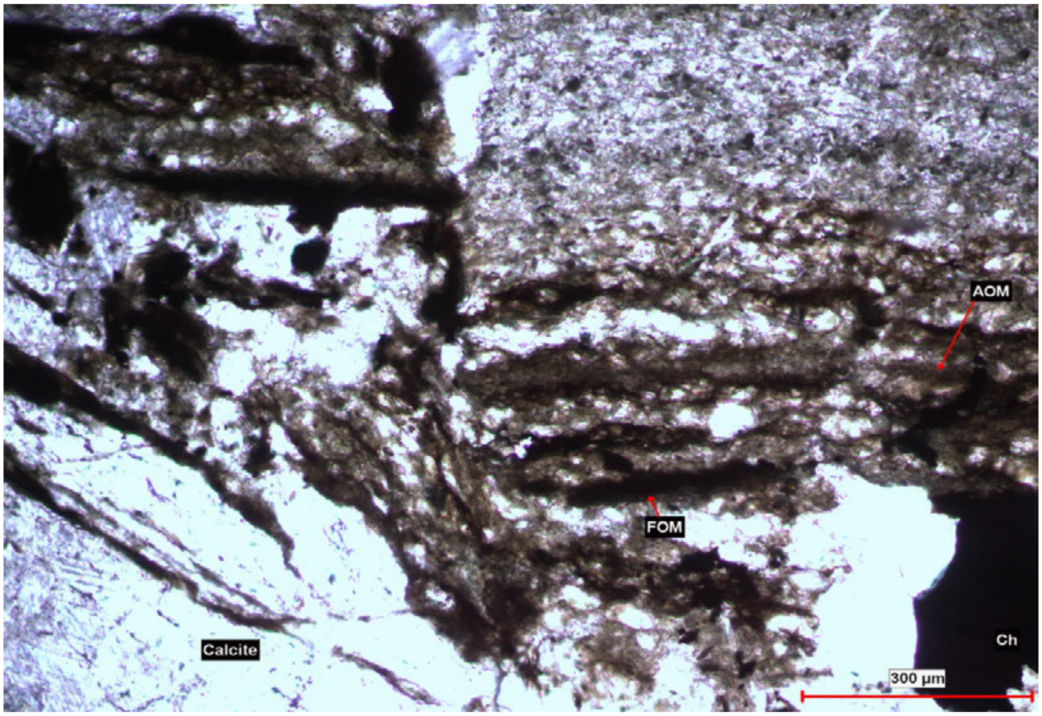

Figure A71: PPL, chalcocite (Ch) grain adjacent to FOM apparent in shale clasts as black opaque (TAI = 3.9) lamellar material associated with dark brown AOM, faintly translucent (TAI = 3.8). Sample BIR 10.

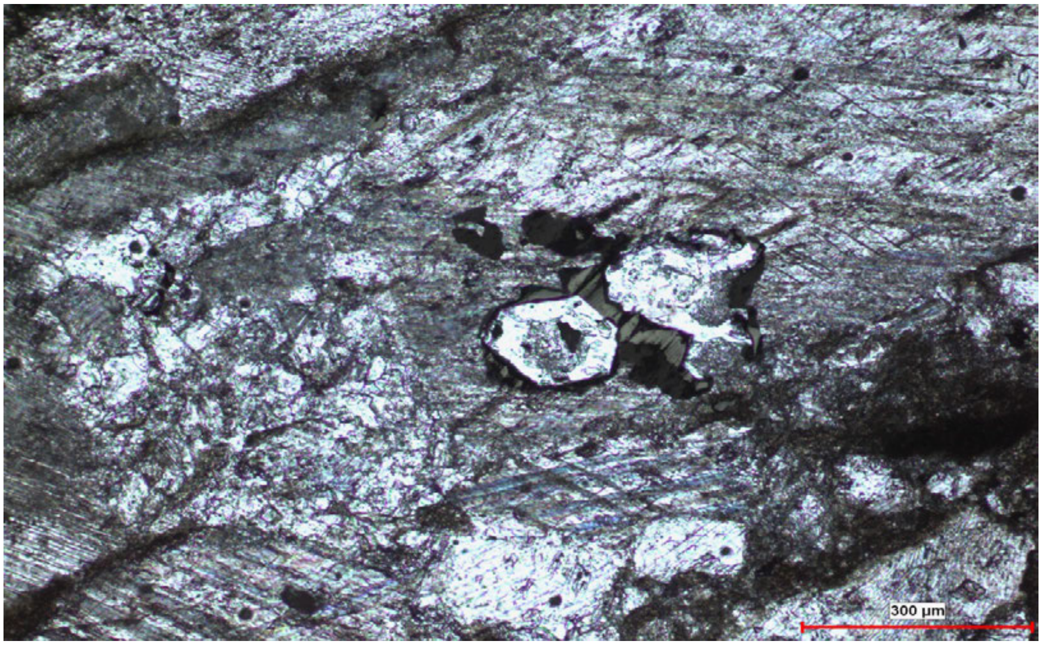

Figure A72: Chalcocite encasing adularia, both suspended in vein calcite, PPL REFL. Sample BIR 10.

**BIR 11**, 800 m downstream from Nonesuch Formation top

This is a gray laminated siltstone with darker gray shale laminae, even and parallel. Syneresis cracks present. Discontinuous, locally disrupted/breached phyllosilicate-rich shale laminations are present, varying in thickness and in places disturbed by calcite blebs. Concave up patterns in shale portion may represent lode structures. Isolated, clay mineral-associated brown lamellar wavy isotropic translucent AOM present, brown (TAI = 3.2), with some possible FOM, also brown and translucent (compacted AOM?) No Cu minerals present, pyrite dominates the opaque reflective fraction.

**BIR 13**, 850 m downstream from Nonesuch Formation top

This is a gray siltstone and interlaminated dark gray shale, ripple-laminated, with bed-concordant phyllosilicates apparent in hand sample; laminations are disrupted by a large (2 x 4 cm) concretion (calcareous). Translucent AOM is intimately associated with v.f.g. clay mineral accumulations (layer parallel aligned); AOM is orange (TAI = 2.55); significant black (TAI = 3.9) opaque lamellar FOM dominates (85% of OM) intimately associated with translucent AOM. Tarnished f.g. chalcocite is widespread as incipient pyrite replacements, some of which show bornite and covellite after chalcocite. This material is analogous to Figure 6’s Top Zone of WP nomenclature.

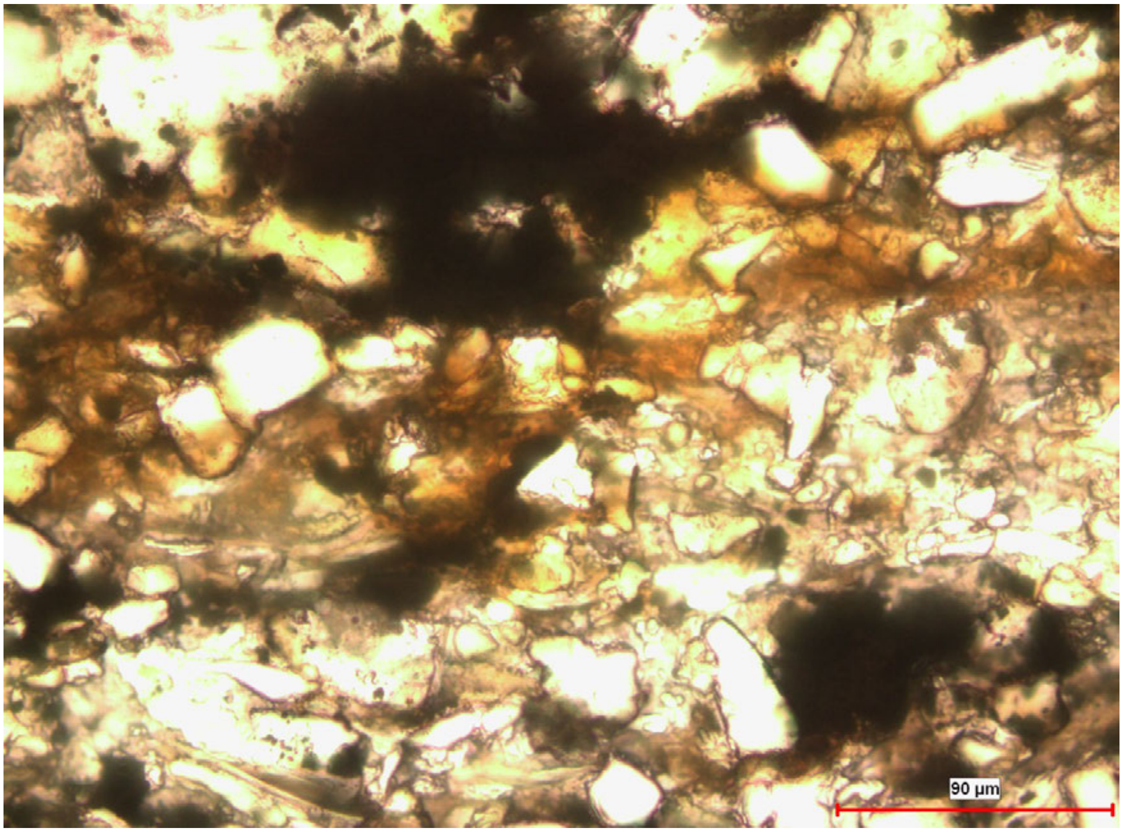

Figure A73: PPL AOM as orange brown (TAI = 2.8) pseudo-lamellar material, in association with pyrite. Sample BIR 13.

**BIR 14**, 850 m downstream from Nonesuch Formation top

This sample was reported by Colbert (2011) as bearing native Cu in the same shale layer as syneresis cracks. It shows cross-bedding and ripple marks in light gray silt layers and dark gray shaley laminae; 65% silt, 35% shale. This sample is analogous to the Top Zone of WP nomenclature (Figure 6). Chalcocite is present, tarnished, widespread, f.g. to m.g., and with bornite/covellite replacements apparent together within individual grains. Rare brown (TAI = 3.2) AOM in association with FOM. FOM is black opaque (TAI = 3.9) wisps most concentrated at silt-shale grain size interfaces, in association with chalcocite. Shaley laminations breached by silty material are apparent but not widespread.

**BIR 15**, 880 m downstream from Nonesuch Formation top

Colbert (2011) described this as a large lithic nodule. The sample is a large concretion of calcareous shale (5 x 5 cm) showing small-scale crossbedding and lenticular discontinuous laminae. This sample is analogous to the dark gray massive of WP nomenclature (Figure 6). It is pyritic, with rare chalcocite incipient replacements. Brown AOM is apparent (TAI = 3.2) as compacted wavy laminar masses distorted about silicate grains - similar appearance to FOM (which is absent).

**BIR 16**, 900 m downstream from Nonesuch Formation top

This sample contains a quartz and calcite vein with pyrite visible in hand sample (Colbert, 2011); fluorescent blue oil inclusions are present with homogenization temperature reported as 159° C. This is the Marker Bed of Figure 6. Pyrite as widespread disseminated f.g. subhedra commonly rounded, with some framboids, many of which show incipient chalcocite replacement. Brown AOM is apparent (TAI = 3.2) as compacted wavy laminar masses distorted about silicate grains - similar appearance to FOM (which is absent).

## *Appendix B: Sample and Analysis Listing*

The listing at each locality is from stratigraphic base to top. Stratigraphic heights for outcrop sections are estimated from dip, deviation from perpendicular transect, and distance from a contact of the Nonesuch Formation and are shown in italics. Informal stratigraphic units within the Nonesuch Formation are given where they can be identified and are indicated with UPPER CASE. The units follow schemes developed by the White Pine Mine staff (e.g. Ensign, *et al*., 1968) and for the Copperwood Project (Bornhorst and Williams, 2013).

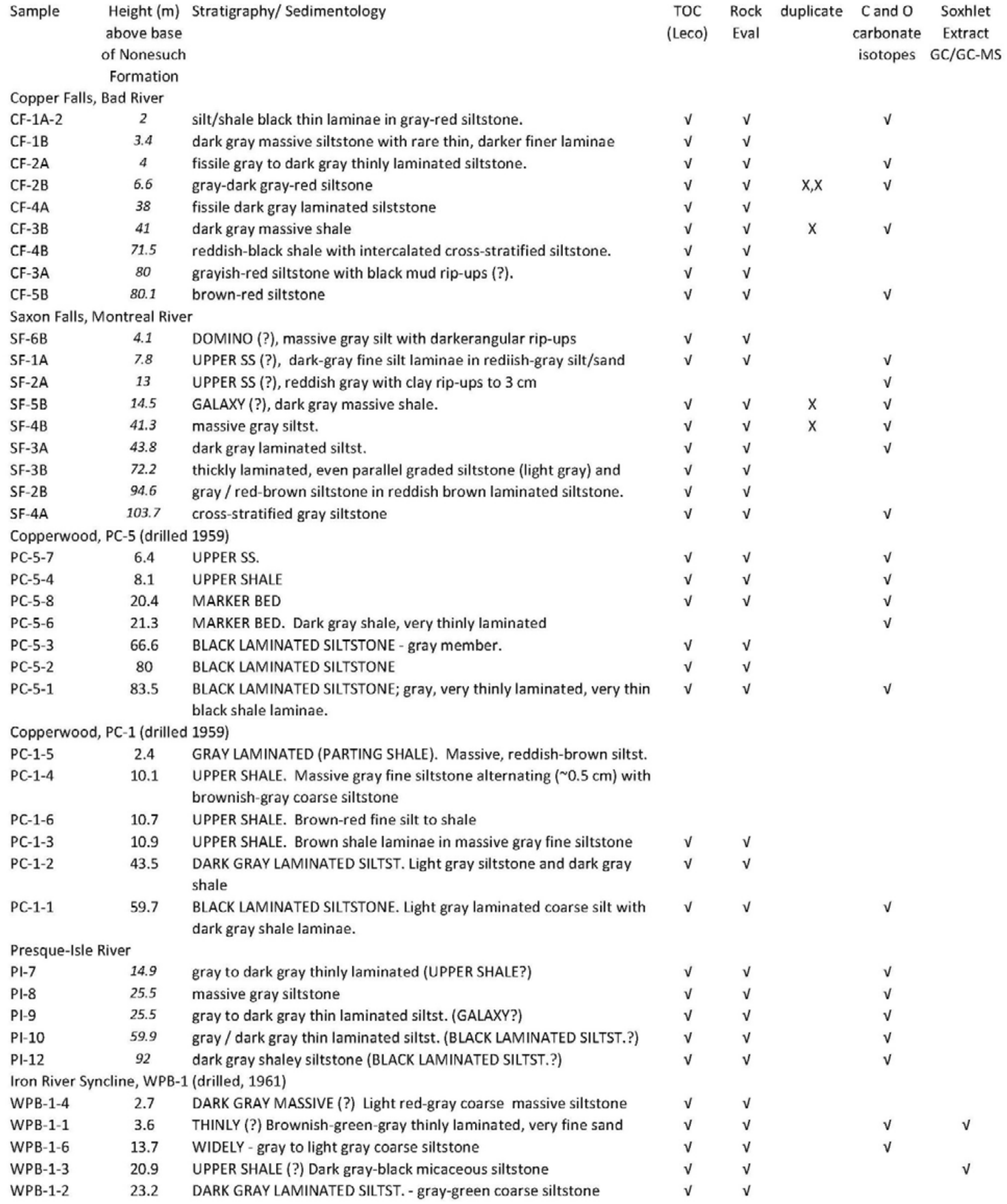

| Sample | Height (m) above base of Nonesuch Formation | Stratigraphy/ Sedimentology | TOC (Leco) | Rock Eval | duplicate | C and O carbonate isotopes | Soxhlet Extract GC/GC-MS |
|---|---|---|---|---|---|---|---|
| Copper Falls, Bad River | | | | | | | |
| CF-1A-2 | *2* | silt/shale black thin laminae in gray-red siltstone. | √ | √ | | √ | |
| CF-1B | *3.4* | dark gray massive siltstone with rare thin, darker finer laminae | √ | √ | | | |
| CF-2A | *4* | fissile gray to dark gray thinly laminated siltstone. | √ | √ | | √ | |
| CF-2B | *6.6* | gray-dark gray-red siltsone | √ | √ | X,X | √ | |
| CF-4A | *38* | fissile dark gray laminated silststone | √ | √ | | | |
| CF-3B | *41* | dark gray massive shale | √ | √ | X | √ | |
| CF-4B | *71.5* | reddish-black shale with intercalated cross-stratified siltstone. | √ | √ | | | |
| CF-3A | *80* | grayish-red siltstone with black mud rip-ups (?). | √ | √ | | | |
| CF-5B | *80.1* | brown-red siltstone | √ | √ | | √ | |
| Saxon Falls, Montreal River | | | | | | | |
| SF-6B | *4.1* | DOMINO (?), massive gray silt with darkerangular rip-ups | √ | √ | | | |
| SF-1A | *7.8* | UPPER SS (?), dark-gray fine silt laminae in rediish-gray silt/sand | √ | √ | | √ | |
| SF-2A | *13* | UPPER SS (?), reddish gray with clay rip-ups to 3 cm | | | | √ | |
| SF-5B | *14.5* | GALAXY (?), dark gray massive shale. | √ | √ | X | √ | |
| SF-4B | *41.3* | massive gray siltst. | √ | √ | X | √ | |
| SF-3A | *43.8* | dark gray laminated siltst. | √ | √ | | √ | |
| SF-3B | *72.2* | thickly laminated, even parallel graded siltstone (light gray) and | √ | √ | | | |
| SF-2B | *94.6* | gray / red-brown siltstone in reddish brown laminated siltstone. | √ | √ | | | |
| SF-4A | *103.7* | cross-stratified gray siltstone | √ | √ | | √ | |
| Copperwood, PC-5 (drilled 1959) | | | | | | | |
| PC-5-7 | 6.4 | UPPER SS. | √ | √ | | √ | |
| PC-5-4 | 8.1 | UPPER SHALE | √ | √ | | √ | |
| PC-5-8 | 20.4 | MARKER BED | √ | √ | | √ | |
| PC-5-6 | 21.3 | MARKER BED. Dark gray shale, very thinly laminated | | | | √ | |
| PC-5-3 | 66.6 | BLACK LAMINATED SILTSTONE - gray member. | √ | √ | | | |
| PC-5-2 | 80 | BLACK LAMINATED SILTSTONE | √ | √ | | | |
| PC-5-1 | 83.5 | BLACK LAMINATED SILTSTONE; gray, very thinly laminated, very thin black shale laminae. | √ | √ | | √ | |
| Copperwood, PC-1 (drilled 1959) | | | | | | | |
| PC-1-5 | 2.4 | GRAY LAMINATED (PARTING SHALE). Massive, reddish-brown siltst. | | | | | |
| PC-1-4 | 10.1 | UPPER SHALE. Massive gray fine siltstone alternating (~0.5 cm) with brownish-gray coarse siltstone | | | | | |
| PC-1-6 | 10.7 | UPPER SHALE. Brown-red fine silt to shale | | | | | |
| PC-1-3 | 10.9 | UPPER SHALE. Brown shale laminae in massive gray fine siltstone | √ | √ | | | |
| PC-1-2 | 43.5 | DARK GRAY LAMINATED SILTST. Light gray siltstone and dark gray shale | √ | √ | | | |
| PC-1-1 | 59.7 | BLACK LAMINATED SILTSTONE. Light gray laminated coarse silt with dark gray shale laminae. | √ | √ | | √ | |
| Presque-Isle River | | | | | | | |
| PI-7 | *14.9* | gray to dark gray thinly laminated (UPPER SHALE?) | √ | √ | | √ | |
| PI-8 | *25.5* | massive gray siltstone | √ | √ | | √ | |
| PI-9 | *25.5* | gray to dark gray thin laminated siltst. (GALAXY?) | √ | √ | | √ | |
| PI-10 | *59.9* | gray / dark gray thin laminated siltst. (BLACK LAMINATED SILTST.?) | √ | √ | | √ | |
| PI-12 | *92* | dark gray shaley siltstone (BLACK LAMINATED SILTST.?) | √ | √ | | √ | |
| Iron River Syncline, WPB-1 (drilled, 1961) | | | | | | | |
| WPB-1-4 | 2.7 | DARK GRAY MASSIVE (?) Light red-gray coarse massive siltstone | √ | √ | | | |
| WPB-1-1 | 3.6 | THINLY (?) Brownish-green-gray thinly laminated, very fine sand | √ | √ | | √ | √ |
| WPB-1-6 | 13.7 | WIDELY - gray to light gray coarse siltstone | √ | √ | | √ | |
| WPB-1-3 | 20.9 | UPPER SHALE (?) Dark gray-black micaceous siltstone | √ | √ | | | √ |
| WPB-1-2 | 23.2 | DARK GRAY LAMINATED SILTST. - gray-green coarse siltstone | √ | √ | | | |

*Appendix B, ctd.*

| Sample | Height (m) above base of Nonesuch Formation | Stratigraphy/ Sedimentology | TOC (Leco) | Rock Eval | duplicate | C and O carbonate isotopes | Soxhlet Extract GC/GC-MS |
|---|---|---|---|---|---|---|---|
| WPB-1-7 | 49.9 | gray - red-brown interbedded siltstone (with black mudstone | √ | √ | | | |
| WPB-1-5 | 100 | light gray - dark gray laminated siltstone | √ | √ | | √ | |
| Little Iron River, Silver City | | | | | | | |
| LIR-2 | *0.8* | PARTING SHALE | √ | | | | |
| LIR-3 | *5* | UPPER SHALE | √ | | | | |
| LIR-4 | *9* | UPPER SHALE. Massive gray siltst., non-calcareous | √ | | | | |
| LIR-6 | *13* | UPPER SHALE. Massive gray siltst. | √ | √ | | | |
| LIR-10 | *17* | UPPER SHALE. Massive gray siltst. | √ | | | | |
| Big Iron River, Silver City | | | | | | | |
| BIR-16 | *4.5* | DOMINO (PARTING SHALE). Dark gray green, thinly laminated | √ | √ | | | √ |
| BIR-15 | *13* | DARK GRAY MASSIVE, calcareous concretion 4x4x2 cm | √ | √ | | | √ |
| BIR-14 | *18* | TOP ZONE, light gray silt, discontinuous dark gray shale laminae. | √ | √ | | | |
| BIR-13 | *19* | TOP ZONE, coarse gray silt with fine shaley laminae | √ | √ | | | √ |
| BIR-11 | *32* | gray laminated siltstone, showing syneresis cracks | √ | √ | | | |
| BIR-10 | *39* | black shale | √ | √ | | | |
| BIR-8 | *44* | light gray laminated siltstone | √ | √ | | | |
| BIR-7 | *48* | cross-stratified gray siltstone, finely laminated | √ | √ | | | |
| White Pine, 28G (drilled 1965) | | | | | | | |
| 28G-572 | 0.5 | DOMINO | √ | | | | |
| 28G-571 | 1 | RED MASSIVE; massive shale | √ | | | | |
| 28G-539 | 11 | UPPER SHALE (massive gray, pyritiferous.) | | | | | |
| 28G-520 | 17 | MARKER BED | √ | √ | | | |
| 28G-514 | 19 | MARKER BED | √ | √ | | | |
| White Pine, 517 (drilled 1995) | | | | | | | |
| 517-6 | 0.5 | DOMINO; thinly laminated green-gray fine silt and light gray to gray-black coarse siltstone | √ | √ | | | |
| 517-5 | 3.2 | RED MASSIVE; brown-gray, massive coarse silt with black laminae | √ | √ | | | |
| 517-2 | 4.8 | UPPER SAND; massive light gray siltstone | √ | √ | | √ | |
| 517-1.5 | 9.8 | BROWN MASSIVE (?) dark gray-green coarse micaceous siltstone. | √ | √ | | | |
| 517-4 | 11.1 | WIDELY; Massive gray siltstone | √ | √ | | | |
| 517-2.5 | 19.5 | UPPER SHALE; dark gray laminated siltstone | √ | √ | | | √ |
| 517-3 | 22.1 | GALAXY; black laminated siltstone and shale | √ | √ | | | √ |
| 517-1 | 206.7 | gray laminated siltst | √ | √ | | √ | |
| White Pine, 523 (drilled 1995) | | | | | | | |
| 523-5 | 1 | DOMINO; light gray-green massive siltstone | √ | √ | | | |
| 523-2 | 3.7 | UPPER TRANSITION; wispy black thin laminations in dark gray siltstone | √ | √ | | √ | |
| 523-3 | 15.9 | STRIPEY; dark gray shaley siltstone. | √ | √ | | √ | √ |
| 523-1 | 17.3 | MARKER BED; dark gray thinly laminated siltstone with gray-black shale laminae. | √ | √ | | √ | √ |
| 523-4 | 21.3 | GALAXY; lenticular fine black silt in gray very fine sandstone. | √ | √ | | | |
| 523-6 | 44.3 | gray massive siltstone, subhedral pyrites | √ | √ | | | |
| 523-7 | 59.5 | gray / red brown siltst. | | | | √ | |

## *Appendix C: Locality, Field, and Prior Core Log Sample Descriptions*

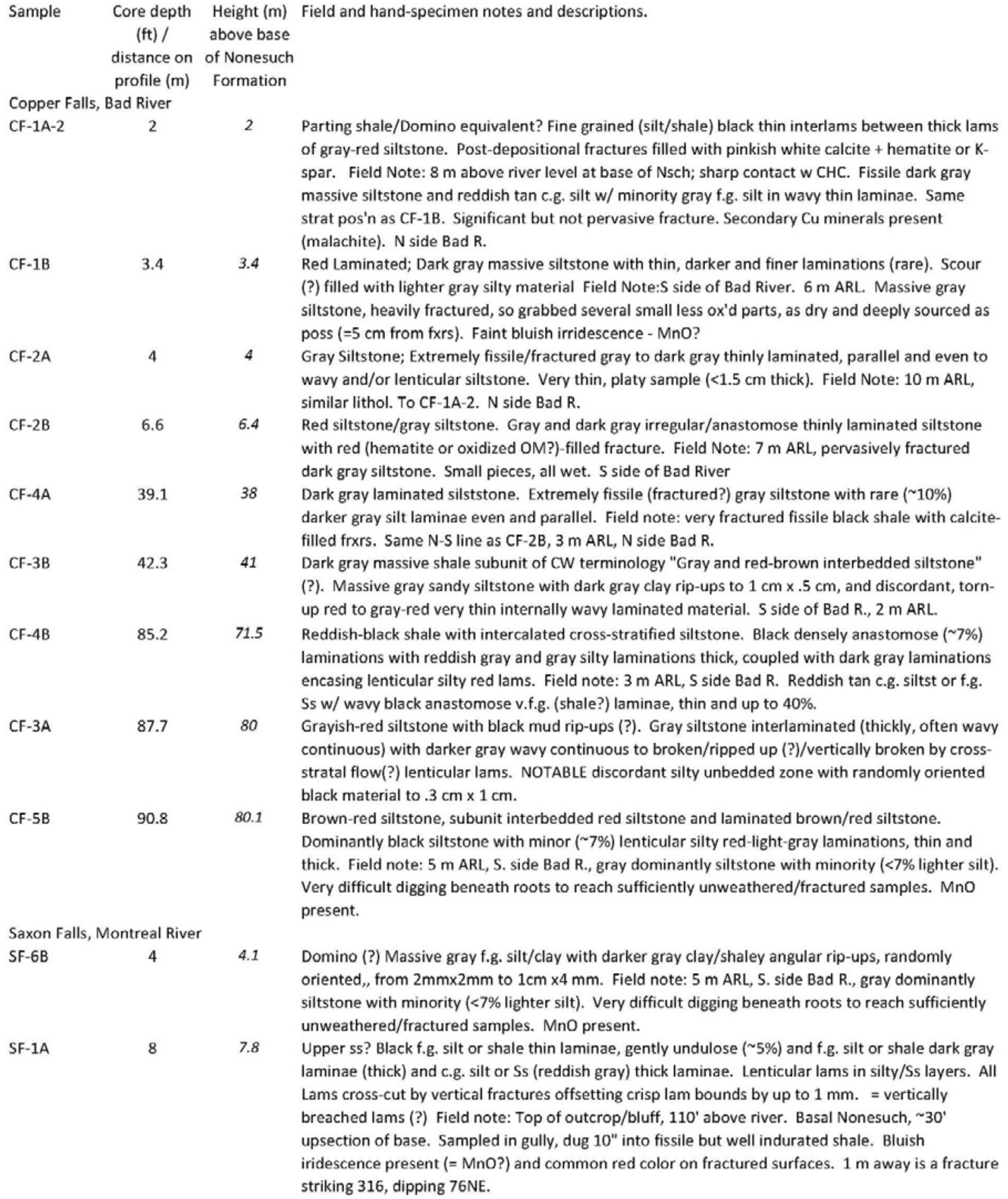

| Sample | Core depth (ft) / distance on profile (m) | Height (m) above base of Nonesuch Formation | Field and hand-specimen notes and descriptions. |
|---|---|---|---|
| Copper Falls, Bad River | | | |
| CF-1A-2 | 2 | *2* | Parting shale/Domino equivalent? Fine grained (silt/shale) black thin interlams between thick lams of gray-red siltstone. Post-depositional fractures filled with pinkish white calcite + hematite or K-spar. Field Note: 8 m above river level at base of Nsch; sharp contact w CHC. Fissile dark gray massive siltstone and reddish tan c.g. silt w/ minority gray f.g. silt in wavy thin laminae. Same strat pos'n as CF-1B. Significant but not pervasive fracture. Secondary Cu minerals present (malachite). N side Bad R. |
| CF-1B | 3.4 | *3.4* | Red Laminated; Dark gray massive siltstone with thin, darker and finer laminations (rare). Scour (?) filled with lighter gray silty material Field Note:S side of Bad River. 6 m ARL. Massive gray siltstone, heavily fractured, so grabbed several small less ox'd parts, as dry and deeply sourced as poss (=5 cm from fxrs). Faint bluish irridescence - MnO? |
| CF-2A | 4 | *4* | Gray Siltstone; Extremely fissile/fractured gray to dark gray thinly laminated, parallel and even to wavy and/or lenticular siltstone. Very thin, platy sample (<1.5 cm thick). Field Note: 10 m ARL, similar lithol. To CF-1A-2. N side Bad R. |
| CF-2B | 6.6 | *6.4* | Red siltstone/gray siltstone. Gray and dark gray irregular/anastomose thinly laminated siltstone with red (hematite or oxidized OM?)-filled fracture. Field Note: 7 m ARL, pervasively fractured dark gray siltstone. Small pieces, all wet. S side of Bad River |
| CF-4A | 39.1 | *38* | Dark gray laminated silststone. Extremely fissile (fractured?) gray siltstone with rare (~10%) darker gray silt laminae even and parallel. Field note: very fractured fissile black shale with calcite-filled frxrs. Same N-S line as CF-2B, 3 m ARL, N side Bad R. |
| CF-3B | 42.3 | *41* | Dark gray massive shale subunit of CW terminology "Gray and red-brown interbedded siltstone" (?). Massive gray sandy siltstone with dark gray clay rip-ups to 1 cm x .5 cm, and discordant, torn-up red to gray-red very thin internally wavy laminated material. S side of Bad R., 2 m ARL. |
| CF-4B | 85.2 | *71.5* | Reddish-black shale with intercalated cross-stratified siltstone. Black densely anastomose (~7%) laminations with reddish gray and gray silty laminations thick, coupled with dark gray laminations encasing lenticular silty red lams. Field note: 3 m ARL, S side Bad R. Reddish tan c.g. siltst or f.g. Ss w/ wavy black anastomose v.f.g. (shale?) laminae, thin and up to 40%. |
| CF-3A | 87.7 | *80* | Grayish-red siltstone with black mud rip-ups (?). Gray siltstone interlaminated (thickly, often wavy continuous) with darker gray wavy continuous to broken/ripped up (?)/vertically broken by cross-stratal flow(?) lenticular lams. NOTABLE discordant silty unbedded zone with randomly oriented black material to .3 cm x 1 cm. |
| CF-5B | 90.8 | *80.1* | Brown-red siltstone, subunit interbedded red siltstone and laminated brown/red siltstone. Dominantly black siltstone with minor (~7%) lenticular silty red-light-gray laminations, thin and thick. Field note: 5 m ARL, S. side Bad R., gray dominantly siltstone with minority (<7% lighter silt). Very difficult digging beneath roots to reach sufficiently unweathered/fractured samples. MnO present. |
| Saxon Falls, Montreal River | | | |
| SF-6B | 4 | *4.1* | Domino (?) Massive gray f.g. silt/clay with darker gray clay/shaley angular rip-ups, randomly oriented,, from 2mmx2mm to 1cm x4 mm. Field note: 5 m ARL, S. side Bad R., gray dominantly siltstone with minority (<7% lighter silt). Very difficult digging beneath roots to reach sufficiently unweathered/fractured samples. MnO present. |
| SF-1A | 8 | *7.8* | Upper ss? Black f.g. silt or shale thin laminae, gently undulose (~5%) and f.g. silt or shale dark gray laminae (thick) and c.g. silt or Ss (reddish gray) thick laminae. Lenticular lams in silty/Ss layers. All Lams cross-cut by vertical fractures offsetting crisp lam bounds by up to 1 mm. = vertically breached lams (?) Field note: Top of outcrop/bluff, 110' above river. Basal Nonesuch, ~30' upsection of base. Sampled in gully, dug 10" into fissile but well indurated shale. Bluish iridescence present (= MnO?) and common red color on fractured surfaces. 1 m away is a fracture striking 316, dipping 76NE. |

*Appendix C, ctd.*

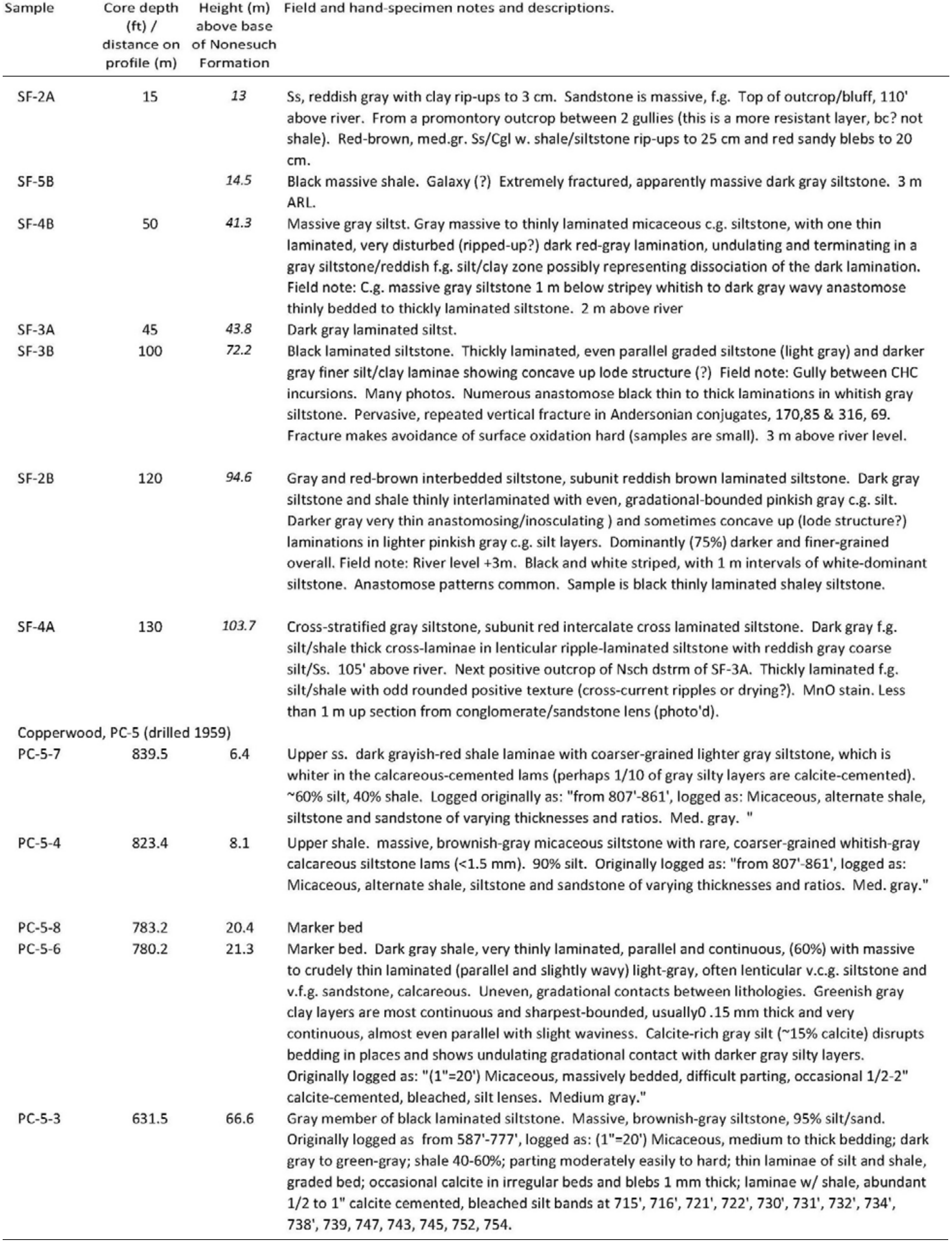

| Sample | Core depth (ft) / distance on profile (m) | Height (m) above base of Nonesuch Formation | Field and hand-specimen notes and descriptions. |
|---|---|---|---|
| SF-2A | 15 | *13* | Ss, reddish gray with clay rip-ups to 3 cm. Sandstone is massive, f.g. Top of outcrop/bluff, 110' above river. From a promontory outcrop between 2 gullies (this is a more resistant layer, bc? not shale). Red-brown, med.gr. Ss/Cgl w. shale/siltstone rip-ups to 25 cm and red sandy blebs to 20 cm. |
| SF-5B | | *14.5* | Black massive shale. Galaxy (?) Extremely fractured, apparently massive dark gray siltstone. 3 m ARL. |
| SF-4B | 50 | *41.3* | Massive gray siltst. Gray massive to thinly laminated micaceous c.g. siltstone, with one thin laminated, very disturbed (ripped-up?) dark red-gray lamination, undulating and terminating in a gray siltstone/reddish f.g. silt/clay zone possibly representing dissociation of the dark lamination. Field note: C.g. massive gray siltstone 1 m below stripey whitish to dark gray wavy anastomose thinly bedded to thickly laminated siltstone. 2 m above river |
| SF-3A | 45 | *43.8* | Dark gray laminated siltst. |
| SF-3B | 100 | *72.2* | Black laminated siltstone. Thickly laminated, even parallel graded siltstone (light gray) and darker gray finer silt/clay laminae showing concave up lode structure (?) Field note: Gully between CHC incursions. Many photos. Numerous anastomose black thin to thick laminations in whitish gray siltstone. Pervasive, repeated vertical fracture in Andersonian conjugates, 170,85 & 316, 69. Fracture makes avoidance of surface oxidation hard (samples are small). 3 m above river level. |
| SF-2B | 120 | *94.6* | Gray and red-brown interbedded siltstone, subunit reddish brown laminated siltstone. Dark gray siltstone and shale thinly interlaminated with even, gradational-bounded pinkish gray c.g. silt. Darker gray very thin anastomosing/inosculating ) and sometimes concave up (lode structure?) laminations in lighter pinkish gray c.g. silt layers. Dominantly (75%) darker and finer-grained overall. Field note: River level +3m. Black and white striped, with 1 m intervals of white-dominant siltstone. Anastomose patterns common. Sample is black thinly laminated shaley siltstone. |
| SF-4A | 130 | *103.7* | Cross-stratified gray siltstone, subunit red intercalate cross laminated siltstone. Dark gray f.g. silt/shale thick cross-laminae in lenticular ripple-laminated siltstone with reddish gray coarse silt/Ss. 105' above river. Next positive outcrop of Nsch dstrm of SF-3A. Thickly laminated f.g. silt/shale with odd rounded positive texture (cross-current ripples or drying?). MnO stain. Less than 1 m up section from conglomerate/sandstone lens (photo'd). |
| Copperwood, PC-5 (drilled 1959) | | | |
| PC-5-7 | 839.5 | 6.4 | Upper ss. dark grayish-red shale laminae with coarser-grained lighter gray siltstone, which is whiter in the calcareous-cemented lams (perhaps 1/10 of gray silty layers are calcite-cemented). ~60% silt, 40% shale. Logged originally as: "from 807'-861', logged as: Micaceous, alternate shale, siltstone and sandstone of varying thicknesses and ratios. Med. gray. " |
| PC-5-4 | 823.4 | 8.1 | Upper shale. massive, brownish-gray micaceous siltstone with rare, coarser-grained whitish-gray calcareous siltstone lams (<1.5 mm). 90% silt. Originally logged as: "from 807'-861', logged as: Micaceous, alternate shale, siltstone and sandstone of varying thicknesses and ratios. Med. gray." |
| PC-5-8 | 783.2 | 20.4 | Marker bed |
| PC-5-6 | 780.2 | 21.3 | Marker bed. Dark gray shale, very thinly laminated, parallel and continuous, (60%) with massive to crudely thin laminated (parallel and slightly wavy) light-gray, often lenticular v.c.g. siltstone and v.f.g. sandstone, calcareous. Uneven, gradational contacts between lithologies. Greenish gray clay layers are most continuous and sharpest-bounded, usually0 .15 mm thick and very continuous, almost even parallel with slight waviness. Calcite-rich gray silt (~15% calcite) disrupts bedding in places and shows undulating gradational contact with darker gray silty layers. Originally logged as: "(1"=20') Micaceous, massively bedded, difficult parting, occasional 1/2-2" calcite-cemented, bleached, silt lenses. Medium gray." |
| PC-5-3 | 631.5 | 66.6 | Gray member of black laminated siltstone. Massive, brownish-gray siltstone, 95% silt/sand. Originally logged as from 587'-777', logged as: (1"=20') Micaceous, medium to thick bedding; dark gray to green-gray; shale 40-60%; parting moderately easily to hard; thin laminae of silt and shale, graded bed; occasional calcite in irregular beds and blebs 1 mm thick; laminae w/ shale, abundant 1/2 to 1" calcite cemented, bleached silt bands at 715', 716', 721', 722', 730', 731', 732', 734', 738', 739, 747, 743, 745, 752, 754. |

*Appendix C, ctd.*

| Sample | Core depth (ft) / distance on profile (m) | Height (m) above base of Nonesuch Formation | Field and hand-specimen notes and descriptions. |
|---|---|---|---|
| PC-5-2 | 587.2 | 80 | Black Laminated Siltstone: Calcareous, gray siltstone, v.c.g.,very thinly laminated, with very thin dark gray/black, laterally continuous OM-rich wavy laminae, often encasing lenticles of silt ~ <1mm; several anastomose carbonaceous lams. 60-40 silt/shale. Originally logged as "from 587'-777', logged as: (1"=20') Micaceous, medium to thick bedding; dark gray to green-gray; shale 40-60%; parting moderately easily to hard; thin laminae of silt and shale, graded bed; occasional calcite in irregular beds and blebs 1 mm thick; laminae w/ shale, abundant 1/2 to 1" calcite cemented, bleached silt bands at 715', 716', 721', 722', 730', 731', 732', 734', 738', 739, 747, 743, 745, 752, 754." |
| PC-5-1 | 576.1 | 83.5 | Black laminated siltst. Gray siltstone, very thinly laminated, with very thin black, organic-rich shale laminae. OM-rich lams are wavy and parallel. Dark gray lams shift gradually up to light gray shale then up into gray siltstone. Non-calcareous (although vuggy fracture may represent calcite diss'ln void). 80 to 95% silt, 5 to 20% shale/clay. V.f.g. oxidized sulfide present. Majority of lams are continuous and very thin, but the very finest - ~50 microns thick - show rare, 3-4 stacked black OM-rich laminations in a convex geometry, nearly or completely encasing gray lenticular silt lam (red arrow) up to 3 mm wide. Very very thin gray-green clay lams and very very thin OM-rich black lams do show some tears/detachments that may indicate disturbance on compaction. Originally logged as "from 576'-589', logged as: (1"=20') Micaceous, thinly bedded, varying amounts of shale from 50-90%, parting easily, thinly laminated, graded bedding, silt and shale layers less than 1 mm thick; dark gray to green-gray; uniform texture; massive siltstone bed." |
| Copperwood, PC-1 (drilled 1959) | | | |
| PC-1-5 | 888.4 | 2.4 | Gray laminated. Massive, reddish-brown siltstone and shale, micaceous. A single black wisp, 1 mm wide, 0.05 mm thick, exists, no grains visible; some, very rare, darker brown round to irregular clay particles (<0.5 mm, rip-ups?) wide. 95+% silt. Originally logged as "(1"=2') Micaceous, thinly to medium bedded, shale 70-90%, parting easily, reddish gray. Limey Marker at 896.6 My Notes: Gray massive siltstone" |
| PC-1-4 | 864.2 | 10.1 | Upper shale. Massive gray f.g. siltstone alternating (~0.5 cm) with brownish-gray c.g. siltstone and v.f.g. sandstone, calcareous. Some rare unID'd black wisps (no grains visible ~ 1 wide, 0.1 mm thick.). Black wisps more prevalent in brownish coarser layers. 95% silt. Original Logged as: (1"=2') "Micaceous, moderately to thickly bedded, uniform texture, shale 50-70%, parting moderately easily, varies to thin-bedded at base. Dark gray to reddish brown." My Notes: Gray massive siltstone |
| PC-1-6 | 862.2 | 10.7 | Upper shale. Brownish-red v.f.g. silt to shale crisply changing to greenish-gray c.g. silt, irregular subhorizontal boundaries (blotchy at times), largely massive texture. Some thin alternate laminae of both are present. 60% silt/sand, 40% shale/fine silt. Isolated clay-rich rip-up, darker and randomly oriented <1mm oblong, with a second, smaller similar clast at random orientation several mm away. Originally logged as : (1"=2') "Micaceous, thinly bedded alternate laminae of siltstone and shale 1-2mm thick, shale 70-90%, easily parting." |
| PC-1-3 | 861.4 | 10.9 | Upper shale. Very thin, brown, lenticular to continuous and parallel shale laminae in massive gray f.g. siltstone, micaceous and massive . Rare, faint light gray zones apparent, ~1 mm thick and semi-continuous across core, in f.g. siltstone. Transition at end of sample is black wavy-crinkly, 0.1 mm thick semi-continuous fracture-fil or wispy lamination grading through gray f.g. siltstone to brown, f.g. siltstone/shale. Non-calcareous throughout. 75% silt/sand, 25% brown/black shale/clay. Original: Logged as "(1"=2') Micaceous thinly bedded alternate laminae of silststone and shale 1-2 mm thick, shale 70-90%, easily parting." |
| PC-1-2 | 754 | 43.5 | Dark gray laminated siltst. Light gray siltstone and dark gey shale laminae, both very thin, continuous across core. Whitish-gray , v.f.g. silt laminae anastomose/inosculate in places, leaving lenticular light gray siltstone lams (6 mm x .5mm). Laminae show small-amplitude wavy texture, and are generally. 0.5 mm thick, vuggy-centered fracture in c.g. gray siltstone bounded by brownish black f.g. siltstone lams (0.1 mm thick); f.g. brown bounding lams anastomose after ~1 cm. 65% shale, 35% silt. Original:"Logged as: (1"=20') Micaceous, massively bedded, shale <30%, no parting, 45 degree fracture; occasional 1-3mm calcite laminae, dark gray" My Notes: gray laminated siltstone. |

*Appendix C, ctd.*

| Sample | Core depth (ft) / distance on profile (m) | Height (m) above base of Nonesuch Formation | Field and hand-specimen notes and descriptions. |
|---|---|---|---|
| PC-1-1 | 701.3 | 59.7 | Black laminated siltst. Light gray very thinly to thickly laminated, v.c.g. siltstone laminae (some calcareous) with dark gray to grayish black shale laminae. Graded laminations, with silty material fining upward to clay/shale. Laminations are wavy and parallel, continuous. Oxidized pyrite up to 0.1 mm present. 0.05 mm thick wavy/irregular black calcareous fracture (?) w/o visible constituent grains, continuous across width of core (1"); (black color is discontinuous). UnID'd non-carbonate whitish-gray thin (<0.5 mm) shale laminae (no grains visible, likely very fine phyllos) show internal, concordant, discontinuous wisps of black material or possibly, voids, (~1 mm wide but linking to ~1 cm); (photo 2, 40x and Leica 2). Subvertical, calcite-filled fracture at margin. 70% silt, 30% shale. Originally logged as (1"=20') "Micaceous med bed., sh. 50-70%, parts mod. Easily; calcareous vuggy?, brecciated?, dark gray in color." My Notes: gray laminated siltstone |
| Presque-Isle River | | | |
| PI-7 | 48.2 | *14.9* | Gray to dark gray thinly laminated to disrupted/ripped-up interlaminations of darker, OM-rich material at ~30 deg to horiz, to 2.5 cm wide. Silty lams are even and lenticular. Sample note: 2 m above river level, brownish gray fissile f.g. siltstone, just 3 m upsection of very thin CHC-esque lens (.3 m thick). Cu stain, as photo'd. Cherty lenticular concretions, non-calcareous, parallel to bedding, 5cm x 20 cm. Ex-situ (but most likely local, ie: Nsch) micaceous siltstone w/ rip-ups and mudcracks. E side of river |
| PI-8 | 82.7 | *25.5* | Massive gray siltstone. Uniform, unlaminated, with minor pyrite, dominant qtz. |
| PI-9 | 82.7 | *25.5* | Gray to dark gray very thin laminated (even parallel near to straight with some gently undulose and some crossbedded fine lams against massive-bedded) siltstone. Lenticular dark lam .5 cm wide present, isolate in lighter gray silt. |
| PI-10 | 193.8 | *59.9* | Very finely laminated gently undulose to wavy dark gray to gray silty and shaly laminae. |
| PI-12 | 298.2 | *92* | Shaley siltstone. Indistinctly bedded dark gray with blotchy pink calcite blobs (to .5mm) coloring ~45% of sample light gray. Silty to shaly. |
| Iron River Syncline, WPB-1 (drilled, 1961) | | | |
| WPB-1-4 | 521.1 | 2.7 | Dark Gray Massive equiv? Light reddish-gray coarse and massive siltstone, well-sorted and with very rare, faintly visible thin laminae of darker and finer-grained silt particles. Lamination is not ubiquitous and not observed in lighter areas, which appear massive. Calcite cement throughout. Rusty red 0.05 mm weathered pyrite and smaller, less-oxidized chalcopyrite (BLUE DOTS). 100% siltstone. Pyrite or chalcopyrite, phyllosilicates. Some sub-parallel alignment of phyllosilicate grains. 1961 Drill log: "Logged as: (1"=50') Interbedded siltstone and shale and massive sandstone. (1"=10') Well-bedded thinly laminated even-grained micaceous siltstone. Pyrite/Chalcopyrite in limey layers" |
| WPB-1-1 | 518.1 | 3.6 | Thinly equiv? Brownish-green-gray thinly laminated, v.f.g. sandstone and coarse siltstone. Laminae are wavy, parallel and often discontinuous or lenticular and commonly ~ 1 cm or less in width. Extensively (>70% of lams) calcite cemented, with some coarser-grained laminae light gray in color (>40% CaCO3), while more organic-rich shale laminae are near-black. 50% silt, 50% shale. Black, OM-rich lams are wavy/undulating, with anastomose and possible folded geometry. conjecture: brown blotchy exterior = oxidation?; wavy, undulose/possibly folded laminae - possible algal mats? 1961 logged as: (1"=50') Interbedded siltstone and shale and massive sandstone. (1"=10') Well-bedded thinly laminated even-grained micaceous siltstone. |
| WPB-1-6 | 485 | 13.7 | Widely, gray to light gray coarse siltstone, massive to very thinly laminated with most laminae lenticular and <~2mm wide. Multiple 1 cm thick layers of very thinly laminated grayish-black shale alternate with coarse gray siltstone - black lams here are more continuous and parallel - despite some distortion as in photo 29 Notable thicker, darker gray-brown, and finer-grained but rare laminae are significant - more laterally continuous and showing both irregular anastomosing and near-parallel forms. Calcite-filled fractures crosscut bedding at ~60°. Pyritic, micaceous, with isolated pinkish-white calcite blebs (<1 mm) and some rare thin (<0.5mm thick), lat. discont. subhoriz. calcite filled fxrs. Mud rip-ups present on bed-parallel end of sample, darker gray shale fragments to 3 mm. 85% silt, 15% shale. 1961 logged as: (1"=50') Interbedded siltstone and shale. Massive sandstone w/ thin shaley limestone bed. (1"=10') gray-green and dark gray thick bedded (2-10 cm), v.f.g sandstone or coarse siltstone and fine grained siltstone or shale. Varve-like graded beds, each bed graded from coarse siltstone to shale. |

*Appendix C, ctd.*

| Sample | Core depth (ft) / distance on profile (m) | Height (m) above base of Nonesuch Formation | Field and hand-specimen notes and descriptions. |
|---|---|---|---|
| WPB-1-3 | 461.5 | 20.9 | Upper Shale equiv? Dark gray-black micaceous siltstone with fracture-fill calcite, (subhedral xtals up to 0.1 mm) some fillings up to 1 mm max. dimension. Calcite blebs to 0.2 mm wide present, discordant to bedding. Massive to irregular bedding, rare darker gray rip-ups of shale, lenticular and discontinuous, to 2 mm, within a dark brownish-gray to dark gray (coloration is blotchy) matrix, heavily fractured m.g. quartzose siltstone blotchy coloration of cement and distorted bedding = (higher-E deposition storm, or perhaps early diagene fluid movement?) Fractured surfaces showing fairly uniform pseudofoliated near-metamorphic fabric and reflective, greasy lustre. 60% silt, 40% shale. 1961 Log: "(1"=50') Interbedded siltstone and shale.: (1"=10') Brown sandstone, well bedded and fine to c.g." ??Fractured surfaces showing fairly uniform pseudofoliated near-metamorphic fabric and reflective, greasy lustre may represent chloritization/greenschist metamorphism.?? |
| WPB-1-2 | 454 | 23.2 | Dark Gray Laminated Siltstone equiv., Micaceous, gray-green coarse-grained siltstone, in irregular, contorted thin laminae (some partially encasing rare darker, black shale laminae, wavy and somewhat discordant wisps up to 1mm wide). Lacking calcareous laminae, and cement is non-calcareous. One piece shows massive and distorted irregular bedding, with a brownish-gray domain and more definite rip-ups (photo 23). Fracture-fill calcite and pink (K-spar?) rimey coating on fracture oblique to bedding. Similar-oriented phyllosilicate grains may reflect gravity settling or some degree of imbrication (?). 70% siltstone, 30% shale. 1961 Logged as: (1"=50') Interbedded siltstone and shale. (1"=10') Brown and gray interbedded v.f.g. sandstone or coarse siltstone and fine grained siltstone or shale, w/ varve-like graded beds, each bed graded from coarse siltstone to shale. Individual beds are from 1 mm to 10 cm thick. Mud-chip tear-up (interformational) conglomerate and some slump structures. Some isolate lenses or thin beds of pebble conglomerate (particles >5 mm diameter). Conjecture: represent interformational conglomerate (BLUE-DOTTED SAMPLES). With rip-ups of clay and poss carb material as well. |
| WPB-1-7 | 366.2 | 49.9 | Similar to gray and red-brown interbedded siltstone (subunit black mudstone ripups). Dark greenish-gray micaceous siltstone, coarse-grained with rare dark gray to gray-brown shale laminae. Very weak calc-cement. Massive to crudely thinly laminated, most distinct bedding is apparent as 2 mm-wide darker, finer-grained wispy parallel to discordant, sub-parallel laminae/rip-ups. 85% silt/sand, 15% shale. "1961 logged as: (1"=50') Thinly laminated highly micaceous, siltstone and shale." Conjecture: Wet-sed def'mn? Or rip-ups = intraformational conglomerate? Brown blotchy exterior = oxidation? |
| WPB-1-5 | 201.9 | 100 | Gray siltstone; Wavy parallel, alternate laminae of light whitish-gray and dark gray f.g. siltstone/OM-rich shale. Individual laminae are very very thin and largely continuous across core, though discontinuous lams (40%) are lenticular. Lamina-sets of dominantly (>75%) darker material vs dominantly lighter material are ~.5-1 cm thick. Darker, gray-black, greasier-looking thin (<0.1 mm thick) wavier (concave up and down in small amplitude, ~0.5 cm alternations) laminations of clay-size particles present. Calcareous cement, rare, in light grayish white siltstone lams - calcareous lams encase dark gray silty lenticular lams in places, with sharp, irregular contact. 40% shale, 60% silt. Epoxy/resin on outer edge? Multiple irregular, bedding parallel fractures present, several calcite-cemented; one of same in irregular vertical orientation. Finely interlaminated clay-rich layers (enriched in ?bitumen, as rounded opaque blebs ?) and siltstone layers. Fine, continuous strand of ?migrated HCs? focused along a clay-rich layer, crosscut by?later calcite?. Bedding-oblique fractures appear to show darkening (HCs?) along their axis, but some show unilateral darkening on one side (R for the main one) relative to the other. 1961 drill logger:" Logged as (1"=50') Interbedded siltstone and shale in thin varve-like beds. Symbol: Interbedded v.f.g. sandstone or coarse siltstone and fine grained siltstone or shale. Varve-like graded beds, each bed graded from coarse siltstone to shale. Individual beds are from 1 mm to 10 cm thick." |
| Little Iron River, Silver City | | | |
| LIR-2 | regular | *0.8* | Parting shale |
| LIR-3 | sampling: | *5* | Upper shale |
| LIR-4 | dip = 18° | *9* | Massive gray siltst., non-calcareous, reg. sampling between CHC top and Parting Ss |
| LIR-6 | | *13* | Massive gray siltst. |
| LIR-10 | | *17* | Massive gray siltst. |
| Big Iron River, Silver City | | | |

*Appendix C, ctd.*

| Sample | Core depth (ft) / distance on profile (m) | Height (m) above base of Nonesuch Formation | Field and hand-specimen notes and descriptions. |
|---|---|---|---|
| BIR-16 | 900 | *4.5* | Domino. Calcareous, silty shale, thinly laminated with thick calcite vein (3mm wide) Fissile and thinly bedded on the larger scale. Dark gray green overall. |
| BIR-15 | 850 | *13* | Dark Gray Massive, concretion 4x4x2 cm, calcareous. |
| BIR-14 | 850 | *18* | Top Zone, calcareous coarser-grained silty light gray matrix with discontinuous darker gray shale interlaminae. |
| BIR-13 | 850 | *19* | Top Zone, Calcareous cemented in coarser gray silty layers, with large white calcareous concreti apparently disrupting fine-grained shaley silt interlaminae in a light gray coarser matrix. |
| BIR-11 | 800 | *32* | Gray laminated siltstone, showing syneresis cracks |
| BIR-10 | 760 | *39* | Black shale, with brecciated/foliated appearance, significant secondary malachite, calcareous an very fragile due to pervasive fracturing |
| BIR-8 | 720 | *44* | Light gray laminated siltstone |
| BIR-7 | 700 | *48* | Cross-stratified gray siltstone, fine laminated |
| White Pine, 28G (drilled 1965) | | | |
| 28G-572 | 572 | 0.5 | Domino |
| 28G-571 | 571 | 1 | Red massive. Massive shale with sulfides, non-calcareous. |
| 28G-539 | 539 | 11 | Upper shale (massive gray, pyritiferous.) |
| 28G-520 | 520 | 17 | Marker bed. sparry Calcite vein, anastomose and inosculate, to 2mm wide; massive dark gray shaley siltstone with thin even parallel to wavy parallel alternate dark gray and light gray (coarse material, silty). |
| 28G-514 | 514 | 19 | Marker bed. dark gray shaley siltstone with calcite nodules to 3 mm wide by 1 mm thick. Vertic calcite vein .5 mm thick, irregular, anastomose/inosculate, disturbs bedding in places. Thin, eve parallel to wavy parallel laminations of darker gray finer lams with thicker siltier-sized lighter gra laminations. |
| White Pine, 517 (drilled 1995) | | | |
| 517-6 | 3136.15 | 0.5 | Domino. Crude, very thinly laminated alternate layers of greenish-gray shale/v.f.g. siltstone and light gray to gray-black coarse siltstone. Non-calcareous. V.f.g. sulfides present in finer-grained, green-gray laminae, gently undulating in geometry, sometimes anastomosing. some brown oxidation(of ore?) on v.f.g. silt/shale layers. 60% silt, 40% shale. Originally logged as" Domino: Sandy siltstone; gray-green (5E 2/1); shale, well-laminated at base, grading upward to crudely laminated chloritic micaceous sandy siltstone. Just below "Junior Lime" - crudely laminated w/ mudcracks." |
| 517-5 | 3127.5 | 3.2 | Red Massive; Brownish-Gray, massive coarse-grained siltstone with very thin black, OM-rich laminae, (undulating lenticular, f.g. silt or shale) in laminasets (<0.3 cm) with bronzy-reddish brown massive fine-grained thicker lams of probable sulfide ore. Coarser layers appear to bear more chlorite and finer laminae show reddish, v.f.g. probable sulfide. Non-calcareous. "ore" bar overlies the very thin OM-rich black lam and appears to have a very very fine black OM-rich lam above it. noncalcareous. 65% silt, 35% shale. Possible mig'd bitumen.Originally Logged as Tiger Ss. Graded beds (<4 in.) Med/-gray (N3-> N5); siltstone dark-brown (5R 2/2), v.f.g., gray Ss, grading upward to hematitic siltstone and shale laminae as graded beds; shale laminae are commonly truncated and distorted w/ loadcasts and flame structures. |
| 517-2 | 3122.25 | 4.8 | Upper sand. Massive light gray siltstone with 1 mm thick continuous and discontinuous (lenticular) pinkish-white pseudo laminae (even, parallel; no grain size change visible). Lighter layers are strongly calcite-cemented. Significant massive light gray = 85%. Reddish/pink tint to calcite cemented layers (hematite or kspar?). Significant iron oxide stain on ext of core - ox'd pyrite/sulfide? 80% silt, 30% sand/silt. Whitest lams have sparry-looking calcite cement (up to 40% locally) and few to no dark grains, instead supporting pinkish white translucent subangular grains of probable qtz. 1961 Logged as "middle of a 2 ft long fining upward sequence. Upper Ss Ss, brown-gray (5YR6/1) to med-gray (N4->N6); siltstone, gray-green (5YR3/2) to med-gray (N4->N6); shale, dark-gray (N1_>N2), course to v.f.g. poor to well-sorted, calcareous +/- lithic Ss w/ subangular to subround lithic frags and mudchip intraclasts (2mm-1cm diam.); interbedded w/ crudely laminated siltstone and shale; shale partings and lenses throughout." Conjecture: Laminations are actually just differential cementation (no grain size change, or apparent lineations, associated) |

*Appendix C, ctd.*

| Sample | Core depth (ft) / distance on profile (m) | Height (m) above base of Nonesuch Formation | Field and hand-specimen notes and descriptions. |
|---|---|---|---|
| 517-1.5 | 3106.9 | 9.8 | Brown massive? Dark grayish-green massively bedded coarse-grained micaceous siltstone. No calcite cement. Bedding-sub-parallel fracture with (?) silica (noneffervescent) cement. 85% silt/Ss, 15% shale. Originally logged as Tiebel Ss as above, w/ dissem. pyrite in siltstone/shale beds. (N4->N7 Munsell) |
| 517-4 | 3101.5 | 11.1 | Widely; Massive gray siltstone and lighter gray siltstone, with rare thin discontinuous laminae, trough-shaped. Micaceous and bearing uneven subhorizontal (concave up/down on a 2 inch wavelength, .5 cm amplitude) calcite-filled fractures. Some (<25% total) calcite cemented zones. One lone very thin, planar and parallel black OM-rich shale layer, with rips/folds/irregularities as in photo 41. 90%silt/Ss, 10% shale.Originally logged as Tiebel Ss (Predom. Planar-bedded v.f.g. Ss w. minor siltstone, shale laminae and partings. Ss is predom. Planar-bedded with minor trough xbeds and convolute beds (ripple x-laminae). Fining upward from 3108 to 3101'. (N4->N7 Munsell) |
| 517-2.5 | 3078 | 19.5 | Dark gray laminated siltstone; Very thin, continuous and parallel laminae in alternate dark gray fine grained siltstone/shale and lighter gray coarse-grained siltstone, both micaceous. Some lams undulate, with darker gray staying similar thickness and lighter gray changing thickness. Calcite cements lighter colored layers. Subhorizontal fracture-fill calcite present at base of core sample. Subvertical fracture showing calcite and void at either end (photo 39). 50% f.g. silt/shale, 50% silt/Ss.1995 logged as calcareous crudely laminated siltstone (N1->N2 Munsell) with non-calcareous well-laminated shale. |
| 517-3 | 3074.6 | 22.1 | Galaxy (black laminated siltstone and shale). Very very thin, alternate, gradationally-bounded, laminae of dark gray (f.g. silt/shale) to gray c.g. siltstone, with lighter layers commonly calcite-cemented. Laminae are wavy to gently undulating, often lenticular and <1 mm wide. 0.5 mm wide dark silty blebs and blotchy, finer-grained stain (bedding-parallel fracture assoc.) of possible HCs visible on outside of core. Fracture-assoc. blotchy dark oil? stain on exterior (photo 38). 90% f.g. silt/shale, 10% c.g. silt. Basal 1 cm of sample is lighter gray and shows clay-sized bronzy gray blebs subconcordant with bedding up to 1 mm wide and fat but lenticular. |
| 517-1 | 3065 | 206.7 | Gray laminated siltst.Gray laminated siltstone with soft-sed def'mn (my interpretive term). Thin to very thin laminae in laminasets of OM-rich black, clay-rich layers alternating with grayish-white coarse siltstone layers. grayish-black shale, variably continuous to <2 mm wide, in laminasets to ~0.5 cm thick, wavy and parallel to wavy discontinuous laminated, between light grayish white coarse grained siltstone. Variable calcite content, with some lighter-color laminae very calcite-rich but others less so; calcite cement NOT disseminated throughout. Concave up patterning in bases of light laminae, and some anastomosing/possibly folded dark, OM-rich black lams. 50% silt, 50% shale. Upward concavities may represent load structures - the cohesiveness of the darker shale contrasts the pillowy structures. Thickly striped appearance (~.5 cm thick alternate white/gray banding = very thin lamina composite bedsets) |
| White Pine, 523 (drilled 1995) | | | |
| 523-5 | 2868.1 | 1 | Domino. Light gray-green massive siltstone hosting bronzy-gray shale (irregular lenticular lamina 2 mm thick at bottom) with numerous discontinuous wispy black ?rip-ups? (some approaching 45° to bedding) of higher apparent [OM]. Brecciated/slumped disturbance texture. Wispy black rip-ups offset by .1 mm wide calcite-filled fracture (some brecciation of light gray massive siltstone). At least 7 subhorizontal, .05 mm wide calcite-filled fractures, some offset by the subvertical one. Some of the subhorizontal fractures anastomose. Anhedral, unoxidized chalcocite ? visible on fresh surface. irregular, blotchy brown bounding green color, across beds = oxidation of sulfides? Some pieces show different, more cohesive and subparallel (but still very wavy/irregular) thin laminations of all three lithologies listed above. 70% shale, 30% silt. Originally logged as: "Lower Transition: Ss, siltstone, brown-pink, (5YR 6/1) to green-gray (5E 4/1); shale, dark-gray (N1-->N2); coarse to v.f.g. poor-to-well-sorted, hematitic to chloritic to gray (OM-rich), calcareous lithic Ss w/ subangular to subrounded lithic fragments and angular mudchip intraclasts; Ss interbedded w/siltstoneand shale beds and laminae, and shale partings; beds become thinner and finer-grained upwards. Planar bedded Ss w/ siltstone/shale partings. Just above calcite& red (Kspar?) filled veins < 2mm wide at 10-45 deg to L.A.?" My Notes: gray-green siltstone |

*Appendix C, ctd.*

| Sample | Core depth (ft) / distance on profile (m) | Height (m) above base of Nonesuch Formation | Field and hand-specimen notes and descriptions. |
|---|---|---|---|
| 523-2 | 2859.1 | 3.7 | Upper transition. Wispy black subparallel very thin laminations in dark gray siltstone at top 1 cm. Massive, dark gray siltstone with irregular, darker gray-black rip-up clast-rich, wispy black laminated finer silt and shale. A very small minority of rip-up clasts appears to be calcite-cemented, light gray siltstone. Interformational rip-up conglomeratic siltstone. 1, 0.1 mm thick pink and white fracture-filling calcite/?k-spar? zone at base. Pink and white calcite/kpar also from a 0.5 mm thick subvertical fracture-fill which offsets a 0.05mm fracture of the same color/app. mineralogy. 85% silt, 15% shale. Originally logged as "Upper Transition: med. to v.f.g., well-sorted, calcareous hematitic or chloritic Ss and Ss w/ interbedded shale laminae and shale partings; Ss, siltstone bed decrease in width upward, fining upward unit. (5E 4/1, N5-->N7, N1-->N2)." My notes: Greenish-gray siltstone, with fracture-fill calcite, just above UZV |
| 523-3 | 2819 | 15.9 | Stripey. Overall dark gray shaley siltstone. Very thin bronzy-gray shale laminae between dark-gray f.g. silt laminae and v.c.g. siltstone/v.f.g. qtzose sandstone laminae (high calcite, white to gray-white). Bronzy-gray shale and dark gray silt lams are sometimes irregular, wavy and ?anastomose/inosc?, while white/gray-white c.g. silt/f.g. Ss layers are often lenticular/pseudo-boudin'd; even parallel lamination dominates, overall. Bronzy-gray shale = 20%, dark gray silt =45%, v.c.g. silt/v.f.g. sand = 35%. Originally logged as: "Massive black siltstone: shale, siltstone. Dark gray (N3) to gray-black (N2); shale and siltstone laminae (<??0.3mm/3mm wide??); well-indurated, calcareous; greater concentration of calcite laminae near center of unit w/ wisps of shale/discontinuous shale laminae; calcareous nodules (1.5cmx2mm) sub-parallel to horizontal near base of unit. Traces of v.f.g. disseminated pyrite throughout." My Notes: Dark gray wavy laminated siltstone |
| 523-1 | 2814.7 | 17.3 | Marker bed; Dark gray very thinly laminated siltstone and darker gray-black shale laminae. Laminations are very very thin, subhorizontal, even parallel to wavy, and commonly distorted by concretionary calcite. Numerous calcite concretions, some subhedral (up to 0.1 x 0.8 cm but mostly ~0.5 mm max dim.), some having a greenish cast(chlorite?), with very little silt/shale suspended. Concretions locally disturb bedding, contorting dark layers concentrically or in lenticular bulges about concretions, large and small. This sample has the most intense calcite cement of the suite. 65% shale, 35% silt. Originally logged as "Marker siltstone and shale - gray-black (N2) to very light gray (N8); shale laminae (< .5mm wide) alternating with discontinuous calcareous siltstone laminae (<1.0 mm wide) giving the unit an overally blotchy appearand; small-scale calcareous nodules (1.0cmx2.0mm) cross-cut laminites throughout; randomly located zones of continuous silstone, shale laminae that give the appearance of dark stripes throughout the marker bed: Tr. v.f.g. disseminated pyrite throughout." My Notes: Dark gray laminated siltstone with calcite concretions. |
| 523-4 | 2801.5 | 21.3 | Galaxy. Very thin, lenticular (lat. discont.) laminae of finer-grained black silt or clay (OM?) intercalated with gray v.f.g. sandstone. Multiple 4mm wide, very thin lenticular but mostly parallel and slightly undulating whiter-gray silt laminae. Some of the black laminae anastomose and inosculate. Two subhorizontal, high calcite-content fractures (<0.1 mm thick). One laterally continuous fracture showing voids (calcite diss'ln?). Oxidized pyrites (<0.3 mm) present on exterior of core. Calcite cement present in lighter colored laminae. 65% shale, 35% silt/Ss. |
| 523-6 | 2726.7 | 44.3 | Gray Massive siltstone (my term) Subhedral pyrites (<0.5 mm), oxidized, in both Ss/silt and shale. Sharp transition from massive reddish-gray v.f.g. silt/shale to massive dark gray v.f.g sandstone. Some interlamination in thin gradational wavy parallel to even parallel lams. Transition shows undulating contact - in places the lower sandstone protrudes up into siltstone and "overhangs" siltstone (more gradational transition here, as in photo 59). Subvertical calcite-filled fracture (0.1 mm wide) and black subvertical fracture 0.05 mm wide (bitumen migration?) Rare very thin blackish-gray discontinuous and wispy laminae. Massive dark gray sandstone grades back to v.f.g. reddish-gray siltstone/shale at base. 75% silt, 25% shale. |
| 523-7 |  | 59.5 | Gray / red brown siltst. Parallel, even, with some minor irregularities, crisp to gradational bounded, thin to thick laminae of v.c.g. green-gray siltstone and maroon/red shale/v.f.g. siltstone. Very narrow (<0.1 mm) vertical calcite-filled fracture, with subhorizontal fxrs joining at high angles - each with diffuse fxr-assoc'd calcite blebs to 0.25 mm around. 60% shale, 40% silt. |

# *Appendix D: LECO TOC and Rock-Eval II Pyrolysis Data*

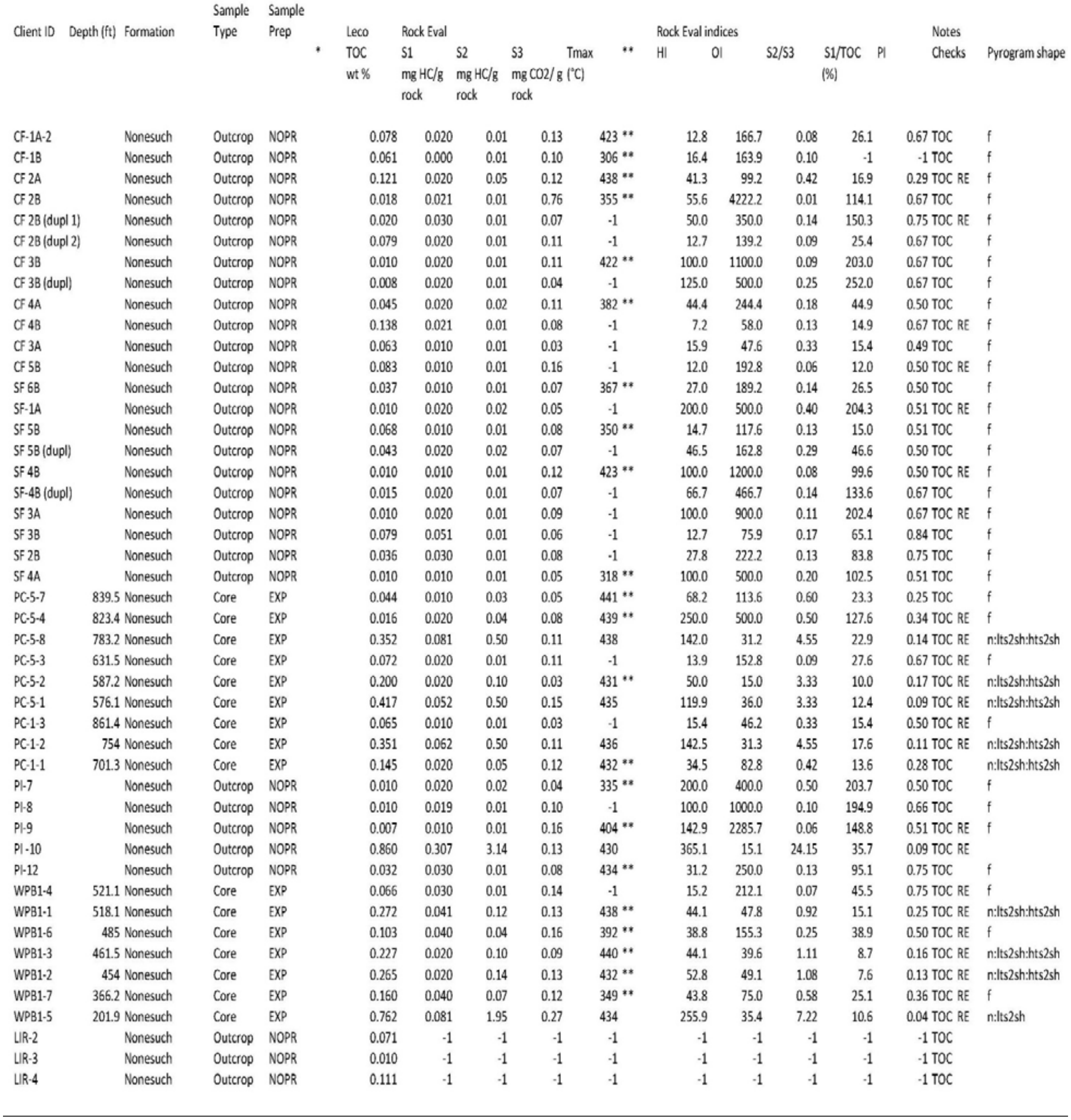

| Client ID | Depth (ft) | Formation | Sample Type | Sample Prep |  | Leco | Rock Eval |  |  |  |  | Rock Eval indices |  |  |  |  | Notes |  |
|---|---|---|---|---|---|---|---|---|---|---|---|---|---|---|---|---|---|---|
|  |  |  |  |  | * | TOC wt % | S1 mg HC/g rock | S2 mg HC/g rock | S3 mg CO2/ g rock | Tmax (°C) | ** | HI | OI | S2/S3 | S1/TOC (%) | PI | Checks | Pyrogram shape |
| CF-1A-2 |  | Nonesuch | Outcrop | NOPR |  | 0.078 | 0.020 | 0.01 | 0.13 | 423 | ** | 12.8 | 166.7 | 0.08 | 26.1 | 0.67 | TOC | f |
| CF-1B |  | Nonesuch | Outcrop | NOPR |  | 0.061 | 0.000 | 0.01 | 0.10 | 306 | ** | 16.4 | 163.9 | 0.10 | -1 | -1 | TOC | f |
| CF 2A |  | Nonesuch | Outcrop | NOPR |  | 0.121 | 0.020 | 0.05 | 0.12 | 438 | ** | 41.3 | 99.2 | 0.42 | 16.9 | 0.29 | TOC RE | f |
| CF 2B |  | Nonesuch | Outcrop | NOPR |  | 0.018 | 0.021 | 0.01 | 0.76 | 355 | ** | 55.6 | 4222.2 | 0.01 | 114.1 | 0.67 | TOC | f |
| CF 2B (dupl 1) |  | Nonesuch | Outcrop | NOPR |  | 0.020 | 0.030 | 0.01 | 0.07 | -1 |  | 50.0 | 350.0 | 0.14 | 150.3 | 0.75 | TOC RE | f |
| CF 2B (dupl 2) |  | Nonesuch | Outcrop | NOPR |  | 0.079 | 0.020 | 0.01 | 0.11 | -1 |  | 12.7 | 139.2 | 0.09 | 25.4 | 0.67 | TOC | f |
| CF 3B |  | Nonesuch | Outcrop | NOPR |  | 0.010 | 0.020 | 0.01 | 0.11 | 422 | ** | 100.0 | 1100.0 | 0.09 | 203.0 | 0.67 | TOC | f |
| CF 3B (dupl) |  | Nonesuch | Outcrop | NOPR |  | 0.008 | 0.020 | 0.01 | 0.04 | -1 |  | 125.0 | 500.0 | 0.25 | 252.0 | 0.67 | TOC | f |
| CF 4A |  | Nonesuch | Outcrop | NOPR |  | 0.045 | 0.020 | 0.02 | 0.11 | 382 | ** | 44.4 | 244.4 | 0.18 | 44.9 | 0.50 | TOC | f |
| CF 4B |  | Nonesuch | Outcrop | NOPR |  | 0.138 | 0.021 | 0.01 | 0.08 | -1 |  | 7.2 | 58.0 | 0.13 | 14.9 | 0.67 | TOC RE | f |
| CF 3A |  | Nonesuch | Outcrop | NOPR |  | 0.063 | 0.010 | 0.01 | 0.03 | -1 |  | 15.9 | 47.6 | 0.33 | 15.4 | 0.49 | TOC | f |
| CF 5B |  | Nonesuch | Outcrop | NOPR |  | 0.083 | 0.010 | 0.01 | 0.16 | -1 |  | 12.0 | 192.8 | 0.06 | 12.0 | 0.50 | TOC RE | f |
| SF 6B |  | Nonesuch | Outcrop | NOPR |  | 0.037 | 0.010 | 0.01 | 0.07 | 367 | ** | 27.0 | 189.2 | 0.14 | 26.5 | 0.50 | TOC | f |
| SF-1A |  | Nonesuch | Outcrop | NOPR |  | 0.010 | 0.020 | 0.02 | 0.05 | -1 |  | 200.0 | 500.0 | 0.40 | 204.3 | 0.51 | TOC RE | f |
| SF 5B |  | Nonesuch | Outcrop | NOPR |  | 0.068 | 0.010 | 0.01 | 0.08 | 350 | ** | 14.7 | 117.6 | 0.13 | 15.0 | 0.51 | TOC | f |
| SF 5B (dupl) |  | Nonesuch | Outcrop | NOPR |  | 0.043 | 0.020 | 0.02 | 0.07 | -1 |  | 46.5 | 162.8 | 0.29 | 46.6 | 0.50 | TOC | f |
| SF 4B |  | Nonesuch | Outcrop | NOPR |  | 0.010 | 0.010 | 0.01 | 0.12 | 423 | ** | 100.0 | 1200.0 | 0.08 | 99.6 | 0.50 | TOC RE | f |
| SF-4B (dupl) |  | Nonesuch | Outcrop | NOPR |  | 0.015 | 0.020 | 0.01 | 0.07 | -1 |  | 66.7 | 466.7 | 0.14 | 133.6 | 0.67 | TOC | f |
| SF 3A |  | Nonesuch | Outcrop | NOPR |  | 0.010 | 0.020 | 0.01 | 0.09 | -1 |  | 100.0 | 900.0 | 0.11 | 202.4 | 0.67 | TOC RE | f |
| SF 3B |  | Nonesuch | Outcrop | NOPR |  | 0.079 | 0.051 | 0.01 | 0.06 | -1 |  | 12.7 | 75.9 | 0.17 | 65.1 | 0.84 | TOC | f |
| SF 2B |  | Nonesuch | Outcrop | NOPR |  | 0.036 | 0.030 | 0.01 | 0.08 | -1 |  | 27.8 | 222.2 | 0.13 | 83.8 | 0.75 | TOC | f |
| SF 4A |  | Nonesuch | Outcrop | NOPR |  | 0.010 | 0.010 | 0.01 | 0.05 | 318 | ** | 100.0 | 500.0 | 0.20 | 102.5 | 0.51 | TOC | f |
| PC-5-7 | 839.5 | Nonesuch | Core | EXP |  | 0.044 | 0.010 | 0.03 | 0.05 | 441 | ** | 68.2 | 113.6 | 0.60 | 23.3 | 0.25 | TOC | f |
| PC-5-4 | 823.4 | Nonesuch | Core | EXP |  | 0.016 | 0.020 | 0.04 | 0.08 | 439 | ** | 250.0 | 500.0 | 0.50 | 127.6 | 0.34 | TOC RE | f |
| PC-5-8 | 783.2 | Nonesuch | Core | EXP |  | 0.352 | 0.081 | 0.50 | 0.11 | 438 |  | 142.0 | 31.2 | 4.55 | 22.9 | 0.14 | TOC RE | n:lts2sh:hts2sh |
| PC-5-3 | 631.5 | Nonesuch | Core | EXP |  | 0.072 | 0.020 | 0.01 | 0.11 | -1 |  | 13.9 | 152.8 | 0.09 | 27.6 | 0.67 | TOC RE | f |
| PC-5-2 | 587.2 | Nonesuch | Core | EXP |  | 0.200 | 0.020 | 0.10 | 0.03 | 431 | ** | 50.0 | 15.0 | 3.33 | 10.0 | 0.17 | TOC RE | n:lts2sh:hts2sh |
| PC-5-1 | 576.1 | Nonesuch | Core | EXP |  | 0.417 | 0.052 | 0.50 | 0.15 | 435 |  | 119.9 | 36.0 | 3.33 | 12.4 | 0.09 | TOC RE | n:lts2sh:hts2sh |
| PC-1-3 | 861.4 | Nonesuch | Core | EXP |  | 0.065 | 0.010 | 0.01 | 0.03 | -1 |  | 15.4 | 46.2 | 0.33 | 15.4 | 0.50 | TOC RE | f |
| PC-1-2 | 754 | Nonesuch | Core | EXP |  | 0.351 | 0.062 | 0.50 | 0.11 | 436 |  | 142.5 | 31.3 | 4.55 | 17.6 | 0.11 | TOC RE | n:lts2sh:hts2sh |
| PC-1-1 | 701.3 | Nonesuch | Core | EXP |  | 0.145 | 0.020 | 0.05 | 0.12 | 432 | ** | 34.5 | 82.8 | 0.42 | 13.6 | 0.28 | TOC | n:lts2sh:hts2sh |
| PI-7 |  | Nonesuch | Outcrop | NOPR |  | 0.010 | 0.020 | 0.02 | 0.04 | 335 | ** | 200.0 | 400.0 | 0.50 | 203.7 | 0.50 | TOC | f |
| PI-8 |  | Nonesuch | Outcrop | NOPR |  | 0.010 | 0.019 | 0.01 | 0.10 | -1 |  | 100.0 | 1000.0 | 0.10 | 194.9 | 0.66 | TOC | f |
| PI-9 |  | Nonesuch | Outcrop | NOPR |  | 0.007 | 0.010 | 0.01 | 0.16 | 404 | ** | 142.9 | 2285.7 | 0.06 | 148.8 | 0.51 | TOC RE | f |
| PI -10 |  | Nonesuch | Outcrop | NOPR |  | 0.860 | 0.307 | 3.14 | 0.13 | 430 |  | 365.1 | 15.1 | 24.15 | 35.7 | 0.09 | TOC RE |  |
| PI-12 |  | Nonesuch | Outcrop | NOPR |  | 0.032 | 0.030 | 0.01 | 0.08 | 434 | ** | 31.2 | 250.0 | 0.13 | 95.1 | 0.75 | TOC | f |
| WPB1-4 | 521.1 | Nonesuch | Core | EXP |  | 0.066 | 0.030 | 0.01 | 0.14 | -1 |  | 15.2 | 212.1 | 0.07 | 45.5 | 0.75 | TOC RE | f |
| WPB1-1 | 518.1 | Nonesuch | Core | EXP |  | 0.272 | 0.041 | 0.12 | 0.13 | 438 | ** | 44.1 | 47.8 | 0.92 | 15.1 | 0.25 | TOC RE | n:lts2sh:hts2sh |
| WPB1-6 | 485 | Nonesuch | Core | EXP |  | 0.103 | 0.040 | 0.04 | 0.16 | 392 | ** | 38.8 | 155.3 | 0.25 | 38.9 | 0.50 | TOC RE | f |
| WPB1-3 | 461.5 | Nonesuch | Core | EXP |  | 0.227 | 0.020 | 0.10 | 0.09 | 440 | ** | 44.1 | 39.6 | 1.11 | 8.7 | 0.16 | TOC RE | n:lts2sh:hts2sh |
| WPB1-2 | 454 | Nonesuch | Core | EXP |  | 0.265 | 0.020 | 0.14 | 0.13 | 432 | ** | 52.8 | 49.1 | 1.08 | 7.6 | 0.13 | TOC RE | n:lts2sh:hts2sh |
| WPB1-7 | 366.2 | Nonesuch | Core | EXP |  | 0.160 | 0.040 | 0.07 | 0.12 | 349 | ** | 43.8 | 75.0 | 0.58 | 25.1 | 0.36 | TOC RE | f |
| WPB1-5 | 201.9 | Nonesuch | Core | EXP |  | 0.762 | 0.081 | 1.95 | 0.27 | 434 |  | 255.9 | 35.4 | 7.22 | 10.6 | 0.04 | TOC RE | n:lts2sh |
| LIR-2 |  | Nonesuch | Outcrop | NOPR |  | 0.071 | -1 | -1 | -1 | -1 |  | -1 | -1 | -1 | -1 | -1 | TOC |  |
| LIR-3 |  | Nonesuch | Outcrop | NOPR |  | 0.010 | -1 | -1 | -1 | -1 |  | -1 | -1 | -1 | -1 | -1 | TOC |  |
| LIR-4 |  | Nonesuch | Outcrop | NOPR |  | 0.111 | -1 | -1 | -1 | -1 |  | -1 | -1 | -1 | -1 | -1 | TOC |  |

*Appendix D, ctd.*

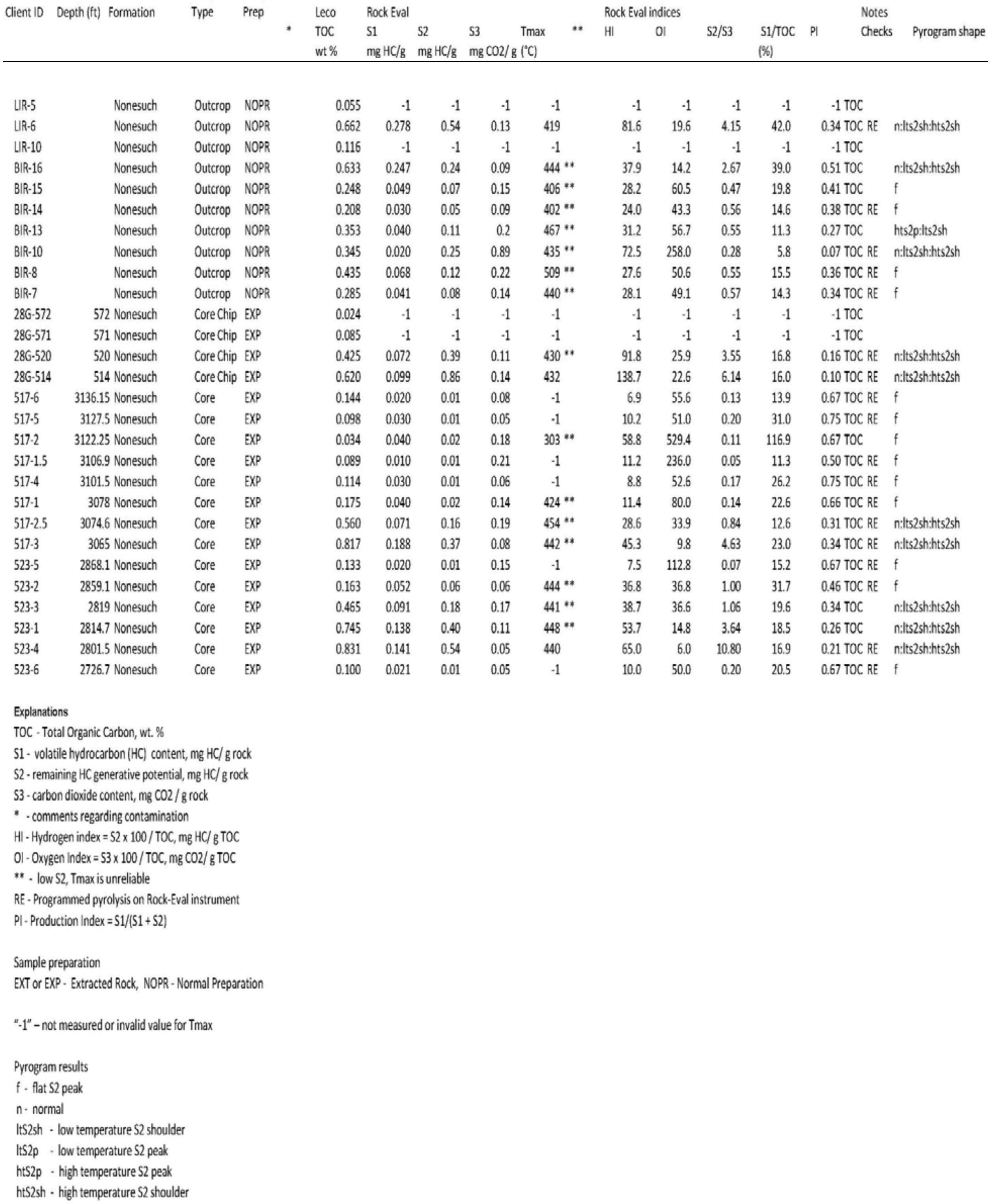

|  |  |  | Sample | Sample |  | Leco | Rock Eval |  |  |  |  | Rock Eval indices |  |  |  |  | Notes |  |
|---|---|---|---|---|---|---|---|---|---|---|---|---|---|---|---|---|---|---|
| Client ID | Depth (ft) | Formation | Type | Prep | * | TOC wt % | S1 mg HC/g | S2 mg HC/g | S3 mg CO2/ g | Tmax (°C) | ** | HI | OI | S2/S3 | S1/TOC (%) | PI | Checks | Pyrogram shape |
| LIR-5 |  | Nonesuch | Outcrop | NOPR |  | 0.055 | -1 | -1 | -1 | -1 |  | -1 | -1 | -1 | -1 | -1 | TOC |  |
| LIR-6 |  | Nonesuch | Outcrop | NOPR |  | 0.662 | 0.278 | 0.54 | 0.13 | 419 |  | 81.6 | 19.6 | 4.15 | 42.0 | 0.34 | TOC RE | n:lts2sh:hts2sh |
| LIR-10 |  | Nonesuch | Outcrop | NOPR |  | 0.116 | -1 | -1 | -1 | -1 |  | -1 | -1 | -1 | -1 | -1 | TOC |  |
| BIR-16 |  | Nonesuch | Outcrop | NOPR |  | 0.633 | 0.247 | 0.24 | 0.09 | 444 | ** | 37.9 | 14.2 | 2.67 | 39.0 | 0.51 | TOC | n:lts2sh:hts2sh |
| BIR-15 |  | Nonesuch | Outcrop | NOPR |  | 0.248 | 0.049 | 0.07 | 0.15 | 406 | ** | 28.2 | 60.5 | 0.47 | 19.8 | 0.41 | TOC | f |
| BIR-14 |  | Nonesuch | Outcrop | NOPR |  | 0.208 | 0.030 | 0.05 | 0.09 | 402 | ** | 24.0 | 43.3 | 0.56 | 14.6 | 0.38 | TOC RE | f |
| BIR-13 |  | Nonesuch | Outcrop | NOPR |  | 0.353 | 0.040 | 0.11 | 0.2 | 467 | ** | 31.2 | 56.7 | 0.55 | 11.3 | 0.27 | TOC | hts2p:lts2sh |
| BIR-10 |  | Nonesuch | Outcrop | NOPR |  | 0.345 | 0.020 | 0.25 | 0.89 | 435 | ** | 72.5 | 258.0 | 0.28 | 5.8 | 0.07 | TOC RE | n:lts2sh:hts2sh |
| BIR-8 |  | Nonesuch | Outcrop | NOPR |  | 0.435 | 0.068 | 0.12 | 0.22 | 509 | ** | 27.6 | 50.6 | 0.55 | 15.5 | 0.36 | TOC RE | f |
| BIR-7 |  | Nonesuch | Outcrop | NOPR |  | 0.285 | 0.041 | 0.08 | 0.14 | 440 | ** | 28.1 | 49.1 | 0.57 | 14.3 | 0.34 | TOC RE | f |
| 28G-572 | 572 | Nonesuch | Core Chip | EXP |  | 0.024 | -1 | -1 | -1 | -1 |  | -1 | -1 | -1 | -1 | -1 | TOC |  |
| 28G-571 | 571 | Nonesuch | Core Chip | EXP |  | 0.085 | -1 | -1 | -1 | -1 |  | -1 | -1 | -1 | -1 | -1 | TOC |  |
| 28G-520 | 520 | Nonesuch | Core Chip | EXP |  | 0.425 | 0.072 | 0.39 | 0.11 | 430 | ** | 91.8 | 25.9 | 3.55 | 16.8 | 0.16 | TOC RE | n:lts2sh:hts2sh |
| 28G-514 | 514 | Nonesuch | Core Chip | EXP |  | 0.620 | 0.099 | 0.86 | 0.14 | 432 |  | 138.7 | 22.6 | 6.14 | 16.0 | 0.10 | TOC RE | n:lts2sh:hts2sh |
| 517-6 | 3136.15 | Nonesuch | Core | EXP |  | 0.144 | 0.020 | 0.01 | 0.08 | -1 |  | 6.9 | 55.6 | 0.13 | 13.9 | 0.67 | TOC RE | f |
| 517-5 | 3127.5 | Nonesuch | Core | EXP |  | 0.098 | 0.030 | 0.01 | 0.05 | -1 |  | 10.2 | 51.0 | 0.20 | 31.0 | 0.75 | TOC RE | f |
| 517-2 | 3122.25 | Nonesuch | Core | EXP |  | 0.034 | 0.040 | 0.02 | 0.18 | 303 | ** | 58.8 | 529.4 | 0.11 | 116.9 | 0.67 | TOC | f |
| 517-1.5 | 3106.9 | Nonesuch | Core | EXP |  | 0.089 | 0.010 | 0.01 | 0.21 | -1 |  | 11.2 | 236.0 | 0.05 | 11.3 | 0.50 | TOC RE | f |
| 517-4 | 3101.5 | Nonesuch | Core | EXP |  | 0.114 | 0.030 | 0.01 | 0.06 | -1 |  | 8.8 | 52.6 | 0.17 | 26.2 | 0.75 | TOC RE | f |
| 517-1 | 3078 | Nonesuch | Core | EXP |  | 0.175 | 0.040 | 0.02 | 0.14 | 424 | ** | 11.4 | 80.0 | 0.14 | 22.6 | 0.66 | TOC RE | f |
| 517-2.5 | 3074.6 | Nonesuch | Core | EXP |  | 0.560 | 0.071 | 0.16 | 0.19 | 454 | ** | 28.6 | 33.9 | 0.84 | 12.6 | 0.31 | TOC RE | n:lts2sh:hts2sh |
| 517-3 | 3065 | Nonesuch | Core | EXP |  | 0.817 | 0.188 | 0.37 | 0.08 | 442 | ** | 45.3 | 9.8 | 4.63 | 23.0 | 0.34 | TOC RE | n:lts2sh:hts2sh |
| 523-5 | 2868.1 | Nonesuch | Core | EXP |  | 0.133 | 0.020 | 0.01 | 0.15 | -1 |  | 7.5 | 112.8 | 0.07 | 15.2 | 0.67 | TOC RE | f |
| 523-2 | 2859.1 | Nonesuch | Core | EXP |  | 0.163 | 0.052 | 0.06 | 0.06 | 444 | ** | 36.8 | 36.8 | 1.00 | 31.7 | 0.46 | TOC RE | f |
| 523-3 | 2819 | Nonesuch | Core | EXP |  | 0.465 | 0.091 | 0.18 | 0.17 | 441 | ** | 38.7 | 36.6 | 1.06 | 19.6 | 0.34 | TOC | n:lts2sh:hts2sh |
| 523-1 | 2814.7 | Nonesuch | Core | EXP |  | 0.745 | 0.138 | 0.40 | 0.11 | 448 | ** | 53.7 | 14.8 | 3.64 | 18.5 | 0.26 | TOC | n:lts2sh:hts2sh |
| 523-4 | 2801.5 | Nonesuch | Core | EXP |  | 0.831 | 0.141 | 0.54 | 0.05 | 440 |  | 65.0 | 6.0 | 10.80 | 16.9 | 0.21 | TOC RE | n:lts2sh:hts2sh |
| 523-6 | 2726.7 | Nonesuch | Core | EXP |  | 0.100 | 0.021 | 0.01 | 0.05 | -1 |  | 10.0 | 50.0 | 0.20 | 20.5 | 0.67 | TOC RE | f |

**Explanations**

TOC - Total Organic Carbon, wt. %
S1 - volatile hydrocarbon (HC) content, mg HC/ g rock
S2 - remaining HC generative potential, mg HC/ g rock
S3 - carbon dioxide content, mg CO2 / g rock
* - comments regarding contamination
HI - Hydrogen index = S2 x 100 / TOC, mg HC/ g TOC
OI - Oxygen Index = S3 x 100 / TOC, mg CO2/ g TOC
** - low S2, Tmax is unreliable
RE - Programmed pyrolysis on Rock-Eval instrument
PI - Production Index = S1/(S1 + S2)

Sample preparation
EXT or EXP - Extracted Rock, NOPR - Normal Preparation

"-1" – not measured or invalid value for Tmax

Pyrogram results
f - flat S2 peak
n - normal
ltS2sh - low temperature S2 shoulder
ltS2p - low temperature S2 peak
htS2p - high temperature S2 peak
htS2sh - high temperature S2 shoulder

*Appendix D, ctd.*

Kerogen Type Plots
Batch 1

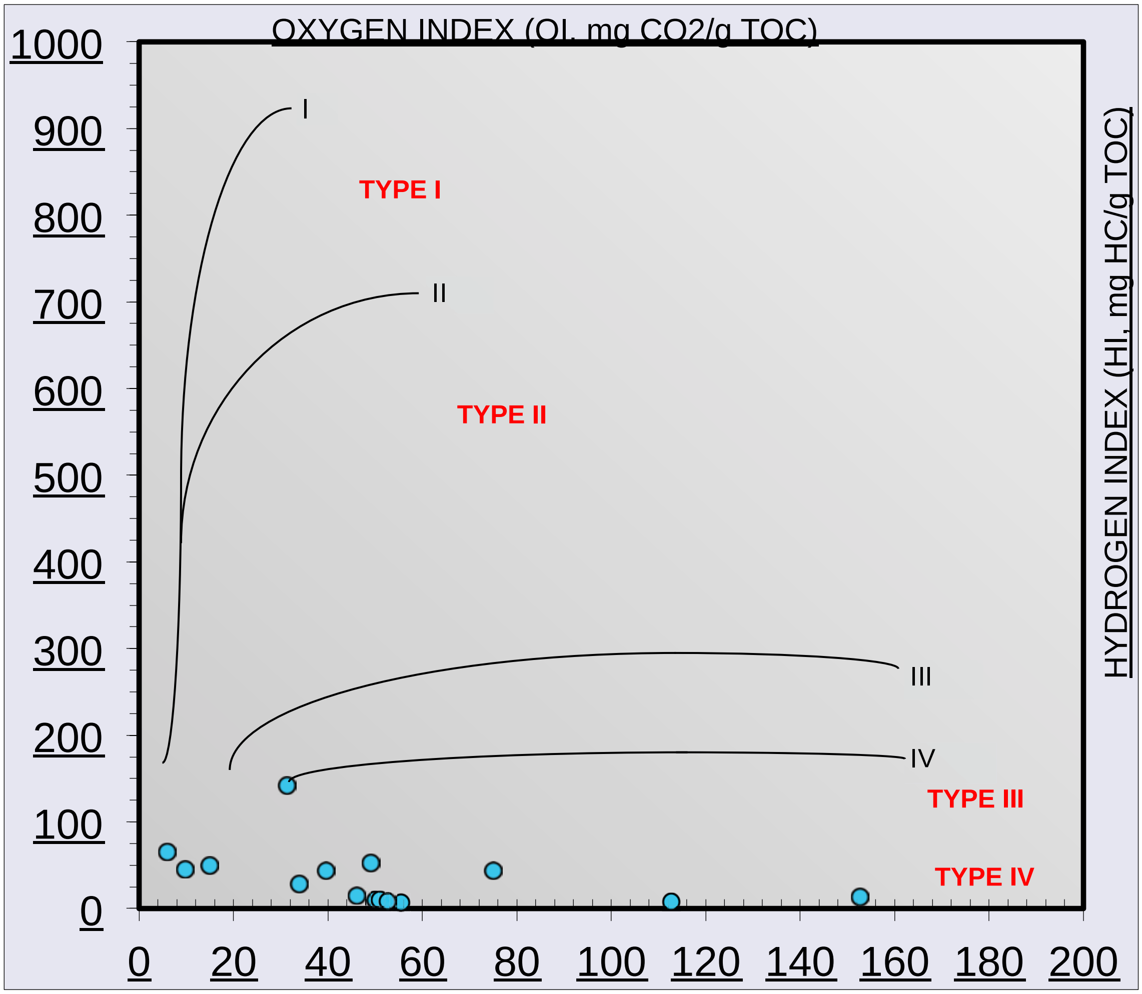

*Appendix D, ctd.*

Batch 2

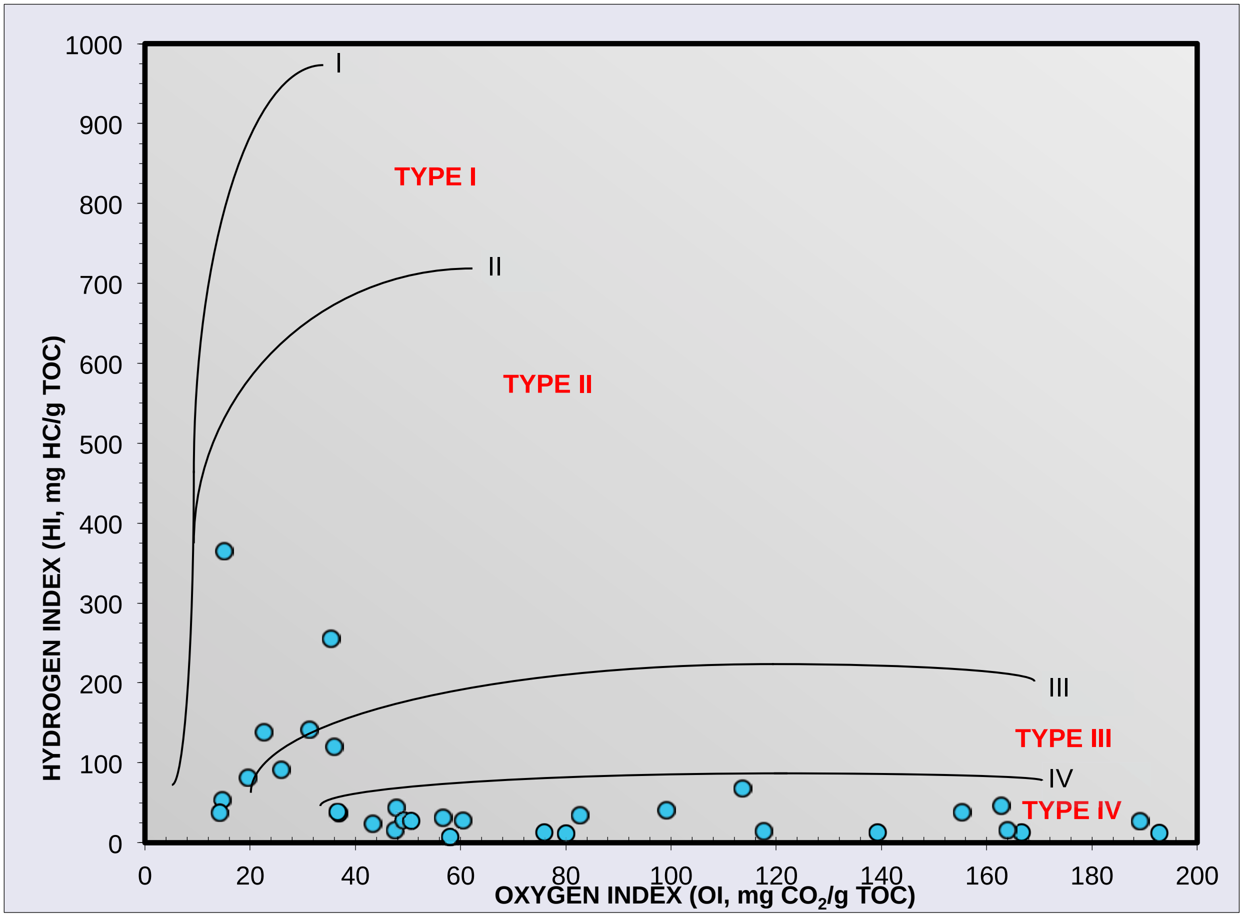

*Appendix D, ctd.*

## Kerogen Type and Maturity

### Batch 1

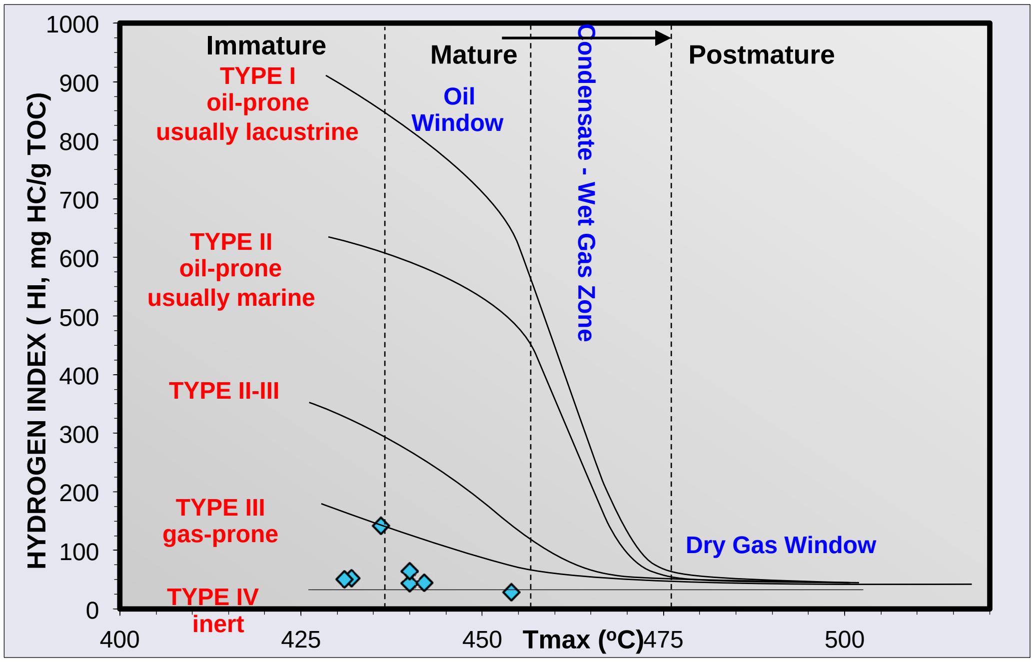

### Batch 2

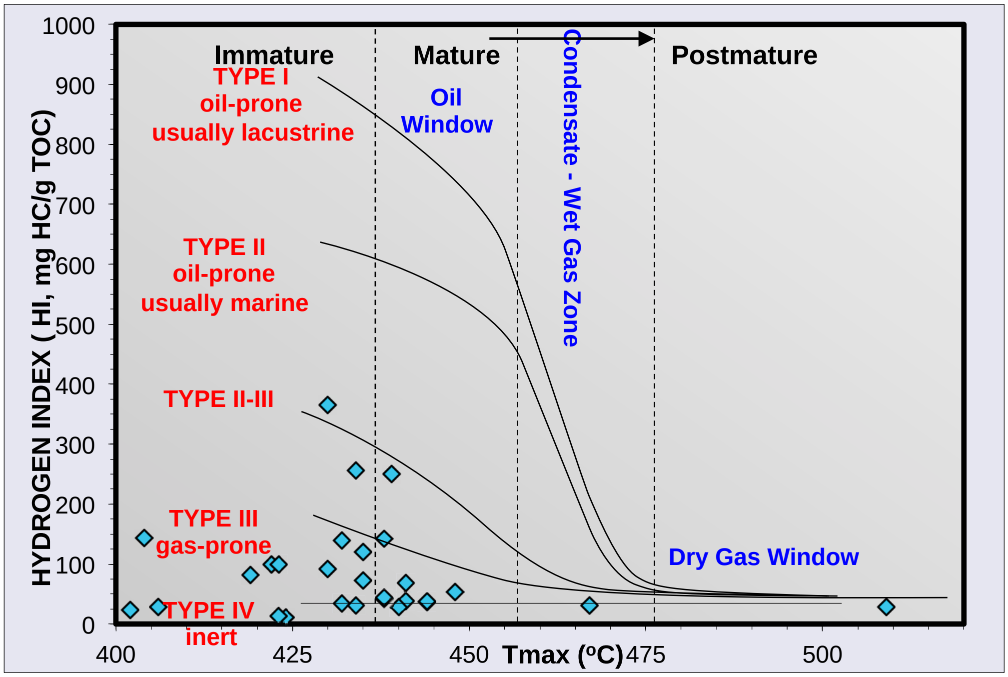

*Appendix D, ctd.*

Kerogen Quality

Batch 1

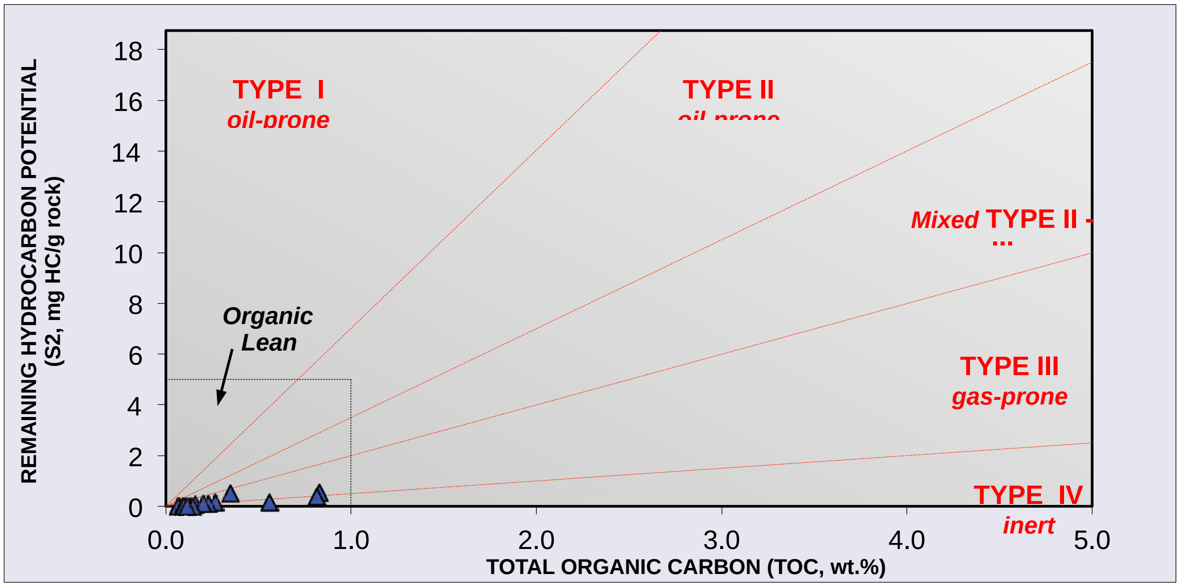

Batch 2

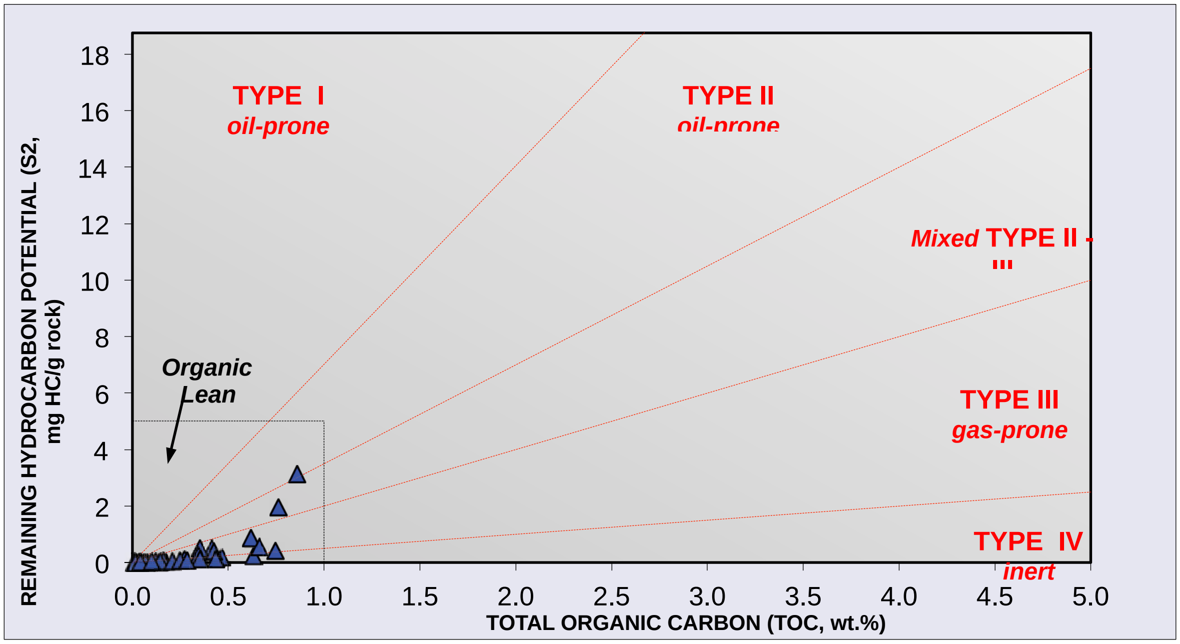

*Appendix E: Carbonate Carbon and Oxygen Stable Isotope Data*
Insuff. = insufficient carbonate in sample for analysis

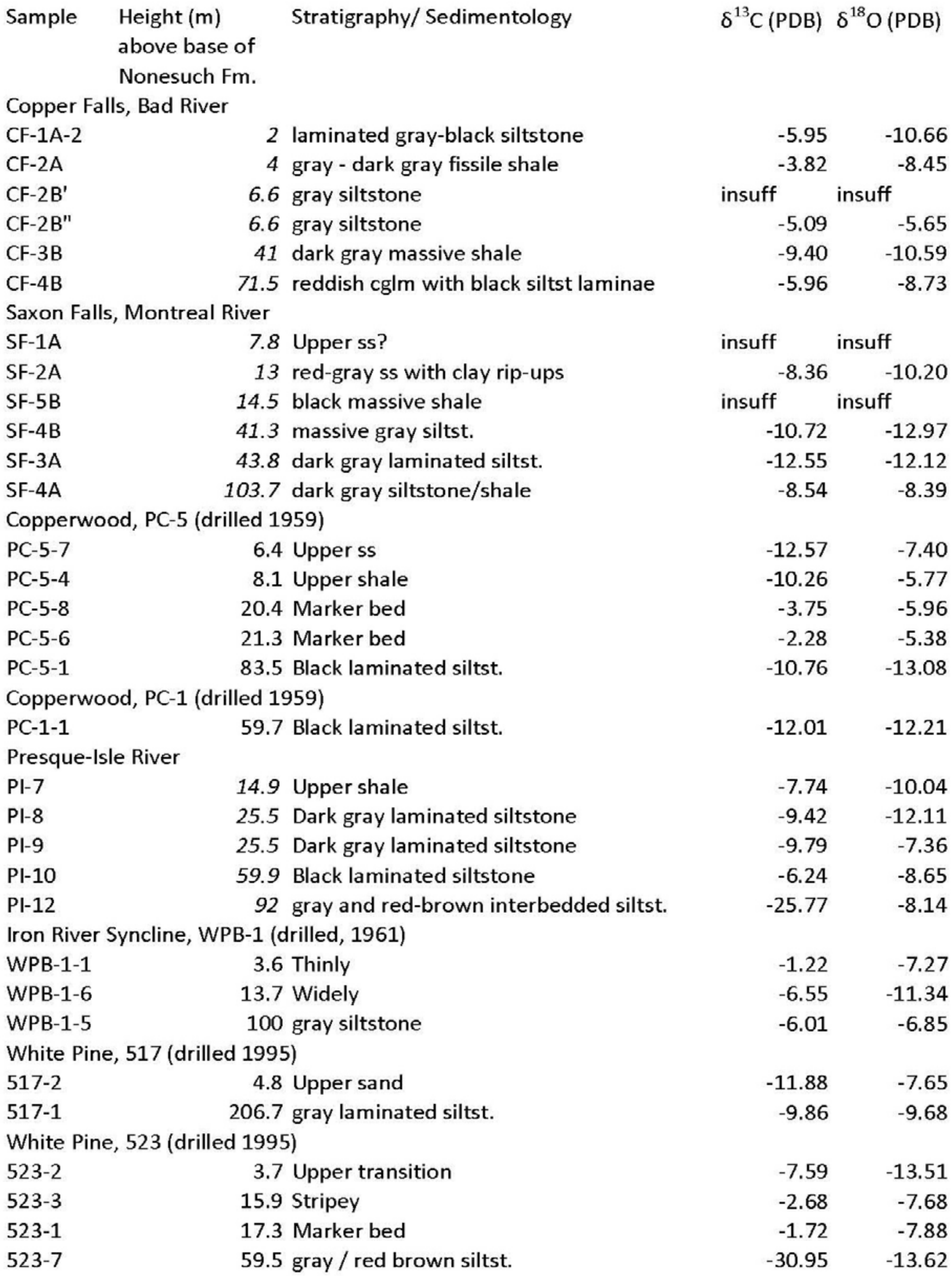

| Sample | Height (m) above base of Nonesuch Fm. | Stratigraphy/ Sedimentology | $\delta^{13}C$ (PDB) | $\delta^{18}O$ (PDB) |
|---|---|---|---|---|
| Copper Falls, Bad River | | | | |
| CF-1A-2 | *2* | laminated gray-black siltstone | -5.95 | -10.66 |
| CF-2A | *4* | gray - dark gray fissile shale | -3.82 | -8.45 |
| CF-2B' | *6.6* | gray siltstone | insuff | insuff |
| CF-2B" | *6.6* | gray siltstone | -5.09 | -5.65 |
| CF-3B | *41* | dark gray massive shale | -9.40 | -10.59 |
| CF-4B | *71.5* | reddish cglm with black siltst laminae | -5.96 | -8.73 |
| Saxon Falls, Montreal River | | | | |
| SF-1A | *7.8* | Upper ss? | insuff | insuff |
| SF-2A | *13* | red-gray ss with clay rip-ups | -8.36 | -10.20 |
| SF-5B | *14.5* | black massive shale | insuff | insuff |
| SF-4B | *41.3* | massive gray siltst. | -10.72 | -12.97 |
| SF-3A | *43.8* | dark gray laminated siltst. | -12.55 | -12.12 |
| SF-4A | *103.7* | dark gray siltstone/shale | -8.54 | -8.39 |
| Copperwood, PC-5 (drilled 1959) | | | | |
| PC-5-7 | 6.4 | Upper ss | -12.57 | -7.40 |
| PC-5-4 | 8.1 | Upper shale | -10.26 | -5.77 |
| PC-5-8 | 20.4 | Marker bed | -3.75 | -5.96 |
| PC-5-6 | 21.3 | Marker bed | -2.28 | -5.38 |
| PC-5-1 | 83.5 | Black laminated siltst. | -10.76 | -13.08 |
| Copperwood, PC-1 (drilled 1959) | | | | |
| PC-1-1 | 59.7 | Black laminated siltst. | -12.01 | -12.21 |
| Presque-Isle River | | | | |
| PI-7 | *14.9* | Upper shale | -7.74 | -10.04 |
| PI-8 | *25.5* | Dark gray laminated siltstone | -9.42 | -12.11 |
| PI-9 | *25.5* | Dark gray laminated siltstone | -9.79 | -7.36 |
| PI-10 | *59.9* | Black laminated siltstone | -6.24 | -8.65 |
| PI-12 | *92* | gray and red-brown interbedded siltst. | -25.77 | -8.14 |
| Iron River Syncline, WPB-1 (drilled, 1961) | | | | |
| WPB-1-1 | 3.6 | Thinly | -1.22 | -7.27 |
| WPB-1-6 | 13.7 | Widely | -6.55 | -11.34 |
| WPB-1-5 | 100 | gray siltstone | -6.01 | -6.85 |
| White Pine, 517 (drilled 1995) | | | | |
| 517-2 | 4.8 | Upper sand | -11.88 | -7.65 |
| 517-1 | 206.7 | gray laminated siltst. | -9.86 | -9.68 |
| White Pine, 523 (drilled 1995) | | | | |
| 523-2 | 3.7 | Upper transition | -7.59 | -13.51 |
| 523-3 | 15.9 | Stripey | -2.68 | -7.68 |
| 523-1 | 17.3 | Marker bed | -1.72 | -7.88 |
| 523-7 | 59.5 | gray / red brown siltst. | -30.95 | -13.62 |

*Appendix F1: Total Extract Gas Chromatography Data*

Definitions on page 319.

**Weatherford**
LABORATORIES

**EXTRACT GC**

| | | | |
|---|---|---|---|
| **Company:** | **Colorado State University** | **Client ID:** | **WPB1-1** |
| **Country:** | | **Project #:** | **BH-79915** |
| **Basin:** | | **Lab ID:** | **6121836392** |
| **Lease:** | | **Sample Type:** | **Core** |
| **Block:** | | **Sampling Point:** | |
| **Field:** | | **Formation:** | |
| **Well Name:** | **Colorado State University Samples** | **Geologic Age:** | |
| **Latitude:** | | **Top Depth:** | **518.10** |
| **Longitude:** | | **Bottom Depth:** | |
| **Preparation:** | | **GC Method:** | **G02G** |

**Extract GC Trace** G2160497.D

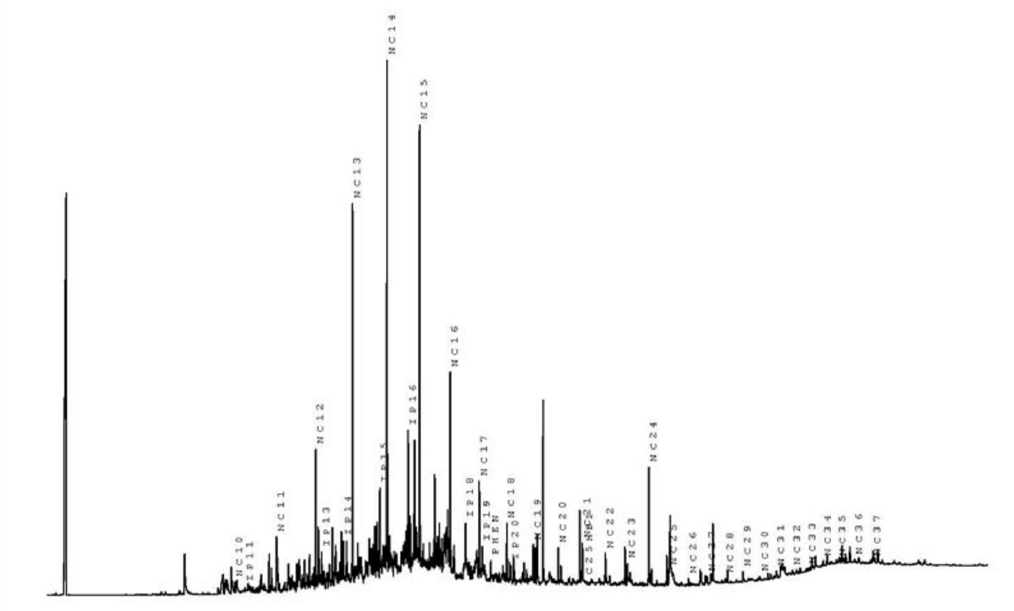

| WGC parameters | |
|---|---|
| Pristane/Phytane | 1.81 |
| Pristane/$nC_{17}$ | 0.45 |
| Phytane/$nC_{18}$ | 0.45 |
| $nC_{18}/(nC_{18}+nC_{19})$ | 0.60 |
| $nC_{17}/(nC_{17}+nC_{29})$ | 0.90 |
| CPI Hunt[4] | 0.42 |
| Normal Paraffins | 20.4 |
| Isoprenoids | 4.6 |
| Cycloparaffins | |
| Branched (iso-) Paraffins | |
| BTX aromatics | |
| Resolved unknowns | 74.8 |

| Thompson[1] | | |
|---|---|---|
| A. | BZ/$nC_6$ | |
| B. | TOL/$nC_7$ | |
| C. | $(nC_6+nC_7)/(CH+MCH)$ | |
| I. | Isoheptane Value | |
| F. | $nC_7$/MCH | |
| U. | CH/MCP | |
| R. | $nC_7$/2MH | |
| S. | $nC_6$/22DMB | |
| H. | Heptane Value | |
| | MCH/$nC_7$ | |
| | mpXYL/$nC_8$ | |
| | | |

| Mango[2] | |
|---|---|
| $P_1$ | |
| $P_2$ | |
| $P_3$ | |
| $5N_1$ | |
| $N_2$ | |
| $6N_1$ | |
| $K_1$ | |
| $K_2$ | |
| $5N_1/6N_1$ | |
| $P_3/N_2$ | |
| ln(24DMP/23DMP) | |
| | |

| Halpern[3] | |
|---|---|
| $Tr_1$ | |
| $Tr_2$ | |
| $Tr_3$ | |
| $Tr_4$ | |
| $Tr_5$ | |
| $Tr_7$ | |
| $Tr_8$ | |
| $C_1$ | |
| $C_2$ | |
| $C_3$ | |
| $C_4$ | |
| $C_5$ | |

[1] Thompson, K.F.M.,1983.GCA:V.47, p.303. [2] Mango, F.D.,1994.GCA: V.58, p.895. [3] Halpern,H.I.,1995,AAPG Bull.: V.79, p.801. [4] Hunt, 1979

*Appendix F1, ctd.*

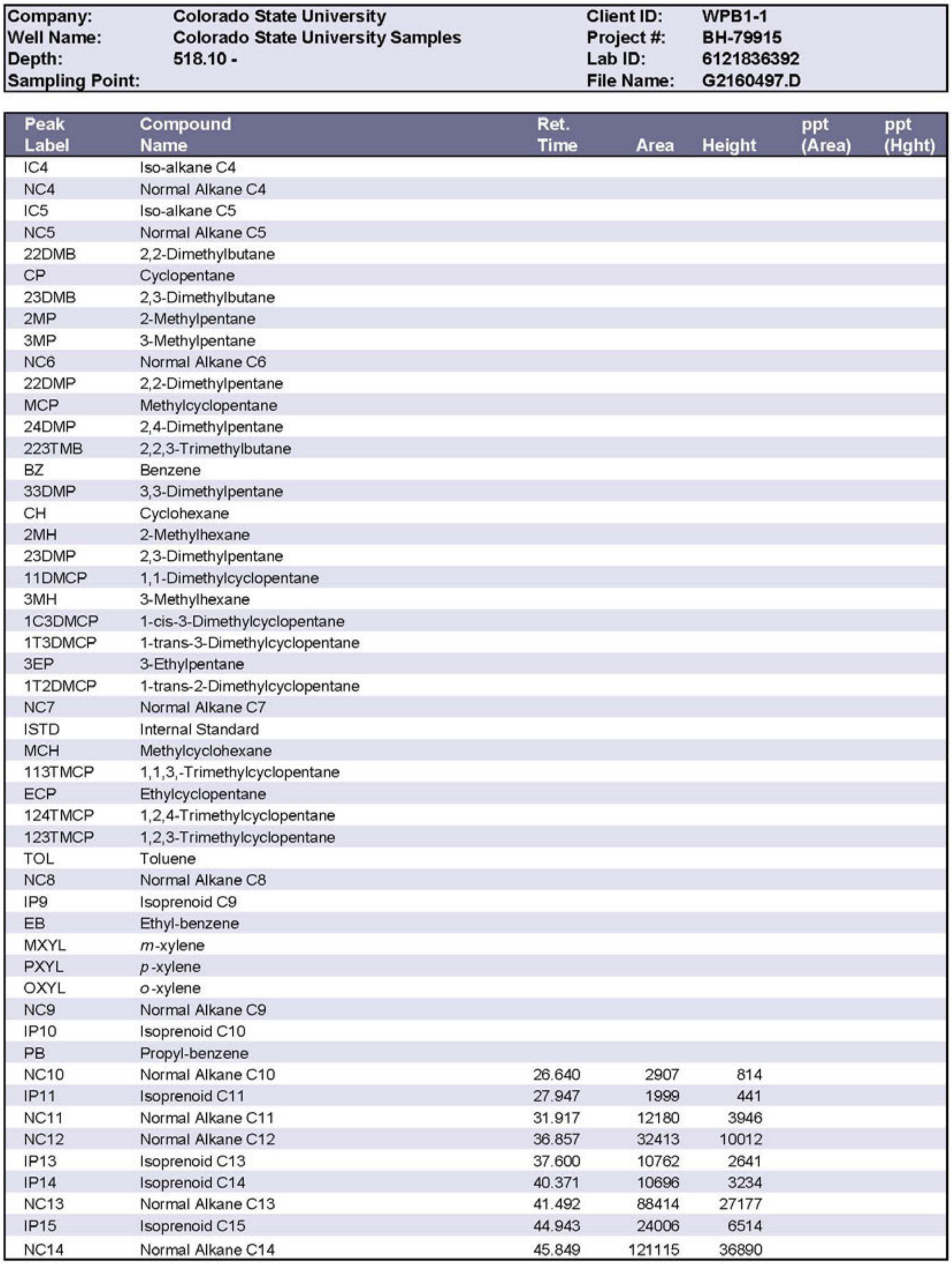

| | | | |
|---|---|---|---|
| **Company:** | **Colorado State University** | **Client ID:** | **WPB1-1** |
| **Well Name:** | **Colorado State University Samples** | **Project #:** | **BH-79915** |
| **Depth:** | **518.10 -** | **Lab ID:** | **6121836392** |
| **Sampling Point:** | | **File Name:** | **G2160497.D** |

| Peak Label | Compound Name | Ret. Time | Area | Height | ppt (Area) | ppt (Hght) |
|---|---|---|---|---|---|---|
| IC4 | Iso-alkane C4 | | | | | |
| NC4 | Normal Alkane C4 | | | | | |
| IC5 | Iso-alkane C5 | | | | | |
| NC5 | Normal Alkane C5 | | | | | |
| 22DMB | 2,2-Dimethylbutane | | | | | |
| CP | Cyclopentane | | | | | |
| 23DMB | 2,3-Dimethylbutane | | | | | |
| 2MP | 2-Methylpentane | | | | | |
| 3MP | 3-Methylpentane | | | | | |
| NC6 | Normal Alkane C6 | | | | | |
| 22DMP | 2,2-Dimethylpentane | | | | | |
| MCP | Methylcyclopentane | | | | | |
| 24DMP | 2,4-Dimethylpentane | | | | | |
| 223TMB | 2,2,3-Trimethylbutane | | | | | |
| BZ | Benzene | | | | | |
| 33DMP | 3,3-Dimethylpentane | | | | | |
| CH | Cyclohexane | | | | | |
| 2MH | 2-Methylhexane | | | | | |
| 23DMP | 2,3-Dimethylpentane | | | | | |
| 11DMCP | 1,1-Dimethylcyclopentane | | | | | |
| 3MH | 3-Methylhexane | | | | | |
| 1C3DMCP | 1-cis-3-Dimethylcyclopentane | | | | | |
| 1T3DMCP | 1-trans-3-Dimethylcyclopentane | | | | | |
| 3EP | 3-Ethylpentane | | | | | |
| 1T2DMCP | 1-trans-2-Dimethylcyclopentane | | | | | |
| NC7 | Normal Alkane C7 | | | | | |
| ISTD | Internal Standard | | | | | |
| MCH | Methylcyclohexane | | | | | |
| 113TMCP | 1,1,3,-Trimethylcyclopentane | | | | | |
| ECP | Ethylcyclopentane | | | | | |
| 124TMCP | 1,2,4-Trimethylcyclopentane | | | | | |
| 123TMCP | 1,2,3-Trimethylcyclopentane | | | | | |
| TOL | Toluene | | | | | |
| NC8 | Normal Alkane C8 | | | | | |
| IP9 | Isoprenoid C9 | | | | | |
| EB | Ethyl-benzene | | | | | |
| MXYL | *m*-xylene | | | | | |
| PXYL | *p*-xylene | | | | | |
| OXYL | *o*-xylene | | | | | |
| NC9 | Normal Alkane C9 | | | | | |
| IP10 | Isoprenoid C10 | | | | | |
| PB | Propyl-benzene | | | | | |
| NC10 | Normal Alkane C10 | 26.640 | 2907 | 814 | | |
| IP11 | Isoprenoid C11 | 27.947 | 1999 | 441 | | |
| NC11 | Normal Alkane C11 | 31.917 | 12180 | 3946 | | |
| NC12 | Normal Alkane C12 | 36.857 | 32413 | 10012 | | |
| IP13 | Isoprenoid C13 | 37.600 | 10762 | 2641 | | |
| IP14 | Isoprenoid C14 | 40.371 | 10696 | 3234 | | |
| NC13 | Normal Alkane C13 | 41.492 | 88414 | 27177 | | |
| IP15 | Isoprenoid C15 | 44.943 | 24006 | 6514 | | |
| NC14 | Normal Alkane C14 | 45.849 | 121115 | 36890 | | |

*Appendix F1, ctd.*

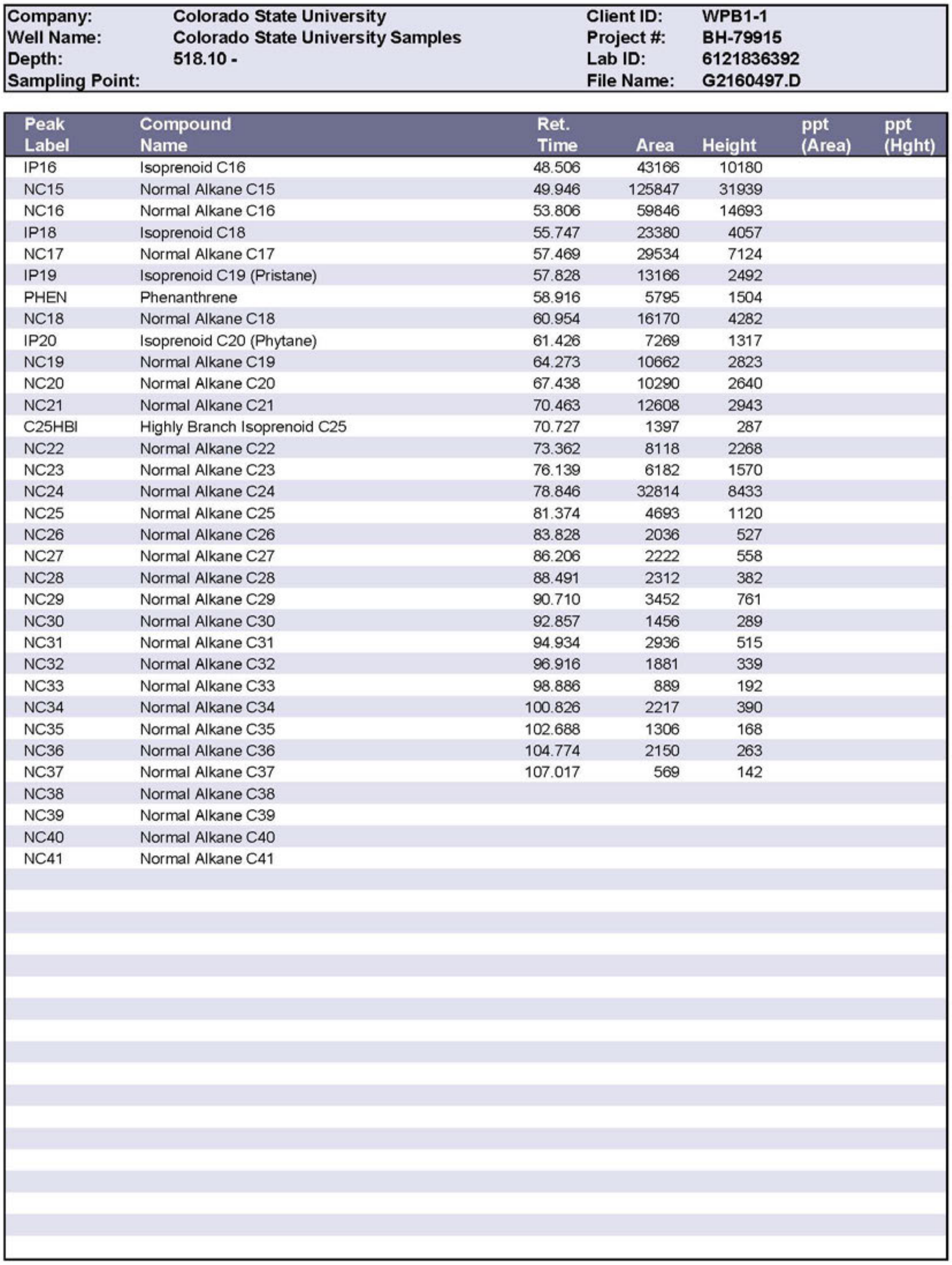

| | | | |
|---|---|---|---|
| **Company:** | **Colorado State University** | **Client ID:** | **WPB1-1** |
| **Well Name:** | **Colorado State University Samples** | **Project #:** | **BH-79915** |
| **Depth:** | **518.10 -** | **Lab ID:** | **6121836392** |
| **Sampling Point:** | | **File Name:** | **G2160497.D** |

| Peak Label | Compound Name | Ret. Time | Area | Height | ppt (Area) | ppt (Hght) |
|---|---|---|---|---|---|---|
| IP16 | Isoprenoid C16 | 48.506 | 43166 | 10180 | | |
| NC15 | Normal Alkane C15 | 49.946 | 125847 | 31939 | | |
| NC16 | Normal Alkane C16 | 53.806 | 59846 | 14693 | | |
| IP18 | Isoprenoid C18 | 55.747 | 23380 | 4057 | | |
| NC17 | Normal Alkane C17 | 57.469 | 29534 | 7124 | | |
| IP19 | Isoprenoid C19 (Pristane) | 57.828 | 13166 | 2492 | | |
| PHEN | Phenanthrene | 58.916 | 5795 | 1504 | | |
| NC18 | Normal Alkane C18 | 60.954 | 16170 | 4282 | | |
| IP20 | Isoprenoid C20 (Phytane) | 61.426 | 7269 | 1317 | | |
| NC19 | Normal Alkane C19 | 64.273 | 10662 | 2823 | | |
| NC20 | Normal Alkane C20 | 67.438 | 10290 | 2640 | | |
| NC21 | Normal Alkane C21 | 70.463 | 12608 | 2943 | | |
| C25HBI | Highly Branch Isoprenoid C25 | 70.727 | 1397 | 287 | | |
| NC22 | Normal Alkane C22 | 73.362 | 8118 | 2268 | | |
| NC23 | Normal Alkane C23 | 76.139 | 6182 | 1570 | | |
| NC24 | Normal Alkane C24 | 78.846 | 32814 | 8433 | | |
| NC25 | Normal Alkane C25 | 81.374 | 4693 | 1120 | | |
| NC26 | Normal Alkane C26 | 83.828 | 2036 | 527 | | |
| NC27 | Normal Alkane C27 | 86.206 | 2222 | 558 | | |
| NC28 | Normal Alkane C28 | 88.491 | 2312 | 382 | | |
| NC29 | Normal Alkane C29 | 90.710 | 3452 | 761 | | |
| NC30 | Normal Alkane C30 | 92.857 | 1456 | 289 | | |
| NC31 | Normal Alkane C31 | 94.934 | 2936 | 515 | | |
| NC32 | Normal Alkane C32 | 96.916 | 1881 | 339 | | |
| NC33 | Normal Alkane C33 | 98.886 | 889 | 192 | | |
| NC34 | Normal Alkane C34 | 100.826 | 2217 | 390 | | |
| NC35 | Normal Alkane C35 | 102.688 | 1306 | 168 | | |
| NC36 | Normal Alkane C36 | 104.774 | 2150 | 263 | | |
| NC37 | Normal Alkane C37 | 107.017 | 569 | 142 | | |
| NC38 | Normal Alkane C38 | | | | | |
| NC39 | Normal Alkane C39 | | | | | |
| NC40 | Normal Alkane C40 | | | | | |
| NC41 | Normal Alkane C41 | | | | | |

*Appendix F1, ctd.*

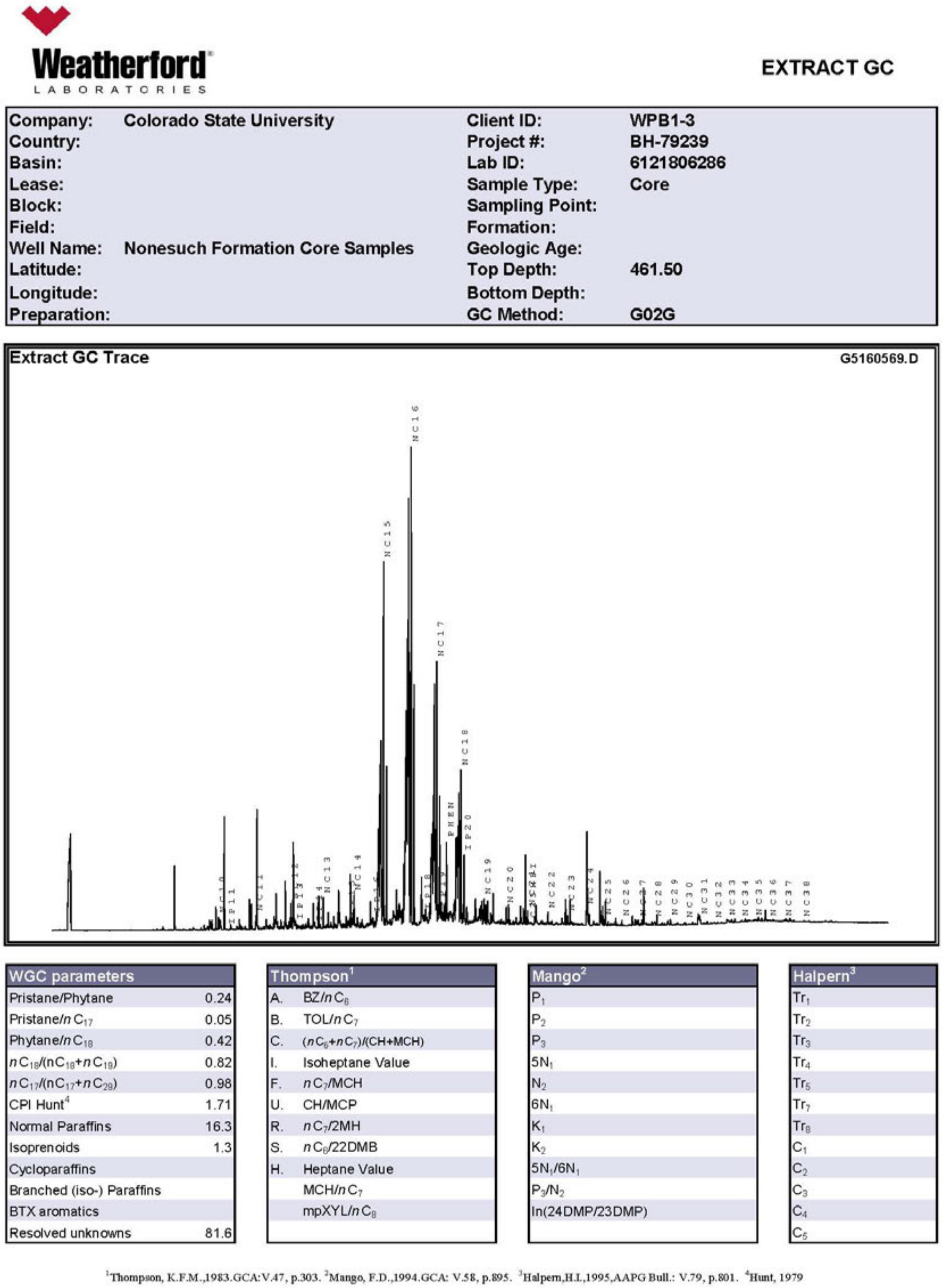

**Weatherford** LABORATORIES

**EXTRACT GC**

| | | | |
|---|---|---|---|
| **Company:** | **Colorado State University** | **Client ID:** | **WPB1-3** |
| **Country:** | | **Project #:** | **BH-79239** |
| **Basin:** | | **Lab ID:** | **6121806286** |
| **Lease:** | | **Sample Type:** | **Core** |
| **Block:** | | **Sampling Point:** | |
| **Field:** | | **Formation:** | |
| **Well Name:** | **Nonesuch Formation Core Samples** | **Geologic Age:** | |
| **Latitude:** | | **Top Depth:** | **461.50** |
| **Longitude:** | | **Bottom Depth:** | |
| **Preparation:** | | **GC Method:** | **G02G** |

**Extract GC Trace** G5160569.D

| WGC parameters | |
|---|---|
| Pristane/Phytane | 0.24 |
| Pristane/$nC_{17}$ | 0.05 |
| Phytane/$nC_{18}$ | 0.42 |
| $nC_{18}/(nC_{18}+nC_{19})$ | 0.82 |
| $nC_{17}/(nC_{17}+nC_{29})$ | 0.98 |
| CPI Hunt[4] | 1.71 |
| Normal Paraffins | 16.3 |
| Isoprenoids | 1.3 |
| Cycloparaffins | |
| Branched (iso-) Paraffins | |
| BTX aromatics | |
| Resolved unknowns | 81.6 |

| Thompson[1] | | |
|---|---|---|
| A. | BZ/$nC_6$ | |
| B. | TOL/$nC_7$ | |
| C. | $(nC_6+nC_7)$/(CH+MCH) | |
| I. | Isoheptane Value | |
| F. | $nC_7$/MCH | |
| U. | CH/MCP | |
| R. | $nC_7$/2MH | |
| S. | $nC_6$/22DMB | |
| H. | Heptane Value | |
| | MCH/$nC_7$ | |
| | mpXYL/$nC_8$ | |

| Mango[2] | |
|---|---|
| $P_1$ | |
| $P_2$ | |
| $P_3$ | |
| $5N_1$ | |
| $N_2$ | |
| $6N_1$ | |
| $K_1$ | |
| $K_2$ | |
| $5N_1/6N_1$ | |
| $P_3/N_2$ | |
| ln(24DMP/23DMP) | |

| Halpern[3] |
|---|
| $Tr_1$ |
| $Tr_2$ |
| $Tr_3$ |
| $Tr_4$ |
| $Tr_5$ |
| $Tr_7$ |
| $Tr_8$ |
| $C_1$ |
| $C_2$ |
| $C_3$ |
| $C_4$ |
| $C_5$ |

[1] Thompson, K.F.M.,1983.GCA:V.47, p.303. [2] Mango, F.D.,1994.GCA: V.58, p.895. [3] Halpern,H.I.,1995,AAPG Bull.: V.79, p.801. [4] Hunt, 1979

*Appendix F1, ctd.*

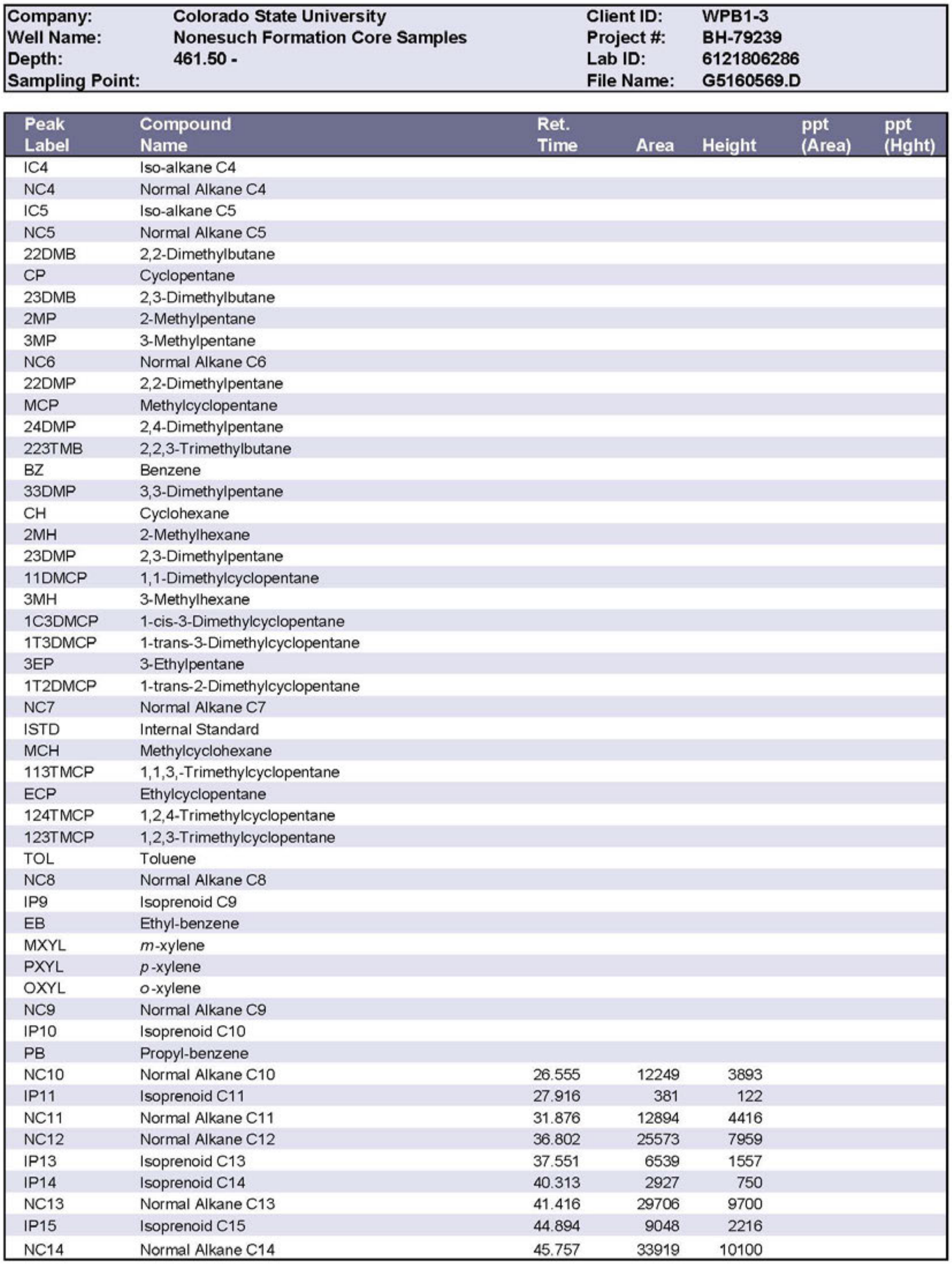

| | | | |
|---|---|---|---|
| **Company:** | **Colorado State University** | **Client ID:** | **WPB1-3** |
| **Well Name:** | **Nonesuch Formation Core Samples** | **Project #:** | **BH-79239** |
| **Depth:** | **461.50 -** | **Lab ID:** | **6121806286** |
| **Sampling Point:** | | **File Name:** | **G5160569.D** |

| Peak Label | Compound Name | Ret. Time | Area | Height | ppt (Area) | ppt (Hght) |
|---|---|---|---|---|---|---|
| IC4 | Iso-alkane C4 | | | | | |
| NC4 | Normal Alkane C4 | | | | | |
| IC5 | Iso-alkane C5 | | | | | |
| NC5 | Normal Alkane C5 | | | | | |
| 22DMB | 2,2-Dimethylbutane | | | | | |
| CP | Cyclopentane | | | | | |
| 23DMB | 2,3-Dimethylbutane | | | | | |
| 2MP | 2-Methylpentane | | | | | |
| 3MP | 3-Methylpentane | | | | | |
| NC6 | Normal Alkane C6 | | | | | |
| 22DMP | 2,2-Dimethylpentane | | | | | |
| MCP | Methylcyclopentane | | | | | |
| 24DMP | 2,4-Dimethylpentane | | | | | |
| 223TMB | 2,2,3-Trimethylbutane | | | | | |
| BZ | Benzene | | | | | |
| 33DMP | 3,3-Dimethylpentane | | | | | |
| CH | Cyclohexane | | | | | |
| 2MH | 2-Methylhexane | | | | | |
| 23DMP | 2,3-Dimethylpentane | | | | | |
| 11DMCP | 1,1-Dimethylcyclopentane | | | | | |
| 3MH | 3-Methylhexane | | | | | |
| 1C3DMCP | 1-cis-3-Dimethylcyclopentane | | | | | |
| 1T3DMCP | 1-trans-3-Dimethylcyclopentane | | | | | |
| 3EP | 3-Ethylpentane | | | | | |
| 1T2DMCP | 1-trans-2-Dimethylcyclopentane | | | | | |
| NC7 | Normal Alkane C7 | | | | | |
| ISTD | Internal Standard | | | | | |
| MCH | Methylcyclohexane | | | | | |
| 113TMCP | 1,1,3,-Trimethylcyclopentane | | | | | |
| ECP | Ethylcyclopentane | | | | | |
| 124TMCP | 1,2,4-Trimethylcyclopentane | | | | | |
| 123TMCP | 1,2,3-Trimethylcyclopentane | | | | | |
| TOL | Toluene | | | | | |
| NC8 | Normal Alkane C8 | | | | | |
| IP9 | Isoprenoid C9 | | | | | |
| EB | Ethyl-benzene | | | | | |
| MXYL | *m*-xylene | | | | | |
| PXYL | *p*-xylene | | | | | |
| OXYL | *o*-xylene | | | | | |
| NC9 | Normal Alkane C9 | | | | | |
| IP10 | Isoprenoid C10 | | | | | |
| PB | Propyl-benzene | | | | | |
| NC10 | Normal Alkane C10 | 26.555 | 12249 | 3893 | | |
| IP11 | Isoprenoid C11 | 27.916 | 381 | 122 | | |
| NC11 | Normal Alkane C11 | 31.876 | 12894 | 4416 | | |
| NC12 | Normal Alkane C12 | 36.802 | 25573 | 7959 | | |
| IP13 | Isoprenoid C13 | 37.551 | 6539 | 1557 | | |
| IP14 | Isoprenoid C14 | 40.313 | 2927 | 750 | | |
| NC13 | Normal Alkane C13 | 41.416 | 29706 | 9700 | | |
| IP15 | Isoprenoid C15 | 44.894 | 9048 | 2216 | | |
| NC14 | Normal Alkane C14 | 45.757 | 33919 | 10100 | | |

| | | | |
|---|---|---|---|
| **Company:** | **Colorado State University** | **Client ID:** | **WPB1-3** |
| **Well Name:** | **Nonesuch Formation Core Samples** | **Project #:** | **BH-79239** |
| **Depth:** | **461.50 -** | **Lab ID:** | **6121806286** |
| **Sampling Point:** | | **File Name:** | **G5160569.D** |

| Peak Label | Compound Name | Ret. Time | Area | Height | ppt (Area) | ppt (Hght) |
|---|---|---|---|---|---|---|
| IP16 | Isoprenoid C16 | 48.427 | 17877 | 2959 | | |
| NC15 | Normal Alkane C15 | 49.969 | 474087 | 113668 | | |
| NC16 | Normal Alkane C16 | 53.867 | 694945 | 148903 | | |
| IP18 | Isoprenoid C18 | 55.675 | 19549 | 3452 | | |
| NC17 | Normal Alkane C17 | 57.482 | 350783 | 82237 | | |
| IP19 | Isoprenoid C19 (Pristane) | 57.774 | 18403 | 4000 | | |
| PHEN | Phenanthrene | 58.865 | 102930 | 25673 | | |
| NC18 | Normal Alkane C18 | 60.935 | 184967 | 48159 | | |
| IP20 | Isoprenoid C20 (Phytane) | 61.368 | 77811 | 21587 | | |
| NC19 | Normal Alkane C19 | 64.189 | 39417 | 8009 | | |
| NC20 | Normal Alkane C20 | 67.339 | 21449 | 5485 | | |
| NC21 | Normal Alkane C21 | 70.359 | 14885 | 4396 | | |
| C25HBI | Highly Branch Isoprenoid C25 | 70.546 | 2484 | 624 | | |
| NC22 | Normal Alkane C22 | 73.252 | 14279 | 3976 | | |
| NC23 | Normal Alkane C23 | 76.028 | 11605 | 3029 | | |
| NC24 | Normal Alkane C24 | 78.664 | 4906 | 2617 | | |
| NC25 | Normal Alkane C25 | 81.251 | 7408 | 1983 | | |
| NC26 | Normal Alkane C26 | 83.712 | 6279 | 1686 | | |
| NC27 | Normal Alkane C27 | 86.086 | 6364 | 1654 | | |
| NC28 | Normal Alkane C28 | 88.375 | 7119 | 1312 | | |
| NC29 | Normal Alkane C29 | 90.590 | 7589 | 1666 | | |
| NC30 | Normal Alkane C30 | 92.731 | 2761 | 723 | | |
| NC31 | Normal Alkane C31 | 94.802 | 10243 | 1751 | | |
| NC32 | Normal Alkane C32 | 96.813 | 2173 | 463 | | |
| NC33 | Normal Alkane C33 | 98.752 | 4568 | 861 | | |
| NC34 | Normal Alkane C34 | 100.661 | 1299 | 352 | | |
| NC35 | Normal Alkane C35 | 102.521 | 3456 | 407 | | |
| NC36 | Normal Alkane C36 | 104.544 | 1371 | 218 | | |
| NC37 | Normal Alkane C37 | 106.797 | 883 | 174 | | |
| NC38 | Normal Alkane C38 | 109.367 | 622 | 108 | | |
| NC39 | Normal Alkane C39 | | | | | |
| NC40 | Normal Alkane C40 | | | | | |
| NC41 | Normal Alkane C41 | | | | | |

*Appendix F1, ctd.*

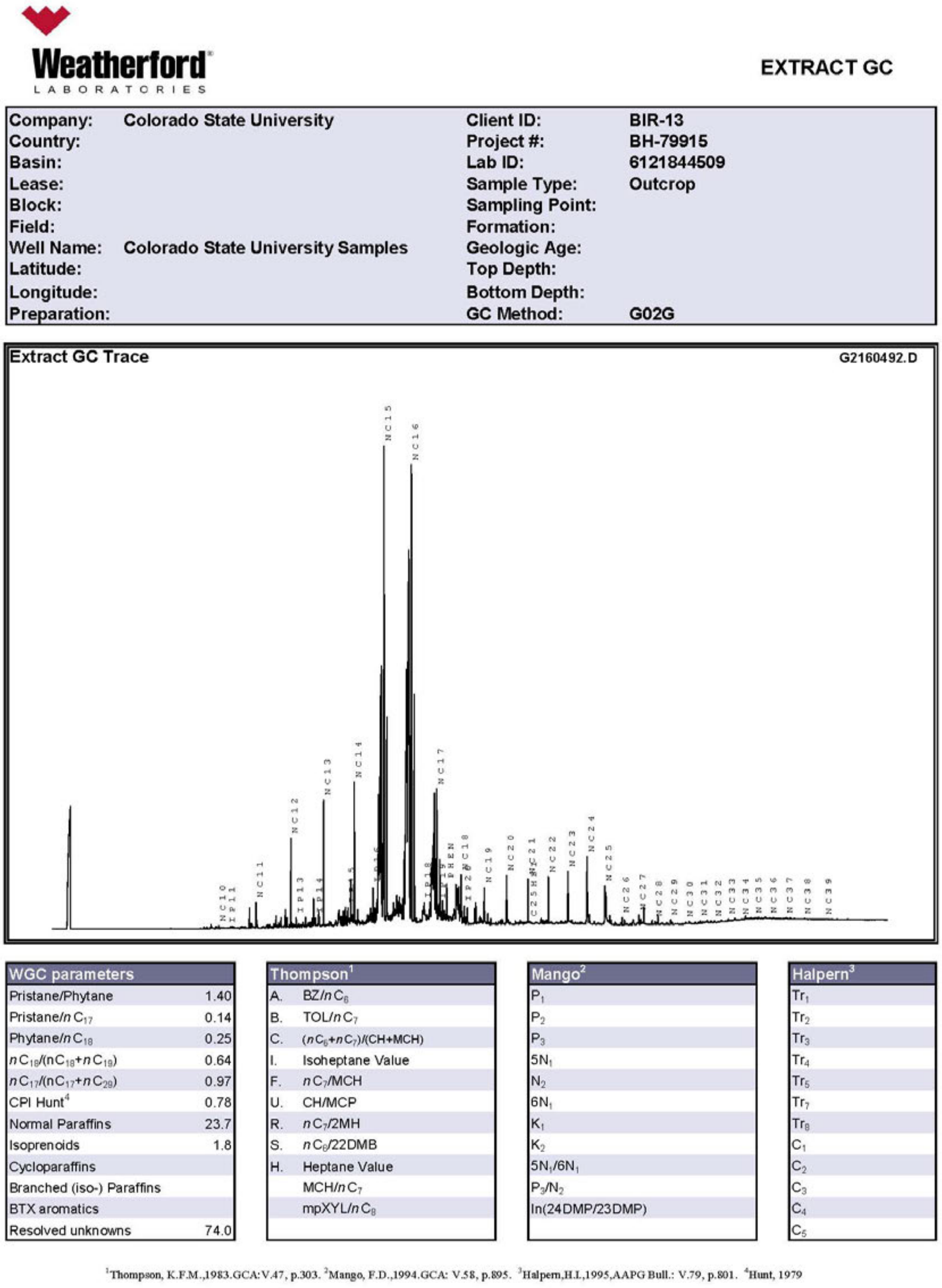

Weatherford LABORATORIES

**EXTRACT GC**

| | | | |
|---|---|---|---|
| **Company:** | **Colorado State University** | **Client ID:** | **BIR-13** |
| **Country:** | | **Project #:** | **BH-79915** |
| **Basin:** | | **Lab ID:** | **6121844509** |
| **Lease:** | | **Sample Type:** | **Outcrop** |
| **Block:** | | **Sampling Point:** | |
| **Field:** | | **Formation:** | |
| **Well Name:** | **Colorado State University Samples** | **Geologic Age:** | |
| **Latitude:** | | **Top Depth:** | |
| **Longitude:** | | **Bottom Depth:** | |
| **Preparation:** | | **GC Method:** | **G02G** |

**Extract GC Trace**

G2160492.D

| WGC parameters | |
|---|---|
| Pristane/Phytane | 1.40 |
| Pristane/$n$C$_{17}$ | 0.14 |
| Phytane/$n$C$_{18}$ | 0.25 |
| $n$C$_{18}$/(nC$_{18}$+$n$C$_{19}$) | 0.64 |
| $n$C$_{17}$/(nC$_{17}$+$n$C$_{29}$) | 0.97 |
| CPI Hunt[4] | 0.78 |
| Normal Paraffins | 23.7 |
| Isoprenoids | 1.8 |
| Cycloparaffins | |
| Branched (iso-) Paraffins | |
| BTX aromatics | |
| Resolved unknowns | 74.0 |

| Thompson[1] | | |
|---|---|---|
| A. | BZ/$n$C$_6$ | |
| B. | TOL/$n$C$_7$ | |
| C. | ($n$C$_6$+$n$C$_7$)/(CH+MCH) | |
| I. | Isoheptane Value | |
| F. | $n$C$_7$/MCH | |
| U. | CH/MCP | |
| R. | $n$C$_7$/2MH | |
| S. | $n$C$_6$/22DMB | |
| H. | Heptane Value | |
| | MCH/$n$C$_7$ | |
| | mpXYL/$n$C$_8$ | |

| Mango[2] | |
|---|---|
| $P_1$ | |
| $P_2$ | |
| $P_3$ | |
| 5N$_1$ | |
| N$_2$ | |
| 6N$_1$ | |
| K$_1$ | |
| K$_2$ | |
| 5N$_1$/6N$_1$ | |
| P$_3$/N$_2$ | |
| ln(24DMP/23DMP) | |

| Halpern[3] | |
|---|---|
| Tr$_1$ | |
| Tr$_2$ | |
| Tr$_3$ | |
| Tr$_4$ | |
| Tr$_5$ | |
| Tr$_7$ | |
| Tr$_8$ | |
| C$_1$ | |
| C$_2$ | |
| C$_3$ | |
| C$_4$ | |
| C$_5$ | |

[1]Thompson, K.F.M.,1983.GCA:V.47, p.303. [2]Mango, F.D.,1994.GCA: V.58, p.895. [3]Halpern,H.I.,1995,AAPG Bull.: V.79, p.801. [4]Hunt, 1979

*Appendix F1, ctd.*

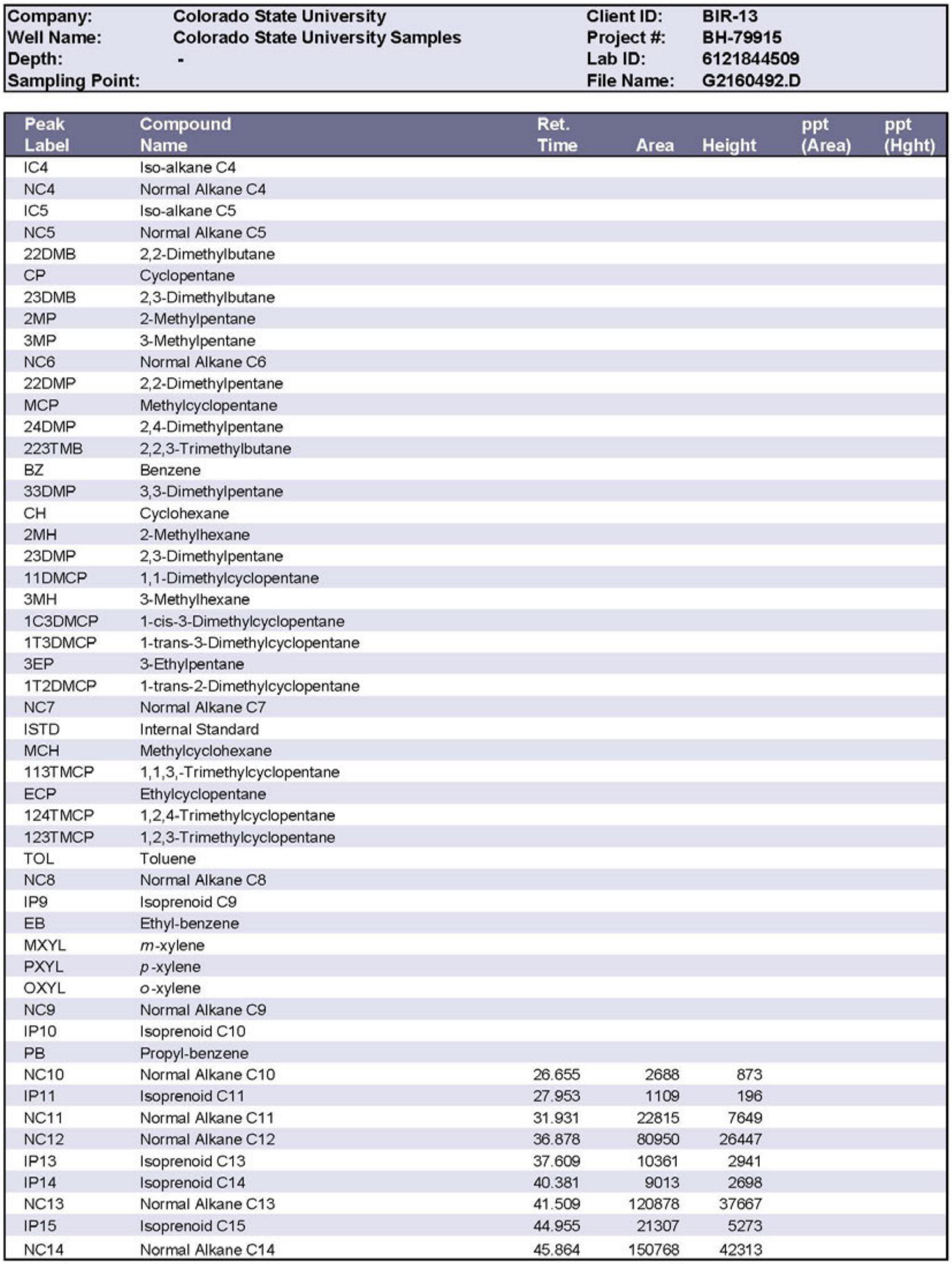

| | | | |
|---|---|---|---|
| **Company:** | **Colorado State University** | **Client ID:** | **BIR-13** |
| **Well Name:** | **Colorado State University Samples** | **Project #:** | **BH-79915** |
| **Depth:** | **-** | **Lab ID:** | **6121844509** |
| **Sampling Point:** | | **File Name:** | **G2160492.D** |

| Peak Label | Compound Name | Ret. Time | Area | Height | ppt (Area) | ppt (Hght) |
|---|---|---|---|---|---|---|
| IC4 | Iso-alkane C4 | | | | | |
| NC4 | Normal Alkane C4 | | | | | |
| IC5 | Iso-alkane C5 | | | | | |
| NC5 | Normal Alkane C5 | | | | | |
| 22DMB | 2,2-Dimethylbutane | | | | | |
| CP | Cyclopentane | | | | | |
| 23DMB | 2,3-Dimethylbutane | | | | | |
| 2MP | 2-Methylpentane | | | | | |
| 3MP | 3-Methylpentane | | | | | |
| NC6 | Normal Alkane C6 | | | | | |
| 22DMP | 2,2-Dimethylpentane | | | | | |
| MCP | Methylcyclopentane | | | | | |
| 24DMP | 2,4-Dimethylpentane | | | | | |
| 223TMB | 2,2,3-Trimethylbutane | | | | | |
| BZ | Benzene | | | | | |
| 33DMP | 3,3-Dimethylpentane | | | | | |
| CH | Cyclohexane | | | | | |
| 2MH | 2-Methylhexane | | | | | |
| 23DMP | 2,3-Dimethylpentane | | | | | |
| 11DMCP | 1,1-Dimethylcyclopentane | | | | | |
| 3MH | 3-Methylhexane | | | | | |
| 1C3DMCP | 1-cis-3-Dimethylcyclopentane | | | | | |
| 1T3DMCP | 1-trans-3-Dimethylcyclopentane | | | | | |
| 3EP | 3-Ethylpentane | | | | | |
| 1T2DMCP | 1-trans-2-Dimethylcyclopentane | | | | | |
| NC7 | Normal Alkane C7 | | | | | |
| ISTD | Internal Standard | | | | | |
| MCH | Methylcyclohexane | | | | | |
| 113TMCP | 1,1,3,-Trimethylcyclopentane | | | | | |
| ECP | Ethylcyclopentane | | | | | |
| 124TMCP | 1,2,4-Trimethylcyclopentane | | | | | |
| 123TMCP | 1,2,3-Trimethylcyclopentane | | | | | |
| TOL | Toluene | | | | | |
| NC8 | Normal Alkane C8 | | | | | |
| IP9 | Isoprenoid C9 | | | | | |
| EB | Ethyl-benzene | | | | | |
| MXYL | *m*-xylene | | | | | |
| PXYL | *p*-xylene | | | | | |
| OXYL | *o*-xylene | | | | | |
| NC9 | Normal Alkane C9 | | | | | |
| IP10 | Isoprenoid C10 | | | | | |
| PB | Propyl-benzene | | | | | |
| NC10 | Normal Alkane C10 | 26.655 | 2688 | 873 | | |
| IP11 | Isoprenoid C11 | 27.953 | 1109 | 196 | | |
| NC11 | Normal Alkane C11 | 31.931 | 22815 | 7649 | | |
| NC12 | Normal Alkane C12 | 36.878 | 80950 | 26447 | | |
| IP13 | Isoprenoid C13 | 37.609 | 10361 | 2941 | | |
| IP14 | Isoprenoid C14 | 40.381 | 9013 | 2698 | | |
| NC13 | Normal Alkane C13 | 41.509 | 120878 | 37667 | | |
| IP15 | Isoprenoid C15 | 44.955 | 21307 | 5273 | | |
| NC14 | Normal Alkane C14 | 45.864 | 150768 | 42313 | | |

*Appendix F1, ctd.*

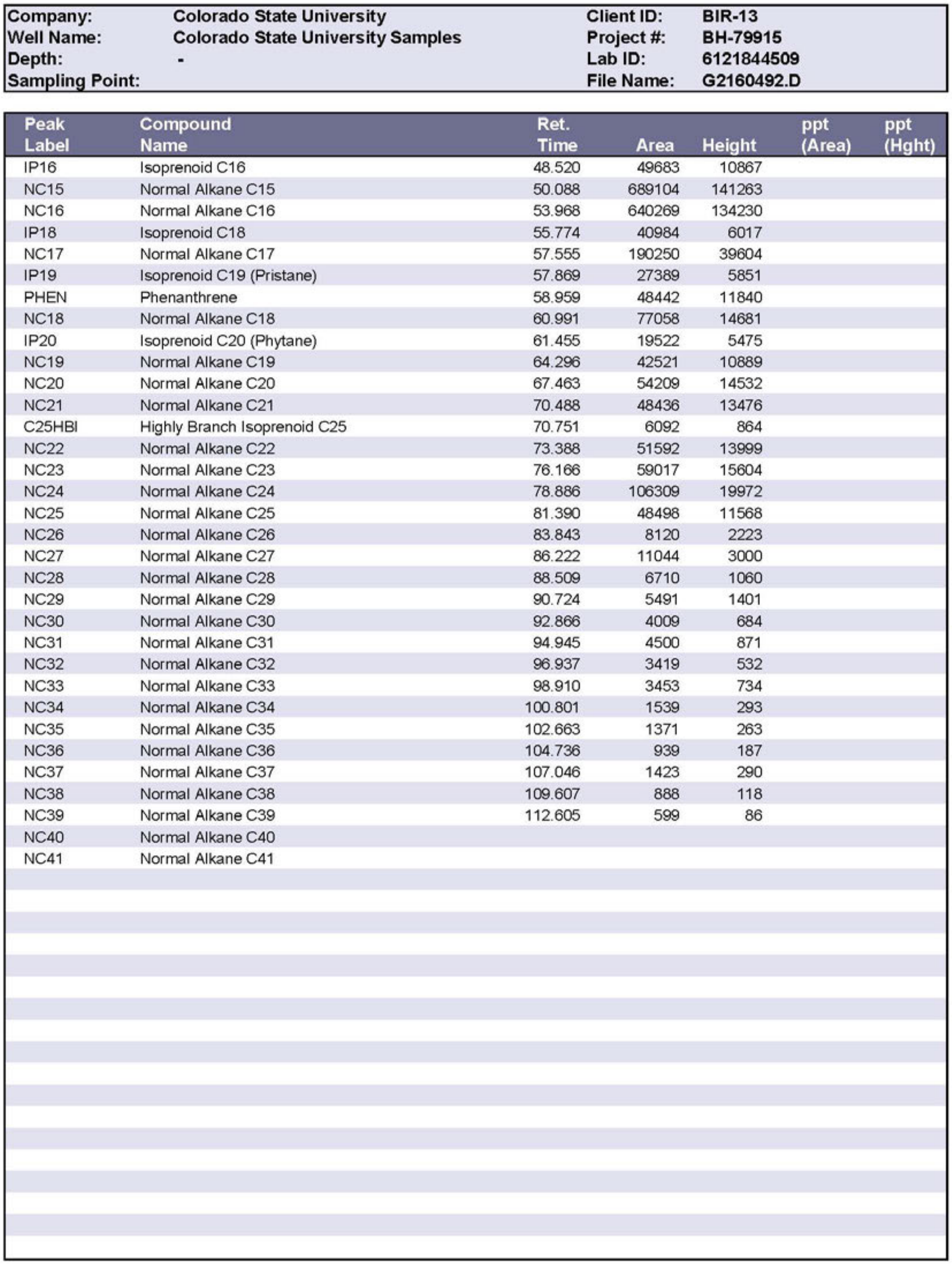

**Company:** Colorado State University
**Well Name:** Colorado State University Samples
**Depth:** -
**Sampling Point:**
**Client ID:** BIR-13
**Project #:** BH-79915
**Lab ID:** 6121844509
**File Name:** G2160492.D

| Peak Label | Compound Name | Ret. Time | Area | Height | ppt (Area) | ppt (Hght) |
|---|---|---|---|---|---|---|
| IP16 | Isoprenoid C16 | 48.520 | 49683 | 10867 | | |
| NC15 | Normal Alkane C15 | 50.088 | 689104 | 141263 | | |
| NC16 | Normal Alkane C16 | 53.968 | 640269 | 134230 | | |
| IP18 | Isoprenoid C18 | 55.774 | 40984 | 6017 | | |
| NC17 | Normal Alkane C17 | 57.555 | 190250 | 39604 | | |
| IP19 | Isoprenoid C19 (Pristane) | 57.869 | 27389 | 5851 | | |
| PHEN | Phenanthrene | 58.959 | 48442 | 11840 | | |
| NC18 | Normal Alkane C18 | 60.991 | 77058 | 14681 | | |
| IP20 | Isoprenoid C20 (Phytane) | 61.455 | 19522 | 5475 | | |
| NC19 | Normal Alkane C19 | 64.296 | 42521 | 10889 | | |
| NC20 | Normal Alkane C20 | 67.463 | 54209 | 14532 | | |
| NC21 | Normal Alkane C21 | 70.488 | 48436 | 13476 | | |
| C25HBI | Highly Branch Isoprenoid C25 | 70.751 | 6092 | 864 | | |
| NC22 | Normal Alkane C22 | 73.388 | 51592 | 13999 | | |
| NC23 | Normal Alkane C23 | 76.166 | 59017 | 15604 | | |
| NC24 | Normal Alkane C24 | 78.886 | 106309 | 19972 | | |
| NC25 | Normal Alkane C25 | 81.390 | 48498 | 11568 | | |
| NC26 | Normal Alkane C26 | 83.843 | 8120 | 2223 | | |
| NC27 | Normal Alkane C27 | 86.222 | 11044 | 3000 | | |
| NC28 | Normal Alkane C28 | 88.509 | 6710 | 1060 | | |
| NC29 | Normal Alkane C29 | 90.724 | 5491 | 1401 | | |
| NC30 | Normal Alkane C30 | 92.866 | 4009 | 684 | | |
| NC31 | Normal Alkane C31 | 94.945 | 4500 | 871 | | |
| NC32 | Normal Alkane C32 | 96.937 | 3419 | 532 | | |
| NC33 | Normal Alkane C33 | 98.910 | 3453 | 734 | | |
| NC34 | Normal Alkane C34 | 100.801 | 1539 | 293 | | |
| NC35 | Normal Alkane C35 | 102.663 | 1371 | 263 | | |
| NC36 | Normal Alkane C36 | 104.736 | 939 | 187 | | |
| NC37 | Normal Alkane C37 | 107.046 | 1423 | 290 | | |
| NC38 | Normal Alkane C38 | 109.607 | 888 | 118 | | |
| NC39 | Normal Alkane C39 | 112.605 | 599 | 86 | | |
| NC40 | Normal Alkane C40 | | | | | |
| NC41 | Normal Alkane C41 | | | | | |

*Appendix F1, ctd.*

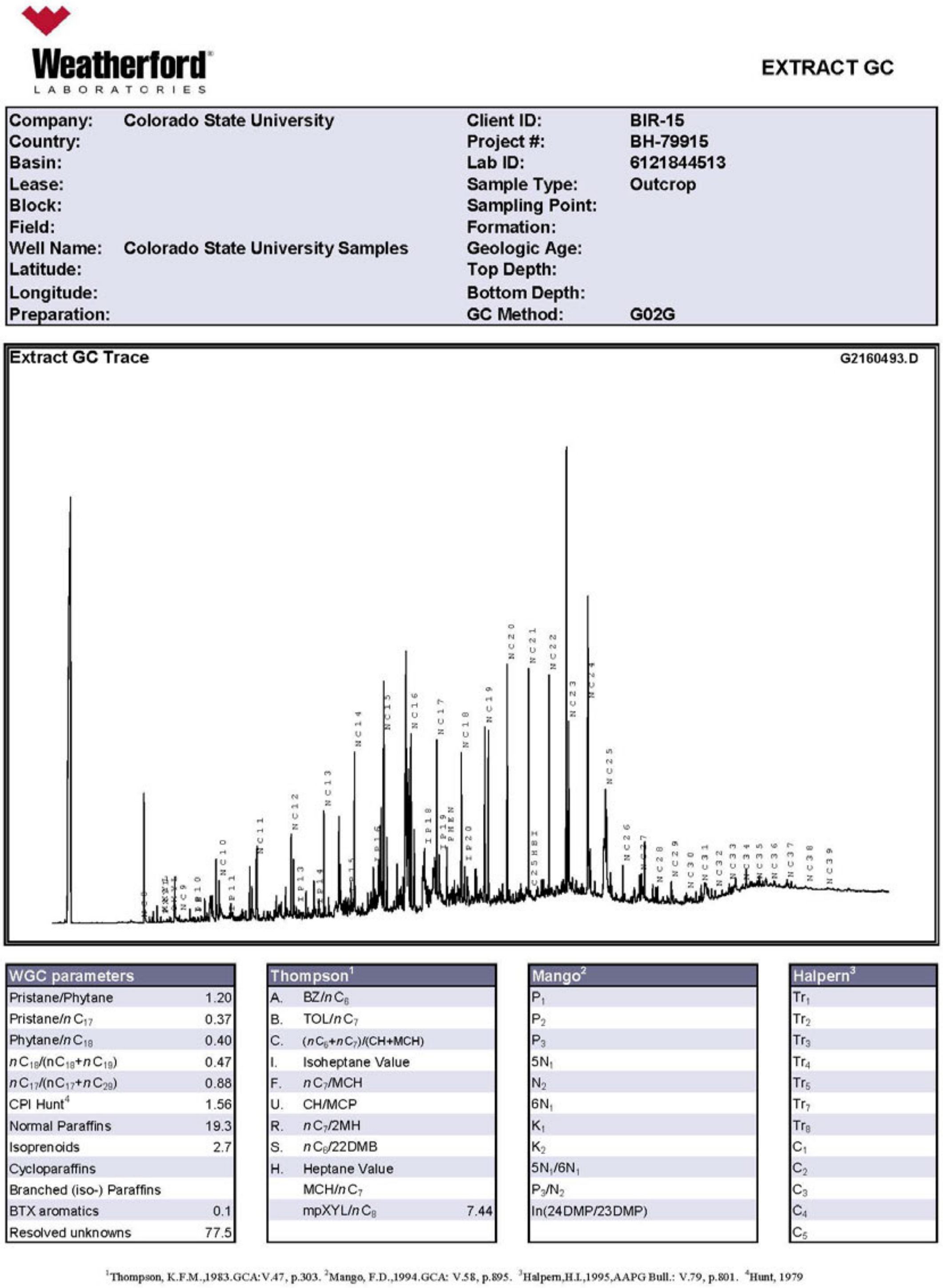

Weatherford LABORATORIES

**EXTRACT GC**

| | | | |
|---|---|---|---|
| **Company:** | **Colorado State University** | **Client ID:** | **BIR-15** |
| **Country:** | | **Project #:** | **BH-79915** |
| **Basin:** | | **Lab ID:** | **6121844513** |
| **Lease:** | | **Sample Type:** | **Outcrop** |
| **Block:** | | **Sampling Point:** | |
| **Field:** | | **Formation:** | |
| **Well Name:** | **Colorado State University Samples** | **Geologic Age:** | |
| **Latitude:** | | **Top Depth:** | |
| **Longitude:** | | **Bottom Depth:** | |
| **Preparation:** | | **GC Method:** | **G02G** |

**Extract GC Trace**

G2160493.D

| WGC parameters | |
|---|---|
| Pristane/Phytane | 1.20 |
| Pristane/$nC_{17}$ | 0.37 |
| Phytane/$nC_{18}$ | 0.40 |
| $nC_{18}/(nC_{18}+nC_{19})$ | 0.47 |
| $nC_{17}/(nC_{17}+nC_{29})$ | 0.88 |
| CPI Hunt[4] | 1.56 |
| Normal Paraffins | 19.3 |
| Isoprenoids | 2.7 |
| Cycloparaffins | |
| Branched (iso-) Paraffins | |
| BTX aromatics | 0.1 |
| Resolved unknowns | 77.5 |

| Thompson[1] | | |
|---|---|---|
| A. | BZ/$nC_6$ | |
| B. | TOL/$nC_7$ | |
| C. | $(nC_6+nC_7)/(CH+MCH)$ | |
| I. | Isoheptane Value | |
| F. | $nC_7$/MCH | |
| U. | CH/MCP | |
| R. | $nC_7$/2MH | |
| S. | $nC_6$/22DMB | |
| H. | Heptane Value | |
| | MCH/$nC_7$ | |
| | mpXYL/$nC_8$ | 7.44 |

| Mango[2] | |
|---|---|
| $P_1$ | |
| $P_2$ | |
| $P_3$ | |
| $5N_1$ | |
| $N_2$ | |
| $6N_1$ | |
| $K_1$ | |
| $K_2$ | |
| $5N_1/6N_1$ | |
| $P_3/N_2$ | |
| ln(24DMP/23DMP) | |

| Halpern[3] | |
|---|---|
| $Tr_1$ | |
| $Tr_2$ | |
| $Tr_3$ | |
| $Tr_4$ | |
| $Tr_5$ | |
| $Tr_7$ | |
| $Tr_8$ | |
| $C_1$ | |
| $C_2$ | |
| $C_3$ | |
| $C_4$ | |
| $C_5$ | |

[1] Thompson, K.F.M.,1983.GCA:V.47, p.303. [2] Mango, F.D.,1994.GCA: V.58, p.895. [3] Halpern,H.I.,1995,AAPG Bull.: V.79, p.801. [4] Hunt, 1979

*Appendix F1, ctd.*

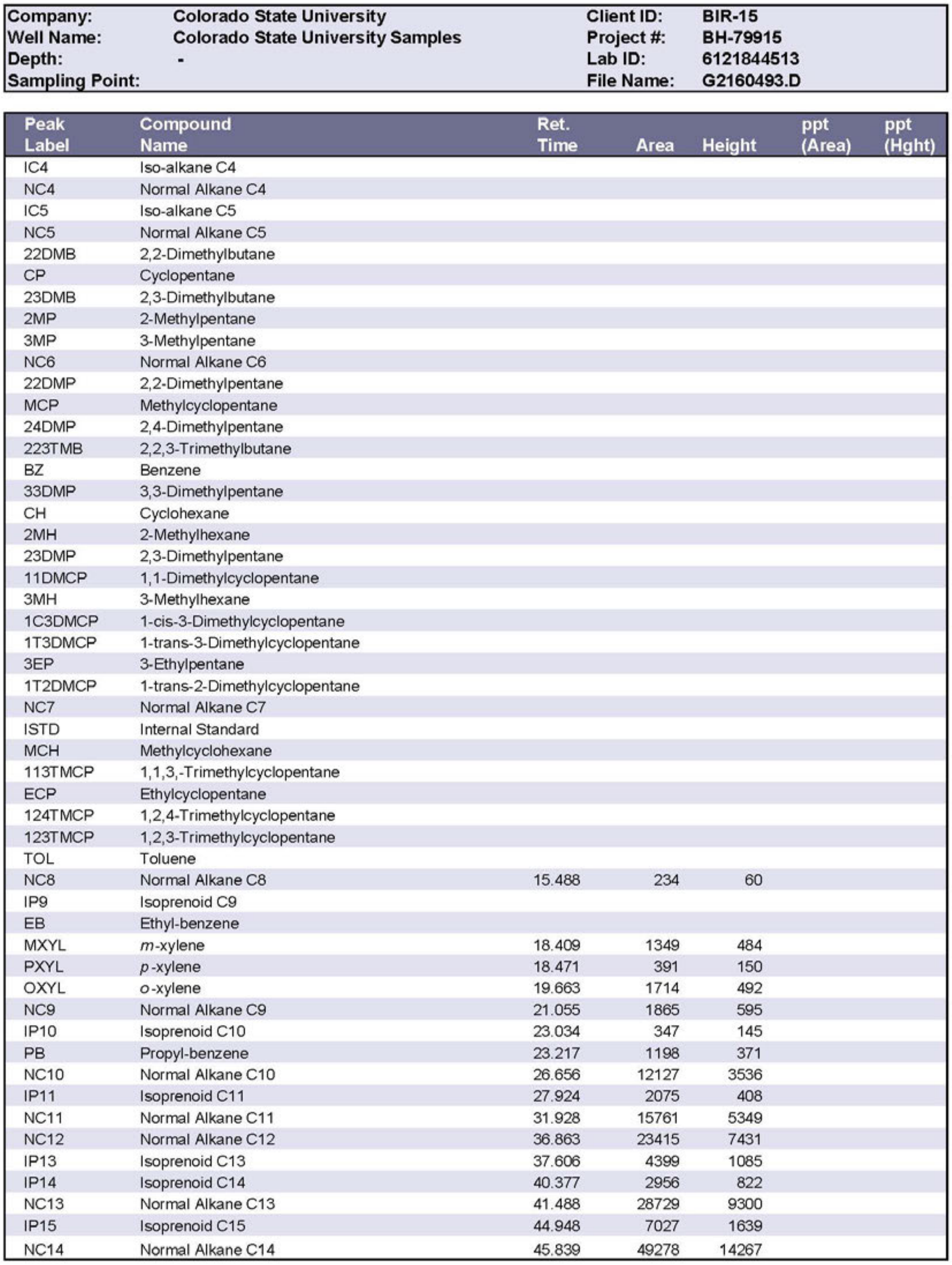

| | | | |
|---|---|---|---|
| **Company:** | **Colorado State University** | **Client ID:** | **BIR-15** |
| **Well Name:** | **Colorado State University Samples** | **Project #:** | **BH-79915** |
| **Depth:** | **-** | **Lab ID:** | **6121844513** |
| **Sampling Point:** | | **File Name:** | **G2160493.D** |

| Peak Label | Compound Name | Ret. Time | Area | Height | ppt (Area) | ppt (Hght) |
|---|---|---|---|---|---|---|
| IC4 | Iso-alkane C4 | | | | | |
| NC4 | Normal Alkane C4 | | | | | |
| IC5 | Iso-alkane C5 | | | | | |
| NC5 | Normal Alkane C5 | | | | | |
| 22DMB | 2,2-Dimethylbutane | | | | | |
| CP | Cyclopentane | | | | | |
| 23DMB | 2,3-Dimethylbutane | | | | | |
| 2MP | 2-Methylpentane | | | | | |
| 3MP | 3-Methylpentane | | | | | |
| NC6 | Normal Alkane C6 | | | | | |
| 22DMP | 2,2-Dimethylpentane | | | | | |
| MCP | Methylcyclopentane | | | | | |
| 24DMP | 2,4-Dimethylpentane | | | | | |
| 223TMB | 2,2,3-Trimethylbutane | | | | | |
| BZ | Benzene | | | | | |
| 33DMP | 3,3-Dimethylpentane | | | | | |
| CH | Cyclohexane | | | | | |
| 2MH | 2-Methylhexane | | | | | |
| 23DMP | 2,3-Dimethylpentane | | | | | |
| 11DMCP | 1,1-Dimethylcyclopentane | | | | | |
| 3MH | 3-Methylhexane | | | | | |
| 1C3DMCP | 1-cis-3-Dimethylcyclopentane | | | | | |
| 1T3DMCP | 1-trans-3-Dimethylcyclopentane | | | | | |
| 3EP | 3-Ethylpentane | | | | | |
| 1T2DMCP | 1-trans-2-Dimethylcyclopentane | | | | | |
| NC7 | Normal Alkane C7 | | | | | |
| ISTD | Internal Standard | | | | | |
| MCH | Methylcyclohexane | | | | | |
| 113TMCP | 1,1,3,-Trimethylcyclopentane | | | | | |
| ECP | Ethylcyclopentane | | | | | |
| 124TMCP | 1,2,4-Trimethylcyclopentane | | | | | |
| 123TMCP | 1,2,3-Trimethylcyclopentane | | | | | |
| TOL | Toluene | | | | | |
| NC8 | Normal Alkane C8 | 15.488 | 234 | 60 | | |
| IP9 | Isoprenoid C9 | | | | | |
| EB | Ethyl-benzene | | | | | |
| MXYL | *m*-xylene | 18.409 | 1349 | 484 | | |
| PXYL | *p*-xylene | 18.471 | 391 | 150 | | |
| OXYL | *o*-xylene | 19.663 | 1714 | 492 | | |
| NC9 | Normal Alkane C9 | 21.055 | 1865 | 595 | | |
| IP10 | Isoprenoid C10 | 23.034 | 347 | 145 | | |
| PB | Propyl-benzene | 23.217 | 1198 | 371 | | |
| NC10 | Normal Alkane C10 | 26.656 | 12127 | 3536 | | |
| IP11 | Isoprenoid C11 | 27.924 | 2075 | 408 | | |
| NC11 | Normal Alkane C11 | 31.928 | 15761 | 5349 | | |
| NC12 | Normal Alkane C12 | 36.863 | 23415 | 7431 | | |
| IP13 | Isoprenoid C13 | 37.606 | 4399 | 1085 | | |
| IP14 | Isoprenoid C14 | 40.377 | 2956 | 822 | | |
| NC13 | Normal Alkane C13 | 41.488 | 28729 | 9300 | | |
| IP15 | Isoprenoid C15 | 44.948 | 7027 | 1639 | | |
| NC14 | Normal Alkane C14 | 45.839 | 49278 | 14267 | | |

*Appendix F1, ctd.*

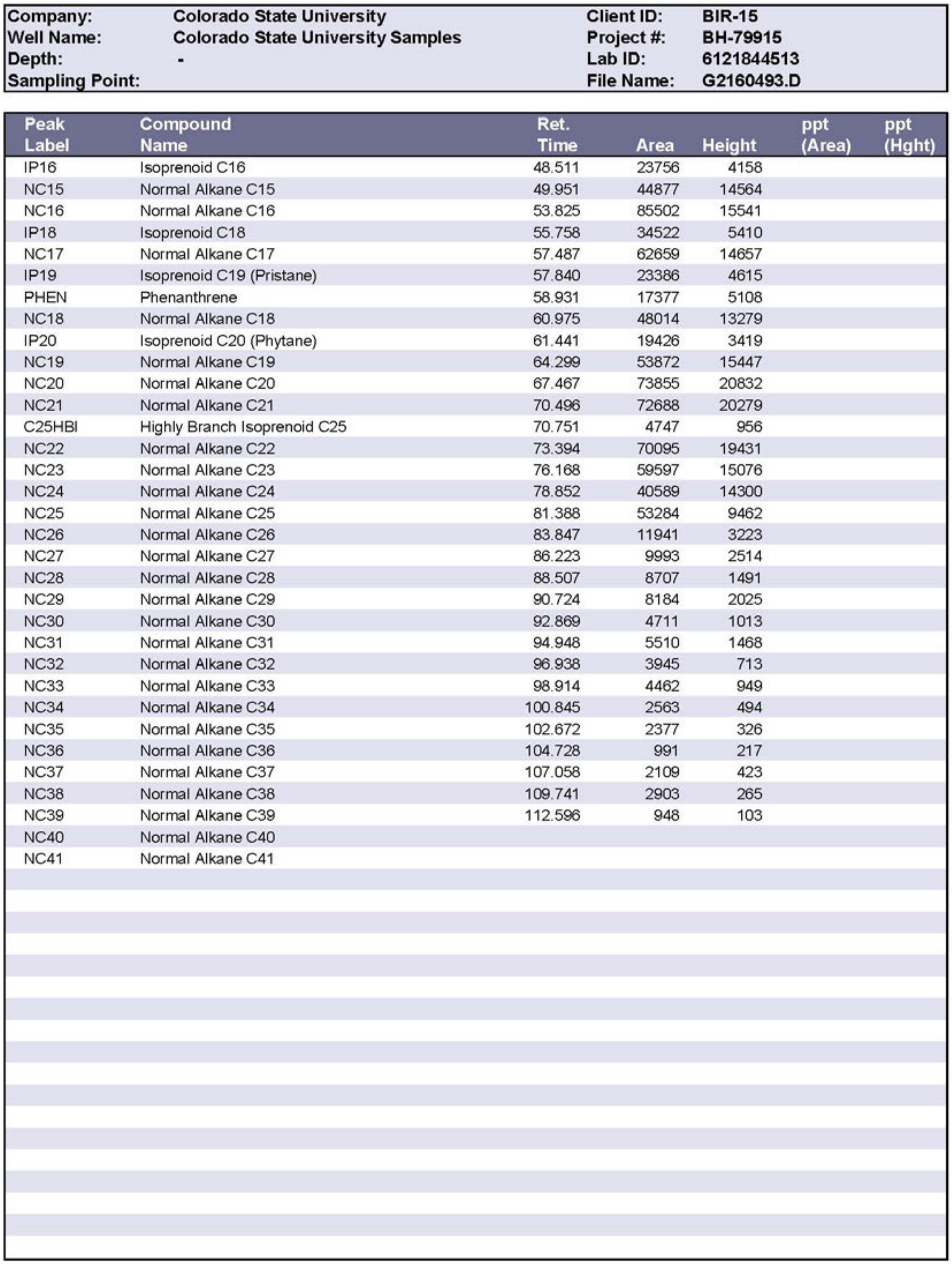

| | | | |
|---|---|---|---|
| **Company:** | **Colorado State University** | **Client ID:** | **BIR-15** |
| **Well Name:** | **Colorado State University Samples** | **Project #:** | **BH-79915** |
| **Depth:** | **-** | **Lab ID:** | **6121844513** |
| **Sampling Point:** | | **File Name:** | **G2160493.D** |

| Peak Label | Compound Name | Ret. Time | Area | Height | ppt (Area) | ppt (Hght) |
|---|---|---|---|---|---|---|
| IP16 | Isoprenoid C16 | 48.511 | 23756 | 4158 | | |
| NC15 | Normal Alkane C15 | 49.951 | 44877 | 14564 | | |
| NC16 | Normal Alkane C16 | 53.825 | 85502 | 15541 | | |
| IP18 | Isoprenoid C18 | 55.758 | 34522 | 5410 | | |
| NC17 | Normal Alkane C17 | 57.487 | 62659 | 14657 | | |
| IP19 | Isoprenoid C19 (Pristane) | 57.840 | 23386 | 4615 | | |
| PHEN | Phenanthrene | 58.931 | 17377 | 5108 | | |
| NC18 | Normal Alkane C18 | 60.975 | 48014 | 13279 | | |
| IP20 | Isoprenoid C20 (Phytane) | 61.441 | 19426 | 3419 | | |
| NC19 | Normal Alkane C19 | 64.299 | 53872 | 15447 | | |
| NC20 | Normal Alkane C20 | 67.467 | 73855 | 20832 | | |
| NC21 | Normal Alkane C21 | 70.496 | 72688 | 20279 | | |
| C25HBI | Highly Branch Isoprenoid C25 | 70.751 | 4747 | 956 | | |
| NC22 | Normal Alkane C22 | 73.394 | 70095 | 19431 | | |
| NC23 | Normal Alkane C23 | 76.168 | 59597 | 15076 | | |
| NC24 | Normal Alkane C24 | 78.852 | 40589 | 14300 | | |
| NC25 | Normal Alkane C25 | 81.388 | 53284 | 9462 | | |
| NC26 | Normal Alkane C26 | 83.847 | 11941 | 3223 | | |
| NC27 | Normal Alkane C27 | 86.223 | 9993 | 2514 | | |
| NC28 | Normal Alkane C28 | 88.507 | 8707 | 1491 | | |
| NC29 | Normal Alkane C29 | 90.724 | 8184 | 2025 | | |
| NC30 | Normal Alkane C30 | 92.869 | 4711 | 1013 | | |
| NC31 | Normal Alkane C31 | 94.948 | 5510 | 1468 | | |
| NC32 | Normal Alkane C32 | 96.938 | 3945 | 713 | | |
| NC33 | Normal Alkane C33 | 98.914 | 4462 | 949 | | |
| NC34 | Normal Alkane C34 | 100.845 | 2563 | 494 | | |
| NC35 | Normal Alkane C35 | 102.672 | 2377 | 326 | | |
| NC36 | Normal Alkane C36 | 104.728 | 991 | 217 | | |
| NC37 | Normal Alkane C37 | 107.058 | 2109 | 423 | | |
| NC38 | Normal Alkane C38 | 109.741 | 2903 | 265 | | |
| NC39 | Normal Alkane C39 | 112.596 | 948 | 103 | | |
| NC40 | Normal Alkane C40 | | | | | |
| NC41 | Normal Alkane C41 | | | | | |

*Appendix F1, ctd.*

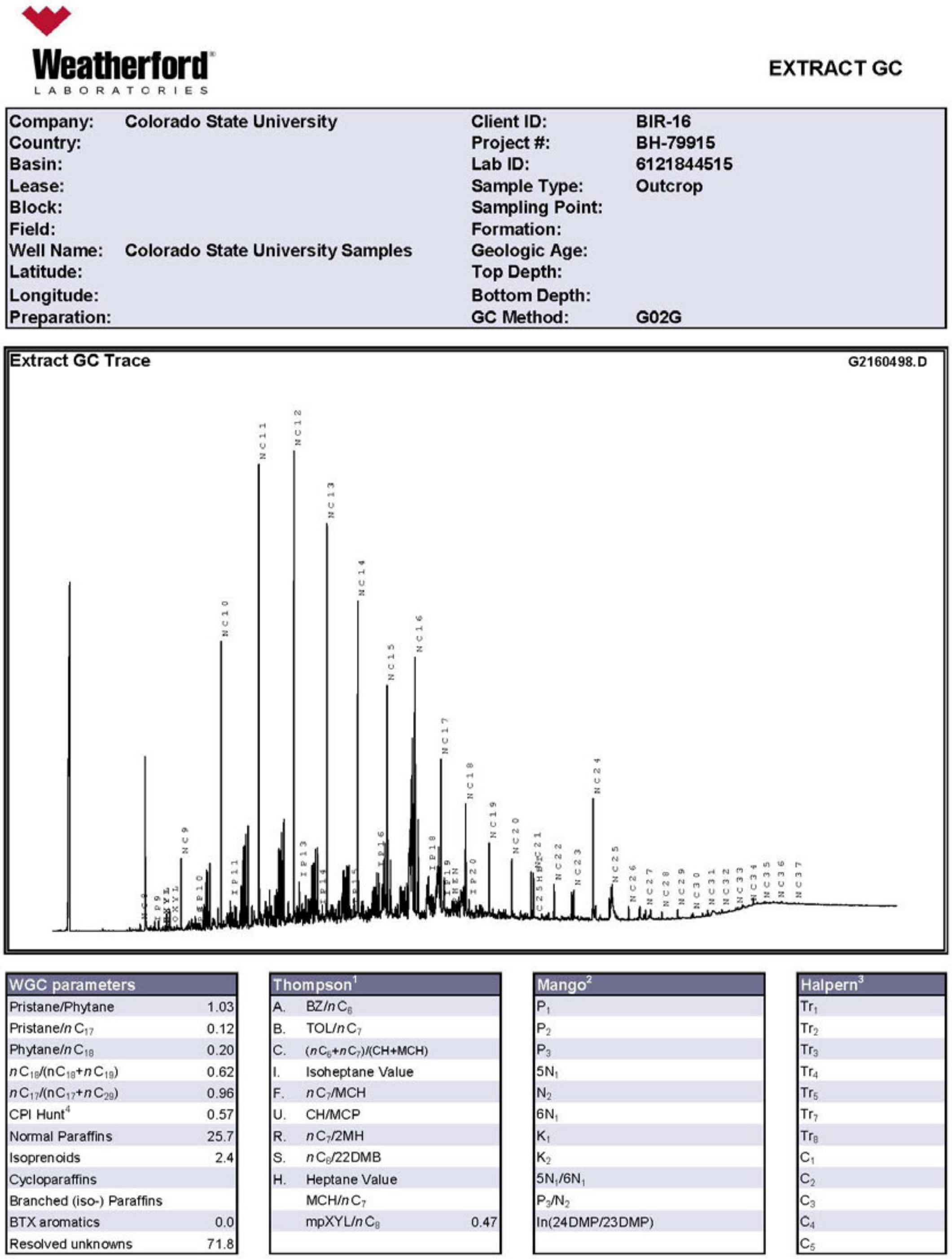

**Weatherford**
LABORATORIES

**EXTRACT GC**

| | | | |
|---|---|---|---|
| **Company:** | **Colorado State University** | **Client ID:** | **BIR-16** |
| **Country:** | | **Project #:** | **BH-79915** |
| **Basin:** | | **Lab ID:** | **6121844515** |
| **Lease:** | | **Sample Type:** | **Outcrop** |
| **Block:** | | **Sampling Point:** | |
| **Field:** | | **Formation:** | |
| **Well Name:** | **Colorado State University Samples** | **Geologic Age:** | |
| **Latitude:** | | **Top Depth:** | |
| **Longitude:** | | **Bottom Depth:** | |
| **Preparation:** | | **GC Method:** | **G02G** |

**Extract GC Trace**

**G2160498.D**

| WGC parameters | |
|---|---|
| Pristane/Phytane | 1.03 |
| Pristane/$nC_{17}$ | 0.12 |
| Phytane/$nC_{18}$ | 0.20 |
| $nC_{18}/(nC_{18}+nC_{19})$ | 0.62 |
| $nC_{17}/(nC_{17}+nC_{29})$ | 0.96 |
| CPI Hunt[4] | 0.57 |
| Normal Paraffins | 25.7 |
| Isoprenoids | 2.4 |
| Cycloparaffins | |
| Branched (iso-) Paraffins | |
| BTX aromatics | 0.0 |
| Resolved unknowns | 71.8 |

| Thompson[1] | | |
|---|---|---|
| A. | BZ/$nC_6$ | |
| B. | TOL/$nC_7$ | |
| C. | $(nC_6+nC_7)$/(CH+MCH) | |
| I. | Isoheptane Value | |
| F. | $nC_7$/MCH | |
| U. | CH/MCP | |
| R. | $nC_7$/2MH | |
| S. | $nC_6$/22DMB | |
| H. | Heptane Value | |
| | MCH/$nC_7$ | |
| | mpXYL/$nC_8$ | 0.47 |

| Mango[2] | |
|---|---|
| $P_1$ | |
| $P_2$ | |
| $P_3$ | |
| $5N_1$ | |
| $N_2$ | |
| $6N_1$ | |
| $K_1$ | |
| $K_2$ | |
| $5N_1/6N_1$ | |
| $P_3/N_2$ | |
| ln(24DMP/23DMP) | |

| Halpern[3] | |
|---|---|
| $Tr_1$ | |
| $Tr_2$ | |
| $Tr_3$ | |
| $Tr_4$ | |
| $Tr_5$ | |
| $Tr_7$ | |
| $Tr_8$ | |
| $C_1$ | |
| $C_2$ | |
| $C_3$ | |
| $C_4$ | |
| $C_5$ | |

[1] Thompson, K.F.M.,1983.GCA:V.47, p.303. [2] Mango, F.D.,1994.GCA: V.58, p.895. [3] Halpern,H.I.,1995,AAPG Bull.: V.79, p.801. [4] Hunt, 1979

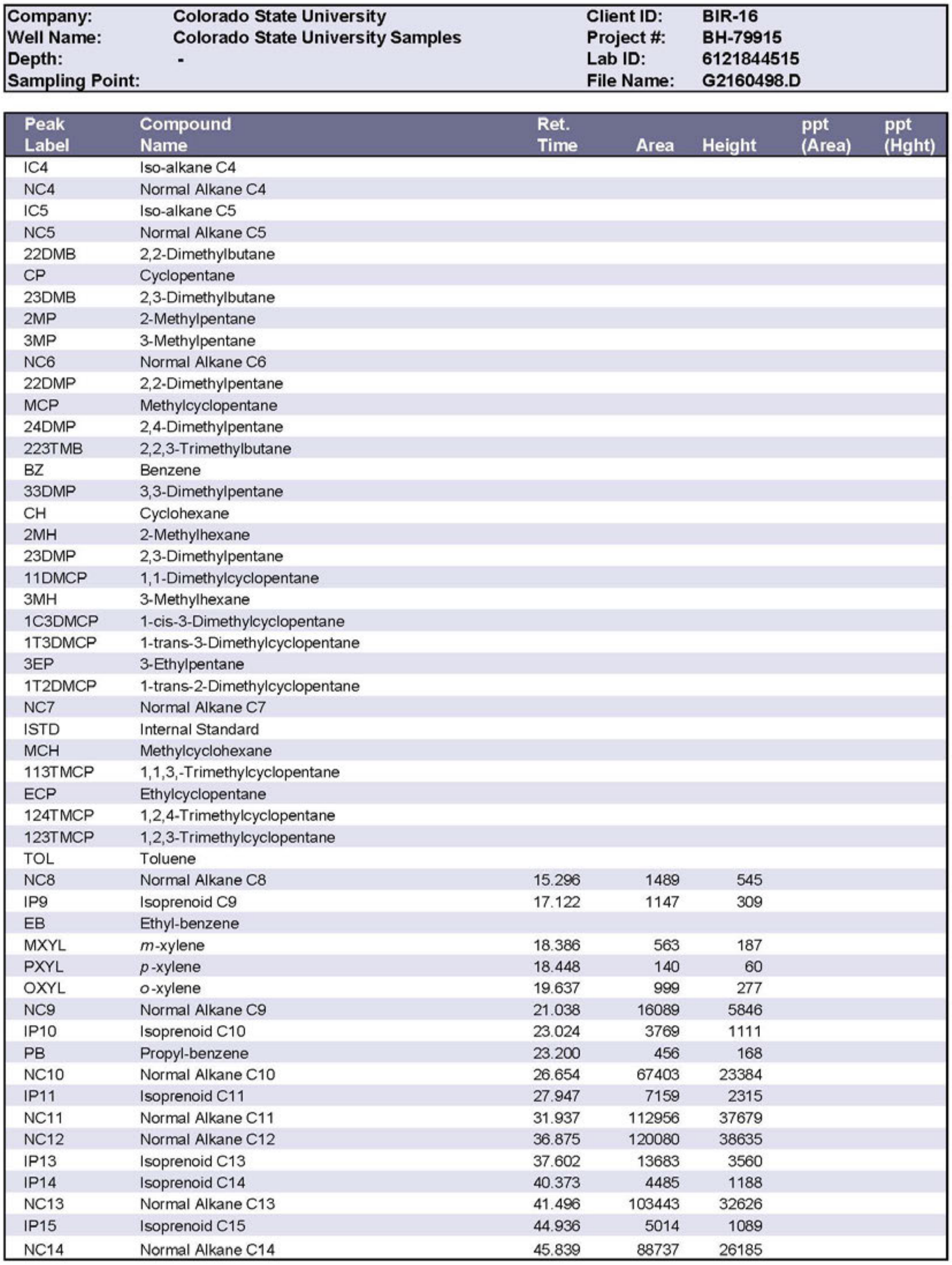

| | | | |
|---|---|---|---|
| **Company:** | **Colorado State University** | **Client ID:** | **BIR-16** |
| **Well Name:** | **Colorado State University Samples** | **Project #:** | **BH-79915** |
| **Depth:** | **-** | **Lab ID:** | **6121844515** |
| **Sampling Point:** | | **File Name:** | **G2160498.D** |

| Peak Label | Compound Name | Ret. Time | Area | Height | ppt (Area) | ppt (Hght) |
|---|---|---|---|---|---|---|
| IC4 | Iso-alkane C4 | | | | | |
| NC4 | Normal Alkane C4 | | | | | |
| IC5 | Iso-alkane C5 | | | | | |
| NC5 | Normal Alkane C5 | | | | | |
| 22DMB | 2,2-Dimethylbutane | | | | | |
| CP | Cyclopentane | | | | | |
| 23DMB | 2,3-Dimethylbutane | | | | | |
| 2MP | 2-Methylpentane | | | | | |
| 3MP | 3-Methylpentane | | | | | |
| NC6 | Normal Alkane C6 | | | | | |
| 22DMP | 2,2-Dimethylpentane | | | | | |
| MCP | Methylcyclopentane | | | | | |
| 24DMP | 2,4-Dimethylpentane | | | | | |
| 223TMB | 2,2,3-Trimethylbutane | | | | | |
| BZ | Benzene | | | | | |
| 33DMP | 3,3-Dimethylpentane | | | | | |
| CH | Cyclohexane | | | | | |
| 2MH | 2-Methylhexane | | | | | |
| 23DMP | 2,3-Dimethylpentane | | | | | |
| 11DMCP | 1,1-Dimethylcyclopentane | | | | | |
| 3MH | 3-Methylhexane | | | | | |
| 1C3DMCP | 1-cis-3-Dimethylcyclopentane | | | | | |
| 1T3DMCP | 1-trans-3-Dimethylcyclopentane | | | | | |
| 3EP | 3-Ethylpentane | | | | | |
| 1T2DMCP | 1-trans-2-Dimethylcyclopentane | | | | | |
| NC7 | Normal Alkane C7 | | | | | |
| ISTD | Internal Standard | | | | | |
| MCH | Methylcyclohexane | | | | | |
| 113TMCP | 1,1,3,-Trimethylcyclopentane | | | | | |
| ECP | Ethylcyclopentane | | | | | |
| 124TMCP | 1,2,4-Trimethylcyclopentane | | | | | |
| 123TMCP | 1,2,3-Trimethylcyclopentane | | | | | |
| TOL | Toluene | | | | | |
| NC8 | Normal Alkane C8 | 15.296 | 1489 | 545 | | |
| IP9 | Isoprenoid C9 | 17.122 | 1147 | 309 | | |
| EB | Ethyl-benzene | | | | | |
| MXYL | *m*-xylene | 18.386 | 563 | 187 | | |
| PXYL | *p*-xylene | 18.448 | 140 | 60 | | |
| OXYL | *o*-xylene | 19.637 | 999 | 277 | | |
| NC9 | Normal Alkane C9 | 21.038 | 16089 | 5846 | | |
| IP10 | Isoprenoid C10 | 23.024 | 3769 | 1111 | | |
| PB | Propyl-benzene | 23.200 | 456 | 168 | | |
| NC10 | Normal Alkane C10 | 26.654 | 67403 | 23384 | | |
| IP11 | Isoprenoid C11 | 27.947 | 7159 | 2315 | | |
| NC11 | Normal Alkane C11 | 31.937 | 112956 | 37679 | | |
| NC12 | Normal Alkane C12 | 36.875 | 120080 | 38635 | | |
| IP13 | Isoprenoid C13 | 37.602 | 13683 | 3560 | | |
| IP14 | Isoprenoid C14 | 40.373 | 4485 | 1188 | | |
| NC13 | Normal Alkane C13 | 41.496 | 103443 | 32626 | | |
| IP15 | Isoprenoid C15 | 44.936 | 5014 | 1089 | | |
| NC14 | Normal Alkane C14 | 45.839 | 88737 | 26185 | | |

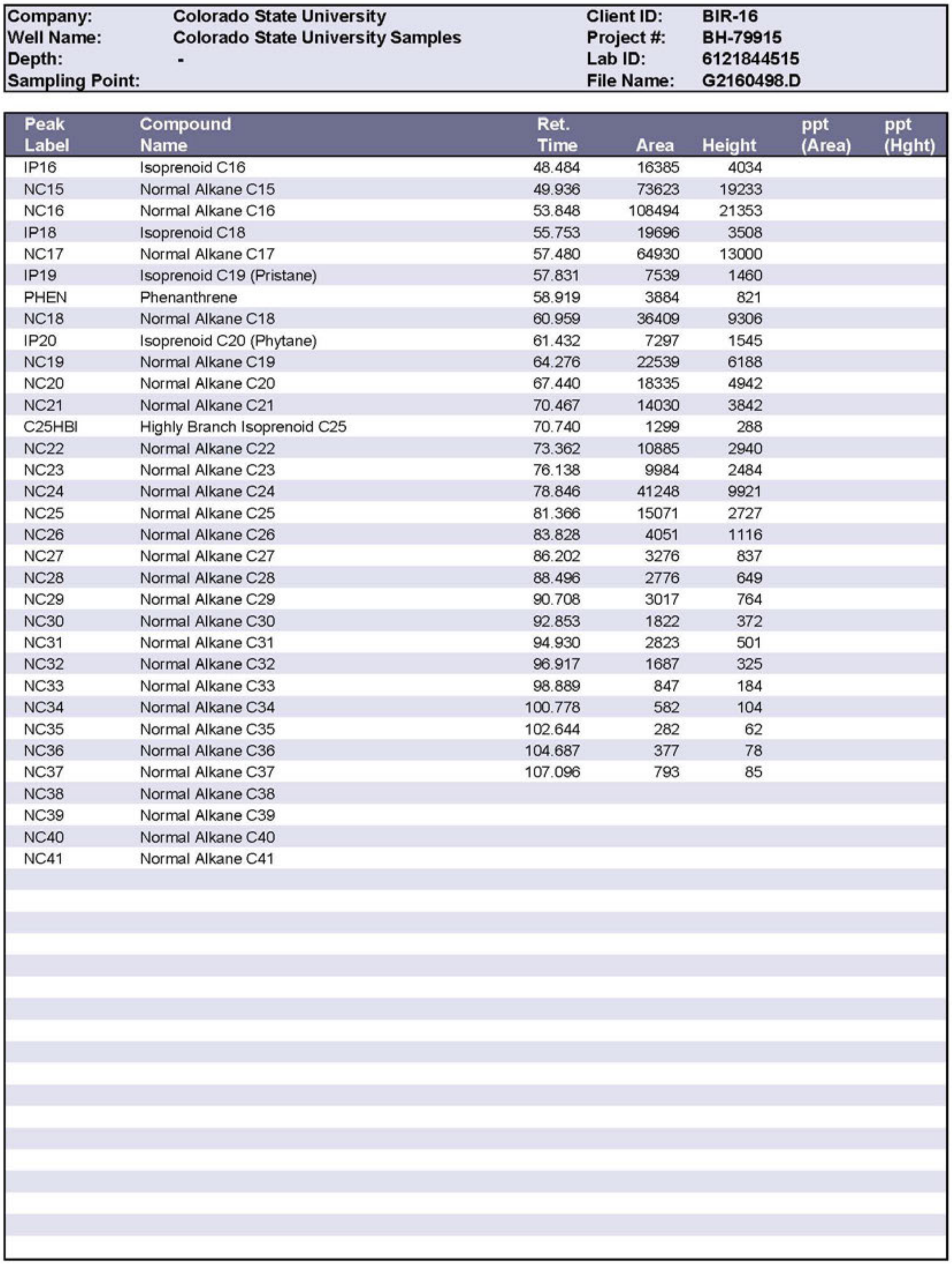

**Company:** Colorado State University
**Well Name:** Colorado State University Samples
**Depth:** -
**Sampling Point:**
**Client ID:** BIR-16
**Project #:** BH-79915
**Lab ID:** 6121844515
**File Name:** G2160498.D

| Peak Label | Compound Name | Ret. Time | Area | Height | ppt (Area) | ppt (Hght) |
|---|---|---|---|---|---|---|
| IP16 | Isoprenoid C16 | 48.484 | 16385 | 4034 | | |
| NC15 | Normal Alkane C15 | 49.936 | 73623 | 19233 | | |
| NC16 | Normal Alkane C16 | 53.848 | 108494 | 21353 | | |
| IP18 | Isoprenoid C18 | 55.753 | 19696 | 3508 | | |
| NC17 | Normal Alkane C17 | 57.480 | 64930 | 13000 | | |
| IP19 | Isoprenoid C19 (Pristane) | 57.831 | 7539 | 1460 | | |
| PHEN | Phenanthrene | 58.919 | 3884 | 821 | | |
| NC18 | Normal Alkane C18 | 60.959 | 36409 | 9306 | | |
| IP20 | Isoprenoid C20 (Phytane) | 61.432 | 7297 | 1545 | | |
| NC19 | Normal Alkane C19 | 64.276 | 22539 | 6188 | | |
| NC20 | Normal Alkane C20 | 67.440 | 18335 | 4942 | | |
| NC21 | Normal Alkane C21 | 70.467 | 14030 | 3842 | | |
| C25HBI | Highly Branch Isoprenoid C25 | 70.740 | 1299 | 288 | | |
| NC22 | Normal Alkane C22 | 73.362 | 10885 | 2940 | | |
| NC23 | Normal Alkane C23 | 76.138 | 9984 | 2484 | | |
| NC24 | Normal Alkane C24 | 78.846 | 41248 | 9921 | | |
| NC25 | Normal Alkane C25 | 81.366 | 15071 | 2727 | | |
| NC26 | Normal Alkane C26 | 83.828 | 4051 | 1116 | | |
| NC27 | Normal Alkane C27 | 86.202 | 3276 | 837 | | |
| NC28 | Normal Alkane C28 | 88.496 | 2776 | 649 | | |
| NC29 | Normal Alkane C29 | 90.708 | 3017 | 764 | | |
| NC30 | Normal Alkane C30 | 92.853 | 1822 | 372 | | |
| NC31 | Normal Alkane C31 | 94.930 | 2823 | 501 | | |
| NC32 | Normal Alkane C32 | 96.917 | 1687 | 325 | | |
| NC33 | Normal Alkane C33 | 98.889 | 847 | 184 | | |
| NC34 | Normal Alkane C34 | 100.778 | 582 | 104 | | |
| NC35 | Normal Alkane C35 | 102.644 | 282 | 62 | | |
| NC36 | Normal Alkane C36 | 104.687 | 377 | 78 | | |
| NC37 | Normal Alkane C37 | 107.096 | 793 | 85 | | |
| NC38 | Normal Alkane C38 | | | | | |
| NC39 | Normal Alkane C39 | | | | | |
| NC40 | Normal Alkane C40 | | | | | |
| NC41 | Normal Alkane C41 | | | | | |

Weatherford LABORATORIES

**EXTRACT GC**

| | | | |
|---|---|---|---|
| **Company:** | **Colorado State University** | **Client ID:** | **517-2.5** |
| **Country:** | | **Project #:** | **BH-79239** |
| **Basin:** | | **Lab ID:** | **6121806260** |
| **Lease:** | | **Sample Type:** | **Core** |
| **Block:** | | **Sampling Point:** | |
| **Field:** | | **Formation:** | |
| **Well Name:** | **Nonesuch Formation Core Samples** | **Geologic Age:** | |
| **Latitude:** | | **Top Depth:** | **3074.60** |
| **Longitude:** | | **Bottom Depth:** | |
| **Preparation:** | | **GC Method:** | **G02G** |

**Extract GC Trace**

G5160570.D

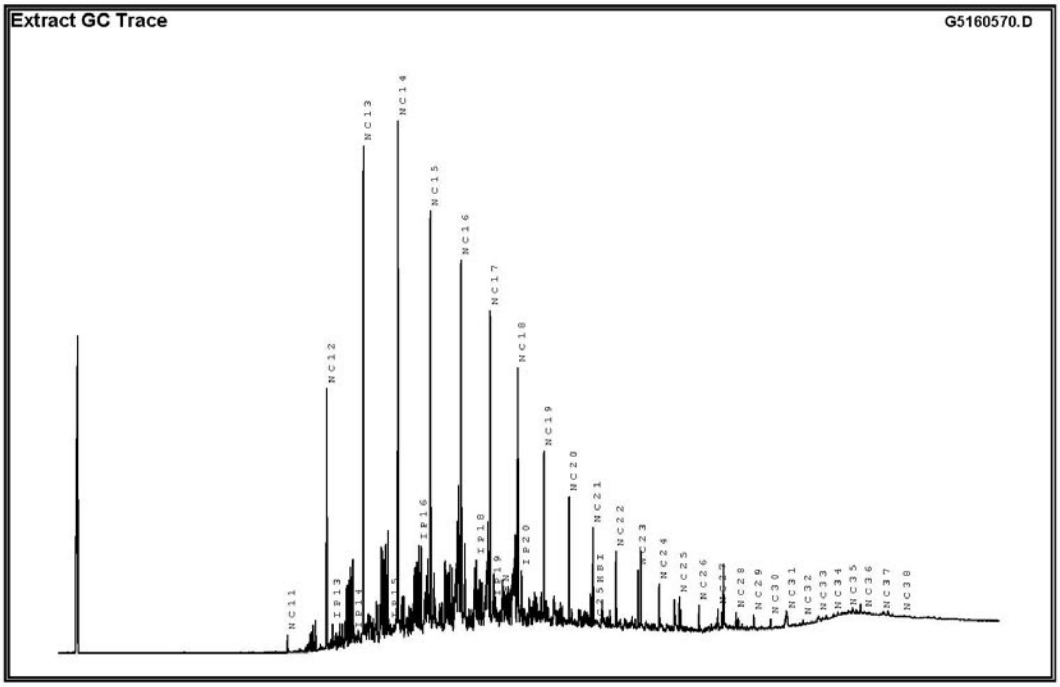

| WGC parameters | |
|---|---|
| Pristane/Phytane | 0.67 |
| Pristane/$n$C$_{17}$ | 0.10 |
| Phytane/$n$C$_{18}$ | 0.19 |
| $n$C$_{18}$/(nC$_{18}$+$n$C$_{19}$) | 0.64 |
| $n$C$_{17}$/(nC$_{17}$+$n$C$_{29}$) | 0.96 |
| CPI Hunt[4] | 1.16 |
| Normal Paraffins | 26.5 |
| Isoprenoids | 2.5 |
| Cycloparaffins | |
| Branched (iso-) Paraffins | |
| BTX aromatics | |
| Resolved unknowns | 71.0 |

| Thompson[1] | | |
|---|---|---|
| A. | BZ/$n$C$_6$ | |
| B. | TOL/$n$C$_7$ | |
| C. | ($n$C$_6$+$n$C$_7$)/(CH+MCH) | |
| I. | Isoheptane Value | |
| F. | $n$C$_7$/MCH | |
| U. | CH/MCP | |
| R. | $n$C$_7$/2MH | |
| S. | $n$C$_6$/22DMB | |
| H. | Heptane Value | |
| | MCH/$n$C$_7$ | |
| | mpXYL/$n$C$_8$ | |

| Mango[2] | |
|---|---|
| P$_1$ | |
| P$_2$ | |
| P$_3$ | |
| 5N$_1$ | |
| N$_2$ | |
| 6N$_1$ | |
| K$_1$ | |
| K$_2$ | |
| 5N$_1$/6N$_1$ | |
| P$_3$/N$_2$ | |
| ln(24DMP/23DMP) | |

| Halpern[3] | |
|---|---|
| Tr$_1$ | |
| Tr$_2$ | |
| Tr$_3$ | |
| Tr$_4$ | |
| Tr$_5$ | |
| Tr$_7$ | |
| Tr$_8$ | |
| C$_1$ | |
| C$_2$ | |
| C$_3$ | |
| C$_4$ | |
| C$_5$ | |

[1]Thompson, K.F.M.,1983.GCA:V.47, p.303. [2]Mango, F.D.,1994.GCA: V.58, p.895. [3]Halpern,H.I.,1995,AAPG Bull.: V.79, p.801. [4]Hunt, 1979

*Appendix F1, ctd.*

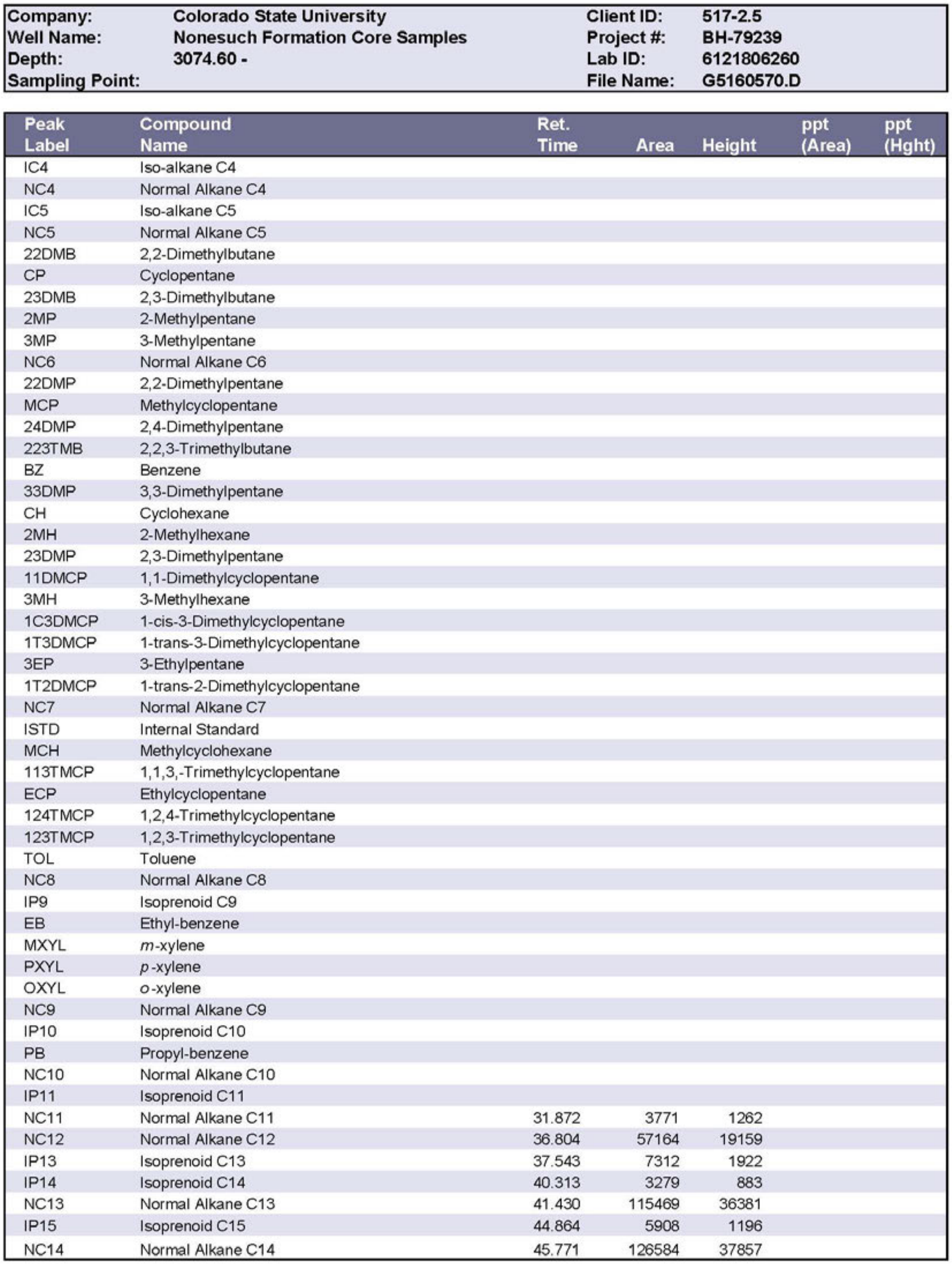

| | | | |
|---|---|---|---|
| **Company:** | **Colorado State University** | **Client ID:** | **517-2.5** |
| **Well Name:** | **Nonesuch Formation Core Samples** | **Project #:** | **BH-79239** |
| **Depth:** | **3074.60 -** | **Lab ID:** | **6121806260** |
| **Sampling Point:** | | **File Name:** | **G5160570.D** |

| Peak Label | Compound Name | Ret. Time | Area | Height | ppt (Area) | ppt (Hght) |
|---|---|---|---|---|---|---|
| IC4 | Iso-alkane C4 | | | | | |
| NC4 | Normal Alkane C4 | | | | | |
| IC5 | Iso-alkane C5 | | | | | |
| NC5 | Normal Alkane C5 | | | | | |
| 22DMB | 2,2-Dimethylbutane | | | | | |
| CP | Cyclopentane | | | | | |
| 23DMB | 2,3-Dimethylbutane | | | | | |
| 2MP | 2-Methylpentane | | | | | |
| 3MP | 3-Methylpentane | | | | | |
| NC6 | Normal Alkane C6 | | | | | |
| 22DMP | 2,2-Dimethylpentane | | | | | |
| MCP | Methylcyclopentane | | | | | |
| 24DMP | 2,4-Dimethylpentane | | | | | |
| 223TMB | 2,2,3-Trimethylbutane | | | | | |
| BZ | Benzene | | | | | |
| 33DMP | 3,3-Dimethylpentane | | | | | |
| CH | Cyclohexane | | | | | |
| 2MH | 2-Methylhexane | | | | | |
| 23DMP | 2,3-Dimethylpentane | | | | | |
| 11DMCP | 1,1-Dimethylcyclopentane | | | | | |
| 3MH | 3-Methylhexane | | | | | |
| 1C3DMCP | 1-cis-3-Dimethylcyclopentane | | | | | |
| 1T3DMCP | 1-trans-3-Dimethylcyclopentane | | | | | |
| 3EP | 3-Ethylpentane | | | | | |
| 1T2DMCP | 1-trans-2-Dimethylcyclopentane | | | | | |
| NC7 | Normal Alkane C7 | | | | | |
| ISTD | Internal Standard | | | | | |
| MCH | Methylcyclohexane | | | | | |
| 113TMCP | 1,1,3,-Trimethylcyclopentane | | | | | |
| ECP | Ethylcyclopentane | | | | | |
| 124TMCP | 1,2,4-Trimethylcyclopentane | | | | | |
| 123TMCP | 1,2,3-Trimethylcyclopentane | | | | | |
| TOL | Toluene | | | | | |
| NC8 | Normal Alkane C8 | | | | | |
| IP9 | Isoprenoid C9 | | | | | |
| EB | Ethyl-benzene | | | | | |
| MXYL | *m*-xylene | | | | | |
| PXYL | *p*-xylene | | | | | |
| OXYL | *o*-xylene | | | | | |
| NC9 | Normal Alkane C9 | | | | | |
| IP10 | Isoprenoid C10 | | | | | |
| PB | Propyl-benzene | | | | | |
| NC10 | Normal Alkane C10 | | | | | |
| IP11 | Isoprenoid C11 | | | | | |
| NC11 | Normal Alkane C11 | 31.872 | 3771 | 1262 | | |
| NC12 | Normal Alkane C12 | 36.804 | 57164 | 19159 | | |
| IP13 | Isoprenoid C13 | 37.543 | 7312 | 1922 | | |
| IP14 | Isoprenoid C14 | 40.313 | 3279 | 883 | | |
| NC13 | Normal Alkane C13 | 41.430 | 115469 | 36381 | | |
| IP15 | Isoprenoid C15 | 44.864 | 5908 | 1196 | | |
| NC14 | Normal Alkane C14 | 45.771 | 126584 | 37857 | | |

*Appendix F1, ctd.*

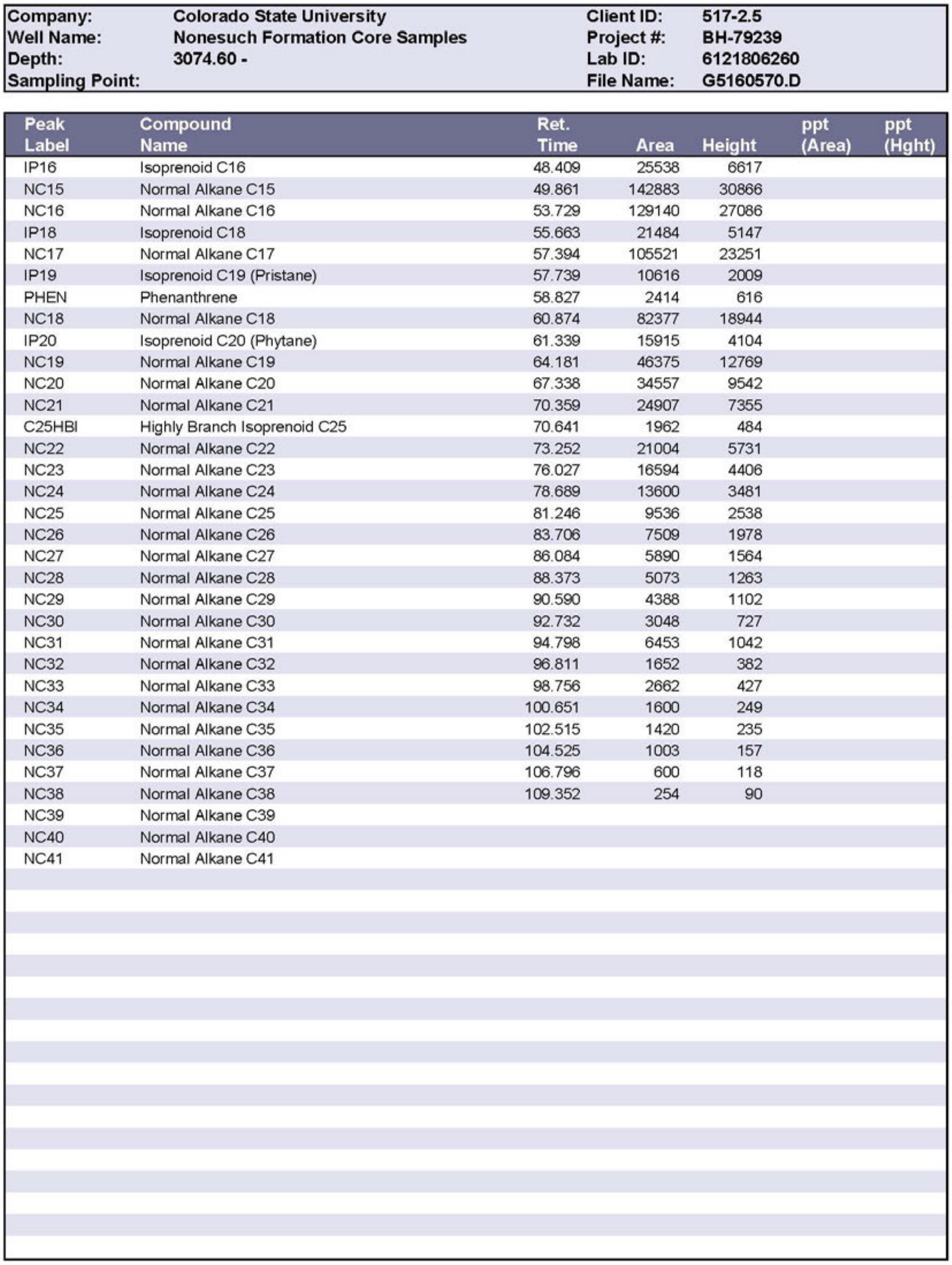

| | | | |
|---|---|---|---|
| **Company:** | **Colorado State University** | **Client ID:** | **517-2.5** |
| **Well Name:** | **Nonesuch Formation Core Samples** | **Project #:** | **BH-79239** |
| **Depth:** | **3074.60 -** | **Lab ID:** | **6121806260** |
| **Sampling Point:** | | **File Name:** | **G5160570.D** |

| Peak Label | Compound Name | Ret. Time | Area | Height | ppt (Area) | ppt (Hght) |
|---|---|---|---|---|---|---|
| IP16 | Isoprenoid C16 | 48.409 | 25538 | 6617 | | |
| NC15 | Normal Alkane C15 | 49.861 | 142883 | 30866 | | |
| NC16 | Normal Alkane C16 | 53.729 | 129140 | 27086 | | |
| IP18 | Isoprenoid C18 | 55.663 | 21484 | 5147 | | |
| NC17 | Normal Alkane C17 | 57.394 | 105521 | 23251 | | |
| IP19 | Isoprenoid C19 (Pristane) | 57.739 | 10616 | 2009 | | |
| PHEN | Phenanthrene | 58.827 | 2414 | 616 | | |
| NC18 | Normal Alkane C18 | 60.874 | 82377 | 18944 | | |
| IP20 | Isoprenoid C20 (Phytane) | 61.339 | 15915 | 4104 | | |
| NC19 | Normal Alkane C19 | 64.181 | 46375 | 12769 | | |
| NC20 | Normal Alkane C20 | 67.338 | 34557 | 9542 | | |
| NC21 | Normal Alkane C21 | 70.359 | 24907 | 7355 | | |
| C25HBI | Highly Branch Isoprenoid C25 | 70.641 | 1962 | 484 | | |
| NC22 | Normal Alkane C22 | 73.252 | 21004 | 5731 | | |
| NC23 | Normal Alkane C23 | 76.027 | 16594 | 4406 | | |
| NC24 | Normal Alkane C24 | 78.689 | 13600 | 3481 | | |
| NC25 | Normal Alkane C25 | 81.246 | 9536 | 2538 | | |
| NC26 | Normal Alkane C26 | 83.706 | 7509 | 1978 | | |
| NC27 | Normal Alkane C27 | 86.084 | 5890 | 1564 | | |
| NC28 | Normal Alkane C28 | 88.373 | 5073 | 1263 | | |
| NC29 | Normal Alkane C29 | 90.590 | 4388 | 1102 | | |
| NC30 | Normal Alkane C30 | 92.732 | 3048 | 727 | | |
| NC31 | Normal Alkane C31 | 94.798 | 6453 | 1042 | | |
| NC32 | Normal Alkane C32 | 96.811 | 1652 | 382 | | |
| NC33 | Normal Alkane C33 | 98.756 | 2662 | 427 | | |
| NC34 | Normal Alkane C34 | 100.651 | 1600 | 249 | | |
| NC35 | Normal Alkane C35 | 102.515 | 1420 | 235 | | |
| NC36 | Normal Alkane C36 | 104.525 | 1003 | 157 | | |
| NC37 | Normal Alkane C37 | 106.796 | 600 | 118 | | |
| NC38 | Normal Alkane C38 | 109.352 | 254 | 90 | | |
| NC39 | Normal Alkane C39 | | | | | |
| NC40 | Normal Alkane C40 | | | | | |
| NC41 | Normal Alkane C41 | | | | | |

*Appendix F1, ctd.*

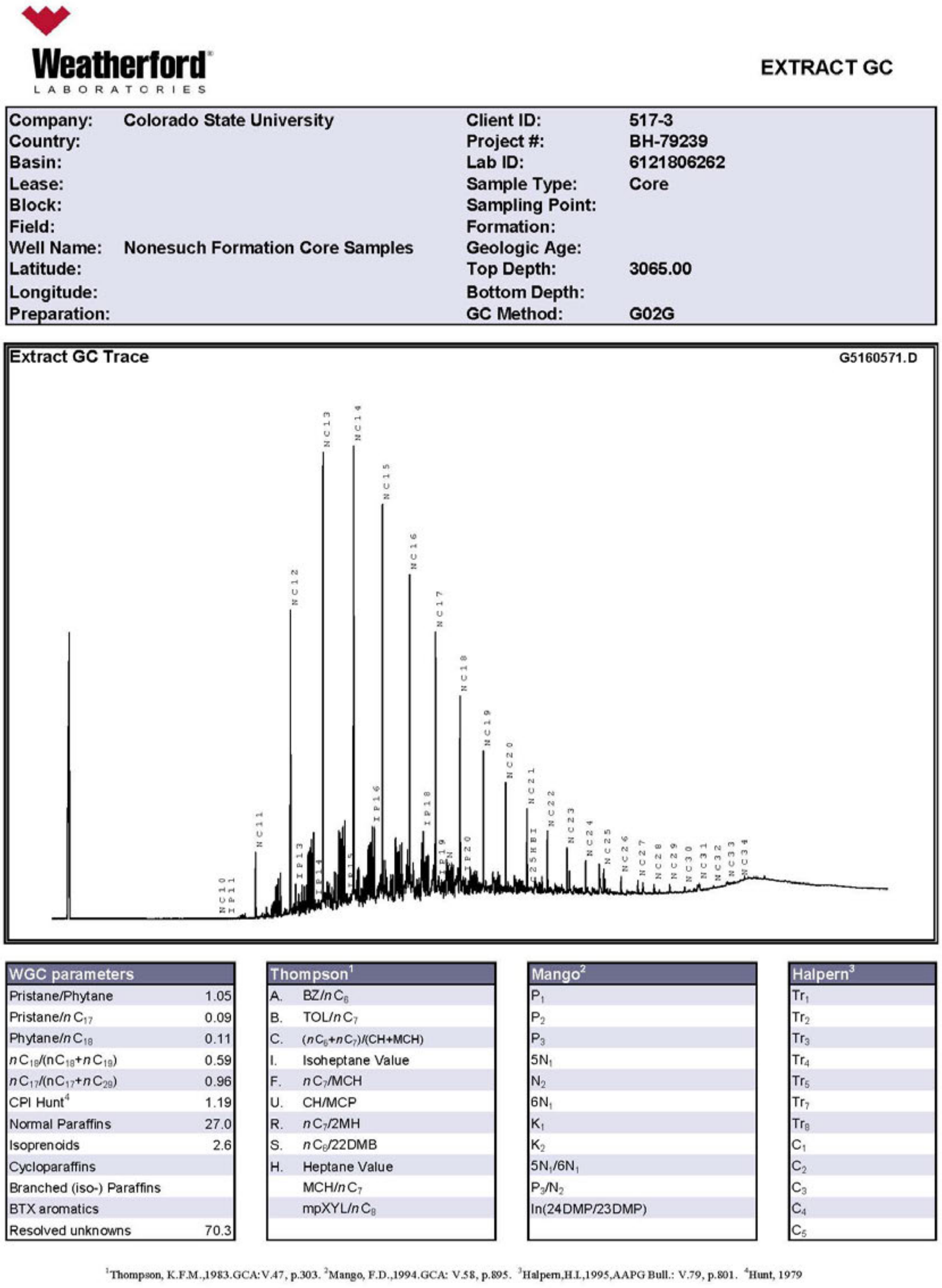

Weatherford LABORATORIES

**EXTRACT GC**

| | | | |
|---|---|---|---|
| **Company:** | **Colorado State University** | **Client ID:** | **517-3** |
| **Country:** | | **Project #:** | **BH-79239** |
| **Basin:** | | **Lab ID:** | **6121806262** |
| **Lease:** | | **Sample Type:** | **Core** |
| **Block:** | | **Sampling Point:** | |
| **Field:** | | **Formation:** | |
| **Well Name:** | **Nonesuch Formation Core Samples** | **Geologic Age:** | |
| **Latitude:** | | **Top Depth:** | **3065.00** |
| **Longitude:** | | **Bottom Depth:** | |
| **Preparation:** | | **GC Method:** | **G02G** |

**Extract GC Trace**

**G5160571.D**

| WGC parameters | |
|---|---|
| Pristane/Phytane | 1.05 |
| Pristane/$n\,C_{17}$ | 0.09 |
| Phytane/$n\,C_{18}$ | 0.11 |
| $n\,C_{18}/(nC_{18}+n\,C_{19})$ | 0.59 |
| $n\,C_{17}/(nC_{17}+n\,C_{29})$ | 0.96 |
| CPI Hunt[4] | 1.19 |
| Normal Paraffins | 27.0 |
| Isoprenoids | 2.6 |
| Cycloparaffins | |
| Branched (iso-) Paraffins | |
| BTX aromatics | |
| Resolved unknowns | 70.3 |

| Thompson[1] | | |
|---|---|---|
| A. | BZ/$n\,C_6$ | |
| B. | TOL/$n\,C_7$ | |
| C. | $(n\,C_6+n\,C_7)$/(CH+MCH) | |
| I. | Isoheptane Value | |
| F. | $n\,C_7$/MCH | |
| U. | CH/MCP | |
| R. | $n\,C_7$/2MH | |
| S. | $n\,C_6$/22DMB | |
| H. | Heptane Value | |
| | MCH/$n\,C_7$ | |
| | mpXYL/$n\,C_8$ | |

| Mango[2] | |
|---|---|
| $P_1$ | |
| $P_2$ | |
| $P_3$ | |
| $5N_1$ | |
| $N_2$ | |
| $6N_1$ | |
| $K_1$ | |
| $K_2$ | |
| $5N_1/6N_1$ | |
| $P_3/N_2$ | |
| ln(24DMP/23DMP) | |

| Halpern[3] | |
|---|---|
| $Tr_1$ | |
| $Tr_2$ | |
| $Tr_3$ | |
| $Tr_4$ | |
| $Tr_5$ | |
| $Tr_7$ | |
| $Tr_8$ | |
| $C_1$ | |
| $C_2$ | |
| $C_3$ | |
| $C_4$ | |
| $C_5$ | |

[1] Thompson, K.F.M.,1983.GCA:V.47, p.303. [2] Mango, F.D.,1994.GCA: V.58, p.895. [3] Halpern,H.I.,1995,AAPG Bull.: V.79, p.801. [4] Hunt, 1979

*Appendix F1, ctd.*

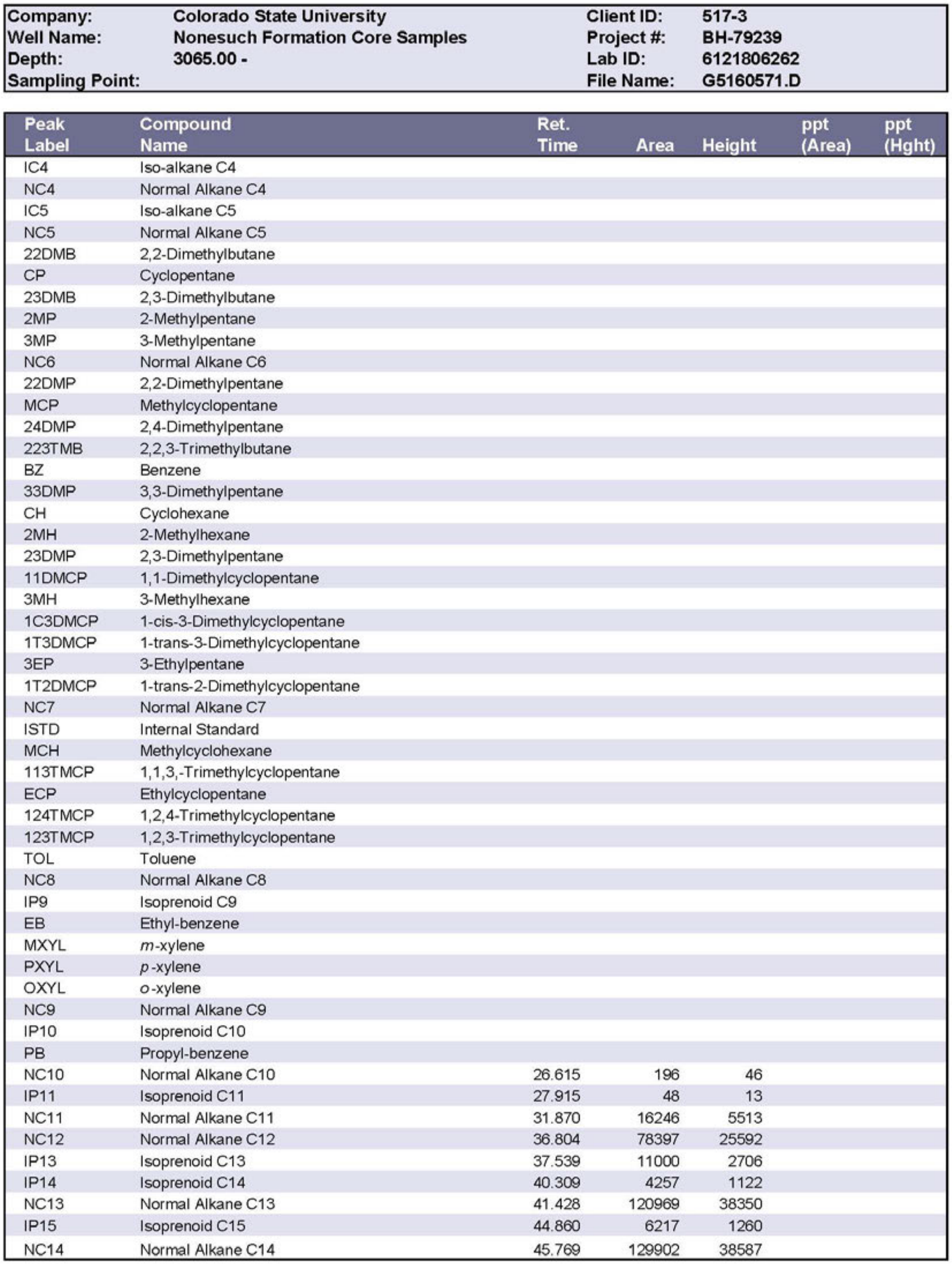

| | | | |
|---|---|---|---|
| **Company:** | **Colorado State University** | **Client ID:** | **517-3** |
| **Well Name:** | **Nonesuch Formation Core Samples** | **Project #:** | **BH-79239** |
| **Depth:** | **3065.00 -** | **Lab ID:** | **6121806262** |
| **Sampling Point:** | | **File Name:** | **G5160571.D** |

| Peak Label | Compound Name | Ret. Time | Area | Height | ppt (Area) | ppt (Hght) |
|---|---|---|---|---|---|---|
| IC4 | Iso-alkane C4 | | | | | |
| NC4 | Normal Alkane C4 | | | | | |
| IC5 | Iso-alkane C5 | | | | | |
| NC5 | Normal Alkane C5 | | | | | |
| 22DMB | 2,2-Dimethylbutane | | | | | |
| CP | Cyclopentane | | | | | |
| 23DMB | 2,3-Dimethylbutane | | | | | |
| 2MP | 2-Methylpentane | | | | | |
| 3MP | 3-Methylpentane | | | | | |
| NC6 | Normal Alkane C6 | | | | | |
| 22DMP | 2,2-Dimethylpentane | | | | | |
| MCP | Methylcyclopentane | | | | | |
| 24DMP | 2,4-Dimethylpentane | | | | | |
| 223TMB | 2,2,3-Trimethylbutane | | | | | |
| BZ | Benzene | | | | | |
| 33DMP | 3,3-Dimethylpentane | | | | | |
| CH | Cyclohexane | | | | | |
| 2MH | 2-Methylhexane | | | | | |
| 23DMP | 2,3-Dimethylpentane | | | | | |
| 11DMCP | 1,1-Dimethylcyclopentane | | | | | |
| 3MH | 3-Methylhexane | | | | | |
| 1C3DMCP | 1-cis-3-Dimethylcyclopentane | | | | | |
| 1T3DMCP | 1-trans-3-Dimethylcyclopentane | | | | | |
| 3EP | 3-Ethylpentane | | | | | |
| 1T2DMCP | 1-trans-2-Dimethylcyclopentane | | | | | |
| NC7 | Normal Alkane C7 | | | | | |
| ISTD | Internal Standard | | | | | |
| MCH | Methylcyclohexane | | | | | |
| 113TMCP | 1,1,3,-Trimethylcyclopentane | | | | | |
| ECP | Ethylcyclopentane | | | | | |
| 124TMCP | 1,2,4-Trimethylcyclopentane | | | | | |
| 123TMCP | 1,2,3-Trimethylcyclopentane | | | | | |
| TOL | Toluene | | | | | |
| NC8 | Normal Alkane C8 | | | | | |
| IP9 | Isoprenoid C9 | | | | | |
| EB | Ethyl-benzene | | | | | |
| MXYL | *m*-xylene | | | | | |
| PXYL | *p*-xylene | | | | | |
| OXYL | *o*-xylene | | | | | |
| NC9 | Normal Alkane C9 | | | | | |
| IP10 | Isoprenoid C10 | | | | | |
| PB | Propyl-benzene | | | | | |
| NC10 | Normal Alkane C10 | 26.615 | 196 | 46 | | |
| IP11 | Isoprenoid C11 | 27.915 | 48 | 13 | | |
| NC11 | Normal Alkane C11 | 31.870 | 16246 | 5513 | | |
| NC12 | Normal Alkane C12 | 36.804 | 78397 | 25592 | | |
| IP13 | Isoprenoid C13 | 37.539 | 11000 | 2706 | | |
| IP14 | Isoprenoid C14 | 40.309 | 4257 | 1122 | | |
| NC13 | Normal Alkane C13 | 41.428 | 120969 | 38350 | | |
| IP15 | Isoprenoid C15 | 44.860 | 6217 | 1260 | | |
| NC14 | Normal Alkane C14 | 45.769 | 129902 | 38587 | | |

*Appendix F1, ctd.*

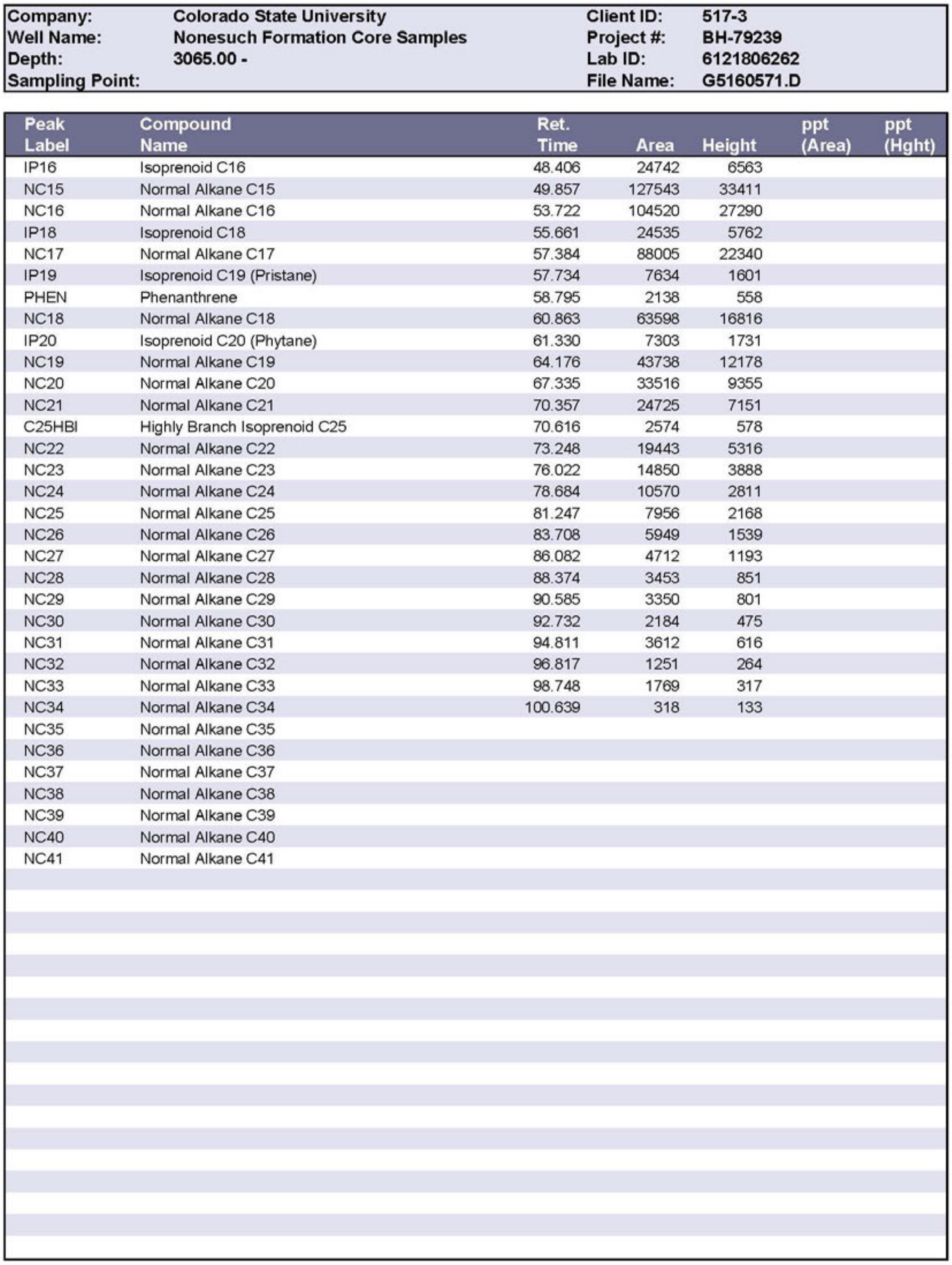

| | | | |
|---|---|---|---|
| **Company:** | **Colorado State University** | **Client ID:** | **517-3** |
| **Well Name:** | **Nonesuch Formation Core Samples** | **Project #:** | **BH-79239** |
| **Depth:** | **3065.00 -** | **Lab ID:** | **6121806262** |
| **Sampling Point:** | | **File Name:** | **G5160571.D** |

| Peak Label | Compound Name | Ret. Time | Area | Height | ppt (Area) | ppt (Hght) |
|---|---|---|---|---|---|---|
| IP16 | Isoprenoid C16 | 48.406 | 24742 | 6563 | | |
| NC15 | Normal Alkane C15 | 49.857 | 127543 | 33411 | | |
| NC16 | Normal Alkane C16 | 53.722 | 104520 | 27290 | | |
| IP18 | Isoprenoid C18 | 55.661 | 24535 | 5762 | | |
| NC17 | Normal Alkane C17 | 57.384 | 88005 | 22340 | | |
| IP19 | Isoprenoid C19 (Pristane) | 57.734 | 7634 | 1601 | | |
| PHEN | Phenanthrene | 58.795 | 2138 | 558 | | |
| NC18 | Normal Alkane C18 | 60.863 | 63598 | 16816 | | |
| IP20 | Isoprenoid C20 (Phytane) | 61.330 | 7303 | 1731 | | |
| NC19 | Normal Alkane C19 | 64.176 | 43738 | 12178 | | |
| NC20 | Normal Alkane C20 | 67.335 | 33516 | 9355 | | |
| NC21 | Normal Alkane C21 | 70.357 | 24725 | 7151 | | |
| C25HBI | Highly Branch Isoprenoid C25 | 70.616 | 2574 | 578 | | |
| NC22 | Normal Alkane C22 | 73.248 | 19443 | 5316 | | |
| NC23 | Normal Alkane C23 | 76.022 | 14850 | 3888 | | |
| NC24 | Normal Alkane C24 | 78.684 | 10570 | 2811 | | |
| NC25 | Normal Alkane C25 | 81.247 | 7956 | 2168 | | |
| NC26 | Normal Alkane C26 | 83.708 | 5949 | 1539 | | |
| NC27 | Normal Alkane C27 | 86.082 | 4712 | 1193 | | |
| NC28 | Normal Alkane C28 | 88.374 | 3453 | 851 | | |
| NC29 | Normal Alkane C29 | 90.585 | 3350 | 801 | | |
| NC30 | Normal Alkane C30 | 92.732 | 2184 | 475 | | |
| NC31 | Normal Alkane C31 | 94.811 | 3612 | 616 | | |
| NC32 | Normal Alkane C32 | 96.817 | 1251 | 264 | | |
| NC33 | Normal Alkane C33 | 98.748 | 1769 | 317 | | |
| NC34 | Normal Alkane C34 | 100.639 | 318 | 133 | | |
| NC35 | Normal Alkane C35 | | | | | |
| NC36 | Normal Alkane C36 | | | | | |
| NC37 | Normal Alkane C37 | | | | | |
| NC38 | Normal Alkane C38 | | | | | |
| NC39 | Normal Alkane C39 | | | | | |
| NC40 | Normal Alkane C40 | | | | | |
| NC41 | Normal Alkane C41 | | | | | |

*Appendix F1, ctd.*

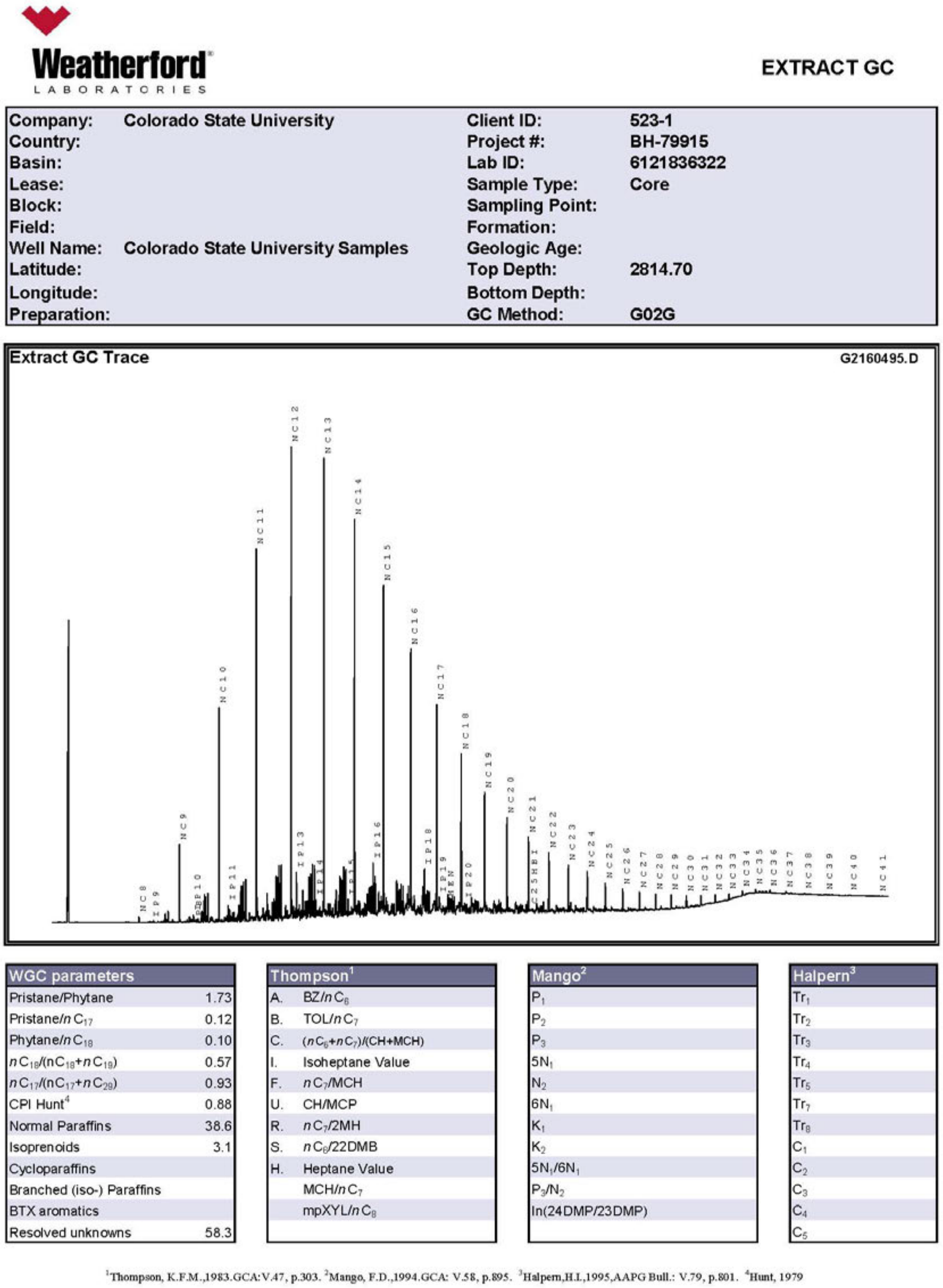

**Weatherford** LABORATORIES

**EXTRACT GC**

| | | | |
|---|---|---|---|
| **Company:** | **Colorado State University** | **Client ID:** | **523-1** |
| **Country:** | | **Project #:** | **BH-79915** |
| **Basin:** | | **Lab ID:** | **6121836322** |
| **Lease:** | | **Sample Type:** | **Core** |
| **Block:** | | **Sampling Point:** | |
| **Field:** | | **Formation:** | |
| **Well Name:** | **Colorado State University Samples** | **Geologic Age:** | |
| **Latitude:** | | **Top Depth:** | **2814.70** |
| **Longitude:** | | **Bottom Depth:** | |
| **Preparation:** | | **GC Method:** | **G02G** |

**Extract GC Trace**

**G2160495.D**

| WGC parameters | |
|---|---|
| Pristane/Phytane | 1.73 |
| Pristane/$nC_{17}$ | 0.12 |
| Phytane/$nC_{18}$ | 0.10 |
| $nC_{18}$/($nC_{18}$+$nC_{19}$) | 0.57 |
| $nC_{17}$/($nC_{17}$+$nC_{29}$) | 0.93 |
| CPI Hunt[4] | 0.88 |
| Normal Paraffins | 38.6 |
| Isoprenoids | 3.1 |
| Cycloparaffins | |
| Branched (iso-) Paraffins | |
| BTX aromatics | |
| Resolved unknowns | 58.3 |

| Thompson[1] | | |
|---|---|---|
| A. | BZ/$nC_6$ | |
| B. | TOL/$nC_7$ | |
| C. | ($nC_6$+$nC_7$)/(CH+MCH) | |
| I. | Isoheptane Value | |
| F. | $nC_7$/MCH | |
| U. | CH/MCP | |
| R. | $nC_7$/2MH | |
| S. | $nC_6$/22DMB | |
| H. | Heptane Value | |
| | MCH/$nC_7$ | |
| | mpXYL/$nC_8$ | |

| Mango[2] | |
|---|---|
| $P_1$ | |
| $P_2$ | |
| $P_3$ | |
| $5N_1$ | |
| $N_2$ | |
| $6N_1$ | |
| $K_1$ | |
| $K_2$ | |
| $5N_1/6N_1$ | |
| $P_3/N_2$ | |
| ln(24DMP/23DMP) | |

| Halpern[3] | |
|---|---|
| $Tr_1$ | |
| $Tr_2$ | |
| $Tr_3$ | |
| $Tr_4$ | |
| $Tr_5$ | |
| $Tr_7$ | |
| $Tr_8$ | |
| $C_1$ | |
| $C_2$ | |
| $C_3$ | |
| $C_4$ | |
| $C_5$ | |

[1]Thompson, K.F.M.,1983.GCA:V.47, p.303. [2]Mango, F.D.,1994.GCA: V.58, p.895. [3]Halpern,H.I.,1995,AAPG Bull.: V.79, p.801. [4]Hunt, 1979

*<u>Appendix F1, ctd.</u>*

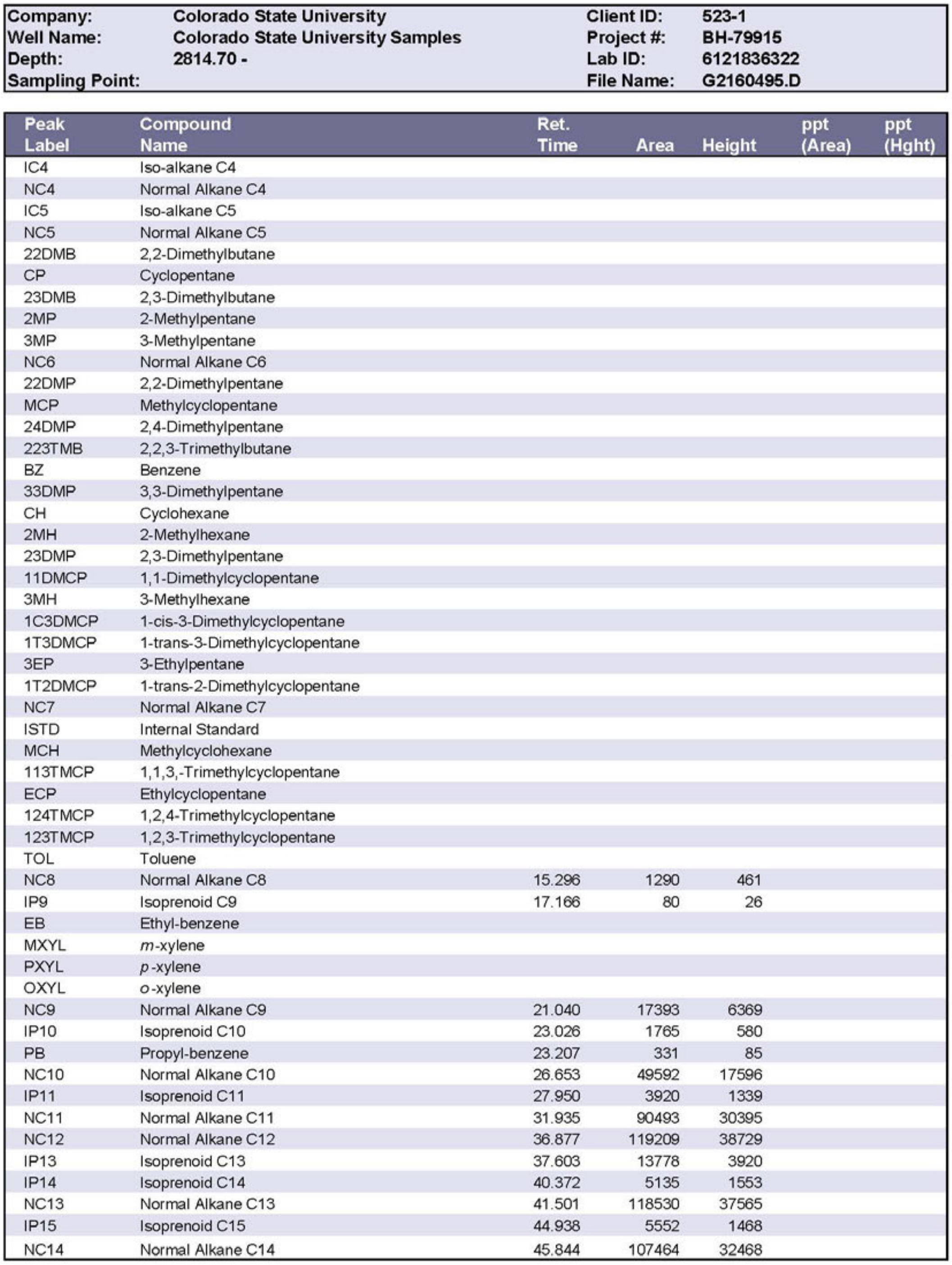

| | | | |
|---|---|---|---|
| **Company:** | **Colorado State University** | **Client ID:** | **523-1** |
| **Well Name:** | **Colorado State University Samples** | **Project #:** | **BH-79915** |
| **Depth:** | **2814.70 -** | **Lab ID:** | **6121836322** |
| **Sampling Point:** | | **File Name:** | **G2160495.D** |

| Peak Label | Compound Name | Ret. Time | Area | Height | ppt (Area) | ppt (Hght) |
|---|---|---|---|---|---|---|
| IC4 | Iso-alkane C4 | | | | | |
| NC4 | Normal Alkane C4 | | | | | |
| IC5 | Iso-alkane C5 | | | | | |
| NC5 | Normal Alkane C5 | | | | | |
| 22DMB | 2,2-Dimethylbutane | | | | | |
| CP | Cyclopentane | | | | | |
| 23DMB | 2,3-Dimethylbutane | | | | | |
| 2MP | 2-Methylpentane | | | | | |
| 3MP | 3-Methylpentane | | | | | |
| NC6 | Normal Alkane C6 | | | | | |
| 22DMP | 2,2-Dimethylpentane | | | | | |
| MCP | Methylcyclopentane | | | | | |
| 24DMP | 2,4-Dimethylpentane | | | | | |
| 223TMB | 2,2,3-Trimethylbutane | | | | | |
| BZ | Benzene | | | | | |
| 33DMP | 3,3-Dimethylpentane | | | | | |
| CH | Cyclohexane | | | | | |
| 2MH | 2-Methylhexane | | | | | |
| 23DMP | 2,3-Dimethylpentane | | | | | |
| 11DMCP | 1,1-Dimethylcyclopentane | | | | | |
| 3MH | 3-Methylhexane | | | | | |
| 1C3DMCP | 1-cis-3-Dimethylcyclopentane | | | | | |
| 1T3DMCP | 1-trans-3-Dimethylcyclopentane | | | | | |
| 3EP | 3-Ethylpentane | | | | | |
| 1T2DMCP | 1-trans-2-Dimethylcyclopentane | | | | | |
| NC7 | Normal Alkane C7 | | | | | |
| ISTD | Internal Standard | | | | | |
| MCH | Methylcyclohexane | | | | | |
| 113TMCP | 1,1,3,-Trimethylcyclopentane | | | | | |
| ECP | Ethylcyclopentane | | | | | |
| 124TMCP | 1,2,4-Trimethylcyclopentane | | | | | |
| 123TMCP | 1,2,3-Trimethylcyclopentane | | | | | |
| TOL | Toluene | | | | | |
| NC8 | Normal Alkane C8 | 15.296 | 1290 | 461 | | |
| IP9 | Isoprenoid C9 | 17.166 | 80 | 26 | | |
| EB | Ethyl-benzene | | | | | |
| MXYL | *m*-xylene | | | | | |
| PXYL | *p*-xylene | | | | | |
| OXYL | *o*-xylene | | | | | |
| NC9 | Normal Alkane C9 | 21.040 | 17393 | 6369 | | |
| IP10 | Isoprenoid C10 | 23.026 | 1765 | 580 | | |
| PB | Propyl-benzene | 23.207 | 331 | 85 | | |
| NC10 | Normal Alkane C10 | 26.653 | 49592 | 17596 | | |
| IP11 | Isoprenoid C11 | 27.950 | 3920 | 1339 | | |
| NC11 | Normal Alkane C11 | 31.935 | 90493 | 30395 | | |
| NC12 | Normal Alkane C12 | 36.877 | 119209 | 38729 | | |
| IP13 | Isoprenoid C13 | 37.603 | 13778 | 3920 | | |
| IP14 | Isoprenoid C14 | 40.372 | 5135 | 1553 | | |
| NC13 | Normal Alkane C13 | 41.501 | 118530 | 37565 | | |
| IP15 | Isoprenoid C15 | 44.938 | 5552 | 1468 | | |
| NC14 | Normal Alkane C14 | 45.844 | 107464 | 32468 | | |

*Appendix F1, ctd.*

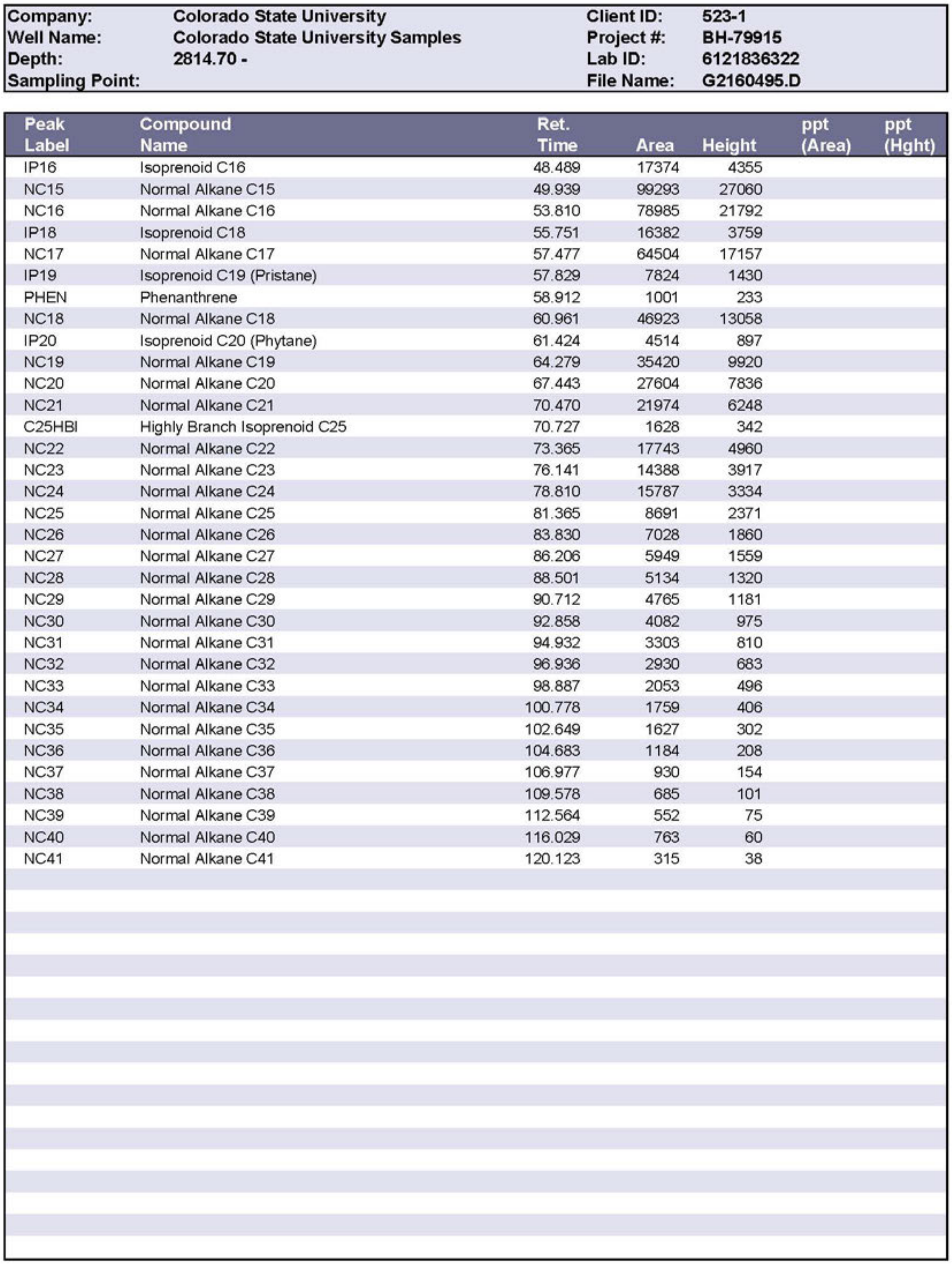

| | | | |
|---|---|---|---|
| **Company:** | **Colorado State University** | **Client ID:** | **523-1** |
| **Well Name:** | **Colorado State University Samples** | **Project #:** | **BH-79915** |
| **Depth:** | **2814.70 -** | **Lab ID:** | **6121836322** |
| **Sampling Point:** | | **File Name:** | **G2160495.D** |

| Peak Label | Compound Name | Ret. Time | Area | Height | ppt (Area) | ppt (Hght) |
|---|---|---|---|---|---|---|
| IP16 | Isoprenoid C16 | 48.489 | 17374 | 4355 | | |
| NC15 | Normal Alkane C15 | 49.939 | 99293 | 27060 | | |
| NC16 | Normal Alkane C16 | 53.810 | 78985 | 21792 | | |
| IP18 | Isoprenoid C18 | 55.751 | 16382 | 3759 | | |
| NC17 | Normal Alkane C17 | 57.477 | 64504 | 17157 | | |
| IP19 | Isoprenoid C19 (Pristane) | 57.829 | 7824 | 1430 | | |
| PHEN | Phenanthrene | 58.912 | 1001 | 233 | | |
| NC18 | Normal Alkane C18 | 60.961 | 46923 | 13058 | | |
| IP20 | Isoprenoid C20 (Phytane) | 61.424 | 4514 | 897 | | |
| NC19 | Normal Alkane C19 | 64.279 | 35420 | 9920 | | |
| NC20 | Normal Alkane C20 | 67.443 | 27604 | 7836 | | |
| NC21 | Normal Alkane C21 | 70.470 | 21974 | 6248 | | |
| C25HBI | Highly Branch Isoprenoid C25 | 70.727 | 1628 | 342 | | |
| NC22 | Normal Alkane C22 | 73.365 | 17743 | 4960 | | |
| NC23 | Normal Alkane C23 | 76.141 | 14388 | 3917 | | |
| NC24 | Normal Alkane C24 | 78.810 | 15787 | 3334 | | |
| NC25 | Normal Alkane C25 | 81.365 | 8691 | 2371 | | |
| NC26 | Normal Alkane C26 | 83.830 | 7028 | 1860 | | |
| NC27 | Normal Alkane C27 | 86.206 | 5949 | 1559 | | |
| NC28 | Normal Alkane C28 | 88.501 | 5134 | 1320 | | |
| NC29 | Normal Alkane C29 | 90.712 | 4765 | 1181 | | |
| NC30 | Normal Alkane C30 | 92.858 | 4082 | 975 | | |
| NC31 | Normal Alkane C31 | 94.932 | 3303 | 810 | | |
| NC32 | Normal Alkane C32 | 96.936 | 2930 | 683 | | |
| NC33 | Normal Alkane C33 | 98.887 | 2053 | 496 | | |
| NC34 | Normal Alkane C34 | 100.778 | 1759 | 406 | | |
| NC35 | Normal Alkane C35 | 102.649 | 1627 | 302 | | |
| NC36 | Normal Alkane C36 | 104.683 | 1184 | 208 | | |
| NC37 | Normal Alkane C37 | 106.977 | 930 | 154 | | |
| NC38 | Normal Alkane C38 | 109.578 | 685 | 101 | | |
| NC39 | Normal Alkane C39 | 112.564 | 552 | 75 | | |
| NC40 | Normal Alkane C40 | 116.029 | 763 | 60 | | |
| NC41 | Normal Alkane C41 | 120.123 | 315 | 38 | | |

*Appendix F1, ctd.*

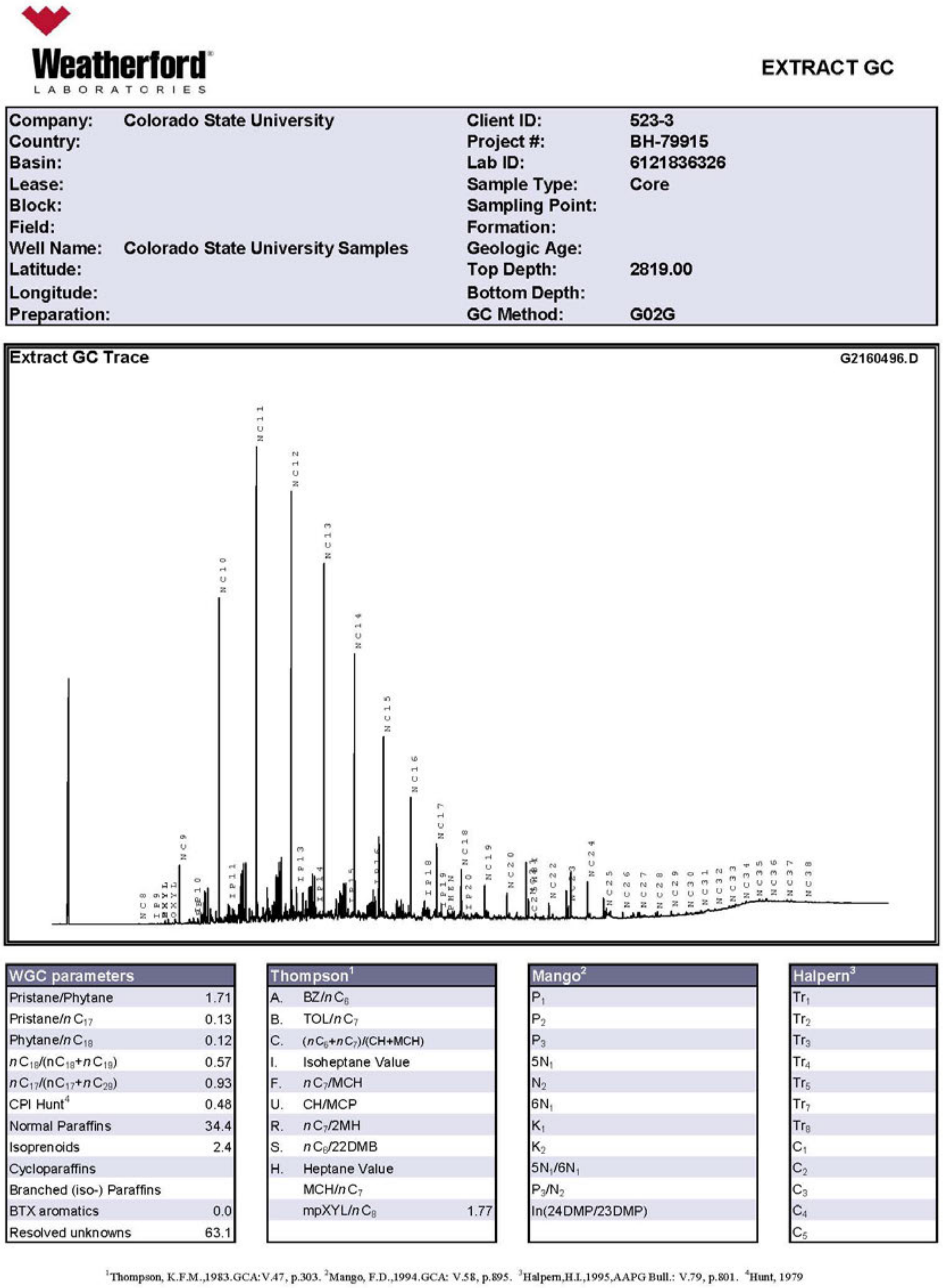

**Weatherford** LABORATORIES

**EXTRACT GC**

| | | | |
|---|---|---|---|
| **Company:** | **Colorado State University** | **Client ID:** | **523-3** |
| **Country:** | | **Project #:** | **BH-79915** |
| **Basin:** | | **Lab ID:** | **6121836326** |
| **Lease:** | | **Sample Type:** | **Core** |
| **Block:** | | **Sampling Point:** | |
| **Field:** | | **Formation:** | |
| **Well Name:** | **Colorado State University Samples** | **Geologic Age:** | |
| **Latitude:** | | **Top Depth:** | **2819.00** |
| **Longitude:** | | **Bottom Depth:** | |
| **Preparation:** | | **GC Method:** | **G02G** |

**Extract GC Trace**

| WGC parameters | |
|---|---|
| Pristane/Phytane | 1.71 |
| Pristane/$nC_{17}$ | 0.13 |
| Phytane/$nC_{18}$ | 0.12 |
| $nC_{18}/(nC_{18}+nC_{19})$ | 0.57 |
| $nC_{17}/(nC_{17}+nC_{29})$ | 0.93 |
| CPI Hunt[4] | 0.48 |
| Normal Paraffins | 34.4 |
| Isoprenoids | 2.4 |
| Cycloparaffins | |
| Branched (iso-) Paraffins | |
| BTX aromatics | 0.0 |
| Resolved unknowns | 63.1 |

| Thompson[1] | | |
|---|---|---|
| A. | BZ/$nC_6$ | |
| B. | TOL/$nC_7$ | |
| C. | $(nC_6+nC_7)/(CH+MCH)$ | |
| I. | Isoheptane Value | |
| F. | $nC_7$/MCH | |
| U. | CH/MCP | |
| R. | $nC_7$/2MH | |
| S. | $nC_6$/22DMB | |
| H. | Heptane Value | |
| | MCH/$nC_7$ | |
| | mpXYL/$nC_8$ | 1.77 |

| Mango[2] | |
|---|---|
| $P_1$ | |
| $P_2$ | |
| $P_3$ | |
| $5N_1$ | |
| $N_2$ | |
| $6N_1$ | |
| $K_1$ | |
| $K_2$ | |
| $5N_1/6N_1$ | |
| $P_3/N_2$ | |
| ln(24DMP/23DMP) | |

| Halpern[3] | |
|---|---|
| $Tr_1$ | |
| $Tr_2$ | |
| $Tr_3$ | |
| $Tr_4$ | |
| $Tr_5$ | |
| $Tr_7$ | |
| $Tr_8$ | |
| $C_1$ | |
| $C_2$ | |
| $C_3$ | |
| $C_4$ | |
| $C_5$ | |

[1] Thompson, K.F.M.,1983.GCA:V.47, p.303. [2] Mango, F.D.,1994.GCA: V.58, p.895. [3] Halpern,H.I.,1995,AAPG Bull.: V.79, p.801. [4] Hunt, 1979

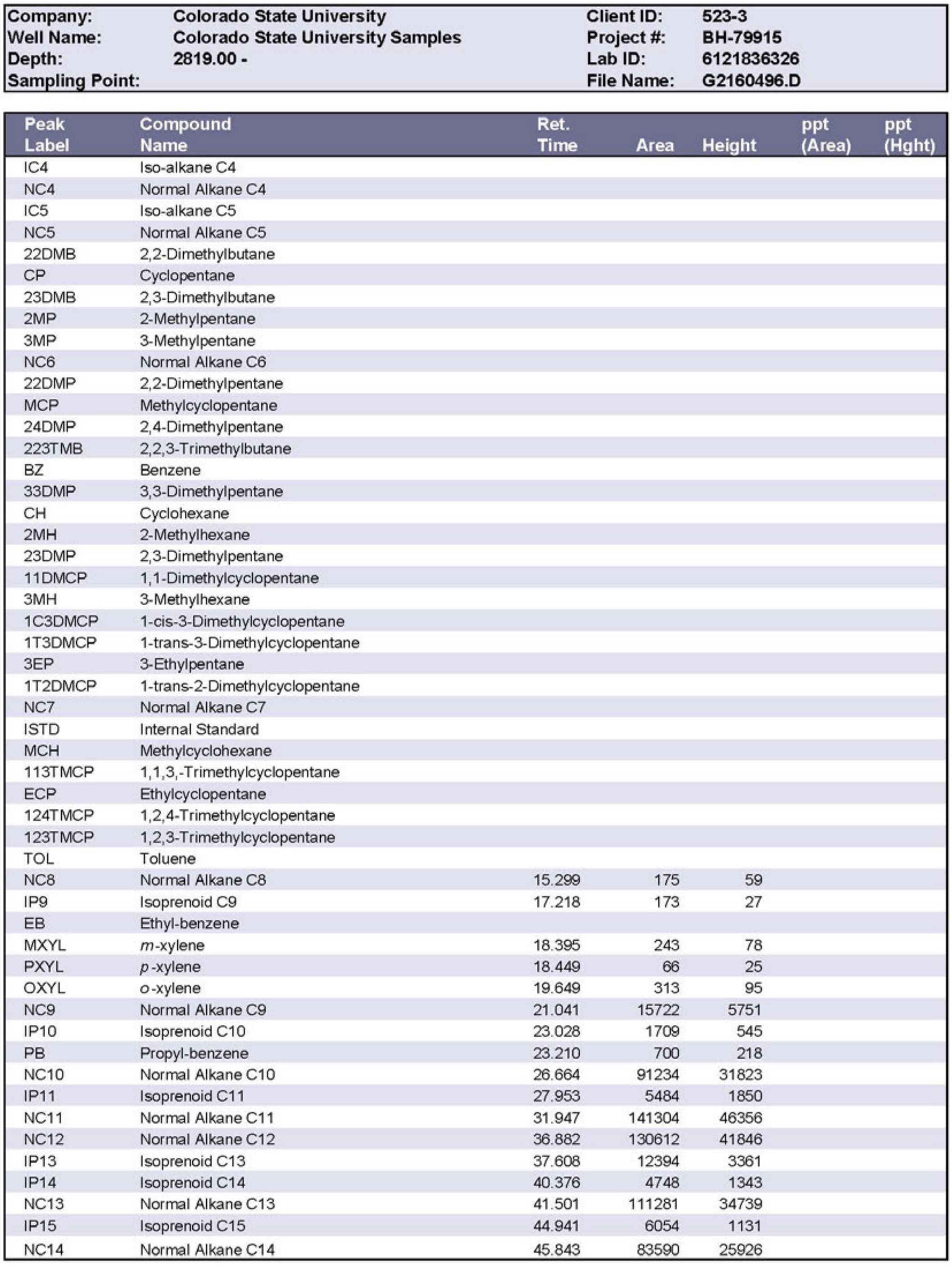

| | | | |
|---|---|---|---|
| **Company:** | **Colorado State University** | **Client ID:** | **523-3** |
| **Well Name:** | **Colorado State University Samples** | **Project #:** | **BH-79915** |
| **Depth:** | **2819.00 -** | **Lab ID:** | **6121836326** |
| **Sampling Point:** | | **File Name:** | **G2160496.D** |

| Peak Label | Compound Name | Ret. Time | Area | Height | ppt (Area) | ppt (Hght) |
|---|---|---|---|---|---|---|
| IC4 | Iso-alkane C4 | | | | | |
| NC4 | Normal Alkane C4 | | | | | |
| IC5 | Iso-alkane C5 | | | | | |
| NC5 | Normal Alkane C5 | | | | | |
| 22DMB | 2,2-Dimethylbutane | | | | | |
| CP | Cyclopentane | | | | | |
| 23DMB | 2,3-Dimethylbutane | | | | | |
| 2MP | 2-Methylpentane | | | | | |
| 3MP | 3-Methylpentane | | | | | |
| NC6 | Normal Alkane C6 | | | | | |
| 22DMP | 2,2-Dimethylpentane | | | | | |
| MCP | Methylcyclopentane | | | | | |
| 24DMP | 2,4-Dimethylpentane | | | | | |
| 223TMB | 2,2,3-Trimethylbutane | | | | | |
| BZ | Benzene | | | | | |
| 33DMP | 3,3-Dimethylpentane | | | | | |
| CH | Cyclohexane | | | | | |
| 2MH | 2-Methylhexane | | | | | |
| 23DMP | 2,3-Dimethylpentane | | | | | |
| 11DMCP | 1,1-Dimethylcyclopentane | | | | | |
| 3MH | 3-Methylhexane | | | | | |
| 1C3DMCP | 1-cis-3-Dimethylcyclopentane | | | | | |
| 1T3DMCP | 1-trans-3-Dimethylcyclopentane | | | | | |
| 3EP | 3-Ethylpentane | | | | | |
| 1T2DMCP | 1-trans-2-Dimethylcyclopentane | | | | | |
| NC7 | Normal Alkane C7 | | | | | |
| ISTD | Internal Standard | | | | | |
| MCH | Methylcyclohexane | | | | | |
| 113TMCP | 1,1,3,-Trimethylcyclopentane | | | | | |
| ECP | Ethylcyclopentane | | | | | |
| 124TMCP | 1,2,4-Trimethylcyclopentane | | | | | |
| 123TMCP | 1,2,3-Trimethylcyclopentane | | | | | |
| TOL | Toluene | | | | | |
| NC8 | Normal Alkane C8 | 15.299 | 175 | 59 | | |
| IP9 | Isoprenoid C9 | 17.218 | 173 | 27 | | |
| EB | Ethyl-benzene | | | | | |
| MXYL | *m*-xylene | 18.395 | 243 | 78 | | |
| PXYL | *p*-xylene | 18.449 | 66 | 25 | | |
| OXYL | *o*-xylene | 19.649 | 313 | 95 | | |
| NC9 | Normal Alkane C9 | 21.041 | 15722 | 5751 | | |
| IP10 | Isoprenoid C10 | 23.028 | 1709 | 545 | | |
| PB | Propyl-benzene | 23.210 | 700 | 218 | | |
| NC10 | Normal Alkane C10 | 26.664 | 91234 | 31823 | | |
| IP11 | Isoprenoid C11 | 27.953 | 5484 | 1850 | | |
| NC11 | Normal Alkane C11 | 31.947 | 141304 | 46356 | | |
| NC12 | Normal Alkane C12 | 36.882 | 130612 | 41846 | | |
| IP13 | Isoprenoid C13 | 37.608 | 12394 | 3361 | | |
| IP14 | Isoprenoid C14 | 40.376 | 4748 | 1343 | | |
| NC13 | Normal Alkane C13 | 41.501 | 111281 | 34739 | | |
| IP15 | Isoprenoid C15 | 44.941 | 6054 | 1131 | | |
| NC14 | Normal Alkane C14 | 45.843 | 83590 | 25926 | | |

*Appendix F1, ctd.*

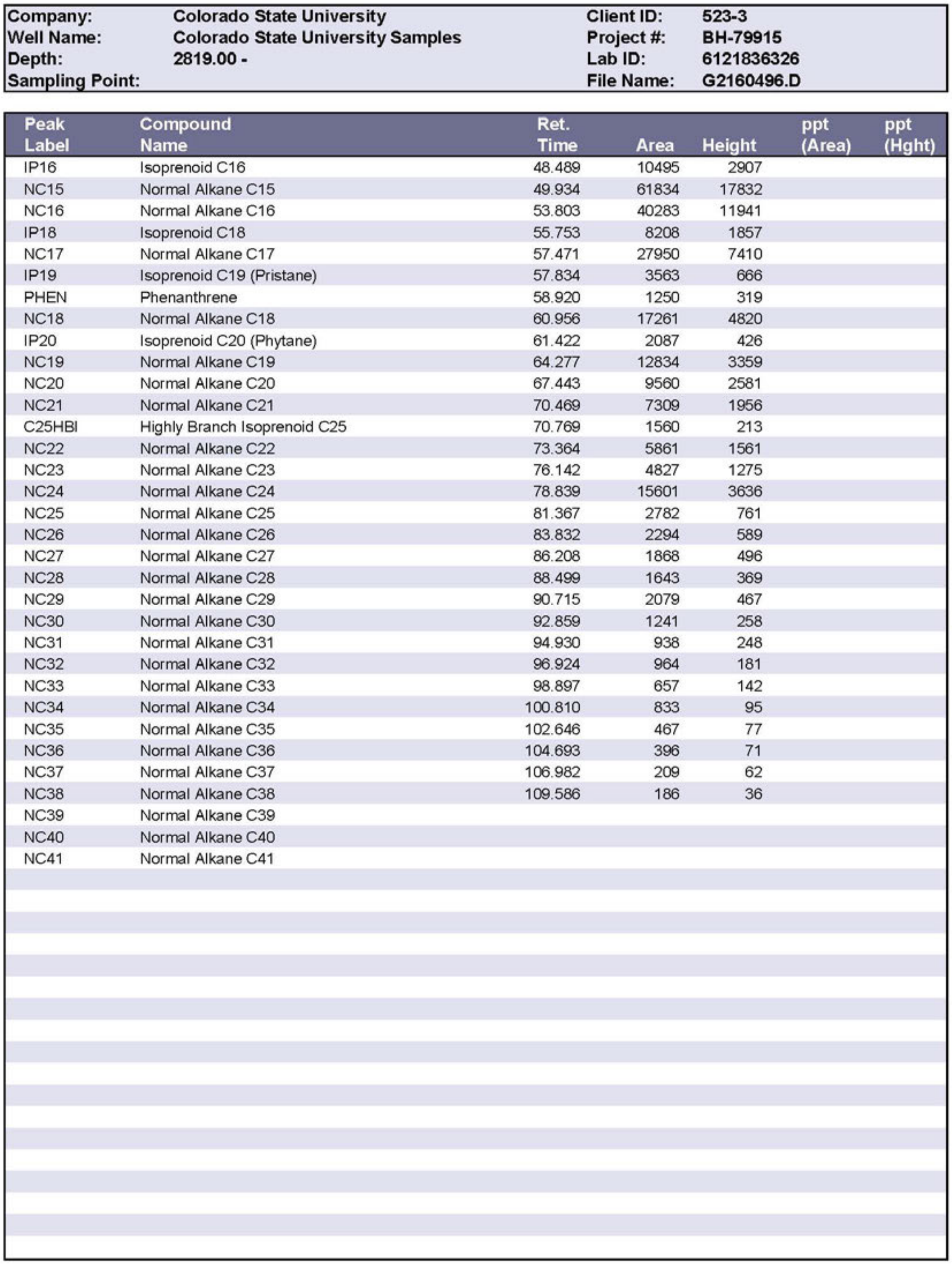

| | | | |
|---|---|---|---|
| **Company:** | **Colorado State University** | **Client ID:** | **523-3** |
| **Well Name:** | **Colorado State University Samples** | **Project #:** | **BH-79915** |
| **Depth:** | **2819.00 -** | **Lab ID:** | **6121836326** |
| **Sampling Point:** | | **File Name:** | **G2160496.D** |

| Peak Label | Compound Name | Ret. Time | Area | Height | ppt (Area) | ppt (Hght) |
|---|---|---|---|---|---|---|
| IP16 | Isoprenoid C16 | 48.489 | 10495 | 2907 | | |
| NC15 | Normal Alkane C15 | 49.934 | 61834 | 17832 | | |
| NC16 | Normal Alkane C16 | 53.803 | 40283 | 11941 | | |
| IP18 | Isoprenoid C18 | 55.753 | 8208 | 1857 | | |
| NC17 | Normal Alkane C17 | 57.471 | 27950 | 7410 | | |
| IP19 | Isoprenoid C19 (Pristane) | 57.834 | 3563 | 666 | | |
| PHEN | Phenanthrene | 58.920 | 1250 | 319 | | |
| NC18 | Normal Alkane C18 | 60.956 | 17261 | 4820 | | |
| IP20 | Isoprenoid C20 (Phytane) | 61.422 | 2087 | 426 | | |
| NC19 | Normal Alkane C19 | 64.277 | 12834 | 3359 | | |
| NC20 | Normal Alkane C20 | 67.443 | 9560 | 2581 | | |
| NC21 | Normal Alkane C21 | 70.469 | 7309 | 1956 | | |
| C25HBI | Highly Branch Isoprenoid C25 | 70.769 | 1560 | 213 | | |
| NC22 | Normal Alkane C22 | 73.364 | 5861 | 1561 | | |
| NC23 | Normal Alkane C23 | 76.142 | 4827 | 1275 | | |
| NC24 | Normal Alkane C24 | 78.839 | 15601 | 3636 | | |
| NC25 | Normal Alkane C25 | 81.367 | 2782 | 761 | | |
| NC26 | Normal Alkane C26 | 83.832 | 2294 | 589 | | |
| NC27 | Normal Alkane C27 | 86.208 | 1868 | 496 | | |
| NC28 | Normal Alkane C28 | 88.499 | 1643 | 369 | | |
| NC29 | Normal Alkane C29 | 90.715 | 2079 | 467 | | |
| NC30 | Normal Alkane C30 | 92.859 | 1241 | 258 | | |
| NC31 | Normal Alkane C31 | 94.930 | 938 | 248 | | |
| NC32 | Normal Alkane C32 | 96.924 | 964 | 181 | | |
| NC33 | Normal Alkane C33 | 98.897 | 657 | 142 | | |
| NC34 | Normal Alkane C34 | 100.810 | 833 | 95 | | |
| NC35 | Normal Alkane C35 | 102.646 | 467 | 77 | | |
| NC36 | Normal Alkane C36 | 104.693 | 396 | 71 | | |
| NC37 | Normal Alkane C37 | 106.982 | 209 | 62 | | |
| NC38 | Normal Alkane C38 | 109.586 | 186 | 36 | | |
| NC39 | Normal Alkane C39 | | | | | |
| NC40 | Normal Alkane C40 | | | | | |
| NC41 | Normal Alkane C41 | | | | | |

*Appendix F1, ctd.*

| Parameter | Formula |
|---|---|
| **EGC Parameters** | |
| Pristane/Phytane | IP19/IP20 |
| Pristane/nC17 | IP19/NC17 |
| Phytane/nC18 | IP20/NC18 |
| $nC_{18}/(nC_{18}+nC_{19})$ | NC18/(NC18+NC19) |
| $nC_{17}/(nC_{17}+nC_{29})$ | NC17/(NC17+NC29) |
| CPI Hunt[4] | ((NC23+NC25+NC27+NC29+NC31)+(NC25+NC27+NC29+NC31+NC33))/(2*(NC24+NC26+NC28+NC30+ NC32)) |
| Normal Paraffins | 100*(NC4+NC5+NC6+NC7+NC8+NC9+NC10+NC11+NC12+NC13+NC14+NC15+NC16+NC17+NC18+NC19+NC20+NC21+NC22+NC23+NC24+NC25+NC26+NC27+NC28+NC29+NC30+NC31+NC32+NC33+NC34+NC35+NC36+NC37+NC38+NC39+NC40+NC41)/TOTAL_RESOLVED |
| Isoprenoids | 100*(IP9+IP10+IP11+IP13+IP14+IP15+IP16+IP18+IP19+IP20+C25HBI)/TOTAL_RESOLVED |
| Cycloparaffins | 100*(CP+MCP+CH+11DMCP+1T3DMCP+1T2DMCP+MCH+113TMCP+ECP+124TMCP+123TMCP+1C3DMCP+1C2DMCP)/TOTAL_RESOLVED |
| Branched (iso-) Paraffins | 100*(IC4+IC5+22DMB+23DMB+2MP+3MP+22DMP+24DMP+223TMB+33DMP+2MH+23DMP+3MH+3EP)/TOTAL_RESOLVED |
| BTX aromatics | 100*(BZ+TOL+MXYL+PXYL+OXYL)/TOTAL_RESOLVED (*OXYL added 05/21/2007) |
| **Thompson**[1] | |
| BZ/nC6 | BZ/NC6 |
| TOL/nC7 | TOL/NC7 |
| (nC6+nC7)/(CH+MCH) | (NC6+NC7)/(CH+MCH) |
| Isoheptane Value | (2MH+3MH)/(1C3DMCP+1T3DMCP+1T2DMCP) |
| nC7/MCH | NC7/MCH |
| CH/MCP | CH/MCP |
| nC7/2MH | NC7/2MH |
| nC6/22DMB | NC6/22DMB |
| Heptane Value | 100*NC7/(CH+2MH+23DMP+11DMCP+3MH+1C3DMCP+1T3DMCP+1T2DMCP+MCH+NC7) |
| MCH/nC7 | MCH/NC7 |
| mpXYL/nC8 | (MXYL+PXYL)/NC8 |
| **Mango**[2] | |
| P1 | 100*NC7/(22DMP+24DMP+223TMB+33DMP+2MH+23DMP+11DMCP+3MH+1C3DMCP+1T3DMCP+3EP+1T2DMCP+NC7+MCH+ECP+TOL) |
| P2 | 100*(2MH+3MH)/(22DMP+24DMP+223TMB+33DMP+2MH+23DMP+11DMCP+3MH+1C3DMCP+1T3DMCP+3EP+1T2DMCP+NC7+MCH+ECP+TOL) |
| P3 | 100*(3EP+33DMP+23DMP+24DMP+22DMP+223TMB)/(22DMP+24DMP+223TMB+33DMP+2MH+23DMP+11DMCP+3MH+1C3DMCP+1T3DMCP+3EP+1T2DMCP+NC7+MCH+ECP+TOL) |
| 5N1 | 100*(ECP+1T2DMCP)/(22DMP+24DMP+223TMB+33DMP+2MH+23DMP+11DMCP+3MH+1C3DMCP+1T3DMCP+3EP+1T2DMCP+NC7+MCH+ECP+TOL) |
| N2 | 100*(11DMCP+1C3DMCP+1T3DMCP)/(22DMP+24DMP+223TMB+33DMP+2MH+23DMP+11DMCP+3MH+1C3DMCP+1T3DMCP+3EP+1T2DMCP+NC7+MCH+ECP+TOL) |
| 6N1 | 100*(MCH+TOL)/(22DMP+24DMP+223TMB+33DMP+2MH+23DMP+11DMCP+3MH+1C3DMCP+1T3DMCP+3EP+1T2DMCP+NC7+MCH+ECP+TOL) |
| K1 | (2MH+23DMP)/(3MH+24DMP) |
| K2 | (3EP+33DMP+23DMP+24DMP+22DMP+223TMB)/(2MH+3MH+11DMCP+1C3DMCP+1T3DMCP) |
| 5N1/6N1 | (ECP+1T2DMCP)/(MCH+TOL) |
| P3/N2 | (3EP+33DMP+23DMP+24DMP+22DMP+223TMB)/(11DMCP+1C3DMCP+1T3DMCP) |
| ln(24DMP/23DMP) | ln(24DMP/23DMP) |
| **Halpern**[3] | |
| Tr1 | TOL/11DMCP |
| Tr2 | NC7/11DMCP |
| Tr3 | 3MH/11DMCP |
| Tr4 | 2MH/11DMCP |
| Tr5 | (2MH+3MH)/11DMCP |
| Tr7 | 1T3DMCP/11DMCP |
| Tr8 | (2MH+3MH)/(22DMP+23DMP+24DMP+33DMP+3EP) |
| C1 | 22DMP/(22DMP+23DMP+24DMP+33DMP+3EP) |
| C2 | 23DMP/(22DMP+23DMP+24DMP+33DMP+3EP) |
| C3 | 24DMP/(22DMP+23DMP+24DMP+33DMP+3EP) |
| C4 | 33DMP/(22DMP+23DMP+24DMP+33DMP+3EP) |
| C5 | 3EP/(22DMP+23DMP+24DMP+33DMP+3EP) |

---

*Appendix F2: Aromatic Gas Chromatography-Mass Spectroscopy Data*
Definitions on page 366.

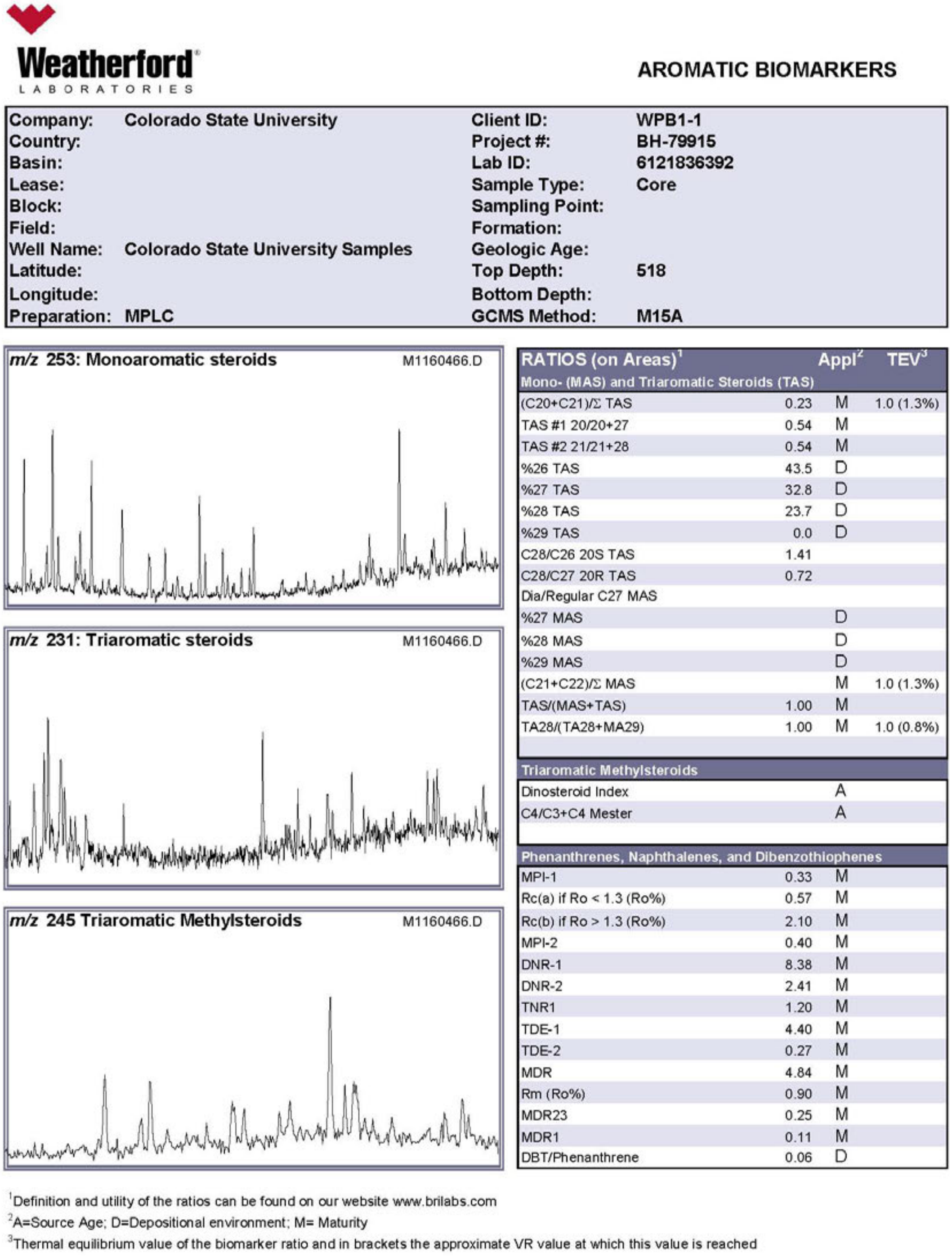

**Weatherford**
LABORATORIES

**AROMATIC BIOMARKERS**

| | | | |
|---|---|---|---|
| **Company:** | **Colorado State University** | **Client ID:** | **WPB1-1** |
| **Country:** | | **Project #:** | **BH-79915** |
| **Basin:** | | **Lab ID:** | **6121836392** |
| **Lease:** | | **Sample Type:** | **Core** |
| **Block:** | | **Sampling Point:** | |
| **Field:** | | **Formation:** | |
| **Well Name:** | **Colorado State University Samples** | **Geologic Age:** | |
| **Latitude:** | | **Top Depth:** | **518** |
| **Longitude:** | | **Bottom Depth:** | |
| **Preparation:** | **MPLC** | **GCMS Method:** | **M15A** |

***m/z* 253: Monoaromatic steroids** M1160466.D

***m/z* 231: Triaromatic steroids** M1160466.D

***m/z* 245 Triaromatic Methylsteroids** M1160466.D

| RATIOS (on Areas)[1] | | Appl[2] | TEV[3] |
|---|---|---|---|
| **Mono- (MAS) and Triaromatic Steroids (TAS)** | | | |
| (C20+C21)/Σ TAS | 0.23 | M | 1.0 (1.3%) |
| TAS #1 20/20+27 | 0.54 | M | |
| TAS #2 21/21+28 | 0.54 | M | |
| %26 TAS | 43.5 | D | |
| %27 TAS | 32.8 | D | |
| %28 TAS | 23.7 | D | |
| %29 TAS | 0.0 | D | |
| C28/C26 20S TAS | 1.41 | | |
| C28/C27 20R TAS | 0.72 | | |
| Dia/Regular C27 MAS | | | |
| %27 MAS | | D | |
| %28 MAS | | D | |
| %29 MAS | | D | |
| (C21+C22)/Σ MAS | | M | 1.0 (1.3%) |
| TAS/(MAS+TAS) | 1.00 | M | |
| TA28/(TA28+MA29) | 1.00 | M | 1.0 (0.8%) |
| **Triaromatic Methylsteroids** | | | |
| Dinosteroid Index | | A | |
| C4/C3+C4 Mester | | A | |
| **Phenanthrenes, Naphthalenes, and Dibenzothiophenes** | | | |
| MPI-1 | 0.33 | M | |
| Rc(a) if Ro < 1.3 (Ro%) | 0.57 | M | |
| Rc(b) if Ro > 1.3 (Ro%) | 2.10 | M | |
| MPI-2 | 0.40 | M | |
| DNR-1 | 8.38 | M | |
| DNR-2 | 2.41 | M | |
| TNR1 | 1.20 | M | |
| TDE-1 | 4.40 | M | |
| TDE-2 | 0.27 | M | |
| MDR | 4.84 | M | |
| Rm (Ro%) | 0.90 | M | |
| MDR23 | 0.25 | M | |
| MDR1 | 0.11 | M | |
| DBT/Phenanthrene | 0.06 | D | |

[1] Definition and utility of the ratios can be found on our website www.brilabs.com

[2] A=Source Age; D=Depositional environment; M= Maturity

[3] Thermal equilibrium value of the biomarker ratio and in brackets the approximate VR value at which this value is reached

*Appendix F2, ctd.*

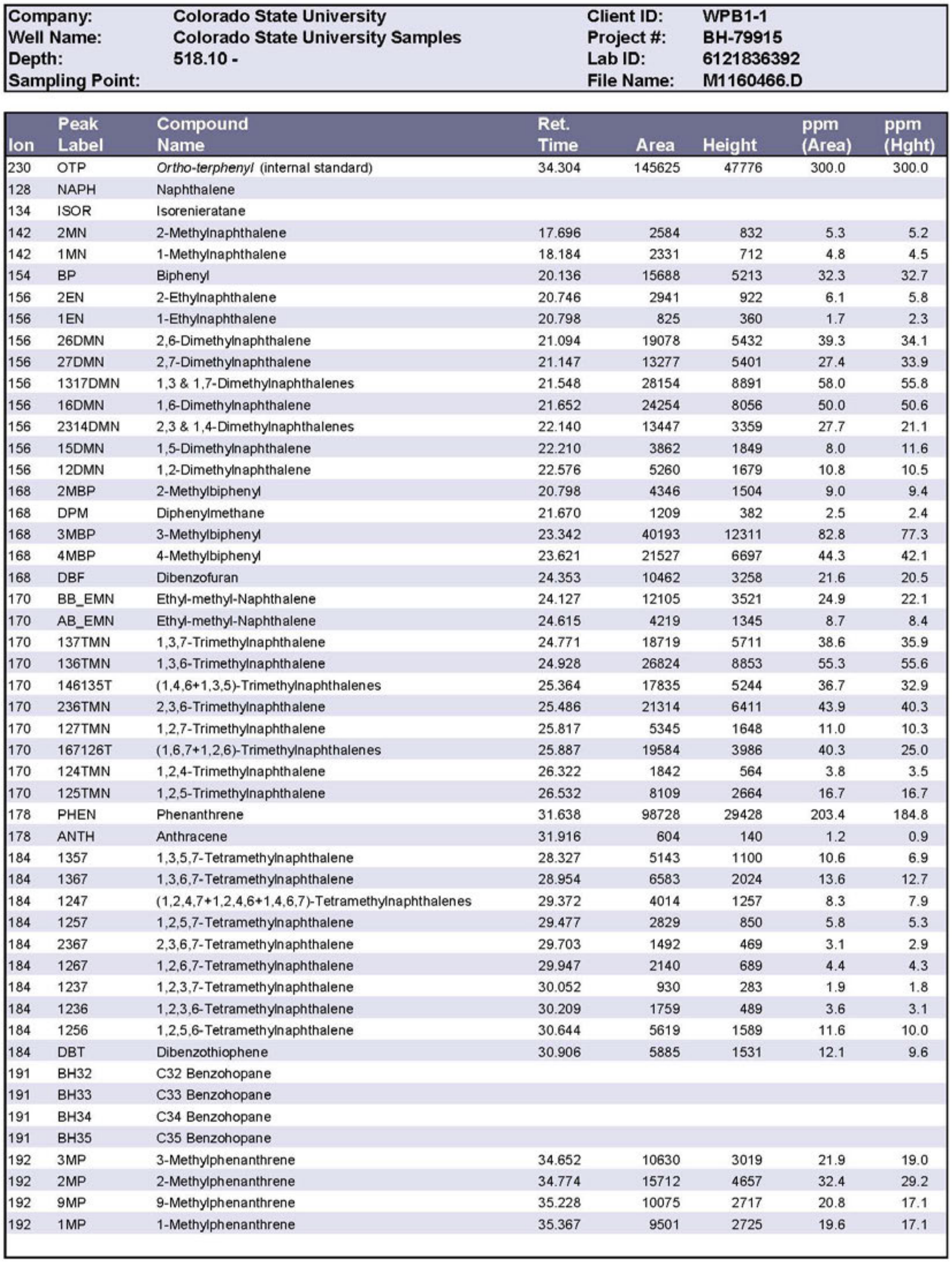

| | | | |
|---|---|---|---|
| **Company:** | **Colorado State University** | **Client ID:** | **WPB1-1** |
| **Well Name:** | **Colorado State University Samples** | **Project #:** | **BH-79915** |
| **Depth:** | **518.10 -** | **Lab ID:** | **6121836392** |
| **Sampling Point:** | | **File Name:** | **M1160466.D** |

| Ion | Peak Label | Compound Name | Ret. Time | Area | Height | ppm (Area) | ppm (Hght) |
|---|---|---|---|---|---|---|---|
| 230 | OTP | *Ortho-terphenyl* (internal standard) | 34.304 | 145625 | 47776 | 300.0 | 300.0 |
| 128 | NAPH | Naphthalene | | | | | |
| 134 | ISOR | Isorenieratane | | | | | |
| 142 | 2MN | 2-Methylnaphthalene | 17.696 | 2584 | 832 | 5.3 | 5.2 |
| 142 | 1MN | 1-Methylnaphthalene | 18.184 | 2331 | 712 | 4.8 | 4.5 |
| 154 | BP | Biphenyl | 20.136 | 15688 | 5213 | 32.3 | 32.7 |
| 156 | 2EN | 2-Ethylnaphthalene | 20.746 | 2941 | 922 | 6.1 | 5.8 |
| 156 | 1EN | 1-Ethylnaphthalene | 20.798 | 825 | 360 | 1.7 | 2.3 |
| 156 | 26DMN | 2,6-Dimethylnaphthalene | 21.094 | 19078 | 5432 | 39.3 | 34.1 |
| 156 | 27DMN | 2,7-Dimethylnaphthalene | 21.147 | 13277 | 5401 | 27.4 | 33.9 |
| 156 | 1317DMN | 1,3 & 1,7-Dimethylnaphthalenes | 21.548 | 28154 | 8891 | 58.0 | 55.8 |
| 156 | 16DMN | 1,6-Dimethylnaphthalene | 21.652 | 24254 | 8056 | 50.0 | 50.6 |
| 156 | 2314DMN | 2,3 & 1,4-Dimethylnaphthalenes | 22.140 | 13447 | 3359 | 27.7 | 21.1 |
| 156 | 15DMN | 1,5-Dimethylnaphthalene | 22.210 | 3862 | 1849 | 8.0 | 11.6 |
| 156 | 12DMN | 1,2-Dimethylnaphthalene | 22.576 | 5260 | 1679 | 10.8 | 10.5 |
| 168 | 2MBP | 2-Methylbiphenyl | 20.798 | 4346 | 1504 | 9.0 | 9.4 |
| 168 | DPM | Diphenylmethane | 21.670 | 1209 | 382 | 2.5 | 2.4 |
| 168 | 3MBP | 3-Methylbiphenyl | 23.342 | 40193 | 12311 | 82.8 | 77.3 |
| 168 | 4MBP | 4-Methylbiphenyl | 23.621 | 21527 | 6697 | 44.3 | 42.1 |
| 168 | DBF | Dibenzofuran | 24.353 | 10462 | 3258 | 21.6 | 20.5 |
| 170 | BB_EMN | Ethyl-methyl-Naphthalene | 24.127 | 12105 | 3521 | 24.9 | 22.1 |
| 170 | AB_EMN | Ethyl-methyl-Naphthalene | 24.615 | 4219 | 1345 | 8.7 | 8.4 |
| 170 | 137TMN | 1,3,7-Trimethylnaphthalene | 24.771 | 18719 | 5711 | 38.6 | 35.9 |
| 170 | 136TMN | 1,3,6-Trimethylnaphthalene | 24.928 | 26824 | 8853 | 55.3 | 55.6 |
| 170 | 146135T | (1,4,6+1,3,5)-Trimethylnaphthalenes | 25.364 | 17835 | 5244 | 36.7 | 32.9 |
| 170 | 236TMN | 2,3,6-Trimethylnaphthalene | 25.486 | 21314 | 6411 | 43.9 | 40.3 |
| 170 | 127TMN | 1,2,7-Trimethylnaphthalene | 25.817 | 5345 | 1648 | 11.0 | 10.3 |
| 170 | 167126T | (1,6,7+1,2,6)-Trimethylnaphthalenes | 25.887 | 19584 | 3986 | 40.3 | 25.0 |
| 170 | 124TMN | 1,2,4-Trimethylnaphthalene | 26.322 | 1842 | 564 | 3.8 | 3.5 |
| 170 | 125TMN | 1,2,5-Trimethylnaphthalene | 26.532 | 8109 | 2664 | 16.7 | 16.7 |
| 178 | PHEN | Phenanthrene | 31.638 | 98728 | 29428 | 203.4 | 184.8 |
| 178 | ANTH | Anthracene | 31.916 | 604 | 140 | 1.2 | 0.9 |
| 184 | 1357 | 1,3,5,7-Tetramethylnaphthalene | 28.327 | 5143 | 1100 | 10.6 | 6.9 |
| 184 | 1367 | 1,3,6,7-Tetramethylnaphthalene | 28.954 | 6583 | 2024 | 13.6 | 12.7 |
| 184 | 1247 | (1,2,4,7+1,2,4,6+1,4,6,7)-Tetramethylnaphthalenes | 29.372 | 4014 | 1257 | 8.3 | 7.9 |
| 184 | 1257 | 1,2,5,7-Tetramethylnaphthalene | 29.477 | 2829 | 850 | 5.8 | 5.3 |
| 184 | 2367 | 2,3,6,7-Tetramethylnaphthalene | 29.703 | 1492 | 469 | 3.1 | 2.9 |
| 184 | 1267 | 1,2,6,7-Tetramethylnaphthalene | 29.947 | 2140 | 689 | 4.4 | 4.3 |
| 184 | 1237 | 1,2,3,7-Tetramethylnaphthalene | 30.052 | 930 | 283 | 1.9 | 1.8 |
| 184 | 1236 | 1,2,3,6-Tetramethylnaphthalene | 30.209 | 1759 | 489 | 3.6 | 3.1 |
| 184 | 1256 | 1,2,5,6-Tetramethylnaphthalene | 30.644 | 5619 | 1589 | 11.6 | 10.0 |
| 184 | DBT | Dibenzothiophene | 30.906 | 5885 | 1531 | 12.1 | 9.6 |
| 191 | BH32 | C32 Benzohopane | | | | | |
| 191 | BH33 | C33 Benzohopane | | | | | |
| 191 | BH34 | C34 Benzohopane | | | | | |
| 191 | BH35 | C35 Benzohopane | | | | | |
| 192 | 3MP | 3-Methylphenanthrene | 34.652 | 10630 | 3019 | 21.9 | 19.0 |
| 192 | 2MP | 2-Methylphenanthrene | 34.774 | 15712 | 4657 | 32.4 | 29.2 |
| 192 | 9MP | 9-Methylphenanthrene | 35.228 | 10075 | 2717 | 20.8 | 17.1 |
| 192 | 1MP | 1-Methylphenanthrene | 35.367 | 9501 | 2725 | 19.6 | 17.1 |

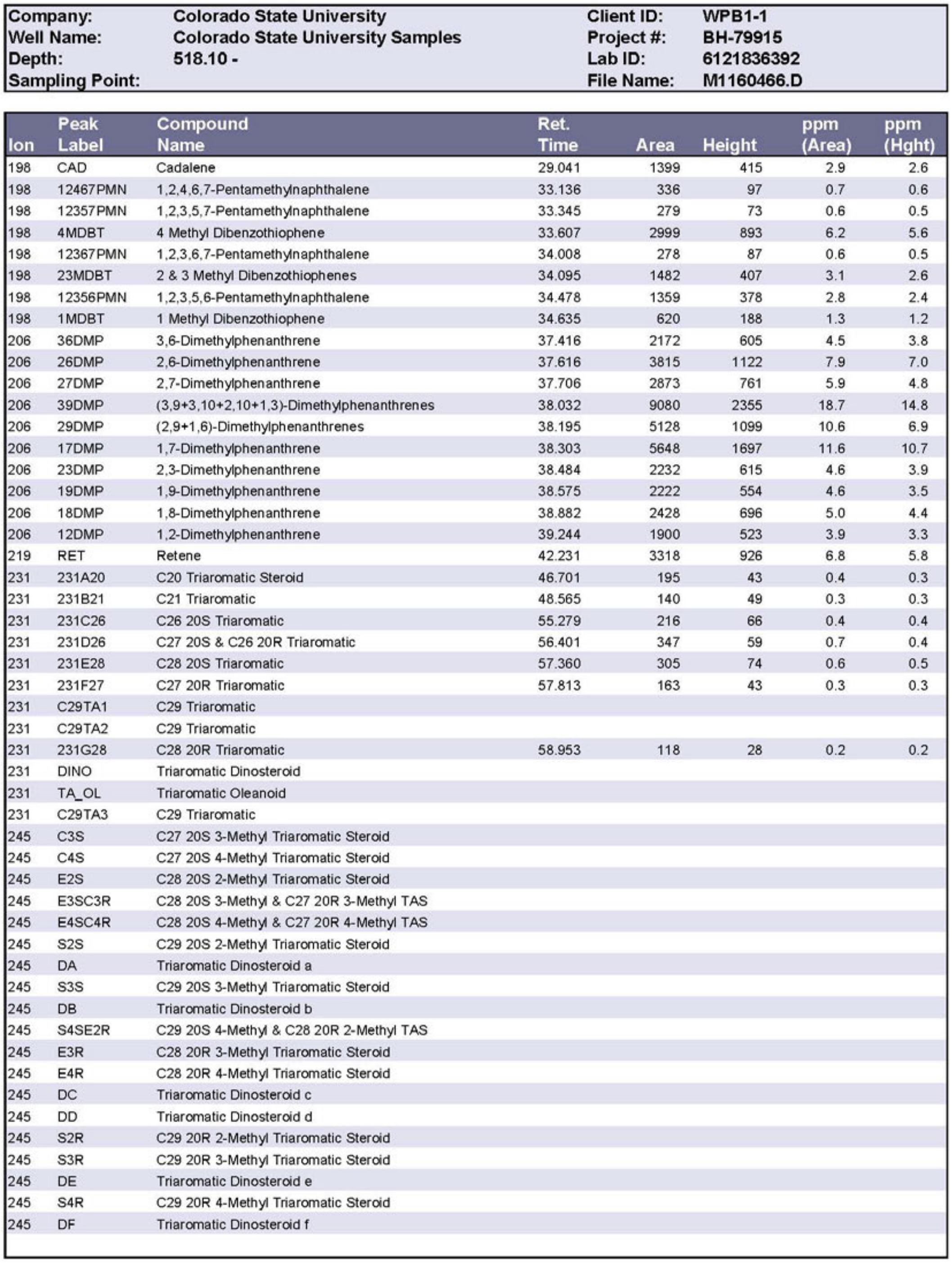

| | | | |
|---|---|---|---|
| **Company:** | **Colorado State University** | **Client ID:** | **WPB1-1** |
| **Well Name:** | **Colorado State University Samples** | **Project #:** | **BH-79915** |
| **Depth:** | **518.10 -** | **Lab ID:** | **6121836392** |
| **Sampling Point:** | | **File Name:** | **M1160466.D** |

| Ion | Peak Label | Compound Name | Ret. Time | Area | Height | ppm (Area) | ppm (Hght) |
|---|---|---|---|---|---|---|---|
| 198 | CAD | Cadalene | 29.041 | 1399 | 415 | 2.9 | 2.6 |
| 198 | 12467PMN | 1,2,4,6,7-Pentamethylnaphthalene | 33.136 | 336 | 97 | 0.7 | 0.6 |
| 198 | 12357PMN | 1,2,3,5,7-Pentamethylnaphthalene | 33.345 | 279 | 73 | 0.6 | 0.5 |
| 198 | 4MDBT | 4 Methyl Dibenzothiophene | 33.607 | 2999 | 893 | 6.2 | 5.6 |
| 198 | 12367PMN | 1,2,3,6,7-Pentamethylnaphthalene | 34.008 | 278 | 87 | 0.6 | 0.5 |
| 198 | 23MDBT | 2 & 3 Methyl Dibenzothiophenes | 34.095 | 1482 | 407 | 3.1 | 2.6 |
| 198 | 12356PMN | 1,2,3,5,6-Pentamethylnaphthalene | 34.478 | 1359 | 378 | 2.8 | 2.4 |
| 198 | 1MDBT | 1 Methyl Dibenzothiophene | 34.635 | 620 | 188 | 1.3 | 1.2 |
| 206 | 36DMP | 3,6-Dimethylphenanthrene | 37.416 | 2172 | 605 | 4.5 | 3.8 |
| 206 | 26DMP | 2,6-Dimethylphenanthrene | 37.616 | 3815 | 1122 | 7.9 | 7.0 |
| 206 | 27DMP | 2,7-Dimethylphenanthrene | 37.706 | 2873 | 761 | 5.9 | 4.8 |
| 206 | 39DMP | (3,9+3,10+2,10+1,3)-Dimethylphenanthrenes | 38.032 | 9080 | 2355 | 18.7 | 14.8 |
| 206 | 29DMP | (2,9+1,6)-Dimethylphenanthrenes | 38.195 | 5128 | 1099 | 10.6 | 6.9 |
| 206 | 17DMP | 1,7-Dimethylphenanthrene | 38.303 | 5648 | 1697 | 11.6 | 10.7 |
| 206 | 23DMP | 2,3-Dimethylphenanthrene | 38.484 | 2232 | 615 | 4.6 | 3.9 |
| 206 | 19DMP | 1,9-Dimethylphenanthrene | 38.575 | 2222 | 554 | 4.6 | 3.5 |
| 206 | 18DMP | 1,8-Dimethylphenanthrene | 38.882 | 2428 | 696 | 5.0 | 4.4 |
| 206 | 12DMP | 1,2-Dimethylphenanthrene | 39.244 | 1900 | 523 | 3.9 | 3.3 |
| 219 | RET | Retene | 42.231 | 3318 | 926 | 6.8 | 5.8 |
| 231 | 231A20 | C20 Triaromatic Steroid | 46.701 | 195 | 43 | 0.4 | 0.3 |
| 231 | 231B21 | C21 Triaromatic | 48.565 | 140 | 49 | 0.3 | 0.3 |
| 231 | 231C26 | C26 20S Triaromatic | 55.279 | 216 | 66 | 0.4 | 0.4 |
| 231 | 231D26 | C27 20S & C26 20R Triaromatic | 56.401 | 347 | 59 | 0.7 | 0.4 |
| 231 | 231E28 | C28 20S Triaromatic | 57.360 | 305 | 74 | 0.6 | 0.5 |
| 231 | 231F27 | C27 20R Triaromatic | 57.813 | 163 | 43 | 0.3 | 0.3 |
| 231 | C29TA1 | C29 Triaromatic | | | | | |
| 231 | C29TA2 | C29 Triaromatic | | | | | |
| 231 | 231G28 | C28 20R Triaromatic | 58.953 | 118 | 28 | 0.2 | 0.2 |
| 231 | DINO | Triaromatic Dinosteroid | | | | | |
| 231 | TA_OL | Triaromatic Oleanoid | | | | | |
| 231 | C29TA3 | C29 Triaromatic | | | | | |
| 245 | C3S | C27 20S 3-Methyl Triaromatic Steroid | | | | | |
| 245 | C4S | C27 20S 4-Methyl Triaromatic Steroid | | | | | |
| 245 | E2S | C28 20S 2-Methyl Triaromatic Steroid | | | | | |
| 245 | E3SC3R | C28 20S 3-Methyl & C27 20R 3-Methyl TAS | | | | | |
| 245 | E4SC4R | C28 20S 4-Methyl & C27 20R 4-Methyl TAS | | | | | |
| 245 | S2S | C29 20S 2-Methyl Triaromatic Steroid | | | | | |
| 245 | DA | Triaromatic Dinosteroid a | | | | | |
| 245 | S3S | C29 20S 3-Methyl Triaromatic Steroid | | | | | |
| 245 | DB | Triaromatic Dinosteroid b | | | | | |
| 245 | S4SE2R | C29 20S 4-Methyl & C28 20R 2-Methyl TAS | | | | | |
| 245 | E3R | C28 20R 3-Methyl Triaromatic Steroid | | | | | |
| 245 | E4R | C28 20R 4-Methyl Triaromatic Steroid | | | | | |
| 245 | DC | Triaromatic Dinosteroid c | | | | | |
| 245 | DD | Triaromatic Dinosteroid d | | | | | |
| 245 | S2R | C29 20R 2-Methyl Triaromatic Steroid | | | | | |
| 245 | S3R | C29 20R 3-Methyl Triaromatic Steroid | | | | | |
| 245 | DE | Triaromatic Dinosteroid e | | | | | |
| 245 | S4R | C29 20R 4-Methyl Triaromatic Steroid | | | | | |
| 245 | DF | Triaromatic Dinosteroid f | | | | | |

*Appendix F2, ctd.*

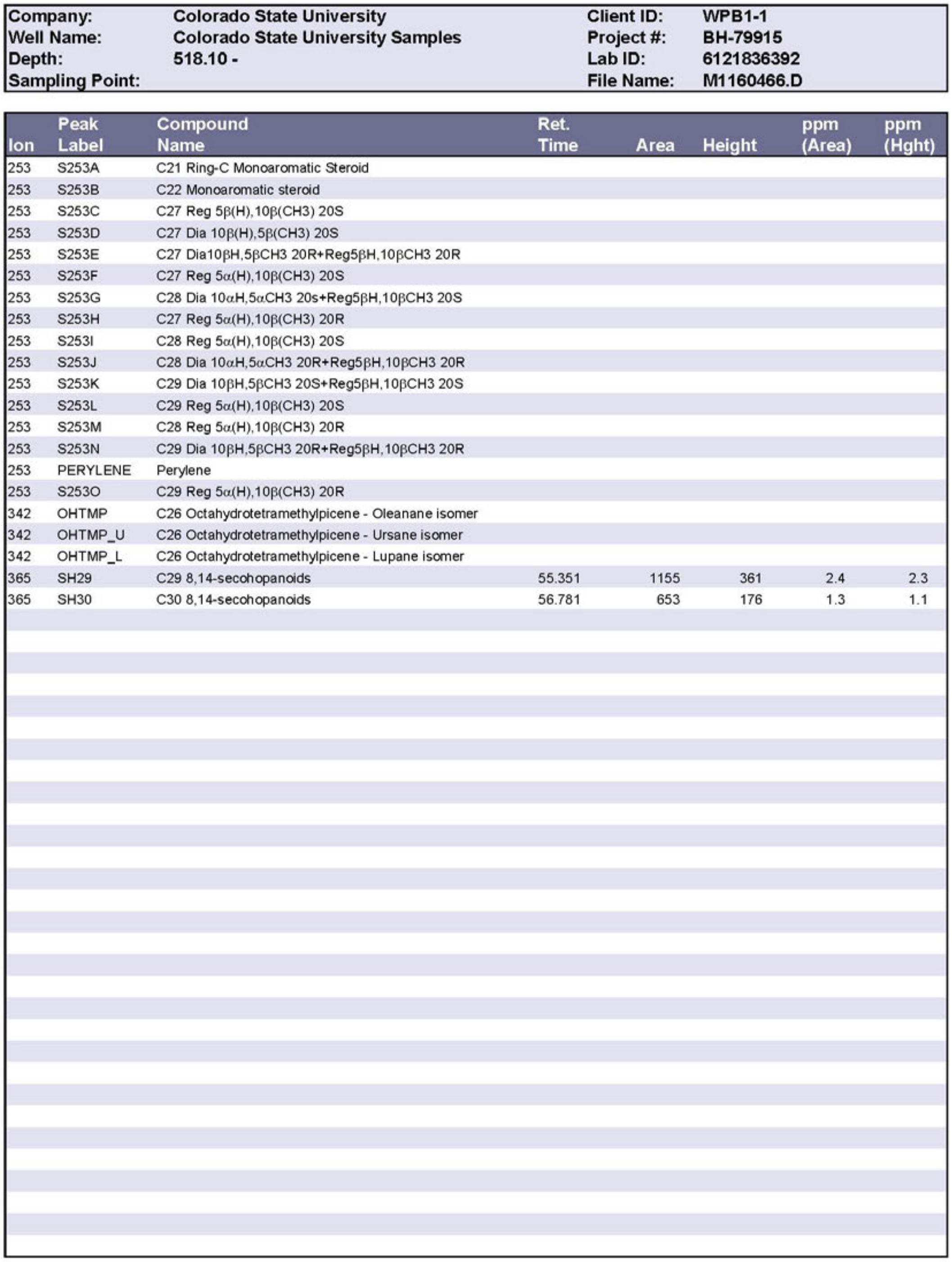

| | | | |
|---|---|---|---|
| **Company:** | **Colorado State University** | **Client ID:** | **WPB1-1** |
| **Well Name:** | **Colorado State University Samples** | **Project #:** | **BH-79915** |
| **Depth:** | **518.10 -** | **Lab ID:** | **6121836392** |
| **Sampling Point:** | | **File Name:** | **M1160466.D** |

| Ion | Peak Label | Compound Name | Ret. Time | Area | Height | ppm (Area) | ppm (Hght) |
|---|---|---|---|---|---|---|---|
| 253 | S253A | C21 Ring-C Monoaromatic Steroid | | | | | |
| 253 | S253B | C22 Monoaromatic steroid | | | | | |
| 253 | S253C | C27 Reg 5β(H),10β(CH3) 20S | | | | | |
| 253 | S253D | C27 Dia 10β(H),5β(CH3) 20S | | | | | |
| 253 | S253E | C27 Dia10βH,5βCH3 20R+Reg5βH,10βCH3 20R | | | | | |
| 253 | S253F | C27 Reg 5α(H),10β(CH3) 20S | | | | | |
| 253 | S253G | C28 Dia 10αH,5αCH3 20s+Reg5βH,10βCH3 20S | | | | | |
| 253 | S253H | C27 Reg 5α(H),10β(CH3) 20R | | | | | |
| 253 | S253I | C28 Reg 5α(H),10β(CH3) 20S | | | | | |
| 253 | S253J | C28 Dia 10αH,5αCH3 20R+Reg5βH,10βCH3 20R | | | | | |
| 253 | S253K | C29 Dia 10βH,5βCH3 20S+Reg5βH,10βCH3 20S | | | | | |
| 253 | S253L | C29 Reg 5α(H),10β(CH3) 20S | | | | | |
| 253 | S253M | C28 Reg 5α(H),10β(CH3) 20R | | | | | |
| 253 | S253N | C29 Dia 10βH,5βCH3 20R+Reg5βH,10βCH3 20R | | | | | |
| 253 | PERYLENE | Perylene | | | | | |
| 253 | S253O | C29 Reg 5α(H),10β(CH3) 20R | | | | | |
| 342 | OHTMP | C26 Octahydrotetramethylpicene - Oleanane isomer | | | | | |
| 342 | OHTMP_U | C26 Octahydrotetramethylpicene - Ursane isomer | | | | | |
| 342 | OHTMP_L | C26 Octahydrotetramethylpicene - Lupane isomer | | | | | |
| 365 | SH29 | C29 8,14-secohopanoids | 55.351 | 1155 | 361 | 2.4 | 2.3 |
| 365 | SH30 | C30 8,14-secohopanoids | 56.781 | 653 | 176 | 1.3 | 1.1 |

*Appendix F2, ctd.*

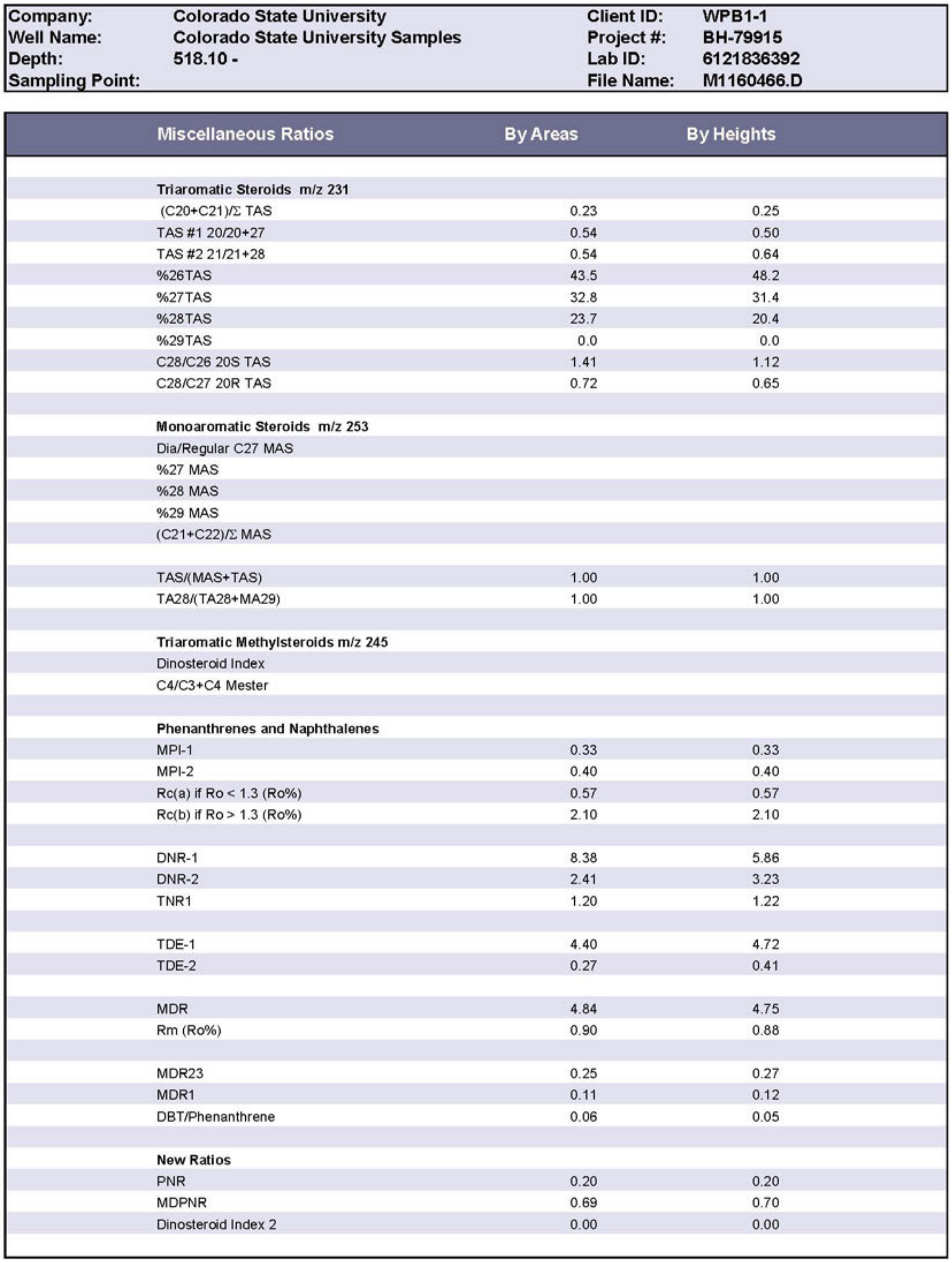

| | | | |
|---|---|---|---|
| **Company:** | **Colorado State University** | **Client ID:** | **WPB1-1** |
| **Well Name:** | **Colorado State University Samples** | **Project #:** | **BH-79915** |
| **Depth:** | **518.10 -** | **Lab ID:** | **6121836392** |
| **Sampling Point:** | | **File Name:** | **M1160466.D** |

| Miscellaneous Ratios | By Areas | By Heights |
|---|---|---|
| **Triaromatic Steroids m/z 231** | | |
| (C20+C21)/Σ TAS | 0.23 | 0.25 |
| TAS #1 20/20+27 | 0.54 | 0.50 |
| TAS #2 21/21+28 | 0.54 | 0.64 |
| %26TAS | 43.5 | 48.2 |
| %27TAS | 32.8 | 31.4 |
| %28TAS | 23.7 | 20.4 |
| %29TAS | 0.0 | 0.0 |
| C28/C26 20S TAS | 1.41 | 1.12 |
| C28/C27 20R TAS | 0.72 | 0.65 |
| | | |
| **Monoaromatic Steroids m/z 253** | | |
| Dia/Regular C27 MAS | | |
| %27 MAS | | |
| %28 MAS | | |
| %29 MAS | | |
| (C21+C22)/Σ MAS | | |
| | | |
| TAS/(MAS+TAS) | 1.00 | 1.00 |
| TA28/(TA28+MA29) | 1.00 | 1.00 |
| | | |
| **Triaromatic Methylsteroids m/z 245** | | |
| Dinosteroid Index | | |
| C4/C3+C4 Mester | | |
| | | |
| **Phenanthrenes and Naphthalenes** | | |
| MPI-1 | 0.33 | 0.33 |
| MPI-2 | 0.40 | 0.40 |
| Rc(a) if Ro < 1.3 (Ro%) | 0.57 | 0.57 |
| Rc(b) if Ro > 1.3 (Ro%) | 2.10 | 2.10 |
| | | |
| DNR-1 | 8.38 | 5.86 |
| DNR-2 | 2.41 | 3.23 |
| TNR1 | 1.20 | 1.22 |
| | | |
| TDE-1 | 4.40 | 4.72 |
| TDE-2 | 0.27 | 0.41 |
| | | |
| MDR | 4.84 | 4.75 |
| Rm (Ro%) | 0.90 | 0.88 |
| | | |
| MDR23 | 0.25 | 0.27 |
| MDR1 | 0.11 | 0.12 |
| DBT/Phenanthrene | 0.06 | 0.05 |
| | | |
| **New Ratios** | | |
| PNR | 0.20 | 0.20 |
| MDPNR | 0.69 | 0.70 |
| Dinosteroid Index 2 | 0.00 | 0.00 |

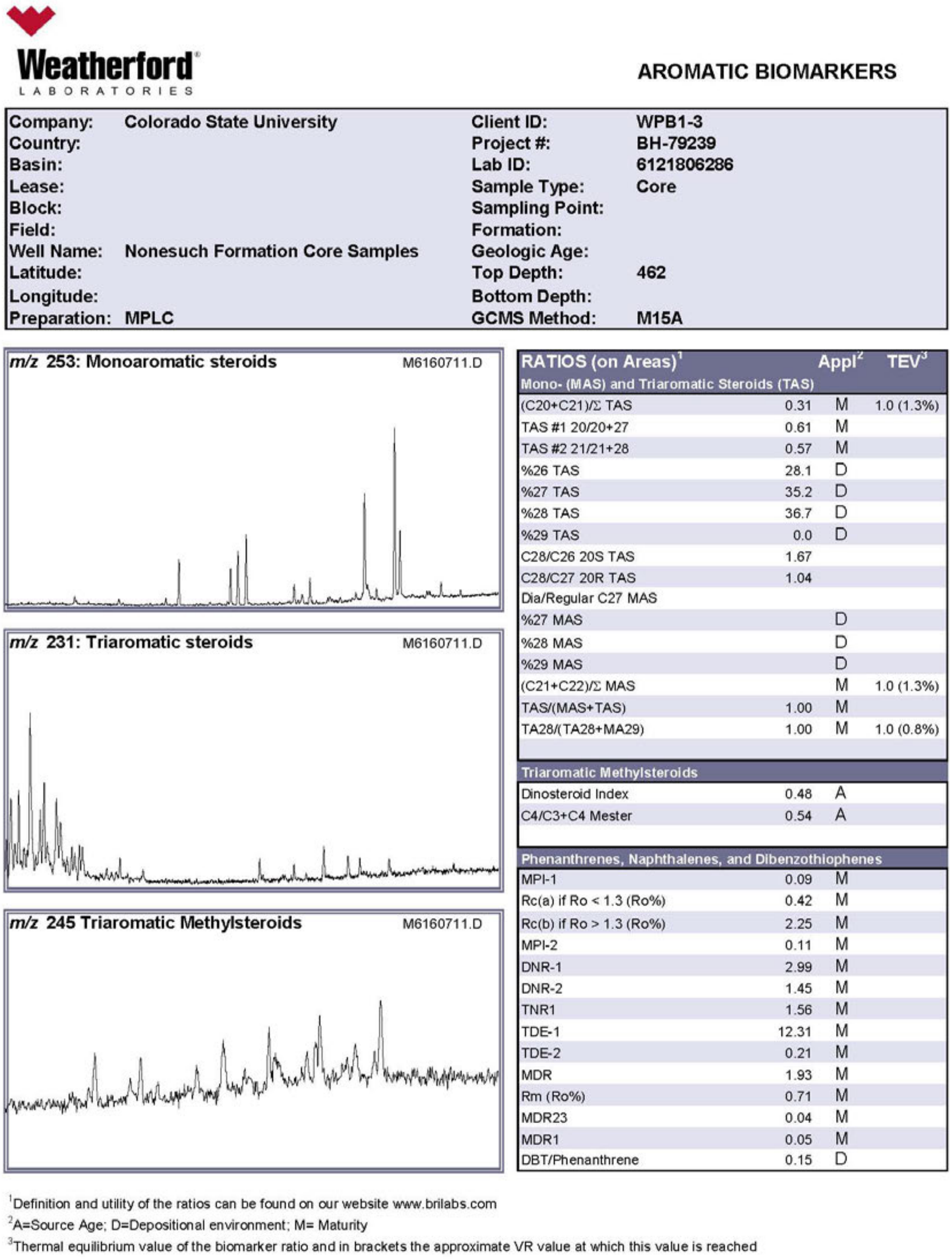

**Weatherford**
LABORATORIES

## AROMATIC BIOMARKERS

| | | | |
|---|---|---|---|
| **Company:** | **Colorado State University** | **Client ID:** | **WPB1-3** |
| **Country:** | | **Project #:** | **BH-79239** |
| **Basin:** | | **Lab ID:** | **6121806286** |
| **Lease:** | | **Sample Type:** | **Core** |
| **Block:** | | **Sampling Point:** | |
| **Field:** | | **Formation:** | |
| **Well Name:** | **Nonesuch Formation Core Samples** | **Geologic Age:** | |
| **Latitude:** | | **Top Depth:** | **462** |
| **Longitude:** | | **Bottom Depth:** | |
| **Preparation:** | **MPLC** | **GCMS Method:** | **M15A** |

***m/z* 253: Monoaromatic steroids** M6160711.D

***m/z* 231: Triaromatic steroids** M6160711.D

***m/z* 245 Triaromatic Methylsteroids** M6160711.D

| RATIOS (on Areas)[1] | | Appl[2] | TEV[3] |
|---|---|---|---|
| **Mono- (MAS) and Triaromatic Steroids (TAS)** | | | |
| (C20+C21)/Σ TAS | 0.31 | M | 1.0 (1.3%) |
| TAS #1 20/20+27 | 0.61 | M | |
| TAS #2 21/21+28 | 0.57 | M | |
| %26 TAS | 28.1 | D | |
| %27 TAS | 35.2 | D | |
| %28 TAS | 36.7 | D | |
| %29 TAS | 0.0 | D | |
| C28/C26 20S TAS | 1.67 | | |
| C28/C27 20R TAS | 1.04 | | |
| Dia/Regular C27 MAS | | | |
| %27 MAS | | D | |
| %28 MAS | | D | |
| %29 MAS | | D | |
| (C21+C22)/Σ MAS | | M | 1.0 (1.3%) |
| TAS/(MAS+TAS) | 1.00 | M | |
| TA28/(TA28+MA29) | 1.00 | M | 1.0 (0.8%) |
| **Triaromatic Methylsteroids** | | | |
| Dinosteroid Index | 0.48 | A | |
| C4/C3+C4 Mester | 0.54 | A | |
| **Phenanthrenes, Naphthalenes, and Dibenzothiophenes** | | | |
| MPI-1 | 0.09 | M | |
| Rc(a) if Ro < 1.3 (Ro%) | 0.42 | M | |
| Rc(b) if Ro > 1.3 (Ro%) | 2.25 | M | |
| MPI-2 | 0.11 | M | |
| DNR-1 | 2.99 | M | |
| DNR-2 | 1.45 | M | |
| TNR1 | 1.56 | M | |
| TDE-1 | 12.31 | M | |
| TDE-2 | 0.21 | M | |
| MDR | 1.93 | M | |
| Rm (Ro%) | 0.71 | M | |
| MDR23 | 0.04 | M | |
| MDR1 | 0.05 | M | |
| DBT/Phenanthrene | 0.15 | D | |

[1] Definition and utility of the ratios can be found on our website www.brilabs.com

[2] A=Source Age; D=Depositional environment; M= Maturity

[3] Thermal equilibrium value of the biomarker ratio and in brackets the approximate VR value at which this value is reached

*Appendix F2, ctd.*

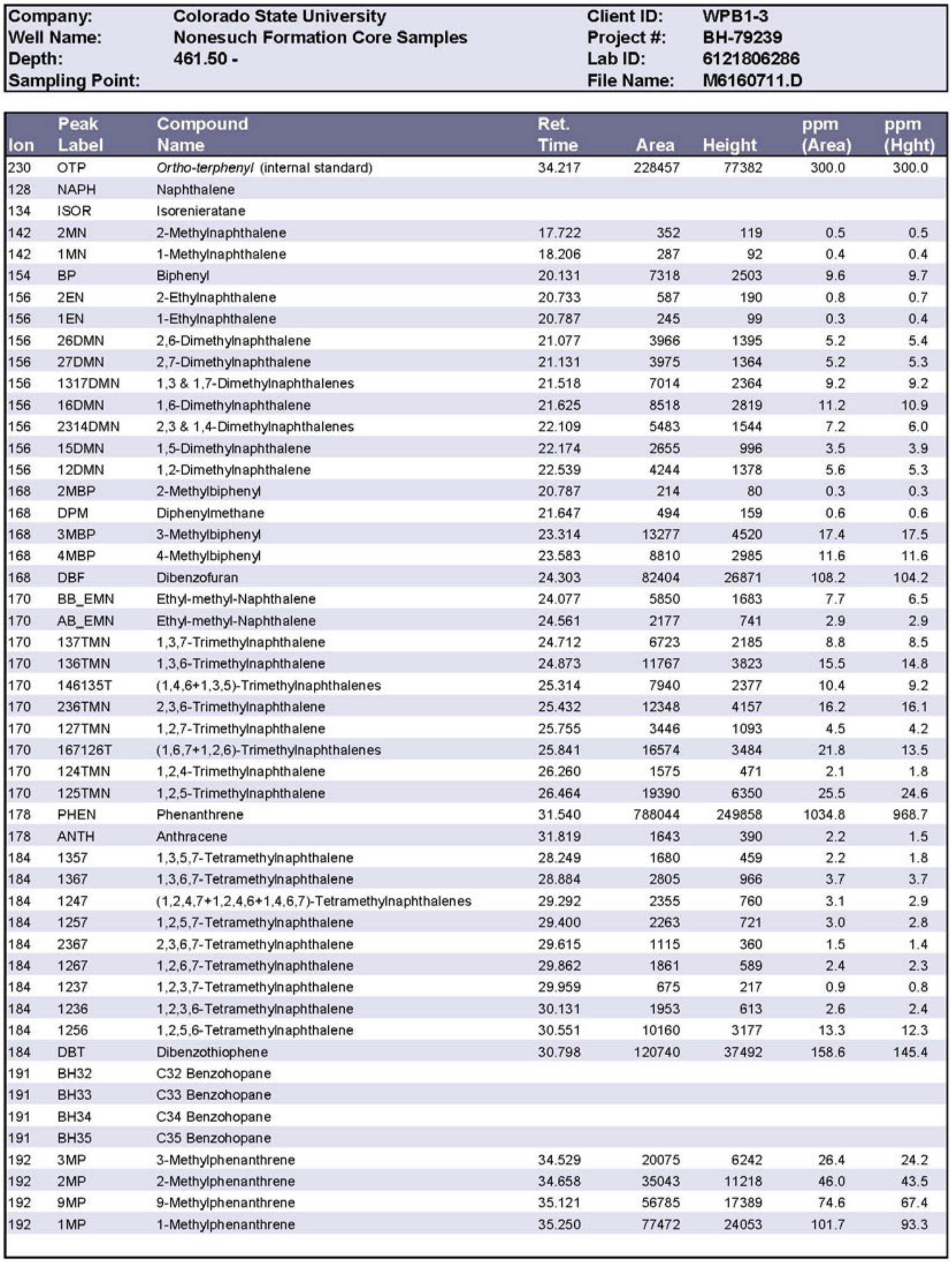

| | | | |
|---|---|---|---|
| **Company:** | **Colorado State University** | **Client ID:** | **WPB1-3** |
| **Well Name:** | **Nonesuch Formation Core Samples** | **Project #:** | **BH-79239** |
| **Depth:** | **461.50 -** | **Lab ID:** | **6121806286** |
| **Sampling Point:** | | **File Name:** | **M6160711.D** |

| Ion | Peak Label | Compound Name | Ret. Time | Area | Height | ppm (Area) | ppm (Hght) |
|---|---|---|---|---|---|---|---|
| 230 | OTP | *Ortho-terphenyl* (internal standard) | 34.217 | 228457 | 77382 | 300.0 | 300.0 |
| 128 | NAPH | Naphthalene | | | | | |
| 134 | ISOR | Isorenieratane | | | | | |
| 142 | 2MN | 2-Methylnaphthalene | 17.722 | 352 | 119 | 0.5 | 0.5 |
| 142 | 1MN | 1-Methylnaphthalene | 18.206 | 287 | 92 | 0.4 | 0.4 |
| 154 | BP | Biphenyl | 20.131 | 7318 | 2503 | 9.6 | 9.7 |
| 156 | 2EN | 2-Ethylnaphthalene | 20.733 | 587 | 190 | 0.8 | 0.7 |
| 156 | 1EN | 1-Ethylnaphthalene | 20.787 | 245 | 99 | 0.3 | 0.4 |
| 156 | 26DMN | 2,6-Dimethylnaphthalene | 21.077 | 3966 | 1395 | 5.2 | 5.4 |
| 156 | 27DMN | 2,7-Dimethylnaphthalene | 21.131 | 3975 | 1364 | 5.2 | 5.3 |
| 156 | 1317DMN | 1,3 & 1,7-Dimethylnaphthalenes | 21.518 | 7014 | 2364 | 9.2 | 9.2 |
| 156 | 16DMN | 1,6-Dimethylnaphthalene | 21.625 | 8518 | 2819 | 11.2 | 10.9 |
| 156 | 2314DMN | 2,3 & 1,4-Dimethylnaphthalenes | 22.109 | 5483 | 1544 | 7.2 | 6.0 |
| 156 | 15DMN | 1,5-Dimethylnaphthalene | 22.174 | 2655 | 996 | 3.5 | 3.9 |
| 156 | 12DMN | 1,2-Dimethylnaphthalene | 22.539 | 4244 | 1378 | 5.6 | 5.3 |
| 168 | 2MBP | 2-Methylbiphenyl | 20.787 | 214 | 80 | 0.3 | 0.3 |
| 168 | DPM | Diphenylmethane | 21.647 | 494 | 159 | 0.6 | 0.6 |
| 168 | 3MBP | 3-Methylbiphenyl | 23.314 | 13277 | 4520 | 17.4 | 17.5 |
| 168 | 4MBP | 4-Methylbiphenyl | 23.583 | 8810 | 2985 | 11.6 | 11.6 |
| 168 | DBF | Dibenzofuran | 24.303 | 82404 | 26871 | 108.2 | 104.2 |
| 170 | BB_EMN | Ethyl-methyl-Naphthalene | 24.077 | 5850 | 1683 | 7.7 | 6.5 |
| 170 | AB_EMN | Ethyl-methyl-Naphthalene | 24.561 | 2177 | 741 | 2.9 | 2.9 |
| 170 | 137TMN | 1,3,7-Trimethylnaphthalene | 24.712 | 6723 | 2185 | 8.8 | 8.5 |
| 170 | 136TMN | 1,3,6-Trimethylnaphthalene | 24.873 | 11767 | 3823 | 15.5 | 14.8 |
| 170 | 146135T | (1,4,6+1,3,5)-Trimethylnaphthalenes | 25.314 | 7940 | 2377 | 10.4 | 9.2 |
| 170 | 236TMN | 2,3,6-Trimethylnaphthalene | 25.432 | 12348 | 4157 | 16.2 | 16.1 |
| 170 | 127TMN | 1,2,7-Trimethylnaphthalene | 25.755 | 3446 | 1093 | 4.5 | 4.2 |
| 170 | 167126T | (1,6,7+1,2,6)-Trimethylnaphthalenes | 25.841 | 16574 | 3484 | 21.8 | 13.5 |
| 170 | 124TMN | 1,2,4-Trimethylnaphthalene | 26.260 | 1575 | 471 | 2.1 | 1.8 |
| 170 | 125TMN | 1,2,5-Trimethylnaphthalene | 26.464 | 19390 | 6350 | 25.5 | 24.6 |
| 178 | PHEN | Phenanthrene | 31.540 | 788044 | 249858 | 1034.8 | 968.7 |
| 178 | ANTH | Anthracene | 31.819 | 1643 | 390 | 2.2 | 1.5 |
| 184 | 1357 | 1,3,5,7-Tetramethylnaphthalene | 28.249 | 1680 | 459 | 2.2 | 1.8 |
| 184 | 1367 | 1,3,6,7-Tetramethylnaphthalene | 28.884 | 2805 | 966 | 3.7 | 3.7 |
| 184 | 1247 | (1,2,4,7+1,2,4,6+1,4,6,7)-Tetramethylnaphthalenes | 29.292 | 2355 | 760 | 3.1 | 2.9 |
| 184 | 1257 | 1,2,5,7-Tetramethylnaphthalene | 29.400 | 2263 | 721 | 3.0 | 2.8 |
| 184 | 2367 | 2,3,6,7-Tetramethylnaphthalene | 29.615 | 1115 | 360 | 1.5 | 1.4 |
| 184 | 1267 | 1,2,6,7-Tetramethylnaphthalene | 29.862 | 1861 | 589 | 2.4 | 2.3 |
| 184 | 1237 | 1,2,3,7-Tetramethylnaphthalene | 29.959 | 675 | 217 | 0.9 | 0.8 |
| 184 | 1236 | 1,2,3,6-Tetramethylnaphthalene | 30.131 | 1953 | 613 | 2.6 | 2.4 |
| 184 | 1256 | 1,2,5,6-Tetramethylnaphthalene | 30.551 | 10160 | 3177 | 13.3 | 12.3 |
| 184 | DBT | Dibenzothiophene | 30.798 | 120740 | 37492 | 158.6 | 145.4 |
| 191 | BH32 | C32 Benzohopane | | | | | |
| 191 | BH33 | C33 Benzohopane | | | | | |
| 191 | BH34 | C34 Benzohopane | | | | | |
| 191 | BH35 | C35 Benzohopane | | | | | |
| 192 | 3MP | 3-Methylphenanthrene | 34.529 | 20075 | 6242 | 26.4 | 24.2 |
| 192 | 2MP | 2-Methylphenanthrene | 34.658 | 35043 | 11218 | 46.0 | 43.5 |
| 192 | 9MP | 9-Methylphenanthrene | 35.121 | 56785 | 17389 | 74.6 | 67.4 |
| 192 | 1MP | 1-Methylphenanthrene | 35.250 | 77472 | 24053 | 101.7 | 93.3 |

*Appendix F2, ctd.*

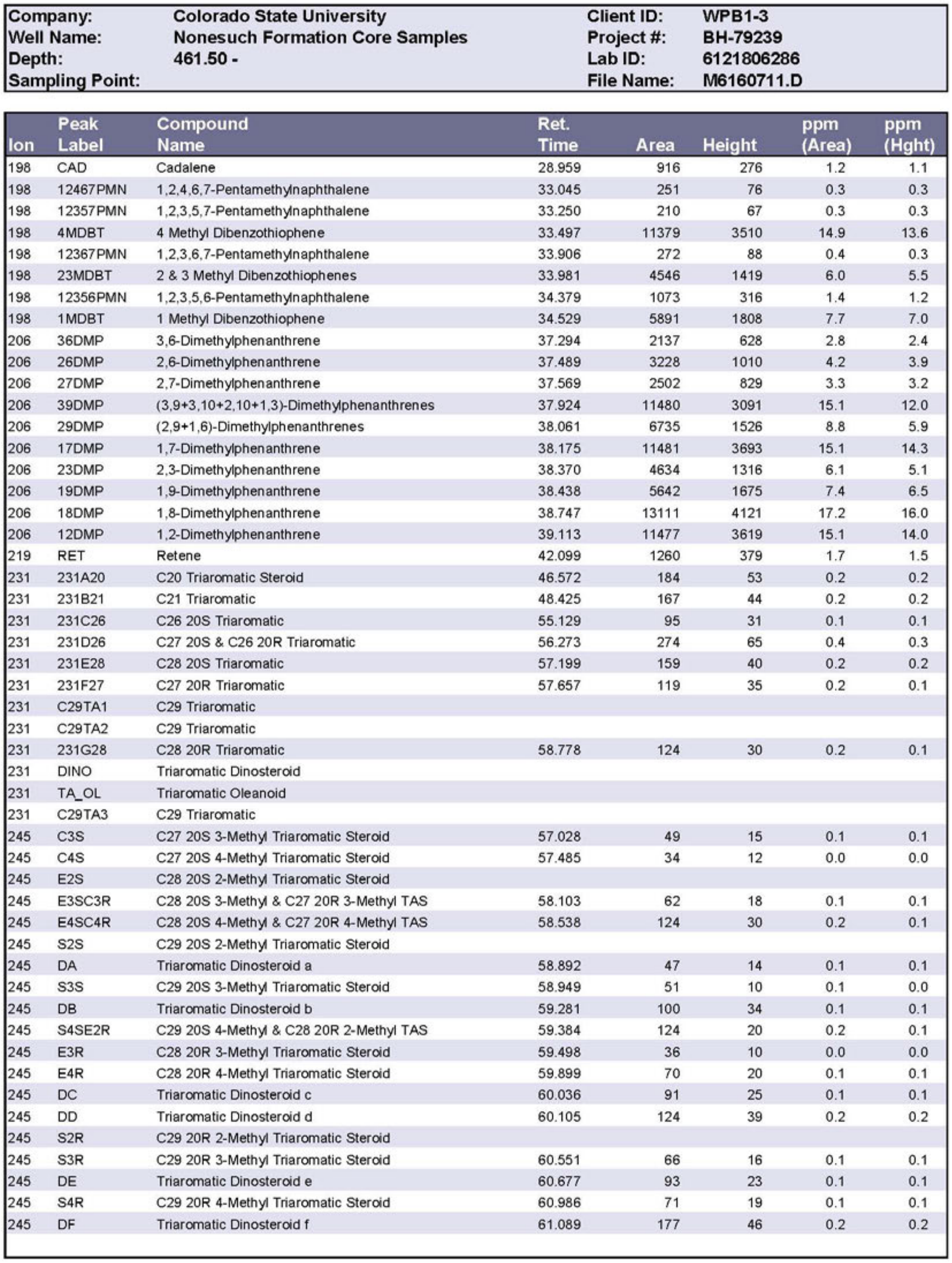

| | | | |
|---|---|---|---|
| **Company:** | **Colorado State University** | **Client ID:** | **WPB1-3** |
| **Well Name:** | **Nonesuch Formation Core Samples** | **Project #:** | **BH-79239** |
| **Depth:** | **461.50 -** | **Lab ID:** | **6121806286** |
| **Sampling Point:** | | **File Name:** | **M6160711.D** |

| Ion | Peak Label | Compound Name | Ret. Time | Area | Height | ppm (Area) | ppm (Hght) |
|---|---|---|---|---|---|---|---|
| 198 | CAD | Cadalene | 28.959 | 916 | 276 | 1.2 | 1.1 |
| 198 | 12467PMN | 1,2,4,6,7-Pentamethylnaphthalene | 33.045 | 251 | 76 | 0.3 | 0.3 |
| 198 | 12357PMN | 1,2,3,5,7-Pentamethylnaphthalene | 33.250 | 210 | 67 | 0.3 | 0.3 |
| 198 | 4MDBT | 4 Methyl Dibenzothiophene | 33.497 | 11379 | 3510 | 14.9 | 13.6 |
| 198 | 12367PMN | 1,2,3,6,7-Pentamethylnaphthalene | 33.906 | 272 | 88 | 0.4 | 0.3 |
| 198 | 23MDBT | 2 & 3 Methyl Dibenzothiophenes | 33.981 | 4546 | 1419 | 6.0 | 5.5 |
| 198 | 12356PMN | 1,2,3,5,6-Pentamethylnaphthalene | 34.379 | 1073 | 316 | 1.4 | 1.2 |
| 198 | 1MDBT | 1 Methyl Dibenzothiophene | 34.529 | 5891 | 1808 | 7.7 | 7.0 |
| 206 | 36DMP | 3,6-Dimethylphenanthrene | 37.294 | 2137 | 628 | 2.8 | 2.4 |
| 206 | 26DMP | 2,6-Dimethylphenanthrene | 37.489 | 3228 | 1010 | 4.2 | 3.9 |
| 206 | 27DMP | 2,7-Dimethylphenanthrene | 37.569 | 2502 | 829 | 3.3 | 3.2 |
| 206 | 39DMP | (3,9+3,10+2,10+1,3)-Dimethylphenanthrenes | 37.924 | 11480 | 3091 | 15.1 | 12.0 |
| 206 | 29DMP | (2,9+1,6)-Dimethylphenanthrenes | 38.061 | 6735 | 1526 | 8.8 | 5.9 |
| 206 | 17DMP | 1,7-Dimethylphenanthrene | 38.175 | 11481 | 3693 | 15.1 | 14.3 |
| 206 | 23DMP | 2,3-Dimethylphenanthrene | 38.370 | 4634 | 1316 | 6.1 | 5.1 |
| 206 | 19DMP | 1,9-Dimethylphenanthrene | 38.438 | 5642 | 1675 | 7.4 | 6.5 |
| 206 | 18DMP | 1,8-Dimethylphenanthrene | 38.747 | 13111 | 4121 | 17.2 | 16.0 |
| 206 | 12DMP | 1,2-Dimethylphenanthrene | 39.113 | 11477 | 3619 | 15.1 | 14.0 |
| 219 | RET | Retene | 42.099 | 1260 | 379 | 1.7 | 1.5 |
| 231 | 231A20 | C20 Triaromatic Steroid | 46.572 | 184 | 53 | 0.2 | 0.2 |
| 231 | 231B21 | C21 Triaromatic | 48.425 | 167 | 44 | 0.2 | 0.2 |
| 231 | 231C26 | C26 20S Triaromatic | 55.129 | 95 | 31 | 0.1 | 0.1 |
| 231 | 231D26 | C27 20S & C26 20R Triaromatic | 56.273 | 274 | 65 | 0.4 | 0.3 |
| 231 | 231E28 | C28 20S Triaromatic | 57.199 | 159 | 40 | 0.2 | 0.2 |
| 231 | 231F27 | C27 20R Triaromatic | 57.657 | 119 | 35 | 0.2 | 0.1 |
| 231 | C29TA1 | C29 Triaromatic | | | | | |
| 231 | C29TA2 | C29 Triaromatic | | | | | |
| 231 | 231G28 | C28 20R Triaromatic | 58.778 | 124 | 30 | 0.2 | 0.1 |
| 231 | DINO | Triaromatic Dinosteroid | | | | | |
| 231 | TA_OL | Triaromatic Oleanoid | | | | | |
| 231 | C29TA3 | C29 Triaromatic | | | | | |
| 245 | C3S | C27 20S 3-Methyl Triaromatic Steroid | 57.028 | 49 | 15 | 0.1 | 0.1 |
| 245 | C4S | C27 20S 4-Methyl Triaromatic Steroid | 57.485 | 34 | 12 | 0.0 | 0.0 |
| 245 | E2S | C28 20S 2-Methyl Triaromatic Steroid | | | | | |
| 245 | E3SC3R | C28 20S 3-Methyl & C27 20R 3-Methyl TAS | 58.103 | 62 | 18 | 0.1 | 0.1 |
| 245 | E4SC4R | C28 20S 4-Methyl & C27 20R 4-Methyl TAS | 58.538 | 124 | 30 | 0.2 | 0.1 |
| 245 | S2S | C29 20S 2-Methyl Triaromatic Steroid | | | | | |
| 245 | DA | Triaromatic Dinosteroid a | 58.892 | 47 | 14 | 0.1 | 0.1 |
| 245 | S3S | C29 20S 3-Methyl Triaromatic Steroid | 58.949 | 51 | 10 | 0.1 | 0.0 |
| 245 | DB | Triaromatic Dinosteroid b | 59.281 | 100 | 34 | 0.1 | 0.1 |
| 245 | S4SE2R | C29 20S 4-Methyl & C28 20R 2-Methyl TAS | 59.384 | 124 | 20 | 0.2 | 0.1 |
| 245 | E3R | C28 20R 3-Methyl Triaromatic Steroid | 59.498 | 36 | 10 | 0.0 | 0.0 |
| 245 | E4R | C28 20R 4-Methyl Triaromatic Steroid | 59.899 | 70 | 20 | 0.1 | 0.1 |
| 245 | DC | Triaromatic Dinosteroid c | 60.036 | 91 | 25 | 0.1 | 0.1 |
| 245 | DD | Triaromatic Dinosteroid d | 60.105 | 124 | 39 | 0.2 | 0.2 |
| 245 | S2R | C29 20R 2-Methyl Triaromatic Steroid | | | | | |
| 245 | S3R | C29 20R 3-Methyl Triaromatic Steroid | 60.551 | 66 | 16 | 0.1 | 0.1 |
| 245 | DE | Triaromatic Dinosteroid e | 60.677 | 93 | 23 | 0.1 | 0.1 |
| 245 | S4R | C29 20R 4-Methyl Triaromatic Steroid | 60.986 | 71 | 19 | 0.1 | 0.1 |
| 245 | DF | Triaromatic Dinosteroid f | 61.089 | 177 | 46 | 0.2 | 0.2 |

*Appendix F2, ctd.*

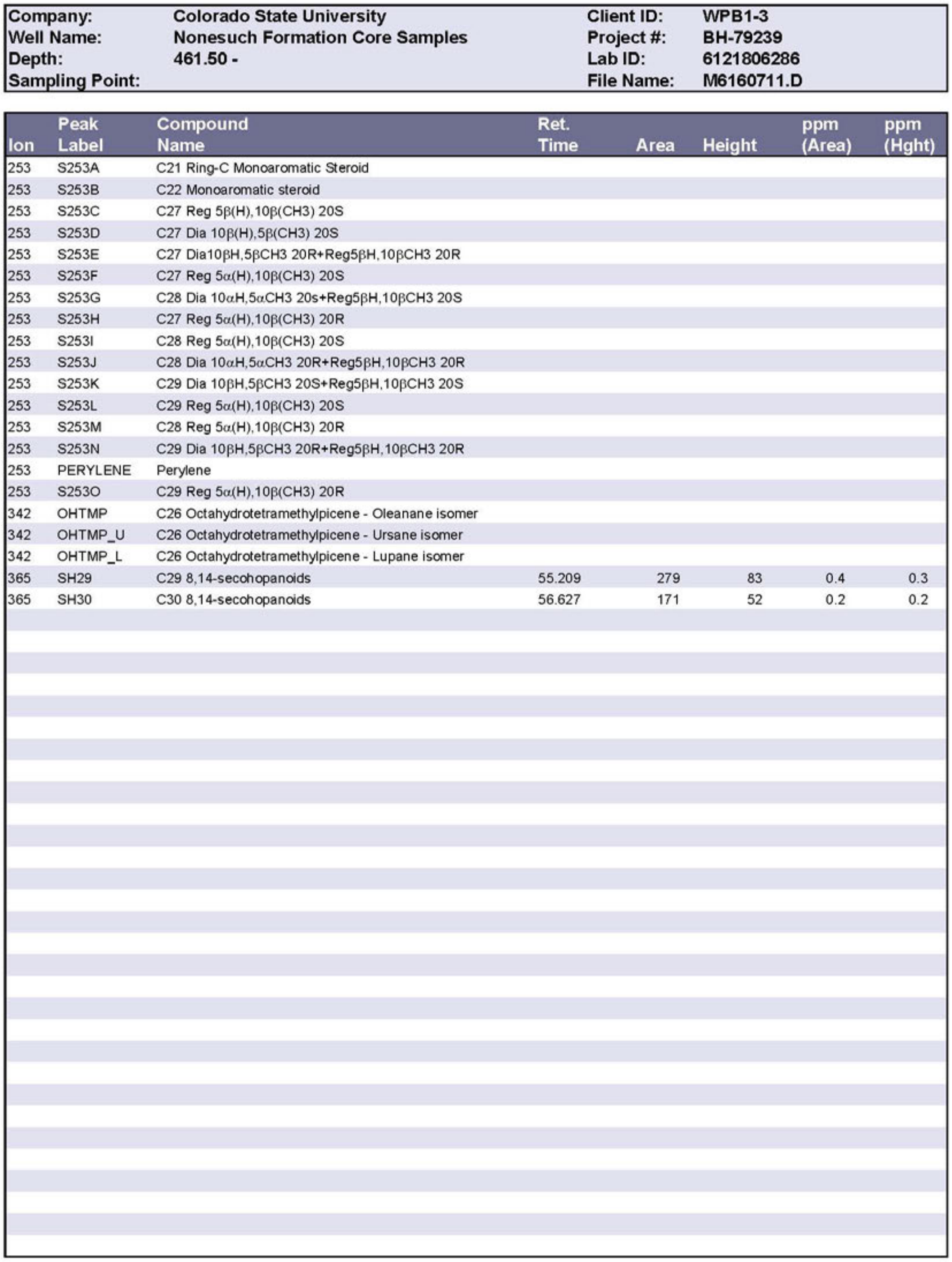

| | | | |
|---|---|---|---|
| **Company:** | **Colorado State University** | **Client ID:** | **WPB1-3** |
| **Well Name:** | **Nonesuch Formation Core Samples** | **Project #:** | **BH-79239** |
| **Depth:** | **461.50 -** | **Lab ID:** | **6121806286** |
| **Sampling Point:** | | **File Name:** | **M6160711.D** |

| Ion | Peak Label | Compound Name | Ret. Time | Area | Height | ppm (Area) | ppm (Hght) |
|---|---|---|---|---|---|---|---|
| 253 | S253A | C21 Ring-C Monoaromatic Steroid | | | | | |
| 253 | S253B | C22 Monoaromatic steroid | | | | | |
| 253 | S253C | C27 Reg 5β(H),10β(CH3) 20S | | | | | |
| 253 | S253D | C27 Dia 10β(H),5β(CH3) 20S | | | | | |
| 253 | S253E | C27 Dia10βH,5βCH3 20R+Reg5βH,10βCH3 20R | | | | | |
| 253 | S253F | C27 Reg 5α(H),10β(CH3) 20S | | | | | |
| 253 | S253G | C28 Dia 10αH,5αCH3 20s+Reg5βH,10βCH3 20S | | | | | |
| 253 | S253H | C27 Reg 5α(H),10β(CH3) 20R | | | | | |
| 253 | S253I | C28 Reg 5α(H),10β(CH3) 20S | | | | | |
| 253 | S253J | C28 Dia 10αH,5αCH3 20R+Reg5βH,10βCH3 20R | | | | | |
| 253 | S253K | C29 Dia 10βH,5βCH3 20S+Reg5βH,10βCH3 20S | | | | | |
| 253 | S253L | C29 Reg 5α(H),10β(CH3) 20S | | | | | |
| 253 | S253M | C28 Reg 5α(H),10β(CH3) 20R | | | | | |
| 253 | S253N | C29 Dia 10βH,5βCH3 20R+Reg5βH,10βCH3 20R | | | | | |
| 253 | PERYLENE | Perylene | | | | | |
| 253 | S253O | C29 Reg 5α(H),10β(CH3) 20R | | | | | |
| 342 | OHTMP | C26 Octahydrotetramethylpicene - Oleanane isomer | | | | | |
| 342 | OHTMP_U | C26 Octahydrotetramethylpicene - Ursane isomer | | | | | |
| 342 | OHTMP_L | C26 Octahydrotetramethylpicene - Lupane isomer | | | | | |
| 365 | SH29 | C29 8,14-secohopanoids | 55.209 | 279 | 83 | 0.4 | 0.3 |
| 365 | SH30 | C30 8,14-secohopanoids | 56.627 | 171 | 52 | 0.2 | 0.2 |

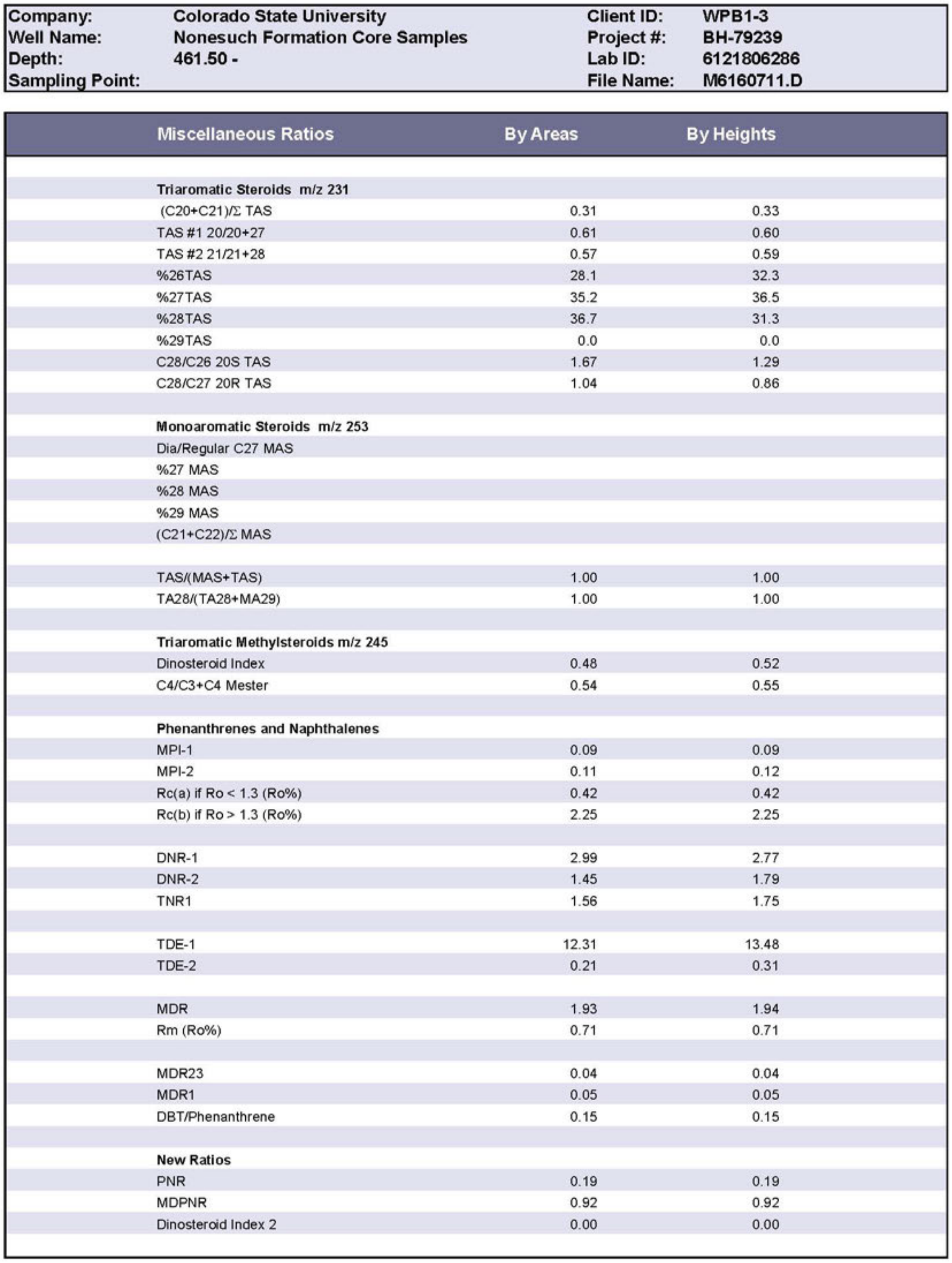

| | | | |
|---|---|---|---|
| **Company:** | **Colorado State University** | **Client ID:** | **WPB1-3** |
| **Well Name:** | **Nonesuch Formation Core Samples** | **Project #:** | **BH-79239** |
| **Depth:** | **461.50 -** | **Lab ID:** | **6121806286** |
| **Sampling Point:** | | **File Name:** | **M6160711.D** |

| Miscellaneous Ratios | By Areas | By Heights |
|---|---|---|
| **Triaromatic Steroids m/z 231** | | |
| (C20+C21)/Σ TAS | 0.31 | 0.33 |
| TAS #1 20/20+27 | 0.61 | 0.60 |
| TAS #2 21/21+28 | 0.57 | 0.59 |
| %26TAS | 28.1 | 32.3 |
| %27TAS | 35.2 | 36.5 |
| %28TAS | 36.7 | 31.3 |
| %29TAS | 0.0 | 0.0 |
| C28/C26 20S TAS | 1.67 | 1.29 |
| C28/C27 20R TAS | 1.04 | 0.86 |
| | | |
| **Monoaromatic Steroids m/z 253** | | |
| Dia/Regular C27 MAS | | |
| %27 MAS | | |
| %28 MAS | | |
| %29 MAS | | |
| (C21+C22)/Σ MAS | | |
| | | |
| TAS/(MAS+TAS) | 1.00 | 1.00 |
| TA28/(TA28+MA29) | 1.00 | 1.00 |
| | | |
| **Triaromatic Methylsteroids m/z 245** | | |
| Dinosteroid Index | 0.48 | 0.52 |
| C4/C3+C4 Mester | 0.54 | 0.55 |
| | | |
| **Phenanthrenes and Naphthalenes** | | |
| MPI-1 | 0.09 | 0.09 |
| MPI-2 | 0.11 | 0.12 |
| Rc(a) if Ro < 1.3 (Ro%) | 0.42 | 0.42 |
| Rc(b) if Ro > 1.3 (Ro%) | 2.25 | 2.25 |
| | | |
| DNR-1 | 2.99 | 2.77 |
| DNR-2 | 1.45 | 1.79 |
| TNR1 | 1.56 | 1.75 |
| | | |
| TDE-1 | 12.31 | 13.48 |
| TDE-2 | 0.21 | 0.31 |
| | | |
| MDR | 1.93 | 1.94 |
| Rm (Ro%) | 0.71 | 0.71 |
| | | |
| MDR23 | 0.04 | 0.04 |
| MDR1 | 0.05 | 0.05 |
| DBT/Phenanthrene | 0.15 | 0.15 |
| | | |
| **New Ratios** | | |
| PNR | 0.19 | 0.19 |
| MDPNR | 0.92 | 0.92 |
| Dinosteroid Index 2 | 0.00 | 0.00 |

*Appendix F2, ctd.*

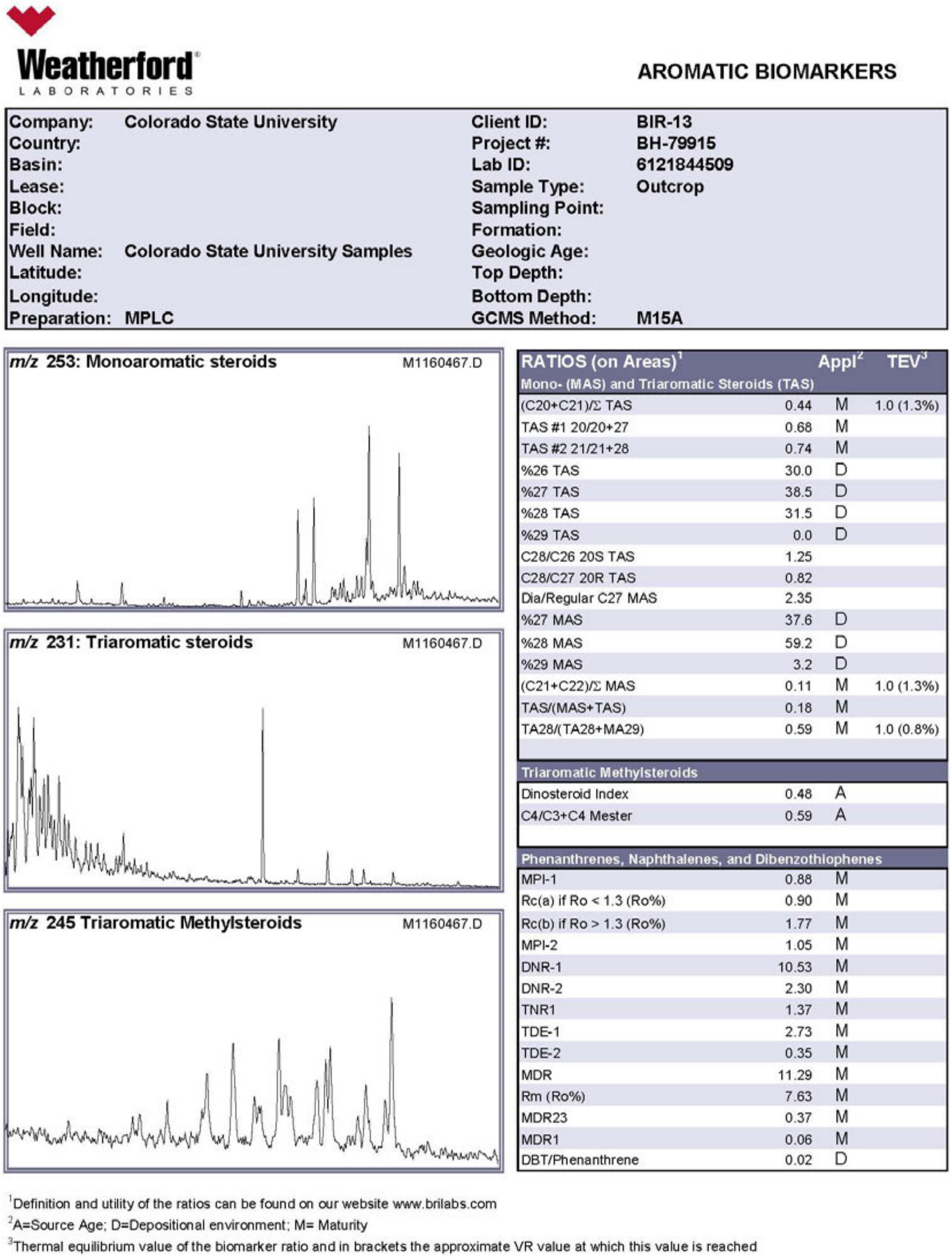

**Weatherford** LABORATORIES

## AROMATIC BIOMARKERS

| | | | |
|---|---|---|---|
| **Company:** | **Colorado State University** | **Client ID:** | **BIR-13** |
| **Country:** | | **Project #:** | **BH-79915** |
| **Basin:** | | **Lab ID:** | **6121844509** |
| **Lease:** | | **Sample Type:** | **Outcrop** |
| **Block:** | | **Sampling Point:** | |
| **Field:** | | **Formation:** | |
| **Well Name:** | **Colorado State University Samples** | **Geologic Age:** | |
| **Latitude:** | | **Top Depth:** | |
| **Longitude:** | | **Bottom Depth:** | |
| **Preparation:** | **MPLC** | **GCMS Method:** | **M15A** |

**m/z 253: Monoaromatic steroids** M1160467.D

**m/z 231: Triaromatic steroids** M1160467.D

**m/z 245 Triaromatic Methylsteroids** M1160467.D

| RATIOS (on Areas)[1] | | Appl[2] | TEV[3] |
|---|---|---|---|
| **Mono- (MAS) and Triaromatic Steroids (TAS)** | | | |
| (C20+C21)/Σ TAS | 0.44 | M | 1.0 (1.3%) |
| TAS #1 20/20+27 | 0.68 | M | |
| TAS #2 21/21+28 | 0.74 | M | |
| %26 TAS | 30.0 | D | |
| %27 TAS | 38.5 | D | |
| %28 TAS | 31.5 | D | |
| %29 TAS | 0.0 | D | |
| C28/C26 20S TAS | 1.25 | | |
| C28/C27 20R TAS | 0.82 | | |
| Dia/Regular C27 MAS | 2.35 | | |
| %27 MAS | 37.6 | D | |
| %28 MAS | 59.2 | D | |
| %29 MAS | 3.2 | D | |
| (C21+C22)/Σ MAS | 0.11 | M | 1.0 (1.3%) |
| TAS/(MAS+TAS) | 0.18 | M | |
| TA28/(TA28+MA29) | 0.59 | M | 1.0 (0.8%) |
| **Triaromatic Methylsteroids** | | | |
| Dinosteroid Index | 0.48 | A | |
| C4/C3+C4 Mester | 0.59 | A | |
| **Phenanthrenes, Naphthalenes, and Dibenzothiophenes** | | | |
| MPI-1 | 0.88 | M | |
| Rc(a) if Ro < 1.3 (Ro%) | 0.90 | M | |
| Rc(b) if Ro > 1.3 (Ro%) | 1.77 | M | |
| MPI-2 | 1.05 | M | |
| DNR-1 | 10.53 | M | |
| DNR-2 | 2.30 | M | |
| TNR1 | 1.37 | M | |
| TDE-1 | 2.73 | M | |
| TDE-2 | 0.35 | M | |
| MDR | 11.29 | M | |
| Rm (Ro%) | 7.63 | M | |
| MDR23 | 0.37 | M | |
| MDR1 | 0.06 | M | |
| DBT/Phenanthrene | 0.02 | D | |

[1] Definition and utility of the ratios can be found on our website www.brilabs.com

[2] A=Source Age; D=Depositional environment; M= Maturity

[3] Thermal equilibrium value of the biomarker ratio and in brackets the approximate VR value at which this value is reached

*Appendix F2, ctd.*

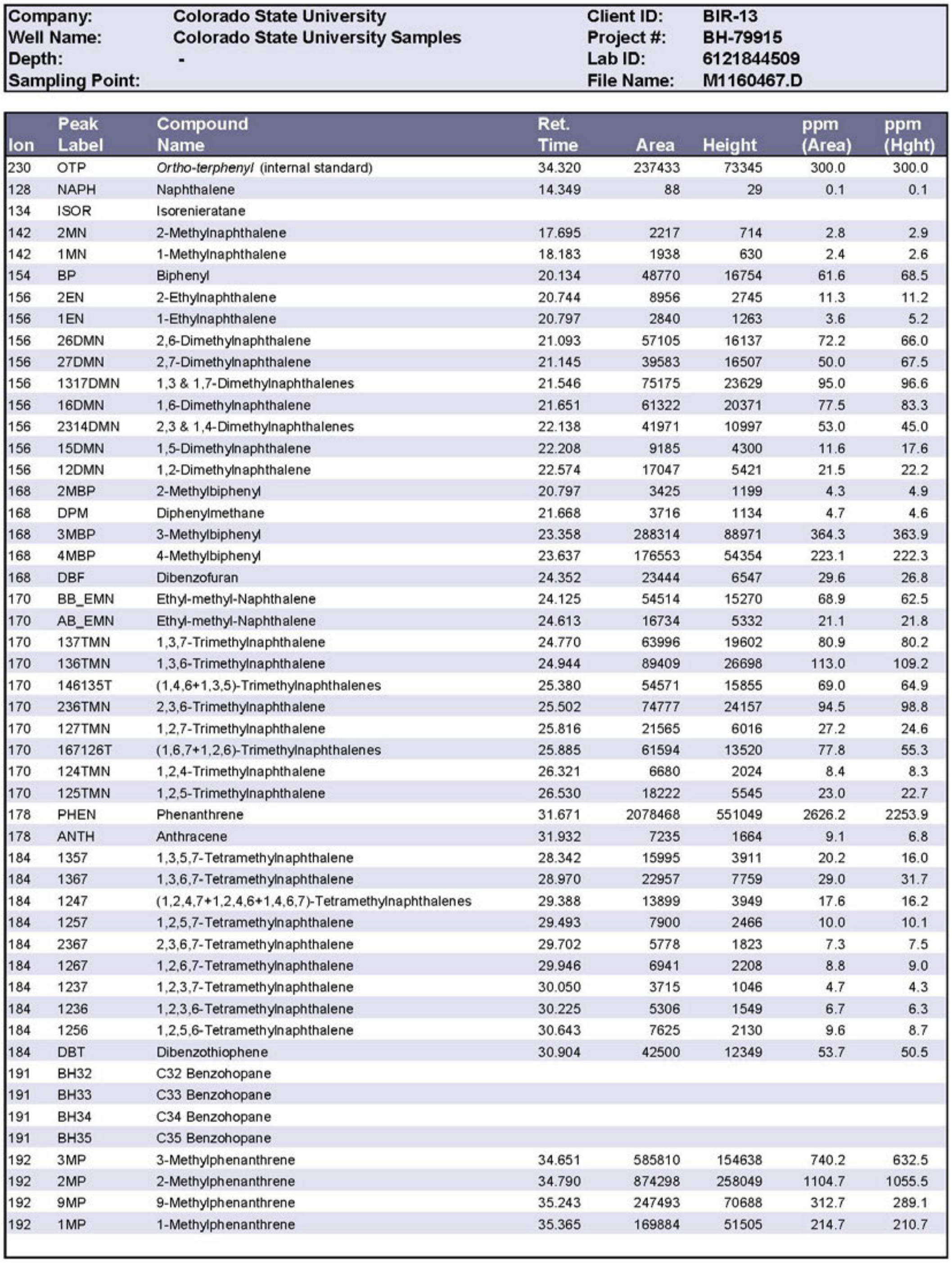

|  |  |  |  |
|---|---|---|---|
| **Company:** | **Colorado State University** | **Client ID:** | **BIR-13** |
| **Well Name:** | **Colorado State University Samples** | **Project #:** | **BH-79915** |
| **Depth:** | **-** | **Lab ID:** | **6121844509** |
| **Sampling Point:** |  | **File Name:** | **M1160467.D** |

| Ion | Peak Label | Compound Name | Ret. Time | Area | Height | ppm (Area) | ppm (Hght) |
|---|---|---|---|---|---|---|---|
| 230 | OTP | *Ortho-terphenyl* (internal standard) | 34.320 | 237433 | 73345 | 300.0 | 300.0 |
| 128 | NAPH | Naphthalene | 14.349 | 88 | 29 | 0.1 | 0.1 |
| 134 | ISOR | Isorenieratane |  |  |  |  |  |
| 142 | 2MN | 2-Methylnaphthalene | 17.695 | 2217 | 714 | 2.8 | 2.9 |
| 142 | 1MN | 1-Methylnaphthalene | 18.183 | 1938 | 630 | 2.4 | 2.6 |
| 154 | BP | Biphenyl | 20.134 | 48770 | 16754 | 61.6 | 68.5 |
| 156 | 2EN | 2-Ethylnaphthalene | 20.744 | 8956 | 2745 | 11.3 | 11.2 |
| 156 | 1EN | 1-Ethylnaphthalene | 20.797 | 2840 | 1263 | 3.6 | 5.2 |
| 156 | 26DMN | 2,6-Dimethylnaphthalene | 21.093 | 57105 | 16137 | 72.2 | 66.0 |
| 156 | 27DMN | 2,7-Dimethylnaphthalene | 21.145 | 39583 | 16507 | 50.0 | 67.5 |
| 156 | 1317DMN | 1,3 & 1,7-Dimethylnaphthalenes | 21.546 | 75175 | 23629 | 95.0 | 96.6 |
| 156 | 16DMN | 1,6-Dimethylnaphthalene | 21.651 | 61322 | 20371 | 77.5 | 83.3 |
| 156 | 2314DMN | 2,3 & 1,4-Dimethylnaphthalenes | 22.138 | 41971 | 10997 | 53.0 | 45.0 |
| 156 | 15DMN | 1,5-Dimethylnaphthalene | 22.208 | 9185 | 4300 | 11.6 | 17.6 |
| 156 | 12DMN | 1,2-Dimethylnaphthalene | 22.574 | 17047 | 5421 | 21.5 | 22.2 |
| 168 | 2MBP | 2-Methylbiphenyl | 20.797 | 3425 | 1199 | 4.3 | 4.9 |
| 168 | DPM | Diphenylmethane | 21.668 | 3716 | 1134 | 4.7 | 4.6 |
| 168 | 3MBP | 3-Methylbiphenyl | 23.358 | 288314 | 88971 | 364.3 | 363.9 |
| 168 | 4MBP | 4-Methylbiphenyl | 23.637 | 176553 | 54354 | 223.1 | 222.3 |
| 168 | DBF | Dibenzofuran | 24.352 | 23444 | 6547 | 29.6 | 26.8 |
| 170 | BB_EMN | Ethyl-methyl-Naphthalene | 24.125 | 54514 | 15270 | 68.9 | 62.5 |
| 170 | AB_EMN | Ethyl-methyl-Naphthalene | 24.613 | 16734 | 5332 | 21.1 | 21.8 |
| 170 | 137TMN | 1,3,7-Trimethylnaphthalene | 24.770 | 63996 | 19602 | 80.9 | 80.2 |
| 170 | 136TMN | 1,3,6-Trimethylnaphthalene | 24.944 | 89409 | 26698 | 113.0 | 109.2 |
| 170 | 146135T | (1,4,6+1,3,5)-Trimethylnaphthalenes | 25.380 | 54571 | 15855 | 69.0 | 64.9 |
| 170 | 236TMN | 2,3,6-Trimethylnaphthalene | 25.502 | 74777 | 24157 | 94.5 | 98.8 |
| 170 | 127TMN | 1,2,7-Trimethylnaphthalene | 25.816 | 21565 | 6016 | 27.2 | 24.6 |
| 170 | 167126T | (1,6,7+1,2,6)-Trimethylnaphthalenes | 25.885 | 61594 | 13520 | 77.8 | 55.3 |
| 170 | 124TMN | 1,2,4-Trimethylnaphthalene | 26.321 | 6680 | 2024 | 8.4 | 8.3 |
| 170 | 125TMN | 1,2,5-Trimethylnaphthalene | 26.530 | 18222 | 5545 | 23.0 | 22.7 |
| 178 | PHEN | Phenanthrene | 31.671 | 2078468 | 551049 | 2626.2 | 2253.9 |
| 178 | ANTH | Anthracene | 31.932 | 7235 | 1664 | 9.1 | 6.8 |
| 184 | 1357 | 1,3,5,7-Tetramethylnaphthalene | 28.342 | 15995 | 3911 | 20.2 | 16.0 |
| 184 | 1367 | 1,3,6,7-Tetramethylnaphthalene | 28.970 | 22957 | 7759 | 29.0 | 31.7 |
| 184 | 1247 | (1,2,4,7+1,2,4,6+1,4,6,7)-Tetramethylnaphthalenes | 29.388 | 13899 | 3949 | 17.6 | 16.2 |
| 184 | 1257 | 1,2,5,7-Tetramethylnaphthalene | 29.493 | 7900 | 2466 | 10.0 | 10.1 |
| 184 | 2367 | 2,3,6,7-Tetramethylnaphthalene | 29.702 | 5778 | 1823 | 7.3 | 7.5 |
| 184 | 1267 | 1,2,6,7-Tetramethylnaphthalene | 29.946 | 6941 | 2208 | 8.8 | 9.0 |
| 184 | 1237 | 1,2,3,7-Tetramethylnaphthalene | 30.050 | 3715 | 1046 | 4.7 | 4.3 |
| 184 | 1236 | 1,2,3,6-Tetramethylnaphthalene | 30.225 | 5306 | 1549 | 6.7 | 6.3 |
| 184 | 1256 | 1,2,5,6-Tetramethylnaphthalene | 30.643 | 7625 | 2130 | 9.6 | 8.7 |
| 184 | DBT | Dibenzothiophene | 30.904 | 42500 | 12349 | 53.7 | 50.5 |
| 191 | BH32 | C32 Benzohopane |  |  |  |  |  |
| 191 | BH33 | C33 Benzohopane |  |  |  |  |  |
| 191 | BH34 | C34 Benzohopane |  |  |  |  |  |
| 191 | BH35 | C35 Benzohopane |  |  |  |  |  |
| 192 | 3MP | 3-Methylphenanthrene | 34.651 | 585810 | 154638 | 740.2 | 632.5 |
| 192 | 2MP | 2-Methylphenanthrene | 34.790 | 874298 | 258049 | 1104.7 | 1055.5 |
| 192 | 9MP | 9-Methylphenanthrene | 35.243 | 247493 | 70688 | 312.7 | 289.1 |
| 192 | 1MP | 1-Methylphenanthrene | 35.365 | 169884 | 51505 | 214.7 | 210.7 |

*Appendix F2, ctd.*

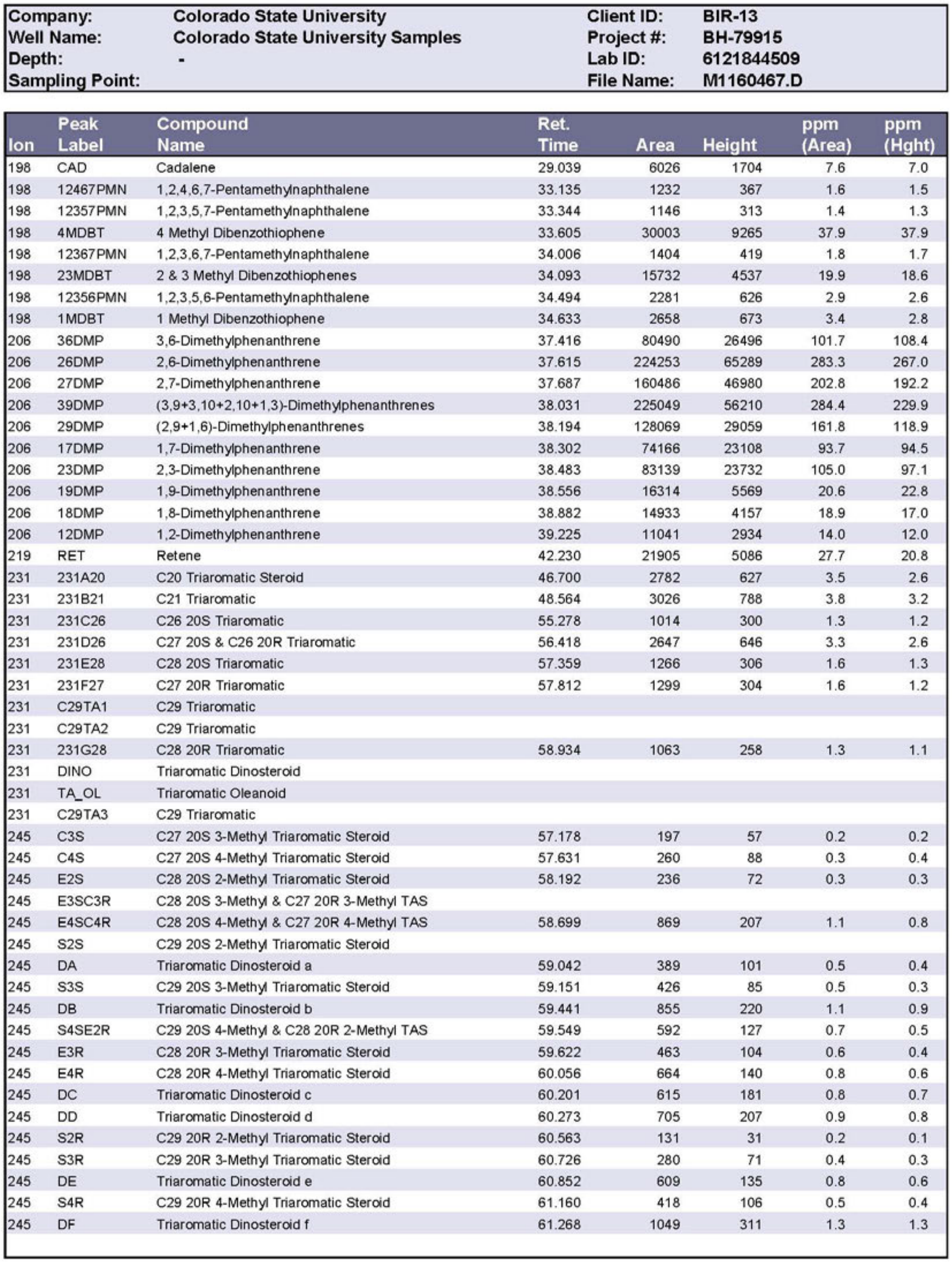

| | | | |
|---|---|---|---|
| **Company:** | **Colorado State University** | **Client ID:** | **BIR-13** |
| **Well Name:** | **Colorado State University Samples** | **Project #:** | **BH-79915** |
| **Depth:** | **-** | **Lab ID:** | **6121844509** |
| **Sampling Point:** | | **File Name:** | **M1160467.D** |

| Ion | Peak Label | Compound Name | Ret. Time | Area | Height | ppm (Area) | ppm (Hght) |
|---|---|---|---|---|---|---|---|
| 198 | CAD | Cadalene | 29.039 | 6026 | 1704 | 7.6 | 7.0 |
| 198 | 12467PMN | 1,2,4,6,7-Pentamethylnaphthalene | 33.135 | 1232 | 367 | 1.6 | 1.5 |
| 198 | 12357PMN | 1,2,3,5,7-Pentamethylnaphthalene | 33.344 | 1146 | 313 | 1.4 | 1.3 |
| 198 | 4MDBT | 4 Methyl Dibenzothiophene | 33.605 | 30003 | 9265 | 37.9 | 37.9 |
| 198 | 12367PMN | 1,2,3,6,7-Pentamethylnaphthalene | 34.006 | 1404 | 419 | 1.8 | 1.7 |
| 198 | 23MDBT | 2 & 3 Methyl Dibenzothiophenes | 34.093 | 15732 | 4537 | 19.9 | 18.6 |
| 198 | 12356PMN | 1,2,3,5,6-Pentamethylnaphthalene | 34.494 | 2281 | 626 | 2.9 | 2.6 |
| 198 | 1MDBT | 1 Methyl Dibenzothiophene | 34.633 | 2658 | 673 | 3.4 | 2.8 |
| 206 | 36DMP | 3,6-Dimethylphenanthrene | 37.416 | 80490 | 26496 | 101.7 | 108.4 |
| 206 | 26DMP | 2,6-Dimethylphenanthrene | 37.615 | 224253 | 65289 | 283.3 | 267.0 |
| 206 | 27DMP | 2,7-Dimethylphenanthrene | 37.687 | 160486 | 46980 | 202.8 | 192.2 |
| 206 | 39DMP | (3,9+3,10+2,10+1,3)-Dimethylphenanthrenes | 38.031 | 225049 | 56210 | 284.4 | 229.9 |
| 206 | 29DMP | (2,9+1,6)-Dimethylphenanthrenes | 38.194 | 128069 | 29059 | 161.8 | 118.9 |
| 206 | 17DMP | 1,7-Dimethylphenanthrene | 38.302 | 74166 | 23108 | 93.7 | 94.5 |
| 206 | 23DMP | 2,3-Dimethylphenanthrene | 38.483 | 83139 | 23732 | 105.0 | 97.1 |
| 206 | 19DMP | 1,9-Dimethylphenanthrene | 38.556 | 16314 | 5569 | 20.6 | 22.8 |
| 206 | 18DMP | 1,8-Dimethylphenanthrene | 38.882 | 14933 | 4157 | 18.9 | 17.0 |
| 206 | 12DMP | 1,2-Dimethylphenanthrene | 39.225 | 11041 | 2934 | 14.0 | 12.0 |
| 219 | RET | Retene | 42.230 | 21905 | 5086 | 27.7 | 20.8 |
| 231 | 231A20 | C20 Triaromatic Steroid | 46.700 | 2782 | 627 | 3.5 | 2.6 |
| 231 | 231B21 | C21 Triaromatic | 48.564 | 3026 | 788 | 3.8 | 3.2 |
| 231 | 231C26 | C26 20S Triaromatic | 55.278 | 1014 | 300 | 1.3 | 1.2 |
| 231 | 231D26 | C27 20S & C26 20R Triaromatic | 56.418 | 2647 | 646 | 3.3 | 2.6 |
| 231 | 231E28 | C28 20S Triaromatic | 57.359 | 1266 | 306 | 1.6 | 1.3 |
| 231 | 231F27 | C27 20R Triaromatic | 57.812 | 1299 | 304 | 1.6 | 1.2 |
| 231 | C29TA1 | C29 Triaromatic | | | | | |
| 231 | C29TA2 | C29 Triaromatic | | | | | |
| 231 | 231G28 | C28 20R Triaromatic | 58.934 | 1063 | 258 | 1.3 | 1.1 |
| 231 | DINO | Triaromatic Dinosteroid | | | | | |
| 231 | TA_OL | Triaromatic Oleanoid | | | | | |
| 231 | C29TA3 | C29 Triaromatic | | | | | |
| 245 | C3S | C27 20S 3-Methyl Triaromatic Steroid | 57.178 | 197 | 57 | 0.2 | 0.2 |
| 245 | C4S | C27 20S 4-Methyl Triaromatic Steroid | 57.631 | 260 | 88 | 0.3 | 0.4 |
| 245 | E2S | C28 20S 2-Methyl Triaromatic Steroid | 58.192 | 236 | 72 | 0.3 | 0.3 |
| 245 | E3SC3R | C28 20S 3-Methyl & C27 20R 3-Methyl TAS | | | | | |
| 245 | E4SC4R | C28 20S 4-Methyl & C27 20R 4-Methyl TAS | 58.699 | 869 | 207 | 1.1 | 0.8 |
| 245 | S2S | C29 20S 2-Methyl Triaromatic Steroid | | | | | |
| 245 | DA | Triaromatic Dinosteroid a | 59.042 | 389 | 101 | 0.5 | 0.4 |
| 245 | S3S | C29 20S 3-Methyl Triaromatic Steroid | 59.151 | 426 | 85 | 0.5 | 0.3 |
| 245 | DB | Triaromatic Dinosteroid b | 59.441 | 855 | 220 | 1.1 | 0.9 |
| 245 | S4SE2R | C29 20S 4-Methyl & C28 20R 2-Methyl TAS | 59.549 | 592 | 127 | 0.7 | 0.5 |
| 245 | E3R | C28 20R 3-Methyl Triaromatic Steroid | 59.622 | 463 | 104 | 0.6 | 0.4 |
| 245 | E4R | C28 20R 4-Methyl Triaromatic Steroid | 60.056 | 664 | 140 | 0.8 | 0.6 |
| 245 | DC | Triaromatic Dinosteroid c | 60.201 | 615 | 181 | 0.8 | 0.7 |
| 245 | DD | Triaromatic Dinosteroid d | 60.273 | 705 | 207 | 0.9 | 0.8 |
| 245 | S2R | C29 20R 2-Methyl Triaromatic Steroid | 60.563 | 131 | 31 | 0.2 | 0.1 |
| 245 | S3R | C29 20R 3-Methyl Triaromatic Steroid | 60.726 | 280 | 71 | 0.4 | 0.3 |
| 245 | DE | Triaromatic Dinosteroid e | 60.852 | 609 | 135 | 0.8 | 0.6 |
| 245 | S4R | C29 20R 4-Methyl Triaromatic Steroid | 61.160 | 418 | 106 | 0.5 | 0.4 |
| 245 | DF | Triaromatic Dinosteroid f | 61.268 | 1049 | 311 | 1.3 | 1.3 |

*Appendix F2, ctd.*

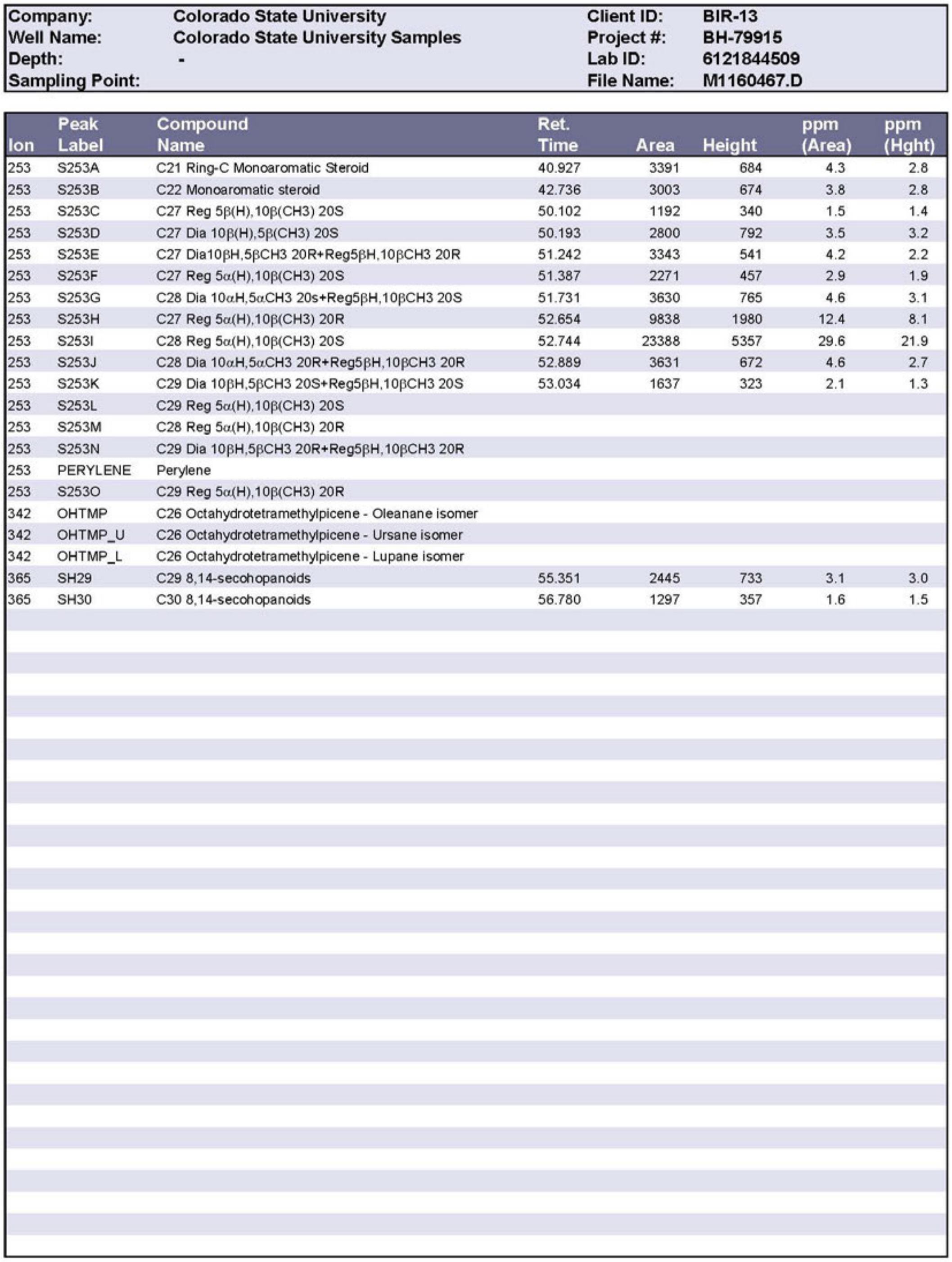

| | | | |
|---|---|---|---|
| **Company:** | **Colorado State University** | **Client ID:** | **BIR-13** |
| **Well Name:** | **Colorado State University Samples** | **Project #:** | **BH-79915** |
| **Depth:** | **-** | **Lab ID:** | **6121844509** |
| **Sampling Point:** | | **File Name:** | **M1160467.D** |

| Ion | Peak Label | Compound Name | Ret. Time | Area | Height | ppm (Area) | ppm (Hght) |
|---|---|---|---|---|---|---|---|
| 253 | S253A | C21 Ring-C Monoaromatic Steroid | 40.927 | 3391 | 684 | 4.3 | 2.8 |
| 253 | S253B | C22 Monoaromatic steroid | 42.736 | 3003 | 674 | 3.8 | 2.8 |
| 253 | S253C | C27 Reg 5β(H),10β(CH3) 20S | 50.102 | 1192 | 340 | 1.5 | 1.4 |
| 253 | S253D | C27 Dia 10β(H),5β(CH3) 20S | 50.193 | 2800 | 792 | 3.5 | 3.2 |
| 253 | S253E | C27 Dia10βH,5βCH3 20R+Reg5βH,10βCH3 20R | 51.242 | 3343 | 541 | 4.2 | 2.2 |
| 253 | S253F | C27 Reg 5α(H),10β(CH3) 20S | 51.387 | 2271 | 457 | 2.9 | 1.9 |
| 253 | S253G | C28 Dia 10αH,5αCH3 20s+Reg5βH,10βCH3 20S | 51.731 | 3630 | 765 | 4.6 | 3.1 |
| 253 | S253H | C27 Reg 5α(H),10β(CH3) 20R | 52.654 | 9838 | 1980 | 12.4 | 8.1 |
| 253 | S253I | C28 Reg 5α(H),10β(CH3) 20S | 52.744 | 23388 | 5357 | 29.6 | 21.9 |
| 253 | S253J | C28 Dia 10αH,5αCH3 20R+Reg5βH,10βCH3 20R | 52.889 | 3631 | 672 | 4.6 | 2.7 |
| 253 | S253K | C29 Dia 10βH,5βCH3 20S+Reg5βH,10βCH3 20S | 53.034 | 1637 | 323 | 2.1 | 1.3 |
| 253 | S253L | C29 Reg 5α(H),10β(CH3) 20S | | | | | |
| 253 | S253M | C28 Reg 5α(H),10β(CH3) 20R | | | | | |
| 253 | S253N | C29 Dia 10βH,5βCH3 20R+Reg5βH,10βCH3 20R | | | | | |
| 253 | PERYLENE | Perylene | | | | | |
| 253 | S253O | C29 Reg 5α(H),10β(CH3) 20R | | | | | |
| 342 | OHTMP | C26 Octahydrotetramethylpicene - Oleanane isomer | | | | | |
| 342 | OHTMP_U | C26 Octahydrotetramethylpicene - Ursane isomer | | | | | |
| 342 | OHTMP_L | C26 Octahydrotetramethylpicene - Lupane isomer | | | | | |
| 365 | SH29 | C29 8,14-secohopanoids | 55.351 | 2445 | 733 | 3.1 | 3.0 |
| 365 | SH30 | C30 8,14-secohopanoids | 56.780 | 1297 | 357 | 1.6 | 1.5 |

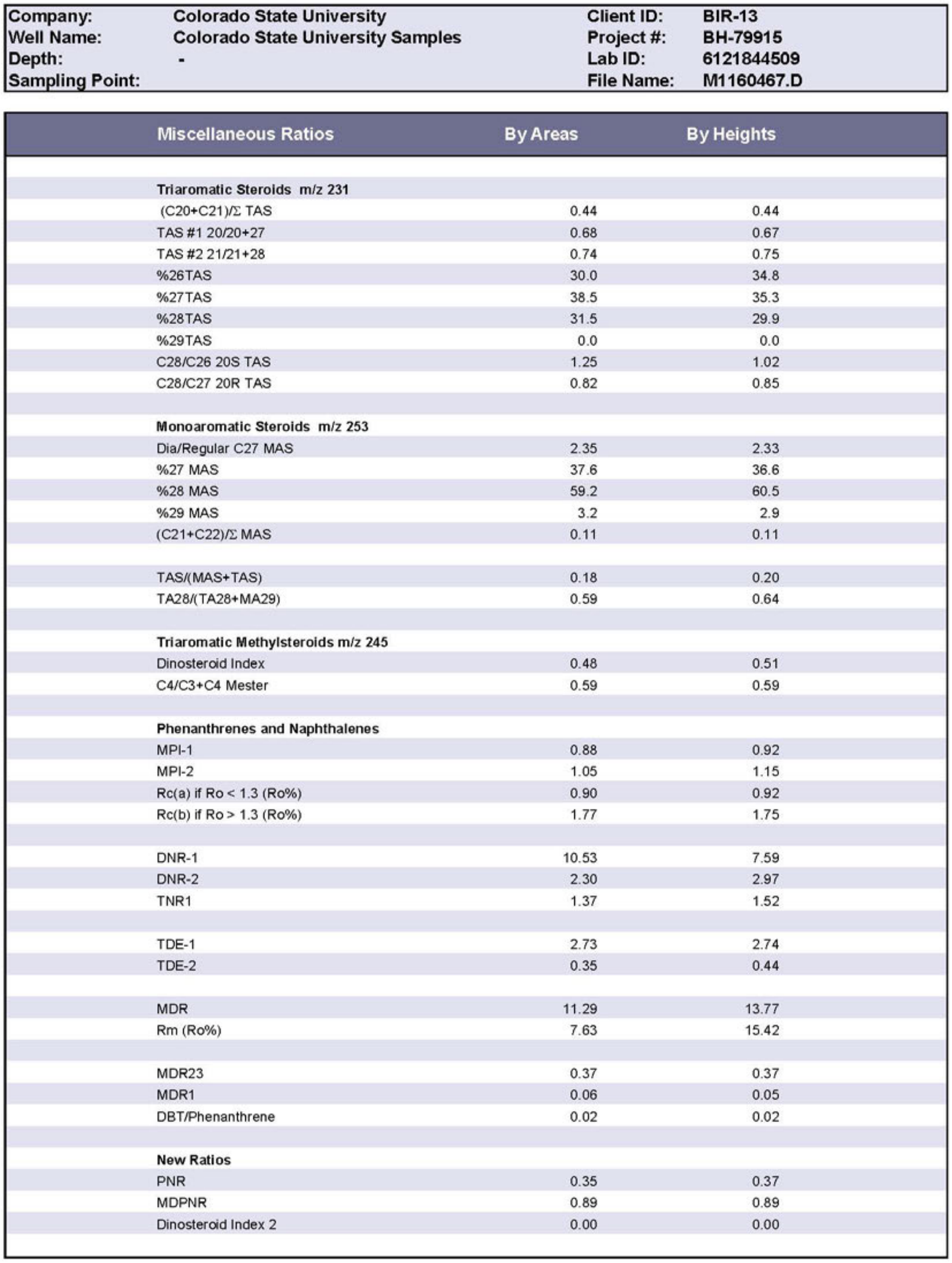

| | | | |
|---|---|---|---|
| **Company:** | **Colorado State University** | **Client ID:** | **BIR-13** |
| **Well Name:** | **Colorado State University Samples** | **Project #:** | **BH-79915** |
| **Depth:** | **-** | **Lab ID:** | **6121844509** |
| **Sampling Point:** | | **File Name:** | **M1160467.D** |

| Miscellaneous Ratios | By Areas | By Heights |
|---|---|---|
| **Triaromatic Steroids m/z 231** | | |
| (C20+C21)/Σ TAS | 0.44 | 0.44 |
| TAS #1 20/20+27 | 0.68 | 0.67 |
| TAS #2 21/21+28 | 0.74 | 0.75 |
| %26TAS | 30.0 | 34.8 |
| %27TAS | 38.5 | 35.3 |
| %28TAS | 31.5 | 29.9 |
| %29TAS | 0.0 | 0.0 |
| C28/C26 20S TAS | 1.25 | 1.02 |
| C28/C27 20R TAS | 0.82 | 0.85 |
| | | |
| **Monoaromatic Steroids m/z 253** | | |
| Dia/Regular C27 MAS | 2.35 | 2.33 |
| %27 MAS | 37.6 | 36.6 |
| %28 MAS | 59.2 | 60.5 |
| %29 MAS | 3.2 | 2.9 |
| (C21+C22)/Σ MAS | 0.11 | 0.11 |
| | | |
| TAS/(MAS+TAS) | 0.18 | 0.20 |
| TA28/(TA28+MA29) | 0.59 | 0.64 |
| | | |
| **Triaromatic Methylsteroids m/z 245** | | |
| Dinosteroid Index | 0.48 | 0.51 |
| C4/C3+C4 Mester | 0.59 | 0.59 |
| | | |
| **Phenanthrenes and Naphthalenes** | | |
| MPI-1 | 0.88 | 0.92 |
| MPI-2 | 1.05 | 1.15 |
| Rc(a) if Ro < 1.3 (Ro%) | 0.90 | 0.92 |
| Rc(b) if Ro > 1.3 (Ro%) | 1.77 | 1.75 |
| | | |
| DNR-1 | 10.53 | 7.59 |
| DNR-2 | 2.30 | 2.97 |
| TNR1 | 1.37 | 1.52 |
| | | |
| TDE-1 | 2.73 | 2.74 |
| TDE-2 | 0.35 | 0.44 |
| | | |
| MDR | 11.29 | 13.77 |
| Rm (Ro%) | 7.63 | 15.42 |
| | | |
| MDR23 | 0.37 | 0.37 |
| MDR1 | 0.06 | 0.05 |
| DBT/Phenanthrene | 0.02 | 0.02 |
| | | |
| **New Ratios** | | |
| PNR | 0.35 | 0.37 |
| MDPNR | 0.89 | 0.89 |
| Dinosteroid Index 2 | 0.00 | 0.00 |

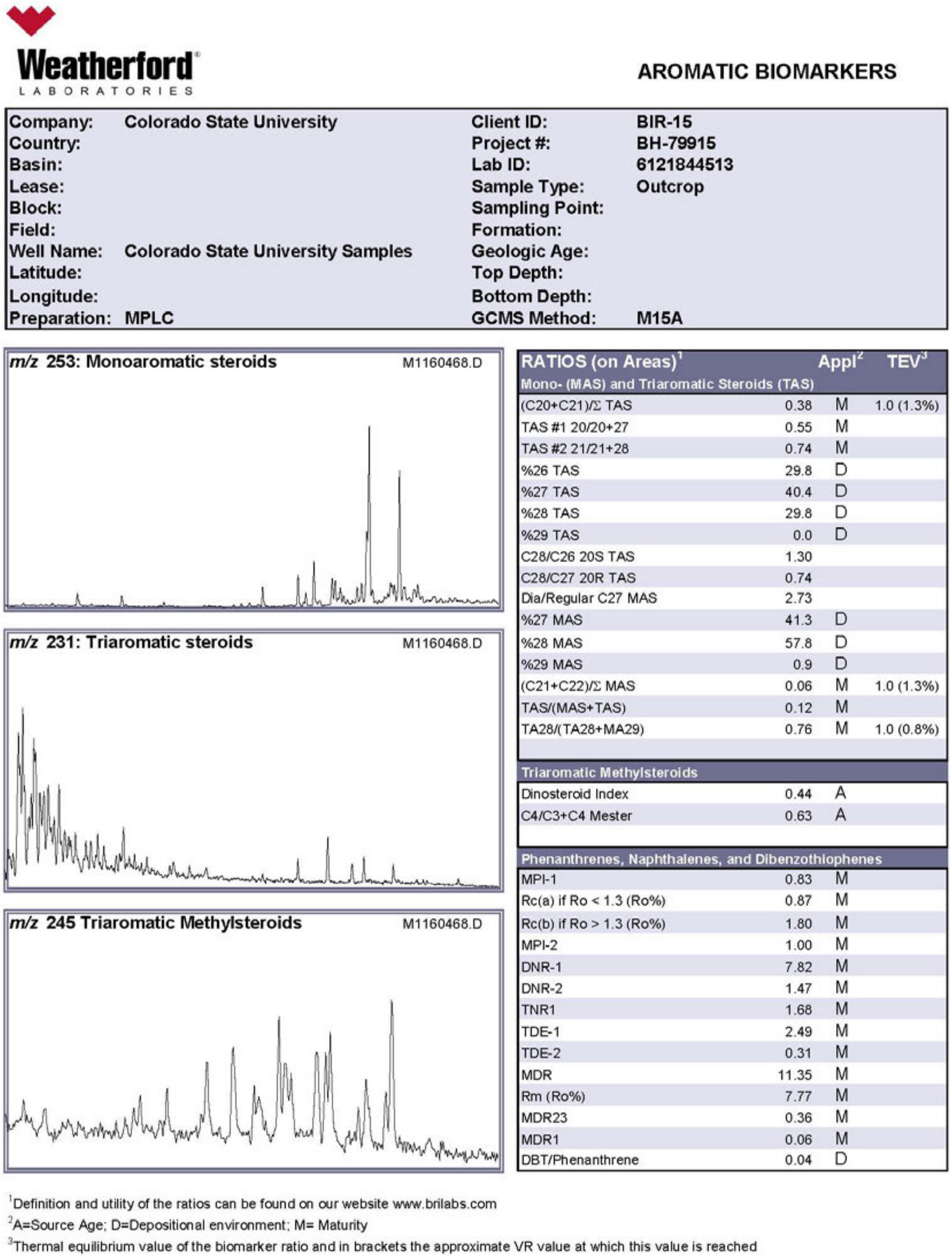

Weatherford LABORATORIES

## AROMATIC BIOMARKERS

|  |  |  |  |
|---|---|---|---|
| **Company:** | **Colorado State University** | **Client ID:** | **BIR-15** |
| **Country:** |  | **Project #:** | **BH-79915** |
| **Basin:** |  | **Lab ID:** | **6121844513** |
| **Lease:** |  | **Sample Type:** | **Outcrop** |
| **Block:** |  | **Sampling Point:** |  |
| **Field:** |  | **Formation:** |  |
| **Well Name:** | **Colorado State University Samples** | **Geologic Age:** |  |
| **Latitude:** |  | **Top Depth:** |  |
| **Longitude:** |  | **Bottom Depth:** |  |
| **Preparation:** | **MPLC** | **GCMS Method:** | **M15A** |

***m/z* 253: Monoaromatic steroids** M1160468.D

***m/z* 231: Triaromatic steroids** M1160468.D

***m/z* 245 Triaromatic Methylsteroids** M1160468.D

| RATIOS (on Areas)[1] |  | Appl[2] | TEV[3] |
|---|---|---|---|
| **Mono- (MAS) and Triaromatic Steroids (TAS)** |  |  |  |
| (C20+C21)/Σ TAS | 0.38 | M | 1.0 (1.3%) |
| TAS #1 20/20+27 | 0.55 | M |  |
| TAS #2 21/21+28 | 0.74 | M |  |
| %26 TAS | 29.8 | D |  |
| %27 TAS | 40.4 | D |  |
| %28 TAS | 29.8 | D |  |
| %29 TAS | 0.0 | D |  |
| C28/C26 20S TAS | 1.30 |  |  |
| C28/C27 20R TAS | 0.74 |  |  |
| Dia/Regular C27 MAS | 2.73 |  |  |
| %27 MAS | 41.3 | D |  |
| %28 MAS | 57.8 | D |  |
| %29 MAS | 0.9 | D |  |
| (C21+C22)/Σ MAS | 0.06 | M | 1.0 (1.3%) |
| TAS/(MAS+TAS) | 0.12 | M |  |
| TA28/(TA28+MA29) | 0.76 | M | 1.0 (0.8%) |
| **Triaromatic Methylsteroids** |  |  |  |
| Dinosteroid Index | 0.44 | A |  |
| C4/C3+C4 Mester | 0.63 | A |  |
| **Phenanthrenes, Naphthalenes, and Dibenzothiophenes** |  |  |  |
| MPI-1 | 0.83 | M |  |
| Rc(a) if Ro < 1.3 (Ro%) | 0.87 | M |  |
| Rc(b) if Ro > 1.3 (Ro%) | 1.80 | M |  |
| MPI-2 | 1.00 | M |  |
| DNR-1 | 7.82 | M |  |
| DNR-2 | 1.47 | M |  |
| TNR1 | 1.68 | M |  |
| TDE-1 | 2.49 | M |  |
| TDE-2 | 0.31 | M |  |
| MDR | 11.35 | M |  |
| Rm (Ro%) | 7.77 | M |  |
| MDR23 | 0.36 | M |  |
| MDR1 | 0.06 | M |  |
| DBT/Phenanthrene | 0.04 | D |  |

[1] Definition and utility of the ratios can be found on our website www.brilabs.com

[2] A=Source Age; D=Depositional environment; M= Maturity

[3] Thermal equilibrium value of the biomarker ratio and in brackets the approximate VR value at which this value is reached

<u>*Appendix F2, ctd.*</u>

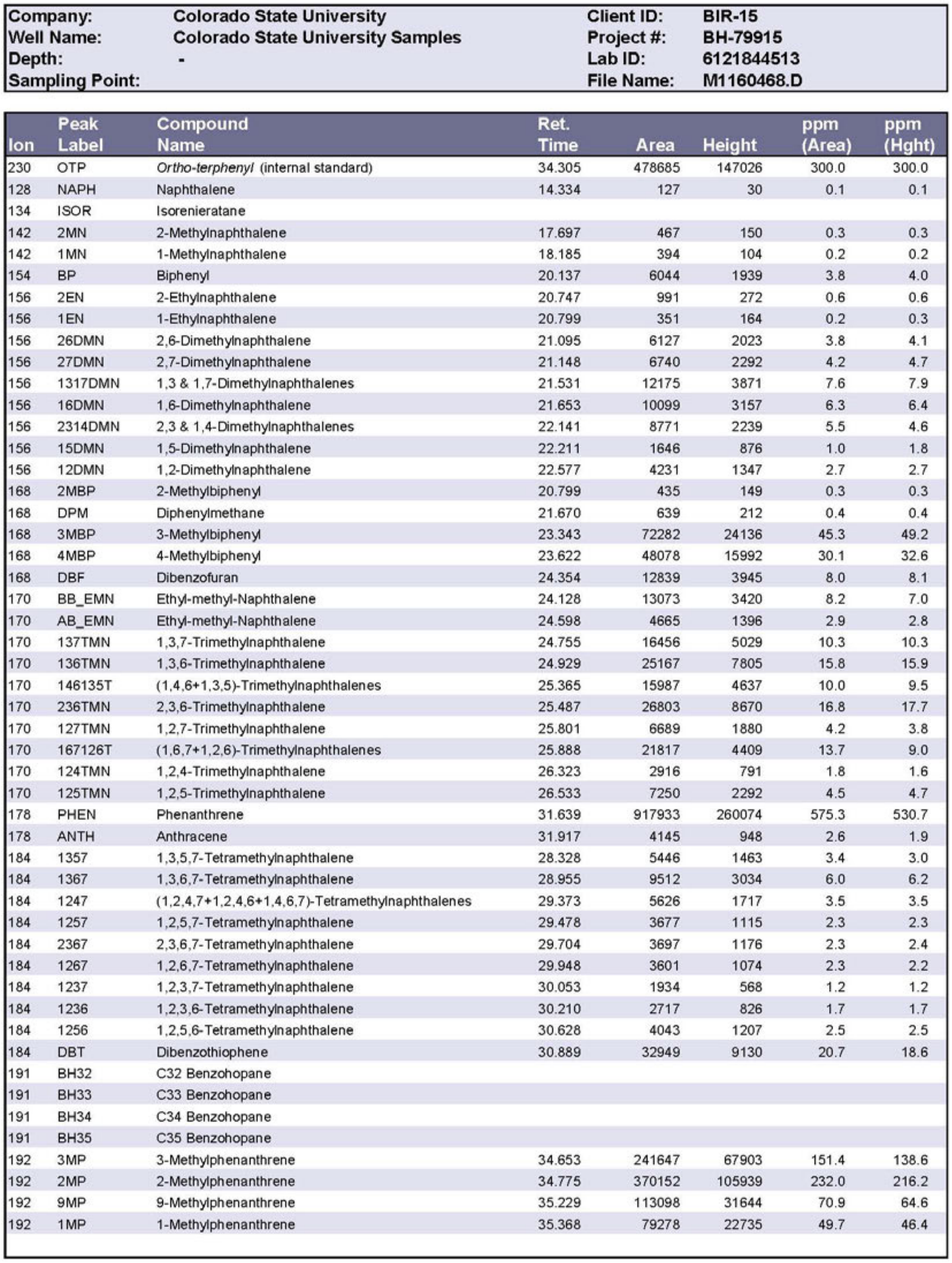

| | | | |
|---|---|---|---|
| **Company:** | **Colorado State University** | **Client ID:** | **BIR-15** |
| **Well Name:** | **Colorado State University Samples** | **Project #:** | **BH-79915** |
| **Depth:** | **-** | **Lab ID:** | **6121844513** |
| **Sampling Point:** | | **File Name:** | **M1160468.D** |

| Ion | Peak Label | Compound Name | Ret. Time | Area | Height | ppm (Area) | ppm (Hght) |
|---|---|---|---|---|---|---|---|
| 230 | OTP | *Ortho-terphenyl* (internal standard) | 34.305 | 478685 | 147026 | 300.0 | 300.0 |
| 128 | NAPH | Naphthalene | 14.334 | 127 | 30 | 0.1 | 0.1 |
| 134 | ISOR | Isorenieratane | | | | | |
| 142 | 2MN | 2-Methylnaphthalene | 17.697 | 467 | 150 | 0.3 | 0.3 |
| 142 | 1MN | 1-Methylnaphthalene | 18.185 | 394 | 104 | 0.2 | 0.2 |
| 154 | BP | Biphenyl | 20.137 | 6044 | 1939 | 3.8 | 4.0 |
| 156 | 2EN | 2-Ethylnaphthalene | 20.747 | 991 | 272 | 0.6 | 0.6 |
| 156 | 1EN | 1-Ethylnaphthalene | 20.799 | 351 | 164 | 0.2 | 0.3 |
| 156 | 26DMN | 2,6-Dimethylnaphthalene | 21.095 | 6127 | 2023 | 3.8 | 4.1 |
| 156 | 27DMN | 2,7-Dimethylnaphthalene | 21.148 | 6740 | 2292 | 4.2 | 4.7 |
| 156 | 1317DMN | 1,3 & 1,7-Dimethylnaphthalenes | 21.531 | 12175 | 3871 | 7.6 | 7.9 |
| 156 | 16DMN | 1,6-Dimethylnaphthalene | 21.653 | 10099 | 3157 | 6.3 | 6.4 |
| 156 | 2314DMN | 2,3 & 1,4-Dimethylnaphthalenes | 22.141 | 8771 | 2239 | 5.5 | 4.6 |
| 156 | 15DMN | 1,5-Dimethylnaphthalene | 22.211 | 1646 | 876 | 1.0 | 1.8 |
| 156 | 12DMN | 1,2-Dimethylnaphthalene | 22.577 | 4231 | 1347 | 2.7 | 2.7 |
| 168 | 2MBP | 2-Methylbiphenyl | 20.799 | 435 | 149 | 0.3 | 0.3 |
| 168 | DPM | Diphenylmethane | 21.670 | 639 | 212 | 0.4 | 0.4 |
| 168 | 3MBP | 3-Methylbiphenyl | 23.343 | 72282 | 24136 | 45.3 | 49.2 |
| 168 | 4MBP | 4-Methylbiphenyl | 23.622 | 48078 | 15992 | 30.1 | 32.6 |
| 168 | DBF | Dibenzofuran | 24.354 | 12839 | 3945 | 8.0 | 8.1 |
| 170 | BB_EMN | Ethyl-methyl-Naphthalene | 24.128 | 13073 | 3420 | 8.2 | 7.0 |
| 170 | AB_EMN | Ethyl-methyl-Naphthalene | 24.598 | 4665 | 1396 | 2.9 | 2.8 |
| 170 | 137TMN | 1,3,7-Trimethylnaphthalene | 24.755 | 16456 | 5029 | 10.3 | 10.3 |
| 170 | 136TMN | 1,3,6-Trimethylnaphthalene | 24.929 | 25167 | 7805 | 15.8 | 15.9 |
| 170 | 146135T | (1,4,6+1,3,5)-Trimethylnaphthalenes | 25.365 | 15987 | 4637 | 10.0 | 9.5 |
| 170 | 236TMN | 2,3,6-Trimethylnaphthalene | 25.487 | 26803 | 8670 | 16.8 | 17.7 |
| 170 | 127TMN | 1,2,7-Trimethylnaphthalene | 25.801 | 6689 | 1880 | 4.2 | 3.8 |
| 170 | 167126T | (1,6,7+1,2,6)-Trimethylnaphthalenes | 25.888 | 21817 | 4409 | 13.7 | 9.0 |
| 170 | 124TMN | 1,2,4-Trimethylnaphthalene | 26.323 | 2916 | 791 | 1.8 | 1.6 |
| 170 | 125TMN | 1,2,5-Trimethylnaphthalene | 26.533 | 7250 | 2292 | 4.5 | 4.7 |
| 178 | PHEN | Phenanthrene | 31.639 | 917933 | 260074 | 575.3 | 530.7 |
| 178 | ANTH | Anthracene | 31.917 | 4145 | 948 | 2.6 | 1.9 |
| 184 | 1357 | 1,3,5,7-Tetramethylnaphthalene | 28.328 | 5446 | 1463 | 3.4 | 3.0 |
| 184 | 1367 | 1,3,6,7-Tetramethylnaphthalene | 28.955 | 9512 | 3034 | 6.0 | 6.2 |
| 184 | 1247 | (1,2,4,7+1,2,4,6+1,4,6,7)-Tetramethylnaphthalenes | 29.373 | 5626 | 1717 | 3.5 | 3.5 |
| 184 | 1257 | 1,2,5,7-Tetramethylnaphthalene | 29.478 | 3677 | 1115 | 2.3 | 2.3 |
| 184 | 2367 | 2,3,6,7-Tetramethylnaphthalene | 29.704 | 3697 | 1176 | 2.3 | 2.4 |
| 184 | 1267 | 1,2,6,7-Tetramethylnaphthalene | 29.948 | 3601 | 1074 | 2.3 | 2.2 |
| 184 | 1237 | 1,2,3,7-Tetramethylnaphthalene | 30.053 | 1934 | 568 | 1.2 | 1.2 |
| 184 | 1236 | 1,2,3,6-Tetramethylnaphthalene | 30.210 | 2717 | 826 | 1.7 | 1.7 |
| 184 | 1256 | 1,2,5,6-Tetramethylnaphthalene | 30.628 | 4043 | 1207 | 2.5 | 2.5 |
| 184 | DBT | Dibenzothiophene | 30.889 | 32949 | 9130 | 20.7 | 18.6 |
| 191 | BH32 | C32 Benzohopane | | | | | |
| 191 | BH33 | C33 Benzohopane | | | | | |
| 191 | BH34 | C34 Benzohopane | | | | | |
| 191 | BH35 | C35 Benzohopane | | | | | |
| 192 | 3MP | 3-Methylphenanthrene | 34.653 | 241647 | 67903 | 151.4 | 138.6 |
| 192 | 2MP | 2-Methylphenanthrene | 34.775 | 370152 | 105939 | 232.0 | 216.2 |
| 192 | 9MP | 9-Methylphenanthrene | 35.229 | 113098 | 31644 | 70.9 | 64.6 |
| 192 | 1MP | 1-Methylphenanthrene | 35.368 | 79278 | 22735 | 49.7 | 46.4 |

*Appendix F2, ctd.*

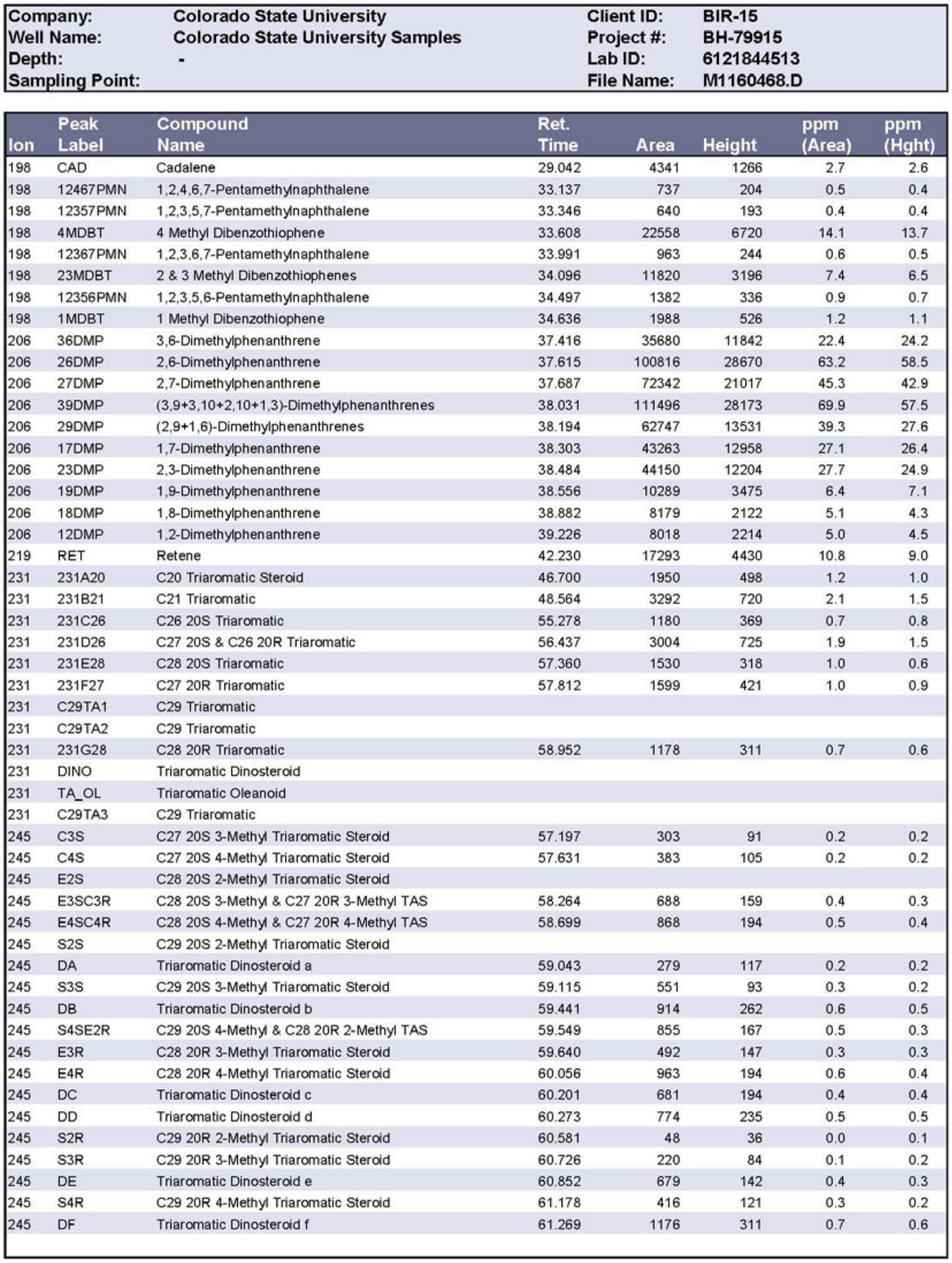

| | | | |
|---|---|---|---|
| **Company:** | **Colorado State University** | **Client ID:** | **BIR-15** |
| **Well Name:** | **Colorado State University Samples** | **Project #:** | **BH-79915** |
| **Depth:** | **-** | **Lab ID:** | **6121844513** |
| **Sampling Point:** | | **File Name:** | **M1160468.D** |

| Ion | Peak Label | Compound Name | Ret. Time | Area | Height | ppm (Area) | ppm (Hght) |
|---|---|---|---|---|---|---|---|
| 198 | CAD | Cadalene | 29.042 | 4341 | 1266 | 2.7 | 2.6 |
| 198 | 12467PMN | 1,2,4,6,7-Pentamethylnaphthalene | 33.137 | 737 | 204 | 0.5 | 0.4 |
| 198 | 12357PMN | 1,2,3,5,7-Pentamethylnaphthalene | 33.346 | 640 | 193 | 0.4 | 0.4 |
| 198 | 4MDBT | 4 Methyl Dibenzothiophene | 33.608 | 22558 | 6720 | 14.1 | 13.7 |
| 198 | 12367PMN | 1,2,3,6,7-Pentamethylnaphthalene | 33.991 | 963 | 244 | 0.6 | 0.5 |
| 198 | 23MDBT | 2 & 3 Methyl Dibenzothiophenes | 34.096 | 11820 | 3196 | 7.4 | 6.5 |
| 198 | 12356PMN | 1,2,3,5,6-Pentamethylnaphthalene | 34.497 | 1382 | 336 | 0.9 | 0.7 |
| 198 | 1MDBT | 1 Methyl Dibenzothiophene | 34.636 | 1988 | 526 | 1.2 | 1.1 |
| 206 | 36DMP | 3,6-Dimethylphenanthrene | 37.416 | 35680 | 11842 | 22.4 | 24.2 |
| 206 | 26DMP | 2,6-Dimethylphenanthrene | 37.615 | 100816 | 28670 | 63.2 | 58.5 |
| 206 | 27DMP | 2,7-Dimethylphenanthrene | 37.687 | 72342 | 21017 | 45.3 | 42.9 |
| 206 | 39DMP | (3,9+3,10+2,10+1,3)-Dimethylphenanthrenes | 38.031 | 111496 | 28173 | 69.9 | 57.5 |
| 206 | 29DMP | (2,9+1,6)-Dimethylphenanthrenes | 38.194 | 62747 | 13531 | 39.3 | 27.6 |
| 206 | 17DMP | 1,7-Dimethylphenanthrene | 38.303 | 43263 | 12958 | 27.1 | 26.4 |
| 206 | 23DMP | 2,3-Dimethylphenanthrene | 38.484 | 44150 | 12204 | 27.7 | 24.9 |
| 206 | 19DMP | 1,9-Dimethylphenanthrene | 38.556 | 10289 | 3475 | 6.4 | 7.1 |
| 206 | 18DMP | 1,8-Dimethylphenanthrene | 38.882 | 8179 | 2122 | 5.1 | 4.3 |
| 206 | 12DMP | 1,2-Dimethylphenanthrene | 39.226 | 8018 | 2214 | 5.0 | 4.5 |
| 219 | RET | Retene | 42.230 | 17293 | 4430 | 10.8 | 9.0 |
| 231 | 231A20 | C20 Triaromatic Steroid | 46.700 | 1950 | 498 | 1.2 | 1.0 |
| 231 | 231B21 | C21 Triaromatic | 48.564 | 3292 | 720 | 2.1 | 1.5 |
| 231 | 231C26 | C26 20S Triaromatic | 55.278 | 1180 | 369 | 0.7 | 0.8 |
| 231 | 231D26 | C27 20S & C26 20R Triaromatic | 56.437 | 3004 | 725 | 1.9 | 1.5 |
| 231 | 231E28 | C28 20S Triaromatic | 57.360 | 1530 | 318 | 1.0 | 0.6 |
| 231 | 231F27 | C27 20R Triaromatic | 57.812 | 1599 | 421 | 1.0 | 0.9 |
| 231 | C29TA1 | C29 Triaromatic | | | | | |
| 231 | C29TA2 | C29 Triaromatic | | | | | |
| 231 | 231G28 | C28 20R Triaromatic | 58.952 | 1178 | 311 | 0.7 | 0.6 |
| 231 | DINO | Triaromatic Dinosteroid | | | | | |
| 231 | TA_OL | Triaromatic Oleanoid | | | | | |
| 231 | C29TA3 | C29 Triaromatic | | | | | |
| 245 | C3S | C27 20S 3-Methyl Triaromatic Steroid | 57.197 | 303 | 91 | 0.2 | 0.2 |
| 245 | C4S | C27 20S 4-Methyl Triaromatic Steroid | 57.631 | 383 | 105 | 0.2 | 0.2 |
| 245 | E2S | C28 20S 2-Methyl Triaromatic Steroid | | | | | |
| 245 | E3SC3R | C28 20S 3-Methyl & C27 20R 3-Methyl TAS | 58.264 | 688 | 159 | 0.4 | 0.3 |
| 245 | E4SC4R | C28 20S 4-Methyl & C27 20R 4-Methyl TAS | 58.699 | 868 | 194 | 0.5 | 0.4 |
| 245 | S2S | C29 20S 2-Methyl Triaromatic Steroid | | | | | |
| 245 | DA | Triaromatic Dinosteroid a | 59.043 | 279 | 117 | 0.2 | 0.2 |
| 245 | S3S | C29 20S 3-Methyl Triaromatic Steroid | 59.115 | 551 | 93 | 0.3 | 0.2 |
| 245 | DB | Triaromatic Dinosteroid b | 59.441 | 914 | 262 | 0.6 | 0.5 |
| 245 | S4SE2R | C29 20S 4-Methyl & C28 20R 2-Methyl TAS | 59.549 | 855 | 167 | 0.5 | 0.3 |
| 245 | E3R | C28 20R 3-Methyl Triaromatic Steroid | 59.640 | 492 | 147 | 0.3 | 0.3 |
| 245 | E4R | C28 20R 4-Methyl Triaromatic Steroid | 60.056 | 963 | 194 | 0.6 | 0.4 |
| 245 | DC | Triaromatic Dinosteroid c | 60.201 | 681 | 194 | 0.4 | 0.4 |
| 245 | DD | Triaromatic Dinosteroid d | 60.273 | 774 | 235 | 0.5 | 0.5 |
| 245 | S2R | C29 20R 2-Methyl Triaromatic Steroid | 60.581 | 48 | 36 | 0.0 | 0.1 |
| 245 | S3R | C29 20R 3-Methyl Triaromatic Steroid | 60.726 | 220 | 84 | 0.1 | 0.2 |
| 245 | DE | Triaromatic Dinosteroid e | 60.852 | 679 | 142 | 0.4 | 0.3 |
| 245 | S4R | C29 20R 4-Methyl Triaromatic Steroid | 61.178 | 416 | 121 | 0.3 | 0.2 |
| 245 | DF | Triaromatic Dinosteroid f | 61.269 | 1176 | 311 | 0.7 | 0.6 |

*Appendix F2, ctd.*

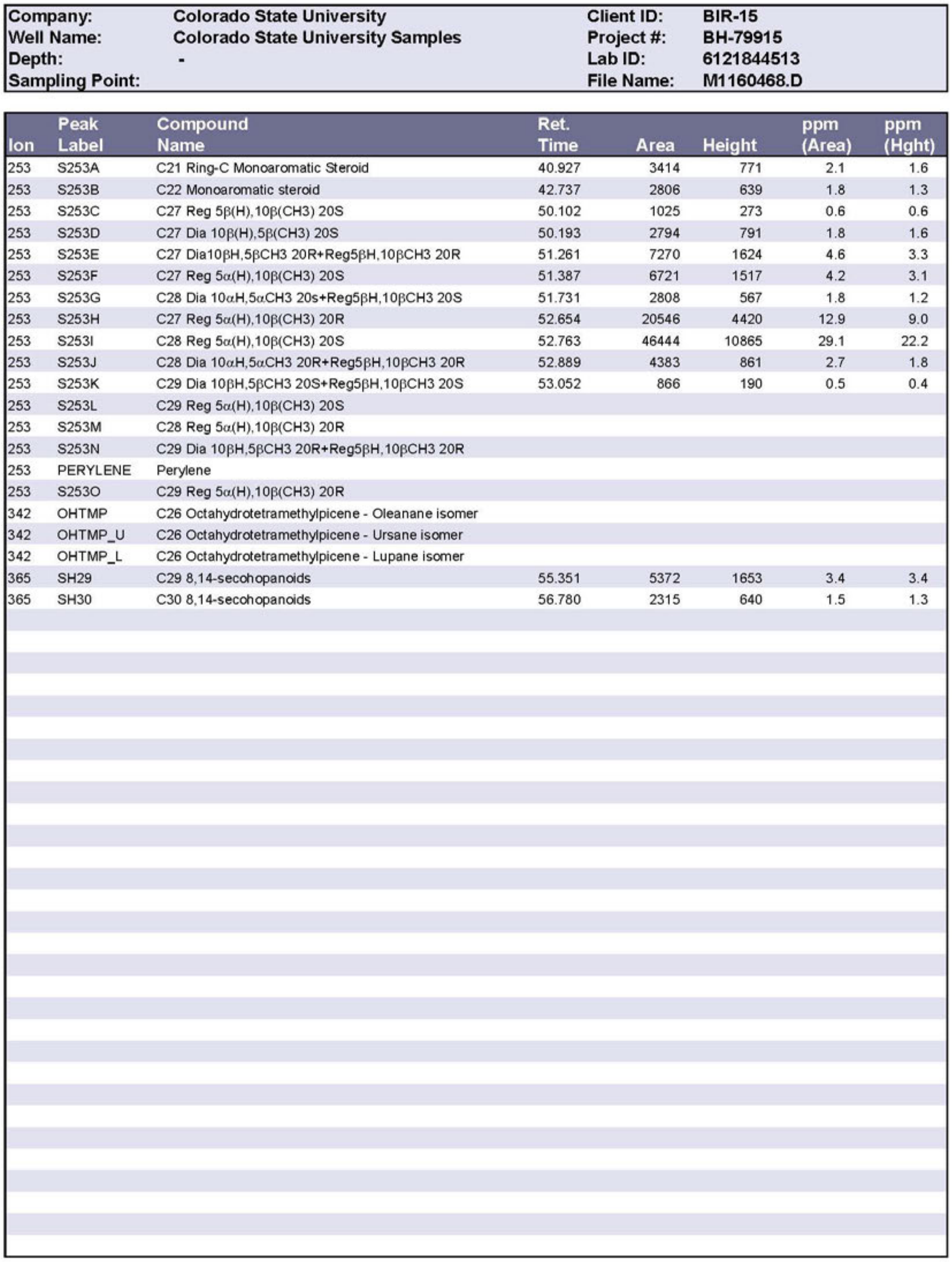

| | | | |
|---|---|---|---|
| **Company:** | **Colorado State University** | **Client ID:** | **BIR-15** |
| **Well Name:** | **Colorado State University Samples** | **Project #:** | **BH-79915** |
| **Depth:** | **-** | **Lab ID:** | **6121844513** |
| **Sampling Point:** | | **File Name:** | **M1160468.D** |

| Ion | Peak Label | Compound Name | Ret. Time | Area | Height | ppm (Area) | ppm (Hght) |
|---|---|---|---|---|---|---|---|
| 253 | S253A | C21 Ring-C Monoaromatic Steroid | 40.927 | 3414 | 771 | 2.1 | 1.6 |
| 253 | S253B | C22 Monoaromatic steroid | 42.737 | 2806 | 639 | 1.8 | 1.3 |
| 253 | S253C | C27 Reg 5β(H),10β(CH3) 20S | 50.102 | 1025 | 273 | 0.6 | 0.6 |
| 253 | S253D | C27 Dia 10β(H),5β(CH3) 20S | 50.193 | 2794 | 791 | 1.8 | 1.6 |
| 253 | S253E | C27 Dia10βH,5βCH3 20R+Reg5βH,10βCH3 20R | 51.261 | 7270 | 1624 | 4.6 | 3.3 |
| 253 | S253F | C27 Reg 5α(H),10β(CH3) 20S | 51.387 | 6721 | 1517 | 4.2 | 3.1 |
| 253 | S253G | C28 Dia 10αH,5αCH3 20s+Reg5βH,10βCH3 20S | 51.731 | 2808 | 567 | 1.8 | 1.2 |
| 253 | S253H | C27 Reg 5α(H),10β(CH3) 20R | 52.654 | 20546 | 4420 | 12.9 | 9.0 |
| 253 | S253I | C28 Reg 5α(H),10β(CH3) 20S | 52.763 | 46444 | 10865 | 29.1 | 22.2 |
| 253 | S253J | C28 Dia 10αH,5αCH3 20R+Reg5βH,10βCH3 20R | 52.889 | 4383 | 861 | 2.7 | 1.8 |
| 253 | S253K | C29 Dia 10βH,5βCH3 20S+Reg5βH,10βCH3 20S | 53.052 | 866 | 190 | 0.5 | 0.4 |
| 253 | S253L | C29 Reg 5α(H),10β(CH3) 20S | | | | | |
| 253 | S253M | C28 Reg 5α(H),10β(CH3) 20R | | | | | |
| 253 | S253N | C29 Dia 10βH,5βCH3 20R+Reg5βH,10βCH3 20R | | | | | |
| 253 | PERYLENE | Perylene | | | | | |
| 253 | S253O | C29 Reg 5α(H),10β(CH3) 20R | | | | | |
| 342 | OHTMP | C26 Octahydrotetramethylpicene - Oleanane isomer | | | | | |
| 342 | OHTMP_U | C26 Octahydrotetramethylpicene - Ursane isomer | | | | | |
| 342 | OHTMP_L | C26 Octahydrotetramethylpicene - Lupane isomer | | | | | |
| 365 | SH29 | C29 8,14-secohopanoids | 55.351 | 5372 | 1653 | 3.4 | 3.4 |
| 365 | SH30 | C30 8,14-secohopanoids | 56.780 | 2315 | 640 | 1.5 | 1.3 |

<u>*Appendix F2, ctd.*</u>

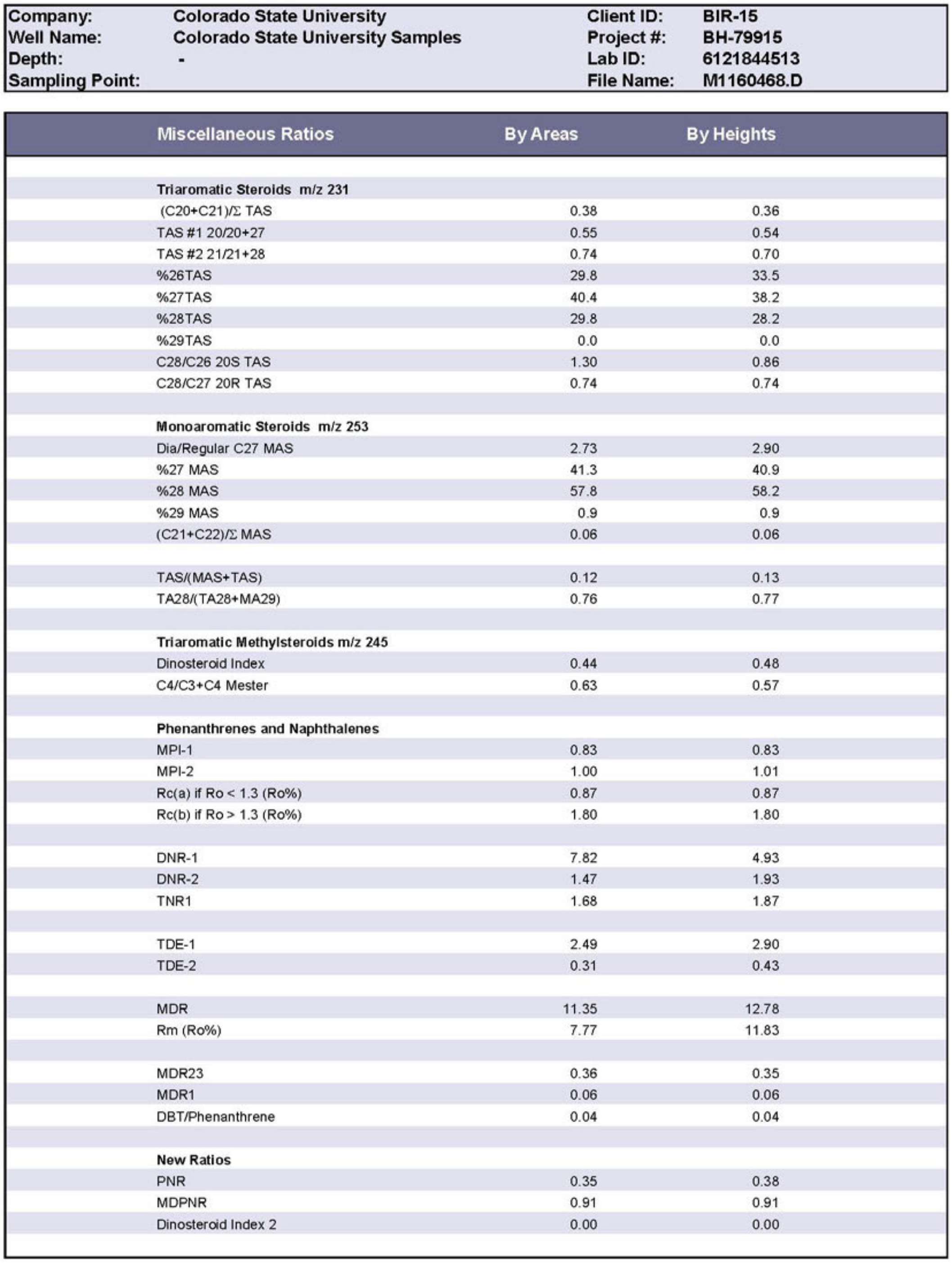

| | | | |
|---|---|---|---|
| **Company:** | **Colorado State University** | **Client ID:** | **BIR-15** |
| **Well Name:** | **Colorado State University Samples** | **Project #:** | **BH-79915** |
| **Depth:** | **-** | **Lab ID:** | **6121844513** |
| **Sampling Point:** | | **File Name:** | **M1160468.D** |

| Miscellaneous Ratios | By Areas | By Heights |
|---|---|---|
| **Triaromatic Steroids m/z 231** | | |
| (C20+C21)/Σ TAS | 0.38 | 0.36 |
| TAS #1 20/20+27 | 0.55 | 0.54 |
| TAS #2 21/21+28 | 0.74 | 0.70 |
| %26TAS | 29.8 | 33.5 |
| %27TAS | 40.4 | 38.2 |
| %28TAS | 29.8 | 28.2 |
| %29TAS | 0.0 | 0.0 |
| C28/C26 20S TAS | 1.30 | 0.86 |
| C28/C27 20R TAS | 0.74 | 0.74 |
| | | |
| **Monoaromatic Steroids m/z 253** | | |
| Dia/Regular C27 MAS | 2.73 | 2.90 |
| %27 MAS | 41.3 | 40.9 |
| %28 MAS | 57.8 | 58.2 |
| %29 MAS | 0.9 | 0.9 |
| (C21+C22)/Σ MAS | 0.06 | 0.06 |
| | | |
| TAS/(MAS+TAS) | 0.12 | 0.13 |
| TA28/(TA28+MA29) | 0.76 | 0.77 |
| | | |
| **Triaromatic Methylsteroids m/z 245** | | |
| Dinosteroid Index | 0.44 | 0.48 |
| C4/C3+C4 Mester | 0.63 | 0.57 |
| | | |
| **Phenanthrenes and Naphthalenes** | | |
| MPI-1 | 0.83 | 0.83 |
| MPI-2 | 1.00 | 1.01 |
| Rc(a) if Ro < 1.3 (Ro%) | 0.87 | 0.87 |
| Rc(b) if Ro > 1.3 (Ro%) | 1.80 | 1.80 |
| | | |
| DNR-1 | 7.82 | 4.93 |
| DNR-2 | 1.47 | 1.93 |
| TNR1 | 1.68 | 1.87 |
| | | |
| TDE-1 | 2.49 | 2.90 |
| TDE-2 | 0.31 | 0.43 |
| | | |
| MDR | 11.35 | 12.78 |
| Rm (Ro%) | 7.77 | 11.83 |
| | | |
| MDR23 | 0.36 | 0.35 |
| MDR1 | 0.06 | 0.06 |
| DBT/Phenanthrene | 0.04 | 0.04 |
| | | |
| **New Ratios** | | |
| PNR | 0.35 | 0.38 |
| MDPNR | 0.91 | 0.91 |
| Dinosteroid Index 2 | 0.00 | 0.00 |

*Appendix F2, ctd.*

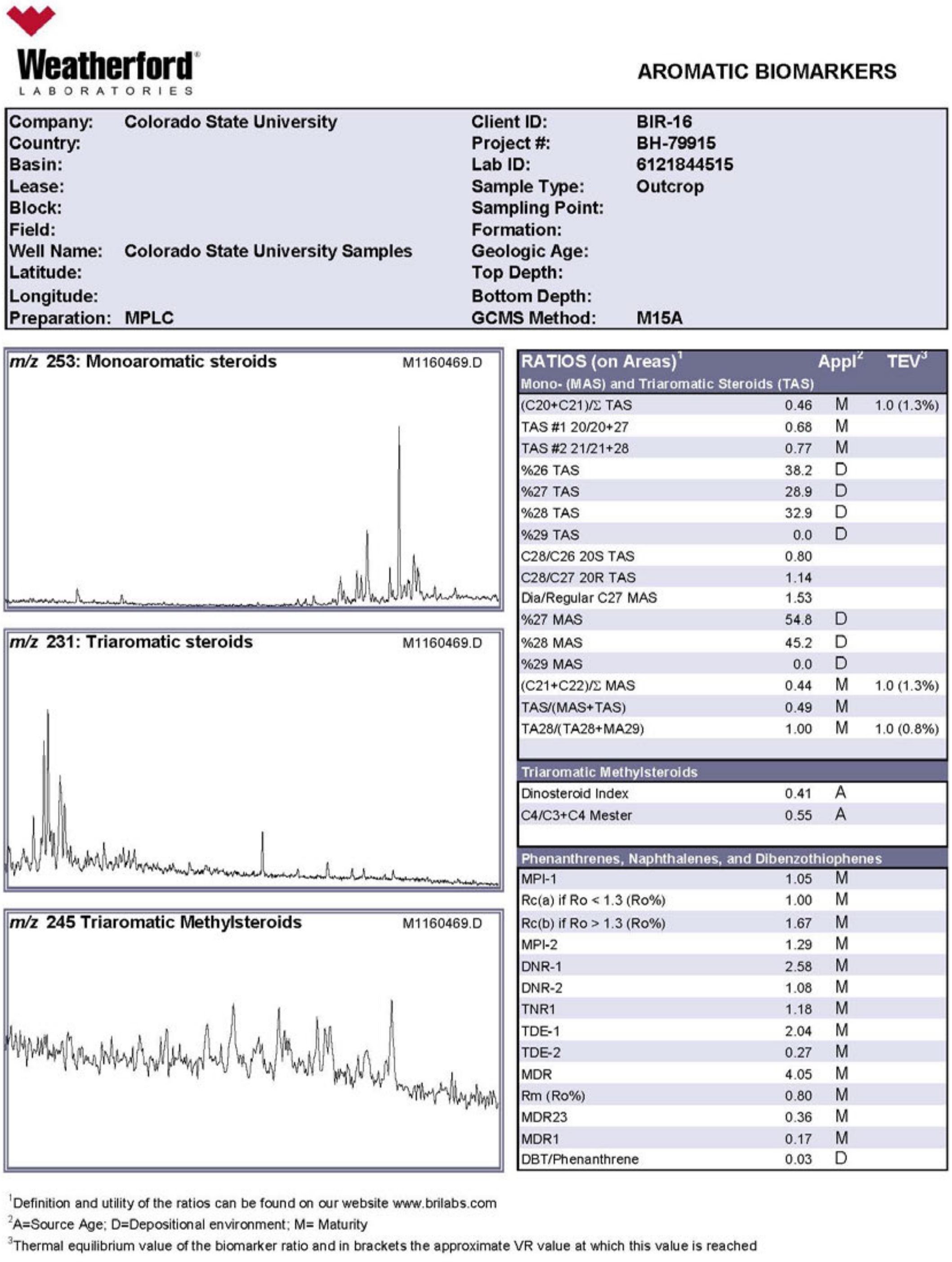

Weatherford LABORATORIES

**AROMATIC BIOMARKERS**

| | | | |
|---|---|---|---|
| **Company:** | **Colorado State University** | **Client ID:** | **BIR-16** |
| **Country:** | | **Project #:** | **BH-79915** |
| **Basin:** | | **Lab ID:** | **6121844515** |
| **Lease:** | | **Sample Type:** | **Outcrop** |
| **Block:** | | **Sampling Point:** | |
| **Field:** | | **Formation:** | |
| **Well Name:** | **Colorado State University Samples** | **Geologic Age:** | |
| **Latitude:** | | **Top Depth:** | |
| **Longitude:** | | **Bottom Depth:** | |
| **Preparation:** | **MPLC** | **GCMS Method:** | **M15A** |

***m/z* 253: Monoaromatic steroids** M1160469.D

***m/z* 231: Triaromatic steroids** M1160469.D

***m/z* 245 Triaromatic Methylsteroids** M1160469.D

| RATIOS (on Areas)[1] | | Appl[2] | TEV[3] |
|---|---|---|---|
| **Mono- (MAS) and Triaromatic Steroids (TAS)** | | | |
| (C20+C21)/Σ TAS | 0.46 | M | 1.0 (1.3%) |
| TAS #1 20/20+27 | 0.68 | M | |
| TAS #2 21/21+28 | 0.77 | M | |
| %26 TAS | 38.2 | D | |
| %27 TAS | 28.9 | D | |
| %28 TAS | 32.9 | D | |
| %29 TAS | 0.0 | D | |
| C28/C26 20S TAS | 0.80 | | |
| C28/C27 20R TAS | 1.14 | | |
| Dia/Regular C27 MAS | 1.53 | | |
| %27 MAS | 54.8 | D | |
| %28 MAS | 45.2 | D | |
| %29 MAS | 0.0 | D | |
| (C21+C22)/Σ MAS | 0.44 | M | 1.0 (1.3%) |
| TAS/(MAS+TAS) | 0.49 | M | |
| TA28/(TA28+MA29) | 1.00 | M | 1.0 (0.8%) |
| **Triaromatic Methylsteroids** | | | |
| Dinosteroid Index | 0.41 | A | |
| C4/C3+C4 Mester | 0.55 | A | |
| **Phenanthrenes, Naphthalenes, and Dibenzothiophenes** | | | |
| MPI-1 | 1.05 | M | |
| Rc(a) if Ro < 1.3 (Ro%) | 1.00 | M | |
| Rc(b) if Ro > 1.3 (Ro%) | 1.67 | M | |
| MPI-2 | 1.29 | M | |
| DNR-1 | 2.58 | M | |
| DNR-2 | 1.08 | M | |
| TNR1 | 1.18 | M | |
| TDE-1 | 2.04 | M | |
| TDE-2 | 0.27 | M | |
| MDR | 4.05 | M | |
| Rm (Ro%) | 0.80 | M | |
| MDR23 | 0.36 | M | |
| MDR1 | 0.17 | M | |
| DBT/Phenanthrene | 0.03 | D | |

[1] Definition and utility of the ratios can be found on our website www.brilabs.com

[2] A=Source Age; D=Depositional environment; M= Maturity

[3] Thermal equilibrium value of the biomarker ratio and in brackets the approximate VR value at which this value is reached

*Appendix F2, ctd.*

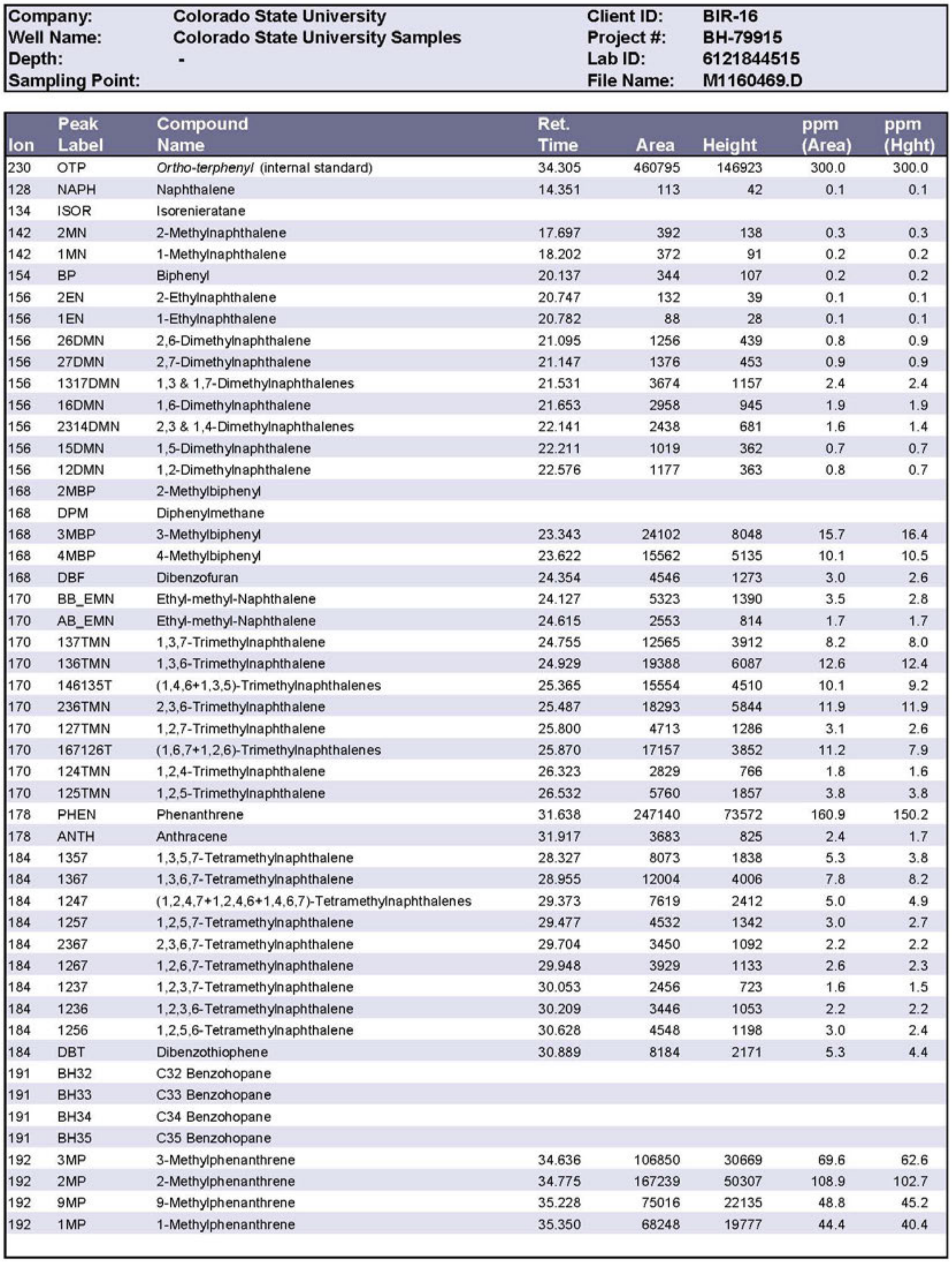

| | | | |
|---|---|---|---|
| **Company:** | **Colorado State University** | **Client ID:** | **BIR-16** |
| **Well Name:** | **Colorado State University Samples** | **Project #:** | **BH-79915** |
| **Depth:** | **-** | **Lab ID:** | **6121844515** |
| **Sampling Point:** | | **File Name:** | **M1160469.D** |

| Ion | Peak Label | Compound Name | Ret. Time | Area | Height | ppm (Area) | ppm (Hght) |
|---|---|---|---|---|---|---|---|
| 230 | OTP | *Ortho-terphenyl* (internal standard) | 34.305 | 460795 | 146923 | 300.0 | 300.0 |
| 128 | NAPH | Naphthalene | 14.351 | 113 | 42 | 0.1 | 0.1 |
| 134 | ISOR | Isorenieratane | | | | | |
| 142 | 2MN | 2-Methylnaphthalene | 17.697 | 392 | 138 | 0.3 | 0.3 |
| 142 | 1MN | 1-Methylnaphthalene | 18.202 | 372 | 91 | 0.2 | 0.2 |
| 154 | BP | Biphenyl | 20.137 | 344 | 107 | 0.2 | 0.2 |
| 156 | 2EN | 2-Ethylnaphthalene | 20.747 | 132 | 39 | 0.1 | 0.1 |
| 156 | 1EN | 1-Ethylnaphthalene | 20.782 | 88 | 28 | 0.1 | 0.1 |
| 156 | 26DMN | 2,6-Dimethylnaphthalene | 21.095 | 1256 | 439 | 0.8 | 0.9 |
| 156 | 27DMN | 2,7-Dimethylnaphthalene | 21.147 | 1376 | 453 | 0.9 | 0.9 |
| 156 | 1317DMN | 1,3 & 1,7-Dimethylnaphthalenes | 21.531 | 3674 | 1157 | 2.4 | 2.4 |
| 156 | 16DMN | 1,6-Dimethylnaphthalene | 21.653 | 2958 | 945 | 1.9 | 1.9 |
| 156 | 2314DMN | 2,3 & 1,4-Dimethylnaphthalenes | 22.141 | 2438 | 681 | 1.6 | 1.4 |
| 156 | 15DMN | 1,5-Dimethylnaphthalene | 22.211 | 1019 | 362 | 0.7 | 0.7 |
| 156 | 12DMN | 1,2-Dimethylnaphthalene | 22.576 | 1177 | 363 | 0.8 | 0.7 |
| 168 | 2MBP | 2-Methylbiphenyl | | | | | |
| 168 | DPM | Diphenylmethane | | | | | |
| 168 | 3MBP | 3-Methylbiphenyl | 23.343 | 24102 | 8048 | 15.7 | 16.4 |
| 168 | 4MBP | 4-Methylbiphenyl | 23.622 | 15562 | 5135 | 10.1 | 10.5 |
| 168 | DBF | Dibenzofuran | 24.354 | 4546 | 1273 | 3.0 | 2.6 |
| 170 | BB_EMN | Ethyl-methyl-Naphthalene | 24.127 | 5323 | 1390 | 3.5 | 2.8 |
| 170 | AB_EMN | Ethyl-methyl-Naphthalene | 24.615 | 2553 | 814 | 1.7 | 1.7 |
| 170 | 137TMN | 1,3,7-Trimethylnaphthalene | 24.755 | 12565 | 3912 | 8.2 | 8.0 |
| 170 | 136TMN | 1,3,6-Trimethylnaphthalene | 24.929 | 19388 | 6087 | 12.6 | 12.4 |
| 170 | 146135T | (1,4,6+1,3,5)-Trimethylnaphthalenes | 25.365 | 15554 | 4510 | 10.1 | 9.2 |
| 170 | 236TMN | 2,3,6-Trimethylnaphthalene | 25.487 | 18293 | 5844 | 11.9 | 11.9 |
| 170 | 127TMN | 1,2,7-Trimethylnaphthalene | 25.800 | 4713 | 1286 | 3.1 | 2.6 |
| 170 | 167126T | (1,6,7+1,2,6)-Trimethylnaphthalenes | 25.870 | 17157 | 3852 | 11.2 | 7.9 |
| 170 | 124TMN | 1,2,4-Trimethylnaphthalene | 26.323 | 2829 | 766 | 1.8 | 1.6 |
| 170 | 125TMN | 1,2,5-Trimethylnaphthalene | 26.532 | 5760 | 1857 | 3.8 | 3.8 |
| 178 | PHEN | Phenanthrene | 31.638 | 247140 | 73572 | 160.9 | 150.2 |
| 178 | ANTH | Anthracene | 31.917 | 3683 | 825 | 2.4 | 1.7 |
| 184 | 1357 | 1,3,5,7-Tetramethylnaphthalene | 28.327 | 8073 | 1838 | 5.3 | 3.8 |
| 184 | 1367 | 1,3,6,7-Tetramethylnaphthalene | 28.955 | 12004 | 4006 | 7.8 | 8.2 |
| 184 | 1247 | (1,2,4,7+1,2,4,6+1,4,6,7)-Tetramethylnaphthalenes | 29.373 | 7619 | 2412 | 5.0 | 4.9 |
| 184 | 1257 | 1,2,5,7-Tetramethylnaphthalene | 29.477 | 4532 | 1342 | 3.0 | 2.7 |
| 184 | 2367 | 2,3,6,7-Tetramethylnaphthalene | 29.704 | 3450 | 1092 | 2.2 | 2.2 |
| 184 | 1267 | 1,2,6,7-Tetramethylnaphthalene | 29.948 | 3929 | 1133 | 2.6 | 2.3 |
| 184 | 1237 | 1,2,3,7-Tetramethylnaphthalene | 30.053 | 2456 | 723 | 1.6 | 1.5 |
| 184 | 1236 | 1,2,3,6-Tetramethylnaphthalene | 30.209 | 3446 | 1053 | 2.2 | 2.2 |
| 184 | 1256 | 1,2,5,6-Tetramethylnaphthalene | 30.628 | 4548 | 1198 | 3.0 | 2.4 |
| 184 | DBT | Dibenzothiophene | 30.889 | 8184 | 2171 | 5.3 | 4.4 |
| 191 | BH32 | C32 Benzohopane | | | | | |
| 191 | BH33 | C33 Benzohopane | | | | | |
| 191 | BH34 | C34 Benzohopane | | | | | |
| 191 | BH35 | C35 Benzohopane | | | | | |
| 192 | 3MP | 3-Methylphenanthrene | 34.636 | 106850 | 30669 | 69.6 | 62.6 |
| 192 | 2MP | 2-Methylphenanthrene | 34.775 | 167239 | 50307 | 108.9 | 102.7 |
| 192 | 9MP | 9-Methylphenanthrene | 35.228 | 75016 | 22135 | 48.8 | 45.2 |
| 192 | 1MP | 1-Methylphenanthrene | 35.350 | 68248 | 19777 | 44.4 | 40.4 |

*Appendix F2, ctd.*

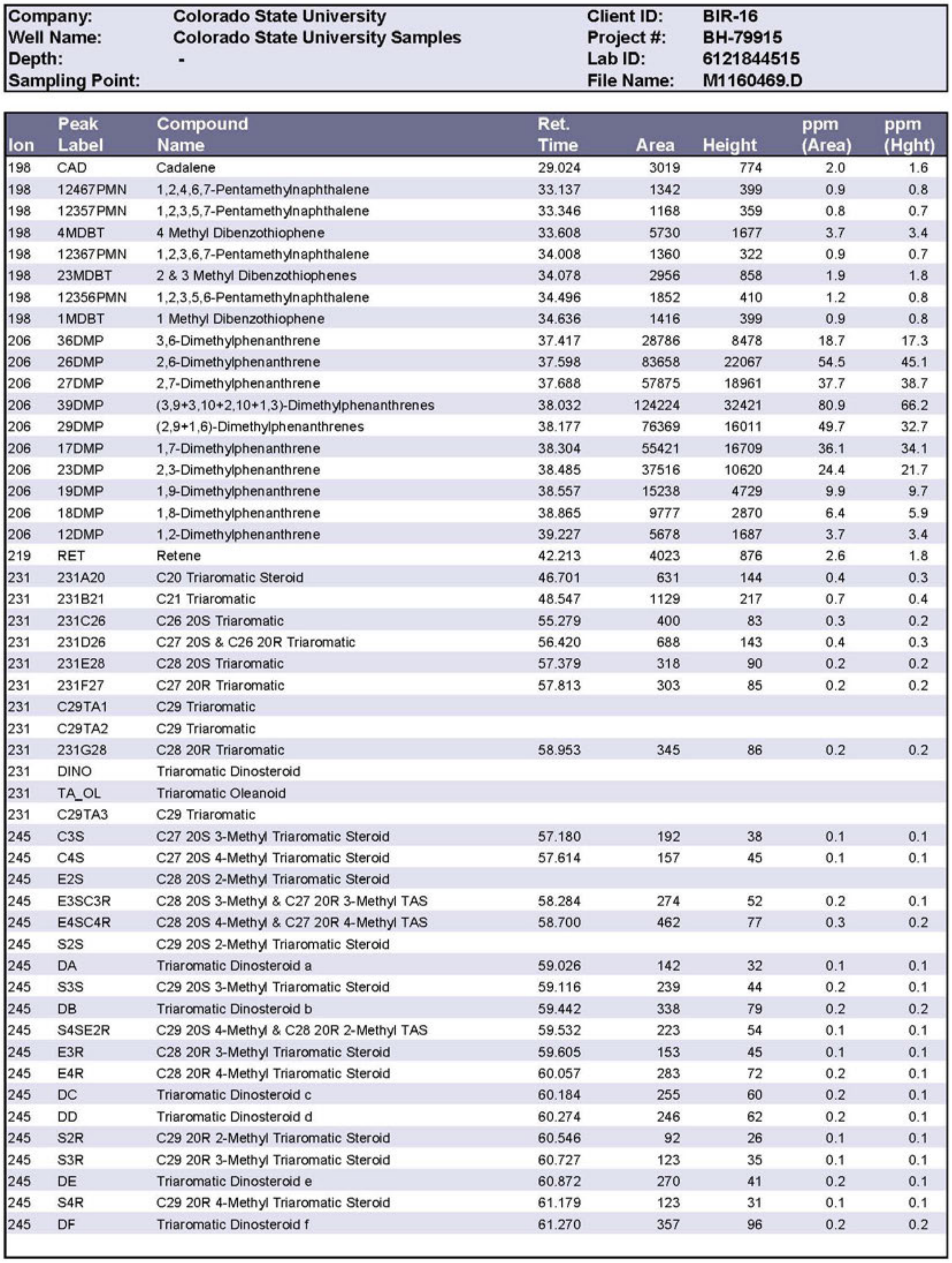

| | | | |
|---|---|---|---|
| **Company:** | **Colorado State University** | **Client ID:** | **BIR-16** |
| **Well Name:** | **Colorado State University Samples** | **Project #:** | **BH-79915** |
| **Depth:** | **-** | **Lab ID:** | **6121844515** |
| **Sampling Point:** | | **File Name:** | **M1160469.D** |

| Ion | Peak Label | Compound Name | Ret. Time | Area | Height | ppm (Area) | ppm (Hght) |
|---|---|---|---|---|---|---|---|
| 198 | CAD | Cadalene | 29.024 | 3019 | 774 | 2.0 | 1.6 |
| 198 | 12467PMN | 1,2,4,6,7-Pentamethylnaphthalene | 33.137 | 1342 | 399 | 0.9 | 0.8 |
| 198 | 12357PMN | 1,2,3,5,7-Pentamethylnaphthalene | 33.346 | 1168 | 359 | 0.8 | 0.7 |
| 198 | 4MDBT | 4 Methyl Dibenzothiophene | 33.608 | 5730 | 1677 | 3.7 | 3.4 |
| 198 | 12367PMN | 1,2,3,6,7-Pentamethylnaphthalene | 34.008 | 1360 | 322 | 0.9 | 0.7 |
| 198 | 23MDBT | 2 & 3 Methyl Dibenzothiophenes | 34.078 | 2956 | 858 | 1.9 | 1.8 |
| 198 | 12356PMN | 1,2,3,5,6-Pentamethylnaphthalene | 34.496 | 1852 | 410 | 1.2 | 0.8 |
| 198 | 1MDBT | 1 Methyl Dibenzothiophene | 34.636 | 1416 | 399 | 0.9 | 0.8 |
| 206 | 36DMP | 3,6-Dimethylphenanthrene | 37.417 | 28786 | 8478 | 18.7 | 17.3 |
| 206 | 26DMP | 2,6-Dimethylphenanthrene | 37.598 | 83658 | 22067 | 54.5 | 45.1 |
| 206 | 27DMP | 2,7-Dimethylphenanthrene | 37.688 | 57875 | 18961 | 37.7 | 38.7 |
| 206 | 39DMP | (3,9+3,10+2,10+1,3)-Dimethylphenanthrenes | 38.032 | 124224 | 32421 | 80.9 | 66.2 |
| 206 | 29DMP | (2,9+1,6)-Dimethylphenanthrenes | 38.177 | 76369 | 16011 | 49.7 | 32.7 |
| 206 | 17DMP | 1,7-Dimethylphenanthrene | 38.304 | 55421 | 16709 | 36.1 | 34.1 |
| 206 | 23DMP | 2,3-Dimethylphenanthrene | 38.485 | 37516 | 10620 | 24.4 | 21.7 |
| 206 | 19DMP | 1,9-Dimethylphenanthrene | 38.557 | 15238 | 4729 | 9.9 | 9.7 |
| 206 | 18DMP | 1,8-Dimethylphenanthrene | 38.865 | 9777 | 2870 | 6.4 | 5.9 |
| 206 | 12DMP | 1,2-Dimethylphenanthrene | 39.227 | 5678 | 1687 | 3.7 | 3.4 |
| 219 | RET | Retene | 42.213 | 4023 | 876 | 2.6 | 1.8 |
| 231 | 231A20 | C20 Triaromatic Steroid | 46.701 | 631 | 144 | 0.4 | 0.3 |
| 231 | 231B21 | C21 Triaromatic | 48.547 | 1129 | 217 | 0.7 | 0.4 |
| 231 | 231C26 | C26 20S Triaromatic | 55.279 | 400 | 83 | 0.3 | 0.2 |
| 231 | 231D26 | C27 20S & C26 20R Triaromatic | 56.420 | 688 | 143 | 0.4 | 0.3 |
| 231 | 231E28 | C28 20S Triaromatic | 57.379 | 318 | 90 | 0.2 | 0.2 |
| 231 | 231F27 | C27 20R Triaromatic | 57.813 | 303 | 85 | 0.2 | 0.2 |
| 231 | C29TA1 | C29 Triaromatic | | | | | |
| 231 | C29TA2 | C29 Triaromatic | | | | | |
| 231 | 231G28 | C28 20R Triaromatic | 58.953 | 345 | 86 | 0.2 | 0.2 |
| 231 | DINO | Triaromatic Dinosteroid | | | | | |
| 231 | TA_OL | Triaromatic Oleanoid | | | | | |
| 231 | C29TA3 | C29 Triaromatic | | | | | |
| 245 | C3S | C27 20S 3-Methyl Triaromatic Steroid | 57.180 | 192 | 38 | 0.1 | 0.1 |
| 245 | C4S | C27 20S 4-Methyl Triaromatic Steroid | 57.614 | 157 | 45 | 0.1 | 0.1 |
| 245 | E2S | C28 20S 2-Methyl Triaromatic Steroid | | | | | |
| 245 | E3SC3R | C28 20S 3-Methyl & C27 20R 3-Methyl TAS | 58.284 | 274 | 52 | 0.2 | 0.1 |
| 245 | E4SC4R | C28 20S 4-Methyl & C27 20R 4-Methyl TAS | 58.700 | 462 | 77 | 0.3 | 0.2 |
| 245 | S2S | C29 20S 2-Methyl Triaromatic Steroid | | | | | |
| 245 | DA | Triaromatic Dinosteroid a | 59.026 | 142 | 32 | 0.1 | 0.1 |
| 245 | S3S | C29 20S 3-Methyl Triaromatic Steroid | 59.116 | 239 | 44 | 0.2 | 0.1 |
| 245 | DB | Triaromatic Dinosteroid b | 59.442 | 338 | 79 | 0.2 | 0.2 |
| 245 | S4SE2R | C29 20S 4-Methyl & C28 20R 2-Methyl TAS | 59.532 | 223 | 54 | 0.1 | 0.1 |
| 245 | E3R | C28 20R 3-Methyl Triaromatic Steroid | 59.605 | 153 | 45 | 0.1 | 0.1 |
| 245 | E4R | C28 20R 4-Methyl Triaromatic Steroid | 60.057 | 283 | 72 | 0.2 | 0.1 |
| 245 | DC | Triaromatic Dinosteroid c | 60.184 | 255 | 60 | 0.2 | 0.1 |
| 245 | DD | Triaromatic Dinosteroid d | 60.274 | 246 | 62 | 0.2 | 0.1 |
| 245 | S2R | C29 20R 2-Methyl Triaromatic Steroid | 60.546 | 92 | 26 | 0.1 | 0.1 |
| 245 | S3R | C29 20R 3-Methyl Triaromatic Steroid | 60.727 | 123 | 35 | 0.1 | 0.1 |
| 245 | DE | Triaromatic Dinosteroid e | 60.872 | 270 | 41 | 0.2 | 0.1 |
| 245 | S4R | C29 20R 4-Methyl Triaromatic Steroid | 61.179 | 123 | 31 | 0.1 | 0.1 |
| 245 | DF | Triaromatic Dinosteroid f | 61.270 | 357 | 96 | 0.2 | 0.2 |

*Appendix F2, ctd.*

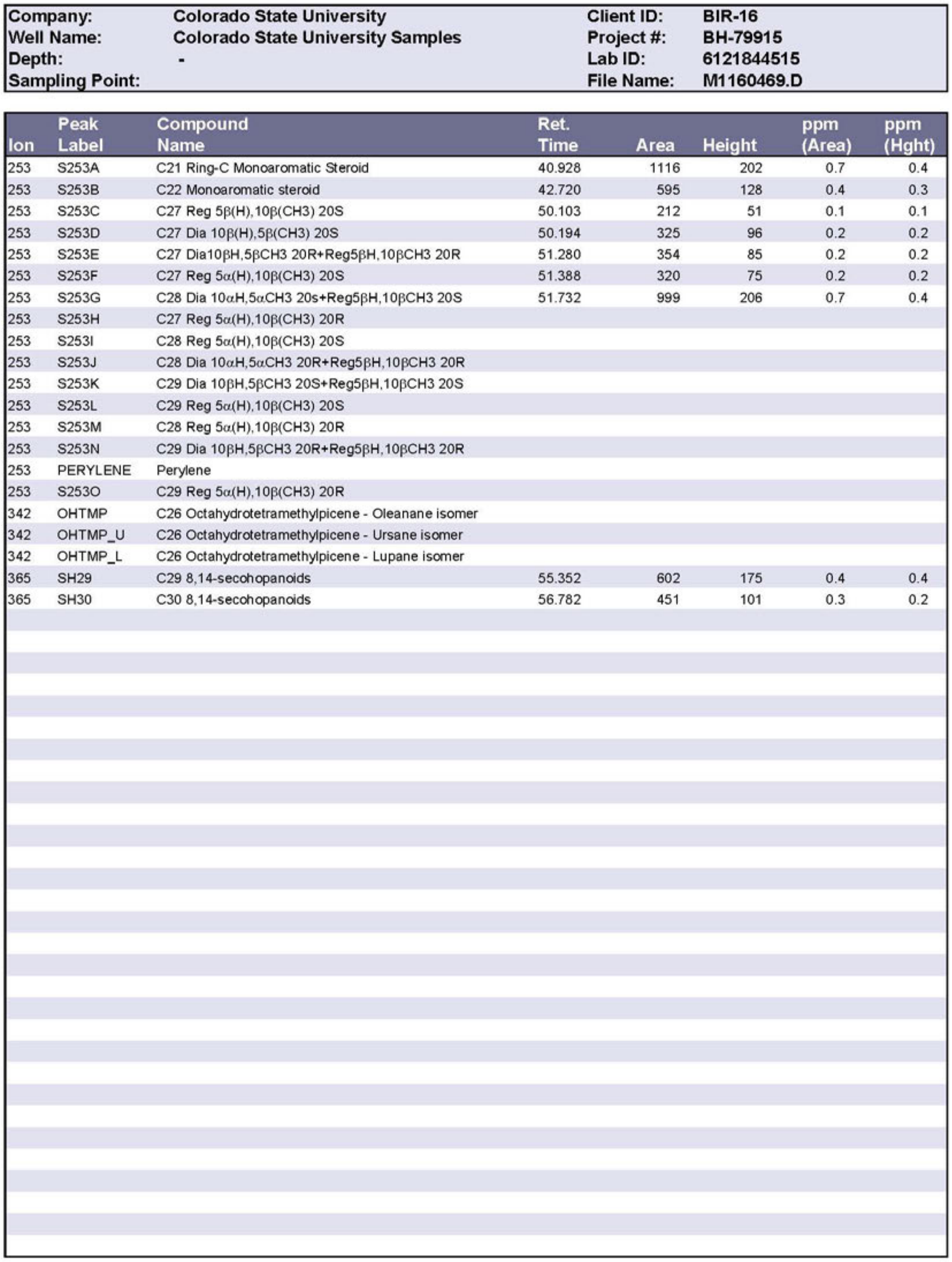

| | | | |
|---|---|---|---|
| **Company:** | **Colorado State University** | **Client ID:** | **BIR-16** |
| **Well Name:** | **Colorado State University Samples** | **Project #:** | **BH-79915** |
| **Depth:** | **-** | **Lab ID:** | **6121844515** |
| **Sampling Point:** | | **File Name:** | **M1160469.D** |

| Ion | Peak Label | Compound Name | Ret. Time | Area | Height | ppm (Area) | ppm (Hght) |
|---|---|---|---|---|---|---|---|
| 253 | S253A | C21 Ring-C Monoaromatic Steroid | 40.928 | 1116 | 202 | 0.7 | 0.4 |
| 253 | S253B | C22 Monoaromatic steroid | 42.720 | 595 | 128 | 0.4 | 0.3 |
| 253 | S253C | C27 Reg 5β(H),10β(CH3) 20S | 50.103 | 212 | 51 | 0.1 | 0.1 |
| 253 | S253D | C27 Dia 10β(H),5β(CH3) 20S | 50.194 | 325 | 96 | 0.2 | 0.2 |
| 253 | S253E | C27 Dia10βH,5βCH3 20R+Reg5βH,10βCH3 20R | 51.280 | 354 | 85 | 0.2 | 0.2 |
| 253 | S253F | C27 Reg 5α(H),10β(CH3) 20S | 51.388 | 320 | 75 | 0.2 | 0.2 |
| 253 | S253G | C28 Dia 10αH,5αCH3 20s+Reg5βH,10βCH3 20S | 51.732 | 999 | 206 | 0.7 | 0.4 |
| 253 | S253H | C27 Reg 5α(H),10β(CH3) 20R | | | | | |
| 253 | S253I | C28 Reg 5α(H),10β(CH3) 20S | | | | | |
| 253 | S253J | C28 Dia 10αH,5αCH3 20R+Reg5βH,10βCH3 20R | | | | | |
| 253 | S253K | C29 Dia 10βH,5βCH3 20S+Reg5βH,10βCH3 20S | | | | | |
| 253 | S253L | C29 Reg 5α(H),10β(CH3) 20S | | | | | |
| 253 | S253M | C28 Reg 5α(H),10β(CH3) 20R | | | | | |
| 253 | S253N | C29 Dia 10βH,5βCH3 20R+Reg5βH,10βCH3 20R | | | | | |
| 253 | PERYLENE | Perylene | | | | | |
| 253 | S253O | C29 Reg 5α(H),10β(CH3) 20R | | | | | |
| 342 | OHTMP | C26 Octahydrotetramethylpicene - Oleanane isomer | | | | | |
| 342 | OHTMP_U | C26 Octahydrotetramethylpicene - Ursane isomer | | | | | |
| 342 | OHTMP_L | C26 Octahydrotetramethylpicene - Lupane isomer | | | | | |
| 365 | SH29 | C29 8,14-secohopanoids | 55.352 | 602 | 175 | 0.4 | 0.4 |
| 365 | SH30 | C30 8,14-secohopanoids | 56.782 | 451 | 101 | 0.3 | 0.2 |

*Appendix F2, ctd.*

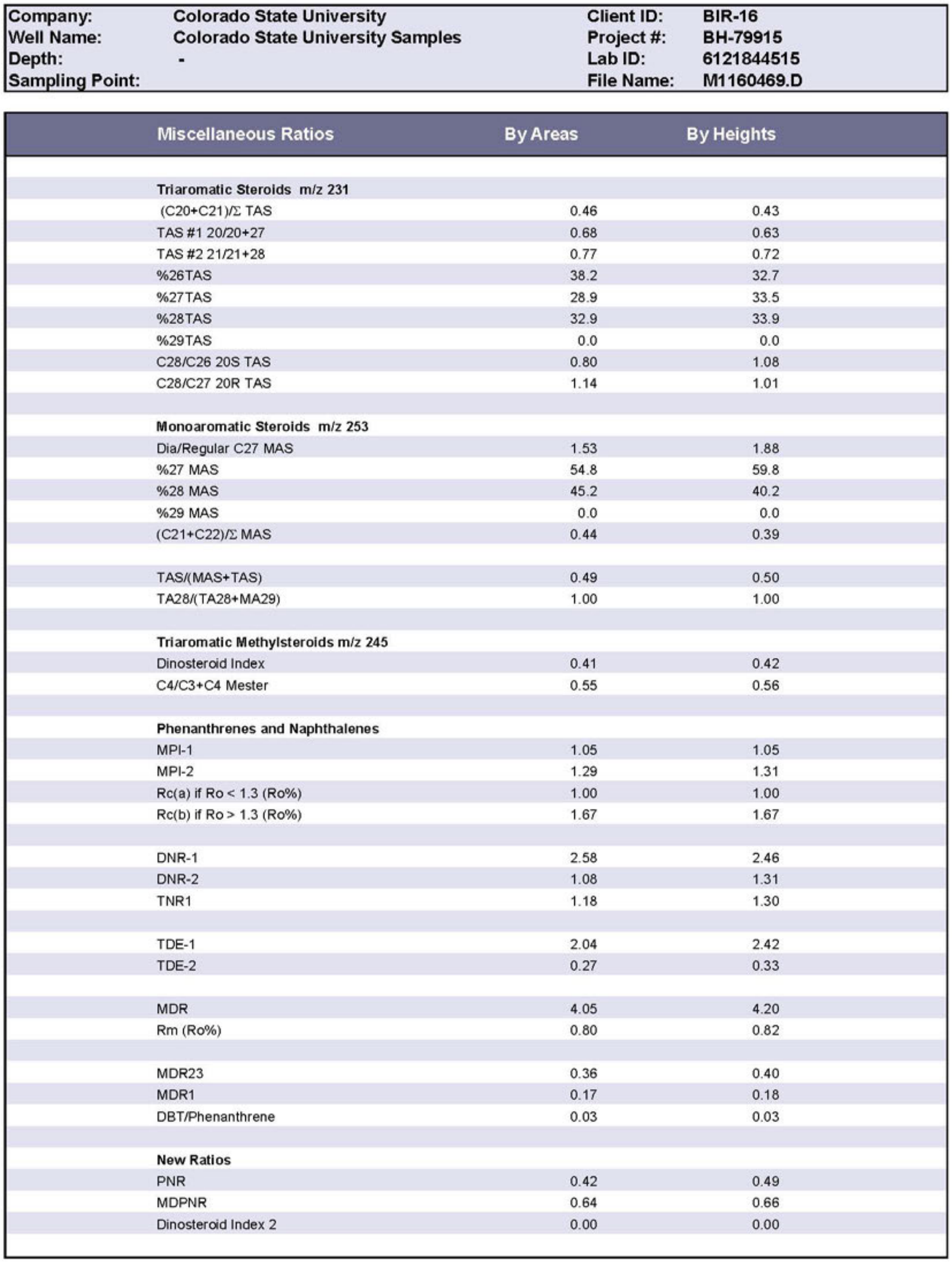

| | | | |
|---|---|---|---|
| **Company:** | **Colorado State University** | **Client ID:** | **BIR-16** |
| **Well Name:** | **Colorado State University Samples** | **Project #:** | **BH-79915** |
| **Depth:** | **-** | **Lab ID:** | **6121844515** |
| **Sampling Point:** | | **File Name:** | **M1160469.D** |

| Miscellaneous Ratios | By Areas | By Heights |
|---|---|---|
| **Triaromatic Steroids  m/z 231** | | |
| (C20+C21)/Σ TAS | 0.46 | 0.43 |
| TAS #1 20/20+27 | 0.68 | 0.63 |
| TAS #2 21/21+28 | 0.77 | 0.72 |
| %26TAS | 38.2 | 32.7 |
| %27TAS | 28.9 | 33.5 |
| %28TAS | 32.9 | 33.9 |
| %29TAS | 0.0 | 0.0 |
| C28/C26 20S TAS | 0.80 | 1.08 |
| C28/C27 20R TAS | 1.14 | 1.01 |
| | | |
| **Monoaromatic Steroids  m/z 253** | | |
| Dia/Regular C27 MAS | 1.53 | 1.88 |
| %27 MAS | 54.8 | 59.8 |
| %28 MAS | 45.2 | 40.2 |
| %29 MAS | 0.0 | 0.0 |
| (C21+C22)/Σ MAS | 0.44 | 0.39 |
| | | |
| TAS/(MAS+TAS) | 0.49 | 0.50 |
| TA28/(TA28+MA29) | 1.00 | 1.00 |
| | | |
| **Triaromatic Methylsteroids m/z 245** | | |
| Dinosteroid Index | 0.41 | 0.42 |
| C4/C3+C4 Mester | 0.55 | 0.56 |
| | | |
| **Phenanthrenes and Naphthalenes** | | |
| MPI-1 | 1.05 | 1.05 |
| MPI-2 | 1.29 | 1.31 |
| Rc(a) if Ro < 1.3 (Ro%) | 1.00 | 1.00 |
| Rc(b) if Ro > 1.3 (Ro%) | 1.67 | 1.67 |
| | | |
| DNR-1 | 2.58 | 2.46 |
| DNR-2 | 1.08 | 1.31 |
| TNR1 | 1.18 | 1.30 |
| | | |
| TDE-1 | 2.04 | 2.42 |
| TDE-2 | 0.27 | 0.33 |
| | | |
| MDR | 4.05 | 4.20 |
| Rm (Ro%) | 0.80 | 0.82 |
| | | |
| MDR23 | 0.36 | 0.40 |
| MDR1 | 0.17 | 0.18 |
| DBT/Phenanthrene | 0.03 | 0.03 |
| | | |
| **New Ratios** | | |
| PNR | 0.42 | 0.49 |
| MDPNR | 0.64 | 0.66 |
| Dinosteroid Index 2 | 0.00 | 0.00 |

*Appendix F2, ctd.*

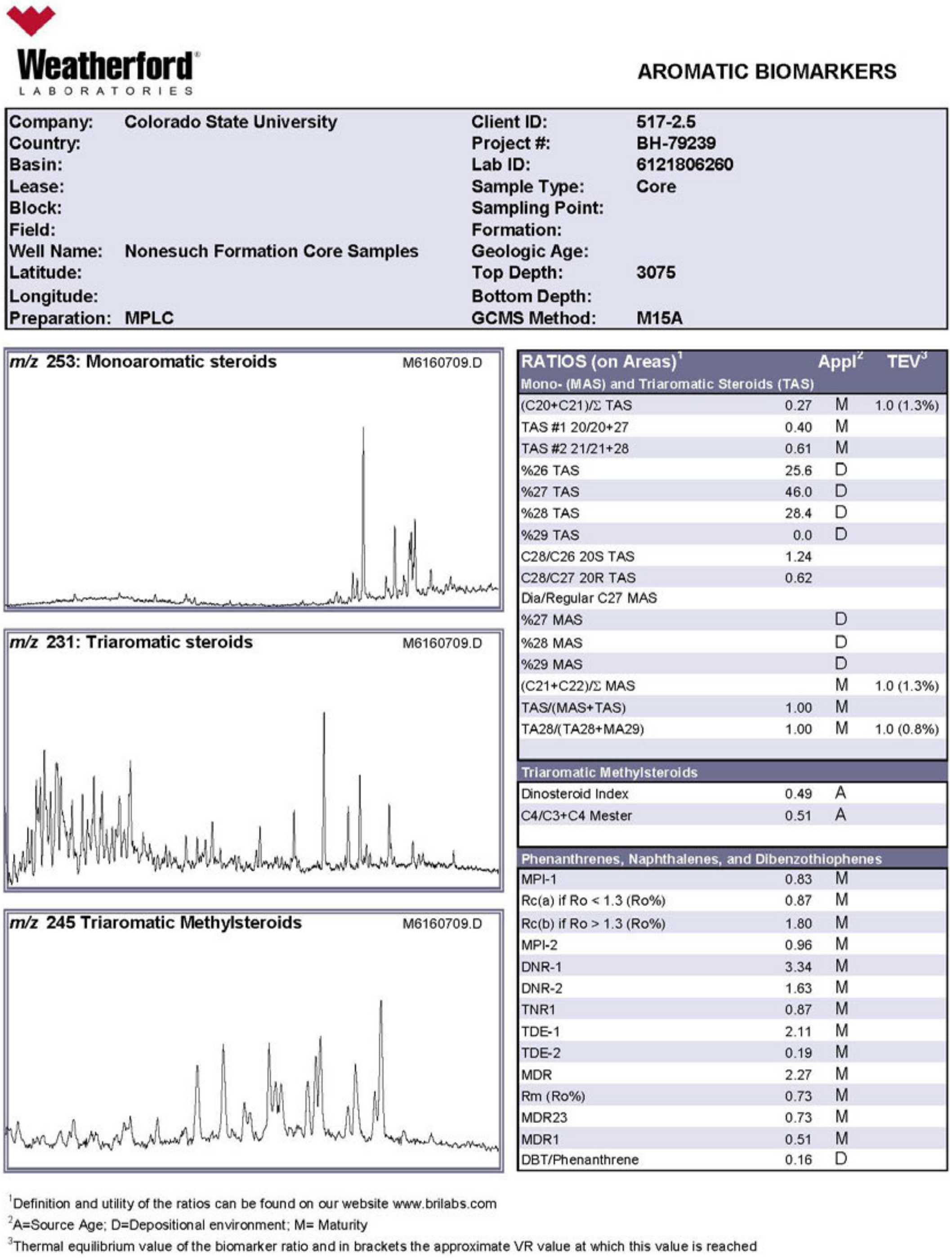

**Weatherford**
LABORATORIES

**AROMATIC BIOMARKERS**

| | | | |
|---|---|---|---|
| **Company:** | **Colorado State University** | **Client ID:** | **517-2.5** |
| **Country:** | | **Project #:** | **BH-79239** |
| **Basin:** | | **Lab ID:** | **6121806260** |
| **Lease:** | | **Sample Type:** | **Core** |
| **Block:** | | **Sampling Point:** | |
| **Field:** | | **Formation:** | |
| **Well Name:** | **Nonesuch Formation Core Samples** | **Geologic Age:** | |
| **Latitude:** | | **Top Depth:** | **3075** |
| **Longitude:** | | **Bottom Depth:** | |
| **Preparation:** | **MPLC** | **GCMS Method:** | **M15A** |

***m/z* 253: Monoaromatic steroids** M6160709.D

***m/z* 231: Triaromatic steroids** M6160709.D

***m/z* 245 Triaromatic Methylsteroids** M6160709.D

| RATIOS (on Areas)[1] | | Appl[2] | TEV[3] |
|---|---|---|---|
| **Mono- (MAS) and Triaromatic Steroids (TAS)** | | | |
| (C20+C21)/Σ TAS | 0.27 | M | 1.0 (1.3%) |
| TAS #1 20/20+27 | 0.40 | M | |
| TAS #2 21/21+28 | 0.61 | M | |
| %26 TAS | 25.6 | D | |
| %27 TAS | 46.0 | D | |
| %28 TAS | 28.4 | D | |
| %29 TAS | 0.0 | D | |
| C28/C26 20S TAS | 1.24 | | |
| C28/C27 20R TAS | 0.62 | | |
| Dia/Regular C27 MAS | | | |
| %27 MAS | | D | |
| %28 MAS | | D | |
| %29 MAS | | D | |
| (C21+C22)/Σ MAS | | M | 1.0 (1.3%) |
| TAS/(MAS+TAS) | 1.00 | M | |
| TA28/(TA28+MA29) | 1.00 | M | 1.0 (0.8%) |
| **Triaromatic Methylsteroids** | | | |
| Dinosteroid Index | 0.49 | A | |
| C4/C3+C4 Mester | 0.51 | A | |
| **Phenanthrenes, Naphthalenes, and Dibenzothiophenes** | | | |
| MPI-1 | 0.83 | M | |
| Rc(a) if Ro < 1.3 (Ro%) | 0.87 | M | |
| Rc(b) if Ro > 1.3 (Ro%) | 1.80 | M | |
| MPI-2 | 0.96 | M | |
| DNR-1 | 3.34 | M | |
| DNR-2 | 1.63 | M | |
| TNR1 | 0.87 | M | |
| TDE-1 | 2.11 | M | |
| TDE-2 | 0.19 | M | |
| MDR | 2.27 | M | |
| Rm (Ro%) | 0.73 | M | |
| MDR23 | 0.73 | M | |
| MDR1 | 0.51 | M | |
| DBT/Phenanthrene | 0.16 | D | |

[1] Definition and utility of the ratios can be found on our website www.brilabs.com

[2] A=Source Age; D=Depositional environment; M= Maturity

[3] Thermal equilibrium value of the biomarker ratio and in brackets the approximate VR value at which this value is reached

*Appendix F2, ctd.*

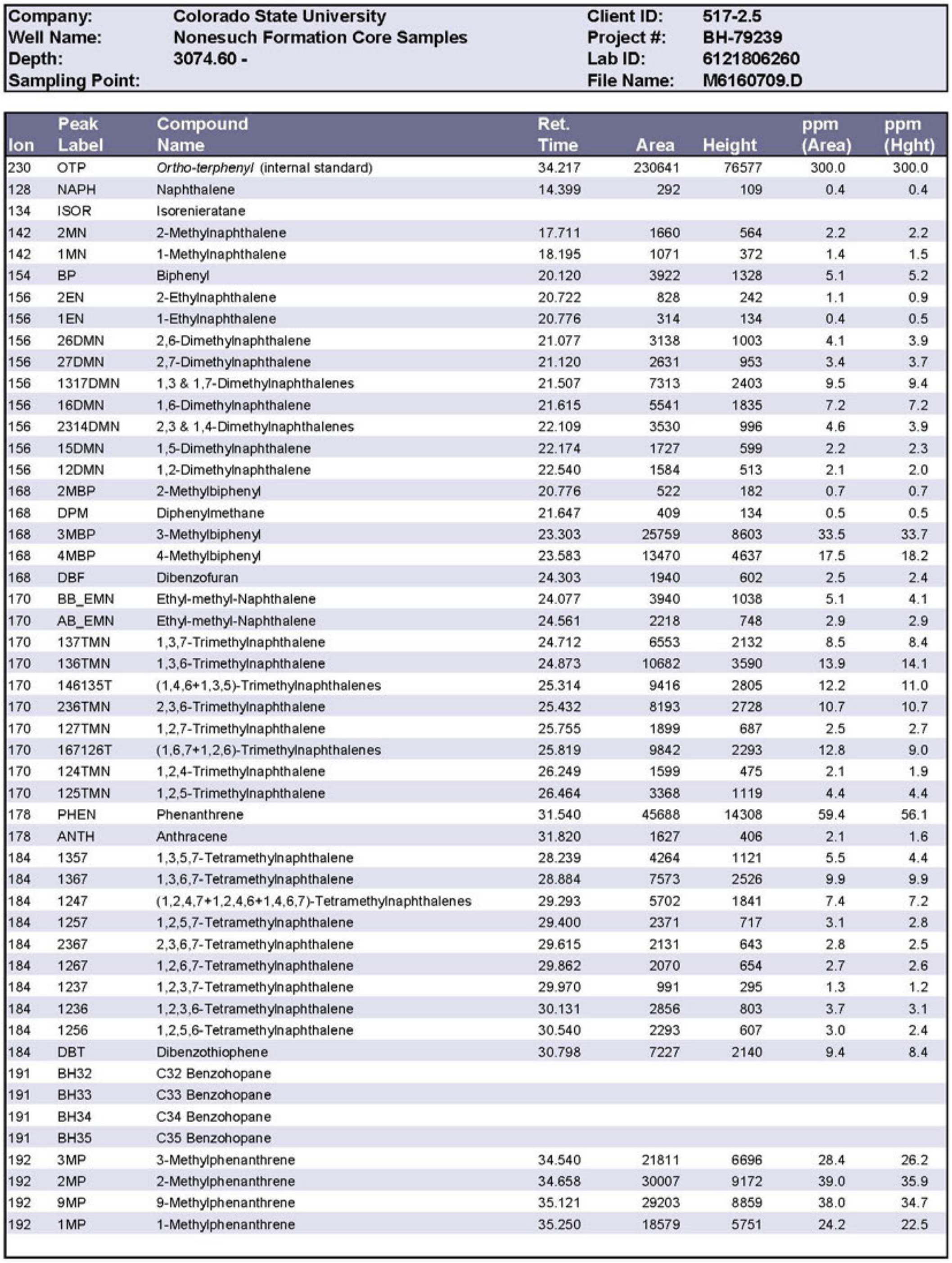

| | | | |
|---|---|---|---|
| **Company:** | **Colorado State University** | **Client ID:** | **517-2.5** |
| **Well Name:** | **Nonesuch Formation Core Samples** | **Project #:** | **BH-79239** |
| **Depth:** | **3074.60 -** | **Lab ID:** | **6121806260** |
| **Sampling Point:** | | **File Name:** | **M6160709.D** |

| Ion | Peak Label | Compound Name | Ret. Time | Area | Height | ppm (Area) | ppm (Hght) |
|---|---|---|---|---|---|---|---|
| 230 | OTP | *Ortho-terphenyl* (internal standard) | 34.217 | 230641 | 76577 | 300.0 | 300.0 |
| 128 | NAPH | Naphthalene | 14.399 | 292 | 109 | 0.4 | 0.4 |
| 134 | ISOR | Isorenieratane | | | | | |
| 142 | 2MN | 2-Methylnaphthalene | 17.711 | 1660 | 564 | 2.2 | 2.2 |
| 142 | 1MN | 1-Methylnaphthalene | 18.195 | 1071 | 372 | 1.4 | 1.5 |
| 154 | BP | Biphenyl | 20.120 | 3922 | 1328 | 5.1 | 5.2 |
| 156 | 2EN | 2-Ethylnaphthalene | 20.722 | 828 | 242 | 1.1 | 0.9 |
| 156 | 1EN | 1-Ethylnaphthalene | 20.776 | 314 | 134 | 0.4 | 0.5 |
| 156 | 26DMN | 2,6-Dimethylnaphthalene | 21.077 | 3138 | 1003 | 4.1 | 3.9 |
| 156 | 27DMN | 2,7-Dimethylnaphthalene | 21.120 | 2631 | 953 | 3.4 | 3.7 |
| 156 | 1317DMN | 1,3 & 1,7-Dimethylnaphthalenes | 21.507 | 7313 | 2403 | 9.5 | 9.4 |
| 156 | 16DMN | 1,6-Dimethylnaphthalene | 21.615 | 5541 | 1835 | 7.2 | 7.2 |
| 156 | 2314DMN | 2,3 & 1,4-Dimethylnaphthalenes | 22.109 | 3530 | 996 | 4.6 | 3.9 |
| 156 | 15DMN | 1,5-Dimethylnaphthalene | 22.174 | 1727 | 599 | 2.2 | 2.3 |
| 156 | 12DMN | 1,2-Dimethylnaphthalene | 22.540 | 1584 | 513 | 2.1 | 2.0 |
| 168 | 2MBP | 2-Methylbiphenyl | 20.776 | 522 | 182 | 0.7 | 0.7 |
| 168 | DPM | Diphenylmethane | 21.647 | 409 | 134 | 0.5 | 0.5 |
| 168 | 3MBP | 3-Methylbiphenyl | 23.303 | 25759 | 8603 | 33.5 | 33.7 |
| 168 | 4MBP | 4-Methylbiphenyl | 23.583 | 13470 | 4637 | 17.5 | 18.2 |
| 168 | DBF | Dibenzofuran | 24.303 | 1940 | 602 | 2.5 | 2.4 |
| 170 | BB_EMN | Ethyl-methyl-Naphthalene | 24.077 | 3940 | 1038 | 5.1 | 4.1 |
| 170 | AB_EMN | Ethyl-methyl-Naphthalene | 24.561 | 2218 | 748 | 2.9 | 2.9 |
| 170 | 137TMN | 1,3,7-Trimethylnaphthalene | 24.712 | 6553 | 2132 | 8.5 | 8.4 |
| 170 | 136TMN | 1,3,6-Trimethylnaphthalene | 24.873 | 10682 | 3590 | 13.9 | 14.1 |
| 170 | 146135T | (1,4,6+1,3,5)-Trimethylnaphthalenes | 25.314 | 9416 | 2805 | 12.2 | 11.0 |
| 170 | 236TMN | 2,3,6-Trimethylnaphthalene | 25.432 | 8193 | 2728 | 10.7 | 10.7 |
| 170 | 127TMN | 1,2,7-Trimethylnaphthalene | 25.755 | 1899 | 687 | 2.5 | 2.7 |
| 170 | 167126T | (1,6,7+1,2,6)-Trimethylnaphthalenes | 25.819 | 9842 | 2293 | 12.8 | 9.0 |
| 170 | 124TMN | 1,2,4-Trimethylnaphthalene | 26.249 | 1599 | 475 | 2.1 | 1.9 |
| 170 | 125TMN | 1,2,5-Trimethylnaphthalene | 26.464 | 3368 | 1119 | 4.4 | 4.4 |
| 178 | PHEN | Phenanthrene | 31.540 | 45688 | 14308 | 59.4 | 56.1 |
| 178 | ANTH | Anthracene | 31.820 | 1627 | 406 | 2.1 | 1.6 |
| 184 | 1357 | 1,3,5,7-Tetramethylnaphthalene | 28.239 | 4264 | 1121 | 5.5 | 4.4 |
| 184 | 1367 | 1,3,6,7-Tetramethylnaphthalene | 28.884 | 7573 | 2526 | 9.9 | 9.9 |
| 184 | 1247 | (1,2,4,7+1,2,4,6+1,4,6,7)-Tetramethylnaphthalenes | 29.293 | 5702 | 1841 | 7.4 | 7.2 |
| 184 | 1257 | 1,2,5,7-Tetramethylnaphthalene | 29.400 | 2371 | 717 | 3.1 | 2.8 |
| 184 | 2367 | 2,3,6,7-Tetramethylnaphthalene | 29.615 | 2131 | 643 | 2.8 | 2.5 |
| 184 | 1267 | 1,2,6,7-Tetramethylnaphthalene | 29.862 | 2070 | 654 | 2.7 | 2.6 |
| 184 | 1237 | 1,2,3,7-Tetramethylnaphthalene | 29.970 | 991 | 295 | 1.3 | 1.2 |
| 184 | 1236 | 1,2,3,6-Tetramethylnaphthalene | 30.131 | 2856 | 803 | 3.7 | 3.1 |
| 184 | 1256 | 1,2,5,6-Tetramethylnaphthalene | 30.540 | 2293 | 607 | 3.0 | 2.4 |
| 184 | DBT | Dibenzothiophene | 30.798 | 7227 | 2140 | 9.4 | 8.4 |
| 191 | BH32 | C32 Benzohopane | | | | | |
| 191 | BH33 | C33 Benzohopane | | | | | |
| 191 | BH34 | C34 Benzohopane | | | | | |
| 191 | BH35 | C35 Benzohopane | | | | | |
| 192 | 3MP | 3-Methylphenanthrene | 34.540 | 21811 | 6696 | 28.4 | 26.2 |
| 192 | 2MP | 2-Methylphenanthrene | 34.658 | 30007 | 9172 | 39.0 | 35.9 |
| 192 | 9MP | 9-Methylphenanthrene | 35.121 | 29203 | 8859 | 38.0 | 34.7 |
| 192 | 1MP | 1-Methylphenanthrene | 35.250 | 18579 | 5751 | 24.2 | 22.5 |

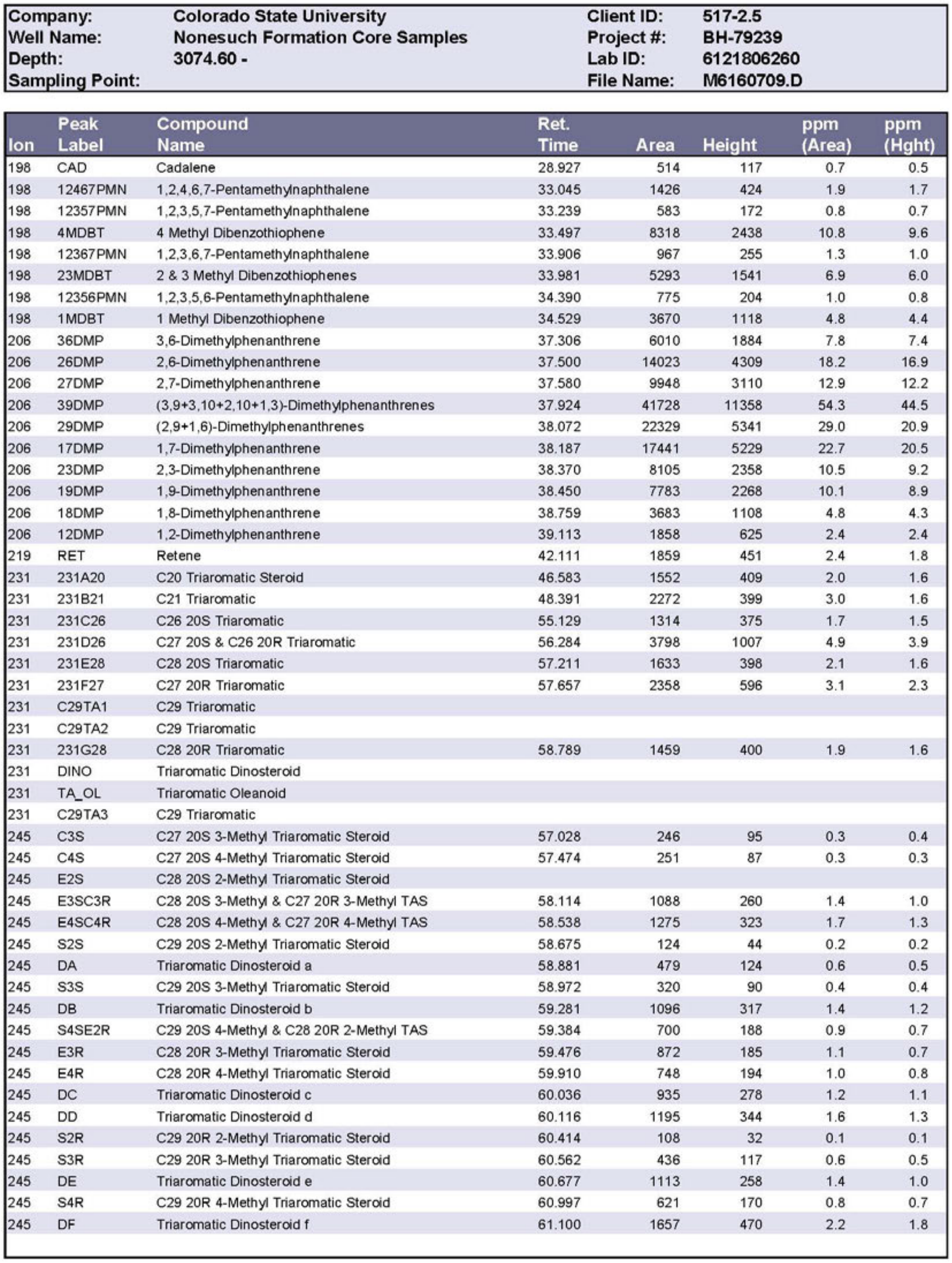

| | | | |
|---|---|---|---|
| **Company:** | **Colorado State University** | **Client ID:** | **517-2.5** |
| **Well Name:** | **Nonesuch Formation Core Samples** | **Project #:** | **BH-79239** |
| **Depth:** | **3074.60 -** | **Lab ID:** | **6121806260** |
| **Sampling Point:** | | **File Name:** | **M6160709.D** |

| Ion | Peak Label | Compound Name | Ret. Time | Area | Height | ppm (Area) | ppm (Hght) |
|---|---|---|---|---|---|---|---|
| 198 | CAD | Cadalene | 28.927 | 514 | 117 | 0.7 | 0.5 |
| 198 | 12467PMN | 1,2,4,6,7-Pentamethylnaphthalene | 33.045 | 1426 | 424 | 1.9 | 1.7 |
| 198 | 12357PMN | 1,2,3,5,7-Pentamethylnaphthalene | 33.239 | 583 | 172 | 0.8 | 0.7 |
| 198 | 4MDBT | 4 Methyl Dibenzothiophene | 33.497 | 8318 | 2438 | 10.8 | 9.6 |
| 198 | 12367PMN | 1,2,3,6,7-Pentamethylnaphthalene | 33.906 | 967 | 255 | 1.3 | 1.0 |
| 198 | 23MDBT | 2 & 3 Methyl Dibenzothiophenes | 33.981 | 5293 | 1541 | 6.9 | 6.0 |
| 198 | 12356PMN | 1,2,3,5,6-Pentamethylnaphthalene | 34.390 | 775 | 204 | 1.0 | 0.8 |
| 198 | 1MDBT | 1 Methyl Dibenzothiophene | 34.529 | 3670 | 1118 | 4.8 | 4.4 |
| 206 | 36DMP | 3,6-Dimethylphenanthrene | 37.306 | 6010 | 1884 | 7.8 | 7.4 |
| 206 | 26DMP | 2,6-Dimethylphenanthrene | 37.500 | 14023 | 4309 | 18.2 | 16.9 |
| 206 | 27DMP | 2,7-Dimethylphenanthrene | 37.580 | 9948 | 3110 | 12.9 | 12.2 |
| 206 | 39DMP | (3,9+3,10+2,10+1,3)-Dimethylphenanthrenes | 37.924 | 41728 | 11358 | 54.3 | 44.5 |
| 206 | 29DMP | (2,9+1,6)-Dimethylphenanthrenes | 38.072 | 22329 | 5341 | 29.0 | 20.9 |
| 206 | 17DMP | 1,7-Dimethylphenanthrene | 38.187 | 17441 | 5229 | 22.7 | 20.5 |
| 206 | 23DMP | 2,3-Dimethylphenanthrene | 38.370 | 8105 | 2358 | 10.5 | 9.2 |
| 206 | 19DMP | 1,9-Dimethylphenanthrene | 38.450 | 7783 | 2268 | 10.1 | 8.9 |
| 206 | 18DMP | 1,8-Dimethylphenanthrene | 38.759 | 3683 | 1108 | 4.8 | 4.3 |
| 206 | 12DMP | 1,2-Dimethylphenanthrene | 39.113 | 1858 | 625 | 2.4 | 2.4 |
| 219 | RET | Retene | 42.111 | 1859 | 451 | 2.4 | 1.8 |
| 231 | 231A20 | C20 Triaromatic Steroid | 46.583 | 1552 | 409 | 2.0 | 1.6 |
| 231 | 231B21 | C21 Triaromatic | 48.391 | 2272 | 399 | 3.0 | 1.6 |
| 231 | 231C26 | C26 20S Triaromatic | 55.129 | 1314 | 375 | 1.7 | 1.5 |
| 231 | 231D26 | C27 20S & C26 20R Triaromatic | 56.284 | 3798 | 1007 | 4.9 | 3.9 |
| 231 | 231E28 | C28 20S Triaromatic | 57.211 | 1633 | 398 | 2.1 | 1.6 |
| 231 | 231F27 | C27 20R Triaromatic | 57.657 | 2358 | 596 | 3.1 | 2.3 |
| 231 | C29TA1 | C29 Triaromatic | | | | | |
| 231 | C29TA2 | C29 Triaromatic | | | | | |
| 231 | 231G28 | C28 20R Triaromatic | 58.789 | 1459 | 400 | 1.9 | 1.6 |
| 231 | DINO | Triaromatic Dinosteroid | | | | | |
| 231 | TA_OL | Triaromatic Oleanoid | | | | | |
| 231 | C29TA3 | C29 Triaromatic | | | | | |
| 245 | C3S | C27 20S 3-Methyl Triaromatic Steroid | 57.028 | 246 | 95 | 0.3 | 0.4 |
| 245 | C4S | C27 20S 4-Methyl Triaromatic Steroid | 57.474 | 251 | 87 | 0.3 | 0.3 |
| 245 | E2S | C28 20S 2-Methyl Triaromatic Steroid | | | | | |
| 245 | E3SC3R | C28 20S 3-Methyl & C27 20R 3-Methyl TAS | 58.114 | 1088 | 260 | 1.4 | 1.0 |
| 245 | E4SC4R | C28 20S 4-Methyl & C27 20R 4-Methyl TAS | 58.538 | 1275 | 323 | 1.7 | 1.3 |
| 245 | S2S | C29 20S 2-Methyl Triaromatic Steroid | 58.675 | 124 | 44 | 0.2 | 0.2 |
| 245 | DA | Triaromatic Dinosteroid a | 58.881 | 479 | 124 | 0.6 | 0.5 |
| 245 | S3S | C29 20S 3-Methyl Triaromatic Steroid | 58.972 | 320 | 90 | 0.4 | 0.4 |
| 245 | DB | Triaromatic Dinosteroid b | 59.281 | 1096 | 317 | 1.4 | 1.2 |
| 245 | S4SE2R | C29 20S 4-Methyl & C28 20R 2-Methyl TAS | 59.384 | 700 | 188 | 0.9 | 0.7 |
| 245 | E3R | C28 20R 3-Methyl Triaromatic Steroid | 59.476 | 872 | 185 | 1.1 | 0.7 |
| 245 | E4R | C28 20R 4-Methyl Triaromatic Steroid | 59.910 | 748 | 194 | 1.0 | 0.8 |
| 245 | DC | Triaromatic Dinosteroid c | 60.036 | 935 | 278 | 1.2 | 1.1 |
| 245 | DD | Triaromatic Dinosteroid d | 60.116 | 1195 | 344 | 1.6 | 1.3 |
| 245 | S2R | C29 20R 2-Methyl Triaromatic Steroid | 60.414 | 108 | 32 | 0.1 | 0.1 |
| 245 | S3R | C29 20R 3-Methyl Triaromatic Steroid | 60.562 | 436 | 117 | 0.6 | 0.5 |
| 245 | DE | Triaromatic Dinosteroid e | 60.677 | 1113 | 258 | 1.4 | 1.0 |
| 245 | S4R | C29 20R 4-Methyl Triaromatic Steroid | 60.997 | 621 | 170 | 0.8 | 0.7 |
| 245 | DF | Triaromatic Dinosteroid f | 61.100 | 1657 | 470 | 2.2 | 1.8 |

*Appendix F2, ctd.*

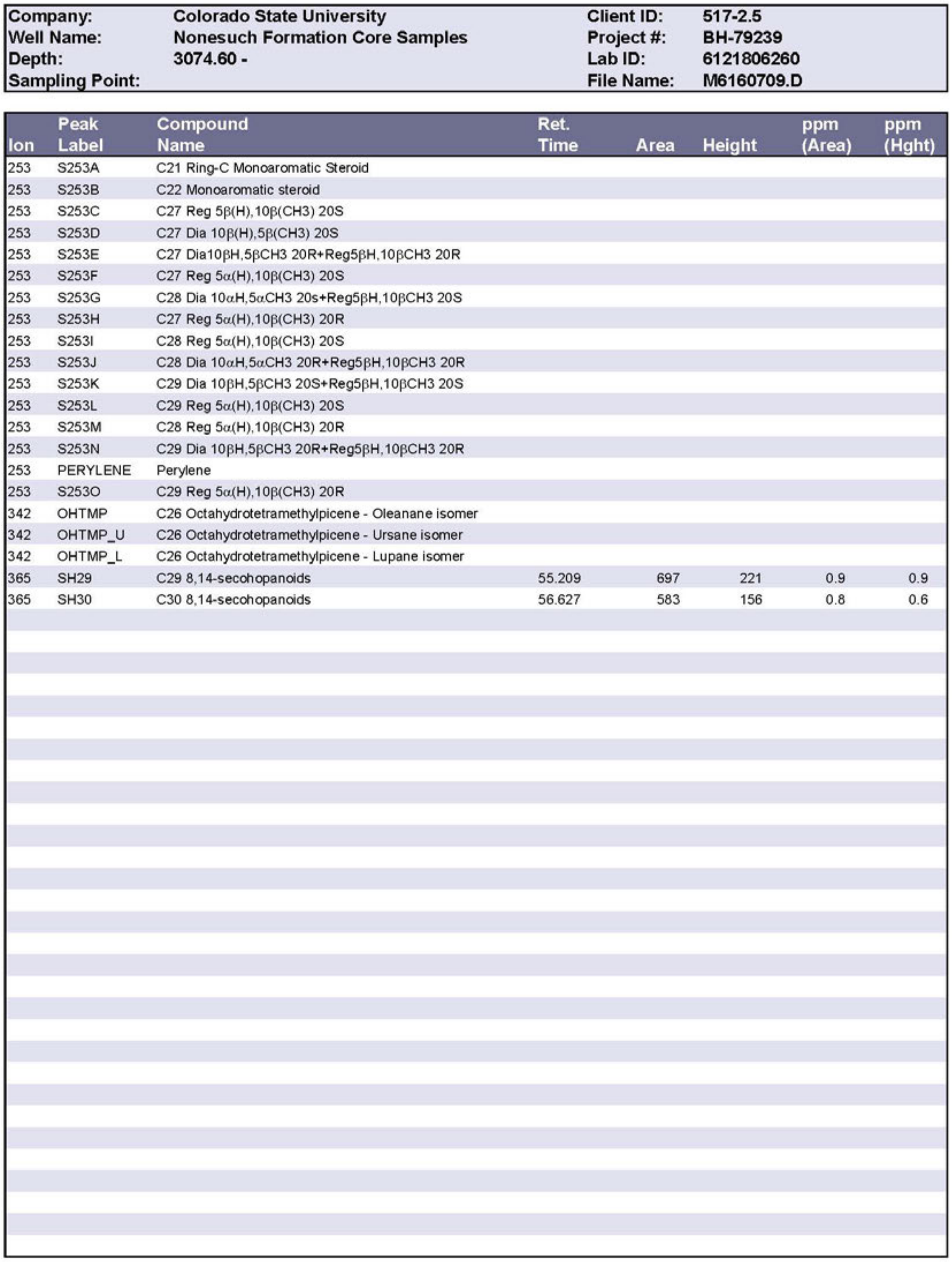

| | | | |
|---|---|---|---|
| **Company:** | **Colorado State University** | **Client ID:** | **517-2.5** |
| **Well Name:** | **Nonesuch Formation Core Samples** | **Project #:** | **BH-79239** |
| **Depth:** | **3074.60 -** | **Lab ID:** | **6121806260** |
| **Sampling Point:** | | **File Name:** | **M6160709.D** |

| Ion | Peak Label | Compound Name | Ret. Time | Area | Height | ppm (Area) | ppm (Hght) |
|---|---|---|---|---|---|---|---|
| 253 | S253A | C21 Ring-C Monoaromatic Steroid | | | | | |
| 253 | S253B | C22 Monoaromatic steroid | | | | | |
| 253 | S253C | C27 Reg 5β(H),10β(CH3) 20S | | | | | |
| 253 | S253D | C27 Dia 10β(H),5β(CH3) 20S | | | | | |
| 253 | S253E | C27 Dia10βH,5βCH3 20R+Reg5βH,10βCH3 20R | | | | | |
| 253 | S253F | C27 Reg 5α(H),10β(CH3) 20S | | | | | |
| 253 | S253G | C28 Dia 10αH,5αCH3 20s+Reg5βH,10βCH3 20S | | | | | |
| 253 | S253H | C27 Reg 5α(H),10β(CH3) 20R | | | | | |
| 253 | S253I | C28 Reg 5α(H),10β(CH3) 20S | | | | | |
| 253 | S253J | C28 Dia 10αH,5αCH3 20R+Reg5βH,10βCH3 20R | | | | | |
| 253 | S253K | C29 Dia 10βH,5βCH3 20S+Reg5βH,10βCH3 20S | | | | | |
| 253 | S253L | C29 Reg 5α(H),10β(CH3) 20S | | | | | |
| 253 | S253M | C28 Reg 5α(H),10β(CH3) 20R | | | | | |
| 253 | S253N | C29 Dia 10βH,5βCH3 20R+Reg5βH,10βCH3 20R | | | | | |
| 253 | PERYLENE | Perylene | | | | | |
| 253 | S253O | C29 Reg 5α(H),10β(CH3) 20R | | | | | |
| 342 | OHTMP | C26 Octahydrotetramethylpicene - Oleanane isomer | | | | | |
| 342 | OHTMP_U | C26 Octahydrotetramethylpicene - Ursane isomer | | | | | |
| 342 | OHTMP_L | C26 Octahydrotetramethylpicene - Lupane isomer | | | | | |
| 365 | SH29 | C29 8,14-secohopanoids | 55.209 | 697 | 221 | 0.9 | 0.9 |
| 365 | SH30 | C30 8,14-secohopanoids | 56.627 | 583 | 156 | 0.8 | 0.6 |

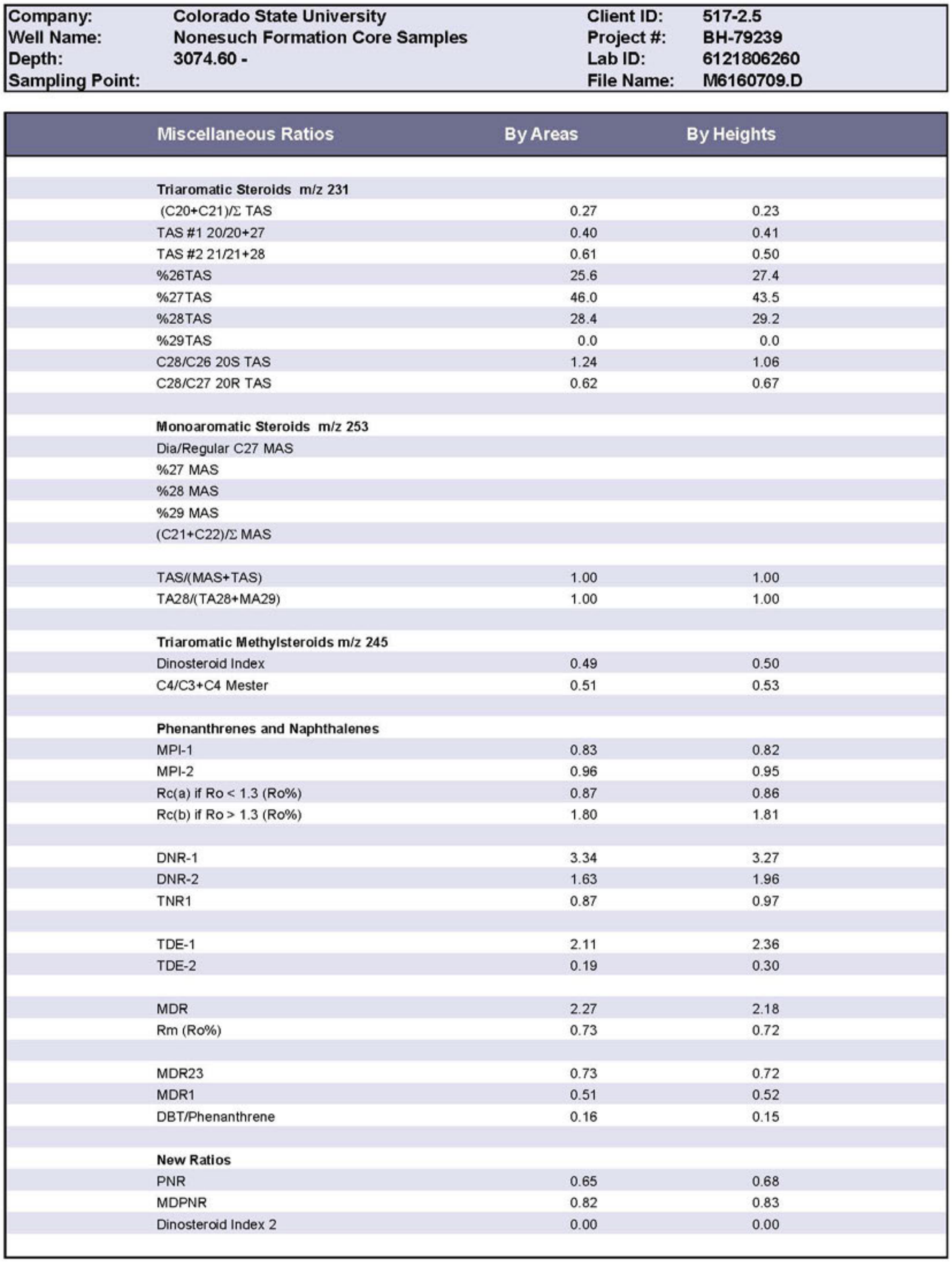

| | | | |
|---|---|---|---|
| **Company:** | **Colorado State University** | **Client ID:** | **517-2.5** |
| **Well Name:** | **Nonesuch Formation Core Samples** | **Project #:** | **BH-79239** |
| **Depth:** | **3074.60 -** | **Lab ID:** | **6121806260** |
| **Sampling Point:** | | **File Name:** | **M6160709.D** |

| Miscellaneous Ratios | By Areas | By Heights |
|---|---|---|
| **Triaromatic Steroids m/z 231** | | |
| (C20+C21)/Σ TAS | 0.27 | 0.23 |
| TAS #1 20/20+27 | 0.40 | 0.41 |
| TAS #2 21/21+28 | 0.61 | 0.50 |
| %26TAS | 25.6 | 27.4 |
| %27TAS | 46.0 | 43.5 |
| %28TAS | 28.4 | 29.2 |
| %29TAS | 0.0 | 0.0 |
| C28/C26 20S TAS | 1.24 | 1.06 |
| C28/C27 20R TAS | 0.62 | 0.67 |
| | | |
| **Monoaromatic Steroids m/z 253** | | |
| Dia/Regular C27 MAS | | |
| %27 MAS | | |
| %28 MAS | | |
| %29 MAS | | |
| (C21+C22)/Σ MAS | | |
| | | |
| TAS/(MAS+TAS) | 1.00 | 1.00 |
| TA28/(TA28+MA29) | 1.00 | 1.00 |
| | | |
| **Triaromatic Methylsteroids m/z 245** | | |
| Dinosteroid Index | 0.49 | 0.50 |
| C4/C3+C4 Mester | 0.51 | 0.53 |
| | | |
| **Phenanthrenes and Naphthalenes** | | |
| MPI-1 | 0.83 | 0.82 |
| MPI-2 | 0.96 | 0.95 |
| Rc(a) if Ro < 1.3 (Ro%) | 0.87 | 0.86 |
| Rc(b) if Ro > 1.3 (Ro%) | 1.80 | 1.81 |
| | | |
| DNR-1 | 3.34 | 3.27 |
| DNR-2 | 1.63 | 1.96 |
| TNR1 | 0.87 | 0.97 |
| | | |
| TDE-1 | 2.11 | 2.36 |
| TDE-2 | 0.19 | 0.30 |
| | | |
| MDR | 2.27 | 2.18 |
| Rm (Ro%) | 0.73 | 0.72 |
| | | |
| MDR23 | 0.73 | 0.72 |
| MDR1 | 0.51 | 0.52 |
| DBT/Phenanthrene | 0.16 | 0.15 |
| | | |
| **New Ratios** | | |
| PNR | 0.65 | 0.68 |
| MDPNR | 0.82 | 0.83 |
| Dinosteroid Index 2 | 0.00 | 0.00 |

*Appendix F2, ctd.*

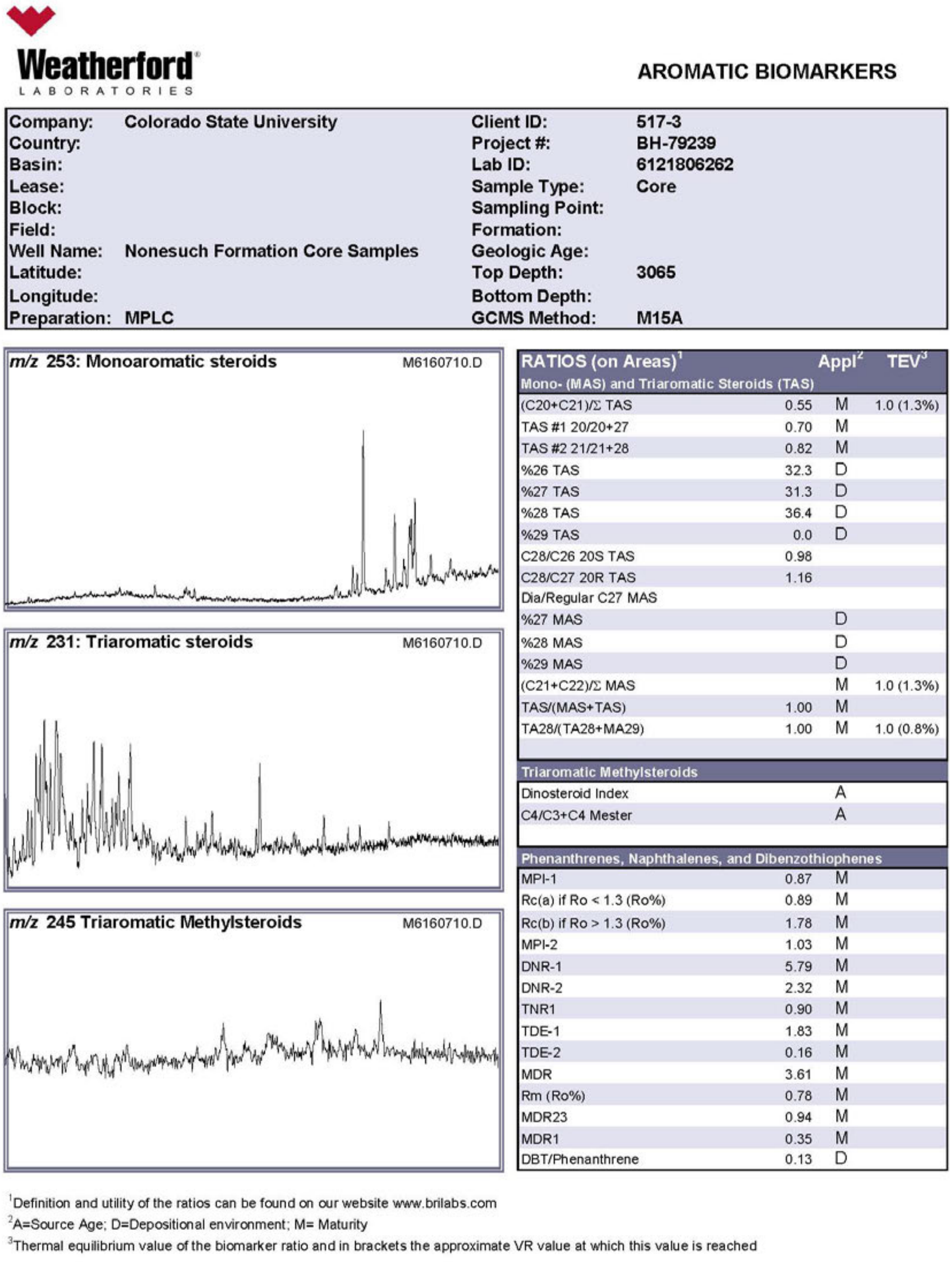

**Weatherford** LABORATORIES

## AROMATIC BIOMARKERS

| | | | |
|---|---|---|---|
| **Company:** | **Colorado State University** | **Client ID:** | **517-3** |
| **Country:** | | **Project #:** | **BH-79239** |
| **Basin:** | | **Lab ID:** | **6121806262** |
| **Lease:** | | **Sample Type:** | **Core** |
| **Block:** | | **Sampling Point:** | |
| **Field:** | | **Formation:** | |
| **Well Name:** | **Nonesuch Formation Core Samples** | **Geologic Age:** | |
| **Latitude:** | | **Top Depth:** | **3065** |
| **Longitude:** | | **Bottom Depth:** | |
| **Preparation:** | **MPLC** | **GCMS Method:** | **M15A** |

| RATIOS (on Areas)[1] | | Appl[2] | TEV[3] |
|---|---|---|---|
| **Mono- (MAS) and Triaromatic Steroids (TAS)** | | | |
| (C20+C21)/Σ TAS | 0.55 | M | 1.0 (1.3%) |
| TAS #1 20/20+27 | 0.70 | M | |
| TAS #2 21/21+28 | 0.82 | M | |
| %26 TAS | 32.3 | D | |
| %27 TAS | 31.3 | D | |
| %28 TAS | 36.4 | D | |
| %29 TAS | 0.0 | D | |
| C28/C26 20S TAS | 0.98 | | |
| C28/C27 20R TAS | 1.16 | | |
| Dia/Regular C27 MAS | | | |
| %27 MAS | | D | |
| %28 MAS | | D | |
| %29 MAS | | D | |
| (C21+C22)/Σ MAS | | M | 1.0 (1.3%) |
| TAS/(MAS+TAS) | 1.00 | M | |
| TA28/(TA28+MA29) | 1.00 | M | 1.0 (0.8%) |
| **Triaromatic Methylsteroids** | | | |
| Dinosteroid Index | | A | |
| C4/C3+C4 Mester | | A | |
| **Phenanthrenes, Naphthalenes, and Dibenzothiophenes** | | | |
| MPI-1 | 0.87 | M | |
| Rc(a) if Ro < 1.3 (Ro%) | 0.89 | M | |
| Rc(b) if Ro > 1.3 (Ro%) | 1.78 | M | |
| MPI-2 | 1.03 | M | |
| DNR-1 | 5.79 | M | |
| DNR-2 | 2.32 | M | |
| TNR1 | 0.90 | M | |
| TDE-1 | 1.83 | M | |
| TDE-2 | 0.16 | M | |
| MDR | 3.61 | M | |
| Rm (Ro%) | 0.78 | M | |
| MDR23 | 0.94 | M | |
| MDR1 | 0.35 | M | |
| DBT/Phenanthrene | 0.13 | D | |

[1] Definition and utility of the ratios can be found on our website www.brilabs.com

[2] A=Source Age; D=Depositional environment; M= Maturity

[3] Thermal equilibrium value of the biomarker ratio and in brackets the approximate VR value at which this value is reached

*Appendix F2, ctd.*

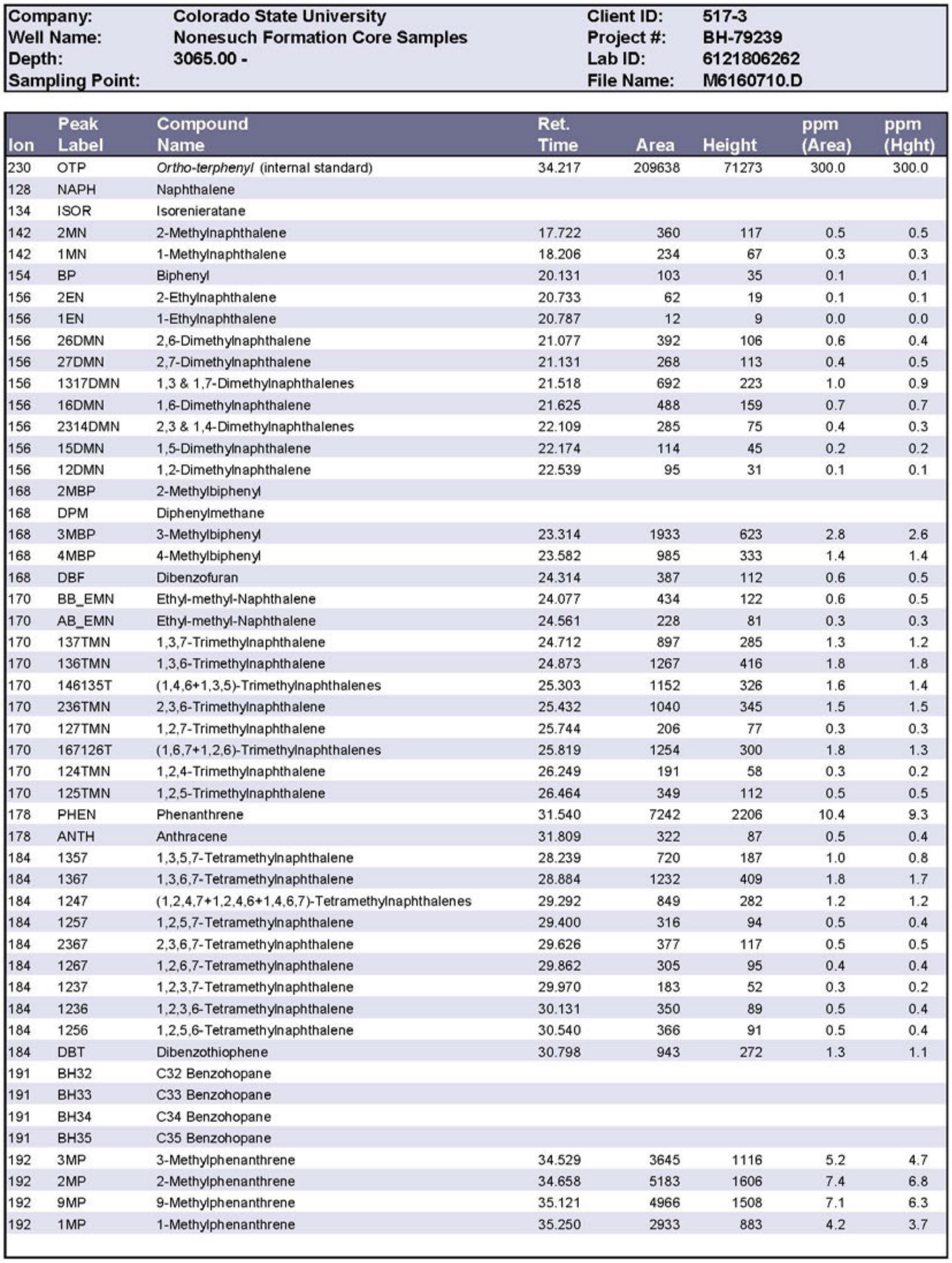

| | | | |
|---|---|---|---|
| **Company:** | **Colorado State University** | **Client ID:** | **517-3** |
| **Well Name:** | **Nonesuch Formation Core Samples** | **Project #:** | **BH-79239** |
| **Depth:** | **3065.00 -** | **Lab ID:** | **6121806262** |
| **Sampling Point:** | | **File Name:** | **M6160710.D** |

| Ion | Peak Label | Compound Name | Ret. Time | Area | Height | ppm (Area) | ppm (Hght) |
|---|---|---|---|---|---|---|---|
| 230 | OTP | *Ortho-terphenyl* (internal standard) | 34.217 | 209638 | 71273 | 300.0 | 300.0 |
| 128 | NAPH | Naphthalene | | | | | |
| 134 | ISOR | Isorenieratane | | | | | |
| 142 | 2MN | 2-Methylnaphthalene | 17.722 | 360 | 117 | 0.5 | 0.5 |
| 142 | 1MN | 1-Methylnaphthalene | 18.206 | 234 | 67 | 0.3 | 0.3 |
| 154 | BP | Biphenyl | 20.131 | 103 | 35 | 0.1 | 0.1 |
| 156 | 2EN | 2-Ethylnaphthalene | 20.733 | 62 | 19 | 0.1 | 0.1 |
| 156 | 1EN | 1-Ethylnaphthalene | 20.787 | 12 | 9 | 0.0 | 0.0 |
| 156 | 26DMN | 2,6-Dimethylnaphthalene | 21.077 | 392 | 106 | 0.6 | 0.4 |
| 156 | 27DMN | 2,7-Dimethylnaphthalene | 21.131 | 268 | 113 | 0.4 | 0.5 |
| 156 | 1317DMN | 1,3 & 1,7-Dimethylnaphthalenes | 21.518 | 692 | 223 | 1.0 | 0.9 |
| 156 | 16DMN | 1,6-Dimethylnaphthalene | 21.625 | 488 | 159 | 0.7 | 0.7 |
| 156 | 2314DMN | 2,3 & 1,4-Dimethylnaphthalenes | 22.109 | 285 | 75 | 0.4 | 0.3 |
| 156 | 15DMN | 1,5-Dimethylnaphthalene | 22.174 | 114 | 45 | 0.2 | 0.2 |
| 156 | 12DMN | 1,2-Dimethylnaphthalene | 22.539 | 95 | 31 | 0.1 | 0.1 |
| 168 | 2MBP | 2-Methylbiphenyl | | | | | |
| 168 | DPM | Diphenylmethane | | | | | |
| 168 | 3MBP | 3-Methylbiphenyl | 23.314 | 1933 | 623 | 2.8 | 2.6 |
| 168 | 4MBP | 4-Methylbiphenyl | 23.582 | 985 | 333 | 1.4 | 1.4 |
| 168 | DBF | Dibenzofuran | 24.314 | 387 | 112 | 0.6 | 0.5 |
| 170 | BB_EMN | Ethyl-methyl-Naphthalene | 24.077 | 434 | 122 | 0.6 | 0.5 |
| 170 | AB_EMN | Ethyl-methyl-Naphthalene | 24.561 | 228 | 81 | 0.3 | 0.3 |
| 170 | 137TMN | 1,3,7-Trimethylnaphthalene | 24.712 | 897 | 285 | 1.3 | 1.2 |
| 170 | 136TMN | 1,3,6-Trimethylnaphthalene | 24.873 | 1267 | 416 | 1.8 | 1.8 |
| 170 | 146135T | (1,4,6+1,3,5)-Trimethylnaphthalenes | 25.303 | 1152 | 326 | 1.6 | 1.4 |
| 170 | 236TMN | 2,3,6-Trimethylnaphthalene | 25.432 | 1040 | 345 | 1.5 | 1.5 |
| 170 | 127TMN | 1,2,7-Trimethylnaphthalene | 25.744 | 206 | 77 | 0.3 | 0.3 |
| 170 | 167126T | (1,6,7+1,2,6)-Trimethylnaphthalenes | 25.819 | 1254 | 300 | 1.8 | 1.3 |
| 170 | 124TMN | 1,2,4-Trimethylnaphthalene | 26.249 | 191 | 58 | 0.3 | 0.2 |
| 170 | 125TMN | 1,2,5-Trimethylnaphthalene | 26.464 | 349 | 112 | 0.5 | 0.5 |
| 178 | PHEN | Phenanthrene | 31.540 | 7242 | 2206 | 10.4 | 9.3 |
| 178 | ANTH | Anthracene | 31.809 | 322 | 87 | 0.5 | 0.4 |
| 184 | 1357 | 1,3,5,7-Tetramethylnaphthalene | 28.239 | 720 | 187 | 1.0 | 0.8 |
| 184 | 1367 | 1,3,6,7-Tetramethylnaphthalene | 28.884 | 1232 | 409 | 1.8 | 1.7 |
| 184 | 1247 | (1,2,4,7+1,2,4,6+1,4,6,7)-Tetramethylnaphthalenes | 29.292 | 849 | 282 | 1.2 | 1.2 |
| 184 | 1257 | 1,2,5,7-Tetramethylnaphthalene | 29.400 | 316 | 94 | 0.5 | 0.4 |
| 184 | 2367 | 2,3,6,7-Tetramethylnaphthalene | 29.626 | 377 | 117 | 0.5 | 0.5 |
| 184 | 1267 | 1,2,6,7-Tetramethylnaphthalene | 29.862 | 305 | 95 | 0.4 | 0.4 |
| 184 | 1237 | 1,2,3,7-Tetramethylnaphthalene | 29.970 | 183 | 52 | 0.3 | 0.2 |
| 184 | 1236 | 1,2,3,6-Tetramethylnaphthalene | 30.131 | 350 | 89 | 0.5 | 0.4 |
| 184 | 1256 | 1,2,5,6-Tetramethylnaphthalene | 30.540 | 366 | 91 | 0.5 | 0.4 |
| 184 | DBT | Dibenzothiophene | 30.798 | 943 | 272 | 1.3 | 1.1 |
| 191 | BH32 | C32 Benzohopane | | | | | |
| 191 | BH33 | C33 Benzohopane | | | | | |
| 191 | BH34 | C34 Benzohopane | | | | | |
| 191 | BH35 | C35 Benzohopane | | | | | |
| 192 | 3MP | 3-Methylphenanthrene | 34.529 | 3645 | 1116 | 5.2 | 4.7 |
| 192 | 2MP | 2-Methylphenanthrene | 34.658 | 5183 | 1606 | 7.4 | 6.8 |
| 192 | 9MP | 9-Methylphenanthrene | 35.121 | 4966 | 1508 | 7.1 | 6.3 |
| 192 | 1MP | 1-Methylphenanthrene | 35.250 | 2933 | 883 | 4.2 | 3.7 |

*Appendix F2, ctd.*

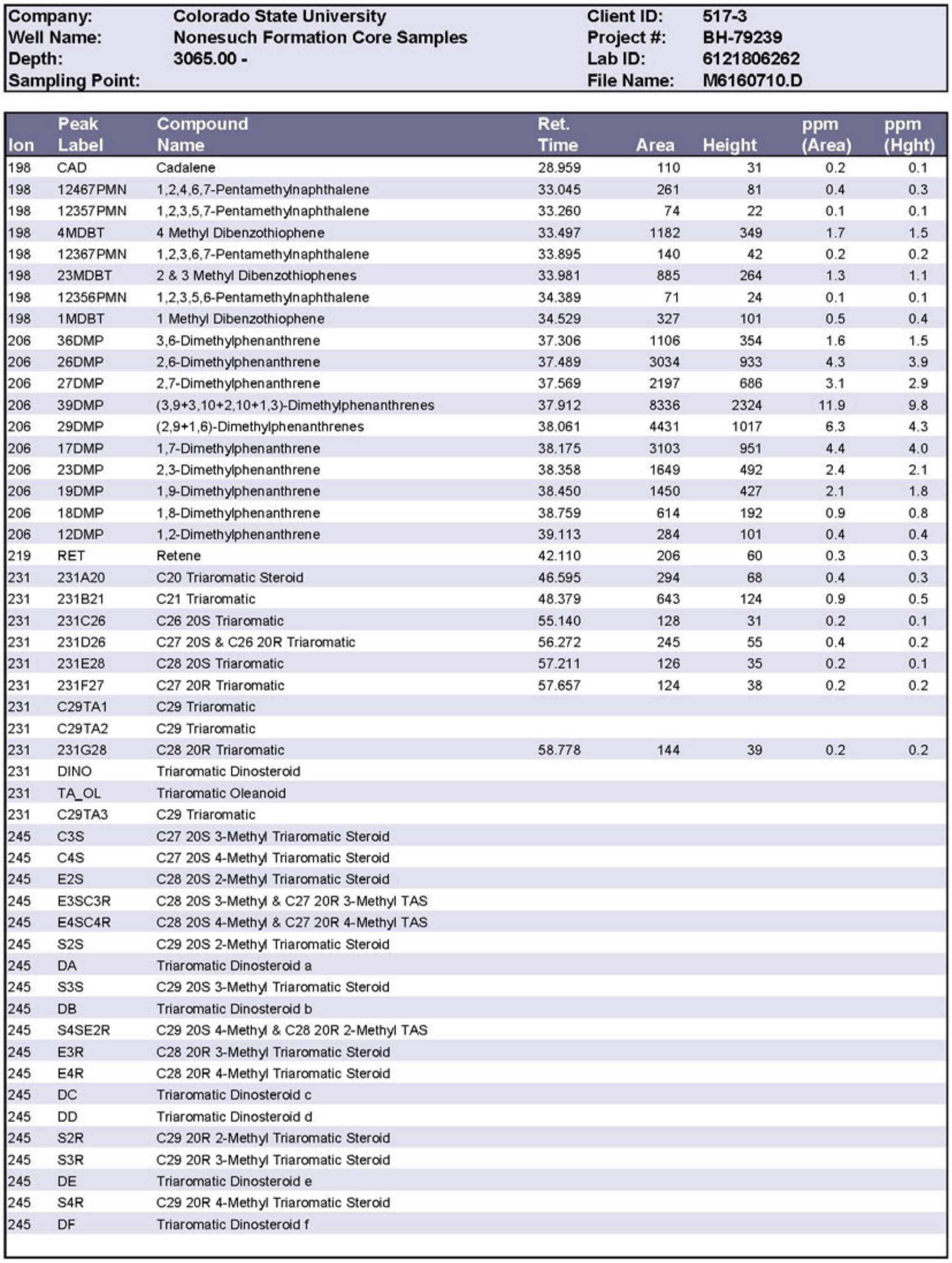

| | | | |
|---|---|---|---|
| **Company:** | **Colorado State University** | **Client ID:** | **517-3** |
| **Well Name:** | **Nonesuch Formation Core Samples** | **Project #:** | **BH-79239** |
| **Depth:** | **3065.00 -** | **Lab ID:** | **6121806262** |
| **Sampling Point:** | | **File Name:** | **M6160710.D** |

| Ion | Peak Label | Compound Name | Ret. Time | Area | Height | ppm (Area) | ppm (Hght) |
|---|---|---|---|---|---|---|---|
| 198 | CAD | Cadalene | 28.959 | 110 | 31 | 0.2 | 0.1 |
| 198 | 12467PMN | 1,2,4,6,7-Pentamethylnaphthalene | 33.045 | 261 | 81 | 0.4 | 0.3 |
| 198 | 12357PMN | 1,2,3,5,7-Pentamethylnaphthalene | 33.260 | 74 | 22 | 0.1 | 0.1 |
| 198 | 4MDBT | 4 Methyl Dibenzothiophene | 33.497 | 1182 | 349 | 1.7 | 1.5 |
| 198 | 12367PMN | 1,2,3,6,7-Pentamethylnaphthalene | 33.895 | 140 | 42 | 0.2 | 0.2 |
| 198 | 23MDBT | 2 & 3 Methyl Dibenzothiophenes | 33.981 | 885 | 264 | 1.3 | 1.1 |
| 198 | 12356PMN | 1,2,3,5,6-Pentamethylnaphthalene | 34.389 | 71 | 24 | 0.1 | 0.1 |
| 198 | 1MDBT | 1 Methyl Dibenzothiophene | 34.529 | 327 | 101 | 0.5 | 0.4 |
| 206 | 36DMP | 3,6-Dimethylphenanthrene | 37.306 | 1106 | 354 | 1.6 | 1.5 |
| 206 | 26DMP | 2,6-Dimethylphenanthrene | 37.489 | 3034 | 933 | 4.3 | 3.9 |
| 206 | 27DMP | 2,7-Dimethylphenanthrene | 37.569 | 2197 | 686 | 3.1 | 2.9 |
| 206 | 39DMP | (3,9+3,10+2,10+1,3)-Dimethylphenanthrenes | 37.912 | 8336 | 2324 | 11.9 | 9.8 |
| 206 | 29DMP | (2,9+1,6)-Dimethylphenanthrenes | 38.061 | 4431 | 1017 | 6.3 | 4.3 |
| 206 | 17DMP | 1,7-Dimethylphenanthrene | 38.175 | 3103 | 951 | 4.4 | 4.0 |
| 206 | 23DMP | 2,3-Dimethylphenanthrene | 38.358 | 1649 | 492 | 2.4 | 2.1 |
| 206 | 19DMP | 1,9-Dimethylphenanthrene | 38.450 | 1450 | 427 | 2.1 | 1.8 |
| 206 | 18DMP | 1,8-Dimethylphenanthrene | 38.759 | 614 | 192 | 0.9 | 0.8 |
| 206 | 12DMP | 1,2-Dimethylphenanthrene | 39.113 | 284 | 101 | 0.4 | 0.4 |
| 219 | RET | Retene | 42.110 | 206 | 60 | 0.3 | 0.3 |
| 231 | 231A20 | C20 Triaromatic Steroid | 46.595 | 294 | 68 | 0.4 | 0.3 |
| 231 | 231B21 | C21 Triaromatic | 48.379 | 643 | 124 | 0.9 | 0.5 |
| 231 | 231C26 | C26 20S Triaromatic | 55.140 | 128 | 31 | 0.2 | 0.1 |
| 231 | 231D26 | C27 20S & C26 20R Triaromatic | 56.272 | 245 | 55 | 0.4 | 0.2 |
| 231 | 231E28 | C28 20S Triaromatic | 57.211 | 126 | 35 | 0.2 | 0.1 |
| 231 | 231F27 | C27 20R Triaromatic | 57.657 | 124 | 38 | 0.2 | 0.2 |
| 231 | C29TA1 | C29 Triaromatic | | | | | |
| 231 | C29TA2 | C29 Triaromatic | | | | | |
| 231 | 231G28 | C28 20R Triaromatic | 58.778 | 144 | 39 | 0.2 | 0.2 |
| 231 | DINO | Triaromatic Dinosteroid | | | | | |
| 231 | TA_OL | Triaromatic Oleanoid | | | | | |
| 231 | C29TA3 | C29 Triaromatic | | | | | |
| 245 | C3S | C27 20S 3-Methyl Triaromatic Steroid | | | | | |
| 245 | C4S | C27 20S 4-Methyl Triaromatic Steroid | | | | | |
| 245 | E2S | C28 20S 2-Methyl Triaromatic Steroid | | | | | |
| 245 | E3SC3R | C28 20S 3-Methyl & C27 20R 3-Methyl TAS | | | | | |
| 245 | E4SC4R | C28 20S 4-Methyl & C27 20R 4-Methyl TAS | | | | | |
| 245 | S2S | C29 20S 2-Methyl Triaromatic Steroid | | | | | |
| 245 | DA | Triaromatic Dinosteroid a | | | | | |
| 245 | S3S | C29 20S 3-Methyl Triaromatic Steroid | | | | | |
| 245 | DB | Triaromatic Dinosteroid b | | | | | |
| 245 | S4SE2R | C29 20S 4-Methyl & C28 20R 2-Methyl TAS | | | | | |
| 245 | E3R | C28 20R 3-Methyl Triaromatic Steroid | | | | | |
| 245 | E4R | C28 20R 4-Methyl Triaromatic Steroid | | | | | |
| 245 | DC | Triaromatic Dinosteroid c | | | | | |
| 245 | DD | Triaromatic Dinosteroid d | | | | | |
| 245 | S2R | C29 20R 2-Methyl Triaromatic Steroid | | | | | |
| 245 | S3R | C29 20R 3-Methyl Triaromatic Steroid | | | | | |
| 245 | DE | Triaromatic Dinosteroid e | | | | | |
| 245 | S4R | C29 20R 4-Methyl Triaromatic Steroid | | | | | |
| 245 | DF | Triaromatic Dinosteroid f | | | | | |

*Appendix F2, ctd.*

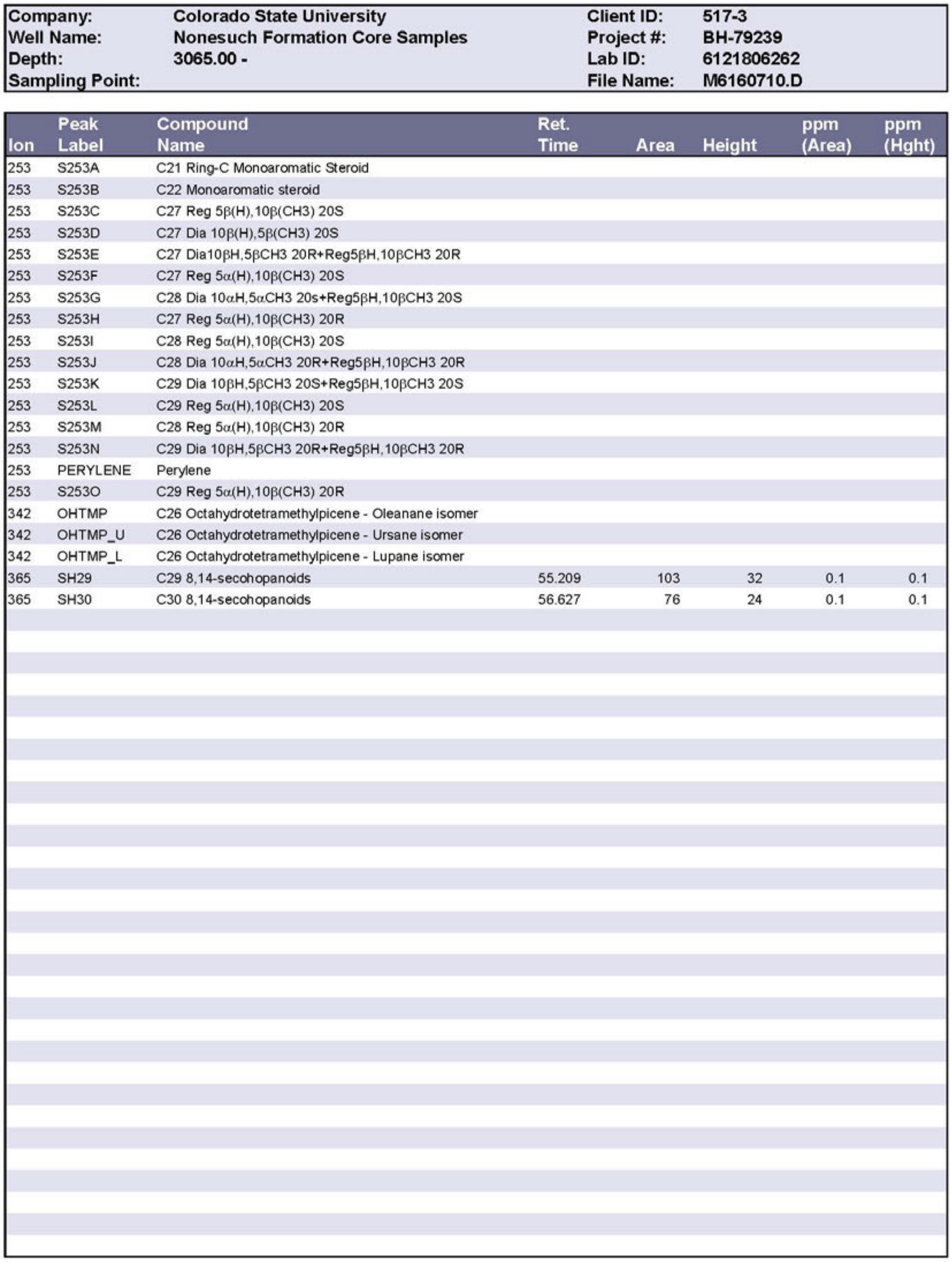

| | | | |
|---|---|---|---|
| **Company:** | **Colorado State University** | **Client ID:** | **517-3** |
| **Well Name:** | **Nonesuch Formation Core Samples** | **Project #:** | **BH-79239** |
| **Depth:** | **3065.00 -** | **Lab ID:** | **6121806262** |
| **Sampling Point:** | | **File Name:** | **M6160710.D** |

| Ion | Peak Label | Compound Name | Ret. Time | Area | Height | ppm (Area) | ppm (Hght) |
|---|---|---|---|---|---|---|---|
| 253 | S253A | C21 Ring-C Monoaromatic Steroid | | | | | |
| 253 | S253B | C22 Monoaromatic steroid | | | | | |
| 253 | S253C | C27 Reg 5β(H),10β(CH3) 20S | | | | | |
| 253 | S253D | C27 Dia 10β(H),5β(CH3) 20S | | | | | |
| 253 | S253E | C27 Dia10βH,5βCH3 20R+Reg5βH,10βCH3 20R | | | | | |
| 253 | S253F | C27 Reg 5α(H),10β(CH3) 20S | | | | | |
| 253 | S253G | C28 Dia 10αH,5αCH3 20s+Reg5βH,10βCH3 20S | | | | | |
| 253 | S253H | C27 Reg 5α(H),10β(CH3) 20R | | | | | |
| 253 | S253I | C28 Reg 5α(H),10β(CH3) 20S | | | | | |
| 253 | S253J | C28 Dia 10αH,5αCH3 20R+Reg5βH,10βCH3 20R | | | | | |
| 253 | S253K | C29 Dia 10βH,5βCH3 20S+Reg5βH,10βCH3 20S | | | | | |
| 253 | S253L | C29 Reg 5α(H),10β(CH3) 20S | | | | | |
| 253 | S253M | C28 Reg 5α(H),10β(CH3) 20R | | | | | |
| 253 | S253N | C29 Dia 10βH,5βCH3 20R+Reg5βH,10βCH3 20R | | | | | |
| 253 | PERYLENE | Perylene | | | | | |
| 253 | S253O | C29 Reg 5α(H),10β(CH3) 20R | | | | | |
| 342 | OHTMP | C26 Octahydrotetramethylpicene - Oleanane isomer | | | | | |
| 342 | OHTMP_U | C26 Octahydrotetramethylpicene - Ursane isomer | | | | | |
| 342 | OHTMP_L | C26 Octahydrotetramethylpicene - Lupane isomer | | | | | |
| 365 | SH29 | C29 8,14-secohopanoids | 55.209 | 103 | 32 | 0.1 | 0.1 |
| 365 | SH30 | C30 8,14-secohopanoids | 56.627 | 76 | 24 | 0.1 | 0.1 |

*Appendix F2, ctd.*

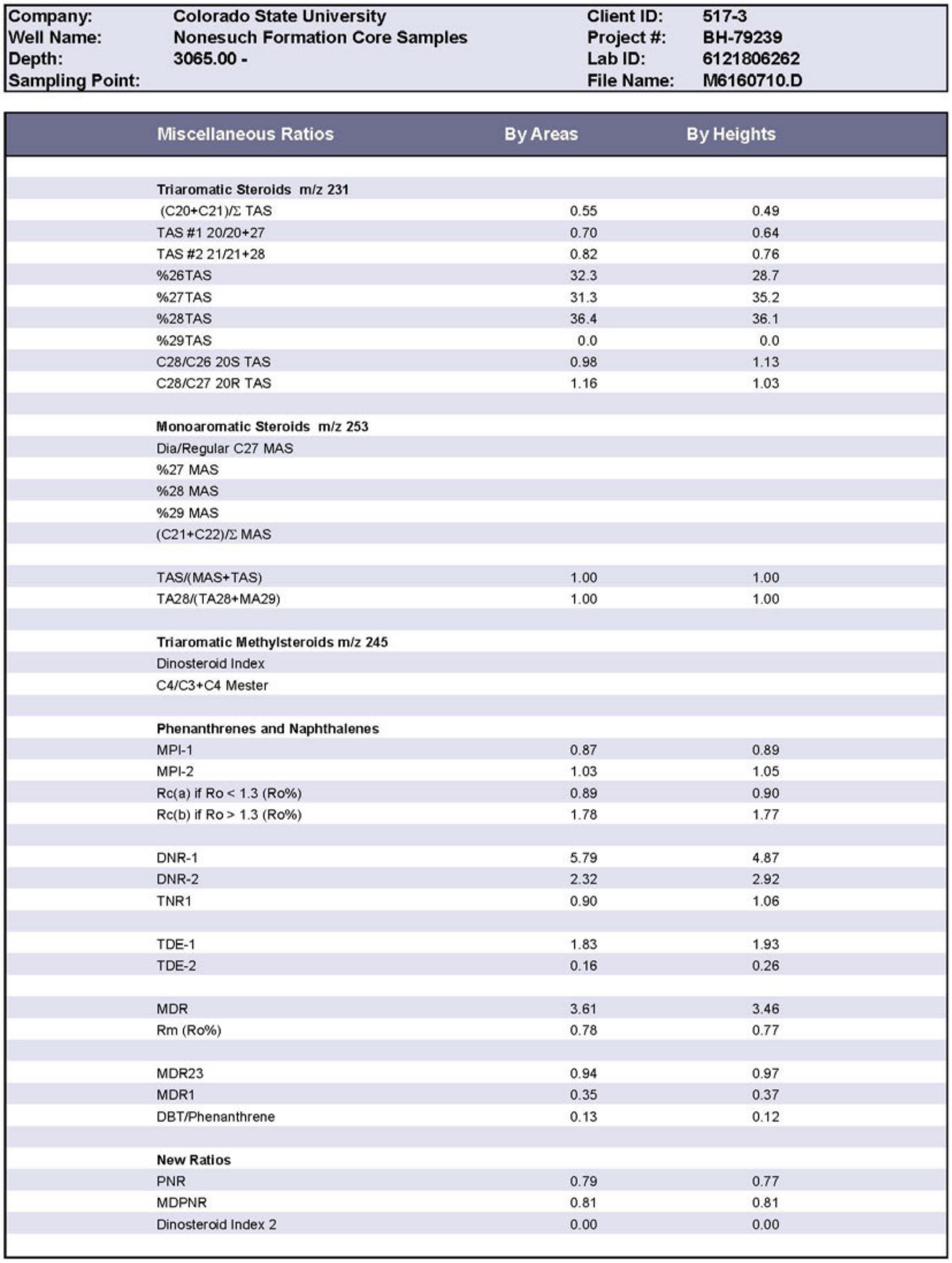

| | | | |
|---|---|---|---|
| **Company:** | **Colorado State University** | **Client ID:** | **517-3** |
| **Well Name:** | **Nonesuch Formation Core Samples** | **Project #:** | **BH-79239** |
| **Depth:** | **3065.00 -** | **Lab ID:** | **6121806262** |
| **Sampling Point:** | | **File Name:** | **M6160710.D** |

| Miscellaneous Ratios | By Areas | By Heights |
|---|---|---|
| **Triaromatic Steroids m/z 231** | | |
| (C20+C21)/Σ TAS | 0.55 | 0.49 |
| TAS #1 20/20+27 | 0.70 | 0.64 |
| TAS #2 21/21+28 | 0.82 | 0.76 |
| %26TAS | 32.3 | 28.7 |
| %27TAS | 31.3 | 35.2 |
| %28TAS | 36.4 | 36.1 |
| %29TAS | 0.0 | 0.0 |
| C28/C26 20S TAS | 0.98 | 1.13 |
| C28/C27 20R TAS | 1.16 | 1.03 |
| | | |
| **Monoaromatic Steroids m/z 253** | | |
| Dia/Regular C27 MAS | | |
| %27 MAS | | |
| %28 MAS | | |
| %29 MAS | | |
| (C21+C22)/Σ MAS | | |
| | | |
| TAS/(MAS+TAS) | 1.00 | 1.00 |
| TA28/(TA28+MA29) | 1.00 | 1.00 |
| | | |
| **Triaromatic Methylsteroids m/z 245** | | |
| Dinosteroid Index | | |
| C4/C3+C4 Mester | | |
| | | |
| **Phenanthrenes and Naphthalenes** | | |
| MPI-1 | 0.87 | 0.89 |
| MPI-2 | 1.03 | 1.05 |
| Rc(a) if Ro < 1.3 (Ro%) | 0.89 | 0.90 |
| Rc(b) if Ro > 1.3 (Ro%) | 1.78 | 1.77 |
| | | |
| DNR-1 | 5.79 | 4.87 |
| DNR-2 | 2.32 | 2.92 |
| TNR1 | 0.90 | 1.06 |
| | | |
| TDE-1 | 1.83 | 1.93 |
| TDE-2 | 0.16 | 0.26 |
| | | |
| MDR | 3.61 | 3.46 |
| Rm (Ro%) | 0.78 | 0.77 |
| | | |
| MDR23 | 0.94 | 0.97 |
| MDR1 | 0.35 | 0.37 |
| DBT/Phenanthrene | 0.13 | 0.12 |
| | | |
| **New Ratios** | | |
| PNR | 0.79 | 0.77 |
| MDPNR | 0.81 | 0.81 |
| Dinosteroid Index 2 | 0.00 | 0.00 |

*Appendix F2, ctd.*

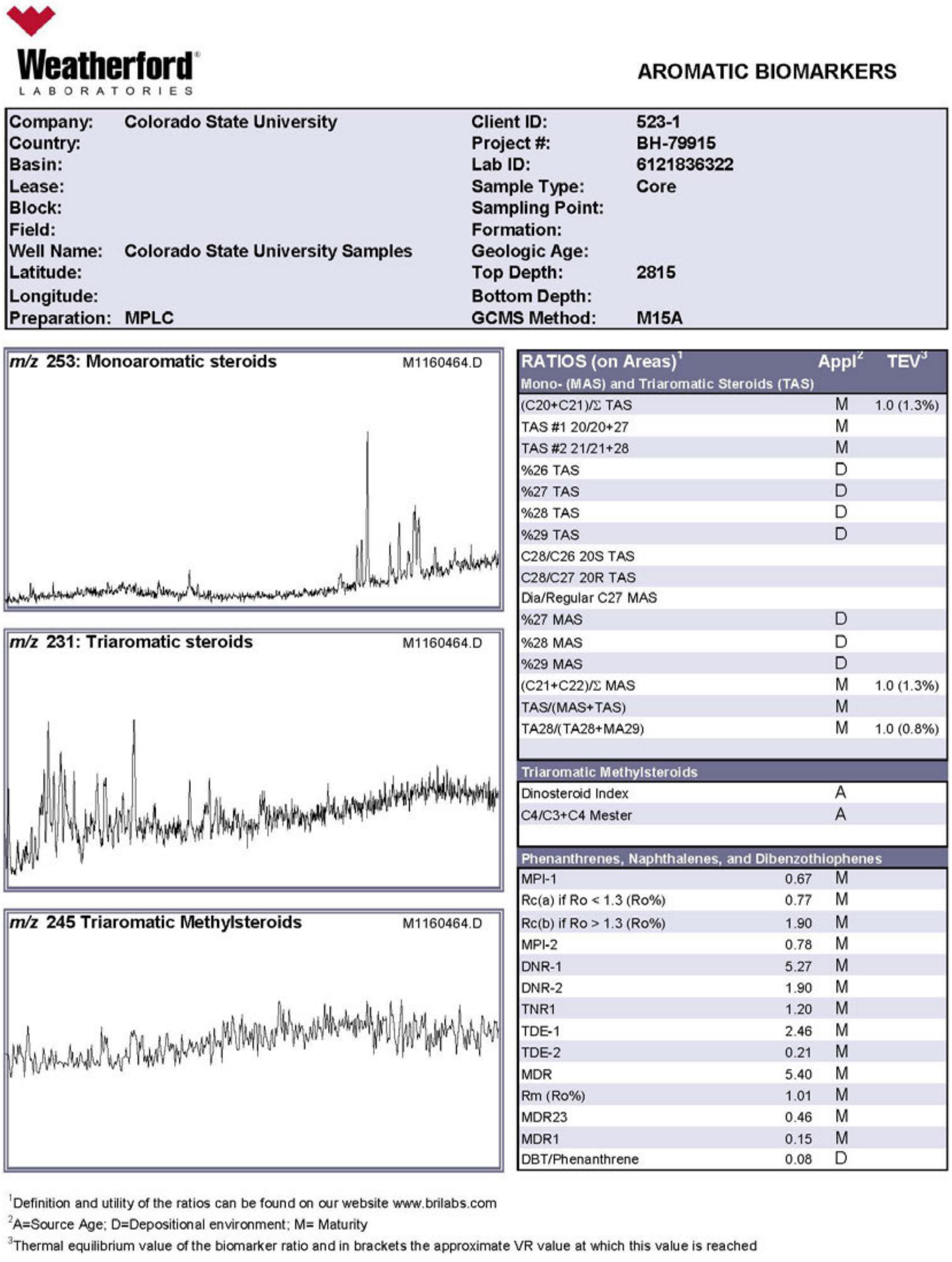

Weatherford LABORATORIES

**AROMATIC BIOMARKERS**

| | | | |
|---|---|---|---|
| **Company:** | **Colorado State University** | **Client ID:** | **523-1** |
| **Country:** | | **Project #:** | **BH-79915** |
| **Basin:** | | **Lab ID:** | **6121836322** |
| **Lease:** | | **Sample Type:** | **Core** |
| **Block:** | | **Sampling Point:** | |
| **Field:** | | **Formation:** | |
| **Well Name:** | **Colorado State University Samples** | **Geologic Age:** | |
| **Latitude:** | | **Top Depth:** | **2815** |
| **Longitude:** | | **Bottom Depth:** | |
| **Preparation:** | **MPLC** | **GCMS Method:** | **M15A** |

***m/z* 253: Monoaromatic steroids** M1160464.D

***m/z* 231: Triaromatic steroids** M1160464.D

***m/z* 245 Triaromatic Methylsteroids** M1160464.D

| RATIOS (on Areas)[1] | | Appl[2] | TEV[3] |
|---|---|---|---|
| **Mono- (MAS) and Triaromatic Steroids (TAS)** | | | |
| (C20+C21)/Σ TAS | | M | 1.0 (1.3%) |
| TAS #1 20/20+27 | | M | |
| TAS #2 21/21+28 | | M | |
| %26 TAS | | D | |
| %27 TAS | | D | |
| %28 TAS | | D | |
| %29 TAS | | D | |
| C28/C26 20S TAS | | | |
| C28/C27 20R TAS | | | |
| Dia/Regular C27 MAS | | | |
| %27 MAS | | D | |
| %28 MAS | | D | |
| %29 MAS | | D | |
| (C21+C22)/Σ MAS | | M | 1.0 (1.3%) |
| TAS/(MAS+TAS) | | M | |
| TA28/(TA28+MA29) | | M | 1.0 (0.8%) |
| **Triaromatic Methylsteroids** | | | |
| Dinosteroid Index | | A | |
| C4/C3+C4 Mester | | A | |
| **Phenanthrenes, Naphthalenes, and Dibenzothiophenes** | | | |
| MPI-1 | 0.67 | M | |
| Rc(a) if Ro < 1.3 (Ro%) | 0.77 | M | |
| Rc(b) if Ro > 1.3 (Ro%) | 1.90 | M | |
| MPI-2 | 0.78 | M | |
| DNR-1 | 5.27 | M | |
| DNR-2 | 1.90 | M | |
| TNR1 | 1.20 | M | |
| TDE-1 | 2.46 | M | |
| TDE-2 | 0.21 | M | |
| MDR | 5.40 | M | |
| Rm (Ro%) | 1.01 | M | |
| MDR23 | 0.46 | M | |
| MDR1 | 0.15 | M | |
| DBT/Phenanthrene | 0.08 | D | |

[1] Definition and utility of the ratios can be found on our website www.brilabs.com

[2] A=Source Age; D=Depositional environment; M= Maturity

[3] Thermal equilibrium value of the biomarker ratio and in brackets the approximate VR value at which this value is reached

*Appendix F2, ctd.*

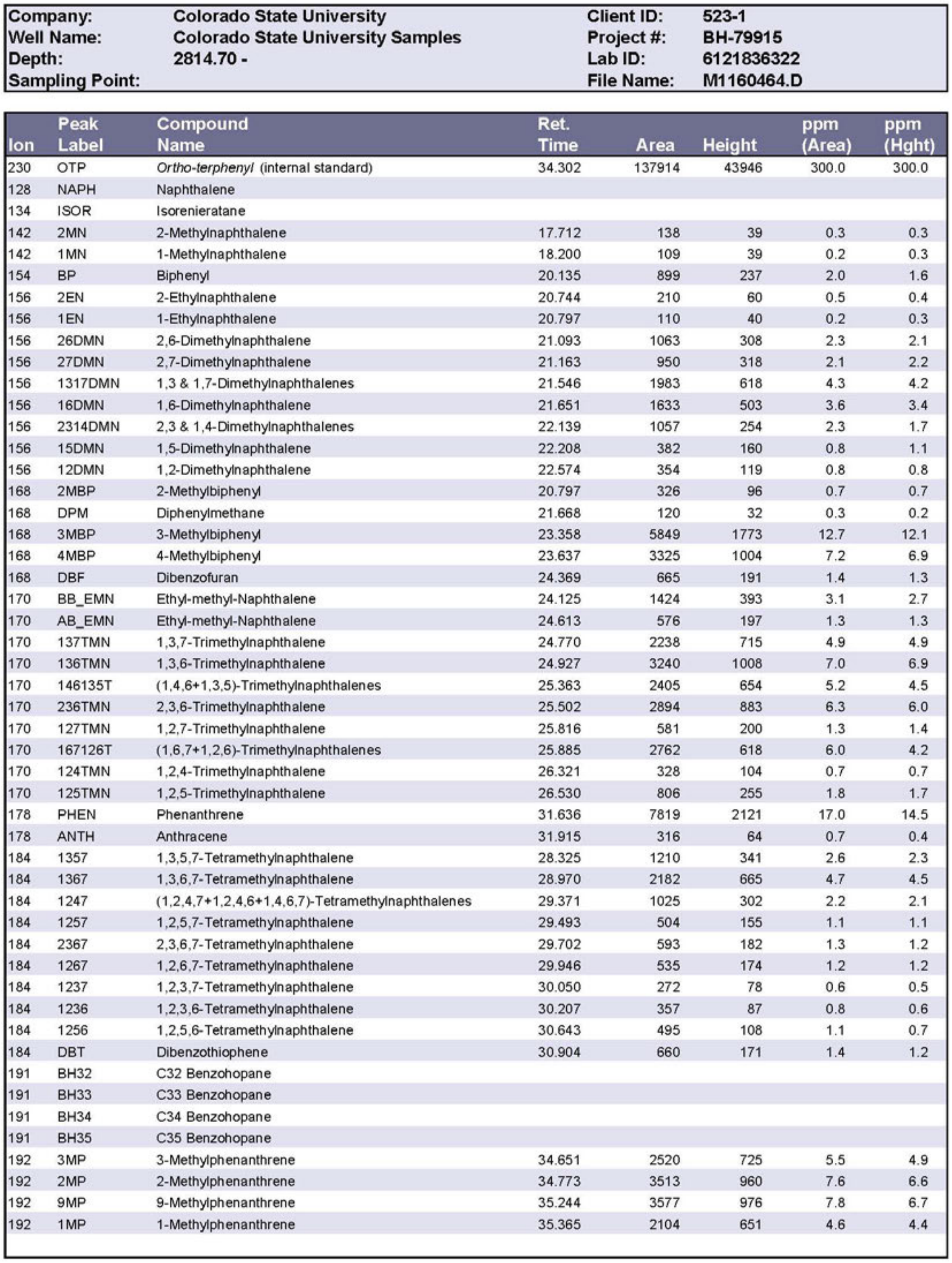

|  |  |  |  |
|---|---|---|---|
| **Company:** | **Colorado State University** | **Client ID:** | **523-1** |
| **Well Name:** | **Colorado State University Samples** | **Project #:** | **BH-79915** |
| **Depth:** | **2814.70 -** | **Lab ID:** | **6121836322** |
| **Sampling Point:** |  | **File Name:** | **M1160464.D** |

| Ion | Peak Label | Compound Name | Ret. Time | Area | Height | ppm (Area) | ppm (Hght) |
|---|---|---|---|---|---|---|---|
| 230 | OTP | *Ortho-terphenyl* (internal standard) | 34.302 | 137914 | 43946 | 300.0 | 300.0 |
| 128 | NAPH | Naphthalene |  |  |  |  |  |
| 134 | ISOR | Isorenieratane |  |  |  |  |  |
| 142 | 2MN | 2-Methylnaphthalene | 17.712 | 138 | 39 | 0.3 | 0.3 |
| 142 | 1MN | 1-Methylnaphthalene | 18.200 | 109 | 39 | 0.2 | 0.3 |
| 154 | BP | Biphenyl | 20.135 | 899 | 237 | 2.0 | 1.6 |
| 156 | 2EN | 2-Ethylnaphthalene | 20.744 | 210 | 60 | 0.5 | 0.4 |
| 156 | 1EN | 1-Ethylnaphthalene | 20.797 | 110 | 40 | 0.2 | 0.3 |
| 156 | 26DMN | 2,6-Dimethylnaphthalene | 21.093 | 1063 | 308 | 2.3 | 2.1 |
| 156 | 27DMN | 2,7-Dimethylnaphthalene | 21.163 | 950 | 318 | 2.1 | 2.2 |
| 156 | 1317DMN | 1,3 & 1,7-Dimethylnaphthalenes | 21.546 | 1983 | 618 | 4.3 | 4.2 |
| 156 | 16DMN | 1,6-Dimethylnaphthalene | 21.651 | 1633 | 503 | 3.6 | 3.4 |
| 156 | 2314DMN | 2,3 & 1,4-Dimethylnaphthalenes | 22.139 | 1057 | 254 | 2.3 | 1.7 |
| 156 | 15DMN | 1,5-Dimethylnaphthalene | 22.208 | 382 | 160 | 0.8 | 1.1 |
| 156 | 12DMN | 1,2-Dimethylnaphthalene | 22.574 | 354 | 119 | 0.8 | 0.8 |
| 168 | 2MBP | 2-Methylbiphenyl | 20.797 | 326 | 96 | 0.7 | 0.7 |
| 168 | DPM | Diphenylmethane | 21.668 | 120 | 32 | 0.3 | 0.2 |
| 168 | 3MBP | 3-Methylbiphenyl | 23.358 | 5849 | 1773 | 12.7 | 12.1 |
| 168 | 4MBP | 4-Methylbiphenyl | 23.637 | 3325 | 1004 | 7.2 | 6.9 |
| 168 | DBF | Dibenzofuran | 24.369 | 665 | 191 | 1.4 | 1.3 |
| 170 | BB_EMN | Ethyl-methyl-Naphthalene | 24.125 | 1424 | 393 | 3.1 | 2.7 |
| 170 | AB_EMN | Ethyl-methyl-Naphthalene | 24.613 | 576 | 197 | 1.3 | 1.3 |
| 170 | 137TMN | 1,3,7-Trimethylnaphthalene | 24.770 | 2238 | 715 | 4.9 | 4.9 |
| 170 | 136TMN | 1,3,6-Trimethylnaphthalene | 24.927 | 3240 | 1008 | 7.0 | 6.9 |
| 170 | 146135T | (1,4,6+1,3,5)-Trimethylnaphthalenes | 25.363 | 2405 | 654 | 5.2 | 4.5 |
| 170 | 236TMN | 2,3,6-Trimethylnaphthalene | 25.502 | 2894 | 883 | 6.3 | 6.0 |
| 170 | 127TMN | 1,2,7-Trimethylnaphthalene | 25.816 | 581 | 200 | 1.3 | 1.4 |
| 170 | 167126T | (1,6,7+1,2,6)-Trimethylnaphthalenes | 25.885 | 2762 | 618 | 6.0 | 4.2 |
| 170 | 124TMN | 1,2,4-Trimethylnaphthalene | 26.321 | 328 | 104 | 0.7 | 0.7 |
| 170 | 125TMN | 1,2,5-Trimethylnaphthalene | 26.530 | 806 | 255 | 1.8 | 1.7 |
| 178 | PHEN | Phenanthrene | 31.636 | 7819 | 2121 | 17.0 | 14.5 |
| 178 | ANTH | Anthracene | 31.915 | 316 | 64 | 0.7 | 0.4 |
| 184 | 1357 | 1,3,5,7-Tetramethylnaphthalene | 28.325 | 1210 | 341 | 2.6 | 2.3 |
| 184 | 1367 | 1,3,6,7-Tetramethylnaphthalene | 28.970 | 2182 | 665 | 4.7 | 4.5 |
| 184 | 1247 | (1,2,4,7+1,2,4,6+1,4,6,7)-Tetramethylnaphthalenes | 29.371 | 1025 | 302 | 2.2 | 2.1 |
| 184 | 1257 | 1,2,5,7-Tetramethylnaphthalene | 29.493 | 504 | 155 | 1.1 | 1.1 |
| 184 | 2367 | 2,3,6,7-Tetramethylnaphthalene | 29.702 | 593 | 182 | 1.3 | 1.2 |
| 184 | 1267 | 1,2,6,7-Tetramethylnaphthalene | 29.946 | 535 | 174 | 1.2 | 1.2 |
| 184 | 1237 | 1,2,3,7-Tetramethylnaphthalene | 30.050 | 272 | 78 | 0.6 | 0.5 |
| 184 | 1236 | 1,2,3,6-Tetramethylnaphthalene | 30.207 | 357 | 87 | 0.8 | 0.6 |
| 184 | 1256 | 1,2,5,6-Tetramethylnaphthalene | 30.643 | 495 | 108 | 1.1 | 0.7 |
| 184 | DBT | Dibenzothiophene | 30.904 | 660 | 171 | 1.4 | 1.2 |
| 191 | BH32 | C32 Benzohopane |  |  |  |  |  |
| 191 | BH33 | C33 Benzohopane |  |  |  |  |  |
| 191 | BH34 | C34 Benzohopane |  |  |  |  |  |
| 191 | BH35 | C35 Benzohopane |  |  |  |  |  |
| 192 | 3MP | 3-Methylphenanthrene | 34.651 | 2520 | 725 | 5.5 | 4.9 |
| 192 | 2MP | 2-Methylphenanthrene | 34.773 | 3513 | 960 | 7.6 | 6.6 |
| 192 | 9MP | 9-Methylphenanthrene | 35.244 | 3577 | 976 | 7.8 | 6.7 |
| 192 | 1MP | 1-Methylphenanthrene | 35.365 | 2104 | 651 | 4.6 | 4.4 |

*Appendix F2, ctd.*

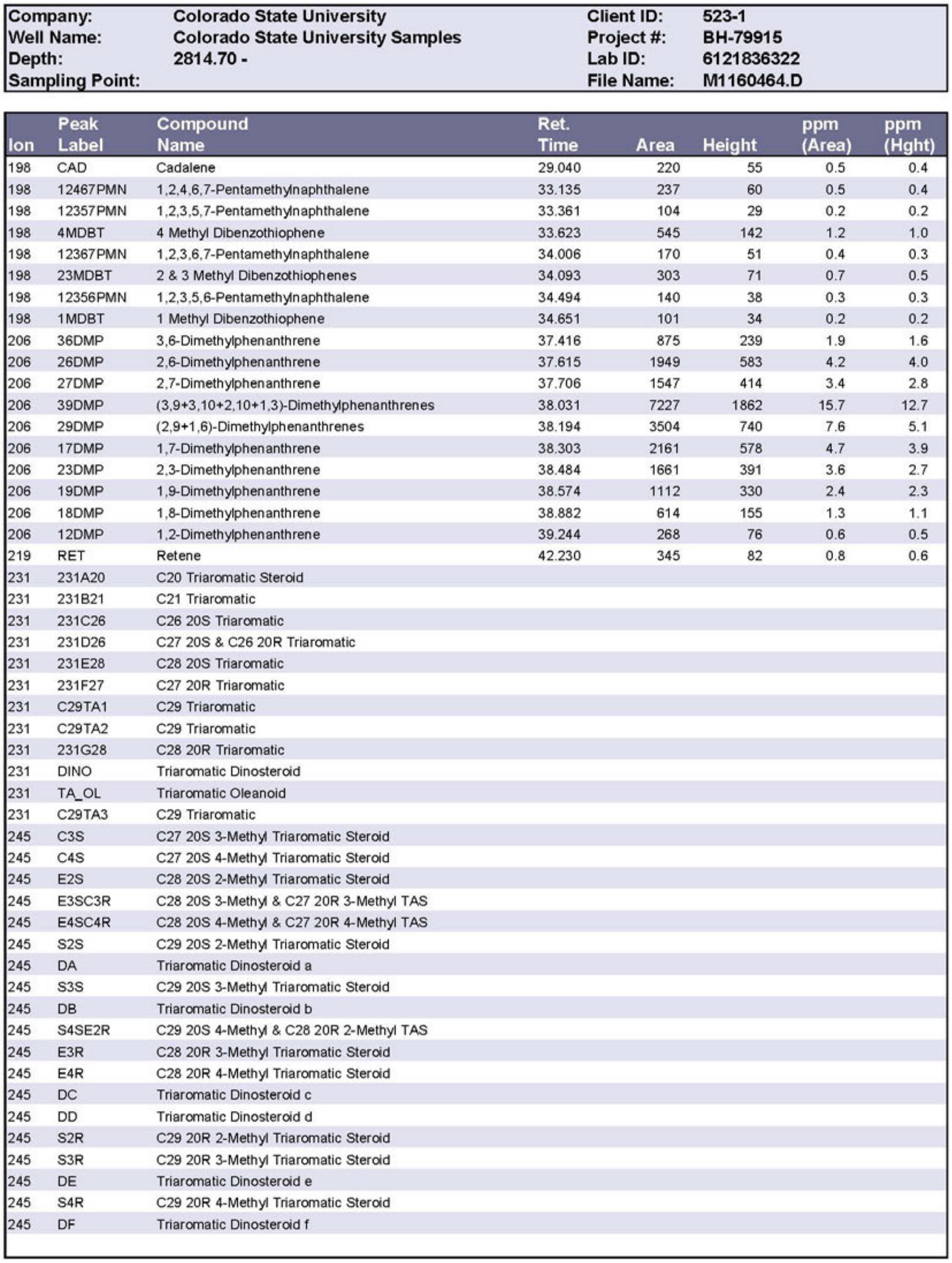

| | | | |
|---|---|---|---|
| **Company:** | **Colorado State University** | **Client ID:** | **523-1** |
| **Well Name:** | **Colorado State University Samples** | **Project #:** | **BH-79915** |
| **Depth:** | **2814.70 -** | **Lab ID:** | **6121836322** |
| **Sampling Point:** | | **File Name:** | **M1160464.D** |

| Ion | Peak Label | Compound Name | Ret. Time | Area | Height | ppm (Area) | ppm (Hght) |
|---|---|---|---|---|---|---|---|
| 198 | CAD | Cadalene | 29.040 | 220 | 55 | 0.5 | 0.4 |
| 198 | 12467PMN | 1,2,4,6,7-Pentamethylnaphthalene | 33.135 | 237 | 60 | 0.5 | 0.4 |
| 198 | 12357PMN | 1,2,3,5,7-Pentamethylnaphthalene | 33.361 | 104 | 29 | 0.2 | 0.2 |
| 198 | 4MDBT | 4 Methyl Dibenzothiophene | 33.623 | 545 | 142 | 1.2 | 1.0 |
| 198 | 12367PMN | 1,2,3,6,7-Pentamethylnaphthalene | 34.006 | 170 | 51 | 0.4 | 0.3 |
| 198 | 23MDBT | 2 & 3 Methyl Dibenzothiophenes | 34.093 | 303 | 71 | 0.7 | 0.5 |
| 198 | 12356PMN | 1,2,3,5,6-Pentamethylnaphthalene | 34.494 | 140 | 38 | 0.3 | 0.3 |
| 198 | 1MDBT | 1 Methyl Dibenzothiophene | 34.651 | 101 | 34 | 0.2 | 0.2 |
| 206 | 36DMP | 3,6-Dimethylphenanthrene | 37.416 | 875 | 239 | 1.9 | 1.6 |
| 206 | 26DMP | 2,6-Dimethylphenanthrene | 37.615 | 1949 | 583 | 4.2 | 4.0 |
| 206 | 27DMP | 2,7-Dimethylphenanthrene | 37.706 | 1547 | 414 | 3.4 | 2.8 |
| 206 | 39DMP | (3,9+3,10+2,10+1,3)-Dimethylphenanthrenes | 38.031 | 7227 | 1862 | 15.7 | 12.7 |
| 206 | 29DMP | (2,9+1,6)-Dimethylphenanthrenes | 38.194 | 3504 | 740 | 7.6 | 5.1 |
| 206 | 17DMP | 1,7-Dimethylphenanthrene | 38.303 | 2161 | 578 | 4.7 | 3.9 |
| 206 | 23DMP | 2,3-Dimethylphenanthrene | 38.484 | 1661 | 391 | 3.6 | 2.7 |
| 206 | 19DMP | 1,9-Dimethylphenanthrene | 38.574 | 1112 | 330 | 2.4 | 2.3 |
| 206 | 18DMP | 1,8-Dimethylphenanthrene | 38.882 | 614 | 155 | 1.3 | 1.1 |
| 206 | 12DMP | 1,2-Dimethylphenanthrene | 39.244 | 268 | 76 | 0.6 | 0.5 |
| 219 | RET | Retene | 42.230 | 345 | 82 | 0.8 | 0.6 |
| 231 | 231A20 | C20 Triaromatic Steroid | | | | | |
| 231 | 231B21 | C21 Triaromatic | | | | | |
| 231 | 231C26 | C26 20S Triaromatic | | | | | |
| 231 | 231D26 | C27 20S & C26 20R Triaromatic | | | | | |
| 231 | 231E28 | C28 20S Triaromatic | | | | | |
| 231 | 231F27 | C27 20R Triaromatic | | | | | |
| 231 | C29TA1 | C29 Triaromatic | | | | | |
| 231 | C29TA2 | C29 Triaromatic | | | | | |
| 231 | 231G28 | C28 20R Triaromatic | | | | | |
| 231 | DINO | Triaromatic Dinosteroid | | | | | |
| 231 | TA_OL | Triaromatic Oleanoid | | | | | |
| 231 | C29TA3 | C29 Triaromatic | | | | | |
| 245 | C3S | C27 20S 3-Methyl Triaromatic Steroid | | | | | |
| 245 | C4S | C27 20S 4-Methyl Triaromatic Steroid | | | | | |
| 245 | E2S | C28 20S 2-Methyl Triaromatic Steroid | | | | | |
| 245 | E3SC3R | C28 20S 3-Methyl & C27 20R 3-Methyl TAS | | | | | |
| 245 | E4SC4R | C28 20S 4-Methyl & C27 20R 4-Methyl TAS | | | | | |
| 245 | S2S | C29 20S 2-Methyl Triaromatic Steroid | | | | | |
| 245 | DA | Triaromatic Dinosteroid a | | | | | |
| 245 | S3S | C29 20S 3-Methyl Triaromatic Steroid | | | | | |
| 245 | DB | Triaromatic Dinosteroid b | | | | | |
| 245 | S4SE2R | C29 20S 4-Methyl & C28 20R 2-Methyl TAS | | | | | |
| 245 | E3R | C28 20R 3-Methyl Triaromatic Steroid | | | | | |
| 245 | E4R | C28 20R 4-Methyl Triaromatic Steroid | | | | | |
| 245 | DC | Triaromatic Dinosteroid c | | | | | |
| 245 | DD | Triaromatic Dinosteroid d | | | | | |
| 245 | S2R | C29 20R 2-Methyl Triaromatic Steroid | | | | | |
| 245 | S3R | C29 20R 3-Methyl Triaromatic Steroid | | | | | |
| 245 | DE | Triaromatic Dinosteroid e | | | | | |
| 245 | S4R | C29 20R 4-Methyl Triaromatic Steroid | | | | | |
| 245 | DF | Triaromatic Dinosteroid f | | | | | |

*Appendix F2, ctd.*

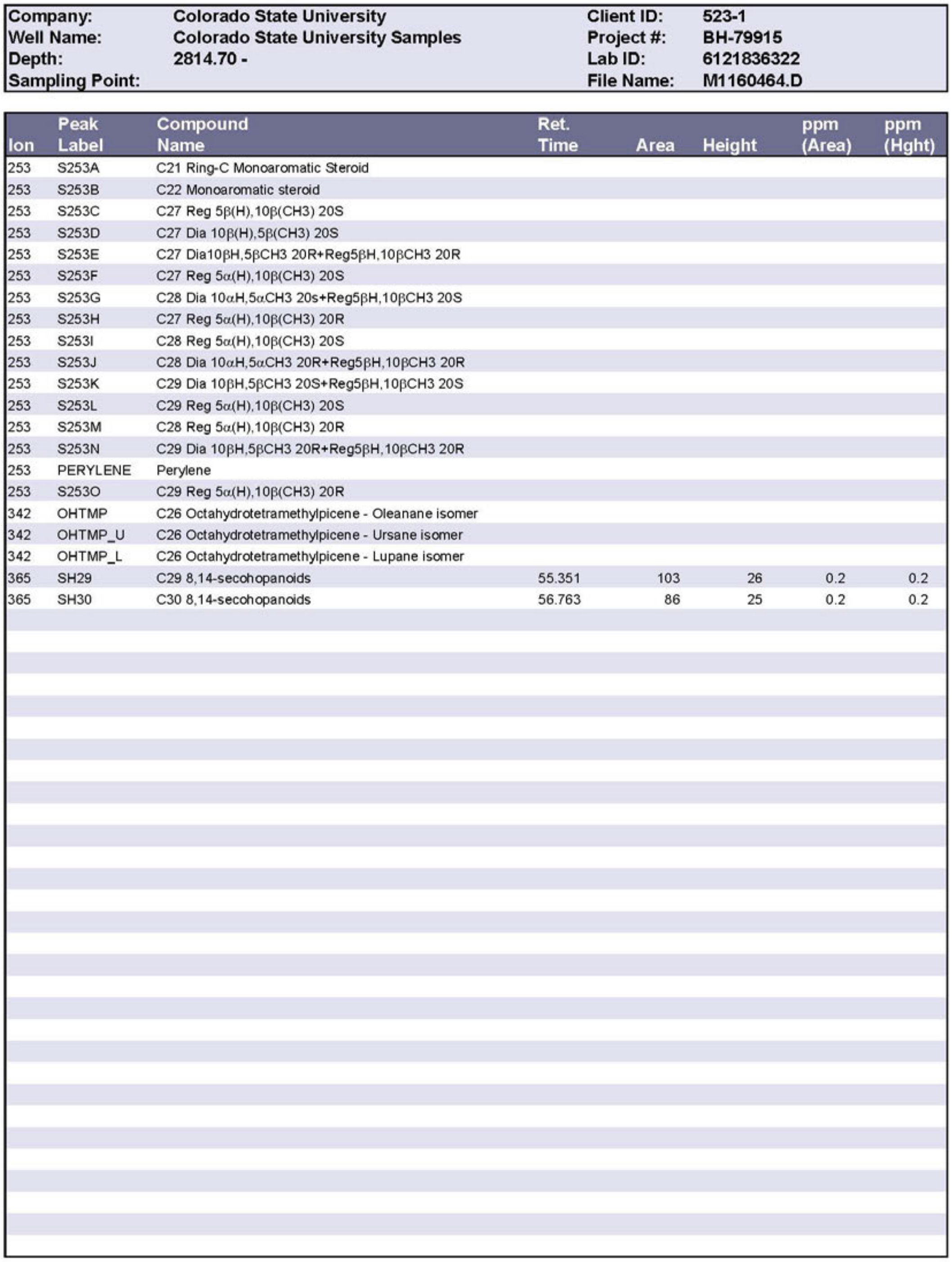

| | | | |
|---|---|---|---|
| **Company:** | **Colorado State University** | **Client ID:** | **523-1** |
| **Well Name:** | **Colorado State University Samples** | **Project #:** | **BH-79915** |
| **Depth:** | **2814.70 -** | **Lab ID:** | **6121836322** |
| **Sampling Point:** | | **File Name:** | **M1160464.D** |

| Ion | Peak Label | Compound Name | Ret. Time | Area | Height | ppm (Area) | ppm (Hght) |
|---|---|---|---|---|---|---|---|
| 253 | S253A | C21 Ring-C Monoaromatic Steroid | | | | | |
| 253 | S253B | C22 Monoaromatic steroid | | | | | |
| 253 | S253C | C27 Reg 5β(H),10β(CH3) 20S | | | | | |
| 253 | S253D | C27 Dia 10β(H),5β(CH3) 20S | | | | | |
| 253 | S253E | C27 Dia10βH,5βCH3 20R+Reg5βH,10βCH3 20R | | | | | |
| 253 | S253F | C27 Reg 5α(H),10β(CH3) 20S | | | | | |
| 253 | S253G | C28 Dia 10αH,5αCH3 20s+Reg5βH,10βCH3 20S | | | | | |
| 253 | S253H | C27 Reg 5α(H),10β(CH3) 20R | | | | | |
| 253 | S253I | C28 Reg 5α(H),10β(CH3) 20S | | | | | |
| 253 | S253J | C28 Dia 10αH,5αCH3 20R+Reg5βH,10βCH3 20R | | | | | |
| 253 | S253K | C29 Dia 10βH,5βCH3 20S+Reg5βH,10βCH3 20S | | | | | |
| 253 | S253L | C29 Reg 5α(H),10β(CH3) 20S | | | | | |
| 253 | S253M | C28 Reg 5α(H),10β(CH3) 20R | | | | | |
| 253 | S253N | C29 Dia 10βH,5βCH3 20R+Reg5βH,10βCH3 20R | | | | | |
| 253 | PERYLENE | Perylene | | | | | |
| 253 | S253O | C29 Reg 5α(H),10β(CH3) 20R | | | | | |
| 342 | OHTMP | C26 Octahydrotetramethylpicene - Oleanane isomer | | | | | |
| 342 | OHTMP_U | C26 Octahydrotetramethylpicene - Ursane isomer | | | | | |
| 342 | OHTMP_L | C26 Octahydrotetramethylpicene - Lupane isomer | | | | | |
| 365 | SH29 | C29 8,14-secohopanoids | 55.351 | 103 | 26 | 0.2 | 0.2 |
| 365 | SH30 | C30 8,14-secohopanoids | 56.763 | 86 | 25 | 0.2 | 0.2 |

*Appendix F2, ctd.*

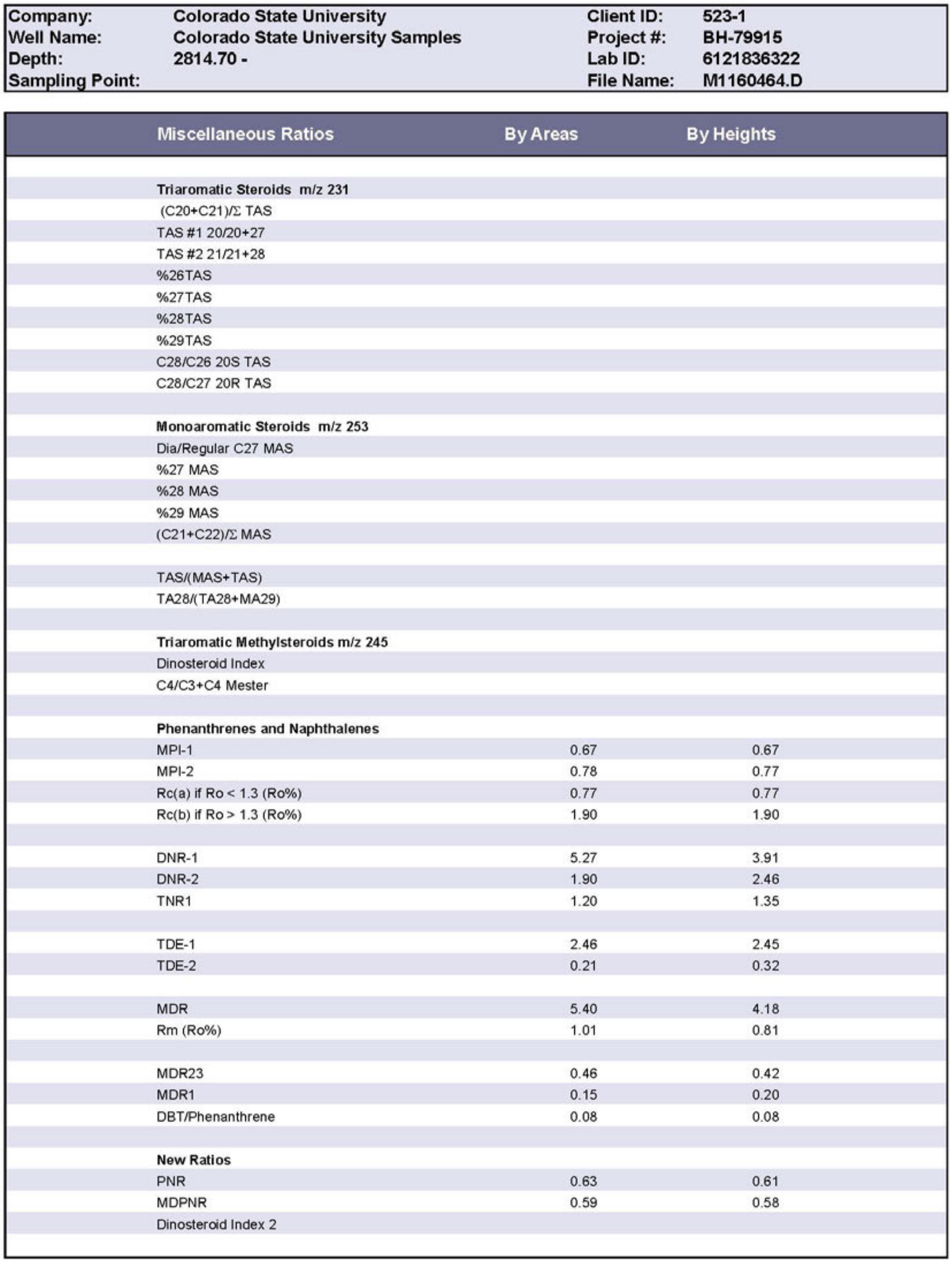

| | | | |
|---|---|---|---|
| **Company:** | **Colorado State University** | **Client ID:** | **523-1** |
| **Well Name:** | **Colorado State University Samples** | **Project #:** | **BH-79915** |
| **Depth:** | **2814.70 -** | **Lab ID:** | **6121836322** |
| **Sampling Point:** | | **File Name:** | **M1160464.D** |

| Miscellaneous Ratios | By Areas | By Heights |
|---|---|---|
| **Triaromatic Steroids m/z 231** | | |
| (C20+C21)/Σ TAS | | |
| TAS #1 20/20+27 | | |
| TAS #2 21/21+28 | | |
| %26TAS | | |
| %27TAS | | |
| %28TAS | | |
| %29TAS | | |
| C28/C26 20S TAS | | |
| C28/C27 20R TAS | | |
| | | |
| **Monoaromatic Steroids m/z 253** | | |
| Dia/Regular C27 MAS | | |
| %27 MAS | | |
| %28 MAS | | |
| %29 MAS | | |
| (C21+C22)/Σ MAS | | |
| | | |
| TAS/(MAS+TAS) | | |
| TA28/(TA28+MA29) | | |
| | | |
| **Triaromatic Methylsteroids m/z 245** | | |
| Dinosteroid Index | | |
| C4/C3+C4 Mester | | |
| | | |
| **Phenanthrenes and Naphthalenes** | | |
| MPI-1 | 0.67 | 0.67 |
| MPI-2 | 0.78 | 0.77 |
| Rc(a) if Ro < 1.3 (Ro%) | 0.77 | 0.77 |
| Rc(b) if Ro > 1.3 (Ro%) | 1.90 | 1.90 |
| | | |
| DNR-1 | 5.27 | 3.91 |
| DNR-2 | 1.90 | 2.46 |
| TNR1 | 1.20 | 1.35 |
| | | |
| TDE-1 | 2.46 | 2.45 |
| TDE-2 | 0.21 | 0.32 |
| | | |
| MDR | 5.40 | 4.18 |
| Rm (Ro%) | 1.01 | 0.81 |
| | | |
| MDR23 | 0.46 | 0.42 |
| MDR1 | 0.15 | 0.20 |
| DBT/Phenanthrene | 0.08 | 0.08 |
| | | |
| **New Ratios** | | |
| PNR | 0.63 | 0.61 |
| MDPNR | 0.59 | 0.58 |
| Dinosteroid Index 2 | | |

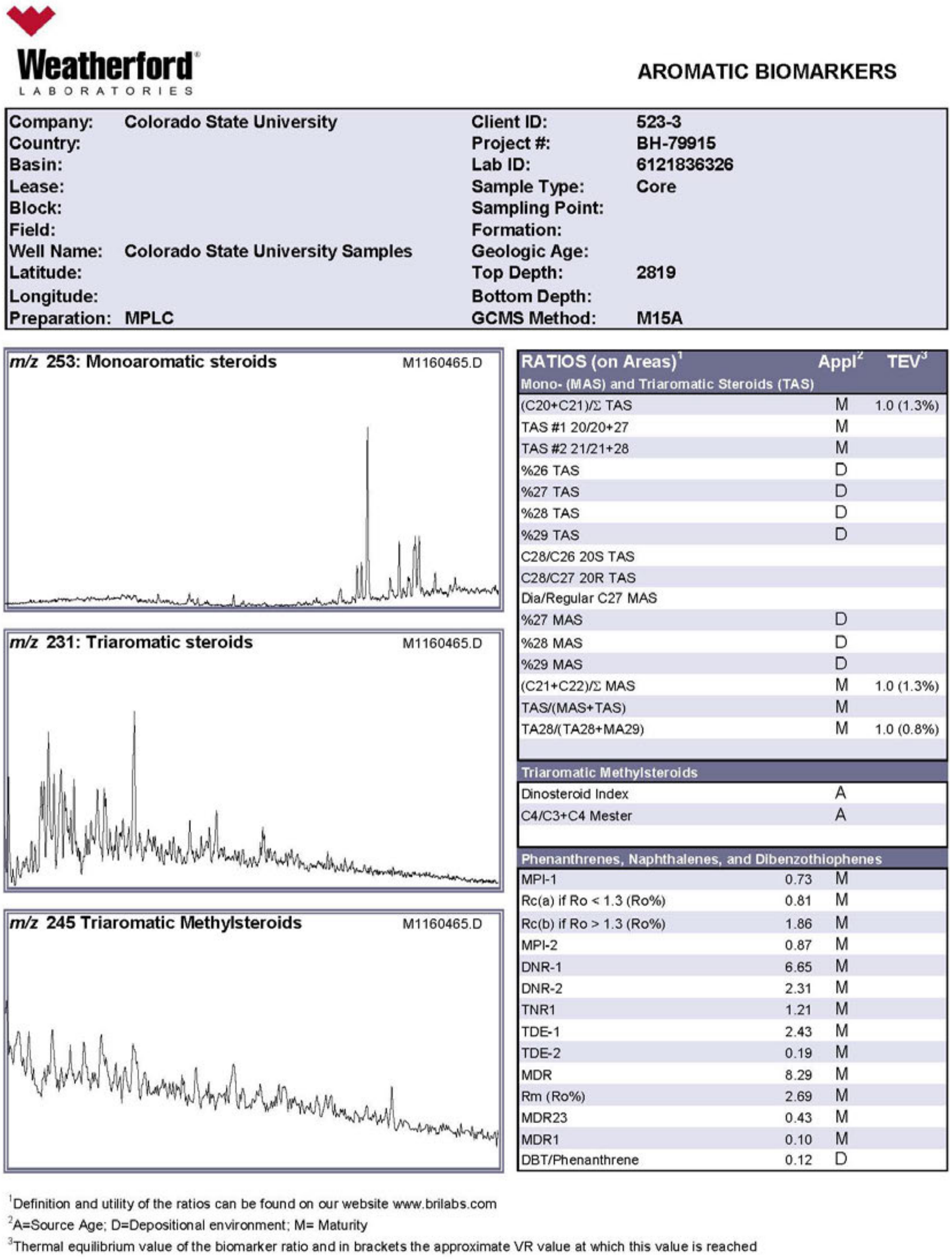

**Weatherford** LABORATORIES

## AROMATIC BIOMARKERS

| | | | |
|---|---|---|---|
| **Company:** | **Colorado State University** | **Client ID:** | **523-3** |
| **Country:** | | **Project #:** | **BH-79915** |
| **Basin:** | | **Lab ID:** | **6121836326** |
| **Lease:** | | **Sample Type:** | **Core** |
| **Block:** | | **Sampling Point:** | |
| **Field:** | | **Formation:** | |
| **Well Name:** | **Colorado State University Samples** | **Geologic Age:** | |
| **Latitude:** | | **Top Depth:** | **2819** |
| **Longitude:** | | **Bottom Depth:** | |
| **Preparation:** | **MPLC** | **GCMS Method:** | **M15A** |

***m/z* 253: Monoaromatic steroids** M1160465.D

***m/z* 231: Triaromatic steroids** M1160465.D

***m/z* 245 Triaromatic Methylsteroids** M1160465.D

| RATIOS (on Areas)[1] | | Appl[2] | TEV[3] |
|---|---|---|---|
| **Mono- (MAS) and Triaromatic Steroids (TAS)** | | | |
| (C20+C21)/Σ TAS | | M | 1.0 (1.3%) |
| TAS #1 20/20+27 | | M | |
| TAS #2 21/21+28 | | M | |
| %26 TAS | | D | |
| %27 TAS | | D | |
| %28 TAS | | D | |
| %29 TAS | | D | |
| C28/C26 20S TAS | | | |
| C28/C27 20R TAS | | | |
| Dia/Regular C27 MAS | | | |
| %27 MAS | | D | |
| %28 MAS | | D | |
| %29 MAS | | D | |
| (C21+C22)/Σ MAS | | M | 1.0 (1.3%) |
| TAS/(MAS+TAS) | | M | |
| TA28/(TA28+MA29) | | M | 1.0 (0.8%) |
| **Triaromatic Methylsteroids** | | | |
| Dinosteroid Index | | A | |
| C4/C3+C4 Mester | | A | |
| **Phenanthrenes, Naphthalenes, and Dibenzothiophenes** | | | |
| MPI-1 | 0.73 | M | |
| Rc(a) if Ro < 1.3 (Ro%) | 0.81 | M | |
| Rc(b) if Ro > 1.3 (Ro%) | 1.86 | M | |
| MPI-2 | 0.87 | M | |
| DNR-1 | 6.65 | M | |
| DNR-2 | 2.31 | M | |
| TNR1 | 1.21 | M | |
| TDE-1 | 2.43 | M | |
| TDE-2 | 0.19 | M | |
| MDR | 8.29 | M | |
| Rm (Ro%) | 2.69 | M | |
| MDR23 | 0.43 | M | |
| MDR1 | 0.10 | M | |
| DBT/Phenanthrene | 0.12 | D | |

[1] Definition and utility of the ratios can be found on our website www.brilabs.com

[2] A=Source Age; D=Depositional environment; M= Maturity

[3] Thermal equilibrium value of the biomarker ratio and in brackets the approximate VR value at which this value is reached

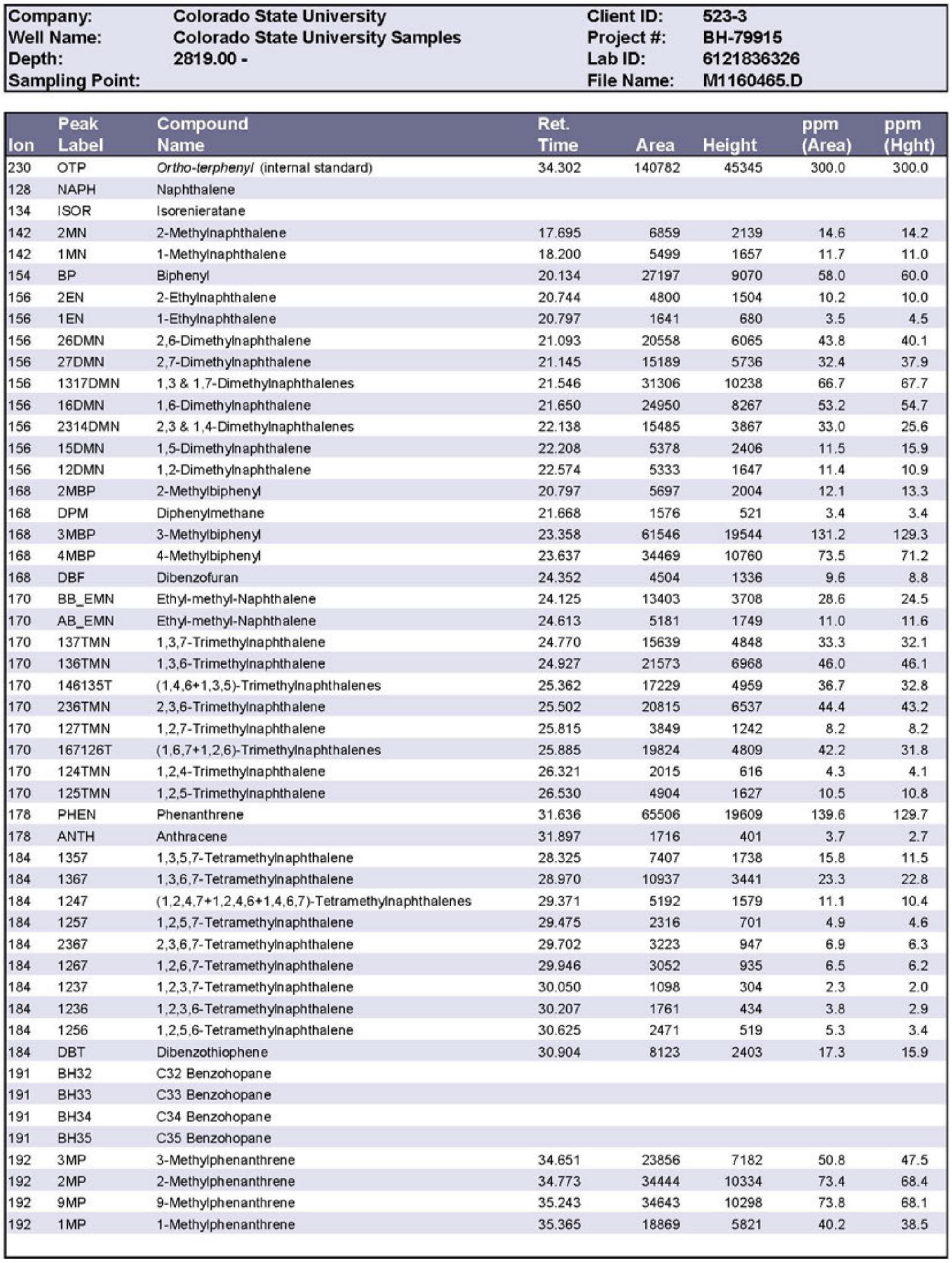

| | | | |
|---|---|---|---|
| **Company:** | **Colorado State University** | **Client ID:** | **523-3** |
| **Well Name:** | **Colorado State University Samples** | **Project #:** | **BH-79915** |
| **Depth:** | **2819.00 -** | **Lab ID:** | **6121836326** |
| **Sampling Point:** | | **File Name:** | **M1160465.D** |

| Ion | Peak Label | Compound Name | Ret. Time | Area | Height | ppm (Area) | ppm (Hght) |
|---|---|---|---|---|---|---|---|
| 230 | OTP | *Ortho-terphenyl* (internal standard) | 34.302 | 140782 | 45345 | 300.0 | 300.0 |
| 128 | NAPH | Naphthalene | | | | | |
| 134 | ISOR | Isorenieratane | | | | | |
| 142 | 2MN | 2-Methylnaphthalene | 17.695 | 6859 | 2139 | 14.6 | 14.2 |
| 142 | 1MN | 1-Methylnaphthalene | 18.200 | 5499 | 1657 | 11.7 | 11.0 |
| 154 | BP | Biphenyl | 20.134 | 27197 | 9070 | 58.0 | 60.0 |
| 156 | 2EN | 2-Ethylnaphthalene | 20.744 | 4800 | 1504 | 10.2 | 10.0 |
| 156 | 1EN | 1-Ethylnaphthalene | 20.797 | 1641 | 680 | 3.5 | 4.5 |
| 156 | 26DMN | 2,6-Dimethylnaphthalene | 21.093 | 20558 | 6065 | 43.8 | 40.1 |
| 156 | 27DMN | 2,7-Dimethylnaphthalene | 21.145 | 15189 | 5736 | 32.4 | 37.9 |
| 156 | 1317DMN | 1,3 & 1,7-Dimethylnaphthalenes | 21.546 | 31306 | 10238 | 66.7 | 67.7 |
| 156 | 16DMN | 1,6-Dimethylnaphthalene | 21.650 | 24950 | 8267 | 53.2 | 54.7 |
| 156 | 2314DMN | 2,3 & 1,4-Dimethylnaphthalenes | 22.138 | 15485 | 3867 | 33.0 | 25.6 |
| 156 | 15DMN | 1,5-Dimethylnaphthalene | 22.208 | 5378 | 2406 | 11.5 | 15.9 |
| 156 | 12DMN | 1,2-Dimethylnaphthalene | 22.574 | 5333 | 1647 | 11.4 | 10.9 |
| 168 | 2MBP | 2-Methylbiphenyl | 20.797 | 5697 | 2004 | 12.1 | 13.3 |
| 168 | DPM | Diphenylmethane | 21.668 | 1576 | 521 | 3.4 | 3.4 |
| 168 | 3MBP | 3-Methylbiphenyl | 23.358 | 61546 | 19544 | 131.2 | 129.3 |
| 168 | 4MBP | 4-Methylbiphenyl | 23.637 | 34469 | 10760 | 73.5 | 71.2 |
| 168 | DBF | Dibenzofuran | 24.352 | 4504 | 1336 | 9.6 | 8.8 |
| 170 | BB_EMN | Ethyl-methyl-Naphthalene | 24.125 | 13403 | 3708 | 28.6 | 24.5 |
| 170 | AB_EMN | Ethyl-methyl-Naphthalene | 24.613 | 5181 | 1749 | 11.0 | 11.6 |
| 170 | 137TMN | 1,3,7-Trimethylnaphthalene | 24.770 | 15639 | 4848 | 33.3 | 32.1 |
| 170 | 136TMN | 1,3,6-Trimethylnaphthalene | 24.927 | 21573 | 6968 | 46.0 | 46.1 |
| 170 | 146135T | (1,4,6+1,3,5)-Trimethylnaphthalenes | 25.362 | 17229 | 4959 | 36.7 | 32.8 |
| 170 | 236TMN | 2,3,6-Trimethylnaphthalene | 25.502 | 20815 | 6537 | 44.4 | 43.2 |
| 170 | 127TMN | 1,2,7-Trimethylnaphthalene | 25.815 | 3849 | 1242 | 8.2 | 8.2 |
| 170 | 167126T | (1,6,7+1,2,6)-Trimethylnaphthalenes | 25.885 | 19824 | 4809 | 42.2 | 31.8 |
| 170 | 124TMN | 1,2,4-Trimethylnaphthalene | 26.321 | 2015 | 616 | 4.3 | 4.1 |
| 170 | 125TMN | 1,2,5-Trimethylnaphthalene | 26.530 | 4904 | 1627 | 10.5 | 10.8 |
| 178 | PHEN | Phenanthrene | 31.636 | 65506 | 19609 | 139.6 | 129.7 |
| 178 | ANTH | Anthracene | 31.897 | 1716 | 401 | 3.7 | 2.7 |
| 184 | 1357 | 1,3,5,7-Tetramethylnaphthalene | 28.325 | 7407 | 1738 | 15.8 | 11.5 |
| 184 | 1367 | 1,3,6,7-Tetramethylnaphthalene | 28.970 | 10937 | 3441 | 23.3 | 22.8 |
| 184 | 1247 | (1,2,4,7+1,2,4,6+1,4,6,7)-Tetramethylnaphthalenes | 29.371 | 5192 | 1579 | 11.1 | 10.4 |
| 184 | 1257 | 1,2,5,7-Tetramethylnaphthalene | 29.475 | 2316 | 701 | 4.9 | 4.6 |
| 184 | 2367 | 2,3,6,7-Tetramethylnaphthalene | 29.702 | 3223 | 947 | 6.9 | 6.3 |
| 184 | 1267 | 1,2,6,7-Tetramethylnaphthalene | 29.946 | 3052 | 935 | 6.5 | 6.2 |
| 184 | 1237 | 1,2,3,7-Tetramethylnaphthalene | 30.050 | 1098 | 304 | 2.3 | 2.0 |
| 184 | 1236 | 1,2,3,6-Tetramethylnaphthalene | 30.207 | 1761 | 434 | 3.8 | 2.9 |
| 184 | 1256 | 1,2,5,6-Tetramethylnaphthalene | 30.625 | 2471 | 519 | 5.3 | 3.4 |
| 184 | DBT | Dibenzothiophene | 30.904 | 8123 | 2403 | 17.3 | 15.9 |
| 191 | BH32 | C32 Benzohopane | | | | | |
| 191 | BH33 | C33 Benzohopane | | | | | |
| 191 | BH34 | C34 Benzohopane | | | | | |
| 191 | BH35 | C35 Benzohopane | | | | | |
| 192 | 3MP | 3-Methylphenanthrene | 34.651 | 23856 | 7182 | 50.8 | 47.5 |
| 192 | 2MP | 2-Methylphenanthrene | 34.773 | 34444 | 10334 | 73.4 | 68.4 |
| 192 | 9MP | 9-Methylphenanthrene | 35.243 | 34643 | 10298 | 73.8 | 68.1 |
| 192 | 1MP | 1-Methylphenanthrene | 35.365 | 18869 | 5821 | 40.2 | 38.5 |

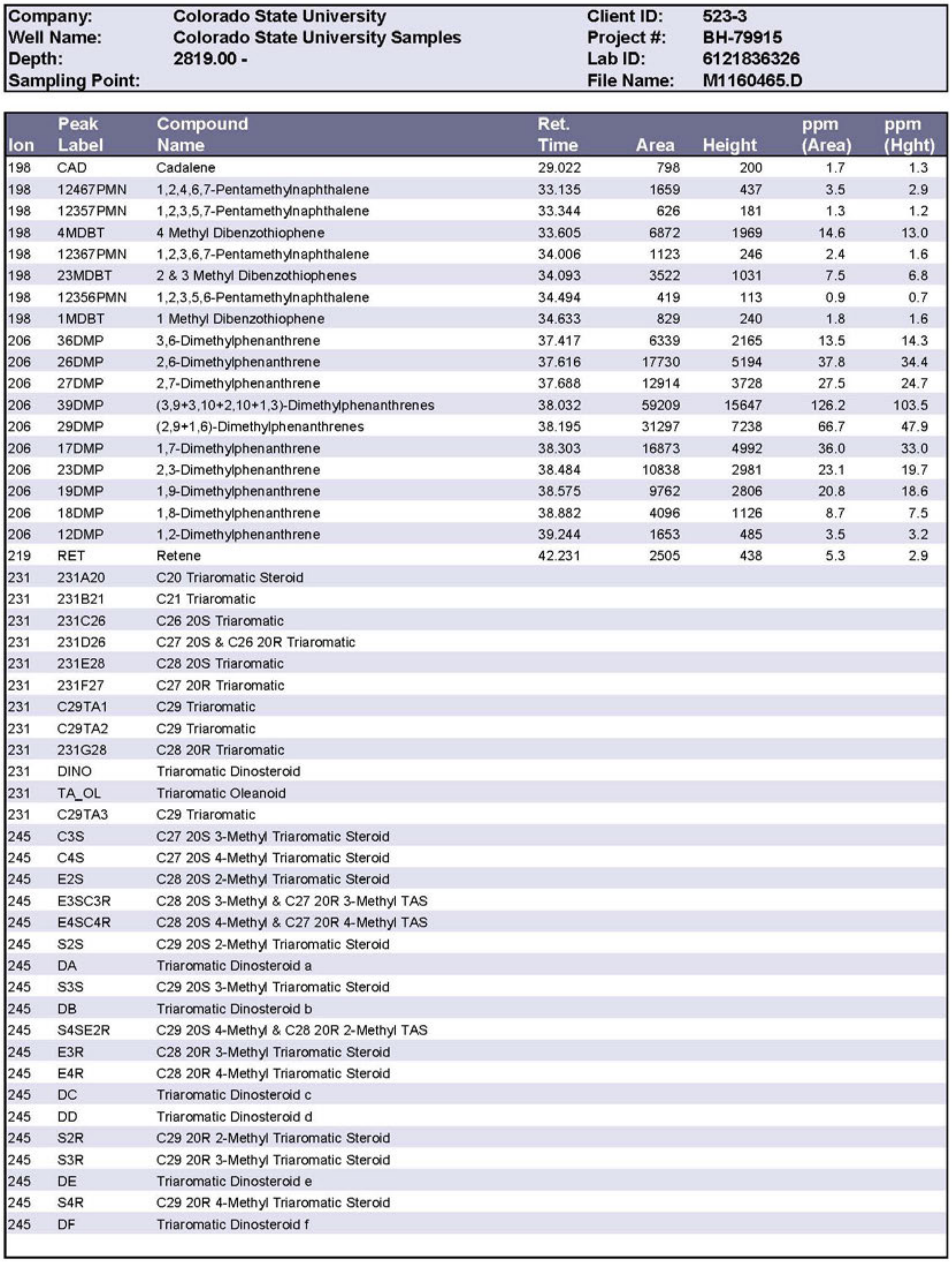

| | | | |
|---|---|---|---|
| **Company:** | **Colorado State University** | **Client ID:** | **523-3** |
| **Well Name:** | **Colorado State University Samples** | **Project #:** | **BH-79915** |
| **Depth:** | **2819.00 -** | **Lab ID:** | **6121836326** |
| **Sampling Point:** | | **File Name:** | **M1160465.D** |

| Ion | Peak Label | Compound Name | Ret. Time | Area | Height | ppm (Area) | ppm (Hght) |
|---|---|---|---|---|---|---|---|
| 198 | CAD | Cadalene | 29.022 | 798 | 200 | 1.7 | 1.3 |
| 198 | 12467PMN | 1,2,4,6,7-Pentamethylnaphthalene | 33.135 | 1659 | 437 | 3.5 | 2.9 |
| 198 | 12357PMN | 1,2,3,5,7-Pentamethylnaphthalene | 33.344 | 626 | 181 | 1.3 | 1.2 |
| 198 | 4MDBT | 4 Methyl Dibenzothiophene | 33.605 | 6872 | 1969 | 14.6 | 13.0 |
| 198 | 12367PMN | 1,2,3,6,7-Pentamethylnaphthalene | 34.006 | 1123 | 246 | 2.4 | 1.6 |
| 198 | 23MDBT | 2 & 3 Methyl Dibenzothiophenes | 34.093 | 3522 | 1031 | 7.5 | 6.8 |
| 198 | 12356PMN | 1,2,3,5,6-Pentamethylnaphthalene | 34.494 | 419 | 113 | 0.9 | 0.7 |
| 198 | 1MDBT | 1 Methyl Dibenzothiophene | 34.633 | 829 | 240 | 1.8 | 1.6 |
| 206 | 36DMP | 3,6-Dimethylphenanthrene | 37.417 | 6339 | 2165 | 13.5 | 14.3 |
| 206 | 26DMP | 2,6-Dimethylphenanthrene | 37.616 | 17730 | 5194 | 37.8 | 34.4 |
| 206 | 27DMP | 2,7-Dimethylphenanthrene | 37.688 | 12914 | 3728 | 27.5 | 24.7 |
| 206 | 39DMP | (3,9+3,10+2,10+1,3)-Dimethylphenanthrenes | 38.032 | 59209 | 15647 | 126.2 | 103.5 |
| 206 | 29DMP | (2,9+1,6)-Dimethylphenanthrenes | 38.195 | 31297 | 7238 | 66.7 | 47.9 |
| 206 | 17DMP | 1,7-Dimethylphenanthrene | 38.303 | 16873 | 4992 | 36.0 | 33.0 |
| 206 | 23DMP | 2,3-Dimethylphenanthrene | 38.484 | 10838 | 2981 | 23.1 | 19.7 |
| 206 | 19DMP | 1,9-Dimethylphenanthrene | 38.575 | 9762 | 2806 | 20.8 | 18.6 |
| 206 | 18DMP | 1,8-Dimethylphenanthrene | 38.882 | 4096 | 1126 | 8.7 | 7.5 |
| 206 | 12DMP | 1,2-Dimethylphenanthrene | 39.244 | 1653 | 485 | 3.5 | 3.2 |
| 219 | RET | Retene | 42.231 | 2505 | 438 | 5.3 | 2.9 |
| 231 | 231A20 | C20 Triaromatic Steroid | | | | | |
| 231 | 231B21 | C21 Triaromatic | | | | | |
| 231 | 231C26 | C26 20S Triaromatic | | | | | |
| 231 | 231D26 | C27 20S & C26 20R Triaromatic | | | | | |
| 231 | 231E28 | C28 20S Triaromatic | | | | | |
| 231 | 231F27 | C27 20R Triaromatic | | | | | |
| 231 | C29TA1 | C29 Triaromatic | | | | | |
| 231 | C29TA2 | C29 Triaromatic | | | | | |
| 231 | 231G28 | C28 20R Triaromatic | | | | | |
| 231 | DINO | Triaromatic Dinosteroid | | | | | |
| 231 | TA_OL | Triaromatic Oleanoid | | | | | |
| 231 | C29TA3 | C29 Triaromatic | | | | | |
| 245 | C3S | C27 20S 3-Methyl Triaromatic Steroid | | | | | |
| 245 | C4S | C27 20S 4-Methyl Triaromatic Steroid | | | | | |
| 245 | E2S | C28 20S 2-Methyl Triaromatic Steroid | | | | | |
| 245 | E3SC3R | C28 20S 3-Methyl & C27 20R 3-Methyl TAS | | | | | |
| 245 | E4SC4R | C28 20S 4-Methyl & C27 20R 4-Methyl TAS | | | | | |
| 245 | S2S | C29 20S 2-Methyl Triaromatic Steroid | | | | | |
| 245 | DA | Triaromatic Dinosteroid a | | | | | |
| 245 | S3S | C29 20S 3-Methyl Triaromatic Steroid | | | | | |
| 245 | DB | Triaromatic Dinosteroid b | | | | | |
| 245 | S4SE2R | C29 20S 4-Methyl & C28 20R 2-Methyl TAS | | | | | |
| 245 | E3R | C28 20R 3-Methyl Triaromatic Steroid | | | | | |
| 245 | E4R | C28 20R 4-Methyl Triaromatic Steroid | | | | | |
| 245 | DC | Triaromatic Dinosteroid c | | | | | |
| 245 | DD | Triaromatic Dinosteroid d | | | | | |
| 245 | S2R | C29 20R 2-Methyl Triaromatic Steroid | | | | | |
| 245 | S3R | C29 20R 3-Methyl Triaromatic Steroid | | | | | |
| 245 | DE | Triaromatic Dinosteroid e | | | | | |
| 245 | S4R | C29 20R 4-Methyl Triaromatic Steroid | | | | | |
| 245 | DF | Triaromatic Dinosteroid f | | | | | |

*Appendix F2, ctd.*

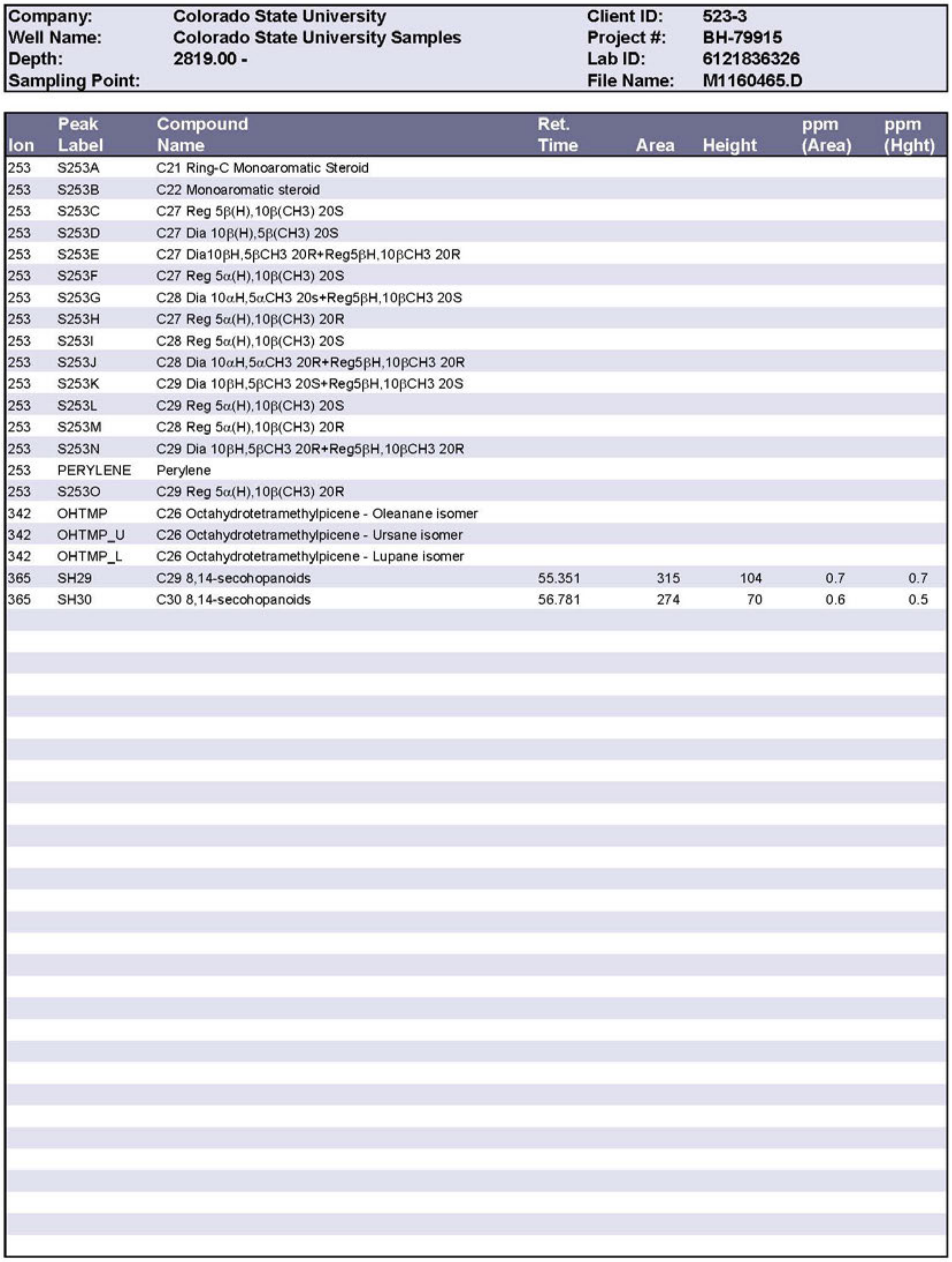

| | | | |
|---|---|---|---|
| **Company:** | **Colorado State University** | **Client ID:** | **523-3** |
| **Well Name:** | **Colorado State University Samples** | **Project #:** | **BH-79915** |
| **Depth:** | **2819.00 -** | **Lab ID:** | **6121836326** |
| **Sampling Point:** | | **File Name:** | **M1160465.D** |

| Ion | Peak Label | Compound Name | Ret. Time | Area | Height | ppm (Area) | ppm (Hght) |
|---|---|---|---|---|---|---|---|
| 253 | S253A | C21 Ring-C Monoaromatic Steroid | | | | | |
| 253 | S253B | C22 Monoaromatic steroid | | | | | |
| 253 | S253C | C27 Reg 5β(H),10β(CH3) 20S | | | | | |
| 253 | S253D | C27 Dia 10β(H),5β(CH3) 20S | | | | | |
| 253 | S253E | C27 Dia10βH,5βCH3 20R+Reg5βH,10βCH3 20R | | | | | |
| 253 | S253F | C27 Reg 5α(H),10β(CH3) 20S | | | | | |
| 253 | S253G | C28 Dia 10αH,5αCH3 20s+Reg5βH,10βCH3 20S | | | | | |
| 253 | S253H | C27 Reg 5α(H),10β(CH3) 20R | | | | | |
| 253 | S253I | C28 Reg 5α(H),10β(CH3) 20S | | | | | |
| 253 | S253J | C28 Dia 10αH,5αCH3 20R+Reg5βH,10βCH3 20R | | | | | |
| 253 | S253K | C29 Dia 10βH,5βCH3 20S+Reg5βH,10βCH3 20S | | | | | |
| 253 | S253L | C29 Reg 5α(H),10β(CH3) 20S | | | | | |
| 253 | S253M | C28 Reg 5α(H),10β(CH3) 20R | | | | | |
| 253 | S253N | C29 Dia 10βH,5βCH3 20R+Reg5βH,10βCH3 20R | | | | | |
| 253 | PERYLENE | Perylene | | | | | |
| 253 | S253O | C29 Reg 5α(H),10β(CH3) 20R | | | | | |
| 342 | OHTMP | C26 Octahydrotetramethylpicene - Oleanane isomer | | | | | |
| 342 | OHTMP_U | C26 Octahydrotetramethylpicene - Ursane isomer | | | | | |
| 342 | OHTMP_L | C26 Octahydrotetramethylpicene - Lupane isomer | | | | | |
| 365 | SH29 | C29 8,14-secohopanoids | 55.351 | 315 | 104 | 0.7 | 0.7 |
| 365 | SH30 | C30 8,14-secohopanoids | 56.781 | 274 | 70 | 0.6 | 0.5 |

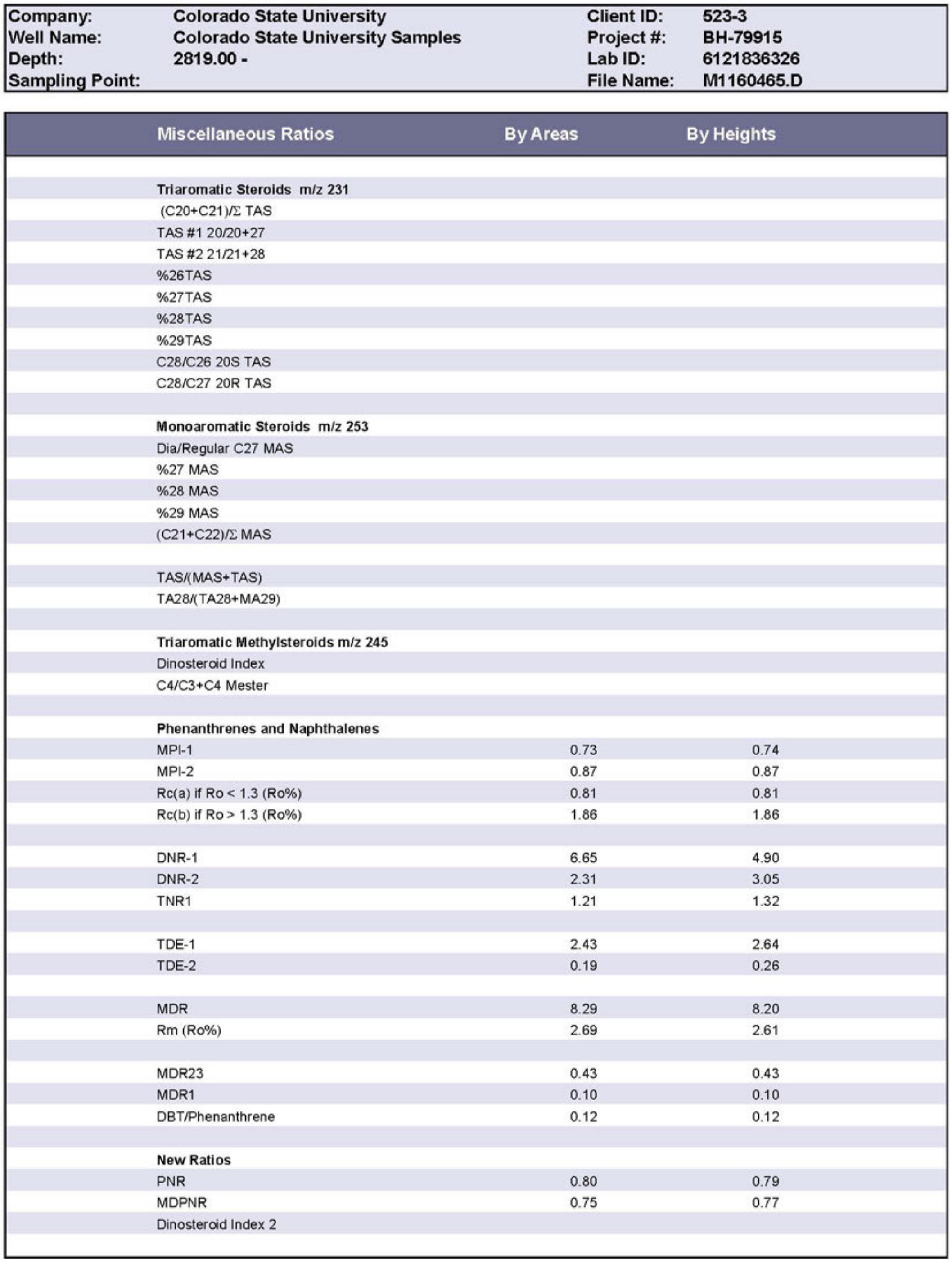

| | | | |
|---|---|---|---|
| **Company:** | **Colorado State University** | **Client ID:** | **523-3** |
| **Well Name:** | **Colorado State University Samples** | **Project #:** | **BH-79915** |
| **Depth:** | **2819.00 -** | **Lab ID:** | **6121836326** |
| **Sampling Point:** | | **File Name:** | **M1160465.D** |

| Miscellaneous Ratios | By Areas | By Heights |
|---|---|---|
| **Triaromatic Steroids m/z 231** | | |
| (C20+C21)/Σ TAS | | |
| TAS #1 20/20+27 | | |
| TAS #2 21/21+28 | | |
| %26TAS | | |
| %27TAS | | |
| %28TAS | | |
| %29TAS | | |
| C28/C26 20S TAS | | |
| C28/C27 20R TAS | | |
| | | |
| **Monoaromatic Steroids m/z 253** | | |
| Dia/Regular C27 MAS | | |
| %27 MAS | | |
| %28 MAS | | |
| %29 MAS | | |
| (C21+C22)/Σ MAS | | |
| | | |
| TAS/(MAS+TAS) | | |
| TA28/(TA28+MA29) | | |
| | | |
| **Triaromatic Methylsteroids m/z 245** | | |
| Dinosteroid Index | | |
| C4/C3+C4 Mester | | |
| | | |
| **Phenanthrenes and Naphthalenes** | | |
| MPI-1 | 0.73 | 0.74 |
| MPI-2 | 0.87 | 0.87 |
| Rc(a) if Ro < 1.3 (Ro%) | 0.81 | 0.81 |
| Rc(b) if Ro > 1.3 (Ro%) | 1.86 | 1.86 |
| | | |
| DNR-1 | 6.65 | 4.90 |
| DNR-2 | 2.31 | 3.05 |
| TNR1 | 1.21 | 1.32 |
| | | |
| TDE-1 | 2.43 | 2.64 |
| TDE-2 | 0.19 | 0.26 |
| | | |
| MDR | 8.29 | 8.20 |
| Rm (Ro%) | 2.69 | 2.61 |
| | | |
| MDR23 | 0.43 | 0.43 |
| MDR1 | 0.10 | 0.10 |
| DBT/Phenanthrene | 0.12 | 0.12 |
| | | |
| **New Ratios** | | |
| PNR | 0.80 | 0.79 |
| MDPNR | 0.75 | 0.77 |
| Dinosteroid Index 2 | | |

## *Appendix F2, ctd.*

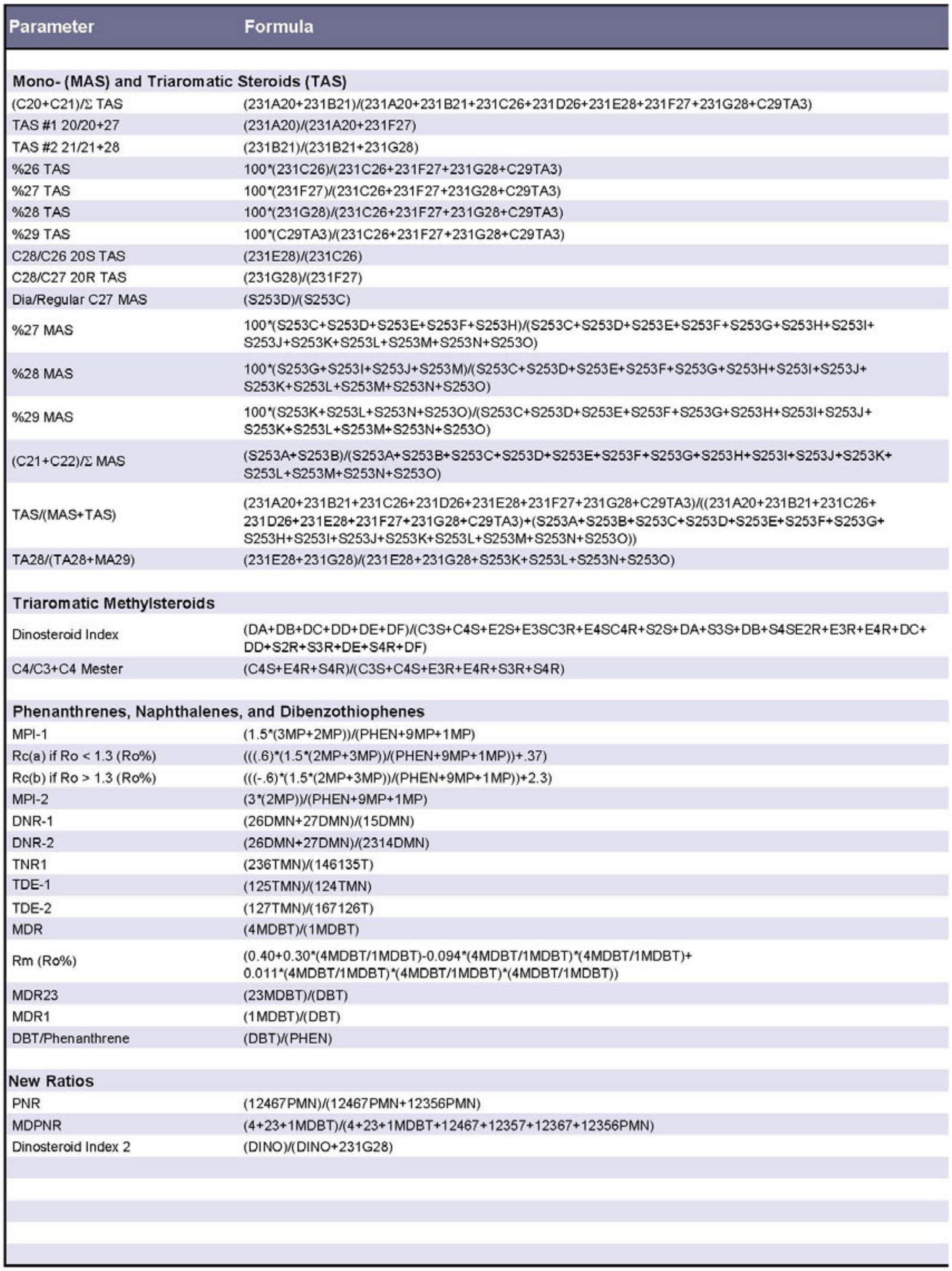

| Parameter | Formula |
|---|---|
| **Mono- (MAS) and Triaromatic Steroids (TAS)** | |
| (C20+C21)/Σ TAS | (231A20+231B21)/(231A20+231B21+231C26+231D26+231E28+231F27+231G28+C29TA3) |
| TAS #1 20/20+27 | (231A20)/(231A20+231F27) |
| TAS #2 21/21+28 | (231B21)/(231B21+231G28) |
| %26 TAS | 100*(231C26)/(231C26+231F27+231G28+C29TA3) |
| %27 TAS | 100*(231F27)/(231C26+231F27+231G28+C29TA3) |
| %28 TAS | 100*(231G28)/(231C26+231F27+231G28+C29TA3) |
| %29 TAS | 100*(C29TA3)/(231C26+231F27+231G28+C29TA3) |
| C28/C26 20S TAS | (231E28)/(231C26) |
| C28/C27 20R TAS | (231G28)/(231F27) |
| Dia/Regular C27 MAS | (S253D)/(S253C) |
| %27 MAS | 100*(S253C+S253D+S253E+S253F+S253H)/(S253C+S253D+S253E+S253F+S253G+S253H+S253I+S253J+S253K+S253L+S253M+S253N+S253O) |
| %28 MAS | 100*(S253G+S253I+S253J+S253M)/(S253C+S253D+S253E+S253F+S253G+S253H+S253I+S253J+S253K+S253L+S253M+S253N+S253O) |
| %29 MAS | 100*(S253K+S253L+S253N+S253O)/(S253C+S253D+S253E+S253F+S253G+S253H+S253I+S253J+S253K+S253L+S253M+S253N+S253O) |
| (C21+C22)/Σ MAS | (S253A+S253B)/(S253A+S253B+S253C+S253D+S253E+S253F+S253G+S253H+S253I+S253J+S253K+S253L+S253M+S253N+S253O) |
| TAS/(MAS+TAS) | (231A20+231B21+231C26+231D26+231E28+231F27+231G28+C29TA3)/((231A20+231B21+231C26+231D26+231E28+231F27+231G28+C29TA3)+(S253A+S253B+S253C+S253D+S253E+S253F+S253G+S253H+S253I+S253J+S253K+S253L+S253M+S253N+S253O)) |
| TA28/(TA28+MA29) | (231E28+231G28)/(231E28+231G28+S253K+S253L+S253N+S253O) |
| | |
| **Triaromatic Methylsteroids** | |
| Dinosteroid Index | (DA+DB+DC+DD+DE+DF)/(C3S+C4S+E2S+E3SC3R+E4SC4R+S2S+DA+S3S+DB+S4SE2R+E3R+E4R+DC+DD+S2R+S3R+DE+S4R+DF) |
| C4/C3+C4 Mester | (C4S+E4R+S4R)/(C3S+C4S+E3R+E4R+S3R+S4R) |
| | |
| **Phenanthrenes, Naphthalenes, and Dibenzothiophenes** | |
| MPI-1 | (1.5*(3MP+2MP))/(PHEN+9MP+1MP) |
| Rc(a) if Ro < 1.3 (Ro%) | (((.6)*(1.5*(2MP+3MP))/(PHEN+9MP+1MP))+.37) |
| Rc(b) if Ro > 1.3 (Ro%) | (((-.6)*(1.5*(2MP+3MP))/(PHEN+9MP+1MP))+2.3) |
| MPI-2 | (3*(2MP))/(PHEN+9MP+1MP) |
| DNR-1 | (26DMN+27DMN)/(15DMN) |
| DNR-2 | (26DMN+27DMN)/(2314DMN) |
| TNR1 | (236TMN)/(146135T) |
| TDE-1 | (125TMN)/(124TMN) |
| TDE-2 | (127TMN)/(167126T) |
| MDR | (4MDBT)/(1MDBT) |
| Rm (Ro%) | (0.40+0.30*(4MDBT/1MDBT)-0.094*(4MDBT/1MDBT)*(4MDBT/1MDBT)+0.011*(4MDBT/1MDBT)*(4MDBT/1MDBT)*(4MDBT/1MDBT)) |
| MDR23 | (23MDBT)/(DBT) |
| MDR1 | (1MDBT)/(DBT) |
| DBT/Phenanthrene | (DBT)/(PHEN) |
| | |
| **New Ratios** | |
| PNR | (12467PMN)/(12467PMN+12356PMN) |
| MDPNR | (4+23+1MDBT)/(4+23+1MDBT+12467+12357+12367+12356PMN) |
| Dinosteroid Index 2 | (DINO)/(DINO+231G28) |

<u>*Appendix F2, ctd.*</u>

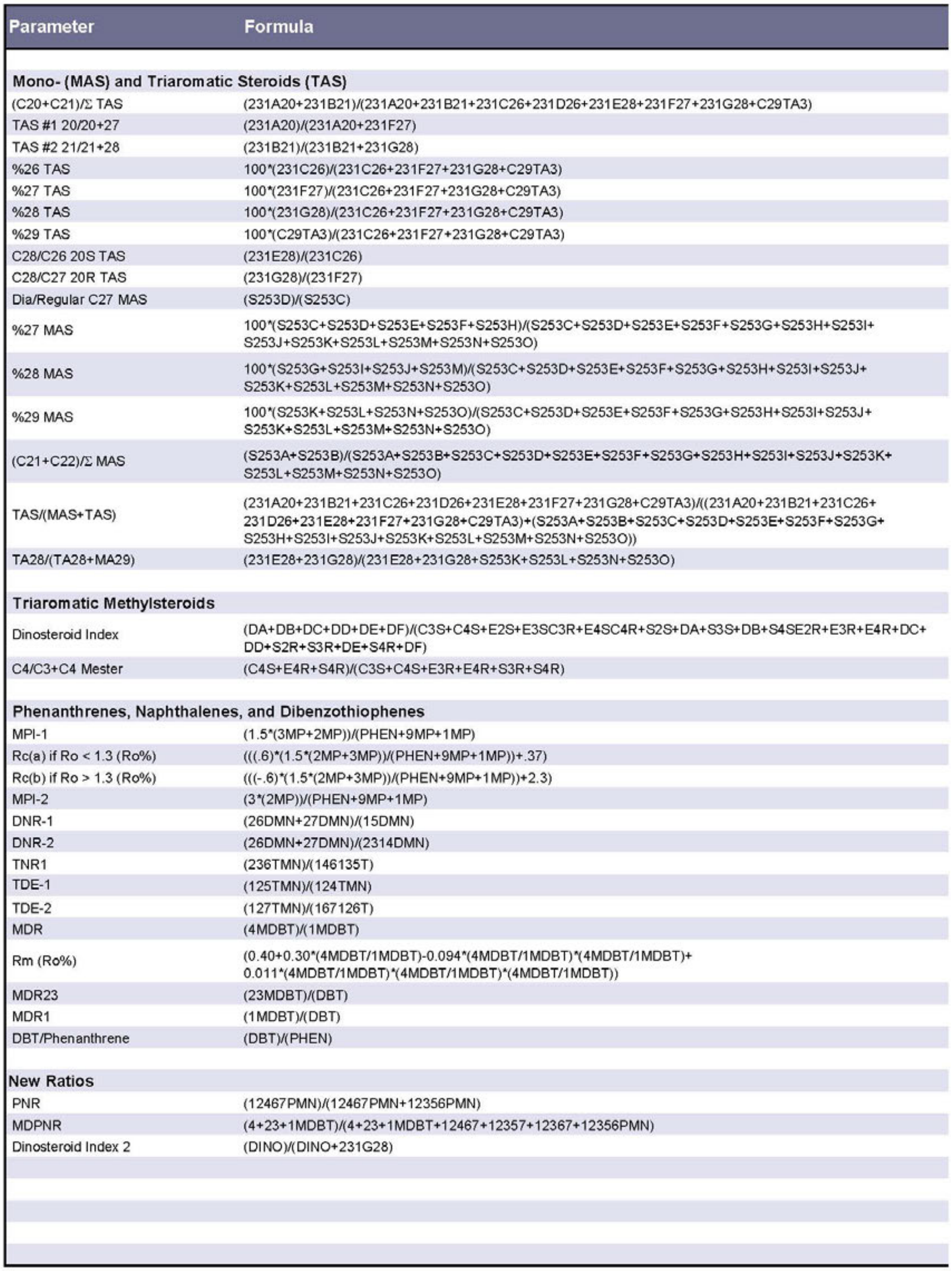

| Parameter | Formula |
|---|---|
| **Mono- (MAS) and Triaromatic Steroids (TAS)** | |
| (C20+C21)/Σ TAS | (231A20+231B21)/(231A20+231B21+231C26+231D26+231E28+231F27+231G28+C29TA3) |
| TAS #1 20/20+27 | (231A20)/(231A20+231F27) |
| TAS #2 21/21+28 | (231B21)/(231B21+231G28) |
| %26 TAS | 100*(231C26)/(231C26+231F27+231G28+C29TA3) |
| %27 TAS | 100*(231F27)/(231C26+231F27+231G28+C29TA3) |
| %28 TAS | 100*(231G28)/(231C26+231F27+231G28+C29TA3) |
| %29 TAS | 100*(C29TA3)/(231C26+231F27+231G28+C29TA3) |
| C28/C26 20S TAS | (231E28)/(231C26) |
| C28/C27 20R TAS | (231G28)/(231F27) |
| Dia/Regular C27 MAS | (S253D)/(S253C) |
| %27 MAS | 100*(S253C+S253D+S253E+S253F+S253H)/(S253C+S253D+S253E+S253F+S253G+S253H+S253I+S253J+S253K+S253L+S253M+S253N+S253O) |
| %28 MAS | 100*(S253G+S253I+S253J+S253M)/(S253C+S253D+S253E+S253F+S253G+S253H+S253I+S253J+S253K+S253L+S253M+S253N+S253O) |
| %29 MAS | 100*(S253K+S253L+S253N+S253O)/(S253C+S253D+S253E+S253F+S253G+S253H+S253I+S253J+S253K+S253L+S253M+S253N+S253O) |
| (C21+C22)/Σ MAS | (S253A+S253B)/(S253A+S253B+S253C+S253D+S253E+S253F+S253G+S253H+S253I+S253J+S253K+S253L+S253M+S253N+S253O) |
| TAS/(MAS+TAS) | (231A20+231B21+231C26+231D26+231E28+231F27+231G28+C29TA3)/((231A20+231B21+231C26+231D26+231E28+231F27+231G28+C29TA3)+(S253A+S253B+S253C+S253D+S253E+S253F+S253G+S253H+S253I+S253J+S253K+S253L+S253M+S253N+S253O)) |
| TA28/(TA28+MA29) | (231E28+231G28)/(231E28+231G28+S253K+S253L+S253N+S253O) |
| **Triaromatic Methylsteroids** | |
| Dinosteroid Index | (DA+DB+DC+DD+DE+DF)/(C3S+C4S+E2S+E3SC3R+E4SC4R+S2S+DA+S3S+DB+S4SE2R+E3R+E4R+DC+DD+S2R+S3R+DE+S4R+DF) |
| C4/C3+C4 Mester | (C4S+E4R+S4R)/(C3S+C4S+E3R+E4R+S3R+S4R) |
| **Phenanthrenes, Naphthalenes, and Dibenzothiophenes** | |
| MPI-1 | (1.5*(3MP+2MP))/(PHEN+9MP+1MP) |
| Rc(a) if Ro < 1.3 (Ro%) | (((.6)*(1.5*(2MP+3MP))/(PHEN+9MP+1MP))+.37) |
| Rc(b) if Ro > 1.3 (Ro%) | (((-.6)*(1.5*(2MP+3MP))/(PHEN+9MP+1MP))+2.3) |
| MPI-2 | (3*(2MP))/(PHEN+9MP+1MP) |
| DNR-1 | (26DMN+27DMN)/(15DMN) |
| DNR-2 | (26DMN+27DMN)/(2314DMN) |
| TNR1 | (236TMN)/(146135T) |
| TDE-1 | (125TMN)/(124TMN) |
| TDE-2 | (127TMN)/(167126T) |
| MDR | (4MDBT)/(1MDBT) |
| Rm (Ro%) | (0.40+0.30*(4MDBT/1MDBT)-0.094*(4MDBT/1MDBT)*(4MDBT/1MDBT)+0.011*(4MDBT/1MDBT)*(4MDBT/1MDBT)*(4MDBT/1MDBT)) |
| MDR23 | (23MDBT)/(DBT) |
| MDR1 | (1MDBT)/(DBT) |
| DBT/Phenanthrene | (DBT)/(PHEN) |
| **New Ratios** | |
| PNR | (12467PMN)/(12467PMN+12356PMN) |
| MDPNR | (4+23+1MDBT)/(4+23+1MDBT+12467+12357+12367+12356PMN) |
| Dinosteroid Index 2 | (DINO)/(DINO+231G28) |

*Appendix F3: Saturate Gas Chromatography-Mass Spectroscopy Data*
Definitions on page 413.

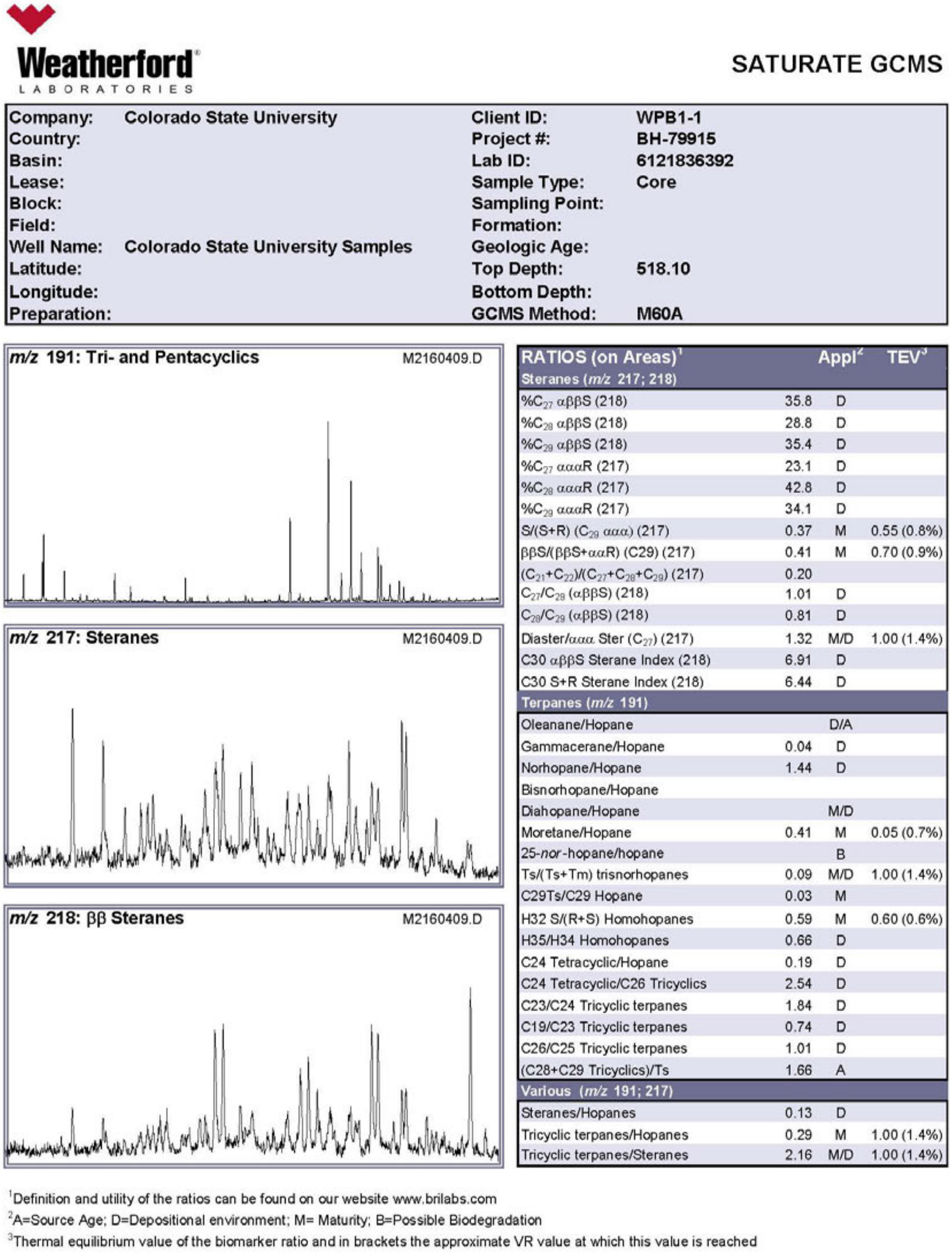

**Weatherford**
LABORATORIES

**SATURATE GCMS**

| | | | |
|---|---|---|---|
| **Company:** | **Colorado State University** | **Client ID:** | **WPB1-1** |
| **Country:** | | **Project #:** | **BH-79915** |
| **Basin:** | | **Lab ID:** | **6121836392** |
| **Lease:** | | **Sample Type:** | **Core** |
| **Block:** | | **Sampling Point:** | |
| **Field:** | | **Formation:** | |
| **Well Name:** | **Colorado State University Samples** | **Geologic Age:** | |
| **Latitude:** | | **Top Depth:** | **518.10** |
| **Longitude:** | | **Bottom Depth:** | |
| **Preparation:** | | **GCMS Method:** | **M60A** |

***m/z* 191: Tri- and Pentacyclics** M2160409.D

***m/z* 217: Steranes** M2160409.D

***m/z* 218: ββ Steranes** M2160409.D

| RATIOS (on Areas)[1] | | Appl[2] | TEV[3] |
|---|---|---|---|
| **Steranes (*m/z* 217; 218)** | | | |
| %$C_{27}$ αββS (218) | 35.8 | D | |
| %$C_{28}$ αββS (218) | 28.8 | D | |
| %$C_{29}$ αββS (218) | 35.4 | D | |
| %$C_{27}$ αααR (217) | 23.1 | D | |
| %$C_{28}$ αααR (217) | 42.8 | D | |
| %$C_{29}$ αααR (217) | 34.1 | D | |
| S/(S+R) ($C_{29}$ ααα) (217) | 0.37 | M | 0.55 (0.8%) |
| ββS/(ββS+ααR) (C29) (217) | 0.41 | M | 0.70 (0.9%) |
| ($C_{21}$+$C_{22}$)/($C_{27}$+$C_{28}$+$C_{29}$) (217) | 0.20 | | |
| $C_{27}$/$C_{29}$ (αββS) (218) | 1.01 | D | |
| $C_{28}$/$C_{29}$ (αββS) (218) | 0.81 | D | |
| Diaster/ααα Ster ($C_{27}$) (217) | 1.32 | M/D | 1.00 (1.4%) |
| C30 αββS Sterane Index (218) | 6.91 | D | |
| C30 S+R Sterane Index (218) | 6.44 | D | |
| **Terpanes (*m/z* 191)** | | | |
| Oleanane/Hopane | | D/A | |
| Gammacerane/Hopane | 0.04 | D | |
| Norhopane/Hopane | 1.44 | D | |
| Bisnorhopane/Hopane | | | |
| Diahopane/Hopane | | M/D | |
| Moretane/Hopane | 0.41 | M | 0.05 (0.7%) |
| 25-*nor*-hopane/hopane | | B | |
| Ts/(Ts+Tm) trisnorhopanes | 0.09 | M/D | 1.00 (1.4%) |
| C29Ts/C29 Hopane | 0.03 | M | |
| H32 S/(R+S) Homohopanes | 0.59 | M | 0.60 (0.6%) |
| H35/H34 Homohopanes | 0.66 | D | |
| C24 Tetracyclic/Hopane | 0.19 | D | |
| C24 Tetracyclic/C26 Tricyclics | 2.54 | D | |
| C23/C24 Tricyclic terpanes | 1.84 | D | |
| C19/C23 Tricyclic terpanes | 0.74 | D | |
| C26/C25 Tricyclic terpanes | 1.01 | D | |
| (C28+C29 Tricyclics)/Ts | 1.66 | A | |
| **Various (*m/z* 191; 217)** | | | |
| Steranes/Hopanes | 0.13 | D | |
| Tricyclic terpanes/Hopanes | 0.29 | M | 1.00 (1.4%) |
| Tricyclic terpanes/Steranes | 2.16 | M/D | 1.00 (1.4%) |

[1] Definition and utility of the ratios can be found on our website www.brilabs.com
[2] A=Source Age; D=Depositional environment; M= Maturity; B=Possible Biodegradation
[3] Thermal equilibrium value of the biomarker ratio and in brackets the approximate VR value at which this value is reached

*Appendix F3, ctd.*

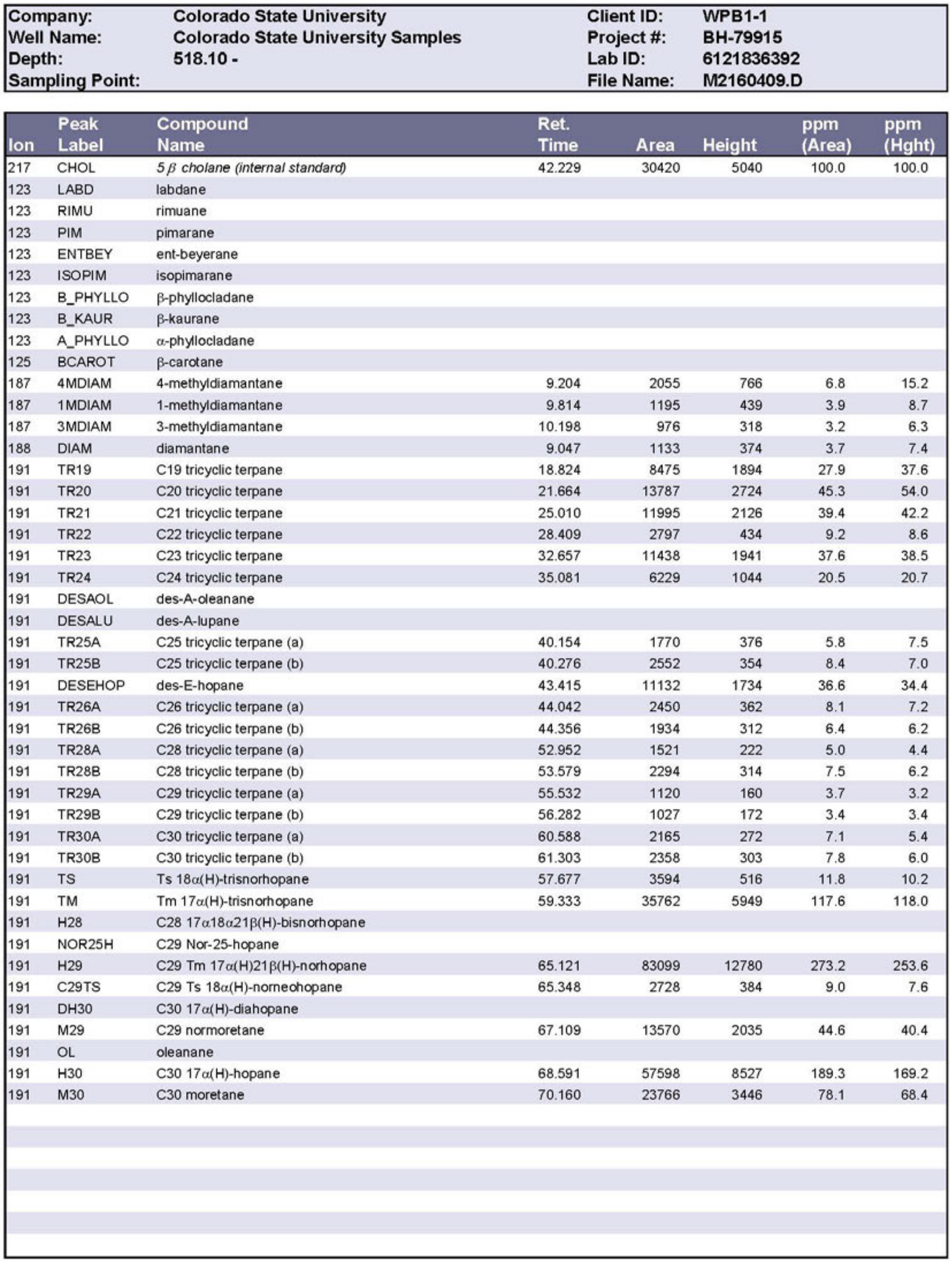

| | | | |
|---|---|---|---|
| **Company:** | **Colorado State University** | **Client ID:** | **WPB1-1** |
| **Well Name:** | **Colorado State University Samples** | **Project #:** | **BH-79915** |
| **Depth:** | **518.10 -** | **Lab ID:** | **6121836392** |
| **Sampling Point:** | | **File Name:** | **M2160409.D** |

| Ion | Peak Label | Compound Name | Ret. Time | Area | Height | ppm (Area) | ppm (Hght) |
|---|---|---|---|---|---|---|---|
| 217 | CHOL | *5β cholane (internal standard)* | 42.229 | 30420 | 5040 | 100.0 | 100.0 |
| 123 | LABD | labdane | | | | | |
| 123 | RIMU | rimuane | | | | | |
| 123 | PIM | pimarane | | | | | |
| 123 | ENTBEY | ent-beyerane | | | | | |
| 123 | ISOPIM | isopimarane | | | | | |
| 123 | B_PHYLLO | β-phyllocladane | | | | | |
| 123 | B_KAUR | β-kaurane | | | | | |
| 123 | A_PHYLLO | α-phyllocladane | | | | | |
| 125 | BCAROT | β-carotane | | | | | |
| 187 | 4MDIAM | 4-methyldiamantane | 9.204 | 2055 | 766 | 6.8 | 15.2 |
| 187 | 1MDIAM | 1-methyldiamantane | 9.814 | 1195 | 439 | 3.9 | 8.7 |
| 187 | 3MDIAM | 3-methyldiamantane | 10.198 | 976 | 318 | 3.2 | 6.3 |
| 188 | DIAM | diamantane | 9.047 | 1133 | 374 | 3.7 | 7.4 |
| 191 | TR19 | C19 tricyclic terpane | 18.824 | 8475 | 1894 | 27.9 | 37.6 |
| 191 | TR20 | C20 tricyclic terpane | 21.664 | 13787 | 2724 | 45.3 | 54.0 |
| 191 | TR21 | C21 tricyclic terpane | 25.010 | 11995 | 2126 | 39.4 | 42.2 |
| 191 | TR22 | C22 tricyclic terpane | 28.409 | 2797 | 434 | 9.2 | 8.6 |
| 191 | TR23 | C23 tricyclic terpane | 32.657 | 11438 | 1941 | 37.6 | 38.5 |
| 191 | TR24 | C24 tricyclic terpane | 35.081 | 6229 | 1044 | 20.5 | 20.7 |
| 191 | DESAOL | des-A-oleanane | | | | | |
| 191 | DESALU | des-A-lupane | | | | | |
| 191 | TR25A | C25 tricyclic terpane (a) | 40.154 | 1770 | 376 | 5.8 | 7.5 |
| 191 | TR25B | C25 tricyclic terpane (b) | 40.276 | 2552 | 354 | 8.4 | 7.0 |
| 191 | DESEHOP | des-E-hopane | 43.415 | 11132 | 1734 | 36.6 | 34.4 |
| 191 | TR26A | C26 tricyclic terpane (a) | 44.042 | 2450 | 362 | 8.1 | 7.2 |
| 191 | TR26B | C26 tricyclic terpane (b) | 44.356 | 1934 | 312 | 6.4 | 6.2 |
| 191 | TR28A | C28 tricyclic terpane (a) | 52.952 | 1521 | 222 | 5.0 | 4.4 |
| 191 | TR28B | C28 tricyclic terpane (b) | 53.579 | 2294 | 314 | 7.5 | 6.2 |
| 191 | TR29A | C29 tricyclic terpane (a) | 55.532 | 1120 | 160 | 3.7 | 3.2 |
| 191 | TR29B | C29 tricyclic terpane (b) | 56.282 | 1027 | 172 | 3.4 | 3.4 |
| 191 | TR30A | C30 tricyclic terpane (a) | 60.588 | 2165 | 272 | 7.1 | 5.4 |
| 191 | TR30B | C30 tricyclic terpane (b) | 61.303 | 2358 | 303 | 7.8 | 6.0 |
| 191 | TS | Ts 18α(H)-trisnorhopane | 57.677 | 3594 | 516 | 11.8 | 10.2 |
| 191 | TM | Tm 17α(H)-trisnorhopane | 59.333 | 35762 | 5949 | 117.6 | 118.0 |
| 191 | H28 | C28 17α18α21β(H)-bisnorhopane | | | | | |
| 191 | NOR25H | C29 Nor-25-hopane | | | | | |
| 191 | H29 | C29 Tm 17α(H)21β(H)-norhopane | 65.121 | 83099 | 12780 | 273.2 | 253.6 |
| 191 | C29TS | C29 Ts 18α(H)-norneohopane | 65.348 | 2728 | 384 | 9.0 | 7.6 |
| 191 | DH30 | C30 17α(H)-diahopane | | | | | |
| 191 | M29 | C29 normoretane | 67.109 | 13570 | 2035 | 44.6 | 40.4 |
| 191 | OL | oleanane | | | | | |
| 191 | H30 | C30 17α(H)-hopane | 68.591 | 57598 | 8527 | 189.3 | 169.2 |
| 191 | M30 | C30 moretane | 70.160 | 23766 | 3446 | 78.1 | 68.4 |

*Appendix F3, ctd.*

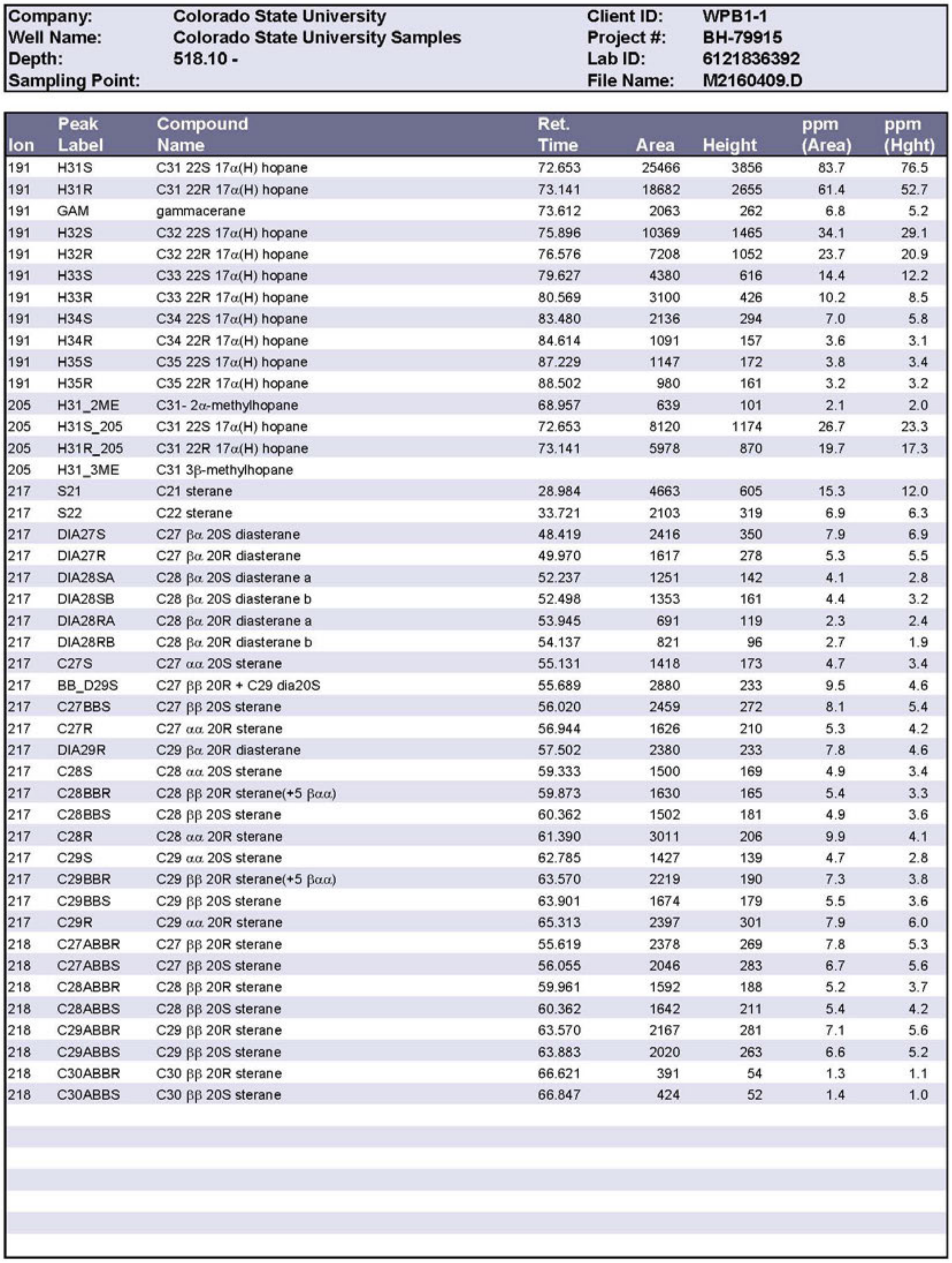

| | | | |
|---|---|---|---|
| **Company:** | **Colorado State University** | **Client ID:** | **WPB1-1** |
| **Well Name:** | **Colorado State University Samples** | **Project #:** | **BH-79915** |
| **Depth:** | **518.10 -** | **Lab ID:** | **6121836392** |
| **Sampling Point:** | | **File Name:** | **M2160409.D** |

| Ion | Peak Label | Compound Name | Ret. Time | Area | Height | ppm (Area) | ppm (Hght) |
|---|---|---|---|---|---|---|---|
| 191 | H31S | C31 22S 17α(H) hopane | 72.653 | 25466 | 3856 | 83.7 | 76.5 |
| 191 | H31R | C31 22R 17α(H) hopane | 73.141 | 18682 | 2655 | 61.4 | 52.7 |
| 191 | GAM | gammacerane | 73.612 | 2063 | 262 | 6.8 | 5.2 |
| 191 | H32S | C32 22S 17α(H) hopane | 75.896 | 10369 | 1465 | 34.1 | 29.1 |
| 191 | H32R | C32 22R 17α(H) hopane | 76.576 | 7208 | 1052 | 23.7 | 20.9 |
| 191 | H33S | C33 22S 17α(H) hopane | 79.627 | 4380 | 616 | 14.4 | 12.2 |
| 191 | H33R | C33 22R 17α(H) hopane | 80.569 | 3100 | 426 | 10.2 | 8.5 |
| 191 | H34S | C34 22S 17α(H) hopane | 83.480 | 2136 | 294 | 7.0 | 5.8 |
| 191 | H34R | C34 22R 17α(H) hopane | 84.614 | 1091 | 157 | 3.6 | 3.1 |
| 191 | H35S | C35 22S 17α(H) hopane | 87.229 | 1147 | 172 | 3.8 | 3.4 |
| 191 | H35R | C35 22R 17α(H) hopane | 88.502 | 980 | 161 | 3.2 | 3.2 |
| 205 | H31_2ME | C31- 2α-methylhopane | 68.957 | 639 | 101 | 2.1 | 2.0 |
| 205 | H31S_205 | C31 22S 17α(H) hopane | 72.653 | 8120 | 1174 | 26.7 | 23.3 |
| 205 | H31R_205 | C31 22R 17α(H) hopane | 73.141 | 5978 | 870 | 19.7 | 17.3 |
| 205 | H31_3ME | C31 3β-methylhopane | | | | | |
| 217 | S21 | C21 sterane | 28.984 | 4663 | 605 | 15.3 | 12.0 |
| 217 | S22 | C22 sterane | 33.721 | 2103 | 319 | 6.9 | 6.3 |
| 217 | DIA27S | C27 βα 20S diasterane | 48.419 | 2416 | 350 | 7.9 | 6.9 |
| 217 | DIA27R | C27 βα 20R diasterane | 49.970 | 1617 | 278 | 5.3 | 5.5 |
| 217 | DIA28SA | C28 βα 20S diasterane a | 52.237 | 1251 | 142 | 4.1 | 2.8 |
| 217 | DIA28SB | C28 βα 20S diasterane b | 52.498 | 1353 | 161 | 4.4 | 3.2 |
| 217 | DIA28RA | C28 βα 20R diasterane a | 53.945 | 691 | 119 | 2.3 | 2.4 |
| 217 | DIA28RB | C28 βα 20R diasterane b | 54.137 | 821 | 96 | 2.7 | 1.9 |
| 217 | C27S | C27 αα 20S sterane | 55.131 | 1418 | 173 | 4.7 | 3.4 |
| 217 | BB_D29S | C27 ββ 20R + C29 dia20S | 55.689 | 2880 | 233 | 9.5 | 4.6 |
| 217 | C27BBS | C27 ββ 20S sterane | 56.020 | 2459 | 272 | 8.1 | 5.4 |
| 217 | C27R | C27 αα 20R sterane | 56.944 | 1626 | 210 | 5.3 | 4.2 |
| 217 | DIA29R | C29 βα 20R diasterane | 57.502 | 2380 | 233 | 7.8 | 4.6 |
| 217 | C28S | C28 αα 20S sterane | 59.333 | 1500 | 169 | 4.9 | 3.4 |
| 217 | C28BBR | C28 ββ 20R sterane(+5 βαα) | 59.873 | 1630 | 165 | 5.4 | 3.3 |
| 217 | C28BBS | C28 ββ 20S sterane | 60.362 | 1502 | 181 | 4.9 | 3.6 |
| 217 | C28R | C28 αα 20R sterane | 61.390 | 3011 | 206 | 9.9 | 4.1 |
| 217 | C29S | C29 αα 20S sterane | 62.785 | 1427 | 139 | 4.7 | 2.8 |
| 217 | C29BBR | C29 ββ 20R sterane(+5 βαα) | 63.570 | 2219 | 190 | 7.3 | 3.8 |
| 217 | C29BBS | C29 ββ 20S sterane | 63.901 | 1674 | 179 | 5.5 | 3.6 |
| 217 | C29R | C29 αα 20R sterane | 65.313 | 2397 | 301 | 7.9 | 6.0 |
| 218 | C27ABBR | C27 ββ 20R sterane | 55.619 | 2378 | 269 | 7.8 | 5.3 |
| 218 | C27ABBS | C27 ββ 20S sterane | 56.055 | 2046 | 283 | 6.7 | 5.6 |
| 218 | C28ABBR | C28 ββ 20R sterane | 59.961 | 1592 | 188 | 5.2 | 3.7 |
| 218 | C28ABBS | C28 ββ 20S sterane | 60.362 | 1642 | 211 | 5.4 | 4.2 |
| 218 | C29ABBR | C29 ββ 20R sterane | 63.570 | 2167 | 281 | 7.1 | 5.6 |
| 218 | C29ABBS | C29 ββ 20S sterane | 63.883 | 2020 | 263 | 6.6 | 5.2 |
| 218 | C30ABBR | C30 ββ 20R sterane | 66.621 | 391 | 54 | 1.3 | 1.1 |
| 218 | C30ABBS | C30 ββ 20S sterane | 66.847 | 424 | 52 | 1.4 | 1.0 |

*Appendix F3, ctd.*

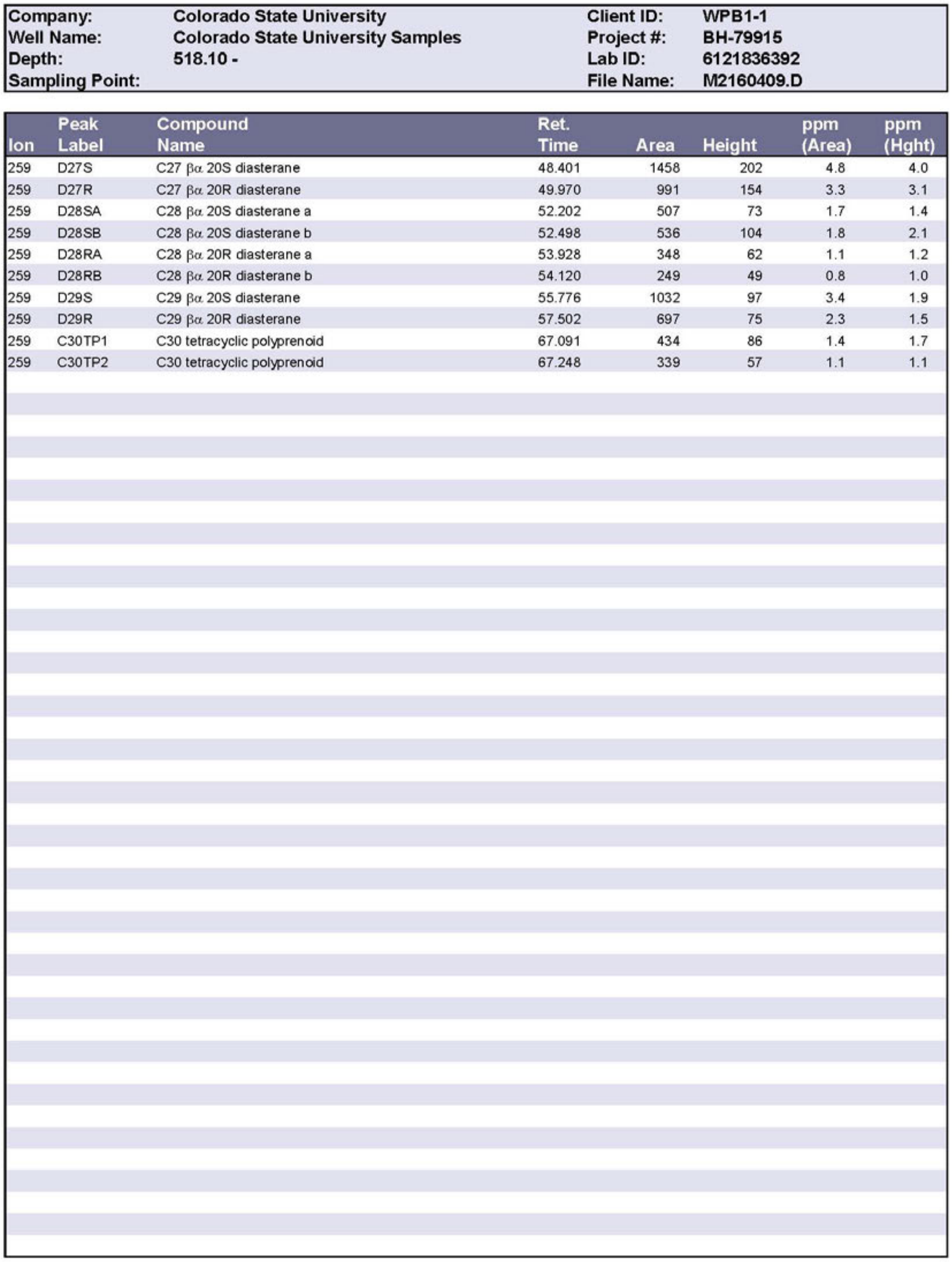

| | | | |
|---|---|---|---|
| **Company:** | **Colorado State University** | **Client ID:** | **WPB1-1** |
| **Well Name:** | **Colorado State University Samples** | **Project #:** | **BH-79915** |
| **Depth:** | **518.10 -** | **Lab ID:** | **6121836392** |
| **Sampling Point:** | | **File Name:** | **M2160409.D** |

| Ion | Peak Label | Compound Name | Ret. Time | Area | Height | ppm (Area) | ppm (Hght) |
|---|---|---|---|---|---|---|---|
| 259 | D27S | C27 βα 20S diasterane | 48.401 | 1458 | 202 | 4.8 | 4.0 |
| 259 | D27R | C27 βα 20R diasterane | 49.970 | 991 | 154 | 3.3 | 3.1 |
| 259 | D28SA | C28 βα 20S diasterane a | 52.202 | 507 | 73 | 1.7 | 1.4 |
| 259 | D28SB | C28 βα 20S diasterane b | 52.498 | 536 | 104 | 1.8 | 2.1 |
| 259 | D28RA | C28 βα 20R diasterane a | 53.928 | 348 | 62 | 1.1 | 1.2 |
| 259 | D28RB | C28 βα 20R diasterane b | 54.120 | 249 | 49 | 0.8 | 1.0 |
| 259 | D29S | C29 βα 20S diasterane | 55.776 | 1032 | 97 | 3.4 | 1.9 |
| 259 | D29R | C29 βα 20R diasterane | 57.502 | 697 | 75 | 2.3 | 1.5 |
| 259 | C30TP1 | C30 tetracyclic polyprenoid | 67.091 | 434 | 86 | 1.4 | 1.7 |
| 259 | C30TP2 | C30 tetracyclic polyprenoid | 67.248 | 339 | 57 | 1.1 | 1.1 |

*Appendix F3, ctd.*

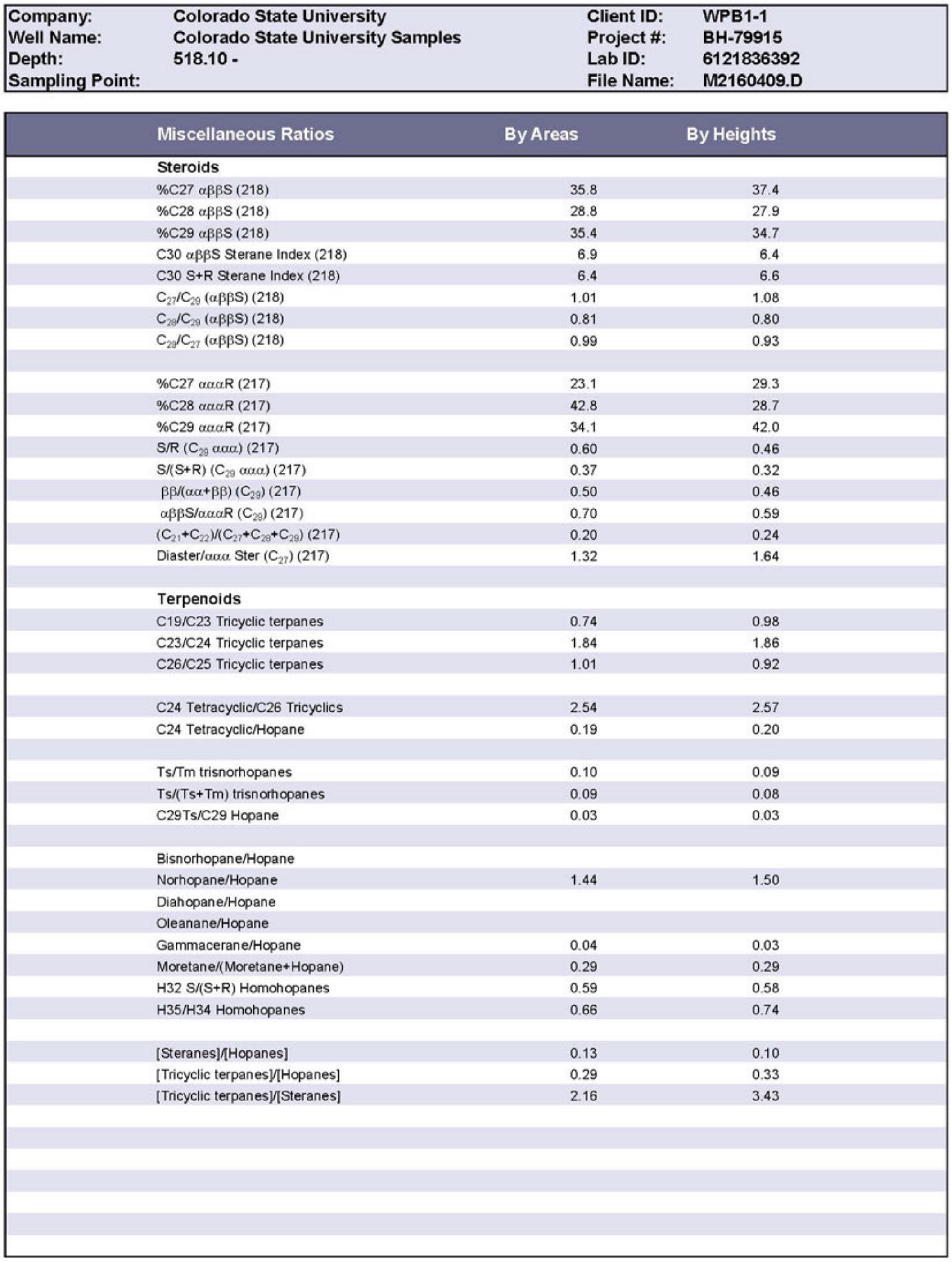

| | | | |
|---|---|---|---|
| **Company:** | **Colorado State University** | **Client ID:** | **WPB1-1** |
| **Well Name:** | **Colorado State University Samples** | **Project #:** | **BH-79915** |
| **Depth:** | **518.10 -** | **Lab ID:** | **6121836392** |
| **Sampling Point:** | | **File Name:** | **M2160409.D** |

| Miscellaneous Ratios | By Areas | By Heights |
|---|---|---|
| **Steroids** | | |
| %C27 αββS (218) | 35.8 | 37.4 |
| %C28 αββS (218) | 28.8 | 27.9 |
| %C29 αββS (218) | 35.4 | 34.7 |
| C30 αββS Sterane Index (218) | 6.9 | 6.4 |
| C30 S+R Sterane Index (218) | 6.4 | 6.6 |
| $C_{27}/C_{29}$ (αββS) (218) | 1.01 | 1.08 |
| $C_{28}/C_{29}$ (αββS) (218) | 0.81 | 0.80 |
| $C_{29}/C_{27}$ (αββS) (218) | 0.99 | 0.93 |
| | | |
| %C27 αααR (217) | 23.1 | 29.3 |
| %C28 αααR (217) | 42.8 | 28.7 |
| %C29 αααR (217) | 34.1 | 42.0 |
| S/R ($C_{29}$ ααα) (217) | 0.60 | 0.46 |
| S/(S+R) ($C_{29}$ ααα) (217) | 0.37 | 0.32 |
| ββ/(αα+ββ) ($C_{29}$) (217) | 0.50 | 0.46 |
| αββS/αααR ($C_{29}$) (217) | 0.70 | 0.59 |
| ($C_{21}+C_{22}$)/($C_{27}+C_{28}+C_{29}$) (217) | 0.20 | 0.24 |
| Diaster/ααα Ster ($C_{27}$) (217) | 1.32 | 1.64 |
| | | |
| **Terpenoids** | | |
| C19/C23 Tricyclic terpanes | 0.74 | 0.98 |
| C23/C24 Tricyclic terpanes | 1.84 | 1.86 |
| C26/C25 Tricyclic terpanes | 1.01 | 0.92 |
| | | |
| C24 Tetracyclic/C26 Tricyclics | 2.54 | 2.57 |
| C24 Tetracyclic/Hopane | 0.19 | 0.20 |
| | | |
| Ts/Tm trisnorhopanes | 0.10 | 0.09 |
| Ts/(Ts+Tm) trisnorhopanes | 0.09 | 0.08 |
| C29Ts/C29 Hopane | 0.03 | 0.03 |
| | | |
| Bisnorhopane/Hopane | | |
| Norhopane/Hopane | 1.44 | 1.50 |
| Diahopane/Hopane | | |
| Oleanane/Hopane | | |
| Gammacerane/Hopane | 0.04 | 0.03 |
| Moretane/(Moretane+Hopane) | 0.29 | 0.29 |
| H32 S/(S+R) Homohopanes | 0.59 | 0.58 |
| H35/H34 Homohopanes | 0.66 | 0.74 |
| | | |
| [Steranes]/[Hopanes] | 0.13 | 0.10 |
| [Tricyclic terpanes]/[Hopanes] | 0.29 | 0.33 |
| [Tricyclic terpanes]/[Steranes] | 2.16 | 3.43 |

*Appendix F3, ctd.*

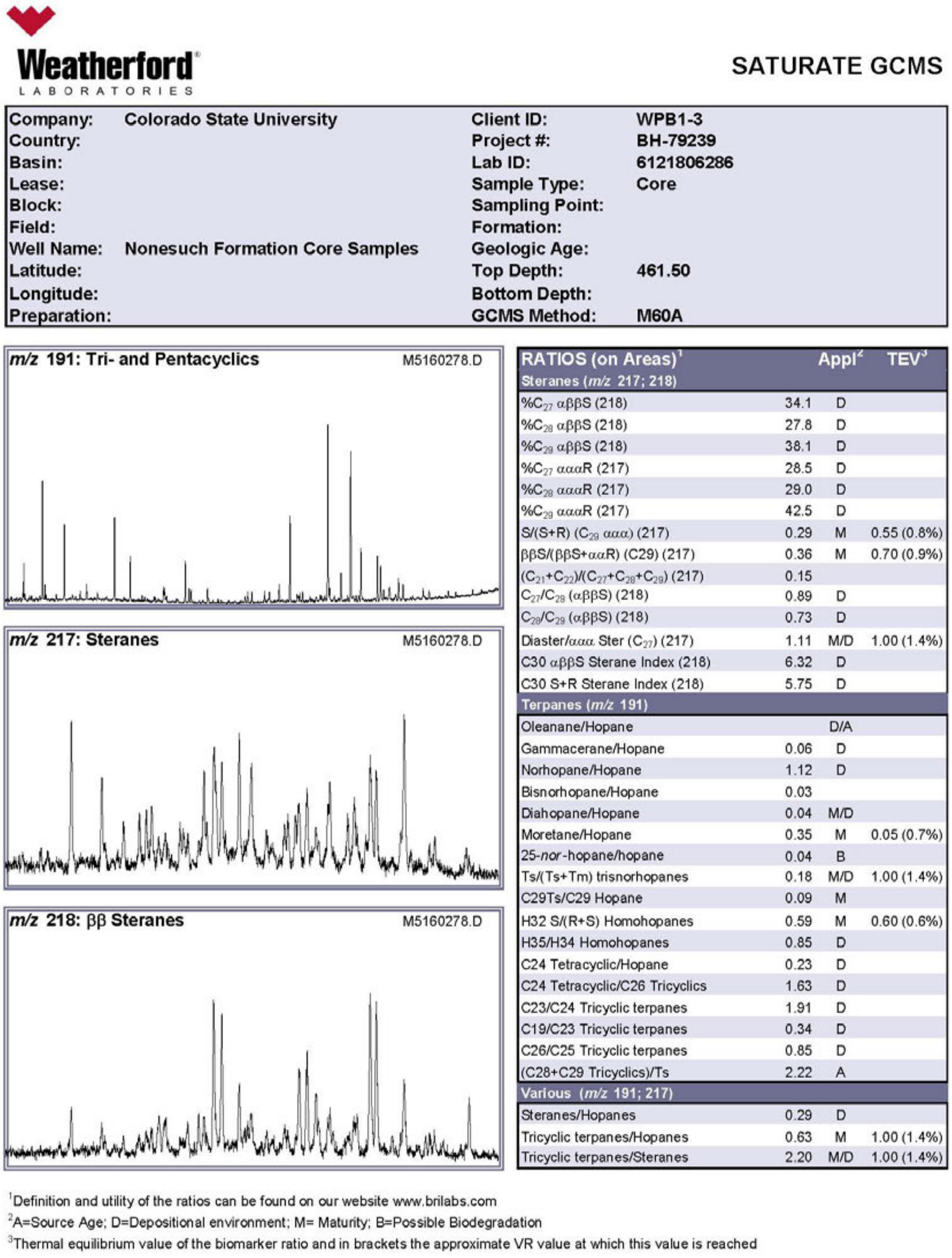

**Weatherford**
LABORATORIES

## SATURATE GCMS

| | | | |
|---|---|---|---|
| **Company:** | **Colorado State University** | **Client ID:** | **WPB1-3** |
| **Country:** | | **Project #:** | **BH-79239** |
| **Basin:** | | **Lab ID:** | **6121806286** |
| **Lease:** | | **Sample Type:** | **Core** |
| **Block:** | | **Sampling Point:** | |
| **Field:** | | **Formation:** | |
| **Well Name:** | **Nonesuch Formation Core Samples** | **Geologic Age:** | |
| **Latitude:** | | **Top Depth:** | **461.50** |
| **Longitude:** | | **Bottom Depth:** | |
| **Preparation:** | | **GCMS Method:** | **M60A** |

***m/z* 191: Tri- and Pentacyclics** M5160278.D

***m/z* 217: Steranes** M5160278.D

***m/z* 218: ββ Steranes** M5160278.D

| RATIOS (on Areas)[1] | | Appl[2] | TEV[3] |
|---|---|---|---|
| **Steranes (*m/z* 217; 218)** | | | |
| %$C_{27}$ αββS (218) | 34.1 | D | |
| %$C_{28}$ αββS (218) | 27.8 | D | |
| %$C_{29}$ αββS (218) | 38.1 | D | |
| %$C_{27}$ αααR (217) | 28.5 | D | |
| %$C_{28}$ αααR (217) | 29.0 | D | |
| %$C_{29}$ αααR (217) | 42.5 | D | |
| S/(S+R) ($C_{29}$ ααα) (217) | 0.29 | M | 0.55 (0.8%) |
| ββS/(ββS+ααR) (C29) (217) | 0.36 | M | 0.70 (0.9%) |
| ($C_{21}$+$C_{22}$)/($C_{27}$+$C_{28}$+$C_{29}$) (217) | 0.15 | | |
| $C_{27}$/$C_{29}$ (αββS) (218) | 0.89 | D | |
| $C_{28}$/$C_{29}$ (αββS) (218) | 0.73 | D | |
| Diaster/ααα Ster ($C_{27}$) (217) | 1.11 | M/D | 1.00 (1.4%) |
| C30 αββS Sterane Index (218) | 6.32 | D | |
| C30 S+R Sterane Index (218) | 5.75 | D | |
| **Terpanes (*m/z* 191)** | | | |
| Oleanane/Hopane | | D/A | |
| Gammacerane/Hopane | 0.06 | D | |
| Norhopane/Hopane | 1.12 | D | |
| Bisnorhopane/Hopane | 0.03 | | |
| Diahopane/Hopane | 0.04 | M/D | |
| Moretane/Hopane | 0.35 | M | 0.05 (0.7%) |
| 25-*nor*-hopane/hopane | 0.04 | B | |
| Ts/(Ts+Tm) trisnorhopanes | 0.18 | M/D | 1.00 (1.4%) |
| C29Ts/C29 Hopane | 0.09 | M | |
| H32 S/(R+S) Homohopanes | 0.59 | M | 0.60 (0.6%) |
| H35/H34 Homohopanes | 0.85 | D | |
| C24 Tetracyclic/Hopane | 0.23 | D | |
| C24 Tetracyclic/C26 Tricyclics | 1.63 | D | |
| C23/C24 Tricyclic terpanes | 1.91 | D | |
| C19/C23 Tricyclic terpanes | 0.34 | D | |
| C26/C25 Tricyclic terpanes | 0.85 | D | |
| (C28+C29 Tricyclics)/Ts | 2.22 | A | |
| **Various (*m/z* 191; 217)** | | | |
| Steranes/Hopanes | 0.29 | D | |
| Tricyclic terpanes/Hopanes | 0.63 | M | 1.00 (1.4%) |
| Tricyclic terpanes/Steranes | 2.20 | M/D | 1.00 (1.4%) |

[1] Definition and utility of the ratios can be found on our website www.brilabs.com

[2] A=Source Age; D=Depositional environment; M= Maturity; B=Possible Biodegradation

[3] Thermal equilibrium value of the biomarker ratio and in brackets the approximate VR value at which this value is reached

*Appendix F3, ctd.*

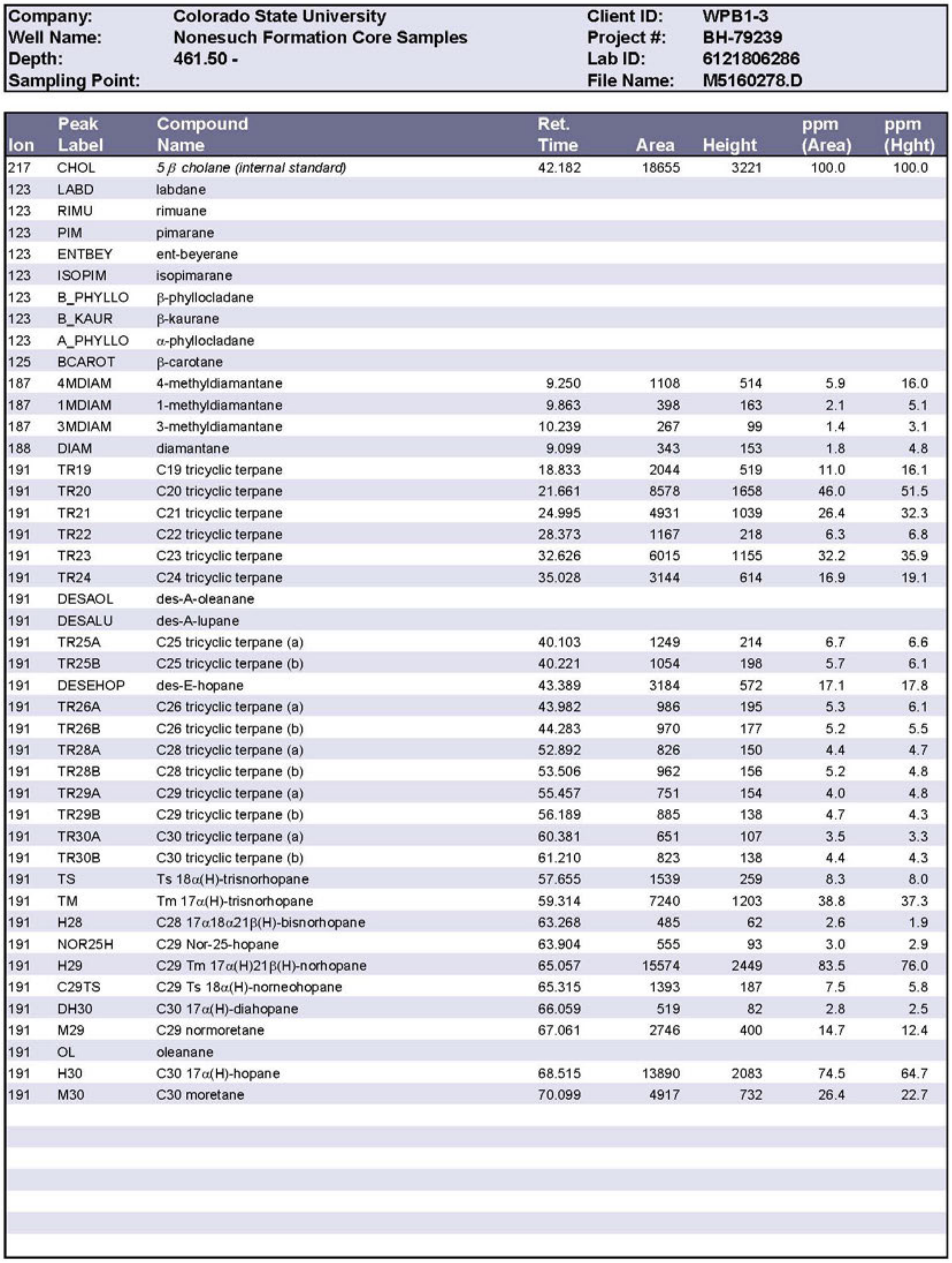

| | | | |
|---|---|---|---|
| **Company:** | **Colorado State University** | **Client ID:** | **WPB1-3** |
| **Well Name:** | **Nonesuch Formation Core Samples** | **Project #:** | **BH-79239** |
| **Depth:** | **461.50 -** | **Lab ID:** | **6121806286** |
| **Sampling Point:** | | **File Name:** | **M5160278.D** |

| Ion | Peak Label | Compound Name | Ret. Time | Area | Height | ppm (Area) | ppm (Hght) |
|---|---|---|---|---|---|---|---|
| 217 | CHOL | *5β cholane (internal standard)* | 42.182 | 18655 | 3221 | 100.0 | 100.0 |
| 123 | LABD | labdane | | | | | |
| 123 | RIMU | rimuane | | | | | |
| 123 | PIM | pimarane | | | | | |
| 123 | ENTBEY | ent-beyerane | | | | | |
| 123 | ISOPIM | isopimarane | | | | | |
| 123 | B_PHYLLO | β-phyllocladane | | | | | |
| 123 | B_KAUR | β-kaurane | | | | | |
| 123 | A_PHYLLO | α-phyllocladane | | | | | |
| 125 | BCAROT | β-carotane | | | | | |
| 187 | 4MDIAM | 4-methyldiamantane | 9.250 | 1108 | 514 | 5.9 | 16.0 |
| 187 | 1MDIAM | 1-methyldiamantane | 9.863 | 398 | 163 | 2.1 | 5.1 |
| 187 | 3MDIAM | 3-methyldiamantane | 10.239 | 267 | 99 | 1.4 | 3.1 |
| 188 | DIAM | diamantane | 9.099 | 343 | 153 | 1.8 | 4.8 |
| 191 | TR19 | C19 tricyclic terpane | 18.833 | 2044 | 519 | 11.0 | 16.1 |
| 191 | TR20 | C20 tricyclic terpane | 21.661 | 8578 | 1658 | 46.0 | 51.5 |
| 191 | TR21 | C21 tricyclic terpane | 24.995 | 4931 | 1039 | 26.4 | 32.3 |
| 191 | TR22 | C22 tricyclic terpane | 28.373 | 1167 | 218 | 6.3 | 6.8 |
| 191 | TR23 | C23 tricyclic terpane | 32.626 | 6015 | 1155 | 32.2 | 35.9 |
| 191 | TR24 | C24 tricyclic terpane | 35.028 | 3144 | 614 | 16.9 | 19.1 |
| 191 | DESAOL | des-A-oleanane | | | | | |
| 191 | DESALU | des-A-lupane | | | | | |
| 191 | TR25A | C25 tricyclic terpane (a) | 40.103 | 1249 | 214 | 6.7 | 6.6 |
| 191 | TR25B | C25 tricyclic terpane (b) | 40.221 | 1054 | 198 | 5.7 | 6.1 |
| 191 | DESEHOP | des-E-hopane | 43.389 | 3184 | 572 | 17.1 | 17.8 |
| 191 | TR26A | C26 tricyclic terpane (a) | 43.982 | 986 | 195 | 5.3 | 6.1 |
| 191 | TR26B | C26 tricyclic terpane (b) | 44.283 | 970 | 177 | 5.2 | 5.5 |
| 191 | TR28A | C28 tricyclic terpane (a) | 52.892 | 826 | 150 | 4.4 | 4.7 |
| 191 | TR28B | C28 tricyclic terpane (b) | 53.506 | 962 | 156 | 5.2 | 4.8 |
| 191 | TR29A | C29 tricyclic terpane (a) | 55.457 | 751 | 154 | 4.0 | 4.8 |
| 191 | TR29B | C29 tricyclic terpane (b) | 56.189 | 885 | 138 | 4.7 | 4.3 |
| 191 | TR30A | C30 tricyclic terpane (a) | 60.381 | 651 | 107 | 3.5 | 3.3 |
| 191 | TR30B | C30 tricyclic terpane (b) | 61.210 | 823 | 138 | 4.4 | 4.3 |
| 191 | TS | Ts 18α(H)-trisnorhopane | 57.655 | 1539 | 259 | 8.3 | 8.0 |
| 191 | TM | Tm 17α(H)-trisnorhopane | 59.314 | 7240 | 1203 | 38.8 | 37.3 |
| 191 | H28 | C28 17α18α21β(H)-bisnorhopane | 63.268 | 485 | 62 | 2.6 | 1.9 |
| 191 | NOR25H | C29 Nor-25-hopane | 63.904 | 555 | 93 | 3.0 | 2.9 |
| 191 | H29 | C29 Tm 17α(H)21β(H)-norhopane | 65.057 | 15574 | 2449 | 83.5 | 76.0 |
| 191 | C29TS | C29 Ts 18α(H)-norneohopane | 65.315 | 1393 | 187 | 7.5 | 5.8 |
| 191 | DH30 | C30 17α(H)-diahopane | 66.059 | 519 | 82 | 2.8 | 2.5 |
| 191 | M29 | C29 normoretane | 67.061 | 2746 | 400 | 14.7 | 12.4 |
| 191 | OL | oleanane | | | | | |
| 191 | H30 | C30 17α(H)-hopane | 68.515 | 13890 | 2083 | 74.5 | 64.7 |
| 191 | M30 | C30 moretane | 70.099 | 4917 | 732 | 26.4 | 22.7 |

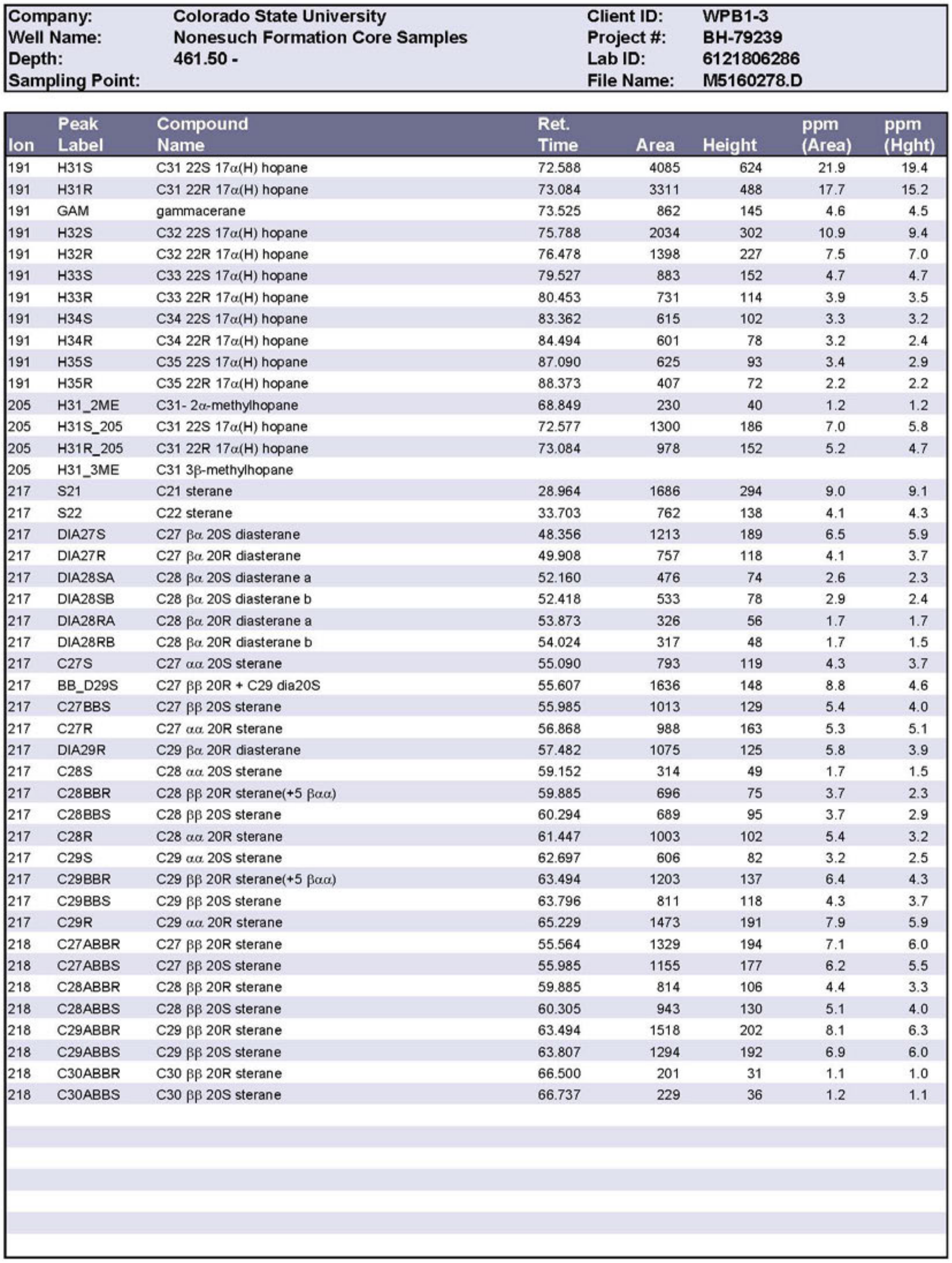

| | | | |
|---|---|---|---|
| **Company:** | **Colorado State University** | **Client ID:** | **WPB1-3** |
| **Well Name:** | **Nonesuch Formation Core Samples** | **Project #:** | **BH-79239** |
| **Depth:** | **461.50 -** | **Lab ID:** | **6121806286** |
| **Sampling Point:** | | **File Name:** | **M5160278.D** |

| Ion | Peak Label | Compound Name | Ret. Time | Area | Height | ppm (Area) | ppm (Hght) |
|---|---|---|---|---|---|---|---|
| 191 | H31S | C31 22S 17α(H) hopane | 72.588 | 4085 | 624 | 21.9 | 19.4 |
| 191 | H31R | C31 22R 17α(H) hopane | 73.084 | 3311 | 488 | 17.7 | 15.2 |
| 191 | GAM | gammacerane | 73.525 | 862 | 145 | 4.6 | 4.5 |
| 191 | H32S | C32 22S 17α(H) hopane | 75.788 | 2034 | 302 | 10.9 | 9.4 |
| 191 | H32R | C32 22R 17α(H) hopane | 76.478 | 1398 | 227 | 7.5 | 7.0 |
| 191 | H33S | C33 22S 17α(H) hopane | 79.527 | 883 | 152 | 4.7 | 4.7 |
| 191 | H33R | C33 22R 17α(H) hopane | 80.453 | 731 | 114 | 3.9 | 3.5 |
| 191 | H34S | C34 22S 17α(H) hopane | 83.362 | 615 | 102 | 3.3 | 3.2 |
| 191 | H34R | C34 22R 17α(H) hopane | 84.494 | 601 | 78 | 3.2 | 2.4 |
| 191 | H35S | C35 22S 17α(H) hopane | 87.090 | 625 | 93 | 3.4 | 2.9 |
| 191 | H35R | C35 22R 17α(H) hopane | 88.373 | 407 | 72 | 2.2 | 2.2 |
| 205 | H31_2ME | C31- 2α-methylhopane | 68.849 | 230 | 40 | 1.2 | 1.2 |
| 205 | H31S_205 | C31 22S 17α(H) hopane | 72.577 | 1300 | 186 | 7.0 | 5.8 |
| 205 | H31R_205 | C31 22R 17α(H) hopane | 73.084 | 978 | 152 | 5.2 | 4.7 |
| 205 | H31_3ME | C31 3β-methylhopane | | | | | |
| 217 | S21 | C21 sterane | 28.964 | 1686 | 294 | 9.0 | 9.1 |
| 217 | S22 | C22 sterane | 33.703 | 762 | 138 | 4.1 | 4.3 |
| 217 | DIA27S | C27 βα 20S diasterane | 48.356 | 1213 | 189 | 6.5 | 5.9 |
| 217 | DIA27R | C27 βα 20R diasterane | 49.908 | 757 | 118 | 4.1 | 3.7 |
| 217 | DIA28SA | C28 βα 20S diasterane a | 52.160 | 476 | 74 | 2.6 | 2.3 |
| 217 | DIA28SB | C28 βα 20S diasterane b | 52.418 | 533 | 78 | 2.9 | 2.4 |
| 217 | DIA28RA | C28 βα 20R diasterane a | 53.873 | 326 | 56 | 1.7 | 1.7 |
| 217 | DIA28RB | C28 βα 20R diasterane b | 54.024 | 317 | 48 | 1.7 | 1.5 |
| 217 | C27S | C27 αα 20S sterane | 55.090 | 793 | 119 | 4.3 | 3.7 |
| 217 | BB_D29S | C27 ββ 20R + C29 dia20S | 55.607 | 1636 | 148 | 8.8 | 4.6 |
| 217 | C27BBS | C27 ββ 20S sterane | 55.985 | 1013 | 129 | 5.4 | 4.0 |
| 217 | C27R | C27 αα 20R sterane | 56.868 | 988 | 163 | 5.3 | 5.1 |
| 217 | DIA29R | C29 βα 20R diasterane | 57.482 | 1075 | 125 | 5.8 | 3.9 |
| 217 | C28S | C28 αα 20S sterane | 59.152 | 314 | 49 | 1.7 | 1.5 |
| 217 | C28BBR | C28 ββ 20R sterane(+5 βαα) | 59.885 | 696 | 75 | 3.7 | 2.3 |
| 217 | C28BBS | C28 ββ 20S sterane | 60.294 | 689 | 95 | 3.7 | 2.9 |
| 217 | C28R | C28 αα 20R sterane | 61.447 | 1003 | 102 | 5.4 | 3.2 |
| 217 | C29S | C29 αα 20S sterane | 62.697 | 606 | 82 | 3.2 | 2.5 |
| 217 | C29BBR | C29 ββ 20R sterane(+5 βαα) | 63.494 | 1203 | 137 | 6.4 | 4.3 |
| 217 | C29BBS | C29 ββ 20S sterane | 63.796 | 811 | 118 | 4.3 | 3.7 |
| 217 | C29R | C29 αα 20R sterane | 65.229 | 1473 | 191 | 7.9 | 5.9 |
| 218 | C27ABBR | C27 ββ 20R sterane | 55.564 | 1329 | 194 | 7.1 | 6.0 |
| 218 | C27ABBS | C27 ββ 20S sterane | 55.985 | 1155 | 177 | 6.2 | 5.5 |
| 218 | C28ABBR | C28 ββ 20R sterane | 59.885 | 814 | 106 | 4.4 | 3.3 |
| 218 | C28ABBS | C28 ββ 20S sterane | 60.305 | 943 | 130 | 5.1 | 4.0 |
| 218 | C29ABBR | C29 ββ 20R sterane | 63.494 | 1518 | 202 | 8.1 | 6.3 |
| 218 | C29ABBS | C29 ββ 20S sterane | 63.807 | 1294 | 192 | 6.9 | 6.0 |
| 218 | C30ABBR | C30 ββ 20R sterane | 66.500 | 201 | 31 | 1.1 | 1.0 |
| 218 | C30ABBS | C30 ββ 20S sterane | 66.737 | 229 | 36 | 1.2 | 1.1 |

*Appendix F3, ctd.*

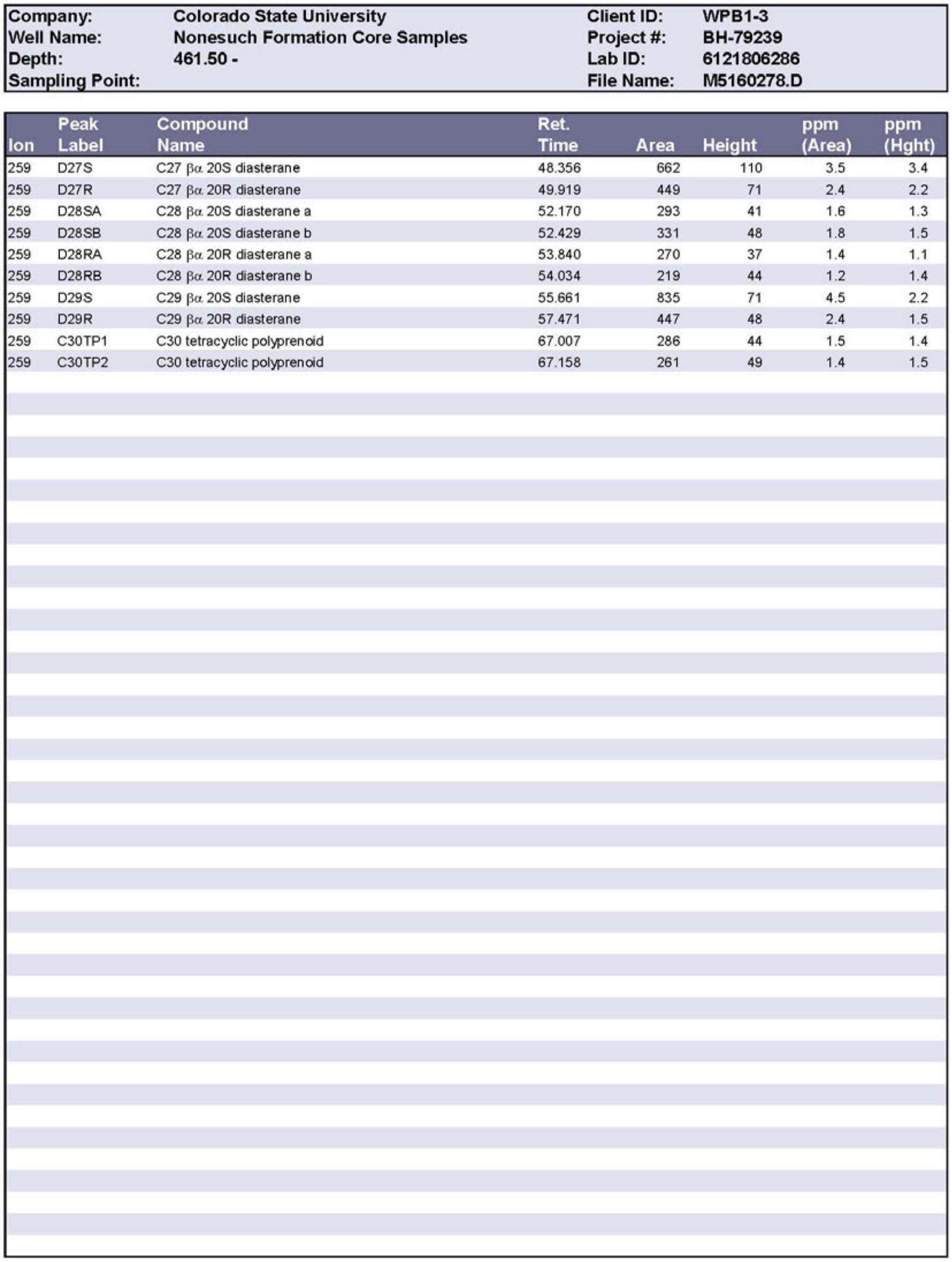

| | | | |
|---|---|---|---|
| **Company:** | **Colorado State University** | **Client ID:** | **WPB1-3** |
| **Well Name:** | **Nonesuch Formation Core Samples** | **Project #:** | **BH-79239** |
| **Depth:** | **461.50 -** | **Lab ID:** | **6121806286** |
| **Sampling Point:** | | **File Name:** | **M5160278.D** |

| Ion | Peak Label | Compound Name | Ret. Time | Area | Height | ppm (Area) | ppm (Hght) |
|---|---|---|---|---|---|---|---|
| 259 | D27S | C27 βα 20S diasterane | 48.356 | 662 | 110 | 3.5 | 3.4 |
| 259 | D27R | C27 βα 20R diasterane | 49.919 | 449 | 71 | 2.4 | 2.2 |
| 259 | D28SA | C28 βα 20S diasterane a | 52.170 | 293 | 41 | 1.6 | 1.3 |
| 259 | D28SB | C28 βα 20S diasterane b | 52.429 | 331 | 48 | 1.8 | 1.5 |
| 259 | D28RA | C28 βα 20R diasterane a | 53.840 | 270 | 37 | 1.4 | 1.1 |
| 259 | D28RB | C28 βα 20R diasterane b | 54.034 | 219 | 44 | 1.2 | 1.4 |
| 259 | D29S | C29 βα 20S diasterane | 55.661 | 835 | 71 | 4.5 | 2.2 |
| 259 | D29R | C29 βα 20R diasterane | 57.471 | 447 | 48 | 2.4 | 1.5 |
| 259 | C30TP1 | C30 tetracyclic polyprenoid | 67.007 | 286 | 44 | 1.5 | 1.4 |
| 259 | C30TP2 | C30 tetracyclic polyprenoid | 67.158 | 261 | 49 | 1.4 | 1.5 |

*Appendix F3, ctd.*

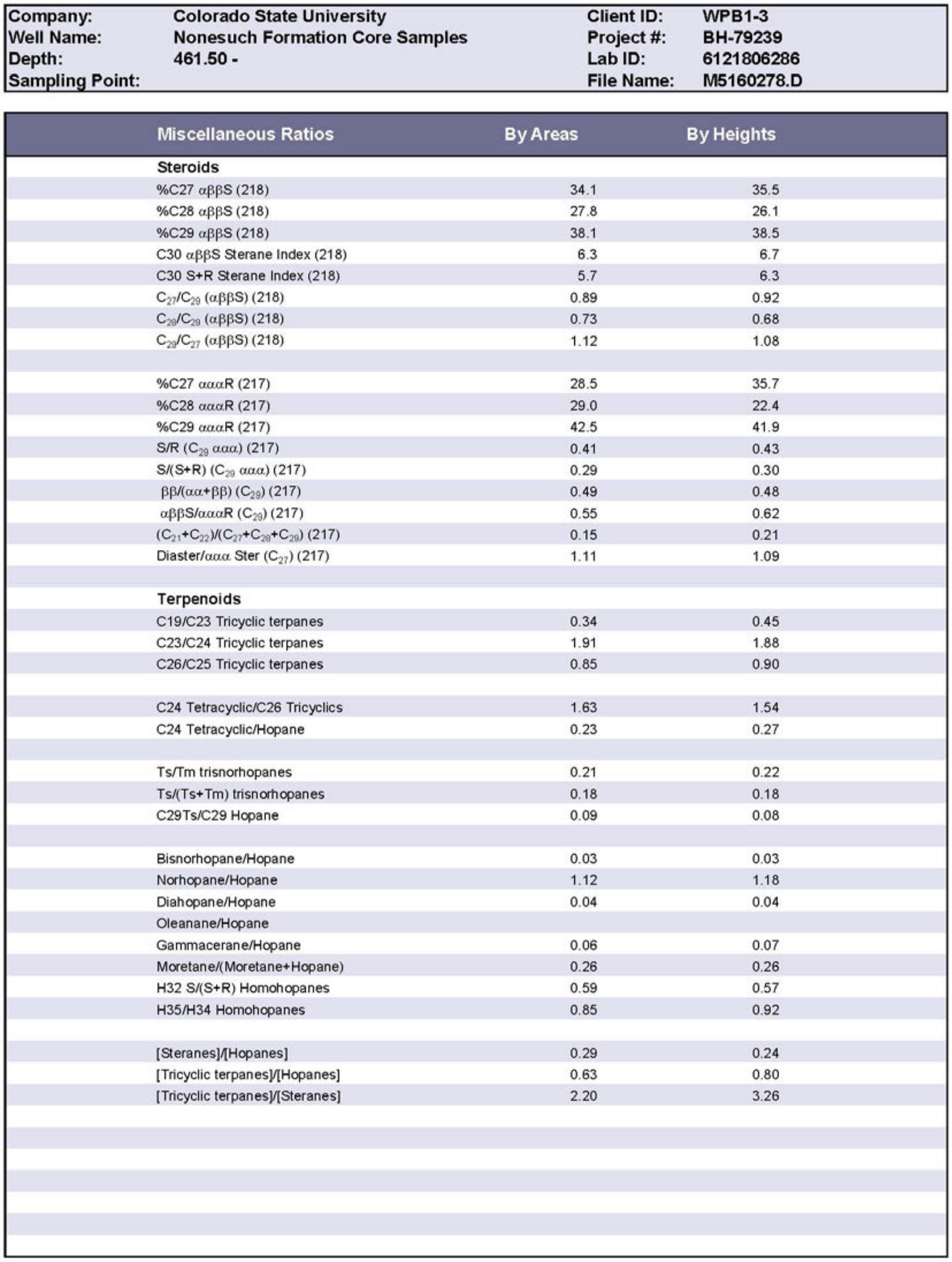

| | | | |
|---|---|---|---|
| **Company:** | **Colorado State University** | **Client ID:** | **WPB1-3** |
| **Well Name:** | **Nonesuch Formation Core Samples** | **Project #:** | **BH-79239** |
| **Depth:** | **461.50 -** | **Lab ID:** | **6121806286** |
| **Sampling Point:** | | **File Name:** | **M5160278.D** |

| Miscellaneous Ratios | By Areas | By Heights |
|---|---|---|
| **Steroids** | | |
| %C27 αββS (218) | 34.1 | 35.5 |
| %C28 αββS (218) | 27.8 | 26.1 |
| %C29 αββS (218) | 38.1 | 38.5 |
| C30 αββS Sterane Index (218) | 6.3 | 6.7 |
| C30 S+R Sterane Index (218) | 5.7 | 6.3 |
| $C_{27}/C_{29}$ (αββS) (218) | 0.89 | 0.92 |
| $C_{28}/C_{29}$ (αββS) (218) | 0.73 | 0.68 |
| $C_{29}/C_{27}$ (αββS) (218) | 1.12 | 1.08 |
| | | |
| %C27 αααR (217) | 28.5 | 35.7 |
| %C28 αααR (217) | 29.0 | 22.4 |
| %C29 αααR (217) | 42.5 | 41.9 |
| S/R ($C_{29}$ ααα) (217) | 0.41 | 0.43 |
| S/(S+R) ($C_{29}$ ααα) (217) | 0.29 | 0.30 |
| ββ/(αα+ββ) ($C_{29}$) (217) | 0.49 | 0.48 |
| αββS/αααR ($C_{29}$) (217) | 0.55 | 0.62 |
| ($C_{21}$+$C_{22}$)/($C_{27}$+$C_{28}$+$C_{29}$) (217) | 0.15 | 0.21 |
| Diaster/ααα Ster ($C_{27}$) (217) | 1.11 | 1.09 |
| | | |
| **Terpenoids** | | |
| C19/C23 Tricyclic terpanes | 0.34 | 0.45 |
| C23/C24 Tricyclic terpanes | 1.91 | 1.88 |
| C26/C25 Tricyclic terpanes | 0.85 | 0.90 |
| | | |
| C24 Tetracyclic/C26 Tricyclics | 1.63 | 1.54 |
| C24 Tetracyclic/Hopane | 0.23 | 0.27 |
| | | |
| Ts/Tm trisnorhopanes | 0.21 | 0.22 |
| Ts/(Ts+Tm) trisnorhopanes | 0.18 | 0.18 |
| C29Ts/C29 Hopane | 0.09 | 0.08 |
| | | |
| Bisnorhopane/Hopane | 0.03 | 0.03 |
| Norhopane/Hopane | 1.12 | 1.18 |
| Diahopane/Hopane | 0.04 | 0.04 |
| Oleanane/Hopane | | |
| Gammacerane/Hopane | 0.06 | 0.07 |
| Moretane/(Moretane+Hopane) | 0.26 | 0.26 |
| H32 S/(S+R) Homohopanes | 0.59 | 0.57 |
| H35/H34 Homohopanes | 0.85 | 0.92 |
| | | |
| [Steranes]/[Hopanes] | 0.29 | 0.24 |
| [Tricyclic terpanes]/[Hopanes] | 0.63 | 0.80 |
| [Tricyclic terpanes]/[Steranes] | 2.20 | 3.26 |

*Appendix F3, ctd.*

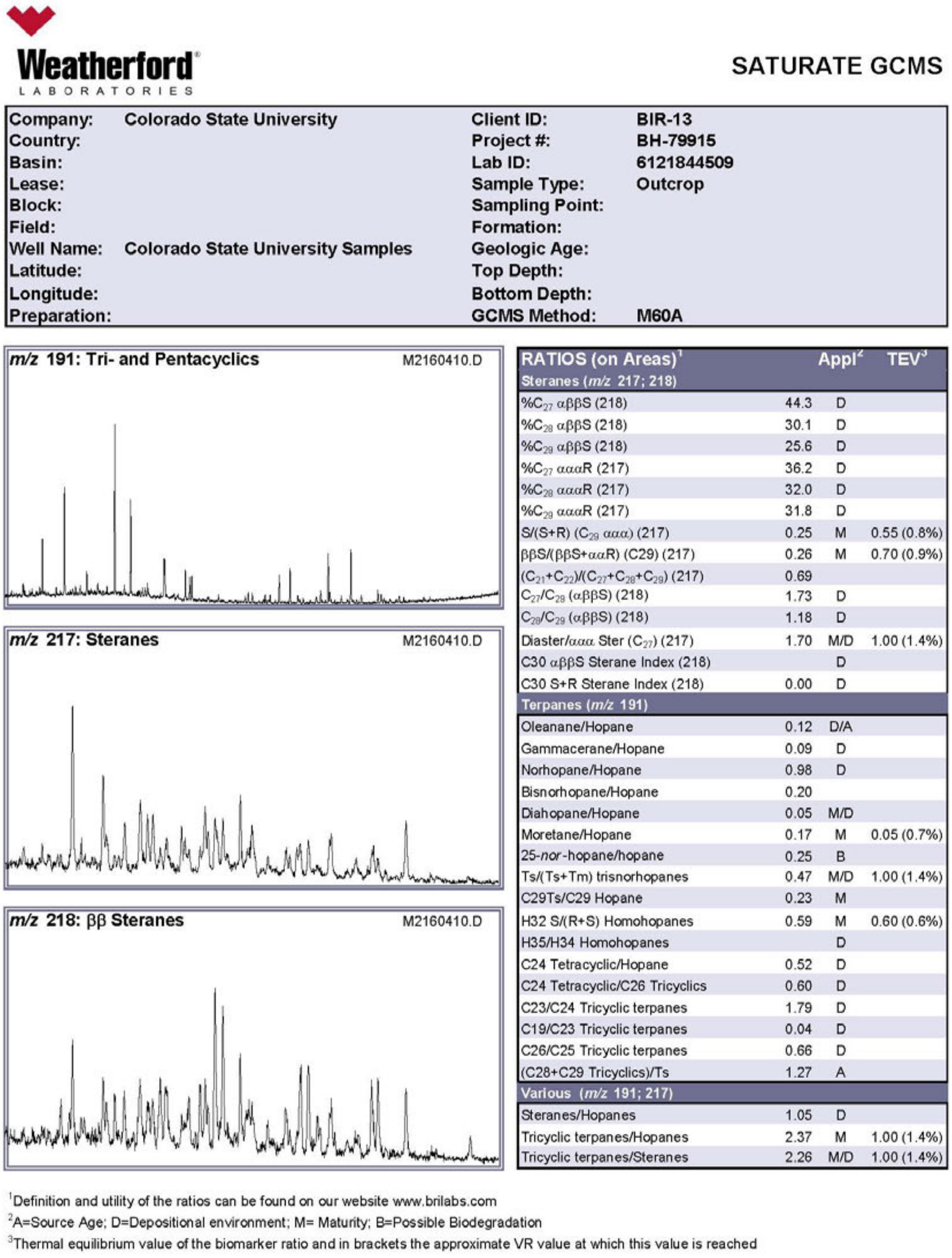

**Weatherford** LABORATORIES

**SATURATE GCMS**

| | | | |
|---|---|---|---|
| **Company:** | **Colorado State University** | **Client ID:** | **BIR-13** |
| **Country:** | | **Project #:** | **BH-79915** |
| **Basin:** | | **Lab ID:** | **6121844509** |
| **Lease:** | | **Sample Type:** | **Outcrop** |
| **Block:** | | **Sampling Point:** | |
| **Field:** | | **Formation:** | |
| **Well Name:** | **Colorado State University Samples** | **Geologic Age:** | |
| **Latitude:** | | **Top Depth:** | |
| **Longitude:** | | **Bottom Depth:** | |
| **Preparation:** | | **GCMS Method:** | **M60A** |

***m/z* 191: Tri- and Pentacyclics** M2160410.D

***m/z* 217: Steranes** M2160410.D

***m/z* 218: ββ Steranes** M2160410.D

| **RATIOS (on Areas)**[1] | | **Appl**[2] | **TEV**[3] |
|---|---|---|---|
| **Steranes (*m/z* 217; 218)** | | | |
| %$C_{27}$ αββS (218) | 44.3 | D | |
| %$C_{28}$ αββS (218) | 30.1 | D | |
| %$C_{29}$ αββS (218) | 25.6 | D | |
| %$C_{27}$ αααR (217) | 36.2 | D | |
| %$C_{28}$ αααR (217) | 32.0 | D | |
| %$C_{29}$ αααR (217) | 31.8 | D | |
| S/(S+R) ($C_{29}$ ααα) (217) | 0.25 | M | 0.55 (0.8%) |
| ββS/(ββS+ααR) (C29) (217) | 0.26 | M | 0.70 (0.9%) |
| ($C_{21}$+$C_{22}$)/($C_{27}$+$C_{28}$+$C_{29}$) (217) | 0.69 | | |
| $C_{27}$/$C_{29}$ (αββS) (218) | 1.73 | D | |
| $C_{28}$/$C_{29}$ (αββS) (218) | 1.18 | D | |
| Diaster/ααα Ster ($C_{27}$) (217) | 1.70 | M/D | 1.00 (1.4%) |
| C30 αββS Sterane Index (218) | | D | |
| C30 S+R Sterane Index (218) | 0.00 | D | |
| **Terpanes (*m/z* 191)** | | | |
| Oleanane/Hopane | 0.12 | D/A | |
| Gammacerane/Hopane | 0.09 | D | |
| Norhopane/Hopane | 0.98 | D | |
| Bisnorhopane/Hopane | 0.20 | | |
| Diahopane/Hopane | 0.05 | M/D | |
| Moretane/Hopane | 0.17 | M | 0.05 (0.7%) |
| 25-*nor*-hopane/hopane | 0.25 | B | |
| Ts/(Ts+Tm) trisnorhopanes | 0.47 | M/D | 1.00 (1.4%) |
| C29Ts/C29 Hopane | 0.23 | M | |
| H32 S/(R+S) Homohopanes | 0.59 | M | 0.60 (0.6%) |
| H35/H34 Homohopanes | | D | |
| C24 Tetracyclic/Hopane | 0.52 | D | |
| C24 Tetracyclic/C26 Tricyclics | 0.60 | D | |
| C23/C24 Tricyclic terpanes | 1.79 | D | |
| C19/C23 Tricyclic terpanes | 0.04 | D | |
| C26/C25 Tricyclic terpanes | 0.66 | D | |
| (C28+C29 Tricyclics)/Ts | 1.27 | A | |
| **Various (*m/z* 191; 217)** | | | |
| Steranes/Hopanes | 1.05 | D | |
| Tricyclic terpanes/Hopanes | 2.37 | M | 1.00 (1.4%) |
| Tricyclic terpanes/Steranes | 2.26 | M/D | 1.00 (1.4%) |

[1] Definition and utility of the ratios can be found on our website www.brilabs.com

[2] A=Source Age; D=Depositional environment; M= Maturity; B=Possible Biodegradation

[3] Thermal equilibrium value of the biomarker ratio and in brackets the approximate VR value at which this value is reached

*Appendix F3, ctd.*

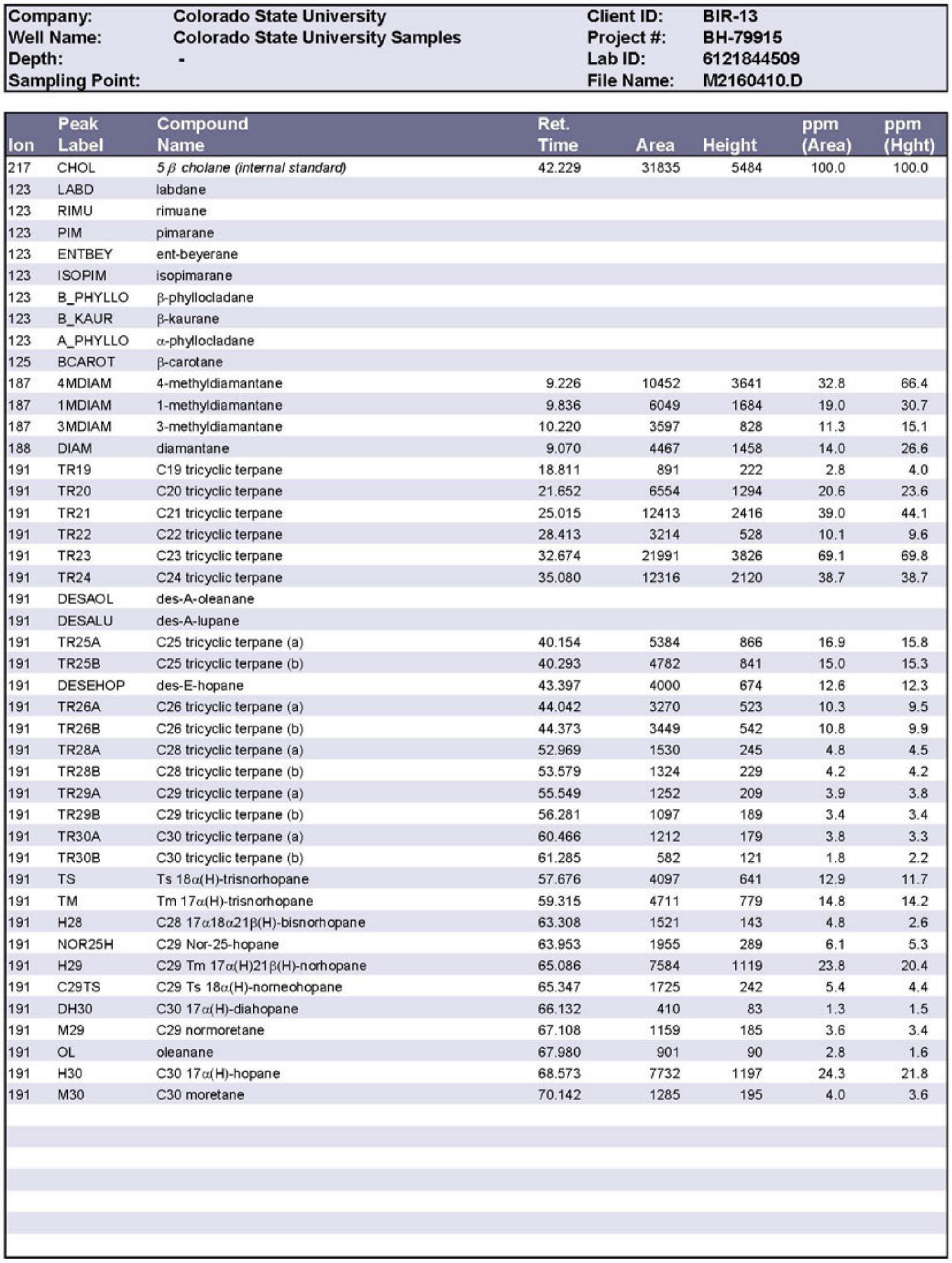

| | | | |
|---|---|---|---|
| **Company:** | **Colorado State University** | **Client ID:** | **BIR-13** |
| **Well Name:** | **Colorado State University Samples** | **Project #:** | **BH-79915** |
| **Depth:** | **-** | **Lab ID:** | **6121844509** |
| **Sampling Point:** | | **File Name:** | **M2160410.D** |

| Ion | Peak Label | Compound Name | Ret. Time | Area | Height | ppm (Area) | ppm (Hght) |
|---|---|---|---|---|---|---|---|
| 217 | CHOL | *5 β cholane (internal standard)* | 42.229 | 31835 | 5484 | 100.0 | 100.0 |
| 123 | LABD | labdane | | | | | |
| 123 | RIMU | rimuane | | | | | |
| 123 | PIM | pimarane | | | | | |
| 123 | ENTBEY | ent-beyerane | | | | | |
| 123 | ISOPIM | isopimarane | | | | | |
| 123 | B_PHYLLO | β-phyllocladane | | | | | |
| 123 | B_KAUR | β-kaurane | | | | | |
| 123 | A_PHYLLO | α-phyllocladane | | | | | |
| 125 | BCAROT | β-carotane | | | | | |
| 187 | 4MDIAM | 4-methyldiamantane | 9.226 | 10452 | 3641 | 32.8 | 66.4 |
| 187 | 1MDIAM | 1-methyldiamantane | 9.836 | 6049 | 1684 | 19.0 | 30.7 |
| 187 | 3MDIAM | 3-methyldiamantane | 10.220 | 3597 | 828 | 11.3 | 15.1 |
| 188 | DIAM | diamantane | 9.070 | 4467 | 1458 | 14.0 | 26.6 |
| 191 | TR19 | C19 tricyclic terpane | 18.811 | 891 | 222 | 2.8 | 4.0 |
| 191 | TR20 | C20 tricyclic terpane | 21.652 | 6554 | 1294 | 20.6 | 23.6 |
| 191 | TR21 | C21 tricyclic terpane | 25.015 | 12413 | 2416 | 39.0 | 44.1 |
| 191 | TR22 | C22 tricyclic terpane | 28.413 | 3214 | 528 | 10.1 | 9.6 |
| 191 | TR23 | C23 tricyclic terpane | 32.674 | 21991 | 3826 | 69.1 | 69.8 |
| 191 | TR24 | C24 tricyclic terpane | 35.080 | 12316 | 2120 | 38.7 | 38.7 |
| 191 | DESAOL | des-A-oleanane | | | | | |
| 191 | DESALU | des-A-lupane | | | | | |
| 191 | TR25A | C25 tricyclic terpane (a) | 40.154 | 5384 | 866 | 16.9 | 15.8 |
| 191 | TR25B | C25 tricyclic terpane (b) | 40.293 | 4782 | 841 | 15.0 | 15.3 |
| 191 | DESEHOP | des-E-hopane | 43.397 | 4000 | 674 | 12.6 | 12.3 |
| 191 | TR26A | C26 tricyclic terpane (a) | 44.042 | 3270 | 523 | 10.3 | 9.5 |
| 191 | TR26B | C26 tricyclic terpane (b) | 44.373 | 3449 | 542 | 10.8 | 9.9 |
| 191 | TR28A | C28 tricyclic terpane (a) | 52.969 | 1530 | 245 | 4.8 | 4.5 |
| 191 | TR28B | C28 tricyclic terpane (b) | 53.579 | 1324 | 229 | 4.2 | 4.2 |
| 191 | TR29A | C29 tricyclic terpane (a) | 55.549 | 1252 | 209 | 3.9 | 3.8 |
| 191 | TR29B | C29 tricyclic terpane (b) | 56.281 | 1097 | 189 | 3.4 | 3.4 |
| 191 | TR30A | C30 tricyclic terpane (a) | 60.466 | 1212 | 179 | 3.8 | 3.3 |
| 191 | TR30B | C30 tricyclic terpane (b) | 61.285 | 582 | 121 | 1.8 | 2.2 |
| 191 | TS | Ts 18α(H)-trisnorhopane | 57.676 | 4097 | 641 | 12.9 | 11.7 |
| 191 | TM | Tm 17α(H)-trisnorhopane | 59.315 | 4711 | 779 | 14.8 | 14.2 |
| 191 | H28 | C28 17α18α21β(H)-bisnorhopane | 63.308 | 1521 | 143 | 4.8 | 2.6 |
| 191 | NOR25H | C29 Nor-25-hopane | 63.953 | 1955 | 289 | 6.1 | 5.3 |
| 191 | H29 | C29 Tm 17α(H)21β(H)-norhopane | 65.086 | 7584 | 1119 | 23.8 | 20.4 |
| 191 | C29TS | C29 Ts 18α(H)-norneohopane | 65.347 | 1725 | 242 | 5.4 | 4.4 |
| 191 | DH30 | C30 17α(H)-diahopane | 66.132 | 410 | 83 | 1.3 | 1.5 |
| 191 | M29 | C29 normoretane | 67.108 | 1159 | 185 | 3.6 | 3.4 |
| 191 | OL | oleanane | 67.980 | 901 | 90 | 2.8 | 1.6 |
| 191 | H30 | C30 17α(H)-hopane | 68.573 | 7732 | 1197 | 24.3 | 21.8 |
| 191 | M30 | C30 moretane | 70.142 | 1285 | 195 | 4.0 | 3.6 |

*Appendix F3, ctd.*

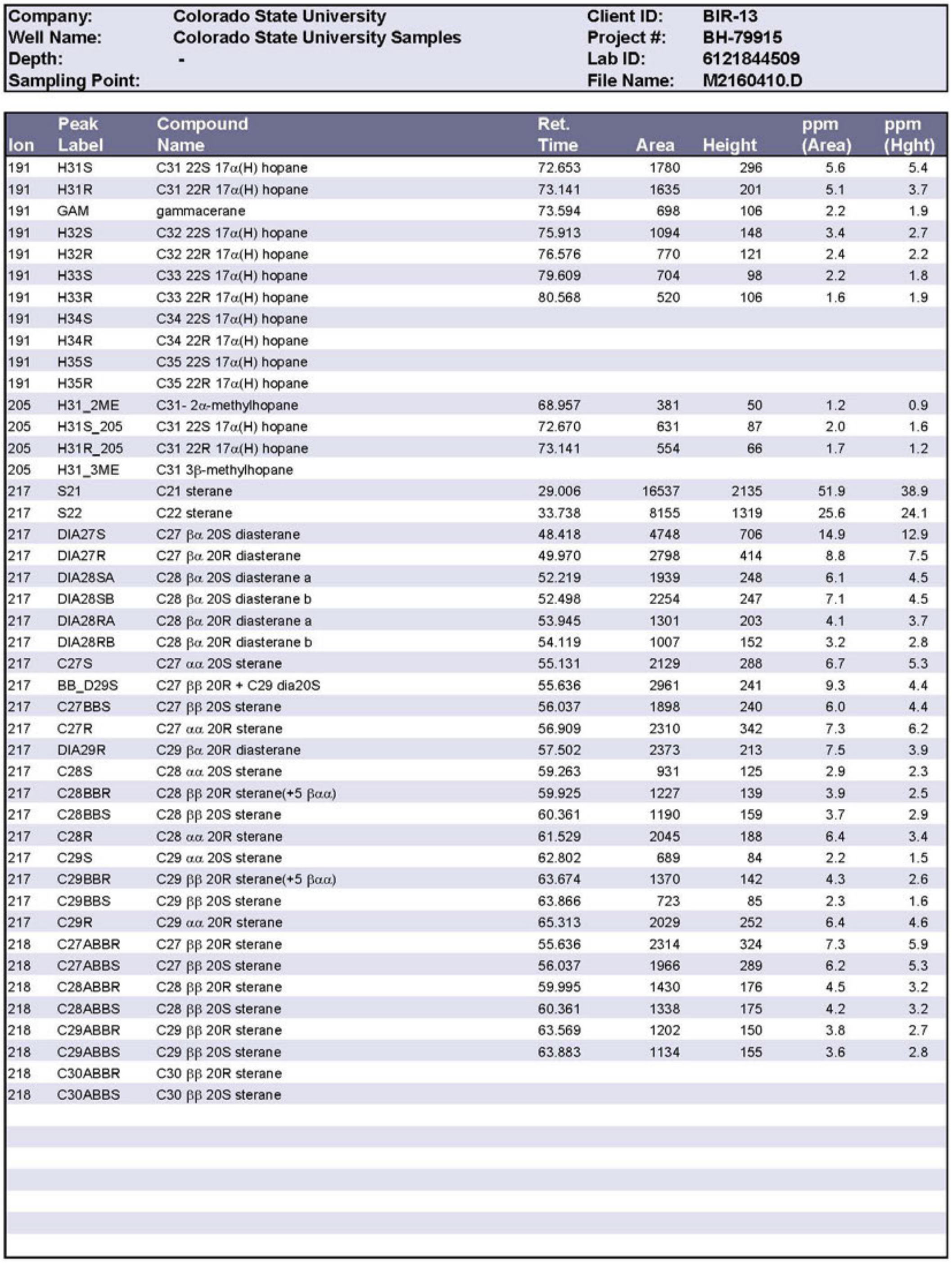

| | | | |
|---|---|---|---|
| **Company:** | **Colorado State University** | **Client ID:** | **BIR-13** |
| **Well Name:** | **Colorado State University Samples** | **Project #:** | **BH-79915** |
| **Depth:** | **-** | **Lab ID:** | **6121844509** |
| **Sampling Point:** | | **File Name:** | **M2160410.D** |

| Ion | Peak Label | Compound Name | Ret. Time | Area | Height | ppm (Area) | ppm (Hght) |
|---|---|---|---|---|---|---|---|
| 191 | H31S | C31 22S 17α(H) hopane | 72.653 | 1780 | 296 | 5.6 | 5.4 |
| 191 | H31R | C31 22R 17α(H) hopane | 73.141 | 1635 | 201 | 5.1 | 3.7 |
| 191 | GAM | gammacerane | 73.594 | 698 | 106 | 2.2 | 1.9 |
| 191 | H32S | C32 22S 17α(H) hopane | 75.913 | 1094 | 148 | 3.4 | 2.7 |
| 191 | H32R | C32 22R 17α(H) hopane | 76.576 | 770 | 121 | 2.4 | 2.2 |
| 191 | H33S | C33 22S 17α(H) hopane | 79.609 | 704 | 98 | 2.2 | 1.8 |
| 191 | H33R | C33 22R 17α(H) hopane | 80.568 | 520 | 106 | 1.6 | 1.9 |
| 191 | H34S | C34 22S 17α(H) hopane | | | | | |
| 191 | H34R | C34 22R 17α(H) hopane | | | | | |
| 191 | H35S | C35 22S 17α(H) hopane | | | | | |
| 191 | H35R | C35 22R 17α(H) hopane | | | | | |
| 205 | H31_2ME | C31- 2α-methylhopane | 68.957 | 381 | 50 | 1.2 | 0.9 |
| 205 | H31S_205 | C31 22S 17α(H) hopane | 72.670 | 631 | 87 | 2.0 | 1.6 |
| 205 | H31R_205 | C31 22R 17α(H) hopane | 73.141 | 554 | 66 | 1.7 | 1.2 |
| 205 | H31_3ME | C31 3β-methylhopane | | | | | |
| 217 | S21 | C21 sterane | 29.006 | 16537 | 2135 | 51.9 | 38.9 |
| 217 | S22 | C22 sterane | 33.738 | 8155 | 1319 | 25.6 | 24.1 |
| 217 | DIA27S | C27 βα 20S diasterane | 48.418 | 4748 | 706 | 14.9 | 12.9 |
| 217 | DIA27R | C27 βα 20R diasterane | 49.970 | 2798 | 414 | 8.8 | 7.5 |
| 217 | DIA28SA | C28 βα 20S diasterane a | 52.219 | 1939 | 248 | 6.1 | 4.5 |
| 217 | DIA28SB | C28 βα 20S diasterane b | 52.498 | 2254 | 247 | 7.1 | 4.5 |
| 217 | DIA28RA | C28 βα 20R diasterane a | 53.945 | 1301 | 203 | 4.1 | 3.7 |
| 217 | DIA28RB | C28 βα 20R diasterane b | 54.119 | 1007 | 152 | 3.2 | 2.8 |
| 217 | C27S | C27 αα 20S sterane | 55.131 | 2129 | 288 | 6.7 | 5.3 |
| 217 | BB_D29S | C27 ββ 20R + C29 dia20S | 55.636 | 2961 | 241 | 9.3 | 4.4 |
| 217 | C27BBS | C27 ββ 20S sterane | 56.037 | 1898 | 240 | 6.0 | 4.4 |
| 217 | C27R | C27 αα 20R sterane | 56.909 | 2310 | 342 | 7.3 | 6.2 |
| 217 | DIA29R | C29 βα 20R diasterane | 57.502 | 2373 | 213 | 7.5 | 3.9 |
| 217 | C28S | C28 αα 20S sterane | 59.263 | 931 | 125 | 2.9 | 2.3 |
| 217 | C28BBR | C28 ββ 20R sterane(+5 βαα) | 59.925 | 1227 | 139 | 3.9 | 2.5 |
| 217 | C28BBS | C28 ββ 20S sterane | 60.361 | 1190 | 159 | 3.7 | 2.9 |
| 217 | C28R | C28 αα 20R sterane | 61.529 | 2045 | 188 | 6.4 | 3.4 |
| 217 | C29S | C29 αα 20S sterane | 62.802 | 689 | 84 | 2.2 | 1.5 |
| 217 | C29BBR | C29 ββ 20R sterane(+5 βαα) | 63.674 | 1370 | 142 | 4.3 | 2.6 |
| 217 | C29BBS | C29 ββ 20S sterane | 63.866 | 723 | 85 | 2.3 | 1.6 |
| 217 | C29R | C29 αα 20R sterane | 65.313 | 2029 | 252 | 6.4 | 4.6 |
| 218 | C27ABBR | C27 ββ 20R sterane | 55.636 | 2314 | 324 | 7.3 | 5.9 |
| 218 | C27ABBS | C27 ββ 20S sterane | 56.037 | 1966 | 289 | 6.2 | 5.3 |
| 218 | C28ABBR | C28 ββ 20R sterane | 59.995 | 1430 | 176 | 4.5 | 3.2 |
| 218 | C28ABBS | C28 ββ 20S sterane | 60.361 | 1338 | 175 | 4.2 | 3.2 |
| 218 | C29ABBR | C29 ββ 20R sterane | 63.569 | 1202 | 150 | 3.8 | 2.7 |
| 218 | C29ABBS | C29 ββ 20S sterane | 63.883 | 1134 | 155 | 3.6 | 2.8 |
| 218 | C30ABBR | C30 ββ 20R sterane | | | | | |
| 218 | C30ABBS | C30 ββ 20S sterane | | | | | |

*Appendix F3, ctd.*

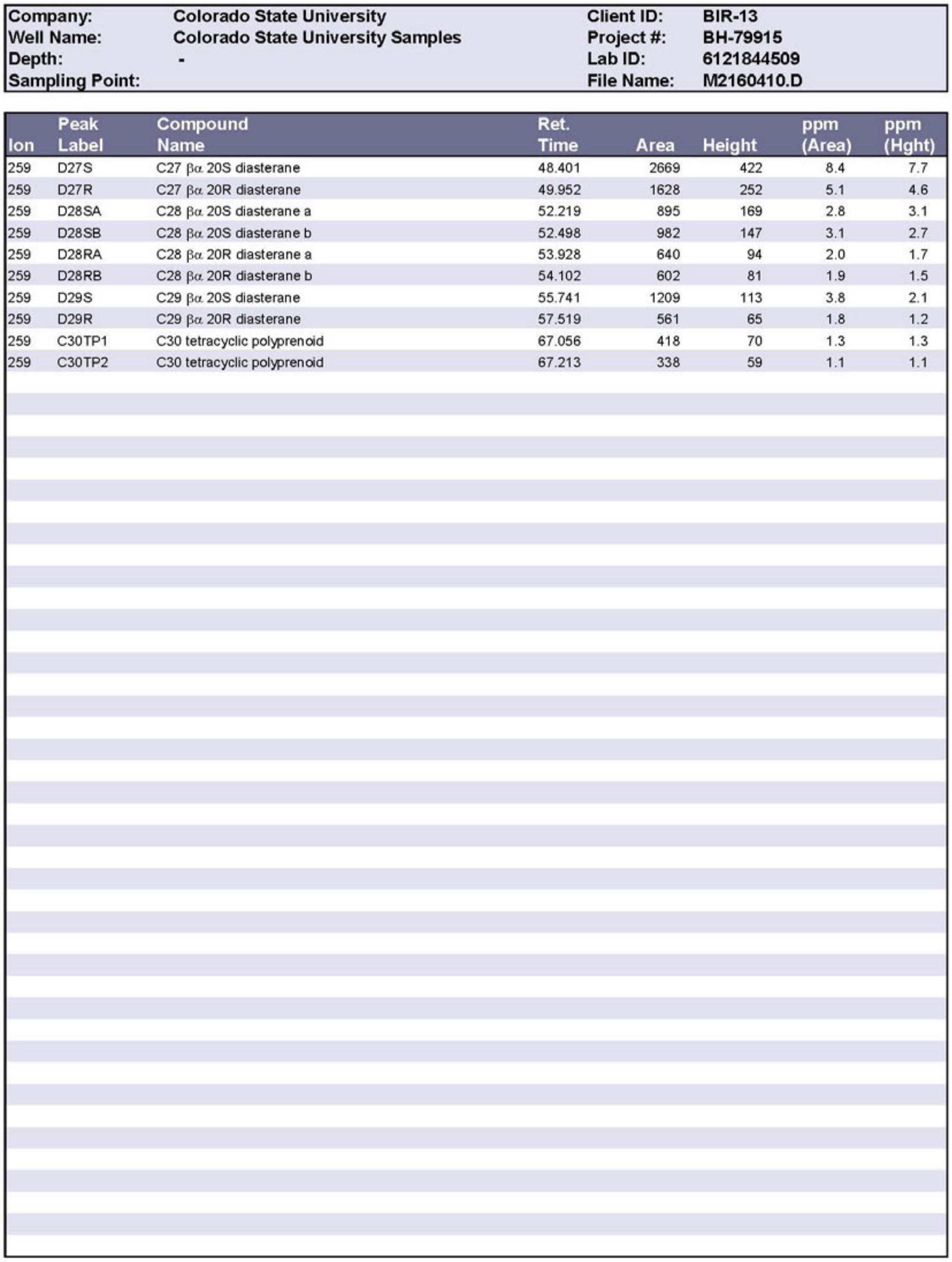

| | | | |
|---|---|---|---|
| **Company:** | **Colorado State University** | **Client ID:** | **BIR-13** |
| **Well Name:** | **Colorado State University Samples** | **Project #:** | **BH-79915** |
| **Depth:** | **-** | **Lab ID:** | **6121844509** |
| **Sampling Point:** | | **File Name:** | **M2160410.D** |

| Ion | Peak Label | Compound Name | Ret. Time | Area | Height | ppm (Area) | ppm (Hght) |
|---|---|---|---|---|---|---|---|
| 259 | D27S | C27 βα 20S diasterane | 48.401 | 2669 | 422 | 8.4 | 7.7 |
| 259 | D27R | C27 βα 20R diasterane | 49.952 | 1628 | 252 | 5.1 | 4.6 |
| 259 | D28SA | C28 βα 20S diasterane a | 52.219 | 895 | 169 | 2.8 | 3.1 |
| 259 | D28SB | C28 βα 20S diasterane b | 52.498 | 982 | 147 | 3.1 | 2.7 |
| 259 | D28RA | C28 βα 20R diasterane a | 53.928 | 640 | 94 | 2.0 | 1.7 |
| 259 | D28RB | C28 βα 20R diasterane b | 54.102 | 602 | 81 | 1.9 | 1.5 |
| 259 | D29S | C29 βα 20S diasterane | 55.741 | 1209 | 113 | 3.8 | 2.1 |
| 259 | D29R | C29 βα 20R diasterane | 57.519 | 561 | 65 | 1.8 | 1.2 |
| 259 | C30TP1 | C30 tetracyclic polyprenoid | 67.056 | 418 | 70 | 1.3 | 1.3 |
| 259 | C30TP2 | C30 tetracyclic polyprenoid | 67.213 | 338 | 59 | 1.1 | 1.1 |

*Appendix F3, ctd.*

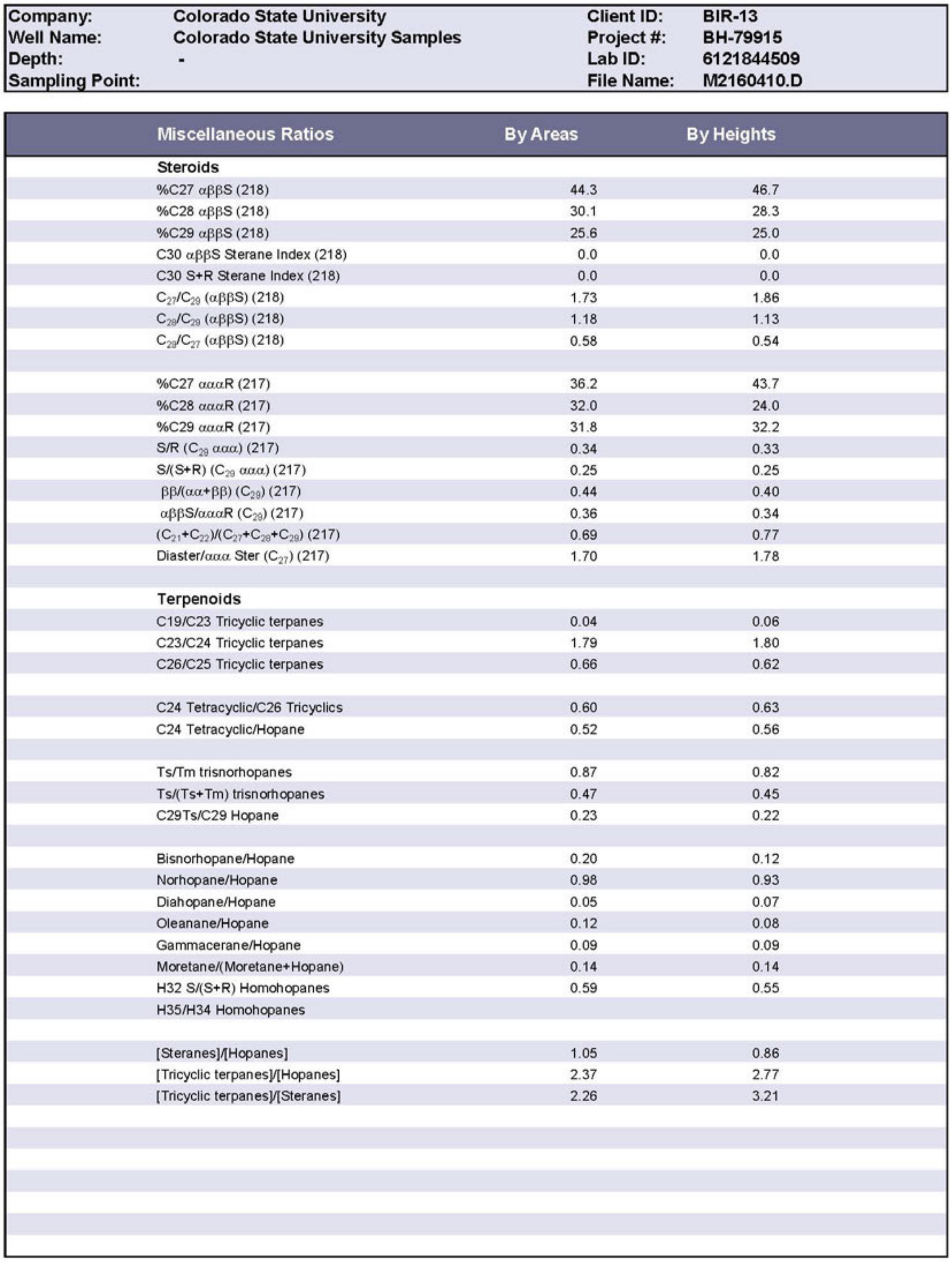

| | | | |
|---|---|---|---|
| **Company:** | **Colorado State University** | **Client ID:** | **BIR-13** |
| **Well Name:** | **Colorado State University Samples** | **Project #:** | **BH-79915** |
| **Depth:** | **-** | **Lab ID:** | **6121844509** |
| **Sampling Point:** | | **File Name:** | **M2160410.D** |

| Miscellaneous Ratios | By Areas | By Heights |
|---|---|---|
| **Steroids** | | |
| %C27 αββS (218) | 44.3 | 46.7 |
| %C28 αββS (218) | 30.1 | 28.3 |
| %C29 αββS (218) | 25.6 | 25.0 |
| C30 αββS Sterane Index (218) | 0.0 | 0.0 |
| C30 S+R Sterane Index (218) | 0.0 | 0.0 |
| $C_{27}/C_{29}$ (αββS) (218) | 1.73 | 1.86 |
| $C_{28}/C_{29}$ (αββS) (218) | 1.18 | 1.13 |
| $C_{29}/C_{27}$ (αββS) (218) | 0.58 | 0.54 |
| | | |
| %C27 αααR (217) | 36.2 | 43.7 |
| %C28 αααR (217) | 32.0 | 24.0 |
| %C29 αααR (217) | 31.8 | 32.2 |
| S/R ($C_{29}$ ααα) (217) | 0.34 | 0.33 |
| S/(S+R) ($C_{29}$ ααα) (217) | 0.25 | 0.25 |
| ββ/(αα+ββ) ($C_{29}$) (217) | 0.44 | 0.40 |
| αββS/αααR ($C_{29}$) (217) | 0.36 | 0.34 |
| ($C_{21}$+$C_{22}$)/($C_{27}$+$C_{28}$+$C_{29}$) (217) | 0.69 | 0.77 |
| Diaster/ααα Ster ($C_{27}$) (217) | 1.70 | 1.78 |
| | | |
| **Terpenoids** | | |
| C19/C23 Tricyclic terpanes | 0.04 | 0.06 |
| C23/C24 Tricyclic terpanes | 1.79 | 1.80 |
| C26/C25 Tricyclic terpanes | 0.66 | 0.62 |
| | | |
| C24 Tetracyclic/C26 Tricyclics | 0.60 | 0.63 |
| C24 Tetracyclic/Hopane | 0.52 | 0.56 |
| | | |
| Ts/Tm trisnorhopanes | 0.87 | 0.82 |
| Ts/(Ts+Tm) trisnorhopanes | 0.47 | 0.45 |
| C29Ts/C29 Hopane | 0.23 | 0.22 |
| | | |
| Bisnorhopane/Hopane | 0.20 | 0.12 |
| Norhopane/Hopane | 0.98 | 0.93 |
| Diahopane/Hopane | 0.05 | 0.07 |
| Oleanane/Hopane | 0.12 | 0.08 |
| Gammacerane/Hopane | 0.09 | 0.09 |
| Moretane/(Moretane+Hopane) | 0.14 | 0.14 |
| H32 S/(S+R) Homohopanes | 0.59 | 0.55 |
| H35/H34 Homohopanes | | |
| | | |
| [Steranes]/[Hopanes] | 1.05 | 0.86 |
| [Tricyclic terpanes]/[Hopanes] | 2.37 | 2.77 |
| [Tricyclic terpanes]/[Steranes] | 2.26 | 3.21 |

*Appendix F3, ctd.*

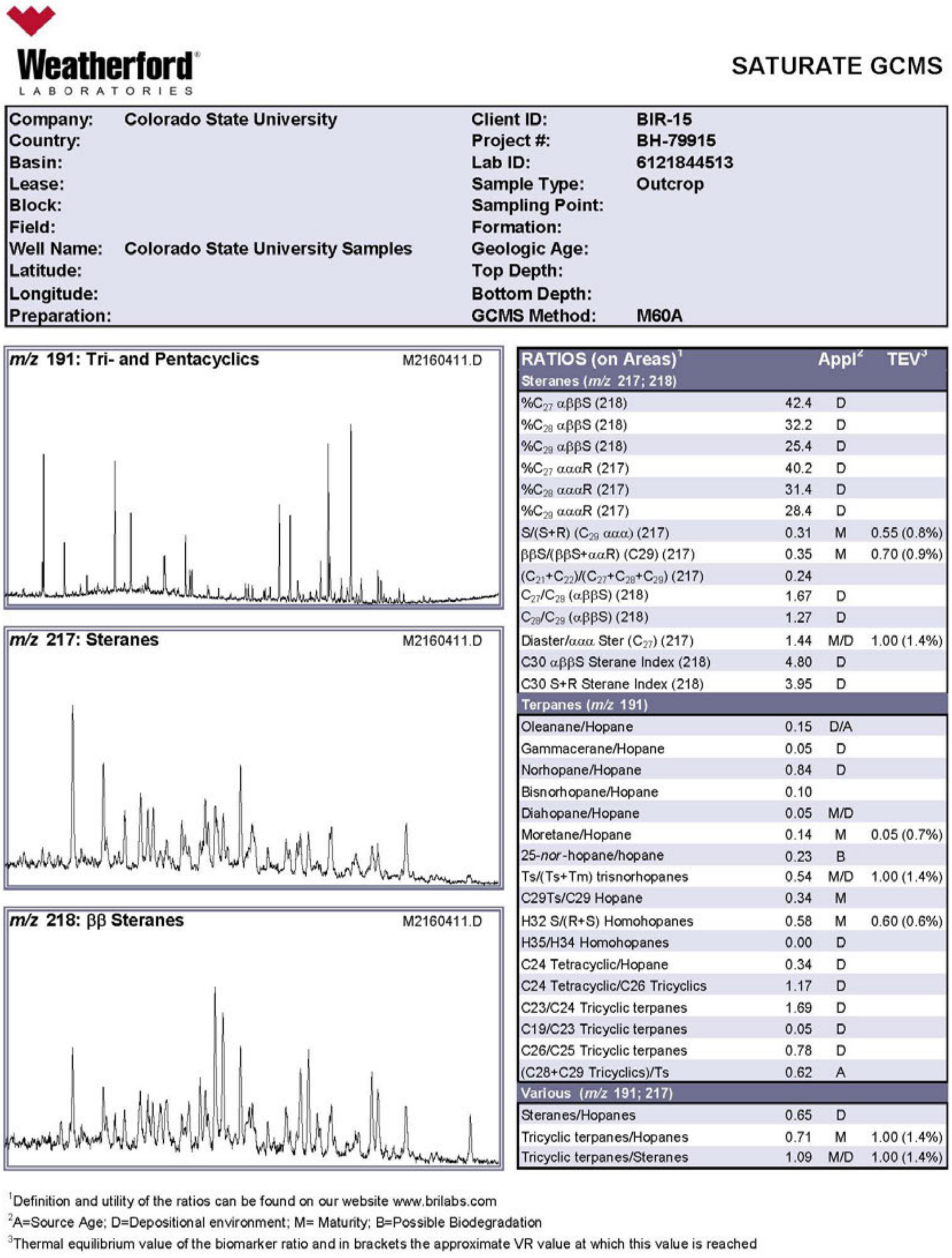

**Weatherford** LABORATORIES

**SATURATE GCMS**

| | | | |
|---|---|---|---|
| **Company:** | **Colorado State University** | **Client ID:** | **BIR-15** |
| **Country:** | | **Project #:** | **BH-79915** |
| **Basin:** | | **Lab ID:** | **6121844513** |
| **Lease:** | | **Sample Type:** | **Outcrop** |
| **Block:** | | **Sampling Point:** | |
| **Field:** | | **Formation:** | |
| **Well Name:** | **Colorado State University Samples** | **Geologic Age:** | |
| **Latitude:** | | **Top Depth:** | |
| **Longitude:** | | **Bottom Depth:** | |
| **Preparation:** | | **GCMS Method:** | **M60A** |

***m/z* 191: Tri- and Pentacyclics** M2160411.D

***m/z* 217: Steranes** M2160411.D

***m/z* 218: ββ Steranes** M2160411.D

| **RATIOS (on Areas)**[1] | | **Appl**[2] | **TEV**[3] |
|---|---|---|---|
| **Steranes (*m/z* 217; 218)** | | | |
| %$C_{27}$ αββS (218) | 42.4 | D | |
| %$C_{28}$ αββS (218) | 32.2 | D | |
| %$C_{29}$ αββS (218) | 25.4 | D | |
| %$C_{27}$ αααR (217) | 40.2 | D | |
| %$C_{28}$ αααR (217) | 31.4 | D | |
| %$C_{29}$ αααR (217) | 28.4 | D | |
| S/(S+R) ($C_{29}$ ααα) (217) | 0.31 | M | 0.55 (0.8%) |
| ββS/(ββS+ααR) (C29) (217) | 0.35 | M | 0.70 (0.9%) |
| ($C_{21}$+$C_{22}$)/($C_{27}$+$C_{28}$+$C_{29}$) (217) | 0.24 | | |
| $C_{27}$/$C_{28}$ (αββS) (218) | 1.67 | D | |
| $C_{28}$/$C_{29}$ (αββS) (218) | 1.27 | D | |
| Diaster/ααα Ster ($C_{27}$) (217) | 1.44 | M/D | 1.00 (1.4%) |
| C30 αββS Sterane Index (218) | 4.80 | D | |
| C30 S+R Sterane Index (218) | 3.95 | D | |
| **Terpanes (*m/z* 191)** | | | |
| Oleanane/Hopane | 0.15 | D/A | |
| Gammacerane/Hopane | 0.05 | D | |
| Norhopane/Hopane | 0.84 | D | |
| Bisnorhopane/Hopane | 0.10 | | |
| Diahopane/Hopane | 0.05 | M/D | |
| Moretane/Hopane | 0.14 | M | 0.05 (0.7%) |
| 25-*nor*-hopane/hopane | 0.23 | B | |
| Ts/(Ts+Tm) trisnorhopanes | 0.54 | M/D | 1.00 (1.4%) |
| C29Ts/C29 Hopane | 0.34 | M | |
| H32 S/(R+S) Homohopanes | 0.58 | M | 0.60 (0.6%) |
| H35/H34 Homohopanes | 0.00 | D | |
| C24 Tetracyclic/Hopane | 0.34 | D | |
| C24 Tetracyclic/C26 Tricyclics | 1.17 | D | |
| C23/C24 Tricyclic terpanes | 1.69 | D | |
| C19/C23 Tricyclic terpanes | 0.05 | D | |
| C26/C25 Tricyclic terpanes | 0.78 | D | |
| (C28+C29 Tricyclics)/Ts | 0.62 | A | |
| **Various (*m/z* 191; 217)** | | | |
| Steranes/Hopanes | 0.65 | D | |
| Tricyclic terpanes/Hopanes | 0.71 | M | 1.00 (1.4%) |
| Tricyclic terpanes/Steranes | 1.09 | M/D | 1.00 (1.4%) |

[1] Definition and utility of the ratios can be found on our website www.brilabs.com

[2] A=Source Age; D=Depositional environment; M= Maturity; B=Possible Biodegradation

[3] Thermal equilibrium value of the biomarker ratio and in brackets the approximate VR value at which this value is reached

*Appendix F3, ctd.*

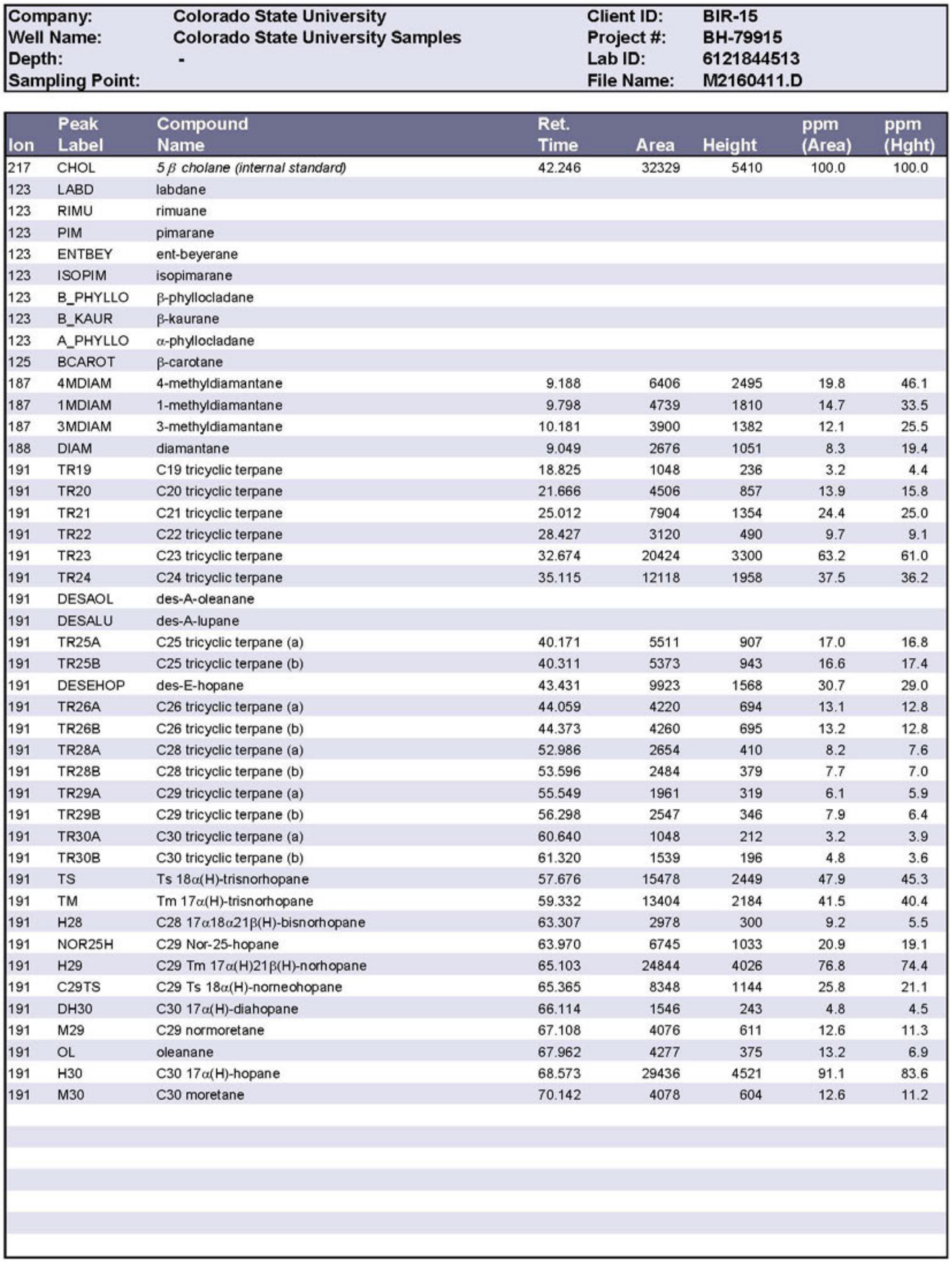

| | | | |
|---|---|---|---|
| **Company:** | **Colorado State University** | **Client ID:** | **BIR-15** |
| **Well Name:** | **Colorado State University Samples** | **Project #:** | **BH-79915** |
| **Depth:** | **-** | **Lab ID:** | **6121844513** |
| **Sampling Point:** | | **File Name:** | **M2160411.D** |

| Ion | Peak Label | Compound Name | Ret. Time | Area | Height | ppm (Area) | ppm (Hght) |
|---|---|---|---|---|---|---|---|
| 217 | CHOL | *5β cholane (internal standard)* | 42.246 | 32329 | 5410 | 100.0 | 100.0 |
| 123 | LABD | labdane | | | | | |
| 123 | RIMU | rimuane | | | | | |
| 123 | PIM | pimarane | | | | | |
| 123 | ENTBEY | ent-beyerane | | | | | |
| 123 | ISOPIM | isopimarane | | | | | |
| 123 | B_PHYLLO | β-phyllocladane | | | | | |
| 123 | B_KAUR | β-kaurane | | | | | |
| 123 | A_PHYLLO | α-phyllocladane | | | | | |
| 125 | BCAROT | β-carotane | | | | | |
| 187 | 4MDIAM | 4-methyldiamantane | 9.188 | 6406 | 2495 | 19.8 | 46.1 |
| 187 | 1MDIAM | 1-methyldiamantane | 9.798 | 4739 | 1810 | 14.7 | 33.5 |
| 187 | 3MDIAM | 3-methyldiamantane | 10.181 | 3900 | 1382 | 12.1 | 25.5 |
| 188 | DIAM | diamantane | 9.049 | 2676 | 1051 | 8.3 | 19.4 |
| 191 | TR19 | C19 tricyclic terpane | 18.825 | 1048 | 236 | 3.2 | 4.4 |
| 191 | TR20 | C20 tricyclic terpane | 21.666 | 4506 | 857 | 13.9 | 15.8 |
| 191 | TR21 | C21 tricyclic terpane | 25.012 | 7904 | 1354 | 24.4 | 25.0 |
| 191 | TR22 | C22 tricyclic terpane | 28.427 | 3120 | 490 | 9.7 | 9.1 |
| 191 | TR23 | C23 tricyclic terpane | 32.674 | 20424 | 3300 | 63.2 | 61.0 |
| 191 | TR24 | C24 tricyclic terpane | 35.115 | 12118 | 1958 | 37.5 | 36.2 |
| 191 | DESAOL | des-A-oleanane | | | | | |
| 191 | DESALU | des-A-lupane | | | | | |
| 191 | TR25A | C25 tricyclic terpane (a) | 40.171 | 5511 | 907 | 17.0 | 16.8 |
| 191 | TR25B | C25 tricyclic terpane (b) | 40.311 | 5373 | 943 | 16.6 | 17.4 |
| 191 | DESEHOP | des-E-hopane | 43.431 | 9923 | 1568 | 30.7 | 29.0 |
| 191 | TR26A | C26 tricyclic terpane (a) | 44.059 | 4220 | 694 | 13.1 | 12.8 |
| 191 | TR26B | C26 tricyclic terpane (b) | 44.373 | 4260 | 695 | 13.2 | 12.8 |
| 191 | TR28A | C28 tricyclic terpane (a) | 52.986 | 2654 | 410 | 8.2 | 7.6 |
| 191 | TR28B | C28 tricyclic terpane (b) | 53.596 | 2484 | 379 | 7.7 | 7.0 |
| 191 | TR29A | C29 tricyclic terpane (a) | 55.549 | 1961 | 319 | 6.1 | 5.9 |
| 191 | TR29B | C29 tricyclic terpane (b) | 56.298 | 2547 | 346 | 7.9 | 6.4 |
| 191 | TR30A | C30 tricyclic terpane (a) | 60.640 | 1048 | 212 | 3.2 | 3.9 |
| 191 | TR30B | C30 tricyclic terpane (b) | 61.320 | 1539 | 196 | 4.8 | 3.6 |
| 191 | TS | Ts 18α(H)-trisnorhopane | 57.676 | 15478 | 2449 | 47.9 | 45.3 |
| 191 | TM | Tm 17α(H)-trisnorhopane | 59.332 | 13404 | 2184 | 41.5 | 40.4 |
| 191 | H28 | C28 17α18α21β(H)-bisnorhopane | 63.307 | 2978 | 300 | 9.2 | 5.5 |
| 191 | NOR25H | C29 Nor-25-hopane | 63.970 | 6745 | 1033 | 20.9 | 19.1 |
| 191 | H29 | C29 Tm 17α(H)21β(H)-norhopane | 65.103 | 24844 | 4026 | 76.8 | 74.4 |
| 191 | C29TS | C29 Ts 18α(H)-norneohopane | 65.365 | 8348 | 1144 | 25.8 | 21.1 |
| 191 | DH30 | C30 17α(H)-diahopane | 66.114 | 1546 | 243 | 4.8 | 4.5 |
| 191 | M29 | C29 normoretane | 67.108 | 4076 | 611 | 12.6 | 11.3 |
| 191 | OL | oleanane | 67.962 | 4277 | 375 | 13.2 | 6.9 |
| 191 | H30 | C30 17α(H)-hopane | 68.573 | 29436 | 4521 | 91.1 | 83.6 |
| 191 | M30 | C30 moretane | 70.142 | 4078 | 604 | 12.6 | 11.2 |

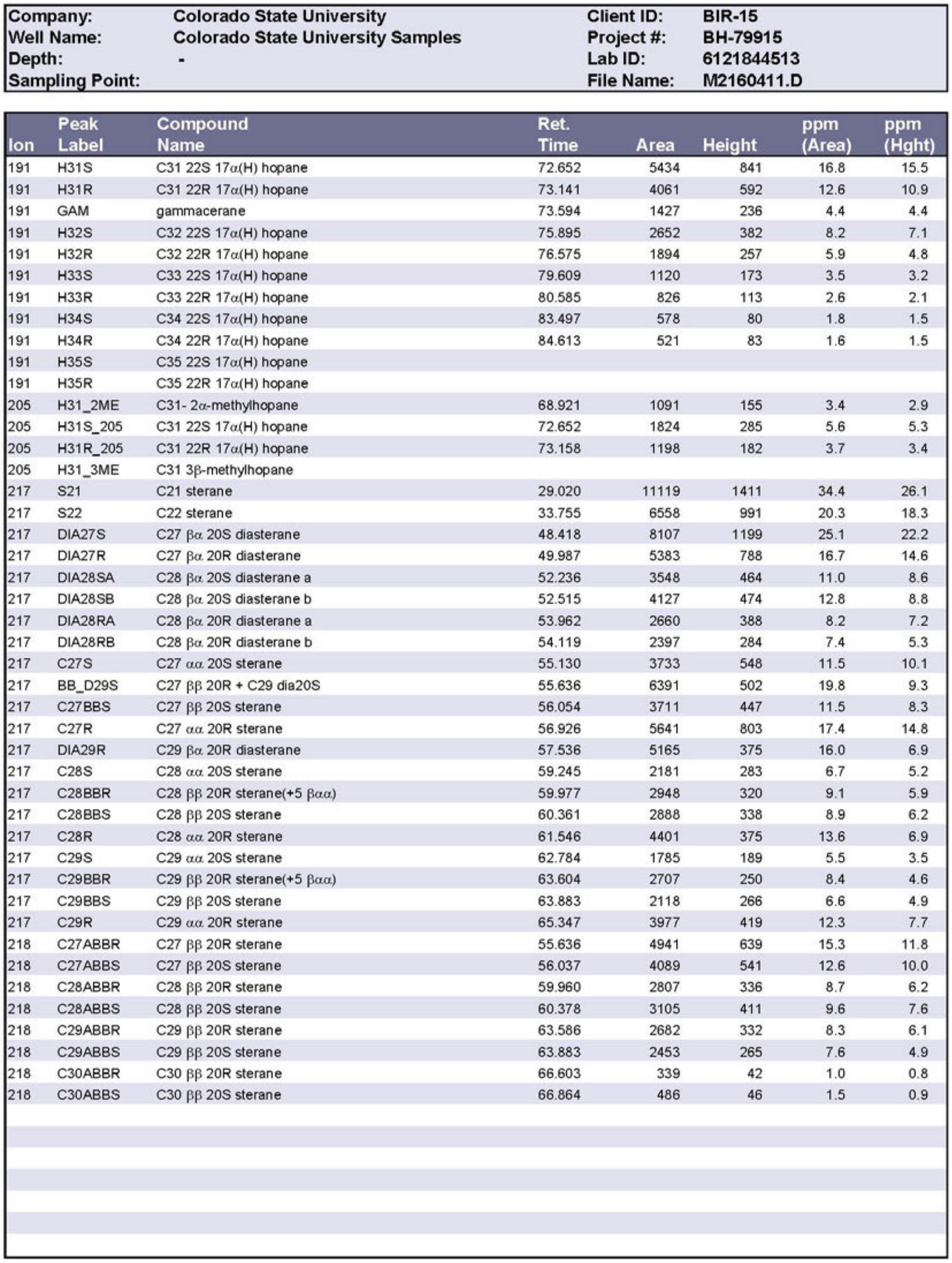

| | | | |
|---|---|---|---|
| **Company:** | **Colorado State University** | **Client ID:** | **BIR-15** |
| **Well Name:** | **Colorado State University Samples** | **Project #:** | **BH-79915** |
| **Depth:** | **-** | **Lab ID:** | **6121844513** |
| **Sampling Point:** | | **File Name:** | **M2160411.D** |

| Ion | Peak Label | Compound Name | Ret. Time | Area | Height | ppm (Area) | ppm (Hght) |
|---|---|---|---|---|---|---|---|
| 191 | H31S | C31 22S 17α(H) hopane | 72.652 | 5434 | 841 | 16.8 | 15.5 |
| 191 | H31R | C31 22R 17α(H) hopane | 73.141 | 4061 | 592 | 12.6 | 10.9 |
| 191 | GAM | gammacerane | 73.594 | 1427 | 236 | 4.4 | 4.4 |
| 191 | H32S | C32 22S 17α(H) hopane | 75.895 | 2652 | 382 | 8.2 | 7.1 |
| 191 | H32R | C32 22R 17α(H) hopane | 76.575 | 1894 | 257 | 5.9 | 4.8 |
| 191 | H33S | C33 22S 17α(H) hopane | 79.609 | 1120 | 173 | 3.5 | 3.2 |
| 191 | H33R | C33 22R 17α(H) hopane | 80.585 | 826 | 113 | 2.6 | 2.1 |
| 191 | H34S | C34 22S 17α(H) hopane | 83.497 | 578 | 80 | 1.8 | 1.5 |
| 191 | H34R | C34 22R 17α(H) hopane | 84.613 | 521 | 83 | 1.6 | 1.5 |
| 191 | H35S | C35 22S 17α(H) hopane | | | | | |
| 191 | H35R | C35 22R 17α(H) hopane | | | | | |
| 205 | H31_2ME | C31- 2α-methylhopane | 68.921 | 1091 | 155 | 3.4 | 2.9 |
| 205 | H31S_205 | C31 22S 17α(H) hopane | 72.652 | 1824 | 285 | 5.6 | 5.3 |
| 205 | H31R_205 | C31 22R 17α(H) hopane | 73.158 | 1198 | 182 | 3.7 | 3.4 |
| 205 | H31_3ME | C31 3β-methylhopane | | | | | |
| 217 | S21 | C21 sterane | 29.020 | 11119 | 1411 | 34.4 | 26.1 |
| 217 | S22 | C22 sterane | 33.755 | 6558 | 991 | 20.3 | 18.3 |
| 217 | DIA27S | C27 βα 20S diasterane | 48.418 | 8107 | 1199 | 25.1 | 22.2 |
| 217 | DIA27R | C27 βα 20R diasterane | 49.987 | 5383 | 788 | 16.7 | 14.6 |
| 217 | DIA28SA | C28 βα 20S diasterane a | 52.236 | 3548 | 464 | 11.0 | 8.6 |
| 217 | DIA28SB | C28 βα 20S diasterane b | 52.515 | 4127 | 474 | 12.8 | 8.8 |
| 217 | DIA28RA | C28 βα 20R diasterane a | 53.962 | 2660 | 388 | 8.2 | 7.2 |
| 217 | DIA28RB | C28 βα 20R diasterane b | 54.119 | 2397 | 284 | 7.4 | 5.3 |
| 217 | C27S | C27 αα 20S sterane | 55.130 | 3733 | 548 | 11.5 | 10.1 |
| 217 | BB_D29S | C27 ββ 20R + C29 dia20S | 55.636 | 6391 | 502 | 19.8 | 9.3 |
| 217 | C27BBS | C27 ββ 20S sterane | 56.054 | 3711 | 447 | 11.5 | 8.3 |
| 217 | C27R | C27 αα 20R sterane | 56.926 | 5641 | 803 | 17.4 | 14.8 |
| 217 | DIA29R | C29 βα 20R diasterane | 57.536 | 5165 | 375 | 16.0 | 6.9 |
| 217 | C28S | C28 αα 20S sterane | 59.245 | 2181 | 283 | 6.7 | 5.2 |
| 217 | C28BBR | C28 ββ 20R sterane(+5 βαα) | 59.977 | 2948 | 320 | 9.1 | 5.9 |
| 217 | C28BBS | C28 ββ 20S sterane | 60.361 | 2888 | 338 | 8.9 | 6.2 |
| 217 | C28R | C28 αα 20R sterane | 61.546 | 4401 | 375 | 13.6 | 6.9 |
| 217 | C29S | C29 αα 20S sterane | 62.784 | 1785 | 189 | 5.5 | 3.5 |
| 217 | C29BBR | C29 ββ 20R sterane(+5 βαα) | 63.604 | 2707 | 250 | 8.4 | 4.6 |
| 217 | C29BBS | C29 ββ 20S sterane | 63.883 | 2118 | 266 | 6.6 | 4.9 |
| 217 | C29R | C29 αα 20R sterane | 65.347 | 3977 | 419 | 12.3 | 7.7 |
| 218 | C27ABBR | C27 ββ 20R sterane | 55.636 | 4941 | 639 | 15.3 | 11.8 |
| 218 | C27ABBS | C27 ββ 20S sterane | 56.037 | 4089 | 541 | 12.6 | 10.0 |
| 218 | C28ABBR | C28 ββ 20R sterane | 59.960 | 2807 | 336 | 8.7 | 6.2 |
| 218 | C28ABBS | C28 ββ 20S sterane | 60.378 | 3105 | 411 | 9.6 | 7.6 |
| 218 | C29ABBR | C29 ββ 20R sterane | 63.586 | 2682 | 332 | 8.3 | 6.1 |
| 218 | C29ABBS | C29 ββ 20S sterane | 63.883 | 2453 | 265 | 7.6 | 4.9 |
| 218 | C30ABBR | C30 ββ 20R sterane | 66.603 | 339 | 42 | 1.0 | 0.8 |
| 218 | C30ABBS | C30 ββ 20S sterane | 66.864 | 486 | 46 | 1.5 | 0.9 |

*Appendix F3, ctd.*

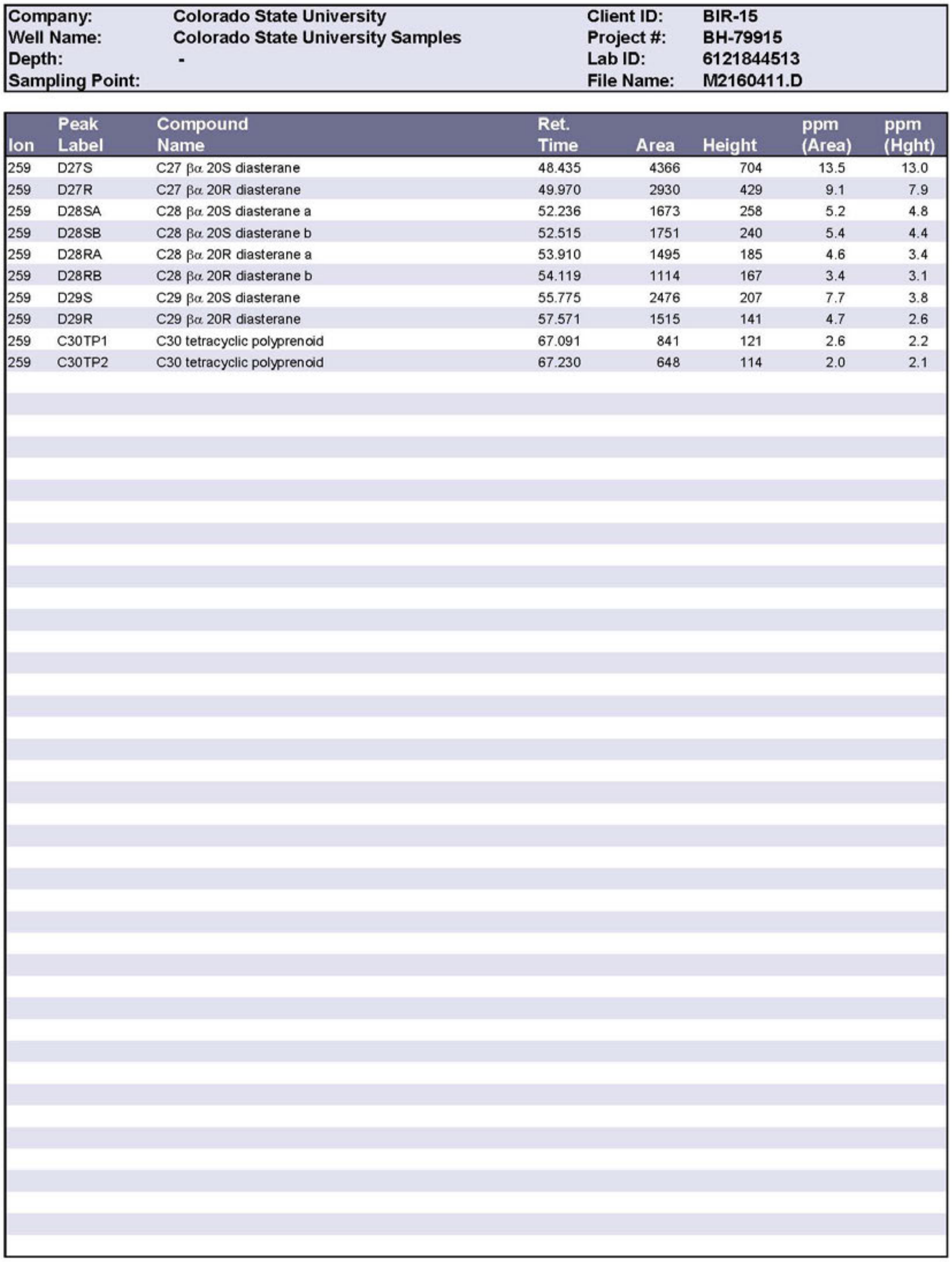

| | | | |
|---|---|---|---|
| **Company:** | **Colorado State University** | **Client ID:** | **BIR-15** |
| **Well Name:** | **Colorado State University Samples** | **Project #:** | **BH-79915** |
| **Depth:** | **-** | **Lab ID:** | **6121844513** |
| **Sampling Point:** | | **File Name:** | **M2160411.D** |

| Ion | Peak Label | Compound Name | Ret. Time | Area | Height | ppm (Area) | ppm (Hght) |
|---|---|---|---|---|---|---|---|
| 259 | D27S | C27 βα 20S diasterane | 48.435 | 4366 | 704 | 13.5 | 13.0 |
| 259 | D27R | C27 βα 20R diasterane | 49.970 | 2930 | 429 | 9.1 | 7.9 |
| 259 | D28SA | C28 βα 20S diasterane a | 52.236 | 1673 | 258 | 5.2 | 4.8 |
| 259 | D28SB | C28 βα 20S diasterane b | 52.515 | 1751 | 240 | 5.4 | 4.4 |
| 259 | D28RA | C28 βα 20R diasterane a | 53.910 | 1495 | 185 | 4.6 | 3.4 |
| 259 | D28RB | C28 βα 20R diasterane b | 54.119 | 1114 | 167 | 3.4 | 3.1 |
| 259 | D29S | C29 βα 20S diasterane | 55.775 | 2476 | 207 | 7.7 | 3.8 |
| 259 | D29R | C29 βα 20R diasterane | 57.571 | 1515 | 141 | 4.7 | 2.6 |
| 259 | C30TP1 | C30 tetracyclic polyprenoid | 67.091 | 841 | 121 | 2.6 | 2.2 |
| 259 | C30TP2 | C30 tetracyclic polyprenoid | 67.230 | 648 | 114 | 2.0 | 2.1 |

*Appendix F3, ctd.*

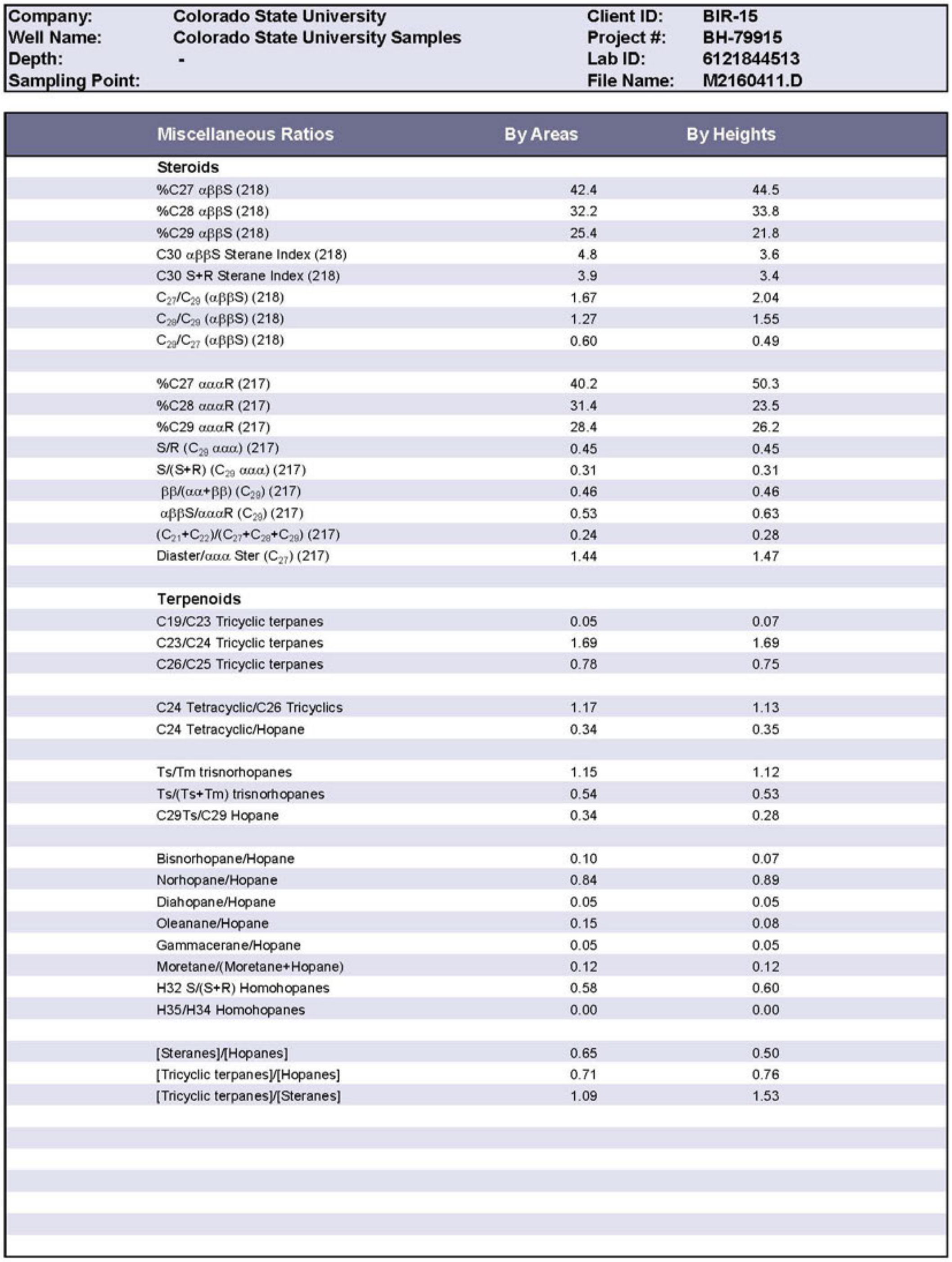

| | | | |
|---|---|---|---|
| **Company:** | **Colorado State University** | **Client ID:** | **BIR-15** |
| **Well Name:** | **Colorado State University Samples** | **Project #:** | **BH-79915** |
| **Depth:** | **-** | **Lab ID:** | **6121844513** |
| **Sampling Point:** | | **File Name:** | **M2160411.D** |

| Miscellaneous Ratios | By Areas | By Heights |
|---|---|---|
| **Steroids** | | |
| %C27 αββS (218) | 42.4 | 44.5 |
| %C28 αββS (218) | 32.2 | 33.8 |
| %C29 αββS (218) | 25.4 | 21.8 |
| C30 αββS Sterane Index (218) | 4.8 | 3.6 |
| C30 S+R Sterane Index (218) | 3.9 | 3.4 |
| $C_{27}$/$C_{29}$ (αββS) (218) | 1.67 | 2.04 |
| $C_{28}$/$C_{29}$ (αββS) (218) | 1.27 | 1.55 |
| $C_{29}$/$C_{27}$ (αββS) (218) | 0.60 | 0.49 |
| | | |
| %C27 αααR (217) | 40.2 | 50.3 |
| %C28 αααR (217) | 31.4 | 23.5 |
| %C29 αααR (217) | 28.4 | 26.2 |
| S/R ($C_{29}$ ααα) (217) | 0.45 | 0.45 |
| S/(S+R) ($C_{29}$ ααα) (217) | 0.31 | 0.31 |
| ββ/(αα+ββ) ($C_{29}$) (217) | 0.46 | 0.46 |
| αββS/αααR ($C_{29}$) (217) | 0.53 | 0.63 |
| ($C_{21}$+$C_{22}$)/($C_{27}$+$C_{28}$+$C_{29}$) (217) | 0.24 | 0.28 |
| Diaster/ααα Ster ($C_{27}$) (217) | 1.44 | 1.47 |
| | | |
| **Terpenoids** | | |
| C19/C23 Tricyclic terpanes | 0.05 | 0.07 |
| C23/C24 Tricyclic terpanes | 1.69 | 1.69 |
| C26/C25 Tricyclic terpanes | 0.78 | 0.75 |
| | | |
| C24 Tetracyclic/C26 Tricyclics | 1.17 | 1.13 |
| C24 Tetracyclic/Hopane | 0.34 | 0.35 |
| | | |
| Ts/Tm trisnorhopanes | 1.15 | 1.12 |
| Ts/(Ts+Tm) trisnorhopanes | 0.54 | 0.53 |
| C29Ts/C29 Hopane | 0.34 | 0.28 |
| | | |
| Bisnorhopane/Hopane | 0.10 | 0.07 |
| Norhopane/Hopane | 0.84 | 0.89 |
| Diahopane/Hopane | 0.05 | 0.05 |
| Oleanane/Hopane | 0.15 | 0.08 |
| Gammacerane/Hopane | 0.05 | 0.05 |
| Moretane/(Moretane+Hopane) | 0.12 | 0.12 |
| H32 S/(S+R) Homohopanes | 0.58 | 0.60 |
| H35/H34 Homohopanes | 0.00 | 0.00 |
| | | |
| [Steranes]/[Hopanes] | 0.65 | 0.50 |
| [Tricyclic terpanes]/[Hopanes] | 0.71 | 0.76 |
| [Tricyclic terpanes]/[Steranes] | 1.09 | 1.53 |

*Appendix F3, ctd.*

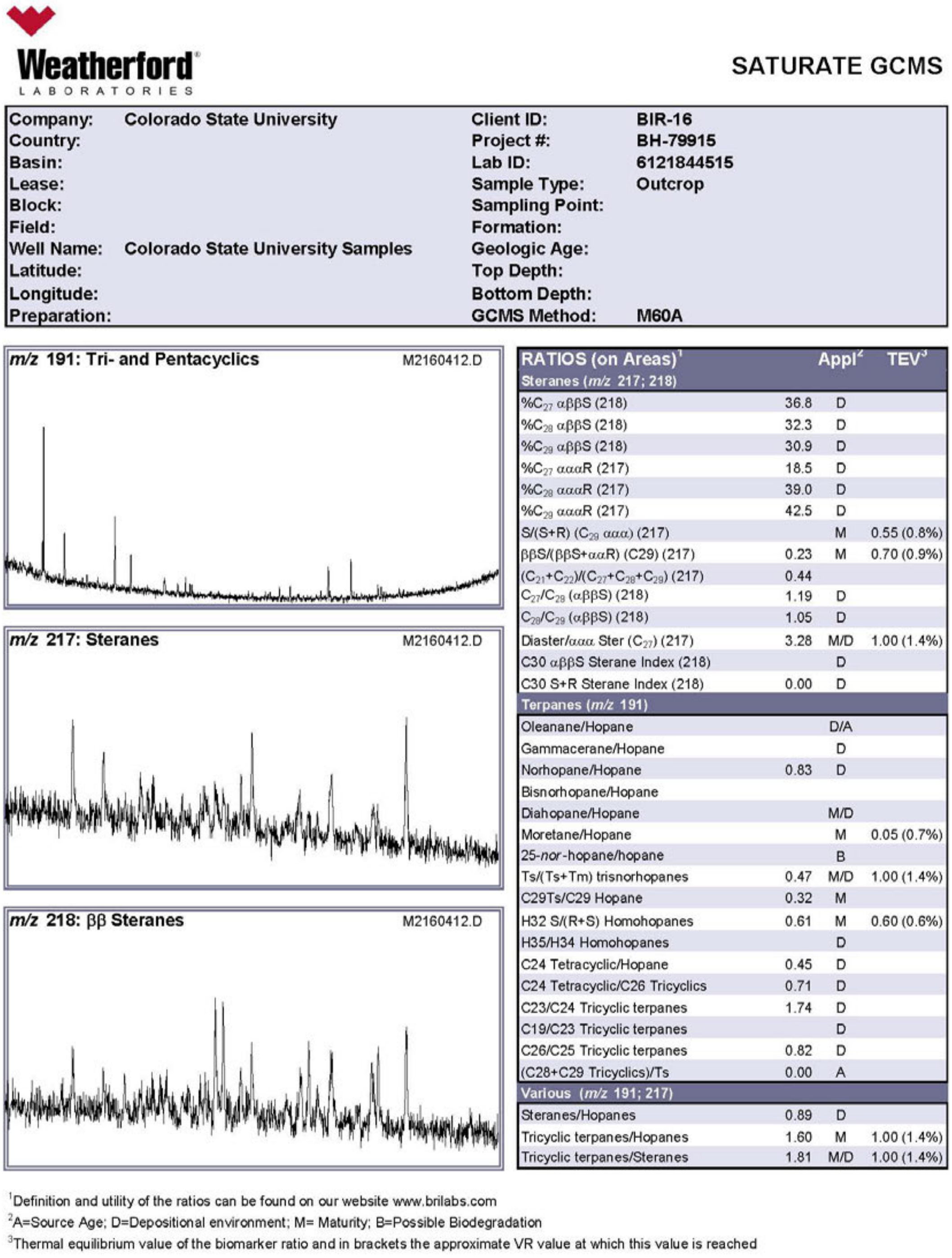

Weatherford LABORATORIES

**SATURATE GCMS**

| | | | |
|---|---|---|---|
| **Company:** | **Colorado State University** | **Client ID:** | **BIR-16** |
| **Country:** | | **Project #:** | **BH-79915** |
| **Basin:** | | **Lab ID:** | **6121844515** |
| **Lease:** | | **Sample Type:** | **Outcrop** |
| **Block:** | | **Sampling Point:** | |
| **Field:** | | **Formation:** | |
| **Well Name:** | **Colorado State University Samples** | **Geologic Age:** | |
| **Latitude:** | | **Top Depth:** | |
| **Longitude:** | | **Bottom Depth:** | |
| **Preparation:** | | **GCMS Method:** | **M60A** |

***m/z* 191: Tri- and Pentacyclics** M2160412.D

***m/z* 217: Steranes** M2160412.D

***m/z* 218: ββ Steranes** M2160412.D

| RATIOS (on Areas)[1] | | Appl[2] | TEV[3] |
|---|---|---|---|
| **Steranes (*m/z* 217; 218)** | | | |
| %$C_{27}$ αββS (218) | 36.8 | D | |
| %$C_{28}$ αββS (218) | 32.3 | D | |
| %$C_{29}$ αββS (218) | 30.9 | D | |
| %$C_{27}$ αααR (217) | 18.5 | D | |
| %$C_{28}$ αααR (217) | 39.0 | D | |
| %$C_{29}$ αααR (217) | 42.5 | D | |
| S/(S+R) ($C_{29}$ ααα) (217) | | M | 0.55 (0.8%) |
| ββS/(ββS+ααR) (C29) (217) | 0.23 | M | 0.70 (0.9%) |
| ($C_{21}$+$C_{22}$)/($C_{27}$+$C_{28}$+$C_{29}$) (217) | 0.44 | | |
| $C_{27}$/$C_{29}$ (αββS) (218) | 1.19 | D | |
| $C_{28}$/$C_{29}$ (αββS) (218) | 1.05 | D | |
| Diaster/ααα Ster ($C_{27}$) (217) | 3.28 | M/D | 1.00 (1.4%) |
| C30 αββS Sterane Index (218) | | D | |
| C30 S+R Sterane Index (218) | 0.00 | D | |
| **Terpanes (*m/z* 191)** | | | |
| Oleanane/Hopane | | D/A | |
| Gammacerane/Hopane | | D | |
| Norhopane/Hopane | 0.83 | D | |
| Bisnorhopane/Hopane | | | |
| Diahopane/Hopane | | M/D | |
| Moretane/Hopane | | M | 0.05 (0.7%) |
| 25-*nor*-hopane/hopane | | B | |
| Ts/(Ts+Tm) trisnorhopanes | 0.47 | M/D | 1.00 (1.4%) |
| C29Ts/C29 Hopane | 0.32 | M | |
| H32 S/(R+S) Homohopanes | 0.61 | M | 0.60 (0.6%) |
| H35/H34 Homohopanes | | D | |
| C24 Tetracyclic/Hopane | 0.45 | D | |
| C24 Tetracyclic/C26 Tricyclics | 0.71 | D | |
| C23/C24 Tricyclic terpanes | 1.74 | D | |
| C19/C23 Tricyclic terpanes | | D | |
| C26/C25 Tricyclic terpanes | 0.82 | D | |
| (C28+C29 Tricyclics)/Ts | 0.00 | A | |
| **Various (*m/z* 191; 217)** | | | |
| Steranes/Hopanes | 0.89 | D | |
| Tricyclic terpanes/Hopanes | 1.60 | M | 1.00 (1.4%) |
| Tricyclic terpanes/Steranes | 1.81 | M/D | 1.00 (1.4%) |

[1] Definition and utility of the ratios can be found on our website www.brilabs.com

[2] A=Source Age; D=Depositional environment; M= Maturity; B=Possible Biodegradation

[3] Thermal equilibrium value of the biomarker ratio and in brackets the approximate VR value at which this value is reached

*Appendix F3, ctd.*

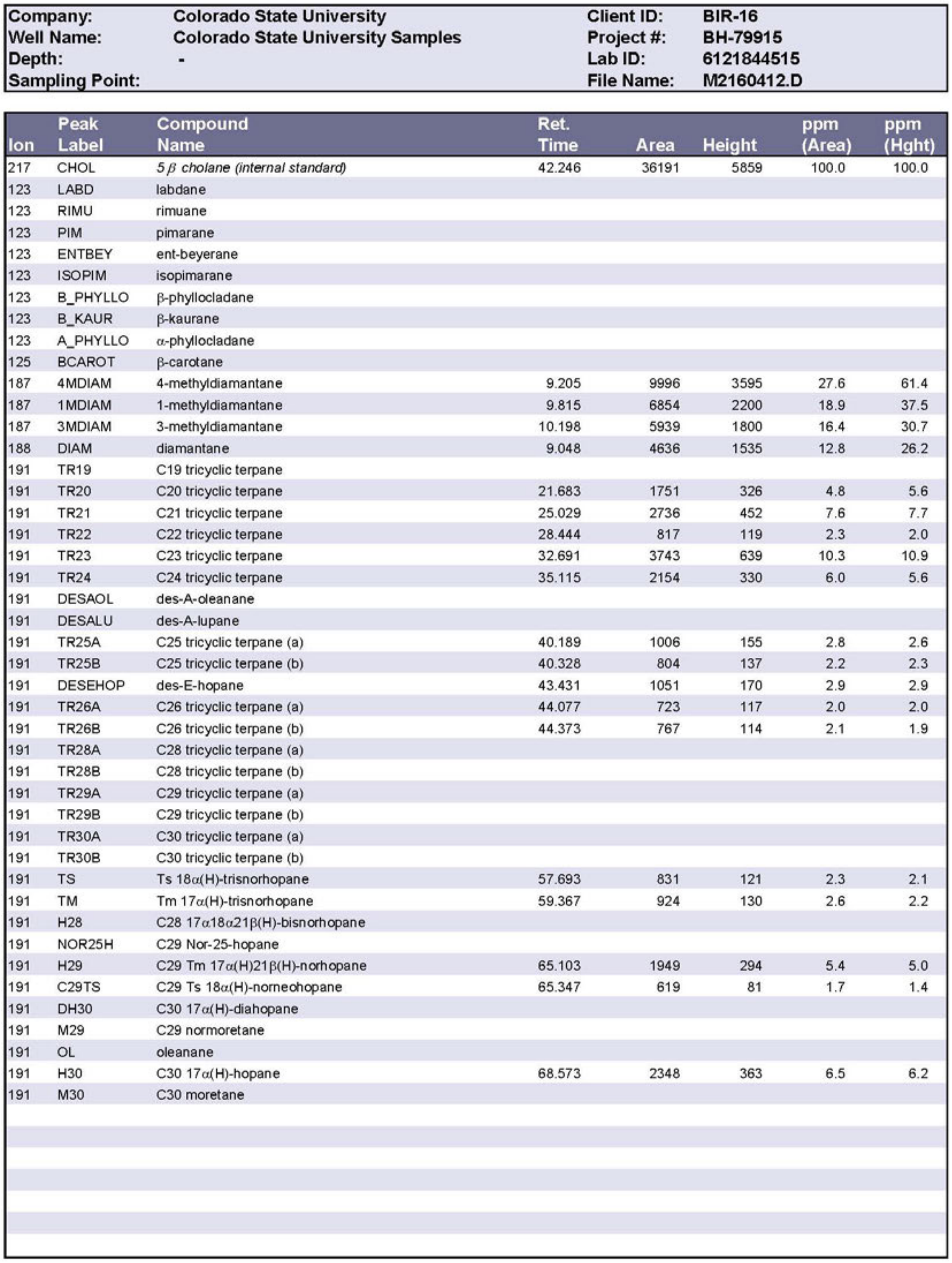

| | | | |
|---|---|---|---|
| **Company:** | **Colorado State University** | **Client ID:** | **BIR-16** |
| **Well Name:** | **Colorado State University Samples** | **Project #:** | **BH-79915** |
| **Depth:** | **-** | **Lab ID:** | **6121844515** |
| **Sampling Point:** | | **File Name:** | **M2160412.D** |

| Ion | Peak Label | Compound Name | Ret. Time | Area | Height | ppm (Area) | ppm (Hght) |
|---|---|---|---|---|---|---|---|
| 217 | CHOL | *5β cholane (internal standard)* | 42.246 | 36191 | 5859 | 100.0 | 100.0 |
| 123 | LABD | labdane | | | | | |
| 123 | RIMU | rimuane | | | | | |
| 123 | PIM | pimarane | | | | | |
| 123 | ENTBEY | ent-beyerane | | | | | |
| 123 | ISOPIM | isopimarane | | | | | |
| 123 | B_PHYLLO | β-phyllocladane | | | | | |
| 123 | B_KAUR | β-kaurane | | | | | |
| 123 | A_PHYLLO | α-phyllocladane | | | | | |
| 125 | BCAROT | β-carotane | | | | | |
| 187 | 4MDIAM | 4-methyldiamantane | 9.205 | 9996 | 3595 | 27.6 | 61.4 |
| 187 | 1MDIAM | 1-methyldiamantane | 9.815 | 6854 | 2200 | 18.9 | 37.5 |
| 187 | 3MDIAM | 3-methyldiamantane | 10.198 | 5939 | 1800 | 16.4 | 30.7 |
| 188 | DIAM | diamantane | 9.048 | 4636 | 1535 | 12.8 | 26.2 |
| 191 | TR19 | C19 tricyclic terpane | | | | | |
| 191 | TR20 | C20 tricyclic terpane | 21.683 | 1751 | 326 | 4.8 | 5.6 |
| 191 | TR21 | C21 tricyclic terpane | 25.029 | 2736 | 452 | 7.6 | 7.7 |
| 191 | TR22 | C22 tricyclic terpane | 28.444 | 817 | 119 | 2.3 | 2.0 |
| 191 | TR23 | C23 tricyclic terpane | 32.691 | 3743 | 639 | 10.3 | 10.9 |
| 191 | TR24 | C24 tricyclic terpane | 35.115 | 2154 | 330 | 6.0 | 5.6 |
| 191 | DESAOL | des-A-oleanane | | | | | |
| 191 | DESALU | des-A-lupane | | | | | |
| 191 | TR25A | C25 tricyclic terpane (a) | 40.189 | 1006 | 155 | 2.8 | 2.6 |
| 191 | TR25B | C25 tricyclic terpane (b) | 40.328 | 804 | 137 | 2.2 | 2.3 |
| 191 | DESEHOP | des-E-hopane | 43.431 | 1051 | 170 | 2.9 | 2.9 |
| 191 | TR26A | C26 tricyclic terpane (a) | 44.077 | 723 | 117 | 2.0 | 2.0 |
| 191 | TR26B | C26 tricyclic terpane (b) | 44.373 | 767 | 114 | 2.1 | 1.9 |
| 191 | TR28A | C28 tricyclic terpane (a) | | | | | |
| 191 | TR28B | C28 tricyclic terpane (b) | | | | | |
| 191 | TR29A | C29 tricyclic terpane (a) | | | | | |
| 191 | TR29B | C29 tricyclic terpane (b) | | | | | |
| 191 | TR30A | C30 tricyclic terpane (a) | | | | | |
| 191 | TR30B | C30 tricyclic terpane (b) | | | | | |
| 191 | TS | Ts 18α(H)-trisnorhopane | 57.693 | 831 | 121 | 2.3 | 2.1 |
| 191 | TM | Tm 17α(H)-trisnorhopane | 59.367 | 924 | 130 | 2.6 | 2.2 |
| 191 | H28 | C28 17α18α21β(H)-bisnorhopane | | | | | |
| 191 | NOR25H | C29 Nor-25-hopane | | | | | |
| 191 | H29 | C29 Tm 17α(H)21β(H)-norhopane | 65.103 | 1949 | 294 | 5.4 | 5.0 |
| 191 | C29TS | C29 Ts 18α(H)-norneohopane | 65.347 | 619 | 81 | 1.7 | 1.4 |
| 191 | DH30 | C30 17α(H)-diahopane | | | | | |
| 191 | M29 | C29 normoretane | | | | | |
| 191 | OL | oleanane | | | | | |
| 191 | H30 | C30 17α(H)-hopane | 68.573 | 2348 | 363 | 6.5 | 6.2 |
| 191 | M30 | C30 moretane | | | | | |

*Appendix F3, ctd.*

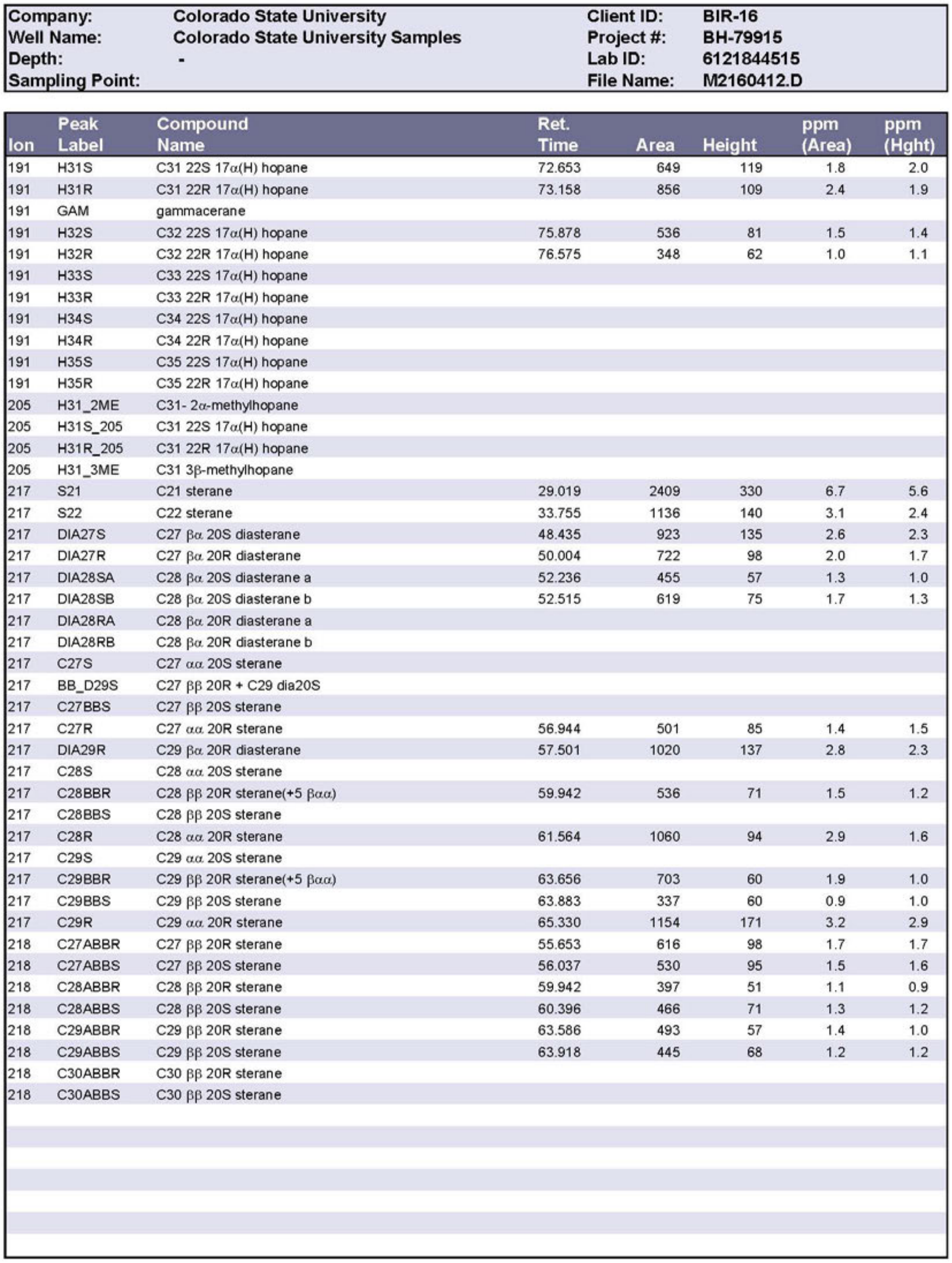

| | | | |
|---|---|---|---|
| **Company:** | **Colorado State University** | **Client ID:** | **BIR-16** |
| **Well Name:** | **Colorado State University Samples** | **Project #:** | **BH-79915** |
| **Depth:** | **-** | **Lab ID:** | **6121844515** |
| **Sampling Point:** | | **File Name:** | **M2160412.D** |

| Ion | Peak Label | Compound Name | Ret. Time | Area | Height | ppm (Area) | ppm (Hght) |
|---|---|---|---|---|---|---|---|
| 191 | H31S | C31 22S 17α(H) hopane | 72.653 | 649 | 119 | 1.8 | 2.0 |
| 191 | H31R | C31 22R 17α(H) hopane | 73.158 | 856 | 109 | 2.4 | 1.9 |
| 191 | GAM | gammacerane | | | | | |
| 191 | H32S | C32 22S 17α(H) hopane | 75.878 | 536 | 81 | 1.5 | 1.4 |
| 191 | H32R | C32 22R 17α(H) hopane | 76.575 | 348 | 62 | 1.0 | 1.1 |
| 191 | H33S | C33 22S 17α(H) hopane | | | | | |
| 191 | H33R | C33 22R 17α(H) hopane | | | | | |
| 191 | H34S | C34 22S 17α(H) hopane | | | | | |
| 191 | H34R | C34 22R 17α(H) hopane | | | | | |
| 191 | H35S | C35 22S 17α(H) hopane | | | | | |
| 191 | H35R | C35 22R 17α(H) hopane | | | | | |
| 205 | H31_2ME | C31- 2α-methylhopane | | | | | |
| 205 | H31S_205 | C31 22S 17α(H) hopane | | | | | |
| 205 | H31R_205 | C31 22R 17α(H) hopane | | | | | |
| 205 | H31_3ME | C31 3β-methylhopane | | | | | |
| 217 | S21 | C21 sterane | 29.019 | 2409 | 330 | 6.7 | 5.6 |
| 217 | S22 | C22 sterane | 33.755 | 1136 | 140 | 3.1 | 2.4 |
| 217 | DIA27S | C27 βα 20S diasterane | 48.435 | 923 | 135 | 2.6 | 2.3 |
| 217 | DIA27R | C27 βα 20R diasterane | 50.004 | 722 | 98 | 2.0 | 1.7 |
| 217 | DIA28SA | C28 βα 20S diasterane a | 52.236 | 455 | 57 | 1.3 | 1.0 |
| 217 | DIA28SB | C28 βα 20S diasterane b | 52.515 | 619 | 75 | 1.7 | 1.3 |
| 217 | DIA28RA | C28 βα 20R diasterane a | | | | | |
| 217 | DIA28RB | C28 βα 20R diasterane b | | | | | |
| 217 | C27S | C27 αα 20S sterane | | | | | |
| 217 | BB_D29S | C27 ββ 20R + C29 dia20S | | | | | |
| 217 | C27BBS | C27 ββ 20S sterane | | | | | |
| 217 | C27R | C27 αα 20R sterane | 56.944 | 501 | 85 | 1.4 | 1.5 |
| 217 | DIA29R | C29 βα 20R diasterane | 57.501 | 1020 | 137 | 2.8 | 2.3 |
| 217 | C28S | C28 αα 20S sterane | | | | | |
| 217 | C28BBR | C28 ββ 20R sterane(+5 βαα) | 59.942 | 536 | 71 | 1.5 | 1.2 |
| 217 | C28BBS | C28 ββ 20S sterane | | | | | |
| 217 | C28R | C28 αα 20R sterane | 61.564 | 1060 | 94 | 2.9 | 1.6 |
| 217 | C29S | C29 αα 20S sterane | | | | | |
| 217 | C29BBR | C29 ββ 20R sterane(+5 βαα) | 63.656 | 703 | 60 | 1.9 | 1.0 |
| 217 | C29BBS | C29 ββ 20S sterane | 63.883 | 337 | 60 | 0.9 | 1.0 |
| 217 | C29R | C29 αα 20R sterane | 65.330 | 1154 | 171 | 3.2 | 2.9 |
| 218 | C27ABBR | C27 ββ 20R sterane | 55.653 | 616 | 98 | 1.7 | 1.7 |
| 218 | C27ABBS | C27 ββ 20S sterane | 56.037 | 530 | 95 | 1.5 | 1.6 |
| 218 | C28ABBR | C28 ββ 20R sterane | 59.942 | 397 | 51 | 1.1 | 0.9 |
| 218 | C28ABBS | C28 ββ 20S sterane | 60.396 | 466 | 71 | 1.3 | 1.2 |
| 218 | C29ABBR | C29 ββ 20R sterane | 63.586 | 493 | 57 | 1.4 | 1.0 |
| 218 | C29ABBS | C29 ββ 20S sterane | 63.918 | 445 | 68 | 1.2 | 1.2 |
| 218 | C30ABBR | C30 ββ 20R sterane | | | | | |
| 218 | C30ABBS | C30 ββ 20S sterane | | | | | |

*Appendix F3, ctd.*

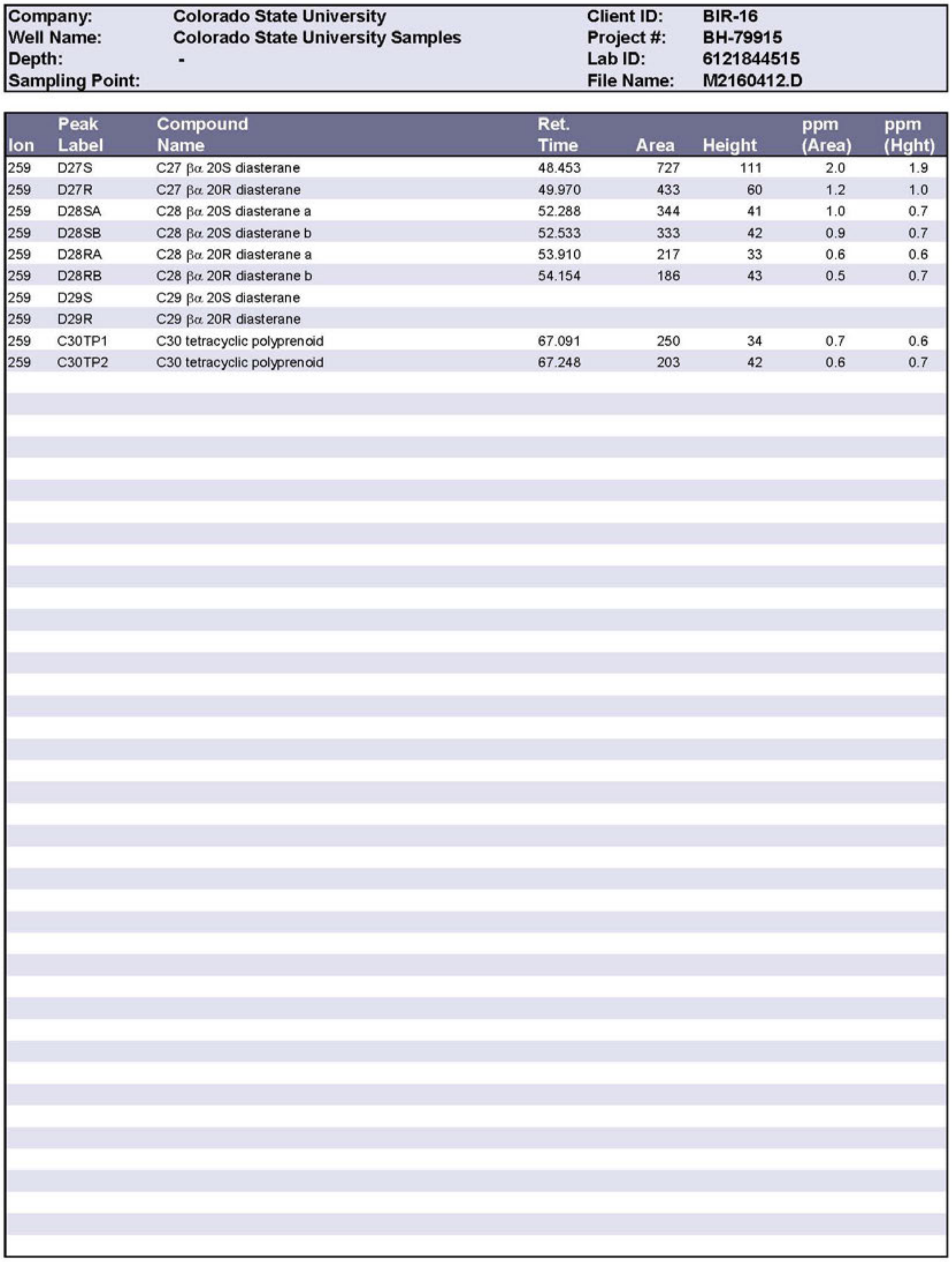

| | | | |
|---|---|---|---|
| **Company:** | **Colorado State University** | **Client ID:** | **BIR-16** |
| **Well Name:** | **Colorado State University Samples** | **Project #:** | **BH-79915** |
| **Depth:** | **-** | **Lab ID:** | **6121844515** |
| **Sampling Point:** | | **File Name:** | **M2160412.D** |

| Ion | Peak Label | Compound Name | Ret. Time | Area | Height | ppm (Area) | ppm (Hght) |
|---|---|---|---|---|---|---|---|
| 259 | D27S | C27 βα 20S diasterane | 48.453 | 727 | 111 | 2.0 | 1.9 |
| 259 | D27R | C27 βα 20R diasterane | 49.970 | 433 | 60 | 1.2 | 1.0 |
| 259 | D28SA | C28 βα 20S diasterane a | 52.288 | 344 | 41 | 1.0 | 0.7 |
| 259 | D28SB | C28 βα 20S diasterane b | 52.533 | 333 | 42 | 0.9 | 0.7 |
| 259 | D28RA | C28 βα 20R diasterane a | 53.910 | 217 | 33 | 0.6 | 0.6 |
| 259 | D28RB | C28 βα 20R diasterane b | 54.154 | 186 | 43 | 0.5 | 0.7 |
| 259 | D29S | C29 βα 20S diasterane | | | | | |
| 259 | D29R | C29 βα 20R diasterane | | | | | |
| 259 | C30TP1 | C30 tetracyclic polyprenoid | 67.091 | 250 | 34 | 0.7 | 0.6 |
| 259 | C30TP2 | C30 tetracyclic polyprenoid | 67.248 | 203 | 42 | 0.6 | 0.7 |

*Appendix F3, ctd.*

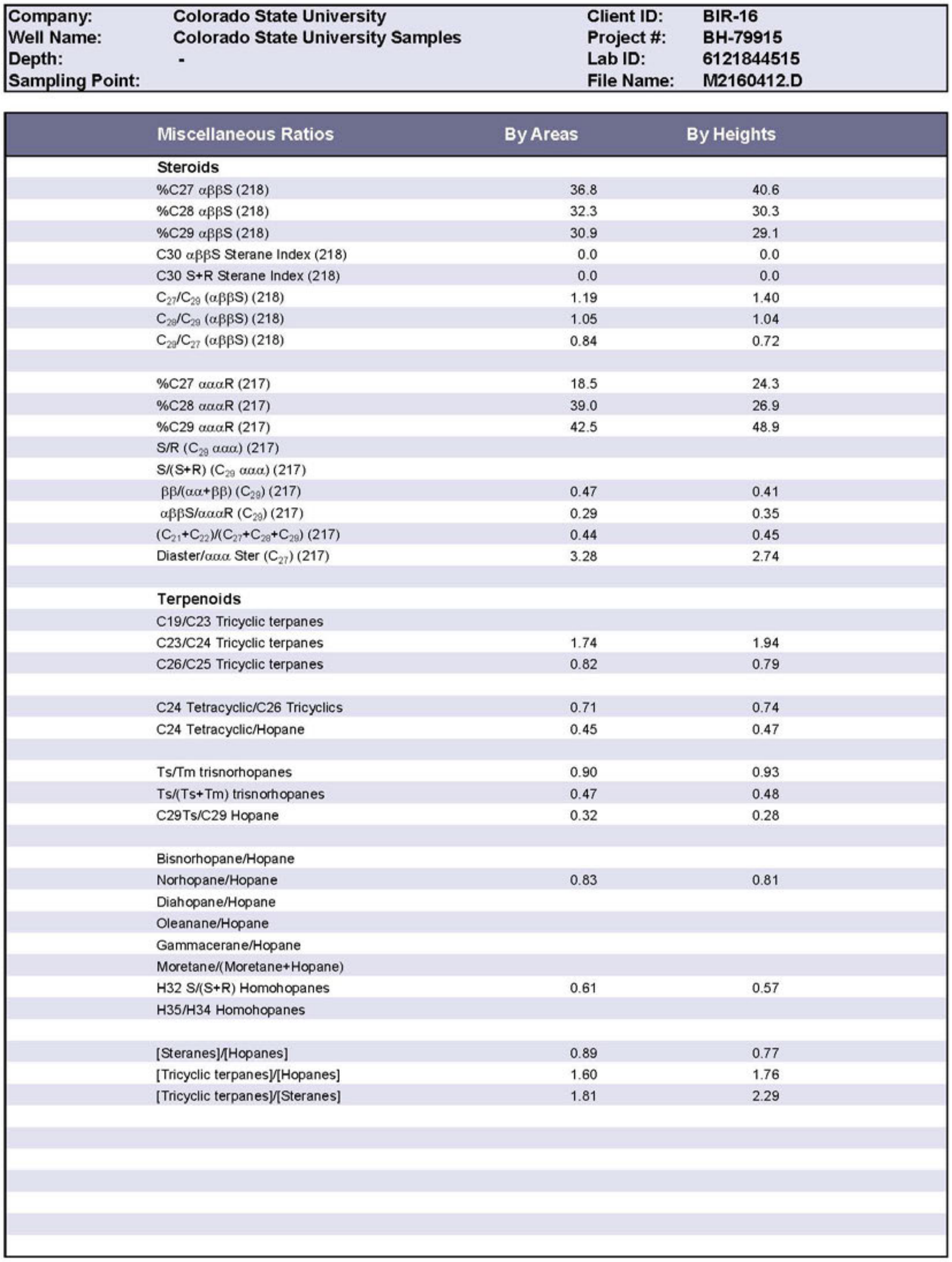

| | | | |
|---|---|---|---|
| **Company:** | **Colorado State University** | **Client ID:** | **BIR-16** |
| **Well Name:** | **Colorado State University Samples** | **Project #:** | **BH-79915** |
| **Depth:** | **-** | **Lab ID:** | **6121844515** |
| **Sampling Point:** | | **File Name:** | **M2160412.D** |

| Miscellaneous Ratios | By Areas | By Heights |
|---|---|---|
| **Steroids** | | |
| %C27 αββS (218) | 36.8 | 40.6 |
| %C28 αββS (218) | 32.3 | 30.3 |
| %C29 αββS (218) | 30.9 | 29.1 |
| C30 αββS Sterane Index (218) | 0.0 | 0.0 |
| C30 S+R Sterane Index (218) | 0.0 | 0.0 |
| $C_{27}/C_{29}$ (αββS) (218) | 1.19 | 1.40 |
| $C_{28}/C_{29}$ (αββS) (218) | 1.05 | 1.04 |
| $C_{29}/C_{27}$ (αββS) (218) | 0.84 | 0.72 |
| %C27 αααR (217) | 18.5 | 24.3 |
| %C28 αααR (217) | 39.0 | 26.9 |
| %C29 αααR (217) | 42.5 | 48.9 |
| S/R ($C_{29}$ ααα) (217) | | |
| S/(S+R) ($C_{29}$ ααα) (217) | | |
| ββ/(αα+ββ) ($C_{29}$) (217) | 0.47 | 0.41 |
| αββS/αααR ($C_{29}$) (217) | 0.29 | 0.35 |
| ($C_{21}+C_{22}$)/($C_{27}+C_{28}+C_{29}$) (217) | 0.44 | 0.45 |
| Diaster/ααα Ster ($C_{27}$) (217) | 3.28 | 2.74 |
| **Terpenoids** | | |
| C19/C23 Tricyclic terpanes | | |
| C23/C24 Tricyclic terpanes | 1.74 | 1.94 |
| C26/C25 Tricyclic terpanes | 0.82 | 0.79 |
| C24 Tetracyclic/C26 Tricyclics | 0.71 | 0.74 |
| C24 Tetracyclic/Hopane | 0.45 | 0.47 |
| Ts/Tm trisnorhopanes | 0.90 | 0.93 |
| Ts/(Ts+Tm) trisnorhopanes | 0.47 | 0.48 |
| C29Ts/C29 Hopane | 0.32 | 0.28 |
| Bisnorhopane/Hopane | | |
| Norhopane/Hopane | 0.83 | 0.81 |
| Diahopane/Hopane | | |
| Oleanane/Hopane | | |
| Gammacerane/Hopane | | |
| Moretane/(Moretane+Hopane) | | |
| H32 S/(S+R) Homohopanes | 0.61 | 0.57 |
| H35/H34 Homohopanes | | |
| [Steranes]/[Hopanes] | 0.89 | 0.77 |
| [Tricyclic terpanes]/[Hopanes] | 1.60 | 1.76 |
| [Tricyclic terpanes]/[Steranes] | 1.81 | 2.29 |

*Appendix F3, ctd.*

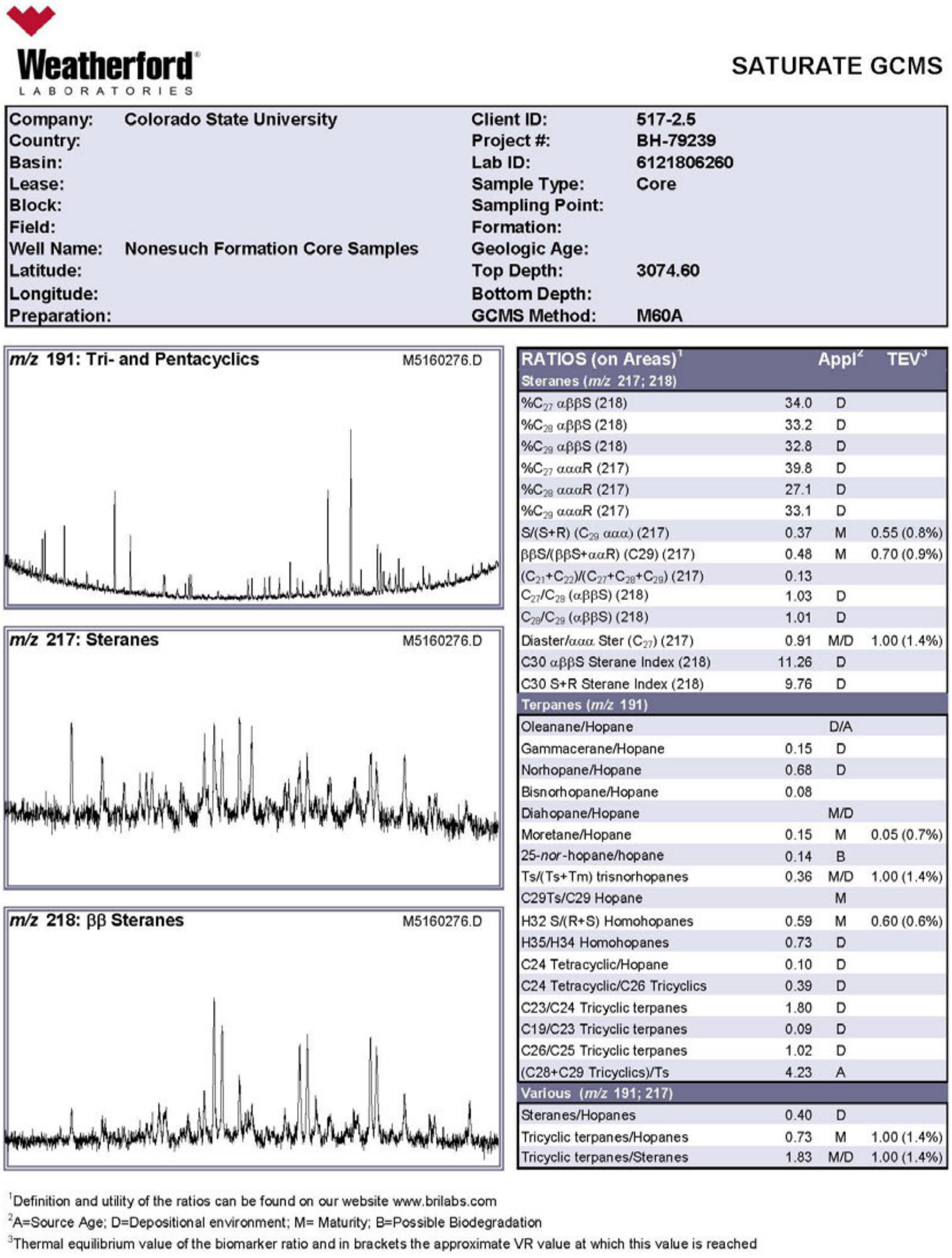

Weatherford LABORATORIES

## SATURATE GCMS

| | | | |
|---|---|---|---|
| **Company:** | **Colorado State University** | **Client ID:** | **517-2.5** |
| **Country:** | | **Project #:** | **BH-79239** |
| **Basin:** | | **Lab ID:** | **6121806260** |
| **Lease:** | | **Sample Type:** | **Core** |
| **Block:** | | **Sampling Point:** | |
| **Field:** | | **Formation:** | |
| **Well Name:** | **Nonesuch Formation Core Samples** | **Geologic Age:** | |
| **Latitude:** | | **Top Depth:** | **3074.60** |
| **Longitude:** | | **Bottom Depth:** | |
| **Preparation:** | | **GCMS Method:** | **M60A** |

***m/z* 191: Tri- and Pentacyclics** M5160276.D

***m/z* 217: Steranes** M5160276.D

***m/z* 218: ββ Steranes** M5160276.D

| RATIOS (on Areas)[1] | | Appl[2] | TEV[3] |
|---|---|---|---|
| Steranes (*m/z* 217; 218) | | | |
| %$C_{27}$ αββS (218) | 34.0 | D | |
| %$C_{28}$ αββS (218) | 33.2 | D | |
| %$C_{29}$ αββS (218) | 32.8 | D | |
| %$C_{27}$ αααR (217) | 39.8 | D | |
| %$C_{28}$ αααR (217) | 27.1 | D | |
| %$C_{29}$ αααR (217) | 33.1 | D | |
| S/(S+R) ($C_{29}$ ααα) (217) | 0.37 | M | 0.55 (0.8%) |
| ββS/(ββS+ααR) (C29) (217) | 0.48 | M | 0.70 (0.9%) |
| ($C_{21}$+$C_{22}$)/($C_{27}$+$C_{28}$+$C_{29}$) (217) | 0.13 | | |
| $C_{27}$/$C_{29}$ (αββS) (218) | 1.03 | D | |
| $C_{28}$/$C_{29}$ (αββS) (218) | 1.01 | D | |
| Diaster/ααα Ster ($C_{27}$) (217) | 0.91 | M/D | 1.00 (1.4%) |
| C30 αββS Sterane Index (218) | 11.26 | D | |
| C30 S+R Sterane Index (218) | 9.76 | D | |
| Terpanes (*m/z* 191) | | | |
| Oleanane/Hopane | | D/A | |
| Gammacerane/Hopane | 0.15 | D | |
| Norhopane/Hopane | 0.68 | D | |
| Bisnorhopane/Hopane | 0.08 | | |
| Diahopane/Hopane | | M/D | |
| Moretane/Hopane | 0.15 | M | 0.05 (0.7%) |
| 25-*nor*-hopane/hopane | 0.14 | B | |
| Ts/(Ts+Tm) trisnorhopanes | 0.36 | M/D | 1.00 (1.4%) |
| C29Ts/C29 Hopane | | M | |
| H32 S/(R+S) Homohopanes | 0.59 | M | 0.60 (0.6%) |
| H35/H34 Homohopanes | 0.73 | D | |
| C24 Tetracyclic/Hopane | 0.10 | D | |
| C24 Tetracyclic/C26 Tricyclics | 0.39 | D | |
| C23/C24 Tricyclic terpanes | 1.80 | D | |
| C19/C23 Tricyclic terpanes | 0.09 | D | |
| C26/C25 Tricyclic terpanes | 1.02 | D | |
| (C28+C29 Tricyclics)/Ts | 4.23 | A | |
| Various (*m/z* 191; 217) | | | |
| Steranes/Hopanes | 0.40 | D | |
| Tricyclic terpanes/Hopanes | 0.73 | M | 1.00 (1.4%) |
| Tricyclic terpanes/Steranes | 1.83 | M/D | 1.00 (1.4%) |

[1] Definition and utility of the ratios can be found on our website www.brilabs.com

[2] A=Source Age; D=Depositional environment; M= Maturity; B=Possible Biodegradation

[3] Thermal equilibrium value of the biomarker ratio and in brackets the approximate VR value at which this value is reached

*Appendix F3, ctd.*

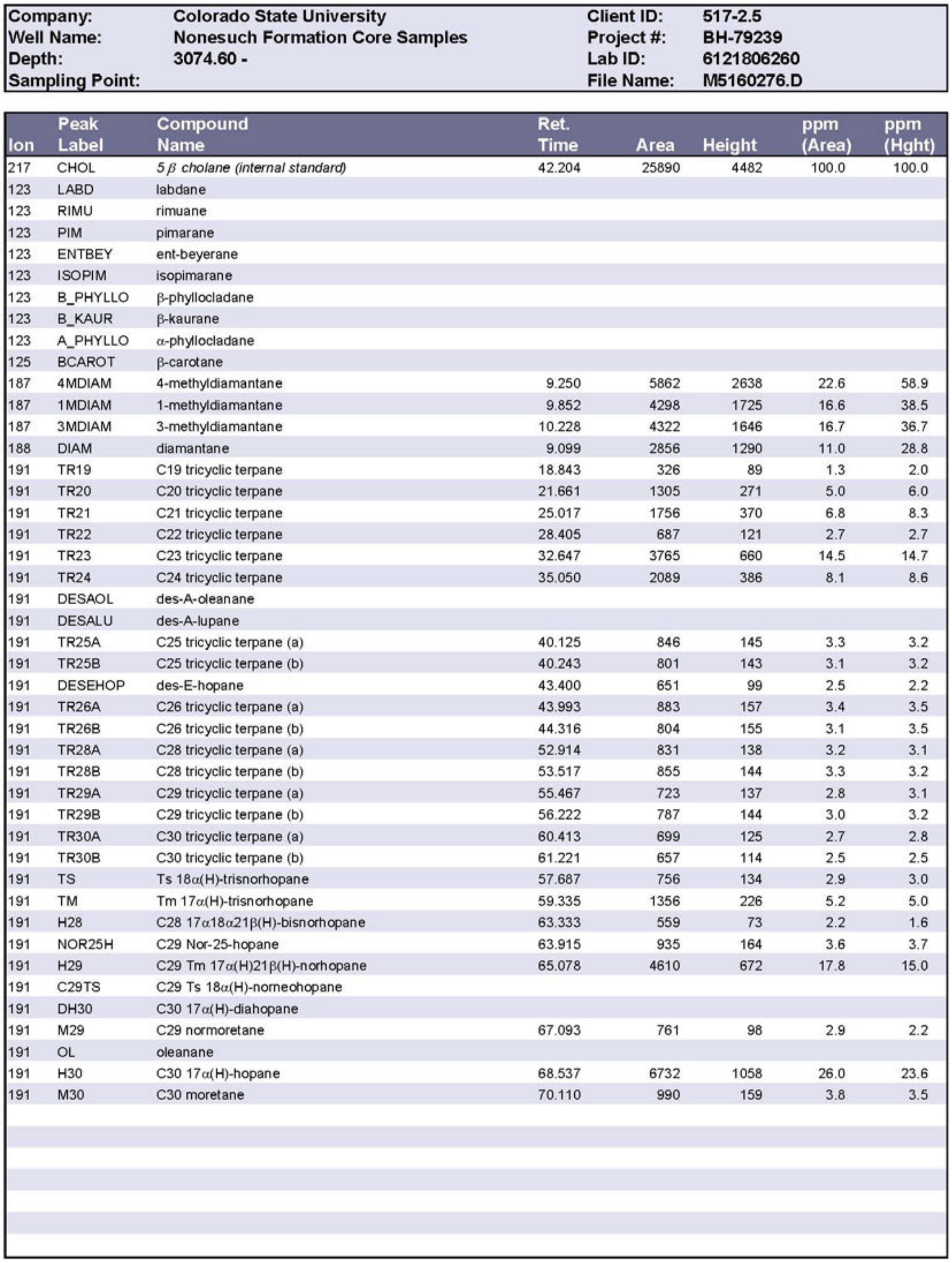

| | | | |
|---|---|---|---|
| **Company:** | **Colorado State University** | **Client ID:** | **517-2.5** |
| **Well Name:** | **Nonesuch Formation Core Samples** | **Project #:** | **BH-79239** |
| **Depth:** | **3074.60 -** | **Lab ID:** | **6121806260** |
| **Sampling Point:** | | **File Name:** | **M5160276.D** |

| Ion | Peak Label | Compound Name | Ret. Time | Area | Height | ppm (Area) | ppm (Hght) |
|---|---|---|---|---|---|---|---|
| 217 | CHOL | *5 β cholane (internal standard)* | 42.204 | 25890 | 4482 | 100.0 | 100.0 |
| 123 | LABD | labdane | | | | | |
| 123 | RIMU | rimuane | | | | | |
| 123 | PIM | pimarane | | | | | |
| 123 | ENTBEY | ent-beyerane | | | | | |
| 123 | ISOPIM | isopimarane | | | | | |
| 123 | B_PHYLLO | β-phyllocladane | | | | | |
| 123 | B_KAUR | β-kaurane | | | | | |
| 123 | A_PHYLLO | α-phyllocladane | | | | | |
| 125 | BCAROT | β-carotane | | | | | |
| 187 | 4MDIAM | 4-methyldiamantane | 9.250 | 5862 | 2638 | 22.6 | 58.9 |
| 187 | 1MDIAM | 1-methyldiamantane | 9.852 | 4298 | 1725 | 16.6 | 38.5 |
| 187 | 3MDIAM | 3-methyldiamantane | 10.228 | 4322 | 1646 | 16.7 | 36.7 |
| 188 | DIAM | diamantane | 9.099 | 2856 | 1290 | 11.0 | 28.8 |
| 191 | TR19 | C19 tricyclic terpane | 18.843 | 326 | 89 | 1.3 | 2.0 |
| 191 | TR20 | C20 tricyclic terpane | 21.661 | 1305 | 271 | 5.0 | 6.0 |
| 191 | TR21 | C21 tricyclic terpane | 25.017 | 1756 | 370 | 6.8 | 8.3 |
| 191 | TR22 | C22 tricyclic terpane | 28.405 | 687 | 121 | 2.7 | 2.7 |
| 191 | TR23 | C23 tricyclic terpane | 32.647 | 3765 | 660 | 14.5 | 14.7 |
| 191 | TR24 | C24 tricyclic terpane | 35.050 | 2089 | 386 | 8.1 | 8.6 |
| 191 | DESAOL | des-A-oleanane | | | | | |
| 191 | DESALU | des-A-lupane | | | | | |
| 191 | TR25A | C25 tricyclic terpane (a) | 40.125 | 846 | 145 | 3.3 | 3.2 |
| 191 | TR25B | C25 tricyclic terpane (b) | 40.243 | 801 | 143 | 3.1 | 3.2 |
| 191 | DESEHOP | des-E-hopane | 43.400 | 651 | 99 | 2.5 | 2.2 |
| 191 | TR26A | C26 tricyclic terpane (a) | 43.993 | 883 | 157 | 3.4 | 3.5 |
| 191 | TR26B | C26 tricyclic terpane (b) | 44.316 | 804 | 155 | 3.1 | 3.5 |
| 191 | TR28A | C28 tricyclic terpane (a) | 52.914 | 831 | 138 | 3.2 | 3.1 |
| 191 | TR28B | C28 tricyclic terpane (b) | 53.517 | 855 | 144 | 3.3 | 3.2 |
| 191 | TR29A | C29 tricyclic terpane (a) | 55.467 | 723 | 137 | 2.8 | 3.1 |
| 191 | TR29B | C29 tricyclic terpane (b) | 56.222 | 787 | 144 | 3.0 | 3.2 |
| 191 | TR30A | C30 tricyclic terpane (a) | 60.413 | 699 | 125 | 2.7 | 2.8 |
| 191 | TR30B | C30 tricyclic terpane (b) | 61.221 | 657 | 114 | 2.5 | 2.5 |
| 191 | TS | Ts 18α(H)-trisnorhopane | 57.687 | 756 | 134 | 2.9 | 3.0 |
| 191 | TM | Tm 17α(H)-trisnorhopane | 59.335 | 1356 | 226 | 5.2 | 5.0 |
| 191 | H28 | C28 17α18α21β(H)-bisnorhopane | 63.333 | 559 | 73 | 2.2 | 1.6 |
| 191 | NOR25H | C29 Nor-25-hopane | 63.915 | 935 | 164 | 3.6 | 3.7 |
| 191 | H29 | C29 Tm 17α(H)21β(H)-norhopane | 65.078 | 4610 | 672 | 17.8 | 15.0 |
| 191 | C29TS | C29 Ts 18α(H)-norneohopane | | | | | |
| 191 | DH30 | C30 17α(H)-diahopane | | | | | |
| 191 | M29 | C29 normoretane | 67.093 | 761 | 98 | 2.9 | 2.2 |
| 191 | OL | oleanane | | | | | |
| 191 | H30 | C30 17α(H)-hopane | 68.537 | 6732 | 1058 | 26.0 | 23.6 |
| 191 | M30 | C30 moretane | 70.110 | 990 | 159 | 3.8 | 3.5 |

*Appendix F3, ctd.*

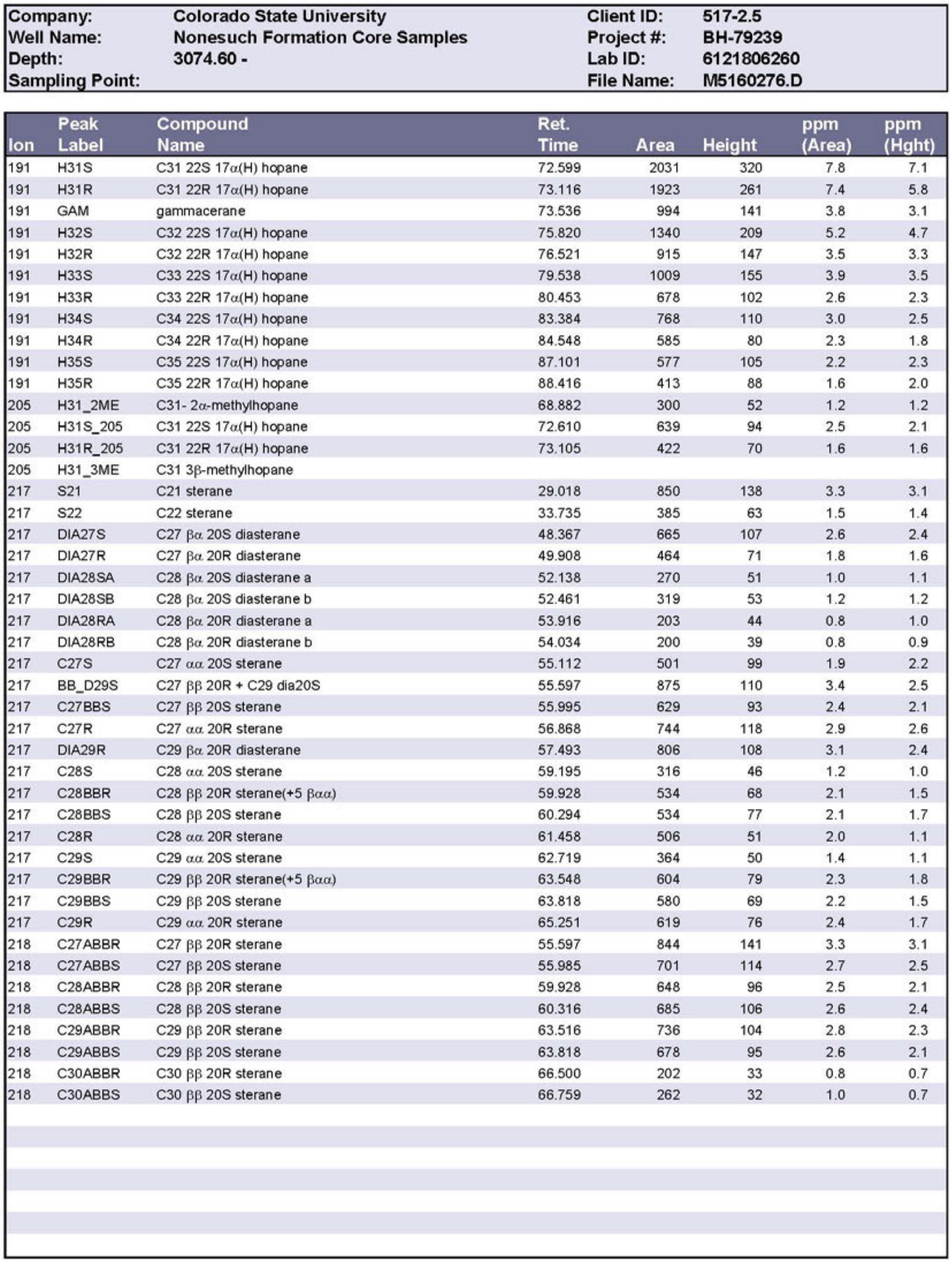

| | | | |
|---|---|---|---|
| **Company:** | **Colorado State University** | **Client ID:** | **517-2.5** |
| **Well Name:** | **Nonesuch Formation Core Samples** | **Project #:** | **BH-79239** |
| **Depth:** | **3074.60 -** | **Lab ID:** | **6121806260** |
| **Sampling Point:** | | **File Name:** | **M5160276.D** |

| Ion | Peak Label | Compound Name | Ret. Time | Area | Height | ppm (Area) | ppm (Hght) |
|---|---|---|---|---|---|---|---|
| 191 | H31S | C31 22S 17α(H) hopane | 72.599 | 2031 | 320 | 7.8 | 7.1 |
| 191 | H31R | C31 22R 17α(H) hopane | 73.116 | 1923 | 261 | 7.4 | 5.8 |
| 191 | GAM | gammacerane | 73.536 | 994 | 141 | 3.8 | 3.1 |
| 191 | H32S | C32 22S 17α(H) hopane | 75.820 | 1340 | 209 | 5.2 | 4.7 |
| 191 | H32R | C32 22R 17α(H) hopane | 76.521 | 915 | 147 | 3.5 | 3.3 |
| 191 | H33S | C33 22S 17α(H) hopane | 79.538 | 1009 | 155 | 3.9 | 3.5 |
| 191 | H33R | C33 22R 17α(H) hopane | 80.453 | 678 | 102 | 2.6 | 2.3 |
| 191 | H34S | C34 22S 17α(H) hopane | 83.384 | 768 | 110 | 3.0 | 2.5 |
| 191 | H34R | C34 22R 17α(H) hopane | 84.548 | 585 | 80 | 2.3 | 1.8 |
| 191 | H35S | C35 22S 17α(H) hopane | 87.101 | 577 | 105 | 2.2 | 2.3 |
| 191 | H35R | C35 22R 17α(H) hopane | 88.416 | 413 | 88 | 1.6 | 2.0 |
| 205 | H31_2ME | C31- 2α-methylhopane | 68.882 | 300 | 52 | 1.2 | 1.2 |
| 205 | H31S_205 | C31 22S 17α(H) hopane | 72.610 | 639 | 94 | 2.5 | 2.1 |
| 205 | H31R_205 | C31 22R 17α(H) hopane | 73.105 | 422 | 70 | 1.6 | 1.6 |
| 205 | H31_3ME | C31 3β-methylhopane | | | | | |
| 217 | S21 | C21 sterane | 29.018 | 850 | 138 | 3.3 | 3.1 |
| 217 | S22 | C22 sterane | 33.735 | 385 | 63 | 1.5 | 1.4 |
| 217 | DIA27S | C27 βα 20S diasterane | 48.367 | 665 | 107 | 2.6 | 2.4 |
| 217 | DIA27R | C27 βα 20R diasterane | 49.908 | 464 | 71 | 1.8 | 1.6 |
| 217 | DIA28SA | C28 βα 20S diasterane a | 52.138 | 270 | 51 | 1.0 | 1.1 |
| 217 | DIA28SB | C28 βα 20S diasterane b | 52.461 | 319 | 53 | 1.2 | 1.2 |
| 217 | DIA28RA | C28 βα 20R diasterane a | 53.916 | 203 | 44 | 0.8 | 1.0 |
| 217 | DIA28RB | C28 βα 20R diasterane b | 54.034 | 200 | 39 | 0.8 | 0.9 |
| 217 | C27S | C27 αα 20S sterane | 55.112 | 501 | 99 | 1.9 | 2.2 |
| 217 | BB_D29S | C27 ββ 20R + C29 dia20S | 55.597 | 875 | 110 | 3.4 | 2.5 |
| 217 | C27BBS | C27 ββ 20S sterane | 55.995 | 629 | 93 | 2.4 | 2.1 |
| 217 | C27R | C27 αα 20R sterane | 56.868 | 744 | 118 | 2.9 | 2.6 |
| 217 | DIA29R | C29 βα 20R diasterane | 57.493 | 806 | 108 | 3.1 | 2.4 |
| 217 | C28S | C28 αα 20S sterane | 59.195 | 316 | 46 | 1.2 | 1.0 |
| 217 | C28BBR | C28 ββ 20R sterane(+5 βαα) | 59.928 | 534 | 68 | 2.1 | 1.5 |
| 217 | C28BBS | C28 ββ 20S sterane | 60.294 | 534 | 77 | 2.1 | 1.7 |
| 217 | C28R | C28 αα 20R sterane | 61.458 | 506 | 51 | 2.0 | 1.1 |
| 217 | C29S | C29 αα 20S sterane | 62.719 | 364 | 50 | 1.4 | 1.1 |
| 217 | C29BBR | C29 ββ 20R sterane(+5 βαα) | 63.548 | 604 | 79 | 2.3 | 1.8 |
| 217 | C29BBS | C29 ββ 20S sterane | 63.818 | 580 | 69 | 2.2 | 1.5 |
| 217 | C29R | C29 αα 20R sterane | 65.251 | 619 | 76 | 2.4 | 1.7 |
| 218 | C27ABBR | C27 ββ 20R sterane | 55.597 | 844 | 141 | 3.3 | 3.1 |
| 218 | C27ABBS | C27 ββ 20S sterane | 55.985 | 701 | 114 | 2.7 | 2.5 |
| 218 | C28ABBR | C28 ββ 20R sterane | 59.928 | 648 | 96 | 2.5 | 2.1 |
| 218 | C28ABBS | C28 ββ 20S sterane | 60.316 | 685 | 106 | 2.6 | 2.4 |
| 218 | C29ABBR | C29 ββ 20R sterane | 63.516 | 736 | 104 | 2.8 | 2.3 |
| 218 | C29ABBS | C29 ββ 20S sterane | 63.818 | 678 | 95 | 2.6 | 2.1 |
| 218 | C30ABBR | C30 ββ 20R sterane | 66.500 | 202 | 33 | 0.8 | 0.7 |
| 218 | C30ABBS | C30 ββ 20S sterane | 66.759 | 262 | 32 | 1.0 | 0.7 |

*Appendix F3, ctd.*

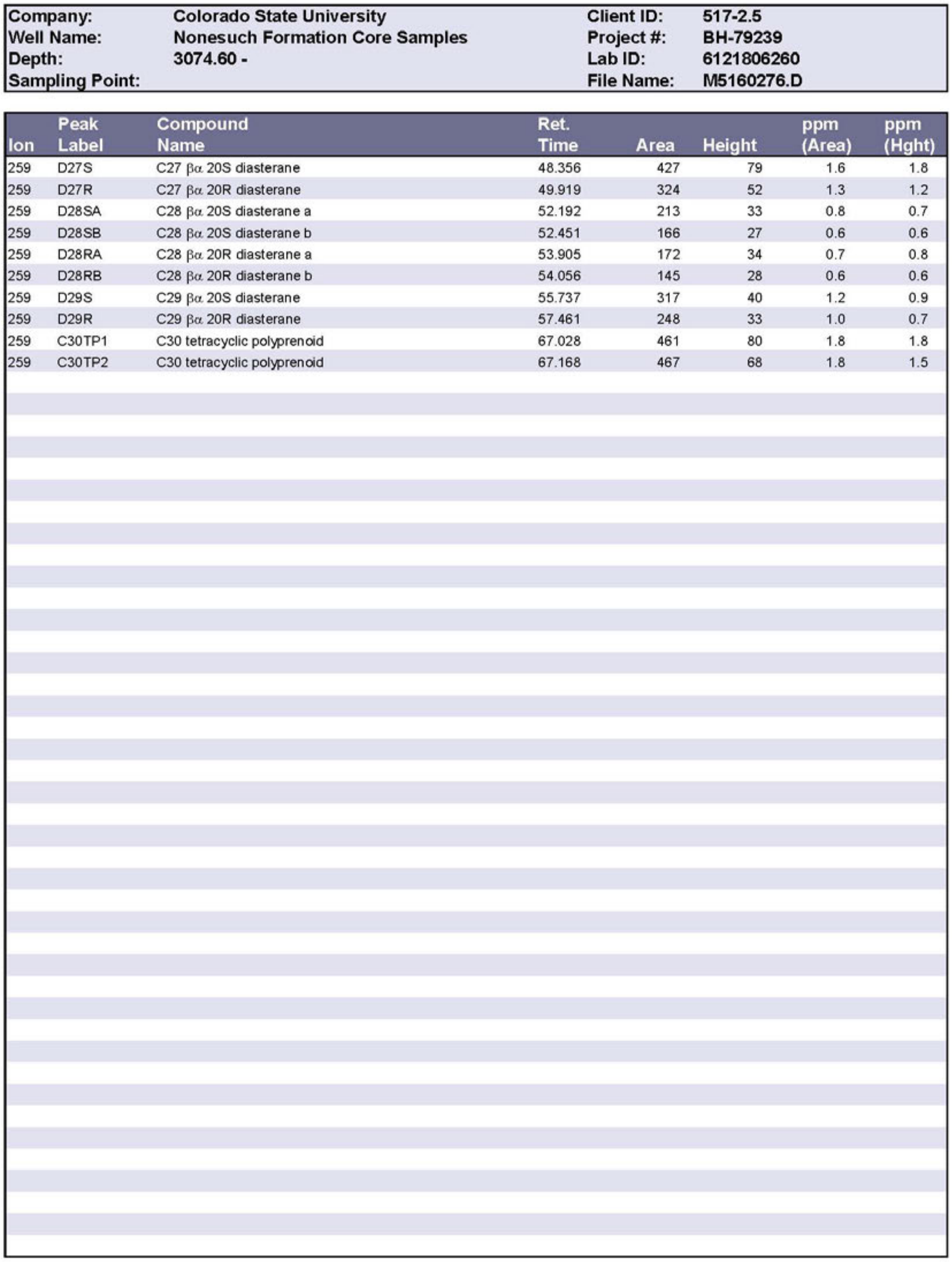

| | | | |
|---|---|---|---|
| **Company:** | **Colorado State University** | **Client ID:** | **517-2.5** |
| **Well Name:** | **Nonesuch Formation Core Samples** | **Project #:** | **BH-79239** |
| **Depth:** | **3074.60 -** | **Lab ID:** | **6121806260** |
| **Sampling Point:** | | **File Name:** | **M5160276.D** |

| Ion | Peak Label | Compound Name | Ret. Time | Area | Height | ppm (Area) | ppm (Hght) |
|---|---|---|---|---|---|---|---|
| 259 | D27S | C27 βα 20S diasterane | 48.356 | 427 | 79 | 1.6 | 1.8 |
| 259 | D27R | C27 βα 20R diasterane | 49.919 | 324 | 52 | 1.3 | 1.2 |
| 259 | D28SA | C28 βα 20S diasterane a | 52.192 | 213 | 33 | 0.8 | 0.7 |
| 259 | D28SB | C28 βα 20S diasterane b | 52.451 | 166 | 27 | 0.6 | 0.6 |
| 259 | D28RA | C28 βα 20R diasterane a | 53.905 | 172 | 34 | 0.7 | 0.8 |
| 259 | D28RB | C28 βα 20R diasterane b | 54.056 | 145 | 28 | 0.6 | 0.6 |
| 259 | D29S | C29 βα 20S diasterane | 55.737 | 317 | 40 | 1.2 | 0.9 |
| 259 | D29R | C29 βα 20R diasterane | 57.461 | 248 | 33 | 1.0 | 0.7 |
| 259 | C30TP1 | C30 tetracyclic polyprenoid | 67.028 | 461 | 80 | 1.8 | 1.8 |
| 259 | C30TP2 | C30 tetracyclic polyprenoid | 67.168 | 467 | 68 | 1.8 | 1.5 |

*Appendix F3, ctd.*

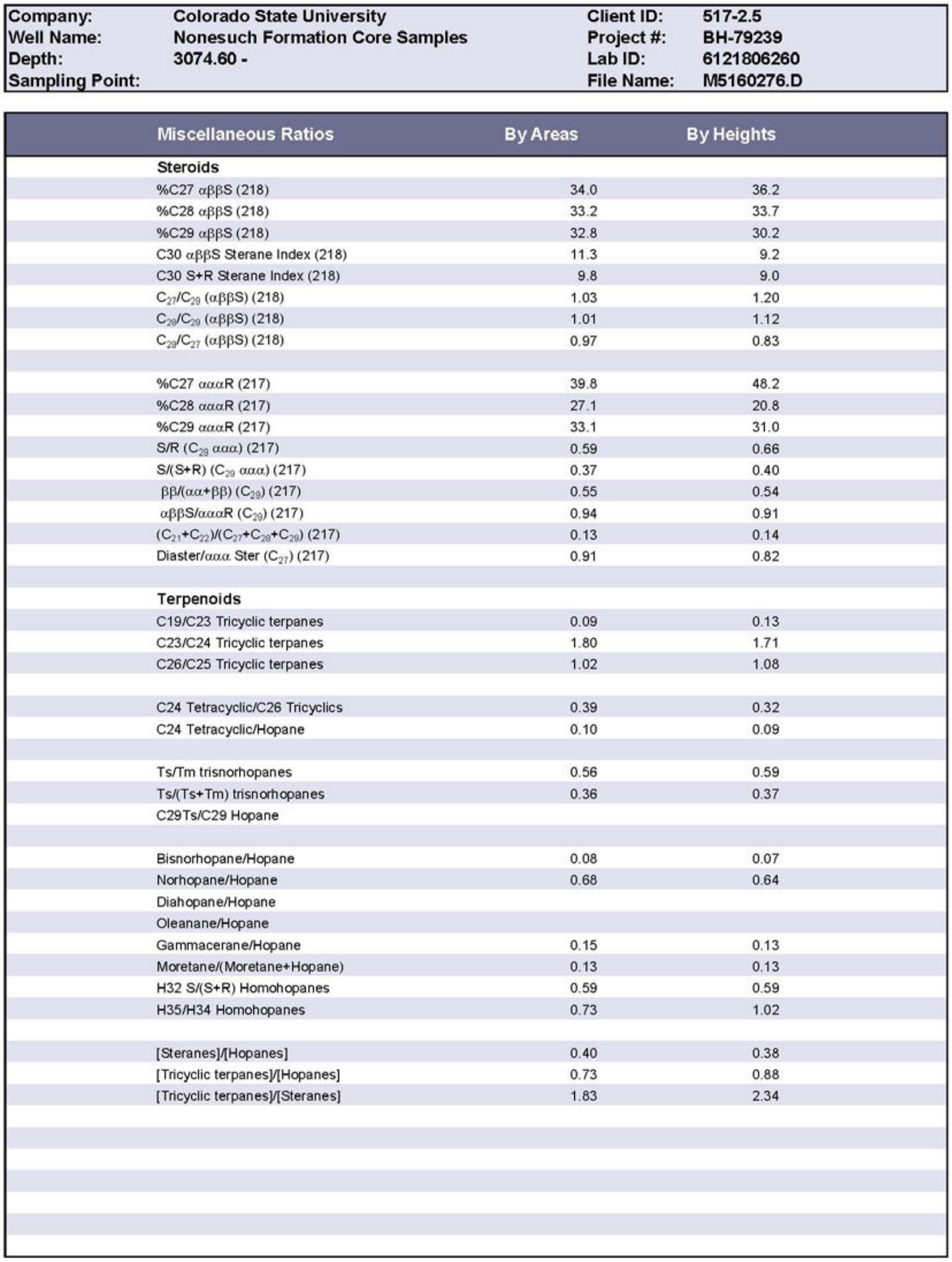

| | | | |
|---|---|---|---|
| **Company:** | **Colorado State University** | **Client ID:** | **517-2.5** |
| **Well Name:** | **Nonesuch Formation Core Samples** | **Project #:** | **BH-79239** |
| **Depth:** | **3074.60 -** | **Lab ID:** | **6121806260** |
| **Sampling Point:** | | **File Name:** | **M5160276.D** |

| Miscellaneous Ratios | By Areas | By Heights |
|---|---|---|
| **Steroids** | | |
| %C27 αββS (218) | 34.0 | 36.2 |
| %C28 αββS (218) | 33.2 | 33.7 |
| %C29 αββS (218) | 32.8 | 30.2 |
| C30 αββS Sterane Index (218) | 11.3 | 9.2 |
| C30 S+R Sterane Index (218) | 9.8 | 9.0 |
| $C_{27}/C_{29}$ (αββS) (218) | 1.03 | 1.20 |
| $C_{28}/C_{29}$ (αββS) (218) | 1.01 | 1.12 |
| $C_{29}/C_{27}$ (αββS) (218) | 0.97 | 0.83 |
| | | |
| %C27 αααR (217) | 39.8 | 48.2 |
| %C28 αααR (217) | 27.1 | 20.8 |
| %C29 αααR (217) | 33.1 | 31.0 |
| S/R ($C_{29}$ ααα) (217) | 0.59 | 0.66 |
| S/(S+R) ($C_{29}$ ααα) (217) | 0.37 | 0.40 |
| ββ/(αα+ββ) ($C_{29}$) (217) | 0.55 | 0.54 |
| αββS/αααR ($C_{29}$) (217) | 0.94 | 0.91 |
| ($C_{21}+C_{22}$)/($C_{27}+C_{28}+C_{29}$) (217) | 0.13 | 0.14 |
| Diaster/ααα Ster ($C_{27}$) (217) | 0.91 | 0.82 |
| | | |
| **Terpenoids** | | |
| C19/C23 Tricyclic terpanes | 0.09 | 0.13 |
| C23/C24 Tricyclic terpanes | 1.80 | 1.71 |
| C26/C25 Tricyclic terpanes | 1.02 | 1.08 |
| | | |
| C24 Tetracyclic/C26 Tricyclics | 0.39 | 0.32 |
| C24 Tetracyclic/Hopane | 0.10 | 0.09 |
| | | |
| Ts/Tm trisnorhopanes | 0.56 | 0.59 |
| Ts/(Ts+Tm) trisnorhopanes | 0.36 | 0.37 |
| C29Ts/C29 Hopane | | |
| | | |
| Bisnorhopane/Hopane | 0.08 | 0.07 |
| Norhopane/Hopane | 0.68 | 0.64 |
| Diahopane/Hopane | | |
| Oleanane/Hopane | | |
| Gammacerane/Hopane | 0.15 | 0.13 |
| Moretane/(Moretane+Hopane) | 0.13 | 0.13 |
| H32 S/(S+R) Homohopanes | 0.59 | 0.59 |
| H35/H34 Homohopanes | 0.73 | 1.02 |
| | | |
| [Steranes]/[Hopanes] | 0.40 | 0.38 |
| [Tricyclic terpanes]/[Hopanes] | 0.73 | 0.88 |
| [Tricyclic terpanes]/[Steranes] | 1.83 | 2.34 |

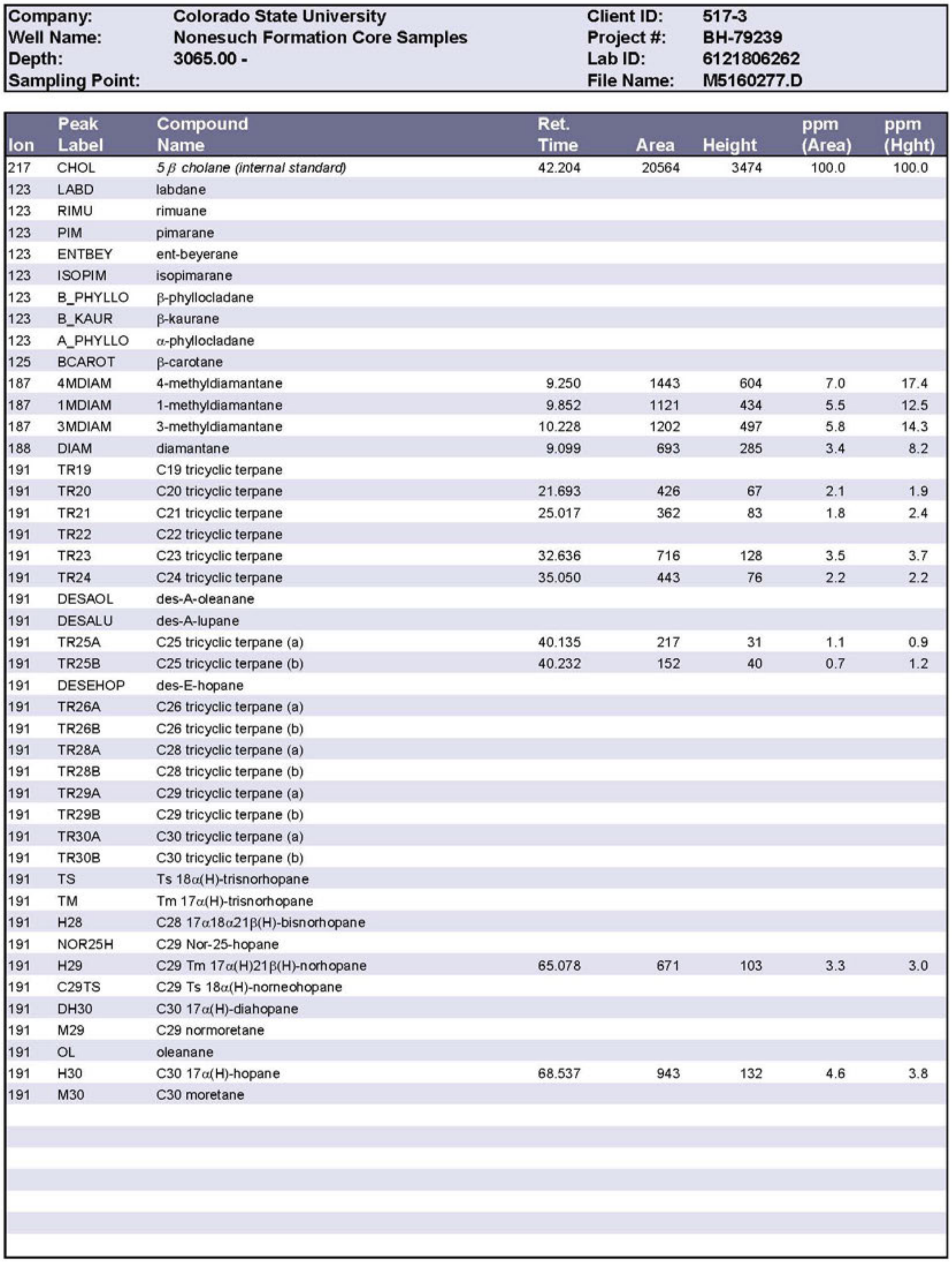

| | | | |
|---|---|---|---|
| **Company:** | **Colorado State University** | **Client ID:** | **517-3** |
| **Well Name:** | **Nonesuch Formation Core Samples** | **Project #:** | **BH-79239** |
| **Depth:** | **3065.00 -** | **Lab ID:** | **6121806262** |
| **Sampling Point:** | | **File Name:** | **M5160277.D** |

| Ion | Peak Label | Compound Name | Ret. Time | Area | Height | ppm (Area) | ppm (Hght) |
|---|---|---|---|---|---|---|---|
| 217 | CHOL | *5β cholane (internal standard)* | 42.204 | 20564 | 3474 | 100.0 | 100.0 |
| 123 | LABD | labdane | | | | | |
| 123 | RIMU | rimuane | | | | | |
| 123 | PIM | pimarane | | | | | |
| 123 | ENTBEY | ent-beyerane | | | | | |
| 123 | ISOPIM | isopimarane | | | | | |
| 123 | B_PHYLLO | β-phyllocladane | | | | | |
| 123 | B_KAUR | β-kaurane | | | | | |
| 123 | A_PHYLLO | α-phyllocladane | | | | | |
| 125 | BCAROT | β-carotane | | | | | |
| 187 | 4MDIAM | 4-methyldiamantane | 9.250 | 1443 | 604 | 7.0 | 17.4 |
| 187 | 1MDIAM | 1-methyldiamantane | 9.852 | 1121 | 434 | 5.5 | 12.5 |
| 187 | 3MDIAM | 3-methyldiamantane | 10.228 | 1202 | 497 | 5.8 | 14.3 |
| 188 | DIAM | diamantane | 9.099 | 693 | 285 | 3.4 | 8.2 |
| 191 | TR19 | C19 tricyclic terpane | | | | | |
| 191 | TR20 | C20 tricyclic terpane | 21.693 | 426 | 67 | 2.1 | 1.9 |
| 191 | TR21 | C21 tricyclic terpane | 25.017 | 362 | 83 | 1.8 | 2.4 |
| 191 | TR22 | C22 tricyclic terpane | | | | | |
| 191 | TR23 | C23 tricyclic terpane | 32.636 | 716 | 128 | 3.5 | 3.7 |
| 191 | TR24 | C24 tricyclic terpane | 35.050 | 443 | 76 | 2.2 | 2.2 |
| 191 | DESAOL | des-A-oleanane | | | | | |
| 191 | DESALU | des-A-lupane | | | | | |
| 191 | TR25A | C25 tricyclic terpane (a) | 40.135 | 217 | 31 | 1.1 | 0.9 |
| 191 | TR25B | C25 tricyclic terpane (b) | 40.232 | 152 | 40 | 0.7 | 1.2 |
| 191 | DESEHOP | des-E-hopane | | | | | |
| 191 | TR26A | C26 tricyclic terpane (a) | | | | | |
| 191 | TR26B | C26 tricyclic terpane (b) | | | | | |
| 191 | TR28A | C28 tricyclic terpane (a) | | | | | |
| 191 | TR28B | C28 tricyclic terpane (b) | | | | | |
| 191 | TR29A | C29 tricyclic terpane (a) | | | | | |
| 191 | TR29B | C29 tricyclic terpane (b) | | | | | |
| 191 | TR30A | C30 tricyclic terpane (a) | | | | | |
| 191 | TR30B | C30 tricyclic terpane (b) | | | | | |
| 191 | TS | Ts 18α(H)-trisnorhopane | | | | | |
| 191 | TM | Tm 17α(H)-trisnorhopane | | | | | |
| 191 | H28 | C28 17α18α21β(H)-bisnorhopane | | | | | |
| 191 | NOR25H | C29 Nor-25-hopane | | | | | |
| 191 | H29 | C29 Tm 17α(H)21β(H)-norhopane | 65.078 | 671 | 103 | 3.3 | 3.0 |
| 191 | C29TS | C29 Ts 18α(H)-norneohopane | | | | | |
| 191 | DH30 | C30 17α(H)-diahopane | | | | | |
| 191 | M29 | C29 normoretane | | | | | |
| 191 | OL | oleanane | | | | | |
| 191 | H30 | C30 17α(H)-hopane | 68.537 | 943 | 132 | 4.6 | 3.8 |
| 191 | M30 | C30 moretane | | | | | |

*Appendix F3, ctd.*

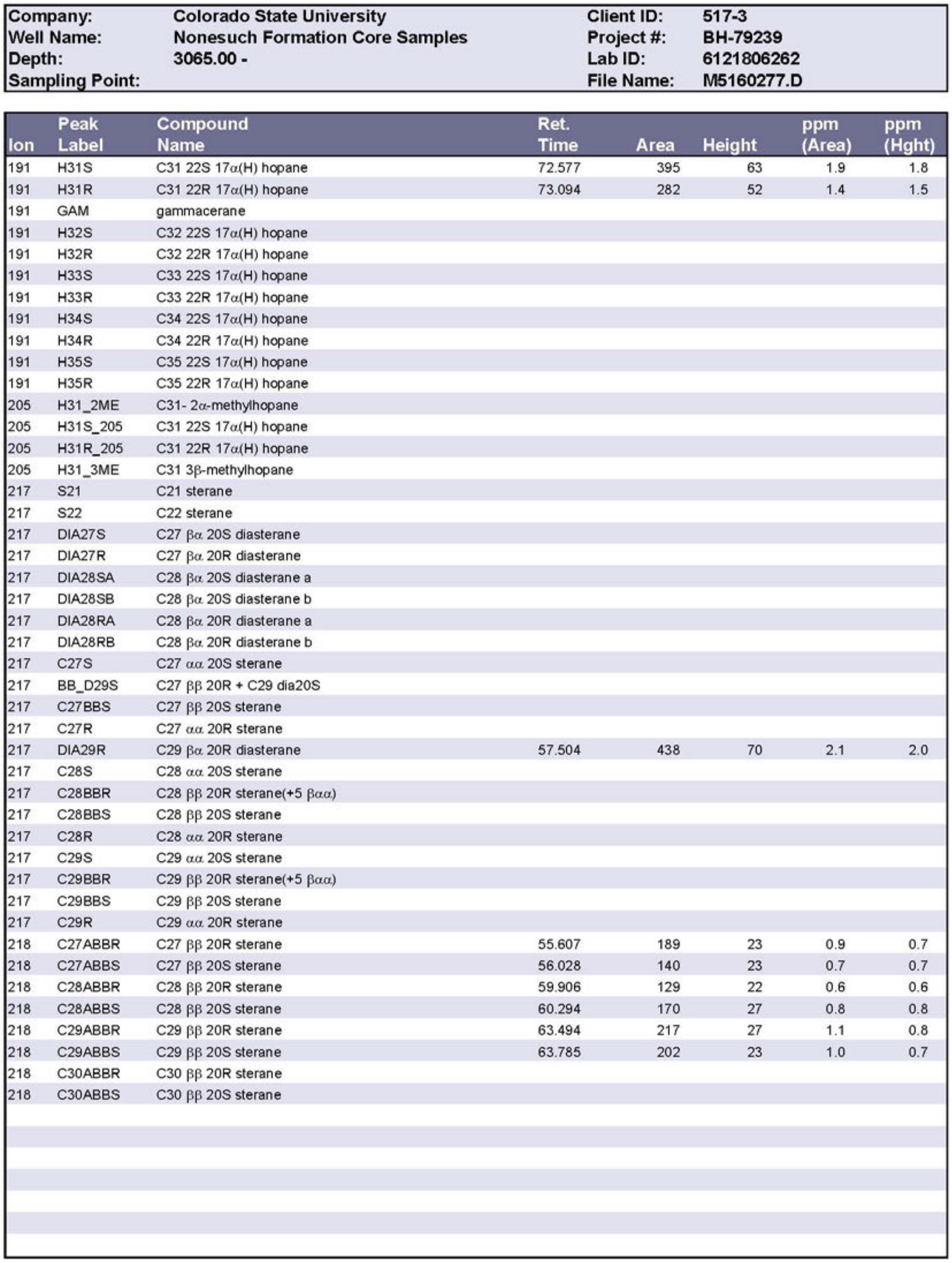

| | | | |
|---|---|---|---|
| **Company:** | **Colorado State University** | **Client ID:** | **517-3** |
| **Well Name:** | **Nonesuch Formation Core Samples** | **Project #:** | **BH-79239** |
| **Depth:** | **3065.00 -** | **Lab ID:** | **6121806262** |
| **Sampling Point:** | | **File Name:** | **M5160277.D** |

| Ion | Peak Label | Compound Name | Ret. Time | Area | Height | ppm (Area) | ppm (Hght) |
|---|---|---|---|---|---|---|---|
| 191 | H31S | C31 22S 17α(H) hopane | 72.577 | 395 | 63 | 1.9 | 1.8 |
| 191 | H31R | C31 22R 17α(H) hopane | 73.094 | 282 | 52 | 1.4 | 1.5 |
| 191 | GAM | gammacerane | | | | | |
| 191 | H32S | C32 22S 17α(H) hopane | | | | | |
| 191 | H32R | C32 22R 17α(H) hopane | | | | | |
| 191 | H33S | C33 22S 17α(H) hopane | | | | | |
| 191 | H33R | C33 22R 17α(H) hopane | | | | | |
| 191 | H34S | C34 22S 17α(H) hopane | | | | | |
| 191 | H34R | C34 22R 17α(H) hopane | | | | | |
| 191 | H35S | C35 22S 17α(H) hopane | | | | | |
| 191 | H35R | C35 22R 17α(H) hopane | | | | | |
| 205 | H31_2ME | C31- 2α-methylhopane | | | | | |
| 205 | H31S_205 | C31 22S 17α(H) hopane | | | | | |
| 205 | H31R_205 | C31 22R 17α(H) hopane | | | | | |
| 205 | H31_3ME | C31 3β-methylhopane | | | | | |
| 217 | S21 | C21 sterane | | | | | |
| 217 | S22 | C22 sterane | | | | | |
| 217 | DIA27S | C27 βα 20S diasterane | | | | | |
| 217 | DIA27R | C27 βα 20R diasterane | | | | | |
| 217 | DIA28SA | C28 βα 20S diasterane a | | | | | |
| 217 | DIA28SB | C28 βα 20S diasterane b | | | | | |
| 217 | DIA28RA | C28 βα 20R diasterane a | | | | | |
| 217 | DIA28RB | C28 βα 20R diasterane b | | | | | |
| 217 | C27S | C27 αα 20S sterane | | | | | |
| 217 | BB_D29S | C27 ββ 20R + C29 dia20S | | | | | |
| 217 | C27BBS | C27 ββ 20S sterane | | | | | |
| 217 | C27R | C27 αα 20R sterane | | | | | |
| 217 | DIA29R | C29 βα 20R diasterane | 57.504 | 438 | 70 | 2.1 | 2.0 |
| 217 | C28S | C28 αα 20S sterane | | | | | |
| 217 | C28BBR | C28 ββ 20R sterane(+5 βαα) | | | | | |
| 217 | C28BBS | C28 ββ 20S sterane | | | | | |
| 217 | C28R | C28 αα 20R sterane | | | | | |
| 217 | C29S | C29 αα 20S sterane | | | | | |
| 217 | C29BBR | C29 ββ 20R sterane(+5 βαα) | | | | | |
| 217 | C29BBS | C29 ββ 20S sterane | | | | | |
| 217 | C29R | C29 αα 20R sterane | | | | | |
| 218 | C27ABBR | C27 ββ 20R sterane | 55.607 | 189 | 23 | 0.9 | 0.7 |
| 218 | C27ABBS | C27 ββ 20S sterane | 56.028 | 140 | 23 | 0.7 | 0.7 |
| 218 | C28ABBR | C28 ββ 20R sterane | 59.906 | 129 | 22 | 0.6 | 0.6 |
| 218 | C28ABBS | C28 ββ 20S sterane | 60.294 | 170 | 27 | 0.8 | 0.8 |
| 218 | C29ABBR | C29 ββ 20R sterane | 63.494 | 217 | 27 | 1.1 | 0.8 |
| 218 | C29ABBS | C29 ββ 20S sterane | 63.785 | 202 | 23 | 1.0 | 0.7 |
| 218 | C30ABBR | C30 ββ 20R sterane | | | | | |
| 218 | C30ABBS | C30 ββ 20S sterane | | | | | |

*Appendix F3, ctd.*

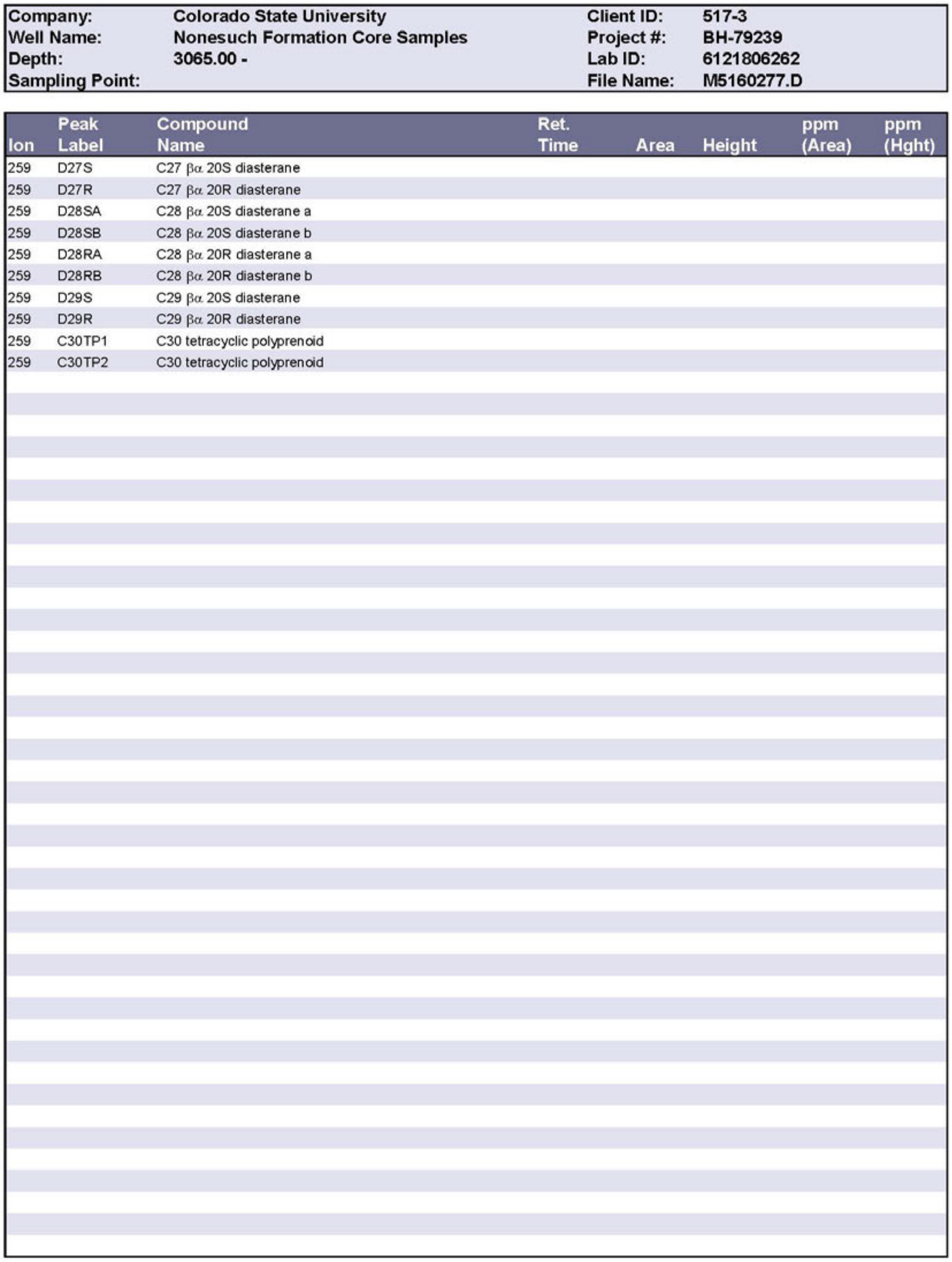

| | | | |
|---|---|---|---|
| **Company:** | **Colorado State University** | **Client ID:** | **517-3** |
| **Well Name:** | **Nonesuch Formation Core Samples** | **Project #:** | **BH-79239** |
| **Depth:** | **3065.00 -** | **Lab ID:** | **6121806262** |
| **Sampling Point:** | | **File Name:** | **M5160277.D** |

| Ion | Peak Label | Compound Name | Ret. Time | Area | Height | ppm (Area) | ppm (Hght) |
|---|---|---|---|---|---|---|---|
| 259 | D27S | C27 βα 20S diasterane | | | | | |
| 259 | D27R | C27 βα 20R diasterane | | | | | |
| 259 | D28SA | C28 βα 20S diasterane a | | | | | |
| 259 | D28SB | C28 βα 20S diasterane b | | | | | |
| 259 | D28RA | C28 βα 20R diasterane a | | | | | |
| 259 | D28RB | C28 βα 20R diasterane b | | | | | |
| 259 | D29S | C29 βα 20S diasterane | | | | | |
| 259 | D29R | C29 βα 20R diasterane | | | | | |
| 259 | C30TP1 | C30 tetracyclic polyprenoid | | | | | |
| 259 | C30TP2 | C30 tetracyclic polyprenoid | | | | | |

*Appendix F3, ctd.*

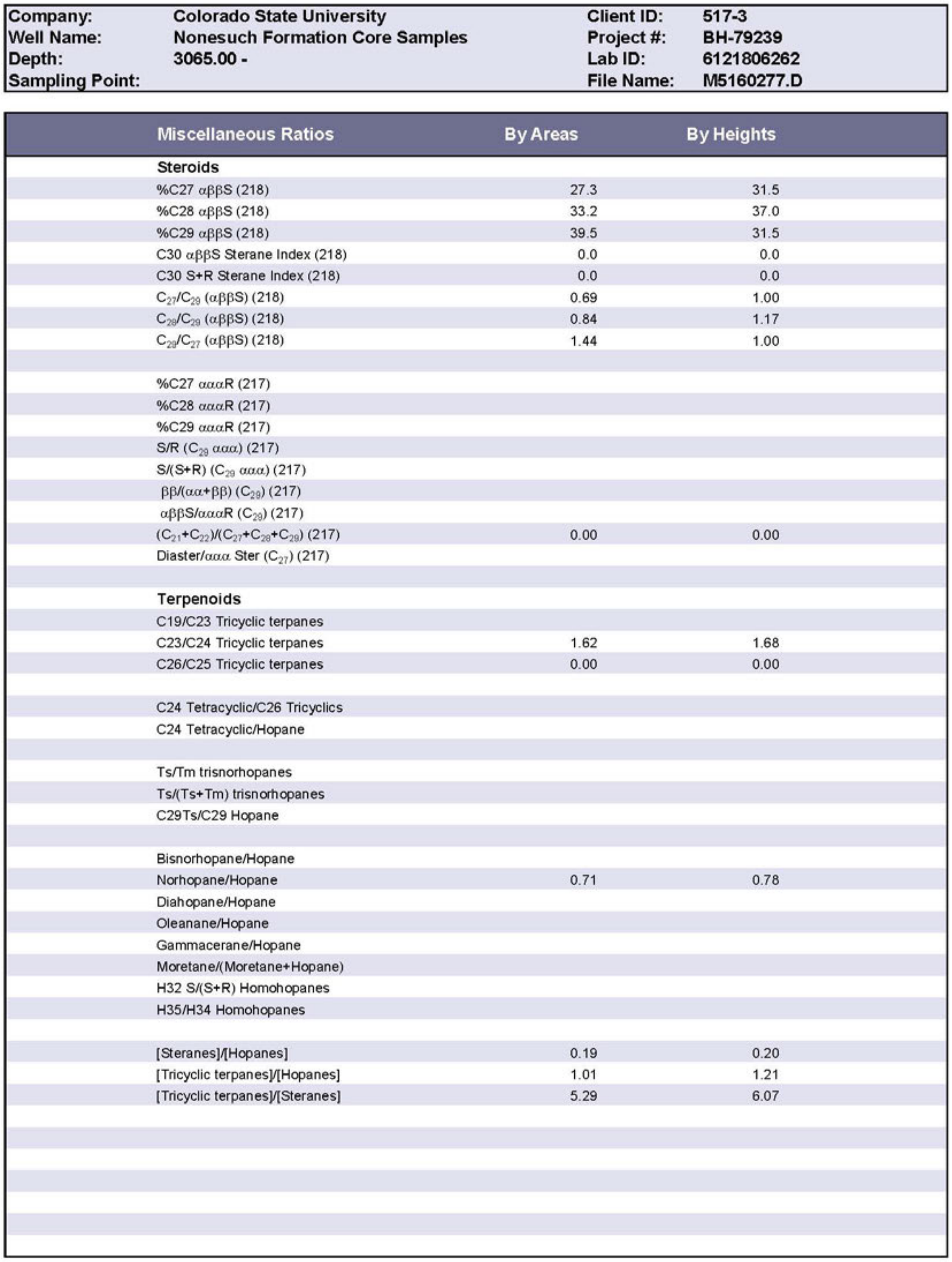

| | | | |
|---|---|---|---|
| **Company:** | **Colorado State University** | **Client ID:** | **517-3** |
| **Well Name:** | **Nonesuch Formation Core Samples** | **Project #:** | **BH-79239** |
| **Depth:** | **3065.00 -** | **Lab ID:** | **6121806262** |
| **Sampling Point:** | | **File Name:** | **M5160277.D** |

| Miscellaneous Ratios | By Areas | By Heights |
|---|---|---|
| **Steroids** | | |
| %C27 αββS (218) | 27.3 | 31.5 |
| %C28 αββS (218) | 33.2 | 37.0 |
| %C29 αββS (218) | 39.5 | 31.5 |
| C30 αββS Sterane Index (218) | 0.0 | 0.0 |
| C30 S+R Sterane Index (218) | 0.0 | 0.0 |
| $C_{27}/C_{29}$ (αββS) (218) | 0.69 | 1.00 |
| $C_{28}/C_{29}$ (αββS) (218) | 0.84 | 1.17 |
| $C_{29}/C_{27}$ (αββS) (218) | 1.44 | 1.00 |
| | | |
| %C27 αααR (217) | | |
| %C28 αααR (217) | | |
| %C29 αααR (217) | | |
| S/R ($C_{29}$ ααα) (217) | | |
| S/(S+R) ($C_{29}$ ααα) (217) | | |
| ββ/(αα+ββ) ($C_{29}$) (217) | | |
| αββS/αααR ($C_{29}$) (217) | | |
| ($C_{21}$+$C_{22}$)/($C_{27}$+$C_{28}$+$C_{29}$) (217) | 0.00 | 0.00 |
| Diaster/ααα Ster ($C_{27}$) (217) | | |
| | | |
| **Terpenoids** | | |
| C19/C23 Tricyclic terpanes | | |
| C23/C24 Tricyclic terpanes | 1.62 | 1.68 |
| C26/C25 Tricyclic terpanes | 0.00 | 0.00 |
| | | |
| C24 Tetracyclic/C26 Tricyclics | | |
| C24 Tetracyclic/Hopane | | |
| | | |
| Ts/Tm trisnorhopanes | | |
| Ts/(Ts+Tm) trisnorhopanes | | |
| C29Ts/C29 Hopane | | |
| | | |
| Bisnorhopane/Hopane | | |
| Norhopane/Hopane | 0.71 | 0.78 |
| Diahopane/Hopane | | |
| Oleanane/Hopane | | |
| Gammacerane/Hopane | | |
| Moretane/(Moretane+Hopane) | | |
| H32 S/(S+R) Homohopanes | | |
| H35/H34 Homohopanes | | |
| | | |
| [Steranes]/[Hopanes] | 0.19 | 0.20 |
| [Tricyclic terpanes]/[Hopanes] | 1.01 | 1.21 |
| [Tricyclic terpanes]/[Steranes] | 5.29 | 6.07 |

*Appendix F3, ctd.*

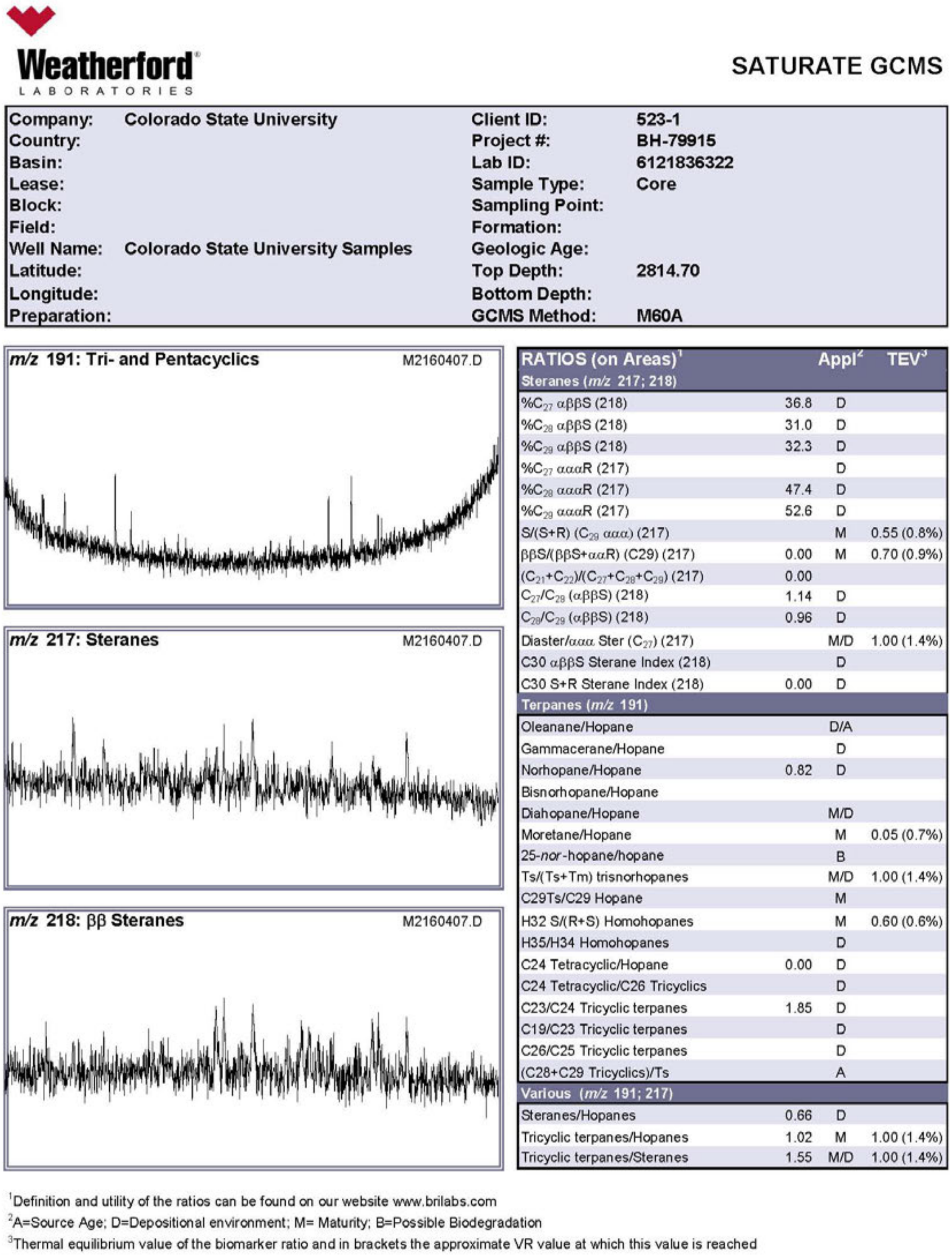

**Weatherford**
LABORATORIES

## SATURATE GCMS

| | | | |
|---|---|---|---|
| **Company:** | **Colorado State University** | **Client ID:** | **523-1** |
| **Country:** | | **Project #:** | **BH-79915** |
| **Basin:** | | **Lab ID:** | **6121836322** |
| **Lease:** | | **Sample Type:** | **Core** |
| **Block:** | | **Sampling Point:** | |
| **Field:** | | **Formation:** | |
| **Well Name:** | **Colorado State University Samples** | **Geologic Age:** | |
| **Latitude:** | | **Top Depth:** | **2814.70** |
| **Longitude:** | | **Bottom Depth:** | |
| **Preparation:** | | **GCMS Method:** | **M60A** |

***m/z*** **191: Tri- and Pentacyclics** M2160407.D

***m/z*** **217: Steranes** M2160407.D

***m/z*** **218: ββ Steranes** M2160407.D

| RATIOS (on Areas)[1] | | Appl[2] | TEV[3] |
|---|---|---|---|
| Steranes (*m/z* 217; 218) | | | |
| %$C_{27}$ αββS (218) | 36.8 | D | |
| %$C_{28}$ αββS (218) | 31.0 | D | |
| %$C_{29}$ αββS (218) | 32.3 | D | |
| %$C_{27}$ αααR (217) | | D | |
| %$C_{28}$ αααR (217) | 47.4 | D | |
| %$C_{29}$ αααR (217) | 52.6 | D | |
| S/(S+R) ($C_{29}$ ααα) (217) | | M | 0.55 (0.8%) |
| ββS/(ββS+ααR) (C29) (217) | 0.00 | M | 0.70 (0.9%) |
| ($C_{21}$+$C_{22}$)/($C_{27}$+$C_{28}$+$C_{29}$) (217) | 0.00 | | |
| $C_{27}$/$C_{29}$ (αββS) (218) | 1.14 | D | |
| $C_{28}$/$C_{29}$ (αββS) (218) | 0.96 | D | |
| Diaster/ααα Ster ($C_{27}$) (217) | | M/D | 1.00 (1.4%) |
| C30 αββS Sterane Index (218) | | D | |
| C30 S+R Sterane Index (218) | 0.00 | D | |
| Terpanes (*m/z* 191) | | | |
| Oleanane/Hopane | | D/A | |
| Gammacerane/Hopane | | D | |
| Norhopane/Hopane | 0.82 | D | |
| Bisnorhopane/Hopane | | | |
| Diahopane/Hopane | | M/D | |
| Moretane/Hopane | | M | 0.05 (0.7%) |
| 25-*nor*-hopane/hopane | | B | |
| Ts/(Ts+Tm) trisnorhopanes | | M/D | 1.00 (1.4%) |
| C29Ts/C29 Hopane | | M | |
| H32 S/(R+S) Homohopanes | | M | 0.60 (0.6%) |
| H35/H34 Homohopanes | | D | |
| C24 Tetracyclic/Hopane | 0.00 | D | |
| C24 Tetracyclic/C26 Tricyclics | | D | |
| C23/C24 Tricyclic terpanes | 1.85 | D | |
| C19/C23 Tricyclic terpanes | | D | |
| C26/C25 Tricyclic terpanes | | D | |
| (C28+C29 Tricyclics)/Ts | | A | |
| Various (*m/z* 191; 217) | | | |
| Steranes/Hopanes | 0.66 | D | |
| Tricyclic terpanes/Hopanes | 1.02 | M | 1.00 (1.4%) |
| Tricyclic terpanes/Steranes | 1.55 | M/D | 1.00 (1.4%) |

[1] Definition and utility of the ratios can be found on our website www.brilabs.com

[2] A=Source Age; D=Depositional environment; M= Maturity; B=Possible Biodegradation

[3] Thermal equilibrium value of the biomarker ratio and in brackets the approximate VR value at which this value is reached

*Appendix F3, ctd.*

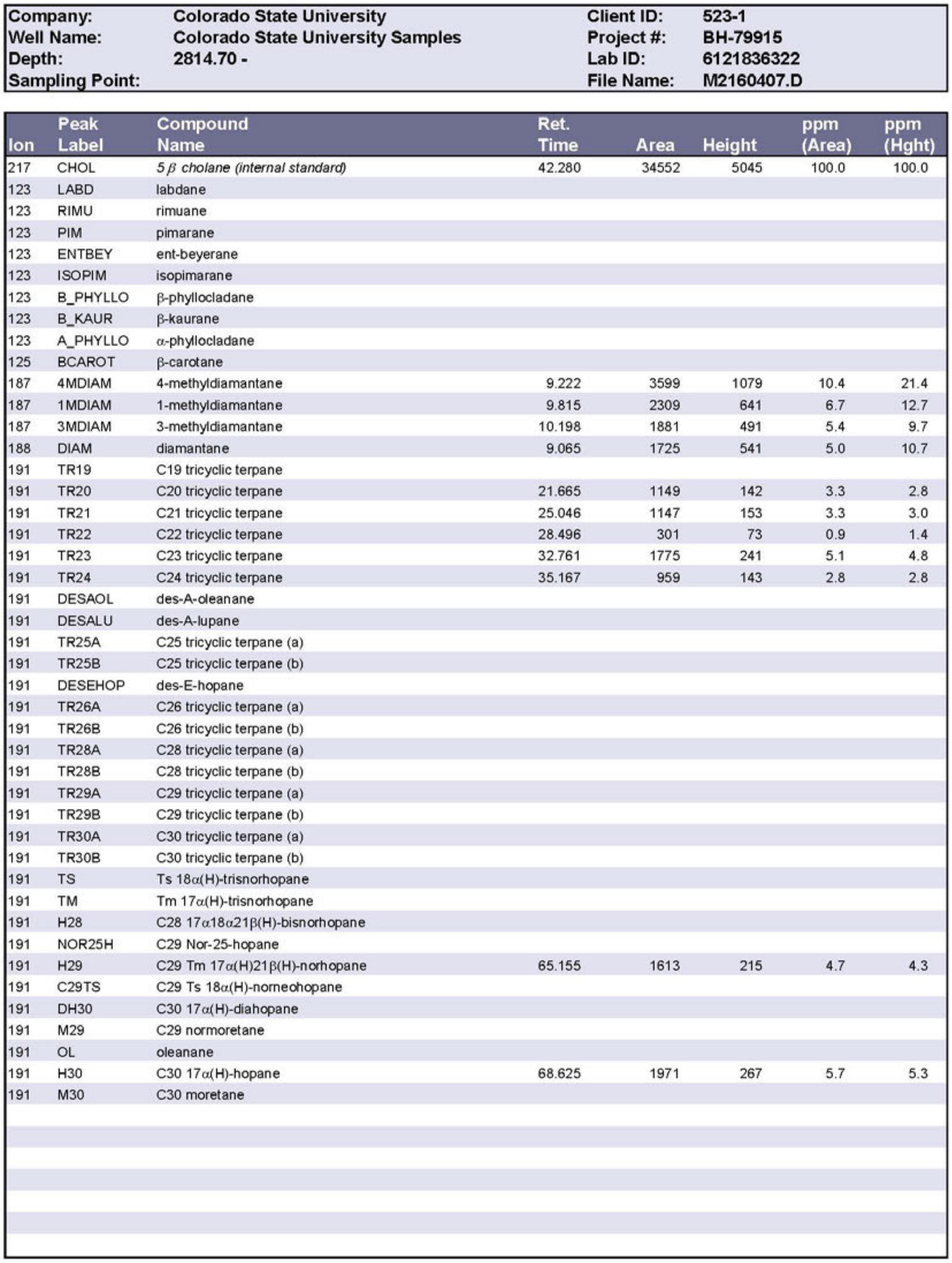

| | | | |
|---|---|---|---|
| **Company:** | **Colorado State University** | **Client ID:** | **523-1** |
| **Well Name:** | **Colorado State University Samples** | **Project #:** | **BH-79915** |
| **Depth:** | **2814.70 -** | **Lab ID:** | **6121836322** |
| **Sampling Point:** | | **File Name:** | **M2160407.D** |

| Ion | Peak Label | Compound Name | Ret. Time | Area | Height | ppm (Area) | ppm (Hght) |
|---|---|---|---|---|---|---|---|
| 217 | CHOL | *5β cholane (internal standard)* | 42.280 | 34552 | 5045 | 100.0 | 100.0 |
| 123 | LABD | labdane | | | | | |
| 123 | RIMU | rimuane | | | | | |
| 123 | PIM | pimarane | | | | | |
| 123 | ENTBEY | ent-beyerane | | | | | |
| 123 | ISOPIM | isopimarane | | | | | |
| 123 | B_PHYLLO | β-phyllocladane | | | | | |
| 123 | B_KAUR | β-kaurane | | | | | |
| 123 | A_PHYLLO | α-phyllocladane | | | | | |
| 125 | BCAROT | β-carotane | | | | | |
| 187 | 4MDIAM | 4-methyldiamantane | 9.222 | 3599 | 1079 | 10.4 | 21.4 |
| 187 | 1MDIAM | 1-methyldiamantane | 9.815 | 2309 | 641 | 6.7 | 12.7 |
| 187 | 3MDIAM | 3-methyldiamantane | 10.198 | 1881 | 491 | 5.4 | 9.7 |
| 188 | DIAM | diamantane | 9.065 | 1725 | 541 | 5.0 | 10.7 |
| 191 | TR19 | C19 tricyclic terpane | | | | | |
| 191 | TR20 | C20 tricyclic terpane | 21.665 | 1149 | 142 | 3.3 | 2.8 |
| 191 | TR21 | C21 tricyclic terpane | 25.046 | 1147 | 153 | 3.3 | 3.0 |
| 191 | TR22 | C22 tricyclic terpane | 28.496 | 301 | 73 | 0.9 | 1.4 |
| 191 | TR23 | C23 tricyclic terpane | 32.761 | 1775 | 241 | 5.1 | 4.8 |
| 191 | TR24 | C24 tricyclic terpane | 35.167 | 959 | 143 | 2.8 | 2.8 |
| 191 | DESAOL | des-A-oleanane | | | | | |
| 191 | DESALU | des-A-lupane | | | | | |
| 191 | TR25A | C25 tricyclic terpane (a) | | | | | |
| 191 | TR25B | C25 tricyclic terpane (b) | | | | | |
| 191 | DESEHOP | des-E-hopane | | | | | |
| 191 | TR26A | C26 tricyclic terpane (a) | | | | | |
| 191 | TR26B | C26 tricyclic terpane (b) | | | | | |
| 191 | TR28A | C28 tricyclic terpane (a) | | | | | |
| 191 | TR28B | C28 tricyclic terpane (b) | | | | | |
| 191 | TR29A | C29 tricyclic terpane (a) | | | | | |
| 191 | TR29B | C29 tricyclic terpane (b) | | | | | |
| 191 | TR30A | C30 tricyclic terpane (a) | | | | | |
| 191 | TR30B | C30 tricyclic terpane (b) | | | | | |
| 191 | TS | Ts 18α(H)-trisnorhopane | | | | | |
| 191 | TM | Tm 17α(H)-trisnorhopane | | | | | |
| 191 | H28 | C28 17α18α21β(H)-bisnorhopane | | | | | |
| 191 | NOR25H | C29 Nor-25-hopane | | | | | |
| 191 | H29 | C29 Tm 17α(H)21β(H)-norhopane | 65.155 | 1613 | 215 | 4.7 | 4.3 |
| 191 | C29TS | C29 Ts 18α(H)-norneohopane | | | | | |
| 191 | DH30 | C30 17α(H)-diahopane | | | | | |
| 191 | M29 | C29 normoretane | | | | | |
| 191 | OL | oleanane | | | | | |
| 191 | H30 | C30 17α(H)-hopane | 68.625 | 1971 | 267 | 5.7 | 5.3 |
| 191 | M30 | C30 moretane | | | | | |

*Appendix F3, ctd.*

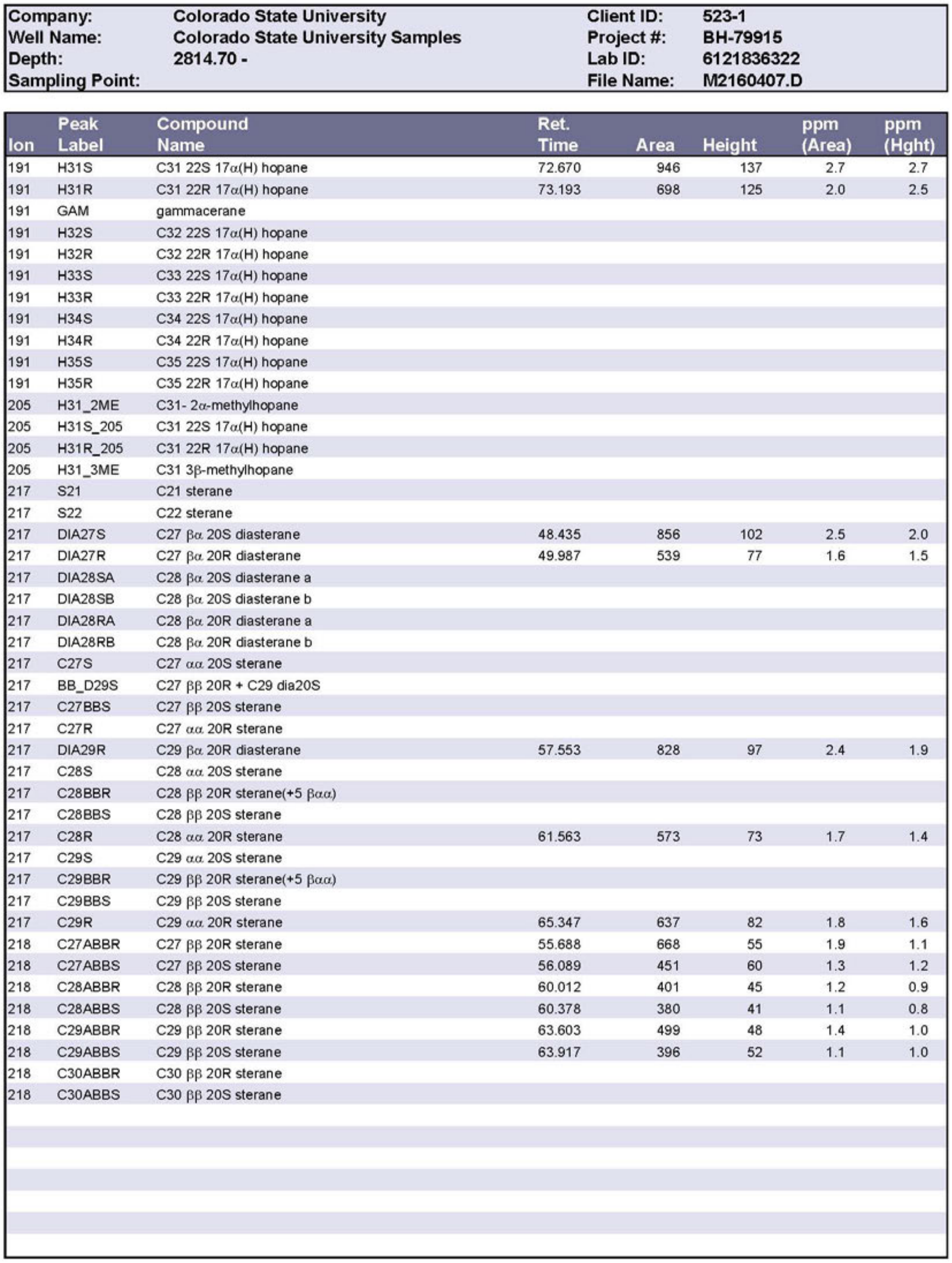

| | | | |
|---|---|---|---|
| **Company:** | **Colorado State University** | **Client ID:** | **523-1** |
| **Well Name:** | **Colorado State University Samples** | **Project #:** | **BH-79915** |
| **Depth:** | **2814.70 -** | **Lab ID:** | **6121836322** |
| **Sampling Point:** | | **File Name:** | **M2160407.D** |

| Ion | Peak Label | Compound Name | Ret. Time | Area | Height | ppm (Area) | ppm (Hght) |
|---|---|---|---|---|---|---|---|
| 191 | H31S | C31 22S 17α(H) hopane | 72.670 | 946 | 137 | 2.7 | 2.7 |
| 191 | H31R | C31 22R 17α(H) hopane | 73.193 | 698 | 125 | 2.0 | 2.5 |
| 191 | GAM | gammacerane | | | | | |
| 191 | H32S | C32 22S 17α(H) hopane | | | | | |
| 191 | H32R | C32 22R 17α(H) hopane | | | | | |
| 191 | H33S | C33 22S 17α(H) hopane | | | | | |
| 191 | H33R | C33 22R 17α(H) hopane | | | | | |
| 191 | H34S | C34 22S 17α(H) hopane | | | | | |
| 191 | H34R | C34 22R 17α(H) hopane | | | | | |
| 191 | H35S | C35 22S 17α(H) hopane | | | | | |
| 191 | H35R | C35 22R 17α(H) hopane | | | | | |
| 205 | H31_2ME | C31- 2α-methylhopane | | | | | |
| 205 | H31S_205 | C31 22S 17α(H) hopane | | | | | |
| 205 | H31R_205 | C31 22R 17α(H) hopane | | | | | |
| 205 | H31_3ME | C31 3β-methylhopane | | | | | |
| 217 | S21 | C21 sterane | | | | | |
| 217 | S22 | C22 sterane | | | | | |
| 217 | DIA27S | C27 βα 20S diasterane | 48.435 | 856 | 102 | 2.5 | 2.0 |
| 217 | DIA27R | C27 βα 20R diasterane | 49.987 | 539 | 77 | 1.6 | 1.5 |
| 217 | DIA28SA | C28 βα 20S diasterane a | | | | | |
| 217 | DIA28SB | C28 βα 20S diasterane b | | | | | |
| 217 | DIA28RA | C28 βα 20R diasterane a | | | | | |
| 217 | DIA28RB | C28 βα 20R diasterane b | | | | | |
| 217 | C27S | C27 αα 20S sterane | | | | | |
| 217 | BB_D29S | C27 ββ 20R + C29 dia20S | | | | | |
| 217 | C27BBS | C27 ββ 20S sterane | | | | | |
| 217 | C27R | C27 αα 20R sterane | | | | | |
| 217 | DIA29R | C29 βα 20R diasterane | 57.553 | 828 | 97 | 2.4 | 1.9 |
| 217 | C28S | C28 αα 20S sterane | | | | | |
| 217 | C28BBR | C28 ββ 20R sterane(+5 βαα) | | | | | |
| 217 | C28BBS | C28 ββ 20S sterane | | | | | |
| 217 | C28R | C28 αα 20R sterane | 61.563 | 573 | 73 | 1.7 | 1.4 |
| 217 | C29S | C29 αα 20S sterane | | | | | |
| 217 | C29BBR | C29 ββ 20R sterane(+5 βαα) | | | | | |
| 217 | C29BBS | C29 ββ 20S sterane | | | | | |
| 217 | C29R | C29 αα 20R sterane | 65.347 | 637 | 82 | 1.8 | 1.6 |
| 218 | C27ABBR | C27 ββ 20R sterane | 55.688 | 668 | 55 | 1.9 | 1.1 |
| 218 | C27ABBS | C27 ββ 20S sterane | 56.089 | 451 | 60 | 1.3 | 1.2 |
| 218 | C28ABBR | C28 ββ 20R sterane | 60.012 | 401 | 45 | 1.2 | 0.9 |
| 218 | C28ABBS | C28 ββ 20S sterane | 60.378 | 380 | 41 | 1.1 | 0.8 |
| 218 | C29ABBR | C29 ββ 20R sterane | 63.603 | 499 | 48 | 1.4 | 1.0 |
| 218 | C29ABBS | C29 ββ 20S sterane | 63.917 | 396 | 52 | 1.1 | 1.0 |
| 218 | C30ABBR | C30 ββ 20R sterane | | | | | |
| 218 | C30ABBS | C30 ββ 20S sterane | | | | | |

*Appendix F3, ctd.*

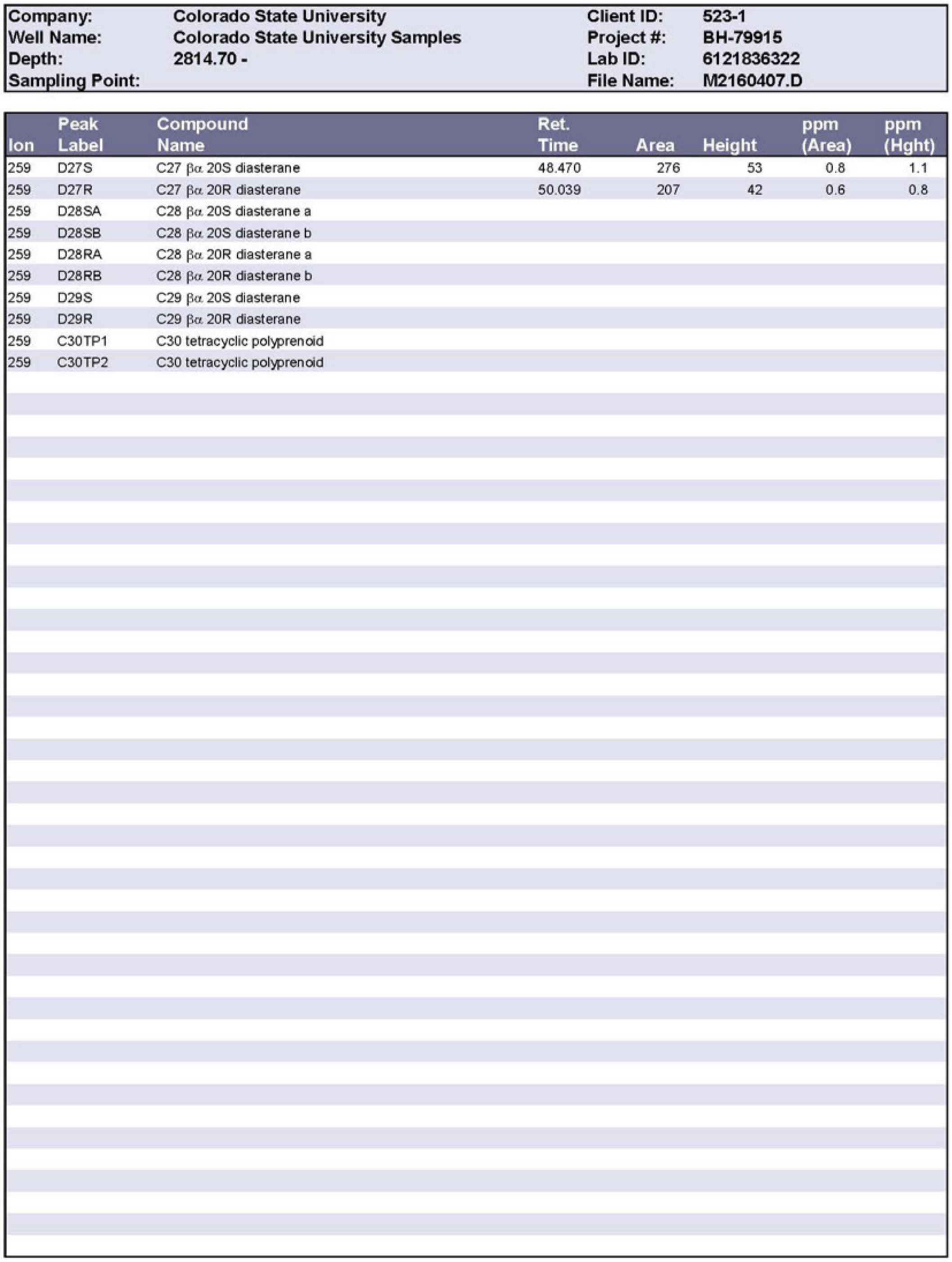

| | | | |
|---|---|---|---|
| **Company:** | **Colorado State University** | **Client ID:** | **523-1** |
| **Well Name:** | **Colorado State University Samples** | **Project #:** | **BH-79915** |
| **Depth:** | **2814.70 -** | **Lab ID:** | **6121836322** |
| **Sampling Point:** | | **File Name:** | **M2160407.D** |

| Ion | Peak Label | Compound Name | Ret. Time | Area | Height | ppm (Area) | ppm (Hght) |
|---|---|---|---|---|---|---|---|
| 259 | D27S | C27 βα 20S diasterane | 48.470 | 276 | 53 | 0.8 | 1.1 |
| 259 | D27R | C27 βα 20R diasterane | 50.039 | 207 | 42 | 0.6 | 0.8 |
| 259 | D28SA | C28 βα 20S diasterane a | | | | | |
| 259 | D28SB | C28 βα 20S diasterane b | | | | | |
| 259 | D28RA | C28 βα 20R diasterane a | | | | | |
| 259 | D28RB | C28 βα 20R diasterane b | | | | | |
| 259 | D29S | C29 βα 20S diasterane | | | | | |
| 259 | D29R | C29 βα 20R diasterane | | | | | |
| 259 | C30TP1 | C30 tetracyclic polyprenoid | | | | | |
| 259 | C30TP2 | C30 tetracyclic polyprenoid | | | | | |

*Appendix F3, ctd.*

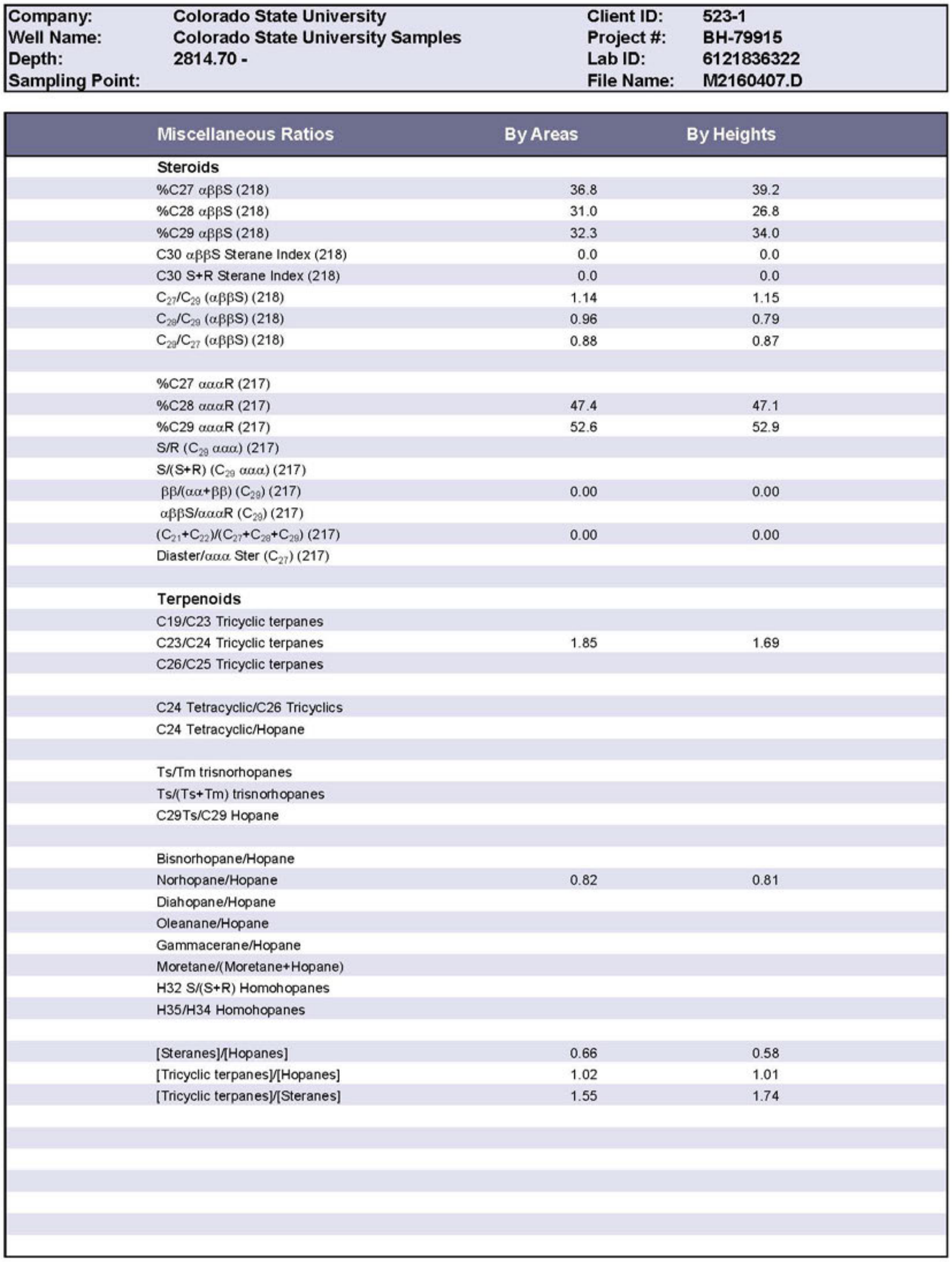

| | | | |
|---|---|---|---|
| **Company:** | **Colorado State University** | **Client ID:** | **523-1** |
| **Well Name:** | **Colorado State University Samples** | **Project #:** | **BH-79915** |
| **Depth:** | **2814.70 -** | **Lab ID:** | **6121836322** |
| **Sampling Point:** | | **File Name:** | **M2160407.D** |

| Miscellaneous Ratios | By Areas | By Heights |
|---|---|---|
| **Steroids** | | |
| %C27 αββS (218) | 36.8 | 39.2 |
| %C28 αββS (218) | 31.0 | 26.8 |
| %C29 αββS (218) | 32.3 | 34.0 |
| C30 αββS Sterane Index (218) | 0.0 | 0.0 |
| C30 S+R Sterane Index (218) | 0.0 | 0.0 |
| $C_{27}/C_{29}$ (αββS) (218) | 1.14 | 1.15 |
| $C_{28}/C_{29}$ (αββS) (218) | 0.96 | 0.79 |
| $C_{29}/C_{27}$ (αββS) (218) | 0.88 | 0.87 |
| | | |
| %C27 αααR (217) | | |
| %C28 αααR (217) | 47.4 | 47.1 |
| %C29 αααR (217) | 52.6 | 52.9 |
| S/R ($C_{29}$ ααα) (217) | | |
| S/(S+R) ($C_{29}$ ααα) (217) | | |
| ββ/(αα+ββ) ($C_{29}$) (217) | 0.00 | 0.00 |
| αββS/αααR ($C_{29}$) (217) | | |
| ($C_{21}$+$C_{22}$)/($C_{27}$+$C_{28}$+$C_{29}$) (217) | 0.00 | 0.00 |
| Diaster/ααα Ster ($C_{27}$) (217) | | |
| | | |
| **Terpenoids** | | |
| C19/C23 Tricyclic terpanes | | |
| C23/C24 Tricyclic terpanes | 1.85 | 1.69 |
| C26/C25 Tricyclic terpanes | | |
| | | |
| C24 Tetracyclic/C26 Tricyclics | | |
| C24 Tetracyclic/Hopane | | |
| | | |
| Ts/Tm trisnorhopanes | | |
| Ts/(Ts+Tm) trisnorhopanes | | |
| C29Ts/C29 Hopane | | |
| | | |
| Bisnorhopane/Hopane | | |
| Norhopane/Hopane | 0.82 | 0.81 |
| Diahopane/Hopane | | |
| Oleanane/Hopane | | |
| Gammacerane/Hopane | | |
| Moretane/(Moretane+Hopane) | | |
| H32 S/(S+R) Homohopanes | | |
| H35/H34 Homohopanes | | |
| | | |
| [Steranes]/[Hopanes] | 0.66 | 0.58 |
| [Tricyclic terpanes]/[Hopanes] | 1.02 | 1.01 |
| [Tricyclic terpanes]/[Steranes] | 1.55 | 1.74 |

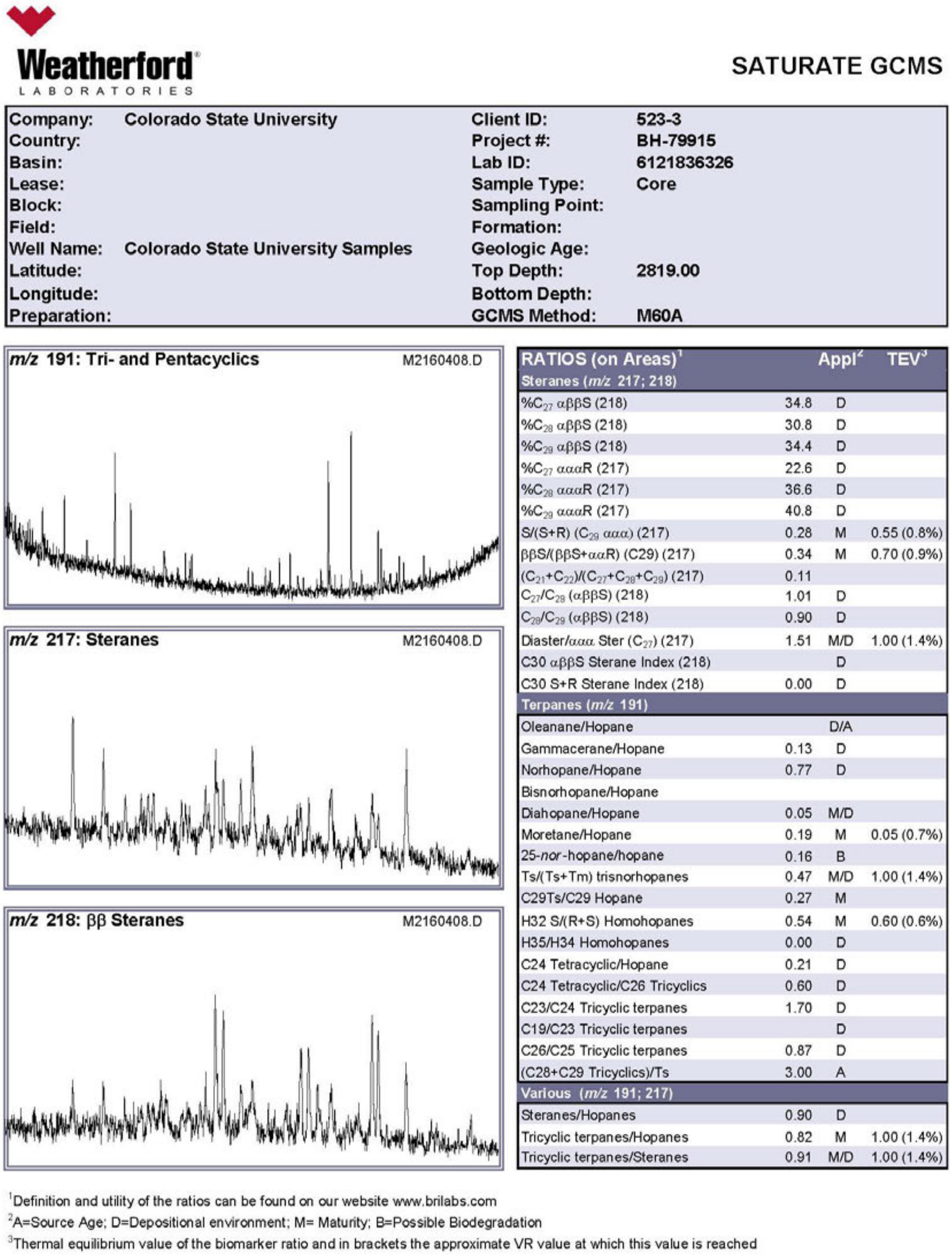

Weatherford LABORATORIES

## SATURATE GCMS

| | | | |
|---|---|---|---|
| **Company:** | **Colorado State University** | **Client ID:** | **523-3** |
| **Country:** | | **Project #:** | **BH-79915** |
| **Basin:** | | **Lab ID:** | **6121836326** |
| **Lease:** | | **Sample Type:** | **Core** |
| **Block:** | | **Sampling Point:** | |
| **Field:** | | **Formation:** | |
| **Well Name:** | **Colorado State University Samples** | **Geologic Age:** | |
| **Latitude:** | | **Top Depth:** | **2819.00** |
| **Longitude:** | | **Bottom Depth:** | |
| **Preparation:** | | **GCMS Method:** | **M60A** |

***m/z* 191: Tri- and Pentacyclics** M2160408.D

***m/z* 217: Steranes** M2160408.D

***m/z* 218: ββ Steranes** M2160408.D

| RATIOS (on Areas)[1] | | Appl[2] | TEV[3] |
|---|---|---|---|
| **Steranes (*m/z* 217; 218)** | | | |
| %$C_{27}$ αββS (218) | 34.8 | D | |
| %$C_{28}$ αββS (218) | 30.8 | D | |
| %$C_{29}$ αββS (218) | 34.4 | D | |
| %$C_{27}$ αααR (217) | 22.6 | D | |
| %$C_{28}$ αααR (217) | 36.6 | D | |
| %$C_{29}$ αααR (217) | 40.8 | D | |
| S/(S+R) ($C_{29}$ ααα) (217) | 0.28 | M | 0.55 (0.8%) |
| ββS/(ββS+ααR) (C29) (217) | 0.34 | M | 0.70 (0.9%) |
| ($C_{21}$+$C_{22}$)/($C_{27}$+$C_{28}$+$C_{29}$) (217) | 0.11 | | |
| $C_{27}$/$C_{29}$ (αββS) (218) | 1.01 | D | |
| $C_{28}$/$C_{29}$ (αββS) (218) | 0.90 | D | |
| Diaster/ααα Ster ($C_{27}$) (217) | 1.51 | M/D | 1.00 (1.4%) |
| C30 αββS Sterane Index (218) | | D | |
| C30 S+R Sterane Index (218) | 0.00 | D | |
| **Terpanes (*m/z* 191)** | | | |
| Oleanane/Hopane | | D/A | |
| Gammacerane/Hopane | 0.13 | D | |
| Norhopane/Hopane | 0.77 | D | |
| Bisnorhopane/Hopane | | | |
| Diahopane/Hopane | 0.05 | M/D | |
| Moretane/Hopane | 0.19 | M | 0.05 (0.7%) |
| 25-*nor*-hopane/hopane | 0.16 | B | |
| Ts/(Ts+Tm) trisnorhopanes | 0.47 | M/D | 1.00 (1.4%) |
| C29Ts/C29 Hopane | 0.27 | M | |
| H32 S/(R+S) Homohopanes | 0.54 | M | 0.60 (0.6%) |
| H35/H34 Homohopanes | 0.00 | D | |
| C24 Tetracyclic/Hopane | 0.21 | D | |
| C24 Tetracyclic/C26 Tricyclics | 0.60 | D | |
| C23/C24 Tricyclic terpanes | 1.70 | D | |
| C19/C23 Tricyclic terpanes | | D | |
| C26/C25 Tricyclic terpanes | 0.87 | D | |
| (C28+C29 Tricyclics)/Ts | 3.00 | A | |
| **Various (*m/z* 191; 217)** | | | |
| Steranes/Hopanes | 0.90 | D | |
| Tricyclic terpanes/Hopanes | 0.82 | M | 1.00 (1.4%) |
| Tricyclic terpanes/Steranes | 0.91 | M/D | 1.00 (1.4%) |

[1] Definition and utility of the ratios can be found on our website www.brilabs.com

[2] A=Source Age; D=Depositional environment; M= Maturity; B=Possible Biodegradation

[3] Thermal equilibrium value of the biomarker ratio and in brackets the approximate VR value at which this value is reached

*Appendix F3, ctd.*

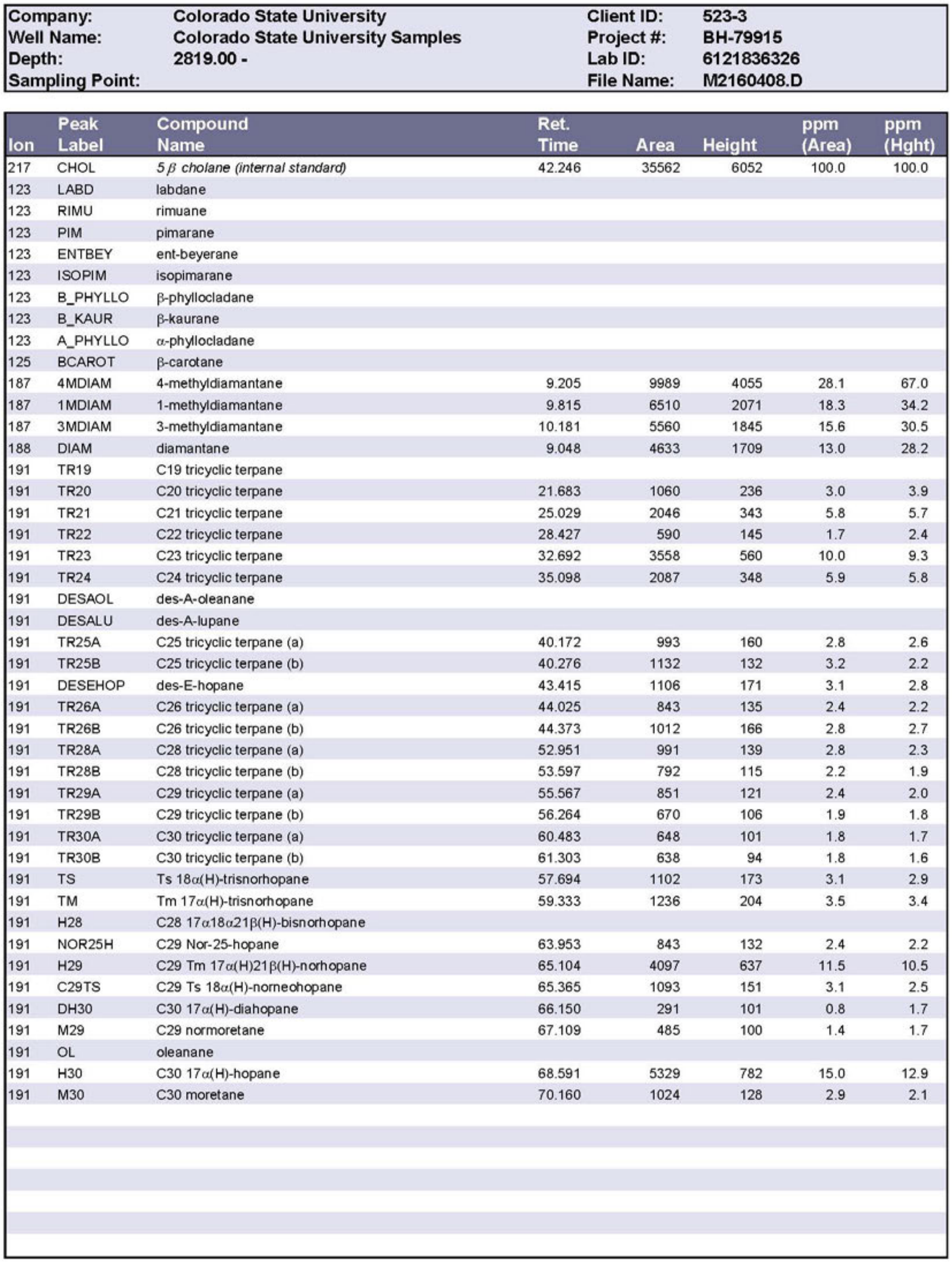

| | | | |
|---|---|---|---|
| **Company:** | **Colorado State University** | **Client ID:** | **523-3** |
| **Well Name:** | **Colorado State University Samples** | **Project #:** | **BH-79915** |
| **Depth:** | **2819.00 -** | **Lab ID:** | **6121836326** |
| **Sampling Point:** | | **File Name:** | **M2160408.D** |

| Ion | Peak Label | Compound Name | Ret. Time | Area | Height | ppm (Area) | ppm (Hght) |
|---|---|---|---|---|---|---|---|
| 217 | CHOL | *5β cholane (internal standard)* | 42.246 | 35562 | 6052 | 100.0 | 100.0 |
| 123 | LABD | labdane | | | | | |
| 123 | RIMU | rimuane | | | | | |
| 123 | PIM | pimarane | | | | | |
| 123 | ENTBEY | ent-beyerane | | | | | |
| 123 | ISOPIM | isopimarane | | | | | |
| 123 | B_PHYLLO | β-phyllocladane | | | | | |
| 123 | B_KAUR | β-kaurane | | | | | |
| 123 | A_PHYLLO | α-phyllocladane | | | | | |
| 125 | BCAROT | β-carotane | | | | | |
| 187 | 4MDIAM | 4-methyldiamantane | 9.205 | 9989 | 4055 | 28.1 | 67.0 |
| 187 | 1MDIAM | 1-methyldiamantane | 9.815 | 6510 | 2071 | 18.3 | 34.2 |
| 187 | 3MDIAM | 3-methyldiamantane | 10.181 | 5560 | 1845 | 15.6 | 30.5 |
| 188 | DIAM | diamantane | 9.048 | 4633 | 1709 | 13.0 | 28.2 |
| 191 | TR19 | C19 tricyclic terpane | | | | | |
| 191 | TR20 | C20 tricyclic terpane | 21.683 | 1060 | 236 | 3.0 | 3.9 |
| 191 | TR21 | C21 tricyclic terpane | 25.029 | 2046 | 343 | 5.8 | 5.7 |
| 191 | TR22 | C22 tricyclic terpane | 28.427 | 590 | 145 | 1.7 | 2.4 |
| 191 | TR23 | C23 tricyclic terpane | 32.692 | 3558 | 560 | 10.0 | 9.3 |
| 191 | TR24 | C24 tricyclic terpane | 35.098 | 2087 | 348 | 5.9 | 5.8 |
| 191 | DESAOL | des-A-oleanane | | | | | |
| 191 | DESALU | des-A-lupane | | | | | |
| 191 | TR25A | C25 tricyclic terpane (a) | 40.172 | 993 | 160 | 2.8 | 2.6 |
| 191 | TR25B | C25 tricyclic terpane (b) | 40.276 | 1132 | 132 | 3.2 | 2.2 |
| 191 | DESEHOP | des-E-hopane | 43.415 | 1106 | 171 | 3.1 | 2.8 |
| 191 | TR26A | C26 tricyclic terpane (a) | 44.025 | 843 | 135 | 2.4 | 2.2 |
| 191 | TR26B | C26 tricyclic terpane (b) | 44.373 | 1012 | 166 | 2.8 | 2.7 |
| 191 | TR28A | C28 tricyclic terpane (a) | 52.951 | 991 | 139 | 2.8 | 2.3 |
| 191 | TR28B | C28 tricyclic terpane (b) | 53.597 | 792 | 115 | 2.2 | 1.9 |
| 191 | TR29A | C29 tricyclic terpane (a) | 55.567 | 851 | 121 | 2.4 | 2.0 |
| 191 | TR29B | C29 tricyclic terpane (b) | 56.264 | 670 | 106 | 1.9 | 1.8 |
| 191 | TR30A | C30 tricyclic terpane (a) | 60.483 | 648 | 101 | 1.8 | 1.7 |
| 191 | TR30B | C30 tricyclic terpane (b) | 61.303 | 638 | 94 | 1.8 | 1.6 |
| 191 | TS | Ts 18α(H)-trisnorhopane | 57.694 | 1102 | 173 | 3.1 | 2.9 |
| 191 | TM | Tm 17α(H)-trisnorhopane | 59.333 | 1236 | 204 | 3.5 | 3.4 |
| 191 | H28 | C28 17α18α21β(H)-bisnorhopane | | | | | |
| 191 | NOR25H | C29 Nor-25-hopane | 63.953 | 843 | 132 | 2.4 | 2.2 |
| 191 | H29 | C29 Tm 17α(H)21β(H)-norhopane | 65.104 | 4097 | 637 | 11.5 | 10.5 |
| 191 | C29TS | C29 Ts 18α(H)-norneohopane | 65.365 | 1093 | 151 | 3.1 | 2.5 |
| 191 | DH30 | C30 17α(H)-diahopane | 66.150 | 291 | 101 | 0.8 | 1.7 |
| 191 | M29 | C29 normoretane | 67.109 | 485 | 100 | 1.4 | 1.7 |
| 191 | OL | oleanane | | | | | |
| 191 | H30 | C30 17α(H)-hopane | 68.591 | 5329 | 782 | 15.0 | 12.9 |
| 191 | M30 | C30 moretane | 70.160 | 1024 | 128 | 2.9 | 2.1 |

*Appendix F3, ctd.*

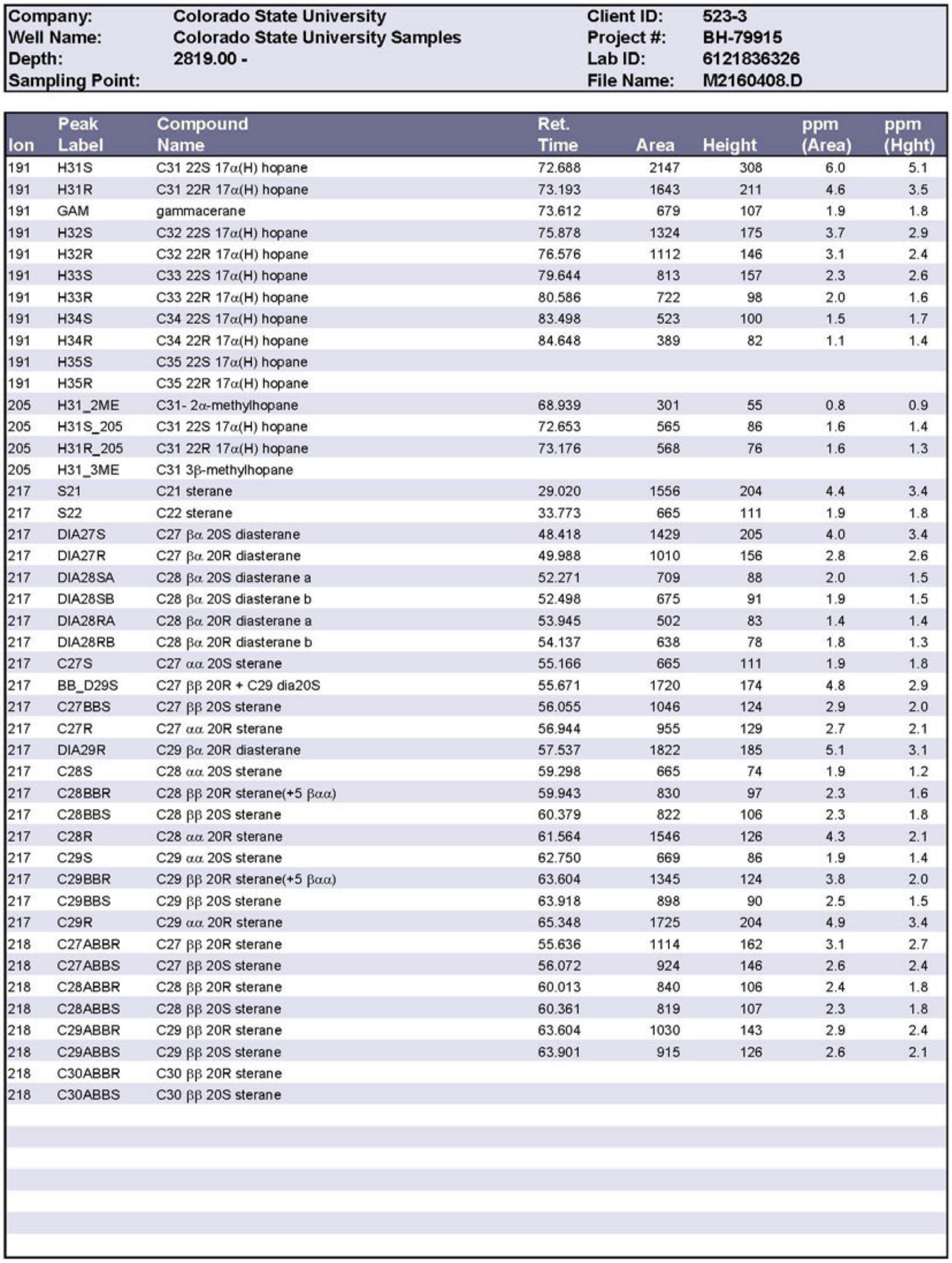

| | | | |
|---|---|---|---|
| **Company:** | **Colorado State University** | **Client ID:** | **523-3** |
| **Well Name:** | **Colorado State University Samples** | **Project #:** | **BH-79915** |
| **Depth:** | **2819.00 -** | **Lab ID:** | **6121836326** |
| **Sampling Point:** | | **File Name:** | **M2160408.D** |

| Ion | Peak Label | Compound Name | Ret. Time | Area | Height | ppm (Area) | ppm (Hght) |
|---|---|---|---|---|---|---|---|
| 191 | H31S | C31 22S 17α(H) hopane | 72.688 | 2147 | 308 | 6.0 | 5.1 |
| 191 | H31R | C31 22R 17α(H) hopane | 73.193 | 1643 | 211 | 4.6 | 3.5 |
| 191 | GAM | gammacerane | 73.612 | 679 | 107 | 1.9 | 1.8 |
| 191 | H32S | C32 22S 17α(H) hopane | 75.878 | 1324 | 175 | 3.7 | 2.9 |
| 191 | H32R | C32 22R 17α(H) hopane | 76.576 | 1112 | 146 | 3.1 | 2.4 |
| 191 | H33S | C33 22S 17α(H) hopane | 79.644 | 813 | 157 | 2.3 | 2.6 |
| 191 | H33R | C33 22R 17α(H) hopane | 80.586 | 722 | 98 | 2.0 | 1.6 |
| 191 | H34S | C34 22S 17α(H) hopane | 83.498 | 523 | 100 | 1.5 | 1.7 |
| 191 | H34R | C34 22R 17α(H) hopane | 84.648 | 389 | 82 | 1.1 | 1.4 |
| 191 | H35S | C35 22S 17α(H) hopane | | | | | |
| 191 | H35R | C35 22R 17α(H) hopane | | | | | |
| 205 | H31_2ME | C31- 2α-methylhopane | 68.939 | 301 | 55 | 0.8 | 0.9 |
| 205 | H31S_205 | C31 22S 17α(H) hopane | 72.653 | 565 | 86 | 1.6 | 1.4 |
| 205 | H31R_205 | C31 22R 17α(H) hopane | 73.176 | 568 | 76 | 1.6 | 1.3 |
| 205 | H31_3ME | C31 3β-methylhopane | | | | | |
| 217 | S21 | C21 sterane | 29.020 | 1556 | 204 | 4.4 | 3.4 |
| 217 | S22 | C22 sterane | 33.773 | 665 | 111 | 1.9 | 1.8 |
| 217 | DIA27S | C27 βα 20S diasterane | 48.418 | 1429 | 205 | 4.0 | 3.4 |
| 217 | DIA27R | C27 βα 20R diasterane | 49.988 | 1010 | 156 | 2.8 | 2.6 |
| 217 | DIA28SA | C28 βα 20S diasterane a | 52.271 | 709 | 88 | 2.0 | 1.5 |
| 217 | DIA28SB | C28 βα 20S diasterane b | 52.498 | 675 | 91 | 1.9 | 1.5 |
| 217 | DIA28RA | C28 βα 20R diasterane a | 53.945 | 502 | 83 | 1.4 | 1.4 |
| 217 | DIA28RB | C28 βα 20R diasterane b | 54.137 | 638 | 78 | 1.8 | 1.3 |
| 217 | C27S | C27 αα 20S sterane | 55.166 | 665 | 111 | 1.9 | 1.8 |
| 217 | BB_D29S | C27 ββ 20R + C29 dia20S | 55.671 | 1720 | 174 | 4.8 | 2.9 |
| 217 | C27BBS | C27 ββ 20S sterane | 56.055 | 1046 | 124 | 2.9 | 2.0 |
| 217 | C27R | C27 αα 20R sterane | 56.944 | 955 | 129 | 2.7 | 2.1 |
| 217 | DIA29R | C29 βα 20R diasterane | 57.537 | 1822 | 185 | 5.1 | 3.1 |
| 217 | C28S | C28 αα 20S sterane | 59.298 | 665 | 74 | 1.9 | 1.2 |
| 217 | C28BBR | C28 ββ 20R sterane(+5 βαα) | 59.943 | 830 | 97 | 2.3 | 1.6 |
| 217 | C28BBS | C28 ββ 20S sterane | 60.379 | 822 | 106 | 2.3 | 1.8 |
| 217 | C28R | C28 αα 20R sterane | 61.564 | 1546 | 126 | 4.3 | 2.1 |
| 217 | C29S | C29 αα 20S sterane | 62.750 | 669 | 86 | 1.9 | 1.4 |
| 217 | C29BBR | C29 ββ 20R sterane(+5 βαα) | 63.604 | 1345 | 124 | 3.8 | 2.0 |
| 217 | C29BBS | C29 ββ 20S sterane | 63.918 | 898 | 90 | 2.5 | 1.5 |
| 217 | C29R | C29 αα 20R sterane | 65.348 | 1725 | 204 | 4.9 | 3.4 |
| 218 | C27ABBR | C27 ββ 20R sterane | 55.636 | 1114 | 162 | 3.1 | 2.7 |
| 218 | C27ABBS | C27 ββ 20S sterane | 56.072 | 924 | 146 | 2.6 | 2.4 |
| 218 | C28ABBR | C28 ββ 20R sterane | 60.013 | 840 | 106 | 2.4 | 1.8 |
| 218 | C28ABBS | C28 ββ 20S sterane | 60.361 | 819 | 107 | 2.3 | 1.8 |
| 218 | C29ABBR | C29 ββ 20R sterane | 63.604 | 1030 | 143 | 2.9 | 2.4 |
| 218 | C29ABBS | C29 ββ 20S sterane | 63.901 | 915 | 126 | 2.6 | 2.1 |
| 218 | C30ABBR | C30 ββ 20R sterane | | | | | |
| 218 | C30ABBS | C30 ββ 20S sterane | | | | | |

*Appendix F3, ctd.*

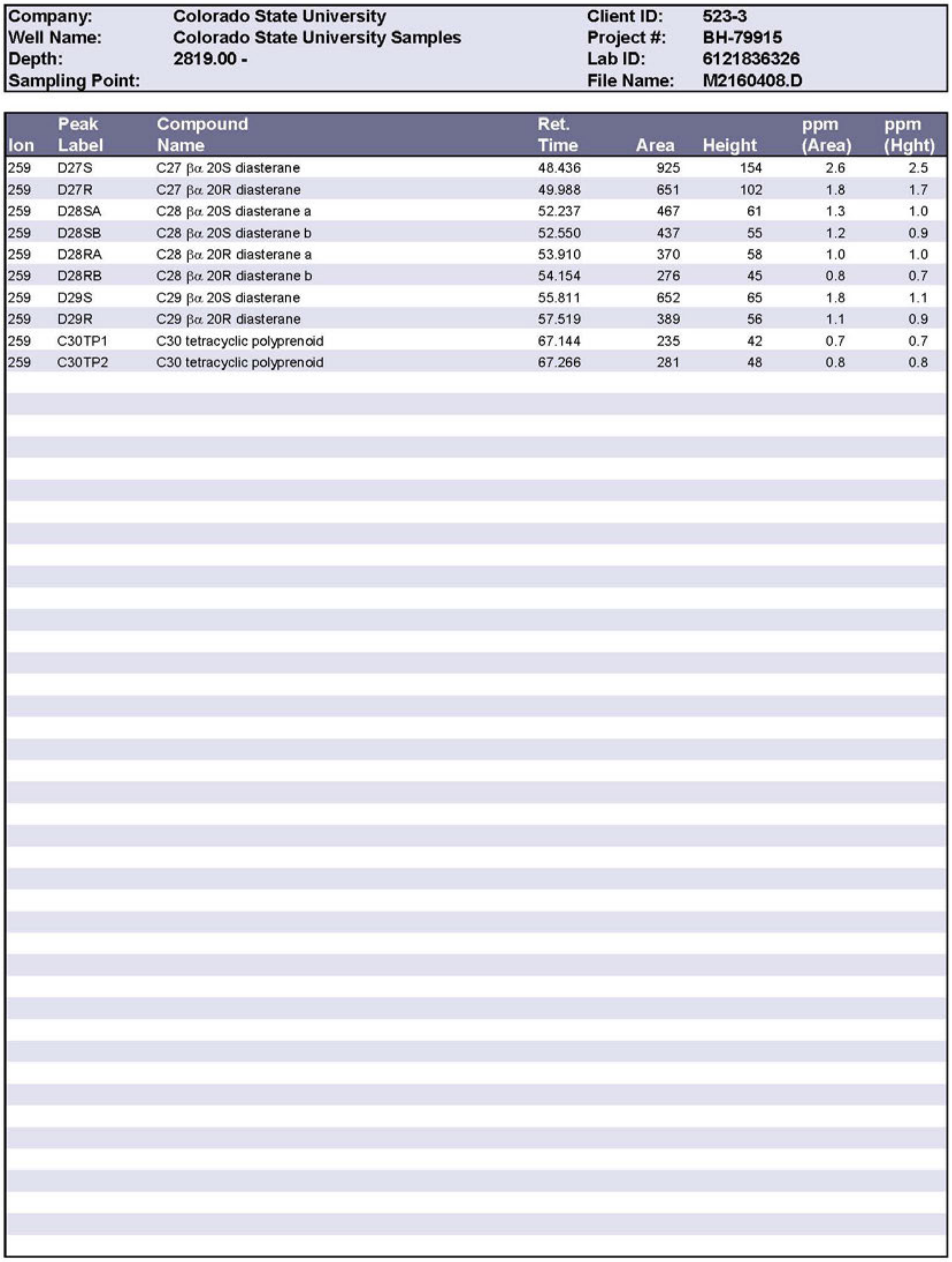

| | | | |
|---|---|---|---|
| **Company:** | **Colorado State University** | **Client ID:** | **523-3** |
| **Well Name:** | **Colorado State University Samples** | **Project #:** | **BH-79915** |
| **Depth:** | **2819.00 -** | **Lab ID:** | **6121836326** |
| **Sampling Point:** | | **File Name:** | **M2160408.D** |

| Ion | Peak Label | Compound Name | Ret. Time | Area | Height | ppm (Area) | ppm (Hght) |
|---|---|---|---|---|---|---|---|
| 259 | D27S | C27 βα 20S diasterane | 48.436 | 925 | 154 | 2.6 | 2.5 |
| 259 | D27R | C27 βα 20R diasterane | 49.988 | 651 | 102 | 1.8 | 1.7 |
| 259 | D28SA | C28 βα 20S diasterane a | 52.237 | 467 | 61 | 1.3 | 1.0 |
| 259 | D28SB | C28 βα 20S diasterane b | 52.550 | 437 | 55 | 1.2 | 0.9 |
| 259 | D28RA | C28 βα 20R diasterane a | 53.910 | 370 | 58 | 1.0 | 1.0 |
| 259 | D28RB | C28 βα 20R diasterane b | 54.154 | 276 | 45 | 0.8 | 0.7 |
| 259 | D29S | C29 βα 20S diasterane | 55.811 | 652 | 65 | 1.8 | 1.1 |
| 259 | D29R | C29 βα 20R diasterane | 57.519 | 389 | 56 | 1.1 | 0.9 |
| 259 | C30TP1 | C30 tetracyclic polyprenoid | 67.144 | 235 | 42 | 0.7 | 0.7 |
| 259 | C30TP2 | C30 tetracyclic polyprenoid | 67.266 | 281 | 48 | 0.8 | 0.8 |

*Appendix F3, ctd.*

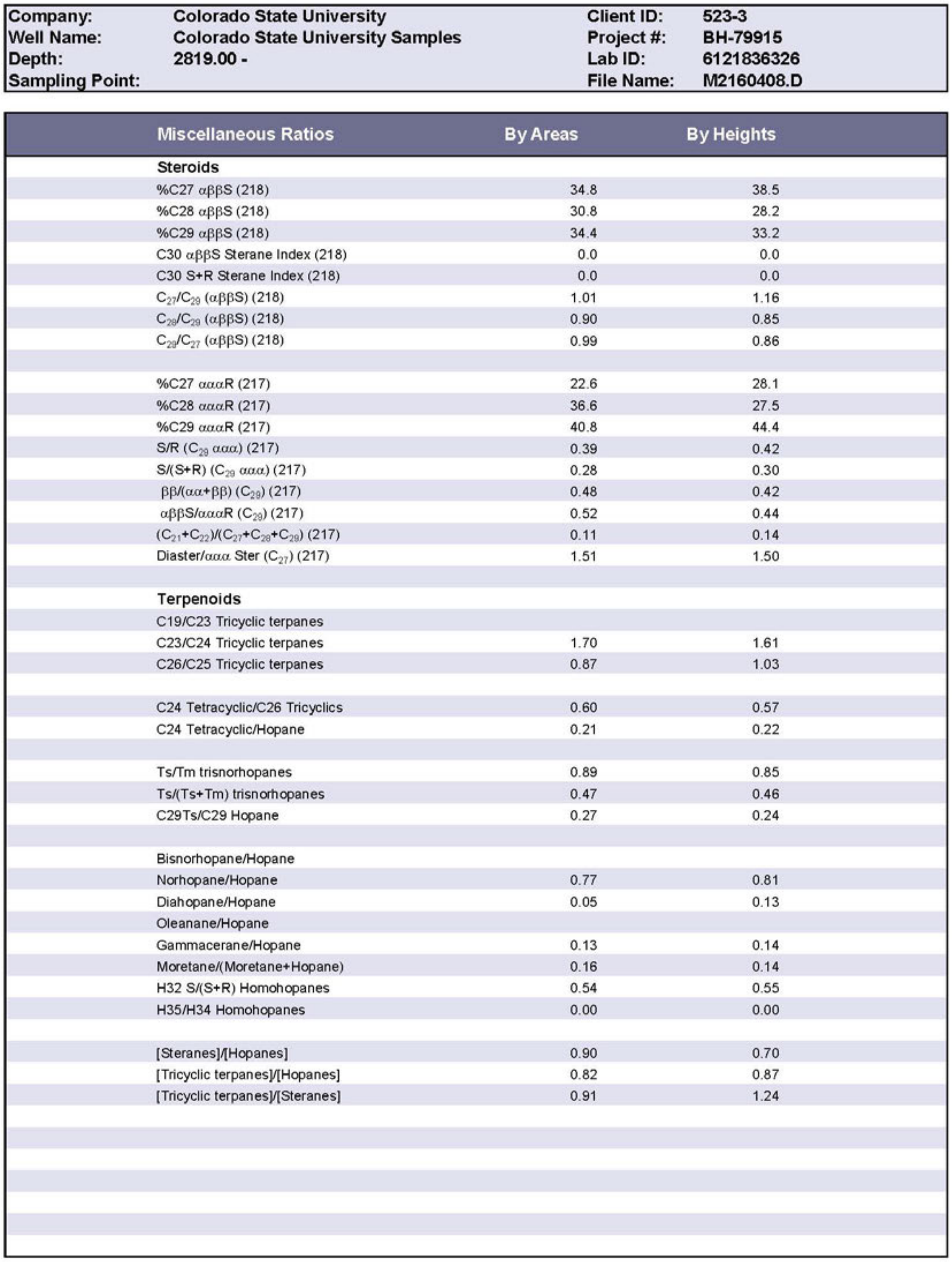

| | | | |
|---|---|---|---|
| **Company:** | **Colorado State University** | **Client ID:** | **523-3** |
| **Well Name:** | **Colorado State University Samples** | **Project #:** | **BH-79915** |
| **Depth:** | **2819.00 -** | **Lab ID:** | **6121836326** |
| **Sampling Point:** | | **File Name:** | **M2160408.D** |

| Miscellaneous Ratios | By Areas | By Heights |
|---|---|---|
| **Steroids** | | |
| %C27 αββS (218) | 34.8 | 38.5 |
| %C28 αββS (218) | 30.8 | 28.2 |
| %C29 αββS (218) | 34.4 | 33.2 |
| C30 αββS Sterane Index (218) | 0.0 | 0.0 |
| C30 S+R Sterane Index (218) | 0.0 | 0.0 |
| $C_{27}/C_{29}$ (αββS) (218) | 1.01 | 1.16 |
| $C_{28}/C_{29}$ (αββS) (218) | 0.90 | 0.85 |
| $C_{28}/C_{27}$ (αββS) (218) | 0.99 | 0.86 |
| | | |
| %C27 αααR (217) | 22.6 | 28.1 |
| %C28 αααR (217) | 36.6 | 27.5 |
| %C29 αααR (217) | 40.8 | 44.4 |
| S/R ($C_{29}$ ααα) (217) | 0.39 | 0.42 |
| S/(S+R) ($C_{29}$ ααα) (217) | 0.28 | 0.30 |
| ββ/(αα+ββ) ($C_{29}$) (217) | 0.48 | 0.42 |
| αββS/αααR ($C_{29}$) (217) | 0.52 | 0.44 |
| ($C_{21}$+$C_{22}$)/($C_{27}$+$C_{28}$+$C_{29}$) (217) | 0.11 | 0.14 |
| Diaster/ααα Ster ($C_{27}$) (217) | 1.51 | 1.50 |
| | | |
| **Terpenoids** | | |
| C19/C23 Tricyclic terpanes | | |
| C23/C24 Tricyclic terpanes | 1.70 | 1.61 |
| C26/C25 Tricyclic terpanes | 0.87 | 1.03 |
| | | |
| C24 Tetracyclic/C26 Tricyclics | 0.60 | 0.57 |
| C24 Tetracyclic/Hopane | 0.21 | 0.22 |
| | | |
| Ts/Tm trisnorhopanes | 0.89 | 0.85 |
| Ts/(Ts+Tm) trisnorhopanes | 0.47 | 0.46 |
| C29Ts/C29 Hopane | 0.27 | 0.24 |
| | | |
| Bisnorhopane/Hopane | | |
| Norhopane/Hopane | 0.77 | 0.81 |
| Diahopane/Hopane | 0.05 | 0.13 |
| Oleanane/Hopane | | |
| Gammacerane/Hopane | 0.13 | 0.14 |
| Moretane/(Moretane+Hopane) | 0.16 | 0.14 |
| H32 S/(S+R) Homohopanes | 0.54 | 0.55 |
| H35/H34 Homohopanes | 0.00 | 0.00 |
| | | |
| [Steranes]/[Hopanes] | 0.90 | 0.70 |
| [Tricyclic terpanes]/[Hopanes] | 0.82 | 0.87 |
| [Tricyclic terpanes]/[Steranes] | 0.91 | 1.24 |

*Appendix F3, ctd.*

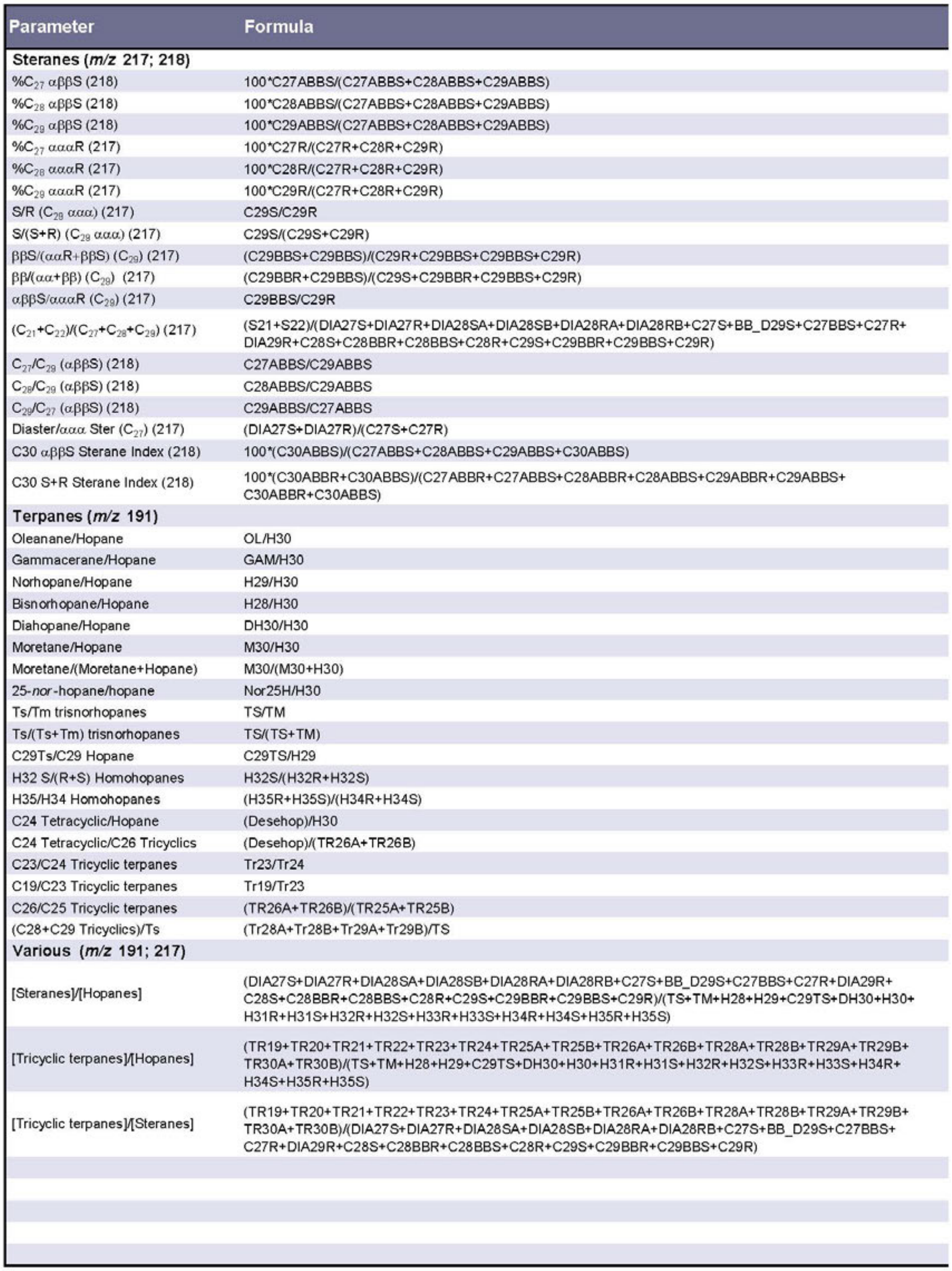

| Parameter | Formula |
|---|---|
| **Steranes (*m/z* 217; 218)** | |
| %$C_{27}$ αββS (218) | 100*C27ABBS/(C27ABBS+C28ABBS+C29ABBS) |
| %$C_{28}$ αββS (218) | 100*C28ABBS/(C27ABBS+C28ABBS+C29ABBS) |
| %$C_{29}$ αββS (218) | 100*C29ABBS/(C27ABBS+C28ABBS+C29ABBS) |
| %$C_{27}$ αααR (217) | 100*C27R/(C27R+C28R+C29R) |
| %$C_{28}$ αααR (217) | 100*C28R/(C27R+C28R+C29R) |
| %$C_{29}$ αααR (217) | 100*C29R/(C27R+C28R+C29R) |
| S/R ($C_{29}$ ααα) (217) | C29S/C29R |
| S/(S+R) ($C_{29}$ ααα) (217) | C29S/(C29S+C29R) |
| ββS/(ααR+ββS) ($C_{29}$) (217) | (C29BBS+C29BBS)/(C29R+C29BBS+C29BBS+C29R) |
| ββ/(αα+ββ) ($C_{29}$) (217) | (C29BBR+C29BBS)/(C29S+C29BBR+C29BBS+C29R) |
| αββS/αααR ($C_{29}$) (217) | C29BBS/C29R |
| ($C_{21}$+$C_{22}$)/($C_{27}$+$C_{28}$+$C_{29}$) (217) | (S21+S22)/(DIA27S+DIA27R+DIA28SA+DIA28SB+DIA28RA+DIA28RB+C27S+BB_D29S+C27BBS+C27R+DIA29R+C28S+C28BBR+C28BBS+C28R+C29S+C29BBR+C29BBS+C29R) |
| $C_{27}$/$C_{29}$ (αββS) (218) | C27ABBS/C29ABBS |
| $C_{28}$/$C_{29}$ (αββS) (218) | C28ABBS/C29ABBS |
| $C_{29}$/$C_{27}$ (αββS) (218) | C29ABBS/C27ABBS |
| Diaster/ααα Ster ($C_{27}$) (217) | (DIA27S+DIA27R)/(C27S+C27R) |
| C30 αββS Sterane Index (218) | 100*(C30ABBS)/(C27ABBS+C28ABBS+C29ABBS+C30ABBS) |
| C30 S+R Sterane Index (218) | 100*(C30ABBR+C30ABBS)/(C27ABBR+C27ABBS+C28ABBR+C28ABBS+C29ABBR+C29ABBS+C30ABBR+C30ABBS) |
| **Terpanes (*m/z* 191)** | |
| Oleanane/Hopane | OL/H30 |
| Gammacerane/Hopane | GAM/H30 |
| Norhopane/Hopane | H29/H30 |
| Bisnorhopane/Hopane | H28/H30 |
| Diahopane/Hopane | DH30/H30 |
| Moretane/Hopane | M30/H30 |
| Moretane/(Moretane+Hopane) | M30/(M30+H30) |
| 25-*nor*-hopane/hopane | Nor25H/H30 |
| Ts/Tm trisnorhopanes | TS/TM |
| Ts/(Ts+Tm) trisnorhopanes | TS/(TS+TM) |
| C29Ts/C29 Hopane | C29TS/H29 |
| H32 S/(R+S) Homohopanes | H32S/(H32R+H32S) |
| H35/H34 Homohopanes | (H35R+H35S)/(H34R+H34S) |
| C24 Tetracyclic/Hopane | (Desehop)/H30 |
| C24 Tetracyclic/C26 Tricyclics | (Desehop)/(TR26A+TR26B) |
| C23/C24 Tricyclic terpanes | Tr23/Tr24 |
| C19/C23 Tricyclic terpanes | Tr19/Tr23 |
| C26/C25 Tricyclic terpanes | (TR26A+TR26B)/(TR25A+TR25B) |
| (C28+C29 Tricyclics)/Ts | (Tr28A+Tr28B+Tr29A+Tr29B)/TS |
| **Various (*m/z* 191; 217)** | |
| [Steranes]/[Hopanes] | (DIA27S+DIA27R+DIA28SA+DIA28SB+DIA28RA+DIA28RB+C27S+BB_D29S+C27BBS+C27R+DIA29R+C28S+C28BBR+C28BBS+C28R+C29S+C29BBR+C29BBS+C29R)/(TS+TM+H28+H29+C29TS+DH30+H30+H31R+H31S+H32R+H32S+H33R+H33S+H34R+H34S+H35R+H35S) |
| [Tricyclic terpanes]/[Hopanes] | (TR19+TR20+TR21+TR22+TR23+TR24+TR25A+TR25B+TR26A+TR26B+TR28A+TR28B+TR29A+TR29B+TR30A+TR30B)/(TS+TM+H28+H29+C29TS+DH30+H30+H31R+H31S+H32R+H32S+H33R+H33S+H34R+H34S+H35R+H35S) |
| [Tricyclic terpanes]/[Steranes] | (TR19+TR20+TR21+TR22+TR23+TR24+TR25A+TR25B+TR26A+TR26B+TR28A+TR28B+TR29A+TR29B+TR30A+TR30B)/(DIA27S+DIA27R+DIA28SA+DIA28SB+DIA28RA+DIA28RB+C27S+BB_D29S+C27BBS+C27R+DIA29R+C28S+C28BBR+C28BBS+C28R+C29S+C29BBR+C29BBS+C29R) |

*Appendix F3, ctd.*

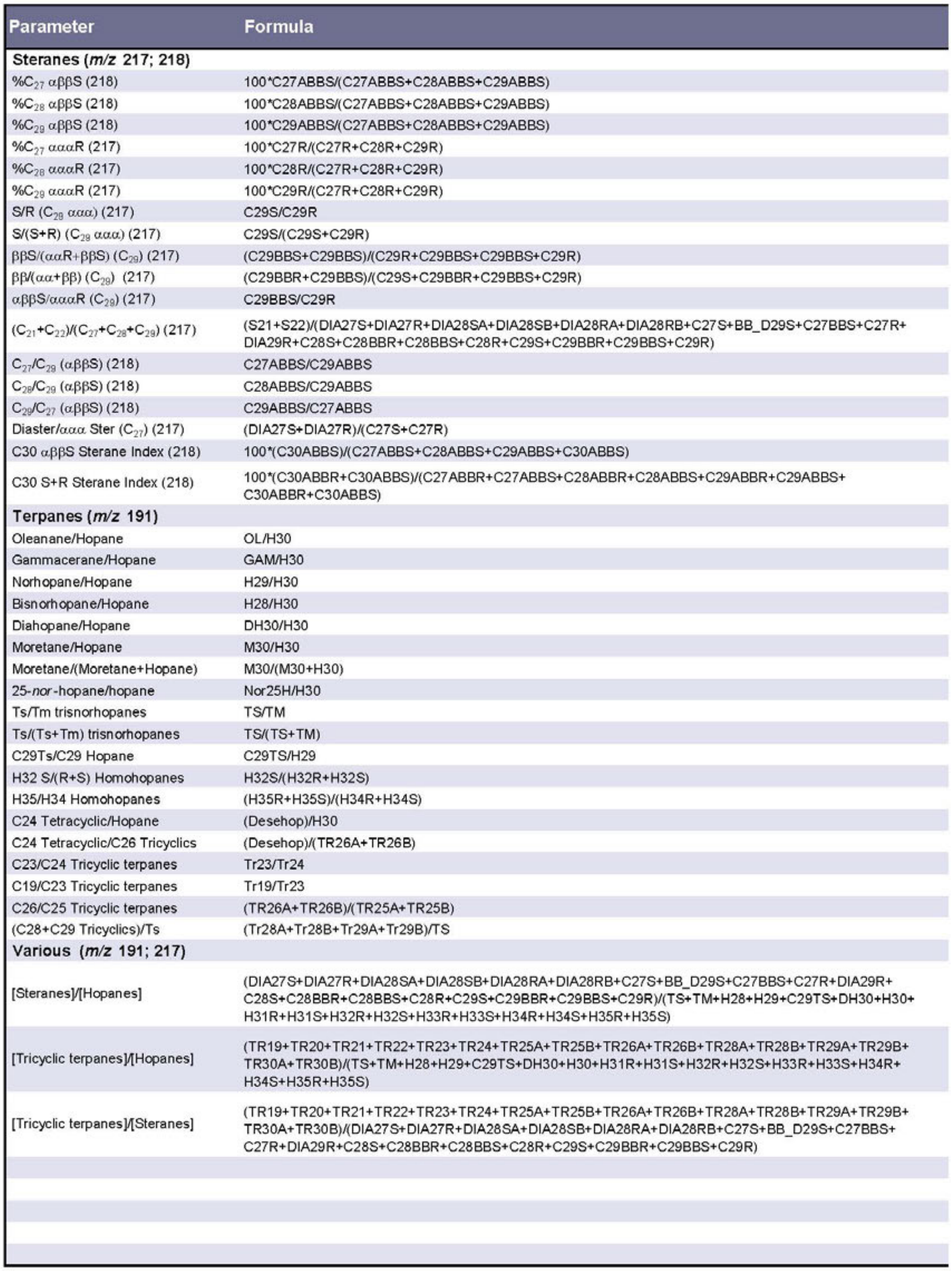

| Parameter | Formula |
|---|---|
| **Steranes (*m/z* 217; 218)** | |
| %$C_{27}$ $\alpha\beta\beta$S (218) | 100*C27ABBS/(C27ABBS+C28ABBS+C29ABBS) |
| %$C_{28}$ $\alpha\beta\beta$S (218) | 100*C28ABBS/(C27ABBS+C28ABBS+C29ABBS) |
| %$C_{29}$ $\alpha\beta\beta$S (218) | 100*C29ABBS/(C27ABBS+C28ABBS+C29ABBS) |
| %$C_{27}$ $\alpha\alpha\alpha$R (217) | 100*C27R/(C27R+C28R+C29R) |
| %$C_{28}$ $\alpha\alpha\alpha$R (217) | 100*C28R/(C27R+C28R+C29R) |
| %$C_{29}$ $\alpha\alpha\alpha$R (217) | 100*C29R/(C27R+C28R+C29R) |
| S/R ($C_{29}$ $\alpha\alpha\alpha$) (217) | C29S/C29R |
| S/(S+R) ($C_{29}$ $\alpha\alpha\alpha$) (217) | C29S/(C29S+C29R) |
| $\beta\beta$S/($\alpha\alpha$R+$\beta\beta$S) ($C_{29}$) (217) | (C29BBS+C29BBS)/(C29R+C29BBS+C29BBS+C29R) |
| $\beta\beta$/($\alpha\alpha$+$\beta\beta$) ($C_{29}$) (217) | (C29BBR+C29BBS)/(C29S+C29BBR+C29BBS+C29R) |
| $\alpha\beta\beta$S/$\alpha\alpha\alpha$R ($C_{29}$) (217) | C29BBS/C29R |
| ($C_{21}$+$C_{22}$)/($C_{27}$+$C_{28}$+$C_{29}$) (217) | (S21+S22)/(DIA27S+DIA27R+DIA28SA+DIA28SB+DIA28RA+DIA28RB+C27S+BB_D29S+C27BBS+C27R+DIA29R+C28S+C28BBR+C28BBS+C28R+C29S+C29BBR+C29BBS+C29R) |
| $C_{27}$/$C_{29}$ ($\alpha\beta\beta$S) (218) | C27ABBS/C29ABBS |
| $C_{28}$/$C_{29}$ ($\alpha\beta\beta$S) (218) | C28ABBS/C29ABBS |
| $C_{29}$/$C_{27}$ ($\alpha\beta\beta$S) (218) | C29ABBS/C27ABBS |
| Diaster/$\alpha\alpha\alpha$ Ster ($C_{27}$) (217) | (DIA27S+DIA27R)/(C27S+C27R) |
| C30 $\alpha\beta\beta$S Sterane Index (218) | 100*(C30ABBS)/(C27ABBS+C28ABBS+C29ABBS+C30ABBS) |
| C30 S+R Sterane Index (218) | 100*(C30ABBR+C30ABBS)/(C27ABBR+C27ABBS+C28ABBR+C28ABBS+C29ABBR+C29ABBS+C30ABBR+C30ABBS) |
| **Terpanes (*m/z* 191)** | |
| Oleanane/Hopane | OL/H30 |
| Gammacerane/Hopane | GAM/H30 |
| Norhopane/Hopane | H29/H30 |
| Bisnorhopane/Hopane | H28/H30 |
| Diahopane/Hopane | DH30/H30 |
| Moretane/Hopane | M30/H30 |
| Moretane/(Moretane+Hopane) | M30/(M30+H30) |
| 25-*nor*-hopane/hopane | Nor25H/H30 |
| Ts/Tm trisnorhopanes | TS/TM |
| Ts/(Ts+Tm) trisnorhopanes | TS/(TS+TM) |
| C29Ts/C29 Hopane | C29TS/H29 |
| H32 S/(R+S) Homohopanes | H32S/(H32R+H32S) |
| H35/H34 Homohopanes | (H35R+H35S)/(H34R+H34S) |
| C24 Tetracyclic/Hopane | (Desehop)/H30 |
| C24 Tetracyclic/C26 Tricyclics | (Desehop)/(TR26A+TR26B) |
| C23/C24 Tricyclic terpanes | Tr23/Tr24 |
| C19/C23 Tricyclic terpanes | Tr19/Tr23 |
| C26/C25 Tricyclic terpanes | (TR26A+TR26B)/(TR25A+TR25B) |
| (C28+C29 Tricyclics)/Ts | (Tr28A+Tr28B+Tr29A+Tr29B)/TS |
| **Various (*m/z* 191; 217)** | |
| [Steranes]/[Hopanes] | (DIA27S+DIA27R+DIA28SA+DIA28SB+DIA28RA+DIA28RB+C27S+BB_D29S+C27BBS+C27R+DIA29R+C28S+C28BBR+C28BBS+C28R+C29S+C29BBR+C29BBS+C29R)/(TS+TM+H28+H29+C29TS+DH30+H30+H31R+H31S+H32R+H32S+H33R+H33S+H34R+H34S+H35R+H35S) |
| [Tricyclic terpanes]/[Hopanes] | (TR19+TR20+TR21+TR22+TR23+TR24+TR25A+TR25B+TR26A+TR26B+TR28A+TR28B+TR29A+TR29B+TR30A+TR30B)/(TS+TM+H28+H29+C29TS+DH30+H30+H31R+H31S+H32R+H32S+H33R+H33S+H34R+H34S+H35R+H35S) |
| [Tricyclic terpanes]/[Steranes] | (TR19+TR20+TR21+TR22+TR23+TR24+TR25A+TR25B+TR26A+TR26B+TR28A+TR28B+TR29A+TR29B+TR30A+TR30B)/(DIA27S+DIA27R+DIA28SA+DIA28SB+DIA28RA+DIA28RB+C27S+BB_D29S+C27BBS+C27R+DIA29R+C28S+C28BBR+C28BBS+C28R+C29S+C29BBR+C29BBS+C29R) |

# LIST OF ACRONYMS AND ABBREVIATIONS

| | |
|---|---|
| BIR | Big Iron River |
| $C_{carb}$ | carbonate carbon |
| CF | Copper Falls, Bad River, WI |
| c.g. | coarse grained |
| $C_n$ | hydrocarbon containing *n* carbon atoms |
| $C_{org}$ | organic carbon |
| DBF | dibenzofuran |
| DBT | dibenzothiophene |
| DMDBF | dimethyldibenzofuran |
| DMDBT | dimethyldibenzothiophene |
| DMN | dimethylnaphthalene |
| DNx | dimethylnaphthalene index = (1,3-DMN+1,6-DMN)/(1,4-DMN+1,5-DMN) [after Radke *et al.*, 1987] |
| EOM | extractable organic matter |
| f.g. | fine grained |
| FI | fluid inclusion |
| FL | fluorene |
| GC | gas chromatography |
| GC-MS | gas chromatography-mass spectroscopy |
| HC | hydrocarbon |
| HI | hydrogen index |
| LIR | Little Iron River |
| MDEQ | Michigan Department of Environmental Quality |
| MDBF | methyldibenzofuran |
| MDBT | methyldibenzothiophene |
| MDR | methyldibenzothiophene ratio (per Radke *et al.*, 1986) = 4-MDBT/1-MDBT |
| methyldiamantane index | 4-methyldiamantane/[4- + 1- + 3-methyldiamantanes] (after Fang *et al*., 2016) |
| m.g. | medium grained |
| MP | methylphenanthrene |
| MPI1 | methylphenanthrene index (per Radke *et al*., 1982) =1.5 (2-MP + 3-MP) / (P+1-MP+9-MP) |
| MS | mass spectrometry |
| MSD | mass selective detector |
| OI | oxygen index |
| OM | organic matter |
| P | phenanthrene |
| PAH | polycyclic aromatic hydrocarbon |
| PH | pyrolysis, hydrous |
| Ph | phytane |
| PIR | Presque Isle River |
| Pr | pristine |
| PPL | plane polarized light |
| RE or RE II | Rock-Eval II |
| REFL | reflected light |
| SF | Saxon Falls, Montreal River, MI |
| SI | stable isotope |
| Ss | sandstone |

|  |  |
|---|---|
| SSC | sediment hosted stratiform copper |
| TAI | Thermal Alteration Index (after Jones and Edison, 1978) |
| TDS | total dissolved solids |
| TMN | trimethylnaphthalene |
| TNy | trimethylnaphthalene index<br>= (1,3,6-TMN+1,3,7-TMN)/(1,3,5-TMN+1,4,6-TMN) [after Radke *et al.*, 1987] |
| TSR | thermochemical sulfate reduction |
| UCM | unresolved complex mixture |
| VR | vitrinite reflectance |
| v.f.g. | very fine grained (likewise, v.c.g. means "very coarse grained") |
| VPDB | Vienna Pee Dee Belemnite |
| WP | White Pine, MI |
| XPL | cross polarized light |